VOLUME 79 DECEMBER 18, 1975 NUMBER 26

JPCHAx

THE JOURNAL OF PHYSICAL CHEMISTRY

Colloque Weyl IV

ELECTRONS IN FLUIDS—THE NATURE OF METAL–AMMONIA SOLUTIONS

MICHIGAN STATE UNIVERSITY • JUNE 30–JULY 3, 1975

PUBLISHED BIWEEKLY BY THE AMERICAN CHEMICAL SOCIETY

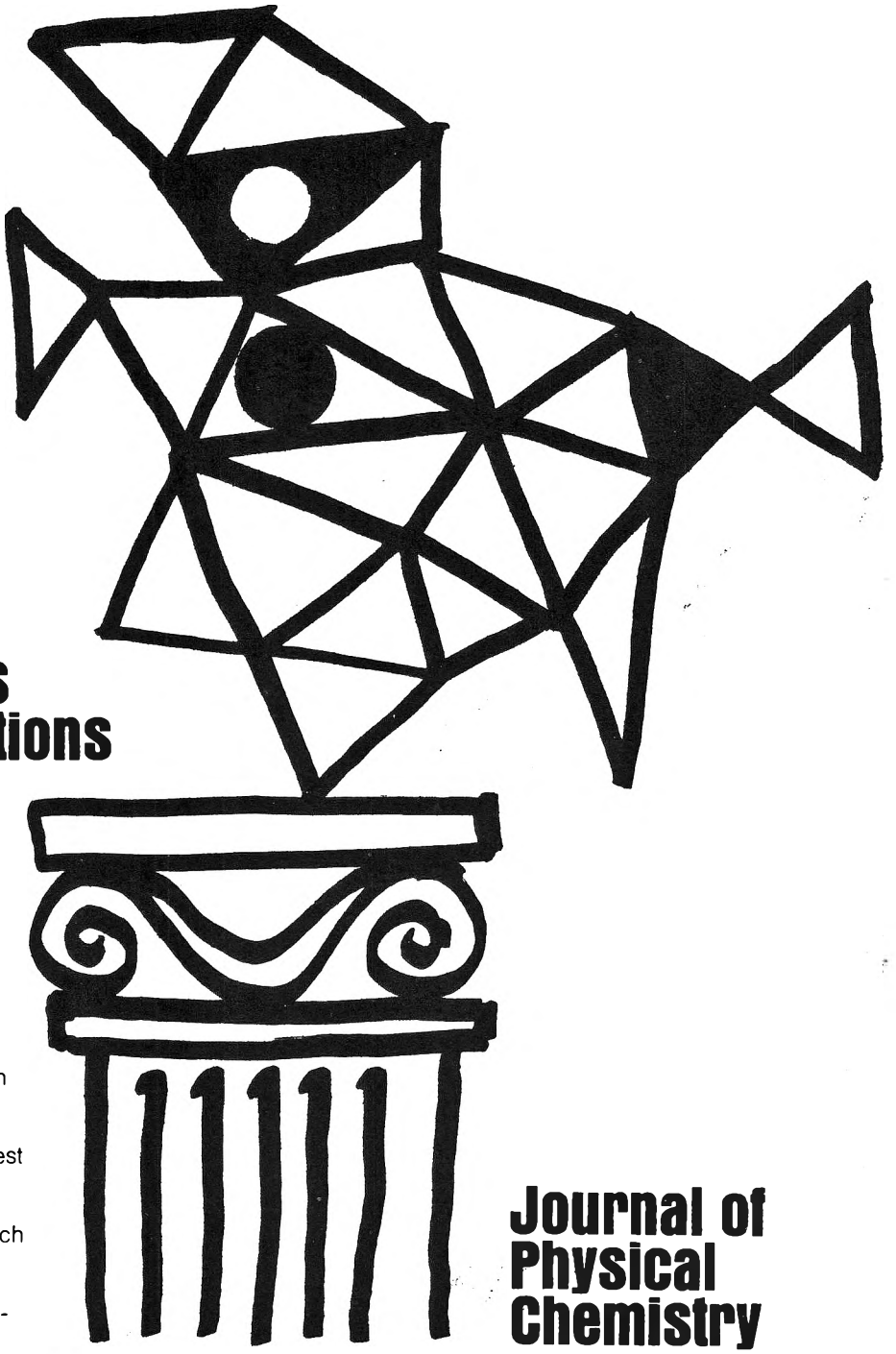

New concepts new techniques new interpretations

. . . together with valuable reports on classical areas

They are all waiting for you between the covers of our well-balanced JOURNAL OF PHYSICAL CHEMISTRY. Whatever your particular interest in physical chemistry, you'll find the JOURNAL's broad range of experimental and theoretical research reports are relevant and beneficial to your work. Each biweekly issue brings you an average of 30 authoritative, comprehensive reports on fundamental aspects of atomic and molecular phenomena, as well as timely notes, communications and reports plus the proceedings of selected symposia.

Join your fellow physical chemists who rely on JPC as an excellent biweekly source of data in both new and classical areas. Just complete and return the form to start your own subscription.

. . . *another ACS service*

Journal of Physical Chemistry

The Journal of Physical Chemistry
American Chemical Society **1976**
1155 Sixteenth Street, N.W.
Washington, D.C. 20036

Yes, I would like to receive the JOURNAL OF PHYSICAL CHEMISTRY at the one-year rate checked below:

	U.S.	*Canada***	*Latin America***	*Other Nations***
ACS Member One-Year Rate*	☐ $24.00	☐ $30.25	☐ $29.75	☐ $30.25
Nonmember	☐ $96.00	☐ $102.25	☐ $101.75	☐ $102.25

Bill me ☐ Bill company ☐ Payment enclosed ☐

Air freight rates available on request.

Name _____

Street _____ Home ☐ Business ☐

City _____ State _____ Zip _____

Journal subscriptions start January '76

*NOTE: Subscriptions at ACS member rates are for personal use only. **Payment must be made in U.S. currency, by international money order, UNESCO coupons, U.S. bank draft, or order through your book dealer.

THE JOURNAL OF

PHYSICAL CHEMISTRY

AMERICAN CHEMICAL SOCIETY, *1155 Sixteenth St., N.W., Washington, D.C. 20036*

Books and Journals Division

D. H. MICHAEL BOWEN *Director*

CHARLES R. BERTSCH *Head, Editorial Department*
BACIL GUILEY *Head, Graphics and Production Department*
SELDON W. TERRANT *Head, Research and Development Department*

 Published biweekly by the American Chemical Society at 20th and Northampton Sts., Easton, Pa. 18042. Second-class postage paid at Washington, D.C., and at additional mailing offices.

All manuscripts should be sent to *The Journal of Physical Chemistry,* Department of Chemistry, University of Minnesota, Minneapolis, Minn. 55455.

Additions and Corrections are published once yearly in the final issue. See Volume 78, Number 26 for the proper form.

Extensive or unusual alterations in an article after it has been set in type are made at the author's expense, and it is understood that by requesting such alterations the author agrees to defray the cost thereof.

The American Chemical Society and the Editor of *The Journal of Physical Chemistry* assume no responsibility for the statements and opinions advanced by contributors.

Correspondence regarding accepted copy, proofs, and reprints should be directed to Editorial Department, American Chemical Society, 20th and Northampton Sts., Easton, Pa. 18042. Department Head: CHARLES R. BERTSCH. Associate Department Head: MARIANNE C. BROGAN, Assistant Editors: CELIA B. MCFARLAND, JOSEPH E. YURVATI.

Advertising Office: Centcom, Ltd., 50 W. State St., Westport, Conn. 06880.

Business and Subscription Information

Send all new and renewal subscriptions *with payment* to: Office of the Controller, 1155 16th Street, N.W., Washington, D.C. 20036. Subscriptions should be renewed promptly to avoid a break in your series. All correspondence and telephone calls regarding changes of address, claims for missing issues, subscription service, the status of records, and accounts should be directed to Manager, Membership and Subscription Services, American Chemical Society, P.O. Box 3337, Columbus, Ohio 43210. Telephone (614) 421-7230. For microfiche service, contact ACS Microfiche Service, 1155 16th St. N.W., Washington, D.C. 20036. Telephone (202) 872-4444.

On changes of address, include both old and new addresses with ZIP code numbers, accompanied by mailing label from a recent issue. Allow four weeks for change to become effective.

Claims for missing numbers will not be allowed (1) if loss was due to failure of notice of change in address to be received before the date specified, (2) if received more than sixty days from date of issue plus time normally required for postal delivery of journal and claim, or (3) if the reason for the claim is "issue missing from files."

Subscription rates (hard copy or microfiche) in 1975: $20.00 for 1 year to ACS members; $80.00 to nonmembers. Extra postage $4.50 in Canada and PUAS, $5.00 other foreign. Supplementary material (on microfiche only) available on subscription basis, 1975 rates: $15.00 in U.S., $19.00 in Canada and PUAS, $20.00 elsewhere. All microfiche airmailed to non-U.S. addresses; air freight rates for hard-copy subscriptions available on request.

Single copies for current year: $4.00. Rates for back issues from Volume 56 to date are available from the Special Issues Sales Department, 1155 Sixteenth St., N.W., Washington, D.C. 20036.

Subscriptions to this and the other ACS periodical publications are available on microfilm. For information on microfilm write Special Issues Sales Department at the address above.

Notice to Authors last printed in the issue of July 3, 1975

Research Reviewed

Authoritative critical discussions by internationally recognized chemists in

CHEMICAL REVIEWS

Reactions, mechanisms, syntheses, spectroscopy and more—the many facets of theoretical chemistry explored in comprehensive, authoritative and critical articles in CHEMICAL REVIEWS. A timesaver for the serious scientist, bimonthly CHEMICAL REVIEWS covers in single articles the material that might otherwise require reading many papers from many sources. To keep current on new chemical insights and new correlations, mail the coupon below.

CHEMICAL REVIEWS **1976**
American Chemical Society
1155 Sixteenth Street, N.W.
Washington, D.C. 20036

Yes, I would like to receive CHEMICAL REVIEWS at the one-year rate checked below:

	U.S.	*Canada***	*Latin America***	*Other Nations***
ACS Member One-Year Rate*	☐ $15.00	☐ $18.50	☐ $18.25	☐ $18.50
Nonmember	☐ $60.00	☐ $63.50	☐ $63.25	☐ $63.50

Bill me ☐ Bill company ☐ Payment enclosed ☐

Air freight rates available on request.

Name _____

Street _____ Home ☐ Business ☐

City _____ State _____ Zip _____

Journal subscriptions start January '76

*NOTE: Subscriptions at ACS member rates are for personal use only. **Payment must be made in U.S. currency, by international money order, UNESCO coupons, U.S. bank draft, or order through your book dealer.

THE JOURNAL OF
PHYSICAL CHEMISTRY

Volume 79, Number 26 December 18, 1975

JPCHAx 79(26) 2789-3114 (1975)
ISSN 0022-3654

Colloque Weyl IV. Electrons in Fluids—The Nature of Metal-Ammonia Solutions

■ Supplementary material for this paper is available separately, in photocopy or microfiche form. Ordering information is given in the paper.

* In papers with more than one author, the asterisk indicates the name of the author to whom inquiries about the paper should be addressed.

AUTHOR INDEX

THE JOURNAL OF PHYSICAL CHEMISTRY

Volume 79

JANUARY—JUNE 1975

PAGES 1–1326

JPCHAx 79(1–13) 1–1326 (1975)
ISSN 0022-3654

THE JOURNAL OF PHYSICAL CHEMISTRY

Volume 79

JULY—DECEMBER 1975

PAGES 1327–3114

JPCHAx 79(14–26) 1327–3114 (1975)
ISSN 0022-3654

THE JOURNAL OF
PHYSICAL CHEMISTRY

VOLUME 79, NUMBER 26 DECEMBER 18, 1975

Colloque Weyl IV

Electrons in Fluids— The Nature of Metal–Ammonia Solutions

MICHIGAN STATE UNIVERSITY, EAST LANSING, MICHIGAN

MONDAY JUNE 30–THURSDAY JULY 3, 1975

Introductory Remarks

James L. Dye

Department of Chemistry, Michigan State University, East Lansing, Michigan 48824

Publication costs assisted by Colloque Weyl IV

The fourth international conference on metal–ammonia solutions was held June 29–July 3, 1975 at Michigan State University, East Lansing, Michigan. The original Colloque Weyl was held on the occasion of the 100th anniversary of Weyl's discovery of metal–ammonia solutions. It convened in June 1963 at the Catholic University of Lille, France under the direction of Professor Gerard Lepoutre and marked the first time that chemists and physicists with a common interest in the solvated electron met to exchange ideas about this interesting species in metal–ammonia solutions. Through the years, as the importance of electrons in fluids, not only in ammonia, but also in other polar and nonpolar solvents became apparent to workers in a variety of fields ranging from radiation chemistry to the physics of liquid metals, the scope of the conference expanded to include more than just metal solutions in ammonia. However, the major goal of the Weyl colloquium is to contribute to the understanding of metal–ammonia solutions.

After a lapse of 6 years, Colloque Weyl II was held at Cornell University, Ithaca, New York in June 1969, with Professor M. J. Sienko directing the arrangements. At that time an informal agreement was reached to hold such a conference every 3 years and to meet in the United States for alternate meetings. Colloque Weyl III was convened by Professor J. Jortner of Tel Aviv University, Israel, at Kibbutz Hanita in June 1972. At that time, tentative plans were made to hold the fourth conference at Michigan State University in 1975.

In view of the interdisciplinary nature of this field, the scope of the meeting included related work on electrons in polar and nonpolar fluids, the problem of electronic states in disordered systems, and the metal–insulator transition.

The organizers of Colloque Weyl IV are grateful to the National Science Foundation, the donors of the Petroleum Research Fund (administered by the American Chemical Society) and the Dow Chemical Company for partial support of the conference. We also acknowledge the cooperation of the Department of Chemistry and the Continuing Education Service of Michigan State University. We are grateful to the Session Chairmen for their help with the program. Special thanks are due Ann Tsiminakis of the Continuing Education Service for her skillful handling of arrangements for the conference and to Naomi Hack, who worked very effectively with the Chairman of the Organizing Committee from the inception of the conference to the publication of the manuscripts and discussion.

Organizing Committee: R. Dewald (Tufts), J. Jortner (Tel Aviv), G. Lepoutre (Lille), U. Schindewolf (Karlsruhe), M. Sienko (Cornell), J. Thompson (Texas).

List of Participants and Affiliation

J. Acrivos — San Jose State University
C. Andrews — Michigan State University
S. Arai — Wako-Shi, Japan
D. A. Armstrong — University of Calgary, Canada
J. K. Baird — Oak Ridge National Laboratory
G. Bakale — Case-Western Reserve University
H. Bale — University of North Dakota
J. Belloni — University of Paris, Orsay, France
A. Bernas — University of Paris, Orsay, France
B. Bockrath — Energy Research and Development Administration, Pittsburgh, Pa.
D. Bowen — University of Texas—El Paso
G. Caflisch — University of Wisconsin—Madison
R. Catterall — University of Salford, England
J. Ceraso — Michigan State University
J. Chase — University of Toronto, Canada
L. Chia — New York University
P. Chieux — Institut Laue-Langevin, Grenoble, France
M. Cohen — University of Chicago
L. V. Coulter — Boston University
M. DaGue — Michigan State University
P. Damay — Lille, France
M. DeBacker — Lille, France
B. J. DeBettignies, Villeneuve, France
P. Delahay — New York University
R. Dewald — Tufts University
L. Dorfman — Ohio State University
R. Firestone — Ohio State University
J. W. Fletcher — AEC, Chalk River, Ontario, Canada
G. Freeman — University of Alberta, Canada
K. Fueki — Nagoya University, Japan
W. S. Glaunsinger — Arizona State University
S. Golden — Brandeis University
G. Hall — University of Toronto, Canada
T. Higashimura — Kyoto University, Japan
R. Holroyd — Brookhaven National Laboratory
J. W. Hunt — University of Toronto, Canada
D. Huppert — Bell Laboratories, Murray Hill, N.J.
C. Subhash Jain — University of Chicago
J. Jortner — University of Tel-Aviv, Israel
M. Katsumoto — Lille, France
N. Kestner — Louisiana State University
L. Kevan — Wayne State University
N. Klassen — National Research Council of Canada
W. Koehler — Texas Christian University
A. M. Koulkes-Pujo — C.E.N. Saclay, France
P. Krebs — University of Karlsruhe, Germany
J. J. Lagowski — University of Texas—Austin
N. Lau — Tufts University
J. P. Lelieur — Lille, France
G. Lepoutre — Lille, France
W. Love — Arizona State University
R. F. Marzke — Arizona State University
E. Mei — Michigan State University
E. Minnich — Elmira College, New York
S. Nehari — Brandeis University and Tel-Aviv University
L. Nemec — New York University
M. Newton — Brookhaven National Laboratory
S. O. Nielsen — AECRE, Denmark
A. Patterson, Jr. — Yale University
W. Peer — University of Texas—Austin
A. K. Pikaev, Academy of Sciences, Moscow, USSR
K. Plowman — McGill University, Montreal, Canada
S. Rice — Oxford University, England
P. Rusch — Chemical Abstracts Service, Columbus, Ohio
P. Schettler — Juniata College, Pennsylvania
U. Schindewolf — University of Karlsruhe, Germany
W. A. Seddon — AEC, Chalk River, Ontario, Canada
M. Sienko — Cornell University
M. Silver — University of North Carolina
W. S. Struve — Iowa State University
J. Thompson — University of Texas—Austin
T. Tuttle — Bandeis University
R. VonDreele — Arizona State University
B. Webster — University of Glasgow, Scotland
T. White — Arizona State University
J. E. Willard — University of Wisconsin
M. Yemen — Michigan State University

COLLOQUE WEYL IV FINAL PROGRAM

(Papers as presented at the sessions.)

SESSION A: Theories and Models of Electrons in Polar Fluids
Session Chairman: J. Jortner, Tel Aviv University, Israel

Marshall D. Newton, Chemistry Department, Brookhaven National Laboratory, Upton, N.Y. 11973
The Role of ab Initio Calculations in Elucidating Properties of Hydrated and Ammoniated Electrons

Brian Webster, Chemistry Department, University of Glasgow, Glasgow G12 8QQ , Scotland
Ab Initio Studies into the Mechanisms of Formation of the Hydrated Electron

Neil R. Kestner and Jean Logan, Chemistry Department, Louisiana State University, Baton Rouge, La. 70803
Theoretical Studies on the Composition of the Absorption Spectrum of the Solvated Electron

Sidney Golden, Chemistry Department, Brandeis University, Waltham, Mass. 02154
Model Adiabaticity Effects on Solvation Free-Energies of Electrons

Paul D. Schettler, Jr., Lille, France and Juniata College, Pa., **and Gerard Lepoutre,** Lille, France
Interactions between Solvated Electrons. I. Electron–Electron, Electron–Solvent, Solvent–Solvent Interactions in Ammonia. Valence Bond Approximation

* **K. Plowman,** McGill University, Canada, **and J. J. Lagowski,** University of Texas at Austin
A Vibrational Analysis of the Solvent as It Pertains to the Nature of Metal–Ammonia Solutions

R. R. Dogonadze, E. M. Itskovitch, A. M. Kuznetsov, and M. A. Vorotyntsev, Institute of Electrochemistry of the Academy of Sciences of the USSR, Moscow State University
Theory of Light Absorption by Ions in Solution

SESSION B: The Electron Localization Process
Session Chairman: U. Schindewolf, Karlsruhe, Germany

John W. Hunt and W. John Chase, Ontario Cancer Institute and Department of Medical Biophysics, University of Toronto, Toronto, Ontario, Canada M4X 1K9
Solvation Time of the Electron in Polar Liquids. Water and Alcohols

Larry Kevan, Department of Chemistry, Wayne State University, Detroit, Mich. 48202
Pulse Radiolysis Study of Solvated Electrons in Water–Ethanol Glasses at 76 K. Structure of the First Solvation Shell Around the Electron

J. Belloni, E. Saito, and M. Clerc, Orsay, France
Solvation Time of Electrons in Liquid Ammonia

** **P. M. Rentzepis, W. Struve, and D. Huppert,** Bell Laboratories, Murray Hill, N.J. 07974
Dynamics of the Solvating Electron and the Hole Burning in NH_3–Na Solutions by Picosecond Pulses

** **P. M. Rentzepis and D. Huppert,** Bell Laboratories, Murray Hill, N.J. 07974
Kinetics of Electrons in Methylamine–Sodium Solutions by Picosecond Pulses

SESSION C: Electrons in Dense Vapors and Nonpolar Liquids
Session Chairman: G. R. Freeman, University of Alberta, Edmonton, Canada

Richard Holroyd, Steven Tames, and Alvin Kennedy, Chemistry Department, Brookhaven National Laboratory, Upton, N.Y. 11973
The Effect of Temperature on Conduction Band Energies and on Reactions of Electrons in Nonpolar Liquids

* **S. O. Nielsen,** AECRE, Denmark
Localization of Excess Electrons in Liquid Alkanes

J. K. Baird, Oak Ridge National Laboratory, Health Physics Division, Oak Ridge, Tenn. 37830
Continuum Dielectric Model for an Electron in a Nonpolar Fluid

Shoji Noda, Larry Kevan, Department of Chemistry, Wayne State University, Detroit, Mich. 48202, **and Kenji Fueki,** Department of Synthetic Chemistry, Faculty of Engineering, Nagoya University, Nagoya, Japan
Conduction State Energy of Excess Electrons in Condensed Media. Liquid Methane, Ethane, and Argon and Glassy Matrices

* **M. Silver and J. P. Hernandez,** Physics Department, University of North Carolina, Chapel Hill, N.C. 27514
Electron Transport and O_2^- Formation in Fluid Helium

D. A. Armstrong and S. S. Nagra, Department of Chemistry, The University of Calgary, Calgary, Alberta, Canada
Mechanisms of Thermal Electron Capture by HCl and HBr

J.-P. Dodelet, F.-Y. Jou, and G. R. Freeman, Chemistry Department, University of Alberta, Edmonton, Canada, T6G 2E1
An Electron Mobility Transition in Liquid Ethers

SESSION D: The Metal–Nonmetal Transition in Metal–Ammonia Solutions
Session Chairmen: T. Tuttle, Brandeis University, and J. C. Thompson, University of Texas

J. P. Lelieur, P. Damay, and G. Lepoutre, 13 rue de Toul, 49000 Lille, France
Magnetic Properties and the Metal–Nonmetal Transition in Metal–Ammonia Solutions

Sidney Golden, Chemistry Department, Brandeis University, Waltham, Mass. 02154; Isotope Department, The Weizmann Institute of Science, Rehovot, Israel; and Physical Chemistry Department, The Hebrew University, Jerusalem, Israel.
Magnetic Similarities and Differences of Some Chemical Models of Alkali Metal–Ammonia Solutions

* **D. N. Knapp and H. D. Bale,** University of North Dakota, Grand Forks, N.D.
Small Angle X-Ray Scattering from Metal–Ammonia Solutions

P. Chieux, Institut Laue Langevin, Grenoble, France
Concentration Fluctuations in the Nonmetal to Metal Transition Range of the ^7Li–ND_3 System. A Neutron Small Angle Scattering Experiment

D. E. Bowen, Physics Department, The University of Texas at El Paso, El Paso, Tex.
Ultrasound Absorption Studies in the Critical Region of Lithium–Ammonia Solutions

Morrel H. Cohen, The James Franck Institute and Department of Physics, The University of Chicago, Chicago, Ill. 60637, **and Joshua Jortner,** Department of Chemistry, Tel-Aviv University, Tel-Aviv, Israel
Metal–Nonmetal Transition in Metal–Ammonia Solutions via the Inhomogeneous Transport Regime

N. F. Mott, Cavendish Laboratory, University of Cambridge, England
The Metal–Insulator Transition in Metal–Ammonia Solutions

K. G. Breitschwerdt and H. Radscheit, Institute fur Angewandte Physik, Universitat Heidelberg, Heidelberg, Germany
Microwave Electronic Properties of Metal–Ammonia Solutions

S. Hahne and U. Schindewolf, Institut fur Physikalische Chemie und Elektrochemie, Universitat Karlsruhe, Germany
Temperature- and Pressure-Dependence of the Nonmetal–Metal Transition in Sodium–Ammonia Solutions (Electrical Conductivity and *PVT* Data up to 150°C and 1000 bars)

Masayuki Katsumoto and Pierre Damay, 13 rue de Toul, 59000 Lille, France
Phase Diagram for Liquid–Liquid Coexistence in the Li–ND_3 System

* **J. C. Thompson,** Department of Physics, The University of Texas at Austin, Tex. 78712
Phase Separation of Mixed Solutes in Liquid Ammonia

* **B. DeBettignies,** Universite des Sciences et Techniques de Lille, F-59650 Villeneuve d'ASCQ, France, **and M. G. DeBacker,** CNRS ERA 126, 13 rue de Toul, F-59046, Lille, France
Raman Spectra of Li–$4NH_3$ and Li–$4ND_3$ Solutions

Pierre Damay, Lille, France, **and Paul Schettler,** Lille, France and Juniata College, Juniata Pa.
Fluctuations in Metal–Ammonia Solutions

SESSION E: Optical Properties
Session Chairman: G. Lepoutre, Lille, France

Ladislav Nemec, Lucille Chia, and Paul Delahay, Department of Chemistry, New York University, 4 Washington Place, Room 514, New York, N.Y. 10003
Photoionization Spectra of Solutions as Obtained by Photoelectron Spectroscopy

P. Krebs, Institut fur Physikalische Chemie und Elektrochemie, Universitat Karlsruhe, Germany
Continuous Registration of Optical Absorption Spectra of Periodically Produced Solvated Electrons

W. Schmitt and U. Schindewolf, Institut fur Physikalische Chemie und Elektrochemie, Universitat Karlsruhe, Germany
Absorption Spectra of Excess Electrons in Alkali-Halide Salt Melts

* **Judith B. Weinstein and R. F. Firestone,** Department of Chemistry, The Ohio State University, Columbus, Ohio 43210
Dependence of the Thermodynamic Stability of the Solvated Electron in Binary Liquid Solutions on Thermodynamic Solution Stability Prior to Electron Injection

T. R. White and W. S. Glaunsinger, Arizona State University
Laser Raman Investigation of Dilute Metal–Ammonia Solution

W. F. Love, C. T. Walker, and W. S. Glaunsinger, Arizona State University
Brillouin Scattering in Dilute Metal–Ammonia Solutions

William Peer and J. J. Lagowski, The Robert A. Welch Laboratories, The University of Texas at Austin, Austin, Tex.
Metal–Ammonia Solutions. IX. Matrix Rank Analysis as an Indicator of the Number of Species Present

James W. Lundeen and William H. Koehler, Department of Chemistry, Texas Christian University, Fort Worth, Tex. 76129
Liquid Ammonia. A Comparative Study of Models via Raman Spectroscopy

G. Rubinstein, Ramapo College of New Jersey, Mahwah, N.J. 07430
Correlation of Optical and Magnetic Data for Na–NH_3 Solutions

SESSION F: Electrons in Disordered Solids
Session Chairman: L. Kevan, Wayne State University

John E. Willard, Department of Chemistry, University of Wisconsin, Madison Wis. 53706
Trapped Electrons in Organic Glasses

A. Bernas, D. Grand, and T. B. Truong, Orsay, France
Trapped Electrons Studied through Stimulated Neutralization Luminescence

A. Namiki, M. Noda, and T. Higashimura, Research Reactor Institute, Kyoto University, Japan
Capture of the Trapped Electron in Alcohol Glasses

SESSION G: Properties of Solid Metal–Amines and Related Compounds
Session Chairman: M. Sienko, Cornell University

R. F. Marzke and W. S. Glaunsinger, Arizona State University
Proton Magnetic Resonance Study of Metal–Ammonia Compounds

W. H. McKnight and J. C. Thompson, The University of Texas at Austin
Optical Properties of Concentrated Li–NH_3 Solutions and Solid $Li(NH_3)_4$

Therese David Pfeuty and M. J. Sienko, Baker Laboratory of Chemistry, Cornell University, Ithaca, N.Y. 14853
Electron Band Structure in Solid Hexaamminecalcium(0)

R. B. Von Dreele, W. S. Glaunsinger, Arizona State University, **A. L. Bowman, and J. L. Yarnell,** Los Alamos Scientific Laboratory
Neutron Diffraction Study of Hexaammine-d_3-calcium(0) at 75 K

P. Chieux, Grenoble, France, **M. J. Sienko,** Cornell University, **and F. DeBaecker,** Lille, France
Neutron Diffraction Study and Phase Diagram Investigation of the Solid Lithium–Ammonia Compound

Pierre Damay, Lille, France, **and M. J. Sienko,** Cornell University
Conduction Electron Spin Resonance of Lithium Tetraammine, $Li(NH_3)_4$

J. V. Acrivos, C. Delios, N. Y. Topsøe, and J. R. Salem, San Jose State University, San Jose, Calif. 95194
Insertion of NH_3 and N_2H_4 into Layer Disulfides

R. Catterall and P. P. Edwards, University of Salford, England
Electron Spin Resonance Studies of Localized Excess Electron States in Frozen Solutions of Alkali Metals in Hexamethylphosphoramide

R. Catterall and P. P. Edwards, University of Salford, England
Electron Spin Resonance Studies of Extended Excess Electron States in Frozen Solutions of Alkali Metals in Hexamethylphosphoramide

SESSION H: Reactions of Electrons
Session Chairman: L. Dorfman, Ohio State University

A. K. Pikaev, B. G. Erskov, and I. E. Makarov, Institute of Physical Chemistry of the Academy of Sciences of the USSR, Moscow, USSR
Influence of Nature of Matrix on Reactivity of Electrons in Irradiated Systems

M. J. Pilling and Stephen A. Rice, Physical Chemistry Laboratory, South Parks Road, Oxford, OX1 3QZ, England
The Effect of the Charge of an Electron Scavenger on the Rate of Electron Tunneling in Glasses and Liquids

A. M. Koulkes-Pujo, C.N.R.S., France, **L. Gilles, and J. Sutton,** Cen. Saclay, France
Kinetics Study of Selective Solvation of Electrons in Water–Dimethyl Sulfoxide Mixtures

Leon M. Dorfman and Bradley Bockrath, Department of Chemistry, The Ohio State University, Columbus, Ohio, 43210
The Solvated Electron as Reducing Species in the Submicrosecond Formation of Reactive Transients. Carbanions in Solution

George Bakale, Department of Radiology, Case Western Reserve University, Cleveland, Ohio 44106, **U. Sowada, and W. F. Schmidt,** Hahn-Meitner-Institut fur Kernforschung Berlin GmbH, Bereich Strahlenchemie, 1 Berlin 39, Germany
Electron Attachment to SF_6 in Nonpolar Liquids

SESSION I: Kinetics and Thermodynamics of Metal–Ammonia Solutions
Session Chairman: L. V. Coulter, Boston University

Robert R. Dewald, Tufts University, Medford, Mass. 02155
Mechanistic Studies of Metal–Ammonia Reductions

Pierre Damay, 13 rue de Toul, Lille 59046, France
Surface Tension of Metal–Ammonia Solutions

Gerard Billaud and Antoine Demortier, 13 rue de Toul, 59000 Lille, France
Dielectric Constant of Liquid Ammonia from −35 to +50°C and Its Influence on the Association between Solvated Electrons and Cations

J. W. Fletcher and W. A. Seddon, Physical Chemistry Branch, Atomic Energy of Canada, Limited, Chalk River Nuclear Laboratories, Chalk River, Ontario, K0J 1J0, Canada
Alkali Metal Species in Liquid Amines, Ammonia, and Ethers. Formation by Pulse Radiolysis

SESSION J: Alkali Metal Monomers and Anions
Session Chairmen: J. J. Lagowski, University of Texas and G. Lepoutre, Lille, France

Bradley Bockrath, James F. Gavlas, and Leon M. Dorfman, Department of Chemistry, The Ohio State University, Columbus, Ohio 43210
Spectra of e_{sol}^- Coupled with Metal Cations. Lithium in Tetrahydrofuran

James L. Dye, Charles W. Andrews, and S. E. Mathews, Department of Chemistry, Michigan State University, East Lansing, Mich. 48824
Strategies for the Preparation of Compounds of Alkali Metal Anions

T. R. Tuttle, Jr., Brandeis University
The Monomer and Its Paramagnetic Companion in Some Potassium Solutions in Alkylated Amines

James L. Dye, Charles W. Andrews, and Joseph M. Ceraso, Department of Chemistry, Michigan State University, East Lansing, Mich. 48824
NMR Studies of Alkali Anions

* **S. Nehari and K. Bar-Eli,** Department of Chemistry, Tel-Aviv University, Ramat-Aviv, Israel
On the Optical, Electrical, and Magnetic Properties of Alkali Metal Amine Solutions

* **J. V. Acrivos,** Department of Chemistry, San Jose State University, San Jose, California 95194
On the Dilemma of $M–NH_3$ Solutions

* Papers marked with a single asterisk were presented for discussion at the Colloquium but, for various reasons, are not included in this symposium issue.

** These papers have been combined into one paper by D. Huppert, P. M. Rentzepis, and W. S. Struve, Picosecond Dynamics of Localized Electrons in Metal–Ammonia and Metal–Methylamine Solutions

The Role of ab Initio Calculations in Elucidating Properties of Hydrated and Ammoniated Electrons

Marshall D. Newton

Chemistry Department, Brookhaven National Laboratory, Upton, New York 11973 *(Received August 14, 1975)*

Publication costs assisted by Brookhaven National Laboratory

The properties of solvated electrons are analyzed in terms of a self-consistent modified continuum model based on the techniques of ab initio molecular quantum mechanics. The model is semiclassical in spirit, employing the quantum mechanical density for the excess charge and the first solvation shell in conjunction with classical electrostatics, and is developed in a general form which can be straightforwardly applied to special cases of interest, such as the solvated mono- and dielectron complexes. The advantages and disadvantages of the technique are discussed in relation to other, more empirical approaches. Computational results are presented for excess electrons (mono- and dielectrons) in water and ammonia, and the role of long-range polarization of the medium in localizing the excess charge is analyzed. The variationally determined ground states are characterized in terms of equilibrium solvation shell geometry (appreciable cavities are implied for both water and ammonia), solvation energy, photoionization energy, and charge distribution. The finding of negative spin densities at the first solvent shell protons underscores the importance of a many electron theoretical treatment. Preliminary results for excited states are also reported. The calculated results are compared with experimental and other theoretical data, and the sensitivity of the results to various features of the model are discussed. Particular attention is paid to the number of solvent molecules required to trap the excess electron.

I. Introduction

The nature of excess electrons in polar fluids has been the focus of increasingly intense theoretical efforts in the past 30 years.[1] Early cavity models for electrons in liquid ammonia were developed and refined by Ogg,[2] Lipscomb,[3] and Stairs.[4] Many of the more elaborate models which have subsequently evolved were inspired in large part by a pivotal contribution of Jortner[5] in 1959. He developed a detailed theory based on the concept of the polaron,[6] but modified to include a cavity, which accounted for both spectroscopic and thermodynamic data. Theories for the properties of electrons in ammonia and other polar solvents have recently been reviewed by Webster and Howat[7] and by Kestner.[8]

The challenge to theory posed by excess electrons in polar fluids (and nonpolar fluids as well) is especially broad since the degree of localization of the excess electron may vary widely, ranging from the quasifree state down to the highly localized state characteristic of solvated anions. This situation is to be contrasted with species such as the hydronium or hydroxide ion in aqueous solution, where the excess charge appears to be fairly well localized on electron and vibrational time scales.[9,10] The nature of the stabilization of electrons in liquids like water and ammonia is of particular interest since the electron affinity of the monomers in the gas phase appears to be negative. One may also consider the possibility that under appropriate circumstances unpaired excess electrons in the liquid would prefer energetically to coalesce into solvated dielectrons.[11] The degree of localization of excess electrons is, of course, coupled to the polarization and configuration of the surrounding solvent, and a paramount theoretical question is the role of various short- and long-range solvent interactions in determining the electronic states available to the excess electron.

Stringent tests for current theories of electrons in polar fluids and glasses are provided by a growing body of thermodynamic, spectroscopic, magnetic, and conductivity data.[1] Recent electron and nuclear spin resonance studies of aqueous alkaline glasses give promise of yielding detailed microscopic information about the geometry of the first solvent shell and the extent of the excess electron density.[12] Also of great significance is recent work on excess electrons in dense water and ammonia vapor,[13] which allows earlier models based on the liquid to be extended, thereby helping to bridge the gap between liquids and low-density ($<10^{-3}$ g/cc) vapor. Studies of excess electrons in dilute solutions of polar molecules provide yet another probe of trapped electrons.[14] While experiments of the type just mentioned should help to answer the question as to how many polar molecules are needed to trap an electron, one must recognize that the occurrence of density or concentration fluctuations complicates the interpretation of such experiments.

Table I schematically summarizes some of the current semiempirical and ab initio models for excess electrons in polar fluids.[15-29] The terms "self-consistent field" and "adiabatic" appearing in Table I refer to models in which the excess electrons are assumed to move at frequencies respectively similar to or much less than those of the solvent molecule electrons. Hence the medium electrons "see" the effective "self-consistent field" (SCF) of the excess charge or respond adiabatically to its instantaneous field, in the SCF and adiabatic models, respectively.[30] Most of the theories in use today are semiempirical, either of the one-electron continuum (or semicontinuum) or valence-electron cluster type. In the cluster model the emphasis is on the microscopic details of the short-range interactions, with the cluster typically containing the excess electron and a first solvation shell of four to six molecules.[31] Simpler cluster models have considered the interaction of an electron with only one (monomer model)[16] or two (dimer model)[20,32]

TABLE I: Outline of Recent Theoretical Models for Solvated Electrons in Polar Liquids

Type of model	Investigators	Ref
A. Cluster models		
(1) Semiempirical (INDO)[a]	Cohan, Finkelstein, Weissmann	15
	Howat, Webster	16
	Ishimaru et al.	17
	Kerr, Williams	18
(2) Semiempirical (point dipole)	Tachiya, Mozumder	19
(3) Ab initio (LCAO SCF)	Naleway, Schwartz	20
	Newton	21
	Ishimaru et al.	17
	Webster	22
B. Continuum models		
(1) Configuration coordinate model	Tachiya, Tabata, Oshima	23
(2) Ab inito (SCF)[b]	Waber, Liberman	24
C. Semicontinuum models		
(1) Semiempirical (point dipole)		
(a) Adiabatic	Copeland, Kestner, Jortner	25
	Gaathon, Jortner	26
(b) Self-consistent field	Fueki, Feng, Kevan	27
(2) Ab initio		
(a) LCAO SCF	Newton	21,28
(b) Multiple scattering-Xα	Moskowitz, Boring, Wood	29

[a] For earlier non-INDO cluster models see ref 31 and 32. [b] The excess charge in this work was in the form of atomic anions.

solvent molecules. In the semicontinuum models the cluster, often simulated by point dipoles surrounding a cavity,[25-27] is embedded in a polarizable dielectric continuum. In this paper we concentrate on elucidating the powerful role which can now be played by the techniques of ab initio molecular quantum mechanics, thanks to the availability of high-speed digital computers.[33] Many electron ab initio techniques have been used in the context of both cluster[16,20-22] and semicontinuum models.[21,29] In the latter case it should be emphasized that since the simulation of the continuum invariably involves empirical parameters, the use of the term ab initio must be qualified. It is preferable to say that the ab initio treatment of a small cluster can be modified by a suitably simulated polarized continuum surrounding the cluster, thus yielding more general models which efficiently combine the requisite short- and long-range aspects of the problem, while retaining most of the usual advantages of conventional ab initio treatments. The continuum is characterized by empirical quantities such as temperature, dielectric constant, fluid density, surface tension, etc. The bearing of these empirical parameters on the validity of the variational principle will be discussed when the formalism is presented below.

Before turning to the details of the formalism, we make a few general qualitative comments about the semicontinuum approach, which will then be implemented in an ab initio framework in the remainder of the paper. The contributions to the electron solvation energy in the semicontinuum model (where the discrete cluster is identified with the inner solvation shell) can be classified as shown below. In this breakdown of the various interactions we have distinguished the excess electrons from those of the solvent molecules in the discrete cluster. While such a distinction is required in the "adiabatic" model as discussed above, it should be noted that in the SCF model which is adopted for most of our calculations, the excess electrons and those of the discrete cluster are indistinguishable.[30]

(1) Excess electron–solvent interactions: (a) short-range attractive and repulsive interactions with the discrete cluster, including electron exchange; (b) interaction with the polarized continuum, including orientational and electronic contributions; short-range interactions with the continuum which are not included by simple classical electrostatics can be simulated by a constant effective potential.[34]

(2) Medium rearrangement energy (relative to ordinary bulk liquid): (a) discrete cluster contribution (permanent and induced multipole interactions, H-bond breakage, etc.); (b) variation in effective number of "surface" molecules associated with cavity formation (can be simulated through surface tension term) and the interaction between the discrete cluster and the polarized continuum; (c) self-energy of the polarized continuum.

(3) Self-energy of the excess charge: (a) electronic kinetic energy; (b) Coulombic repulsion in the case of the dielectron.

Item 2b takes into account the fact that as the inner shell with a fixed number of solvent molecules expands so as to form a void space, some of the molecules in the next solvent shell (simulated by the continuum) begin to attain the character of surface molecules. Among the factors contributing to this phenomenon would be variations in H bonding between the two shells, an effect which clearly cannot be explicitly considered in the semicontinuum model.

Common to any semicontinuum approach are the problems involved in specifying (1) the boundary between the continuum and the microscopic cluster; and (2) the detailed nature of the dielectric response of the continuum. Thus while the full continuum polarization, including electronic and orientational terms, may contribute to the solvation energy, the electronic term does not contribute to the trapping potential if the excess electron is very weakly bound, as in the "adiabatic" model.[25,30]

The principal attractiveness of an ab initio formulation of the semicontinuum model is, of course, the proven ability of ab initio techniques to give a reliable account of short-range interactions in solvation phenomena.[9b,35] In the present application we add to the usual short-range terms, those long-range terms needed to specify completely the liquid solvation phenomenon. An ab initio approach allows the detailed energetic contributions outlined above to be handled in an objective and unified manner. Some obvious disadvantages of an ab initio approach are the fact that pertinent solvent properties such as dipole moments and polarizabilities are quantitatively reproduced only with the most elaborate ab initio models, usually at the level of Hartree–Fock or better. Nevertheless, ab initio models short of the Hartree–Fock limit can still provide systematic and accurate structural and energetic information.[36,37] Even at the Hartree–Fock level, calculated energetics suffer from correlation energy effects. While in many cases these effects may largely cancel out, this may not always be so. For example, correlation energy is not expected to be as critical a factor in calculating the solvation energy of a single excess electron, as it is in assessing the relative energies of the solvated electron and dielectron in a Hartree–Fock framework.[38] The above points will receive further attention in sections IV and V.

The next section will illustrate how simple one-electron

formulations of the semicontinuum model can be straightforwardly generalized so as to accommodate a many electron ab initio treatment. One particular reason for developing many electron models (either semiempirical or ab initio) is that there is evidence for *negative* spin densities on the protons in dilute metal ammonia solutions, an effect which appears to involve the ammoniated electron (e_{am}^-).[39] Calculations lead to similar results for the hydrated electron (e_{aq}^-).[16,21] In sections III and IV we shall discuss the structural and computational models chosen for implementing the formalism in a study of the e_{am}^- and e_{aq}^-. Section V contains the computational results and discussion, including a comparison of the present results with those of semiempirical theories and with available experimental data. While most of the results pertain to the ground states of e_{am}^- and e_{aq}^-, preliminary results for excitation and ionization processes are also given, and the relative stability of the solvated dielectron is also examined.

II. Formalism

General Considerations. This section provides a detailed formulation of an ab initio model for solvated electrons in the limiting case of the SCF approximation, described above. Most of the calculations reported below are based on this model. At the end of the section we shall comment briefly on the changes in the formalism needed to implement the ab initio model under the adiabatic approximation. The present formalism may be considered to be an extension of earlier continuum and semicontinuum approaches in which only the excess charge (one or two electrons) was treated quantum mechanically.[25,27,30] We adopt the Hartree–Fock framework and approximate the n-electron wave function corresponding to the discrete cluster and the excess charge as an antisymmetrized product of real occupied spin orbitals, ϕ_i:

$$\psi(\vec{r}_1, \cdots, \vec{r}_n) = \mathcal{A} \prod_i^n \phi_i(\vec{r}_i) \tag{1}$$

Energy Expressions. The starting point for the development of the formalism is the classical polarization energy of a fully relaxed dielectric continuum, which can be equated with the (free) energy required to transfer a fixed polarizing charge distribution $\rho(\vec{r})$ from vacuum to a dielectric with which it is in electrostatic equilibrium:[21]

$$U = -\left(\frac{1}{8\pi}\right)\left(1 - \frac{1}{D_s}\right)\int_V D^2 \, d\tau \tag{2}$$

where D_s is the static dielectric constant (taken as constant within volume V)

$$\vec{\nabla}\cdot\vec{D} = 4\pi\rho(\vec{r}) \tag{3}$$

and

$$\vec{D} = \int_{\text{all space}} \rho(\vec{r}')(\vec{r} - \vec{r}')/|\vec{r} - \vec{r}'|^3 \, d\tau' \tag{4}$$

In the Hartree–Fock framework represented by eq 1, the charge density $\rho(\vec{r})$, which includes the discrete solvent cluster and the excess charge, can be expressed as follows:

$$\rho(\vec{r}) = \sum_i^n \phi_i^2(\vec{r}) - \sum_k^{\text{atoms}} Z_k \delta(\vec{r} - \vec{r}_k) \tag{5}$$

where the Z_k are nuclear charges. The electronic part of this density can be decomposed into contributions from electrons of α and β spin, denoted, respectively, as $\rho^\alpha(\vec{r})$ and $\rho^\beta(\vec{r})$. If the number of α spin electrons exceeds the number of β spin electrons, then *negative* spin density is said to occur at those points in space for which $\rho^\beta(\vec{r}) > \rho^\alpha(\vec{r})$. Negative spin densities are possible within the Hartree–Fock formalism only if the spin-unrestricted version (UHF)[40] is employed, as is done in the present work, i.e., paired electrons are not constrained to have identical spatial orbitals.

The quantity $\rho(\vec{r})$ plays a crucial role in linking the quantum mechanical wave function (eq 1) with the classical polarization energy (eq 2). Equation 2 is consistent with the SCF approximation for the interaction between medium and excess electrons,[30] since it corresponds to the full continuum dielectric response (represented by D_s) in equilibrium with the effective or average (as opposed to instantaneous) charge distribution $\rho(\vec{r})$ given by eq 5. We determine $\rho(\vec{r})$ by minimizing the following energy expression:

$$E = E_0 + U \tag{6}$$

where E_0 is the self-energy of $\rho(\vec{r})$ in the Hartree–Fock framework

$$E_0 = \sum_i^n h_i + (1/2)\sum_{i,j}^n (J_{ij} - K_{ij}) + \sum_{k,l}^{\text{atoms}} (Z_k Z_l)/r_{kl} \tag{7}$$

In eq 7 the quantities h_i, J_{ij}, and K_{ij} are the usual one-electron, two-electron Coulomb, and two-electron exchange integrals over spin orbitals.[40] The reader is reminded that K_{ij} is nonzero only for cases where spin–orbitals i and j have the same spin. Furthermore, the net contribution to the two-electron energy for cases where $i = j$ is zero, due to cancellation of J_{ii} and K_{ii}. Anticipating further developments below, we note that the total "Coulomb" contribution to eq 7 can be expressed as a simple functional of the electronic charge density, $\rho^{el}(\vec{r})$, defined by the first term in eq 5:

$$(1/2)\sum_{i,j} J_{ij} = 1/2 \int \rho^{el}(\vec{r}_1)(1/r_{12})\rho^{el}(\vec{r}_2) \, d\tau_1 \, d\tau_2 \tag{8}$$

Our task now is to transform eq 2 into a form which resembles eq 8 and is thus easily incorporated into the conventional Hartree–Fock formalism. The integration in eq 2 can, of course, involve any volume V. In our applications below, V will correspond to an infinite dielectric with a spherical cavity of variable radius, r_c. In addition, we simplify the problem by employing only the spherical component (with respect to the cavity origin) of $\rho(\vec{r})$ in evaluating the polarization energy (eq 2). This is a reasonable approximation, since the discrete clusters studied here will generally have a high degree of symmetry. Clearly in cases of neutral clusters or clusters strongly departing from spherical symmetry, the contribution of dipole and higher multipoles would be more important. Under the above assumptions, U can be expressed as follows:

$$U = \frac{1}{2}\left(1 - \frac{1}{D_s}\right)\int\int_{\text{all space}} \rho(\vec{r}_1)\, g(r_1, r_2)\rho(\vec{r}_2) \, d\tau_1 \, d\tau_2 \tag{9}$$

where the truncated Coulomb interaction associated with the finite cavity is defined in terms of the maximum of r_1, r_2, and r_c:

$$g(r_1, r_2) = -1/\max(r_1, r_2, r_c) \tag{10}$$

Equation 9 can be expressed either in terms of $\rho(\vec{r})$ or its spherical average $\rho(r)$, since $g(r_1, r_2)$ depends only on the magnitudes of $\vec{r}_1$ and $\vec{r}_2$.

The Variational Principle. Comparison of eq 8 and 9 re-

veals that U is just an additional Coulomb-type integral which leads naturally via eq 6 to a generalized Hartree–Fock energy. Note, however, that there is no "exchange" term corresponding to eq 9. This is related to the fact that the energy of eq 6, while quite meaningful physically, is not expressible as the expectation value of the Schroedinger Hamiltonian with respect to a wave function of the type given in eq 1 (as opposed to the case for E_0 by itself, eq 7). Thus the justification for applying the variational principle to $E_0 + U$ requires appeal to other physical considerations. At constant temperature (T) and pressure (P), thermodynamic equilibrium requires minimization of the free enthalpy or Gibbs free energy (G). The condition $dG_{T,P} = 0$ can be expanded in a form appropriate for our semicontinuum model:

$$dG_{T,P} = 0 = dU + dE_0 + P\,dV_0 - T\,dS_0 + dW_0 \quad (11)$$

where, in addition to the free energy (dU) and internal energy (dE_0) terms already discussed, we have contributions associated with the discrete cluster (designated by a subscript of zero): $P\,dV_0$ is the pressure–volume work done to maintain a finite void within the first solvent shell (negligible for normal pressures), $T\,dS_0$ the entropy change involved in converting bulk solvent molecules into inner-shell solvent molecules, and dW_0 other reversible work terms, such as work done against surface tension in creating a void.

At this point, a word is in order regarding the incorporation of temperature into the present formalism. The continuum polarization energy depends on temperature through the dielectric constant. Temperature can be introduced into the discrete cluster by carrying out a Boltzmann averaging over various possible configurations of the solvent molecules; i.e., an ab initio semicontinuum calculation is performed for each configuration, and then the averaging is carried out. This procedure, which has been referred to as the "temperature-independent potential" approach,[41] is the only one easily incorporated into an ab initio Hartree–Fock model, and is to be contrasted with the more common temperature-dependent potential used in semiempirical calculations, which is based on the Langevin function for the average orientation of the solvent molecule dipole moments.[25-27] In our applications, the wave function (eq 1) and density (eq 5) will be determined by minimizing $E_0 + U$ in the spirit of the temperature-independent cluster potential. A complete calculation of the free energy of solvation would require determination of the frequencies associated with distortions in the discrete cluster as well as Boltzmann averaging of E_0, and will not be attempted in the present paper. However, crude estimates of the temperature dependence of some properties will be made.

Minimization of $E_0 + U$ leads to a generalized Hartree–Fock one-electron Schroedinger equation:

$$F'\phi = (F + f')\phi = \epsilon\phi \quad (12)$$

where F is the ordinary Hartree–Fock potential and f' is the contribution from the polarized dielectric

$$f'(r) = (1 - 1/D_s) \int_{\text{all space}} \rho(\vec{r}')\, g(r, r')\, d\tau' \quad (13)$$

The prime is added to $f(r)$ to distinguish it from earlier formulations which did not include the factor $(1 - 1/D_s)$ in the definition of $f(r)$.[30] The operator $g(r, r')$ is defined by eq 10. The integration in eq 13 is over all space in spite of the finite cavity. The portion of $\rho(\vec{r})$ within the cavity contributes to the fictitious charge density at the cavity surface. Certain properties of $f'(r)$ should be noted: (1) The factor $(1 - 1/D_s)$ corresponds to the SCF approximation, in which both orientational and electronic polarization of the continuum contribute to the trapping potential for the excess charge. The total trapping potential consists of $f'(r)$ and the contribution of the solvent molecules in the discrete cluster. (2) Due to the definition of $g(r, r')$, $f'(r)$ is constant within the cavity, and thus will not directly affect the charge density of solvent molecules which lie completely within the cavity. In our applications r_c is chosen so that the solvent molecules included in $\rho(\vec{r})$ are essentially contained within the cavity.[42]

More General Energy Expressions. The above treatment of the continuum polarization (based on eq 2) is somewhat oversimplified in situations where a significant portion of $\rho(\vec{r})$ penetrates the continuum. This is because eq 2 ignores short-range repulsive interactions between the excess charge and the solvent in the continuum, and assumes a simplified model for the local field inside the continuum.[43] The ground-state energies of quasifree electrons in dense nonpolar fluids have been calculated by Springett, Jortner, and Cohen[44] and are usually designated by the constant effective energy term V_0. Attempts have also been made to calculate the corresponding V_0 quantities for quasifree electrons in polar fluids, including water and ammonia,[26] and V_0 has also been employed as a measure of the energy of that part of the trapped electron which penetrates the solvent medium.[25-27] Even though V_0 is difficult to estimate for polar media it appears to be quite important in determining the density dependence of properties of electrons trapped in such media.[26,45] We can accordingly generalize our formalism to include V_0 in a manner analogous to that employed in earlier semiempirical approaches:[25-27]

$$E' = E_0 + U + [1 - q(r_c)]V_0 \quad (14)$$

where the quantity $q(r_c)$ represents the component of $\rho(\vec{r})$ inside the cavity:

$$q(r_c) = \int_0^{r_c} \int_0^{4\pi} d\Omega\, \rho(\vec{r}) r^2\, dr \quad (15)$$

In the semiempirical versions of the semicontinuum model, however, V_0 is also used to simulate interactions between the excess charge and the solvent molecules in the discrete cluster, interactions automatically included in the present ab initio approach.

The preceding equations have been general in that they pertain to any state (ground or excited) of the excess charge for which the medium is completely relaxed with respect to the average charge distribution (eq 5). Excitation or ionization of excess electrons will be followed by nearly instantaneous electronic relaxation of the medium, while the orientational polarization will stay frozen for long periods on an electronic time scale. Hence the energy of a vertically excited state must be corrected for this effect:[30]

$$E^{ex} = E_0^{ex} + U^{ex} + [1 - q(r_c)^{ex}]V_0 \quad (16)$$

where

$$U^{ex} = (1/2)(1 - 1/D_{op}) \int \rho^{ex}(\vec{r}_1)\, g(r_1, r_2) \rho^{ex}(\vec{r}_2)\, d\tau_1\, d\tau_2 + (1/D_{op} - 1/D_s) \int \rho^{ex}(\vec{r}_1)\, g(r_1, r_2) \rho^{gnd}(r_2)\, d\tau_1\, d\tau_2 - (1/2)(1/D_{op} - 1/D_s) \int \rho^{gnd}(\vec{r}_1)\, g(r_1, r_2) \rho^{gnd}(\vec{r}_2)\, d\tau_1\, d\tau_2$$

"ex" and "gnd" refer to (vertically) excited and ground

electronic states, and D_{op} is the optical dielectric constant. The first term in eq 16 gives the electronic polarization contribution to U^{ex}, while the last two terms give the contribution from the orientational polarization for the medium induced by $\rho^{gnd}(\vec{r})$. Equation 16 can also be used for vertical ionization, if $\rho^{ex}(\vec{r})$ is identified with the density of the vertically ionized state.

The Adiabatic Approximation. In the adiabatic approximation the electrons of the medium are assumed to respond instantaneously to the excess charge, with the result that only the orientational polarization contributes to the trapping potential.[30] In simple semicontinuum models, where $\rho(\vec{r})$ refers only to the excess charge, the trapping potential in the adiabatic approximation is obtained by changing the prefactor in eq 13 from $(1 - 1/D_s)$ to $(1/D_{op} - 1/D_s)$. The latter factor corresponds to orientational polarization of the medium and is usually designated as β. In more general cases where $\rho(\vec{r})$ contains both excess charge and solvent charge, the trapping potential would have to be split up into an SCF and an adiabatic contribution. Actually, in the cases we shall consider, the solvent portion of $\rho(\vec{r})$ is essentially contained within the dielectric cavity and makes very little contribution to $f'(\vec{r})$. Thus to very good approximation, we may use eq 15 for the full density $\rho(\vec{r})$, with a prefactor of β.

Although the electronic polarization does not contribute to the trapping potential of the excess charge, it must be included in the total solvation energy. This can be added as a first-order perturbation term, after $\rho(\vec{r})$ has been determined by the adiabatic potential, thus leading once again to a total polarization energy of the form given in eq 2. In semiempirical models, some of the electronic polarization energy is included in V_0, and care must be exercised in avoiding redundancies between the U and V_0 contributions to the electronic polarization energy.[25-27] Expressions for the energy of excited states in the adiabatic approximation have been given by Jortner,[30] and they can be generalized in a manner similar to that used in the rest of this section.

The choice as to whether the adiabatic or SCF approximation is physically preferable depends on the particular system under consideration. Electrons trapped in polar media appear to represent an intermediate situation, since the electrons are rather strongly bound, but less strongly than the medium electrons. Most of our calculations are based on the SCF approximation, but some comparisons of the two approximations have also been made.[46]

The Dielectron. The general formalism just outlined applies, of course, to the special case of the solvated dielectron. One novel feature of the dielectron in contrast to the monoelectron is that the self-energy of the dielectron has an electron repulsion term as well as a kinetic energy term. The expression "self-energy" in this context refers only to the self-energy of the dielectron contribution to the cluster charge distribution (call it $\rho'(\vec{r})$), as opposed to the self-energy of the entire discrete cluster given by eq 7. In addition to the self-energy term, the two excess electrons are also coupled indirectly via the medium polarization. For a given dielectron charge distribution, $\rho'(\vec{r})$, the resultant Coulomb repulsion energy between the two excess electrons, E^{rep}, is the same in the SCF and adiabatic approximations, but the individual contributions from the self-energy and the medium polarization energy differ. In the SCF approximation for the dielectron, the self-energy is simply the two-electron Coulomb integral J_{12}, i.e., the interaction between the charge density of one electron and the effective Hartree–Fock potential created by the other. The medium then contributes an additional term corresponding to eq 2, with $\rho(r)$ replaced by $\rho'(r)$.[47] In the usual formulation of the adiabatic approximation for the dielectron, the corresponding effective potential of the electron is modified by the electronic polarization of the medium (via D_{op}), as discussed by Land and O'Reilly,[48] and the remainder of E^{rep} arises from the orientational polarization of the medium.

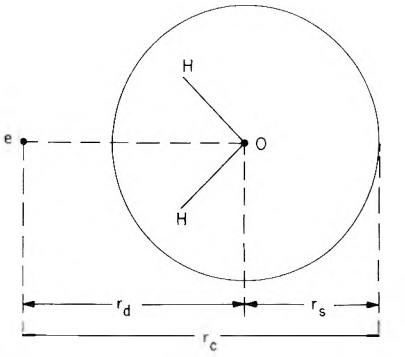

Figure 1. Definition of radii in the semicontinuum model. The spherical cavity origin is at e and the origin of the effective sphere representing the water molecule is at the oxygen atom.

III. Geometrical Configurations

Calculations were carried out for various geometrical configurations of the discrete cluster represented by $\rho(\vec{r})$, corresponding to four or five H_2O or NH_3 molecules plus one to two excess electrons. The clusters consisted of three or four solvent molecules, disposed about a void or an additional solvent molecule at the center of the dielectric cavity. The heavy atoms (O or N) of the peripheral solvent molecules were constrained for simplicity to be a common distance, r_d, from the center of the cavity. If the effective radius of a solvent molecule is defined as r_s, then the cavity radius r_c is equal to $r_d + r_s$, as illustrated for H_2O in Figure 1, where the cavity origin is designated by e. The effective origin of each solvent molecule was located at its heavy atom. For H_2O or NH_3 the centroids of both the nuclear and electronic charge are within 0.1 Å of the heavy atom. Hence the solvent molecules are reasonably well centered about their heavy atoms in spite of the deceptive appearance of Figure 1, which, of course, does not indicate the back side lone pairs of the molecule.

The only consequence that changing the effective solvent origin would have on the calculations is to change the value of r_c, which determines the beginning of the continuum. Numerical tests indicated that calculated results for a given r_d are relatively insensitive to changes in r_c of $\lesssim$0.1 Å. Energies were determined for the lowest energy structures of various point group symmetries, and then in the spirit of the temperature-independent-potential approach for the discrete cluster mentioned in section II, various hindered translations and rotations of the solvent molecules were studied so as to help anticipate the effect of thermal fluctuations on calculated properties. Some of the basic symmetrical structures are illustrated in Figures 2–5. Figures 2 and 3 correspond to the dipole and OH-bond-oriented void models for the hydrated electron. The H_2O molecules have been rotated so that the overall symmetry is D_{2d} (the principal twofold axis bisects the angle formed by the origin and O_1 and O_2) and the oxygen atom configurations corre-

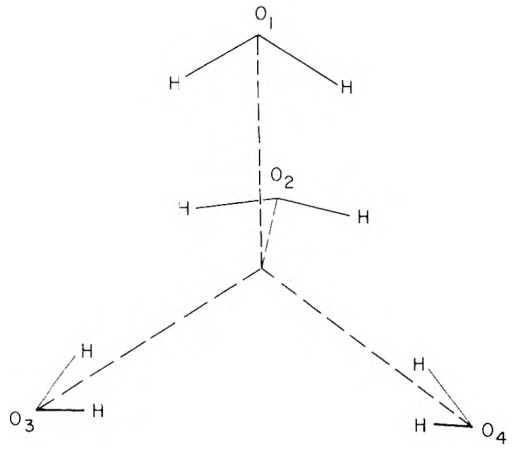

Figure 2. Dipole-oriented cluster model for $(H_2O)_4^-$.

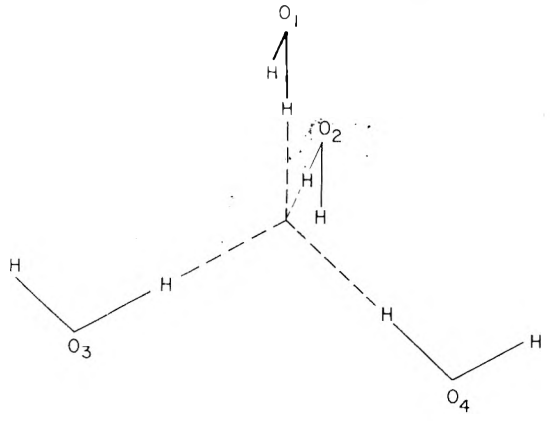

Figure 3. OH-bond-oriented cluster model for $(H_2O)_4^-$.

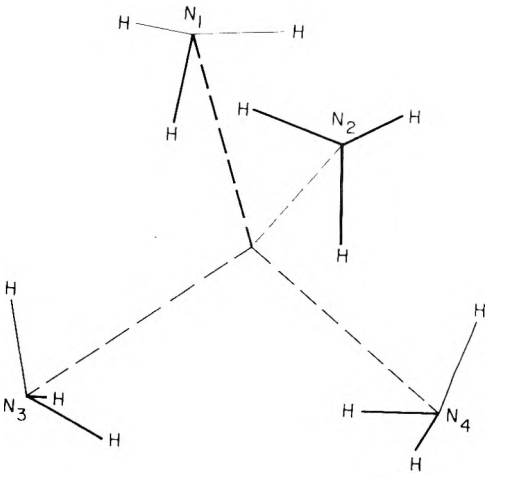

Figure 4. Dipole-oriented cluster model for $(NH_3)_4^-$.

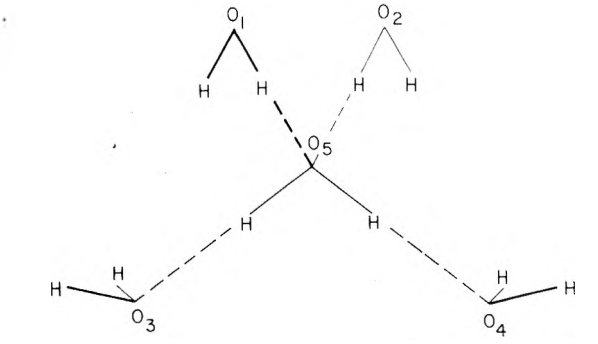

Figure 5. Ice-like pentamer model for $(H_2O)_5^-$.

spond to T_d symmetry. The dipole oriented void model for $(NH_3)_4^-$ in Figure 4 has T_d symmetry. Figure 5 offers an example of a hydrogen-bonded ice-like pentamer (C_{2v} symmetry) as an alternative to the previous structures which contain voids. For comparison with the non-hydrogen-bonded structures of Figures 2 and 3 we have also looked at branched H-bonded water tetramers of C_s symmetry, obtained by removing a proton donor or proton accepting water molecule from the periphery of the pentamer (Figure 5).

IV. Computational Details

The unrestricted Hartree–Fock (UHF) calculations were carried out both with and without the polarized dielectric, using a reasonably flexible basis of contracted Gaussian-type orbitals (CGTO's) commonly referred to as the 4-31G basis.[49] Matrix elements of the polarization potential $f'(r)$ in a GTO basis involve one- and two-electron integrals which are discussed in the Appendix. The 4-31G basis was supplemented with two additional 1s (for the ground state) or 2p (for the lowest excited state) GTO's located at the center of the dielectric cavity. This basis was selected as a compromise between the requirements of computer time and the need to provide a measure of basis set flexibility both on the solvent molecules and in the void space, thereby allowing an objective determination of the degree of localization of the excess charge. The use of GTO's in the void region is preferable to the use of Slater-type orbitals, which introduce spurious cusps.[21] This fact has also been recognized in the context of semiempirical calculations.[50] It is important to note that in contrast to most semicontinuum models, the excess charge is not forced to correspond to pure s or p symmetry since the solvent orbitals are mixed in with the extra s- and p-type GTO's. The orbital exponents of the extra GTO's were taken as 0.01 and $0.05a_0^{-2}$, based on energy optimization for the ground states of the dipole-oriented structures (Figures 2 and 4) in the presence of the polarized continuum. Readjustments of the excess charge for other structures or for excited states is thus governed by variations in the linear coefficients of the extra GTO's as well as the solvent orbitals.

The effectiveness of the 4-31G basis in solvation studies has been thoroughly documented for the case of hydrated hydroxyl and hydronium ions, where detailed structural and energetic information was obtained in good agreement with available experimental data.[9b] For example, trends in incremental hydration energies were systematically reproduced, typically exceeding experimental values by 10–20%, and relaxation of O···O distances in the vicinity of H_3O^+ and OH^- was accurately accounted for. In this earlier work attention was drawn to the fact that typical atom-centered basis sets short of the Hartree–Fock limit tend to favor intermolecular complexes relative to isolated monomers, since the latter cannot share basis functions on other monomers, as occurs in the complex. For example, the 4-31G basis leads to exaggerated H-bond energies for water clusters corresponding to ~1.2 kcal/H bond, as inferred by calculating the H_2O monomer energy in the presence of basis functions from other H_2O molecules in H-bonded geometries. In the present work the effective monomer energy (i.e., that obtained from the entire basis set for a given discrete cluster) involves not only other monomers but also

the extra s or p GTO's. Thus, for example, the effective H_2O monomer energy based on the dipole-oriented $(H_2O)_4^-$ structure (Figure 2) varies with r_d (see Figure 1) at a rate of ~0.075 eV/Å near the equilibrium r_d value (see below). The corresponding quantity for $(NH_3)_4^-$ (Figure 3) is ~0.073 eV/Å. Since basis set effects of this type have a bearing on cluster energies calculated relative to isolated monomers and also on equilibrium cluster size (r_d^0), we have made appropriate corrections when calculating such quantities, based on the differences between the isolated monomer energies and the effective energies as defined above. This procedure is clearly an approximate one, but should provide an upper limit for differential basis set effects.[51] Energy differences between charged and neutral clusters of the same geometry are of course unaffected by such considerations.

The monomer bond angles were kept fixed at 109° for water and 113° for NH_3. These values correspond to energy-optimized values for the dipole-oriented structures (Figures 2 and 4) near their equilibrium r_d values and are about two degrees smaller than the equilibrium angles for the isolated monomers in the 4-31G basis. The 4-31G HXH angles are systematically larger than experimental values, as noted elsewhere.[9b]

It remains to consider the parameters which specify the continuum. For water, we assume T = 298 K, D_s = 78.5, D_{op} = 1.78, and γ (the surface energy coefficient) = 72 erg/cm^2.[52] For ammonia, T = 240 K (boiling point at 1 atm), D_s = 22, D_{op} = 1.756, and γ = 40.[52] The surface energy was calculated in the same manner as reported earlier.[21] The effective solvent radius, r_s (Figure 1), was taken as 1.5 Å for both H_2O and NH_3. Such values have been used in earlier semicontinuum calculations.[25] Calculations for e_{aq}^- with r_s = 1.4 Å give results similar to those for r_s = 1.5 Å, as noted in section III. Sensitivity to the V_0 parameter (eq 14) was tested by using a value of +0.04 au (~1 eV), which is likely to be an upper limit for the corrections due to short-range effects between the excess charge and the continuum.

A final comment regards the measure of charge localization $q(r_c)$ defined in eq 15. With the values of r_d and r_s (Figure 1) used in the present calculations, the tails of the peripheral neutral H_2O and NH_3 monomers typically contributed, respectively, ~0.014 and ~0.040 electrons/molecule to the continuum. Accordingly the $q(r_c)$ values for $(H_2O)_{4,5}^-$ and $(NH_3)_4^-$ clusters (see below) have been corrected for these neutral monomer contributions, so as to provide a better picture of the penetration of the *excess* charge into the continuum. These corrected $q(r_c)$ values, denoted as $q'(r_c)$, are found to be similar to those based simply on the density of the highest occupied MO of each anion cluster. The reader should note that 1 au = 27.21 eV (cf. the hartree, which is half as large).

V. Results and Discussion

This section is concerned with properties of the energy and charge density of excess electrons in a variety of trapping sites. The most informative total energies are not the absolute energies (E_0, U, etc.) but relative energies, such as those for different anion complexes or for anion complexes and the corresponding neutral complexes. To the extent that the latter neutral complexes represent preexisting clusters in the polar medium, then the relative energies for the neutral and charged species provide rough estimates of the electron solvation energy. More refined estimates of the latter would have to consider the "medium rearrangement" energy corresponding to a given cluster geometry. In this connection, the energies of the charged clusters relative to isolated neutral monomer molecules are also useful, especially when the clusters are isolated in the gas phase, although as calculated here such energies do not contain the $T\Delta S$ term needed to obtain the complete free energy of solvation (see section II). We first consider electron trapping by four dipoles directed at the center of a void (Figures 2 and 4) whose size is estimated variationally. Then the picture is rounded out by consideration of alternative solvent configurations. We shall find that structures close to the dipole-oriented model lead to the greatest solvation energy relative to the neutral complex of the same geometry.

TABLE II: Effect of Continuum on Dipole-Oriented $(H_2O)_4^-$

r_d, Å	Status of continuum	$E_{(H_2O)_4^-}$, eV[a]	$q'(r_c)$[b]
2.65[b]	Absent	−0.06[c] (+0.34)[d]	0.72
	Present	−1.62[c] (−0.88)[d,e]	0.84
4.00[f]	Absent	−0.30[c] (−0.16)[d]	0.84[g]

[a] Relative to $(H_2O)_4$ with the same geometry. The continuum has a negligible effect on the energy of the neutral cluster. [b] r_c continues to equal $r_d + r_s$ and represents the effective size of the cluster even in the absence of the dielectric, when the term cavity has no meaning. [c] The corresponding total energies, $E_0 + U$ (eq 6), are −303.6291, −303.6864, and −303.6412 au, respectively (1 au = 27.21 eV). In the absence of the continuum, U is of course equal to zero. [d] Relative to four times the effective isolated monomer energy (see section IV). [e] Includes an effective surface energy contribution (0.34 eV). [f] Near-equilibrium value of r_d in the absence of a continuum. [g] Corresponds to considerably less localization than the similar values of q' found for r_d = 2.65 Å.

Dipole-Oriented Models. Before the results are presented in detail it is important to document the importance of the long-range continuum contribution to the localization phenomenon. Table II contains results for $(H_2O)_4^-$ based on the structure of Figure 2. The value of 2.65 Å for r_d is close to the equilibrium value when the polarized continuum is included (see below). If the continuum polarization is not included the $(H_2O)_4^-$ cluster characterized by r_d = 2.65 is unbound relative to isolated neutral monomers, even though it is slightly stable with respect to vertical ionization; i.e., when the isolated cluster is frozen at r_d = 2.65 Å, some trapping occurs so as to offset repulsive solvent interactions. A minimum in the absolute energy of the isolated $(H_2O)_4^-$ cluster occurs for $r_d \sim 4$ Å, corresponding to a potential well of ~0.16 eV. Clearly a well of this magnitude will not lead to room-temperature stability if thermal population of intermolecular vibrational modes and entropy effects are taken into consideration. Even at 0 K, zero-point effects would probably eliminate the stability of a dipole-oriented $(H_2O)_4^-$ cluster. Furthermore we have found hydrogen-bonded $(H_2O)_4^-$ clusters which have lower total energies, but they are unstable with respect to autoionization. Similar calculations for $(NH_3)_4^-$ suggest even greater instability in the absence of additional solvent. We thus predict that more than four H_2O or NH_3 molecules are needed for observable electron trapping under equilibrium conditions at room temperature or above, and trapping by ammonia appears to require more solvent molecules than is the case for water. These conclusions, while admittedly based on an approximate *ab initio* model, nevertheless seem to be consistent with other results, both theoretical and experimental. Clusters of the type $(H_2O)_4^-$ or $(NH_3)_4^-$

TABLE III: Structure and Energetics for the Dipole-Oriented Model with Polarized Continuum[a]

Solvent	H_2O	NH_3
r_d[b], Å	2.65	2.75
$q'(r_c)$	0.84 (0.92)	0.43 (0.56)
Rel total energy, eV[c]	−1.62 (−1.50)	−0.82 (−0.26)
Continuum polarization energy, eV[d]	−1.59 (−1.65)	−1.25 (−1.32)
Lowest vertical excitation energy, eV[e]	1.20 (1.78)	0.50 (0.80)
Vertical ionization energy, eV	2.51 (2.42)	1.51 (1.00)

[a] The quantities in parentheses are based on V_0 = 0.04 au (~1 eV). [b] Near-equilibrium values, as discussed in text. [c] Relative to neutral clusters with same geometry. With V_0 = 0.0, $E_0 + U$ for e_{am}^- is −224.46257 au; see Table II for e_{aq}^-. [d] U, as defined by eq 9. [e] Based on eq 14 and 16, and corrected for the small difference in effective monomer energy in the ground and excited state.[51]

have not been directly observed in the gas phase, and pulse radiolysis studies of ammonia at temperatures well above the liquid–vapor coexistence curve (CEC) have revealed density thresholds below which electron trapping is not observed.[53] The trapped electron yields from these experiments have been analyzed in terms of semi-empirical calculations which lead to reasonable density thresholds at temperatures above the CEC, and which suggest that clusters of 10–12 NH_3 molecules may be necessary for trapping, at least at the temperatures corresponding to the experimental work.[54] Water vapor at densities as low as ~5×10^{-3} g/cc still appears to trap electrons at temperatures near the CEC,[55] but there is the possibility that a threshold may appear at higher temperatures where density fluctuations are less important.

Detailed results for the dipole-oriented clusters immersed in the continuum are presented in Table III, allowing a comparison of e_{aq}^- and e_{am}^-. Some results based on V_0 = +0.04 au (see eq 14) are given in parentheses. Since all calculated quantities are based on the listed r_d values, the source of these values must be discussed. Straightforward minimization of $E_0 + U$ (see eq 6), with adjustment for the variation of effective monomer energy with r_d (section IV),[51] yields equilibrium r_d values (r_d^0) for e_{aq}^- and e_{am}^- in excess of 3 Å. Inclusion of a surface energy term in the energy minimization leads to $r_d^0 \sim 2.8$ and 2.9 Å, respectively, for e_{aq}^- and e_{am}^-.[56] Since our procedure of adjusting for variations in basis set quality with r_d is thought to provide only an upper limit for the effect, the above r_d values are undoubtedly somewhat exaggerated. Due to this and other factors (e.g., detailed H-bonding effects between cluster and continuum, which have only been crudely simulated; temperature effects due to anharmonicity of the potential energy curve; and variations of monomer bond angle with r_d) our calculated r_d^0 values must be considered uncertain by at least 0.1 Å, and values of 2.7 ± 0.1 (e_{aq}^-) and 2.8 ± 0.1 (e_{am}^-) are the best estimates. Most of our numerical results happen to be based on 2.65 Å (e_{aq}^-) and 2.75 Å (e_{am}^-), and accordingly, these r_d values are used for the most part in presenting the data.

The upshot of our r_d^0 calculations is the prediction of appreciable effective void space for both e_{aq}^- and e_{am}^-, based on the dipole-oriented model, with r_d^0 slightly larger for e_{am}^-. Pressure-dependent pulse radiolysis studies have suggested significant but appreciably different effective partial molal volumes for e_{aq}^- (~7 ml/mol) and e_{am}^- (~98 ml/mol), based on reaction activation volumes.[57] The absorption maxima of e_{aq}^- and e_{am}^- (on an eV scale) show similar blue shifts (~0.2–0.3 eV) in the pressure range ~0–6 kbars near room temperature, although a larger inferred compressibility of e_{am}^- in the low pressure limit once again suggests a larger effective void.[58] Returning to our calculations, we note that in spite of similar r_d^0 values, the force constant for breathing of the e_{am}^- cavity (~0.1 mdyn/Å) is markedly smaller than the e_{aq}^- value (~0.3 mdyn/Å), qualitatively consistent with the inferred relative compressibilities. Furthermore the "size" of e_{am}^- as measured by the average distance of the trapped electron from the cavity origin[59]

$$\bar{r} = \int \rho'(\vec{r})|\vec{r}|\, d\tau \qquad (17)$$

is quite large (~3.9 Å), compared with a value for e_{aq}^- (~2.6 Å), which nearly coincides with r_d^0. The $q'(r_c)$ values also suggest much greater size of e_{am}^-. A relatively large and diffuse e_{am}^- is consistent with the large *positive* partial molal entropy determined for e_{am}^- (~36 eu), as opposed to the value of ~3 eu for e_{aq}^- and the negative values typical of highly localized structure-making ions.[60]

Although magnetic structural data are not directly available for e_{aq}^- and e_{am}^-, a wealth of data has recently been obtained by Kevan and coworkers for electrons trapped in 10 *M* aqueous NaOH glasses.[12] In spite of the high concentration of alkali, these glasses may provide trapping sites similar to those in pure water, and it is of great interest to note that the r_d^0 value inferred from the glass (~2.4 Å) lies within the range of r_d^0 values for e_{aq}^- calculated here and in recent previous work (~2.3–2.9 Å).[26,29,61] At present Kevan's data seem most compatible with six protons adjacent to the void, and models based on dipole oriented clusters [$(H_2O)_3^-$] or OH-bond oriented clusters [$(H_2O)_6^-$] clusters have been proposed. Further ab initio calculations are now in progress to test these models and compare them with the $(H_2O)_4^-$ models presented for e_{aq}^- in the current paper. The structural predictions from experiment are, of course, related to spin densities, which are discussed below.

The remainder of Table III concerns the energetics of e_{aq}^- and e_{am}^-. The listed total energies are relative to neutral clusters. The energies relative to isolated monomers are reduced to −0.9 and −0.4 eV for e_{aq}^- and e_{am}^-, respectively (with V_0 = 0.0 eV), corresponding to inclusion of the positive medium rearrangement energy associated with the discrete cluster. Although these energies cannot be directly identified with the solvation energies, as noted above, they do indicate the expected greater solvation energy of the more compact e_{aq}^-, as compared with e_{am}^-. Some recent estimates of solvation energy (ΔG) based on experiment, are respectively −1.6 eV for e_{aq}^- (25°C) and −1.1 eV for e_{am}^- (−35°C).[62] The long-range or continuum contribution to the total energy (U) is seen to be comparable in magnitude to the total solvation energy, which of course is the resultant of several attractive and repulsive contributions. The final two rows of Table III give calculated excitation energies. For V_0 = 0.0, the lowest energy excitations are calculated to be ~70 and ~60% of the respective experimental $h\nu_{max}$ values for e_{aq}^- (1.72 eV)[63] and e_{am}^- (0.80 eV).[64] The e_{aq}^- transition involves an $a_1 \rightarrow e$ excitation. The $a_1 \rightarrow b_2$ transition (corresponding roughly to an excitation to the remaining component of the 2p orbital in D_{2d} symmetry) is calculated to lie ~0.15 eV higher.[65] The lowest e_{am}^- excited state involves the triply degenerate t_2 or-

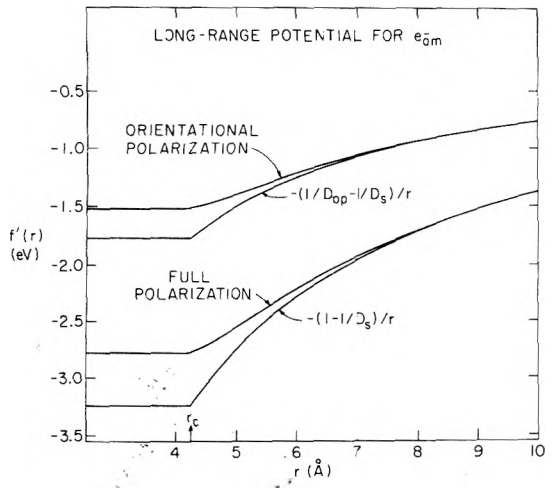

Figure 6. Continuum trapping potentials for e_{am}^-. The upper two curves pertain to the adiabatic approximation and the lower two, to the SCF approximation. Within each pair of curves, the upper member represents the complete, density-dependent potential, $f'(r)$, while the lower member is the corresponding truncated Coulomb potential.

bital. The calculated vertical ionization energy of e_{am}^- should provide a lower bound for the photoionization threshold and is indeed found to lie below the experimental threshold of 1.6 eV.[66]

Not surprisingly, the relatively diffuse e_{am}^- is more sensitive to V_0 than is e_{aq}^-, and excitation energies in general are more sensitive than ground state properties. The positive V_0 tends to force more excess charge into the cavity. From the point of view of reproducing the excitation energies, it is clear that a positive value of V_0 near 1 eV would be optimal for both e_{aq}^- and e_{am}^-. The values of V_0 for e_{aq}^- and e_{am}^- estimated by Gaathon and Jortner[26] are also close to each other, although their magnitudes are smaller (+0.2 and −0.2 eV, respectively), as expected in view of the somewhat different role played by V_0 in their formalism (see section II).

Since e_{am}^- is more delocalized than e_{aq}^-, it should be more sensitive to the difference between the adiabatic and SCF approximations. Even for e_{am}^-, however, the difference in the ground state is rather small, as indicated by the fact that $q'(r_c)$ is found to be only 0.02 less, when the adiabatic approximation is used. In Figure 6 the associated continuum trapping potentials for e_{am}^- ($f'(r)$, as defined in section II) are displayed along with the corresponding truncated Coulomb potentials. The deviation of $f'(r)$ from the simple coulombic model for $r > r_c$ is related to the appreciable leakage of e_{am}^- into the continuum.

Calculated proton spin densities and hyperfine splittings are given in Table IV, and negative values are found for both e_{aq}^- and e_{am}^-. The negative spin persists when the dipole-oriented structures are distorted, as discussed below. Negative electronic spin densities on protons in metal-ammonia solution have been inferred from Knight shift data and most likely correspond to e_{am}^-.[39] For sodium solutions, the experimental data imply a total contact spin density of $-17 \times 10^{-3} a_0^{-3}$ at the protons surrounding the trapped electrons. The 12 NH_3 protons on the cavity surface in our model correspond to a total calculated spin density of $\sim -8 a_0^{-3}$ (based on $V_0 = 0.0$). With $V_0 = 0.04$ au the calculated spin density is 67% larger.[67] Hyperfine splittings for e_{aq}^- have only been reported for alkaline ices or glasses.[12,68] Earlier work suggested $|a_H|$ values in the range 5–6 G,[68] while more recent detailed analysis of data for 10 *M* NaOH glasses has allowed a separation of isotropic and anisotropic coupling and appears to be most consistent with an a_H magnitude near 2 G. In the present work positive spin densities are calculated at the O and N nuclei in e_{aq}^- and e_{am}^-: $+0.08 a_0^{-3}$ and $+0.05 a_0^{-3}$, respectively. A positive value for N is also obtained from Knight shift data.[39]

TABLE IV: Calculated Spin Densities and Hyperfine Coupling Constants for First Shell Protons in the Dipole-Oriented Model for e_{aq}^- and e_{am}^-

Solvent	ρ_H^{spin}, a_0^{-3}	a_H, G[a]
H_2O[a]	-2.9×10^{-3}	−4.6
NH_3[a]	-0.63×10^{-3}	−1.0

[a] Based on r_d = 2.65 Å (H_2O), 2.75 Å (NH_3), and V_0 = 0.0.

TABLE V: Symmetric[a] Deformation of the Dipole-Oriented Configuration for e_{aq}^- [b]

	Rel energy, kcal/mol of e_{aq}^-	$q'(r_c)$	ρ_H^{spin}, a_0^{-3}
A. Departures from the dipole-oriented model			
Undistorted	0.00	0.84	-2.9×10^{-3}
Dipoles rotated by ±15°[c,d]	1.20	0.81	-2.6×10^{-3}
Dipoles rotated by ±30°[c,d]	4.04	0.72	-1.8×10^{-3}
B. OH-bond oriented model[e]	6.2	0.83	-5.4×10^{-3}

[a] With respect to D_{2d} symmetry. [b] Based on r_d = 2.65 Å, V_0 = 0.0. [c] Dipole moment rotations with respect to r_d are defined as positive or negative in the sense of the water protons attached to O_1 (Figure 2) moving respectively toward or away from the water molecule containing O_2, etc. The equilibrium dipole moment angle is +11°. [d] The quantities listed represent average values for positive and negative rotations. [e] Figure 3. The spin densities refer to the four innermost protons. The outer four protons also have negative contact spin densities, but smaller by an order of magnitude.

Distortions of the Dipole-Oriented Model for e_{aq}^-. We now consider how closely the dipole-oriented structure for e_{aq}^- (Figure 2) corresponds to the equilibrium structure in D_{2d} symmetry, and what types of fluctuation of the dipole orientations from equilibrium are expected to be important at room temperature. Some pertinent relative energies corresponding to totally symmetric deformations of the D_{2d} dipole-oriented e_{aq}^- structure are given in Table V, based on r_d = 2.65 Å. The equilibrium dipole orientation is found to be close (within 11°) to perfect alignment (see footnote *c* of Table V), and the slight deviation reflects the balance of charge-dipole interactions and dipole–dipole and proton–proton repulsions. The average deformation energy per solvent molecule is ~0.3 and ~1.0 kcal, respectively, for rotations of 15 and 30° with respect to the equilibrium orientation (Table VA). Since room temperature thermal energy is ~0.6 kcal/mol, we can anticipate that dipole fluctuations of at least 15° will be statistically important at room temperature. Other concerted hindered rotations corresponding to nontotally symmetric deformations are found to make even larger dipole fluctuations (up to 30°) thermally accessible. The 30° dipole fluctuations are seen to be accompanied by a significant reduction in the magnitude of the proton spin densities. Table VB shows that a more drastic distortion (to the oriented OH-bond model (Figure 3)) costs 6 kcal/

TABLE VI: The Ice-like Pentamer Model[a] for $(H_2O)_5^-$

Status of continuum	Energy relative to $(H_2O)_5$, eV[c]	$q'(r_c)$[b]
Absent	+0.65	0.28
Present	−0.59	0.33

[a] See Figure 5. [b] See footnote *b* of Table II. [c] r_d = 2.75 Å.

mol, significantly above thermal energies on a per solvent molecule basis. This model also yields negative spin densities at the water protons.

Other e_{aq}^- Structures. As an alternative to the traditional trapping model based on a cluster with a void at the center, we briefly consider the ability of hydrogen-bonded clusters to trap electrons. Table VI gives some data for an ice-like pentamer (Figure 5). In contrast to the dipole-oriented configuration (Table II), H-bonded $(H_2O)_5$ is *not* stabilized by addition of an electron in the absence of additional solvent. The $(H_2O)_5^-$ cluster without a surrounding continuum *is* stable relative to five isolated monomers, but such a cluster would have a short lifetime due to autoionization since the neutral cluster with the same geometry is more stable. When embedded in the continuum, $(H_2O)_5^-$ is stable relative to the neutral cluster, but the stabilization and degree of excess charge localization $[q'(r_c)]$ is much less than in the case of the dipole-oriented cluster (Table II). The calculated stabilization of $(H_2O)_5^-$ in the continuum is even less when the outer H_2O molecules in $(H_2O)_5$ are rotated so as to facilitate charge-dipole interactions at the expense of broken H bonds. Thus fully H-bonded water molecules do not appear to offer especially favorable trapping sites, and preexisting groups of water molecules with free OH bonds would seem to be more effective sites. Similar results are found for the H-bonded tetramers obtained by removing a peripheral water molecule from the $(H_2O)_5$ cluster. The solvation energy in the case of the H-bonded tetramer plus the continuum is appreciably less than that for the dipole-oriented tetramer, as mesaured relative to the respective neutral clusters. Nevertheless, the total energies $(E_0 + U)$ of the two anion clusters are actually within 0.1 eV of each other, due to the energy of the H bonds.

A model of e_{aq}^- based on a solvated monomer anion, $(H_2O)^-$, has previously been suggested.[69] Our results for $(H_2O)_5^-$ plus continuum yield small $q'(r)$ values which are not consistent with the concept of a well-defined monomer anion surrounded by additional solvent.

The Dielectron. A discussion of excess electrons is incomplete without some mention of the dielectron, whose possible existence has been postulated both in aqueous media and in liquid ammonia.[11] Energies for the solvated mono- and dielectrons in water and ammonia are compared in Table VII, based on the dipole-oriented solvent cluster (Figures 2 and 3). The equilibrium values of r_d for the dielectron were estimated from a rough grid of r_d values to be fairly close to and probably somewhat less than the corresponding r_d^0 values for the solvated monoelectrons. Table VII reveals that for both solvents, two single solvated electrons are more stable than a solvated dielectron, based on a comparison of $E_0 + U$ values (eq 6). The hydrated dielectron is more unstable than the ammoniated dielectron. In assessing our results one must recognize that inclusion of electron correlation would probably reduce the dielectron energy by a few tenths of an electron volt, while the entropy term would tend to offset the stability. Hence the safest

TABLE VII: Comparison of Energies for Solvated Mono- and Dielectrons (eV)[a]

Solvent	r_d, Å	E_1[b]	E_2[c]	$E_2/2 - E_1$[d]
H_2O	2.65	−1.62	−2.38	+0.43
NH_3	2.75	−0.82	−1.39	+0.12

[a] Based on V_0 = 0.0. [b] Energy of solvated monoelectron relative to neutral cluster. [c] Energy of solvated dielectron relative to neutral cluster. [d] Half the dielectron energy relative to that of the monoelectron.

conclusion from the present limited calculations is that a marginal stability may be possible for the ammoniated case, but probably not for the case of water. Previous semiempirical calculations have indicated stability for the dielectron, although no estimates of the entropy effect have been included so far.[70]

VI. Summary

We have demonstrated that the traditional semicontinuum model for trapped excess electrons can be generalized into a many electron treatment which self-consistently combines short-range microscopic solvent effects and long-range continuum interactions, using the techniques of ab initio molecular quantum mechanics. This formalism has been implemented within the unrestricted Hartree–Fock framework, using an extended atomic orbital basis set. The calculations strongly indicate that significant electron trapping by ammonia or water requires more than a single solvent shell of four molecules. A variety of properties have been calculated for the ground and lowest excited states, among which we emphasize the following: (1) appreciable voids are found for both e_{aq}^- and e_{am}^-, based on the dipole-oriented model; (2) the ammoniated electron is calculated to be appreciably less strongly bound than its aqueous counterpart, and is found to be much more diffuse, in spite of similar r_d^0 values for e_{aq}^- and e_{am}^-; (3) the protons of the inner solvent shells in e_{aq}^- and e_{am}^- have negative spin densities, both for the dipole- and OH bond-oriented models; (4) fully H-bonded water molecules are relatively ineffective in trapping electrons; (5) stability of the dielectron relative to two single solvated electrons appears marginal at best for ammonia and unlikely for water; (6) the SCF and adiabatic approximations are found to yield similar results for ground state properties; (7) within the SCF approximation, agreement between calculated and experimental excitation energies for e_{aq}^- and e_{am}^- appears to be best when the short-range interaction of the excess electron with the continuum is simulated by an effective potential energy of $\lesssim$1 eV.

The encouraging results presented here in an ab initio framework suggest that many electron semicontinuum models for trapped electrons might also be effectively studied in a semiempirical framework, where great reductions in cost would allow a much larger variety of systems to be studied.

Acknowledgments. We gratefully acknowledge receipt of material prior to publication and numerous informative discussions with Professor N. Kestner, Professor L. Kevan, Professor J. Jortner, Professor J. W. Moscowitz, and Dr. M. Tachiya. Figures 2–5 were generated by the CRYSNET computer graphics facilities in the Brookhaven Chemistry Department, with assistance from Dr. L. Andrews.

Research performed under the auspices of the U.S. Energy Research and Development Administration.

Appendix

Matrix elements of the effective one-electron potential $f'(r)$ lead to one- and two-electron integrals arising respectively from $g(r_c, r')$ and $g(r, r')$, as can be easily seen by inserting the two contributions to the density (eq 5) into eq 13, with the additional proviso that all nuclear charges Z_k lie within the cavity specified by r_c.[42] The necessary one-electron integrals are dealt with first. We shall explicitly consider only those integrals which arise from 1s-type GTO's. Integrals involving 2p and higher order GTO's can be straightforwardly obtained by differentiation (see below).

The product of two 1s-type GTO's on different centers gives another 1s-type GTO, denoted here as $\phi_p(\vec{r})$, whose origin, $\vec{r}_p$, lies along the vector between the original two centers, and whose orbital exponent, p, is the sum of the original orbital components.[71] We shall derive integrals for the charge distribution $\phi_p(\vec{r})$ in its unnormalized form:

$$\phi_p(\vec{r}) = e^{-p(\vec{r}-\vec{r}_p)^2} \tag{A1}$$

Integrals over the original basis of GTO's require additional factors.[71]

Two basic types of integral are needed:

$$S(r_c) = \int_0^{r_c} r^2\,dr \int_0^{4\pi} d\Omega\,\phi_p(\vec{r}) \tag{A2}$$

and

$$V(r_c) = \int_0^{r_c} (1/r) r^2\,dr \int_0^{4\pi} d\Omega\,\phi_p(\vec{r}) \tag{A3}$$

These integrals resemble overlap and one-electron Coulomb integrals but are truncated at $r = r_c$. Whereas the usual overlap integrals over GTO's can be expressed in analytical form, the truncated function $S(r_c)$, with $r_c < \infty$, requires the use of the incomplete gamma function[71]

$$F_0(x) = \int_0^1 e^{-xu^2}\,du \tag{A4}$$

which can also be related to the familiar error function:

$$F_0(x) = (1/2)\sqrt{(\pi/x)}\,\mathrm{erf}\,(\sqrt{x}) \tag{A5}$$

Straightforward integration based on the preceding equations yields:

$$S(r_c) = -(2\pi r_c/p)\{\exp\{-p(r_c^2 + R^2)\}\sinh(2pr_cR)/(2pr_cR) + (\pi/p)[(r_c - R)F_0\{p(r_c - R)^2\} + (r_c - R)F_0\{p(r_c + R)^2\}] \tag{A6}$$

where $R = |\vec{r}_p|$ is the distance from the origin of the coordinate system to the origin for ϕ_p (eq A1). The corresponding expression for $V(r_c)$ is

$$V(r_c) = (2\pi/p)\,F_0(pR^2) + (\pi/pR)[(r_c - R) \times F_0\{p(r_c - R)^2\} - (r_c + R)\,F_0\{p(r_c + R)^2\}] \tag{A7}$$

In the limit $r_c \to \infty$, $S(r_c)$ and $V(r_c)$ yield the standard forms for overlap and one-electron Coulomb integrals. The quantity $q(r_c)$ defined in eq 15 is evaluated in terms of the $S(r_c)$ integrals and the appropriate density matrix coefficients.

It is clear from eq A6 and A7 that special consideration is required in the case where $R \to 0$. We have accordingly derived expressions for $S(r_c)$ and $V(r_c)$ which are Taylor expansions about $R = 0$.[72] The formulae are as follows:

$$S(r_c) = S_0 + S_2R^2 + S_4R^4 + \ldots$$

with

$$S_0 = 4\pi r_c^3 F_1(pr_c^2)$$

$$S_2 = -(4\pi p r_c^3/3)\exp(-pr_c^2)$$

$$S_4 = (11\pi p r_c)F_2(pr_c^2) - (275/12)\pi p^2 r_c^3 F_3(pr_c^2) + (31/2)\pi p^3 r_c^5\{F_4(pr_c^2) - (8/465)\exp(-pr_c^2)\} \tag{A8}$$

and

$$V(r_c) = V_0 + V_2R^2 + V_4R^4 + \ldots$$

with

$$V_0 = (2\pi/p)[F_0(0) - F_0(pr_c^2) + 2pr_c^2\,F_1(pr_c^2)]$$

$$V_2 = -2\pi\{F_1(0) - F_1(pr_c^2) + 4pr_c^2\,F_2(pr_c^2) - (4p^2r_c^4/3)\,F_3(pr_c^2)\}$$

$$V_4 = \pi p\{F_2(0) - F_2(pr_c^2) + 6pr_c^2\,F_3(pr_c^2) - 4p^2r_c^4\,F_4(pr_c^2) + (8/15)p^3r_c^6\,F_5(pr_c^2)\} \tag{A9}$$

Equations A8 and A9 employ the higher order incomplete gamma functions defined by[71] $F_m(x) = \int_0^1 (u)^{2m} e^{-xu^2} du$. With $G_p(r)$ defined as

$$G_p(r) = \int_{\text{all space}} \phi_p(\vec{r}')\,g(r, r')\,d\tau' \tag{A10}$$

The desired integral over $g(r_c, r')$ can now be expressed as

$$G_p(r_c) = -(1/r_c)\int_0^{r_c} r^2\,dr \int_0^{4\pi} d\pi\,\phi_p(\vec{r}) - \int_{r_c}^{\infty} (1/r) r^2\,dr \int_0^{4\pi} d\Omega\,\phi_p(\vec{r}) = -S(r_c)/r_c - (V(\infty) - V(r_c)) \tag{A11}$$

Turning now to two-electron integrals over $g(r, r')$, we find that

$$\int \phi_p(\vec{r})\,g(r, r')\phi_q(\vec{r}')\,d\tau\,d\tau' = S_p(r_c)G_q(r_c) + \int_{r_c}^{\infty} r^2\,dr \left(\int_0^{4\pi} d\Omega\,\phi_p(\vec{r})\right) G_q(r) \tag{A12}$$

Note also that by symmetry the right-hand side of eq A12 is invariant if the subscripts p and q are interchanged. The one-dimensional integral over r in eq A12 is evaluated by Gaussian quadrature (the upper limit of the integration is truncated between 50 and 100 au, depending on the spatial extent of the GTO's), after the angular integration has been carried out analytically:

$$\int_0^{4\pi} d\Omega\,\phi_p(\vec{r}) = 4\pi e^{-p(r^2+R^2)}\sinh(2prR)/(2prR) \tag{A13}$$

For small values of the argument, $\sinh(x)/x$ can be expanded in a Taylor series, analogously to eq A8 and A9.

The above formulae pertain to charge distributions, $\phi_p(\vec{r})$, arising from 1s-type GTO's. More general Cartesian GTO's of the form $x^iy^jz^ke^{-ar^2}$ can be generated by repeated differentiation.[71] For example, a $2p_x$ GTO is defined as follows:

$$(x - x_A)\exp\{-a(\vec{r} - \vec{r}_A)^2\} = (\tfrac{1}{2}a)\partial/\partial x_A\{\exp[-a(r - r_A)^2]\} \tag{A14}$$

where the GTO is centered at $\vec{r}_A$. Consequently, if $\phi_p(\vec{r})$ is a product of 1s GTO's centered at $\vec{r}_A$ and $\vec{r}_B$, differentiation of the above integral expressions (eq A6–A9 and eq A13 and A14) with respect to the appropriate Cartesian components of $\vec{r}_A$ and $\vec{r}_B$ will yield the corresponding integrals for 2p GTO's.

Some attention must be paid to the numerical accuracy to be expected from the above formulae. The Taylor expansions of the integrals for the 1s-type GTO's were truncated after terms of order R^4 and errors of order R^6, R^5, and R^4 are introduced into the 1s–1s, 1s–2p, and 2p–2p integrals, respectively. For typical GTO basis sets, such as that used in the present calculations, it was found that adequate accuracy could be obtained (i.e., errors $<10^{-6}$ au) for the overlap integrals, provided that either the general equations [(A6) or (A13)] or the Taylor expansions were used, depending on whether the quantity $(pr_cR)^2$ was, respectively, greater or less than $\sim 10^{-5}$. Similarly, for the $V(r_c)$ integrals, a criterion of $\sim 10^{-5}$ was applied to the quantity pR^2.

References and Notes

(1) (a) "Metal Ammonia Solutions", Colloque Weyl I, G. Lepoutre and M. J. Sienko, Ed., W. A. Benjamin, New York, N.Y., 1964; (b) *Adv. Chem. Ser.*, **No. 50** (1964); (c) "Metal-Ammonia Solutions", Colloque Weyl II, J. J. Lagowski and M. J. Sienko, Ed., Butterworths, London, 1970; (d) E. J. Hart and M. Anbar, "The Hydrated Electron", Wiley, New York, N.Y., 1970; (e) "Electrons in Fluids", J. Jortner and N. R. Kestner, Ed., Springer-Verlag; Berlin, 1973.

(2) R. A. Ogg, *J. Am. Chem. Soc.*, **68**, 155 (1946); *J. Chem. Phys.*, **14**, 114, 295 (1946); *Phys. Rev.*, **69**, 243, 668 (1946).

(3) W. N. Libscomb, *J. Chem. Phys.*, **21**, 52 (1953).

(4) R. A. Stairs, *J. Chem. Phys.*, **27**, 1431 (1957)

(5) J. Jortner, *J. Chem. Phys.*, **30**, 839 (1959).

(6) L. Landau, *Phys. Z. Sowjetunion*, **3**, 664 (1933); A. S. Davydov, *J. Exp. Theor. Phys. USSR*, **18**, 913 (1948); M. F. Deigen, *Zh. Eksp. Teor. Fiz.*, **26**, 300 (1954); R. L. Platzman and J. Franck, *Z. Phys.*, **138**, 411 (1954).

(7) B. C. Webster and G. Howat, *Radiat. Res. Rev.*, **4**, 259 (1972).

(8) N. R. Kestner, in ref 1e, p 1; N. R. Kestner, Proceeding of the 5th International Radiation Congress, Seattle, Wash., 1974, in press.

(9) (a) The excess charge distribution has been analyzed theoretically in terms of the static electronic structure of various hydrate clusters.[9b] (b) M. D. Newton and S. Ehrenson, *J. Am. Chem. Soc.*, **93**, 4971 (1971).

(10) (a) Discrete vibrational spectra attributable to the localized protons and hydroxide ions in aqueous solution have been analyzed by W. R. Busing and D. F. Hornig, *J. Phys. Chem.*, **65**, 284 (1961); (b) NMR relaxation data of S. Meiboom, *J. Chem. Phys.*, **34**, 375 (1961), implies a lifetime of picoseconds for these ions.

(11) (a) Experimental evidence for dielectrons has been discussed by J. Zimbrick and L. Kevan, *J. Am. Chem. Soc.*, **89**, 2484 (1967); N. Basco, G. A. Kenney-Wallace, S. K. Vidyarthi, and D. C. Walker, *Can. J. Chem.*, **50**, 2059 (1972); R. Catterall and M. C. R. Symons, *J. Chem. Soc. A*, 13 (1966). (b) Recent work by G. Czapski and E. Peled [*J. Chem. Soc., Chem. Commun.*, 1303 (1970)] and D. Meisel, G. Czapski, M. S. Matheson, and W. A. Mulac [*Int. J. Radiat. Phys. Chem.*, **7**, 233 (1975).] suggests that if the aqueous dielectron absorbs significantly in the visible or near-uv region its lifetime must be very short relative to that of e_{aq}^-.

(12) B. L. Bales, J. Helbert, and L. Kevan, *J. Phys. Chem.*, **78**, 221 (1974); B. L. Bales, M. K. Bowman, L. Kevan, and R. N. Schwartz, *J. Chem. Phys.*, **63**, 3008 (1975); P. A. Narayana, M. K. Bowman, L. Kevan, V. F. Yudanov, and Yu. D. Tsvetkov, *ibid.*, **63**, 3365 (1965).

(13) A. Gaathon, G. Czapski, and J. Jortner, *J. Chem. Phys.*, **58**, 2648 (1973).

(14) J. R. Brandon and R. F. Firestone, *J. Phys. Chem.*, **78**, 792 (1974).

(15) M. Weissmann and N. V. Cohan, *Chem. Phys. Lett.*, **7**, 445 (1970); *J. Chem. Phys.*, **59**, 1385 (1973); N. V. Cohan, G. Finkelstein, and M. Weissmann, *Chem. Phys. Lett.*, **26**, 93 (1974).

(16) G. Howat and B. C. Webster, *J. Phys. Chem.*, **76**, 3714 (1972).

(17) S. Ishimaru, H. Kato, T. Yamabe, and K. Fukui, *J. Phys. Chem.*, **77**, 1450 (1973); *Chem. Phys. Lett.*, **17**, 264 (1972); S. Ishimaru, H. Tomita, T. Yamabe, K. Fukui, and H. Kato, *ibid.*, **23**, 106 (1973).

(18) C. M. L. Kerr and F. Williams, *J. Phys. Chem.*, **76**, 3838 (1972).

(19) M. Tachiya and A. Mozumder, *J. Chem. Phys.*, **60**, 3037 (1974); **61**, 3690 (1974).

(20) C. A. Naleway and M. E. Schwartz, *J. Phys. Chem.*, **76**, 3905 (1972).

(21) M. D. Newton, *J. Chem. Phys.*, **58**, 5833 (1973).

(22) B. Webster, *J. Phys. Chem.*, this issue.

(23) M. Tachiya, Y. Tabata, and K. Oshima, *J. Phys. Chem.*, **77**, 263 (1973); M. Tachiya, *J. Chem. Phys.*, **60**, 2275 (1974); see earlier related work by K. Iguchi, *J. Chem. Phys.*, **48**, 1735 (1968); numerical solution of the wave function for the continuum model has been reported by I. Carmichael and B. Webster, *J. Chem. Soc., Faraday Trans. 2*, **70**, 1570 (1974).

(24) J. T. Waber and D. A. Liberman, *J. Chem. Phys.*, **57**, 967 (1972).

(25) (a) D. A. Copeland, N. R. Kestner, and J. Jortner, *J. Chem. Phys.*, **53**, 1189 (1970). (b) Earlier semicontinuum models were developed by D. E. O'Reilly, *J. Chem. Phys.*, **41**, 3736 (1964).

(26) A. Gaathon and J. Jortner, ref 1e, p 429.

(27) (a) K. Fueki, D. F. Feng, L. Kevan, and R. Christoffersen, *J. Phys. Chem.*, **75**, 2291 (1971); (b) K. Fueki, D. F. Feng, and L. Kevan, *J. Am. Chem. Soc.*, **95**, 1398 (1973).

(28) Present work.

(29) J. W. Moskowitz, M. Boring, and J. H. Wood, *J. Chem. Phys.*, **62**, 2254 (1975).

(30) (a) J. Jortner, *Mol. Phys.*, **5**, 257 (1962). (b) The term "self-consistent" or "SCF" is used in two different senses. First, SCF refers to a model for treating the excess electron vis a vis the medium electrons; secondly, within both the SCF and adiabatic models one obtains a self-consistent field trapping potential; i.e., the medium polarization modes which are involved in the trapping "see" the self-consistent field of the excess electron.[30a]

(31) Tetramer anions were first studied by M. Natori, *J. Phys. Soc. Jpn.*, **27**, 1309 (1969); **24**, 913 (1968); M. Natori and T. Watanabe, *ibid.*, **21**, 1573 (1966).

(32) A prototype dimer calculation was carried out by L. Raff and H. A. Pohl, ref 1b, p 173.

(33) A preliminary account of the present work is given in ref 21.

(34) Effective potentials of this type are usually designated by the symbol V_0,[25a] and will be discussed below.

(35) (a) W. P. Kraemer and G. H. F. Diercksen, *Chem. Phys. Lett.*, **5**, 463 (1970); (b) P. A. Kollmann and L. C. Allen, *J. Am. Chem. Soc.*, **92**, 6101 (1970); (c) W. P. Kraemer and G. H. F. Diercksen, *Theor. Chim. Acta*, **23**, 398 (1972); (d) G. H. F. Diercksen and W. P. Kraemer, *ibid.*, **36**, 249 (1975); (e) H. Kistenmacher, H. Popkie, and E. Clementi, *J. Chem. Phys.*, **59**, 5842 (1973).

(36) H. F. Schaefer, III, "The Electronic Structure of Atoms and Molecules", Addison Wesley, Reading, Mass., 1972.

(37) L. Radom, W. J. Hehre, and J. A. Pople, *J. Am. Chem. Soc.*, **93**, 289 (1971); *J. Chem. Soc. A*, 2299 (1971).

(38) (a) D. E. O'Reilly, *J. Chem. Phys.*, **55**, 474 (1971); (b) D. A. Copeland and N. R. Kestner, *ibid.*, **58**, 3500 (1973).

(39) (a) T. R. Hughes, Jr., *J. Chem. Phys.*, **38**, 202 (1963); (b) B. B. Wayland and W. L. Rice, *J. Chem. Phys.*, **45**, 3150 (1966).

(40) J. A. Pople and R. K. Nesbet, *J. Chem. Phys.*, **22**, 571 (1954).

(41) N. R. Kestner and J. Jortner, *J. Phys. Chem.*, **77**, 1040 (1973).

(42) All the atomic nuclei lie within the cavity and only the long-range orbital tails of the solvent molecules penetrate the continuum.

(43) J. Lekner, *Phys. Rev.*, **158**, 130 (1967).

(44) B. E. Springett, M. H. Cohen, and J. Jortner, *Phys. Rev.*, **159**, 183 (1967).

(45) D.-F. Feng, K. Fueki, and L. Kevan, *J. Chem. Phys.*, **57**, 1253 (1972).

(46) Although the two approximations often give similar results, especially for ground state properties, the adiabatic approximation appears to be preferable for studying the density dependence of λ_{max} in gases, due to the different variations of D_s and β with density.[26]

(47) M. Tachiya (*Chem. Phys. Lett.*, **34**, 588 (1975)) has reached similar conclusions, based on a simple continuum model.

(48) R. H. Land and D. E. O'Reilly, *J. Chem. Phys.*, **46**, 4496 (1967).

(49) R. Ditchfield, W. J. Hehre, and J. A. Pople, *J. Chem. Phys.*, **54**, 724 (1971).

(50) D.-F. Feng, D. Ebbing, and L. Kevan, *J. Chem. Phys.*, **61**, 249 (1974).

(51) The effective monomer corrections for the ground state of e_{aq}^- and e_{am}^- (relative to the energy of the isolated monomer in the 4-31G basis) are as follows: −0.053 eV (dipole-oriented hydrate cluster, r_d = 2.65 Å); −0.023 eV (OH-bond-oriented hydrate cluster, r_d = 2.65 Å); and −0.076 eV (dipole-oriented ammonia cluster, r_d = 2.75 Å). For the excited states of the dipole-oriented structures, the corresponding corrections are −0.093 eV (H_2O) and −0.063 eV (NH_3).

(52) These physical parameters of the medium have been used in previous studies.[25-27] Most of the data are cited in "Handbook of Chemistry and Physics", R. C. Weast, Ed., 50th ed, The Chemical Rubber Company, Cleveland, Ohio, 1969.

(53) R. Olinger, S. Hahne, and U. Schindewolf, *Ber. Bunsenges. Phys. Chem.*, **76**, 349 (1972); A. Gaathon and J. Jortner, unpublished work.

(54) A. Gaathon, Ph.D. Dissertation, Hebrew University, 1974.

(55) A. Gaathon and J. Jortner, unpublished work.

(56) The value of r_d^0 published previously[21] for e_{aq}^- (2.68 Å) was shorter, because the energies had not been corrected for effective monomer energy.

(57) R. R. Hentz, Farhataziz, and E. M. Hansen, *J. Chem. Phys.*, **57**, 2959 (1972); U. Schindewolf, ref 1c, p 207.

(58) R. R. Hentz, Farhataziz, and E. M. Hensen, *J. Chem. Phys.*, **55**, 4974 (1971) (H_2O data); Farhataziz, L. M. Perkey, and R. R. Hentz, *ibid.*, **60**, 4383 (1974) (NH_3 data).

(59) The density of the excess charge, $\rho'(r)$ in eq 17, is based on the highest occupied molecular orbital. Similar results would be obtained if $\rho'(r)$ is defined as the difference in the total densities ($\rho(r)$, eq 5) for the charged and neutral clusters.

(60) (a) G. Lepoutre and A. Demortier, *Ber. Bensenges. Phys. Chem.*, **75**, 647 (1971); (b) G. Lepoutre and J. Jortner, *J. Phys. Chem.*, **76**, 53 (1972).

(61) A somewhat shorter r_d^0 value for e_{aq}^- (1.93 Å) was obtained by Kevan et al.[27b] using a semicontinuum approach which does not include H–H repulsions between the water molecules.
(62) See ref 60b and previous work cited therein.
(63) E. J. Hart and W. C. Gottschall, *J. Phys. Chem.*, **71**, 2102 (1967), T = 300 K.
(64) A similar small splitting was found by Moskowitz et al.[29] although the ordering was reversed.
(66) G. V. Teal, *Phys. Rev.*, **71**, 138 (1948).
(67) By analogy with e_{aq}^- (see Table VI), thermal fluctuations would be expected to reduce the spin density magnitudes somewhat.
(68) J. E. Bennett, B. Mile, and A. Thomas, *J. Chem. Soc. A*, 1393 (1967); 1502 (1969); K. Ohno, I. Takemura, and J. Sohma, *J. Chem. Phys.*, **56**, 1202 (1972); B. G. Ershov and A. K. Pikaev, *Radiat. Res. Rev.*, **2**, 1 (1969).
(69) S. Ray, *Chem. Phys. Lett.*, **11**, 573 (1971).
(70) D.-F. Feng, K. Feuki, and L. Kevan, *J. Chem. Phys.*, **58**, 3281 (1973).
(71) I. Shavitt, "Methods in Computational Physics", Vol. 2, Academic Press, New York, N.Y., 1963, p 1.
(72) For the case R = 0, these integral formulae were previously given in ref 50.

Discussion

R. CATTERALL. Have you found any change in the geometry of the water or ammonia molecules when they take part in the solvated electron?

In related calculations within an INDO approximation on ammoniated lithium atoms I have found a decrease of up to 3° in the Li–N–H angle in the optimum geometry. Since the dipole is reversed in this system relative to your solvated electrons, this is very similar to the decrease of this order you found for the H–O–H angle.

M. D. NEWTON. We have found a decrease of 2° in the angle for the case of H_2O. This is a small effect.

T. TUTTLE. Have you estimated the spin density at the nitrogen nleus for your model?

M. D. NEWTON. Yes. As I recall, we obtained a positive value with a magnitude of $\sim 10^{-1} a_0^{-3}$.

L. KEVAN. (1) I would like to point out that there is a way to experimentally distinguish between the dipole orientation and OH bond orientation models for H_2O around an electron. From our electron spin echo modulation results for electrons in alkaline ice we deduce that there are six nearest neighbor protons at an average distance of 2.1 Å (*J. Chem. Phys.*, **63**, 3365 (1975)). Now, for the dipole orientation model the oxygens are at 2.4 Å while for the OH bond orientation model the oxygens are at 3.2 Å. Your value of r_d is between these two values. By using ^{17}O ice we are presently analyzing EPR line widths and shapes due to hyperfine coupling of the electron with ^{17}O. Preliminary analysis appears to support the OH bond orientation model for electrons in alkaline ice.

(2) I would also like to comment that the isotopic hyperfine constant to protons for electrons in alkaline ice cannot be larger than ~2 G from recent second moment EPR line width analyses at both 9 and 35 GHz by Bales, Bowman, Schwartz, and Kevan (*J. Chem. Phys.*, **63**, 3008 (1975)). How strongly would your calculation be affected if you were required to obtain an isotopic coupling constant only half as large as you now obtain?

M. D. NEWTON. Our calculations were carried out within the unrestricted Hartree–Fock framework, which leads to a certain amount of contamination of the doublet spin state by quartet and higher spin states. In view of your experimental results, we should remove the contaminating quartet component and ascertain what effect this improvement has on our calculated spin densities. However, the effect will probably be very small, since our calculated value of $\langle \hat{S}^2 \rangle$ for e_{aq}^-, 0.7509, is quite close to the correct eigenvalue for the doublet. Furthermore, we can calculate the equilibrium geometry of various OH-bond oriented models to allow comparisons with your geometric predictions with regard to the distance of the closest protons from the electron.

S. GOLDEN. Can you state just how the solvent–solvent interactions were taken into account in your calculations?

M. D. NEWTON. All interactions within the first solvation shell, and between the first solvation shell and the excess electron, are explicitly included quantum mechanically (i.e., this is what the self-energy of $\rho(\vec{r})$ corresponds to).

P. DELAHAY. Is it fair to say that one essential difference between your approach and previous semicontinuum models is the taking into account of *structure*? Cavity models do not work well when there is hydrogen bonding, e.g., Onsager's theory of dielectrics.

M. D. NEWTON. There is no straightforward comprehensive answer to your question. Symmetry corresponding to s or p orbitals should only be considered as a zeroth-order approximation. In fact, our calculations, like those of Moskowitz et al., correspond to D_{2d} symmetry which implies a closely spaced e and b_2 set of lowest-lying excited states, separated by about 0.2 eV.

G. R. FREEMAN. You mentioned s → p excitation energies. In your ab initio calculations it is not assumed that the ground state is s-like, but this approximation is frequently made in continuum and semicontinuum models. What would be the effect on the calculated transition energy if the ground state symmetry were closer to p or d than to s?

M. D. NEWTON. There is no straightforward comprehensive answer to your question. Symmetry corresponding to s or p orbitals should only be considered as a zeroth-order approximation. In fact, our calculations, like those of Moskowitz et al., correspond to D_{2d} symmetry which implies a closely spaced e and b_2 set of lowest-lying excited states, separated by about 0.2 eV.

A. BERNAS. The ionization energy and excitation energy values calculated by the author, I guess, apply to liquid phase conditions. How would these values be affected by shifting from the liquid to solid phase conditions? In particular, how would this affect the energy difference between ionization and excitation energy? For crystalline H_2O and D_2O ices, stimulated luminescence experiments have in fact shown that the photodetachment threshold energy is very close to the hc/λ_{max} value of the trapped electron: ~1 eV.

M. D. NEWTON. Shifting from the liquid to ice in our framework, would require the use of a considerably smaller effective dielectric constant. Such calculations have not yet been carried out, but would certainly be worthwhile in view of the experimental data which you have mentioned.

P. DELAHAY. The term "threshold" is often quoted, but one should be very careful in the case of solutions. A threshold defined in an operational manner has no well-defined significance. One needs an equation for the photoionization spectrum.

M. D. NEWTON. Clearly the calculated ionization energy in principle only provides a lower limit to the threshold.

N. KLASSEN. Your calculations show that in ice-like structures e_t^- is stabilized to the extent of ~0.5 eV. This is close to the maximum of an infrared band (λ_{max} ~3600 nm) which we have observed in D_2O crystals and D_2O glasses which we attribute to a type of e_t^- unlike the well-known e_t^- which absorbs in the visible. Which ice-like structures have you examined and do they include D and L defects?

M. D. NEWTON. Our calculations were for an ice-like pentamer, with an excess electron in diffuse orbitals centered about the central water molecule. Although various distortions corresponding to orientational relaxation of the outer water molecules were considered, the H-bonded ice-like configuration was energetically favored.

J. JORTNER. I would like to raise the issue of the energetic stability of the dielectron, that is two electrons trapped in a single cavity. The old calculations of O'Reilly indicated that this species is unstable in ammonia. Recent calculations by Kevan, Kestner, and the present work indicate that it is on the verge of stability. From the experimental point of view, the optical data, which indicate only a small spectral shift of the absorption maximum of the electron center in the concentration range where spin pairing occurs, provide strong evidence against the stability of the dielectron.

M. H. COHEN. Not only do the optical properties change only slightly in the region where spin pairing takes place but so does the excess volume per electron. For the dielectron to be stable and give

agreement with the optical and volume data would therefore require two accidents.

T. TUTTLE. I want to emphasize that the optical spectrum of sodium ammonia solution is not invariant to changes in composition (see G. Rubinstein, T. R. Tuttle, Jr., and S. Golden, *J. Phys. Chem.*, **77**, 2872 (1973)). We have found that changes in the optical spectra do occur and from these changes the presence of a species with the composition of M^- may be inferred in dilute, i.e., 10^{-4} to 10^{-3} *M* sodium–ammonia solutions.

J. V. ACRIVOS. Even if the optical data give little evidence for the pairing of electrons near the MNM transition, the magnetic data (NMR and ESR) give unambiguous evidence for spin pairing. Therefore the theory should concentrate on explaining the difference.

J. JORTNER. Spin pairing does not necessarily require the formation of the dielectron and can originate from the well triplets or quartets, where spin pairing between a pair of single electron centers occurs.

R. CATTERALL. Regarding the experimental evidence for solvated dielectrons, I would like to recall the exceptionally long lifetime ($>10^{-6}$ sec) of the electron–electron spin pairing interaction required to maintain the electron spin state lifetimes required by the line width of ESR spectra of metal–ammonia solutions. Equilibria of the type

$$e^- + e^- \rightleftarrows \text{(spin paired species)}$$

must limit the lifetime of unpaired electron spin states, but the observed spin relaxation rates are approximately independent of metal concentration (and hence concentration of spin paired species) up to about 0.2 *M*. Such long lifetimes argue strongly for strong spin-pairing processes. [R. Catterall and M. C. R. Symons, *J. Chem. Soc.*, 3763 (1965); *J. Chem. Soc. A*, 13 (1966).]

N. KLASSEN. I should like to present a cautionary note regarding experiments designed to observe the optical absorption spectra of dielectrons. We irradiated alkaline ice glasses at 76 K with doses of about 1 Mrad and then bleached at 650 nm. After bleaching quickly we observed the transmission of the sample in the near-infrared to slowly decrease. This appeared to be due to a physical change in the glass rather than dielectrons and on warming the glass many tiny bubbles were seen.

B. WEBSTER. Concerning the comments on the mobilities of the dielectron within the semicontinuum models, it may be recalled that according to the calculations of Kestner e_2^{2-} was unstable with respect to two one-electron cavities, while within the SCF model the dielectron is stable. Recent studies, calculating the wave functions numerically (Webster and Carmichael, unpublished), show that in both approximations the dielectron is predicted to be stable, and also the use of analytic wave functions leads to differences in calculated energies of ~10%, and significantly influence properties.

M. D. NEWTON. It should be noted that the difference between Kestner and Kevan et al. regarding the stability of the dielectron does not now exist, in view of recent work of Kestner which has superseded earlier results.

B. WEBSTER. I should like to ask with respect to the dielectron calculations whether the lowest state is a singlet or triplet. Some recent ab initio work on dimers seems to suggest that depending on the orientation of the molecules, triplet states are energetically preferred over singlets and vice-versa. Also has the triplet dielectron species any relation to so-called "excited water"?

M. D. NEWTON. In our ab initio calculations we did not look directly at triplet states. However, we did some spin-unrestricted calculations, which gave no indications of low-lying triplets.

P. DELAHAY. Are calculations really sufficiently realistic to allow the settling of a fine point (dielectron existence)?

M. D. NEWTON. Our ab initio calculations provide a well-defined reference energy, which indicates that the stability of the dielectron relative to two monoelectrons is marginal. Refined calculations would have to consider the correlation energy (beyond the Hartree–Fock framework) and the entropy term in the free energy.

N. KESTNER. The stability of the dielectron is very dependent on the long-range electron–solvent interaction which is the weakest part of the theory. A very small modification of the long-range interaction makes the dielectron unstable. Thus present theories probably overestimate dielectron stability.

M. D. NEWTON. I agree. Our ab initio calculations are quite consistent with your suggestions. In particular, our calculations in the adiabatic approximation give even greater instability than that which we obtain when the full dielectric response (orientational and electronic) is included.

J. JORTNER. This work provides the first complete theoretical approach to the problem of structure and energetics of the solvated electron. This ab-initio approach is inherently limited to a quantum mechanical treatment of the first coordination layer. It will be very interesting to incorporate the molecular structure in the second layer in relation to recent experimental work on electron localization in dense polar vapors. In this context there is a promising alternative approach to the problem which rests on the work of Gordon and Kim at Harvard on the intermolecular interaction between rare gas atoms. Their approach rests on a free electron approximation for the charge densities of the interacting atoms. A theoretical justification for this method was provided by the interesting work of Harris, Gelbert, and Heller at Berkeley, based on the density functional method. It will be interesting to apply the same approach to the ground state of the solvated electron. Such an approach may provide an alternative to the $X\alpha$ method recently used by Moskowitz et al. and may be more reliable.

M. D. NEWTON. This is an interesting possibility.

Ab-Initio Studies into the Mechanisms of Formation of the Hydrated Electron

Brian Webster

Chemistry Department, University of Glasgow, Glasgow G12 8QQ, Scotland *(Received July 23, 1975)*

This study concerns events occurring between the time of thermalization of electrons generated in radiolyzed water and the appearance of the fully developed absorption spectrum of e_{aq}^-. First, the significance of including diffuse orbitals in ab-initio calculations on solvated electrons is illustrated by reference to H^- and the structures of the oxonium family H_3O^+, H_3O, H_3O^-. Five mechanisms proposed for the formation of e_{aq}^- are then examined: (a) formation via the radical intermediate H_3O; (b) direct electron capture by a water molecule; (c) selective electron attachment, and attachment through a favorable vibrational mode of an n-mer; (d) attachment via the excited state $H_2O(^3B_1)$; (e) attachment arising from medium interactions. Finally attention is directed to the structure of the hydrated electron.

Introduction

The mechanisms which lead to the generation of hydrated electrons on the pulse radiolysis of water still remain rather obscure. It was emphasized some years ago by Magee that the oxonium ion H_3O^+ produced in the ion–molecule reaction

$$H_2O + H_2O^+ = H_3O^+ + OH \quad (1)$$

occurring in $\sim 10^{-14}$ sec, may capture an electron to form the oxonium radical

$$H_3O^+ + e^- = H_3O \quad (2)$$

This radical then either may undergo dissociation to yield hydrogen atoms

$$H_3O = H_2O + H \quad (3)$$

or serve as an intermediate on the path to e_{aq}^-.[1]

$$H_3O = (H_3O^+)_{solv} + e_{solv}^- \quad (4)$$

Such a view for the formation of the hydrated electron is in contrast with the models developed to account for the structure and properties of solvated electrons, in which excess electrons are considered to range through the liquid until they are self-trapped, or captured by a group of molecules arranged at some favorable orientation. A review of these theories is given by Webster and Howat.[2] In Magee's opinion of 1964, it is unlikely that many of the hydrated electrons are formed by hydration of electrons which remain free of their parent ions after the initial action with high-energy radiation.

In this study the results of some ab-initio molecular orbital calculations are interwoven with experimental data pertaining to the hydrated electron, in order to ascertain whether current models for electron solvation are adequately founded with regard to events occurring after thermalization at $\sim 10^{-14}$ sec and the onset of the fully developed spectrum of e_{aq}^- at ~ 4 psec.[3]

Computational Details

The ab-initio calculations reported here have been performed within an LCGO spherical Gaussian approximation using the program MOLPRO III, written by Meyers and Pulay at the University of Stuttgart. Where equilibrium structures are given, these have been obtained using the force methods of Pulay.[4] A variety of basis sets have been employed, the primitive bases are those given by Huzinaga,[5] with the contractions proposed by Dunning.[6] The coarsest basis used is [9, 5; 4] → [4, 3; 3] referring for water to the use of nine s-type and five p-type primitive functions on oxygen, and four s-type functions on hydrogen, contracted as indicated.

Basis sets have been supplemented with polarization functions having exponents, noted in parentheses, optimized upon a water molecule lying in the xy plane. These bases will be referred to as follows:

basis A: [9, 5; 4] → [4, 3; 3]
basis B: basis A + d_{xy}^O (1.28) + p_x^H, p_y^H (0.79) + p_z^H (0.55)
basis C: [10, 6; 5] + full d set^O + p_x^H, p_y^H, p_z^H

For comparison, total energies, equilibrium geometries, and dipole moments for the water molecule obtained for these bases are listed in Table I. Conversion factors are taken from Taylor, Parker, and Langenburg.[7] (1 Bohr = 0.529177 Å, 1 Hartree = 27.211652 eV, 1 au = 2.54177 D).

Calculations on the water molecule have been reviewed recently by Kern and Karplus,[8] and it is well known that the inclusion of polarization functions has an ameliorative effect upon computed energies and structure. This may be seen from Table I, a detailed discussion of which is not pertinent. The bases have also been supplemented by a set of diffuse Gaussian functions. It is the role of these functions which will now be illustrated.

Orbitals and Structure

In an early semiempirical molecular orbital study on the hydrated and ammoniated electron, cognizance was taken of the need to introduce into the calculation a set of functions to allow for the possible diffuse character of the orbital of the excess electron.[9] Such practice is now common in molecular calculations on excess electrons, a number of diffuse Gaussian functions for example being included in the basis set. These functions are of the type

$$\phi = (2k/\pi)^{3/4} \exp(-kr^2) \quad (5)$$

with k having values as 0.07, 0.0175, and $0.0044 a_0^{-1}$.[10]

TABLE I: Equilibrium Structures Calculated for the Water Molecule

Basis	E, au	O–H, Å	HOH, deg	μ, au	q_O	q_H
A	−76.010468	0.952	112.01	0.985	8.77	0.615
B	−76.042046	0.945	106.57	0.870	8.45	0.774
C	−76.057178	0.942	106.08	0.853	8.52	0.740
Obsd[a]	−76.431	0.9572	104.52	0.741 ± 0.004,		
	H–F limit					
	−76.066 ± 0.002					

[a] Reference 9.

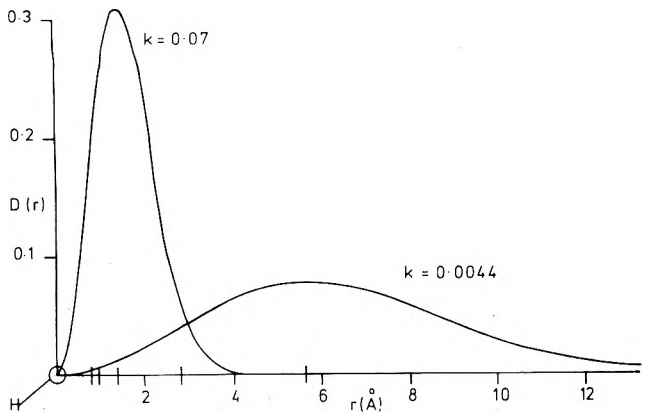

Figure 1. Radial distribution function D(r) for diffuse orbitals with k = 0.07 and $k = 0.0044a_0^{-1}$, as compared with the O–H distance in water. Maxima noted along abscissa.

To illustrate the diffuse character of such functions, the radial distribution $4\pi r^2\phi^2$ is shown in Figure 1; for k = 0.07 the maximum occurs at 1.41 Å, for k = 0.0044 the maximum is at 5.64 Å with the tail extending many units further. It would however be inaccurate to compare such distance with the O–H internuclear distance of 0.9572 Å, for the electron density of the water molecule extends over a much wider region. Even allowing for the global nature of the molecular electron density, diffuse orbitals centered upon the oxygen nucleus with exponents as given are quite peripheral, and would have little influence upon the energy and structure of the neutral molecule. If added to basis B, the energy of a water molecule is lowered from −76.042046 to −76.043355 au; as the HOH angle decreases by 0.46° to 106.12°, the O–H distance is unaffected. Yet when one comes to consider an electron attachment process, the inclusion of diffuse functions in the basis is of prime importance if one is to secure an adequate representation for the additional electron. Two examples will illustrate this role of the diffuse functions. The exponents are as given above.

(a) *The Hydrogen Negative Ion* $H^-(^1S)$. With the five term Gaussian representation for the 1s orbital of the hydrogen atom, of basis C, the energy of $H(^2S)$ is computed to be −13.601 eV. The four term contracted function of basis B yields a value of −13.588 eV compared with the exact value of −13.606 eV. It is known that within the single particle approximation the H^- anion is calculated to be unbound by 0.33 eV, the Hartree–Fock limit being placed at −13.275 eV.

Using the five term function, the Hartree–Fock limit of H^- is not even approached, with E = −12.723 eV. Yet should the less accurate four term function be taken supplemented with the three diffuse functions, the energy of H^- is calculated to be −13.258 eV, an improvement in the energy of −0.535 eV over the five term function. That the additional electron is not autoionizing is suggested by the magnitudes of the coefficients of the diffuse functions in the expansion of the molecular orbital. These are 0.2736, 0.2884, and 0.0108, respectively, in order of diffuseness, with no particular dominance of the most diffuse orbital.

The exact solution for $H^-(^1S)$ is −14.361 eV, the additional electron being bound by −0.755 eV, for comparison a numerical calculation using a pair function method yields −14.299 eV.[11] It might be noted that the Hartree–Fock limit lies 1.09 eV above the exact solution. This is of the order of magnitude sought for the electron affinity of water clusters toward excess electrons. It so might seem that any ab-initio calculation performed even with a sufficient basis to approach the Hartree–Fock limit will through the omission of two particle and higher order interactions be inadequate to allow any definite statement to be made on the subject.

(b) *The Oxonium Sequence* H_3O^+, H_3O, H_3O^-. Experimental data on these species are rather rare. From a crystallographic analysis of the p-toluenesulfonate salt H_3O^+ $CH_3C_6H_4SO_3^-$, the H_3O^+ ion is identified as a discrete entity in the crystal, of flat pyramidal structure O–H = 1.01 Å, HOH = 110.4°.[12] Initial reports of the formation of H_3O in a perchlorate glass at −180°C under uv irradiation have subsequently been refuted, although Melton and Joy have suggested that H_3O is formed in water vapor under the action of ionizing radiation.[13-15] Of the hydrated hydrogen anion, little if anything is known.

The structure of H_3O^+ using basis A is calculated to be of regular D_{3h} symmetry, HOH = 120°, O–H = 0.96 Å, E = −76.300158 au. Inclusion of diffuse functions has no effect on the structure, the energy being lowered by only 0.008 eV to −76.300466 au. Retention of D_{3h} symmetry and the use of basis C allows the Hartree–Fock limit to be placed at near −76.335563 au with no change found in the structure.

For the radical H_3O, a slight departure from a regular planar structure is found with basis A, though equal O–H distances of 0.987 Å are restored when diffuse functions are centered on the oxygen nucleus. The variations in structure are shown in Figure 2. The total energy is lowered by −0.80 eV from −76.438036 to −76.467600 au with the Hartree–Fock limit (H_3O^+ geometry) placed at near −76.50207 au. It is with H_3O^- that the diffuse functions come into dominance, bringing an energy decrease of −3.83 eV from −76.323987 to −76.464591 au, the Hartree–Fock limit is near −76.49879 au (H_3O^+ geometry). As with the radical, slight differences in structure with basis A are removed with the use of diffuse functions. Also given in Figure 2 are the orbital energies for the additional electron. Compared with H_3O in which the orbital energy is lowered by −0.41 eV, from −4.24 eV, for the anion the diffuse functions bring a computed unbound level of +2.19 eV to a bound level of energy −0.33 eV.

Variations in charge density with inclusion of diffuse

TABLE II: Variation in the Charge Distribution for the Oxonium Sequence H_3O^+, H_3O, and H_3O^- at Equilibrium Structures Calculated for D_{3h} Symmetry with Changing Basis Sets

	H^2 H^1 O^+—H^3				H^2 H^1 O—H^3				H^2 H^1 O^-—H^3			
	q_O	q_{H^1}	q_{H^2}	q_{H^3}	q_O	q_{H^1}	q_{H^2}	q_{H^3}	q_O	q_{H^1}	q_{H^2}	q_{H^3}
[9, 5; 4] ↓ [4, 3; 3]	8.70	0.43_3	0.43_3	0.43_3	8.57	0.81	0.80	0.82	8.45	1.19	1.17	1.19
With diffuse s	8.87	0.41	0.41	0.41	9.23	0.59	0.59	0.59	10.16	0.61_4	0.61_4	0.61_2
[10 6; 5] with polzn and diffuse s	8.35	0.55	0.55	0.55	8.58_7	0.80_5	0.80_5	0.80_3	9.51	0.83	0.83	0.83

functions are noted in Table II. For H_3O^+ the change is minor and the positive charge resides on the hydrogen nuclei. Addition of an electron tends to equalize this distribution within basis A but with the use of the diffuse set, the density comes to be partitioned as to appear predominantly on the oxygen atom. That this is due to imbalance in the basis set is shown by the distribution obtained with basis C in which the additional charge is distributed equally over all the nuclei. In the case of H_3O^- the changing pattern of charge with the smaller bases becomes unacceptable, with basis C the additional electron appears associated with the oxygen nucleus to a measure of 0.92 unit.

The H_3O^- anion should it be formed would seem to consist of an excess electron lightly held by −0.33 eV, outside the molecular density of the parent, and serves as a prototype of a diffuse anion.

It should be stated that the structure for H_3O^+ as obtained with basis C is, in fact, a flat pyramid, O–H = 0.96 Å, mean HOH = 112.8°, E = −76.336921 au with an inversion barrier of 0.85 kcal/mol. For comparison, in a recent study of correlation effects on hydrogen bonding, Diercksen, Kraemer, and Roos found the SCF structure to be O–H = 0.959 Å, HOH = 113.5°, E = −76.329776 au. Allowing for correlation leads to a lengthening of the O–H distance to 0.972 Å, HOH = 111.6°. The correlation energy is given as −0.212 au which increases the barrier to inversion from 1.30 to 2.05 kcal/mol.[16]

A species H_3O^- formed by electron attachment without structural modification of H_3O^+ has an energy of −76.502088 au representing an inversion barrier of 2.07 kcal/mol.

With respect to dissociation into $H_2O(^1A_1) + H^-(^1S)$, the anion is calculated to be unstable by +14.2 kcal/mol. Similarly, Gangi and Bader, in considering the possible formation of H_3O, found this radical to be unstable with respect to dissociation to $H_2O(^1A_1) + H(^2S)$ by 14 kcal/mol, although a barrier ~6.6 kcal/mol was noted on the dissociation path.[17]

On comparing the charge distributions for H_3O^+ and H_3O^- at a pyramidal structure, just as with the planar structure nearly one unit of the additional charge is dispersed on the hydrogen nuclei, and one unit associated with the oxygen nucleus.

In anions of the type exemplified by H_3O^-, the additional electron appears to occupy a Rydberg type orbital, and in order to achieve an adequate representation of the orbital it is necessary to include a number of diffuse functions in the basis set. Since the additional electron is so peripheral, behaving rather as an independent single particle, the correlation corrections which are of importance to obtain an accurate description for the structure of H^- may not be as significant for the diffuse anion. Pacansky, Wahlgren, and Bagus in a study of the energy surface of the CO_2^- anion express a similar view.[18]

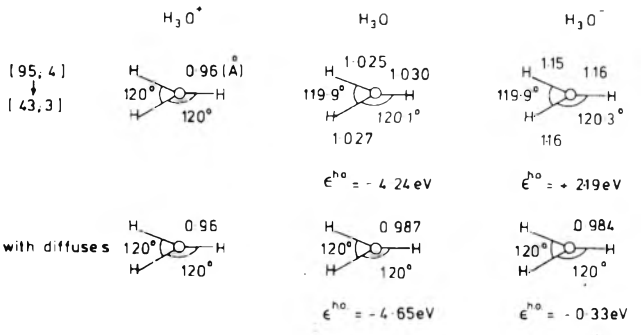

Figure 2. Variation in equilibrium structures of the oxonium sequence with inclusion of diffuse functions. Energies of highest occupied orbitals $\epsilon^{h.o.}$ are noted.

Mechanisms of Formation

Five mechanisms which could be proposed to account for the formation of hydrated electrons in radiolyzed water will now be considered.

(a) *Formation via the Radical Intermediate H_3O.* Examination of the electronic structures and total energies of the oxonium sequence H_3O^+, H_3O, H_3O^- lends some credence to the possibility that thermalized electrons could be withheld by H_3O^+ for form H_3O as in reaction 2, although the radical would be expected to dissociate according to reaction 3. In order for solvation step 4 to occur, molecular orientation needs to take place, and this seems inconsistent with the time scale of molecular events, even accepting that microscopic relaxation processes may occur prior to $\sim 10^{-10}$ sec.

Fast electron shake-off with electron transfer to a neighboring water molecule might be postulated

$$H_3O + H_2O = H_2O^- + H_3O^+ \qquad (6)$$

In such circumstances H_2O^- would be a precursor of e_{aq}^-.

(b) *Direct Electron Capture by H_2O.* The interaction of a water molecule with an incident electron is usually considered to lead to a dissociative attachment process, yielding H^-, O^-, and OH among the products. Claydon, Segal, and Taylor in reviewing the available data emphasize the fact that OH^- is not a primary product.[19] They conclude that the $^2A_1$ state of H_2O^- is stable with respect to disso-

TABLE III: Equilibrium Structures Calculated for H_2O^-

Basis	E, au	O–H, Å	HOH, deg	q_O	q_H	EA, eV
A	−75.854720	1.03	104.61	8.71	1.15	−4.24
B	−75.876817	1.01	99.86	8.45	1.27,	−4.50
B + diffuse s	−76.036659	0.952	107.4	9.44	0.78	−0.18

ciation into $H(^2S) + OH^-(^1\Sigma^+)$ and that it is the $^2B_1$ and $^2B_2$ states which dissociate to $H^-(^1S) + OH(^2\Pi)$.

Structures for H_2O^-, calculated over bases A, B, and B with diffuse s, are given in Table III together with energies and charge distributions. In no case is the additional electron found to be bound, while the last structure noted is only approximate, the geometry cycle proving to be nonconvergent. With diffuse functions, it is seen that the total energy is considerably lowered, from −75.876817 to −76.036659 au. That Claydon, Segal, and Taylor arbitrarily lowered their H_2O^- surface by 3 eV then might seem justified.

Taking the equilibrium structure for H_2O^- in basis B and considering dissociation into OH^- at an equilibrium O–H calculated distance of 0.955 Å, E = −75.369237 au, and H for which E = −0.499277 au, the $^2A_1$ state of H_2O^- at equilibrium is found to be stable by 5.2 kcal/mol with respect to dissociation. In view of the quality of the basis, and the lack of account for correlation, this value serves only to illustrate the argument of Claydon, Segal, and Taylor that $H_2O^-(^2A_1)$, if formed, would dissociate to $H_2O + e^-$, rather than yielding OH^-.

Electron capture, in the sense noted, refers to capture during the course of a molecular vibration of the water molecule; Franck–Condon capture at the equilibrium structure of neutral water would tend to be less stable with respect to dissociation, though not likely to exceed the dissociation limit. If the attachment time is of order $\gtrsim 10^{-12}$ sec, then

$$e^- + H_2O = H_2O^- \qquad (7)$$

might constitute a possible mechanism leading to the formation of e_{aq}^-, as has been noted by Ballard.[20]

(c) *Selective Attachment and Attachment through a Favorable Vibrational Mode of an n-mer.* In Figure 3a is depicted the equilibrium structure of the water dimer $(H_2O)_2$, as obtained over basis A, with the geometries of the individual water molecules unconstrained. The total energy is −152.032330 au which in comparison with the energy of the component molecules at equilibrium, given in Table I, provides a value of −7.14 kcal/mol as a measure of the energetic stability of the dimer. Slight differences are seen in the structures of the two components: molecule 1 lying in the xy plane has HOH = 111.8°, O–H = 0.95 Å; molecule 2 in the xz plane has HOH = 112.7°, O–H···O = 3.008 Å, with O–H = 0.957 Å and the outer O–H distance is 0.951 Å. Comparison with the structure of an individual molecule for basis A, noted in Table I, shows the unit to be an assembly of two molecules with little structural modification.

On addition of an electron, both molecules undergo considerable structural deformation, as calculated in this basis. The HOH angle of molecule 1 opens to 115.2°, the O–H distance increases to 1.019 Å, there is a decrease in the O–H···O distance to 2.45 Å yet with O–H becoming 1.026 Å, and the outer O–H bond shortens to 0.948 Å. The energy of the dimer is −151.899253 au and with respect to H_2O and H_2O^- is stable by −21.37 kcal/mol. At this geometry the energy of the neutral dimer is −152.011819 au and adiabatic removal of the electron would be accompanied by cleavage of the hydrogen bond.

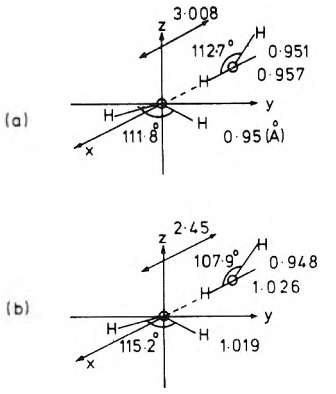

Figure 3. Equilibrium structures calculated for the water dimer $(H_2O)_2$ (a) and the negative ion $(H_2O)_2^-$ (b).

A comparison of the structures of the component molecules of the dimer with those of the individual H_2O^- or H_2O structures, Tables I and III, would suggest that the structure is not an assembly of two distinct units, unless molecule 2 is compared with H_2O^- in the diffuse basis. However, the charge of the extra electron, as partitioned in the Mulliken analysis, appears exclusively on molecule 1, and similar distributions have been obtained previously in semiempirical calculations. Charge distributions are given in Table IV. As has been commented previously for the oxonium sequence, such distributions are likely to be considerably basis dependent, and should a diffuse set of functions be placed on the oxygen molecule of molecule 2, then the electron will be localized on that center. The energy of $(H_2O)_2^-$ is then lowered to −152.005564 au. For comparison, Naleway and Schwartz found $E(H_2O)_2^-$ = −152.0078 au for a linear hydrogen bonded structure.[21]

Two questions concerning mechanism are raised by these calculations. First, are there sites of preferential attachment within a molecular cluster, for example, the molecule which donates the hydrogen atom in the hydrogen bond, bringing the electron to reside upon a specific molecule of the cluster to form a species $(H_2O)^-(H_2O)_{n-1}$? Secondly, on viewing the structural modifications concomitant with the additional electron not being held totally outside the molecular density of the neutral substrate, are there vibrational modes of a dimer, or n-mer, which would lead to the trapping of an excess electron by virtue of the energy surface of the negative ion state falling below that of the neutral species at a structure distant from equilibrium for the neutral system? This latter type of attachment has been reported to occur for CO_2 which when linear displays a negative electron affinity, yet proceeding through a bending mode will attach an electron at OCO angles in the neighborhood of 135°. The electron is lightly bound by 0.3 eV.[22,23]

(d) *Attachment via the Excited State $H_2O(^3B_1)$.* Figure 4 shows some qualitative energy curves derived from calcu-

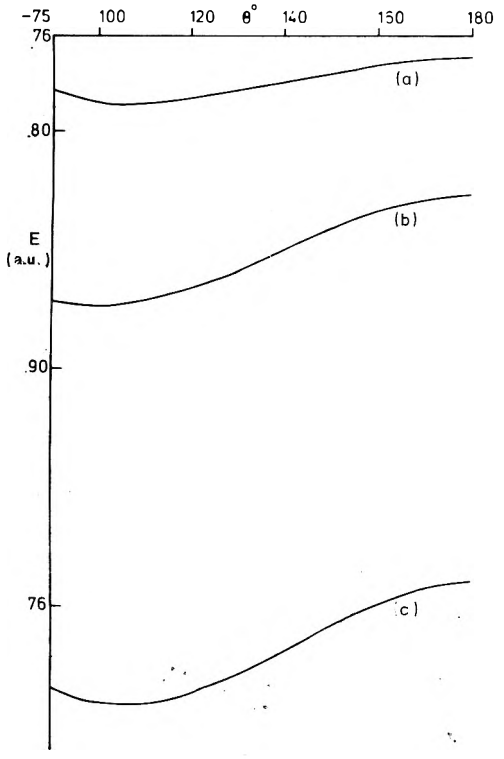

Figure 4. Qualitative curves showing the variation in energy with HOH angle: curve a, $H_2O(^3B_1)$; curve b, $H_2O^-(^2A_1)$; curve c, $H_2O(^1A_1)$.

TABLE IV: Charge Distributions for the Dimers $(H_2O)_2$, $(H_2O)_2^-$

	Molecule 1 xy plane		Molecule 2 xz plane		
	q_O	q_H	q_O	q_H	q_H^{outer}
$(H_2O)_2$	8.80	0.59,	8.82	0.56	0.63
$(H_2O)_2^-$	8.72	1.11	8.89	0.44	0.73
$(H_2O)_2^-$ diffuse s molecule 2	8.86	0.55	9.88	0.51	0.65

lations within basis B, for the ground state of water, curve c, the excited state $^3B_1$, curve a, and the negative ion $H_2O^-(^2A_1)$, curve b. The O–H distance is maintained at 0.945 Å the equilibrium value for the ground state in this basis.

For variation of the HOH angle between 90 and 180° the $^3B_1$ surface lies considerably above the H_2O^- surface. The lowest point found on the excited state surface is for the linear structure with O–H = 1.17 Å, E = −75.813294 au. Accordingly, with the excited state surface placed at energies >6.2 eV above the ground state, and the $^2A_1$ surface of H_2O^- at <4.5 eV, electron attachment through the excited state to yield H_2O^- is a possibility.

The argument occasionally presented in favor of capture via the excited state, in which comparison is made between the $4a_1$ virtual orbital of water and the occupied orbital of H_2O^- to show their similarity, is noted as false. The virtual orbitals of the neutral molecule directly pertain to the N + 1 electron system.[10,22,23]

(e) *Attachment Arising from Medium Interactions.* At Colloque Weyl III, Gaathon and Jortner noted that a water cluster $(H_2O)_n$ if formed in a dense vapor would display little affinity toward excess electrons, though with increasing cluster size, $n \geq 4$, the tendency for attachment increases.[25] This is in agreement with molecular orbital calculations performed on groups of water molecules at semiempirical and ab-initio levels.[21,26,28] For example, trial calculations on a trimer with a [9,5;3] basis and very diffuse functions suggest the electron affinity of a trimer is of order +0.01 eV within the restricted Hartree–Fock approximation.

The orbitals of a water molecule placed in a solvation field will undergo a certain distortion. If diffuse functions are involved in fields of near spherical symmetry, studies on orbital contraction of diffuse orbitals in ligand fields indicate that significant radial contraction may occur, amounting to as much as a factor of 0.5 of the original size. Diffuse anions should accordingly be stabilized in solvation fields, and excess electron states which are represented by diffuse functions centered on a vacancy found to be more strongly localized and bound.

According to the calculations of Ray, the energy of a water molecule placed in a tetrahedral dipole field at a specific alignment is lowered by −56.78 eV from −75.97089 to −78.05757 au, and H_2O^- by a further −1.80 eV.[27] For a tetrahedral vacancy with diffuse functions located on the center, Newton has demonstrated that the polarization field of a continuous dielectric will lower the energy of $(H_2O)_4e^-$ to produce a strongly bound state for the excess electron.[28] Recently, Moscowitz, Boring, and Wood have reported an $X\alpha$ calculation on a similar tetrahedral model, finding a localized species.[29]

Concluding Discussion

In developing theoretical models to account for the behavior of solvated electrons less attention perhaps has been directed toward the mechanism of formation of these species, than, for example, the optical properties. Often, the excess electron is assumed to have attained a localized state occupying a void region, with a solvation shell forming about the localization site. It is the expectation that if short-range interactions are treated either as in semicontinuum models, or by recourse to ab-initio calculations, and with allowance for long-range interactions, that the structure of the solvated electron will be open to incisive determination. Certainly, should only a coarse representation of the molecular density of the solvation shell be taken, as basis A, this would seem a considerable improvement over a point multipole approximation. Yet if accuracy is sought then as illustrated by the oxonium sequence larger bases need be deployed. Such calculations are founded usually on the assumption that e_{aq}^- should be formulated as $(H_2O)_ne^-$.

Except for mechanism e which is concerned more with energetic stabilization than mechanism, the alternative mechanisms are characterized by electron capture upon a single molecule, or selective attachment to a molecule within a H-bonded network. Although it could be contended that the electron is only transiently held upon the molecule, or undergoes a series of radiationless transitions,[3] consideration of the time scale of formation and the detection of long-lived anionic species in the gas phase as CO_2^- does not permit the formulation of e_{aq}^- as a hydrated diffuse anion to be totally precluded.

The term "diffuse anion" is taken to signify a species in which the additional electron remains exterior to the neutral molecule, being attached through a Rydberg-type orbital, rather than as an additional electron which is incorporated into the molecular density of the neutral molecule.

Stabilization of the anion through medium interactions may be expected to occur, but in contrast to $(H_2O)_n e^-$, the anion remains as a distinct entity with e_{aq}^- formulated as $(H_2O)_{aq}^-$. In such circumstances, solvated electrons would constitute a class of diffuse anions, open to formation in liquids of great variety in structure and yet being characterized by an absorption band arising from a series of molecular Rydberg transitions. Such resemblances that exist between solvated halide ions and solvated electrons would also find a natural explanation.[30]

Three structures which might be assumed to represent e_{aq}^- are the solvated localized electron $(H_2O)_n e^-$, the solvated diffuse anion $(H_2O)_{aq}^-$, and the polaron $(H_2O)_n^-$. It is not the purpose here to distinguish between these possibilities, although structure $(H_2O)_n e^-$ is currently most favored, yet it would be informative if one could ascertain which, if any, of the structures is adequate to describe a solvated electron. For such a purpose, the measurement of Verdet constants for solvated electrons could be of value, as these depend upon the polarizabilities of e_{solv}^- and accordingly would provide a sensitive probe for assessing the accuracy of the wave function.

Acknowledgments. I wish to express my sincere thanks to Professor H. Preuss, Institut für Theoretische Chemie, Universität Stuttgart, for hospitality during the year 1973–1974 and for his interest in this work. I also thank Dr. Rudolf Janoschek for some useful discussions. The work was performed during the tenure of a CIBA-GEIGY Senior Fellowship whom I thank for their kind support.

References and Notes

(1) J. L. Magee, *Radiat. Pes. Suppl.*, **4**, 20 (1964).
(2) B. C. Webster and G. Howat, *Radiat. Res. Rev.*, **4**, 259 (1972).
(3) P. M. Rentzepis, R. P. Jones, and J. Jortner, *J. Chem. Phys.*, **59**, 766 (1973).
(4) W. Meyer and P. Pulay, MOLPRO III, Institut fur Theoretische Chemie, Universitat Stuttgart, 1972; P. Pulay, *Mol. Phys.*, **17**, 197 (1969).
(5) S. Huzinaga, *J. Chem. Phys.*, **42**, 1293 (1965).
(6) T. H. Dunning, *J. Chem. Phys.*, **53**, 2823 (1970).
(7) B. N. Taylor, W. H. Parker, and D. N. Langenburg, *Rev. Mod. Phys.*, **41**, 375 (1969).
(8) C. W. Kern and M. Karplus, "Water: A Comprehensive Treatise," F. Francks, Ed., Plenum Press, New York, N.Y., 1972, pp 21–91.
(9) B. J. McAloon and B. C. Webster, *Theor. Chim. Acta*, **15**, 385 (1969).
(10) For exponents used in calculations of excited states of H_2O, see W. J. Hunt and W. Goddard, *Chem. Phys. Lett.*, **3**, 414 (1969).
(11) R. F. Stewart, Ph.D. Thesis, University of Glasgow, 1973; B. C. Webster and R. F. Stewart, *Theor. Chim. Acta*, **27**, 355 (1972). For the exact energy value for H^-, see C. L. Pekeris, *Phys. Rev.*, **127**, 509 (1962). See also W. Goddard, *Phys. Rev.*, **172**, 7 (1968), for a discussion of H^-. I thank a referee for drawing my attention to this work.
(12) J. O. Lundgren and J. M. Williams, *J. Chem. Phys.*, **58**, 789 (1973).
(13) T. W. Martin and L. L. Swift, *J. Am. Chem. Soc.*, **93**, 2788 (1971).
(14) J. A. Wargon and F. Williams, *Chem. Phys. Lett.*, **13**, 579 (1972).
(15) C. F. Melton and H. W. Joy, *J. Chem. Phys.*, **46**, 4275 (1967).
(16) G. H. F. Diercksen, W. P. Kraemer, and B. O. Roos, *Theor. Chim. Acta*, **36**, 249 (1975).
(17) R. A. Gangi and R. F. W. Bader, *Chem. Phys. Lett.*, **11**, 216 (1971).
(18) J. Pacansky, U. Wahlgren, and P. S. Bagus, *J. Chem. Phys.*, **62**, 2740 (1975).
(19) C. R. Claydon, G. A. Segal, and H. S. Taylor, *J. Chem. Phys.*, **54**, 3799 (1971).
(20) R. F. Ballard, *Chem. Phys. Lett.*, **16**, 300 (1972).
(21) C. A. Naleway and M. E. Schwartz, *J. Phys. Chem.*, **76**, 3905 (1972).
(22) C. D. Cooper and R. N. Compton, *Chem. Phys. Lett.*, **14**, 29 (1972).
(23) C. D. Cooper and R. N. Compton, *J. Chem. Phys.*, **59**, 3550 (1973).
(24) R. F. Stewart and B. C. Webster, *J. Chem. Soc., Faraday Trans. 2*, **70**, 524 (1973).
(25) A. Gaathon and J. Jortner, "Electrons in Fluids", J. Jortner and N. R. Kestner, Ed., Springer-Verlag, Heidelberg, 1973, p 429.
(26) G. Howat and B. C. Webster, *J. Phys. Chem.*, **76**, 3714 (1972); M. Weissmann and N. V. Cohan, *J. Chem. Phys.*, **59**, 1385 (1973).
(27) S. Ray, *Chem. Phys. Lett.*, **11**, 573 (1971).
(28) M. D. Newton, *J. Chem. Phys.*, **58**, 5833 (1973).
(29) J. M. Moscowitz, M. Boring, and J. H. Wood, *J. Chem. Phys.*, **62**, 2254 (1975).
(30) M. C. R. Symons in "Electron-Solvent and Anion-Solvent Interactions", L. Kevan and B. C. Webster, Ed., Elsevier, Amsterdam, Chapter 9, in press.

Discussion

M. NEWTON. You have pointed out that electron correlation has an obvious effect in lowering the energy of an electron pair. This would of course have a bearing on the dielectron, as Kestner has shown, but would not be nearly so crucial for solvated monoelectrons, where there is only a single electron in the diffuse orbital. Thus your 1-eV correlation effect in H^- certainly does not indicate that a transition energy of ~1–2 eV for the solvated electron could not be reasonably calculated.

B. WEBSTER. A contrast was drawn between correlation effects in H^-, where the Hartree–Fock limit lies ~1.09 eV above the exact solution, and diffuse anions as illustrated by the oxonium sequence. For a diffuse anion with the additional electron peripheral in character, then indeed the one-electron approximation is likely to be valid, as is since to be evidenced by the agreement between observed and calculated electron affinities for CO_2^-. However, I am still of the opinion that if e_{aq}^- is taken to be a diffuse anion $(H_2O)^-(H_2O)_n$ stabilized in a liquid, correlation effects will be important.

P. DELAHAY. It may be noted that the photoionization spectrum of solvated electrons and iodide ion in solution are quite similar. This tells us something about models.

B. WEBSTER. Yes, this is certainly the case, and since resemblances exist between the spectral properties of solvated electrons and solvated halide ions, this seems to favor a solvated diffuse anion $(H_2O)^-(H_2O)_{n-1}$ formulation for the structure of e_{aq}^-.

Theoretical Studies on the Composition of the Absorption Spectrum of the Solvated Electron

Neil R. Kestner* and Jean Logan

Chemistry Department, Louisiana State University, Baton Rouge, Louisiana 70803 *(Received July 23, 1975)*

Our studies on the optical spectrum of electrons in polar fluids are extended to study the influence of cavity distortions, the higher excited states, and the role of the two electron cavity species. The higher excited states with $l = 1$ were studied by simple models using numerical solutions of the differential equations and by solutions of the Copeland–Kestner–Jortner model (CKJ). In ammonia the second excited state is predicted to lie about 0.44–0.52 eV above the first, depending on the technique used. Most cavity distortions do not split the $l = 1$ components. Those that do, yield only a small difference in energy of the levels. Improved calculations of the two electron cavity species are presented. That species is larger than the one electron cavity. Calculations using a screened interelectronic interaction predict a stable two electron species which becomes marginally stable when solvent effects are included. Thus none of these studies can explain the observed spectrum. A reinvestigation of the long-range electron–solvent interaction is needed. Preliminary results of such studies, using the recent work of Dogonadze et al. are included. Agreement with experimental results is greatly improved.

I. Introduction

The study of electrons in polar fluids can be roughly divided into studies which primarily investigate the long-range electron–solvent interaction and those that primarily explore the short-range or local interactions. The most recent calculations have attempted to include both effects but in comparing the results to experimental data, one or the other region is often emphasized.

The recent models[1,2] and a priori calculations[3] have been quite successful in discussing ground state properties and the band maximum. The model calculations have had great difficulty explaining the shape of the absorption spectrum. The most successful calculations of the absorption spectrum have assumed a very simple short-range interaction and *no* long-range interaction, i.e., a particle in a box model.[4,5]

Because of the failure of our original model to explain the absorption spectra we have initiated several studies[6] into possible causes for the observed spectrum. While our studies will concentrate on electrons in ammonia the arguments apply to other fluids as well. The questions we shall address are as follows. (1) Is the line really homogeneously broadened? (2) What is the role of higher excited states? (3) What is the importance of cavity distortions? (4) What contribution does the two electron cavity species make to the optical spectrum? (5) What is the limitation of the present model? Finally we will present initial attempts at producing a new model which can explain the experimental data and reconciles the previous successes of the model with its chief failures. The new approach is also in accord with the previous arbitrary "particle in a box" models.

II. Homogeneous vs. Inhomogeneous Broadening

In principle the observed broad absorption spectrum could be due to a variety of "trapping sites" whose spectra differ slightly from one another rather than from a peculiar nature of one or more excitations of the solvated electrons which are almost identical. The former type of broadening is called inhomogeneous and the latter, homogeneous. Rather than try to decide between these on theoretical grounds, we will recite recent laser experiments which have indicated the broadening is homogeneous. The work of Hupert, Struve, Rentzepis, and Jortner[7] and preliminary results from Walker[8] show that hole burning of the absorption peak probably is not possible; rather one obtains a uniform reduction of the intensity of the line. This indicates that all "components" of the line originate from the same "species". In contrast to this Hager and Willard,[9] in studies of organic glasses, find a large amount of inhomogeneous broadening, although their results also suggest that each component is also homogeneously broadened primarily to the high-energy side.

Generalizing these results we will assume, in general, that the primary cause of the broad spectrum is homogeneous and the study of the most stable species should explain the experimental data. It can also be pointed out here that this conclusion is in accord with our previous theoretical calculations.[1,6]

III. Higher Excited States

We have previously touched on the role of higher excited states in several papers.[6,10] In particular we have explored the position of the second s state in ammonia relative to the 2p state, since this could be studied by two photon absorption and would be a nice test of the model.[10] We also indicated previously the location of the higher excited states if we could neglect the short-range electron–medium interaction. This last assumption has been of concern to us and therefore we undertook more accurate calculations of the higher excited states, not only to verify the location of these levels within our model but also to explore the relative roles of the long- and short-range electron medium interactions. In addition, we wanted to be sure our results were not biased by our choice of basis set.

In Table I we present the results from the Copeland–Kestner–Jortner (CKJ) model for three p and one s state as well as finite difference calculations for the potential which

TABLE I: Higher Excited States

CKJ model[a]					
	Simpler model[b]				
Usual calculation, eV	Usual calculation	Finite difference, eV	Simple model by finite difference,[c] eV	Rydberg levels, eV	
2p −1.031	−1.117	−1.176	−1.025	−0.933	(−1.153)[b]
3p −0.598	−0.621	−0.639	−0.417	−0.415	(−0.635)
4p −0.437	−0.448	−0.455	−0.232	−0.233	(0.453)
5p unknown	inknown	−0.363	−0.157	−0.150	(0.370)
2s −0.854	−0.867	−0.913	−0.603	−0.933	(−1.153)
$h\nu$(1s → 2p) 1.011	1.050	1.249	0.814	2.80	(2.80)

[a] With $V_0 = -0.22$ eV included as in eq 3 in text. [b] With constant potential up to center of dipole and long-range potential beyond.

$$\begin{bmatrix} V(r) = -N\mu e/r_d^2 - \beta e^2/r_e \\ = -\beta e^2/r + V_0 \end{bmatrix} \begin{matrix} 0 < r < r_e \\ r > r_e \end{matrix}$$

[c] Using a potential defined by fitting the CKJ model to a potential similar to that discussed in footnote *b* adjusted such that the first transition energy is in reasonable agreement with experimental data (see eq 1).

originates from that model and for a potential which yields reasonable agreement with the experimental band maximum and has a potential well of reasonable dimensions. The well depth was

$$-2.808 \text{ eV} = -1.088 - \beta e^2/a \qquad \text{for } r \leq a \tag{1}$$

where

$$a = 4.39 \text{ Å}$$

$$\beta = 0.514 = (1/D_{op} - 1/D_s) \tag{2}$$

with D_{op} the optical dielectric constant and D_s the static dielectric constant. The long-range potential was of the adiabatic form $-\beta e^2/r$. The finite difference method used was that originated by McKoy and coworkers[11] using a transformation $r = x^2$ to allow the range of radii to become quite large with ease.

From these results and from the numerical calculations of Carmichael and Webster[12] on the continuum model it is apparent that the next p state lies at much too high an energy to be the cause of the observed line shape. This is also not the fault of the particular basis set (see the finite difference calculations) nor the particular form of the model.

From Table I we see that the results are simply due to the long-range potential ($-\beta e^2/r$). All of the models approach those in the last column of Table I which is based on

$$En = -\frac{\beta^2}{2n^2} + V_0 \tag{3}$$

if V_0 is included.

The finite difference calculations also point out the dependence on the potential at large radii in another way. In order to obtain good energies for a coulombic potential which is as weak as this one, we need to carry out the calculation to radii over one hundred Bohr radii. In most of our results the cut off was 250 bohrs. This implies that we need a very great degree of uniformity or conversely, very little fluctuation in the polarization of the medium over large distances.

IV. Cavity Distortions

The contribution to the line shape of some simple cavity distortions is being investigated, although it appears at this time that the significance of such distortions is negligible. Assuming the existence of some bound states (2p, 2s), a mechanism for mixing 2p and 2s states, thus splitting the 2p's allows for the possibility of optical transitions to several states, resulting in a broadening of the absorption band.

Most distortions and vibrations do not do this but one suitable mechanism involves a particular arrangement of dipoles in the first layer so that for points in the medium (continuum), the cavity itself appears to have a total dipole moment. This induces a "reaction field" in the cavity due to response of the medium. This contributes a term to the electronic potential which involves an angular dependence. This angular dependence leads to nonzero matrix elements between s and p states.

Those configurations which lead to a total dipole moment outside the cavity involve a rotation of one (or more) dipoles about their equilibrium positions. Deformation away from general tetrahedral symmetry would also lead to a total dipole moment but these were not investigated. A simple displacement of a dipole along the radius vector makes a negligible contribution.

For the case where only one dipole is allowed to rotate, the dipole contribution to the electronic potential inside the cavity is altered to

$$-(\mu/r_a^2)(3 + \cos\psi) + 2(\mu/A^3)(1 - D)r(\cos\theta(\cos\psi - 1) + \sin\psi\cos\varphi\sin\theta)/(2D + 1)$$

while outside it is

$$(3\mu/r^2(2D + 1))(\cos\theta(\cos\psi - 1) + \sin\psi\sin\theta\cos\varphi)$$

where ψ is the angle of the dipole with respect to the radius vector, D is the dielectric constant, and A is the radius of the cavity, R_c, while θ and φ are the usual spherical polar coordinates centered at the origin of the cavity.

The results yield a splitting of the p states by a small amount, about 0.003 eV, for reasonable changes in ψ. This calculation and others of a similar nature have convinced us that distortions of the cavity cannot lead to the correct line shape.

V. Two Electron Cavity Species

One other suggested cause for the line shape (and for the diamagnetic behavior of metal–ammonia solutions) is the presence of stable species containing two electrons in a single cavity. Very little experimental evidence supports this, however.

A great many calculations have been made on this species and when all errors are corrected, all calculations

TABLE II: Two Electron Cavity[a]

	One term wave function	Two term wave function
One electron cavity		
ΔH_1, eV	−1.0801	−1.0061
$h\nu$, eV	1.0251	1.10
	(N = 4, r_d^0 = 2.7 Å)	(N = 4, r_d^0 = 2.7 Å)
Two electron cavity		
ΔH_2, eV	−2.508	−3.0106
$h\nu$, eV	1.23	1.68
	(N = 4, r_d^0 = 2.60 Å)	(N = 12, r_d^0 = 4.15 Å)
ΔH_{21} (eV) = $^1/_2\,\Delta H_2 - \Delta H_1$	−0.174	−0.499

[a] Screened $1/r_{12}$ interaction. (Pure adiabatic model, ammonia, 203 K), V_0 = −0.220 eV.

TABLE III: Two Electron Cavity[a]

	One term wave function	Two term wave function
Two electron cavity		
ΔH_2, eV	−1.261	−1.546
$h\nu$, eV	0.554	0.882
	(N = 4)	(N = 12)
ΔH_{21} (eV) = $^1/_2\,\Delta H_2 - \Delta H_1$	+0.450	+0.233
	One term[b] wave function	
Two electron cavity		
ΔH_2, eV	−2.306	
$h\nu$, eV	0.992	
	(N = 4)	
ΔH_{21}, eV	−0.073	

[a] Not pure adiabatic model. Unscreened $1/r_{12}$ interaction. Ammonia, 203 K; V_0 = −0.220 eV. [b] Pure adiabatic model with screening only beyond R_c; start of continuum.

had suggested such a stable species. Land and O'Reilly[13] made the first detailed calculation. This was followed by papers by Fueki[14] using a continuum model and two calculations using both long- and short-range electron–solvent interactions, one by Feng, Fueki and Kevin[15] and one by Copeland and Kestner.[16] The latter paper contained a serious error and when it is corrected all calculations agree.

The basic Hamiltonian for a two electron species by the simple CKJ model is

$$H = H_1(2\beta) + H_2(2\beta) + U(r_{12}) \qquad (4)$$

where H_1 and H_2 are one electron Hamiltonians like those in the one electron cavity, except that 2β appears in place of β because the medium is being polarized by two electrons. If we use the expression for $U(r_{12})$ as given by Land and O'Reilly[13] and used by almost all workers since, using the same procedures as in earlier papers we get the results in Table II which are referred to as the screened calculations. The word screened is used since we assumed that the $1/r_{12}$ interaction was reduced by the optical dielectric constant when an electron was outside the cavity. The one term results are very similar to those of Feng et al.[15] As we see in Table II the cavity species is stable and more accurate calculations suggest that it has a higher energy optical transition. Such results are consistent with the results of Vannikov et al. in HMPA[17] but seem unsupported in ammonia.

Very recently Tachiya[18] reviewed this problem again and points out correctly that in the SCF theory as used by Feng et al.[15] one should use an unscreened interelectronic interaction since the medium does not follow the motion of the electrons. In the adiabatic theory the screened result should be correct. This leads to a significant difference between the two approaches. Using continuum theories the two approaches are in reasonable agreement with the two electron cavity being stable only at low static dielectric constants.[18]

In Table III we present two alternative approaches to the treatment of the electronic interaction, i.e., no screening and screening only in the continuum (as compared with screening in the continuum and the first coordination layer). Although the definition of the adiabatic model requires the screening of the electron's interaction, in actual fact the screening of highly localized electrons should be much less than this, closer in fact to no screening, the SCF limit. Calculations using screening in Table III indicate the dielectron is unstable on an energy scale.

There are other considerations which make the two electron species unstable. First of all, we have been using enthalpy and not free energy as a criterion as is proper. We have also been neglecting energies and entropies required to change the liquid structure to accommodate the two electron cavity. The two term wave functions suggest that the dielectron has a larger number of molecules in the first coordination layer than the one electron species. If we assume that the only change in liquid structure can be relat-

TABLE IV: Model Potential Results[a]

State[b]	$\gamma = 0$	$\gamma = {}^1/_{40}a_0^{-1}$	$\gamma = {}^1/_{25}a_0^{-1}$	$\gamma = {}^1/_{20}a_0^{-1}$	$\gamma = {}^1/_{12}a_0^{-1}$
1s	−1.839	−1.768	−1.723	−1.721	−1.661
2s	−0.603	−0.340	−0.231	−0.171	
3s	−0.307	−0.078	−0.020	−0.055	
4s	−0.185	−0.008			
5s	−0.124				
6s	−0.084				
2p	−1.025	−0.858	−0.762	−0.747	−0.619
3p	−0.417	−0.290	−0.080	−0.040	
4p	−0.232	−0.028			
5p	−0.157				
6p	−0.102				
7p	−0.062				
3d	−0.431	−0.167	−0.056	−0.006	
4d	−0.242	−0.025			
5d	−0.154				
6d	−0.106				

[a] Potential used is that discussed in Table I, footnote *b*. [b] States are labeled by hydrogenic notation whereas the results are more closely approximated by a particle in a box model in which case one should use 1p, 2p,..., 6p and 1d, 2d, 3d, 4d.

ed to four extra solvent molecules (12 − 2(4)), the additional terms could include about 4(0.05) eV to break four hydrogen bonds and about 0.18 eV for entropy corrections,[19] thus the stability of the two electron cavity could become something like $\Delta G_{12} = -0.119$ eV. This value is so small that the theoretical results are questionable.

There is another reason for regarding the above calculations suspiciously. A great deal of emphasis is placed on the value and behavior of the long-range potential. If β were reduced or the potential cut off, the two electron species would rapidly become unstable. This fact, coupled with the adiabatic theory's overemphasis on screening of the interelectronic interaction, leads us to say quite confidently that the dielectron species is not thermodynamically stable.

VI. Suggested Improved Models

The major lessons learned from the calculation of the optical spectrum, especially the higher excited states, and the two electron cavity species is that the present models overemphasize the long-range electron–medium interaction. Additional data are contained in the work of Firestone[20] on mixtures of alcohols and hydrocarbons, namely, the absorption maxima is very insensitive to the bulk properties. The finite difference calculations also indicated that the higher excited states require Coulombic behavior out to almost 100 Å. However, as has been stated by Funabashi[4,21] and others, such long-range correlations in the polarization in a liquid is unlikely. Unfortunately no adequate formal development had been available to allow for liquid fluctuations. Within the past few years Dogonadze and his collaborators have developed an extensive quantum theory of the dielectric behavior of a liquid.[22-24] They have applied it to electron transfer reactions,[23] the polaron model,[23] and the solvation energies of ions.[24] Their main point is the introduction of correlation lengths for polarization modes (assuming as a first approximation an exponential decay of correlations).

The meaning of this for our work is that the long-range electron–medium interation is not simply Coulombic but of a screened Coulombic form such as

$$-2\beta e^{-\gamma r}/r \qquad (5)$$

where $\gamma = 1/\lambda_D$, λ_D being a correlation length. We have made finite difference calculations using this potential along with the reasonable short-range interaction, discussed in an earlier section. The results are shown in Table IV. For $\lambda_D = 25a_0$, the assumed value for water and possibly applicable to ammonia, we see that essentially only one p state exists, the other being just barely bound. However, the energy of the bound p and ground state are only slightly affected by the change in the long-range electron–medium interaction. The energy of all other states is greatly affected.

The results of this modifed model are such that the ground state description has not changed greatly. Neither has the description of the band maximum changed, since it is of the same nature as that in the CKJ and semicontinuum models. Thus all of their previous calculations are still qualitatively correct. We now can explain why the long-wavelength part of spectrum behaves as if dominated by a short-range potential (see recent article by Brodskii and Tsarevskii)[25] and the high-energy tail acts like a bound-continuum transition (see work of Delahay et al.[26] on photoemission spectra). While the details of this model need to be explored, especially the details of the line shape, it is consistent with all of the experimental data and unifies most of the many diverse models. For example, both the lack of any observed higher energy transitions[27] and the pressure dependence should be predicted by the new version as well as the older one.

We are currently exploring the detailed correlation function (which probably decays more slowly than exponential) which is appropriate for ammonia and other polar solvents. We are also developing formal theories of the solvated electron, including the medium modes properly. It is obvious that such a theory will also lead to an unstable dielectron.

References and Notes

(1) For a summary, see N. R. Kestner in "Electrons in Fluids", J. Jortner and N. R. Kestner, Ed., Springer-Verlag, Heidelberg, 1973, p 1; N. R. Kestner in "Electron-Solvent and Anion-Solvent Interactions", L. Kevan and B. Webster, Ed., Elsevier, Amsterdam, in press.
(2) For a partial summary, see L. Kevan, *Adv. Radiat. Chem.*, **4**, 881 (1974); K. Fueki, D-F. Feng, and L. Kevan, *J. Am. Chem. Soc.*, **95**, 1398 (1973).
(3) M. Newton, *J. Phys. Chem.*, this issue; *J. Chem. Phys.*, **58**, 5833 (1973).
(4) T. Kajiwara, K. Funabashi, and C. Naleway, *Phys. Rev.*, **6**, 808 (1972).
(5) A. M. Brodskii and A. V. Tsarevskii, *Sov. Electrochem. (Engl. Transl.)*, **9**, 1571 (1973).
(6) The early work is contained in N. R. Kestner and J. Jortner, *J. Phys. Chem.*, **77**, 1040 (1973), as well as N. R. Kestner, in "Proceeding of the Fifth International Congress on Radiation Research", H. F. Adler, O. F. Nygaard, and W. K. Sinclair, Ed., Academic Press, in press.
(7) D. Hupert, W. S. Struve, P. M. Rentzepis, and J. Jortner, *J. Chem. Phys.*, **63**, 1205 (1975), using a 6–8-psec pulse of 30 mJ.

(8) D. C. Walker and R. May, *Int. J. Radiat. Phys. Chem.*, **6**, 345 (1974), and unpublished work.
(9) S. L. Hager and J. E. Willard, *J. Chem. Phys.*, **61**, 3244 (1974).
(10) J. Logan and N. R. Kestner, *J. Phys. Chem.*, **76**, 2738 (1972).
(11) N. W. Winter, D. Diestler, and V. McKoy, *J. Chem. Phys.*, **48**, 1879 (1968); V. McKoy and N. W. Winter, *ibid.*, **48**, 5263 (1968).
(12) I. Carmichael and B. Webster, *J. Chem. Soc., Faraday Trans 2*, **70**, 1570 (1974).
(13) R. H. Land and D. E. O'Reilly, *J. Chem. Phys.*, **46**, 4496 (1967).
(14) K. Fueki, *J. Chem. Phys.*, **50**, 5381 (1969).
(15) D.-F. Feng, K. Fueki, and L. Kevan, *J. Chem. Phys.*, **58**, 3281 (1973).
(16) D. A. Copeland and N. R. Kestner, *J. Chem. Phys.*, **58**, 3500 (1973).
(17) A. V. Vannikov, N. M. Alpatova, E. I. Mal'tsev, and L. I. Krishtalik , *Sov. Electrochem. (Engl. Transl.)*, **10**, 794 (1974). They have probably observed the species Na^- and not (e_2^{2-}).
(18) M. Tachiya, *Chem. Phys. Lett.*, in press.
(19) Based on ΔS° values from G. Lepoutre and A. Demortier, *Ber. Bunsenges. Phys. Chem.*, **75**, 647 (1971).
(20) J. R. Brandon and R. F. Firestone, *J. Phys. Chem.*, **78**, 792 (1974).
(21) K. Funabashi, *Adv. Radiat. Chem.*, **4**, 103 (1974).
(22) R. R. Dogonadze and A. A. Kornyshev, *Phys. Status Solidi b*, **53**, 439 (1972).
(23) R. R. Dogonadze, *Ber. Bunsenges. Phys. Chem.*, **75**, 628 (1971).
(24) R. R. Dogonadze and A. A. Kornyshev, *J. Chem. Soc., Faraday Trans. 2*, **70**, 1121 (1974), and papers referenced there.
(25) A. M. Brodskii and A. V. Tsarevskii, *Dokl. Akad. Nauk SSSR*, **217**, 1110 (1974).
(26) P. Delahay, *J. Phys. Chem.*, this issue, and also earlier work.
(27) Farhataziz, R. R. Hentz, and L. M. Perkey, unpublished results; they have determined the spectrum down to about 0.3 μ at 23°C.
(28) R. R. Hentz, Farhataziz, and E. M. Hansen, *J. Chem. Phys.*, **55**, 4974 (1971) [H_2O data]; Farhataziz, L. M. Perkey, and R. R. Hentz, *ibid.*, **60**, 4383 (1974) [NH_3 data]; U. Schindewolf and R. Olinger reported by U. Schindewolf in "Metal Ammonia Solutions", Colloque Weyl II, J. J. Lagowski and M. J. Sienko, Ed., Butterworths, London, 1970, pp 199–215 [NH_3 data].

Discussion

M. COHEN. If one makes the adiabatic approximation, the wave number dependence or spatial dispersion of the dielectric function does not affect the long-range Coulomb tail. The latter relates only to the zero wave number limit of the static dielectric function which, for an insulating material, is just the appropriate macroscopic dielectric constant; there is no exponential screening as for a metal. However, the time an electron takes to move a distance r into the fluid is r/v, where $v = (2|E - V|/m)$ and V is an appropriate mean potential which approaches V_0 for large enough r. While the electron is outside the cavity and its solvation shell, the ammonia molecules within that shell and even the cavity itself will start to relax. Let us say, therefore, that the effective charge decays exponentially with time as $e^{-t/\tau}$, where τ is the characteristic time of ammonia reorientation. The effective potential is therefore of the form $(1/r)e^{-r/l}$, where $l = v\tau$. Thus, a simple description of the nonadiabatic decay of the polarization leads to the form of the potential used by Kestner, it has nothing to do with spatial dispersion, which affects only the short-range part.

The sensitivity of the stability of the dielectron to cutting off the Coulomb tail may be understood as follows. In the energy of the dielectron there is a compensation of the direct electron–electron interaction by the polarization energy. The result is a small difference between two large quantities and is very sensitive to any change in the polarization energy.

N. R. KESTNER. In Dogonadze's work there are some k dependent effects but you are correct that they would be smaller in the difference in energy levels. This will probably require abandoning the adiabatic approach. Your proposed procedure is exciting and will be pursued. My primary point was to show that even with a small amount of screening in the high excited states (lengths of, e.g., 25 Å) the long-range behavior is reduced drastically. We need many more studies on the exact reason the long-range behavior is washed out. We plan to pursue the ideas you have presented. There is no question that with a small amount of screening the dielectron will be unstable.

P. DELAHAY. I should like to echo Kestner's statement that the semicontinuum model overestimates the Coulombic tail of the potential. In fact, the photoionization spectrum of solvated electrons (in HMPA) fits quite well the particle in a box model (deuteron photodisintegration). It is not even necessary to doctor up the Coulombic potential by a Yukawa potential (as was done by Dogonadze). Of course, this kind of fitting should not be overemphasized because of the complexity of the problem.

N. R. KESTNER. We need to modify our model because the long-range potential is a necessary consequence. If a Coulombic tail does not exist we must provide some theoretical reasons for its vanishing. It seems likely that the best model will appear closer to a particle in a box than a Coulombic potential.

J. JORTNER. I would like to introduce a cautious note regarding the fit to a square well potential. As we now know the short-range part of the potential can indeed be fit well to a spherical well, however, general correlations of optical data are not always accurate. To demonstrate this point let me remind you of the Ivey law for correlating the energies of optical excitation of F centers in alkali halides, which fit extremely well to the particle in a box model, although in that case it is obvious that the asymptotic form of the potential is Coulombic.

W. H. KOEHLER. We have seen data suggesting that energies are dependent on the number of solvent molecules, their orientation (i.e., whether the dipole is oriented or the O–H is oriented), and long-range forces. Can we expect a definitive model which excludes time as a variable, that is a model which ignores molecular dynamics?

N. R. KESTNER. The theories should be very good in predicting general features. In cases where the time scale of the experiment is short there probably will be or could be major effects. In general, however, we should be able to deal with time-independent models.

S. GOLDEN. The data of Gunn and coworkers of some years ago, based upon a volumetric-differential analysis provide the best experimental argument against the existence of a minimum in the molar volume–composition diagram.

N. R. KESTNER. I agree. There is no experimental evidence for the existence of the dielectron from volume expansion data.

Model Adiabaticity Effects on Solvation Free Energies of Electrons

Sidney Golden

Chemistry Department, Brandeis University, Waltham, Massachussetts 02154 *(Received July 23, 1975)*

A class of quasi-classical adiabatic statistical models is introduced for the solvated electron. Based upon the statistical thermodynamic analogue of the extended Born–Oppenheimer approximation, these models permit an assessment to be made of the effect of various adiabatic approximations on resulting theoretical expressions for the free energy of solvation of solvated electrons. In terms of these models, adiabatic approximations, which may be invoked for the solvated electron and any others, will always result in an estimated solvation free energy for the solvated electron that ascribes a greater thermodynamic stability to that species than is actually the case or may be attained in the absence of such approximations. A similar role is to be anticipated for the adiabatic approximations which have been incorporated in most current models of the solvated electron.

Introduction

Although the solvated electron has received no little experimental and theoretical attention from chemists and physicists during the past century or so, interest in this unusual chemical species continues unabated even at the present time.[1] It is no great surprise to find, as a result, that several theoretical models now exist in terms of which this species can be characterized.[2] What is remarkable, perhaps, is that each of the models gives a quite good quantitative account of certain of the solvated electron's properties, even while invoking basic ideas and procedures of approximation that differ from those invoked by other models. In fact, if only such performance were the criterion of a model's adequacy, little basic discrimination between the several models seems likely.

Matters would be obviously eased in this respect if a tractable exact theory of the solvated electron were to become available, but it seems almost inconceivable at the present time that any successful model of this species—either now existing or yet to be developed—can avoid including approximations of the type exemplified by the extended Born–Oppenheimer approximation[3,4] in quantum mechanics. Furthermore, any such model which is designed to account for equilibrium properties can scarcely avoid dealing with such approximations in statistical thermodynamic terms. Since none of the current models appear to have dealt directly with a proper statistical-thermodynamically formulated model of the solvated electron, it is to provide some rectification of the latter omission that the present paper is primarily directed.

In order to do so, it proves useful to introduce a class of quasi-classical adiabatic statistical models (QUASM) of the solvated electron, in terms of which the adequacy of many of its members often can be assessed on purely formal theoretical grounds. Based upon the recently developed theory of quasi-classical adiabatic approximations,[5] which provides the statistical thermodynamic analogue of the extended Born–Oppenheimer approximation, each QUASM differs from another one only in the manner and extent by which adiabatic approximations are incorporated in them. Each such model is so constructed that it provides a characteristic partition function and associated Helmholtz function for the electron–solvent system under consideration, and a corresponding free energy of solvation for the solvated electron. The latter serves as a proper criterion of the adequacy of the model whereby the role of various adiabatic approximations involved in certain QUASM's can be assessed; thereby, some indication can be had of the role they play in more tractable models of the solvated electron.

Quasi-Classical Adiabatic Statistical Models of the Solvated Electron. The QUASM's for the electron–solvent system under consideration are characterized as follows: (1) all models have the same Hamiltonian, which is exact; (2) each model is identified with a stipulated set of adiabatically designated degrees of freedom and the sequence by which they are so treated and eliminated or retained as such; (3) every model has a partition function which is evaluated quasi-classically in accord with the adiabatic treatment sequence which has been stipulated. By construction, the exact statistical thermodynamic treatment of the solvated electron is included among these models; i.e., no degrees of freedom are treated adiabatically.

We now render the foregoing characterization in mathematical terms.

With no undue loss of generality, the system under consideration will be supposed to have a fixed number of molecules of a chemically unreactive solvent, confined to a fixed volume in space with the spin-free Hamiltonian

$$H_S = K_x + K_y + V_{xx} + V_{xy} + V_{yy} + \Omega(x) + \Omega(y) \quad (1)$$

where x and y represent all the electronic and nuclear degrees of freedom, respectively, of the solvent; K refers to the kinetic energy operator for the indicated particles, V to the interaction operator of the indicated particles, and Ω to a "boxlike" potential which confines the indicated particles to a specified region in space.

In similar terms, an unsolvated electron which is presumably confined to the same specified region in space has the Hamiltonian

$$H_\epsilon = K_z + \Omega(z) \quad (2)$$

where z designates the degrees of freedom of the additional electron.

Finally, the electron–solvent system has the Hamiltonian

$$H_{S+\epsilon} = H_S + H_\epsilon + V_{zx} + V_{zy} \quad (3)$$

In terms of the foregoing, the electron–solvent system under consideration has the partition function[6]

$$Z_{\text{exact}} = \text{Tr}_{xyz}\, \mathcal{A}(x + z)e^{-H_{S+\epsilon}/kT} \quad (4)$$

where k is Boltzmann's constant, T is the absolute temperature, and $\mathcal{A}$ is the total antisymmetrizing projection for the indicated set of electrons.

The essence of a particular QUASM for the solvated electron is to be found in the expression which is used to evaluate its partition function. This can be made clear by means of explicit expressions. Thus,[6]

$$Z_{\text{QUASM}}(y) \equiv \text{Tr}_y e^{-(K_y + A_y)/kT} \quad (5)$$

where

$$A_y \equiv -kT \ln \text{Tr}_{xz}\, \mathcal{A}(x + z)e^{-(H_{S+\epsilon} - K_y)/kT} \quad (6)$$

is a partition function in which all the electronic coordinates implicit in x and z have been treated as averageable,[5] while only the nuclear coordinates implicit in y have been dealt with as adiabatic;[5] this is the essence of (6). The QUASM described by (5) and (6) corresponds to the single adiabatic procedure involving nuclear coordinates ordinarily associated with the extended Born–Oppenheimer approximation.

As an example of a simple sequence of adiabatic procedures, we consider[6]

$$Z_{\text{QUASM}}(y; y + z) \equiv \text{Tr}_y e^{-(K_y + B_y)/kT} \quad (7)$$

where

$$B_y \equiv -kT \ln \text{Tr}_z e^{-(K_z + C_{yz})/kT} \quad (8)$$

and

$$C_{yz} \equiv -kT \ln \text{Tr}_x\, \mathcal{A}(x)e^{-(H_{S+\epsilon} - K_y - K_z)/kT} \quad (9)$$

For the QUASM characterized by (7)–(9), just the electronic coordinates implicit in x have first been treated as averageable,[5] while a combination of electronic and nuclear coordinates, the y and z, have been dealt with as adiabatic;[5] this is the essence of (9). A subsequent adiabatic procedure retains as adiabatic,[5] only the nuclear coordinates implicit in y; this is the essence of (8), which follows (9) in execution.

A QUASM which involves a more elaborate sequence of adiabatic procedures is that for which[6]

$$Z_{\text{QUASM}}(y; y + z; x_1 + y + z) = \text{Tr}_y e^{-(K_y + D_y)/kT} \quad (10)$$

where

$$D_y \equiv -kT \ln \text{Tr}_z e^{-(K_z + E_{yz})/kT} \quad (11)$$

$$E_{yz} \equiv -kT \ln \text{Tr}_{x_1}\, \mathcal{A}(x_1)e^{-(K_{x_1} + G_{x_1 yz})/kT} \quad (12)$$

and

$$G_{x_1 yz} \equiv -kT\, \text{Tr}_{x_2}\, \mathcal{A}(x_2)e^{-(H_{S+\epsilon} - K_{x_1} - K_y - K_z)/kT} \quad (13)$$

Here, x_1 and x_2 represent disjoint electronic degrees of freedom of which the latter have first been treated as averageable,[5] followed by the former; this is the essence of (13) followed by (12). The subsequent retention of the nuclear coordinates as adiabatic[5] is indicated by (11), which follows (12) in execution.

It is evident that the exact partition function of the electron–solvent system under consideration is readily accommodated as a member of those of the class of QUASM's as asserted.

A comparison of (6), (9), (12), and (13) emphasizes the imposed relaxation of total exchange antisymmetry when proper subsets of electrons are treated either[5] as adiabatic or averageable. This is especially prominent in (8) and (11) where, because of the succeeding (9) and (12), respectively, the solvated electron has been ascribed an adiabatic individuality that renders it distinct from all the other electrons that are present. The notational differences between (5) and (7), or (10), reflect this ascribed behavior.

Each of the foregoing partition functions has an associated Helmholtz function, which we list:

$$F_{\text{exact}} \equiv -kT \ln Z_{\text{exact}} \quad (14)$$

$$F_{\text{QUASM}}(y) \equiv -kT \ln Z_{\text{QUASM}}(y) \quad (15)$$

$$F_{\text{QUASM}}(y; y + z) \equiv -kT \ln Z_{\text{QUASM}}(y; y + z) \quad (16)$$

$$F_{\text{QUASM}}(y; y + z; x_1 + y + z) \equiv -kT \ln Z_{\text{QUASM}}(y; y + z; x_1 + y + z) \quad (17)$$

Here, also, the notational differences between the various Helmholtz functions reflect the character of the QUASM approximations which have been imposed on the partition functions of the solvated electron.

Quasi-Classical Adiabatic Statistical Model Solvation Free Energies. In the absence of interaction between the unsolvated electron and the solvent system, we have the Hamiltonian

$$H^0_{S+\epsilon} = H_S + H_\epsilon \quad (18)$$

with the corresponding partition function for the reference state

$$Z^0_{\text{ref}} = \text{Tr}_{xyz}\, \mathcal{A}(x)e^{-H^0_{S+\epsilon}/kT} = \text{Tr}_{xy}\, \mathcal{A}(x)e^{-H_S/kT}\text{Tr}_z e^{-H_\epsilon/kT} \equiv Z^0_S Z^0_\epsilon \quad (19)$$

and the corresponding Helmholtz function

$$F^0_{\text{ref}} = -kT \ln Z^0_S - kT \ln Z^0_\epsilon \equiv F^0_S + F^0_\epsilon \quad (20)$$

In terms of the exact Helmholtz functions of (14) and (20), the exact solvation free energy of a solvated electron then is given by

$$\Delta F_{\text{solv}} \equiv F_{\text{exact}} - F^0_S - F^0_\epsilon \quad (21)$$

In similar terms, the QUASM solvation free energy of a solvated electron is obtained from the relevant QUASM Helmholtz function and (20). For example, the Helmholtz functions in (15)–(17) yield[7]

$$\Delta F_{\text{solv}}(y) \equiv F_{\text{QUASM}}(y) - F^0_S - F^0_\epsilon \quad (22)$$

$$\Delta F_{\text{solv}}(y; y + z) \equiv F_{\text{QUASM}}(y; y + z) - F^0_S - F^0_\epsilon \quad (23)$$

$$\Delta F_{\text{solv}}(y; y + z; x_1 + y + z) \equiv F_{\text{QUASM}}(y; y + z; x_1 + y + z) - F^0_S - F^0_\epsilon \quad (24)$$

Now, an essential property of the QUASM Helmholtz functions is that they all provide lower bounds to the exact Helmholtz functions.[5,8] This means that solvation free energies are similarly bounded by QUASM values, e.g., in terms of the previous values

$$\Delta F_{\text{solv}} \geq \Delta F_{\text{solv}}(y)$$

$$\Delta F_{\text{solv}} \geq \Delta F_{\text{solv}}(y; y + z), \text{ etc.} \quad (25)$$

In addition, any QUASM Helmholtz function which corresponds to a sequence of adiabatic approximations is demonstrably greater in value than one in which the sequence has been eliminated.[5,8] This means, in the case of the sequences which have been considered here, that

$$\Delta F_{solv} \geq \Delta F_{solv}(y) \geq \Delta F_{solv}(y; y+z) \geq \Delta F_{solv}(y; y+z; x_1+y+z) \quad (26)$$

As expressed by (25), the use of a QUASM Helmholtz function for the electron–solvent system comprising the solvated electron system will nearly always ascribe a greater thermodynamic stability to that species than will actually be the case.[9] This ascribed greater thermodynamic stability is to be associated with the quasi-classical nature of the adiabatic approximations which may have been introduced.[5] Moreover, when sequences of such approximations are employed, the result, illustrated by (26), is to ascribe even greater thermodynamic stability to the solvated electron than is actually the case. Such ascribed greater thermodynamic stability is, of course, purely an artifact (arising from the quasi-classical adiabatic approximations). To the extent that all existing theories of the solvated electron do invoke such adiabatic approximations for electrons,[10] the results that these theories produce must be regarded with reserve: that QUASM, which produces the lowest ground-state energy is by no means the "best" theory of the solvated electron.

References and Notes

(1) See, for example, the summaries of preceding Colloque Weyls: "Metal–Ammonia Solutions", G. Lepoutre and M. J. Sienko, Ed., W. A. Benjamin, New York, N.Y., 1964; "Metal–Ammonia Solutions", J. J. Lagowski and M. J. Sienko, Ed., Butterworths, London, 1970; "Electrons in Fluids", J. Jortner and N. R. Kestner, Ed., Springer-Verlag, New York, N.Y., 1973. See, in adcition, E. J. Hart and M. Anbar, "The Hydrated Electron", Wiley, New York, N.Y., 1970.

(2) An especially pertinent brief historical account can be found in J. M. Moskowitz, M. Boring, and J. H. Wood, *J. Chem. Phys.*, **62**, 2254 (1975).

(3) M. Born and R. Oppenheimer, *Ann. Phys. (Leipzig)*, **84**, 457 (1927).

(4) M. Born, *Nachr. Akad. Wiss. Göttingen Math-Phys. Kl.* **2**, no. 6 (1951). See, in this connection, C. J. Ballhausen and A. E. Hansen, *Annu. Rev. Phys. Chem.*, **23**, 15 (1972).

(5) S. Golden, *Phys. Rev. A.*, **9**, 530 (1974). See this reference for a clarification of the terminology used.

(6) We tacitly assume that all traces exist, the subscripts thereto denoting the particles to which the relevant degrees of freedom pertain. Any restrictions of symmetry not expressed are implicit.

(7) Particular notice should be taken of the fact that no approximations are involved since the quantities introduced define the relevant QUASM.

(8) S. Golden, *Chem. Phys. Lett.*, **33**, 899 (1975). For the sake of brevity, we will give no explicit proof here.

(9) In a mathematical sense the relationship involves the possibility of equality, but such equality is presumably apt to be accidental.

(10) Note the absence of "kinetic energy" corrections associated with the adiabatically treated electrons in existing theories of the solvated electron. For the appropriate statistical-thermodynamic theory that can take such corrections into account, see S. Golden, *Phys. Rev. A.*, **10**, 1740 (1974). For a discussion of the adiabatic principle pertaining here, see J. M. Zimar, "Electrons and Phonons", Clarendon Press, Oxford, 1963, Chapter V.

Discussion

M. NEWTON. I would like to point out an additional thermodynamic complication; i.e., most of us who perform semicontinuum calculations are actually applying the variational energy to a sum of a free energy (continuum) and enthalpy (discrete solvent shell). In addition, it seems to me that you will obtain an upper or lower bound to the exact energy depending on whether or not you include the so-called diagonal correction to the vibronic energy.

S. GOLDEN. The analysis I have described pertains to that adiabatic approximation due to Born and Oppenheimer in which the so-called diagonal correction is neglected altogether. This, it seems, is precisely what is done in solvated-electron theories to date: if the so-called diagonal contribution were to be included, it would be proportional to the reciprocal mass of the particle treated adiabatically and therefore very large when electronic masses are involved. For the statistical thermodynamic extension of the Born–Oppenheimer approximation, see S. Golden, *Phys. Rev. A.*, **9**, 540 (1974). For the statistical thermodynamic extension which involves the so-called diagonal contribution see S. Golden, *Phys. Rev. A.*, **10**, 1740 (1974).

Interactions between Solvated Electrons. I. Electron–Electron, Electron–Solvent, Solvent–Solvent Interactions in Ammonia. Valence Bond Approximation

Paul D. Schettler, Jr.,* and Gerard Lepoutre

Department of Chemistry, Juniata College, Huntingdon, Pennsylvania 16652 *(Received July 23, 1975)*

The binary interaction between two electrons solvated in ammonia is considered by treating the electrons in the valence bond approximation with dispersion forces added. Solvent–solvent and solvent–electron interactions vary as a function of distance between the solvated electrons. These changes are considered within the continuum approximation along with the electronic interaction. A major result of this study is that the ground (singlet state) is separated from the lowest triplet state by kT at distances of separation as large as 10.5 Å. The theoretical treatment is general in that it does not need to be restricted to the valence bond approach or to two electron problems.

Introduction

The general properties of metal–ammonia solutions are well known and have been amply documented elsewhere.[1-6] Basically the solutions show strong deviations from "ideality" as measured by many thermodynamic and nonequilibrium methods but surprisingly no deviation from ideality as measured by others. Although the concept of a solvated electron has been successful in explaining experimental results extrapolated to infinite dilution, the attempts to explain the interactions of solvated electrons in terms of chemical species (e.g., e_2^{2-} (solvated), dimers) has not enjoyed a similar success. The most explicit statement of the problems involved has been presented by Dye[7] who points out that existing (and generally accepted) data are paradoxical when interpretation is attempted in terms of models involving only the formation of (various) chemical species as a description of interelectronic interaction. As a specific example the solutions, initially paramagnetic due to all electrons being unpaired, become primarily diamagnetic at concentration as low as 0.05 M (0.1 MPM). This has been widely interpreted in terms of the formation of some sort of paired electron chemical species whereas data from optical and infrared spectroscopy would seem to mitigate against the formation of any such species. It should be noted that the problem is common to all models of solvated electron–electron interaction which seek explanation in terms of the appearance of any species (e.g., e_2^{2-}) as a chemical entity. Thus the dilemma raises a number of important theoretical questions.

Dye's dilemma would apply at concentrations of 0.005 M and above as this concentration is the lower limit of paramagnetic susceptibility data which demonstrate the significant presence of spin pairing.[8] This is well below the concentration range of most recent theoretical attention which has focused on the nonmetal–metal transition and formation of metallic clusters[8] as explanations of properties above 0.4 M (1 MPM). Whereas critical fluctuations formation may be important at high concentrations, the results of studying binary interactions should help to explicate properties at low concentration.

Work has already been done for two important cases of trap separation, $R = \infty$ corresponding to the energy of two single solvated electrons[10-12] and $R = 0$ corresponding to two electrons in the same trap.[13-15] In this previous work the presupposition of spherical symmetry allows consideration of the effects of cavity formation and a partial treatment of the discrete nature of the solvent as well. This has not been attempted here for the new problem at hand.

Theoretical

Treatments of bonding in the valence bond approximation are plentiful and need not be discussed here.[16,17] However for the case of solvated electrons two important modifications are necessary. First the diffuse nature of the trapping potential (as contrasted to the point–point $1/r$ interaction for electrons with a nucleus) necessitates the replacement of algebraic operators by integral operators in the Hamiltonian since the solvent orientation at all points contributes to the potential of an electron. Second, as bonding arises from changes in the electronic wave function as a function of R, these changes will be reflected in changes in solvent orientation. This consideration is one of utmost importance as solvent and electronic wave function have a "bootstrapping" interrelationship. Thus the effect of perturbations on the electronic wave function is intensified by the inclusion of solvent changes. Attention here is focused on these necessary modifications to the ordinary valence bond treatment.

The total Hamiltonian will contain terms dealing with the electron–trap interaction and the trap–trap interaction and these terms will be considered now. This problem has two components: first, the electrostatic potential created by the trap and, second, the nonelectrostatic work necessary to create that potential.

Electrostatic Terms. If the charge density of an electron is associated with the electric displacement, $\mathbf{D}$, Poissons equation gives

$$\nabla\cdot\vec{\mathbf{D}} = -4\pi e\psi\psi^* \tag{1}$$

where ψ is a normalized electronic wave function. Following standard treatment[18,19] the trapping effect of the solvent continuum can be described by a polarization vector, $\mathbf{P}_D$, associated with that part of the total polarization which is associated with a long time constant.

$$4\pi\vec{\mathbf{P}}_D = \left(\frac{1}{\epsilon_s} - \frac{1}{\epsilon_0}\right)\vec{\mathbf{D}} \tag{2}$$

where ϵ_s and ϵ_0 are the low and high frequency (static and optical) dielectric constants, respectively. The vector $\vec{P}_D$ arises because solvent dipole orientations create a net local charge distribution, ρ', in the solvent. Thus, whereas ρ refers to solute charge distribution, ρ' refers to the charge distribution hence induced in the solvent. The standard treatment then calculates the electrostatic trapping potential due to the electric charge enclosed within a sphere. However, with problems without spherical symmetry, it is simpler to consider ρ' directly. The relationship between ρ' and $\mathbf{P}_D$ is

$$\nabla \cdot 4\pi \mathbf{P}_D = \frac{4\pi\rho'}{\epsilon_0} \tag{3}$$

hence

$$\rho' = \beta\rho + c$$

$$\beta = \left(\frac{\epsilon_0}{\epsilon_s} - 1\right) \tag{4}$$

It is assumed in all of this that both dielectric constants are constant and that the solvent has in fact relaxed to its equilibrium (lowest free energy) configuration. Within these approximations eq 4 is a general relationship between the electronic charge density function and solvent orientation. The constant c is chosen so that $\int_v \rho'\, d\tau = 0$; if ρ includes both cationic and anionic contributions of a normal solute, $c = 0$. The close relationship between ρ and ρ' leads to the bootstrapping effect mentioned. If some external perturbation changes ρ, the resulting change will change ρ' also; since β is negative this "induced" perturbation intensifies the effect of the original perturbation.

In general

$$\rho_{Av'} \equiv \rho'/N = \frac{1}{N}\sum_{j=1}^{N} \int\int \cdots \int \psi\psi^*\, d\tau, \ldots d\tau_N \tag{5}$$

where N is the number of electrons, ψ is the N electron wave function, and the integrations are over the space of all the electrons except the coordinates of electron j which are held fixed at the point under consideration. (For the special case wherein ψ is given by a product of molecular orbitals ρ' is simply the sum of charge densities associated with each orbital.)

Thus the total Hamiltonian operator is

$$\hat{H} = T + V_{te} + V_{ee} + V_{tt} \tag{6}$$

$$T = \frac{\hbar^2}{2m}\sum_{i=1}^{N} \nabla_i^2$$

$$V_{te} = \frac{eN}{\epsilon_0}\sum_{i=1}^{N} \int \frac{\rho_{Av'}(\mathbf{r})\, d\mathbf{r}}{|\mathbf{r}_i - \mathbf{r}|}$$

$$V_{ee} = \frac{e^2}{\epsilon_0}\sum_{i=1}^{N-1}\sum_{j=i+1}^{N} \frac{1}{\mathbf{r}_{ij}}$$

$$V_{tt} = \frac{N^2}{2\epsilon_0}\int\int \frac{\rho_{Av'}(\mathbf{r})\rho_{Av}(\mathbf{r}')}{|\mathbf{r} - \mathbf{r}'|}\, d\mathbf{r}\, d\mathbf{r}' + A_{or}$$

where $|\mathbf{r}_i - \mathbf{r}|$ represents the distance between the position of electron i and the position $\mathbf{r}$ being integrated over, $|\mathbf{r} - \mathbf{r}'|$ is the distance between two points in the solvent (with integration over both). A_{or} is the nonelectrostatic part of the work necessary to create ρ' (ignoring the effects of volume change), and the other terms have their usual meaning. T and the various V's represent kinetic and potential energy contributions to $\hat{H}$, respectively. V_{te} is the trap–electron energy and is an integral (in contrast to the atomic case) because of the diffuse nature of the trapping charge, ρ'. V_{ee} takes account of the interelectron repulsions screened by ϵ_0, and V_{tt} takes account of the energy required to form ρ'.

Nonelectrolyte Solvent Contributions. A_{or}, β, and ρ have a functional relationship. β is a function of the dielectric constants which are determined at constant temperature rather than constant entropy. Therefore[20] it is more appropriate to consider a minimization of A rather than E but we are then restricted within the approximations noted.[21] The relationship between A_{or}, β, and ρ can be ascertained by associating charging parameters α and α' with ρ_{Av} and ρ_{Av}', respectively.

In this case upon application of ψ_N to (6) and integrating, V_{te} and V_{tt} combine

$$V_{te} + V_{tt} = \left(\frac{\beta N^2\alpha\alpha'}{\epsilon_0} + \frac{\beta^2 N^2\alpha'^2}{\epsilon_0^2}\right)\mathcal{G} + A_{or} \tag{7}$$

$$\mathcal{G} = \int \frac{\rho_{Av}(r)\rho_{Av}(r)}{|\mathbf{r} - \mathbf{r}'|}\, d\mathbf{r}\, d\mathbf{r}'$$

The total free energy is a min when $(\partial A/\partial\alpha')_\alpha = 0$. This can only happen when $\alpha = \alpha'$ and implies

$$\frac{dA_{or}}{d\alpha'} = -\left(\frac{\beta N^2\alpha}{\epsilon_0} + \frac{\beta^2 N^2\alpha'}{\epsilon_0}\right)\mathcal{G}$$

and upon integrating α from zero to one ($\alpha' = \alpha$)

$$A_{or} = -\left(\frac{\beta N^2}{\epsilon_0} + \frac{\beta^2 N^2}{\epsilon_0}\right)\frac{\mathcal{G}}{2} \tag{8}$$

and

$$A = -\frac{\hbar^2}{2m}\sum_i^N \langle \psi_N^* \nabla_i^2 \psi_N\rangle + \frac{N^2\beta}{2\epsilon_0}\mathcal{G} + \frac{1}{\epsilon_0}\sum_i\sum_j \left\langle \psi_N \frac{1}{r_{ij}} \psi_N^* \right\rangle \tag{9}$$

The Two Electron Valence Bond Application. Equation 9 is simple enough to allow a number of multiple solvated electron problems to be solved. In the case where ψ_N is approximated by molecular orbitals a further simplification occurs because

$$\sum_i\sum_j \left\langle \text{MO}\psi_N^* \left|\frac{1}{r_{ij}}\right| \text{MO}\psi_N \right\rangle = N(N-1)\mathcal{G} \tag{10}$$

Here we report the results of (9) when ψ_N is a two electron wave function of the valence bond type

$$\psi = \frac{1}{2 \pm 2S^2}(U_A(1)U_B(2) \pm U_A(2)U_B(1)) \tag{11}$$

For this case

$$\rho_{Av} = \frac{e^2}{2(1 \pm S^2)}[U_A^2 + U_B^2 \pm 2U_AU_BS] \tag{12}$$

Upon utilizing 1S hydrogenic functions ($U_A = (\varkappa^3/\pi)^{1/2} e^{-\varkappa r_A}$ and keeping $\varkappa$ as a variational parameter we obtain

$$A = \frac{\hbar^2\varkappa^2}{m}\left[\frac{1 \pm SY}{1 \pm S^2}\right] + \frac{\beta e^2}{\epsilon_0 R}\times \left[\frac{AR + J' \pm 4BS + 2K'S^2}{(1 \pm S^2)^2}\right] + \frac{e^2}{\epsilon_0 R}\left[\frac{J' \pm K'}{1 \pm S^2}\right] \tag{13}$$

The integrals J'/R, K'/R, are the familiar coulombic and exchange integrals.[22] In addition

$$B = \int U_A^2(1)U_B(1)U_B(2)\, d\mathbf{r}_1\, d\mathbf{r}_2$$

$$Y = \frac{1}{\varkappa^2} \int \frac{U_A^2(1) U_A^2(2)}{r_{12}} d\mathbf{r}_1 d\mathbf{r}_2$$

With respect to eq 13 it is interesting to note that the first and last terms are essentially the same as the kinetic energy and electronic repulsion terms, respectively, in the valence bond treatment of the hydrogen atom. The second term is quite different both in conception and effect from the valence bond treatment of electron–nucleus interactions; nevertheless the integrals are the same as those commonly encountered in dealing with electronic repulsions.[23]

Generalization. As a conclusion to the discussion of the general method summarized in eq 9 it should be noted that it is applicable to a number of different one and multiple electron problems. For a wide number of cases the integrals which appear will be identical with those encountered in analogous atomic or molecular problems. For MO treatments the application of (10) implies that the only integrals which will occur will be those involved in evaluating electron–electron repulsions in the molecular analog; in particular electron cloud–nucleus interactions will be absent. This latter fact means that although an analogy appears between solvated electron–electron interactions and atom–atom interactions it is a formal one only; the results can be expected to be quite different.

The simplicity of the approach is the result of the approximation of a continuum and the limitations of such models should not be overlooked. To deal with this point and the more recent models for the single and dielectron species replace the continuum at the trap center with a cavity formed by a discrete structure of oriented dipoles. However the rigorous inclusion of structure is a difficult many body problem even in the case of a spherical symmetry; and becomes formidable when this symmetry disappears.

Inclusion of London Forces. The discussion so far does not include van der Waal or London forces arising from the tendency of the electrons to avoid each other. Normal treatments must be modified in order to include the effects of the solvent and the size of the solvated electron. A simple treatment closely paralleling that in Pauling[17] for hydrogen but maintaining $\varkappa$ as a parameter and including a factor $1/\epsilon_0$ in the perturbing Hamiltonian in order to include the effect of solvent screening results in

$$E_L = -\frac{6me^4}{h^2\epsilon_0^2(\varkappa R)^6} \qquad (14)$$

This $1/R^6$ dependence is an approximate result strictly valid only at relatively large R; however, its use is usually extended down to the potential minima ($R \sim 2/\varkappa$) for the case of molecules. However for solvated electrons there exists a critical distance below which E_L as calculated by eq 14 becomes the predominant term in the total Hamiltonian, and no minimum value of $\varkappa$ is found, but rather $\varkappa$ decreases to zero and E goes to negative infinity. For solvated electrons in ammonia this critical distance is around 10.5 Å. However it would appear that the notion of catastrophic trap destruction (explosion) at 10.5 Å is not well based but rather there is a difficulty in using eq 14 for solvated electrons even at this large distance of separation. Equation 14 has been subject to numerous refinements that suggest that it is actually the lead term in a series, $E_L = -a_1/R^6 - a_2/R^8 - a_3/R^{10} + \ldots$.[24] It would seem however that the effect of this kind of refinement would be to increase the radius at which catastropic destruction occurs; in any event an expansion in inverse powers of R will always have a singularity at $R = 0$.

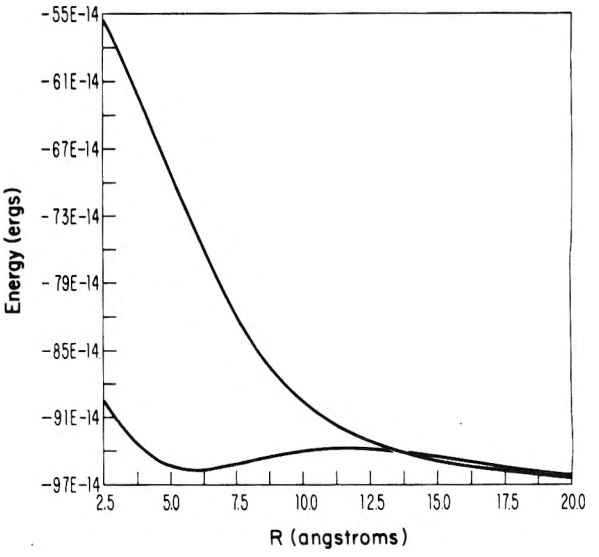

Figure 1. Energy of interaction in the valence bond approximation of two solvated electrons in ammonia as a function of distance of separation. London forces are not included. The lower state is a singlet (electron paired) state, the upper is a triplet.

The approximations in eq 14 are of a twofold nature. First it is assumed that the atom can be replaced by a *point* instantaneous dipole. Second, various nonessential mathematical approximations are made with a view to arriving at a simple result valid at large R. For the present work we assumed that the perturbing Hamiltonian should be

$$H' = -\frac{e^2}{R_{eff}^3\epsilon_0}(2z_1z_2 - x_1x_2 - y_1y_2)$$

where $R_{eff} = (R^2 + 4/\varkappa^2)^{1/2}$ is an approximate evaluation of the actual interelectronic distance as opposed to the distance separating two theoretical point dipoles.

Following the usual variational treatment for hydrogenic wave functions $\psi = \psi_0(1 + aH')$ from which (by excluding the usual mathematical simplifications which result in eq 14) we obtained

$$E_L = \frac{A'a + B'a^2}{1 + Da^2} \qquad (15)$$

$$A' = 12\alpha^2/\varkappa^4$$

$$B' = -6\alpha^2h^2/\varkappa^2m$$

$$D = 6\alpha^2/\varkappa^4$$

$$\alpha = -e^2/\epsilon_0 R_{eff}^3$$

with the parameter a determined from $a^2(B'C - A'D) + 2aB' + A' = 0$ for each R. At large R (15) reduces to (14); however as $R \to 0$ (15) remains finite, approaching the value 0.72×10^{-12} erg which compares nicely with the value that Copeland and Kestner estimate for the correlation energy of the dielectron, 0.65×10^{-12} erg. (Since the major component of London forces is electron correlation-at-a-distance, this is a proper comparison for any method claiming validity at all R.)

Results

In Figure 1 is shown the results of the valence bond calculation for both the symmetric (singlet) and the antisymmetric (triplet) configuration. There are several distinctive

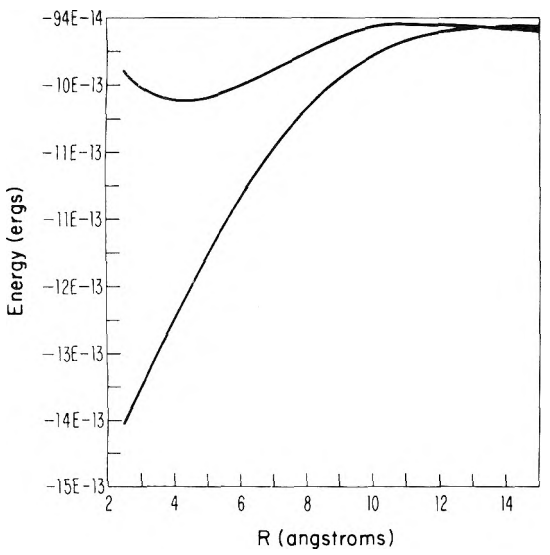

Figure 2. Energy of interaction of two solvated electrons in ammonia as a function of distance of separation including both valence and London forces. The lower state is a singlet (electron paired) state, the upper is a triplet.

features. First, the two states, symmetric and antisymmetric, are distinctly separate at distances of separation as large as 14 Å, thus affording a mechanism for the appearance of spin pairing for traps that are separated by large distances. A second feature is the appearance of a maximum at 11.5 Å and a minimum at 6.0 Å. The minimum is metastable in respect to the traps separated at infinity. Both of these features are relatively small in that their magnitude is comparable with kT (computed at T = 240 K).

Figure 2 shows the interaction energy with London forces included. For all cases the total Hamiltonian was minimized in respect to the parameter $\varkappa$.[25] Thus $\varkappa$ is a function of the symmetry, the inclusion or exclusion of London forces, and of R. It is evident that the London forces make a major contribution to the energy of interaction. It is clear that the London dispersion forces are a predominant term of the energy of interaction.

Discussion

The calculations thus far invite more elaborate consideration but several major points would seem inescapable. Non-Coulombic interactions between two electrons solvated in ammonia are clearly discernible at distances of separation as large as 14 Å. Below this distance of separation both spin pairing effects and London dispersion forces become important. The mechanism for these effects is fundamentally analogous to the interaction of ordinary atoms (or ions) but because of the unusual nature of the solvated electron wave function (primarily its diffusiveness) these "close range" interactions occur at unusually large distances of separation.

It should be noted that the 14 Å mentioned above corresponds roughly to the Bjerrum distance in liquid ammonia. This distance plays an important role in the theory of dilute electrolytes; for example, it is used as the distance of separation defining association between ions of opposite sign.[26] The long range solvated electron–electron interaction suggests a closer analogy with ionic association in the Bjerrum sense as opposed to bonding in the ordinary chemical sense. Association in the Bjerrum sense is accompanied by relatively small energies of association (a few kT), however, the volume in phase space attributable to association of this kind is very large. The non-Coulombic solvated electron–electron interaction is similar in these respects and it should not be surprising to find that the result is a somewhat analogous type of association between these ions (of the *same* charge) resulting in a dissociation constant of the order of 10^{-3}. However, again because of the large volume in phase space associated with the large distances of association, this dissociation constant is a result of bonding forces which are however very weak in comparison to ordinary chemical bonding. (See Figure 2.) Thus the variation of energy of the ground state with distance of separation is small in comparison with the energy associated with the optical transition. Unfortunately our calculations do not yet include a consideration of excited singlet states, but it is reasonable to suppose that the R dependence of energy is similar in magnitude to the ground state. If this is so it furnishes an explanation for the apparent discrepancy between magnetic and optical data as considerable spin pairing would be expected as R decreases without a great change in the optical spectrum.

Acknowledgment. The authors thank Drs. Pierre Damay, Jean-Pierre Lelieur, and Marc Debacker for helpful discussions. In addition one of the authors wishes to thank Juniata College and CNRS for funds for a sabbatical leave that made this work possible.

References and Notes

(1) J. Jortner, N. R. Kestner, Ed., "Electrons in Fluids", Colloquium Weyl III, Springer-Verlag, New York, N.Y., 1973.
(2) J. J. Lagowski, M. J. Sienko, Ed., "Metal Ammonia Solutions", Colloquium Weyl II, Butterworths, London, 1970.
(3) G. Lepoutre and M. J. Sienko, Ed., "Solutions Métal-Ammoniac", Colloquium Weyl I, Benjamin, New York, N.Y., 1964.
(4) M. H. Coehn and J. C. Thompson, *Adv. Phys.*, **17**, 857–907 (1968).
(5) T. P. Das in "Advances in Chemical Physics", Vol. IV, I. Prigogene, Ed., Interscience, New York, N.Y., 1962, pp 303–388.
(6) W. H. Jolly in "Progress in Inorganic Chemistry", F. A. Cotton, Ed., Interscience, New York, N.Y., 1959, pp 235–281.
(7) J. L. Dye, ref 2, pp 1–15.
(8) R. Catterall, ref 2, p 106.
(9) M. H. Cohen, ref 1, p 282.
(10) D. A. Copeland, N. R. Kestner, and J. Jortner, *J. Chem. Phys.*, **53**, 1189 (1970). See also J. Jortner, *ibid.*, **57**, 587 (1972).
(11) D. Feng, D. Ebbing, and L. Kevan, *J. Chem. Phys.*, **61**, 249 (1974).
(12) I. Carmichael and B. Webster, *J. Chem. Soc., Faraday Trans 2*, **70**, 1570 (1974).
(13) D. A. Copeland and N. R. Kestner, *J. Chem. Phys.*, **58**, 3500 (1973).
(14) D. E. O'Reilly, *J. Chem. Phys.*, **55**, 474 (1971).
(15) J. Fueki, *J. Chem. Phys.*, **50**, 5381 (1969).
(16) J. C. Slater, "Quantum Theory of Molecules and Solids", Vol. 1, McGraw-Hill, New York, N.Y., 1963.
(17) L. Pauling, "Introduction to Quantum Mechanics", McGraw-Hill, New York, N.Y., 1935.
(18) J. Jortner, *J. Chem. Phys.*, **30**, 839 (1959).
(19) D. E. O'Reilly, *J. Chem. Phys.*, **41**, 3736 (1964).
(20) L. D. Landau and E. M. Liftshitz, "Electrodynamics of Continuous Media", Pergamon Press, New York, N.Y., 1960.
(21) These restrictions are not peculiar to this method but are common to all methods to date which utilize ensemble averages in dealing with the solvent.
(22) Reference 17, p 342.
(23) M. P. Barnett in "Methods in Computational Physics", Vol. II, B. Alder, S. Fernback, and M. Rosenberg, Ed., Academic Press, New York, N.Y., 1963, pp 95–153.
(24) See for example ref 17.
(25) See Slater's discussion of the procedure, ref 16, p. 54.
(26) For an excellent discussion of electrolyte theory see M.-C. Justice, Ph.D. Thesis, Université de Paris VI, CNRS No. A.O.10140, 1974.

Discussion

M. NEWTON. I would like to ask how you describe the limiting energy when the two electrons coalesce into the dielectron, and what you mean by correlation energy. Correlation energy is gener-

ally defined as energy lowering relative to the Hartree–Fock energy.

B. WEBSTER. Perhaps I could just clarify the point with respect to correlation energy. As I understand this model, the interactions between two electrons in a continuum have been evaluated with an estimate being made of long range forces via a dispersion term. The term correlation energy pertains to the difference between the observed energy of an atom, for example, computed at the Hartree–Fock limit, and the experimental energy corrected for relativistic effects.

N. R. KESTNER. What is the definition of London forces and how does it arise from calculations?

P. D. SCHETTLER. Although correlation energy is defined in terms of a difference between experimental and a calculated quantity, it is estimated by further refinements to the Hartree–Fock wave functions by the inclusion of the interelectronic distances in the wave function. In this sense the approach of London for the separated atom case is quite analogous to the approach of Hylleras for the united atom case. The inclusion of interelectronic distances in the wave function (leading to London forces) is a relatively minor component of the hydrogen–hydrogen atom interaction but is of major concern for the interaction of solvated electrons even at long distances of separation.

T. TUTTLE. What is the stabilizing effect in your model which overcomes the Coulombic repulsion between the electrons and the destabilization caused by the interpenetration of solvation spheres?

P. D. SCHETTLER. There are several stabilizing effects that are partially analogous to the bonding effects in ordinary atom–atom interaction. Briefly, for atoms, the Coulombic electron–electron, electron–nucleus, and nucleus–nucleus interactions do not simply cancel out but rather combine in a way that may result in bonding. Slater in ref 16 has a particularly complete discussion of the separate effects for hydrogen. In ammonia some 95% of the electron–electron interaction that would be present in vacuo is shielded (cancelled out) by the solvent. This solvent polarization results in effects that are reminiscent of the effects of nuclei.

R. CATTERALL. Your long range spin-pairing process is very difficult to reconcile with the long electron–electron spin pairing interaction lifetimes required by electron relaxation data (see discussion of M. Newton paper by R. C.). In the related Bjerrum ion-pairing formalism, the lifetime of Na^+ e_{sol}^- ion pairs is only $\sim 10^{-12}$ sec as indicated by the Na nuclear relaxation rate. In contrast the lifetime of the spin-paired state must be $>10^{-6}$ sec.

P. D. SCHETTLER. Since we included no kinetic parameters in our model we hesitate to come to any conclusion about predicting the lifetime of a Bjerrum electron–electron association except to agree with you that a simple Arrhenius model would seem to be excluded.

Theory of Light Absorption by Ions in Solution

R. R. Dogonadze,* E. M. Itskovitch, A. M. Kuznetsov, and M. A. Vorotyntsev

Institute of Electrochemistry of the Academy of Sciences of the USSR, Moscow State University, Moscow, USSR
(Received June 20, 1975)

Absorption and emission spectra of molecules in solutions are widely used for investigation of the properties of the medium and interactions of the absorbing molecules with the solvent. Spectroscopic characteristics give the important information about ionic solvation in solutions, properties of solvated electrons, ionic pairs, etc.

I. Introduction

There are many papers devoted to the theoretical description of the absorption and emission spectra of molecules in solutions. These may be separated into two main groups. The first approach uses the methods of calculation developed for the investigation of molecular spectra in gases. Such an approach is used in many papers (see, e.g., ref 1, and references there). Weak coupling of the molecule with its environment is essentially adopted in these works leading naturally to the Lorentzian-type absorption band. The second approach uses the methods developed in the theory of polarons and color centers in polar crystals (see, e.g., ref 2 and 3). This approximation leads to Gaussian-type absorption bands for ions.

As it will be shown in the present paper, the quantitative criteria of weak and strong coupling, given in ref 4, is not quite complete for the description of the radiation and radiationless transitions in a medium. Applicability of the approximation of strong or weak coupling of the electronic subsystem with the solvent proves to be dependent on the value of the reorganization of the solvent degrees of freedom. Similarly the concept of strong or weak coupling with the intramolecular vibrations depending on the degree of their reorganization may be introduced.

At present there are some difficulties in explaining the more complex shape of the experimentally observed absorption bands, their temperature dependence, and in describing the processes of light absorption involving the rearrangement of intramolecular degrees of freedom. These difficulties arise from the application of an insufficiently exact model for the medium and the absorbing centers.

There are many common features in the processes of light absorption and in other charge transfer processes, viz., in chemical and electrochemical reaction in liquids.

In the last few years a number of essential results were obtained in this field. That is why the attempt was made to

* Author to whom correspondence should be addressed at the Institute of Electrochemistry, Academy of Science of the USSR, Moscow, V71, Leninsky Prospeht, 31, USSR.

extend the methods developed in the theory of chemical kinetics to the description of light absorption processes. In this sense the process of light absorption may be formally considered as a chemical reaction, caused by the interaction with the electromagnetic field of the light wave. The dependence of the absorption coefficient on the light frequency ν is the analogue of the dependence of the reaction rate constant on the heat of reaction or that of the electric current on the overpotential for the electrochemical reaction. The transition probability $W(\nu)$ of light absorption per unit time is described by[9]

$$W(\nu) = \frac{2\pi|d|^2}{\hbar} \mathrm{Av_i} \sum_{\mathrm{f}} |\langle\psi_{\mathrm{f}}|\psi_{\mathrm{i}}\rangle|^2 \delta(E_{\mathrm{i}} + h\nu - E_{\mathrm{f}}) \quad (1)$$

where d is the electron–photon matrix element of the operator of the molecule interaction with the electromagnetic field, ψ_{i} and ψ_{f} are the vibronic wave functions of the initial and final states, $\mathrm{Av_i}$ denotes averaging over the initial states, E_{i} is the energy of the initial state with no account of the electromagnetic field, E_{f} is the energy of the final state. The energy conservation condition has a form

$$E_{\mathrm{i}} + h\nu = E_{\mathrm{f}} \quad (2)$$

We consider the transition between two specific electronic states that experimentally corresponds to the transition between two discrete electronic states. To take into account the continuous electronic spectrum the results obtained should be integrated over the electronic spectrum.

For the sake of definiteness we consider the process of light absorption in the system where the "entangling" of the vibrational degrees of freedom of the medium with the intramolecular vibrations and with the vibrations in the coordination layer is absent.[8]

The system Hamiltonians (without accounting for the interaction with the electromagnetic wave) in the initial H_{i} and final H_{f} states have the form[5,8]

$$H_{\mathrm{i}} = \sum_{\kappa} \frac{1}{2} \hbar\omega_{\kappa} \left[q_{\kappa}^2 - \frac{\partial^2}{\partial q_{\kappa}^2} \right] + T_{\mathrm{R}} + U_{\mathrm{i}}(R_{\mathrm{j}}) + h\nu$$

$$H_{\mathrm{f}} = \sum_{\kappa} \frac{1}{2} \hbar\omega_{\kappa} \left[(q_{\kappa} - q_{\kappa 0})^2 - \frac{\partial^2}{\partial q_{\kappa}^2} \right] + T_{\mathrm{R}} + U_{\mathrm{f}}(R_{\mathrm{j}}) + \Delta I \quad (3)$$

where $\{q_{\kappa}\}$ is the set of dimensionless normal coordinates of medium, $\{\omega_{\kappa}\}$ are the vibration frequencies of the medium, $\{q_{\kappa 0}\}$ characterizes the displacement of the minimum of the final potential energy surface with respect to the initial one, T_{R} is the kinetic energy of the intramolecular vibrations, $U_{\mathrm{i}}(R_{\mathrm{j}})$ and $U_{\mathrm{f}}(R_{\mathrm{j}})$ are their potential energy surfaces in the initial and final states, R_{j} are their coordinates, and ΔI is the difference of the minimal energies of the final and initial states.

The transition probability may be written in the form[5]

$$W(\nu) = \frac{\beta|d|^2}{i\hbar} \int_{C-i\infty}^{C+i\infty} \mathrm{d}\theta \exp\{\beta\theta(h\nu - \Delta I) - \mathrm{F}(\theta)\} \times e^{\beta F} \mathrm{Tr}\{\rho_{\beta(1-\theta)}{}^{\mathrm{i}} \rho_{\beta\theta}{}^{\mathrm{f}}\} \quad (4)$$

$$\mathrm{F}(\theta) = \frac{2}{\pi\hbar} \sum_{k} |\Delta D_k|^2 \int_0^{\infty} \frac{\mathrm{d}\omega}{\omega^2} \mathrm{Im}\, \mathrm{G}(k, \omega) \times \frac{\sinh\frac{1}{2}\beta\hbar\omega\theta \sinh\frac{1}{2}\beta\hbar\omega(1-\theta)}{\sinh\frac{1}{2}\beta\hbar\omega} \quad (5)$$

Here ΔD_k is the difference of the Fourier amplitudes of the electric induction in the initial and final states, $\mathrm{G}(k, \omega)$ is the retarded Green's function for the polarization operators of the liquid, $\rho_{\beta}{}^{\mathrm{i}}$ and $\rho_{\beta}{}^{\mathrm{f}}$ are the density matrices in the initial and final states for the intramolecular vibrations at the temperature T without accounting for ΔI, F is the free energy of the intramolecular vibrations in the initial state. Tr denotes trace only for the intramolecular degrees of freedom.

II. Outersphere Transitions

The simplest case to consider is the light absorption not involving the change of state of the intramolecular degrees of freedom (outersphere transitions). Such a situation takes place, e.g., for light absorption by halide ions, in cases where ions do not form strong covalent bonds with the molecules. Then, using

$$e^{\beta F} \mathrm{Tr}\{\rho_{\beta(1-\theta)}{}^{\mathrm{i}} \rho_{\beta\theta}{}^{\mathrm{f}}\} = 1 \quad (4')$$

the transition probability may be rewritten in the form

$$W(\nu) = \frac{\beta|d|^2}{i\hbar} \int_{C-i\infty}^{C+i\infty} \mathrm{d}\theta \exp\{\beta\theta(h\nu - \Delta I) - \mathrm{F}(\theta)\} \quad (6)$$

where $\mathrm{F}(\theta)$ is defined by eq 5.

An analysis of the integrand shows that two limiting cases may be distinguished. If the process involves a large enough charge redistribution (ΔD_k's are sufficiently large), the major contribution to the integral derives from the values of θ near the real axis (this is strong coupling). In this case for the frequency interval inside the absorption band half-width, the integral may be calculated by the steepest descent method (in the neighborhood of the saddle point only the second-order term in θ usually may be retained in the power series for $\mathrm{F}(\theta)$). Outside the half-width additional effects usually have to be taken into account (see section II). If a large charge redistribution does not occur (small ΔD_k), the steepest descent method is not applicable because of the very large interval of the variable values contributing to the integral. In this case the major contribution to the integral derives from the large $|\mathrm{Im}\,\theta|$, for which the asymptotic behavior of $\mathrm{F}(\theta)$ is a linear function of θ (weak coupling).

Below we consider these cases separately and shall derive the quantitative criterion of weak or strong coupling with the medium. As for the properties of the medium, characterized by $\mathrm{Im}\, \mathrm{G}(k, \omega)$, we shall assume at first that the medium has a single rather wide absorption band, as is usual for polar liquids.[6] This condition is satisfied, e.g., for the Debye-type absorption spectrum of liquids[7]

$$\sum_{k} |\Delta D_k|^2 \mathrm{Im}\, \mathrm{G}(k, \omega) = \frac{2E_{\mathrm{r}}{}^{\mathrm{m}}\omega_{\mathrm{D}}\omega}{\omega^2 + \omega_{\mathrm{D}}{}^2} \quad (7)$$

($E_{\mathrm{r}}{}^{\mathrm{m}}$ is the medium reorganization energy, ω_{D} is the characteristic frequency of the medium) or for a smoothed resonance

$$\sum_{k} |\Delta D_k|^2 \mathrm{Im}\, \mathrm{G}(k, \omega) = E_{\mathrm{r}}{}^{\mathrm{m}} \left[\frac{\omega\Gamma}{(\omega - \omega_{\mathrm{r}})^2 + \Gamma^2} + \frac{\omega\Gamma}{(\omega + \omega_{\mathrm{r}})^2 + \Gamma^2} \right] \quad (8)$$

if its half-width Γ is not very small compared to ω_{r}. If the function $\mathrm{G}(k, \omega)$ has narrow maxima, the situation is similar to processes involving the reorganization of the discrete vibrational degrees of freedom in addition to that of the de-

grees of freedom of the medium, characterized by the continuous vibrational spectrum (see section III). In this case the absorption band $W(\nu)$ may reveal some structure.

It is important for further consideration that Im $G(\bar{k}, \omega)$ decreases linearily at $\omega \to 0$

$$\frac{1}{\pi\hbar}\sum_{k}|\Delta D_k|^2 \operatorname{Im} G(\bar{k}, \omega) \simeq a\omega \qquad (9)$$

$$(\omega \to 0)$$

It should be noted that just this condition is necessary for the convergence of the integral over θ in eq 6.

1. Weak Coupling. (a) High-Temperature Approximation. We assume that the condition $\beta\hbar\omega_m \ll 1$ is satisfied for the characteristic frequencies of the medium ω_m. Then for $\beta\hbar\omega_m|\theta| \ll 1$ we have

$$F(\theta) \simeq \beta E_r^m\theta - \beta E_r^m\theta^2 \qquad (10)$$

where

$$\beta E_r^m = \frac{\beta}{\pi}\sum_{k}|\Delta D_k|^2\int_0^\infty \frac{d\omega}{\omega}\operatorname{Im} G(\bar{k}, \omega) \qquad (11)$$

whereas for $\beta\hbar\omega_m|y| \gg 1$ ($y = \operatorname{Im}\theta$, $x = \operatorname{Re}\theta \sim 1$) $F(\theta)$ has the form

$$F(\theta) \simeq \pi a|y| + ia\frac{\pi}{2}\operatorname{sign} y \qquad (12)$$

In this case

$$a = \lim_{\omega\to 0}\frac{1}{\pi\omega\hbar}\sum_{k}|\Delta D_k|^2 \operatorname{Im} G(\bar{k}, \omega) \sim \frac{E_r^m}{\hbar\omega_m} \qquad (12')$$

is a sufficient condition of the smoothness of Im G. Then the major contribution to βE_r^m derives from $\omega \lesssim \omega_m$ for which eq 9 is valid. The inequality

$$\beta E_r^m \ll (\beta\hbar\omega_m)^2 \qquad (13)$$

is the criterion of weak coupling. When condition 13 is satisfied, the steepest descent method for the calculation of the integral in eq 6 is not applicable. The major contribution to the integral derives from the region where asymptotic relation 12 is valid. Near the maximum of the absorption band $|h\nu - h\nu_{max}| \ll \gamma(\beta\hbar\omega_m/\beta E_r^m)$ the absorption line is described by the Lorentzian-type formula

$$W(\nu) = W_{max}\frac{\gamma^2}{(h\nu - h\nu_{max})^2 + \gamma^2} \qquad (14)$$

$$W_{max} = \frac{2\beta|d|^2}{\pi a\hbar} = \frac{2|d|^2}{\hbar\gamma} \qquad \gamma = \frac{\pi a}{\beta} \qquad (14')$$

$$h\nu_{max} = \Delta I + E_r^m \qquad (15)$$

(See Figure 9.)

(b) Low-Temperature Approximation. At low temperature, when the characteristic vibration frequencies satisfy the condition $\beta\hbar\omega_m \gg 1$, some relations change their form but the qualitative picture is retained. Sufficient criterion of the smoothness of the function Im G is the same as in case a. At Im $\theta \gg \ln \beta\hbar\omega_m$ the asymptotic formula 12 for $F(\theta)$ is valid. The criterion of weak coupling is described now by

$$\beta E_r^m \ll \beta\hbar\omega_m \qquad (16)$$

When eq 16 is satisfied $W(\nu)$ near the maximum is also described by Lorentzian-type formula 14 (see Figure 9). In this region the main contribution is the "classical" degrees of freedom having low vibration frequencies.

It is worth noting in this case that the presence of narrow resonances of the function $G(\bar{k}, \omega)$ may cause the appearance of a structure in the absorption spectrum.

Thus we see that coupling with the medium depends on the value of reorganization of the medium in the course of the transition (see eq 13 and 16). It should be emphasized, that both at high and at low temperatures, the width of the Lorentzian curve γ is proportional to T, indicating the important role played by the low-frequency vibration degrees of freedom.

2. Strong Coupling. The criterion of weak coupling with the medium was derived in section II.1. We assume now that if the ΔD_k's are sufficiently large the conditions for eq 13 and 16 are fulfilled. Then the absorption line in the neighborhood of its maximum has a Gaussian shape

$$W = W_{max}\exp\left|-\frac{(\Delta I + E_r^m - h\nu)^2}{\Delta_m^2}\right| \qquad (17)$$

$$h\nu_{max} = \Delta I + E_r^m = \Delta I + \frac{1}{\pi}\sum_{k}|\Delta D_k|^2 \times$$

$$\int_0^\infty \frac{d\omega}{\omega}\operatorname{Im} G(\bar{k}, \omega) = \Delta I + \sum_{k}|\Delta D_k|^2 \operatorname{Re} G(\bar{k}, 0) \qquad (18)$$

$$W_{max} = 2\sqrt{\pi}|d|^2/\hbar\Delta_m \qquad (19)$$

where Δ_m is the half-width of the line. (See Figure 10.)

This result is obtained by using the steepest descent method for calculation of the integral over θ. The quantity $h\nu_{max}$ is determined by (a) thermodynamic characteristics ΔI, which with the use of the thermodynamic cycle method may be related to the excitation energy of the molecule in the gas phase ΔI_g and equilibrium solvation energies of the molecule in the ground (E_p^i) and excited (E_p^f) states ($\Delta I = \Delta I_g + E_p^i - E_p^f$); and (b) kinetic characteristics E_r^m, which depend on both the properties of the medium and the redistribution of the charge density. The half-width Δ_m depends on the behavior of the function Im G. If Im G decreases more rapidly than $1/\omega$ at $\omega \to \infty$, then we have

$$\Delta_m = \left|\frac{2\hbar}{\pi}\sum_{k}|\Delta D_k|^2\int_0^\infty d\omega \operatorname{Im} G(\bar{k}, \omega)\coth\frac{1}{2}\beta\hbar\omega\right|^{1/2} \qquad (20)$$

Thus the half-width depends explicitly on the temperature ($G(\bar{k}, \omega)$ also depends on the temperature, but this effect is usually rather weak[8]). If the contribution to the reorganization energy from the degrees of freedom characterized by intermediate frequencies $\omega \sim kT/\hbar$ is sufficiently small (see, e.g., ref 8), more simple relations for E_r^m and Δ_m may be obtained

$$E_r^m = E_{Cl}^m + E_Q^m$$

$$\Delta_m^2 = 4kTE_{Cl}^m + 2\hbar\omega_Q E_Q^m \qquad (20')$$

where E_{Cl}^m and E_Q^m are the total reorganization energies of the classical and quantum degrees of freedom, respectively, and ω_Q is the mean frequency of the quantum degrees of freedom:

$$E_{Cl}^m = \frac{1}{\pi}\sum_{k}|\Delta D_k|^2\int_0^{kT/\hbar}\frac{d\omega}{\omega}\operatorname{Im} G(\bar{k}, \omega)$$

$$E_Q^m = \frac{1}{\pi}\sum_{k}|\Delta D_k|^2\int_{kT/\hbar}^\infty\frac{d\omega}{\omega}\operatorname{Im} G(\bar{k}, \omega)$$

$$\omega_Q E_Q^m = \frac{1}{\pi}\sum_{k}|\Delta D_k|^2\int_{kT/\hbar}^\infty d\omega \operatorname{Im} G(\bar{k}, \omega) \qquad (21)$$

If Im $G(\vec{k}, \omega)$ decreases as $C(\vec{k})/\omega$ (e.g., for the Debye-type spectrum), the Gaussian-type line, described by eq 17, has slowly varying width

$$\Delta_m = \left\{\frac{2\hbar}{\pi}\left[\sum_k |\Delta D_k|^2 C(\vec{k})\right][\ln|h\nu - \Delta I - E_r^m| + \text{constant}]\right\}^{1/2} \quad (22)$$

Outside the half-width the band becomes gradually unsymmetric and non-Gaussian. In this region the quantum degrees of freedom usually play the main role. The behavior of Im $G(\vec{k}, \omega)$ at $\omega \to \infty$ is especially important. First we consider a rather sharp decrease of Im $G(\vec{k}, \omega)$ at $\omega \to \infty$. Then the deviation of the band shape from the symmetrical Gaussian form occurs gradually. The curve $W(\nu)$ becomes asymmetrical, the short wavelength branch decreasing more slowly. The deviation of the curve ln $W(\nu)$ from the parabolic form occurs at somewhat larger values of $|\nu - \nu_{max}|$.

In all cases the last effect is due to the subbarrier transition along some coordinates of the vibrational subsystem (for details see section IV).

The above results were obtained by using the steepest descent method in formula 6. However, if Im $G(\vec{k}, \omega)$ decreases at $\omega \to \infty$ as a power of $1/\omega$, the integrand must be analytically continued before calculating the integral over θ, because at Re $\theta < 0$ the integral over ω in eq 5 diverges.

$$F(\theta) = \frac{2}{\pi\hbar}\sum_k |\Delta D_k|^2 \int_0^\infty \frac{d\omega}{\omega^2} \text{Im } G(\vec{k}, \omega) \times \frac{\sinh\frac{1}{2}\beta\hbar\omega\theta \sinh\frac{1}{2}\beta\hbar\omega(1-\theta)}{\sinh\frac{1}{2}\beta\hbar\omega} \quad (23)$$

Calculations show that at rather general assumptions on the properties of the function Im $G(\vec{k}, \omega)$ there is only one (logarithmic) branch point of the function $F(\theta)$. Choosing the cut along the half-axis, Im $\theta = 0$, Re $\theta < 0$, one may determine the values of the analytical continuation of the function $F(\theta)$ on upper and lower edges of the cut. Thus we obtain

$$F_0(-\tau) \equiv \frac{1}{2}\{F(-\tau + iO) + F(-\tau - iO)\} = F(\tau) - \frac{4i}{\beta\hbar^2}\sum_k |\Delta D_k|^2 \sum_j \frac{1}{\omega_j^2} \sinh\beta\hbar\omega_j\tau \cdot \text{res}_{\omega_j} \text{Im } G(\vec{k}, \omega)$$

$$\Delta F(-\tau) \equiv F(-\tau + iO) - F(-\tau - iO) = \frac{|G_i|}{\beta\hbar^2}\sum_k |\Delta D_k|^2 \sum_j \frac{1}{\omega_j^2} \sinh^2\frac{1}{2}\beta\hbar\omega_j\tau \cdot \text{res}_{\omega_j} \text{Im } G(\vec{k}, \omega)$$

The summation in these formulas is performed over all singularities of the function Im $G(\vec{k}, \omega)$ in the upper half-plane of the ω variable. It is the difference between $F_0(-\tau)$ and $F_0(\tau)$ which leads to the gradual destruction of the symmetry of the curve $W(\nu)$ mentioned above. At values of $h\nu - h\nu_{max} > 0$ which are not very large, there is only one saddle point on each edge of the cut, and the result is essentially identical with that obtained by the formal application of the steepest descent method for the function $F_0(-\tau)$. However at higher values of $h\nu - h\nu_{max} > 0$ the major contribution to the integral over θ derives from integration along the cut near the point $\theta = 0$, but not from the neighborhood of the saddle points. In this case $W(\nu)$ decreases as a power of $(h\nu - h\nu_{max})^{-1}$: $W \sim (h\nu - h\nu_{max})^{-n}$. The value n depends on the decreasing character of Im $G(\vec{k}, \omega)$ at $\omega \to \infty$. Thus $n = 5$ for Im $G \sim 1/\omega^3$ (e.g., for smoothed resonance), whereas at more slowly decreasing Im G (Im $G \sim 1/\omega$ as, e.g., for the Debye-type spectrum), n is equal to 3. This difference is due to the fact that at small values of τ the function $\Delta F(-\tau)$ contains a term of the order of τ^2 only if the condition

$$\sum_j \text{res}_{\omega_j} \text{Im } G(\vec{k}, \omega) = \lim_{R\to\infty} \int_{\substack{\omega=\text{Re}^{i\varphi} \\ (\varphi_1 \le \varphi \le \varphi_2)}} \text{Im } G(\vec{k}, \omega) \neq 0$$

is fulfilled, i.e., for Im $G(\vec{k}, \omega) \sim 1/\omega$ at $\omega \to \infty$. It is worth noting that the exponential decrease of $W(\nu)$ is changed by a factor of 1 outside the half-width in the rather narrow interval of the frequency values whose position is determined partly by the multiplier of the quantity ω^{-k}.

Thus the deviation of $W(\nu)$ from the symmetrical Gaussian-shape curve (having constant or varying width) occurs outside the half-width of the line and is due to the subbarrier transition along the vibrational degrees of freedom. Therefore it is weakly expressed at sufficiently high temperatures (when the inequality $\beta\hbar\omega_m \ll 1$ holds for all the characteristic frequencies of medium), and is revealed as the temperature is lowered.

III. Effect of the Reorganization of the Intramolecular Vibrations

A more complex situation takes place when the electron transition results in the reorganization of both the medium and the intramolecular vibrations. In this case condition 4′ is not satisfied and the term $F_C(\theta)$, dependent on the characteristics of the reorganizing intramolecular vibrations, must be added to $F(\theta)$ in eq 6. Then the expression for the transition probability takes the form

$$W(\nu) = \frac{\beta|d|^2}{i\hbar}\int_{C-i\infty}^{C+i\infty} d\theta \exp\{\beta\theta(h\nu - \Delta I) - F(\theta) - F_c(\theta)\} \quad (24)$$

To obtain $F_c(\theta)$ it is necessary to integrate over q_k and q_k' calculating Tr $\{\rho_{\beta(1-\theta)}{}^i \rho_{\beta\theta}{}^f\}$. The exponent in eq 24 in addition to $F(\theta)$ contains now the periodic or quasiperiodic function of the θ variable, so that depending on the value of the reorganization energy of the medium E_r^m the major contribution to the integral may derive from one or from many saddle points dissimilar from the case of outersphere transitions. Unlike section II.2 where the major contribution to the integral was due to a single saddle point, here many saddle points contribute to $W(\nu)$ with about the same order of magnitude at not too large E_r^m (see below).

Before considering the effects caused by the reorganization of the intramolecular degrees of freedom we introduce the concept of strong or weak coupling of the electronic subsystem with the intramolecular vibrations. For this purpose it is useful to consider the process of light absorption by the isolated molecule. The transition probability $W(\nu)$ for this process is of resonance-type character, i.e., it is described by the discrete sum of the delta functions multiplied by weight factors. (This may be seen from a general eq 1 without any assumptions about the shape of the intramolecular potential energy surfaces.) The quantity $W(\nu)$ may be formally presented in the form

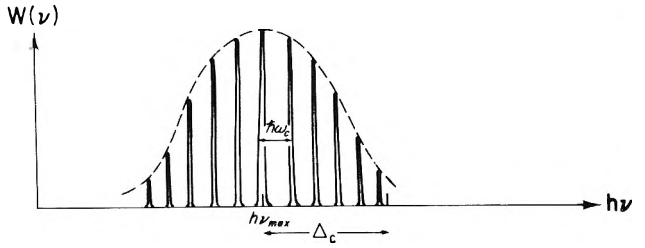

Figure 1. $\beta\hbar\omega_c > 1$, $\beta\hbar\omega_m < 1$, $q_{co} > 1$, $\beta E_r^m = 0$, $\Delta_c = \hbar\omega_c q_{co}$, $\Delta_m = 0$, $\hbar\nu_{max} = \Delta I + E_r^c$.

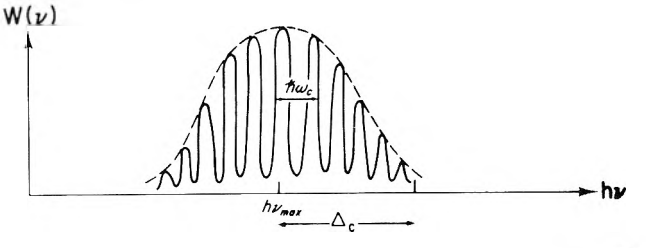

Figure 2. $\beta\hbar\omega_c > 1$, $\beta\omega_m < 1$, $q_{co} > 1$, $\beta E_r^m < (\beta\hbar\omega_m)^2$, $\Delta_c = \hbar\omega_c q_{co}$, $\Delta_m = \gamma = \pi akT$, $\hbar\nu_{max} = \Delta I + E_r^c + E_r^m$.

$$W(\nu) = \sum_{m,n} f_{mn}\delta(h\nu + E_m{}^i - E_n{}^f) \tag{25}$$

where $E_m{}^i$ and $E_n{}^f$ are the total energies of the initial and final states. The factors f_{mn} may be shown to take maximum values at $m = 0$ (unexcited initial state) and $n \approx n_{max}$ where n_{max} is determined by the condition $E_{n_{max}} = E_r^c$ (E_r^c is the reorganization energy of all the intramolecular degrees of freedom).

If there is a large group of the final states for which all the quantities f_{0n} have approximately the same values ($f_{0n} \sim f_{0n_{max}}$), the coupling with the intramolecular vibrations will be called strong. In this case according to eq 25, there are large numbers of separate resonances of approximately equal intensities. In the opposite case when only one resonance dominates, the coupling will be called weak. For the case of only one intramolecular degree of freedom the strong coupling corresponds to $n_{max} \gg 1$ (i.e., to large reorganization along this degree of freedom). For multidimensional intramolecular potential energy surfaces, when the movement along different degrees of freedom is separated, the strong coupling at least with one vibration is sufficient so that the coupling with the molecule as a whole will be strong.

We consider now the role played by the medium in the process of light absorption by the molecules, involving the reorganization of intramolecular degrees of freedom, for strong and finally for weak couplings.

1. Strong Coupling with the Intramolecular Vibrations. To obtain a qualitative picture we consider first the case where the reorganization of only one intramolecular oscillator having a constant (in the course of the process) quantum frequency ω_c ($\beta\hbar\omega_c \gg 1$) takes part.

Then $F_c(\theta)$ has the form

$$F_c(\theta) = q_{co}{}^2 \frac{\sinh\frac{1}{2}\beta\hbar\omega_c\theta \sinh\frac{1}{2}\beta\hbar\omega_c(1-\theta)}{\sinh\frac{1}{2}\beta\hbar\omega_c} \tag{26}$$

where q_{co} is the displacement of the equilibrium dimensionless coordinate of the oscillator: $q_{co} = (n_c\omega_c/\hbar)^{1/2}(R_{co}' - R_{co})$, R_{co} (R_{co}') is the equilibrium dimensional coordinate of the oscillator in the initial (final) state. (In the case of harmonic approximation, integration over the intramolecular coordinates, while calculating $\mathrm{Tr}\{\rho_{\beta(1-\theta)}{}^i, \rho_{\beta\theta}{}^f\}$, may be performed exactly.[8] The qualitative picture, obtained below for this particular case, may be directly extended to more general situations (see below).

As was noted above $W(\nu)$ for an isolated molecule has a resonance form as shown in Figure 1 (the height of the maximum is proportional to f_{0n}). For the case under consideration the envelope curve may be shown to have a Gaussian-type form (cf. eq 17 of section II.2):

$$\exp\left\{-\frac{(h\nu - h\nu_{max})^2}{\Delta_c{}^2}\right\} \tag{27}$$

where $h\nu_{max} = \Delta I + E_r^c$, $E_r^c = \frac{1}{2}\hbar\omega_c q_{co}{}^2$ is the reorganization energy of the intramolecular degree of freedom, $\Delta_c = (2E_r^c\hbar\omega_c)^{1/2}$ is the half-width of the line.

The distance between the neighboring maxima is equal to $\hbar\omega_c$. The number of the maxima inside the half-width of the envelope curve is equal to $q_{co} \gg 1$ (strong coupling with the intramolecular vibration).

Now we investigate the effect of coupling strength with the medium (i.e., E_r^m) on the shape of the absorption line $W(\nu)$. For the sake of definiteness we assume that the characteristic frequencies of the medium ω_m are classical, $\beta\hbar\omega_m \ll 1$, and the spectrum of the medium is sufficiently broad (see eq 12').

(a) Weak coupling with the medium:

$$\beta E_r^m \ll (\beta\hbar\omega_m)^2 \tag{28}$$

The calculation shows that due to the inequality $q_{co} \gg 1$ the calculation of (24) may be performed by using the steepest descent method (cf. section II.2), but a great number of saddle points ($\sim(\beta\hbar\omega_m)^2/\beta E_r^m$) make approximately the same contribution to expression 24 because of the smallness of βE_r^m (it is caused by the periodicity of $F_c(\theta)$). Calculating each of the summand corresponding to one of these saddle points it is necessary to take into account that in the neighborhood of these saddle points $F(\theta)$ has the asymptotic form described by eq 12 (weak coupling with the medium).

Because of very weak coupling with the medium each maximum of absorption of $W(\nu)$ in Figure 1 is broadened according to Lorentzian type formula with the width equal to $\gamma = \pi akT$ whereas the envelope curve is still of Gaussian form 27 with the half-width Δ_c and $h\nu_{max} = \Delta I + E_r^c + E_r^m$. The spacing of the broadened maxima is still equal to $\hbar\omega_c$ (see Figure 2, where $\gamma \ll \hbar\omega_c \ll \Delta_c$).

The maximum value of W is equal to

$$W_{max} = \frac{2|d|^2}{\hbar q_{co}\gamma\pi^{1/2}} \tag{29}$$

(b) Now we consider the case when coupling with the medium is strong ($\beta E_r^m \gg (\beta\hbar\omega_m)^2$), but βE_r^m is not too large

$$(\beta\hbar\omega_m)^2 \ll \beta E_r^m \ll (\beta\hbar\omega_c)^2 \tag{30}$$

As above the steepest descent method is applicable and the large number of saddle points (now it is of the order $(\beta\hbar\omega_c)^2/\beta E_r^m$) contribute to (24) (due to the second inequality in eq 30). However, now the asymptotic form of $F(\theta)$ in the neighborhood of the saddle points is described by eq 10 (strong coupling with the medium). Coupling with the medium is strong enough that each maximum is

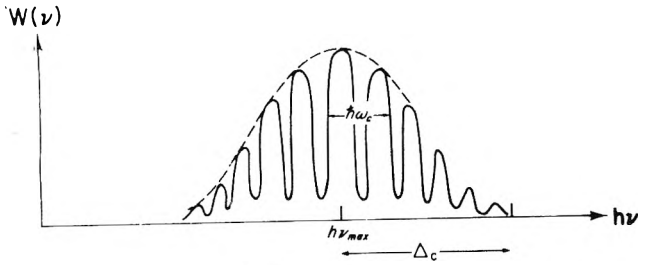

Figure 3. $\beta\hbar\omega_c > 1$, $\beta\hbar\omega_m < 1$, $q_{co} > 1$, $(\beta\hbar\omega_m)^2 < E_r^m < (\beta\hbar\omega_c)^2$, $\Delta_c = \hbar\omega_c q_{co}$, $\Delta_m = 2(kTE_r^m)^{1/2}$, $\hbar\nu_{max} = \Delta I + E_r^c + E_r^m$.

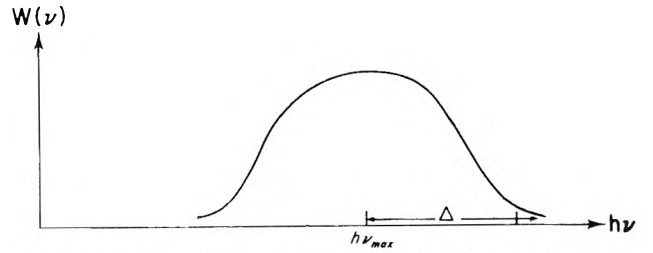

Figure 4. $\beta\hbar\omega_c > 1$, $\beta\hbar\omega_m < 1$, $q_{co} > 1$, $\beta E_r^m > (\beta\hbar\omega_c)^2$, $\Delta = 2\{kT[E_r^m + (\hbar\omega_c/2kT)E_r^c]\}^{1/2}$, (a) $E_r^m < (\hbar\omega_c/2kT)E_r^c$, $\Delta \simeq \Delta_c = \hbar\omega_c q_{co}$, (δ) $E_c^m > (\hbar\omega_c/2kT)\,E_r^c$, $\Delta \simeq \Delta_m = 2(kTE_r^m)^{1/2}$, $\hbar\nu_{max} = \Delta I + E_r^c + E_r^m$.

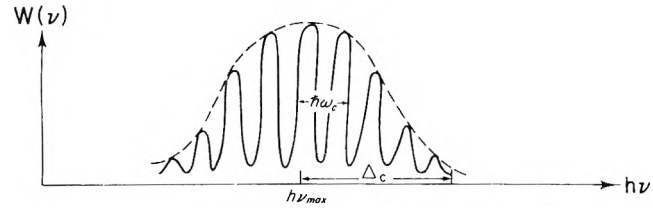

Figure 5. $(\beta\hbar\omega_c)^2 < \beta E_r^c < (\beta\hbar\omega_m)^2 < 1$, $\beta E_r^m < \beta\hbar\omega_c{\cdot}\beta\hbar\omega_m$, $\Delta_c = 2(kTE_r^c)^{1/2}$, $\Delta_m = \gamma = \pi akT$, $\hbar\nu_{max} = \Delta I + E_r^c + E_r^m$.

smoothed according to Gaussian-type formula (with the half-width $\Delta_m = 2(kTE_r^m)^{1/2}$), but it is not too strong to destroy the structure of the absorption band $W(\nu)$ (spacing of the neighboring broadened maxima is much more than their width: $\hbar\omega_c \gg 2(kTE_r^m)^{1/2}$. The envelope curve, as previously, has the form (27), where $h\nu_{max} = \Delta I + E_r^c + E_r^m$ (see Figure 3, where $\Delta_m \ll \hbar\omega_c \ll \Delta_c$)

$$W_{max} = \frac{\beta}{\hbar}|d|^2 \frac{1}{q_{co}(\beta E_r^m)^{1/2}} = \frac{2|d|^2}{\hbar q_{co}\Delta_m} \tag{31}$$

The quantity $h\nu_{max}$ may be calculated by the method described in section II.2.

(c) Finally we consider the case when the reorganization energy of the medium E_r^m is sufficiently large:

$$\beta E_r^m \gg (\beta\hbar\omega_c)^2 \tag{32}$$

Now coupling with the medium is strong it being so strong that only one saddle point contributes to (24), and $W(\nu)$ has the form of a Gaussian-type curve (see Figure 4):

$$W(\nu) = \frac{2\sqrt{\pi}}{\hbar\Delta}|d|^2 \exp\left\{-\frac{(h\nu - h\nu_{max})^2}{\Delta^2}\right\} \tag{33}$$

where $h\nu_{max} = \Delta I + E_r^m + E_r^c$, $E_r^c = \frac{1}{2}\hbar\omega_c q_{co}^2$, and $\Delta = 2\{kT[E_r^m + (\hbar\omega_c/2kT)E_r^c]\}^{1/2}$ is the half-width. When E_r^m increases, Δ is determined at first [at $E_r^m \ll (\hbar\omega_c/kT)E_r^c$] by the intramolecular characteristics, and then [at $E_r^m \gg (\hbar\omega_c/kT)E_r^c$] by the properties of the medium.

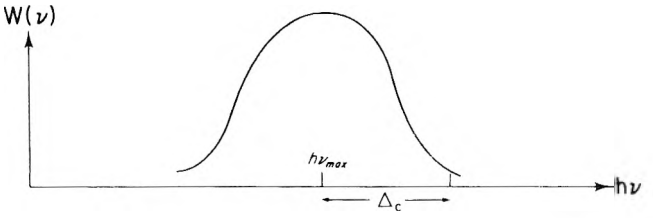

Figure 6. $(\beta\hbar\omega_c)^2 < \beta E_r^c < (\beta\hbar\omega_m)^2 < 1$, $\beta\hbar\omega_m{\cdot}\beta\hbar\omega_c < \beta E_r^m < \beta\hbar\omega_m(\beta E_r^c)^{1/2}$, $\Delta_c = 2(kTE_r^c)^{1/2}$, $\hbar\nu_{max} = \Delta I + E_r^c + E_r^m$.

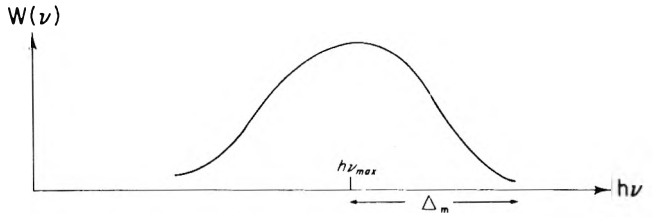

Figure 7. $(\beta\hbar\omega_c)^2 < \beta E_r^c < (\beta\hbar\omega_m)^2 < 1$, $\beta\hbar\omega_m(\beta E_r^c)^{1/2} < \beta E_r^m < (\beta\hbar\omega_m)^2$, $\Delta_m = \gamma = \pi akT$, $\hbar\nu_{max} = \Delta I + E_r^c + E_r^m$.

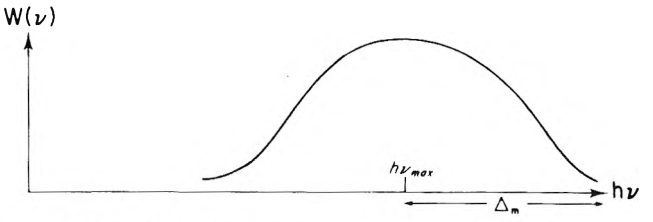

Figure 8. $(\beta\hbar\omega_c)^2 < \beta E_r^c < (\beta\hbar\omega_m)^2 < 1$, $\beta E_r^m > (\beta\hbar\omega_m)^2$, $\Delta_m = 2(kTE_r^m)^{1/2}$, $\hbar\nu_{max} = \Delta I + E_r^c + E_r^m$.

Thus we see that the role of the medium consists in the broadening of the resonance lines and the shifting of $h\nu_{max}$ to the uv region by the quantity E_r^m. In the case of strong coupling with the medium the shape of the absorption band may be essentially changed (see Figure 4).

We have considered above the cases when the intramolecular frequency was quantum, $\beta\hbar\omega_c \gg 1$, and the characteristic frequency of the medium was classical, $\beta\hbar\omega_m \ll 1$. A general qualitative picture will be the same also for other situations, some of which are cited below.

Thus, for example, if the intramolecular frequency is classical $\beta\hbar\omega_c \ll 1$ and $\omega_c \gg \omega_m$, the change is only in the half-width of the envelope curve in Figures 1–3 (Δ_c is equal now to $2(kTE_r^c)^{1/2}$) and in the half-width of $W(\nu)$ in Figure 4 ($\Delta = 2[kT(E_r^c + E_r^m)]^{1/2}$). If $\omega_c \ll \omega_m$, two additional cases are possible ($(\beta\hbar\omega_m)^2 \gg \beta E_r^c$ or $(\beta\hbar\omega_m)^2 \ll \beta E_r^c$). For the sake of definiteness we assume that

$$(\beta\hbar\omega_c)^2 \ll \beta E_r^c \ll (\beta\hbar\omega_m)^2 \tag{34}$$

Then under the condition $\beta E_r^m \ll \beta\hbar\omega_c{\cdot}\beta\hbar\omega_m$ the resonant maxima are broadened according to a Lorentzian-type formula with the width γ, and the envelope curve is of a Gaussian form with a half-width of $2(kTE_r^c)^{1/2}$. If $\beta\hbar\omega_c{\cdot}\beta\hbar\omega_m \ll \beta E_r^m \ll \beta\hbar\omega_m(\beta E_r^c)^{1/2}$, the transition probability $W(\nu)$ is described by a Gaussian-type curve of half-width $2(kTE_r^c)^{1/2}$ (Figure 6). If $\beta\hbar\omega_m(\beta E_r^c)^{1/2} \ll \beta E_r^m \ll (\beta\hbar\omega_m)^2$, then $W(\nu)$ is described by a Lorentzian-type curve of the width γ (Figure 7). Finally if $\beta E_r^m \gg \beta\hbar\omega_m)^2$, $W(\nu)$ is of a Gaussian form with a half-width of $2(kTE_r^m)^{1/2}$ (Figure 8). Thus even weak coupling with the medium ($\beta E_r^m \ll (\beta\hbar\omega_m)^2$) does not lead always to the structure and Lorentzian-type shape of the absorption band $W(\nu)$.

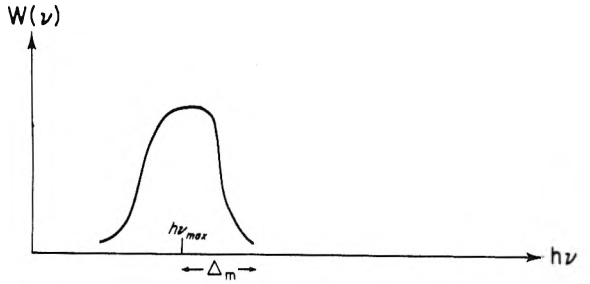

Figure 9. $\Delta_m = \gamma = \pi akT$, $\hbar\nu_{max} = \Delta I + E_r^c + E_r^m$.

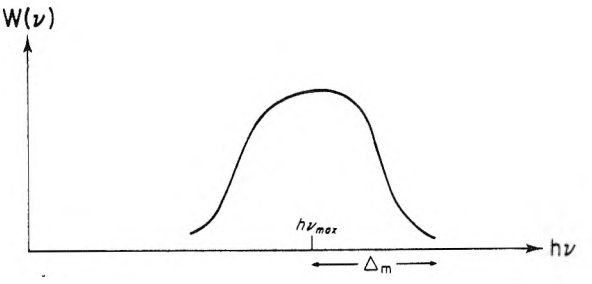

Figure 10. $\Delta_m = 2(kTE_r^m)^{1/2}$ if $\beta\hbar\omega_m < 1$, $\Delta_m = 2(\hbar\omega_q E_q)^{1/2}$ if $\beta\hbar\omega_m > 1$, $\hbar\nu_{max} = \Delta I + E_r^c + E_r^m$.

If the characteristic frequencies of the medium are quantum, the qualitative picture is also retained, and only the values of W_{max} and the half-width of the Gaussian-shaped maxima and conditions of the type (28) and (30) are changed (see section II.1).

The qualitative picture described above is valid also for more general case, when the reorganization of several intramolecular vibrations involving "entangling" of normal coordinates takes place, though the shape of the absorption curve may be essentially complicated (in particular, the envelope curve may consist of several Gaussian-type curves of various amplitudes). The result may be extended also to the case, when the harmonic approximation is not applicable to the final state. For the processes of light absorption in the medium the harmonic approximation is always applicable for the initial state in the region of the absorption curve maximum:

$$U_i(q_c) \simeq \frac{1}{2}\hbar\omega_c q_c^2 \tag{35}$$

For the final state the quasiclassical approximation for $\rho_{\beta\theta}^f$

$$\rho_{\beta\theta}^f(q_c, q_c') \sim \exp\left\{-\frac{(q_c - q_c')^2}{2\beta\hbar\omega_c\theta} - \beta\theta U_f\left(\frac{q_c + q_c'}{2}\right)\right\} \tag{36}$$

may be used because the major contribution to the transition probability comes from the highly excited energy levels of the final state (strong coupling with the intramolecular vibrations. The expansion of U_f to first-order terms may be used in the neighborhood of the minimum of the initial potential energy surface:

$$U_f(q_c) \simeq E_r^{c'} + F_c' q_c \tag{37}$$

The calculation shows that ν_{max} is determined by the quantity $F_r^{c'}$

$$h\nu_{max} = \Delta I + E_r^m + E_r^{c'} \tag{38}$$

The width of the envelope curve in Figures 1–3

$$\Delta_c^2 = (F_c')^2 \coth\frac{1}{2}\beta\hbar\omega_c \tag{39}$$

and the width of the curve in Figure 4

$$\Delta = 2\left[kT\left(E_r^m + \frac{(F_c')^2 \coth\frac{1}{2}\beta\hbar\omega_c}{4kT}\right)\right]^{1/2} \tag{40}$$

are determined by the linear term in eq 37.

Thus in this case the gradual broadening of the maxima in Figure 1 also occurs, the shape and the heights of the broadened maxima being the same as in Figures 2 and 3, only the quantitative characteristics of the envelope curve (27) (but not its shape) are changed. The expression for the width of the Gaussian-type curve in Figure 4 is also changed.

2. Weak Coupling with the Intramolecular Vibrations. In the case of weak coupling with the intramolecular vibrations there is only one frequency for the isolated molecule, at which the transition really takes place. For light absorption in the medium with weak coupling with the medium this absorption band is broadened according to a Lorentzian formula, the half-width being equal to $\gamma = \pi akT$ (Figure 9). For strong coupling with the medium it is broadened in accordance with a Gaussian-type formula, the half-width being equal to $2(kTE_{Cl}^m)^{1/2}$ if $\beta\hbar\omega_m \ll 1$ or $(2\hbar\omega_Q E_Q)^{1/2}$ if $\beta\hbar\omega_m \gg 1$ (see Figure 10).

IV. Asymmetry of the Intramolecular Lines

All that was said above about the shape of the envelope curves in Figures 1–3 and about the shape of the absorption band in Figure 4 is valid only in the neighborhood of their maxima. The symmetry of these curves may be destroyed outside the half-width only. Some authors relate the asymmetry only with the anharmonicity or with the change of frequencies in the course of the transition. It will be shown in the present paper in particular that the asymmetry may take place also in the framework of the harmonic approximation with unchanged frequencies. The anharmonicity is naturally one of the factors leading to the asymmetry. We consider this problem for the processes with sufficiently strong coupling with the medium the characteristic frequencies of the last ω_m being classical ($\beta\hbar\omega_m \ll 1$).

$$\beta E_r^m \gg \max\{(\beta\hbar\omega_c^{i,f})^2, (\beta\hbar\omega_m)^2\} \tag{41}$$

where ω_c^i and ω_c^f are the frequencies of the intramolecular vibrations in the initial and final states.

We assume also that the decrease of Im $G(\bar{k}, \omega)$ at $\omega \to \infty$ is sufficiently rapid (the effects due to the rapid decreasing of Im G were discussed in Section II).

Under these conditions the major contribution to (24) derives from the single saddle point and the asymmetry is determined by terms higher than second order in the expansion of the exponent in eq 24 in the saddle point θ. Then the probability of the light absorption is described by the expressions

$$W(\nu) = W_{max}\exp\left\{-\frac{(h\nu - h\nu_{max})^2}{\Delta^2}\left[1 - \frac{h\nu - h\nu_{max}}{\Delta\zeta}\right]\right\} \tag{42}$$

$$\Delta^2 = \sum_n F_n'^2 \coth\frac{1}{2}\beta\hbar\omega_n$$

$$F_n' = \left.\frac{\partial U_f}{\partial q_n}\right|_{q_n=0} = -\sum_\rho \hbar\omega_\pi' q_{\rho 0}' \alpha_{\rho n} \tag{43}$$

$$\zeta = \Delta^3 \left| - \sum_n F_n'^2 \frac{\hbar\omega_n}{Ih^2 \frac{1}{2}\beta\hbar\omega_n} + \sum_{n,\rho} U_{n\rho}' F_n' F_\rho' \coth\frac{1}{2}\beta\hbar\omega_n \coth\frac{1}{2}\beta\hbar\omega_\rho - \frac{1}{3}\sum_\rho \frac{1}{2}\hbar^3\omega_\rho'^3 q_{\rho 0}'^2 \right|^{-1}$$

$$U_{n\rho}' = \frac{\partial^2 U_f}{\partial q_n \partial q_\rho} = \sum_\xi \hbar\omega_\xi' \alpha_{\xi n}\alpha_{\xi\rho} \qquad (44)$$

where ω_n and ω_n' are the frequencies of vibrations in the initial and final states, q_n and q_n' are the normal coordinates, $\{\alpha_{\xi n}\}$ is the matrix relating the normal coordinates of the initial and final states: $q_\rho' = \Sigma\alpha_{\rho n} q_n$. $\{q_{n0}'\}$ are the equilibrium values of the coordinates in the final state. Subscripts n, ρ, ... belong to the set of coordinates of the normal vibrations of both the medium and the molecule.

Under the assumptions made above the condition $\zeta \gg 1$ holds and the asymmetry is destroyed far outside the half-width.

If the entangling of the normal coordinates of the medium and the molecule may be neglected, Δ^2 and ζ are the sums of the terms each of them being dependent on either the characteristics of the molecule or those of the medium only.

If the electron transition leads to the change of the vibrational frequencies only, the characteristics of the band are expressed by

$$h\nu_{max} = \Delta I + \sum_k |\Delta D_k|^2 \operatorname{Re} G(\bar{k}, 0) + \sum_c \frac{1}{2}\hbar\omega_c' q_{c0}^2$$

$$\Delta^2 = \frac{2\hbar}{\pi}\sum_k |\Delta D_k|^2 \int_0^\infty d\omega \operatorname{Im} G(\bar{k}, \omega) \coth\frac{1}{2}\beta\hbar\omega + \sum_c \hbar^4\omega_c'^4\omega_c^{-2} q_{c0}^2 \coth\frac{1}{2}\beta\hbar\omega_c \qquad (45)$$

$$\zeta = \Delta^3 \left| \frac{4\hbar^2}{3\pi}\sum_k |\Delta D_k|^2 \int_0^\infty d\omega \operatorname{Im} G(\bar{k}, \omega) + \sum_c \hbar^3\omega_c'^3 q_{c0}'^2 \left[\left(\frac{\omega_c'}{\omega_c}\right)^2 \coth^2\frac{1}{2}\beta\hbar\omega_c + \frac{2}{3} - \coth^2\frac{1}{2}\beta\hbar\omega_c \right] \right|^{-1} \qquad (46)$$

Equation 46 shows that ζ is nonzero and positive even when the frequencies are changed in the course of the transition, i.e., the curve outside its half-width is asymmetric, its short wavelength branch decreasing more slowly than that for the symmetric curve.

Unlike the case of the oscillators having nonvarying frequencies, for $\omega_c' \neq \omega_c$, the quantity ζ may be both positive and negative depending on the character of the frequency change due to the electron transition. This quantity becomes negative at sufficiently large decrease of one or several frequencies of the system. The sign of the quantity ζ determines which of the branches of the absorption curve decreases more slowly: at $\zeta > 0$ the short wavelength branch of $W(\nu)$ decreases more slowly, whereas at $\zeta < 0$ the long wavelength branch does. If the electronic excitation does not lead to the entangling of the normal coordinates, the quantity in eq 46 may become negative owing to only the vibrations of not very high frequencies: $\coth(\frac{1}{2})\beta\hbar\omega_c > \sqrt{2/3}$ and $\omega_c' < \omega_c$.

Similar expressions are also obtained when analyzing the asymmetry of the envelope curve (Figures 2 and 3), but if the rearrangement of several intramolecular vibrations takes place it is necessary to analyze the relative strengths of the coupling of the electron with each of them.

In conclusion we should like to note that we did not attempt to describe in detail all possible types of transitions in the solution involving light absorption (i.e., all the possible cases of the relations between the characteristic parameters and also the processes involving the entangling of the normal coordinates) because of their very large variety.

However the approach suggested enables one to calculate, in principle, the shape of the absorption curve $W(\nu)$ for any possible case in the framework of the model described. The importance of this approach is that it enables us to introduce in a natural manner the concepts of strong and weak coupling of the electronic subsystem with the medium and intramolecular vibrations and to derive both the Gaussian- and Lorenzian-type shape of the absorption curve (having structure or not).

Thus, for example, if the reorganization of only one intramolecular degree of freedom of nonvarying frequency takes place, the values of three quantities are sufficient to describe the shape of the absorption curve. These quantities are:

(1) Δ_m (The width of the absorption curve in the absence of reorganization of the intramolecular degrees of freedom.) Depending on the values of βE_r^m and $\beta\hbar\omega_m$ (see eq 14′ and 20), the expression for Δ_m may have different forms (see eq 14′, 20, 20′, and 22′).

(2) $\hbar\omega_c$ (where ω_c is the intramolecular frequency).

(3) Δ_c (the width of the intramolecular envelope curve). This quantity is equal to $\Delta_c = \hbar\omega_c q_{c0}$ for $\beta\hbar\omega_c \gg 1$ and to $\Delta_c = 2(\frac{1}{2}\hbar\omega_c q_{c0}^2 kT)^{1/2}$ for $\beta\hbar\omega_c \ll 1$).

Three possible cases may take place depending on the relations between these quantities: (a) $\Delta_m \ll \hbar\omega_c \ll \Delta_c$, (b) $\hbar\omega_c \ll \Delta_m \ll \Delta_c$, (c) $\hbar\omega_c \ll \Delta_c \ll \Delta_m$ or $\Delta_c \ll \hbar\omega_c$.

(a) If $\Delta_m \ll \hbar\omega_c \ll \Delta_c$, the band reveals clearly the structure and includes a large number of Gaussian- or Lorentzian-shaped maxima (depending on the strength of the coupling with the medium). The width of these maxima is equal to Δ_m, and their spacing is equal to $\hbar\omega_c$. Their amplitudes decrease slowly in the characteristic energy interval of the order Δ_c (see, e.g., Figures 1–3 and 5).

(b) If $\hbar\omega_c \ll \Delta_m \ll \Delta_c$, the band has no structure and represents a Gaussian-type line of half-width Δ_c (see, e.g., Figure 4a and 6). (More precisely, only one maximum dominates, whereas the amplitudes of the other possible maxima are negligibly small.)

(c) If $\hbar\omega_c \ll \Delta_c \ll \Delta_m$ or $\Delta_c \ll \hbar\omega_c$, the band also has no structure (in the same sense as above) and represents a Gaussian- or Lorentzian-shaped line of width Δ_m depending on the strength of coupling with the medium (see, e.g., Figures 4, 7, and 8–10).

References and Notes

(1) R. Englman and J. Jortner, *Mol. Phys.*, **18**, 145 (1970).
(2) S. Pekar, "Studies in Electronic Theory of Crystals", Fizmatgiz, Moscow, 1951.
(3) T. Franck and M. Platzman, *Z. Phys.*, 138, 411 (1954).
(4) H. Frohlich, "Theory of Dielectrics", Clarendon Press, Oxford, 1958.
(5) M. A. Vorotyntsev, R. R. Dogonadze, and A. M. Kuznetsov, *Dokl. Akad. Nauk. SSSR*, **195**, 1135 (1970).
(6) R. Saxton, *Proc. R. Soc., Ser. A*, **219**, 473 (1952).
(7) A. A. Ovchinnikov and M. Ya. Ovchinnikova, *J. Exp. Theor. Phys.*, **56**, 1278 (1969).
(8) R. R. Dogonadze, A. M. Kuznetsov, "Itogi Nauki i Techniki, Ser. Physical Chemistry. Kinetics", Vol. 2, V. V. Bondar, Ed., Viniti, Moscow, 1973.
(9) The probability of light emission is described by a similar expression with the substitution of $-\nu$ for ν.

Solvation Time of the Electron in Polar Liquids. Water and Alcohols

W. John Chase[1] and John W. Hunt*

The Ontario Cancer Institute and Department of Medical Biophysics, University of Toronto, Toronto, Ontario, M4X 1K9 Canada

(Received August 25, 1975)

Publication costs assisted by The Ontario Cancer Institute

The formation of e_{sol}^- from its precursor, e_t^-, has been investigated in the temperature range from −65 to 60°C using a stroboscopic pulse radiolysis (SPR) system. The rate of formation of e_{sol}^-, measured at 600 nm, and rate of decay of e_t^-, measured at 1300 nm, are the same; the rate of decay of e_t^- is slower by as much as a factor of 2 when measured at 1050 nm. At 20°C the values of τ_{sol} are 10.7 ± 1, 23 ± 2, 54 ± 3, and 39 ± 5 psec for methanol, ethanol, 1-propanol, and 1-butanol, respectively. At 20°C τ_{sol} is estimated to be less than 3 psec for H_2O and D_2O. In all of the alcohols tested there is a good correlation between τ_{sol} and the dielectric relaxation time, τ_2, for rotation of the molecules over a wide range of temperatures; this suggests that intermolecular hydrogen bonding does not limit the rate of electron solvation.

Introduction

Electrons can be separated from their parent molecules by radiation or chemical techniques. These electrons will interact with solvent molecules and, in polar solvents, most of them will become trapped in a "cage" of solvent molecules to form a relatively stable species, the solvated electron, e_{sol}^-.[2] In polar solvents such as H_2O, alcohols, and ammonia, e_{sol}^- is a well-established entity on theoretical and experimental grounds.[3,4] There is also direct evidence that a precursor of e_{sol}^- called the "trapped" or "damp" electron,[2] e_t^-, has been observed in cold glasses and liquids.[5-14] As well, indirect evidence exists from electron scavenging results that precursors of e_{sol}^- [2] take part in early electron processes.[15-19]

Higashimura and his coworkers studied γ-irradiated alcohol glasses at 4 K and found a strong absorption band which peaked at infrared wavelengths.[6-8] This band shifts irreversibly toward blue wavelengths upon warming to 77 K. At the same time, the ESR line width increases, indicating that the cavity around the electron decreases in size and that the electron is stabilized in a deeper trap.[6-8] Pulse radiolysis of alcoholic glasses and liquids shows that the disappearance of the infrared absorption is accompanied concurrently by the appearance of the absorption band of e_{sol}^-.[9-14] In addition to these experimental observations, theoretical calculations also support the concept of a partially stabilized electron, e_t^-. In ethanol, Fueki et al.[20] predicted an optical absorption shift due to dipole orientation of solvent molecules around the electron; this shift was at least 70% of the observed value. Tachiya et al.[21] have shown that excess electrons in a polar glass would initially be trapped in a relatively shallow preexisting trap, a particular arrangement of the molecular dipoles forming a region of low potential energy for the electron. This model indicates that virtually all of the trapping sites would have energies less than 1 eV, well below the energy of the peak absorption of e_{sol}^- (1.77 eV in ethanol[22]).

Photobleaching studies,[6-8] pulse radiolysis studies,[9-12] and theoretical calculations[20,21] indicate that molecular orientation, rather than thermal de- and retrapping of the electron, or tunneling of the electron from a *shallow to a deep trap*, is the probable mechanism for the solvation of e_t^-. If this is the case, the amount of intermolecular hydrogen bonding should affect the rate of molecular reorientation. The variation of the solvation rate with temperature should indicate whether hydrogen bonding hinders the molecular reorientation process.

Several laboratories have made attempts to obtain the formation times of e_{sol}^- in water and alcohols.[11,13,23-27] Using their stroboscopic pulse radiolysis system, Bronskill et al.[23] observed the usual absorption spectrum of e_{sol}^-, and estimated that it was formed in less than 10 psec in water and alcohols. Beck and Thomas[24] used a fast pulse radiolysis system to obtain the formation of e_{sol}^- in alcohols; values of 2–5 and 50 psec were obtained for ethanol and 1-propanol. Recently, Kenney-Wallace and Jonah[25] showed that in normal aliphatic alcohols, the formation time of e_{sol}^- increases with increasing chain length. Baxendale and Wardman[11] monitored the formation of e_{sol}^- indirectly by observing the concurrent decay of e_t^- at 1300 nm in cold, liquid alcohols. Gilles et al.[13] observed the formation of e_{sol}^- in *cool alcohols*, and using the data of Baxendale and Wardman[11] extrapolated to find the formation times of e_{sol}^- at 294 K. In water, Kenney-Wallace and Walker[26] estimated that the formation time of e_{aq}^- was less than 5.5 psec. Rentzepis et al.[27] used a unique picosecond mode-locked laser system where the electrons were produced by the photoionization of a solute molecule. Their studies indicate that e_{sol}^- is formed in water *in* about 2 psec.

There were considerable discrepancies among the values for the formation times of e_{sol}^-: for example, values from 2–5[24] to 18 psec[25] have been published for ethanol. Accurate measurements of the formation times are needed to elucidate the mechanism of the electron solvation process. In particular, we have studied the formation of e_{sol}^- in H_2O, D_2O, ethylene glycol, and the first four normal alcohols by observing the absorption signals from our pulse radiolysis system.

Experimental Section

The stroboscopic pulse radiolysis (SPR) system allows us to observe the formation and decay of transient species in the 350-psec time window between fine-structure electron pulses from the University of Toronto Linear Accelerator. The details of the SPR system are described else-

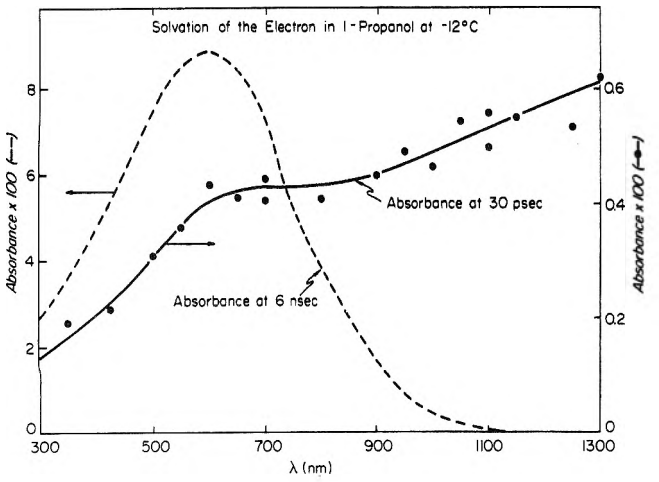

Figure 1. Absorption spectra of the electron at 30 psec and 6 nsec in 1-propanol at −12°C (261 K). For the 30-psec spectrum (●), the absorbance is that produced by a single fine structure pulse, measured at 30 psec after the midpoint of the pulse. The average dose per fine structure pulse was ~220 rads. The solid line (——) was drawn by hand through the points. The 6-nsec spectrum (- - -) was obtained with the facility described by Aldrich et al.[29] Because the 6-nsec absorbance is the integrated absorbance of about 26 fine structure pulses, the 6-nsec absorbance is larger than the 30-psec absorbance from a single fine structure pulse. The absorbance scale for the 6-nsec spectrum is on the left side of the figure while the scale for the 30-psec spectrum is on the right side.

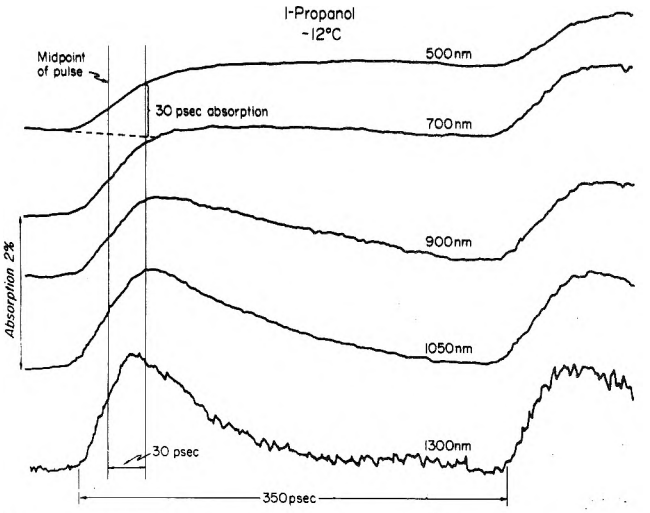

Figure 2. Typical picosecond kinetic traces of absorption vs. time in 1-propanol at −12°C. These traces were among those used to construct the 30-psec spectrum of Figure 1. The two vertical lines mark the middle of the pulse and the point at which the 30-psec spectrum of Figure 1 was calculated. The absorption signal is noisier at 1300 nm because the germanium photodiode was used for this trace, whereas the more sensitive silicon photodiode was used for the other traces.

where,[18,23,28,29] and the effect that some of these details have upon kinetics is described in the Appendix. The width of the fine-structure electron pulse depends upon the alignment of the linear accelerator. This pulse width changes from run to run, and is checked each time by observing the formation of the absorption signal of e_{aq}^-.

Chemicals. The D_2O was supplied by Chalk River Nuclear Laboratories, Atomic Energy of Canada Limited. The D_2O contained less than 1% H_2O and less than 10^{-4} *M* of other impurities. Both D_2O and once-distilled H_2O were not degassed as it has been shown that dissolved oxygen has no effect on the yields or kinetics.[23] Ethanol was obtained from Consolidated Alcohol Limited or from U.S. Industrial Co. and all other alcohols were certified reagent grade from Fisher Scientific Co. The alcohols were not purified but were bubbled with argon gas (prepurified grade) from Canadian Anaesthetics Limited for at least 30 min before use. In alcohols, tests showed that dissolved air decreased the absorbance at 6 nsec by less than 10%, but left e_{sol}^- yields and kinetics at picosecond times unaffected.

Variable Temperature Irradiation Cell. To prevent a buildup of long-lived irradiation products the solutions must be continually flowed through the irradiation cell. At room temperature this presents no special problem and cells with optical path lengths of 0.5, 1, or 2 cm were used.

A specially constructed cell allowed us to vary the temperature at which the liquid was irradiated. A 1-cm irradiation cell was suspended inside an aluminum housing which had windows of Suprasil quartz to allow the electron beam and the analyzing light to reach the cell. A vacuum provided thermal insulation between the aluminum housing and the cell.

The flowing liquid is first cooled by passage through a copper coil immersed in a bath of ethanol–dry ice mixture, and then heated by passage through an externally heated length of copper tubing. The temperature of the liquid can be varied from −65 to 45°C by this method, and by leaving the dry ice out of the cooling bath, temperatures of at least 60°C can be reached. The temperature of the flowing liquid was sensed at the outlet of the cell by a temperature probe and converted to a voltage by a bridge circuit (Rosemount Engineering Co., platinum resistance temperature sensor, Model 146 MA, and linear bridge, Model 414L). The estimated error in the temperature measurement is less than 1°C, although it should be noted that the electron beam heats the liquid by 3 or 4°C. All the temperatures quoted in this paper are those recorded during irradiation.

Signal Detection. In these experiments, solid state photodetectors were used to detect the picosecond absorption signals. In the wavelength range from 300 to 1100 nm a silicon photodiode (United Detector Technology Inc., PIN-10) was used. This detector had a response time of 6 nsec into a 50-Ω load and a maximum quantum efficiency of ~90% at a wavelength of 900 nm. Observations have also been carried out at wavelengths as long as 1300 nm using a planar *passivated* germanium photodiode (RCA Limited, Montreal). This detector had a response time of 10 nsec and a quantum efficiency of about 30% at 1300 nm. The time resolution of the SPR system is not degraded by using this somewhat slower photodetector.

Results

(*1*) *Spectra.* (*a*) *H_2O.* As shown by Lam and Hunt[14] the picosecond and microsecond absorption spectra of e_{aq}^- are very similar. The absorption signal is formed in less than 10 psec and does not grow or decay in 350 psec.[23] There is no indication of a fast decay in the infrared which could be attributed to e_t^-.

(*b*) *Alcohols.* Unlike H_2O, the absorption spectra in alcohols change markedly with time. Baxendale and Wardman[11] observed nanosecond spectral shifts in cold alcohols and we find similar spectral changes in alcohols on a picosecond timescale. A broad absorption band rising into infrared wavelengths is formed very rapidly; Basendale and Wardman observed that it was completely formed by the

end of their 5-nsec pulse and we find that it is formed within the 18-psec response time of the SPR system. We attribute the infrared portion of the absorption band to electrons trapped in shallow potential wells. We have labeled these electrons trapped electrons, e_t^-, to differentiate them from e_{sol}^-, a fully relaxed electron which is presumably in a deeper potential well than e_t^-. As e_t^- becomes solvated

$$e_t^- \xrightarrow{k_{sol}} e_{sol}^- \qquad (1)$$

the shape of the absorption spectrum evolves with time, as shown in Figure 1 for 1-propanol at −12°C (261 K). The 30-psec spectrum changes to that of e_{sol}^-, as shown by the 6-nsec spectrum. The 6-nsec spectrum peaks at 600 nm, compared to the value of 610 nm recorded by Dixon and Lopata[30] at the same temperature. Our 6-nsec spectrum also has a shape similar to that measured for e_{sol}^- at room temperature.[22] The spectra of Figure 1 are typical of those found for the other normal alcohols that we studied.

Some of the picosecond kinetic absorption traces used to construct the 30-psec spectrum of Figure 1 are shown in Figure 2. At all wavelengths a portion of the absorption signal (as indicated by the 30-psec spectrum of Figure 1) is formed rapidly within the fine structure pulse and then either grows or decays, depending upon the wavelength. At short wavelengths (<800 nm) the rapid formation of the signal is followed by a further growth which is complete in 350 psec (500, 700 nm in Figure 2). The final signal is that of e_{sol}^-. At long wavelengths (>1050 nm) the rapidly formed signal decays in 350 psec. At 1300 nm in Figure 2 the absorption signal decays to its baseline and there is no indication of a contribution from e_{sol}^-. At 1050 nm the signal does not decay completely in 350 psec and has a small component apparently due to e_{sol}^-. At intermediate wavelengths the signals form quickly and then decay slowly. At 900 nm in Figure 2, the signal is formed almost within the width of the fine structure pulse and then decays slowly in 350 psec. The fast formation followed by a slower decay agree with the results of Hase et al.[7] and Baxendale and Wardman.[11] These complex kinetics are probably due to a shift in the spectrum of e_t^- as it relaxes into a deeper trap. A detailed analysis of the kinetics is difficult for wavelengths between 800 and 1000 nm.

(2) *Kinetics.* The raw kinetic data are in the form of traces of percentage absorption vs. time, from which the absorbance, $A(t)$, can be calculated. From traces where $A(t)$ returns to its baseline it was found that $A(t)$ follows first-order kinetics at 1050 and 1300 nm

$$A(t) = A(0)\exp(-k_t t) \qquad (I)$$

and it was assumed that all of the solvation kinetics were first order at these wavelengths. The growth of the absorption signal due to e_{sol}^- at wavelengths shorter than ~800 nm was also first order, as determined from traces where the signal is completely formed in 350 psec. For wavelengths less than ~800 nm, $A(t)$ is conveniently given by

$$A(t) = A(\infty)\{(1-\alpha) + \alpha[1 - \exp(-k_{sol}t)]\} \qquad (II)$$

where $A(\infty)$ is the absorbance at infinite time (assuming no other reactions occur), $(1-\alpha)$ is the fraction of the absorbance which is formed during the fine structure pulse of the accelerator, and α is the fraction of the absorbance which grows in with a rate constant, k_{sol}.

Rate constants, k_t and k_{sol}, were calculated from semilog plots of absorbance vs. time. For these plots the *tilt* of the baseline was determined from kinetic traces where the absorbance returned to its baseline, but the *position* of the baseline was shifted until the semilog plot was a straight line. The accuracy of individual rate constants determined from these plots was usually better than 20%, and in no case worse than 35%.

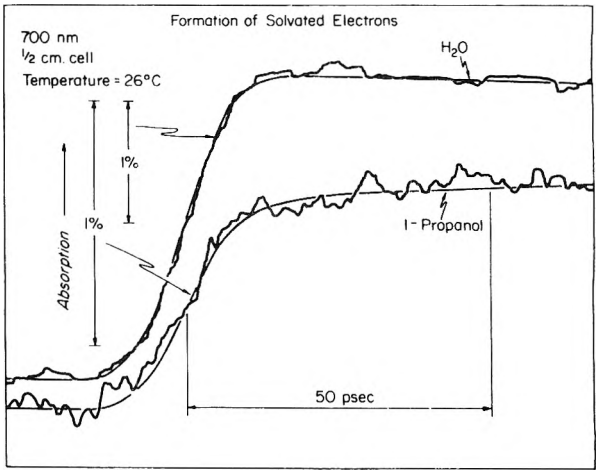

Figure 3. Experimental data and calculated curves for the formation of e_{sol}^-. For both H_2O and 1-propanol the fine structure pulse shape was Gaussian with a σ of 4.4 psec (see Appendix). For H_2O the formation time used was $\tau_{sol} = 0$ psec. For 1-propanol the absorption buildup followed eq II with $\tau_{sol} = 28$ psec and $\alpha = 0.2$.

For lifetimes, $\tau = 1/k$, shorter than about 20-psec kinetics could be altered by the 18-psec response time of the SPR system. For all traces with $\tau < 20$ psec and selected other traces a convolution technique (see Appendix) which accounted for this response time was used to calculate curves which could be compared to the experimental data, thus ensuring that the lifetime obtained from the semilog plot was correct.

(a) *Formation Time of e_{sol}^- in H_2O and D_2O.* The formation time, $\tau_{sol} = 1/k_{sol}$, of e_{aq}^- is known to be very rapid,[13,23,27] and in order to reduce the response time of the SPR system to a minimum, an irradiation cell with a path length of only 0.5 cm was used. As well, a narrow time range was studied so that the absorption buildup could be more closely examined.

According to Bronskill et al.[23] and Aldrich et al.,[18] the shape of the absorption signal is the convolution of the shape of the fine structure pulse, $f(t)$, the desynchronization, $d(t)$, between the electron beam and the slower light beam, and the function assumed for the concentration of the absorbing species, $c(t)$. Details of this calculation are found in the Appendix. Beer's law relates $c(t)$ to the absorbance, as given by eq II. The fine structure electron and Čerenkov light pulses were assumed to be Gaussian in shape and are convoluted together to give $f(t)$, itself a Gaussian.[32]

$$f(t) = \frac{1}{2\sigma\sqrt{\pi}}\exp(-t^2/4\sigma^2) \qquad (III)$$

in which σ is the width of a fine-structure electron pulse.

The formation of e_{sol}^- was observed at 600 and 700 nm in H_2O and at 600 nm in D_2O. A comparison between predicted curves and experimental data (see Figure 3) showed the following: (1) the fine structure pulse shape, $f(t)$, is Gaussian or nearly Gaussian in general agreement with the

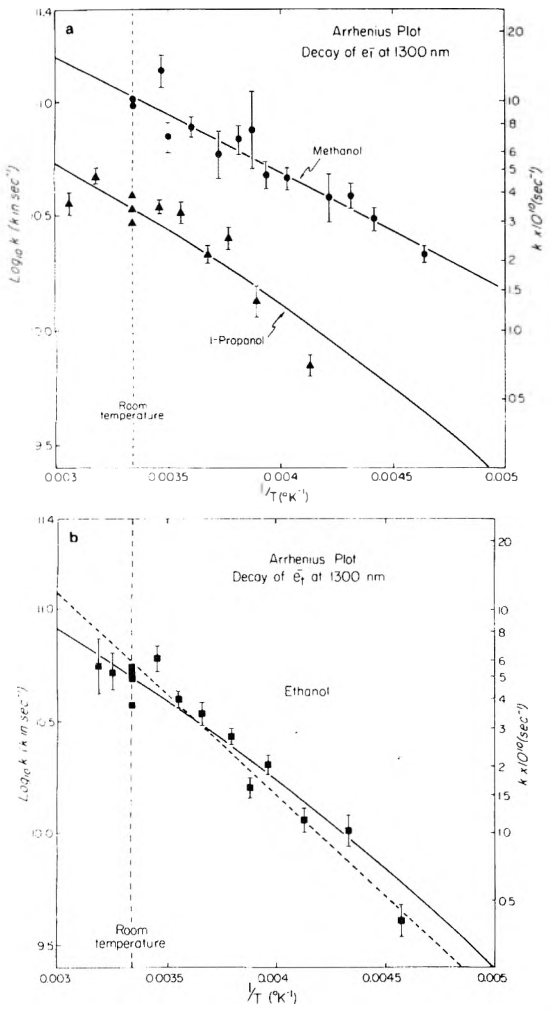

Figure 4. (a) Arrhenius plot of the rate constant for the decay of e_t^- measured at 1300 nm in methanol (●) and 1-propanol (▲). The solid line for methanol is a least-squares fit of the data to the Arrhenius expression (eq IV). The solid line for 1-propanol is a least-squares fit of the data to the Cole–Davidson expression (eq V) with T_0 = 73.5 K. (b) Arrhenius plot of the rate constant for the decay of e_t^- measured at 1300 nm in ethanol (■). The dashed line (- - -) is a least-squares fit to the Arrhenius expression (eq IV). The solid line (—) is a least-squares fit to the Cole–Davidson expression (eq V) with T_0 = 73.5 K. The parameters of the curves in a and b are listed in the supplementary material.

results of Mavrogenes et al.;[31] (2) the formation time, τ_{sol}, of e_{sol}^- in H_2O and D_2O is between 0 and 3 psec. Figure 3 shows that the calculated curve for the absorption buildup (using σ = 4.4 psec and τ_{sol} = 0 psec) agrees extremely well with the experimental data. It should be noted, however, that by using σ = 4.0 psec, τ_{sol} = 2.0 psec and α = 1, a curve nearly identical in shape with, but displaced to the right of, the curve in Figure 3 is generated. Unfortunately we do not have an accurate, absolute time marker and thus we cannot distinguish between these two cases. Finally, if α were to have a small value of 0.2, there would be a good fit between the calculated curves and the experimental data for values of τ_{sol} as large as 10 psec. From our picosecond studies of H_2O, there is no evidence for a short-lived absorption in the infrared due to the decay of e_t^-; thus we consider it most unlikely that τ_{sol} could be more than a few picoseconds.

(*b*) *Alcohols.* The rate constants for the decay of e_t^- and for the formation of e_{sol}^-, k_t and k_{sol}, respectively, are first order at all wavelengths. They, are listed elsewhere; see the paragraph at the end of the text regarding supplementary material. At any given temperature k_{sol} has the same value within experimental error at short wavelengths (400–800 nm) as k_t has at long wavelengths (1300 nm). At intermediate wavelengths (900–1050 nm) k_t is as much as 100% slower than the rate constants found in the other part of the spectrum, depending upon the alcohol studied and the temperature. We can accurately determine rate constants for decays of e_t^- whose lifetimes are longer than about 20 psec since the response time of the SPR system with a 1-cm irradiation cell is 18 psec. Because there is such excellent agreement between the theoretical and observed formation of e_{sol}^- in Figure 3 we can use the shape of the fine-structure pulse to calculate a curve for the decay of e_t^-. By matching the theoretical curves to the experimental data we can obtain lifetimes for the decay of e_t^- as short as 10 psec with reasonable accuracy.

The kinetics of the decay of e_t^- at 1300 nm are the least ambiguous because the absorption signal always decays to the zero absorption level as there is no e_{sol}^- absorption signal. For this reason the kinetics of the decay of e_t^- at 1300 nm are discussed first.

(*i*) *1300 nm.* An Arrhenius plot of the rate, k_t, of disappearance of e_t^- is shown in Figure 4a,b for methanol, ethanol, and 1-propanol over a temperature range from −65 to 60°C. The observed decay rates change by a factor ranging from 5 to 10 over this temperature range. At 20°C the values of $\tau(e_t^-)_{1300\ nm}$ are 10.7 ± 1, 23 ± 2, and 34 ± 3 psec in methanol, ethanol, and 1-propanol, respectively. In Figure 4a the line for methanol is a least-squares fit of the data to an Arrhenius expression

$$k = A \exp(-E_a/RT) \qquad \text{(IV)}$$

while for 1-propanol the curve is a fit to a modification of eq IV due to Cole and Davidson.[33]

$$k = A \exp(-E_a/R(T - T_0)) \qquad \text{(V)}$$

In this equation, T_0 represents a glass transition temperature. In agreement with dielectric relaxation data,[33] a value of 73.5 K was chosen for Figure 4a. The least-squares fit for 1-propanol includes recent new data from Baxendale.[34] In Figure 4b the dashed and solid lines are least-squares fits to Arrhenius and Cole–Davidson expressions, respectively.

(*ii*) *1050 nm.* At 1050 nm the decay of the absorption signal is similar to that seen at 1300 nm except that a component due to e_{sol}^- may remain, depending upon the temperature and the particular liquid used. After accounting for this the data can be analyzed exactly like the data at 1300 nm. As shown in the Arrhenius plot of Figure 5a,b the rate constants measured at 1050 nm in methanol, ethanol, 1-propanol, and 1-butanol are somewhat slower than those measured at 1300 nm. The analysis was done carefully and we feel that the differences are real and probably due to complex spectral shifts as e_t^- becomes solvated.[35]

(*iii*) *600 and 700 nm.* The formation of e_{sol}^- was studied at 600 and 700 nm. At 700 nm definitive values of τ_{sol} could not usually be obtained because the fraction of the signal, α, of the slow formation of e_{sol}^- was small (~0.2), but all of the data is consistent with eq II. In Figure 3 the absorption signal of e_{sol}^- in 1-propanol is compared to the calculated curve using α = 0.2 and τ_{sol} = 28 psec. It should be noted that a wide range of values for τ_{sol} (10–50 psec) is consistent with the experimental data.

A more accurate assessment of τ_{sol} was obtained at 600

nm at a variety of temperatures. At 600 nm α is larger and at cold temperatures a definite break can be seen between the fast $(1 - \alpha)$ and slow (α) components of the e_{sol}^- absorption signal. The rate constant, k_{sol}, was calculated from the slow formation component and is plotted in Figure 5a,b for methanol, ethanol, 1-propanol, and 1-butanol. The curves are from the 1300 nm data and those of Figure 4a,b; there is a good agreement between the two sets of data at the different wavelengths.

(c) *Formation Time of e_{sol}^- in Ethylene Glycol.* Because the signals were noisy accurate estimation of τ_{sol} could not be made by observing the formation of e_{sol}^- at 600 nm at room temperature. However, a signal due to e_t^- in ethylene glycol has been observed at 1000 nm by Lam and Hunt.[14] This signal decays at a rate faster than that for the decay of e_t^- in methanol and it is not possible to obtain an accurate rate constant even using a convolution technique.

However, we observe that at cold temperatures the relative absorptions of e_t^- in the different alcohols are the same to within ~30%; these absorption yields are also nearly independent of temperature provided a correction is made for the decay of the absorption during the fine structure pulse. Thus if we assume that the absorption yields are the same in methanol and ethylene glycol we estimate that e_t^- decays twice as fast in ethylene glycol as in methanol. Our crude estimate for the formation time of e_{sol}^- in ethylene glycol is $\tau_{sol} = 5 \pm 3$ psec.

Discussion

We have been studying electron solvation in highly polar liquids that form large numbers of intermolecular H bonds. As a result, these liquids are highly associated and it has been suggested that pure ethanol-d_1 exists primarily as a solution of tetramers.[36] From dielectric relaxation studies the activation energy, E_a, for H bond breakage ranges from 3.5 kcal/mol in methanol[37] to 5.6 kcal/mol in 1-butanol.[38] From our data (Figures 4 and 5) the apparent activation energy for solvation ranges from 2 to 3.5 kcal/mol near room temperature. Thus the solvation process cannot be explained by H-bond breakage alone, nor by viscosity alone, as solvation occurs in alcoholic glasses at 77 K[9,10,12] where the viscosity is very large. Certainly, electron solvation cannot be explained by a single process, as an Arrhenius plot of our data and that of Baxendale[34] shows a distinct curvature. The dielectric relaxation for molecular rotation should perhaps show a good correlation with τ_{sol}, which also involves molecular reorientation. However, there is a fundamental difference in the two processes; in dielectric relaxation the reorienting field is external to the medium while in electron solvation it is internal. Nonetheless, the dielectric relaxation time for molecular reorientation corresponds rather well to the time required for electron solvation.

As well a problem peculiar to ionizing radiation will be considered. The ions and electrons are not distributed randomly, but instead they are clustered along the tracks of the charged particles (spurs). A certain fraction of the energy expended is not expressed in ionization, but instead as local "hot spots" within the spurs. The effect of this temperature jump on the solvation processes will be estimated.

A. Temperature Jump. It was once thought that "point-heat" or local heating effects could account for some of the chemical changes induced by radiation,[39] but subsequent radiation chemical studies proved that ionization and excitation produce most of the chemical changes. In addition, it has been argued for low LET radiation where the energy is deposited in "spurs" or "blobs", that the temperature rise would neither be high enough nor last long enough to significantly alter the reaction rates.[40,41] However, since the solvation process has a rate constant of 10^{10} to 10^{11} sec^{-1} around room temperatures in the alcohols and takes place entirely in the spur, it is necessary to reconsider whether a temperature jump could affect the rate of solvation.

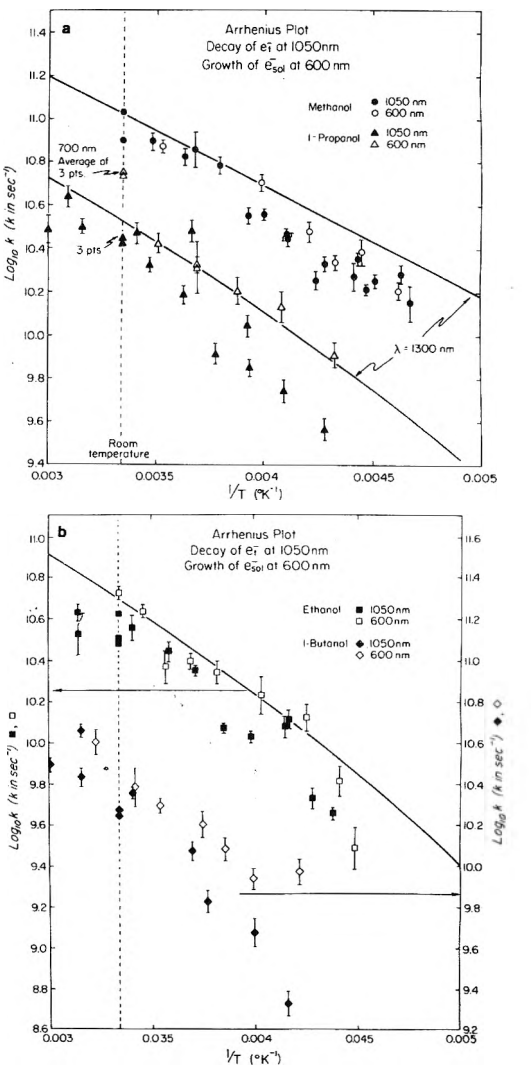

Figure 5. Arrhenius plot of the rate constants for the decay of e_t^- (solid symbols, measured at 1050 nm) and for the formation of e_{sol}^- (open symbols, measured at 600 nm). The curves are from Figure 4a,b.

Following the theoretical analysis of Magee et al.[40] and Mozumder,[41] we can obtain an estimate of the temperature jump. If we assume that the ionizing radiation deposits its energy in a spherical spur of radius r_0, the excess temperature $T_{ex}(t)$ relaxes in time, t, as given by[40,41]

$$T_{ex}(t) = \Delta T\{(1 + 4Dt/r_0^2)^{-3/2} \exp[-r^2/(r_0^2 + 4Dt)]\} \quad \text{(VI)}$$

where ΔT is the maximum temperature rise at the center of this spur and r is the distance from the center of the spur. The quantity D is the thermal diffusivity, given by

$$D = K/\rho C_v \quad \text{(VII)}$$

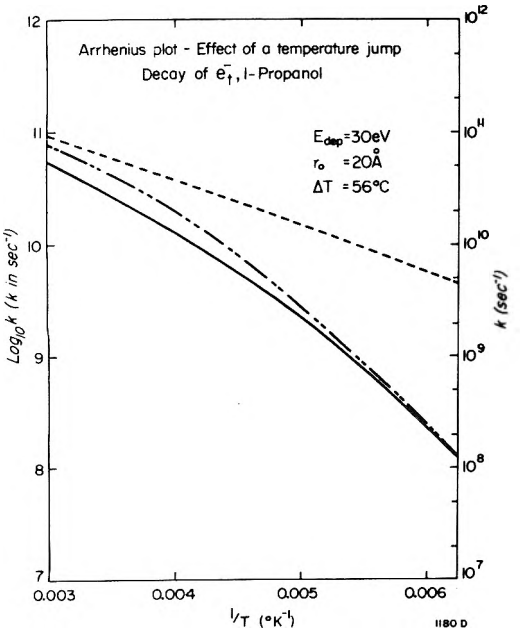

Figure 6. The effects of a time dependent temperature jump, $T_{ex}(t)$, in altering the effective rate constant, $k = 1/\tau_{eff}$ of $e_t^- \rightarrow e_{sol}^-$ in 1-propanol at the center of the spur ($r = 0$ in eq VI). The effective lifetime, τ_{eff}, is calculated from equation (X). The solid curve (—) is calculated using $T_{ex}(t) = 0$ (no temperature jump) and is the same as the curves in Figures 4a and 5a. The curve (– – –) is the effect of $T_{ex}(t)$, given by eq VI, when the maximum temperature jump is $\Delta T = 56°C$. The curve (- - -) for $T_{ex}(t)$ shows the effect of neglecting thermal diffusion; this is an upper limit to the effect of the temperature jump.

where K is the thermal conductivity, ρ is the density, and C_v the specific heat at constant volume. The maximum temperature rise at the center of the spur is therefore given by

$$\Delta T = E_{dep}/\pi^{3/2}r_0^3\rho C_v \qquad \text{(VIII)}$$

where E_{dep} is the energy deposited in the spur that becomes heat. The time required for the excess temperature to drop to one-half of its original value is given by the solution of

$$(1 + 4Dt/r_0^2)^{-3/2} = 1/2 \qquad \text{(IX)}$$

which for 1-propanol (using $K = 1.409 \times 10^{-3}$ J sec^{-1} cm^{-1} K^{-1}) is 15 psec. Depending upon the temperature sensitivity (apparent activation energy) of the reaction rates, a temperature jump could alter the rate of reactions, such as electron solvation, having reaction lifetimes from 10 to 100 psec.

Let us now consider the effect of the temperature jump on reaction 1. The differential equation for the rate of disappearance of e_t^- is

$$d[e_t^-]/dt = -k[e_t^-] \qquad \text{(X)}$$

where k, instead of being a constant as is usually the case, is now time dependent. If k shows an altered Arrhenius type temperature dependence of the Cole–Davidson type (eq V), the instantaneous value of k is given by combining eq V and VI

$$k(t) = A \exp[-E/R(T - T_0 + T_{ex}(t))] \qquad \text{(XI)}$$

where T is the ambient temperature.

A computer program was written to solve eq X with a time dependent rate constant given by eq XI. In order to compare reaction rates, an effective rate constant for the solution of eq X can be defined as $k_{eff} = 1/\tau_{eff}$, where τ_{eff} is the time required for $[e_t^-]$ to be reduced to $1/e$ of its original value. Unfortunately, accurate values for the spur parameters are not available because of the apparent discrepancies between the theoretical and observed decay of e_{aq}^- in spurs.[41-44] Mozumder[41] has made an estimate of $E_{dep} = 30$ eV and $r_0 = 20$ Å in H_2O. Using these values in eq VIII, for 1-propanol the maximum temperature at the center of the spur is $\Delta T = 56°C$, which would increase k considerably. This is illustrated in Figure 6, an Arrhenius plot of the effect of a 56°C temperature jump on the decay of e_t^- in 1-propanol. The lower curve is the one for 1-propanol used in Figures 4a and 5a. The middle curve is the effective rate constant, k_{eff}, for $\Delta T = 56°C$. At room temperature k_{eff} is ~50% greater than the rate constant for no temperature jump. Note that this suggests the formation time of e_{sol}^- produced by an ionizing beam could be considerably faster than for e_{sol}^- produced a photoionization process.[27] The upper curve is a calculation using $T_{ex}(t) = \Delta T = 56°C$ and is an upper limit to the effect of the temperature jump, since $T_{ex}(t) \leq \Delta T$ for all time and space.

It should be pointed out that the spur theories do not agree with the observed spur decays,[43] therefore the corrections to k_{sol} by the temperature jump might be incorrect. For example, Kupperman[44] has recently suggested that the spatial distribution of e_{aq}^- in the spur might be wrong. He estimates that the spur contains 6.7 ion pairs and has an initial radius, r_0, of 60 Å. Using this data, $E_{dep} \sim 95$ eV, but the temperature jump is only ~7°C; this temperature jump is so small that no corrections would be needed. Because of the uncertainty of the possible temperature jump correction, no such correction was applied to the observed rate constants in this paper.

B. The Solvation Time of the Electron in Liquid Alcohols. (a) Dielectric Relaxation. As background before considering the solvation process in detail it is useful to discuss the theory of dielectric relaxation. On a molecular level these two phenomena are similar and it might be expected that τ_{sol} should be correlated with one of the characteristic dielectric relaxation times.

When an electric field is applied to a dielectric medium, the resulting polarization is proportional to the dielectric constant, ϵ. If the electric field is changing rapidly, the polarization will lag behind the electric field and the dielectric constant now is a complex quantity. The imaginary part of ϵ is the dielectric loss factor, ϵ''. Frequency regions where the dielectric losses are nonzero are called dispersion regions.

Dielectric relaxation measurements have shown that there are three distinct dispersion regions in the normal alcohols for 1-propanol and its higher homologues.[38,45] Only two distinct dispersion regions have been observed in methanol and ethanol.[46,47] For each dispersion region, x, the real part of the dielectric constant, ϵ', can be described by

$$\epsilon' = \epsilon_{\infty x} - (\epsilon_{0x} - \epsilon_{\infty x})/(1 + \omega^2\tau_x^2) \qquad \text{(XII)}$$

where τ_x is the dielectric relaxation time in the region x. The dielectric constants, ϵ_{0x} and $\epsilon_{\infty x}$, are the limiting low and high frequency dielectric constants in each region.

The longest dielectric relaxation time, τ_1, is the time required for the breaking of intermolecular H bonds followed by reorientation of the liberated molecules. Most of the

TABLE I: Picosecond Solvation Times in Electrons, τ_{sol}, in Alcohols and Water at 293 K

	Observed results	Theoretical estimates					
		Dielectric relaxation times			Constant charge[i]		
	$\tau_{sol} = 1/k_{obsd}$	τ_1	τ_2	τ_3	$\tau_1' = \tau_1'$ $(\epsilon_{\infty 1}/\epsilon_{01})$	$(t_{ma}t_{mb})^{1/2}$/.	$\tau_r(\theta_0 = 80, N = 6)^k$
H_2O	<3[a] 2[b]	9.2[c]			0.2	0.2	
Methanol	10.7 ± 1[a]	52[d,e]	12.6[g]	1.4[d]	9	3.5	1.9
Ethanol	23 ± 2[a]	191[d,f]	16.4[g]	1.6[d]	30	8.6	7
1-Propanol	34 ± 3[a]	430[h]	22[h]	2.1[h]	81	18	17
1-Butanol	39 ± 5[a]	670[h]	27[h]	2.4[h]	127		

[a] This work. [b] Rentzepis et al, ref 27. [c] E. H. Grant, T. J. Buchanan, and H. F. Cook, *J. Chem. Phys.*, 26, 156 (1957). [d] Saxton et al, ref 46. [e] G. Barbenza, ref 37. [f] M. W. Sagal, *J. Chem. Phys.*, 36, 2437 (1962). [g] Extrapolation from the data of Garg and Smyth, ref 38. [h] Garg and Smyth, ref 38. [i] Calculated from the constant charge approximation (eq XIII) of ref 48 and 49. [j] Wave packet model (see text) of Schiller and Vass, ref 53. [k] Semicontinuum model (see text) of Fueki et al., ref 54.

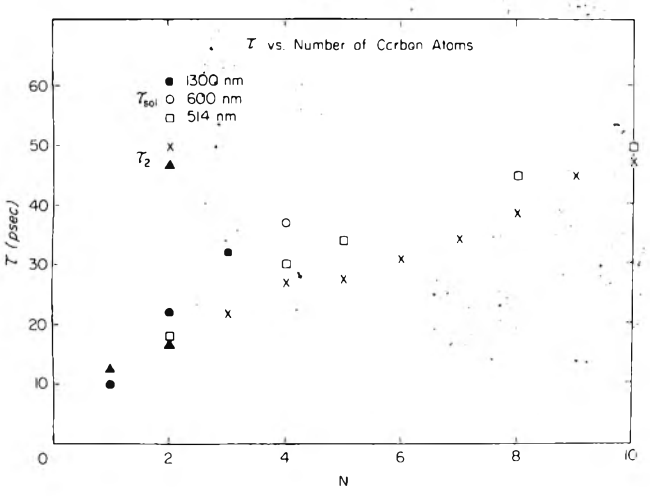

Figure 7. Electron solvation times, τ_{sol}, and dielectric relaxation times for molecular rotation, τ_2, vs. the number of carbon atoms in normal alcohols at 20°C. The values for τ_{sol} at 1300 nm (●) and at 600 nm (○) were obtained from this work while those at 514 nm (□) are from the work of Kenney-Wallace et al.[25] The points (×) are dielectric relaxation times, τ_2, from Garg and Smyth,[38] while the points (▲) are values for τ_2 extrapolated from the data of Garg and Smyth.[38]

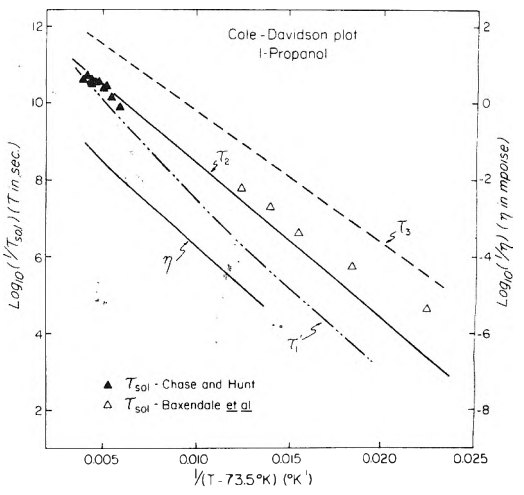

Figure 8. A Cole–Davidson plot of characteristic relaxation times in 1-propanol over a temperature range of 60 to −160°C. For τ_{sol}, the solid points (▲) are from this work and the open points (△) are from Baxendale.[34] Curves are drawn through the dielectric relaxation data from ref 33, 37, and 50 for τ_2 and τ_3 while τ_1' is the data for τ_1 modified according to eq XIII. The data for the viscosity, η, from ref 51 and 52 and uses the scale on the right side of the figure.

changes in the dielectric constant occur in the first dispersion region which implies that most of the molecules must break intermolecular H bonds before they can rotate. The intermediate relaxation time, τ_2, is the time required to reorient a monomer in the liquid. The shortest time, τ_3, is the reorientation time of OH dipoles.

When an electron is injected into a medium, the charge of the electron is thought to speed up the process of dielectric relaxation[48,49] and a dielectric relaxation time, τ', at constant charge (the "constant charge approximation") is given by

$$\tau_x' = \tau_x \epsilon_{\infty x}/\epsilon_{0x} \qquad \text{(XIII)}$$

where τ_x, $\epsilon_{\infty x}$, and ϵ_{0x} have been previously defined. The possible effect of the "constant charge approximation" is particularly important for τ_1; for the *other* dispersion regions, $\epsilon_{\infty x}/\epsilon_{0x}$ changes τ_x by less than a factor of 2. Because the alcohols are strongly associative liquids[36] it might be expected that τ_{sol} and τ_1' should be correlated.

(*b*) *Comparison of Dielectric Times and* τ_{sol}. The dielectric relaxation times, τ_1, τ_2, τ_3, and τ_1', are compared to τ_{sol} in Table I for H_2O and the first four primary alcohols. The values of τ_1 are much larger, and τ_3 much smaller, than τ_{sol}, while τ_2 is similar to τ_{sol}. As well, the modified dielectric relaxation time τ_1' of Schiller[48] and Mozumder[49] (see eq XIII) corresponds closely to the observed τ_{sol} for methanol and ethanol. However, the ratio, τ_1'/τ_{sol} increases as the number of carbon atoms in the alcohol also increases. Therefore, it appears that τ_{sol} is not closely correlated to τ_1'; for example, τ_1'/τ_{sol} in 1-butanol is 3.4.

The close relationship between τ_2 and τ_{sol} is emphasized in Figure 7, where τ_{sol} and τ_2 are compared for a number of primary alcohols. The values of τ_{sol} and τ_2 agree to within a factor of 1.5. The correlation between τ_{sol} and τ_2 at different temperatures is shown in Figure 8, in which the values of τ_{sol} in our work and the work of Baxendale[34] are plotted in a Cole–Davidson plot.[33] As well, dielectric relaxation times[33,37,50] τ_1, τ_3 and τ_1', and the viscosity,[51,52] η, are compared to τ_{sol}. This plot indicates that τ_{sol} corresponds closely to τ_2 over the 215 K temperature range. The modified time, τ_1', is considerably slower than τ_{sol}, particularly at the lower temperatures. One should note as well that viscosity data are parallel to the τ_{sol} data. Plots similar to Figure 8 are obtained for methanol, ethanol, and 1-butanol; there

are similar correlations between τ_2 and τ_{sol} over a wide range of temperatures.

The correspondence between τ_2 and τ_{sol} rather than τ_1' and τ_{sol} implies that the large amount of intermolecular H bonding present in these alcohols does not play a large part in the process of electron solvation. It is possible that this correspondence is just a coincidence and that the theory of the constant charge modification to τ_1 is correct in principle but not in its detailed application to the dynamics of solvation. It is more probable, however, that the intermolecular H bonds are broken very rapidly by the strong electric field of the electron, and that the rotation of the molecules limits the rates of the solvation processes. If this is true, the solvation time would be τ_2 (or possibly τ_2') as the alcohol molecules reorient around the electron.

Wave Packet Model. In this model by Schiller and Vass[53] a moving electron polarizes the liquid to form a potential well in which the electron becomes self-trapped. The electron is described by a "roof" shaped wave packet. Upper, t_{mb}, and lower, t_{ma}, estimates for τ_{sol} are combined to give the intermediate value $(t_{ma}t_{mb})^{1/2}$, as listed in Table I. It can be seen that τ_{sol} is always larger than $(t_{ma}t_{mb})^{1/2}$ but considering the approximations made in the model the agreement is rather good. In Table I of ref 53 it can be seen that τ_{sol} and $(t_{ma}t_{mb})^{1/2}$ also agree to within a factor of 2–4 at colder temperatures except for methanol. Overall, this model predicts τ_{sol} with reasonable accuracy.

The Fueki–Feng–Kevan Semicontinuum Model. In the Fueki–Feng–Kevan semicontinuum model[54] the medium surrounding the electron is divided into a shell of N ($N = 4$ or 6) symmetrically oriented solvent molecules, and the molecules surrounding the first shell are treated as a continuous dielectric medium. During solvation, the electron reorients the dipoles of the molecules in the first shell by a short-range charge dipole attractive potential and polarizes the surrounding medium by a long-range polarization potential.

An estimate of τ_{sol} was made by calculating the relaxation time, τ_r, for orientation of the dipoles in the first shell using the classical formulation of Debye.[55] The rate of dipole orientation is limited by the microscopic viscosity, η, of the alcohol; in the model it is then assumed that η can be approximated by the microscopic viscosity.

The dipoles are originally oriented at an angle, θ_0, to the central electron. The times, τ_r, for dipole orientation are given in Table I for $\theta_0 = 80°$. For methanol, ethanol, and 1-propanol τ_r is faster than τ_{sol} by factors of 5, 3, and 2, respectively. It should be noted that the two theoretical estimates, $(t_{ma}t_{mb})^{1/2}$ and τ_r, are in very good agreement. In Figures 1–3 of ref 54 the temperature dependence of τ_r is compared to experimental data. The curves for 1-propanol fall on most of the data points and reproduce the form of the curvature shown in Figure 4a of this paper. The experimental data for methanol and ethanol do not fall on the curves for τ_r. In the case of methanol τ_r is much shorter than the experimental values of τ_{sol}. In general the curves for τ_r predict the form of the temperature dependence observed for τ_{sol} but cannot as yet always predict the values of τ_{sol}. Modifications taking into account the change of cavity radius around the electron as the dipoles orient, and polarization of the surrounding continuum do not appreciably alter the predictions of the semicontinuum model.[56] It would seem to us that it is necessary to take into account dipole–dipole interactions before a better agreement between theory and experiment can be reached.

Conclusions

(1) The excellent correlation between the rates of decay of e_t^- and of formation of e_{sol}^- is strong evidence that e_t^- really is the immediate precursor of e_{sol}^-.

(2) The solvation time of the electron is not correlated with the dielectric relaxation times τ_1, for H bond breakage, and τ_3, for OH dipole rotation. When τ_1 is modified to account for the charge of the electron, the modified time, τ_1', agrees with τ_{sol} for methanol and ethanol. However, τ_1' is considerably longer than τ_{sol} for the larger alcohols. This implies that the rate of electron solvation is not limited by the rate of H bond breakage.

(3) The dielectric relaxation time for molecular rotation, τ_2, shows a very good correspondence to τ_{sol} over a wide range of temperatures for the alcohols. Thus molecular reorientation, rather than thermal de- and retrapping or trap-to-trap tunneling of the electron, appears to be the mechanism of electron solvation.

Acknowledgments. The authors thank A. Worthington, D. Bazett-Jones, and M. O'Loughlin for their help in doing the experiments and H. Yee as a summer student for his computer programming. We acknowledge some very useful comments during the preparation of this paper from Drs. G. A. Kenney-Wallace and J. H. Baxendale. Dr. A. D. Singh, Whiteshell Nuclear Research Establishment, Atomic Energy of Canada Limited, arranged the loan of the D_2O. We also acknowledge the continuing help of Mr. T. Horrigan and the staff of the Linac Laboratory of the University of Toronto. The experimental work was supported by the Medical Research Council of Canada and the National Cancer Institute of Canada. Financial support for the operation of the Linear Accelerator at the University of Toronto was provided by the National Research Council of Canada.

Appendix

Because the kinetics that were studied were very rapid it was necessary to be able to compare our experimental results with theoretical calculations which take into account the complexities of the SPR system. To do this computer programs, similar in principle to those previously used,[18] were written to generate theoretical curves of optical absorption vs. time which could be directly compared to our picosecond kinetic traces.

In these calculations the total response function (the fine structure pulse *shape*, $s(t)$) of the SPR system is generated from the individual system response functions and then convoluted[57] with the radiation chemistry that occurs in the cell, the result being the radiation chemical response function of the SPR system to a single fine structure electron pulse (the fine structure pulse chemical *response* function, $r(t)$). Because the electron macropulse consists of a train of fine structure pulses, the overall absorption is the sum of the absorptions of the fine structure pulses, each of which is a different age. To generate the overall response of the system the individual fine structure pulses response functions must, except under certain circumstances (see below), be appropriately summed.

Several factors contribute to the fine structure pulse shape but some of these are not important. The dose delivered to the sample was previously assumed to vary linearly from 1.2 to 0.8 (in relative units) from the front to the back of the cell.[18] It was found that this dose distribution was in-

distinguishable from a uniform dose distribution and therefore the latter was routinely used. The electronic response time, τ_{elec}, depends upon the scanning rate of the light delay mirrors and the smoothing circuit time constant.[18,23] Generally, τ_{elec} is less than the equivalent of 2 psec and for particularly sensitive experiments, such as the formation of e_{aq}^-, τ_{elec} was reduced to the completely negligible value of 0.3 psec.

The important contributions to the fine structure pulse shape are as follows.

(1) The electron distribution is assumed to be a Gaussian of the form $\exp(-t^2/2\sigma^2)$.

(2) The Čerenkov analyzing light pulses are produced by the electron pulses and thus have the same shape. When the two Gaussians are convoluted the σ^2 add and the combined response function is also Gaussian. We shall refer to this function as the *fine* structure pulse function

$$f(t) = \frac{1}{2\sigma\sqrt{\pi}} \exp(-t^2/4\sigma^2) \qquad \text{(XIV)}$$

as shown in Figure 9.

(3) A photon takes T' psec longer than an electron to traverse the sample. This "desynchronization time" is

$$T' = (n - 1)(l/c) \qquad \text{(XV)}$$

where n is the index of refraction of the sample, l the path length of the sample, and c the speed of light. For water in a 2-cm cell $T' = 22$ psec. Thus an instantaneous event is spread out to one over T' psec. The *desynchronization* response function is:

$$d(t) = 1 \qquad 0 < t < T' \qquad \text{(XVI)}$$
$$= 0 \qquad t > T'$$

This function is also shown in Figure 9.

The response functions $f(t)$ and $d(t)$ can now be convoluted together to give the fine structure pulse *shape* $s(t)$ as shown in Figure 9. The function $s(t)$ can now be combined with the *chemical* response to irradiation $c(t)$ to give the overall *response* to a single fine structure pulse, $r(t)$, also shown in Figure 9. The chemical response function $c(t)$ is merely the concentration of the observed species as a function of time. For example, for a simple first-order decay of a species A the concentration of A at any given time is

$$[A(t)] = [A(0)] \exp(-kt) \qquad \text{(XVII)}$$

Thus the chemical response function is

$$c(t) = c(0) \exp(-kt) \qquad \text{(XVIII)}$$

A distinct advantage of this technique over the one we previously used is that the function $c(t)$ need not be exponential. The differential equations for the concentrations of the appropriate species can always be solved numerically, thus $c(t)$ and $r(t)$ can be generated for any arbitrary chemical system.

The electron macropulse from the University of Toronto Linear Accelerator consists of a series of fine structure electron pulses, spaced 350 psec apart, which generate the absorbing species in the sample cell and the Čerenkov analyzing light by which these species are observed, as shown in Figure 2 of ref 18. To obtain the true absorption signal it is necessary to sum the concentrations of the absorbing products and to account for the delay of the analyzing light flashes. However, in order to determine rate constants it was not necessary to do this summation, since we observed

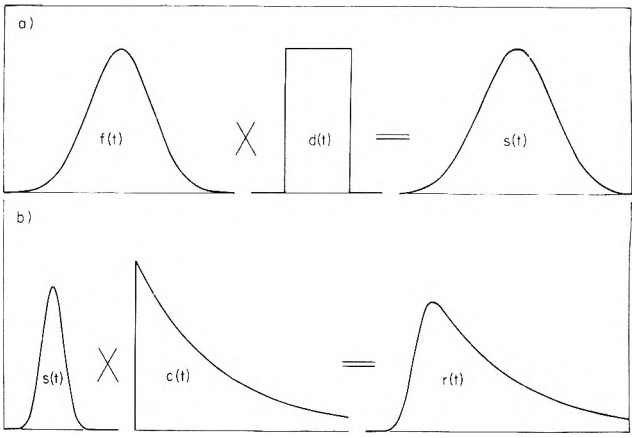

Figure 9. (a) The fine structure electron–Cerenkov pulse shape, f(*t*), with $\sigma = 4.0$ psec, convoluted with the desynchronization response function, d(*t*), for a 1-cm irradiation cell ($T = 12$ psec) to give the fine structure pulse shape, s(*t*). (b) The fine structure pulse shape, s(*t*), convoluted with the chemical response function, c(*t*), for a first-order decay to give the total response to a single fine structure pulse.

first-order kinetics (see eq I) and the sum of a number of exponentials having the same lifetime is still an exponential. It should also be noted that the shape of the absorption buildup is not affected by the summation.

Rate constants were obtained from semilog plots of absorption (or absorbance) vs. time. Although the 10–90% *response* time of the SPR system is about 18 psec with a 1-cm path length irradiation cell, the time *resolution* is somewhat less and depends upon the width of the fine structure pulse.[18] This width is related to σ in eq III and XIV.[32] A value of σ was obtained from the shape of the absorption buildup of e_{aq}^-. For values of τ less than 20 psec, σ and τ were used to calculate $r(t)$ which was then compared to the experimental data. Using this technique we could obtain accurate values for τ as short as 10 psec.

Supplementary Material Available. The rate constants for the decay of e_t^- and for the formation of e_{sol}^- illustrated in Figures 4 and 5, and the parameters of the curves in Figures 4 and 5 will appear following these pages in the microfilm edition of this volume of the journal. Photocopies of the supplementary material from this paper only or microfiche (105 × 148, 24× reduction, negatives) containing all of the supplementary material for the papers in this issue may be obtained from the Business Office, Books and Journals Division, American Chemical Society, 1155 16th St., N.W., Washington, D.C. 20036. Remit check or money order for $4.50 for photocopy or $2.50 for microfiche, referring to code number JPC-75-2835.

References and Notes

(1) Studentship, Medical Research Council of Canada.
(2) In this paper, e^-, is defined as a general class of electrons which have energies below the lowest excited states of the molecules in the medium but are not localized in traps. The e^- includes $e^-_{subexcitation}$, $e^-_{epithermal}$, $e^-_{thermal}$, e^-_{dry}, $e^-_{quasi\text{-}free}$ and e^-_{mobile}. The trapped electron, e^-, is a partially solvated electron localized in a shallow trap and is equivalent to the "damp" electron, e^-_{damp}. The solvated electron, e_{sol}^- or e_s^-, is an electron localized in a deep trap. In water e_{sol}^- is called a hydrated electron, e_{aq}^-.
(3) See, for example, E. J. Hart and M. Anbar, "The Hydrated Electron", Wiley-Interscience, New York, N.Y., 1970.
(4) See, for example, *Adv. Chem. Soc.*, **No. 50** (1965).
(5) (a) L. Kevan in "Advances in Radiation Chemistry," Vol. 4, M. Burton and J. L. Magee, Ed., Wiley-Interscience, New York, N.Y., 1974. (b) L. Kevan, *Int. J. Radiat. Phys. Chem.*, **6**, 297 (1974).
(6) T. Higashimura, *Annu. Rep. Res. Reactor Inst. Kyoto Univ.*, **6**, 38 (1973).
(7) H. Hase, T. Warashina, M. Noda, A. Namiki, and T. Higashimura, *J*

Chem. Phys., **57**, 1039 (1972).
(8) T. Higashimura, M. Noda, T. Warashina, and H. Yoshida, *J. Chem. Phys.*, **53**, 1152 (1970).
(9) J. T. Richards and J. K. Thomas, *J. Chem. Phys.*, **53**, 218 (1970).
(10) (a) L. Kevan, *Chem. Phys. Lett.*, **11**, 140 (1971); (b) L. Kevan, *J. Chem. Phys.*, **56**, 838 (1972).
(11) (a) J. H. Baxendale and P. Wardman, *Nature (London)*, **230**, 449 (1971); (b) J. H. Baxendale and P. Wardman, *J. Chem. Soc., Faraday Trans. 1*, **69**, 584 (1973).
(12) N. V. Klassen, H. A. Gillis, G. G. Tether, and L. Kevan, *J. Chem. Phys.*, **62**, 2474 (1975).
(13) L. Gilles, J. E. Aldrich, and J. W. Hunt, *Nature (London)*, **243**, 70 (1973).
(14) K. Y. Lam and J. W. Hunt, *J. Phys. Chem.*, **78**, 2414 (1974).
(15) W. H. Hamill, *J. Phys. Chem.*, **73**, 1341 (1969).
(16) H. Ogura and W. H. Hamill, *J. Phys. Chem.*, **78**, 504 (1974).
(17) R. K. Wolff, M. J. Bronskill, and J. W. Hunt, *J. Chem. Phys.*, **53**, 4211 (1970).
(18) J. E. Aldrich, M. J. Bronskill, R. K. Wolff, and J. W. Hunt, *J. Chem. Phys.*, **55**, 530 (1971).
(19) R. K. Wolff, J. E. Aldrich, T. L. Penner, and J. W. Hunt, *J. Phys. Chem.*, **79**, 210 (1975).
(20) K. Fueki, D. Feng, and L. Kevan, *J. Chem. Phys.*, **56**, 5351 (1972).
(21) M. Tachiya and A. Mozumder, *J. Chem. Phys.*, **60**, 3037 (1974).
(22) L. M. Dorfman, *Adv. Chem. Ser.*, **No. 50**, 36 (1965).
(23) M. J. Bronskill, R. K. Wolff, and J. W. Hunt, *J. Chem. Phys.*, **53**, 4201 (1970).
(24) G. Beck and J. K. Thomas, *J. Phys. Chem.*, **76**, 3856 (1972).
(25) G. A. Kenney-Wallace and C. D. Jonah, submitted to *J. Chem. Phys.*
(26) G. A. Kenney-Wallace and D. C. Walker, *J. Chem. Phys.*, **55**, 447 (1971).
(27) P. M. Rentzepis, R. P. Jones, and J. Jortner, *J. Chem. Phys.*, **59**, 766 (1973).
(28) M. J. Bronskill, W. B. Taylor, R. K. Wolff, and J. W. Hunt, *Rev. Sci. Instrum.*, **41**, 333 (1970).
(29) J. E. Aldrich, P. Foldvary, J. W. Hunt, W. B. Taylor, and R. K. Wolff, *Rev. Sci. Instrum.*, **43**, 991 (1972).
(30) R. S. Dixon and V. J. Lopata, *J. Phys. Chem.*, **79**, 185 (1975).
(31) G. S. Mavrogenes, C. Jonah, K. H. Schmidt, S. Gordon, G. Tripp, and L. W. Coleman, in press.
(32) The time resolution of the SPR system is determined by the fine structure electron–Cerenkov pulse shape. $f(t)$. The full-width half-maximum (fwhm) of $f(t)$ is equal to $4\sigma\sqrt{\ln 2} = 3.33\sigma$.
(33) R. H. Cole and D. W. Davidson, *J. Chem. Phys.*, **20**, 1389 (1952).
(34) J. H. Baxendale, private communication.
(35) As e_t^- becomes more deeply trapped during solvation, the wavelength of its absorption should shift toward intermediate wavelengths. The number of electrons, e_{int}^-, in traps of intermediate depth depends on the rate of $e_t^- \rightarrow e_{int}^-$ and the rate of $e_{int}^- \rightarrow e_{sol}^-$.
(36) A. N. Fletcher, *J. Phys. Chem.*, **76**, 2562 (1972).
(37) G. Barbenza, *J. Chim. Phys. Phys. Chim. Biol.*, **65**, 906 (1968).
(38) S. K. Garg and C. P. Smyth, *J. Phys. Chem.*, **69**, 1294 (1965).
(39) F. Dessauer, *Z. Phys.*, **20**, 288 (1923).
(40) J. L. Magee, K. Funabashi, and A. Mozumder, *Nippon Isotope Kaigi Hobunshu*, **6**, 755 (1965).
(41) A. Mozumder in "Advances in Radiation Chemistry", Vol. 1, M. Burton and J. L. Magee, Ed., Wiley-Interscience, New York, N.Y., 1969.
(42) (a) A. Kupperman in "Radiation Research", G. Silini, Ed., North-Holland Publishing Co., Amsterdam, 1967. (b) H. A. Schwarz, *J. Phys. Chem.*, **73**, 1928 (1969).
(43) J. W. Hunt, R. K. Wolff, M. J. Bronskill, C. D. Jonah, E. J. Hart, and M. S. Matheson, *J. Phys. Chem.*, **77**, 425 (1973).
(44) A. Kupperman, personal communications.
(45) C. Brot and M. Magat, *J. Chem. Phys.*, **39**, 841 (1963).
(46) J. A. Saxton, R. A. Bond, G. T. Coats, and R. M. Dickinson, *J. Chem. Phys.*, **37**, 2132 (1962).
(47) F. X. Hassion and R. H. Cole, *J. Chem. Phys.*, **23**, 1756 (1955).
(48) (a) R. Schiller, *J. Chem. Phys.*, **43**, 2760 (1965); (b) *Ibid.*, **47**, 2278 (1967); (c) *Chem. Phys. Lett.*, **5**, 176 (1970).
(49) A. Mozumder, *J. Chem. Phys.*, **50**, 3153 (1969).
(50) D. W. Davidson and R. H. Cole, *J. Chem. Phys.*, **19**, 1484 (1951).
(51) "Handbook of Chemistry and Physics", 51st ed, R. C. Weast, Ed., The Chemical Rubber Co., Cleveland, Ohio, 1970, p F37.
(52) M. R. Carpenter, D. B. Davies, and A. J. Matheson, *J. Chem. Phys.*, **46**, 2451 (1967).
(53) R. Schiller and S. Vass, *Int. J. Radiat. Phys. Chem.*, **6**, 223 (1974).
(54) K. Fueki, D. Feng, and L. Kevan, *J. Phys. Chem.*, **78**, 393 (1974).
(55) P. Debye, "Polar Molecules", Dover Publications, New York, N.Y., 1929, p 81.
(56) K. Fueki, private communications.
(57) R. G. Brown and J. W. Nilsson, "Introduction to Linear Systems", Wiley, New York, N.Y., 1962.

Discussion

L. KEVAN. (1) How well do the electron decay times in the infrared correlate with the electron growth times in the visible? Does extension of the initial infrared band of the partially solvated electron into the visible cause problems in evaluating the growth kinetics?

(2) Fueki, Feng, and Kevan's calculations of electron solvation times only include molecular dipole rotation without specifically considering H-bond breaking, yet the calculations are in good agreement with your results. The important point seems to be that the calculation reproduces the non-Arrhenius temperature dependence without including H-bond breaking. Does this affect your inclusion of H-bond breaking?

J. HUNT. (1) In the main text of this paper, a figure compares the observed decay of e_t^- at 1300 and 1050 nm and the formation time of e_{sol}^- at 600 nm. These values at 1300 and 600 nm are quite comparable. At 1050 nm the observed values are about 30% slower. We were expecting larger differences between 1300 and 600 nm, as the peak of the spectrum shifted from infrared to visible wavelengths. This is not observed.

(2) I agree that Fueki, Feng, and Kevan do not specifically mention it in their theory, but the formulation implies that the bulk viscosity η of the solvent is limited by the H-bond breakage. I feel that the rotation of the molecules around the electron must also be considered, particularly around room temperature.

J. CHASE. I would like to point out that there is some evidence from the work of Higashimura et al. for an intermediate species of partially trapped electrons. When γ-irradiated ethanol glass is warmed slowly from 4 to 77 K the absorption spectrum shows a series of "bumps" as it shifts from that of e_t^- to that of e_{sol}^-. These "bumps" are attributed to electrons in various states of solvation. The photobleaching studies carried out at 4 K clearly showed an intermediate electron species peaking at about 1000 nm. An intermediate species might be expected to have somewhat different kinetics and this could account for the fact that the rate of solvation observed at 1050 nm is slightly slower than the rates at 600 and 1300 nm.

R. HOLROYD. In the alcohols is there a formation of the *solvated* electron occurring fast within the time resolution of your apparatus?

J. HUNT. You are correct that the process

$$e^- \xrightarrow{k_{sol}} e_{sol}^-$$

is faster than the ~18 psec time response of the system, i.e., the value of τ_{sol} = 9.6 psec for methanol. These values were obtained by comparing the H_2O formation times, making use of the time desynchronism for a 1 cm cell, a Gaussian distribution for the electron micropulse (σ = 4.4 psec) and an identical pulse width for the Čerenkov light pulse. These factors were convoluted to obtain an excellent agreement to the data in water. Then the same factors were convoluted with first-order decay of e_{sol}^- in methanol at 1300 nm. The curve which agrees best with the observed absorption signals, both in shape and amplitude, was used to obtain the τ_{sol} values.

B. WEBSTER. Concerning the relaxation time, are we referring to macroscopic relaxation $\sim 10^{-10}$ sec *or* microscopic times. For the alcohols there are at least three relaxation times observed corresponding for example to molecular rotation and O–H bond motion. The development of theoretical models must allow for the time scale of events. Statistical fluctuations will give rise to shallow traps in the liquid at early times, prior to say $\sim 10^{-12}$ sec.

J. HUNT. I agree with this comment that three relaxations have been observed in dielectric relaxation studies. Therefore three different trap depths could also be envisioned. At the present time, only one shallow trap has been observed in alcohols, and until fast pulse radiolysis studies at 4 K have been done, we will not know whether intermediate traps will also occur.

R. CATTERALL. The attempt to identify different solvation steps for electrons during the solvation process is surely oversimplifying the matter. If the initial trapping site is a fortuitous, statistically controlled, inhomogeneity in the liquid, the relaxation of this site to the deep solvated electron should surely be a nearly continuous process rather than a stepwise one. In this context it is important to remember that the relaxation of several different molecules is involved.

J. HUNT. Your point is quite valid, since several molecules should be considered as they relax around the electron. However, when different well-spaced relaxations are considered, quite different processes are expected as the electrons relax from $e^-_{quasi\ free} \rightarrow e^-_{trap} \rightarrow e_{sol}^-$ as mentioned above. At the present time, only the latter processes are observed.

J. JORTNER. Regarding the interpretation of your detailed experimental data on the relaxation of the "initially" trapped electron to the normal solvated state, there is an interesting theoretical problem regarding the roles of short-range and long-range reorganization of the medium. In the theoretical studies of the energetics of solvated electrons we separate the short-range interactions with the first coordination layer from long-range dipolar interactions, which as N. Kestner has discussed, persist at least to distances exceeding 100 Å for the trapping center. I thought at one time that the long-range dipolar polarization field relaxes faster than the short-range structure, as the former is related to τ_2 (rotational relaxation) while the former is related to τ_1. However, your data indicate that the experimental solvation time is $\sim\tau_2$, whereupon short-range configurational changes in a strong electric field result in an enhanced breaking of hydrogen bonding, as compared to the situation in the normal liquid.

J. HUNT. As you suggest, there might be some conflict between the short-range and long-range dipole interaction, particularly in the early events in the relaxation process, τ_1 and τ_2, for the H-bond breakage and molecular rotation, respectively. The fair agreement between τ_2 and the observed formation suggest that molecular rotation limits the formation times of e_{sol}^-. However, we must be careful about making large claims about the relationship between τ_2 in different solutions, since different models (i.e., Shiller and Vass, and Fueki et al) both indicate a similar curved Arrhenius plot. Therefore, there is fair agreement between the observed and theoretical data.

J. JORTNER. I would like to comment on your definition of a "dry" electron, which is somewhat misleading, as far as electrons in fluids are concerned. In this context we have to consider two physical aspects of the problem, the electron–medium interaction and the configurational changes in the solvent induced by the excess electron. Your "dry" electron does not modify the solvent structure but does interact with the solvent. This is what we have referred to as the "quasi-free" excess electron state. In liquid Ar the electron remains "quasi-free" but the energetics is drastically modified and it is inappropriate to refer to the electron as "dry".

J. HUNT. I totally agree with Dr. Jortner's comment regarding the interactions between electrons and the medium. However, I have lumped all of the electrons e^-_{dry}, $e^-_{thermal}$, e^-_{subex}, $e^-_{quasi\text{-}free}$, and e^-_{mobile} together as e^-_{dry}, in order to differentiate them from e_t^-. In the literature, the definition of e^-_{dry} is purposely very vague; it is just an operational definition in an attempt to explain the fast electron scavenging process. At the present time the reactions might occur in any of the general e^-_{dry} groups.

N. KLASSEN. I propose a search for weakly trapped electrons in water which are transformed into deeply trapped electrons. In the pulse radiolysis of LiCl–H_2O glass at 76 K the initial spectrum of e_t^- has considerable intensity at 900 nm but this absorption, on the high wavelength side of the spectrum, decays on a time scale in which no change is observed at λ_{max} (625 nm), i.e., the trapped electrons which absorb at 900 nm do not become deeply trapped.

J. HUNT. Our data indicate that, in alcohols, the electrons in the infrared wavelength band decrease as the visible band increases. I believe that the process is very complex in glasses. For example, Hase et al., *J. Chem. Phys.*, 57, 1039 (1972), has found a lower yield of electrons when the sample was warmed slowly from 77 K. When the sample was warmed quickly, the yield of electrons are constant. During this time, the infrared absorption band (e_t) was shifted to visible wavelengths (e_{sol}^-) in agreement with our picosecond studies.

Pulse Radiolysis Study of Solvated Electrons in Water–Ethanol Glasses at 76 K. Structure of the First Solvation Shell around the Electron

Larry Kevan

Department of Chemistry, Wayne State University, Detroit, Michigan 48202 *(Received June 30, 1975)*

The initial spectrum of the trapped electron at ≤200 nsec in anhydrous C_2D_5OD glasses at 76 K has λ_{max} ~1300 nm and shifts with time to a stable position near 540 nm. The presence of water in C_2D_5OD–D_2O glass causes a large increase in the visible portion and a decrease in the infrared portion of the initial spectrum, suggesting that the initial time scale for the solvation process is more rapid when a water molecule is in the first solvation shell of the electron, or that water induces specific structural arrangements of shallow trapping molecular configurations. From the effect of water on the spectra, a simple analysis indicates that there are four molecules in the average first solvation shell of the electron.

Introduction

Solvated electrons are stably trapped in glassy ethanol at 77 K and have a broad structureless absorption band peaking at 540 nm.[1] If 10–20 mol % of water is added to the ethanol, the absorption band remains structureless but its maximum shifts slightly (10–15 nm) toward the red. So the effect of water on the stable spectra of trapped electrons in alcohols is small. Transient spectra of partially solvated electrons in ethanol and deuterated ethanol glasses have been observed by pulse radiolysis at 76 K. The "initial" spectra at 200 nsec after the start of an ionizing electron pulse show a broad structureless absorption band peaking near 1300 nm.[2] These spectra shift to the stable spectra peaking at 540 nm on a microsecond to millisecond time scale. This spectral change reflects the reorientation of surrounding molecular or bond dipoles around the electron in the process of solvation. Some structure seems to be present in the partially relaxed spectra which may result from specific geometrical orientations of the first solvation shell molecules.

In this work we find that the presence of 10–20 mol % of water in an ethanol glass has a dramatic effect on the "initial" spectrum of the trapped electron, suggesting that the time scale for the solvation process is more rapid when a water molecule is in the first solvation shell of the electron or that water induces specific structural arrangements of shallow trapping molecular configurations.

One unknown in the electron solvation process and in the structure of the solvated electron is the number of alcohol molecules in the first solvation shell. An analysis of the water effect on the electron spectra mentioned above allows one to obtain an estimate of this number.

Experimental Section

Anhydrous C_2H_5OD and C_2D_5OD from Merck Sharpe and Dohme and D_2O from Stohler Isotope Chemicals were used as received. All samples were degassed several times by the freeze–pump–thaw method, pumped on at 195 K, and distilled into a Suprasil irradiation cell before being sealed off. The experimental technique and pulse radiolysis apparatus have been described.[2] A linear accelerator produced 40- to 130-nsec pulses of 35-MeV electrons at 3–12 krad per pulse. Spectra were measured at 76 K in cooled liquid nitrogen.

Results and Discussion

Figure 1 shows the effect of water on the "initial" spectra of trapped electrons in ethanol glass measured 130 nsec after the start of a 100-nsec pulse. Although deuterated ethanol is used, previous results[2] demonstrate that the same behavior is expected in protiated systems. In anhydrous ethanol the spectrum is structureless with a long tail toward higher energy. When water is added, definite structure is seen in the spectra which appears to be approximately characterized by an additional band in the 600–800-nm region. All of the spectra in Figure 1 change with time until they reach about the same stable, structureless absorption with a maximum near 540 nm. To test whether the "initial" spectra shown in Figure 1 were really "initial", a 40-nsec pulse was used. Changes of less than 10% were seen in the 700–1400-nm range in the C_2D_5OD + 11 mol % D_2O mixture over the period 60 nsec to 160 nsec after the start of the 40-nsec pulse. Thus, there does not appear to be a more rapid relaxation process taking place in the ethanol–water mixtures than in pure ethanol.

The different spectra in Figure 1 appear to be "initial" and decay little over the first 200 nsec after the start of a pulse, but then all decay to the same final spectrum. Figure 2 shows that the rate of spectral shift, as studied by decay at λ >1300 nm is quite similar in anhydrous ethanol and ethanol–water mixtures. However, there still could be a phase of initial rapid relaxation for an electron with at least one water molecule in its first solvation shell that occurs before our earliest observation and which does not occur for electrons with only ethanol molecules in their first solvation shell.

The structure in the spectra seems to imply that the distribution of shallow trapping, molecular configurations is altered by addition of water to ethanol. The addition of water to ethanol does result in structural reordering of the hydrogen bonds as revealed by a variety of physical measurements, but the specific structural configurations remain unknown.[3] It appears that an electron with at least one water molecule in its first solvation shell has an initial absorption farther toward the visible than does an electron surrounded only by ethanol molecules. Below, an analysis is given which suggests that there are four molecules (ethanol and/or water) in the first solvation shell of the electron.

If the spectrum at >1300 nm represents e_t^- with no

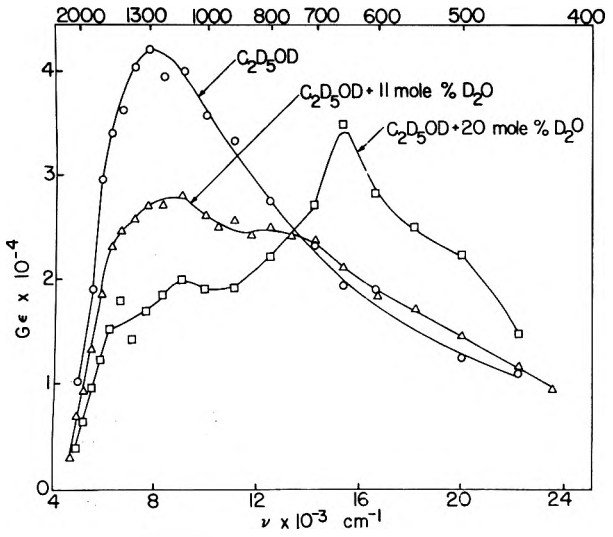

Figure 1. Initial spectra of trapped electrons in C_2D_5OD and C_2D_5OD–D_2O glasses at 76 K measured 130 nsec after the start of a 100-nsec pulse.

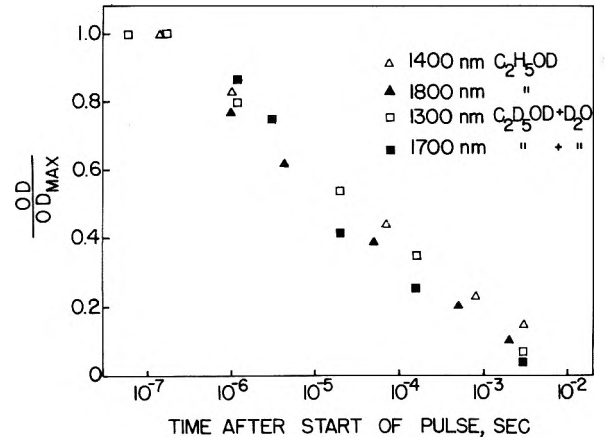

Figure 2. Decay of trapped electron absorption in the infrared for C_2H_5OD and 89 mol % C_2D_5OD–D_2O glasses at 76 K.

water molecules in its first solvation shell, it appears possible to calculate the number of ethanol molecules in the first solvation shell by use of the information in Figure 1. The calculation involves the following assumptions: (i) trapped electrons in a configuration containing a water molecule in the first solvation shell do not absorb at >1300 nm; (ii) each molecule has an equal chance of being in the first solvation shell of a molecular configuration that stabilizes an electron. Then, the absorption at >1300 nm decreases linearly with the probability that the first solvation shell of n molecules does not contain a water molecule. Figure 3 shows the predicted linear decrease at 1300 and 1670 nm. The probability that the first solvation shell contains n_a alcohol molecules and $n_w = n - n_a$ water molecules, given that there are n molecules in the first solvation shell, is

$$P(n_a) = \frac{n!}{n_a! n_w!} X^{n_w}(1 - X)^{n_a} \qquad (1)$$

where X is the mole fraction of water.[4] From this we calculate the probabilities for n = 3, 4, 5 at the water mole fractions of 0.11 and 0.2. The probabilities for $n_a = n$ are shown in Figure 3 where the vertical coordinate is given by $(G\epsilon)_\lambda$ for each water mole fraction. The fit indicates that the first solvation shell contains an average of four mole-

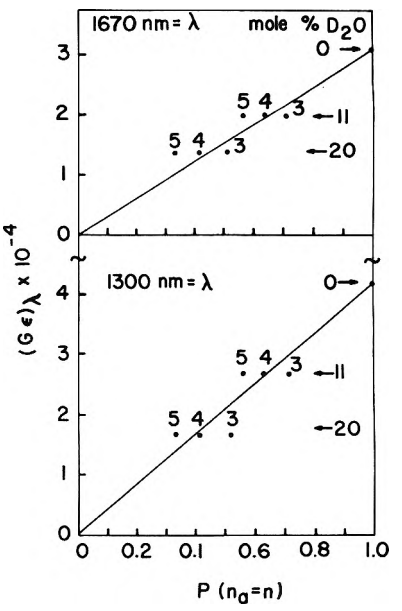

Figure 3. Plot of $(G\epsilon)_\lambda$ for trapped electrons at different mole percent D_2O in C_2D_5OD glass vs. the probability that all n molecules in the first solvation shell are ethanol molecules. Points are calculated for n = 3, 4, and 5 as indicated. The best fit for n = 4 indicates four molecules in the first solvation shell of e_t^-. See text for details.

cules per shell. This result supports theoretical calculations in which the first solvation shell of a trapped electron is often assumed to consist of four point dipoles arranged tetrahedrally.[5] Although the assumptions in this calculation may be criticized, we feel that the method is potentially useful until better experimental estimates of n in alcohol glasses become available. Analysis of electron spin–echo modulation shows promise of providing such information in the future.[6,7]

Acknowledgment. We thank the Energy Research and Development Agency for partial support of this work under Contract E(11-1)-2086, and Drs. N. V. Klassen and H. A. Gillis, National Research Council, Canada, for experimental assistance and critical discussions.

References and Notes

(1) L. Kevan, *Adv. Radiat. Chem.*, **4**, 181 (1974).
(2) N. V. Klassen, H. A. Gillis, G. G. Teather, and L. Kevan, *J. Chem. Phys.*, **62**, 2474 (1975).
(3) F. Franks and D. J. G. Ives, *Q. Rev., Chem. Soc.*, **20**, 1 (1966).
(4) B. L. Bales, J. Helbert, and L. Kevan, *J. Phys. Chem.*, **78**, 221 (1974).
(5) K. Fueki, D. F. Feng, and L. Kevan, *J. Am. Chem. Soc.*, **95**, 1398 (1973).
(6) L. Kevan, M. K. Bowman, P. A. Narayana, R. K. Boeckman, V. F. Yudanov, and Yu. D. Tsvetkov, *J. Chem. Phys.*, **63**, 409 (1975).
(7) P. A. Narayana, M. K. Bowman, L. Kevan, V. F. Yudanov, and Yu. D. Tsvetkov, *J. Chem. Phys.*, in press.

Discussion

R. CATTERALL. I would like to draw attention to the considerably greater asymmetry of the optical absorption band of the "partly solvated" electron relative to the "fully solvated" electron. Also in the spectra of EtOH irradiated at 4 K, the high-energy tail is much more pronounced than in the fully relaxed spectrum obtained after thermal annealing at 77 K.

J. JORTNER. I would like to make two comments.

(1) Your experiment on the water–ethanol mixtures establishes that a trapping center containing water molecule(s) does not absorb at 13000 Å on a time scale of ~200 nsec. This observation can-

not distinguish between two possibilities. Either a preexisting trap containing H_2O does not absorb in the above range, or the rotational relaxation time of H_2O is faster than that of C_2H_5OH. One has to probe shorter time scales to establish this point.

(2) I would like to raise the question of the nature of the preexisting traps in polar glasses and in polar liquids. Obviously, in a glass we have a distribution of local potentials while in the liquid rotational fluctuations will result in essentially the same effect. In your language this corresponds to an electron moving in a "rough" potential. To be more precise, such a situation corresponds to the Anderson problem of an electron moving in a fluctuating potential. Only when the energetic spread of the potentials exceeds a certain "critical" value, relative to the band width, will localization occur. Thus the potential not only has to be "rough" but must also exhibit a large spatial energetic spread.

L. KEVAN. (1) We did try to distinguish these two possibilities by looking at shorter times. With a 40-nsec pulse there is little change in the spectra in Figure 1 for the first 200 nsec after the start of the pulse and *then* all of the spectra with various mole fractions of water begin to shift on about the same time scale to nearly the same final spectrum. On this basis we think that the "initial" spectra presented are initial and characteristic of different types of solvation shells for the electron.

(2) Yes, the "rough" potential I speak of corresponds to a spread of potentials both energetically and spatially. However, we still have no real understanding of the initial localization process of an electron in this "rough" potential. Perhaps it is mainly due to strong scattering events and perhaps resonance capture interactions are important for certain energy ranges.

S. A. RICE. Have electron scavengers been added to glassy ethanol to discover whether the infrared absorption is characteristic of electron-geminate cation pairs?

L. KEVAN. No scavenger experiments have been done in the ethanol–water glasses in these experiments. In earlier work (L. Kevan, *J. Chem. Phys.*, **56**, 838 (1972)) we did add biphenyl as a scavenger. There the intensity of the electron band was decreased because some of the electrons were scavenged, but the shape and time profile of the infrared absorption did not change.

M. NEWTON. How did you simulate the original solvent configuration for the partially solvated electron? Is it not surprising that further solvation leads to an increase in the effective radius for the dipolar interaction?

L. KEVAN. This question refers to our study of average distance changes in the process or solvation (H. Hase et al., *J. Chem. Phys.*, **62**, 985 (1975)). We did not have to assume any particular solvent configuration for the partially solvated electron. We simply simulated the matrix ENDOR line for these electrons. Further solvation leads to an increase in the average distance between the electron and the CH matrix protons, i.e., those protons *that* do not overlap significantly with the electron wave function. The CH dipole has its H end negative so as solvation proceeds the H end of the CH dipole moves slightly away from the electon. The OH protons in alcohol matrices have opposite polarity and probably move the other way. We do not obtain direct information about the OH protons from matrix ENDOR, because there is enough isotropic hyperfine coupling to these protons to move their ENDOR signal away from the free proton frequency where the matrix ENDOR signal appears.

N. R. KESTNER. Is your experiment simply sampling initially only those sites which already contain one water molecule or do you think you see those species in which the electron drags one water molecule into the first coordination layer? How can one be sure which is correct?

L. KEVAN. We have assumed that the experiment samples those electrons which already have a water molecule in the first solvation shell from statistical considerations. In a glassy matrix of high macroscopic viscosity, such as we have, we do not think that the electron will exert much "drag" on water molecules outside the first or perhaps the second solvation shell, especially when the other molecules (ethanol) are also strongly polar.

Solvation Time of Electrons in Liquid Ammonia

J. Belloni,† M. Clerc,‡ P. Goujon,* and E. Saito

DRA, SRIRMA, CEN Saclay, 91190 Gif-sur-Yvette, France *(Received August 1, 1975)*

Publication costs assisted by Service de Documentation, CEN Saclay

The phenomenon of solvation of an electron depends either on the presence of preexisting positive potential wells and/or on the orientation of the surrounding molecules by the field arising from the electron's charge. In our studies we have tried to evaluate the solvation time for an excess electron in liquid ammonia at low temperature (−50°C).

The experiment consists of exciting a $K–NH_3$ solution by a picosecond laser pulse in the absorption band of the solvated electron present, and determining the time of the whole process of detrapping and recovering of the initial absorbance.

We used a dye laser (Rhodamine 6G) pumped by an abrasive lamp, producing a 1.5-μsec train consisting of 300 to 400 pulses, each of 5 to 10 psec and separated by 4-nsec intervals. The wavelength of the beam is 610 nm and the intensity is $\sim 2 \times 10^{14}$ photons per pulse.

The analyzing light (xenon lamp) and the laser beam fall on the 1 mm cell with almost the same incident angle but adjusted so that the laser beam does not fall on the spectrograph slit (Figure 1). The $K–NH_3$ solutions were in the con-

† Laboratoire de Physico-chimie des Rayonnements, Associéan CNRS, 91605 Ordy.

‡ DGI-SEPCP, CEN Saclay.

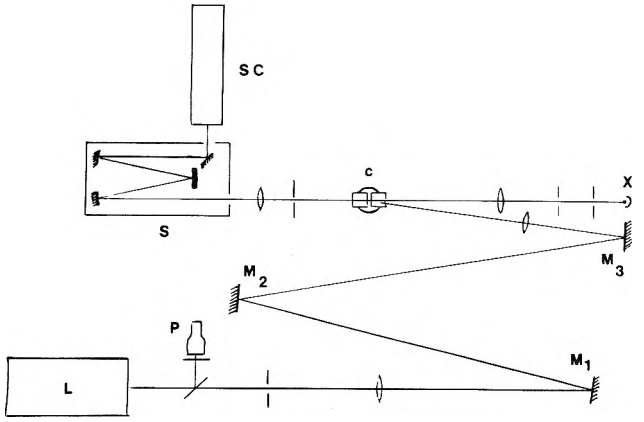

Figure 1. Schematic representation of the experimental setup: (L) dye laser; (P) photodiode; (M_1, M_2, M_3) mirrors; (X) xenon lamp; (c) cell, optical pathlength 1 mm; (S) spectrograph; (SC) streak camera.

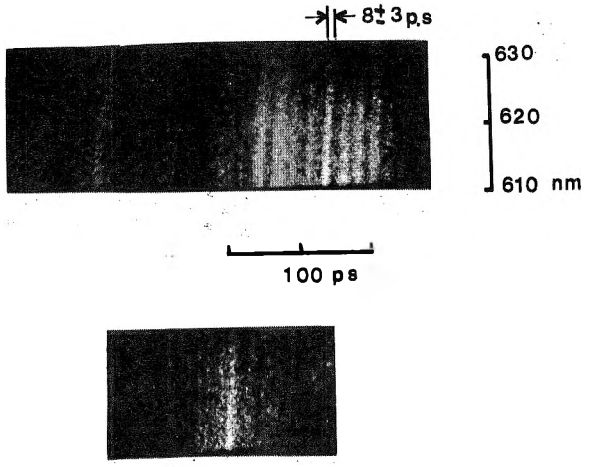

Figure 2. Bleaching of the solvated electron in liquid NH_3 (−50°C).

centration range 10^{-3} to 10^{-2} M. The resolution of the spectrograph allowed us to observe the wavelength range 610–630 nm. The variation of absorbance with time was followed by ultrafast spectroscopy using a picosecond streak camera. The highest scanning rate was 125 psec/cm corresponding to a resolved time of 5 psec.

Although we have not been able to avoid successive reflections of the laser beam on the thick walls of the cell, the main observation derived from these experiments is that the transient transparency due to bleaching and recovering of the initial absorbance lasts no longer than the pulse itself. Supposing that the bleaching process is much shorter than that of solvation, we conclude that the solvation time of electrons in liquid NH_3 at −50°C is ≤5 psec (Figure 2).

This result is discussed in relation to macroscopic and microscopic dielectric relaxation times in liquid ammonia and compared to recent data in other solvants, mainly alcohols.

Discussion

U. SCHINDEWOLF. I would like to raise the question about the process you are observing: by excitation with about 600-nm light you might go to the 2p, 3p, 4p, . . . state with dipole orientation or structure of the ground state. So I would suppose you observe the relaxation back to the ground state, rather than that of solvation, because with the light energy you apply an electron probably cannot be kicked out of its solvation shell.

J. JORTNER. Optical excitation of the solvated electron band can result in two major types of subsequent relaxation processes, depending on the excitation energy. (a) Excitation of a bound–bound transition, e.g., 1s → 2p will result in multiphonon nonradiative relaxation within the single trapping center. (b) Excitation above the threshold for ionization will result in a quasi-free electron which will then be localized. The present experiments correspond to case b, as the excitation energy is 2.0 eV (i.e., 6100 Å).

J. BELLONI. I agree that the energy of the exciting photons is high enough to excite the transition to the continuum. It is likely that in this region of the spectrum the time to recover absorption corresponds to a complete solvation time instead of observations at about 1000 nm where solvation could be only a partial one (work from Bell Laboratories).

Picosecond Dynamics of Localized Electrons in Metal–Ammonia and Metal–Methylamine Solutions

D. Huppert, P. M. Rentzepis,*

Bell Laboratories, Murray Hill, New Jersey 07974

and W. S. Struve

Department of Chemistry, Iowa State University, Ames, Iowa 50010 *(Received September 2, 1975)*

Publication costs assisted by Bell Laboratories

Experimental studies are presented here for time and wavelength resolved optical bleaching of the 1.5-μ solvated electron absorption band in liquid ammonia by 1.06-μ single pulses of ~6 psec duration, and for electron localization in methylamine following photoionization of the M^- species in sodium–methylamine solutions by 530-nm picosecond pulses. Bleaching of the solvated electron band in methylamine by 1.06-μ pumping pulses was also studied. In both ammonia and methylamine solutions, the solvated electron absorption band is found to be homogeneously bleached between ~800 and 1100 nm, and the relaxation time of the 1.06-μ populated excited state of the localized electron is $\sim 2 \times 10^{-13}$ sec. The electron localization process in methylamine occurs within 5 psec of creation of the quasifree electron at temperatures between −40 and −80°C.

Introduction

A great deal of effort has been studied toward understanding the physical properties of dilute ($\lesssim 10^{-3}$ M) metal–ammonia and metal–methylamine solutions.[1] Diverse experimental techniques, including optical absorption spectroscopy,[2] calorimetric[3] and conductance studies,[4] EPR and magnetic susceptibility determinations,[5] and NMR Knight shift measurements,[6] have shaped some consensus concerning the *structure* of such systems. For sufficiently high temperatures and low concentrations, alkali metal–ammonia solutions are considered to contain only independently ammoniated alkali cations and electrons. The latter account for the solutions' broad 1.5-μ optical absorption band,[2] which undergoes blue shifts with decreasing temperature, and varies little for different alkali metals. This spectrum is believed to arise primarily from the 1s → 2p transition between bound states of the trapped electron, though higher transitions (to additional bound states converging to a free-electron continuum[7]) may well cause the band's short-wavelength "tail" extending well into the visible. Electronic structure calculations[8] derived from a simple polaron model for the lowest bound states yield excellent agreement with the spectral transition energy and oscillator strength ($\epsilon \sim 5 \times 10^4$ M^{-1} cm^{-1} at 1.5 μ).

By comparison, dilute metal–amine solutions exhibit optical and EPR spectra which can only be rationalized by the existence of at least three species.[9,10] The solvated electron is believed to be responsible for the single sharp EPR band, as well as for the infrared absorption band (1.3-μ band maximum, $\Delta\nu$ ~6000 cm^{-1}) observed in methylamine–, ethylamine–, and EDA–metal solutions. As in the metal–ammonia solutions, this band's position and shape are independent of the alkali metal. Secondly, a diamagnetic species[11] is responsible for the optical absorption band located in the red and near-infrared region. Unlike the solvated electron band, this band depends markedly on the alkali metal, so that it has been assigned to the alkali metal anion M^-. The band maxima for Na^- and possibly Li^- are situated at 660 nm, while those for K^-, Rb^-, and Cs^- are displaced to 850, 930, and 1030 nm, respectively. Finally, a monomeric M species is likely to be the origin of the hyperfine structure observed in the EPR spectra, though no corresponding optical absorption spectrum has been identified.

By contrast, virtually nothing is known about the relaxation *dynamics* of either quasifree or excited trapped electrons in liquid ammonia or amine solutions. Because of its comparative simplicity in molecular and liquid structure (especially in comparison to strongly hydrogen-bonding solvents), liquid ammonia provides an attractive prototype for phenomenological,[12] SCF,[13] and pseudopotential[14] calculations of excess electron distributions in polar solvents. The ammoniated electron's predicted emission band maximum, originating from a vertical transition between the relaxed 2p state and the 1s state, is drastically red-shifted to ~0.5 eV from the 0.9-eV absorption band owing to the diffuseness of the equilibrium 2p charge density.[15] No such fluorescence has ever been observed[16] in metal ammonia solutions, indicating that nonradiative relaxation of the bound 2p state occurs on a time scale at least two orders of magnitude faster than the pure radiative lifetime τ_r. The latter has been estimated from the 2p → 1s transition moment to be $\tau_r \sim 1$ nsec, so that the 2p state decays within 10 psec or less. Of equal interest is the question of whether the 1.5-μ band (as well as the 1.3-μ band in the metal–amine solutions) arises from *homogeneous* broadening of the trapped electron's lowest allowed electronic transition. If so, the entire spectrum should be proportionately bleached by narrow band pumping ($\Delta\nu \sim 100$ cm^{-1} at 9431 cm^{-1} in the present experiments). Evidence for wavelength-dependent bleaching ("hole burning") has recently been cited[17] as proof of inhomogeneous broadening of trapped electron absorption band in MTHF and 3-methylpentane glasses, indicating those spectra are broadened by local variations in cavity radii or dielectric constant.

The following alternative processes may be visualized for the nonradiative relaxation of electronically excited trapped electrons. (a) The solvated electron absorption

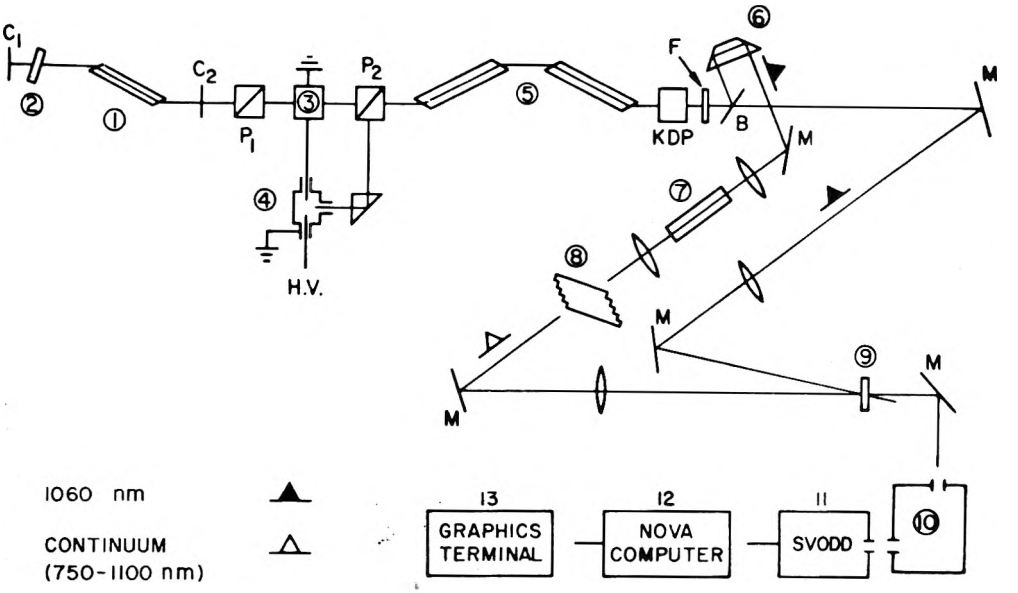

Figure 1. Schematic representation of the experimental system. The components are: (1) Nd^{3+} glass oscillator with cavity mirrors C_1, C_2; (2) saturable dye absorber cell; (3) Pockels cell positioned between crossed Glan polarizers P_1, P_2; (4) spark gap; (5) Nd^{3+} glass amplifiers; (6) translatable prism used to generate variable delay; (7) broad band continuum cell containing CCl_4; (8) stepped-delay transmission echelon; (9) sample cell; (10) monochromator; (11) silicon vidicon optical data digitizer; (12) Nova computer; (13) graphics terminal. Mirrors are denoted by M, beam splitter B, optical filter F.

band originates from the bound–bound 1s → 2p vertical transition. The excited state relaxes to an equilibrium 2p configuration which then crosses to the ground state.[15] Involvement of a long-lived 2s excited state appears to be ruled out here, because the 2s state is of higher energy than the 2s state and cannot be populated without appreciable activation energy. (b) The 1s → 2p transition is followed by thermal ionization of the excited state, yielding a *quasi-free*[18] electron which is trapped to form the 1s ground state. This electron localization process has attracted considerable study in liquid water[18] and alcohols,[19,20] and can be described in terms of two consecutive processes: an ultrafast relaxation process, induced by nonadiabatic coupling between the electron's quasifree and 1s ground states, producing the latter in a nonequilibrium solvent configuration, and subsequent solvent relaxation, occurring on the time scale of dielectric relaxation. (c) The quasifree electron is produced in a bound–continuum transition, and is then trapped to form the localized ground state.

In the present work, we report picosecond bleaching studies of dilute ($\sim 2 \times 10^{-4}$ *M*) Na–NH_3 solutions pumped at 1.06 μ. Pertinent information has been extracted here concerning the line broadening and radiationless relaxation of the solvated electron in liquid NH_3. In addition, we have studied the dynamics of electron localization in Na–methylamine by ejecting an electron with a single 530-nm picosecond pulse overlapping the 660-nm Na^- absorption band. Following the subsequent localization of the solvated electron in methylamine, the optical bleaching of the 1.3-μ band by a 1.06-μ pulse was studied with a view to interpreting the band's broadening mechanism as well as the relaxation behavior of the excited trapped electron.

Experimental Section

Sample Preparation. Concentrated 3-ml samples of Na–NH_3 were prepared in sealed glass vessels comprising vacuum-line optical cells with side arm extensions. Matheson anhydrous NH_3 gas was purified by several liquid N_2 freeze–pump–thaw cycles before purification by reaction with Na metal. After distillation of clean solvent into the sample vessel and addition of ~50 mg of Na metal (Merck, vacuum distilled), additional degassing and baking of the vessel walls were applied before the sample was sealed off. Analogous procedures were followed in the preparation of Na–methylamine solutions. Care was taken to ensure that sample absorption spectra conformed to previously reported bands[2] for M^- and the solvated electron. The use of 2-mm absorption cells reduced the optical density of solvent vibrational overtone bands[21] at 1.06 μ to $\lesssim$0.05, considerably less than the picosecond optical density changes reported in this work. A 7-cm diameter optical Dewar furnished with ~2-cm diameter Pyrex windows housed the sample, which was flushed by N_2 gas streams at −78 and −195°C; sample temperatures were monitored by a Cu–constantan thermocouple suspended ~5 mm from the sample cell. Na–NH_3 solutions had an optical density of ~1.0–1.3, and temperatures were maintained at −60 to −75°C. Na–methylamine solutions were adjusted to have densities of ~0.15–0.4 at 530 nm, and were used from −40 to −80°C. Both types of solution were quite stable at liquid N_2 temperature, though the concentrations of dilute Na–methylamine solutions declined by ~20% after several hours at −80°C. Sample solutions were replaced within 2 weeks of preparation.

Optical Arrangement. Figure 1 summarizes the optical arrangement providing the picosecond bleaching and interrogating pulses in the Na–NH_3 experiments. A Nd^{3+} glass oscillator (Brewster/Brewster rod dimensions ~7 in. long × 0.5 in. diameter) was mode-locked with Eastman Kodak 9860 saturable dye in a 1-cm cell, yielding 1.06-μ pulse trains with average width ~8 psec[21] and separation ~7 nsec. Mode locking was monitored with an ITT F4000 S1 fast photodiode and Tektronix 519 oscilloscope. Single pulse extraction[22] was achieved with a Pockels cell situated between cross Glan polarizers. A 21-kV spark gap triggered by the first few rejected mode-locked pulses supplied a ~4-nsec duration half-wave voltage to the Pockels cell. Amplification of the transmitted 1.06-μ single pulse was

provided by two Brewster/Brewster Nd^{3+} glass amplifiers with a total measured gain of ~50. A multilayer dielectric beam splitter reflected ~45% of the amplified 1.06 μ pulse for sample excitation. The remainder was focussed into a 20-cm path length cell containing CCl_4, where self-phase modulation[23] of the laser fundamental and stimulated Stokes Raman band produced a broad band continuum pulse[24] of duration comparable to the 1.06-μ pulse. This

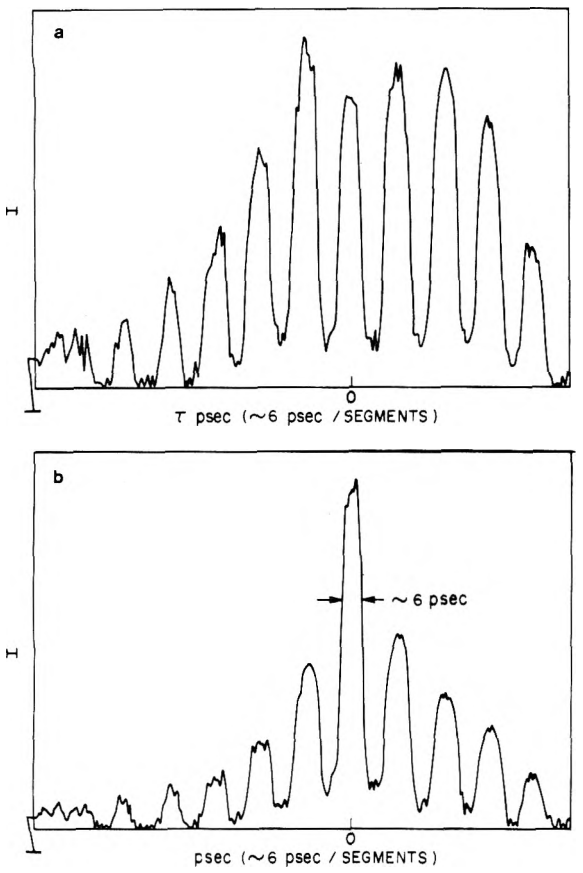

Figure 2. Histogram of echelon pulses traversing through the ND_3–Na 2-mm cell. Intersegment separation 6 psec, wavelength 1100 nm, *I* designates relative transmitted intensity; (a) transmitted echelon segments without excitation; (b) same as (a) with excitation occurring at t = 0 segment.

was split into an interrogating train of 10 pulses separated by 3.3, 6.7, or 20 psec using an appropriate transmission echelon. The echelon train was focussed into a sample cell. After passing through a McPherson 0.3-μ monochromator (53 Å/mm dispersion), each of the interrogating pulses was sharply imaged onto a distinct spatial region[25] of an RCA 4532 silicon vidicon. The vidicon scan was controlled over a programmable two-dimensional grid by a Nova 1230 computer (Data General Corp., interfacing electronics provided by EMR Photoelectric). A liquid N_2 vidicon cooler (Products for Research, Danvers, Mass.) maintained the photocathode temperature at −90°C. Interrogating light intensities from each laser shot were stored by position (256 × 28 resolvable points were read from a thin, rectangular portion of the entire vidicon target for an accelerated readout) onto a moving-head disk file for further processing. These signals were integrated along the axis normal to the time coordinate to produce one-dimensional plots (Figure 2) on a computer graphic terminal. Here, each sharply defined peak corresponds to a particular pulse in the interrogating train.

The principal modification of this apparatus for the Na–methylamine experiments (Figure 3) consists in that two bleaching pulses were directed into the sample rather than one. The first of these, a 530-nm single pulse generated by a second harmonic generator from the 1.06-μ fundamental in a 1-in.^{3} KDP crystal, photoionized the Na^- species to form an ejected electron which became solvated. Approximately 60 psec later, this was followed by a 1.06-μ single pulse which bleached the solvated electron absorption spectrum. When interrogating pulses were required to monitor bleaching of the Na^- absorption band at 600–660 nm, 1-octanol was substituted for CCl_4 as the continuum liquid.

The synchronization of arrival of the 1.06-μ bleaching pulse and the interrogating pulses in the $Na–NH_3$ experiments was verified by placing an Eastman Kodak 9860 dye solution (D ~ 1.0 at 1.06 μ) in place of the sample. Quantitative bleaching of the saturable dye, lasting ~8–10 psec at 1.06 μ, was achieved with unamplified 1.06-μ bleaching pulses (estimated energy ~2 mJ/pulse), but attenuation of these pumping pulses with neutral density filters proportionately diminished the bleaching optical density change. As the extinction coefficient (ϵ ~5 × 10^4 M^{-1} cm^{-1}) and re-

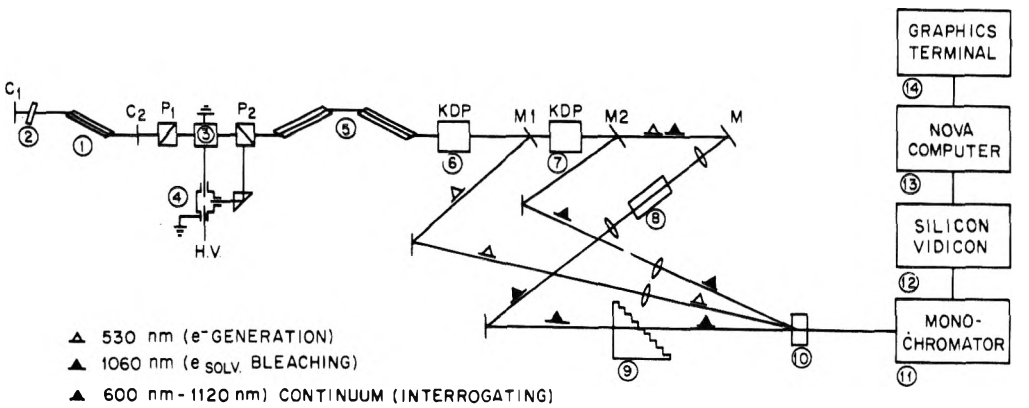

Figure 3. Schematic representation of the experimental system. The components are: (1) Nd^{3+} glass oscillator with cavity mirrors C_1, C_2; (2) saturable dye absorber cell; (3) Pockels cell positioned between crossed Glan polarizers P_1, P_2; (4) spark gap; (5) Nd^{3+} glass amplifiers; (6) second harmonic generator; (7) second harmonic generator; (8) broad band continuum cell containing CCl_4 or 1-octanol; (9) stepped-delay transmission echelon; (10) sample cell; (11) monochromator; (12) silicon vidicon optical data digitizer; (13) Nova computer; (14) graphics terminal. Mirrors are denoted by M, beam splitter B, optical fiber F.

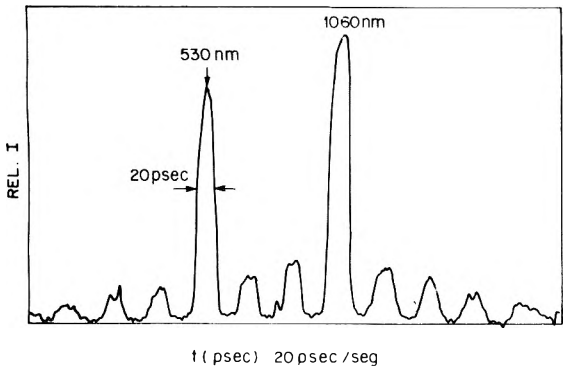

Figure 4. Display of the synchronization of the single 530-nm excitation and 1060-nm bleaching pulses with the 1000-nm interrogating 10 echelon light segments. It is seen that each segment is 20 psec in width, and the 530 nm is coincident with the fourth echelon segment while the 1060 nm arrives three segments later equivalent to 60 psec after the 530 nm-pulse.

laxation time of the dye are independently known, these auxiliary experiments served to calibrate bleaching intensities in $Na-NH_3$.

In the Na–methylamine studies, synchronization of the 530-nm and 1.06-μ pulses and the $t = 0$ interrogating pulse was determined with a CS_2 optical shutter.[26] The CS_2 cell was subsequently replaced by the methylamine sample at exactly the same position. Owing to the effects of wavelength dispersion in the continuum liquid, this synchronization was checked at all wavelengths used. Figure 4 shows the timing of 1000-nm echelon interrogating pulses with the 530-nm and 1.06-μ pumping pulses. It is evident here that the delay between excitation pulses was adjusted at 60 psec, in other cases, the pulse delay was varied between 40 to 80 psec depending on the species studied.

The 1.06-μ pumping pulse energy in both experiments was typically $\sim 30 \pm 10$ mJ, while the 530-nm photoionization pulse contained ~10 mJ. The optical density of the $Na-NH_3$ solution was maintained ~1.3 at 1060 nm while the Na–methylamine was 0.3 at 530 nm. A typical optical density change at 1000 nm was ~0.8 for the formation of the solvated electron band in methylamine. Much smaller density changes were observed for bleaching of the solvated electron band in $Na-NH_3$ and Na–methylamine, however, these were symptomatic of rapid repopulation of the trapped electron's ground state (vide infra). Experimental optical density changes ΔD were determined by firing laser shots alternatively with and without the 530-nm and/or 1.06-μ pulse entering the sample cell. Values for ΔD were computed via $\Delta D = \log (I^w/I^n)$, where I^w and I^n denote the intensity of the particular interrogating pulse in the presence and absence of the pumping pulse(s), respectively.

Results

Ammonia. Bleaching of $Na-NH_3$ and $Na-ND_3$ solutions by 30 ± 10 mJ, 1.06-μ pumping pulses was observed with 10-nm resolution between 850 and 1100 nm with echelon pulse spacings of 20, 6.7, and 3.3 psec. Reduction of raw data similar to that presented in Figure 2 results in the typical results depicted as optical density changes for 940-, 1040-, and 1100-nm interrogation in Figures 5 and 6. When the 20-psec echelon was used, the bleaching and recovery of the solvated electron band occurred within one echelon segment. It is apparent from the data of Figure 7 that the optical density changes ΔD follow qualitatively the same

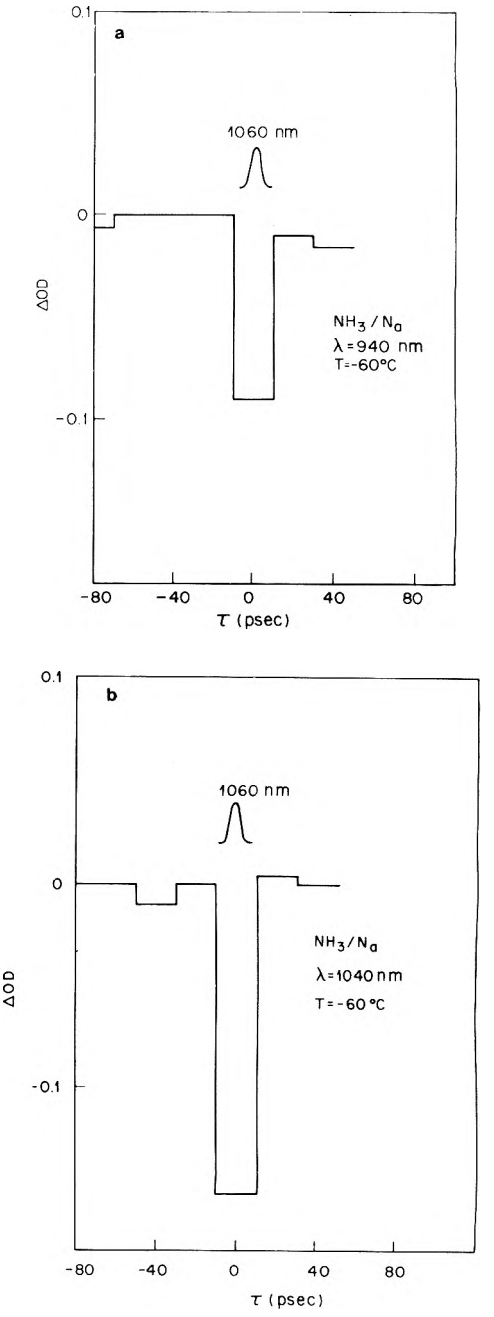

Figure 5. Time-resolved bleaching and recovery of the solvated electron absorption band of the sodium ammonia solution at (a) 940 and (b) 1040 nm. As shown kinetic data are achieved by 20-psec echelon segments. The excitation was performed by a single 1.06μ pulse generated by a mode locked Nd^{3+} glass laser.

wavelength dependence between 850 and 1100 nm as the absorption coefficient of the solvated electron band. These experimental results may be summarized as follows. (a) Bleaching and recovery of the solvated electron band in ammonia occurs within the pumping pulse width of 8 psec, and the symmetrical shape of the ΔD plots is undistorted from that of the pumping pulse. This indicates that bleaching and recovery proceed at least one order of magnitude more rapidly than the experimental time scale, i.e., $\lesssim 8 \times 10^{-13}$ sec. (b) When pumped by a 30 ± 10 mJ 1.06-μ pulse, the solvated electron band (monitored with 6.7-psec echelon pulses at 1100 nm) is bleached with an optical density change $\Delta D = 0.3 \pm 0.05$ for a solution having $D_0 = 1.3$ at

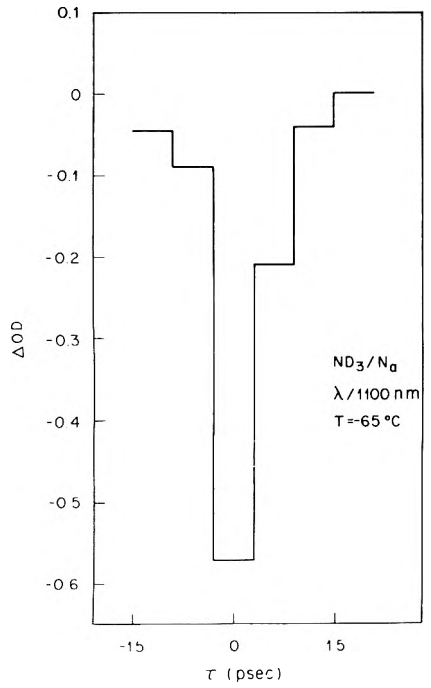

Figure 6. Time-resolved bleaching and recovery of the solvated electron absorption band of sodium deuterated ammonia solution at 1100 nm. In this case, the kinetics were monitored with 6.7 psec echelon/segments. All other experimental parameters same as Figure 3.

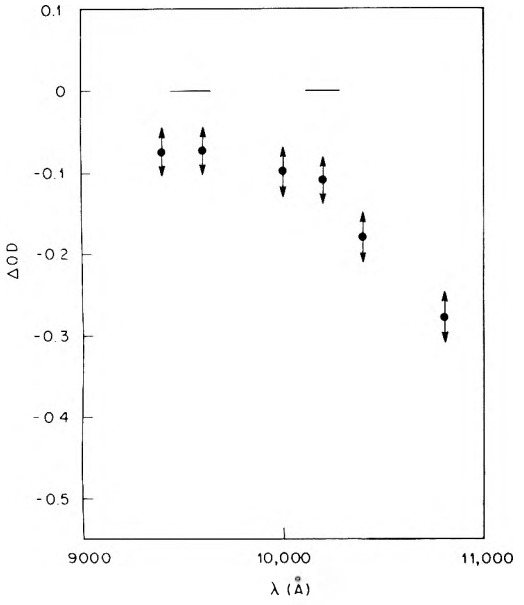

Figure 7. Optical density changes (ΔD) of the ammonia–Na absorption band as a function of wavelength (λ). The excitation was performed by a single 1060-nm pulse generated by a mode locked Nd^{3+} glass laser.

1100 nm, so that $\Delta D/D_0 = 0.23 \pm 0.05$. If the bound electron's excited states has zero extinction coefficient at 1100 nm, $\Delta D/D_0 = x/(1 + x)$, where $x = \tau\epsilon lI$. Here ϵ is the molar absorption coefficient at 1100 nm, l the 2-mm path length, and $I = 4 \times 10^{28}$ photon/cm^2 the photon flux. From this, the relaxation time τ of the excited bound electron is estimated to be $\sim 2 \times 10^{-13}$ sec in NH_3 at −70°C. (c) The solvated electron absorption band is homogeneously broadened between 850 and 1100 nm. The data plotted in Figure 7 are summarized in Table I.

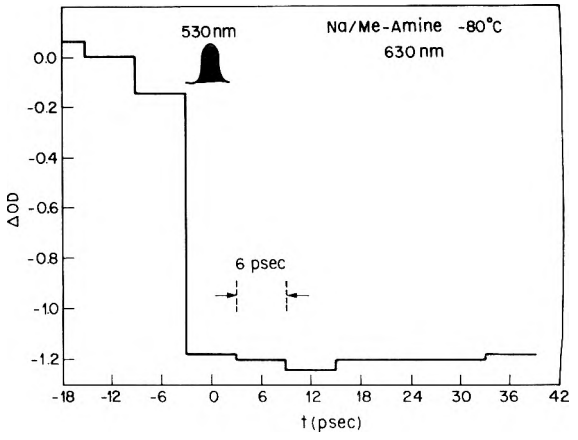

Figure 8. Time-resolved bleaching characteristics of the M^- band of methylamine sodium solution at 630 nm. The interrogating light polarization is parallel to that of the bleaching beam.

TABLE I: Optical Density Changes (ΔD) in NH_3–Na and ND_3–Na Solution Excited by a 1060-nm Pulse and Observed within the Time of the Pulse Width

	$\Delta(D)$	
λ, nm	NH_3	ND_3
1100		−0.44
1080	−0.28	−0.34
1040	−0.18	−0.21
1020	−0.12	
1000	−0.10	−0.17
960	−0.09	
940	−0.08	

Methylamine. Bleaching of the Na^- absorption band in Na–methylamine solution following 530-nm, 10-mJ excitation was monitored between 590 and 650 nm. Bleaching was proved for both interrogating pulse polarizations (orthogonal and parallel) relative to the excitation pulse polarization, in order to avoid errors in interpretation arising from dichroic effects. Figure 8 presents typical data for bleaching of the Na^- band; while only data for parallel interrogation is shown, both polarizations yielded optical density changes of ~1.2. The Na^- band is clearly bleached immediately within experimental time resolution, and no significant recovery of the absorption occurs within 200 psec after excitation. Wavelength dependence studies of bleaching in the Na^- band between 600 and 660 nm lead us to conclude that the Na^- band is homogeneously broadened, in full accord with earlier nanosecond laser photolysis data.[27]

Formation of the solvated electron band was monitored between 770 and 1120 nm at temperatures between −40 and −90°C. This process, as is evidenced by the data in Figure 9, is completed within the 8 psec limit of the picosecond pulse width. Moreover, the solvated electron band does not decay within 200 psec; the normalized optical density changes plotted in Figure 10 vs. wavelength between 770 and 1120 nm, correspond quite well to both the solvated electron absorption spectrum in methylamine and to the absorption band formed in the flash photolysis and nanosecond laser studies.

Data for time-resolved bleaching and recovery of the solvated electron band by a 1.06-μ single pulse, following the 530-nm photoionizing pulse by ~80 psec, are typified by Figure 11 for Na–methylamine at −80°C. Conclusions a–c

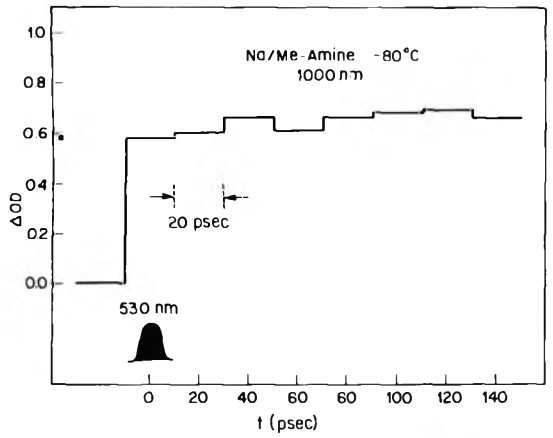

Figure 9. Picosecond formation kinetics of the M^- in methylamine sodium solution at 1000 nm. The formation of the M^- band is immediately after excitation by the 530-nm pulse: solution temperature −80°C; 20 psec/echelon.

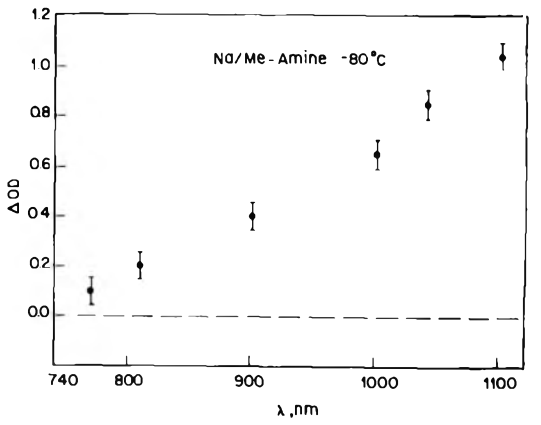

Figure 10. The optical density changes (ΔD) of the M^- band vs. wavelength (λ, nm) in methylamine sodium solution.

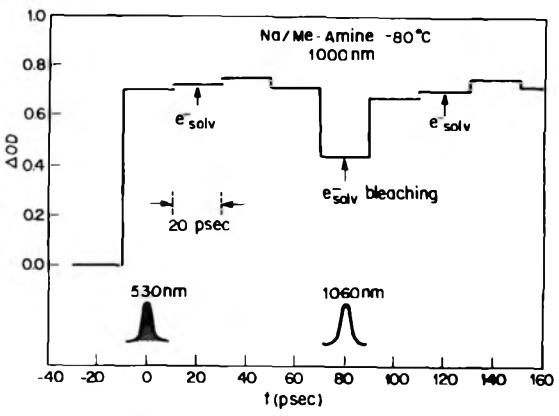

Figure 11. Bleaching kinetics of the electron band, M^-, at 1000 nm. It is seen that the 1000-nm bleaching pulse is delayed by 80 psec with respect to the electron generating 530-nm pulse.

of the preceding summarized data for the Na–NH_3 results apply here as well, and we estimate, as in the Na–NH_3 case, that regeneration of the solvated electron's ground state occurs within $\sim 2 \times 10^{-13}$ sec. The degree of bleaching of the 1.3-μ band by a 1.06-μ pulse, monitored between 850 and 1100 nm, follows the absorption cross section of the solvated electron in methylamine. This suggests, in analogy with the wavelength dependence studies of bleaching in Na–NH_3, that the solvated electron band is homogeneously broadened in methylamine.

Discussion

Any speculations concerning the relaxation mechanisms for excited trapped electrons in liquid ammonia and methylamine are necessarily entwined with assumptions about the levels populated by the 1.06-μ pumping pulse. Though calculated configuration diagrams depicting the solvated electron's 1s and 2p energies as a function of a symmetric cavity radius R have been offered as evidence that thermal fluctuations in R can lead to 1s → 2p transition half-bandwidths commensurate with that observed,[2] the possibility that the solvated electron absorption band is inhomogeneously broadened in liquid ammonia and methylamine is excluded by our present data. Possible refinements of the theory of line broadening in the 1s → 2p and 1s → np^9 transitions include the dependence of the transition moment on the nuclear coordinates together with the incorporation of nontotally symmetric cavity distortions about the electron trapping center. Secondly, while the subpicosecond relaxation time of $\sim 2 \times 10^{-13}$ sec provides us with a first direct clue concerning these systems' relaxation dynamics, we still cannot ascertain whether we are observing a bound–bound 1s → 2p excitation followed by "predissociation-like" relaxation to the ground state, or whether a process involving creation of a localizing quasifree electron is involved. The trapping of a quasifree electron in polar solvents proceeds via initial trapping due to relaxation of long-range polar modes, followed by local relaxation of the first coordination layer which proceeds on the time scale of dielectric relaxation.[18] The overall localization time in H_2O at 300 K has been determined as ~4 psec using picosecond spectroscopy,[18] while pulse radiolysis studies[19,20] led to lifetimes of 2.2 psec in CH_3OH at 300 K, 10 psec in C_2H_5OH at 300 K, and ~2 psec in H_2O at 236 K for the second stage of evolution of the solvated electron. Since these are all approximately one order of magnitude longer than the relaxation time of the solvated electron pumped at 1.06 μ in liquid ammonia and methylamine, it is plausible that "intramolecular" type nonradiative relaxation to the ground state is occurring here. Independent studies of the relaxation of quasifree electrons in liquid ammonia are required to establish this, however.

Our data indicate no change in the rate of formation of the solvated electron band in methylamine following photoionization of Na^- between the temperatures of −40 and −80°C, contrary to a priori expectations based on the behavior of the solvated electron band in water and the alcohols. Conceivable, the increase in dielectric relaxation time in methylamine within that viscosity range is insufficient to dilate the localization time by the one order of magnitude necessary to be detected. Alternatively, hydrogen bonding may prove critical in determining the rate of the dielectric relaxation-limited second step of the localization process in the alcohols, and is much less prevalent in ammonia and the amines. This hypothesis is supported by the low temperature increase in localization time in a hydrogen-bonded system, which is correlated with the known increase in hydrogen-bonding at low temperatures.

Acknowledgment. We gratefully acknowledge the many stimulating and helpful discussions with Professor J. Jortner and the valuable experimental efforts of Mr. J. Marshall.

References and Notes

(1) W. L. Jolly, Ed., "Metal-Ammonia Solutions", Dowden, Hutchinson, and Ross, Inc., Stroudsburg, Pa., 1972.
(2) (a) W. L. Jolly, C. J. Hallada, and M. Gold in "Metal-Ammonia Solutions", Colloque Weyl I, G. Lepoutre and M. J. Sienko, Ed., W. A. Benjamin, New York, N.Y., 1964, p 174; (b) H. Blades and J. W. Hodgins, *Can. J. Chem.*, **33**, 411 (1955).
(3) (a) W. L. Jolly, *Chem. Rev.*, **50**, 351 (1952); (b) L. V. Coulter, *J. Phys. Chem.*, **57**, 553 (1953); (c) L. V. Coulter and L. Monchick, *J. Am. Chem. Soc.*, **73**, 5867 (1951); and references therein.
(4) (a) E. C. Ever and P. W. Frank, *J. Chem. Phys.* **26**, 1517 (1957); (b) C. A. Kraus, *J. Chem. Educ.*, **30**, 83 (1953).
(5) D. E. O'Reilly, *J. Chem. Phys.*, **35**, 1856 (1962); (b) C. A. Hutchinson and R. S. Pastor, *ibid.*, **21**, 1959 (1953); (c) S. Freed and N. Sugarman, *ibid.*, **11**, 354 (1943).
(6) (a) H. M. McConnell and C. A. Holm, *J. Chem. Phys.* **26**, 1517 (1957); (b) J. V. Acrivos and K. S. Pitzer, *J. Phys. Chem.*, **66**, 1693 (1962); (c) T. R. Hughes, *J. Chem. Phys.*, **38**, 202 (1962).
(7) P. F. Rusch, W. H. Koehler, and J. J. Lagowski in "Metal-Ammonia Solutions", Colloque Weyl II, J. J. Lagowski and M. J. Sienko, Ed., Butterworths, London, 1970.
(8) J. Jortner and N. R. Kestner in "Metal-Ammonia Solutions", Colloque Weyl II, J. J. Lagowski and M. J. Sienko, Ed., Butterworths, London, p 49, 1970.
(9) I. Hurley, T. R. Tuttle, Jr., and S. Golden, "Metal-Ammonia Solutions", Colloque Weyl II, J. J. Lagowski and M. J. Sienko, Ed., Butterworths, London, p 449, 1970.
(10) S. Matalon, S. Golden, and M. Ottolenghi, *J. Phys. Chem.*, **73**, 3098 (1969).
(11) See ref 9, p 476.
(12) (a) R. A. Ogg, *Phys. Rev.*, **69**, 668 (1946); (b) R. A. Stairs, *J. Chem. Phys.*, **27**, 431 (1957); (c) J. Jortner, *ibid.*, **30**, 839 (1959).
(13) J. Jortner, S. A. Rice, and E. G. Wilson in "Metal-Ammonia Solutions", Colloque Weyl I, G. Lepoutre and M. J. Sienko, Ed., W. A. Benjamin, New York, N.Y., p 222, 1964.
(14) J. Jortner and N. R. Kestner in "Metal-Ammonia Solutions", Colloque Weyl II, J. J. Lagowski and M. J. Sienko, Ed., Butterworths, London, p 49, 1970.
(15) N. R. Kestner and J. Jortner, *J. Phys. Chem.*, **77**, 1040 (1973).
(16) We are not aware of any negative published report in the literature concerning this point, however, search for emission was performed by several groups without any positive results.
(17) S. L. Hager and J. E. Willard, *J. Chem. Phys.*, **61**, 3244 (1974).
(18) P. M. Rentzepis, R. P. Jones, and J. Jortner, *J. Chem. Phys.*, **59**, 9 (1973).
(19) L. Gilles, J. E. Aldrich, and J. W. Hunt, *Nature (London), Phys. Sci.*, **243**, 70 (1973).
(20) J. H. Baxendale and P. Wardman, *J. Chem. Soc., Faraday Trans. 1*, **69**, 584 (1973).
(21) These pulse widths were ascertained in a separate three-photon fluorescence experiment; see P. M. Rentzepis, C. J. Mitschele, and A. C. Saxman, *Appl. Phys. Lett.*, **17**, 122 (1970).
(22) T. L. Netzel, W. S. Struve, and P. M. Rentzepis, *Annu. Rev. Phys. Chem.*, **24**, 473 (1973).
(23) F. Shimizu, *IBM J. Res. Dev.*, **17**, 286 (1973), and references cited therein.
(24) C. G. O. Varma and P. M. Rentzepis, *J. Chem. Phys.*, **58**, 5237 (1973); M. Clerc, R. P. Jones, and P. M. Rentzepis, *Chem. Phys. Lett.*, **26**, 167 (1974).
(25) A continuous wave Nd^{3+}:YAG laser was used for alignment and focusing of the echelon images.
(26) M. A. Duguay and J. W. Hansen, *Appl. Phys. Lett.*, **15**, 192 (1969).
(27) D. Huppert and K. H. Bar-Eli, *J. Chem. Phys.*, **74**, 3285 (1970).
(28) K. J. Kaufmann, D. Huppert, and P. M. Rentzepis, manuscript in preparation.

Discussion

J. JORTNER. Confronting the experimental data reported by the Bell group (relaxation time $\tau \simeq 2 \times 10^{-13}$ sec) for excitation at 1.06 μ with the results of the Orsay group ($\tau \leq 5 \times 10^{-12}$ sec) for excitation at 6100 Å, it appears that the relaxation times are different. The former experiment corresponds to bound (2p) to bound (1s) relaxation while the latter data pertain to ionization followed by ("two step") relaxation to the ground 1s state.

Furthermore, the observation of homogeneous broadening (or bleaching) of the absorption bond in the range 8000–11000 Å provides support to the theoretical ideas that the 1s → 2p absorption line shape is broadened by the conventional phonon coupling mechanism. What is still missing are optical bleaching experiments at 1.4–1.5 μ. If this experiment yields identical relaxation times with those observed by excitation at 1.06 μ, we shall have strong support for the identification of the broad absorption band in that range with the phonon broadened 1s → 2p bound–bound transition.

T. TUTTLE. (1) How does the value of the relaxation time distinguish between the bound state and the continuum? (2) Does exciting into the continuum give a different relaxation time? (3) What is the mechanism for this very rapid relaxation?

J. JORTNER. The mechanism of electron localization in a polar liquid bears a close analogy to the well-known electron–hole recombination in semiconductors, as studied by Kubo, Toyozawa, and others. The basic physics involved is a nonradiative multiphonon relaxation of the electron from an initial quasifree state to the final bound state. The excess energy is converted into vibrational energy which will involve polar phonon modes of the solvent and possibly also intramolecular vibrational modes of the solvent molecules.

P. DELAHAY. Question to Jortner: Why would you feel reassured by an experiment that shows that you have a bound state? The theoretical problem is a much broader one, anyhow.

J. JORTNER. In response to the comment made by P. Delahay, let me emphasize that when we have complete relaxation data for excitation of electrons in ammonia at 1.4–1.5 μ (τ_1), at 1.06 μ (τ_2), and at 5300 Å (τ_3), and provided that $\tau_1 = \tau_2 < \tau_3$, we shall have a strong basis for distinguishing between bound–bound and bound–continuum excitation, as predicted by current theories.

J. L. DYE. The magnitude of the optical density changes at 600 and at 1000 nm are of interest since the values shown seem to indicate $Na^- \rightarrow 2e^- + Na^+$ (response indicates different intensities). It would be of interest of measure ΔD at both wavelengths with the same intensity pulse in order to determine the extinction coefficients.

D. HUPPERT. The ratio $\Delta D_{600}/\Delta D_{1000} \sim 3$ was measured in 1,3-propylenediamine solution with 20-nsec time resolution. This work appeared in *J. Phys. Chem.*, **74**, 3285 (1970).

Effect of Temperature on Conduction Band Energies of Electrons in Nonpolar Liquids[1]

Richard A. Holroyd,* Steven Tames, and Alvin Kennedy

Chemistry Department, Brookhaven National Laboratory, Upton, New York 11973 *(Received July 23, 1975)*

Publication costs assisted by Brookhaven National Laboratory

The energy of injection of an electron from vacuum into various nonpolar liquids was studied as a function of temperature. The method used was based on the difference in the photoelectric work function of zinc under vacuum and in the liquid; the difference: $\phi_{liq} - \phi_{vac}$, is denoted V_0. Measurements are reported for *n*-pentane, *n*-hexane, 2,2-dimethylbutane, 2,2,4-trimethylpentane, 2,2,5-trimethylhexane, 2,2,4,4-tetramethylpentane, and tetramethylsilane (Me_4Si). In all cases V_0 increases with decreasing temperature. The increase is largest for *n*-hexane (0.0024 eV/°C), less for the branched hydrocarbons (~0.0016 eV/°C), and smallest for Me_4Si (0.0005 eV/°C). The temperature dependence is roughly in accord with the Springett, Jortner, and Cohen model. The data on hydrocarbons show that V_0 increases as the free volume in the liquid decreases.

Introduction

Excess electrons in nonpolar liquids such as hydrocarbons occupy a band of states in which the electron wave function can be either localized or extended. The energy corresponding to the lowest extended state is referred to as the conduction band energy. Its energy relative to the energy of the electron under vacuum is denoted V_0, and the measurement of this quantity as a function of temperature is reported here. In the method used, V_0 is the difference in work function of a metal immersed in the liquid from its value in vacuo; thus $V_0 = \phi_{liq} - \phi_{vac}$. Most previous studies[2-7] utilized this method, but V_0 can also be determined by photoionization of solutes[8] as well as other methods.[9] All earlier photoelectric measurements were done at room temperature. However, the photoionization study[8] spanned a large temperature range and the results suggested that V_0 changes with temperature. Since the photoionization method is complicated by the temperature effect on both ion–electron separation probabilities and threshold behavior, this study utilizing the photoelectric method was undertaken to measure V_0 over a range of temperatures for several liquids.

The temperature dependence of V_0 is of interest because of the suggestion[10] that the rates of electron reactions in hydrocarbons are a function of V_0. It has also been observed that the equilibrium constant of electron attachment reactions is influenced by the energy of the conduction band,[11] and it was hoped that a temperature study would help evaluate the parameters involved.

Calculations utilizing the semicontinuum model indicate that V_0 should decrease with increasing temperature for alcohols.[12] A similar effect would be expected for other liquids since it is a consequence of changes in density with temperature. The model of Springett, Jortner, and Cohen[13] is used to calculate V_0 as a function of temperature for each liquid by normalizing to the value of V_0 at 20°.

Experimental Section

The photocell used in this study could be assembled and disassembled to permit resurfacing of the photocathode. A Varian flange with a copper gasket joined upper and lower parts of the cell. The lower part of the flange was sealed by Kovar to the outer quartz envelope of the photocell. The inner surface of the quartz, with the exception of the flat window, was coated with tin oxide. To the upper part of the flange was connected two stainless steel tubes (A) (see detail Figure 1), through which passed the high voltage and current leads. A valve was attached for connection to the vacuum line. The photocathode (C) was coated in a separate apparatus by slow evaporation of zinc from a tungsten filament. The zinc electrode was then transferred to the cell; this operation was done in a glove bag filled with N_2 to avoid exposure of the zinc to air. After assembly, the cell was washed with dry solvent and evacuated to 10^{-6} Torr. The light beam passed through an oval slot in the anode which was covered with mesh. The anode was maintained at a positive potential and the electrodes were separated by about 1 mm. For high-temperature work, the cell was placed in a temperature-regulated oven. Low temperatures were attained by cooling with a cold nitrogen gas stream.

Work functions were determined by the method outlined previously.[2] First the photoelectric response of the zinc surface as a function of wavelength was determined under vacuum at 20°C. Then the liquid was distilled into the cell and heated or cooled to the appropriate temperature and the response remeasured. After removal of the liquid, the vacuum response was repeated at 20°C.

The current (i) from a phototube is given by

$$i/T^2 = \alpha A F(x) \qquad (1)$$

where $F(x)$ is Fowler's function and x is $(h\nu - \phi)/kT$. The data were fit to this equation to determine the work function (ϕ). A set of data was not accepted unless the two vacuum work functions agreed to within 0.02 eV. Generally for clean zinc surfaces the data gave a reasonably good fit to the Fowler function in both the liquid and the vacuum (see Figures 2 and 3 in Results). Since this function applies only near the threshold, measurements that were more than 30 $h\nu/kT$ units above the work function were not used in the least-squares analysis. Typically a zinc surface could be used over a period of weeks without significant change in the work function.

Most liquids used in this study were first passed through activated silica gel, degassed, and stirred over NaK alloy. The only exception to this treatment was tetramethyltin (Alfa, electronic grade), which was dried over anhydrous

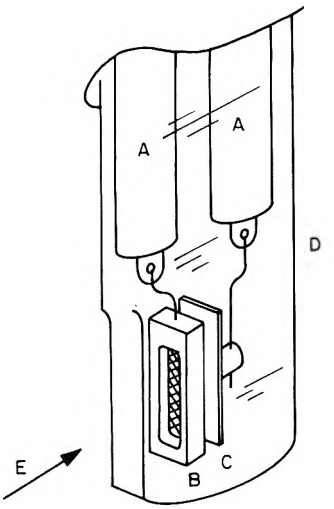

Figure 1. Detail of photocell: (A) stainless steel electrode supports, (B) anode (wire mesh over central hole is 80% transparent), (C) zinc-coated cathode, (D) quartz envelope coated on inside with SnO_2, (E) light beam (enters through flat quartz window).

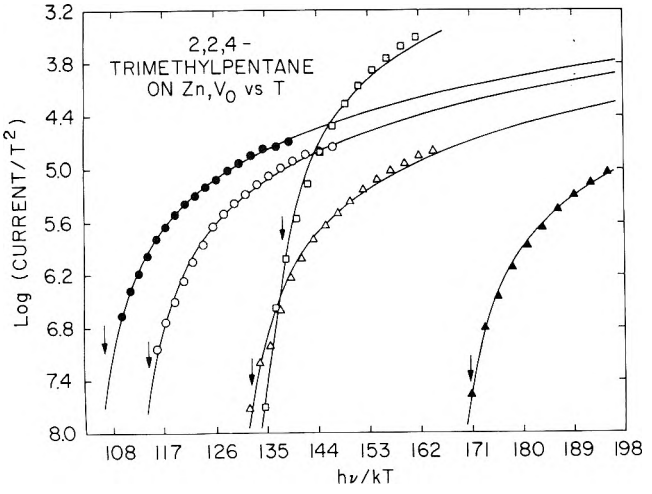

Figure 2. Spectral response of photocell, log (i/T^2) vs. $h\nu/kT$ at E = 10^4 V/cm: □ vacuum at 20°, ϕ = 3.54 eV. Filled with 2,2,4-trimethylpentane: ▲ at −39°, ϕ = 3.44 eV; △ at 18°, ϕ = 3.32 eV; ○ at 53°, ϕ = 3.23 eV; ● at 71°, ϕ = 3.19 eV.

$CaCl_2$ and degassed without NaK treatment. Most hydrocarbons were Phillips Research Grade; 2,2,4,4-tetramethylpentane was from Chemical Samples, 2,2,5-trimethylhexane was Phillips Pure Grade (99%), and 2,3-dimethylbutene-2 was from Aldrich. Densities were taken from published compilations where available or from extrapolations of the type given by Francis.[14]

Results

The work function of Zn immersed in several nonpolar liquids was measured as a function of temperature. Figures 2 and 3 show typical spectral data obtained for 2,2,4-trimethylpentane and 2,2,4,4-tetramethylpentane, respectively. These are plots of $\log(i/T^2)$, where i is the normalized photocurrent vs. the photon energy parameter $h\nu/kT$ (see eq 1). The solid lines are the Fowler curves computed by least squares to fit the set of data at each temperature. The fit of the data to the Fowler curves is as good for the liquid as for the vacuum. The work function is derived from the shift in the Fowler curve along the $h\nu/kT$ axis and corresponds to a specific value of $h\nu_0$ (indicated by the arrows in

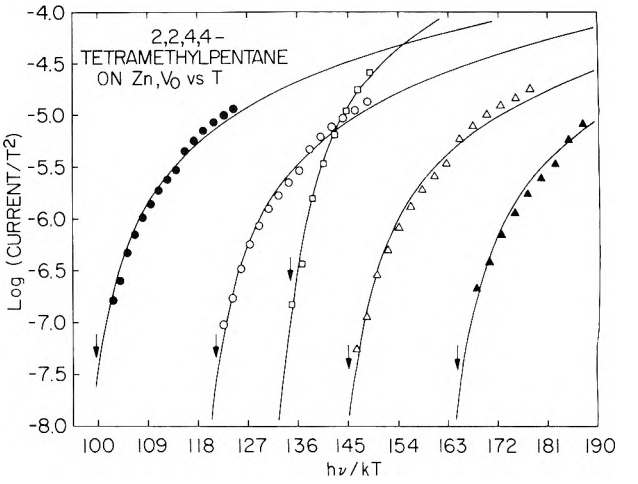

Figure 3. Spectral response of photocell, log (i/T^2) vs. $h\nu/kT$ at E = 5000 V/cm: □, vacuum at 20°, ϕ = 3.41 eV. Filled with 2,2,4,4-tetramethylpentane at: ▲, −53°, ϕ = 3.13 eV; △, −26°, ϕ = 3.09 eV; ○, 21°, ϕ = 3.06 eV; ●, +58°, ϕ = 3.01 eV.

the figures). The figures show clearly that ϕ_{liq} decreases with increasing temperature for both liquids; the actual decrease for 2,2,4-trimethylpentane is −0.18 eV and for 2,2,4,4-tetramethylpentane is −0.14 eV over a 100° temperature range. (Note the use of the parameter $h\nu/kT$ in the figures tends to exaggerate this effect.)

In addition to the two liquids, for which results are given in Figures 2 and 3, detailed measurements of V_0 vs. temperature were also obtained for n-pentane, n-hexane, 2,2-dimethylbutane, 2,2,5-trimethylhexane, and tetramethylsilane (Me_4Si); the results are given in Table I. Also shown are some new work function measurements for *cis*-butene-2, 2,3-dimethylbutene-2, and tetramethyltin. For these liquids, V_0 was measured only at one temperature. For tetramethyltin at 20°, V_0 is −0.75 eV, which is the lowest value reported for any liquid and is attributed to the highly polarizable tin atom which enhances the polarization energy, thus lowering V_0 (see Discussion).

For the liquids studied, V_0 decreases with increasing temperature; this effect for four liquids is shown in Figure 4. The decrease is approximately linear with temperature up to the highest temperatures studied, around 100°C. The slope dV_0/dT is greatest for n-hexane (−0.0024 eV/deg), somewhat less for the branched octanes and nonanes (∼−0.0016 eV/deg), and even less for Me_4Si (−0.0005 eV/deg). A V_0 value less than −0.5 eV has not yet been observed for a hydrocarbon. Comparison of the present results with the earlier photoionization results[8] indicates good agreement for n-hexane, but a much smaller slope for Me_4Si.

From the data in Figure 4, it may be noted that V_0 for n-hexane at +80° is approximately the same as V_0 for 2,2,4-trimethylpentane at −80°. Similarly, V_0 for 2,2,4-trimethylpentane at +70° is comparable to V_0 for neopentane and 2,2,4,4-tetramethylpentane at 20°. Comparable values of V_0 indicate the liquids may correspond in some other property (see Discussion). It is also interesting to note that molecules with similar molecular structure have very similar values of V_0 and similar temperature effects: thus at room temperature neopentane and 2,2,4,4-tetramethylpentane have the same V_0; at all temperatures the V_0 values for 2,2,4-trimethylpentane and 2,2,5-trimethylhexane are similar as are those for n-pentane and n-hexane.

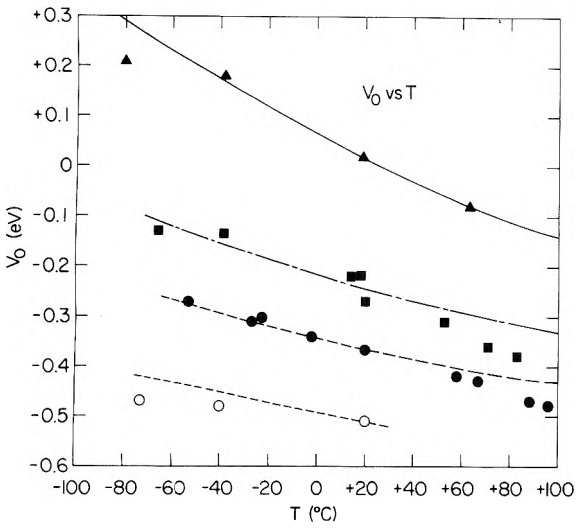

Figure 4. Plot of V_0 vs. temperature. Points are experimental; lines are calculated from Wigner–Seitz method: *n*-hexane (▲, —), 2,2,4-trimethylpentane (■, — - —); 2,2,4,4-tetramethylpentane (●, — — —); tetramethylsilane (○, - - - -).

Results presented here indicate that the magnitude of the photocurrent observed from liquid-filled photocells is not very temperature sensitive. Figures 2 and 3 show that as the temperature increases there is little or no shift in the Fowler curve along the y axis. The current depends on two main factors: the yield of electrons from the photoelectric effect, which varies as T^2 (see eq 1), and the probability of escape from the image potential. The data in Figures 2 and 3 have been plotted as log (i/T^2); thus any vertical shifts in the Fowler curves with temperature must be attributed to changes in the escape probability. This probability is a function of the field, the range of the injected electrons, and the temperature. The theory for this in the one-dimensional Onsager case has been worked out in detail.[3,15,16] The effect of temperature in the diffusion theory has been examined specifically by Blossey.[16] Our results appear to be in reasonable accord with this theory. In most instances the theory predicts the current will decrease with increasing temperature, although if the range is small there will be an increase. For the conditions applicable to Figures 2 and 3, a small decrease (14%) over a 110° temperature rise is predicted, which is in reasonable accord with experiment.

Discussion

Temperature Dependence of V_0. The data in Figures 2–4 and in Table I show that V_0 decreases with increasing temperature. This means that the V_0 level decreases as the free volume in the liquid increases. Since the Springett, Jortner, and Cohen model[13,17] for calculating V_0 predicts a change in this direction, it is of interest to compare the results with those of the model. The method was originally developed for rare gas liquids but has been applied to hydrocarbons[18–20] to calculate the hard core radius a from experimental V_0's (a defines the sphere from which the electron is excluded in the model). Here we use values of V_0 measured at 20° to calculate a from which V_0 is calculated at other temperatures. The conduction band energy is given by

$$V_0 = T_0 + U_p \tag{2}$$

where U_p is the long-range polarization energy assumed to be a constant given by

TABLE I: V_0 vs. Temperature

Liquid	Temp, °C	V_0 Exptl	V_0 Calcd[a]	a
n-Pentane	−61	+0.18	+0.21	
	−39	+0.12	+0.17	
	+17	+0.01	(+0.01)	2.03
n-Hexane	−80	+0.21	+0.29	
	−38	+0.18	+0.17	
	+19	+0.02	(+0.02)	2.17
	+63	−0.08	−0.08	
2,2-Dimethylbutane	−66	−0.17	−0.08	
	−34	−0.20	−0.14	
	+13	−0.22	(−0.22)	2.11
2,2,4-Trimethylpentane	−66	−0.13	−0.11	
	−39	−0.14	−0.16	
	+14	−0.22	−0.24	
	+19	−0.24	(−0.24)	2.34
	+53	−0.31	−0.28	
	+71	−0.36	−0.30	
	+83	−0.38	−0.31	
2,2,5-Trimethylhexane	−53	−0.10	−0.12	
	−46	−0.12	−0.14	
	−32	−0.13	−0.16	
	20	−0.24	(−0.24)	2.45
	45	−0.29	−0.27	
	75	−0.30	−0.31	
	+113	−0.39	−0.34	
2,2,4,4-Tetramethylpentane	−53	−0.27	−0.27	
	−27	−0.31	−0.31	
	−23	−0.30	−0.31	
	−2	−0.34	−0.34	
	20	−0.36	(−0.36)	2.40
	58	−0.42	−0.40	
	67	−0.43	−0.41	
	88	−0.47	−0.42	
	96	−0.48	−0.43	
2,3-Dimethylbutene-2	+13	−0.15	(−0.15)	
cis-Butene-2	−30	−0.16		
Tetramethyltin	20	−0.75		
Tetramethylsilane	+20	−0.51	(−0.51)	2.02
	−40	−0.48	−0.45	
	−73	−0.47	−0.42	

[a] V_0 was calculated for temperatures other than 20° by using the method in ref 12, in which the a value is derived from the value of V_0 at room temperature. Assumed V_0's in parentheses.

$$U_p = \frac{-3\alpha e^2}{2r_s^4}\left[\frac{8}{7} + \left(1 + \frac{8\pi\alpha n}{3}\right)^{-1}\right] \tag{3}$$

α is the molecular polarizability and T_0 is the zero-point kinetic energy given by

$$T_0 = \hbar^2 k_0^2/2m \tag{4}$$

The Wigner–Seitz radius r_s is related to the number density n by $\frac{4}{3}\pi r_s^3 = n^{-1}$ and k_0 is determined by

$$\tan k_0(r_s - a) = k_0 r_s \tag{5}$$

From these equations one expects that T_0 will decrease with decreasing density, that is, as r_s increases. However, from eq 3, U_p also increases as r_s increases and any change in V_0 will be determined by the relative changes in these two energy terms. For these hydrocarbons the calculated change in the T_0 term is greater than the change in the U_p term, and a decrease in V_0 with increasing temperature is expected. The calculated values are shown in the last column of Table I and as the lines in Figure 4. Overall the agreement with experiment is remarkably good, especially for *n*-hexane. Also a smaller change with temperature is

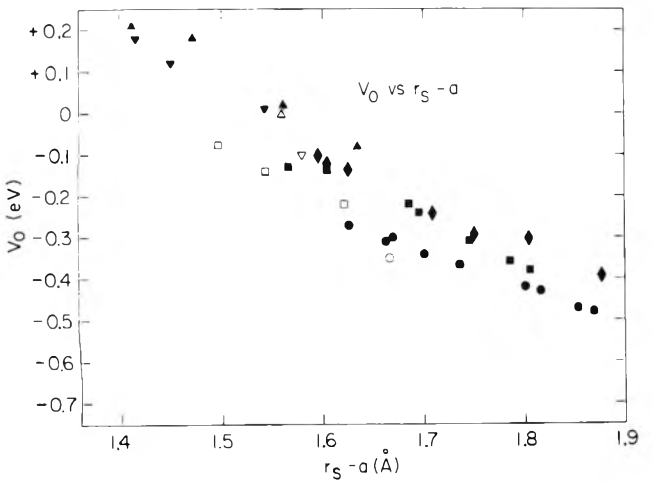

Figure 5. Data on V_0 at different temperatures plotted vs. $r_s - a$. This work: ▲, *n*-hexane; ▼, *n*-pentane; ■, 2,2,4-trimethylpentane; ●, 2,2,4,4-tetramethylpentane; ♦, 2,2,5-trimethylhexane; □, neohexane; ○, neopentane (ref 6, 8); △, 3-methylpentane and 2-methylpentane (ref 3); ▽, 2,3-dimethylbutane (ref 7).

predicted for Me_4Si and 2,2,4,4-tetramethylpentane than for *n*-hexane, as is observed experimentally. Thus it seems justifiable, based on this and other evidence,[20] to employ the Springett–Jortner–Cohen model as we have done. The calculation indicates the change (dV_0/dT) becomes less above 100°.

In order to ascertain the nature of the free volume dependence of V_0 and to show the importance of this parameter, we plotted the data as a function of $r_s - a$ in Figure 5. Figure 5 includes all the data for saturated hydrocarbons reported here and from previous work function data. The points tend to follow a single curve, V_0 decreasing monotonically as the distance $r_s - a$ increases. The points for the more symmetrical molecules like neopentane and 2,2,4,4-tetramethylpentane lie somewhat below the rest. In contrast, in plots of V_0 vs. temperature (as in Figure 4) or vs. density the points for each liquid lie on completely separate curves. The points for Me_4Si and TMT (not shown) lie significantly below the line; which indicates that the presence of a polarizable atom has an added effect on V_0. The correlation with $r_s - a$ thus applies only to hydrocarbons. The assumption of an isotropic value of a derivable from V_0 may not be valid in all cases. It appears to apply here perhaps since most of the molecules studied are not too unspherical. Since molecular volumes can be estimated from V_{crit}, it has been suggested[20] that the electron molecule hard core radius a can likewise be estimated from V_{crit}. From examination of all the available data the relationship $a = 0.303 V_{crit}^{1/3}$ has been suggested[21] (a is in Å and V_{crit} is in cm³/mol). If a is estimated in this way and the data plotted as in Figure 5 the same general trend is obtained. The figure does provide a rationale why V_0 is the same for *n*-hexane near +80° and 2,2,4-trimethylpentane near −80°: because the two liquids have corresponding values of the $r_s - a$ parameter (1.6 Å) at these conditions. The dependence on $r_s - a$ also suggests that high pressures should lead to an increase in V_0. We conclude from these results that in nonpolar liquids there are regions of molecular size from which the electron is at least partly excluded.

It has been known since the early work of DuBridge and others[22,23] that the temperature effect on the vacuum work function is small (~10^{-4} V/deg). However, here we find for injection into a liquid that temperature changes the work function and, consequently, V_0, and the effect is an order of magnitude greater than in vacuo. From the results, this effect can be expressed by

$$V_0(T) = V_0^0 + \alpha T \qquad (6)$$

where α has values from −0.0005 to −0.0024 eV/deg depending on the liquid.

References and Notes

(1) Research performed under the auspices of the U.S. Energy Research and Development Administration.
(2) R. A. Holroyd and M. Allen, *J. Chem. Phys.*, **54**, 5014 (1971).
(3) R. A. Holroyd, B. K. Dietrich, and H. A. Schwarz, *J. Phys. Chem.*, **76**, 3794 (1972).
(4) R. A. Holroyd and W. Tauchert, *J. Chem. Phys.*, **60**, 3715 (1974).
(5) S. Noda and L. Kevan, *J. Chem. Phys.*, **61**, 2467 (1974).
(6) W. Tauchert and W. F. Schmidt, Proceedings of the 5th International Conference on Conduction and Breakdown in Dielectric Liquids, Noordwijkerbrout, The Netherlands, July 1975.
(7) R. Schiller, S. Vass, and J. Mandics, *Int. J. Radiat. Phys. Chem.*, **5**, 491 (1973).
(8) R. A. Holroyd and R. L. Russell, *J. Phys. Chem.*, **78**, 2128 (1974).
(9) B. Raz and J. Jortner, *Chem. Phys. Lett.*, **4**, 155 (1969).
(10) A. O. Allen, T. E. Gangwer, and R. A. Holroyd, *J. Phys. Chem.*, **79**, 25 (1975).
(11) R. A. Holroyd, T. E. Gangwer, and A. O. Allen, *Chem. Phys. Lett.*, **31**, 520 (1975).
(12) K. Fueki, D.-F. Feng, and L. Kevan, *J. Phys. Chem.*, **78**, 393 (1974).
(13) B. E. Springett, J. Jortner, and M. H. Cohen, *J. Chem. Phys.*, **48**, 2720 (1968).
(14) A. W. Francis, *Chem. Eng. Sci.*, **10**, 37 (1959).
(15) R. Haberkorn and M. E. Michel-Beyerle, *Chem. Phys. Lett.*, **23**, 128 (1973).
(16) D. F. Blossey, *Phys. Rev. B*, **9**, 5183 (1974).
(17) B. Raz and J. Jortner, *Proc. R. Soc. London, Ser. A*, **317**, 113 (1970).
(18) H. T. Davis, L. D. Schmidt, and R. M. Minday, *Chem. Phys. Lett.*, **13**, 413 (1972).
(19) K. Fueki, D.-F. Feng, and L. Kevan, *Chem. Phys. Lett.*, **13**, 616 (1972).
(20) H. T. Davis and L. D. Schmidt, *Can. J. Chem.*, **51**, 3443 (1973).
(21) R. A. Holroyd, *Proc. 5th Int. Congr., Radiat. Res.*, in press.
(22) J. A. Becker and W. H. Brattain, *Phys. Rev.*, **45**, 694 (1934).
(23) L. A. DuBridge and W. W. Roehr, *Phys. Rev.*, **39**, 99 (1932); **42**, 52 (1932).

Discussion

M. H. COHEN. The reported correlation of V_0 with $r_s - a$ and therefore free volume suggests a very amusing correlation of V_0 with viscosity and the glass transition which also correlates with free volume. It should also be pointed out that the presence of the liquid outside the metal will reduce the image potential experienced by the electron and affect the injection current thereby.

R. HOLROYD. The correlation with $r_s - a$ is independent of the model we chose.

J. JORTNER. (1) The definite experiment for the determination of V_0 will be the measurement of the threshold, E_I, for internal photoionization of an impurity, as you have done, together with the threshold, E_E, for external photoionization whereupon $V_0 = E_I - E_E$. The only difficulty involves the corrections for the escape length, L, of electrons in the liquid in the determination of E_E. We have conducted such experiments in doped solid rare gases, where L is large (~1000 Å). The latter case is much simpler, while in polar liquids where L is relatively small appropriate corrections have to be introduced.

(2) The model of Springett, Jortner, and Cohen (SJC) for V_0 in nonpolar fluids was advanced for the quasi-free electron state. Without dwelling on technical details, I would like to point out that for liquid hydrocarbons where the electron mobility is low the electron is not quasi-free. Kestner and I attempted to treat this problem in terms of an inhomogeneous percolation picture. In this case the SJC model is inapplicable.

B. WEBSTER. Could I just follow up the earlier remark of J. Jortner. In $[Fe(CN)_6]^{4-}$ an electron ejection into the liquid has an onset at >3.82 eV. Direct emission into the vapor occurs at >5.25 eV. Is the difference really a measure of $V_0 \sim -1.33$ eV or should this be regarded as the electron affinity of water?

J. JORTNER. I am well familiar with the photoemission work from ferrocyanide solutions conducted by Delahay and his colleagues. I wonder whether the experimental value for internal photoionization in this system is reliable. Photochemical evidence can be misleading as excited states such as that of ferrocyanide in solution can yield an electron by thermal ionization.

L. KEVAN. (1) Question: Do V_0 values for methane and ethane fit on the correlation plot of V_0 vs. free volume?

(2) Comment: You pointed out that the temperature dependence of V_0 for alkanes depends theoretically on the balance between the temperature dependence of the two component terms of V_0 ($V_0 = T_0 + U_p$), where T_0 is the kinetic energy and U_p is the polarization energy. In alkanes, including methane in which the electron is in a quasi-free state like in argon, T_0 decreases more than U_p increases with increasing temperature so V_0 becomes more negative. However, in argon the increase in U_p with temperature is almost exactly compensated for by the decrease in T_0 with temperature, so that V_0 is predicted to be essentially temperature independent. Thus the expected temperature dependence of V_0 depends on the medium.

R. HOLROYD. Ethane is on the line. However, methane is somewhat below the line, especially if we use Tauchert and Schmidt's more recent value of $V_0 = -0.2$ eV. But the symmetrical molecules (like neopentane) are all on the low side. It is interesting that argon and methane have the same values for the $r_s - a$ parameter and comparable V_0's, which fits in with our correlation.

M. SILVER. Using the Fowler plot to determine V_0 is very questionable because the Fowler method presumes that the limitation on the current is solely due to the flux of electrons from the electrode capable of entering the medium. However, experimentally one observes a field dependence of current implying that scattering in the medium and the specific potential distribution near the electrode are important. Unless the momentum exchange scattering and the energy loss (inelastic) scattering have the same energy dependence, there will be reflections back into the electrode which vary with $h\nu$. Since one measures a current, the $h\nu$ dependence of the current will reflect the energy dependence of the scattering events as well as the flux of electrons (Fowler emission). A simple calculation involving inelastic scattering and involving the excitation of vibrations could give an *apparent* positive energy shift of V_0 by the vibrational energy of approximately 0.1 or 0.2 eV. This calculation is equivalent to the one-dimensional Onsager escape probability over an arbitrary shaped barrier but including scattering of the hot electrons as well as diffusion of the thermalized electrons. . . . The correct procedure to use to obtain V_0 from photoinjection experiments is a careful study of the current–voltage characteristics at each $h\nu$ to obtain the scattering parameters and, of course, to use the Fowler plot on the current corrected for back scattering.

R. HOLROYD. We use the Fowler function to fit the data in the liquid because empirically the spectral dependence is the same as in vacuo. The current–voltage dependence is nearly ohmic, independent of wavelength, and this dependence is entirely accounted for by diffusion from the image charge under the applied field (see ref 3), and does not in itself imply back scattering. If the fraction of electrons back scattered is independent of wavelength, the Fowler function should apply. Any errors due to this problem are, I believe, minor and the photoelectric effect is at present the best method available to measure V_0

P. DELAHAY. Two comments: (1) A treatment of photoelectron emission into dielectrics is available (Brodskii). If I recall his theory (about 1970), the threshold extrapolation depends on the dielectric constant, e.g., with the power 5/2 of photon energy at high dielectric constants. It can be very different from the Fowler theory. (2) V_0 is a bulk property. Your definition of V_0 involves also the difference between the surface potentials of the metal in vacuo and the surface potential on the metal in the liquid. This term may not be entirely negligible. Moreover, the dipole induced in the electric field at this interface would orient at the interface orientation should be temperature dependent.

R. HOLROYD. The 5/2 power applies only for $\epsilon > 10$; for $\epsilon \sim 2$, the Brodskii treatment shows the Fowler equation is applicable.

G. R. FREEMAN. (1) Although measurements in the 1930's showed little temperature dependence of the work functions of metals, did you check the temperature dependence with your apparatus?

R. HOLROYD. Yes, and we find in agreement with DuBridge et al. little change in ϕ_{vac} with temperature.

G. R. FREEMAN. (2) Calculations with several recent models that correlate V_0 with electron mobilities in hydrocarbons indicate that $(V_0 - \bar{V})$, that is, the difference between the energies of the bound and quasi-free states, is nearly independent of temperature. Would you comment upon why $\bar{V}$ and V_0 should have similar temperature dependences?

R. HOLROYD. I think others here are more qualified than I to comment on this. However, let me suggest that V_0 and $\bar{V}$ change together because the same factors, such as free volume, influence both states.

Continuum Dielectric Model for an Electron in a Nonpolar Fluid

James K. Baird

Health Physics Division, Oak Ridge National Laboratory, Oak Ridge, Tennessee 37830 *(Received August 13, 1975)*

Publication costs assisted by the Oak Ridge National Laboratory

A function expressing the electrostatic polarization energy experienced by an electron immersed in a nonpolar fluid is derived on the basis of classical electrostatics. A continuum dielectric model is used to represent the collective effect of the fluid molecules, which are assumed individually to possess spherical symmetry. The local electric field in the fluid is calculated from the sum of a cavity field and a dielectric reaction field. The model is parametrized by constants (the molecular electric dipole and quadrupole polarizabilities and the effective cavity radius presented by a molecule in the fluid), which for the example of argon can be determined from published literature data. The results obtained from the continuum model are compared with a recent theory dealing with the same question, but based on a model in which the molecules in the fluid are regarded as being discrete, and the local electric field is taken to be the traditional one due to Lorentz.

Introduction

The properties of excess electrons introduced into dielectric fluids by ionizing radiation or by field emission tips have been actively studied in recent years.[1] Part of the effort has centered about attempts to describe the microscopic interactions of the electrons with the molecules of the fluid and to formulate a theory of electron transport.[2-10] Pursuing the problem of microscopic description, we calculate herein the electrostatic polarization energy for an electron immersed in a nonpolar fluid consisting of molecules having spherical symmetry. The electron is taken to be a point charge, while a molecule in the fluid is assumed to consist of point polarizable electric multipoles at the center of a spherical cavity in an otherwise continuous dielectric. This molecular model is a generalization of that introduced by Bell[11] and used by Onsager[12] to calculate the density dependence of the dielectric constant of a polar fluid.

The contributions of Bell and Onsager, taken together, differed from previous investigations[13] in three fundamental ways: (1) the electric lines of force produced by an external field were allowed to bend in the vicinity of the cavity; (2) the cavity was taken to be of approximately molecular size; and (3) the elementary charges making up a molecule were replaced by a point electric dipole at the center of the cavity, and the interaction of the molecule with its neighbors was represented by a dipolar reaction field. Although Onsager was concerned with polar substances, Böttcher[14] has since demonstrated the applicability of his concepts to explain the density dependence of the dielectric constant of nonpolar fluids. In what follows, the model developed by Bell, Onsager, and Böttcher will be used to represent the many body nature of the interaction of the electron with the fluid.

Mathematical Development

Cavity Field. Consider, as shown in Figure 1a, a point charge of magnitude q located a distance b from the center of a spherical cavity of radius a in a uniform dielectric of dielectric constant ϵ. Using standard methods of analysis,[24] we may solve the equation

$$\nabla^2 V(r,\theta) = 0 \qquad r \neq b \tag{1}$$

for the electrostatic potential $V(r,\theta)$ subject to the boundary conditions

$$V(r,\theta) - (q/\epsilon)|\mathbf{r} - b\mathbf{k}|^{-1} = \text{continuous} < \infty \tag{2}$$

$$\frac{\partial V(r,\theta)}{\partial r}\bigg|_{a-0} = \epsilon \frac{\partial V(r,\theta)}{\partial r}\bigg|_{a+0} \tag{3}$$

where $\mathbf{k}$ is a unit vector in the z direction. Of help in matching boundary conditions is the expansion

$$\frac{q}{\epsilon|\mathbf{r} - b\mathbf{k}|} = \frac{q}{\epsilon b}\sum_{l=0}^{\infty}\left(\frac{r}{b}\right)^l P_l(\cos\theta) \tag{4}$$

where $\{P_l(\cos\theta)\}$ are the Legendre polynomials. The results are

$$V(r,\theta) = \frac{q}{b}\sum_{l=0}^{\infty}\left[\frac{(2l+1)}{\epsilon(l+1)+l}\right]\left(\frac{r}{b}\right)^l P_l(\cos\theta) \qquad r < a \tag{5a}$$

$$V(r,\theta) = \frac{q}{\epsilon|\mathbf{r} - b\mathbf{k}|} + \frac{q}{\epsilon b}\sum_{l=0}^{\infty}\left[\frac{l(\epsilon-1)}{\epsilon(l+1)+l}\right]\left(\frac{a}{b}\right)^l\left(\frac{a}{r}\right)^{l+1} P_l(\cos\theta) \qquad r > a \tag{5b}$$

The electric field $\mathbf{G}(r,\theta)$ evaluated at the center of the cavity is given by

$$\mathbf{G}(0,\theta) = -\nabla V(r,\theta)|_{r=0} = -\frac{q}{b^2}\left(\frac{3}{2\epsilon+1}\right)\mathbf{k} \tag{6}$$

The gradient of the cavity field is denoted by $G_{ij}'(r,\theta)$, where the prime and subscripts combine to indicate differentiation of the ith component of $\mathbf{G}(r,\theta)$ with respect to the jth direction. The subscripts i and j may be any of the three coordinates x, y, or z. Because of symmetry with respect to rotations about the z direction, $G_{ij}'(r,\theta)$ satisfies the equations

$$G_{ij}'(0,\theta) = 0 \qquad i \neq j \tag{7a}$$

$$G_{xx}'(0,\theta) = G_{yy}'(0,\theta) = -\frac{1}{2}G_{zz}'(0,\theta) = \frac{q}{b^3}\left(\frac{5}{3\epsilon+2}\right) \tag{7b}$$

Induced Dipole. Consider the point charge q removed and a point polarizable electric dipole of magnitude m

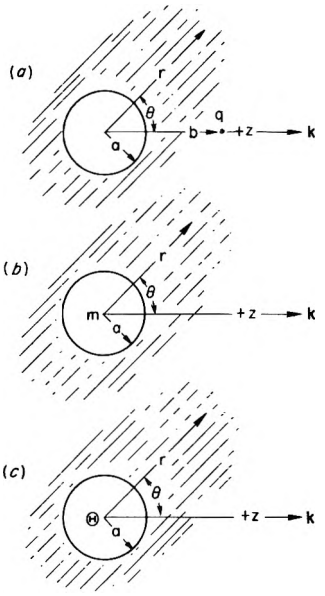

Figure 1. (a) Point charge of magnitude q outside a cavity. (b) Electric dipole of moment m inside a cavity. (c) Electric quadrupole of moment Θ inside a cavity.

placed at the center of the cavity as shown in Figure 1b. The solution to eq 1 (restriction $r \neq b$ now removed) subject to the boundary conditions, eq 3, and the following

$$V(r,\theta) - mr^{-2}\cos\theta = \text{continuous} < \infty \tag{8}$$

has been derived by Onsager.[12,14] The results are

$$V(r,\theta) = \frac{m\cos\theta}{r^2} - \frac{2m}{a^2}\left(\frac{\epsilon-1}{2\epsilon+1}\right)\left(\frac{r}{a}\right)\cos\theta \qquad r < a \tag{9a}$$

$$V(r,\theta) = \left(\frac{3\epsilon}{2\epsilon+1}\right)\left(\frac{m\cos\theta}{\epsilon r^2}\right) \qquad r > a \tag{9b}$$

The dipole reaction field $\mathbf{R}(r,\theta)$ at the cavity center is

$$\mathbf{R}(0,\theta) = -\nabla\left[V(r,\theta) - \frac{m\cos\theta}{r^2}\right]_{r=0} = \frac{2m}{a^3}\left(\frac{\epsilon-1}{2\epsilon+1}\right)\mathbf{k} \tag{10}$$

By the principle of superposition, the local electric field $\mathbf{F}$ is given by

$$\mathbf{F} = \mathbf{G}(0,\theta) + \mathbf{R}(0,\theta) = -\left(\frac{3}{2\epsilon+1}\right)\frac{q}{b^2}\mathbf{k} + \frac{2m}{a^3}\left(\frac{\epsilon-1}{2\epsilon+1}\right)\mathbf{k} \tag{11}$$

The first term of the above equation may be regarded as due to the direct electron–solvent interaction and the second as arising from the solvent–solvent interaction. If α is the electric dipole polarizability of a molecule in the fluid, then

$$m = \alpha F = -\left(\frac{3}{2\epsilon+1}\right)\frac{\alpha q}{b^2} + 2m\left(\frac{\epsilon-1}{2\epsilon+1}\right)\frac{\alpha}{a^3} \tag{12}$$

Solving eq 12 for m, we find

$$m = -\left[\left(\frac{3}{2\epsilon+1}\right)\frac{\alpha q}{b^2}\right]\left[1 - \frac{2\alpha}{a^3}\left(\frac{\epsilon-1}{2\epsilon+1}\right)\right]^{-1} \tag{13}$$

Induced Quadrupole. The induced quadrupole moment tensor Θ_{ij} is given by[15]

$$\Theta_{ij} = \sum_{k,l} C_{ij:kl}F_{kl}' \tag{14}$$

where F_{kl}' is the gradiant of the local electric field, and $C_{ij:kl}$ is the field gradiant quadrupole polarizability tensor.[16] Because the molecule is considered to be spherically symmetric, the nonzero components of this polarizability tensor satisfy the relation[17]

$$C_{ii:ii} - C_{ii:kk} = C \qquad i \neq k \tag{15}$$

Since the cavity field possesses rotational symmetry about the z direction, we also have

$$F_{xx}' = F_{yy}' = -\tfrac{1}{2}F_{zz}' \tag{16}$$

Substituting eq 15 and 16 in eq 14, we find

$$\Theta_{xx} = \Theta_{yy} = -\tfrac{1}{2}\Theta_{zz} = -\tfrac{1}{2}CF_{zz}' = -\tfrac{1}{2}\Theta \tag{17}$$

The electrostatic potential due to a general quadrupole Θ_{ij} is

$$V(r) = \frac{1}{3}\sum_{i,j}\frac{\Theta_{ij}}{r^3}(3r_ir_j - \delta_{ij}r^2) \tag{18}$$

where r_i is the ith component of the vector r, and δ_{ij} is the Kronecker delta.[16] Combination of eq 17 and 18 results in the potential

$$V(r,\theta) = \frac{\Theta}{r^3}P_2(\cos\theta) \tag{19}$$

Consider now a quadrupole with potential given by eq 19 situated at the center of the cavity as shown in Figure 3b. The solution of eq 1 (restriction $r \neq b$ removed) subject to the boundary conditons, eq 3, and

$$V(r,\theta) - \Theta r^{-3}P_2(\cos\theta) = \text{continuous} < \infty \tag{20}$$

may be derived by analogy with that for the case of the induced dipole. The results are

$$V(r,\theta) = \frac{\Theta}{r^3}P_2(\cos\theta) - \frac{3(\epsilon-1)}{(3\epsilon+2)}\frac{\Theta}{a^3}\left(\frac{r}{a}\right)^2 P_2(\cos\theta) \qquad r < a \tag{21a}$$

$$V(r,\theta) = \left(\frac{5\epsilon}{3\epsilon+2}\right)\frac{\Theta}{\epsilon r^3}P_2(\cos\theta) \qquad r > a \tag{21b}$$

The reaction field gradiant is given by

$$R_{ij}'(0,\theta) = 0 \qquad i \neq j \tag{22a}$$

$$R_{xx}'(0,\theta) = R_{yy}'(0,\theta) = -\frac{1}{2}R_{zz}'(0,\theta) = -\frac{3(\epsilon-1)}{(3\epsilon+2)}\frac{\Theta}{a^5} \tag{22b}$$

By adding eq 7 and 22, one finds the local electric field gradiant to be given by

$$F_{zz}' = G_{zz}' + R_{zz}' = -\frac{q}{b^3}\left(\frac{10}{3\epsilon+2}\right) + \frac{6\Theta}{a^5}\left(\frac{\epsilon-1}{3\epsilon+2}\right) \tag{23}$$

Once again, the first term of this equation may be associated with the direct electron–solvent interaction and the second with the solvent–solvent interaction. When eq 23 is substituted into eq 17, there results

$$\Theta = CF_{zz}' = -\left(\frac{10}{3\epsilon+2}\right)\frac{Cq}{b^3} + 6\Theta\left(\frac{\epsilon-1}{3\epsilon+2}\right)\frac{C}{a^5} \tag{24}$$

Hence, the induced quadrupole moment of the molecule is

$$\Theta = -\left[\left(\frac{10}{3\epsilon+2}\right)\frac{qC}{b^3}\right]\left[1 - \frac{6C}{a^5}\left(\frac{\epsilon-1}{3\epsilon+2}\right)\right]^{-1} \tag{25}$$

Electrostatic Potential Energy. The total electrostatic

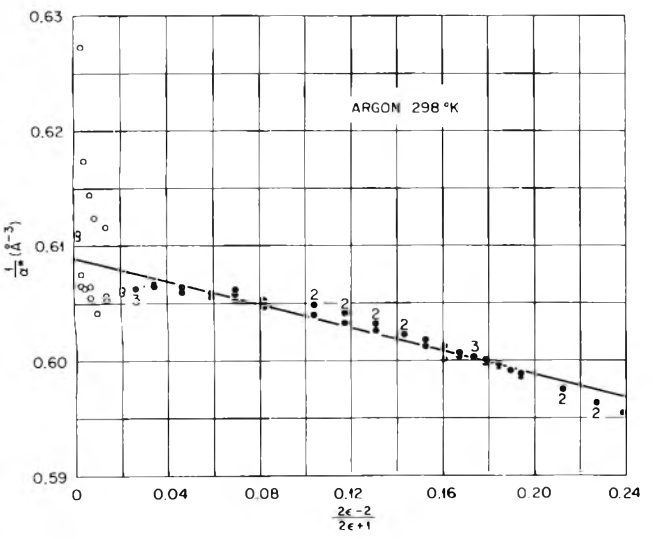

Figure 2. Böttcher plot of the density dependence of the dielectric constant of argon at 298 K. The dielectric constant is ϵ, and $1/\alpha^*$ is as defined in the discussion of eq 31 of the text. The data are taken from ref 19. The straight line was determined by the method of least squares using only the points represented by the filled circles. Where a filled circle represents more than one measurement of ϵ, the number of measurements is given by an integer.

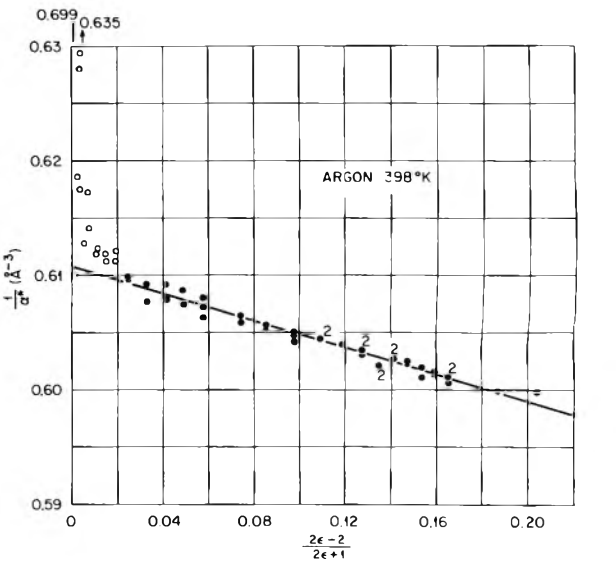

Figure 3. Böttcher plot of the density dependence of the dielectric constant of argon at 398 K. The integers associated with the arrows at the top of the figure give the ordinates of points off the scale of the graph. The horizontal locations of the arrows indicate the abscissas of these points. See Figure 2 for additional information.

potential, evaluated at the position of the point charge for the problem of a point charge outside a cavity containing both a point polarizable electric dipole and a point polarizable electric quadrupole, may now be calculated by adding eq 5b, 9b, and 21b with $(r,\theta) = (b,0)$. In so doing, however, we must ignore the term $(q/\epsilon)|\mathbf{r} - b\mathbf{k}|^{-1}$ which otherwise results in an infinite self-energy for the point charge. Also, we use eq 13 and 25 to evaluate m and Θ, respectively, and combine terms of like values of l. The net result of these operations is

$$V(r) = -\frac{\alpha q}{r^4} f_1(u_1,\epsilon) - \frac{2Cq}{r^6} f_2(u_2,\epsilon) + \frac{q}{\epsilon a}\sum_{l=3}^{\infty}\left[\frac{l(\epsilon-1)}{\epsilon(l+1)+l}\right]\left(\frac{a}{r}\right)^{2(l+1)} \quad (26)$$

wherein the dipole and quadrupole dielectric screening functions, $f_1(u_1,\epsilon)$ and $f_2(u_2,\epsilon)$, are defined, respectively, by

$$f_1(u_1,\epsilon) = \left(\frac{1}{u_1\epsilon}\right)\left[\frac{u_1(\epsilon+2)-(\epsilon-1)}{(2\epsilon+1)-2u_1(\epsilon-1)}\right] \quad (27a)$$

$$u_1 = \alpha/a^3 \quad (27b)$$

$$f_2(u_2,\epsilon) = \left(\frac{1}{u_2\epsilon}\right)\left[\frac{u_2(2\epsilon+3)-(\epsilon-1)}{(3\epsilon+2)-6u_2(\epsilon-1)}\right] \quad (28a)$$

$$u_2 = C/a^5 \quad (28b)$$

If the point charge is increased in magnitude continuously from 0 to q in infinitesimal steps of $q\ d\lambda$ while the electrostatic potential has a magnitude $\lambda V(r)$, $0 < \lambda < 1$, then the electrostatic potential energy $U(r)$ is given by the formula[25]

$$U(r) = \int_0^1 \lambda V(r) q\ d\lambda \quad (29)$$

We have by exclusion of all but the first two terms in eq 26

$$U(r) = -\frac{1}{2}\frac{\alpha q^2}{r^4} f_1(u_1,\epsilon) - \frac{Cq^2}{r^6} f_2(u_2,\epsilon) \quad (30)$$

Our model being restricted to molecules having spherical symmetry, eq 30 is correct up to terms of order $1/r^6$. The term in $1/r^5$ is missing not only from the cavity contribution to this equation, but also because a spherical molecule has no polarizability giving rise to the appropriate multipoles.[16,18] It should be noted that when $\epsilon = 1$, $f_1(u_1,1) = f_2(u_2,1) = 1$, thus leaving eq 30 in the form one would expect for the potential energy associated with an atom in the field of a point charge surrounded by vacuum.

TABLE I: Values of Molecular Constants and Derived Quantities for Argon[a]

T, K	α, Å^3	a, Å	$u_1 \times 10^2$	$u_2 \times 10^2$	ϵ_1	ϵ_2
298	1.642	2.70	8.34	0.760	1.27	1.04
398	1.637	2.58	9.53	0.954	1.32	1.05

[a] The values of u_2 and ϵ_2 were calculated on the basis of $C = 1.09$ Å^5.

Determination of the Molecular Constants α, a, and C. In order to evaluate $f_1(u_1,\epsilon)$ and $f_2(u_2,\epsilon)$ for a given fluid, the constants α, a, and C must first be determined. Two of these, α and a, may be estimated by using Böttcher's method of plotting the density dependence of the dielectric constant.[14] If the Böttcher–Onsager formula is written in the fashion

$$\frac{12\pi\epsilon N}{(\epsilon-1)(2\epsilon+1)} = \frac{1}{\alpha} - \frac{1}{a^3}\left(\frac{2\epsilon-2}{2\epsilon+1}\right) \quad (31)$$

where ϵ is the dielectric constant and N the molecular number density, then a plot of the left-hand side (usually referred to as $1/\alpha^*$) as a function of $(2\epsilon-2)/(2\epsilon+1)$ should give a straight line with intercept α^{-1} and slope $-a^{-3}$.

As an example, plots of the data of Michels et al.[19] for argon at two different temperatures are shown in Figures 2 and 3. In Table I are listed the least-squares values for α and a. In determining these values, the points represented by the open circles in the figures were given zero statistical weight, while all other points were assigned a weight of unity. The points to be zero-weighted were selected on the basis of their obvious scatter about the linear trend suggested by the remainder of the data. The scatter was due

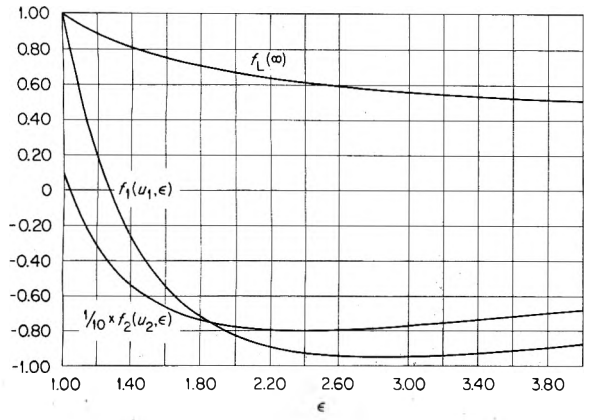

Figure 4. The dipole screening function $f_L(\infty)$ of ref 4, the dipole screening function $f_1(u_1,\epsilon)$, and the quadrupole screening function $f_2(u_2,\epsilon)$.

presumably to the fact that at low densities $\epsilon - 1$ is little different from zero and poorly known. Without specific knowledge of the errors to be associated with particular values of ϵ and N, the present method of weights cannot be improved upon, and the values of α and a listed in Table I are to that extent approximate. The values for a are somewhat larger than the argon atomic radius of 1.92 Å calculated from the length of a side of the face-centered-cubic unit cell observed in solid argon.[20]

There seems to be as yet no experimental value of C for argon, although a calculated value, $C = 1.09$ Å^5, has been given by Burns.[21,22]

Discussion

Plots of $f_1(u_1,\epsilon)$ and $f_2(u_2,\epsilon)$ as functions of ϵ are shown in Figure 4. At certain values of ϵ, namely $\epsilon_1 = (1 + 2u_1)/(1 - u_1)$ and $\epsilon_2 = (1 + 3u_2)/(1 - 2u_2)$, $f_1(u_1,\epsilon_1)$ and $f_2(u_2,\epsilon_2)$, respectively, are zero. This may be interpreted in physical terms as follows. The field lines associated with a point charge in a uniform dielectric extend radially outward from the charge. The presence of an empty cavity in the vicinity of the charge causes these lines to bend. However, the presence of the multipole moments at the center of the cavity also produces a curvilinear system of field lines. When these systems of field lines are superposed, the net bending due to terms proportional to $P_1(\cos\theta)$ is zero at $\epsilon = \epsilon_1$, and likewise the net bending due to terms proportional to $P_2(\cos\theta)$ is zero at $\epsilon = \epsilon_2$.

In a recent paper, Lekner[4] has determined the electric dipole screening function for argon by assuming a model in which all atoms are regarded as point electric dipoles. He calculates the polarization contribution to the local electric field at the position of a given atom by summing the contributions due to the remaining atoms weighted by the radial distribution function for the fluid. Lekner's screening function, which is denoted by $f_L(r)$ and is a function of the distance r between the electron and an atom, takes on the asymptotic value $f_L(\infty) = [1 + (8\pi/3)N\alpha]^{-1} = (\epsilon + 2)/3\epsilon$ for r greater than a few atomic diameters. This fast approach to an asymptotic value appears to be due to the short-range order in the fluid. By contrast, the intermolecular forces responsible for short-range order are largely ignored in the continuum model used herein, so that $f_1(u_1,\epsilon)$ and $f_2(u_2,\epsilon)$ are constants.[27] In Figure 4, $f_L(\infty)$ has been plotted for comparison with $f_1(u_1,\epsilon)$.

In calculation of $f_L(r)$, however, Lekner chose to neglect the effects of statistical fluctuations in the positions and orientations of the point electric dipoles. He assumes that the average electric field due to a dipole is the field of the average dipole. Kirkwood showed in his calculation of the density dependence of the dielectric constant that, by neglecting the effects of fluctuations, one is led to the Lorentz value for the local electric field.[23] Consequently, it is not surprising that the asymptotic value of the Lekner screening function is just that to be expected on the basis of the Lorentz local field, $F_L = [(\epsilon + 2)/3\epsilon]E_0$, where E_0 is the vacuum electric field. For the case when a uniform external electric field induces the polarization in the dielectric, the local electric field based on Lekner's model with fluctuations taken partly into account shows some agreement with the local field calculated on the basis of the Onsager cavity model. That is to say, when the two local fields are each expanded in powers of the parameter $(4\pi/3)N\alpha$, the constant and first-order terms agree.[26] Thus, it is of some general interest to introduce the effects of fluctuations into the Lekner's calculation of the dipole screening function.

The potential energy $U(r)$ specified by eq 30 should find application in calculations based on the Schroedinger equation to determine the scattering cross sections for electrons in monatomic fluids. From these cross sections, one may calculate from kinetic theory[2,4-6] the mobility of excess electrons in argon, which has been extensively investigated experimentally by Jahnke et al.[7] Additionally, $U(r)$ may be employed in the theory of Springett et al.[10] to calculate V_0, the bottom of the electronic conduction band in a fluid.

Acknowledgments. The author would like to acknowledge some helpful conversations concerning this work with James H. Marable and to thank Verner E. Anderson for assistance with the least-squares fits. This research was sponsored by the U.S. Energy Research and Development Administration under contract with Union Carbide Corporation.

References and Notes

(1) A. Hummel and W. F. Schmidt, *Radiat. Res. Rev.*, **5**, 199 (1974).
(2) H. Schnyders, S. A. Rice, and L. Meyer, *Phys. Rev.*, **150**, 127 (1966).
(3) B. Halpern, J. Lekner, S. A. Rice, and R. Gomer, *Phys. Rev.*, **156**, 351 (1967).
(4) J. Lekner, *Phys. Rev.*, **158**, 130 (1967).
(5) M. H. Cohen and J. Lekner, *Phys. Rev.*, **158**, 305 (1967).
(6) J. Lekner, *Philos. Mag.*, **18**, 1281 (1968).
(7) J. A. Jahnke, L. Meyer, and S. A. Rice, *Phys. Rev. A*, **3**, 734 (1971).
(8) H. T. Davis, L. D. Schmidt, and R. M. Minday, *Phys. Rev. A*, **3**, 1027 (1971).
(9) J. A. Jahnke, N. A. W. Holzwarth, and S. A. Rice, *Phys. Rev. A*, **5**, 463 (1972).
(10) B. E. Springett, J. Jortner, and M. H. Cohen, *J. Chem. Phys.*, **48**, 2720 (1968).
(11) R. P. Bell, *Trans. Faraday Soc.*, **27**, 797 (1931).
(12) L. Onsager, *J. Am. Chem. Soc.*, **58**, 1486 (1936).
(13) H. A. Lorentz, "The Theory of Electrons", B. G. Teubner, Leipzig, 1909, Dover Publications, New York, N.Y., 1952.
(14) C. J. F. Böttcher, "Theory of Electric Polarization", Elsevier, New York, N.Y., 1952.
(15) The quadrupole moment Θ_{ij} is defined as in ref 16, namely $\Theta_{ij} = \frac{1}{2}\sum_\alpha e_\alpha(r_{\alpha i}r_{\alpha j} - \delta_{ij}r_\alpha^2)$, where $r_{\alpha i}$ is the ith component of the position vector of the αth charge, e_α, $r_\alpha^2 = \sum_i r_{\alpha i}^2$, and δ_{ij} is the Kronecker delta.
(16) A. D. Buckingham, *Q. Rev., Chem. Soc.*, **13**, 183 (1959).
(17) A. D. Buckingham, *J. Chem. Phys.*, **30**, 1580 (1959).
(18) A. D. Buckingham, *Adv. Chem. Phys.*, **12**, 107–142 (1967).
(19) A. Michels, C. A. Ten Seldam, and S. D. J. Overdijk, *Physica*, **17**, 781 (1951).
(20) E. A. Moelwyn-Hughes, "Physical Chemistry", Pergamon Press, New York, N.Y., 1957, p 527.
(21) G. Burns, *J. Chem. Phys.*, **31**, 1253 (1959); see also A. Dalgarno, *Adv. Phys.*, **11**, 281 (1962).
(22) The quantity C satisfies the equation $C = \alpha_Q/2$ where α_Q is the quadrupole polarizability calculated by Burns (ref. 21). The relationship derives from a factor of 2 difference between the definitions of the quadrupole moment employed by Buckingham and by Burns.

(23) J. G. Kirkwood, *J. Chem. Phys.*, **4**, 592 (1936).
(24) W. Hauser, "Introduction to the Principles of Electromagnetism", Addison-Wesley, Reading, Mass., 1971, p 195.
(25) Reference 24, p 145.
(26) Reference 14, pp 225–226.
(27) One of the reviewers pointed out that the local electric field produced by a point charge immersed in a continuous dielectric (without cavities) is simply q/r^2. In this instance, the dipole screening function would be unity. The argument proceeds as follows. The local electric field is given by the field due to the point charge, namely, q/r^2, plus the sum of the fields due to microscopic electric dipoles induced in the dielectric. Inasmuch as all the polarization in the dielectric is directed radially toward the charge, its contribution to the local field cancels out, making the local electric field simply q/r^2. This argument can in fact be verified by replacing the fluid radial distribution function in eq 11 of ref 4 by unity and performing the indicated integration. A fluid characterized by a radial distribution function, which is unity everywhere, is a fluid in which the molecules may overlap. The physical impossibility of molecules overlapping is in some sense taken into account in the cavity model used in this paper. That is to say, the cavity boundary surrounding the induced multipoles prevents the uniform dielectric representing the remaining molecules from approaching the multipoles too closely. To this extent, the repulsive aspect of the intermolecular force has been taken into account.

Conduction State Energy of Excess Electrons in Condensed Media. Liquid Methane, Ethane, and Argon and Glassy Matrices

Shoji Noda, Larry Kevan,*

Department of Chemistry, Wayne State University, Detroit, Michigan 48202

and Kenji Fueki

Department of Synthetic Chemistry, Faculty of Engineering, Nagoya University, Nagoya, Japan *(Received July 3, 1975)*

The temperature dependence of the conduction electron energy V_0 in liquid methane and ethane has been measured, and the theoretical model of Springett, Jortner, and Cohen (SJC) for the temperature dependence of V_0 is shown to apply to liquid alkanes as well as rare gases. Criteria for electron localization in liquid rare gases, molecular gases, and alkanes are critically discussed. The SJC criterion for electron localization in liquid rare gases is shown not be extendable to liquid alkanes or to molecular gases. In alkanes we assume that transient localization arises from rotational and translational fluctuations leading to cavities of molecular size. Then consideration of the kinetic and electronic polarization energies with a cavity radius given by the Wigner–Seitz radius leads to a new localization criterion that seems generally applicable to alkane systems. Electrons in molecular gases probably move as molecular anions so neither of the above criteria apply to them. An empirical relation between the electron mobility and V_0 is found that seems valid for all alkanes at room temperature for both localized and quasi-free electron states. Values of V_0 for polar and nonpolar glassy matrices at 77 K are derived from experimental data by two independent methods. It is found that V_0 becomes more positive as the glassy matrix polarity decreases.

Introduction

Excess electrons are excellent probes of the complex electron–molecule interactions found in condensed media. Electron mobilities and conduction state energy levels relative to vacuum are the major experimental quantities available to probe the weak interactions of excess electrons, while optical and magnetic resonance spectroscopy of excess electrons can probe stronger interactions leading to electron localization.[1] Rare gases constitute the simplest condensed media. There the electron mobilities and conduction state energies are fairly well understood theoretically[2] although discrepancies do remain, notably in liquid helium.[3]

Condensed alkanes are much more complex and electron interactions in them are the focus of much current interest. Electron mobilities μ have been measured in both liquid[4–6] and glassy[7,8] phases for a wide variety of alkanes, and conduction electron energies V_0 have been reported for several higher molecular weight alkanes.[9–12] The basic question is to what degree the theories of V_0[13] and of μ,[14] which seem rather successful for rare gases, apply to condensed molecular media. Attempts have been made to extend these theories to liquid alkanes.[15–17] It has also been suggested both experimentally[9,18] and theoretically[19,20] that there is a general correlation between μ and V_0 for rare gas and alkane liquids.

In this work we report measurements of V_0 for both liquid ethane and methane over a limited range of temperature to compare with the measured mobilities in these liquids and to test the generality of a correlation between μ and V_0. The correlation appears to fail for methane.[21] We present a simple successful model of the temperature dependence of V_0 and discuss a new approach to the relation between μ and V_0. Finally, we consider photoionization

data in a variety of glassy matrices and derive estimated values of V_0 for organic and aqueous glasses.

Experimental Section

Methane (99.99% Matheson research grade), ethane (99.94% Phillips research grade), and argon (99.995% Matheson research grade) were purified by passing through activated silica gel (activated at 300°C in vacuo for 48 hr) and activated charcoal (activated at 200°C in vacuo for 48 hr) columns at 195 K. Methane and ethane were stored over activated silica gel at 77 K, and argon was stored over activated charcoal at 77 K.

Conduction state energies were measured by work function changes of zinc electrodes in vacuo compared to the liquid. Our apparatus was similar to that described by Holroyd and Allen[9] with modifications for low-temperature work. Light from an air-cooled Philips SP-900W mercury lamp passed through a Bausch and Lamb high-intensity uv monochromator and appropriate filters to eliminate scattered light and higher order diffractions and was reflected 90° by a mirror up through the unsilvered flat bottom of a quartz dewar onto the bottom quartz window of the photoelectric cell. The light passed through an electron collector electrode made of brass mesh to strike the zinc-coated emitting electrode. The electrodes were separated by a 0.5 mm Mylar spacer. The applied voltage was obtained from a Keithley 245B power supply, and the photocurrent was measured with a Keithley 610B electrometer. Temperatures were obtained with liquid argon or by cold nitrogen gas flow and were monitored with a calibrated digital thermocouple thermometer.

The cell and vacuum line were flushed with purified gas and evacuated to <1 Pa (1×10^{-5} Torr). Zinc was freshly deposited on the emitter electrode in vacuo, and the photocurrent was measured between 280 and 400 nm. The liquid was transferred to the cell, the photocurrent remeasured, the cell evacuated, and the photocurrent measured again in vacuo. For variable-temperature runs the emitter electrode was reused until the active metal surface deteriorated as indicated by a significant drop, typically twofold, of the photocurrent in vacuo. The light intensity was measured at the emitter electrode position with a YSI Model 65 radiometer. The work functions were determined by a fit of the data to Fowler's spectral response curve for photocurrents.[22] The applicability of this response curve to dielectric liquids has been verified experimentally[9] and theoretically.[23] The work functions were reproducible to ±0.02 eV between runs on different days.

Results

Table I summarizes the V_0 measurements as a function of temperature. The temperature dependence is also calculated from a simple model discussed below. Figure 1 shows data for one run in argon and demonstrates the reproducibility attainable. Figure 2 shows typical data for ethane at one temperature; a similar plot for methane was published previously in a communication.[21]

Near the boiling points of methane (111 K) and ethane (185 K), the V_0 values are essentially equal. This contrasts strikingly with the electron mobilities in methane (400 $cm^2\ V^{-1}\ sec^{-1}$) and ethane (0.85 $cm^2\ V^{-1}\ sec^{-1}$) at these temperatures and suggests that the theoretical models for V_0 and μ and the relation between them must be reexamined.

TABLE I: Temperature Dependence of V_0 in Liquids

Liquid	T, K[a]	n, $Å^{-3}$	V_0(calcd), eV	V_0(exptl), eV[b]
Methane[c]	109	0.0161	(0.0)[d]	0.0
	91	0.0171	0.07	0.1
Ethane	182	0.0110	(0.02)	0.02
	152	0.0118	0.14	0.15
	130	0.0124	0.21	0.22
	103	0.0131	0.35	0.28
Argon	87			−0.17

[a] ±0.2 K. [b] ±0.02 eV for methane; ±0.03 eV for others. [c] W. Tauchert and W. F. Schmidt [*Z. Naturforsch., Teil A* 29, 1526 (1974)] have recently confirmed our value of V_0 for methane. [d] Values in parentheses are assumed and values at other temperatures are calculated relative to these; see text for details.

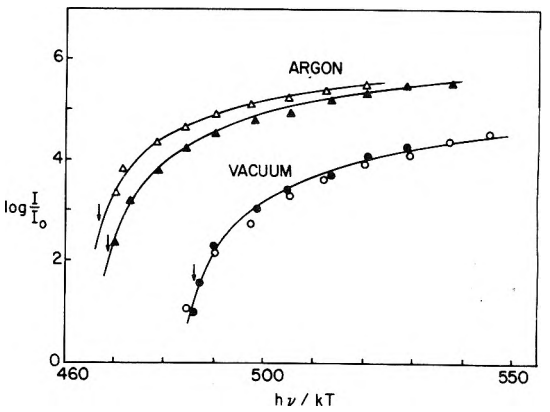

Figure 1. Photoelectric work function plot for argon at 87 K on a zinc electrode at 4 kV/cm field. The solid lines are theoretical Fowler curves fitted to the open experimental points. The arrows indicate the origin of the Fowler curve and therefore the work function. The solid points represent a second experimental run with the same electrode.

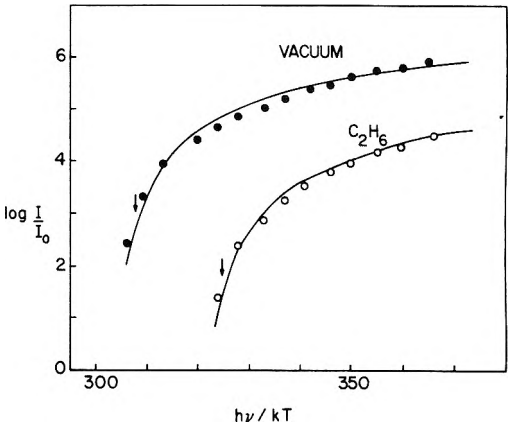

Figure 2. Photoelectric work function plot for ethane at 130 K on a zinc electrode at 2 kV/cm field. The solid lines are theoretical Fowler curves fitted to the experimental points. The arrows indicate the origin of the Fowler curve and therefore the work function.

Discussion

A. Conduction State Electron Energies in Liquid Rare Gases. Calculation of the energy levels of an excess electron in any multiatom system depends upon formulating a tractable potential. For a delocalized electron in condensed media Springett, Jortner, and Cohen[13] did this by using pseudopotential arguments to account for the orthogonality of the excess electron wave function with the bound

TABLE II: Experimental Measurements of Conduction Electron Energies in Liquid Rare Gases

System	Temp, K	V_0, eV	Method	$\bar{a}$(derived),[a] Å
He[b]	1.1	1.02 ± 0.08[c]	Direct, PI, LT[d]	0.68 ± 0.02
He[e]	1.4	1.3 ± 0.4	Indirect[f]	
Ar[g]	87	−0.17 ± 0.03	Direct, PI, FT[h]	0.93 ± 0.05
Ar[i]	85	−0.33 ± 0.05	Direct, PI, LT[d]	0.90 ± 0.09
Ar[j]	105	−0.45 ± 0.2	Indirect[k]	0.87 ± 0.45
Kr[j]	135	−0.78 ± 0.2	Indirect[k]	0.99 ± 0.45

[a] Hard core atomic radius derived from V_0 by the theory of ref 13. The data used are as follows: He, α = 0.204 Å^3 and n(1.1 K) = 0.02189 Å^{-3}; Ar, α = 1.63 Å^3, n(85–87 K) = 0.02096 Å^{-3}, and n(105 K) = 0.01921 Å^{-3}; Kr, α = 2.465 Å^3 and n(135 K) = 0.01648 Å^{-3}. [b] M. A. Woof and G. W. Rayfield, *Phys. Rev. Lett.*, 15, 235 (1965). [c] Independent of temperature from 1.1 to 2.2 K. Note that the density only increases by 0.7% in this range. [d] Direct method by photoelectric injection, linear threshold used. [e] W. T. Sommer, *Phys. Rev. Lett.*, 12, 271 (1964). [f] Indirect method involving analysis of electron passage across the liquid–gas interfact. [g] This work; if a linear threshold is used, V_0 = −0.26 ± 0.2 eV. [h] Direct method by photoelectric injection, Fowler function threshold used. [i] B. Halpern, J. Lekner, S. A. Rice, and R. Gomer, *Phys. Rev.*, 156, 351 (1967). [j] B. Raz and J. Jortner, *Chem. Phys. Lett.*, 4, 155 (1969). [k] Indirect method based on analysis of Wannier type impurity states in Xe-doped liquids and based on calculated polarization energies of the positive ion.

atomic electron wave functions, as required by the Pauli principle, and by using the Wigner–Seitz model to obtain a spherically symmetric potential. In the Wigner–Seitz model each atom is replaced by a sphere of radius r_s given by

$$r_s = (3/4\pi n)^{1/3} \tag{1}$$

where n is the number density. The potential is assumed spherically symmetric and identical in each sphere; thus density fluctuations in the medium are neglected. The eigenvaue equation is then

$$[(-\hbar^2/2m)\nabla^2 + V_m]\phi_0 = V_0\phi_0 \tag{2}$$

where ϕ_0 is a pseudo wave function, which is smooth inside r_s, and V_m is the pseudopotential approximated as ∞ for $r < \bar{a}$ and as U_p for $r > \bar{a}$. This pseudopotential excludes the excess electron from the hard core radius $\bar{a}$ of the atoms. U_p is the polarization potential from the atom inside and the atoms outside r_s which is approximated by

$$U_p = \frac{-3\alpha e^2}{2r_s^4}\left[\frac{8}{7} + \left(1 + \frac{8}{3}\pi\alpha n\right)^{-1}\right] \tag{3}$$

where α is the isotropic polarizability. Then (2) may be solved to yield

$$V_0 = U_p + \hbar^2k_0/2m = U_p + T_0 \tag{4}$$

where the electron wave vector k_0 is obtained from the Wigner–Seitz boundary condition $(d\phi_0/dr)_{r=r_s} = 0$ which gives the equation

$$\tan k_0(r_s - \bar{a}) = k_0 r_s \tag{5}$$

T_0 is the zero point energy which arises because the excess electron is excluded from the hard core region of radius $\bar{a}$ in each Wigner–Seitz sphere.

Assuming the polarizability and density are known, V_0 may be calculated from $\bar{a}$ and vice versa. V_0 may be directly determined experimentally but $\bar{a}$ cannot. Thus, derived experimental values of $\bar{a}$ must come from V_0 measurements. However, $\bar{a}$ can be independently obtained from the calculated effective electron scattering cross section by only the Hartree–Fock potential of an atom or molecule via $\sigma_{HF} = 4\pi\bar{a}^2$. Note that σ_{HF} is *not* the experimental gas-phase scattering cross section because the real total potential includes both Hartree–Fock and polarization components.

There have been few measurements of V_0 in liquid rare gases. The ones extant including ours in argon are summarized in Table II. Direct photoelectric injection methods are felt to be the most accurate. We have used the Fowler function[22] to find the thresholds and believe that this should give more accurate results than thresholds from simple linear extrapolations. Our value (−0.17 eV) is less than a previous direct experiment (−0.33 eV)[24] in which a linear extrapolation was used. If we try to fit Halpern et al.'s data[24] to a Fowler plot, we find that it is all far above the Fowler threshold. This perhaps explains some of the discrepancy between the two sets of results; if we use a linear extrapolation on our data we find $V_0 \sim -0.26$ eV. Raz and Jortner[25] determined V_0 in argon by an interesting indirect method. They interpret the vacuum uv absorption spectrum of 3 ppm Xe impurity in liquid argon as a hydrogenic series and obtain the series ionization limit I_1 from a Rydberg constant modified by the dielectric constant of the medium. Using the expression

$$I_1 = I_g + P^+ + V_0 \tag{6}$$

known values of the gas-phase ionization potential I_g, and calculated values of the polarization energy of the positive ion, P^+, they obtain V_0. Their experimental uncertainty comes from the spectral analysis, but it seems that the calculated values of P^+ in the solid (−1.10 eV), which were assumed to be the same in the liquid, could well be uncertain by several tenths of an electron volt.

Table II also shows values of $\bar{a}$ derived from the experimental V_0 values via eq 1–5. Note that $\bar{a}$ is relatively insensitive to V_0 but that the converse is not true. Thus theoretical V_0 values obtained by using a theoretical calculation or estimate of $\bar{a}$[13] seem subject to large errors which can exceed a factor of 2.

B. Temperature Dependence of V_0. V_0 is only a function of density if $\bar{a}$ is assumed independent of density. Within the framework of the V_0 theory presented, $\bar{a}$ is density independent. Thus a test of the validity of the V_0 theory may be provided by the density dependence of V_0 as obtained by changing temperature or pressure.

Recall that $V_0 = U_p + T_0$. U_p and T_0 change in opposite directions with density, so in principle V_0 may increase, decrease, or be independent of density. We will find that in alkanes V_0 becomes more negative with increasing temperature (decreasing density), but that V_0 is approximately independent of temperature in argon.

Changes in U_p are always dominated by r_s^{-4} or $n^{4/3}$. The term involving αn inside the bracket in eq 3 changes much more slowly for all reasonable values of α and n in atomic or molecular media; and, in fact, this term changes U_p in the opposite direction from the dominant $n^{4/3}$ dependence. So U_p becomes less negative as temperature increases.

T_0 becomes less positive as temperature increases, and it depends on both n and $\bar{a}$. Note that if $\bar{a}$ is changed T_0 changes but U_p does not, so the temperature dependence of V_0 is rather sensitive to $\bar{a}$. This suggests that the temperature dependence of V_0 may serve as a rather sensitive indication of the validity of a particular $\bar{a}$.

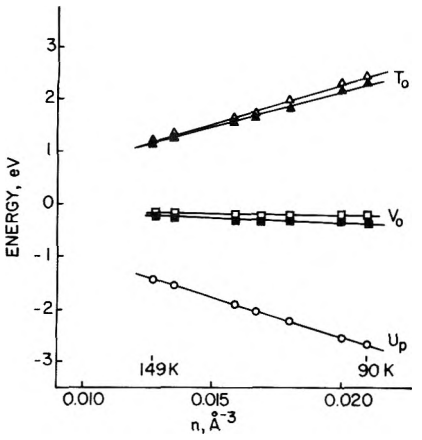

Figure 3. Calculated density dependence (or temperature dependence) of V_0 in liquid argon at 55 atm pressure. The density dependence of the T_0 and U_p components of V_0 is also shown. The open points correspond to $\bar{a}$ = 0.928 Å as determined from V_0 = −0.17 eV at 87 K at 1 atm. The solid points correspond to $\bar{a}$ = 0.904 Å as determined from V_0 = −0.33 eV at 85 K at 0.8 atm.

These points are illustrated in Figure 3 for argon over an extremely large density range. If $\bar{a}$ = 0.928 Å, as determined from V_0 = −0.17 eV at 87 K under 1 atm pressure, V_0 is constant with temperature. But if a = 0.904 Å, as determined from V_0 = −0.33 eV at 85 K under 0.8 atm, V_0 becomes less negative by ~0.1 eV (25%) with increasing temperature.

The only temperature-dependent measurements of V_0 in liquid rare gases are in helium. V_0 is temperature independent from 1.1 to 2.2 K. However, this is a trivial test since there is less than 0.7% change in density over this temperature range. It seems that a critical test of the V_0 theory can be carried out for liquid alkanes. Table I shows that the calculated temperature dependence of V_0 in methane and particularly in ethane agrees well with theory. This is further substantiated by similar good agreement for propane through n-hexane and several other branched alkanes.[11] Thus, all alkanes, including methane, seem to obey the V_0 theory of Springett et al.,[13] at least over the normal range of liquid densities. Furthermore, the temperature-independent values of the hard core radii $\bar{a}$ can be regarded as having some general validity, and trends between these radii are probably meaningful. It would be interesting to measure V_0 vs. temperature in argon and other rare gases to further test the V_0 theory, although we expect the theory to be even more valid for the rare gases. The alkane measurements do not extend into the critical region. There we might expect density fluctuations to be more important and to find a failure of the V_0 theory which ignores these. This could be most easily tested in the liquid rare gases.

C. Electron Localization Criteria. Given a value for V_0 in a condensed medium, one can then ask whether electron localization is possible. The general criterion for localization is that the ground-state energy level be less than the conduction state energy level or

$$E_t < V_0 \tag{7}$$

where E_t is the total ground-state energy relative to vacuum of the electron in the medium. If $E_t > V_0$, we then describe the electron as quasi-free and able to move in the conduction band of the medium. An experimental criterion of localization is the electron mobility and we may specify approximate limits as follows. From this experimental point of view

$$\mu_e \gtrsim 10 \text{ cm}^2 \text{ V}^{-1} \text{ sec}^{-1} \quad \text{quasi-free state stable} \tag{8}$$

$$\mu_e \lesssim 1 \text{ cm}^2 \text{ V}^{-1} \text{ sec}^{-1} \quad \text{localized state stable} \tag{9}$$

excess electrons are localized in the liquid phase of helium (^{3}He and ^{4}He), neon, hydrogen, and most alkanes, and are quasi-free in argon, krypton, xenon, methane, neopentane, and probably 2,2-dimethylbutane and 2,2,4,4-tetramethylpentane.[26]

Let us now examine how to obtain E_t for various media. We will use the general formulation for E_t given by the semicontinuum model.[1,27] E_t is given by

$$E_t = E_k + E_e^s + E_e^l + V_0(1 - C_i) + E_m^s + E_m^l + E_v + E_{pv} \tag{10}$$

where E_k is the kinetic energy, E_e^s and E_e^l are the short-range and long-range attractive electronic energies, $V_0(1 - C_i)$ is the short-range repulsive energy between the medium and the electron whose charge density within a given radius r is C_i, E_m^s and E_m^l are the short-range and long-range medium rearrangement energies due to polarization interactions, E_v is the void or surface tension energy, and E_{pv} is the pressure–volume energy associated with void formation. In media consisting of polar molecules like water, alcohols, etc., the E_e^s term due to charge–dipole interaction is large and negative (−2 to −4 eV) so that the localized state is always energetically favored. This situation has been treated in some detail[27] and will not be considered further. In media consisting of nonpolar molecules (rare gases, homonuclear diatomics, and alkanes) E_e^s and E_m^s = 0 because there are no permanent dipoles (or negligibly small ones in the case of alkanes) and E_m^l = 0 because the static and optical dielectric constants are equal. We will also consider media at low external pressures (<10 atm), so E_{pv} is negligible. Then we may write E_t as

$$E_t(\text{nonpolar}) = E_k + E_e^l + V_0(1 - C_i) + E_v \tag{11}$$

We can then consider two cases: one where the medium is microscopically nonpolar, as in rare gases, and the second where the medium is microscopically polar, as in alkanes. The first case has been treated by Springett, Jortner, and Cohen.[13] They assume that E_e^l can be neglected, which seems only justifiable for helium, and assume a spherical well potential for E_k. If the electron is localized within a spherical well, $C_i \to 1$ and the V_0 term drops out. Then for an infinite spherical well

$$E_t = E_k + E_v = h^2/8mR^2 + 4\pi R^2\gamma \tag{12}$$

where γ is the surface energy of the medium per unit area. Since this E_t is always positive, all rare gases with $V_0 < 0$ are predicted to exhibit quasi-free electrons. $V_0 < 0$ for argon, krypton, and presumably xenon by extrapolation, and electrons in these media do exhibit high mobilities indicating the quasi-free state. However, it is difficult to see how E_e^l can be justifiably neglected in these media. Molecular hydrogen[29] and a variety of alkanes[9] also have $V_0 < 0$, but these media do not exhibit high electron mobilities and hence the above simple model does not apply.

When $V_0 > 0$, a localization criterion has been obtained by Springett et al.[13] by choosing R to minimize E_t. They find

$$2\pi h^2\gamma/mV_0^2 < 1.0 \tag{13}$$

for an infinite spherical well or

$$2\pi h^2\gamma/mV_0^2 < 1.9 \quad (14)$$

for a finite spherical well. By (14), electrons in liquid ^{3}He, ^{4}He, and Ne ($V_0 \sim +0.5$ eV from spectral analysis of Wannier states in the solid[25]) are predicted to exhibit localization, and they do as indicated by low electron mobilities.[26] Whenever $V_0 > 0$ and small (<0.3 eV for typical values of γ), the localization criterion (eq 14) is not satisfied and the quasi-free state is predicted to be most stable. Thus for methane the quasi-free state is predicted which does correlate with the high electron mobility in liquid methane.[26] However, the quasi-free state is also predicted for electrons in ethane and other *n*-alkanes over the temperature ranges where V_0 is positive,[11] and this does not correlate with the low electron mobilities found in these liquids.

It appears that the model for E_t suggested by Springett, Jortner, and Cohen[13] applies only to rare gas liquids and not to molecular liquids. This is what one might expect from the assumptions used. Methane also fits the rare gas model, but we regard this as perhaps fortuitous since methane is microscopically polar.

We now present a model for E_t which appears to work for microscopically polar liquids like alkanes. In such liquids we consider that *transient* values of E_t may be important. E_t(transient) < V_0 is a necessary condition for electron localization, at least transiently. We assume that E_t(transient) can arise from rotational and translational (density) fluctuations in microscopically polar liquids leading to cavities of molecular size. We have recently shown that relatively deep electron binding can occur (~0.5 eV) in alkanes for properly arranged configurations of C–H bond dipoles in CH_2 fragments.[30] We then write

$$E_t(\text{transient}) = E_k + E_e^{\,l} \quad (15)$$

where the dominant contributions are the kinetic energy E_k and the electronic polarization energy $E_e^{\,l}$. The electronic polarization potential energy is given by $(-e^2/2R)(1 - D_{op}^{-1})$, where D_{op} is the optical dielectric constant. For cavity radii R of molecular size or smaller, this term cannot be neglected. However, we do neglect the surface tension energy term E_v because we envision the cavity to be formed by fluctuations rather than by repulsions of the localized electron; also, the cavities are small so the E_v term is small.

To apply this model we consider a finite spherical well for electron localization with the radius R given by the Wigner–Seitz radius r_s (eq 1). The radius r_s is of molecular size and seems appropriate to choose for a transient trap associated with rotational and translational fluctuations. The finite spherical well problem has been solved,[28] and a condition to have at least one bound state relative to the vacuum level and hence the possibility of electron localization in the case of potential $E_e^{\,l}$ is given by

$$0 > E_e^{\,l} + \pi^2\hbar^2/8mr_s^2 \quad (16)$$

This simply states that the total energy is nonpositive for electron binding to occur. In the case of interest here the bound state must be less than the conduction electron level so our criterion for electron localization becomes

$$V_0 > \frac{-e^2}{2r_s}\left(1 - \frac{1}{D_{op}}\right) + \frac{\pi^2\hbar^2}{8mr_s^2} \equiv V_0^* \quad (17)$$

We then have the following localization criteria where approximate mobility ranges are

$$(V_0 - V_0^*) > 0 \rightarrow \text{localization } (\mu_e \lesssim 1 \text{ cm}^2\text{ V}^{-1}\text{ sec}^{-1}) \quad (18)$$

$$(V_0 - V_0^*) < 0 \rightarrow \text{quasi-free } (\mu_e \gtrsim 10 \text{ cm}^2\text{ V}^{-1}\text{ sec}^{-1}) \quad (19)$$

given in accordance with the range above which electron band motion is considered valid. We have therefore found that the general localization criterion, $E_t < V_0$, can be replaced by the localization criterion $V_c^* < V_0$. The advantage is that we have a simple expression for V_0^* that can be simply evaluated, whereas evaluation of E_t requires the nontrivial solution of an eigenvalue equation.

Table III summarizes the data on mobility, V_0, V_0^*, and the two components of V_0^* from eq 17 for electrons in the alkanes plus tetramethylsilane for which V_0 measurements have been reported. Methane, neopentane, and tetramethylsilane are clearly predicted to exhibit the quasi-free electron state, and this is consistent with the high electron mobility in these liquids. The quasi-free electron state is also predicted for 2,2-dimethylbutane and 2,2,4,4-tetramethylpentane as is consistent with their reasonably high electron mobility, but this prediction is borderline. The other alkanes are correctly predicted to exhibit electron localization and a consequent low electron mobility.

As discussed above, V_0 is temperature dependent; for alkanes it decreases with increasing temperature. Thus we must also consider the temperature dependence of V_0^* and how it affects the above correlation. V_0^* depends on the temperature dependence of both r_s and D_{op}, and for alkanes V_0^* increases very slowly with increasing temperature (Table IV). The net result is that $(V_0 - V_0^*)$ decreases with increasing temperature. This suggests that the quasi-free state becomes more favorable at higher temperature. In ethane the onset of the quasi-free state is predicted to occur near 180 K; μ does approach unity near this temperature.[4] In general, Table IV shows that the criteria (18) and (19) still hold over the temperature ranges for which V_0 has been measured in alkane systems.

We point out that our localization criteria, (18) and (19), are not expected to and do not apply to rare gas liquids since our assumption that R equals the Wigner–Seitz radius is then not valid. If one tries to apply (18) and (19) to rare gases, the quasi-free state is always predicted, even for Ne and He.

The liquified molecular gases H_2, D_2, O_2, and N_2 all have low electron mobilities (<3×10^{-2} cm^2 V^{-1} sec^{-1}).[31] V_0 has been measured indirectly only for H_2.[29] The localization criteria that seem successful for rare gases (eq 14) and for alkanes (eq 18) do not seem applicable to these molecular gases. Both localization criteria (eq 14 and 18) predict stability of the quasi-free state for electrons in liquid H_2; this is inconsistent with the low electron mobility. It seems probable that the negative charge carriers in these liquified gases are molecular anions rather than localized excess electrons; thus the localization criteria considered, (14) and (18), are not expected to apply.

D. Relation between V_0 and Critical Volumes. Davis and Schmidt[17] have suggested that the hard core radius $\bar{a}$ derived from V_0 data correlates with the cube root of the critical volume such that $\bar{a}/V_c^{1/3} = 0.305$ Å/(cm^3/mol)$^{1/3}$. This was supported by consideration of V_0 data in nine alkanes at room temperature. We find that this suggested correlation does not apply to methane, ethane, or argon for which $\bar{a}/V_c^{1/3} = 0.454$, 0.425, and 0.220 Å/(cm^3/mol)$^{1/3}$, respectively. The relation between these two size parameters apparently exhibits considerable subtilty.

E. Relation between V_0 and Electron Mobility. Lekner[32] obtained eq 20 for the low-field mobility of quasi-free elec-

TABLE III: Comparison of the Calculated Electron State Energy (V_0*) with the Observed Conduction State Energy (V_0)

Medium	T, K	μ, $cm^2 V^{-1} sec^{-1}$	E_e[l], eV	E_k, eV	V_0*, eV	V_0, eV	$V_0 - V_0$*,[o] eV
Methane	109	400[a]	−1.161	1.566	0.41	0.0[b]	−0.41
Ethane	130	0.014[c,d]	−1.263	1.309	0.05	0.22[b]	+0.17
Propane	175	0.04,[c] 0.05[d]	−1.150	1.044	−0.11	0.11[e]	+0.22
n-Butane	271	0.15[d]	−0.956	0.828	−0.13	0.12[e]	+0.25
n-Pentane	293	0.075,[f] 0.14[g] 0.16[h]	−0.921	0.738	−0.18	−0.01,[i] +0.04[j] +0.02,[k] +0.01[e]	+0.17, +0.22 +0.20, +0.19
Cyclopentane	293	1.1[h]	−1.068	0.848	−0.22	−0.28,[i] −0.17[j] −0.18,[k] −0.21[e]	−0.06, +0.05 +0.04, +0.01
Neopentane	293	50,[l] 54[g] 55,[h] 70[m,n]	−0.900	0.724	−0.18	−0.43,[i,k] −0.35[j] −0.38[e]	−0.25, −0.17 −0.20
n-Hexane	293	0.076,[m] 0.082[g] 0.09[h]	−0.906	0.676	−0.23	0.04,[i] 0.0,[i] 0.16[p] 0.09,[k] 0.10[e]	0.27. 0.23. 0.39 0.32, 0.33
Cyclohexane	293	0.24,[g] 0.35[h] 0.45[l]	−1.035	0.767	−0.27	0.01[e]	+0.28
2-Methylpentane	293		−0.902	0.672	−0.23	−0.20[p]	+0.03
3-Methylpentane	293		−0.912	0.687	−0.23	0.0,[k] 0.01,[e] −0.14[p]	0.23, 0.24, 0.09
2,2-Dimethylbutane	293	10,[h] 12[n]	−0.893	0.668	−0.23	−0.24,[k] −0.26[e] −0.15[p]	−0.01, −0.03 +0.08
2,3-Dimethylbutane	293		−0.918	0.684	−0.23	−0.10[p]	+0.13
2,3-Dimethylbutene-2	293		−0.998	0.725	−0.27	−0.25[e]	+0.02
2,2,4-Trimethylpentane	293	7[h]	−0.858	0.579	−0.28	−0.18,[i] −0.14[j] −0.15,[k] −0.17[e]	+0.10, +0.14 +0.13, +0.11
2,2,4,4-Tetramethylpentane	293	24[l]	−0.863	0.551	−0.31	−0.33[e]	−0.02
Tetramethylsilane	293	90,[h] 100[g]	−0.875	0.661	−0.21	−0.59,[e] −0.62[i] −0.55[j]	−0.38, −0.41 −0.34

[a] G. Bakale and W. F. Schmidt, *Z. Naturforsch., Teil A* 28, 511 (1973). [b] S. Noda and L. Kevan, *J. Chem. Phys.*, **61**, 2467 (1974), and data herein. [c] G. Bakale, U. Sowada, and W. F. Schmidt, *ibid.*, in press. [d] M. G. Robinson and G. R. Freeman, *Can. J. Chem.*, 52, 440 (1974). [e] R. A. Holroyd and R. L. Russell, *J. Phys. Chem.*, 78, 2128 (1974). [f] R. M. Minday, L. D. Schmidt, and H. T. Davis, *J. Chem. Phys.*, 54, 3112 (1971). [g] A. O. Allen and R. A. Holroyd, *J. Phys. Chem.*, 78, 796 (1974). [h] W. F. Schmidt and A. O. Allen, *J. Chem. Phys.*, 52, 4788 (1970). [i] R. A. Holroyd and M. Allen, *ibid.*, 54, 5014 (1971). [j] R. A. Holroyd, B. K. Dietrich, and H. A. Schwarz, *J. Phys. Chem.*, 76, 3794 (1972). [k] R. A. Holroyd, *J. Chem. Phys.*, 57, 3007 (1972). [l] J. P. Dodelet and G. R. Freeman, *Can. J. Chem.*, 50, 2667 (1972). [m] R. M. Minday, L. D. Schmidt, and H. T. Davis, *J. Phys. Chem.*, 76, 442 (1972). [n] G. Bakale and W. F. Schmidt, *Chem. Phys. Lett.*, 22, 164 (1973). [o] Where $(V_0 - V_0^*) > 0$ indicates electron localization and low mobilities and $(V_0 - V_0^*) < 0$ indicates quasi-free electron states and high mobilities. [p] R. Schiller, Sz. Vass, and J. Mandico, *Int. J. Radiat. Phys. Chem.*, 5, 491 (1973).

trons in nonpolar liquids like argon which is equivalent to the equation derived by Bardeen and Shockley[33] for electron mobility in nonpolar crystals. In (20) k is Boltzmann's

$$\mu_0 = \tfrac{2}{3}(2/\pi mkT)^{1/2}[e/n\sigma S(0)] \qquad (20)$$

constant, σ is the electron scattering cross section, and $S(0)$ is the low wave vector limit of the x-ray structure factor which equals $nkT\kappa_T$, where κ_T is the isothermal compressibility. Since κ_T can be measured experimentally, application of this mobility expression only requires a knowledge of σ. Lekner[32] considered coherent single scattering events and wrote $\sigma = 4\pi\tilde{a}^2$, where $\tilde{a}$ is a liquid-phase scattering length. For polyatomic molecules incoherent scattering from internal degrees of freedom can also contribute. This has been considered by Davis, Schmidt, and Minday,[34] but estimates of the effects of incoherent scattering contributions are not normally large, at least for alkanes, so we will not include this complication. Multiple scattering effects have been discussed by Lekner[32] and will also be neglected.

We are then left with the problem of evaluating $\tilde{a}$ in order to calculate the quasi-free electron mobility. Fueki, Feng, and Kevan[15] and Davis, Schmidt, and Minday[16] suggested that $\tilde{a}$ could be equated to $\bar{a}$ determined from experimental values of V_0. Since $\bar{a}$ is determined only by the Hartree–Fock field, this is equivalent to assuming that the polarization potential contributions cancel out for scattering in nonpolar liquids. This assumption seems to be supported for argon by Lekner's calculations.[32] The validity of this assumption for alkanes is more uncertain. Although calculated mobilities using this assumption seem reasonable,[15,16] the mobilities are rather insensitive to the assumption as shown below.

Within the framework of the theories for V_0 and μ_0, together with the assumption that $\tilde{a} = \bar{a}$ it is possible to calculate μ_0 from V_0 and vice versa for quasi-free electrons. Table V summarizes results of some such calculations. It can be seen that the calculated values of μ_0 agree only in order of magnitude with experiment and are rather insensitive to V_0. It appears that "ball park" mobilities may always be calculated because of the insensitivity to V_0. However, it is doubtful that reliable trends in μ_0 can be predicted so the assumption $\tilde{a} = \bar{a}$ is called into question. This assumption may be applicable to argon[32] but not to krypton or xenon because the larger polarization contributions in these heavier gases may not cancel out. Reliable mobilities in these three heavy rare gases are available. However, a set of consistent V_0 values, preferably determined in one laboratory, is needed to better test the connection between the V_0 and μ_0 theories. If V_0 is calculated from μ_0 the results are poor. This is simply a reflection of the insensitivity of V_0 to μ_0 when connected by the assumption $\tilde{a} = \bar{a}$; this is most evident for small values of V_0 near 0.

As shown previously[15] it seems possible to interpret the mobility of localized electrons in alkanes by assuming that the mobility is given by

$$\mu = \mu_0 \exp(-E_a/RT) \qquad (21)$$

where μ_0 is the quasi-free electron mobility calculable from V_0 and E_a is the experimental activation energy. Here we have implicity assumed that the ratio of the density of

TABLE IV: Temperature Dependence of the Electron Stability Criterion ($V_0 - V_0^*$) in Alkanes

T, K	V_0, eV[a,b]	V_0^*, eV	$V_0 - V_0^*$, eV
	Methane		
109	0.0	0.41	−0.41
91	0.1	0.44	−0.30
	Ethane		
182	0.02	0.09	−0.07
152	0.15	0.07	0.08
130	0.22	0.05	0.17
103	0.28	0.02	0.26
	n-Butane		
271	0.12	−0.13	0.25
239	0.23	−0.16	0.39
224	0.27	−0.17	0.44
199	0.35	−0.19	0.54
	n-Pentane		
297	0.02	−0.18	0.20
270	0.12	−0.20	0.32
260	0.14	−0.20	0.34
229	0.20	−0.23	0.45
	n-Hexane		
335	0.01	−0.21	0.22
298	0.10	−0.23	0.33
251	0.22	−0.26	0.48
204	0.34	−0.29	0.63
193	0.37	−0.29	0.66
175	0.40	−0.30	0.70
	2,2,4-Trimethylpentane		
296	−0.17	−0.28	0.11
191	0.08	−0.34	0.42

[a] This work for methane and ethane. [b] R. A. Holroyd and R. L. Russell, *J. Phys. Chem.*, 78, 2128 (1974), for other alkanes.

TABLE V: Calculations of μ_0 from V_0 and Vice Versa for Quasi-Free Electron Systems

Medium	T, K	μ_0, exptl, cm² V⁻¹ sec⁻¹	μ_0 from $V_0(\bar{a})$, cm² V⁻¹ sec⁻¹	V_0 from $\mu_0(\bar{a})$, eV	V_0, exptl, eV
Methane	111	400	272	−1.11	−0.01
Argon	85	450	228	−1.34	−0.17
			245		−0.33
Krypton	117	1800	286	−2.44	−0.78
Neopentane	293	55	275	−2.23	−0.38

states at the bottom of the conduction band to the density of the localized states is near unity. Equation 21 predicts a linear plot for log μ vs. E_a at constant temperature. We may interpret E_a as $|E_\parallel|$(transient) referenced to V_0. We thus expect that ($V_0 - V_0^*$) will qualitatively correlate with the mobility activation energy, E_a. This correlation is only approximate since ($V_0 - V_0^*$) is weakly temperature dependent. Figure 4 appears to support this picture by a roughly linear correlation for a wide variety of alkanes near room temperature, although other interpretations may be possible. It is striking that this correlation seems to include electrons in both localized and quasi-free states. Methane at 109 K is also included in this figure; its mobility has a weak temperature dependence, and if $\mu \propto T^{-3/2}$ is assumed, the extrapolated mobility at 295 K is 100 cm² V⁻¹ sec⁻¹. ($V_0 - V_0^*$) will also become somewhat more negative so the extrapolated point to room temperature will also roughly fit the correlation.

The idea of transient trapping of electrons in alkanes has been used before to suggest quantitative correlations between μ and V_0.[12,19,20] The model of Kestner and Jortner[19] and that of Schiller[20] assume a two-state picture involving high and low mobility regions. Kestner and Jortner emphasize that the medium is microscopically inhomogeneous while Schiller emphasizes energy fluctuations of the electron states in a homogenous medium. Both approaches lead to a nonlinear correlation between log μ and V_0 with two[20] or four[19] parameters. Although a two-state picture of mobility would be expected to extrapolate to the high mobility limit (quasi-free state), both of these correlations predict $V_0 \lesssim -0.8$ eV for the quasi-free state in methane which does not agree with experiment. Schiller has suggested that these two-state mobility models may be brought into agreement with experiment by making other assumptions about the parameters involved.[35] It also seems that the effect of temperature on these correlations should be investigated.

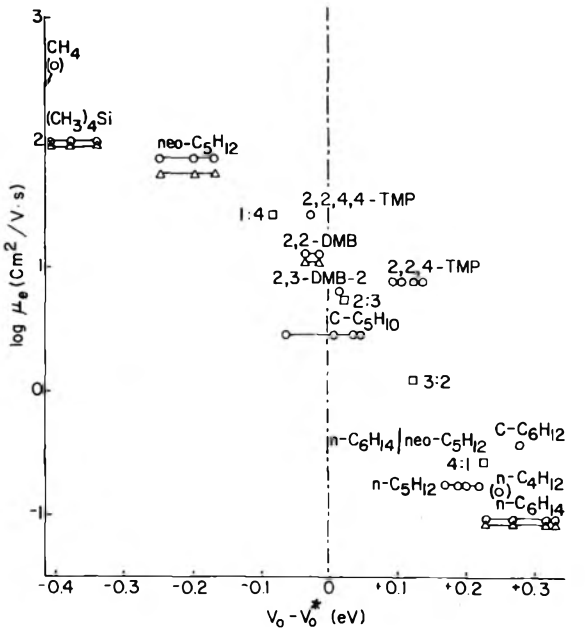

Figure 4. Correlation plot of electron mobility at room temperature (log scale) and the proposed stability criterion ($V_0 - V_0^*$) for excess electrons in liquid hydrocarbons. The electron mobilities and ($V_0 - V_0^*$) values were taken from Table III. The triangles and circles, for the same compound represent two different reported mobilities. The points connected by a line for a single compound correspond to different reported V_0 values. The abbreviations for the compounds may be deduced from the names given in Table III. The values in parentheses indicate results not at room temperature (~295 K). The n-C_4H_{10} results are for 271 K and would not change much when extrapolated to room temperature. The CH_4 results are for 111 K and would extrapolate to higher temperature in the direction of the arrow. The squares represent data from ref 6 and 18 for *n*-hexane–neopentane mixtures with the mole ratio shown.

Holroyd and Tauchert[18] have noted that the following empirical relation holds approximately for alkanes, $\mu = 0.35 \exp(-15.2 V_0)$, where V_0 is in electron volts and μ is in cm² V⁻¹ sec⁻¹. This relation gives $V_0 = -0.47$ eV for liquid methane and $V_0 = -0.06$ eV for liquid ethane and does not agree with the present experiments. Again, the effect of temperature on the above relation should also be explored.

F. V_0 in Glassy Matrices. Attempts were made to measure V_0 in various polar and nonpolar glassy matrices, but the photoemission currents were too small to measure in our apparatus. The addition of a chopped light beam with lock-in detection still did not improve the sensitivity enough. In 2-methyltetrahydrofuran (MTHF) and 3-meth-

TABLE VI: Derived Experimental Values of Conduction Electron Energies (V_0) in Glassy Matrices at 77 K (Method 1; See Text)

Matrix	ΔI	D_{op}	$-P_t$, eV	V_0, eV
Methylcyclohexane	0.85[a]	2.28	2.09	1.24
3-Methylpentane	0.85[a]	2.22	2.05	1.20
2-Methyltetrahydrofuran	1.08[a]	2.23	2.06	0.98
1-Propanol	1.65[b]	2.17	2.01	0.36
Ethanol	1.70[b]	2.08	1.94	0.24
Methanol	1.85[b]	1.97	1.84	−0.01
Ice	(2.0)[b]	1.78	1.64	−0.36
10 *M* KOH–H_2O	2.2[c]	1.96	1.83	−0.37

[a] A. Bernas, M. Gauthier, and D. Grand, *J. Phys. Chem.*, 76, 2236 (1972). [b] A. Bernas, M. Gauthier, D. Grand, and G. Parlant, *Chem. Phys. Lett.*, 17, 439 (1972) the value for ice is extrapolated. [c] R. Santus, A. Hèlene, C. Hèlene, and M. Ptak, *J. Phys. Chem.*, 74, 550 (1970).

ylpentane (3MP) glasses at 77 K, the photoemission current yield was $>10^5$ lower in the glass compared to the vacuum.

Since direct attempts to measure V_0 in glassy matrices failed, we have used the indirect method of eq 6 to obtain V_0. Bernas et al.[36-38] have measured the photoionization threshold I_s of tryptophan and *N,N,N′,N′*-tetramethyl-*p*-phenylenediamine (TMPD) solutes in a range of glassy matrices. Since the gas-phase ionization potential I_g is known for these solutes, values of $\Delta I = I_g - I_s$ are reported.[37-39] Then by calculating the cation polarization energy P^+ we can obtain V_0. We have calculated P^+ from[40]

$$P^+ = \frac{-e^2}{2r_0}\left(1 - \frac{1}{D_{op}}\right) \qquad (22)$$

where r_0 is the effective radius of the positive ion ($TMPD^+$) in the matrix. Instead of estimating a value of r_0 from geometrical considerations, as is typical, we obtain r_0 = 1.93 Å as the only unknown in eq 6 from experimental values of I_1, I_g, and V_0 in liquid *n*-pentane.[11,41] We implicitly assume r_0 to be temperature independent. Values of D_{op} at 77 K were obtained from n_d^2 at 77 K, where n_d is the refractive index. Room-temperature values of n_d were extrapolated to 77 K by analogy to the observed temperature dependence of n_d in glycerol.[42] The temperature coefficients (dn_d/dT) measured in the liquid[43] were extrapolated to the glass transition temperature, and below that the temperature coefficient was assumed to be zero. The values of D_{op} used are given in Table VI.

Table VI summarizes the indirect experimental values of V_0 obtained by this analysis together with ΔI and P^+. For ice and 10 *M* KOH tryptophan was used to measure ΔI and r_0 for $tryptophan^+$ was assumed to be the same as for $TMPD^+$. The matrices are listed in order of increasing polarity, and there appears to be a clear trend of decreasing V_0 with increasing polarity.

It is interesting to compare these V_0 values with the optimized V_0 values used in the semicontinuum model of trapped electron energy levels.[27] In this model V_0 is a limited adjustable parameter. Although the agreement is not quantitative, the trends are similar in polar matrices, and the more positive optimized V_0 values in the glass compared to the liquid are in agreement with what we know of the temperature dependence of V_0. In MTHF, however, there is significant disagreement between the optimized V_0 value from the semicontinuum model and the derived experimental value which deserves further investigation. Thus, in general, the derivation of V_0 values for polar glasses removes the last remaining parameter from the semicontinuum model with the not unexpected consequence of slightly less good agreement with experiment.

TABLE VII: Derived Experimental Values of Conduction Electron Energies (V_0) in Nonpolar Glassy Matrices at 77 K (Method 2; See Text)

Matrix	ρ, g/cm^3	r_s, Å	$\bar{a}$, Å[a]	V_0, eV
Methylcyclohexane	1.02	3.37	2.22	1.21
3-Methylpentane	0.88	3.39	2.16	0.82

[a] R. A. Holroyd and R. L. Russell, *J. Phys. Chem.*, 78, 2128 (1974).

In the photoionization of TMPD in liquid alkanes the value of ΔI is much larger than in the corresponding glassy matrices. For example, ΔI = 1.8 eV in liquid methylcyclohexane (MCH) and in liquid 3-methylpentane (3MP).[11] Since the P^+ energy only decreases by ~0.2–0.3 eV in the glass compared to the liquids, the major factor in changing ΔI is V_0. We have shown that the temperature dependence of V_0 in alkanes seems satisfactorily accounted for by the V_0 theory of Springett et al.,[13] so we may use this theory with directly measured values of V_0 in liquids to derive experimental values of V_0 in glassy matrices. The calculated values of V_0 at 77 K are given in Table VII together with values of the matrix density, ρ, the Wigner–Seitz radius, r_s, and the hard core radius, $\bar{a}$. This independent method of deriving V_0 values for glassy matrices gives results in reasonable agreement with the method summarized in Table VI.

The large positive value of V_0 in 3MP and MCH (~1 eV) is consistent with electron localization and the observed low electron mobilities in such glasses.[7,8] It also implies that the potential a mobile electron "sees" is very "rough" because of the large repulsive forces implied by the large positive V_0. Macroscopic voids in alkane glasses will act as low spots in the potential or as so-called preexisting traps. However, the potential will be considerably modified by bond dipole orientation and molecular configurational rearrangement as indicated by experimental[44,45] and theoretical[30] studies.

Acknowledgment. This research was supported by the U.S. Energy Research and Development Agency under Contract No. E(11-1)-2086.

References and Notes

(1) L. Kevan, *Adv. Radiat. Chem.*, **4**, 181–306 (1974).
(2) J. Jortner, *Ber. Bunsenges. Phys. Chem.*, **75**, 696 (1971).
(3) M. Silver, private communication.
(4) W. F. Schmidt, G. Bakale, and U. Sowada, *J. Chem. Phys.*, **61**, 5275 (1975).
(5) M. G. Robinson and G. R. Freeman, *Can. J. Chem.*, **52**, 440 (1974).
(6) R. M. Minday, L. D. Schmidt, and H. T. Davis, *J. Phys. Chem.*, **76**, 442 (1972), and earlier references cited therein.
(7) Y. Maruyama and K. Funabashi, *J. Chem. Phys.*, **56**, 2342 (1972).
(8) T. Huang and L. Kevan, *J. Chem. Phys.*, **61**, 4660 (1974).
(9) R. A. Holroyd and M. Allen, *J. Chem. Phys.*, **54**, 5014 (1971).
(10) R. A. Holroyd, *J. Chem. Phys.*, **57**, 3007 (1972).
(11) R. A. Holroyd and R. L. Russell, *J. Phys. Chem.*, **78**, 2128 (1974).
(12) R. Schiller, Sz. Vass, and J. Mandics, *Int. J. Radiat. Phys. Chem.*, **5**, 491 (1973).
(13) B. E. Springett, J. Jortner, and M. H. Cohen, *J. Chem. Phys.*, **48**, 2720 (1968).
(14) M. Cohen and J. Lekner, *Phys. Rev.*, **158**, 305 (1967).
(15) K. Fueki, D. F. Feng, and L. Kevan, *Chem. Phys. Lett.*, **13**, 413 (1972).
(16) H. T. Davis, L. D. Schmidt, and R. M. Minday, *Chem. Phys. Lett.*, **13**, 413 (1972).
(17) H. T. Davis and L. D. Schmidt, *Can. J. Chem.*, **51**, 3443 (1973).
(18) R. A. Holroyd and W. Tauchert, *J. Chem. Phys.*, **60**, 715 (1974).
(19) N. R. Kestner and J. Jortner, *J. Chem. Phys.*, **59**, 26 (1973).
(20) R. Schiller, *J. Chem. Phys.*, **57**, 2222 (1972).
(21) S. Noda and L. Kevan, *J. Chem. Phys.*, **61**, 2467 (1974).

(22) R. H. Fowler, *Phys. Rev.*, **38**, 45 (1931).
(23) A. M. Brodskii and Y. Y. Gurevich, *Sov. Phys. JETP (Engl. Trans.)*, **27**, 114 (1968).
(24) B. Halpern, J. Lekner, S. A. Rice, and R. Gomer, *Phys. Rev.*, **156**, 351 (1967).
(25) B. Raz and J. Jortner, *Chem. Phys. Lett.*, **4**, 155 (1969).
(26) W. F. Schmidt in "Electron-Solvent and Anion-Solvent Interactions", L. Kevan and B. Webster, Ed., Elsevier, New York, N.Y., 1975, Chapter **7**.
(27) K. Fueki, D. F. Feng, and L. Kevan, *J. Am. Chem. Soc.*, **95**, 1398 (1973).
(28) L. I. Schiff, "Quantum Mechanics", McGraw-Hill, New York N.Y., 1955, pp 76–77.
(29) A. Gedanken, B. Raz, and J. Jortner, *Chem. Phys. Lett.*, **14**, 326 (1972).
(30) D. F. Feng, H. Yoshida, and L. Kevan, *J. Chem. Phys.*, **61**, 4440 (1974).
(31) B. Halpern and R. Gomer, *J. Chem. Phys.*, **51**, 1031 (1969).
(32) J. Lekner, *Phys. Rev.*, **158**, 130 (1967).
(33) J. Bardeen and W. Shockley, *Phys. Rev.*, **80**, 72 (1950).
(34) H. T. Davis, L. D. Schmidt, and R. M. Minday, *Phys. Rev. A*, **3**, 1027 (1971).
(35) R. Schiller, private communication.
(36) A. Bernas, J. Blais, M. Gauthier, and D. Grand, *Chem. Phys. Lett.*, **30**, 383 (1975).
(37) A. Bernas, M. Gauthier, and D. Grand, *J. Phys. Chem.*, **76**, 2236 (1972).
(38) A. Bernas, M. Gauthier, D. Grand, and G. Parlant, *Chem. Phys. Lett.*, **17**, 439 (1972).
(39) R. Santus, A. Helène, C. Helène, and M. Ptak, *J. Phys. Chem.*, **74**, 550 (1970).
(40) J. Jortner, *J. Chem. Phys.*, **30**, 839 (1959).
(41) Here I_g = 6.6 eV was used to be consistent with the ΔI values reported by Bernas et al.[37,38] If I_g = 6.2 eV is used, P^+ as well as ΔI are both decreased by ~0.4 eV so the derived value of V_0 is unchanged.
(42) K. Schultz, *Kolloid Z.*, **138**, 75 (1954).
(43) Landolt-Bornstein, "Zahlenwerte und Funktionen," Band II, 8 Teil, Springer-Verlag, Berlin, 1962, p 572; when dn_0/dT was not given for a particular compound, it was estimated from data of similar compounds.
(44) N. V. Klassen, H. A. Gillis, and G. G. Teather, *J. Phys. Chem.*, **76**, 3847 (1972).
(45) H. Hase, T. Higashimura, and M. Ogasawara, *Chem. Phys. Lett.*, **16**, 214 (1972).

Discussion

M. H. COHEN. The transition in the mobility from quasi-free electron behavior to that associated with electrons bound within well-defined configurations of the liquid occurs continuously. In the transition region, Anderson localization occurs. Electrons are indeed transiently trapped in fluctuations in the liquid, but the latter are not well defined and cover a broad range of configurations. Moreover, the mobility contains contributions from both extended, i.e., quasi-free, states and from localized states. Thus, arbitrarily to select one as a mobility marking a transition from quasi-free electron behavior to localized behavior when $V_0 = V_0^*$ is an oversimplification. Further, it is only well after the mobility is dominated by localized states that the liquid configuration or trapping configuration becomes sharply enough defined to be obtained from an energy minimization criterion. Any such criterion has to include the energy required to form the fluctuation, which goes over continuously to the surface energy contribution.

L. KEVAN. I agree that the transition from delocalized to localized states of electrons in different alkanes is not a sharp one. And as our correlation between log μ_e vs. $V_0 - V_0^*$ shows, the trend of the points between clearly localized electron states, as in *n*-pentane, to clearly delocalized electron states, as in methane, is roughly continuous. What we think we have provided is a simple criterion that does validly predict both extremes of electron behavior and provides a connection over the entire mobility region. In the mobility range of ~1 to ~10 cm^2 V^{-1} sec^{-1}, we clearly have intermediate behavior as far as localization goes, and likewise when our $V_0 - V_0^*$ criterion is say ~−0.05 to ~+0.05 eV, we clearly have an intermediate range where the predictability of the criterion is not sharp. We have indeed ignored the energy of the fluctuations which produce the transient cavities of molecular size. This assumption seems valid for the extreme cases of electron localization and delocalization which we seem to have accounted for, and this assumption becomes less good in the transition region.

J. JORTNER. (1) Concerning the V_0 for dense rare gases I'm somewhat worried by your statement that this quantity calculated by the SJC model is density independent in liquid Ar due to mutual cancellation between changes in the T_0 and U_p energy terms. We have recently determined experimentally for spectroscopic and photoemission data the value $V_0 = +0.3 \pm 0.1$ eV *for solid Ar*, while the corresponding value in the liquid is -0.33 to -0.17 eV.

(2) Your electron localization picture for hydrocarbons differs from the SJC model originally applied to simple dense fluids. Also in heavier rare gases polarization effects have to be incorporated in the calculation of the energy of the localized state. The main difference between your approach and the SJC model lies in a different treatment of short-range repulsive interactions. I wonder whether a physical argument can be advanced concerning this point. If your model does not work for electron localization in the simple case of liquid rare gases, its detailed justification for hydrocarbons is crucial.

(3) In segregating excess electron states in liquid hydrocarbons into two categories, localized ($\mu < 1$ cm^2 V^{-1} sec^{-1}) and extended ($\mu > 10$ cm^2 V^{-1} sec^{-1}), you disregard the most interesting aspect of the continuous variation of the mobility with the change of molecular structure in these liquids. On the other hand, two such extreme situations prevail for liquid rare gases where $\mu \equiv 10^{-2}$–10^{-3} cm^2 V^{-1} sec^{-1} for liquid He and Ne (i.e., localized state) while $\mu \simeq$ 400–2000 cm^2 V^{-1} sec^{-1} for liquid Ar, Kr, and Xe (i.e., extended quasi-free state), such a sharp distinction does not prevail in liquid hydrocarbon. In the latter case we face the interesting physical situation where local fluctuation (probably orientational fluctuation) determines the transport properties. This is a most interesting and challenging problem.

L. KEVAN. (1) Figure 3 is a plot of the cancellation of the T_0 and U_p terms for liquid argon at 55 atm pressure. As for your V_0 measurement in solid Ar, it would be interesting to measure V_0 vs. temperature in the solid phase and see how this would compare with the SJC model.

(2) I probably overemphasized that our approach does not apply to liquid rare gases. In fact, it does apply to the heavier rare gases (argon, krypton, and xenon) where it correctly predicts electron delocalization. This is what you would expect since our approach emphasizes the polarization contribution, and this contribution is undoubtedly important in the heavier rare gases. It strikes me as perhaps fortuitous that the SJC electron localization criterion "works" for these heavier rare gases when the polarization contribution is ignored.

(3) I think the intermediate range of mobility is indeed an interesting question. What we have done in our simple approach is to explain the two extremes of electron behavior in liquid alkanes which does not appear to have been done before and which is not explained by the model applied to rare gases. In the intermediate mobility range, our model is certainly overly simplified and it is an interesting question as to how far it may be extended. We have of course considered the role of local fluctuations by making them the driving force to form our transient traps of molecular size. By using the Wigner–Seitz radius to "size" these transient traps we have emphasized fluctuations in the intermediate mobility range by considering a distribution of "important" fluctuations.

Mechanisms of Thermal Electron Capture by HCl and HBr

D. A. Armstrong* and S. S. Nagra

Department of Chemistry, The University of Calgary, Calgary, Alberta, Canada *(Received July 23, 1975)*

The capture of electrons in gaseous HCl and HBr produces one molecule of hydrogen per electron.[1,2] Studies of the kinetics of these processes in the presence and absence of nonattaching buffer gases have shown that the majority of electrons captured are of thermal energy, and that the capture reactions are complex multibody events.[3] For the case of HBr, recent experiments have confirmed an earlier conclusion that two molecules of halide are involved in the rate-controlling step, and have shown in addition that the rate is unaltered by the addition of buffer gases.[3] For HCl the rate in the presence of buffer gas is second order with respect to the hydrogen halide, but there is a dependence on the total pressure of the system.[2,3] In the absence of buffer gas the reaction is third order in HCl.

Several possible reaction paths have been examined with the object of developing a unifying capture mechanism for the two closely related molecules. Present evidence suggests that the major route to the formation of the previously proposed $(HX)_2^{-*}$ intermediate[1,2,4] is via $(HX)_2$ dimer molecules:

$$e^- + (HX)_2 \rightleftarrows (HX)_2^{-*} \qquad (1, -1)$$

$$(HX)_2^{-*} \rightarrow H + XHX^- \qquad (2)$$

$$(HX)_2^{-*} + M \rightarrow (HX)_2^- + M \qquad (3)$$

with reaction 2 being the major exit channel for HBr, and reactions −1 and 3 dominating for HCl. Calculations on the energetics of these reactions, based on currently available data, support these conclusions.[3]

References and Notes

(1) D. E. Wilson and D. A. Armstrong, *Radiat. Res. Rev.*, **2**, 297 (1970).
(2) G. R. A. Johnson and J. L. Redpath, *Trans. Faraday Soc.*, **66**, 861 (1970).
(3) S. S. Nagra and D. A. Armstrong, submitted for publication.
(4) L. G. Christophorou, R. N. Compton, and H. W. Dickson, *J. Chem. Phys.*, **48**, 1949 (1968).

Discussion

G. R. FREEMAN. Does electron capture by dimers of HCl and HBr in the gas phase have implications for electron capture by water clusters in the gas phase?

D. A. ARMSTRONG. Optical density measurements have shown that clustered electrons exist in ammonia and water vapor at densities considerably below the normal liquid densities, but the mechanism for the *initial localization of the electrons* does not appear to be known. It seems reasonable to suggest that neutral dimeric (or higher polymeric) species are involved in this process as is $(HCl)_2$ in the initial stage of electron capture in HCl vapors.

J. JORTNER. The problem of electron localization in polar fluids over a broad density range is of considerable interest. In a system where a single molecule or a small cluster cannot localize an excess electron, a dramatic "transition" from a localized to a delocalized state will be exhibited. Helium falls obviously in such a category, and a mobility drop is indeed observed as discussed by Silver. For polar fluids such as H_2O and NH_3, the theoretical calculations of Newton demonstrate that a cluster of four molecules does not localize an excess electron. Our semiempirical model calculations concur with this conclusion. Furthermore, I am *not* aware of any experimental evidence (from mass spectrometry, electron mobility in water vapor, electron swarm experiments, etc.) that electron binding to small water clusters does occur. Led by these considerations, Schindewolf and his group at Karlsruhe, and Gaathon and myself studied the localization of electrons (produced by pulse radiolysis and detected by optical absorption) in subcritical and supercritical H_2O and NH_3 over a broad density range down to 0.01 g cm^{-3}. Studies of lower densities were prohibited by fast (electron–proton) recombination processes, whereupon we were unable to separate kinetic and energetic–structural ingredients. For H_2O, electron localization was observed down to densities of 8×10^{-3} g cm^{-3} over the entire temperature range (from the liquid–vapor coexistence curve up to the thermodynamic critical point). We interpret this result by asserting that an H_2O cluster containing $N = 4$ molecules in the first coordination layer and $N_D \simeq 2 - 3$ molecules in the second coordination layer acts as an initial trap. Density fluctuations are sufficient to ensure the existence of such trapping centers in H_2O. On the other hand, in NH_3 we expect from rough theoretical estimates that a localization center consisting of $N = 4$ and $N_D \simeq 6$–8 is required. The experimental data drastically differ in NH_3 as compared to H_2O. Electron localization is observed in NH_3 vapor near the coexistence curve down to a density of 0.01 g cm^{-3}. However, and most interesting, at temperatures of 40°C above the coexistence curve, electron localization is *not* observed for densities lower than 0.07 g cm^{-3}. Near the coexistence curve, density fluctuations are large (due to the large compressibility) and electron localization there is effective, while this is not the case at higher temperatures. These experiments provide interesting information regarding the role of density fluctuation on electron localization. This is a nice example of how excess electrons can be used to probe the structure of a relatively simple microscopically inhomogeneous system.

M. D. NEWTON. As we noted in our paper, our ab initio calculations employed a large basis set of atomic orbitals, a basis set which in the past has given good quantitative energetic and structural predictions for other solvation clusters. Clearly, more definitive calculations would be desirable, for more accurate estimation of the energies of electrons attached to small water clusters. Obvious improvements would be inclusion of so-called polarization functions (d and p orbitals on oxygen and hydrogen atoms, respectively), and inclusion of correlation energies. Our basis set actually leads to an exaggerated dipole moment for water (the polarizability is somewhat too small), and might well be expected to lead to an upper bound to the stabilization energy, as is the case for hydrates of H_3O^+ and OH^- (M. D. Newton and S. Ehrenson, *J. Am. Chem. Soc.*, **93**, 4971 (1971)). In assessing the importance of correlation energy (i.e., stabilization relative to the Hartree–Fock energy), it is important to make a distinction between anions which involve a pair of electrons (e.g., the dielectron) and doublet radical anions with only a single excess electron. Thus Webster's results for H^- may have some bearing on the dielectron problem, but have no direct bearing on the problem of solvated single electrons.

As a final comment, I should like to make it clear that in fact we calculated a small stabilization of ~4 kcal/mol for $(H_2O)_4^-$ relative to $4H_2O$ with the electron at infinity. Not only is this energy much less than the stabilization possible for the *neutral* H-bonded tetramer, but the entropy factor would make detection of the tetramer anion very unlikely in ordinary gas phase experiments. Nonequilibrium approaches such as nozzle beam techniques should perhaps be considered.

R. CATTERALL. Mane, Leach, and Horani did provide some evidence for electron attachment to gas phase water—they irradiated in the gas phase, and the condensate did contain e_{aq}^-. Some electron attachment must have occurred in the gas phase prior to condensation.

J. JORTNER. I am not sure whether this interesting experiment based on the matrix isolation method is indeed conclusive in providing information on what happens in the gas phase.

An Electron Mobility Transition in Liquid Ethers[1]

J.-P. Dodelet, F.-Y. Jou, and G. R. Freeman*

Chemistry Department, University of Alberta, Edmonton, Canada, T6G 2E1 *(Received July 23, 1975)*

Publication costs assisted by the University of Alberta

Electron mobilities in diethyl, di-*n*-propyl, and di-*n*-butyl ethers undergo a transition in transport mechanism at temperatures in the vicinity of 250 K. The low temperature mechanism appears to involve either ion-like diffusion or phonon-assisted hopping between nearest neighbor sites. The high temperature mechanism involves longer jump distances, perhaps via a conduction band, and has double the activation energy. The mechanisms are discussed. Optical absorption spectrum parameters for electrons in the ethers are reported and compared with the energy parameters for electron migration.

Introduction

The metal–nonmetal transition in the electron transport mechanism in liquids has been well documented in metal–ammonia solutions[2,3] and in fluid metals.[4,5] The transition from a metallic to a nonmetallic mechanism is brought about by decreasing the metal concentration in ammonia or by decreasing the fluid metal density. Thus all these transitions can be attributed to changes in metal concentration. The direct effect of temperature change, for example, when the density of liquid mercury is reduced by greatly increasing the temperature,[5] appears to be secondary.

A similar band–nonband transition occurs for electron transport in liquid xenon.[6] The conduction band in liquid xenon progressively breaks up as the liquid density is decreased below a certain value.

A different type of electron transport transition has been observed in liquid ethers. The transition is related mainly to changes in temperature. The effect of the change in liquid density is in this case secondary.

Experimental Section

The materials and the methods of measuring electron and ion mobilities have been described elsewhere.[7]

Optical absorption measurements were made by methods similar to those used for alcohols.[8] The photocell was an In–Sb diode (Model A-10D/D10S) from Barnes Engineering Co. It was cooled by liquid nitrogen in a Dewar with a sapphire window.

Results and Discussion

Electron and anion mobilities in diethyl, di-*n*-propyl, and di-*n*-butyl ethers are shown as functions of temperature in Figure 1. The anions are heavy molecular ions formed by the capture of electrons by impurities such as aldehydes. Electron conductance transients were measured on a microsecond time scale, whereas ion conductances were measured over milliseconds.

The electron and ion mobilities were independent of field strength up to 20 kV/cm. The anion mobilities u_- give linear Arrhenius plots and they approximately follow Walden's rule.[7] Migration of ions through the liquid requires sympathetic rotational and translational motions of the adjacent solvent molecules.

At low temperatures the electron mobilities u_e are only approximately double those of the anions (Figure 1). The electron transport mechanism at these temperatures has therefore been called ion-like. It apparently involves rotational–translational motions of the molecules surrounding the electron, although the molecules forming the electron trap probably do not migrate with it (the mobility would then be lower).

At higher temperatures the ratio u_e/u_- increases (Figure 1). It has the value 21 in dibutyl ether at 375 K. The activation energy of electron migration increases to slightly more than double that of anion migration. The doubling of the activation energy signifies a change in migration mechanism.

This mobility transition has been reported before,[7] but some of the details of the treatment need to be modified in the light of recent work on a model for electron transport in liquid hydrocarbons[9] and optical absorption measurements reported in this article.

At low temperatures u_e may be represented by

$$u_e(\text{low } T) = u_{il}^0 \exp(-E_{il}/RT) \tag{1}$$

where u_{il}^0 and E_{il} are respectively the preexponential factor and activation energy for ion-like mobility.

Electron migration at high temperatures may be described in terms of thermally activated hopping from site to site, perhaps via a conduction band. For the sake of simplicity it is assumed that the density of states near the top of the occupied solvated state levels is similar to that in the final state of the activated transition. The mobility at high temperatures may then be represented by

$$u_e(\text{high } T) = u_h^0[1 + \exp(E_h/RT)]^{-1} \tag{2}$$

where u_h^0 is the mobility in the activated state and E_h is the activation energy for the high temperature mechanism. The fraction of electrons that are in the activated state at a given time is given by the factor $[1 + \exp(E_h/RT)]^{-1}$, assuming that the entropy difference between the two states is small.

Solvated electrons do not all reside in traps of the same depth, so eq 2 must be integrated over the distribution of trap depths E_h.

$$u_e(\text{high } T) = u_h^0\chi \tag{3}$$

$$\chi = \int_{-\infty}^{\infty} N(E)[1 + \exp(E/RT)]^{-1}\,dE \tag{4}$$

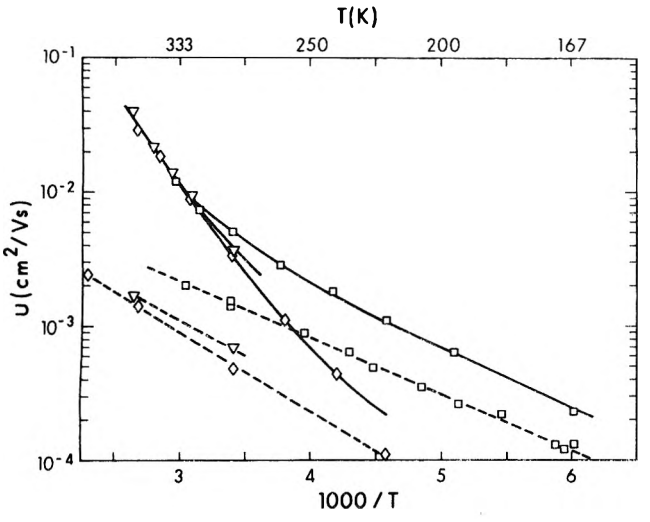

Figure 1. Electron (——) and anion (- - - - -) mobilities in ethers: □, diethyl ether; ▽, di-*n*-propyl ether; ◇, di-*n*-butyl ether. The experimental points were taken from ref 7. The electron mobility curves were calculated from eq 4–10 using parameter values from Table I.

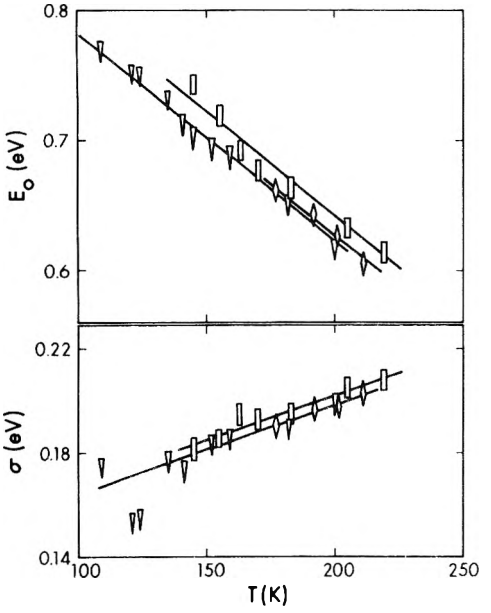

Figure 2. Energies E_0 of the optical absorption maxima and dispersion parameters σ of the low energy side of the absorption spectra of electrons solvated in ethers: □, diethyl ether; ▽, di-*n*-propyl ether; ◇, di-*n*-butyl ether. The lines represent eq 7–10.

where $N(E)\,dE$ is the fraction of solvated electrons with E_h values between E and $E + dE$.

The mobility at any temperature is

$$u_e = (1 - \chi)u_{il}^0 \exp(-E_{il}/RT) + \chi u_h^0 \qquad (5)$$

The calculations with (5) were systematized through the mobilities in diethyl ether, which were measured over the greatest temperature range (Figure 1). The mobilities at low temperatures give $u_{il}^0 = 0.13$ cm²/V sec and $E_{il} = 0.090$ eV in that liquid, compared to the anion values 0.040 cm²/V sec and 0.083 eV, respectively. The mobilities at high temperatures give information about $N(E)$ and u_h^0.

The function $N(E)$ is not known, but it has been compared to the low energy side of the optical absorption spectrum[7] and to the distribution of thermal energy fluctuations.[9,10] In either case the shape is approximately Gaussian and the magnitudes of the dispersion parameters σ are similar.[9]

$$N(E) = \pi^{-1/2}\sigma^{-1} \exp[-(E - E_0)^2/\sigma^2] \qquad (6)$$

where $\pi^{-1/2}\sigma^{-1}$ is a normalization factor and E_0 is the most probable trap depth.

As a first approximation E_0 is taken equal to the energy of the optical absorption maximum in the solvated electron spectrum and σ is taken equal to that for the low-energy side of the spectrum. Optical values of E_0 and σ for electrons in liquid ethers are difficult to measure, due to shortcomings of infrared light sources. Experimental data obtained for electrons in diethyl, di-*n*-propyl, and di-*n*-butyl ethers at low temperatures are displayed in Figure 2. Long extrapolations to temperatures as high as 378 K are needed. In view of the similarities of the high temperature mobilities and of the optical values of E_0 and σ in the three liquids, the extrapolations are made with eq 7–10. In diethyl ether:

$$E_0(\text{eV}) = 0.96 - 0.0016T \qquad (7)$$

$$\sigma(\text{eV}) = 0.134 + 3.4 \times 10^{-4}T \qquad (8)$$

In di-*n*-propyl and di-*n*-butyl ether:

$$E_0(\text{eV}) = 0.94 - 0.0016T \qquad (9)$$

$$\sigma(\text{eV}) = 0.130 + 3.4 \times 10^{-4}T \qquad (10)$$

These quantities are slightly different than those used earlier.[7] For example, the present values of E_0 and σ in diethyl ether at 166–337 K are 0.69–0.42 and 0.19–0.25 eV, respectively, whereas earlier E_0 was taken to be 0.76–0.47 eV and σ was held constant at 0.18 eV. The temperature dependence of the optical absorption σ is smaller than that of the thermal energy fluctuations,[9] $\sigma_{\text{therm}} \approx (5.5 \times 10^{-4}N^{1/2}T)$ eV in fluid cells containing N molecules.

Calculated mobilities can be brought into agreement with the experimental quantities by adjusting u_h^0, provided that $N(E)$ is adequate. In diethyl ether the required value is $u_h^0 = 0.6$ cm²/V sec. The calculated curve is shown in Figure 1.

The mobilities in dipropyl and dibutyl ethers were treated similarly. Values of the parameters are listed in Table I and the curves are displayed in Figure 1. Agreement between calculation and experiment is satisfactory.

In the earlier work[7] the use of larger values of E_0 and smaller, constant values of σ caused calculated values of u_e to vary too rapidly with temperature. It was necessary to divide the optical energies by two to obtain the correct mobility behavior.[7] If one divides the present optical values by two, one can obtain almost the same agreement with the experimental mobilities by making adjustments to the values of u_{il}^0, E_{il}, and u_h^0 (Table I). In diethyl ether the

TABLE I: Parameters for Electron Mobilities in Ethers[a,b]

Ether	u_{il}^0, cm²/V sec	E_{il}, eV	u_h^0, cm²/V sec	E_h[c], eV
Diethyl	0.13 [0.13]	0.09 [0.09]	0.6 [0.3]	~0.2
Di-*n*-propyl	0.15 [0.13]	0.11 [0.13]	0.75 [0.5]	0.26
Di-*n*-butyl	0.19 [0.04]	0.13 [0.12]	0.8 [0.5]	0.26

[a] Equations 4–10. [b] The values in square brackets were obtained when the optical parameters in eq 7–10 were divided by two. [c] Experimental activation energy of the high temperature mechanism.

only change needed is to divide u_h^0 by two. Thus, although there seems to be a correlation between the thermal and optical excitation energies of electrons solvated in ethers, there are still too many adjustable parameters in the model to be able to specify the relationship precisely. However, the extent of agreement attainable between calculated and measured mobilities gets progressively worse when the factor used to divide the optical parameters is smaller than unity or larger than two.

The Magnitudes of u_{il}^0, E_{il}, u_h^0, and E_h. The magnitude of $u_{il}^0 \approx 0.1$ cm^2/V sec may be understood in terms a random walk diffusion mechanism.[11] The mobility is related to the diffusion coefficient D, the average jump distance λ, and average jump frequency ν by

$$u = De/kT = (D^0e/kT)\exp(-E/RT) \quad (11)$$

$$\approx \lambda^2\nu e/2kT = (\lambda^2\nu^0 e/2kT)\exp(-E/RT) \quad (12)$$

where e is the unit electronic charge. The preexponential factors u^0 and D^0 are related to the jump attempt frequency ν^0. The value $u_{il}^0 \approx 0.1$ cm^2/V sec is equivalent to an average jump distance of about one molecular diameter, $\lambda \approx 6$ Å, with an attempt frequency $\nu^0 \approx 10^{12}$ sec^{-1} at temperatures in the vicinity of 200–300 K. The attempt frequency is similar to the frequency of intermolecular motions in the liquid, judging from the energies of absorption maxima in the far infrared (40 cm^{-1}).[12] The preexponential factors of anion mobilities are only 2–3 times smaller than u_{il}^0 and probably reflect smaller values of λ rather than a smaller ν^0.

The magnitude of E_{il} is similar to the activation energy of anion mobility and both reflect the activation energies of intermolecular rotational and translational displacements of the solvent molecules.[7]

The ion-like mechanism is phenomenologically similar to phonon assisted hopping of electrons between nearest neighbor sites in certain semiconductors (small polaron mechanism).[13,14]

The estimated value of u_h^0 in the high temperature mechanism is only about fivefold greater than u_{il}^0 (Table I). This could be attained by simply increasing the average jump distance to two or three molecular diameters (eq 12).[20] The high temperature mechanism may also, therefore, be a phonon assisted process. However, there is a problem concerning the estimated value of u_h^0. Linear extrapolation of the high temperature mobilities in Figure 1 to $T^{-1} = 0$ gives ~100 cm^2/V sec, similar to the extrapolated value obtained for electrons in alkanes.[9,15-17] Electron migration in liquid alkanes appears to involve thermal excitation into a conduction band in which the mobility is $u_{cb} \approx 100$ cm^2/V sec.[9,10] The excitation energy in alkanes has been related theoretically to $(V_0 - \bar{V})$, where V_0 is the potential energy of electrons in the bottom of the band relative to the vacuum level and $\bar{V}$ is the mean energy in the solvated state.[10,18] Values of V_0 were measured[10,18] but $\bar{V}$ was used as an adjustable parameter. The quantity $(V_0 - \bar{V})$ was assumed to be independent of temperature, while σ was assumed to be directly proportional to T.[10] These assumptions might not be accurate.[9] If $d(V_0 - \bar{V})/dT$ were negative and $d\sigma/dT$ were less positive than assumed, the estimated value of u_{cb} in primary alkanes would be <100 cm^2/V sec.

By contrast, if dE_0/dT were less negative and $d\sigma/dT$ more positive for thermal excitation than indicated by eq 7–10, the estimated value of u_h^0 would be >1 cm^2/V sec. It seems probable that electron behavior in n-alkyl ethers is similar to that in n-alkanes. The relative mobilities indicate that $(V_0 - \bar{V})$ is 0.1–0.2 eV greater in an ether than in an alkane of the same molecular weight. The energies of the optical absorption maxima of electrons trapped in glasses of these compounds at 77 K are also ~0.1–0.2 eV greater in ethers than in alkanes.[19]

Measurements of u_e at much higher temperatures and of V_0 as a function of temperature in ethers and hydrocarbons would help to resolve the question of whether $u_h^0 = u_{cb}$ and how this quantity varies with molecular structure.

The experimental activation energy E_h of the *high* temperature mechanism is double that of the ion-like mechanism (Table I). The value of E_h is smaller than that of E_0 in eq 6 because the electrons that migrate most readily are those at the low energy end of the trap depth distribution.

Acknowledgment. We wish to thank the personnel of the Radiation Research Center for aid with the electronics.

References and Notes

(1) Assisted financially by the National Research Council of Canada.
(2) C. A. Kraus, *J. Am. Chem. Soc.*, **43**, 749 (1921), and later work.
(3) "Electrons in Fluids", J. Jortner and N. R. Kestner, Eds., Springer-Verlag, Berlin, 1973.
(4) H. Renkert, F. Hensel, and E. U. Franck, *Ber. Bunsenges. Phys. Chem.*, **75**, 507 (1971).
(5) U. Even and J. Jortner, ref 3, p 363.
(6) T. Kimura and G. R. Freeman, *Can. J. Phys.*, **52**, 2220 (1974).
(7) J.-P. Dodelet and G. R. Freeman, *Can. J. Chem.*, **53**, 1263 (1975).
(8) K. N. Jha, G. L. Bolton, and G. R. Freeman, *J. Phys. Chem.*, **76**, 3876 (1972).
(9) J.-P. Dodelet, K. Shinsaka, and G. R. Freeman, *Can. J. Chem.*, in press.
(10) R. Schiller, Sz. Vass, and J. Mandics, *Int. J. Radiat. Phys. Chem.*, **5**, 491 (1973).
(11) E. W. McDaniel, "Collision Phenomena in Ionized Gases", Wiley, New York, N.Y., 1964.
(12) S. K. Garg, J. E. Bertie, H. Kllp, and C. P. Smyth, *J. Chem. Phys.*, **49**, 2551 (1968).
(13) N. F. Mott and E. A. Davis, "Electronic Processes in Noncrystalline Materials", Clarendon Press, Oxford, 1971.
(14) W. E. Spear, *Adv. Phys.*, **23**, 523 (1974).
(15) W. F. Schmidt and A. O. Allen, *J. Chem. Phys.*, **52**, 4788 (1970).
(16) R. M. Minday, L. D. Schmidt, and H. T. Davis, *J. Chem. Phys.*, **54**, 3112 (1971).
(17) M. G. Robinson and G. R. Freeman, *Can. J. Chem.*, **52**, 440 (1974).
(18) R. A. Holroyd and R. L. Russel, *J. Phys. Chem.*, **78**, 2128 (1974).
(19) T. Shida, S. Iwata, and T. Watanabe, *J. Phys. Chem.*, **76**, 3683 (1972).
(20) The factor corresponding to u_h^0 in the earlier work[7] was assumed to be temperature dependent, as predicted by eq 12. However, the total temperature dependence of the preexponential factor is uncertain. It appears to be small relative to that of the exponential factor and is neglected in the present work.

Discussion

J. JORTNER. There is a basic difference between the Schiller–Freeman approach and the Kestner–Jortner treatment of electron mobility in liquid hydrocarbons. The former approach assumes peaceful coexistence between extended and localized states. In a microscopically homogeneous system bound states overlapping continuum states are metastables and should be envisioned in terms of resonances. The latter model involves the concept of a microscopically inhomogeneous system where localized and extended states can exist *locally*. It is still an open question whether the percolation picture or the Anderson model applies to the problem. Excess electrons in liquid hydrocarbons provide a most interesting system for theoretical and experimental studies of the electron localization problem.

G. R. FREEMAN. Calculations of mobilities in hydrocarbons by three different models indicate that, although percolation might make a contribution near the top of the mobility range (neopentane, isooctane), it does not appear to be the major limiting factor to electron migration in n-hydrocarbons. The interpretation of mobilities at the lower end of the scale (n-hexane) seems to require thermal excitation out of traps (Anderson model), and that model fits the observed mobilities over the entire range.

T. TUTTLE. How does the mobility of the solvated electron in ethers compare with that in ammonia?

G. R. FREEMAN. The electron mobility in low temperature ethers is more ion-like than that in ammonia. The ratio of mobilities (electron/anion) is about five in ammonia at 240 K and only two in low temperature ethers.

M. H. COHEN. The fact that the activation energy for electron mobility at lower temperatures is the same as that of the heavy ion mobility suggests that the mobility mechanism is electron diffusion rather than small polaron hopping from trap to trap. The problem of the larger value of the mobility for the electron occurs also for NH_3 and may arise from the fact that the electron does not possess a rigid structure, as an ion does, and so more rearrangements of the fluid can lead to electron diffusion.

G. R. FREEMAN. The low temperature mechanism of electron migration might simply be diffusion as you say, and as I speculated in the written manuscript. However, the low temperature activation energy is one half of the high temperature activation energy. If the high temperature mechanism involves a conduction band, then that at low temperatures might involve thermal activated hopping in the small polaron fashion.

Magnetic Properties and the Metal–Nonmetal Transition in Metal–Ammonia Solutions

J. P. Lelieur,* P. Damay, and G. Lepoutre

Laboratoire de Chimie Physique, ERA 126 du CNRS, 13, rue de Toul, 59000 Lille, France *(Received July 23, 1975)*

The magnetic properties of metal–ammonia solutions are examined in the dilute, intermediate, and concentrated ranges in the light of the present understanding of these solutions. More attention is given to magnetic data in the intermediate concentration range and to the metal–nonmetal transition problem. A recent model of this transition is analyzed. The analysis of experimental thermodynamic data (activity), in conjunction with a fluctuation correlation length (from neutron scattering), gives the distribution of the concentration fluctuations. This concentration fluctuation distribution around the mean concentration can be used to determine physical properties.

Introduction

In his review given at Colloque Weyl II, Catterall[1] analyzed the magnetic properties of dilute metal–ammonia solutions. Since that time, relatively few papers have been published in this field; however, there has been a number of experimental works dealing with the intermediate concentration range. Therefore, in this paper more attention will be given to the intermediate concentration range and to the problem of metal–nonmetal (MNM) transition. The only solvent considered in this paper will be ammonia.

1. Dilute Solutions

1.1 What about Models of Dilute Metal–Ammonia Solutions? Many measurements of magnetic properties have been performed in the past in the electrolytic dilute metal–ammonia solutions. They have been reviewed in an excellent paper by Catterall;[1] the "dilemma" raised by these dilute solutions have been analyzed by Dye[2] and Lagowski[3]: Are solvated electrons associated (magnetic susceptibilities) or nonassociated (optical spectra)?

Very dilute solutions contain two species: paramagnetic solvated electrons and solvated cations. An increase in metal concentration leads to the formation of electrically neutral ion pairs which, however, remain paramagnetic. It is often assumed that at concentrations larger than about 10^{-3} M, ion pairs associate into quadrupoles where the solvated electrons are spin-paired.

The equilibrium constant for the pairing of ions has the order of magnitude predicted by Bjerrum's theory. Demortier[4] has shown that the constant of association of ion pairs in quadrupoles is much larger than expected. He has therefore suggested that the attractive interactions between solvated electrons are much stronger than between conventional ions.

Justice[5] has shown that Bjerrum's constant for ion pairing, $K_{(+-)}$, can be derived from a statistical treatment of binary interactions between ions, according to Mayer's and Friedman's[6] views. Two interesting results are that the expression of $K_{(+-)}$ is exactly as predicted by Bjerrum, and that two other constants of ion pairing appear as a consequence of the statistical approach: $K_{(--)}$ and $K_{(++)}$. In most cases, these latter constants of association for ions of same sign are very small. Around a given ion, the probability of finding another ion of same sign at a distance shorter than the Bjerrum's distance is usually small and can be neglected.

It is clear that such a statistical treatment of binary interactions cannot lead to quadrupoles. However, it seems to be adequate for most other dilute solutions, and it can be applied at fairly high concentrations for nontransport properties.

Finally, as Schettler[7] shows at the present Colloque, there are unusual attractive interactions between solvated electrons related to their high polarizability and their spin-pairing.

There may be pairs of solvated electrons at distances shorter than the Bjerrum's distance. (This is quite different from two electrons in one cavity. In the present picture,

two solvated electrons are associated and spin-paired but still apart from each other.)

It may therefore be possible to describe dilute metal–ammonia solutions with two ion-pairing constants, $K_{(+-)}$ and $K_{(--)}$, for the two simultaneous equilibria

$$M_{am}^{+} + e_{am}^{-} \rightleftarrows M_{am}^{+}\cdot e_{am}^{-} \quad (1)$$

$$2e_{am}^{-} \rightleftarrows (e_{am}^{-})_2 \quad (2)$$

There would possibly be no need for introducing interactions between more than two particles.

However, the use of pair interactions is not sufficient when the potential energy between two particles is perturbed by a third particle. Such a perturbation occurs when the particles are polarizable. This is the case for solvated electrons, so that triple ions and quadrupole as well as pairs of solvated electrons may occur. A good theory of interactions between solvated electrons would allow a comparison between these various associations.

In any case the pairs of solvated electrons, be it in simple pairs or in triple ions or in quadrupoles, should not be viewed as contact pairs but as a statistical distribution within a critical distance.

The solvated electron remains, therefore, an individual entity in the paramagnetic pair ($M_{am}^{+}\cdot e_{am}^{-}$), the diamagnetic pair $(e_{am}^{-})_2$, in the triple ion, or in the quadrupole. This should help to resolve Dye's dilemma, and reduce the problems of dilute metal–ammonia solutions to the general theories of electrolytic solutions, given a good understanding of interactions between solvated electrons. The range of application to static properties such as magnetic susceptibilities may hopefully be extended to fairly high concentrations, up to the onset of metallic properties (0.4 *M*). Preliminary results of Tehan, Lok, and Dye[8] show that the temperature dependence of the spin-pairing equilibrium in dilute solutions is relatively insensitive to the nature of the cation. This suggests that the diamagnetic species is relatively independent of the cation.

1.2 The Solvated Electron Species from Nuclear Relaxation. All magnetic measurements related to dilute metal–ammonia solutions will not be analyzed here. Only experiments dealing with the correlation time of the interaction between electron and nitrogen, and with the solvation number of the solvated electron, will be considered here.

The electron spin relaxation mechanism, which gives rise to the extremely narrow ESR line width, is the modulated hyperfine interaction of the solvated electron with nitrogen atoms of the solvation shell. The electron relaxation rate is then given by[9]

$$\frac{1}{T_1} = \frac{2}{3} I(I+1) n A^2 \frac{\tau}{1 + (\omega_N - \omega_S)^2 \tau^2} \quad (3)$$

where I is the nitrogen spin, n is the number of nitrogen atoms taking part in the relaxation mechanism, τ is the correlation time of the interaction, ω_N and ω_S are the nitrogen and electron-spin Larmor frequency, respectively, and A is such that $A\hbar\mathbf{I}\cdot\mathbf{S}$ is the energy of the interaction. The latter quantity A can be directly expressed in terms of the spin density P_N on nitrogen atom in the solvated electron:

$$A = (8\pi/3)\gamma_N\gamma_S\hbar P_{N/n} \quad (4)$$

where γ_N and γ_S are the gyromagnetic ratios of nitrogen and electron, respectively. P_N is directly given by the nitrogen Knight shift

$$K(N) = \frac{8\pi}{3} \frac{\chi_m}{N_0} \frac{P_N}{R} \quad (5)$$

where χ_m is the molar paramagnetic susceptibility and R the ammonia-to-metal ratio. It should be noted that this expression defines the average spin density on nitrogen. In the motional narrowing situation, $(\omega_N - \omega_S)^2\tau^2$ is small with respect to (1), and is neglected. From relations 3, 4, and 5, τ/n can be written as:

$$\frac{\tau}{n} = C \frac{1 + (\omega_N - \omega_S)^2\tau^2}{P_N^2 T_1} \simeq \frac{C}{P_N^2 T_1} \quad (6)$$

with

$$\frac{1}{C} = \frac{128\pi^2}{27} \gamma_e^2 \gamma_N^2 \hbar^2 I(I+1) \quad (7)$$

Electron relaxation time T_1 is deduced from ESR linewidth measurements. Published data are in agreement with the values $T_1 \sim 3.1$ μsec at room temperature, and $T_1 \sim 1.1$ μsec at 240 K (Hutchison and Pastor,[10] O'Reilly,[11] Blume,[12] Pollak[13]). Spin density on nitrogen, P_N, is deduced from nitrogen Knight shift measurements (McConnel and Holm,[14] Acrivos and Pitzer,[15] O'Reilly[16]) and from molar paramagnetic susceptibility. For infinitely dilute solutions, it is expected that P_N is independent of the cation in the solution, and P_N can be taken as equal to the values deduced[16] from Na–NH_3 solutions, i.e., $0.77a_0^{-3}$ at room temperature and $1.42a_0^{-3}$ at 240 K. With these values of P_N and T_1, τ/n is equal to 0.85×10^{-13} sec at room temperature and 0.75×10^{-13} sec at 240 K. The value at room temperature is close to the value given by Catterall[1] in his review (0.62×10^{-13} sec). In literature, authors usually give values of τ or n. It should be realized that values of τ or n require hypotheses on n or τ, respectively, because eq 6, for τ/n prevents the independent determination of τ and n. If hypotheses made on τ or n in various papers are removed, it can be shown that τ/n deduced from experiments (and not from theoretical estimation of P_N) have quite close values with different authors.

In fact, such an analysis is only a first approximation. It is well known that, when metal concentration increases, the spin–orbit coupling of the electron with solvent molecules and metal ions makes the electronic relaxation time decrease. With the realistic hypothesis that both relaxation mechanisms (hyperfine interaction and spin–orbit coupling) intervene simultaneously, and with the hypothesis that $n = 24$, O'Reilly[17] was able to obtain the variations of τ with metal concentration. However, if the hypothesis that $n = 24$ is dropped, and if the previously mentioned values of P_N are used, values of τ/n are obtained. The values of τ/n which take account of the spin–orbit coupling are 0.46×10^{-13} sec at 300 K (compared to 0.85×10^{-13} sec without spin–orbit coupling) and 0.58×10^{-13} sec (compared to 0.75×10^{-13} sec). Therefore τ/n values are smaller even at infinite dilution if spin–orbit coupling is accounted for, and the temperature variation of τ/n is inversed. It should be concluded from this work of O'Reilly[17] that the spin–orbit coupling has to be taken into account for the determination of τ/n values.

Swift et al.[18,19] determined τ and n through the analysis of the high-resolution proton magnetic resonance line shape. This proton spectrum in pure liquid ammonia is well known to be a triplet arising from ^{14}N–H coupling. The features of this triplet are determined by the ^{14}N electric quadrupolar relaxation rate. These authors showed that, in dilute K–NH_3 solutions, a large contribution to the

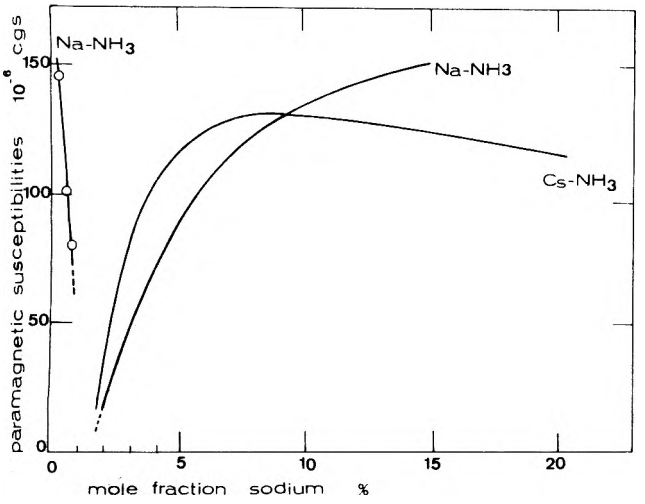

Figure 1. Paramagnetic susceptibility of $Na–NH_3$ and $Cs–NH_3$ solutions, per mole of metal in solution, taken from ref 20, vs. metal concentration. Data on the dilute side (—O—O—) are from ref 46.

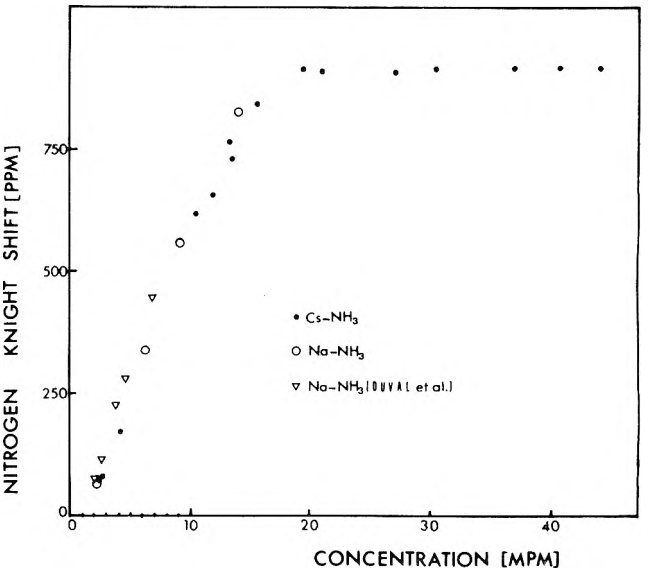

Figure 2. Nitrogen Knight shift, $K(^{14}N)$ (ppm), vs. metal concentration, in $Na–NH_3$ and $Cs–NH_3$. The data (▽) are taken from ref 25.

proton line shape comes from ^{14}N spin–lattice relaxation through magnetic dipolar interaction with unpaired electrons. The fit between theoretical and experimental line shapes gives the value of τ/n. The important point is that the τ/n value is field dependent if $\omega_S^2\tau^2$ (where ω_S is the electron Larmor frequency) is not taken as negligible with respect to (1). Therefore proton line shapes at two different frequencies give the values of τ and n. However, the accuracy of these determinations, particularly for n, was limited for the following reasons. The determination of P_N is based upon the conflicting nitrogen Knight shift values reported in the literature.[14-16] The proton spectra have been taken at two frequencies (60 and 100 MHz) not largely different. The values of τ were found to be of the order of 1 to 2 $\times$ 10^{-12} sec, and the solvation number ranged from approximately 20 to 40. These values are not surprising. However, this technique used with largely different frequencies, combined with simultaneous nitrogen Knight shift measurements to obtain a better accuracy, could prove to be a very powerful tool for the study of metal–ammonia solutions.

2. Intermediate Concentrations

2.1 Magnetic Susceptibility Measurements. In the MNM transition range, i.e., between approximately 1 and 10 MPM, some experiments have been performed since the review made by Catterall for Colloque Weyl II. The magnetic susceptibility[20,21] has been measured for $Na–NH_3$ and $Cs–NH_3$ by the classical Gouy technique (Figure 1). For $Na–NH_3$ solutions, the paramagnetic susceptibility has also been measured[20] directly by the Schumacher–Slichter resonance technique. Both techniques give the same trend of results. The paramagnetic susceptibility increases with the metal concentration; the temperature coefficient of the paramagnetic susceptibility decreases when metal concentration increases. It should be noted that the magnetic susceptibility is not known between approximately 0.5 and 2 MPM. It will be useful to know the concentration of the minimum of the magnetic susceptibility and the concentration of the maximum of its temperature coefficient. The magnetic susceptibility data show that between about 0.5 and 1 MPM most of the solvated electrons are paired. When the metal concentration increases, these solvated electrons become progressively delocalized and behave somewhat as free electrons.

It may be pointed out that the paramagnetic susceptibility is obtained from the Gouy technique, by subtracting the diamagnetic contributions of the ammonia molecules, of the metal cation, and of the Landau diamagnetism of free electrons. This last contribution, taken as equal to $-\frac{1}{3}\chi_P$ as for a free electron gas, is questionable. However, no other estimation can be made, and it does not seem that the paramagnetic susceptibility trend vs. metal concentration would change significantly, even on assuming that the exact diamagnetic contributions could be known and taken into account. It should certainly be useful, as for dilute solutions, to know the magnetic susceptibility deduced from the Gouy technique, and the paramagnetic susceptibility from the resonance technique. However, it is unlikely that the accuracies of these results could make their difference meaningful.

With the measurements of the paramagnetic susceptibility, the ESR line width has been measured[20] at 15 MHz for $Na–NH_3$ solutions. It has also been measured by Chan, Austin, and Paez[22] in the X-band frequency range for $Na–NH_3$ solutions. Damay[23] measured the ESR line width of $Li–NH_3$ solutions in the X-band frequency range. Those results show the change from an ESR line width, typical of the dilute concentration range, i.e., of the order of 50 mG (electronic relaxation time of the order of 1 μsec), to an ESR line width of about 5 G for 10 MPM $Na–NH_3$ solutions, and of about 4 G for 20 MPM $Li–NH_3$ solutions. Therefore the ESR line width displays a rather important change in the intermediate concentration range. On the other hand, it should be noted that there is always a single electron resonance signal, at 15 MHz as at 9000 MHz. As a consequence, if a model of the metal–nonmetal transition assumes the existence of two different electronic states in the solution, for instance, solvated electrons in dilute clusters and free electrons in metallic clusters, the exchange between these states has to be fast.

2.2 Nuclear Resonance Measurements. Nuclear magnetic resonance measurements have been made for sodium– and cesium–ammonia solutions.[20,24] In the intermediate concentration range, the ^{14}N Knight shift has the same values and variations in $Na–NH_3$ and $Cs–NH_3$ solutions up to 15 MPM (Figure 2). This confirms previous observations

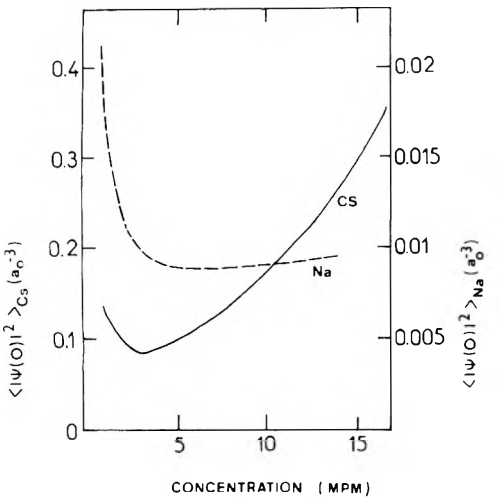

Figure 3. $P_F(Na) = \langle|\Psi_{(0)}|^2\rangle_{Na}$ (a_0^{-3}) for Na–NH_3 at −30°C (right-hand scale) and $P_F(Cs)$ for Cs–NH_3 at −40°C (left-hand scale) vs. metal; concentration expressed in mole per cent (MPM) of metal.

of O'Reilly. It is realized that Knight shifts result from the product of the paramagnetic susceptibility and the electronic density on the nucleus. On the other hand, it has been found[21] by independent measurements that the paramagnetic susceptibilities are similar for Na–NH_3 and Cs–NH_3. It is therefore concluded that the electron densities on the nucleus are similar in both types of solutions. This suggests that the interactions between the nitrogen nucleus and the metal valence electron are similar in Na–NH_3 and in Cs–NH_3. As a consequence it is believed that the solvations of Na and Cs in NH_3 cannot be differentiated on the basis of the ^{14}N Knight shifts. Here again, it should be noted, that a single ^{14}N nuclear resonance signal has been observed. However, ^{14}N nuclear resonance has not been investigated in Li–NH_3 and divalent metal–ammonia solutions.

Cesium Knight shifts have been measured as a function of concentration and temperature.[20,24] With our data of paramagnetic susceptibility,[21] the electronic probability density averaged on the Fermi electronic states, i.e., $P_F(Cs) = \langle|\Psi_F(0)|^2\rangle$, has been obtained. The corresponding quantity $P_F(Na)$ has been obtained from the ^{23}Na Knight shifts measurements[25] and the paramagnetic susceptibility data (Figure 3). The electronic probability densities $P_F(Na)$ and $P_F(Cs)$ decrease up to about 3 MPM. When metal concentration increases above 3 MPM, $P_F(Na)$ is almost constant, while $P_F(Cs)$ increases. This is a quantity where Na–NH_3 and Cs–NH_3 display different trends. These differences could be attributed to the different solvations of Na^+ and Cs^+ cations; but with this hypothesis the similar values of $K(^{14}N)$ for Na–NH_3 and Cs–NH_3 are surprising. It should be noted that a single metal nuclear resonance signal has been observed in alkali metal–ammonia solutions. Therefore, in the framework of an inhomogeneous model, this experimental fact implies a fast exchange between the components of the inhomogeneous model.

Temperature coefficients have also been obtained[20,21,24] for the magnetic susceptibilities and cesium and nitrogen Knight shifts. All these temperature coefficients display the same trend: large positive values at the low concentration end of the intermediate region, and marked decrease when metal concentration increases.

2.3 The Metal–Nonmetal Transition. The main experimental magnetic properties of metal–ammonia solutions in the intermediate concentration range have been summarized. Let us see now which interpretations can be given of these properties. It was recognized early that metal–ammonia solutions display a metal–nonmetal (MNM) transition when metal concentration decreases. However, this idea was discussed only on a qualitative basis for a long time, and often in connection with the liquid–liquid phase separation, the critical concentration of which is about 4 MPM. First, Sienko[26] showed that the criterion for a "Mott transition" predicted a MNM transition at about 4 MPM. The first qualitative inhomogeneous model was proposed by Thompson[27] and Cohen and Thompson.[28] They suggested that between 0.1 and 3 MPM the solutions contain large metallic clusters. At Colloque Weyl II, Lepoutre and Lelieur[29] suggested that, in the range of concentration where phase separation occurs, the solution is composed of a mixture of metallic clusters and the bulk of the solution, metallic clusters beginning to form at about 1 MPM. These suggestions were only qualitative. Lelieur[20] showed that magnetic susceptibility and metal Knight shift measurements could be interpreted in an inhomogeneous model where the solution is composed of dilute and concentrated clusters, a fast exchange between these clusters being assumed.

Acrivos and Mott[30,31] suggested that physical properties of metal–ammonia solutions in the intermediate concentration range could be accounted for in terms of a diffusion type of electron transport. The basic parameter of this model is the Mott g factor (ratio of the density of states to the corresponding free electron density of states), which determines the depth of the pseudogap introduced in this model. It must be noted that this model is basically an homogeneous model. It is difficult to obtain a coherent set of g values from different physical properties. Jortner and Cohen[32] argue that the log–log plot of the electrical conductivity vs. the paramagnetic susceptibility of Na–NH_3 solutions displays a slope of 2.3 instead of 2 as expected in the Mott model.

More recently, Jortner and Cohen[33] proposed the first quantitative inhomogeneous model. They proposed that in the intermediate concentration range, metal–ammonia solutions are microscopically inhomogeneous with a volume fraction C of the material occupied by metallic clusters of a mean concentration 9 MPM, the remaining volume $(1 - C)$ consisting of small solvated electron–cation diamagnetic complexes of a mean concentration of about 1 MPM. It was previously shown[34] that the electrical conductivity problem in such a system, i.e., percolation in a random potential, could be solved with a classical effective medium theory (EMT). Jortner and Cohen were able, with EMT equations, to compute the electrical conductivity of Li–NH_3 solutions.[33] The EMT does not imply a size for metallic or dilute clusters. Jortner and Cohen modified the EMT to account for scattering from the boundaries of the metallic regions. As a consequence, the modified effective medium theory (EMTZ) requires a size for the metallic clusters. Jortner and Cohen found that a good fit with experimental data was obtained with a metallic cluster size of the order of 25 Å. Lelieur[35] used the Jortner–Cohen model to determine the pressure and temperature coefficients of the electrical conductivity, the pressure and temperature dependences of the metallic volume fraction being deduced from the isothermal compressibility and density, respectively. These calculations were able to reproduce the experimental trends of the pressure and temperature coefficients of the electrical conductivity. In the extended version of their

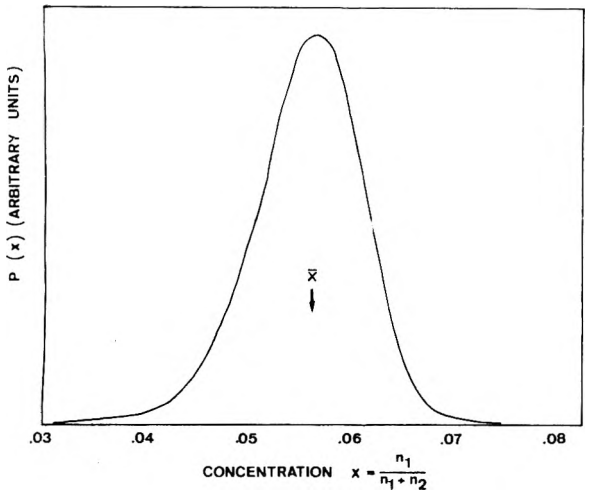

Figure 4. Concentration fluctuations distribution for an average metal concentration of about 5 MPM.

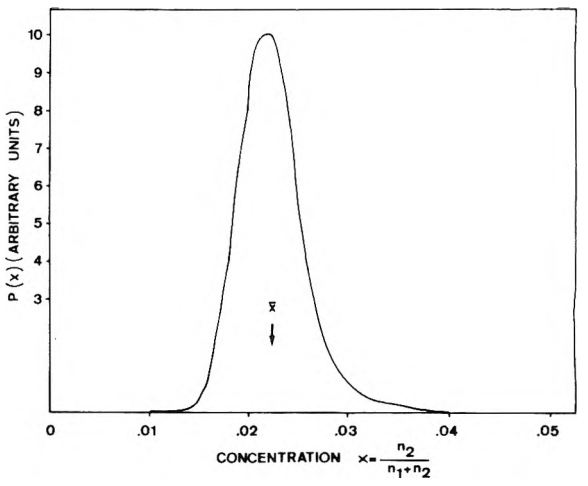

Figure 5. Concentration fluctuations distribution for an average metal concentration of about 2 MPM.

model, Jortner and Cohen[32] proposed that the inhomogeneous regime occurs between $M_1 = 2.3$ MPM and $M_0 = 9$ MPM, mainly on the basis that a fit between experimental data and calculations is possible in this range. The main physical point of this microscopically inhomogeneous model is that the concentration fluctuations are bimodal, varying locally around either of the two well-defined values M_0 and M_1, the concentration appearing to fluctuate abruptly and randomly from M_0 to M_1 or vice versa, with a fluctuation diameter of at least 30 Å for Li–NH_3.

The most controversial idea of the Jortner–Cohen model is the bimodal concentration fluctuation. The physical origin of such a bimodal fluctuation is unclear. More specifically, would it be possible for such clusters of concentrations M_0 and M_1 with a relatively large number of ions to exchange fast enough so that only one ESR and one NMR signal would be observed.[9] As a consequence, the experimental activity data have been analyzed by Damay,[36] in connection with the fluctuation correlation length obtained by Chieux[37] from neutron scattering, to obtain the concentration distribution in a fluctuation model, and this distribution has been used to determine other physical properties.

2.4 Concentration Fluctuations Distribution of a Two-Component Mixture near a Critical Point. The concentration fluctuations of a binary solution correspond to the density fluctuations of a single fluid. They can be represented by[38]

$$P(x) = P_0 \exp\{-n\Delta\mu/RT\} \tag{8}$$

with

$$\Delta\mu = x_1(\mu_1 - \bar{\mu}_1) + x_2(\mu_2 - \bar{\mu}_2)$$

$P(x)$ is the probability of finding a local concentration x_2 within a volume V which has the average concentration $\bar{x}_2$, n is the total number of molecules in V, and $\Delta\mu$ is the local excess free energy. It is the difference between the local free energy $x_1\mu_1 + x_2\mu_2$ of the two components and their free energy if they were at the average chemical potentials, i.e., $x_1\bar{\mu}_1 + x_2\bar{\mu}_2$; P_0 is a normalization factor.

Relation 8 assumes that the pressure work associated with fluctuations is negligible, or that the excess volume of mixing is negligible. $P(x)$ gives the distribution of concentrations around an average concentration $\bar{x}$. It is a Gaussian-like function, more or less skewed. All parameters in $\Delta\mu$ can be computed from vapor pressure data. Ichikawa and Thompson[39] have shown that emf data are consistent with vapor pressure data. Damay[40,41] has shown that, if the two components are taken as pure ammonia and a solvated alkali metal Na–$(NH_3)_n$, the vapor pressure data can be represented by an analytical function. The second and third derivatives of this analytical expression of the chemical potential reproduce the experimental critical temperature and concentration within 0.5%.

The number n of molecules involved in (8) (or the corresponding volume V) has to be chosen carefully. If fluctuations were studied on the overall solution, n would be of the order of 10^{23}, and the distribution function $P(x)$ would be a δ function. The fluctuations cancel each other, and there are no fluctuations on a macroscopic scale.

The local fluctuations do not cancel each other as long as they are correlated. They are correlated[42] over the Debye correlation length L. The smallest volume which has the same properties as the macroscopic properties of the solution is $V = L^3$, and n is the number of molecules in V.

The correlation length has been recently determined by Chieux[37] on the Li–ND_3 system by neutron scattering. His Ornstein–Zernike length is proportional to L, with a numerical factor arising from dimensionality. His results show that the Ornstein–Zernike–Debye variation of the correlation length with temperature is obeyed:

$$L(T) = L_0[(T - T_c)/T]^{1/2} \tag{9}$$

where T_c is the critical temperature and L_0 is a constant which is characteristic of the actual range of interaction. This constant L_0 is assumed to be the same for all alkali metal–ammonia systems, which are much alike with respect to their critical phenomena. For Na–NH_3 solutions at $-35°C$, the volume V corresponding to $L(T)$ contains a few thousand molecules, and thermodynamic properties remain therefore meaningful.

Figures 4 and 5 show the distribution curve which are obtained for two concentrations. Such curves can be used to compute the properties which depend on local fluctuations.

2.5 Determination of Physical Properties from the Concentration Fluctuation Distribution. Let us assume that a theoretical model can predict the values $f(x)$ of a given property as a function of concentrations for an hypothetical metal–ammonia solution without any critical fluctua-

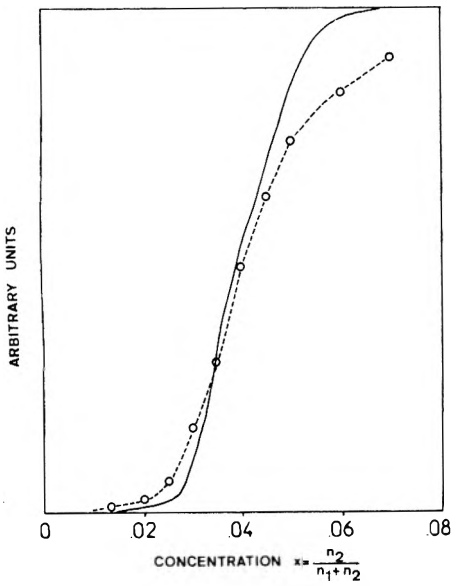

Figure 6. Experimental ESR line width of Na–NH_3 solutions (taken from ref 20) and corresponding calculated values vs. metal concentration (MPM).

tion. It is then possible to calculate the values F(x) of the same property for the real fluctuating system, by use of the distribution curves.

The measured property is given by

$$F(x) = \frac{\int_0^1 P(x)f(x)\,dx}{\int_0^1 P(x)\,dx} \tag{10}$$

In the simplest case f(x) is a step function corresponding to a sharp transition at a critical concentration x_c, with $f(x) = f_1$ for $x < x_c$ and $f(x) = f_2$ for $x > x_c$. Then F(x) is given by

$$F(x) = \frac{f_1\int_0^{x_c} P(x)\,dx + f_2\int_{x_c}^1 P(x)\,dx}{\int_0^1 P(x)\,dx} \tag{11}$$

$$F(x) = f_1 + (A_2/A)(f_2 - f_1) \tag{12}$$

where A_2 is the area under the distribution curve for concentrations going from x_c to 1 and A is the total area under the curve.

The line width of the ESR signal is likely to behave as a step function. A reasonable choice for x_c is the experimental critical concentration for phase separation. Constant values for the line widths may be chosen as 30 mG for the dilute solutions and 4.85 G for the concentrated Na–NH_3 solutions. The values calculated through (12) for ESR line widths are compared with experimental data in Figure 6. The discrepancies at $x_2 > 0.05$ (5 MPM) are explained by the choice of constant value for the line width in concentrated solutions. The difference in the slopes is sensitive to the choice of the correlation length. An almost perfect fit would be obtained if the size of the characteristic volume was decreased by 10 to 15%.

Other properties like the paramagnetic susceptibility can be interpreted in the same way. The theoretical curve is more questionable than for the ESR line width. A step function gives nevertheless a good result.

It is less straightforward to interpret the transport properties. Landauer[43] showed that neither the conductivity nor the resistivity adds up in a microscopically inhomogeneous system. He developed the effective medium theory (EMT) which gives good results for some nonhomogeneous alloys.

For the application of EMT to metal–ammonia solutions, it may be assumed, as a first approximation, that the conductivity would be a step function if the system was free from fluctuations. The results thus obtained would not be essentially different from those obtained by Jortner and Cohen.[32] This comes from the fact that the ratio A_2/A in (12) (i.e., the percentage of the solution at a concentration larger than x_c) gives a concentration scale similar to the Jortner–Cohen scale. The ratio A_2/A comes from the fluctuations and a step function, while the Jortner–Cohen scale comes from a bimodal model.

However, it is possible to use EMT without the model of a step function. The distribution curve can be split into small intervals Δx. The area under the curve for an interval Δx is

$$A_i(\Delta x) = \int_{x_i}^{x_i+\Delta x} P(x)\,dx \tag{13}$$

and the fraction of the solution which has a concentration $x_i \pm (\Delta x/2)$ is

$$y_i = \frac{A_i(\Delta x)}{A} = \frac{\int_{x_i-(\Delta x/2)}^{x_i+(\Delta x/2)} P(x)\,dx}{\int_0^1 P(x)\,dx} \tag{14}$$

If a theoretical conductivity can be ascribed to the nonfluctuating solutions of concentration x_i, it is possible to extend the EMT as follows.

For two states (step function), the conductivity calculated by EMT follows the condition:

$$y_1\left(\frac{\sigma_1 - \bar{\sigma}}{\sigma_1 + 2\bar{\sigma}}\right) + y_2\left(\frac{\sigma_2 - \bar{\sigma}}{\sigma_2 + 2\bar{\sigma}}\right) = 0 \tag{15}$$

where y_2 is the fraction of the solution where $x_2 > x_c$.

The extension to n states is straightforward and the equation

$$\sum_{i=1}^{n} \frac{y_i(\sigma_i - \bar{\sigma})}{\sigma_i + 2\bar{\sigma}} = 0 \tag{16}$$

gives $\bar{\sigma} = f(x_2)$.

Thus even for the transport properties, the above treatment of the fluctuations can help to check a theoretical model against the experimental data, with or without the simplification offered by a step function.

It is clear that the present ideas are profoundly different from the Jortner–Cohen[32] model. Present ideas[36] deal with thermodynamic functions. The concentration fluctuations distribution is calculated in a volume $V = L^3$. This volume is large because of the closeness of the critical point. The concentration fluctuation distribution is around the average concentration. It is an inhomogeneous model because concentrations different from the average concentration have to be taken into account. The application of present ideas to the calculation of physical properties does not imply limits of applicability; i.e., it is not necessary to give the lower and the upper concentration where these ideas are applied. Consequently, these ideas can be used in the whole range of concentrations where MNM transition is known to occur. More calculations are, of course, needed, especially at various temperatures, to check this model.

However, it should be noted that the concentration fluctuations distribution does not depend on model specifically designed for this purpose. The concentration fluctuations distribution is based on experimental values of activity and correlation length, and on the analytical expression of excess thermodynamic functions. This analytical expression is itself based on the assumption that the solution is a mixture of pure ammonia and of solvated alkali metal, $M(NH_3)_n$. The analytical expression of excess thermodynamic functions has been proved successful for the calculation of critical temperature and concentration.

3. Concentrated Solutions

Since the last review about magnetic properties of MAS, some new data have been published in the range of concentrated solutions. The magnetic susceptibilities and nuclear magnetic resonance will be successively considered.

3.1 Magnetic Susceptibility. The magnetic susceptibilities of Na–NH_3 and Cs–NH_3 have been measured[20,21] for concentrated solutions by the Gouy technique. With the Wiedeman additivity law, the paramagnetic susceptibilities have been obtained after the removal of the ammonia, metal cation, and Landau diamagnetic contributions. This last contribution, taken equal to the free electron Landau diamagnetism, is of course more realistic for concentrated than for dilute solutions. It was found that the paramagnetic susceptibilities of solutions more concentrated than, say, 10 MPM have a free electronlike order of magnitude. It was found that, at about 15 MPM, the experimental paramagnetic susceptibility is about twice as large as the noninteracting free electron gas value. This result is not surprising because the free electron formula neglects exchange and correlations effects. Theoretical and experimental works have shown that, for alkali metals, for instance, the ratio of the true spin susceptibility to the value given by the Pauli formula is between 1.5 and 2. From the Pauli formula, the paramagnetic susceptibility per gram atom, χ_P^{at}, is expected to vary as $n^{-2/3}$, where n is the electron density per unit volume. Therefore χ_P^{at} is expected to increase when the metal concentration decreases from saturation in Na–NH_3, or from, say, 15 MPM in Cs–NH_3. This trend is, in fact, observed in Cs–NH_3, but the opposite trend is found in Na–NH_3. It is difficult to speculate about the origin of such a difference.

The temperature coefficient of the paramagnetic susceptibility has been found to be always positive and decreasing when the metal concentration increases. For concentrations of the order of 15 MPM, the temperature coefficient of the paramagnetic susceptibility has been found to have the value expected from the thermal expansion.

Therefore, as far as magnetic susceptibility is concerned, solutions of concentration close to saturation, or close to, say, 15 MPM, appear to have a free electron behavior. However deviations occur for lower metal concentrations.

3.2 Magnetic Resonance. Nitrogen (^{14}N) Knight shifts $K(N)$ have been measured[20,24] for Na–NH_3 and Cs–NH_3 solutions. For concentrations up to about 15 MPM, $K(N)$ is the same for both types of solutions, at the same concentration. It was found also that for concentrations larger than about 20 MPM, $K(^{14}N)$ has constant value. It was not possible to measure $K(N)$ for concentrations larger than about 40 MPM. The general expression of the ^{14}N Knight shift $K(N)$ is

$$K(N) = \frac{8\pi}{3}\chi_P^{at}\frac{P_F(N)}{N_{av}R} \qquad (17)$$

where R is the mole ratio and χ_P^{at} the paramagnetic susceptibility per gram atom. Therefore, the constancy of $K(N)$ between 20 and 40 MPM for Cs–NH_3 solutions means that $\chi_P^{at}P_F(N)$ varies as R does. In fact χ_P^{at} has been found to vary very slightly in this concentration range. Therefore, P_F (N) varies approximately as R does, that is to say that the electron density at the nitrogen nucleus decreases as R does when the cesium concentration increases.

Cesium (^{133}Cs) Knight shifts $K(Cs)$ have been measured[20,24] vs. concentration and temperature. The shifts increase with cesium concentration and with temperature. The values of $K(Cs)$ increase rapidly up to about 25 MPM and show an inflection point between 30 and 35 MPM. With our magnetic susceptibility results, the electronic probability density $P_F = \langle|\Psi_F(0)|^2\rangle$ was obtained for the sodium and for the cesium nucleus and are shown in Figure 3. For concentrated Na–NH_3 solutions, $P_F(Na)$ is almost constant, while for concentrated Cs–NH_3 solutions P_F (Cs) increases rather sharply. These differences in the trends of $P_F(Na)$ and $P_F(Cs)$ are significant. They cannot be accounted for by the uncertainties of the paramagnetic susceptibilities values. These differences are probably a consequence of different solvation for Na^+ and Cs^+ cations. However, no calculation has been made of the conduction electron wave function in concentrated solutions. Such calculations should lead to theoretical values of $P_F(Cs)$ and $P_F(Na)$. Cesium Knight shifts measurements also gave evidence of the liquid–solid equilibrium in the phase diagram of Cs–NH_3 solutions for metal concentrations larger than the eutectic concentration.

Thermal variations of $K(Cs)$ have been measured.[20,24] It was found that $K(Cs)$ always increases with temperature (for concentrations below about 50 MPM), and for temperatures lower than −40°C. $K(Cs)$ should go through a maximum and its temperature coefficient should become negative, but Cs–NH_3 solutions are not stable enough to permit useful measurements at these temperatures. Experimental measurements showed that the positive temperature coefficient decreases when metal concentration increases. Therefore, even for concentrations larger than 10 MPM, increases of metal concentration or temperature make the solutions more metallic, which is a picture coherent with physical properties such as electrical conductivity.

Other NMR measurements have been reported by Garroway and Cotts.[44] They measured self-diffusion coefficients of ^7Li, ^{23}Na, ^1H in Li– and Na–NH_3 by spin-echo technique, in the intermediate and concentrated ranges up to saturation. The purpose of these experiments was to give direct evidence of the solvation of Li^+ and Na^+ by ammonia molecules. They observed that the measured ammonia self-diffusion coefficient is greater than the ^7Li self-diffusion coefficient, except at 20 MPM where they are essentially equal. This result suggests strongly that the Li^+ cation is solvated by four NH_3 molecules, which is an expected result. The similarity of the Na–NH_3 and Li–NH_3 diffusion data indicates that the solvation number is also 4 in the case of Na^+ in Na–NH_3 near saturation. It has been suggested by Sienko that the diffusion coefficient should also be determined for ^{14}N. It would also be interesting to have diffusion measurements in Cs–NH_3, since it is usually expected that the Cs^+ solvation is different (much less tightly bound) from the solvation of other alkali cations.

It should also be noted that the relaxation times and relaxation mechanism for the metal nuclear spin for very

concentrated solutions are not reported.

Let us note also that no other proton Knight shifts measurements have been reported for concentrated solutions since the Hughes measurements[45] of proton Knight shifts in Na–NH_3 solutions. Let us recall that the proton Knight shift $K(^1H)$ was found by Hughes to be negative at all concentrations in Na–NH_3 solutions. It should be noted that the absolute value of $K(^1H)$ increases with metal concentration. Therefore $K(^1H)$ is negative even for concentrations close to saturation, i.e., for concentrations for which there are no more solvated electrons, and for which most of the ammonia molecules are in solvation shells of cations. Therefore, the origin of the negative value of $K(^1H)$ cannot be investigated only in the solvated electron. It should certainly be useful to have data of $K(^1H)$ for other metal–ammonia solutions.

Conclusion

It seems to us that at least the qualitative understanding of metal–ammonia solutions is improving in all the concentration ranges. However, important questions, such as the description of the MNM transition in the intermediate concentration range and the nature of the diamagnetic species in the dilute range, certainly need to receive more attention. About the experimental magnetic data, many have now been collected. However, the magnetic susceptibility is not known between about 0.5 and 2 MPM. Even in very dilute solutions it should be very useful to check the magnetic susceptibility by static and resonance techniques and for different cations. In the intermediate and concentrated ranges, valuable relaxation times studies must still be done.

Acknowledgment. The authors express their thanks to Dr. A. Demortier for helpful discussions.

References and Notes

(1) R. Catterall, "Proceedings Colloque Weyl II", J. J. Lagowski and M. J. Sienko, Ed., Butterworths, London, 1970, pp 105–130.
(2) J. L. Dye, Ref 1, pp 1–17.
(3) J. J. Lagowski, "Electrons in Fluids", J. Jortner and N. R. Kestner, Ed., Springer-Verlag, Berlin, 1973, pp 29–36.
(4) A. Demortier, M. De Backer, and G. Lepoutre, *J. Chimie Phys.* **3**, 380 (1972).
(5) M. C. Justice, Thèse, doctorat d'état, Paris, 1974.
(6) H. L. Friedman, "Ionic Solution Theory", Wiley-Interscience, New York, N.Y., 1962.
(7) P. D. Schettler, this colloque.
(8) F. J. Tehan, M. T. Lok, and J. L. Dye, 165th National Meeting of the American Chemical Society, Dallas, Tex., 1973.
(9) C. Lambert, ref 1, pp 301–308.
(10) C. A. Hutchison and R. C. Pastor, *J. Chem. Phys.*, **21**, 1959 (1953).
(11) D. E. O'Reilly, *J. Chem. Phys.*, **35**, 1856 (1961).
(12) R. J. Blume, *Phys. Rev.*, **109**, 1867 (1958).
(13) V. L. Pollak, *J. Chem. Phys.*, **34**, 864 (1961).
(14) H. M. McConnel and C. H. Holm, *J. Chem. Phys.*, **26**, 1517 (1957).
(15) J. V. Acrivos and K. S. Pitzer, *J. Phys. Chem.*, **66**, 1693 (1962).
(16) D. E. O'Reilly, *J. Chem. Phys.*, **41**, 3729 (1964).
(17) D. E. O'Reilly, *J. Chem. Phys.*, **50**, 4743 (1969).
(18) T. J. Swift, S. B. Marks, and R. A. Pinkowitz, ref 1, pp 133–144.
(19) R. A. Pinkowitz and T. J. Swift, *J. Chem. Phys.*, **54**, 2858 (1971).
(20) J. P. Lelieur, Thèse, doctorat d'état, Orsay, 1972.
(21) J. P. Lelieur and P. Rigny, *J. Chem. Phys.*, **59**, 1142 (1973).
(22) S. I. Chan, J. A. Austin, and O. A. Paez, ref 1, pp 425–438.
(23) P. Damay, this colloque.
(24) J. P. Lelieur and P. Rigny, *J. Chem. Phys.*, **59**, 1148 (1973).
(25) E. Duval, P. Rigny, and G. Lepoutre, *Chem. Phys. Lett.*, **2**, 237 (1968).
(26) M. J. Sienko, "Metal–Ammonia Solutions", G. Lepoutre and M. J. Sienko, W. A. Benjamin, New York, N.Y., 1964, pp 23–40.
(27) J. C. Thompson, *Rev. Mod. Phys.*, **40**, 704 (1968).
(28) M. H. Cohen and J. C. Thompson, *Adv. Phys.*, **17**, 857 (1968).
(29) G. Lepoutre and J. P. Lelieur, ref 1.
(30) J. V. Acrivos and N. F. Mott, *Philos. Mag.*, **24**, 19 (1971).
(31) J. V. Acrivos, *Philos. Mag.*, **25**, 717 (1972).
(32) J. Jortner and M. H. Cohen, "The Metal–Nonmetal Transition in Metal–Ammonia Solutions", unpublished.
(33) J. Jortner and M. H. Cohen, *J. Chem. Phys.*, **58**, 5170 (1973).
(34) S. Kirkpatrick, *Phys. Rev. Lett.*, **27**, 1722 (1971).
(35) J. P. Lelieur, *J. Chem. Phys.*, **59**, 3510 (1973).
(36) P. Damay and P. D. Schettler, *J. Phys. Chem.*, this issue.
(37) P. Chieux, *Phys. Lett. A*, **48**, 493 (1974).
(38) T. L. Hill, "Statistical Mechanics", McGraw-Hill, New York, N.Y., 1956.
(39) K. Ichikawa and J. C. Thompson, *J. Chem. Phys.*, **59**, 1680 (1973).
(40) P. Damay, Thèse, doctorat d'état, Paris, 1972.
(41) P. Damay, ref 3, pp 195–202.
(42) P. Debye, *J. Chem. Phys.*, **31**, 680 (1959).
(43) R. Landauer, *J. Appl. Phys.*, **23**, 779 (1952).
(44) A. N. Garroway and R. M. Cotts, *Phys. Rev. A*, **7**, 635 (1973).
(45) T. R. Hughes, *J. Chem. Phys.*, **38**, 202 (1963).
(46) S. Freed and N. Sugarman, *J. Chem. Phys.*, **11**, 354, (1943).

Discussion

M. H. COHEN AND J. JORTNER. This is an interesting and valuable paper. With regard to our own work, the basic physical idea advanced by us concerning the metal–nonmetal transition in metal–ammonia solutions (MAS) is that those materials fall within the general category of systems where microscopic inhomogeneities determine electronic structure and transport properties within the transition region. We welcome the authors' agreement on this point, but, in our opinion, the question of whether the fluctuations are unimodally or bimodally distributed remains open.

Only unimodal fluctuations can occur within the conventional fluctuation theory used in this paper. Cases of bimodal distributions are, however, also known to occur. Short wavelength fluctuations have been shown to be bimodally distributed in Wilson's theory of phase transitions. The highly developed droplet model of condensation contains bimodally distributed density fluctuations near the liquid–gas critical point. Many examples of clustering are known both near and unrelated to critical points. As the classical thermodynamic analysis used by Lelieur, Damay, and Lepoutre is known not to give a good account of fluctuation phenomena near critical points, and as our proposed bimodal fluctuations are closely connected to the phase separation, the present paper does not clarify the question of unimodal vs. bimodal fluctuations. Our analysis of the electrical conductivity, the optical properties, and the thermoelectric power, however, suggest strongly that bimodally distributed concentration fluctuations occur.

For the Cs solutions, where there is neither a phase separation nor anomalous concentration fluctuations, and for all the solutions at high temperatures, the approach of Lelieur, Damay, and Lepoutre will be very useful.

With regard to details, it is not clear to us why the authors have supposed the Debye correlation length to be proportional to the Ornstein–Zernike correlation length.

A detailed discussion of unimodal inhomogeneous materials and reduction of the theory to that of an equivalent bimodal case has already been given in our paper on expanded liquid Hg [*Phys. Rev.*, **A10**, 978 (1974)].

The effective medium theory is inapplicable for low values of the metallic volume fraction, $C < 0.4$, when the ratio of, e.g., the conductivities, is smaller than 30, as is the case for Li and Na ammonia solutions.

J. P. LELIEUR, P. DAMAY, AND G. LEPOUTRE. The bimodal fluctuation model is obviously successful for the determination of some physical properties. It seems that the existence and origin of these bimodal fluctuations have not been clarified. The bimodal fluctuation model has essentially been introduced to match the electrical conductivity. The physical picture of metal–ammonia solutions in the intermediate range (unimodal or bimodal fluctuation model) has first to consider the structural experimental data (neutron or x ray) rather than the electrical conductivity. The results of Chieux were obtained for temperatures very near the critical point. In the temperature range of Chieux's results, the classical description of Ornstein–Zernike for critical fluctuations in fluids is known to be correct. Chieux's data follow this description. In this framework, the Ornstein–Zernike fluctuation decay length is proportional to the Debye correlation length. Both lengths express the same quantity except for a dimensionality factor [B. Widom, *J. Chem. Phys.*, **43**, 3892 (1965); Sette, Essays in Physics (1973)]. It should also be noted that the bimodal fluctuation model for the description of the nonmetal to metal transition is applicable, according to Jortner and Cohen, only for concentrations larger than 2.3 MPM. It is clear that the experimental onset of metallic characters appears rather for concentrations of the order of 1 MPM. It would be difficult to apply the bimodal fluctuation model to concentrations down to 1 MPM.

Magnetic Similarities and Differences of Some Chemical Models of Alkali Metal–Ammonia Solutions

Sidney Golden*

Chemistry Department, Brandeis University, Waltham, Massachusetts 02154; Isotope Department, The Weizmann Institute of Science, Rehovot, Israel;[1a] and Physical Chemistry Department, The Hebrew University, Jerusalem, Israel[1b] *(Received July 23, 1975)*

Each of six existing chemical models of *alkali metal–ammonia solutions* yields the relationship $\chi_M - \chi_M^{spin} = (1 - y)X_M + yY_M$, independent of the model. The *molar static magnetic susceptibility*, χ_M, the *molar spin susceptibility*, χ_M^{spin}, and the *fraction of unpaired spins*, y, are each measurable quantities which depend implicitly upon the temperature and composition of the solutions and are explicitly independent of the models. The X_M's and Y_M's are characteristic of the models and of the alkali metal M. Existing magnetic susceptibility data, both experimental and theoretical, already give a qualified indication of distinguishability between certain of the models and indicate how a reliable discrimination between them may be effected when data adequate to do so become available.

Introduction

The presence of *alkali metal anions* as essential chemical constituents in *alkali metal–ammonia solutions* was originally conjectured[2a] on the basis of theoretical estimates then available for the positive electron affinities of some of the gaseous alkali atoms and the ensuing stabilization that could be expected from the resulting solvation of the anions that they could form. In terms of these constituents, a good quantitative account could then be given of the compositional behavior of a variety of properties of alkali metal–ammonia solutions.[2b,3] Soon thereafter, based primarily on correlative spectroscopic evidence, the presence of *alkali metal anions* in solutions of *amines*[4] and *ethers*[5] could be inferred—and was.

Somewhat more direct evidence for the real existence of these anions in appropriate solutions of the alkali metals has come forth in just the past 2 years: (1) analysis of the infrared absorption band exhibited by sodium–ammonia solutions, which band had usually been ascribed entirely to the solvated electron, e^-, has revealed the presence of an additional absorbing species (spectrally distinct from the solvated electron) which conforms to the stoichiometry Na^-;[6] (2) the first pure Na^--containing compound (a crystalline salt) has been prepared and identified;[7] (3) precise experimental determinations of the electron affinities of several alkali atoms have established the appreciable stability of their anions, M^-, in the gas phase;[8] (4) theoretical calculations of the electron affinities have been carried out, with results that are in excellent agreement with the measured values;[9] (5) ^{23}Na NMR studies of two nonaqueous solutions of the first prepared sodium anion-containing compound[7] have revealed the presence of a new characteristic resonance (distinct from that to be associated with Na^+) which exhibits a large diamagnetic chemical shift in accord with the expected diamagnetic susceptibility of Na^-.[10]

The foregoing results would seem sufficient to dispel any doubts as to the real existence of *alkali metal anions* as constituents of appropriate solutions of the alkali metals.

However, because of the considerable attention which ammonia solutions of the alkali metals have received during the more than 100 years they have been known,[11] a variety of chemical models has been developed to account for their properties and to correlate them with their presumed compositional behavior. As a consequence, sometimes unusual chemical species have been invoked (depending on the model) which are stoichiometrically equivalent to but differ intrinsically from the alkali metal anions. More importantly, such species are potentially capable of being converted into the anions in pure compounds that may be formed which contain them. Despite the reassuring evidence which has been cited for the real existence of alkali metal anions in appropriate solutions and compounds, therefore, questions regarding the actual nature of the *alkali metal–ammonia solutions* and the adequacy of the chemical models which have been constructed to account for their properties still merit some attention.

It is to the foregoing questions that the present paper is directed. In terms of a fairly general analysis of the magnetic susceptibilities which are to be expected from various chemical models of *alkali metal–ammonia solutions*, a reasonably reliable discrimination between some of them appears to be possible. Although the magnetic data which are currently available are only adequate to *suggest* a qualified distinction, it is hoped that the present paper can encourage the future acquisition of such data (both theoretical and experimental) which are adequate to discriminate between the models in unqualified terms.

Chemical Models of Alkali Metal–Ammonia Solutions

Table I lists the *major chemical species* presumed to be formed and subsequently solvated when an alkali metal, M, is dissolved in ammonia, S, at moderate concentrations, according to six chemical models which have been suggested to describe the compositional behavior of these solutions. The stoichiometric equivalence of the various species in each column of the table is to be noted. Despite any such equivalence, however, the presumed nature of their constitution (reflected in the compositional notation used to describe them) precludes their being regarded as identical. The detailed differences between the various species can be found in the cited references.

*Address correspondence concerning this article to this author at Brandeis University.

TABLE I: Major Stoichiometrically Equivalent Species of Various Chemical Models of Alkali Metal–Ammonia Solutions

Model	Paramagnetic species		Diamagnetic species				Ref
I	$M^+ \cdot e^-$	e^-	M^+	e_2^{2-}	$M^+ \cdot e_2^{2-}$	$M^+ \cdot e_2^{2-} \cdot M^+$	12
II	$M^+ \cdot e^-$	e^-	M^+		$e^- \cdot M^+ \cdot e^-$	$(M^+ \cdot e^-)_2$	13
III	$M^+ \cdot S^-$	S^-	M^+		M^-	$M^+ \cdot M^-$	14
IV		e^-	M^+			M_2	15
V	F	e^-	M^+			F_2	16
VI	F	e^-	M^+		F′	F_2	17, 18

TABLE II: Basic Chemical Species of Various Chemical Models of Alkali Metal–Ammonia Solutions

Model	Paramagnetic species	Diamagnetic species
I	e^-	M^+, e^{2-}
II	e^-	M^+
III	S^-	M^+, M^-, S
IV	e^-	M^+, M_2
V	e^-, F	M^+, F_2
VI	e^-, F	M^+, F_2, F′

The *basic chemical species* involved in each of the models can be ascertained, by inspection, from Table I and are listed in Table II; they are all presumed to be solvated. The latter species are capable of reacting and combining with each other to form the remaining species of Table I as well as larger aggregates, e.g. ion-triples, ion-quadruples, etc., through appropriate chemical equilibria postulated by each model. All the models then give a similar (but not identical) account of the compositional behavior of the solutions as the concentration of dissolved alkali metal is varied.

Since they are not necessary for our purposes, we omit any description of the pertinent equilibria; they, too, can be found in the cited references. We merely note that all the models are constructed so that only *solvated alkali metal cations*, M^+, and *solvated electrons*, e^-, or *solvated anions*, S^-, prevail as solute species when the *alkali metal–ammonia solutions* become increasingly dilute.

Magnetic Susceptibilities of the Models

That the major chemical species invoked by each model are expressible as *composites* of the basic chemical species they also invoke is evident from Tables I and II. A similar composite nature is to be expected for larger aggregates that may be formed. As a result, suitable *additive and constitutive properties*, as regards the basic chemical constituents of the alkali metal–ammonia solutions, can serve to discriminate between some (or all) of the models. In particular, the magnetic susceptibility which is to be ascribed to the dissolved alkali metal, a property which has played a crucial role in our developing understanding of these systems,[15,19,20] will be dealt with here for that purpose.

To be explicit, we assume: (1) the *molar magnetic susceptibility*, χ_k, of the kth *basic chemical species* (Table II) is the algebraic sum[21] of a diamagnetic part, $\chi_k^{\,d}$, and a paramagnetic part, $\chi_k^{\,p}$; (2) the value of $\chi_k^{\,p}$ is entirely due to a common value of the *spin paramagnetic susceptibility* of that species,[22] $\chi_0^{\,spin}$; (3) the *molar diamagnetic susceptibility* of any composite chemical species is the sum of the corresponding quantities of its constituent basic chemical species[23]; (4) the *molar paramagnetic susceptibility* of any composite chemical species arising in models I, III–VI is the sum of the corresponding quantities of its constituent basic chemical species, while for those arising in model II it is just that of the *unpaired* paramagnetic constituent that it contains.[24]

With these assumptions, it follows that the molar *static* magnetic susceptibility,[15,19,25] χ_M, attributable to the dissolved alkali metal, is expressible as

$$\chi_M = \sum_k f_k \chi_k^{\,d} + \left(\sum_k f_k'\right) \chi_0^{\,spin} \tag{1}$$

where f_k is the ratio of the total amount of the kth basic chemical constituent (combined or not) to the total amount of dissolved alkali metal and f_k' is a similar ratio modified in accord with assumption 4. Furthermore, the *molar spin susceptibility*,[20,26,27] $\chi_M^{\,spin}$, attributable to the dissolved alkali metal is expressible as

$$\chi_M^{\,spin} = \left(\sum_k f_k'\right) \chi_0^{\,spin} \tag{2}$$

By merely invoking electrical neutrality of the solutions and material balance among the metal-containing species, we are able to obtain from eq 1 and 2 that

$$\chi_M - \chi_M^{\,spin} = (1 - y)X_M + yY_M \tag{3}$$

where

$$y = \chi_M^{\,spin}/\chi_0^{\,spin} \tag{4}$$

is the fraction of unpaired spins per mole of dissolved alkali metal. The essential invariance of the *form* of eq 3 to the actual model used to obtain it is noteworthy.

The expressions for X_M and Y_M for the various models are given in Table III. Because of the presence of two basic paramagnetic species in models V and VI, viz., e^- and F, and three basic metal-containing diamagnetic species in model VI, viz., M^+, F_2, and F′, we have introduced

$$\Delta\chi_F = \chi_F^{\,d} - (\chi_{e^-}^{\,d} + \chi_{M^+}^{\,d}) \tag{5}$$

$$\Delta\chi_{F_2} = \chi_{F_2}^{\,d} - (\chi_{F'}^{\,d} + \chi_{M^+}^{\,d}) \tag{6}$$

$$\alpha = ([e^-] - [F])/([e^-] + [F]) \tag{7}$$

$$\beta = ([F'] - [F_2])/([F'] + [F_2]) \tag{8}$$

the bracketted quantities being the total concentrations of the indicated species (in combination or not). Apart from the X_M of model VI and the Y_M's of models V and VI, the remaining entries are presumably independent of the detailed compositions that the models ascribe to the solutions and of their temperatures. Such dependence is *implicit* in the χ_M and $\chi_M^{\,spin}$ of eq 3, as is y, which are *measured* quantities that are independent of the specific model considered.

To the extent that the constituent species of an alkali metal–ammonia solution are justifiably composites of the basic chemical species pertinent to a given model, the addition of chemically inert solutes, e.g., unreactive salts having the same metal cation, to the solution will not alter the form of eq 3. Except for model VI, the X_M's will be identical with those already given; except for models V and VI, so will the Y_M's. However, even the exceptions can be expected not to change appreciably in value from that obtained in

TABLE III: Coefficients of Eq 3 for Various Chemical Models of Alkali Metal–Ammonia Solutions

Model	X_M	Y_M
I	$\chi_{M^+}{}^d + \frac{1}{2}\chi_{e^2}{}^{-d}$	$\chi_{M^+}{}^d + \chi_{e^-}{}^d$
II	$\chi_{M^+}{}^d + \chi_{e^-}{}^d$	$\chi_{M^+}{}^d + \chi_{e^-}{}^d$
III	$\frac{1}{2}\left\{\chi_{M^+}{}^d + \chi_{M^-}{}^d\right\}$	$\chi_{M^+}{}^d + \chi_{S^-}{}^d - \chi_S{}^d$
IV	$\frac{1}{2}\chi_{M_2}{}^d$	$\chi_{M^+}{}^d + \chi_{e^-}{}^d$
V	$\frac{1}{2}\chi_{F_2}{}^d$	$\chi_{M^+}{}^d + \chi_{e^-}{}^d + \left(\frac{1-\alpha}{2}\right)\Delta\chi_F{}^d$
VI	$\frac{1}{2}\left\{\chi_{F_2}{}^d - \left(\frac{1+\beta}{2}\right)\Delta\chi_{F_2}\right\}$	$\chi_{M^+}{}^d + \chi_{e^-}{}^d + \left(\frac{1-\alpha}{2}\right)\Delta\chi_F{}^d$

TABLE IV. Some Independently Estimated Values of X_M

Metal, M	X_M(II),[a] 10^{-6} cm³/mol	X_M(III),[b] 10^{-6} cm³/mol	X_M(IV),[c] 10^{-6} cm³/mol
Li	$10^6\chi_{e^-}{}^d - 0.7$	−29	−16; −17
Na	$10^6\chi_{e^-}{}^d - 4$	−37	−67; −40
K	$10^6\chi_{e^-}{}^d - 15$	−58	−87
Rb	$10^6\chi_{e^-}{}^d - 22$	−68	−140
Cs	$10^6\chi_{e^-}{}^d - 35$	−88	−220

[a] Reference 28. [b] Reference 29. [c] Reference 30–32.

TABLE V: Values of X_M Estimated for Experimental Magnetic Susceptibility Data

Metal, M	X_M, 10^{-6} cm³/mol	[M], M	T, K	Ref
Na	<−28	0.4	213	15
	−26	0.5	240	20
	−27	0.06	198	eq 12
K	−26	0.5	240	20
	−47	0.5	240	34
	−45	0.49	227	eq 12

the absence of such added solutes.

The only model dependence to be found in eq 3 lies in the values of X_M and Y_M. To some extent, values of the former can be estimated from independent experimental and theoretical information which is currently available. Some such values are given in Table IV. The values for X_M (I) will be similar to those of X_M (II), but with ($10^6\chi_{e^-}{}^d$) replaced by ($10^6\chi_{e^2-}{}^d/2$). From the intrinsic nature of the species invoked, we can expect that the F and F′ centers, as well as their dimers, will be considerably more diffuse as regards the bound electrons than their alkali metal counterparts in the gas phase. Because of the general correlation between diamagnetic susceptibility and electronic diffuseness[21] we further expect that

$$X_M(\mathrm{IV}) \ll X_M(\mathrm{V}) \doteq X_M(\mathrm{VI}) \qquad (9)$$

but it is evident that the theoretical information needed to verify this relationship still needs to be obtained.

Potential Distinguishability between the Chemical Models

As stated at the outset, there appears to be no adequate experimental data currently available to exploit the analysis of the preceding section for obtaining an unqualified discrimination between the various models which have been considered. In fact, many of the measured values of χ_M and $\chi_M{}^{spin}$ reported by different investigators frequently turn out to be incompatible with a basic requirement of eq 3, viz.

$$\chi_M - \chi_M{}^{spin} \leqslant 0 \qquad (10)$$

The latter condition follows from the observation that the X_M's and Y_M's of Table III are basically *diamagnetic* quantities and, by convention, negative. We shall give no detailed account of the incompatibilities, however, but note that the possibility that solutions of alkali metals can exchange with the constituents of the glass vessels containing them[33] may have a bearing on the matter.

Nevertheless, for not too dilute ammonia solutions of Na and K, the requirement expressed by eq 10 appears to be observed.[20]

The essential idea of using the behavior expressed by eq 3 (but not the equation itself) to provide a *characterization of the diamagnetic species* present in alkali metal–ammonia was first exploited by Huster.[15] He found that the *normally paramagnetic* sodium–ammonia solutions became *diamagnetic* at sufficiently large concentrations and sufficiently low temperatures. Under the conditions of Huster's experiments, it was reasonable to suppose that y was very close to zero, whereupon the most negative value of χ_{Na} that he measured could be taken as a *lower bound* for X_{Na}. This value is given in Table V.

A similar use of the behavior expressed by eq 3 was made by Hutchinson and Pastor[20] in their classic work. By utilizing their measured $\chi_M{}^{spin}$ values for moderately concentrated ammonia solutions of Na and K, where y is presumably quite small, and the corresponding χ_M values measured by Huster[15] and Freed and Sugarman,[19] they obtained estimated values for ($\chi_M - \chi_M{}^{spin}$). The corresponding X_{Na} and X_K values are given in Table V. A subsequent value for ($\chi_K - \chi_K{}^{spin}$) obtained by Hutchinson and O'Reilly[34] yields the X_K value also included in Table V.

The foregoing are the only values obtainable for X_M's estimated from the measured values that have been reported for ($\chi_M - \chi_M{}^{spin}$), by means of eq 3.

An alternative estimate of the X_M's can be made by exploiting the fact that χ_M appears to *vanish* at some appropriate metal concentration and temperature.[15,19] In such circumstances, eq 3 and 4 can be shown to yield

$$X_M = -\left(\frac{\chi_0{}^{spin} - X_M + Y_M}{\chi_0{}^{spin}}\right)\chi_M{}^{spin}\{\chi_M = 0\} \qquad (11)$$

Then, supposing that $|X_M/\chi_0{}^{spin}|, |Y_M/\chi_0{}^{spin}| \ll 1$, we obtain

$$X_M \doteq -\chi_M^{spin} \{\chi_M = 0\} \quad (12)$$

By extrapolating the measured molar spin susceptibilities[20] to the conditions for which the measured static susceptibilities are estimated to vanish,[15,19] additional values of X_{Na} and X_K can be obtained. They are also listed in Table V.

As disclosed by an inspection of the available data there is evident difficulty in obtaining adequately precise measured values of χ_M and χ_M^{spin}. Furthermore, by eq 3, their *differences* are involved in obtaining a relevant X_M. On this account, it would seem that the values given for the latter are probably no more reliable than to within 25% of the correct values. In view of such uncertainty, no unequivocal discrimination between the various models appears to be possible, but a comparison of the values in Tables IV and V (together with eq 9) strongly *suggests* that models IV–VI will be found *not* to be in accord with the magnetic facts once they are adequately determined.

Remarks

An important *caveat* must be kept in mind regarding the preceding results, because of a *metallic state* which has been postulated to occur when the *alkali metal–ammonia solutions* are sufficiently concentrated.[25,35] From Table V, the X_M values do approach conditions propitious for the formation of the *metallic state*, in which case the *chemical models* considered here will require modification. That such a condition may have been attained in some of Huster's experiments[15] is suggested by the *temperature-independent paramagnetic susceptibility* which he reported for very large metal concentrations (~4 *M*). In such cases, χ_0^{spin} will be smaller than the "free-spin" value[22] and y will be larger than that ordinarily estimated.

However, in spite of the foregoing possibilities, the fact that the current data enable any distinction at all to be made between the various chemical models of *alkali metal–ammonia solutions* (as suggested by the results we have described) can be regarded as a satisfactory preview of what may be achieved when adequately precise data, both experimental and theoretical, do become available.

For an unqualified discrimination to be forthcoming it would be desirable to have the requisite experimental data for *all* the alkali metals in ammonia solutions less concentrated than about 0.05 *M*. This would presumably avoid the *metallic state* which has been mentioned[25,35] and the theory which has been used here would then be hardly open to question. With precautions taken to minimize contamination problems[33] and the use of appropriate salts and low temperatures to produce small measured values of both χ_M and χ_M^{spin}, an enhanced reliability can be expected for the X_M's that they would yield.

Adequately precise theoretical values of the X_M's for models IV–VI are also needed in order to assess their reliability.

Acknowledgment. My thanks are due to Professor C. A. Hutchison, Jr., for a stimulating discussion that led to the present investigation. My thanks are also due to Dr. D. W. Norcross for undertaking the calculations of the diamagnetic susceptibilities of the alkali metal anions and, especially, for permitting me to use his preliminary results here prior to their publication.

References and Notes

(1) (a) Senior Weizmann Fellow, 1974–75. (b) Visiting Professor, 1974–75.
(2) (a) S. Golden, C. Guttman, and T. R. Tuttle, Jr., *J. Am. Chem. Soc.*, **87**, 135 (1965); (b) *J. Chem. Phys.*, **44**, 3791 (1966).
(3) T. R. Tuttle, Jr., C. Guttman, and S. Golden, *J. Chem. Phys.*, **45**, 2206 (1966).
(4) S. Matalon, S. Golden, and M. Ottolenghi, *J. Phys. Chem.*, **73**, 3098 (1969).
(5) M. T. Lok, F. J. Tehan, and J. L. Dye, *J. Phys. Chem.*, **76**, 2975 (1972).
(6) G. Rubenstein, T. R. Tuttle, Jr., and S. Golden, *J. Phys. Chem.*, **77**, 2872 (1973).
(7) J. L. Dye, J. M. Ceraso, M. T. Lok, B. L. Barnett, and F. J. Tehan, *J. Am. Chem. Soc.*, **96**, 908 (1974).
(8) T. A. Patterson, H. Hotop, A. Kasdan, D. W. Norcross, and W. C. Lineberger, *Phys. Rev. Lett.*, **32**, 189 (1974). See, also, A. Kasdan and W. C. Lineberger, *Phys. Rev. A.*, **10**, 1658 (1974).
(9) D. W. Norcross, *Phys. Rev. Lett.*, **32**, 192 (1974). See, *also*, D. L. Moores and D. W. Norcross, *Phys. Rev. A*, **10**, 1646 (1974).
(10) J. M. Ceraso and J. L. Dye, *J. Chem. Phys.*, **61**, 1585 (1974).
(11) See, for example (a) "Metal-Ammonia Solutions", W. L. Jolly, Ed., Dowden, Hutchinson, and Ross, Stroudsburg, Pa., 1972; (b) "Metal-Ammonia Solutions", Butterworths, London, 1970; (c) "Solutions Métal-Ammoniac Propriétés Physicochemiques", G. Lepoutre and M. J. Sienko, Ed., W. A. Benjamin, New York, N.Y., 1964.
(12) R. A. Ogg, Jr., *J. Am. Chem. Soc.*, **68**, 155 (1946). See, also, J. Kaplan and C. Kittel, *J. Chem. Phys.*, **21**, 1429 (1953); R. Catterall and M. C. R. Symons, *J. Chem. Soc. A*, 13 (1966).
(13) M. Gold, W. L. Jolly, and K. S. Pitzer, *J. Am. Chem. Soc.*, **84**, 2264 (1962).
(14) Reference 2.
(15) E. Huster, *Ann. Phys. (Leipzig)*, **33**, 477 (1938).
(16) E. Becker, H. Lindquist, and B. Alder, *J. Chem. Phys.*, **25**, 971 (1956).
(17) E. Arnold and A. Patterson, Jr., *J. Chem. Phys.*, **41**, 3089 (1964).
(18) See, also, the article by E. Arnold and A. Patterson, Jr., in ref 11c.
(19) S. Freed and N. Sugarman, *J. Chem. Phys.*, **11**, 354 (1943).
(20) C. A. Hutchinson, Jr., and R. C. Pastor, *J. Chem. Phys.*, **21**, 1959 (1953).
(21) See, in this connection, J. H. Van Vleck, "Electric and Magnetic Susceptibilities", Oxford University Press, London, 1948.
(22) See, for example, Chapter IX of ref 21. Note that the value need not be identical with the "free-spin" value in very concentrated solutions.
(23) A. Pascal, references to whose work can be found in ref 21.
(24) This assumption ensures the presence of a *diamagnetic anion* which is deemed essential in these solutions. Models IV and V are deficient in this regard.
(25) R. G. Suchanneck, S. Naiditch, and O. J. Kleinjot, *J. Appl. Phys.*, **38**, 690 (1967).
(26) A. Demortier and G. Lepoutre, *C. R. Acad. Sci., Ser. C*, **268**, 453 (1969).
(27) A. Demortier, M. DeBacker, and G. Lepoutre, *J. Chim. Phys.*, **69**, 380 (1972).
(28) The cation susceptibilities are those of G. W. Brindley and F. E. Hoare, *Trans. Faraday Soc.*, **33**, 268 (1937); *Proc. Phys. Soc. (London)*, **49**, 619 (1937).
(29) Determined from the anion susceptibilities calculated by Dr. D. W. Norcross, personal communication.
(30) The first Li value is that of M. Karplus and H. J. Kolker, *J. Chem. Phys.*, **38**, 1263 (1963).
(31) The first Na value is the average of two extreme values of $\chi_{Na_2}^{d}$ estimated by Huster, ref 15, who made use of a formula for the susceptibility of a valence electron due to L. Pauling, *Proc. R. Soc. London, Ser. A*, **114**, 181 (1927); see also ref 21, p 211.
(32) The remaining values have been estimated here by Huster's procedure, but with a knowledge of the ionization energies and quantum numbers of the relevant valence electrons, e.g., G. Herzberg, "Atomic Spectra and Atomic Structure", Dover, New York, N.Y., 1941, pp 62–63.
(33) I. Hurley, T. R. Tuttle, Jr., and S. Golden, *J. Chem. Phys.*, **48**, 2818 (1968).
(34) C. A. Hutchison, Jr., and D. E. O'Reilly, *J. Chem. Phys.*, **34**, 163 (1961).
(35) N. F. Mott, *Phil. Mag.*, **6**, 287 (1961).

Discussion

T. TUTTLE. How does your analysis succeed in making a distinction between the trapping center model and the redox model which are stoichiometrically equivalent?

S. GOLDEN. The X_M of the trapping center model can be expected to be considerably greater than that for the redox model, since the value for the latter is already smaller than that estimated for the alkali metal dimers in the gas phase. Although stoichiometric distinctions are absent, the magnetic susceptibilities will differ for the comparable species.

G. LEPOUTRE. A. Demortier (Doctoral Thesis, Paris, 1970) has measured the paramagnetic susceptibility of $K-NH_3$ solutions and his results at −33°C differ from those of Hutchinson and Pastor.

S. A. RICE. The nature of alkali metal–ammonia and also of other such solutions could be probed with ^{133}Cs solutions, since this isotope is Mössbauer active. In particular the nature of the electron orbitals on the metal anion could be investigated.

S. GOLDEN. The only question I would raise here concerns the capability of the Mössbauer effect to distinguish between various stoichiometrically equivalent species which have been proposed in the various chemical models of these solutions. That is, can the Mössbauer effect provide a definitive discrimination between M^- and $e^-{\cdot}M^+{\cdot}e^-$, for example?

S. A. RICE. 10^{-2} *M* solutions of alkali metals in ethers or amines containing "crown" cyclic ethers would provide a sufficient signal in a recoilless medium. To check the interpretation of metal–ammonia solutions, cesium salts in ammonia should also be studied. Cesium halides have been studied and the isomer shift found to vary with the halide (A. J. F. Boyle and C. J. Perlow, *Phys. Rev.*, **149**, 165 (1966)). Thus the nature or existence of Cs (e.g., $6s^2$ or $6s^1$, $6p^1$) could in principle be probed.

R. CATTERALL. If the M^- model is still in the running, where is the M^- band in ammonia? The M^- band has been well characterized in many solvents including, e.g., $MeNH_2$, very close to NH_3. To put the M^- band within 5–600 cm^{-1} of the e_{sol}^- band is a very big coincidence.

S. GOLDEN. Whether the M^- band in NH_3 and the $e_{NH_3}^-$ band are within 500–600 cm^{-1} remains yet to be accepted and confirmed by additional work. Whether such proximity of the bands is to be expected depends upon one's notions as to the species and transitions involved. I do not think currently available theory is either capable of excluding such proximity or of predicting it.

J. L. DYE. The question of the diamagnetic species in metal–ammonia solutions is connected with the presence or absence of diamagnetic species in amines which have a large infrared absorption in addition to the M^- absorption band. Generally one observes a spin concentration by ESR which is far less than that which would be required to give the ir band for any reasonable extinction coefficient. [See, for example, L. R. Dalton, J. D. Rynbrandt, E. M. Hansen, and J. L. Dye, *J. Chem. Phys.*, **44**, 3969 (1966).]

S. GOLDEN. The possibility that diamagnetic species other than alkali anions (and ion multiples of them) may be present in the alkali metal–ammonia solutions surely cannot be ruled out on the basis of the evidence now available. However, any such species can be expected to have diamagnetic susceptibilities which differ from those of the alkali metal anions and so the suggested magnetic analysis could be exploited to possibly rule out their presence.

J. W. FLETCHER. With reference to earlier results of Dye in alkali metal ethylamine–ammonia solutions and our pulse radiolysis data, the visible absorption attributed to Na^- in pure $EtNH_2$ does not appear to shift with added NH_3. Instead the intensity of the visible band decreases whereas the ir band increases with increased NH_3 composition. This and other data lead us to suggest Na^- is not formed in NH_3 solutions.

S. GOLDEN. In the original experiments of Matalon, Golden, and Ottolenghi the position of the M^- band in the amine–ammonia solution was found to shift with changing composition of the solvent, contrary to the observation made by Dr. Fletcher. On the basis of using the position of the I^- band in the same solution as an extrapolating vehicle it was possible to conclude that the visible M^- band in amine solutions did extrapolate essentially to the spectral region of the infrared absorption in metal–ammonia solutions. This led then to the suggestion that the M^- bands are indeed to be found in metal–ammonia solutions, which has been elaborated in more detail by the work of Rubinstein, Tuttle, and Golden [*J. Phys. Chem.*, **77**, 2872 (1973)].

Concentration Fluctuations in the Nonmetal-to-Metal Transition Range of the ^7Li–ND_3 System. A Neutron Small-Angle Scattering Experiment

P. Chieux

Institut Laue–Langevin, 38042 Grenoble Cédex, France *(Received August 11, 1975)*

Publication costs assisted by Institut Laue–Langevin

Correlation lengths for concentration fluctuations in the ^7Li–ND_3 system have been studied by small-angle neutron scattering as a function of the solution concentration in the nonmetal to metal range which is also the region of the liquid–liquid immiscibility. The data fit the Ornstein–Zernike law with maximum fluctuation rather narrowly peaked at the liquid–liquid critical concentration in good qualitative agreement with the thermodynamic predictions.

Some results have already been reported[1] on small-angle neutron scattering experiments performed on the Li–ND_3 system in the nonmetal-to-metal transition region. These results supported the idea of large concentration fluctuations extending several degrees above the liquid–liquid critical temperature near the critical concentration. It was of interest to extend these studies over the concentration scale in the transition region in order to investigate the concentration dependency of the characteristic length for correlated fluctuations. This was considered worthwhile in view of the heterogeneous model developed by Jortner and Cohen[2] to interpret the electronic transport properties over the whole nonmetal-to-metal transition range (~2 to 9 mol % metal (MPM)).

I. Experimental Details

We briefly recall the experimental conditions of the small-angle neutron scattering experiments. They were performed on the D11 machine of the Institut Laue-Langevin in Grenoble. The machine is installed at the end of a neutron guide tube looking at a cold source. A wavelength selector provided us with neutrons of a wavelength λ 7 Å with a resolution $\Delta\lambda/\lambda \approx 9\%$. The sample chamber in which the cryostat is mounted is located at the center of an 80-m-long evacuated system. Forty meters on the reactor side is used for the collimation device ensured by removable sections of guide tube. The detector can be plugged at defined distances up to 40 m on the other side. It is a BF_3-

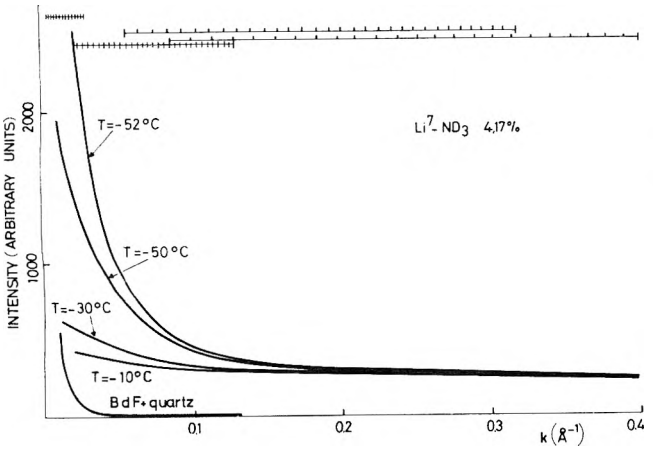

Figure 1. Intensity vs. k plot of a 4.17 MPM Li–ND_3 solution. Four scales representing three different detector positions and a wavelength change are shown. These are raw data. The statistical distribution of the experimental points cannot be represented on this scale.

type planar multidetector composed of 4096 square cells (64 × 64 cm total area) centered perpendicular to the beam direction. A cadmium beam catcher placed in front of the detector protects it from the direct beam and masks about 110 cells.

Since in our case the scattering signal obtained was always centrosymmetric, the neutrons counted in cells equidistant from the detector center could be summed. We usually obtained a series of 30 significant intensity values vs. scattering angle for one detector position. The exposure time was always taken so as to ensure a statistical accuracy of 0.2 to 0.3% for the summed intensity values. Only one detector position at 3.7 m from the sample and covering the k range 1.4×10^{-2} to 8.5×10^{-2} ($Å^{-1}$) (at λ 7 Å) was used to study the concentration effect (Note: $k = (4\pi/\lambda) \sin\theta$, with 2θ being the scattering angle.). The temperature was stabilized to 0.2°C but read only to 2°C which is worse than our previous experimental conditions but was of no importance since we deliberately stayed away from the critical temperature. The background noise (see the BdF + quartz line on Figure 1) comes essentially from the cryostat aluminum tail. It was always corrected for taking into account the transmission of the sample. The transmission was measured in situ, the neutron beam being attenuated by going through a pinhole in a cadmium plate and sent through the sample (in and out position) on the central cell of the multidetector. The beam catcher was removed for this experiment. In the 3m70 detector position (see Figure 1), the background corrections might slightly affect the data over a few cells, say over about three summed intensity values. The sample volume irradiated by the neutron beam was about 7 mm thick over an area 3.5 × 12 mm determined by a cadmium slit mounted on the cell.

A first series of samples consisted of concentrations 1.32, 4.17, 10.9 MPM, plus a pure ND_3 sample and several samples around 20 MPM concentration. More recently a series of concentrations 1.50, 2.50, 3.40, 4.45, 5.30, and 6.50 MPM was also prepared. The solutions were prepared[3] at concentrations known as a priori by weighing the ^7Li, introducing it into the quartz cells, and condensing on it known quantities of ND_3 (99.8% isotopic purity). Several runs were made over a year's time, giving reproducible results. We report essentially on the last most extensive series of concentrations.

II. Data Analysis

The neutron scattering signal is the sum of a coherent, incoherent, inelastic, and multiple term. For a binary system the coherent term can be expressed at $k = 0$, i.e., at zero angle, as in ref 1.

$$\left(\frac{d\sigma}{d\Omega}\right)_{coh} = N\left[\frac{N}{V}k_B T K_T (c_1 b_1 + c_2 b_2)^2 + \frac{N k_B T}{(\partial^2 G/\partial c^2)_{T,P,N}}\left|\frac{N}{V}(V_1 - V_2)(c_1 b_1 + c_2 b_2) - (b_1 - b_2)\right|^2\right] \quad (1)$$

or

$$\left(\frac{d\sigma}{d\Omega}\right)_{coh} = AK_T + BS_{cc}(0) \quad (2)$$

with

$$S_{cc}(0) = N k_B T \Big/ \left(\frac{\partial^2 G}{\partial c^2}\right)_{T,P,N}$$

c_1, c_2 are the mole fractions of the two constituents ($c_1 + c_2 = 1$); b_1, b_2 are the neutron scattering lengths; V_1, V_2 are the partial molar volumes ($c_1 V_1 + c_2 V_2 = V/N$); N is the number of atoms in the system and V the volume of the system; k_B is the Boltzmann constant; K_T is the isothermal compressibility; σ is the scattering cross section; Ω is the solid angle; G is the Gibbs free energy; and $S_{cc}(k)$ is the structure factor for concentration fluctuation. Relation 1 can easily be obtained from the Faber and Ziman expression for the coherent scattering of a binary mixture which is a linear combination of partial structure factors, $S_{ij}(k)$

$$\left(\frac{d\sigma}{d\Omega}\right)_{coh} = N[c_1 b_1^2 + c_2 b_2^2 + c_1^2 b_1^2 (S_{11} - 1) + c_2^2 b_2^2 (S_{22} - 1) + 2c_1 c_2 b_1 b_2 (S_{12} - 1)] \quad (3)$$

and from the Bhatia and Thornton[4] expression for the S_{ij} at $k = 0$ relating them to the thermodynamics of the system. We see, therefore, that from purely thermodynamic values we can predict the possibility of a strong coherent scattering signal in the vicinity of a critical point where the activity vs. concentration curve flattens and therefore the $S_{cc}(0)$ term in eq 2 diverges. The activity vs. concentration has been studied for a long time in metal ammonia. More recent work by Thompson and Ichikawa[5] confirmed the divergency of $S_{cc}(0)$ in the liquid–liquid phase separation region. Of course, the thermodynamics approach does not give any information on the angular dependency of the scattering signal or the $S_{cc}(k)$ values at $k \neq 0$.

In order to obtain experimentally the coherent scattering term all the other terms, incoherent, inelastic, multiple must be subtracted. In the previous study[1] we assumed that all these terms as well as the AK_T term of eq 2 had no angular dependency (gave a flat $I(k)$ signal) and that all the structural information belonged to the $S_{cc}(k)$ term, the concentration fluctuation term. This assumption was carefully checked by several runs away from the critical concentration either on pure ND_3 or on solutions near saturation which gave a perfectly flat $I(k)$ signal. The change of wavelength from 7 to 10 Å did not affect the data at 4 MPM either. The inelasticity effects might therefore be considered as giving also negligible angular dependency.

We are therefore left with a constant term to subtract from the experimental total scattering signal $I(k)$. That

TABLE I

Concentration, MPM	Parameters of eq 5			Correlation length (ξ), Å
	A	B	C	
3.42 ± 0.03	0.0061 ± 0.0003	4.14 ± 0.30	74.6 ± 1.8	26.1 ± 3
4.44 ± 0.04	0.0028 ± 0.0001	2.57 ± 0.10	75.6 ± 1.7	30.3 ± 2
5.32 ± 0.05	0.0032 ± 0.0001	2.74 ± 0.12	82 ± 1.8	29.3 ± 2
6.52 ± 0.06	0.014 ± 0.003	1.86 ± 0.85	65 ± 1.4	11.5 ± 7

term can be determined experimentally from the value of $I(k)$ at large k where the small-angle signal falls off to negligible values. This was done for the 4.17 MPM concentration and is shown on Figure 1. At the top of the drawing we have represented the four k scales 5×10^{-3} to 30×10^{-3} Å^{-1}, 2×10^{-2} to 13×10^{-2} Å^{-1}, 0.08 to 0.3 Å^{-1}, and 0.085 to 0.48 Å^{-1} (partially represented for lack of space) corresponding to the detector positions 10, 2.50, and 0.66 m (with also the λ 10 Å run for that last position). The statistical distribution of the experimental points is too narrow to be represented on the drawing. We see how well under these experimental conditions the constant can be determined. The $S_{cc}(k)$ signal was shown[1] to follow the classical Ornstein–Zernike law (see Figure 2)

$$S_{cc}(k)^{-1} = A(T)[K^2 + k^2] \quad (4)$$

where $\xi = 1/K$ is the correlation length of the fluctuations. $A(T)$ is a constant which might slightly depend on temperature. The Ornstein–Zernike relation was verified over all the investigated k range at the 4.17 MPM concentration. We recall that we are always choosing the wavelength large enough to not see (even at the 180° scattering angle) any feature belonging to the scattering pattern of the intramolecular distances or first neighbor distributions of the ND_3 molecule or of the saturated solutions. These patterns were studied independently on a conventional diffractometer and show up at about 0.7≃0.8 Å^{-1}. We are here truly in the small-angle scattering regime looking at concentration fluctuations extending over several atomic or molecular sites.

In the present study we covered only the 1.4×10^{-2} to 8.5×10^{-2} Å^{-1} range where most of the scattering occurs (see Figure 1). The value of the constant term C to be subtracted from the total scattering intensity $I(k)$ was obtained from a nonlinear least-squares fitting of the data with an Ornstein–Zernike type equation.

$$[I(k) - C]^{-1} = A + Bk^2 \quad (5)$$

III. Results and Discussion

The results are presented in Figure 3 on an intensity vs. k scale for a series of concentrations at a temperature $T = -46 \pm 2$°C. The 20-MPM sample was actually measured at $T = +5$°C and the 10.9-MPM sample was taken from a preliminary series of runs. It is obvious that most of the scattering occurs for concentrations near 4 MPM. We present in Table I the values of the A, B, C parameters of eq 5 as well as the correlation length ξ for concentrations near 4 MPM. No fit of the Ornstein–Zernike equation could actually be made at the other concentrations where the signal is much too flat. It is noticeable that at concentrations near the critical one the correlation length for fluctuations is rather concentration independent.

In Figure 4 we have plotted the extrapolated $I(0) - C$ values (see eq 5) for all the investigated concentrations. (Of course, at the concentrations where the Ornstein–Zernike fit was not feasible the extrapolation is rather conjectural.) We see that these values compare qualitatively well with

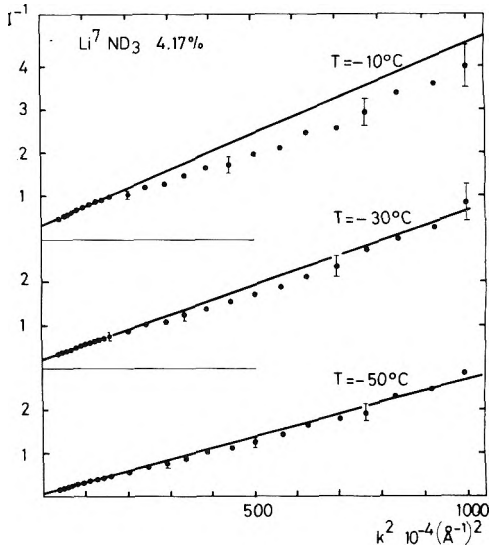

Figure 2. Ornstein–Zernike plots at large k values of a 4.17 MPM Li-ND_3 solution. The error bars represent the statistical accuracy.

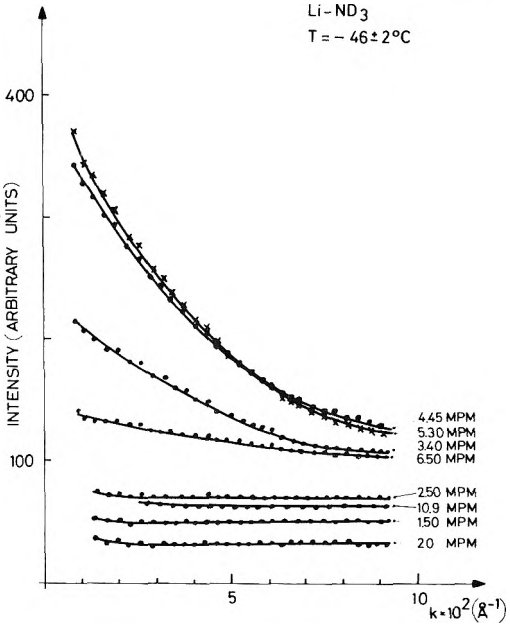

Figure 3. Intensity vs. k plots showing the concentration effect. The 20-MPM sample was measured at +5°C. The 10.9-MPM sample was reported from another series of experiments.

the published $S_{cc}(0)$ obtained from thermodynamics.[5] They are peaked at roughly the critical concentration X_c = 4.5 MPM obtained independently by Katsumoto and Lepoutre (this symposium). If we now consider the Na–NH_3 solutions where $S_{cc}(0)$ has a much broader peak,[5] we might expect to have significant concentration fluctuations extending over a broader concentration scale. This is of real importance since parameters of the lithium solutions are

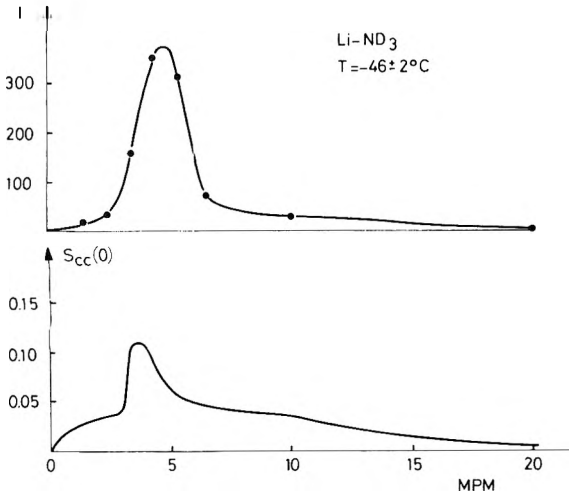

Figure 4. Comparison between the coherent signal at zero angle and $S_{cc}(0)$ (ref 5).

often used by necessity in computations referring to the Na system.

It would be interesting to check in greater detail if the concentration dependency of the slope of the Ornstein–Zernike plots is consistent with the thermodynamic parameters of eq 1. The concentration dependency of the value of C (eq 5) should also be shown to depend entirely on incoherent inelastic and multiple terms. All this would require absolute measurements and careful normalization procedures.

Finally a few words must be added on the interference effects which were detected by Schmidt[6] and more recently by Knapp and Bale (this symposium) using small-angle x-ray techniques. We also detected a strong scattering peak at about 1.0 $Å^{-1}$ with saturated solutions of ^7Li–ND_3 on a conventional neutron diffractometer. This peak shifted to smaller k values with dilution and was no longer detectable below 12 MPM. We believe that it corresponds essentially to the concentration dependent distribution function of the solvated lithium atoms in the system. In the case of the small angle neutron experiments, the choice of a large wavelength avoided any perturbation from these interference terms at high concentration, and at the lowest concentration the effect was not detectable owing to the small scattering length of the lithium atom.

Acknowledgment. Thanks are due to Professor Lepoutre and associates and especially to F. DeBaecker for a very helpful collaboration.

References and Notes

(1) P. Chieux, *Phys. Lett. A.*, **48** (6), 493–4 (1974).
(2) M. H. Cohen and J. Jortner, *Phys. Rev. Lett.*, **30**, 699 (1973).
(3) P. Chieux, M. J. Sienko, and F. DeBaecker, *J. Phys. Chem.*, this issue.
(4) A. B. Bhatia and D. E. Thornton, *Phys. Rev. B.*, **2**, 3004 (1970).
(5) K. Ichikawa and J. C. Thompson, *J. Chem. Phys.*, **59**, 1680 (1973).
(6) P. W. Schmidt, *J. Chem. Phys.*, **27**, 23 (1957).

Discussion

J. JORTNER. An interesting system to study will be Li–CH_3NH_2 solutions where large concentration fluctuations are exhibited in the concentration range above 10 MPM.

P. CHIEUX. These fluctuations are encountered in most of the solutions near saturation and are related to the piling of the solvated ions like large balls. Of course the effect is clearly visible when no anion is present.

M. H. COHEN. I noticed a nonmonotonic variation of the background intensity on top of which the Ornstein–Zernike contribution sits. It reached a maximum near the critical concentration. Do you have any ideas for explaining it?

P. CHIEUX. I think that it should be explained simply by the concentration dependency of the coefficient of the K_T term in the binary scattering law. We should however take as the two species the pure ND_3 and the *solvated* cation. We must also be careful to take the background intensity value at the extrapolated large k value. Finally there is some experimental uncertainty in the relative intensities of these different samples. We will try to prove more quantitatively these points in the near future.

Ultrasound Absorption Studies in the Critical Region of Lithium–Ammonia Solutions

D. E. Bowen

Physics Department, The University of Texas at El Paso, El Paso, Texas *(Received July 23, 1975)*

Publication costs assisted by The University of Texas at El Paso

Values of the absorption coefficient for ultrasound (α/f^2) in lithium–ammonia solutions are presented. These measurements were made in the critical region as a function of metal concentration, temperature, and sound frequency. The absorption is a strong function of the concentration and rises to a maximum at 4.25 MPM (mole percent metal). The absorption increases as either the temperature or the frequency is decreased. The data have been analyzed using a single relaxation theory, the Fixman theory, and the Kawasaki theory. The agreement with the last two theories is not good, leading to unphysical values for the parameters. The large increase in absorption seen may thus be due to causes other than those associated with critical point phenomena.

I. Introduction

Anomalous increases in the sound absorption coefficient have been detected in various liquid–liquid systems near the critical (or consolute) point.[1,2] A moderately successful theory explaining these increases was first given by Fixman.[3] Later theories and their modifications by Kawasaki,[4] Swift,[5] and Mitsura[6] have improved the theoretical explanation of these effects. The application of these theories requires knowledge of several thermodynamic properties of the solutions such as correlation lengths and diffusion coefficients. The assumption that these theories are correct enough to use them to obtain such quantities as the correlation lengths for a complex system such as lithium–ammonia solutions from measurements of the ultrasonic absorption coefficient has prompted us to perform such measurements. We thus present in this paper measurements of the absorption coefficient for lithium–ammonia solutions for concentrations between 12 and 3.25 MPM (mole percent metal) as a function of temperature and frequency. These measurements are then fitted to the theory and values for the correlation lengths obtained.

II. Experimental Section

The experimental apparatus consisted of three major parts: electronics, sample-cell ultrasonic delay-line assembly, and NH_3 preparation apparatus. As all of this apparatus has been described in the literature,[7] we shall only briefly describe it here. The method used is a pulse-echo technique with a variable path length cell. The electronics will allow operation over a 10 to 100 MHz frequency range and is controlled by a programmable calculator which allows very rapid data acquisition and analysis. The system is capable of absorption measurements to within 3%.

The solutions were prepared in a standard manner[8] using high purity NH_3 and lithium metal which was prepared in a helium-filled drybox. For an experimental run, a solution was prepared at a given concentration, and then absorption measurements were made as a function of temperature and frequency. The solution was then diluted by the addition of NH_3.

III. Data

Three separate experimental runs were performed covering the concentration range from 3.25 to 12 MPM. These measurements were made as a function of temperature from −63 to −55°C for most of the concentrations. As the apparatus only operates at odd multiples of the fundamental frequency of the ultrasonic transducer, complete coverage of any given frequency range is difficult. Measurements were made at the following frequencies: 10.4, 14.6, 17.8, 22, 15, 25, 35, 45, and 55 MHz for most of the concentrations studied, although all of the above frequencies were not necessarily used at each concentration and temperature.

Figure 1 shows the absorption (α/f^2) as a function of the metal concentration at 15 MHz and −63°C. There is a significant increase in the absorption between about 8 and 3.25 MPM (the lowest concentration studied); the absorption peaks at 4.25 MPM. Similar curves were obtained for the other temperatures and frequencies. No shift in the location of the absorption maximum was detected with either temperature or frequency, although the resolution in either frequency or concentration is not such as to rule out a small shift.

Figure 2 shows the temperature dependence of α/f^2 for 4.25 and 3.2 MPM both at 10 MHz. We see that there is a nonlinear temperature dependence with the absorption increasing rapidly as the temperature is lowered toward the phase separation temperature. For the critical concentration (we have chosen to call 4.25 MPM the critical concentration since the absorption peaks at this concentration; this is not in exact agreement with the literature values[9]) the temperature dependence is quite strong and falls off as the concentration is either increased or decreased.

Figure 3 is an example of the frequency dependence for the critical concentration at −63°C. These data are the result of two experimental runs using different ultrasonic transducers (2 and 5 MHz fundamentals). While there appears to be good internal consistency within any one run, there seems to be a problem with consistency from run to run (i.e., different solutions, although both are supposed to be at the same concentration). We do not have a good explanation of this effect yet; more data are probably needed. Even with the inconsistency it is seen that there is a rise in the absorption as the frequency is lowered; we take this rise to he evidence for a relaxation effect. We shall return to this in the next section.

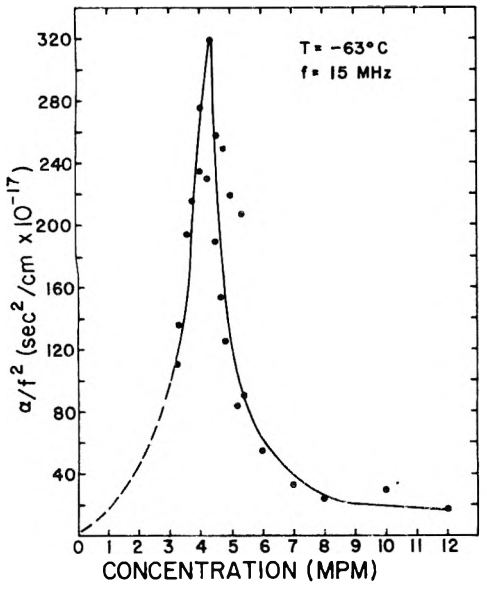

Figure 1. α/f^2 vs. concentration (MPM) at 15 MHz and −63°C.

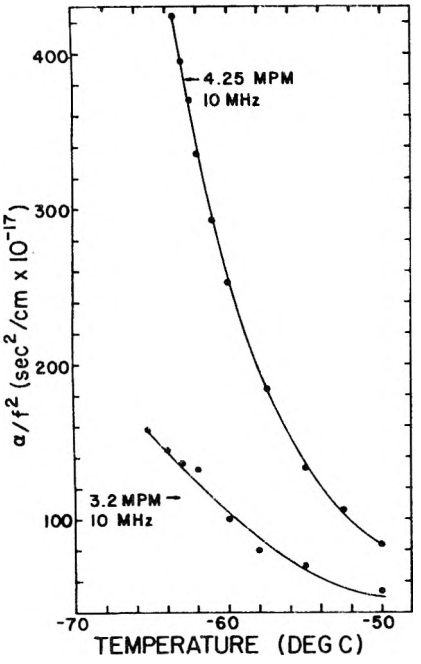

Figure 2. α/f^2 vs. temperature for two solutions.

IV. Interpretation

First we would like to point out that the absorption is far greater than that given by the expression[10]

$$\alpha_c/f^2 = (8\pi^2/3\rho c^3)[\eta_s + 3(\gamma - 1)K/4C_p] \qquad (1)$$

which is known as the classical absorption. Here c is the second velocity, f is the frequency, ρ is the density, η_s is the coefficient of shear viscosity, K is the coefficient of thermal conductivity, γ is the ratio of specific heats (C_p/C_v), and C_p is the specific heat at constant pressure. Using values for the above thermodynamic quantities from the literature, we find that α_c/f^2 varies from 2×10^{-17} to 2.5×10^{-17} cm²/sec as the concentration goes from 15 to 3 MPM. As is evident from Figure 1, the measured absorption is far greater than this and is thus due to mechanisms other than shear viscosity or thermal conductivity.

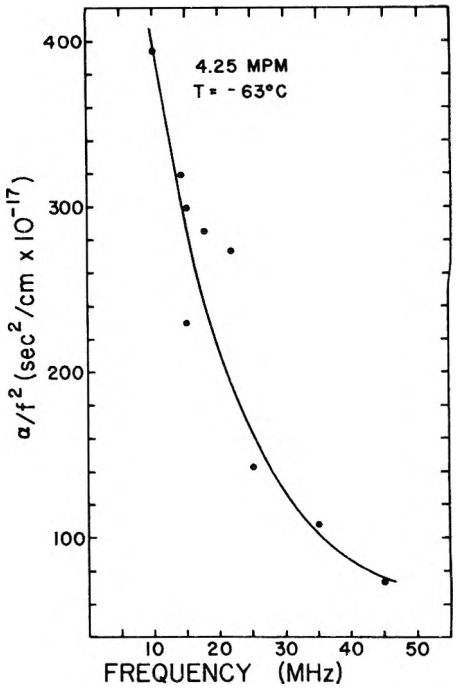

Figure 3. α/f^2 vs. frequency for a 4.25 MPM solution at −63°C.

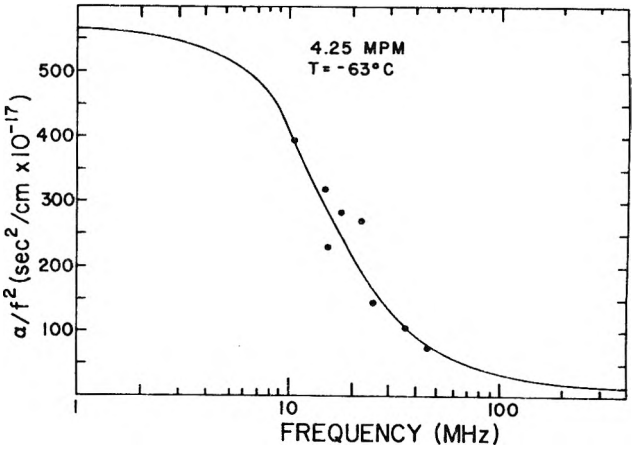

Figure 4. α/f^2 vs. frequency for 4.25 MPM solution at −63°C. The solid line is the fit to eq 2.

Absorption phenomena which depend on frequency such as seen in Figure 3 can be described formally as resulting from relaxation processes. If the process causing the observed absorption is due to a single relaxation, the data should be fitable with an equation of the form:[11]

$$\frac{\alpha}{f^2} = \frac{A}{1 + (f/f_r)^2} + B \qquad (2)$$

where f_r is the relaxation frequency. The term B includes the absorption due to the classical mechanisms given by eq 1 as well as the absorption due to relaxation effects at higher frequencies. Thus the absorption should rise from a value B at high frequencies to the constant value $(A + B)$ at low frequencies. Figure 4 is an example of the data (4.25 MPM at −63°C) fitted to this equation. We get the values: $f_r = 15.4$ MHz; $A = 552 \times 10^{-17}$ sec²/cm; $B = 16.81 \times 10^{-17}$ sec²/cm. This fit appears to be reasonable, but we do not have enough data at either high or low frequencies in order to conclude that a single relaxation effect is responsible for

the absorption. One finds that the exact values for the parameters in eq 2 are quite sensitive to the number of points used. For only two temperatures (−63 and −60°C) do we have enough frequency data to make such a fit, and we feel that the values are only rough indications of the process. We should point out, however, that this fit is better than that which was obtained by Anantaraman et al.[2] in their studies of the absorption in the critical region of the nitrobenzene–isooctane system. They were unable to fit eq 2 to their data at all and concluded that they were looking at a far more complex situation than can be described by a single relaxation expression. This may or may not be the case here.

As we are presenting data taken in the critical region, it is logical to see if the theories for absorption in the critical region have a greater bearing on the data than the above discussed theory. There have been several ultrasonic absorption experiments in critical systems reported both in liquid–gas systems[1,2] and in liquid–liquid systems.[1,2] In all of these experiments, there is an anomalous increase in the absorption near the critical point similar to that reported here (see Figure 1). Possible explanations of these increases can be found in theories first proposed by Fixman[3] and more recently by Kawasaki.[4] Modifications of theories by Mistura[6] may be appropriate for metal–ammonia solutions. We begin with a brief description due to Fixman and then present the mathematical results. We shall limit ourselves to the theory as applied to binary mixtures.

Fixman considers the long-wavelength spatial fluctuations of composition to act as uncontrolled (or hidden) variables which give rise to an anomalous entropy and a complex dynamic heat capacity. Let ξ be the correlation length for concentration fluctuations. Away from the consolute point, ξ is on the order of the range of the intermolecular potential and will not depend strongly on the temperature. As the consolute point is approached, ξ becomes strongly temperature dependent and increases over a macroscopic scale. The strong temperature dependence of the long-range correlation length provides the coupling mechanism between the sound waves and the large concentration fluctuations occurring near the consolute point. Assume we have a situation where the wavelength of the sound is greater than the correlation length (i.e., $\lambda > \xi$; this is likely to be the case in almost all experimental situations). Then in a wavelength will be many coherence regions whose linear dimension ξ will try to follow the temperature variation associated with the sound wave. The ability of a coherence region to respond to a temperature variation is limited by the rapidity with which concentration changes can take place, that is, according to Onsager by diffusion. We thus expect a relaxation process whose characteristic time is the diffusion time for a concentration fluctuation to extend over a region of linear dimension ξ. This time is on the order of ξ^2/D, where D is the diffusion constant.

Using these ideas Fixman arrives at the following expresions for the sound absorption:

$$\alpha/f^2 = A'f^{-5/4}I(d) + B'(T) \tag{3}$$

where

$$d = Cf^{-1/2}|T - T_c| \tag{4}$$

T is the temperature and T_c is the critical temperature. $I(d)$ is a definite integral which is known analytically and numerically.[13] $B'(T)$ represents the frequency independent part of the absorption, presumably representing the "classical" absorption plus the contribution from the bulk viscosity and mechanisms controlled by shorter relaxation times. The constants A' and C are explicitly given in terms of macroscopic heat capacities and composition variables and in terms of the molecular level friction constant β and the coefficients a and l of the long-range correlation function:

$$G(r) \sim (a/r)\exp(-r/\xi) \tag{5}$$

where

$$\xi^{-2} = 6l^{-2}|T - T_c|T_c \tag{6}$$

ξ is the Ornstein–Zernicke long-range correlation length and l is the Debye short-range correlation length.

In application of this theory, values for A', B', and C are obtained by fitting both the temperature and frequency dependence of the data. If sufficient thermodynamic data exist for a particular critical mixture, it is possible to compare the fitted values of these constants and those obtained from the equations given by Fixman. This has been done for several organic mixtures[14] and one liquid metal mixture (Ga–Bi).[1] The agreement is good but not conclusive. It is not clear that one can use this theory along with the ultrasonic measurements to determine unknown quantities such as correlation lengths, but it is tempting to do so.

Since Fixman's theory there have been other theories proposed to explain these anomalous increases in absorption. Detailed expressions for the critical absorption and dispersion of sound have been obtained by Kawasaki[4] within the framework of mode–mode coupling theory. Mistura[6] developed a modified version of Fixman's original approach and has obtained results identical with those presented by Kawasaki. One of the basic results of the theoretical predictions is that the critical absorption depends primarily on a single reduced variable

$$f^* = f/f_D = \omega/\omega_D \tag{7}$$

where ω_D is a characteristic frequency defined by

$$\omega_D = 2D\xi^{-2} \tag{8}$$

where D is the diffusion coefficient. The final expressions for the critical absorption (here expressed as the absorption in a wavelength $\alpha_\lambda = \alpha,\lambda$) are:

$$\alpha_\lambda = 2\pi u^2(\omega)AI(\omega^*) \tag{9}$$

where

$$A = \frac{k_B T^3}{2\pi^2\rho^3}\left(1 - \frac{1}{2}\eta\right)^2 \frac{1}{u^4(0)C_v^2}\left(\frac{\partial P}{\partial T}\right)_u^2 K\left(\frac{\partial K}{\partial T}\right)_s^2 \tag{10}$$

u is the sound velocity, η is the critical exponent arising from the Fisher correction to the Ornstein–Zernicke correlation function, and $K = \xi^{-1}$. $I(\omega^*)$ represents the following integral

$$I(\omega^*) = \int_0^\infty \frac{x^2\,dx}{(1 + x^2)}\frac{\omega^* K(x)}{K^2(x) + \omega^{*2}} \tag{11}$$

where $K(x) = (3/4)(1 + x^2 + (x^3 - x^{-1})\arctan x)$ and $x = q\xi$, with q being the wavenumber of the order parameter fluctuations.

Mistura[6] has shown that good agreement between the above theory and the data for the binary mixture aniline–cyclohexane can be obtained when one plots the data as a function of the reduced frequency.

Starting with the same physical concepts, there are then two theories for explaining the rise in absorption near the

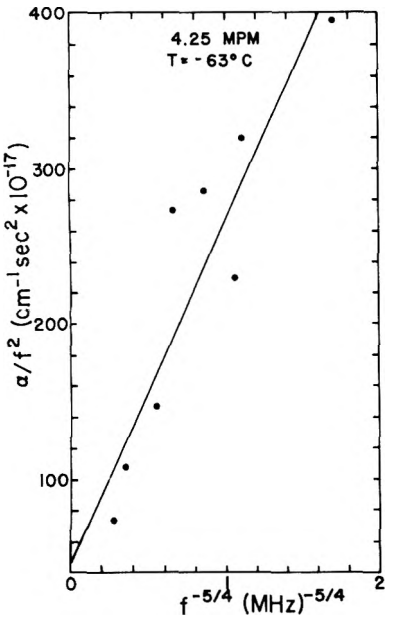

Figure 5. α/f^2 vs. $f^{-5/4}$. The solid line is a least-squares fit to the data points.

TABLE I: Parameters for 4.25 MPM Li–NH_3 Solution

	$T = -63°C$	$T = -60°C$
A_1	3.67×10^{-13} sec²/cm	2.03×10^{-13} sec²/cm
B_1	13.02×10^{-17} sec²/cm	23.41×10^{-17} sec²/cm
f_D	0.85 MHz	0.92 MHz

critical point. Both are currently used in the literature. Recently, Bains and Breazeale[15] have shown that a slight modification of Fixman's original results (eq 3) can be used to satisfactorily fit the data for several binary liquid mixtures (all organic—they did not attempt to fit the liquid metal results). We shall thus present fits to the present data from both the Fixman and the modified Kawasaki results.

As we see from Fixman's equation (eq 3) α/f^2 should vary linearly with $f^{-5/4}$ at a particular temperature (concentration should equal the critical concentration). Figure 5 shows α/f^2 as a function of $f^{-5/4}$, and we see that the agreement is only fair. It should be noted that these data are the result of two runs whose points do not quite agree with one another. However, it is still possible to see the fair agreement with the theory. Previously we reported a portion of these data[16] (the high-frequency part). These data were fitted to the Fixman theory and yielded a value of 51.3 Å for the short-range correlation length (l) at the critical point.

We now turn to the analysis of these data using Mistura's adaptation of Kawasaki's results. To do this we rewrite eq 9 in the form

$$\alpha/f^2 = A_1(T)I(f/f_D) + B_1(T) \qquad (12)$$

where

$$A_1(T) = 2\pi A/uf_D$$

and $I(f/f_D)$ is the integral of eq 11. To obtain values for A_1 and B_1, we have used a computer program which picks a value for f_D, calculates the integral numerically, and then determines A_1 and B_1 by a least-squares fit of the values of α/f^2 at the various frequencies. The value for f_D is then

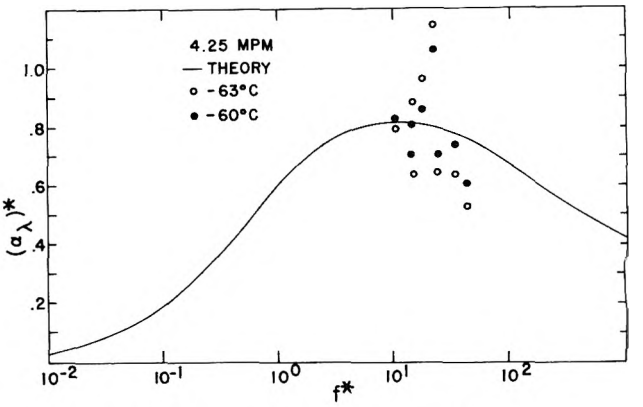

Figure 6. $(\alpha_\lambda)^*$ vs. f^*. The solid line is the result of the theory.

changed and the determination of A_1 and B_1 repeated until the errors are minimized. We thus end up with a "best fit" for f_D, A_1, and B_1. In principle, we can perform this fit on all of the data at the critical concentration. However, the fit involves three parameters using the frequency dependence at a constant temperature. We only have four frequency points for most of the temperatures studied; only at −63 and −60°C are there more points (8). We thus have chosen to perform this fit at only these two temperatures. The values for A_1, B_1, and f_D from this fit are given in Table I. The standard way of presenting these data is to plot $(\alpha_\lambda)^*$ as a function of f^* where

$$(\alpha_\lambda)^* = \frac{(\alpha/f^2) - B_1}{A_1} = 2\pi f^* \int_0^\infty dx \, \frac{x^2}{(1+x^2)^2} \frac{K(x)}{[K(x)]^2 + f^{*2}}$$

This has been done in Figure 6 where the solid line is the value given by the integral. In principle, all of the data at the critical concentration should fall along this line. As can be seen from this figure, our data do not fit the line well at all.

Using eq 8 it is possible to calculate the correlation length for concentration fluctuations if the diffusion coefficient is known. Self-diffusion coefficients in lithium- and sodium–ammonia solutions have been measured by Garroway and Cotts[17] using NMR. Their studies led to the conclusion that the lithium ion is solvated by four ammonia molecules and that this unit persists throughout the concentration region (at least the region of the present studies). We thus use their value for D in eq 8 to calculate ξ. This leads to the value ξ = 259 Å at 4.25 MPM and −63°C.[18] This is a rather unphysical result; it would imply that the correlation extends over 10^5 solvated lithium and electron complexes. It is also in contrast to the value of 41 Å presented by Chieux[19] on the basis of neutron scattering experiments in Li–ND_3 solutions. We thus conclude that our data do not fit this model.

We have attempted to fit our data to three models: single relaxation, Fixman's, and the modified Kawasaki model. Agreement with the latter two models is poor, although the agreement with Fixman's is better than with Kawasaki's. This is not particularly satisfying, as certain assumptions made by Fixman to evaluate his model quantitatively have been found not to be valid and were the stimulus to the derivation of the Kawasaki result. Thus, if critical effects are the reason for the increase in absorption, we should expect agreement with the Kawasaki theory. We do not see this. It is possible that our data are in error especially in the frequency dependence. We are presently repeating these measurements to see if there is a problem here.

It seems that the good agreement with the single relaxation model should not be overlooked. Chieux and Sienko[20] in their study of the coexistence curve for sodium–ammonia solutions concluded that concentration fluctuations over long distances should only occur very near the consolute point (<1.8°C away). Thus we might expect that critical contributions to the absorptions would only occur very near the consolute point—a region which may not have been studied in these experiments. Thus a simple single relaxation effect involving the exchange of free and bound ammonia molecules may suffice to explain the data in the region studied.

It is clear that more experimental data are needed, especially in the frequency coverage. Such measurements are underway and we shall report on them as soon as possible.

References and Notes

(1) M. P. Puls and J. S. Kirkaldy, *J. Chem. Phys.*, **54**, 4468 (1971).
(2) A. V. Anantaraman, A. B. Walters, P. D. Edmonds, and C. J. Pings, *J. Chem. Phys.*, **44**, 2651 (1966).
(3) M. Fixman, *J. Chem. Phys.*, **36**, 1961 (1962).
(4) K. Kawasaki, *Phys. Rev. A*, **1**, 1750 (1970).
(5) J. Swift, *Phys. Rev.*, **173**, 257 (1968).
(6) L. Mistura in "Critical Phenomena", M. S. Green, Ed., Academic Press, New York, N.Y., 1971.
(7) D. E. Bowen and M. A. Priesand, 1974 Ultrasonic Symposium Proceedings, IEEE Cat. No. 74 CHO 896-1SU, 540.
(8) J. A. Morgan, R. L. Schroder, and J. C. Thompson, *J. Chem. Phys.*, **43**, 4494 (1965).
(9) Literature values for Li–NH_3 are 4 MPM at −63.5°C; see P. D. Schlettler and A. Patterson, *J. Phys. Chem.*, **68**, 2865 (1964).
(10) K. F. Hurzfield and T. A. Litovitz, "Absorption and Dispersion of Ultrasonic Waves", Academic Press, New York, N.Y., 1959.
(11) J. H. Andreae, P. D. Edmonds, and J. F. McKellar, *Acoustica*, **15**, 74 (1965).
(12) J. Thoen and C. W. Garland, *Phys. Rev. A*, **10**, 1311 (1974).
(13) A. P. Kendig, R. H. Bigelow, P. D. Edmonds, and C. J. Pings, *J. Chem. Phys.*, **40**, 1451 (1964).
(14) D. Sette in "Critical Phenomena", M. S. Green, Ed., Academic Press, New York, N.Y., 1971.
(15) E. M. Bains and M. A. Breazeale, *J. Chem. Phys.*, **62**, 742 (1975); **61**, 1238 (1974).
(16) D. E. Bowen, *Phys. Lett. A*, **51**, 207 (1975).
(17) A. N. Garroway and R. M. Cotts, *Phys. Rev. A*, **7**, 635 (1973).
(18) As our relaxation frequency at −60°C is the same as that at −63°C, we see only a small temperature change in ξ due to the temperature dependence of D. The difference in ξ is within our error and hence we have no measurement of a temperature dependence of ξ.
(19) P. Chieux, *Phys. Lett. A*, **48**, 493 (1974).
(20) P. Chieux and M. J. Sienko, *J. Chem. Phys.*, **53**, 566 (1970).

Discussion

M. H. COHEN. What is the temperature dependence of the relaxation time in the single relaxation rate experiment? I note that you were concerned for the possible effect of higher values of the attenuation of lower frequencies on the value of the relaxation time. These would lower the relaxation rate so that 20 MHz can be regarded as an upper limit. I note also that in your published paper the anomalous attenuation extended over the entire concentration range you studied. However, it was strongly temperature dependent only in a smaller range of concentrations centered about the critical concentration. This suggests to us the possibility of two distinct mechanisms of attenuation: that due to critical dynamics as studied by Fixman and Kawasaki, and that due to cluster formation and re-formation as suggested by Jortner. Thus your ultrasonic attenuation studies may suggest the existence of concentration fluctuations which are distinct from critical fluctuations and may be the dimodal fluctuations we have proposed.

D. E. BOWEN. We have not determined a temperature dependence for the relaxation frequency, as the change with temperature of this parameter at present is within our error owing to the small number of frequencies studied.

J. JORTNER. I would like to comment on the striking effect reported by you in your recent *Physics Letter* of a broad peak for α/f^2 vs. M at −60°C while at −63°C an additional sharp component is observed near $M \sim 4.5$ MPM. This indicates that appreciable ultrasonic attenuation occurs in the concentration range M = 2.5–9 MPM which is weakly temperature dependent and may be related to clustering. Another interesting observation is the extremely long relaxation time, τ^{-1} = 20 MHz, calculated by you on the basis of the simple relaxation model. M. H. Cohen and myself considered the possibility that this relaxation time monitors breakdown and building of large clusters in the intermediate concentration range. Support for this proposal comes from ultrasonic attenuation studies [P. J. Sams, J. E. Rassing, and E. Wyn-Jones, *Adv. Mol. Relaxation Processes*, **6**, 225 (1975)], an aqueous solution of mixed micelles containing two surfactants. The ultrasonic relaxation times in the latter case are in the range of 5–15 MHz and were assigned to dynamic equilibrium between the miscelle and the monomers.

Metal–Nonmetal Transition in Metal–Ammonia Solutions via the Inhomogeneous Transport Regime[1]

Morrel H. Cohen*

The James Franck Institute and Department of Physics, The University of Chicago, Chicago, Illinois 60637

and Joshua Jortner

Department of Chemistry, Tel-Aviv University, Tel-Aviv, Israel *(Received July 23, 1975)*

In this paper we present a coherent physical picture of the metal–nonmetal transition in metal–ammonia solutions in the intermediate concentration range. We propose that in Li–NH_3 and Na–NH_3 solutions at $T - T_c \simeq 10$–20 K the metallic propagation regime (9–16 MPM) is separated from a nonmetallic pseudointrinsic semiconducting regime (1–2.3 MPM) by a microscopically inhomogeneous regime (2.3–9 MPM) in which the concentration fluctuates locally about either of two well-defined values M_0 and M_1, $M_0 > M_1$, the local concentration remaining near M_0 or M_1 over radii approximately equal to the Debye short correlation length, b, for concentration fluctuations. The limits of the inhomogeneous regime were determined from a combination of concentration fluctuation measurements, electrical conductivity, Hall effect, and paramagnetic susceptibility data to be $M_0 = 9$ MPM and $M_1 = 2.33$ MPM, which yield the C scale, $C = (M - 2.33)/6.66$, for both Li–NH_3 at 223 K and for Na–NH_3 at 240 K. We have also established the consistency of our picture with the available magnetic data for Na solutions. An analysis of electronic transport, thermal transport, optical properties, and sound velocity was carried out in terms of a theory of response functions for microscopically inhomogeneous materials developed by us. Excellent agreement between theory and experiment was obtained throughout the entire inhomogeneous transport regime.

I. Introductory Remarks

In this paper we present a physical picture for the metal–nonmetal transition (MNMT) in metal–ammonia solutions (MAS) in the intermediate concentration range (1–10 MPM).[2-5] The apparently continuous changes of the electronic and thermal transport properties as well as the optical data and thermochemical properties of MAS in the intermediate concentration range provide an important example of a MNMT in a disordered material. Many examples for such MNMT in disordered solids and liquids are now well documented.[6] What is a MNMT in a disordered material? From the point of view of the experimentalist such "transitions" may be roughly classified in terms of the variation of the electrical conductivity, σ, induced by changes in a primary variable of state, such as density in a one-component system or composition in a two-component system:

1. "Abrupt" MNMT. A sharp drop of σ is exhibited in a narrow range of the primary variable of state. We are aware of a single example of such a transition which was observed[7] in amorphous films of Cu–Ar and Pb–Ar at 4 K. σ decreases gradually over the composition range 100–60 mol % metal, exhibiting a "discontinuity" at about ~55 mol % metal. We note in passing that the percolation picture[8-13] which implies that

$$\sigma = 0;\ C < C^*$$

$$\sigma \propto (C - C^*)^{1.6};\ C^* < C < 0.4$$

$$\sigma \propto \left(\frac{3}{2}C - \frac{1}{2}\right);\ 0.4 < C < 1 \qquad \text{(I.1)}$$

where C is the metallic volume fraction and $C^* \simeq 0.17$ is the percolation threshold,[12,13] also provides at least a semiquantitative fit of these experimental data.

2. "Continuous" MNMT. A gradual variation of σ is observed. Many such cases have been recorded in disordered materials. To quote several illustrative examples we mention the MNMT in expanded liquid metals[14-25] and in MAS.[2-5,26-48] Such MNMT's were studied at finite temperatures, and one can argue that thermal excitations will erode any discontinuity in σ.

Two basic theoretical models for the MNMT were advanced by Mott[6,49-57] which rest either on (a) correlation effects or (b) band overlap effects. Mott further invokes the central role of Anderson localization and of polaron effects in determining the features of the MNMT in disordered materials. An alternative model was advanced by the present authors (CJ)[58-63] who argued that in many disordered materials the MNMT occurs via an inhomogeneous transport regime, where microscopic inhomogeneities, e.g., density fluctuations, bonding modifications, or concentration fluctuations, determine the electronic structure and the transport properties. Thus in the CJ approach mechanisms a or b operate *locally*. Mott's picture implies the occurrence of a discrete MNMT at 0 K, while CJ assert that in a disordered material which is characterized by a large correlation length for fluctuations, or by large potential fluctuations, a continuous MNMT will be exhibited. The CJ picture is necessary to overcome serious difficulties encountered in the interpretation of the transport properties of many disordered materials undergoing a MNMT in terms of conventional descriptions of transport mechanisms.

II. Conventional Descriptions of Disordered Metals and Nonmetallic Materials

We wish to understand the nature of the apparently continuous changes of electronic structure and transport properties during the course of a transition from metallic to nonmetallic behavior in disordered systems and in particular in MAS. Let us first characterize the general features of disordered metals and disordered nonmetallic materials in terms of their transport properties. One can specify the transport properties of disordered metals in terms of one of the following transport regimes.

(a) The Metallic Propagation Regime.[64] The mean free path of the conduction electrons considerably exceeds the Fermi wavelength $\lambda_F = k_F^{-1}$, i.e. $l \gg \lambda_F$. The conductivity σ is well represented by the nearly free-electron theory.[64,65] There is no special relation between the Hall coefficient, R, and the conductivity.[66,67] On experimental and theoretical[67] grounds we assert that the latter quantity is close to the free-electron value, R_{FE}, whereupon the Hall mobility $\mu = \sigma R$ is dominated by changes in σ. Correspondingly, the transport properties satisfy the conditions

$$\sigma \gtrsim 3000\ (\Omega\ \text{cm})^{-1} - 1000\ (\Omega\ \text{cm})^{-1} \qquad \text{(II.1a)}$$

$$R \simeq R_{FE} \qquad \text{(II.1b)}$$

$$\mu = R\sigma \simeq R_{FE}\sigma \qquad \text{(II.1c)}$$

A minimum value of $\sim$1000 $(\Omega\ \text{cm})^{-1}$ for the conductivity in the propagation regime is applicable to MAS, where the electron density is low.

(b) The Metallic Diffusion Regime.[50,68-71] As disorder increases the mean free path decreases to a point where $l \sim \lambda_F$. The concept of a mean free path is no longer applicable. However, in the propagation regime l characterizes the distance over which the electronic wave functions retain phase coherence. We can generalize l into a phase coherence length, which can be arbitrarily small. For $l < \lambda_F$ the phase of the electronic wave functions becomes effectively random and interference effects are unimportant. The random phase approximation is applicable within the framework of the Kubo–Greenwood formalism in this problem. Friedman[70] has studied transport in a crystal with a tight-binding s band. He assumes that the wave function amplitudes are everywhere constant but the phases on different sites are random. An extension of this treatment has been provided by Varea de Alvarez and Keller.[72] Friedman's treatment[70] results in

$$\sigma = \frac{2\pi}{3} Z \left(\frac{e^2}{\hbar a}\right) X^2$$

$$R \simeq Z^{-1} R_{FE} X^{-1}$$

$$\mu \simeq \frac{2\pi}{3} \left(\frac{ea^2}{\hbar}\right) X \qquad \text{(II.2)}$$

where a is the internuclear separation, or the intercavity spacing in MAS, z is the number of nearest neighbors, and the parameter

$$X = Ja^3 n(E_F) \qquad \text{(II.2a)}$$

contains J, the nearest neighbor electron transfer integral and the density of states, $n(E_F)$, at the Fermi energy E_F. Two conclusions are immediately apparent. First, the variation of the conductivity in the diffusion regime induced by changes in a primary variable of state is not only determined by the changes of $n(E_F)$ but can be also considerably affected by the changes of J. Thus the Mott relation[51-53] $\sigma = A[n(E_F)]^2$, where $A \sim 2500\ (\Omega\ \text{cm})^{-1}$ and $n(E_F)$ is extracted from the Knight shift or the paramagnetic susceptibility for the conductivity in the diffusion regime, is of limited applicability. Second, one can derive explicit relations between the Hall coefficient and other electrical transport properties

$$\sigma \propto (R_{FE}/R)^2$$

$$\mu \propto (R_{FE}/R) \qquad \text{(II.3)}$$

where the proportionality factors contain parameters which depend either explicitly or weakly on the variable of state. These relations provide an important diagnostic tool for the identification of diffusive or Brownian motion, i.e., the strong scattering regime.

Turning to nonmetallic materials we consider the most common case, that of disordered semiconductors, where there are two transport mechanisms in parallel.

(c) Pseudointrinsic Semiconductivity. In the current picture of disordered semiconductors the band gap is replaced by a mobility gap[69,51,52,73]

$$E_g = E_c - E_v \qquad \text{(II.4)}$$

where E_c and E_v correspond to the mobility edges in the conduction band and in the valence band, respectively. All the states within the mobility gap are localized, and $\sigma = 0$ at $T = 0$. Conduction at sufficiently high temperatures proceeds by thermal excitation of carriers across the mobility gap. The conductivity is[69,73]

$$\sigma \simeq \sigma(E_c) \exp[-(E_c - E_F)/kT]$$

$$\sigma(E_c) = 2n(E_c) e \mu(E_c) kT \qquad \text{(II.5)}$$

where $n(E_c)$ and $\mu(E_c)$ are the density of states and the (mean) mobility near the mobility edge, respectively. To derive a relation between the conducitivity and the thermoelectric power, S, Mott and Cutler started from the relations[74]

$$\sigma = -\int \sigma(E)(\partial f/\partial E)\, dE \qquad \text{(II.6)}$$

$$S\sigma = \frac{k}{e} \int \sigma(E) \left(\frac{E - E_F}{kT}\right) (\partial f/\partial E)\, dE \qquad \text{(II.7)}$$

where f is the Fermi distribution function. Assuming that $\sigma(E)$ is weakly dependent on E above E_c, these formula give

$$\sigma \simeq \sigma(E_c) f(E_c) \qquad \text{(II.8)}$$

which is practically identical with eq I.5, and

$$S = \frac{k}{e} \{\ln(\sigma(E_c)/\sigma) + [1 + (\sigma(E_c)/\sigma)] \ln[1 + (\sigma/\sigma(E_c))]\} \qquad \text{(II.9)}$$

when one band dominates. When $\sigma/\sigma(E_c) \ll 1$, i.e. $E_c - E_F > 4kT$, eq I.9 reduces to the conventional form

$$S = \frac{k}{e} [\ln(\sigma(E_c)/\sigma) + 1] \qquad \text{(II.10)}$$

The σ vs. S relations (II.9) and (II.10) unambiguously specify pseudointrinsic semiconductivity, provided that compensation effects do not affect S.

(d) Pseudoextrinsic Semiconductivity. In general, the Fermi energy is located within the mobility gap and $n(E_F)$ is finite. Consequently, electrons near the Fermi energy

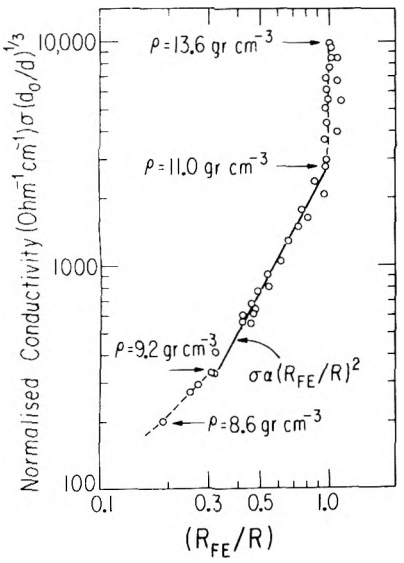

Figure 1. The dependence of the electrical conductivity on R_{FE}/R for expanded liquid Hg, after Even and Jortner (ref 20). The diffusion regime spans the density range 9.3 g cm^{-3} < ρ < 11.0 g cm^{-3}, $\sigma \propto (R_{FE}/R)^2$ in accordance with eq II.3.

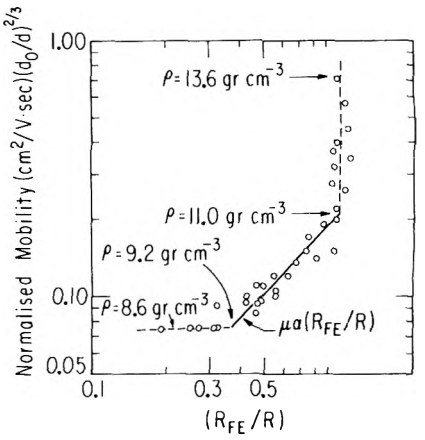

Figure 2. The dependence of the Hall mobility on $(R_{FE}/R)^2$ for expanded liquid Hg, after Even and Jortner (ref 20). In the diffusion regime 9.3 g cm^{-3} < ρ < 11.0 g cm^{-3}, $\mu \propto (R_{FE}/R)$ in agreement with eq II.3.

contribute to the transport via variable range hopping.[54,75] At sufficiently low temperatures this Mott hopping will dominate the conductivity. The thermopower[76] is expected to be small and not related to σ. This mechanism is important only at low temperatures, and we shall not be concerned with it here.

In MAS an additional transport regime is exhibited.

(e) Electrolytic transport regime where conventional electrolytic transport[4] prevails. According to Mott's picture the MNMT in a disordered system will be manifested by an "abrupt" switching of the transport mechanisms from regime b (or regime a) to semiconducting transport (mechanisms c and d) in materials undergoing a metal–semiconductor transition such as expanded liquid Hg. In MAS a switch from regime b to regime e may be exhibited, or alternatively the transition from regime b to regime c will occur. As several of these conventional transport regimes have already been identified[55,56,59,70] in expanded liquid Hg we proceed to the analysis of the experimental evidence for this relatively simple one-component system.

III. Transport in Expanded Liquid Mercury

For expanded liquid Hg the extensive experimental data[14-24] for σ, R, and S over the density range 13.6–5 g cm^{-3} can be partially understood in terms of the following distinct transport regimes: (a) propagation regime, 11 g cm^{-3} < ρ < 13.6 g cm^{-3} where eq II.1 applies, as is evident from the data of Even and Jortner reproduced in Figures 1 and 2; (b) diffusion regime, 9.2 g cm^{-3} < ρ < 11.0 g cm^{-3} where Friedman's relations, eq II.3, apply (Figures 1 and 2); and (c) pseudointrinsic semiconducting regime, ρ < 7.8 g cm^{-3} where the ln σ vs. S relation, eq II.10, holds. In the intermediate density range ρ = 9.2–7.8 g cm^{-3} the electrical conductivity[14-18] at 1550°C varies in the range 500–20 (Ω cm)$^{-1}$, the Hall mobility μ (which was measured down to 8.6 g cm^{-3}) is practically constant,[20] μ = 0.07 cm^2 V^{-1} sec^{-1}, the thermoelectric power[18] exhibits a weak variation with ρ, S = −70 (μV/°C) at ρ = 9.2 g cm^{-3} and S = −150 (μV/°C) at 7.8 g cm^{-3}, while the volume and temperature dependence of σ reveal a fast increase with decreasing density.[16,18] None of the conventional transport regimes appears to be consistent with the transport data in this intermediate density range, in our opinion. However, Mott's picture[55,56] for the metal–nonmetal transition in Hg asserts that the material remains microscopically homogeneous with regard to electronic structure and transport. When the density of states ratio g falls below a critical value $g^* \simeq \frac{1}{3}$, Mott supposes the states to be localized. Accordingly, he proposes that a mobility gap opens at ρ = 9.2 g cm^{-3}, and that for lower densities the transport properties are determined by excitation to the mobility edge, the conductivity being given by eq 1.5. Mott's model encounters three serious difficulties. First, it was argued by Mott[56] that in this model μ is given by the Hall mobility of electrons at the mobility edge and is thus expected to be practically independent of density, in agreement with experiment. However, it should be noted that according to the Friedman theory[70] for the Hall mobility in an amorphous semiconductor $\mu \propto Jn(E_c)$ where $n(E_c)$ is the density of states at the mobility edge. Thus both in the metallic diffusion regime (see, e.g., (II.2)) and in the semiconducting regime the variation of the conductivity and of the Hall mobility with decreasing density will be strongly affected by the decrease of the transfer integral J with decreasing ρ. Thus the Hall mobility is not expected to remain constant throughout the semiconducting regime in expanded Hg. Second, Mott's approach leads to a substantial disagreement between the density variation of the electrical conductivity and the thermoelectric power in the intermediate density range. A recent analysis of the thermoelectric power data of Schmutzler and Hensel[18] demonstrates that eq I.9 and I.10 are not obeyed for Hg in the intermediate density range. If we assume that the mobility gap opens up (i.e., $E_c - E_F = 0$) at 9.2 g cm^{-3} and reaches $4kT$ at 7.8 g cm^{-3}, the highest density for which eq II.10 is obeyed, we have to take $\sigma_M = \sigma$ (9.2 g cm^{-3}) = 550 (Ω cm)$^{-1}$. As is evident from Figure 3, eq II.9 results in a much weaker decrease of σ/σ_M with increasing $|S|$ than is experimentally observed in the intermediate density range. Any other choice of σ_M will not reproduce the experimental σ vs. S relation for 7.8 g cm^{-3} < ρ < 9.2 g cm^{-3}. Thus the discrepancy is a serious one. To overcome this difficulty Mott has recently suggested[56] an additional contribution to the thermoelectric power in the semiconducting range for $E_c - E_F > kT$ which originates from a negative heat of transport. We note in passing that in order

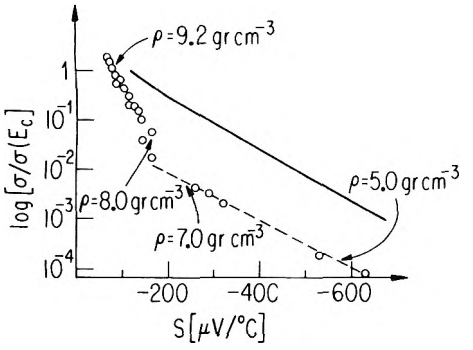

Figure 3. The dependence of ln σ on S for expanded liquid Hg, after Schmutzler and Hensel (ref 18). The solid line represent Mott's analysis (eq II.9). The dashed line corresponds to a slope of (k/e). According to eq II.10 the pseudointrinsic semiconducting regime holds for $\rho < 7.8$ g cm^{-3}.

to provide a quantitative fit of the experimental data Mott had to invoke[56] a change of the negative heat of transport, ΔH, from zero at 9.2 g cm^{-3} to −0.25 eV at 7.8 g cm^{-3}, which is half the energy gap. It is rather difficult to comprehend how the polaron effects proposed by Mott can be operative in a small-gap semiconductor at high temperatures where $4kT > |\Delta H|$. Third, we have pointed out[59] that the density dependence of $E_c - E_F$ which can be extracted from Mott's picture, together with basic thermodynamic considerations concerning the amplitude of the density fluctuations, inevitably leads to the conclusion that the conductivity is nonuniform over distances L which considerably exceed the phase coherence length l for the conduction electrons. For the average density ρ = 8.5 g cm^{-3} we find $\Delta\sigma/\sigma_{mode}$ = 2.7 for L = 15 Å and $\Delta\sigma/\sigma_{mode}$ = 0.5 for L = 40 Å, where σ_{mode} and $\Delta\sigma$ are the most probable conductivity and the spread of the distribution. Thus if we start with a homogeneous material we inescapably wind up with nonuniformity. We thus conclude that Mott's model[55,56] does not provide a self-consistent picture for the variation of the electrical and thermal transport properties in the intermediate density range. In other words, the conventional transport regimes, which assume microscopic homogeneity of the material, appear to be inconsistent with the data in this density range.

We have proposed[59] that the electronic structure and transport properties of expanded liquid Hg in the density range 9.2–8.0 g cm^{-3} are intermediated by density fluctuations. Invoking a unimodal distribution for the density fluctuations, as appropriate for a density range where the Ornstein–Zernicke decay length is of the order the interatomic spacing, we were able to provide a coherent physical picture for the continuous metal–nonmetal transition in this system. In that process we have established[59] the volume fraction, C, of the metallic regions (where the s–p band gap did not open locally). This C scale should be regarded as a theoretical prediction of the Knight shift and paramagnetic susceptibility throughout the inhomogeneous transport regime. The recent Knight shift data of El-Hamary and Warren[77] in the density range 9.2–8.0 g cm^{-3} are in excellent agreement with our predictions.

IV. Transport in MAS

We now turn to the central issue of the present paper and consider the identification of conventional transport regimes in MAS. In concentrated MAS (20–10 MPM), Lepoutre[78] and Thompson[79] find that l = 70 Å and k_F = 0.49 Å^{-1} at 20 MPM decreasing to l = 12 Å and k_F = 0.40 Å^{-1} at 10 MPM, so that the basic condition for the propagation of conduction electrons between scattering events, $k_F l \geq 3$, is satisfied down to about 10 MPM. For expanded liquid Hg the propagation regime terminates at $k_F l$ = 2.3. Thus for concentrated (10–20 MPM) MAS solutions, the propagation regime applies. The decrease of σ with dilution in the propagation regime can be well accounted for in terms of the NFE model and is primarily a consequence of the concentration dependence of the structure factors and the increase of the fraction of unbound ammonia molecules.[80,81] The Hall coefficient[32-35] is $R = R_{FE}$, and the variation of μ is dominated by the changes in σ as expected for the propagation regime.

In the intermediate concentration regime (2–10 MPM), the Friedman relations (II.3) do not hold. (R_{FE}/R) changes only from 1.0 to 0.5. However, σ decreases by three orders of magnitude and μ by two orders of magnitude, so that (R_{FE}/R) should decrease from 1.0 to 0.03 in that concentration range according to the Friedman relations.[70] One could instead attempt to establish whether the conductivity relation (II.2) does hold. From an analysis of the experimental conductivity and volume susceptibility χ_p in this concentration range we have established that $\sigma = A\chi_p^{2.3}$. This power is not so different from the value of 2.0, expected by Mott, however, in the concentration range 10–2 MPM the transfer integral $J \propto \exp[-\beta a]$, where[82] $\beta \sim 0.55$ Å^{-1}, decreases by one order of magnitude due to the decrease of a by a factor of ~2. Thus the correct version of the conductivity relation in the diffusion regime $\sigma \propto \chi_p^2 \exp[-2\beta a]$ does not hold. We thus conclude that the physical properties of MAS in the intermediate region cannot be accounted for in terms of a diffusion type of metallic transport, and that the MNMT in this system is not preceded by a homogeneous diffusion regime as does happen in expanded liquid Hg. The conductivity in the intermediate regime σ = $10^3 - 1$ (Ω cm)$^{-1}$ is so high that it cannot be assigned to semiconducting transport (mechanism c, section II). Furthermore, relations (II.9) and (II.10) do not hold in this range. Obviously, the electrolytic transport regime ((e), section II) also does not apply. Thus none of the conventional transport regimes is applicable in the concentration range from ~2 to ~10 MPM.

We now turn to a brief summary of the transport properties at lower concentrations.[4] At $M \simeq 10^{-1}$ MPM the equivalent conductance, Λ_e, goes through a minimum. It has been suggested that the increase of Λ_e with increasing M is associated with the onset of electronic conduction. For this to occur, spin depairing must be observed. The spin susceptibility reaches a low value $\chi_p \simeq 0$ at 1 MPM and increases slowly in the range 1–2.3 MPM. We thus prefer a physical picture where dissociation of neutral quartets (i.e., $2M^+ 2e^-$) into negative spin paired triplets ($M^+ 2e^-$) and positive ions prevails in the concentration range from 10^{-1} to 1 MPM resulting in an increase of Λ_e, so that the conventional electrolytic transport regime prevails up to at least 0.5 MPM. One can roughly estimate an upper limit to Λ_e expected when dissociation is complete. Coulomb effects, as in the Onsager–Fuoss theory, act so as to reduce the equivalent conductance below its limiting value 760 (Ω mol)$^{-1}$. The latter is, therefore, an upper limit. The equivalent conductance at 0.5 MPM is[4] 550 (Ω mol)$^{-1}$ indicating that dissociation is substantial, if not complete, at that concentration. At 1 MPM Λ_e = 770 (Ω mol)$^{-1}$ and electrolytic transport cannot account for the conductivity above that

TABLE I: Assignments of Conventional Transport Regimes in MAS[a]

M, MPM	Transport regimes	Experimental evidence
16–9	Metallic propagation	$\sigma = 5 \times 10^3 - 10^3\ (\Omega\ \text{cm})^{-1}$ $R = R_{FE}$ $l \simeq 70$–12 Å Applicability of (RMP) Thermal transport and optical properties
9–2.3	?	$\sigma = 10^3 - 1\ (\Omega\ \text{cm})^{-1}$ $R/R_{FE} = 1$–2 Inapplicability of (FR)
2.3–1	Disordered semiconductor	$\sigma = 0.16 - 1\ (\Omega\ \text{cm})^{-1}$ $\chi_p = 0$ at 1 MPM to $\sim 8 \times 10^{-8}$ cgs at 2.3 MPM
<0.5	Electrolytic	$\Lambda_e < 550\ (\Omega\ \text{mol})^{-1}$

[a] M–NH_3 liquid; $T - T_c \sim 10$–20 K; for Li, Na–NH_3. RMP = relations for metallic propagation regime, eq 11.1. FR = Freedman relations for metallic diffusion regime, eq 11.3.

concentration. We suggest that in the concentration range from ~1 to ~2 MPM an electronic transport mechanism sets in. As at ~1 MPM complete spin pairing occurs, we suggest a pseudointrinsic semiconducting transport (mechanism c, section II) to be operative in MAS in the range ~1–2 MPM. The full valence band corresponds to doubly occupied σ_g-type orbitals of electron cavity pairs within triplets. The conduction band consists of a superposition of σ_u-type orbitals. The low density band gap corresponding to the σ_g–σ_u excitation within a single cavity pair is 0.6–0.7 eV. Thus electronic structure and transport in MAS in the latter region are analogous to those exhibited in semiconducting expanded Hg for $\rho < 7.8$ g cm^{-3}.

The present status of our efforts to identify the conventional transport regimes in MAS undergoing a "continuous" MNMT is summarized in Table I. None of the conventional transport regimes is applicable in the intermediate (2.3–9 MPM) concentration range. We have proposed that in Li–NH_3 and Na–NH_3 solutions the metallic propagation regime is separated from a nonmetallic (semiconducting) regime by a microscopically inhomogeneous regime in which concentration fluctuations determine electronic structure and transport properties in this two-component system. We now proceed to a semiquantitative exploration of the effects of microscopic density fluctuations on the electronic properties of MAS.

V. Microscopic Inhomogeneities in MAS

We propose that the metal–nonmetal transition in MAS is intermediated by concentration fluctuations. In the present context the three major questions concerning the fluctuations are: (a) the spatial extent of fluctuations; (b) whether they are of large amplitude; and (c) whether they are unimodally or multimodally distributed. Let us consider the local value $m(r)$ of a configurational parameter which could refer to the local density in a one-component system or to the local concentration in a multicomponent system. The mean value of the configurational parameter is $\langle m(\vec{r}) \rangle = M$ while the autocorrelation function, $A(R)$, is

$$A(R) = \frac{\langle m(\vec{r} + \vec{R}) m(\vec{r}) \rangle - M^2}{M^2} \qquad \text{(V.2)}$$

Condensed systems are stiff, tending to resist rapid change in local configuration so that, roughly speaking, $m(\vec{r})$ varies significantly over distances greater than b, the short correlation length. For liquids we know from the Ornstein–Zernike theory for fluctuations that the asymptotic decay of $A(R)$ is exponential. We can set

$$A(R) \approx \text{constant} \qquad R < b$$
$$A(R) \sim \exp(-R/\zeta)/R \qquad \text{(V.3)}$$

where ζ is the fluctuation decay length. Provided that $b \gg a$ and $b > \zeta$ the values of $m(\vec{r})$ at two points separated by more than b are statistically independent. We can then idealize the physical picture, replacing $A(R)$ by a simple step function

$$A(R) = \text{constant} \qquad R \leq b$$
$$A(R) = 0 \qquad R > b \qquad \text{(V.4)}$$

b thus specifies the spatial extent of the fluctuations. The rms amplitude of the fluctuations is determined by $A(R < b)$. Two examples of the probability distribution $P(m(\vec{r}))$, of the local values of $m(\vec{r})$ are given in Figure 4.

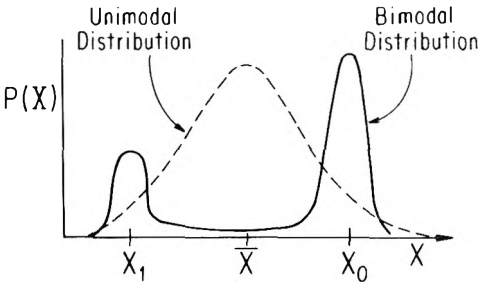

Figure 4. Examples of the probability distribution $P(X(\vec{r}))$ of the local values of the primary variable of state.

There are several experimental techniques available to probe the nature of microscopic inhomogeneities in disordered materials. The spatial extent of fluctuations can be monitored by small angle x-ray and neutron scattering, or by electron microscopy and diffraction. The amplitudes of the fluctuations can be inferred from structure factors, ultrasonic attenuation, and determinations of concentration fluctuations through chemical potential measurements in a multicomponent system. No direct evidence is currently available concerning the probability distribution function $P(m)$ for the local concentration in a two-component liquid. It should be emphasized at this point that the proposed microscopic inhomogeneities are distinct from critical fluctuations; a careful examination of the experimental data is required to separate these two physical effects. We now proceed to explore the nature of microscopic inhomogeneities and consider the experimental evidence for them in MAS.

There is substantial evidence for large amplitude concentration fluctuations in metal–ammonia solutions. Thompson and Ichikawa[83] have found direct evidence for large concentration fluctuations in lithium and sodium ammonia solutions, but not in cesium solutions. They measure the dependence of the chemical potential of the metal on metal concentration at −33 K and from it extract the mean square concentration fluctuation in the form $\langle (\Delta X_M)^2 \rangle$ where ΔX_M is the fluctuation of the mole fraction. Their results are shown in Figures 5–7. Li and Na solutions saturate at 20 and 16 MPM, respectively;[4] the Cs solutions do not saturate.[84] In Figures 5–7 we compare the observed fluctuations with those expected from an ideal mixture of NH_3 and $M(NH_3)_n$, with $n = 4$ for Li and 6 for Na and Cs.

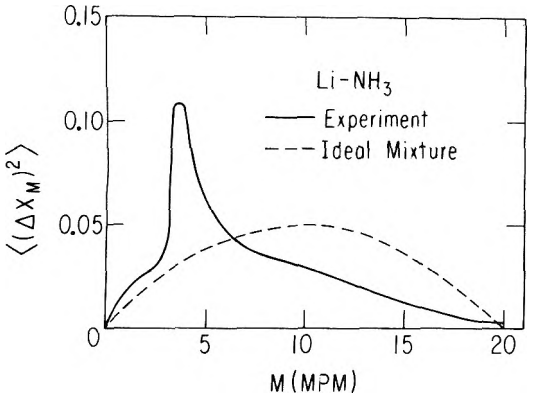

Figure 5. Mean square of concentration fluctuations in $Li–NH_3$ solutions: solid lines, experimental data (ref 83); dashed line, ideal mixture.

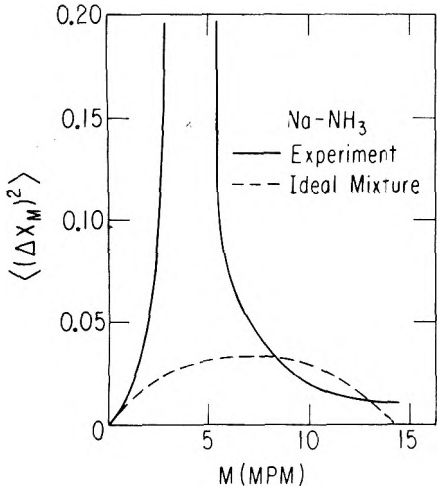

Figure 6. Mean square of concentration fluctuations in $Na–HN_3$ solutions: solid line, experimental data (ref 83); dashed line, ideal mixture.

$$\langle(\Delta X_M)^2\rangle_{ideal} = X_M[1 - (n+1)X_M] \qquad (V.5)$$

where X_M is the mole fraction of metal. The following features of the data are noteworthy. (1) There are large peaks in the Li and Na data centered about 3.6 MPM for Li and a similar value for Na. (2) These peaks are superimposed on a background similar to what is expected from (V.5). (3) The background differs from (V.5) in two respects, being higher at low concentrations and lower at high concentrations. (4) Cs shows no peak and its value of $\langle(\Delta X_M)^2\rangle$ is similar to the backgrounds for Li and Na for $M < 16$ MPM. (5) $\langle(\Delta X_M)^2\rangle$ for Cs above 20 MPM resembles what is expected from (V.5) for an ideal mixture of $Cs(NH_3)_6$ and Cs.

Regarding the distance scale for concentration fluctuations it was pointed out by Thompson and Lelieur[85] that one can infer from the concentration fluctuation data for $Li–NH_3$ and $Na–NH_3$ by a simple argument of Turner[86] the existence of large, high concentration clusters in these materials. Additional evidence for a large distance scale for concentration fluctuations stems from x-ray (X)[87] and neutron (n)[88] small-angle scattering studies. Recent experiments of Chieux[88] on small-angle neutron scattering on 4 MPM $Li–ND_3$ solutions were analyzed in terms of the Ornstein–Zernike picture of concentration fluctuations. The resulting decay length was $4.7[T_c/(T - T_c)]^{1/2}$ Å at a temperature T above the consolute temperature T_c, which is −58°C for $Li–ND_3$. This decay length is unusually large,

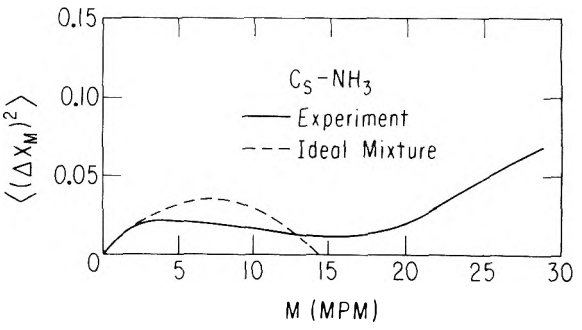

Figure 7. Mean square of concentration fluctuations in $Cs–NH_3$ solutions: solid line, experimental data (ref 83); dashed line, ideal mixture.

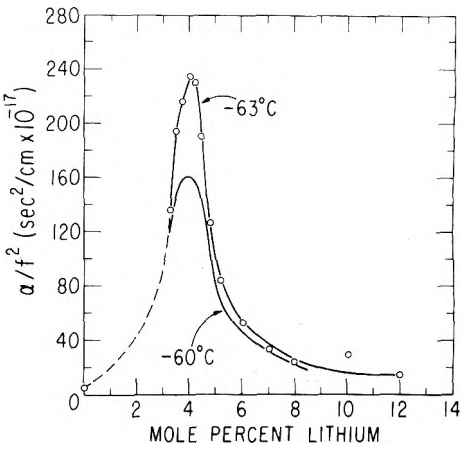

Figure 8. Ultrasonic attenuation in MAS solution after Bowen (ref 89a).

~70 Å at 1 K above T_c and ~10 Å ($>a$) at $T - T_c \simeq 40$ K.

Are these fluctuations distinct from critical fluctuations? Ultrasonic attenuation measurements by Bowen[89] (Figure 8) indicate not only that the fluctuations exist in the 2.3–9 MPM range but that they are distinct from critical fluctuations. The latter are manifested in the ultrasonic attenuation α over a narrow concentration and temperature range about the consolute point as a peak superimposed upon a broad, weakly temperature-dependent maximum. The broad background attenuation we attribute to fluctuations which are, indeed, distinct from critical fluctuations.

Thus, there is strong experimental evidence favoring large amplitude microscopic inhomogeneity at $T - T_c \lesssim 20$ K on a scale of tens of ångströms in NH_3 solutions of Li and Na, but not of Cs. None of the available experiments proves whether these fluctuations in Li and Na solutions are unimodal or bimodal. Only unimodal concentration fluctuations can occur far away (i.e., when $\zeta \lesssim a$) from T_c, and these are well accounted for in terms of conventional fluctuation theory. Cases of bimodal distribution of local concentration (or density) are, however, also known to occur. The highly developed droplet model of condensation rests on bimodally distributed density fluctuations near the liquid–gas critical point. Many examples of clustering are known both near and unrelated to critical points. Indeed, clustering effects provide the extreme case of a bimodal distribution of concentration fluctuations.

We have proposed for Li and Na solutions at $T - T_c \simeq$ 10–20 K a microscopically inhomogeneous region of the phase diagram of MAS in which (1) the concentration fluctuations are bimodal, varying locally about either of two

well-defined values M_0 and M_1, $M_0 > M_1$; (2) the concentration remains near M_0 or M_1 over radii approximately equal to the short correlation length b for concentration fluctuations; and (3) M_0 is the upper and M_1 the lower bound of the microscopically inhomogeneous region. The concentration fluctuations associated with clusters increase monotonically with cluster size. If the Ornstein–Zernike fluctuation decay length ζ is smaller than b, the concentration would appear to fluctuate abruptly and randomly from M_0 to M_1 or vice versa. We have inferred from Figures 5 and 6 that $M_0 \simeq 9$ MPM and $M_1 \simeq 2.5$ MPM.

Weak experimental evidence for a bimodal distribution of density fluctuations originates from the Thompson–Lelieur analysis[85] of the concentration fluctuation data in terms of the Turner model. Furthermore, the ultrasonic relaxation time[89a] found by Bowen is 5×10^{-8} sec (20 MHz) which is surprisingly long. We propose that it is associated with the time variation of the locally inhomogeneous concentration. Comparable ultrasonic relaxation times (in the range 5–10 MHz) were reported[89b] in aqueous solution of mixed micelles containing two surfactants. There is a close analogy between clustering of solvated electrons and solvated cations in MAS (i.e., bimodal distribution of concentration fluctuations) and micelle formation. These experimental data are indicative but by no means conclusive regarding our proposal of a bimodal distribution of fluctuation.

We now proceed to explore the consequences of the inhomogeneous model regarding electronic structure and transport in MAS.

VI. Allowed Volume Concept

In the microscopically inhomogeneous regime in MAS we propose that the concentration fluctuates locally about either of two well-defined values M_0 and M_1, $M_0 > M_1$, the local concentration remaining near M_0 or M_1 over radii approximately equal to the Debye short correlation length, b, for concentration fluctuations. Provided that b constitutes the largest distance scale parameter involved in the problem, and considerably exceeds λ_F (or l whichever is longer) for the conductive electrons as well as the interionic distance a, the concept of local electronic structure and local response functions can be introduced.[58–62] We then can define an allowed volume fraction $C(E)$ as that fraction of the total volume of the material actually allowed to electrons of energy E. Now, the Weyl theorem[90] tells us that as long as the de Broglie wavelength, or the phase coherence length, is sufficiently small compared to the dimensions of the allowed regions, the density of states will be independent of the geometry of the allowed regions and of the boundary conditions presented by the forbidden regions and proportional to the allowed volume. Thus we may take[58–62,91] as a definition of $C(E)$

$$n(E) = n_0(E)C(E) \qquad \text{(VI.1)}$$

where $n_0(E)$ is the density of states per unit volume of a metallic region of macroscopic extent and $n(E)$ is the actual density of states of the microscopically inhomogeneous material. Defined in this way $C(E)$ allows properly for penetration into the excluded regions. However, for it to be a useful concept, tunneling across the excluded regions must be quantitatively unimportant for the physical properties. We have demonstrated elsewhere[61,62] that for such large values of the correlation length b as we are concerned with here or for large fluctuations in the potential, tunneling effects are negligible.

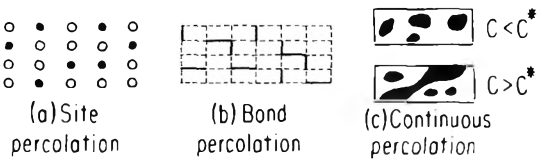

Figure 9. Sketch of different models for classical percolation: (a) site percolation in a two-component system; (b) bond percolation for two types of bonds; (c) continuous percolation for $C < C^*$ and for $C > C^*$.

There are some interesting immediate consequences of this physical picture. The allowed volume concept allows us to establish direct contact with classical percolation theory.[8–13] We are dealing with a continuous site-percolation problem, where any portion of the material can be randomly metallic or nonmetallic. The continuous percolation picture is distinct from the discrete models for site percolation and for bond percolation,[8] as is evident from Figure 9. If $C(E)$ falls below the critical value C^* for classical continuous percolation, percolation theory tells us that a continuous extended path through metallic regions does not exist. The metallic wave functions are therefore localized at that energy. We note in passing that the continuous percolation concept is strictly applicable provided that the conductivity of the nonmetallic regions is vanishingly small. If this is not the case, the concept of a percolation threshold does not strictly apply, but instead we encounter a continuous change of σ, which is finite for all values of C.

The above definition of $C(E)$ should make clear that

$$C(E_F) = C \qquad \text{(VI.2)}$$

is just the metallic volume fraction, that fraction of the volume of the material in which it is locally metallic. Provided the Fermi level E_F lies close to the middle of the fluctuating semiconducting gaps, the condition for a metal–semiconductor transition in the inhomogeneous transport regime is obtained from eq IV.1 and IV.2

$$C = C(E_F) = n(E_F)/n_0(E_F) = C^* \qquad \text{(VI.3)}$$

The continuous site-percolation problem has not yet been solved. Existing numerical studies[8] for three-dimensional lattices give values of C^* ranging from $C^* = 0.195$ for fccub to 0.30 for the single crystal. Zallen and Scher[9] suggest that for percolation in a continuous potential $C^* = 0.15$. Skal, Shklovskii, and Efros[12] find $C^* = 0.17$ for the percolation probability in a particular random potential. Webman, Cohen, and Jortner[13] obtained $C^* = 0.15 \pm 0.02$ from numerical simulations of the conductivity of cubic resistor networks with correlated bonds.

We are dealing with an inhomogeneous transport regime in a disordered system, $0 < C < 1$, $C = C(E_F)$. The inhomogeneous regime can be subdivided into two parts. (a) Pseudometallic regime: $1 > C > C^*$. Above the percolation limit the major contribution to transport originates from the continuous extended metallic paths. The transport properties will exhibit a gradual change from those corresponding to the lower limit of the homogeneous metallic regime. (b) Pseudononmetallic regime: $0 < C < C^*$. Here extended states do not exist and tunneling between isolated metallic regions can be ignored.

Finally, we have to establish the relation between the values of C and the mean value

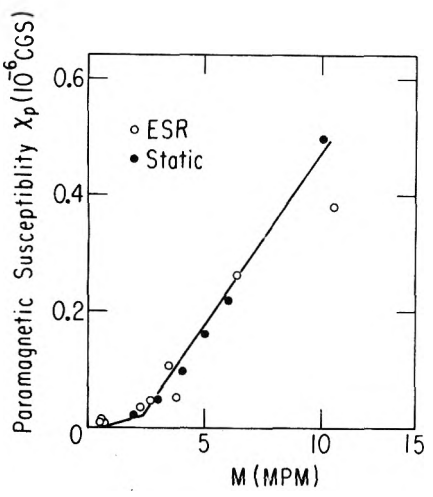

Figure 10. Volume spin susceptibility data for Na–NH_3 solutions (ref 87, 103–106) in the infermediate concentration range. A fit to a two-line-segment function, eq VII.1 and VII.6, is shown.

$$M = \int_0^\infty mP(m)\,dm \qquad \text{(VI.4)}$$

of the mean concentration in MAS. Such a relation we term a C scale. For the special case of a bimodal distribution as we are concerned with here we set approximately

$$P(m) = [(M - M_1)/(M_0 - M_1)]\delta(m - M_0) \times [(M_0 - M)/(M_0 - M_1)]\delta(m - M_1) \qquad \text{(VI.5)}$$

where M_1 and M_0 are the local value of M corresponding to nonmetallic and the metallic regions, respectively. The C scale is

$$C = (M - M_1)/(M_0 - M_1) \qquad \text{(VI.6)}$$

a linear relation between C and M.

We establish the C scale in microscopically inhomogeneous materials in two steps. First, we determine the limits of the inhomogeneous regime from the available structural, thermodynamic, transport, and magnetic data. For a bimodal distribution we take $C = 1$ for $M = M_0$ and $C = 0$ at $M = M_1$. Second, we utilize volume susceptibility data $\chi_p(M)$, when available, to establish the C vs. M relation in the inhomogeneous regime. Because for the materials under consideration local field corrections are negligible in χ_p, the volume spin susceptibility can be written as a superposition

$$\chi_p = C\chi_0 + (1 - C)\chi_1 \qquad \text{(VI.7)}$$

where χ_0 and χ_1 define metallic and nonmetallic susceptibilities at $C = 1$ and at $C = 0$, respectively. Complementary information concerning the C scale originates from Knight shift data.

VII. The C Scale and Analysis of Magnetic Data in MAS

We now establish the relation between the metal concentration M and the metallic volume fraction for metal–ammonia solutions. Regarding the upper limit, $C = 1$, we have already noted that the anomalously large concentration fluctuations[83] disappear into the background at $M \simeq 9$ ppm in the Li and Na solutions, Figures 5 and 6. It is interesting that the Hall constant,[32-35] R, for Li begins to exceed the free electron value R_{fe} for $M < 9$ MPM, and that the conductivity[30,32-35] there becomes of order $10^3\ \Omega^{-1}\ cm^{-1}$ for Li and Na solutions while $k_F l \sim 3$. We recall that for expanded Hg[7] the propagation regime terminates at $k_F l \simeq 2.3$. These three facts together indicate the termination of the homogeneous propagation regime at 9 MPM. Coupling these facts about the transport properties with the evidence for inhomogeneity exposed in section IV leads us to identify the upper limit of the inhomogeneous transport regime as $C = 1$ at 9 MPM in Li and Na solutions. Turning now to the lower limit, $C = 0$, the concentration fluctuations[83] in Li solutions, Figure 5, suggest that the material becomes homogeneous again at $M \simeq 2.5$ MPM. Accordingly, we set $M \simeq 2.5$ MPM as the lowest limit, $C = 0$, of the inhomogeneous regime, and refine this value of M for $C = 0$ to 2.3 MPM by analysis of the magnetic data.

The best available data for the spin susceptibility[39-42,84] are shown in Figure 10. For Na solutions χ_p becomes appreciable above 1 MPM, increasing monotonically with M. It is linear with M in the range $3 < M < 9$ MPM, where it follows

$$\chi_p = \frac{M - 2}{7}\chi_0 \qquad \text{(VII.1)}$$

where $\chi_0 = \chi_p(9)$ is the volume susceptibility in the metallic regions. The bimodal distribution immediately implies that

$$M = 9C + M_1(1 - C) \qquad \text{(VII.2)}$$

which gives us the linear relation

$$C = (M - M_1)/(9 - M_1) \qquad \text{(VII.3)}$$

for the C scale in analogy with eq VI.6. Next, we utilize eq VII.3 for χ_p. Inserting (VII.1) in (VI.7) and defining

$$r = \chi_1/\chi_0 \qquad \text{(VII.4)}$$

where χ_1 is the susceptibility of the nonmetallic regions, yields the relation

$$M_1 = 2 + 7r \qquad \text{(VII.5)}$$

between the two parameters M_1 and r.

Since χ_p is linear in M at least down to 3 MPM and C is linear in M according to (VII.3), (VI.7) plus (VII.5) imply that $2 < M_1 < 3$ MPM. Accordingly we have to introduce a fitting function for χ_p in that range. We have chosen a fit to two linear segments, eq V.12 for $M > 2.33$ MPM and for

$$\chi_p = \frac{M - 1}{28}\chi_0 \qquad \text{(VII.6)}$$

for $M < 2.33$ MPM. Inserting M_1 into (VII.6) give χ_1 and r gives $M_1 = 2.33$. Accordingly we choose our C scale as

$$C = (M - 2.3)/(9 - 2.3) \qquad \text{(VII.7)}$$

and show in Figure 10 the corresponding fit of the χ_p data.

VIII. Response Functions of Microscopically Inhomogeneous Materials

We now address ourselves to the calculation of transport properties of microscopically inhomogeneous materials. We shall refrain from providing detailed derivations and restrict ourselves to quoting mostly new results from our yet unpublished work.

A. Electrical Transport. We now address the problem of calculating the macroscopic transport properties of a material which is locally nonuniform. Consider first the electri-

cal conductivity. In simulating electrical transport properties of a microscopically inhomogeneous material we are dealing with a continuous site-percolation problem in which any portion of the material can be randomly metallic or nonmetallic. To mimic the features of the continuous conduction problem, one can impose correlations on neighboring bonds, so that if a bond is of one type all its neighbors out to the correlation distance b must be of the same type. Together with Webman[13] we have carried out a numerical study of the conductivity of simple cubic resistor networks with correlated bonds. For $x = 0$, the conductivity must vanish for C below the percolation threshold. The major effect of correlations is to shift the percolation threshold from $C^* = 0.25$ for the uncorrelated network[10,11] to $C^* = 0.15 \pm 0.02$, in accord with numerical simulation of the percolation probability[9,12] in the continuous percolation problem. In the particular case of a bimodal distribution of local conductivities, the macroscopic conductivity, σ, was expressed in the form

$$\sigma = \sigma_0 \, \mathrm{f}(x, C) \qquad x = \sigma_1/\sigma_0 \tag{VIII.1}$$

where σ_0 and σ_1 correspond to the conductivities at $C = 1$ and at $C = 0$, respectively. The effective medium theory (EMT) for the conductivity[10,11,58,92-95]

$$\mathrm{f}(x, C) = a + (a^2 + x/2)^{1/2}$$
$$a = \frac{1}{2}\left[\left(\frac{3}{2}C - \frac{1}{2}\right)(1 - x) + \frac{x}{2}\right] \qquad x = \sigma_1/\sigma_0 \tag{VIII.2}$$

was found accurate for $0.4 < C < 1.0$ for all values of the conductivity ratio x, in agreement with Kirkpatrick's original work.[10] Serious deviations from the EMT occur for $C < 0.4$ for small values of x (<0.03). This is not surprising, as the EMT, which rests on a mean field approximation for the local conductivity, overestimates the percolation threshold for $x = 0$, $C_{\mathrm{EMT}}^* = \frac{1}{3}$, and can in general be expected to result in too low values of σ for $C < 0.4$ and $0 \leq x < 3 \times 10^{-2}$.

The above theory of the conductivity of an inhomogeneous system is applicable in the inhomogeneous transport regime provided that the phase coherence length for the conduction electrons within the metallic regions is considerably shorter than the correlation length b. When the transport within extended metallic clusters corresponds to the propagation case, as is the case for metal–ammonia solutions, the mean free path is comparable to the sampling length $L = 2b$. In that case, scattering off metallic cluster boundaries reduces the conductivity below the value σ_0 at $C = 1$. The reduction of the metallic conductivity below σ_0 is concentration dependent because the mean cluster size decreases with decreasing concentration. We have accounted for the consequent dependence of the conductivity of the metallic region on C by a modification of Eggarter's theory for scattering from the boundaries of the allowed regions.[96] The two conductivities are related by

$$\sigma_0(C)/\sigma_0 = \lambda(C)/l \tag{VIII.3}$$

where l is the mean free path at $C = 1$, while $\lambda(C)$ is the mean free path in the allowed volume fraction C. The latter quantity is given by Eggarter in the form[96]

$$\lambda(C) = l\lambda_s/(l + \lambda_s) \tag{VIII.4}$$

where in our case the mean free path λ_s associated with scattering by prohibited regions at the boundaries of the allowed regions is

$$\lambda_s = \sum_{n=1}^{\infty} 2nbC^{n-1}(1 - C) = 2b[1 - C]^{-1} \tag{VIII.5}$$

Thus from eq VIII.3–VIII.6 we obtain

$$D(C) = \frac{\sigma_0(C)}{\sigma_0} = \frac{z}{1 - C + z} \tag{VIII.6}$$

where

$$z = 2b/l \tag{VIII.7}$$

We impose no corresponding correction to σ_1 from scattering from the boundaries of the nonmetallic regions. We should note in passing that when the metallic region corresponds to the diffusion limit $z \geq 2b/a$ holds, where a is the interatomic spacing, so that $z \gg 1$ and $D(C) \to 1$ for all C.

The classical expression for the conductivity, eq VIII.2, has now to be modified by accounting for the dependence of $\sigma_0(C)$ on the fraction of allowed volume so that

$$\sigma = \bar{\mathrm{f}} D(C)\sigma_0 \tag{VIII.8}$$

where

$$\bar{\mathrm{f}} = \mathrm{f}[C, x(C)] \tag{VIII.9}$$

$$x(C) = \frac{\sigma_1}{\sigma_0 D(C)} = \frac{x}{D(C)} \tag{VIII.10}$$

and now $x(C)$, eq VIII.10 replaces x in eq VIII.2. Equations VIII.8–VIII.10 constitute a modified effective medium theory (EMTZ). For materials characterized by $x > 3 \times 10^{-2}$ the EMTZ is applicable throughout the entire range $0 < C < 1$. For materials where $x < 3 \times 10^{-2}$ the EMTZ is valid only for $0.5 < C < 1.0$, while for $C < 0.5$ we have utilized eq VIII.1 where $\bar{\mathrm{f}}$, eq VIII.9, can be obtained from numerical simulations of σ/σ_0 in a correlated cubic network, with $x(C)$ given by eq VIII.10.

We were unable to go beyond the EMT for the galvanomagnetic properties of inhomogeneous materials. The EMT yields[97] for the Hall coefficient, R, and for the Hall mobility, μ

$$\mu/\mu_0 = \mathrm{g}(x, y, \mathrm{f}) = [1 - B(1 - xy)]\mathrm{f}^{-1} \tag{VIII.11}$$

$$R/R_0 = \mathrm{h}(x, y, \mathrm{f}) = [1 - B(1 - xy)]\mathrm{f}^{-2} \tag{VIII.12}$$

$$B = \frac{(2\mathrm{f} + 1)^2(1 - C)}{(2\mathrm{f} + 1)^2(1 - C) + (2\mathrm{f} + x)^2 C} \qquad y = \mu_1/\mu_0 \tag{VIII.13}$$

where μ_0 and μ_1 are the Hall mobilities in the metallic and in the semiconducting regions, corresponding to the Hall mobilities at $C = 1$ and at $C = 0$, respectively. When boundary scattering effects are incorporated EMTZ yields correspondingly

$$R = \bar{\mathrm{h}} R_0 \tag{VIII.14}$$

$$\mu = \bar{\mathrm{g}} D(C)\mu_0 \tag{VIII.15}$$

$$\bar{\mathrm{g}} = \mathrm{g}[C, x(C), y(C), \bar{\mathrm{f}}] \tag{VIII.16}$$

$$\bar{\mathrm{h}} = \bar{\mathrm{g}}/\bar{\mathrm{f}}$$
$$x(C) = x/D(C)$$
$$y(C) = y/D(C) \tag{VIII.17}$$

On the basis of numerical simulations of σ we have concluded that the EMT or the EMTZ hold in general for $C >$

0.4, while for $0 < C < 0.4$ the mean field approximation is adequate for materials where $x > 3 \times 10^{-2}$. We infer that the same will apply for R and μ. On the other hand, for materials where $x < 3 \times 10^{-2}$ for $C < 0.4$ the EMT and the EMTZ provide only a qualitative interpolation formula.

B. Thermal Transport. It is straightforward to carry out an effective medium theory for any tensorial response function, e.g., thermal transport coefficients, optical constants, diffusion coefficients, etc. Such an EMT analysis can be readily generalized into an accurate numerical calculation of a random continuum property for a diagonal response function by the method we have used for the electrical conductivity.

We have carried out an EMT for a system simultaneously subjected to gradients of temperature and electric potential, obtaining explicit expressions for the thermal transport properties of an inhomogeneous material.[58] We start with the microscopic equations

$$\vec{J}' = k'\vec{\nabla}T' + P'T'\vec{\nabla}\varphi'$$
$$\vec{j}' = \sigma'\vec{\nabla}\varphi' + P'\vec{\nabla}T' \qquad \text{(VIII.18)}$$

which holds locally within the inhomogeneous material. Primed quantities indicate local values. J' and j' are the heat and electrical currents, respectively, k' and σ' are thermal and electrical conductivity, respectively. P' is the Peltier coefficient, while φ' and T' are the electrical potential and the temperature, respectively. The corresponding macroscopic equations are identical with (VIII.18) but with unprimed quantities. The relation between the macroscopic and microscopic fluxes and forces is

$$\vec{J} = \langle\vec{J}'\rangle;\ T = \langle T'\rangle$$
$$\vec{j} = \langle\vec{j}'\rangle;\ \varphi = \langle\varphi'\rangle \qquad \text{(VIII.19)}$$

where the average can be taken equivalently over all space or over all local configurations at a given point.

To carry out an effective medium theory of the relation between the macroscopic transport coefficients κ, σ, and P and the corresponding microscopic quantities, we treat the system as though it consisted of a sphere of radius b embedded within a uniform effective medium characterized by the coefficients κ, σ, and P. We use the conservation conditions and Maxwell's equations together with eq VIII.18 to determine J', j', T', and φ' inside the inclusion. Application of eq VIII.19 results in a consistency condition, the EMT condition, which must be satisfied by κ, σ, and P, determining them implicitly in terms of averages over κ', σ', and P'. The result for σ is the usual EMT result, eq VIII.2, that for κ is

$$\left\langle \frac{\kappa - \kappa'}{\kappa' + 2\kappa} \right\rangle = 0 \qquad \text{(VII.20)}$$

while for P we get

$$P = \frac{3\kappa\sigma\langle P'/(\kappa' + 2\kappa)(\sigma' + 2\sigma)\rangle}{\langle(\kappa\sigma' + \sigma\kappa' + 2\kappa\sigma - \kappa'\sigma')/(\kappa' + 2\kappa)(\sigma' + 2\sigma)\rangle} \qquad \text{(VIII.21)}$$

The thermoelectric power, S, can be obtained from eq VIII.21 by substituting

$$S = P/\sigma \qquad \text{(VIII.22)}$$

for primed and unprimed quantities in (VIII.21).

The measured thermal conductivity $\bar{\kappa}$ is given by

$$\bar{\kappa} = \kappa - S^2\sigma T \qquad \text{(VIII.23)}$$

For MAS the second term on the right-hand side of eq VIII.23 is of order $10^{-3}\bar{\kappa}$ and can be neglected.

C. Optical Properties. Finally, we consider the optical properties of microscopically inhomogeneous materials. Together with Webman we have developed[99] an effective-medium theory for the frequency dependent dielectric constant

$$\epsilon(\omega) = \epsilon_1(\omega) + i\epsilon_2(\omega) \qquad \text{(VIII.24)}$$

The EMT condition for $\epsilon(\omega)$ is

$$\left\langle \frac{\epsilon(\omega) - \epsilon^i(\omega)}{2\epsilon(\omega) + \epsilon^i(\omega)} \right\rangle = 0 \qquad \text{(VIII.25)}$$

where $\epsilon^i(\omega)$ is a possible value of the local complex dielectric function and the average is over all such values. For a bimodal distribution of fluctuations $\epsilon^i(\omega)$ takes on a functional form $\epsilon^0(\omega) = \epsilon_1{}^0(\omega) + i\epsilon_2{}^0(\omega)$ characteristic of metallic regions with probability C or $\epsilon^1(\omega) = \epsilon_1{}^1(\omega) + i\epsilon_2{}^1(\omega)$ characteristic of the nonmetallic regions, with a probability $1 - C$. Equation VIII.25 may then be readily solved:

$$\epsilon(\omega) = \epsilon^0(\omega)\, f(C, x(\omega)) \qquad \text{(VIII.26)}$$

$$f(C, x(\omega)) = a(\omega) \pm \left[(a(\omega))^2 + \frac{1}{2}x(\omega)\right]^{1/2} \qquad \text{(VIII.27)}$$

$$a(\omega) = \frac{1}{2}\left[\left(\frac{3}{2}C - \frac{1}{2}\right)(1 - x(\omega)) + \frac{x(\omega)}{2}\right] \qquad \text{(VIII.28)}$$

$$x(\omega) = \epsilon^1(\omega)/\epsilon^0(\omega) \qquad \text{(VIII.29)}$$

The sign in (VIII.27) is chosen to give positive $\epsilon_2(\omega) = |m|[\epsilon(\omega)]$. Equations VIII.26–VIII.29 represent a generalization of the EMT for a real, diagonal, second-order tensor to the complex case. Our experience with the former case leads us to expect that the EMT is accurate for all values of C if $|x(\omega)|$ is within the range 0.03–30. Numerical simulations[99] of $\epsilon(\omega)$ in a simple cubic network bear out this expectation.

D. Sound Velocity. We have recently extended the effective-medium theory to the case of wave propagation in a microscopically inhomogeneous medium[100] in which the propagation velocity takes a random value c_i which remains constant over a correlation radius b. The familiar effective-medium condition

$$\left\langle \frac{c_i{}^2 - \bar{c}^2}{c_i{}^2 + 2\bar{c}^2} \right\rangle = 0 \qquad \text{(VIII.30)}$$

results for the macroscopic propagation velocity $\bar{c}$, where the average is taken over all values of local velocity c_i. For a bimodal distribution of fluctuations c_i takes the values c_0 with probability C or c_i with probability $1 - C$, whereupon (VIII.30) results in

$$\bar{c}^2 = c_0{}^2 f(X_s, C)$$
$$X_s = c_1{}^2/c_0{}^2 \qquad \text{(VIII.31)}$$

and the function $f(X_s, C)$ is defined in terms of eq VIII.2.

IX. Analysis of Response Functions for MAS

We now proceed to the analysis of the transport properties of disordered materials undergoing a metal–nonmetal transition via the inhomogeneous transport regime. In section V we have established the limits of the inhomogeneous transport regime and the C scale. The parameters needed as input data for the analysis of the transport properties are the transport coefficients at $C = 1$ and at $C = 0$. These are taken from experiments and listed in Table II.

TABLE II: Values of the Ratios of Electronic and Thermal Transport Coefficients Associated with the Limits of the Inhomogeneous Regime in MAS

	$C = 0$	$C = 1$	x	y	κ_1/κ_0	S_1/S_0	c_S'/c_S^0	Sources of experimental data
Li–NH_3 (223 K)	M = 2.3 MPM	M = 9 MPM	1.2×10^{-3}	8×10^{-3}			1.33	2–5, 26–38, 43, 44
Na–NH_3 (240 K)	M = 2.3 MPM	M = 9 MPM	2.4×10^{-3}		0.35	20	1.33	101, 102

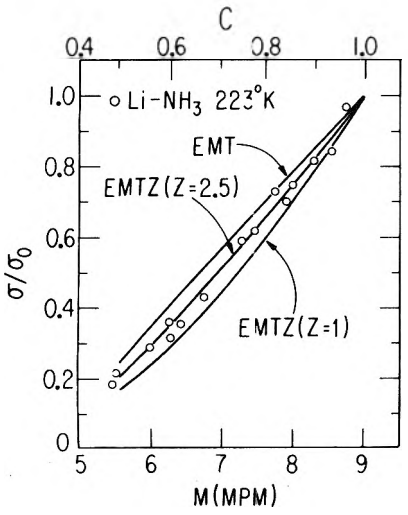

Figure 11. Analysis of the electrical conductivity data of Li–NH_3 solutions, 5.5 MPM < M < 9 MPM, at T = 223 K (ref 30–37), in terms of the modified effective medium theory (EMTZ). The best fit is obtained for z = 2.5. The curves for $z = \infty$ (EMT) and for z = 1 are shown for comparison.

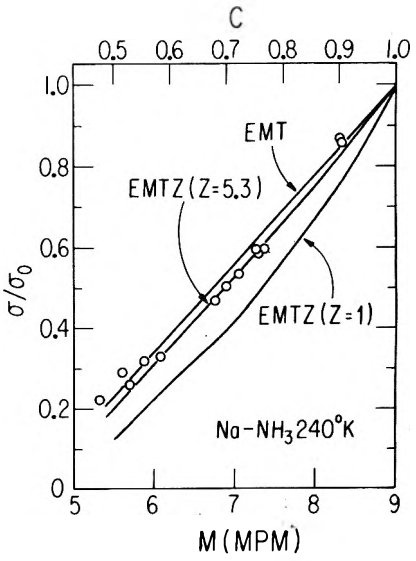

Figure 12. Analysis of the electrical conductivity data of Na–NH_3, 5.5 MPM < M < 9 MPM, at T = 240 K (ref 28 and 29), in terms of the EMTZ. The best fit is obtained for $z = 5.3 \pm 0.6$. Also shown are the curves for $z = \infty$ and z = 1.

For small x and y, i.e., $x \sim 10^{-3}$ to 10^{-4} and $y \sim 10^{-2}$ to 10^{-3}, as is appropriate to metal–ammonia solutions, the transport coefficients in the range $4 < C < 1.0$ are independent of x and y. Thus the EMT equations (VIII.2) or the EMTZ relations (VIII.8–VIII.10) apply for $C > 0.4$. Both σ and μ drop rapidly while R varies slowly in this range of C. The conductivity assumes the simple form

$$\sigma = \sigma_0 \left(\frac{3}{2}C - \frac{1}{2}\right) \qquad 0.4 < C < 1.0 \qquad \text{(IX.1)}$$

while the galvanomagnetic transport coefficients are

$$R = 4R_0/(3C + 1) \qquad \text{(IX.2)}$$

$$\mu = \mu_0 \left(\frac{6C - 2}{3C + 1}\right) \qquad \text{(IX.3)}$$

When boundary scattering corrections are required they do not affect the value of R, eq VIII.14, while σ and μ are modified to

$$\sigma = \sigma_0 D(C) \left(\frac{3}{2}C - \frac{1}{2}\right) \qquad \text{(IX.4)}$$

$$\mu = \mu_0 D(C) \left(\frac{6C - 2}{3C + 1}\right) \qquad \text{(IX.5)}$$

in this range of C. For lower values of C (<0.4) we assert on the basis of numerical simulations that σ continues to decrease. We expect the Hall mobility to exhibit a similar decrease in the range $0 < C < 0.4$.

We now proceed to the analysis of the conductivity data. We have compared σ/σ_0 with eq IX.1 for Li and Na for 9 MPM > M > 5.5 MPM and show the results in Figures 11 and 12. The data fall systematically below the EMT, more so for Li than for Na. We therefore fitted the data to the EMTZ, adjusting the one parameter z to get a best fit. The results are also shown in Figures 11 and 12 for the best fit with z = 2.5 for Li while at least-squares analysis results in $z = 5.3 \pm 0.6$ for Na. Also shown is EMTZ for z = 1 for comparison. From these values of z a rough estimate of b can be obtained. Using the weak scattering, nearly free electron form for σ_0, we estimate the mean free path to be 12 Å for Li and Na. The corresponding values of b from eq VIII.8 are

$$\begin{aligned} b &= 15 \text{ Å} \quad \text{Li–NH}_3,\ T = 223 \text{ K} \\ b &= 32 \text{ Å} \quad \text{Na–NH}_3,\ T = 240 \text{ K} \end{aligned} \qquad \text{(IX.6)}$$

The fit to the EMT breaks down seriously at low concentration, and the EMTZ is little different there. Accordingly, we have compared the experimental data with various numerical simulations in Figures 13 and 14 for Li and for Na. One sees that as the range of correlation is increased so that continuum percolation is approached, the fit becomes excellent over three orders of magnitude of variation in σ. It should be recognized that the theoretical curve is fixed to the experimental data at the C = 0 and C = 1 end points of the inhomogeneous range but that otherwise there are no adjustable parameters. (We have ignored the EMTZ corrections in the present context.) The simulations should be regarded, therefore, as interpolations between the end points and they serve excellently as such. There should be little doubt now as to the existence of an inhomogeneous transport regime for 2.3 MPM < M < 9 MPM.

Next, we consider the Hall data for this system. Since we have been unable to go beyond the EMT for the galvanomagnetic properties, we have compared the available Li Hall data[32–35] to the effective medium theory. As we have already noted, in this material the boundary scattering cor-

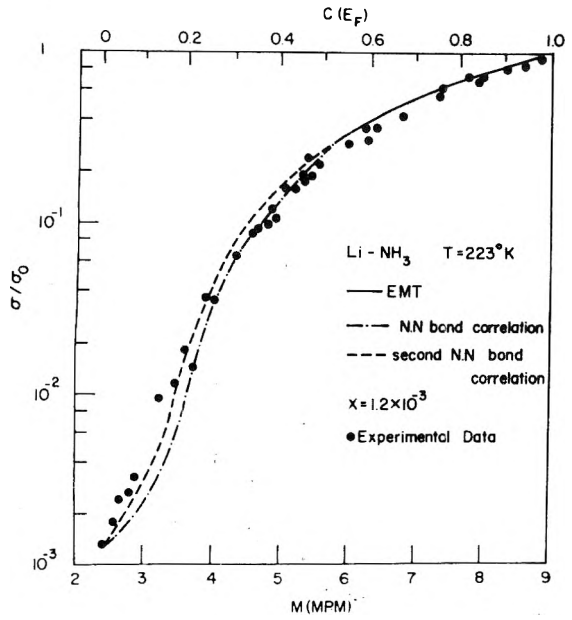

Figure 13. Analysis of the electrical conductivity data of Li–NH_3 solutions at 223 K (ref 32–37) throughout the entire inhomogeneous regime $C = 1$ at 9 MPM and $C = 0$ at 2.33 MPM: solid curve ($C > 0.5$), EMT; dotted-dashed curve, numerical simulation with nearest neighbor bond correlation ($x = 1.2 \times 10^{-3}$); dashed curve, numerical simulation with second nearest neighbor bond correlation ($x = 1.2 \times 10^{-3}$). Circles represent experimental data.

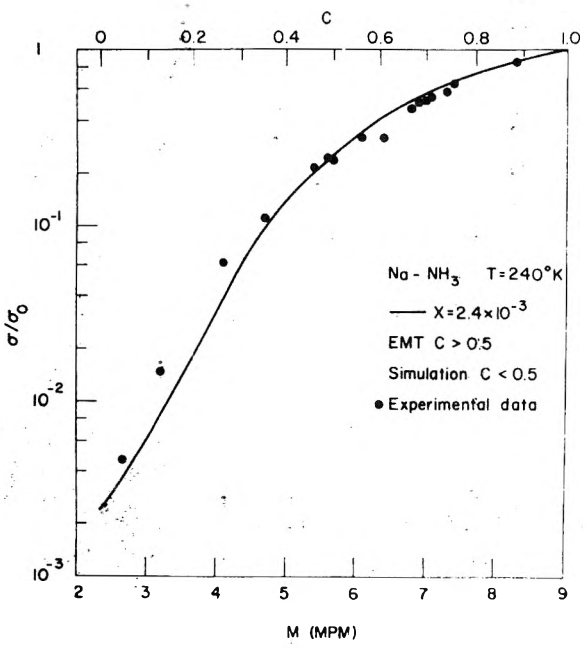

Figure 14. Analysis of the electrical conductivity data of Na–NH_3 solutions at 240 K (ref 28 and 29) throughout the entire inhomogeneous regime C = 1 at 9 MPM and $C = 0$ at 2.33 MPM: solid curve, EMT for $C > 0.5$ and numerical simulations with second nearest neighbor bond correlation ($x = 2.4$ and 10^{-3}) for $C < 0.5$. Circles represent experimental results.

rections to R are negligible for $C > 0.4$, while in the low C range ($0 < C < 0.4$) the EMT is inaccurate and there is little point to introduce the modified EMTZ version of the theory. In Figure 15 we portray the available Li Hall effect data together with the EMT curve using the experimental data at $C = 0$ and $C = 1$ from Table II. In the pseudometallic regime down to $C = 0.4$ the agreement between theory

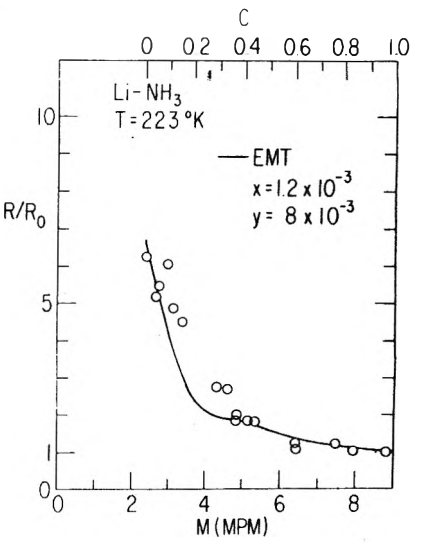

Figure 15. Analysis of Hall effect data (ref 33 and 34) of Li–NH_3 solutions at 223 K in terms of the EMT.

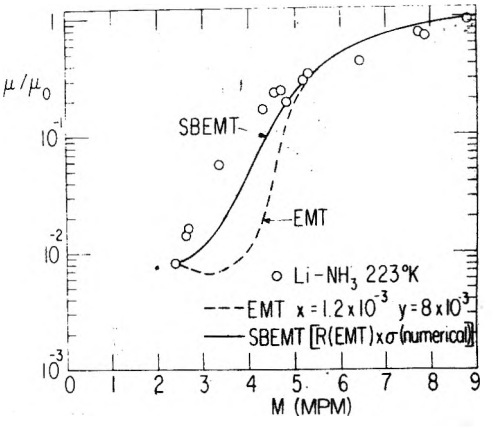

Figure 16. Analysis of the Hall mobility data (ref 33 and 34) for Li–NH_3 solutions at 223 K in terms of the effective-medium theory (dashed line) and the SBEMT (solid line).

and experiment is good, while for $0 < C < 0.4$ the EMT curve provides just an approximate interpolation formula.

In view of the quantitative agreement of σ and the reasonable agreement of R with the predictions of the EMT (and EMTZ) in the range $0.4 < C < 1$ it is apparent that a good fit can be obtained for the concentration dependence of the Hall mobility, μ, in this range as is evident from Figure 16. The small negative deviations of μ from the EMT curve in the concentration range 5 MPM $< M <$ 9 MPM can be readily accounted for in terms of boundary scattering effects; however, the experimental Hall mobility data are not accurate enough to warrant a detailed analysis in terms of the EMTZ. In the lower concentration range $C <$ 0.4 the experimental data exhibit a marked deviation from the EMT curve. This is not surprising as the EMT for σ reveals deviations in that range. In the absence of a numerical simulation scheme for R and μ, we have compromised by taking for μ the product of R obtained from EMT and μ as derived from the numerical simulation. The resulting curve, labeled as SBEMT in Figure 16, substantially improves the agreement with experiment.

We now turn to the analysis of the thermal conductivity[43] and the thermoelectric power[44,45] for Li and Na solutions. The available thermal conductivity data for Na–NH_3

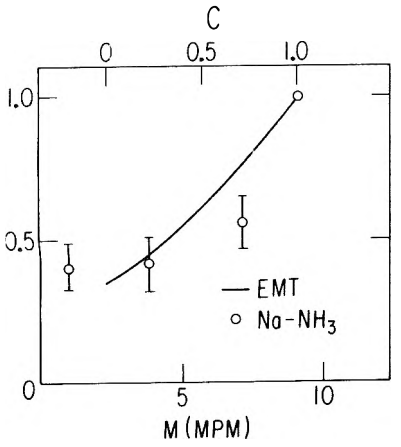

Figure 17. Analysis of the available thermal conductivity data (ref 43) for Na–NH_3 solutions in terms of the EMT.

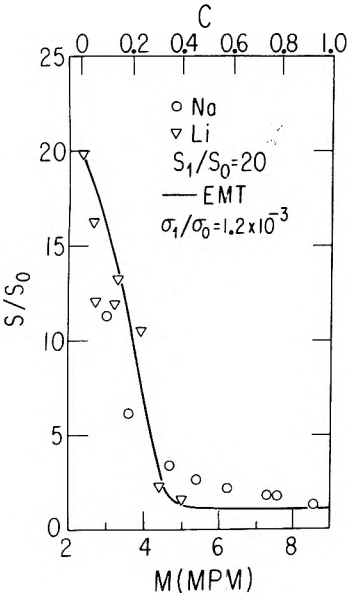

Figure 18. Analysis of the thermoelectric power data (ref 44 and 45) for Na–NH_3 and for Li–NH_3 solutions. The solid EMT curve is drawn for $S_1/S_0 = 20$, $\kappa_1/\kappa_0 = 0.35$, and $\sigma_1/\sigma_0 = 1.2 \times 10^{-3}$. Increasing x by a factor of 2 has small (~1%) effect in the range $C < 0.4$ where the EMT is inaccurate.

can be fitted by the EMT equation with $\kappa_1/\kappa_0 = 0.35$–0.40. The available experimental data,[43] Figure 17, are too sparse and inaccurate to attempt a quantitative correction for boundary scattering. Finally, it is worthwhile to note that for this system the high κ_1/κ_0 ratio implies that the EMT for the thermal conductivity is valid throughout the whole C range.

The thermoelectric power data for Li and Na solutions,[44,45] Figure 18, are in reasonable agreement with the EMT curve calculated from eq VIII.21 and VIII.22 with the parameters shown in Table II. We note in passing that as the general EMT expression, eq VIII.21 and VIII.22 for S, involves the local conductivity σ_1, which exhibits a large fluctuation for this system, we do not expect the EMT for S to be accurate as for κ for $C < 0.4$. It is important to note that the very weak variation of S with C in the range $0.4 < C < 1$ predicted by EMT and found in the data is a feature of the bimodal distribution of M values. A unimodal distribution would give a more nearly linear interpolation between $C = 0$ and $C = 1$.

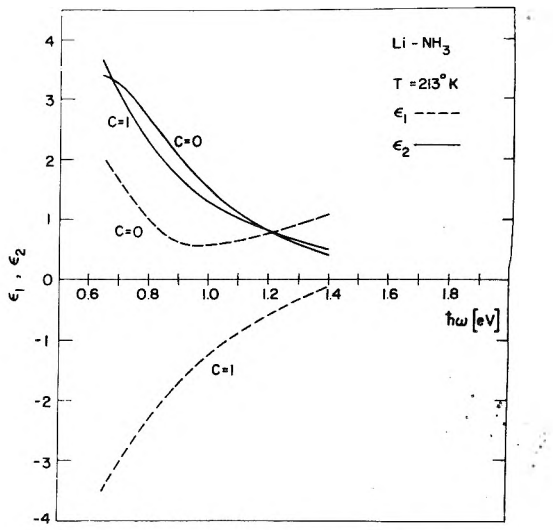

Figure 19. $\epsilon^0(\omega)$ and $\epsilon^1(\omega)$ for Li–NH_3 solutions at 213 K.

We now turn to the optical data of MAS. At concentrations above 8 MPM $\epsilon_1(\omega)$ and $\epsilon_2(\omega)$ differ for Li–NH_3 and Na–NH_3 solutions only in details from the behavior expected for a Drude, free-electron system. In the concentration range 8–2 MPM, which corresponds approximately to the inhomogeneous regime, $\epsilon_1(\omega)$ exhibits a continuous variation from metallic toward a behavior characteristic of a very broad resonance at ~0.6 eV. This is consistent with the behavior of $\epsilon_2(\omega)$, which is Drude-like and shows a slow variation with M in the range 4–8 MPM, with an indication of a resonance around 0.6 eV at 2–3 MPM. Thompson and colleagues[47,48] point out that there are signs of persistence of the bound-electron absorption to quite high concentrations, 6 MPM. This mixed behavior of optical properties is consistent with our model for microscopic inhomogeneities in these solutions in that concentration range and lends further point to our attempts to account for the optical data in terms of our theory. As in these systems $|x(\omega)|$, eq VIII.28, is in the range 0.1–10 the condition for the applicability of the EMT, eq VIII.26–VIII.29 are well met. We now turn to the analysis of Li–NH_3 optical data at 213 K in terms of the EMT. We choose a Drude–Lorentz form for $\epsilon^0(\omega)$

$$\epsilon^0(\omega) = \epsilon_\infty - \frac{\omega_p^2}{\omega(\omega + i/\tau)} \qquad \text{(IX.7)}$$

with the parameters $\epsilon_\infty = 1.35$, $\hbar\omega_p = 1.8$ eV, and $\hbar/\tau = 0.5$ eV. $\epsilon^1(\omega)$ at 2.3 MPM ($C = 0$) is not available, and we had to follow an indirect route in evaluating $\epsilon^1(\omega)$. $\epsilon^1(\omega)$ was determined by inserting (IX.7) and the experimental values of $\epsilon(\omega)$ into (VIII.26)–(VIII.29) for $M = 3$ MPM (i.e., $C = 0.1$) and solving for $\epsilon^1(\omega)$. The results for $\epsilon^0(\omega)$ and $\epsilon^1(\omega)$ are shown in Figure 19. Next, calculations for $\epsilon(\omega)$ were made for $M = 4$ MPM ($C = 0.25$), $M = 5$ MPM ($C = 0.4$), and $M = 8$ MPM ($C = 0.85$). The comparison between theory and experiment (Figures 20 and 21) is as good as can be expected. We therefore believe that bound-electron absorption persists well into the intermediate range and that this persistence is a strong evidence for compositional inhomogeneities in this composition range.

Finally, we consider the sound velocity data for Bowen et al.[101,102] The sound velocity c_0 at 9 MPM is taken as 1678 m sec^{-1} for Li–NH_3 at 223 K and 1376.2 m sec^{-1} for Na–NH_3 at 240 K, while for c_1 we take 1678 m sec^{-1} for Li–

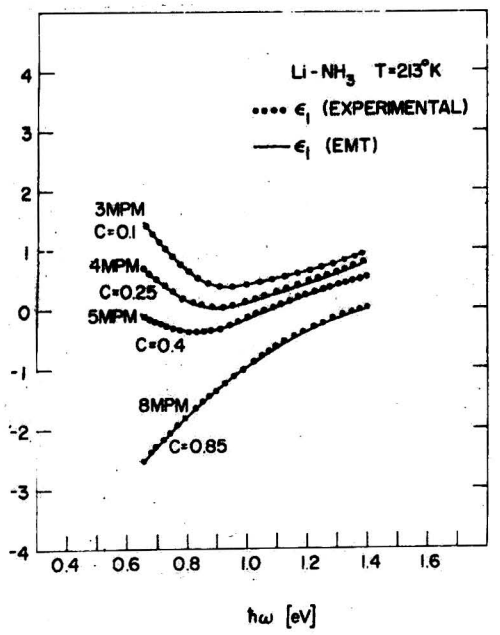

Figure 20. Concentration dependence of $\epsilon_1(\omega)$ of Li–NH_3 solutions at 213 K. Points represent experimental data (ref 47 and 48).

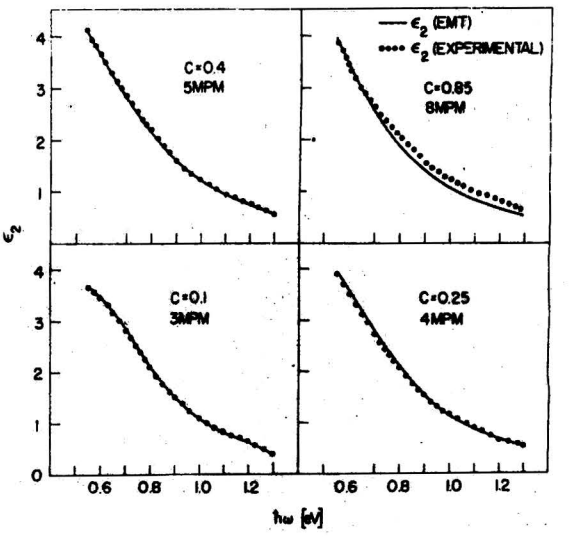

Figure 21. Concentration dependence of $\epsilon_2(\omega)$ for Li–NH_3 solutions at 213 K. Points represent experimental data (ref 47 and 48).

NH_3 at 223 K and 1608.4 m sec^{-1} for Na–NH_3 at 240 K. The fit to the EMT, eq VIII.31, is shown in Figure 22. It should, however, be pointed out that for a value of X_s, 1.32, as large as occurs here, the agreement between theory and experiment for the sound velocity data provides no further confirmation of our model for MAS.

X. Concluding Remarks

We have built up strong evidence for continuous MNMT intermediated by microscopic inhomogeneities in the two component systems Li and Na ammonia solutions at $|T - T_c| \simeq$ 10–20 K. These materials were selected for detailed study because of the availability of extensive experimental data. Our theory provides the first semiquantitative approach for the understanding of the variation of the response functions in a class of disordered materials which undergo a "continuous" MNMT. Concerning the details of the analysis of response functions of inhomogeneous materials we stress that the analysis of transport and optical data in terms of numerical simulations and the EMT does not involve a curve-fitting procedure. Instead, we connect the transport and optical properties to magnetic data, which are used to derive the C scale. Comparison with observations leads to a good fit between theory and experiment for electrical and thermal transport properties, optical data, and sound velocity data and to the determination of the short correlation length from the analysis of the conductivity data.

The validity of our physical picture has been challenged by Mott.[57] All of the published objections to our approach are explicitly or implicitly refuted.[60-62] We note also that the continuous metal–nonmetal transitions considered by us do not involve a Mott transition, as the electrons are confined either to metallic regions or nonmetallic regions. The ideas advanced by Mott regarding the Hubbard bands in a monovalent metal and the band overlap in a divalent metal have to be applied *locally*.

The basic physical idea advanced by us concerning the MNMT in MAS is that microscopic inhomogeneities deter-

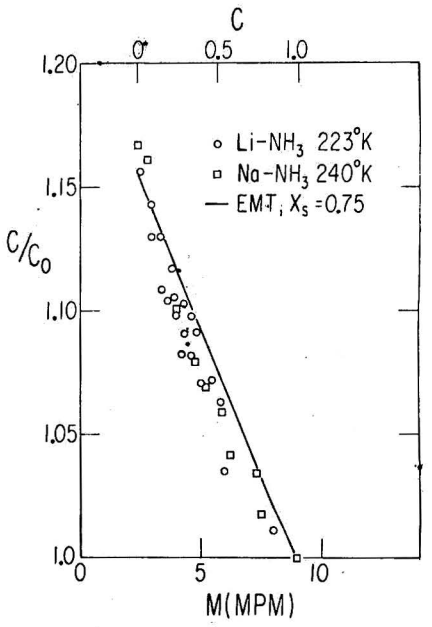

Figure 22. Concentration dependence of the sound velocity data (Bowen, ref 101 and 102) in Li–NH_3 and Na–NH_3.

mine electronic structure and transport properties within the transition region. We have proposed that for Li–NH_3 and Na–NH_3 in the low temperature range ($T - T_c \lesssim 20$K) bimodal concentration fluctuations prevail, constituting essentially a physical situation where clustering of solvated electrons and cations occurs. The following transport data are consistent with the assumption of bimodality. First, our analysis of the electrical conductivity which varies over a range of three orders of magnitude would fail if a unimodal distribution were to prevail. Second, the thermoelectric power calculated for the bimodal distribution (Figure 18) exhibits a weak dependence on C for $0.5 < C < 1$, which is also the trend observed in the experimental data. A unimodal distribution would result in a faster increase of S with decreasing M in that region. Finally, the excellent fit of the optical data over a broad energy range supports the bimodality hypothesis. Nevertheless, in our opinion the question of whether the fluctuations in Li– and Na–NH_3 at

low $T - T_c$ are unimodally or bimodally distributed remains open, providing a challenging theoretical and experimental problem.

At higher temperatures for Li and Na solutions as well as for Cs solutions over the entire temperature range a normal, unimodal distribution of density fluctuations will intermediate the MNMT. The physical situation is analogous to the case of the MNMT in expanded liquid Hg, briefly considered in section III.

The lower limit of the inhomogeneous regime in Li–NH_3 and Na–NH_3 at 2.3 MPM requires a reinterpretation of the transport properties in the range between ~1 and 2.3 MPM, which we have already considered in section IV. We propose that a pseudointrinsic semiconductivity mechanism prevails. The valence and the conduction bands correspond to σ_g and σ_u orbitals of electron cavity pairs, respectively. In view of the low (~0.6–0.7 eV) σ_g–σ_u separation within a single cavity pair reduction of the band gap due to the broadening of the valence and conduction bands will occur at much lower number density than in expanded semiconducting Hg below 7.8 g cm^{-3}. In the intrinsic semiconducting regime in MAS the major contribution to the conductivity and the paramagnetic susceptibility will result from electrons excited near the mobility edge E_c. Thus χ_p is proportional to the conductivity. We expect that in the concentration range 1–2.3 MPM, $\chi_p = \bar{A}\sigma J^{-2}$, where $\bar{A}$ is a constant and J is the transfer integral in Friedman's theory.[70] The sparse experimental data available are not yet sufficient to test this hypothesis. Regarding the galvanomagnetic properties in that concentration range we expect that according to the Friedman relations[70] for a disordered semiconductor $\mu \propto Jn(E_c)$ so that the Hall mobility will decrease with decreasing M due to the reduction of the transfer integral J.

From the foregoing discussion a coherent picture emerges for the electrical transport properties and the MNMT of MAS in the intermediate concentration range 1–9 MPM. We predict that the Hall coefficient for MAS will decrease throughout the entire concentration range 9–1 MPM which spans the inhomogeneous regime and the semiconducting regime. Furthermore, the microwave properties of MAS would provide extremely useful information on the state of these systems in the transition region. We have treated the microwave dielectric constant by numerical simulations. The results are sensitive to the difference between unimodal and bimodal distributions of density fluctuations. Uncertainty in the available experimental data[103] prevents a comparison with theory. Detailed experimental evidence on the microwave properties of MAS will be of considerable importance.

Acknowledgments. We are indebted to I. Webman for his help with the numerical analysis, to S. Kirkpatrick for providing us with his computer program, to J. C. Thompson and to D. A. Bowen for supplying detailed experimental results, and to N. R. Kestner, J. C. Thompson, and I. Webman for helpful discussions.

References and Notes

(1) Based on research supported by the ARO(D), the L. Block Fund, and the Materials Research Laboratory of the National Science Foundation at The University of Chicago, and by the U.S.–Israel Binational Science Foundation at the University of Tel-Aviv.
(2) (a) "Metal Ammonia Solutions", G. Lepoutre and M. J. Sienko, Ed., W. A. Benjamin, New York, N.Y., 1964; (b) "Metal Ammonia Solutions", J. J. Lagowski and M. J. Sienko, Ed., Butterworths, London, 1970.
(3) "Electrons in Fluids", Proceedings of Colloque Weyl III on Metal-Ammonia Solutions, J. Jortner and N. R. Kestner, Ed., Springer-Verlag, Heidelberg, 1973, p 257.
(4) M. H. Cohen and J. C. Thompson, *Adv. Phys.*, **17**, 857 (1968).
(5) R. Catteral and N. F. Mott, *Adv. Phys.*, **18**, 665 (1969).
(6) N. F. Mott, "Metal-Insulator Transitions", Taylor and Francis, London, 1974.
(7) H. Endo, A. I. Eatah, J. G. Wright, and N. Cusack, *J. Phys. Soc. Jpn.*, **34**, 666 (1973).
(8) V. K. S. Shante and S. Kirkpatrick, *Adv. Phys.*, **20**, 325 (1971).
(9) R. Zallen and H. Scher, *Phys. Rev., B*, **4**, 4471 (1971).
(10) S. Kirkpatrick, *Phys. Rev. Lett.*, **27**, 1722 (1971).
(11) S. Kirkpatrick, *Rev. Mod. Phys.*, **45**, 574 (1973).
(12) A. S. Skall, B. I. Shlovskii, and A. L. Efros, *JETP Lett.*, **17**, 522 (1973).
(13) I. Webman, J. Jortner, and Morrel H. Cohen, *Phys. Rev. B*, **11**, 2885 (1975).
(14) F. Hensel and E. U. Franck, *Ber. Bunsenges. Phys. Chem.*, **70**, 1154 (1966).
(15) R. Schmutzler, F. Hensel, and E. U. Franck, *Ber. Bunsenges. Phys. Chem.*, **72**, 1194 (1968).
(16) E. U. Franck and F. Hensel, *Phys. Rev.*, **147**, 109 (1967).
(17) R. W. Schmutzler and F. Hensel, *Ber. Bunsenges. Phys. Chem.*, **76**, 347 (1972).
(18) F. Hensel and R. W. Schmutzler, *J. Non-Cryst. Solids*, **8–10**, 718 (1972).
(19) F. Hensel, *Phys. Lett.*, **31**, 88 (1970).
(20) U. Even and J. Jortner, *Phys. Rev. Lett.*, **28**, 31 (1972); *Phys. Rev. B*, **8**, 2536 (1973).
(21) U. Even and J. Jortner, *Phil. Mag.*, **25**, 715 (1972).
(22) M. Zillgit, Thesis, Karlsruhe University, Germany, 1972.
(23) M. Zillgit and F. Hensel, submitted for publication.
(24) U. Even and J. Jortner, *Phil. Mag.*, **30**, 325 (1974).
(25) W. Freyland, H. P. Pfeiffer, and F. Hensel, "Proceedings of the Fifth International Conference on Amorphous and Liquid Semiconductors", Taylor and Francis, London, 1974.
(26) J. C. Thompson, *Rev. Mod. Phys.*, **40**, 704 (1968).
(27) J. C. Thompson, ref 49, p 231.
(28) C. A. Kraus, *J. Am. Chem. Soc.*, **43**, 741 (1921).
(29) C. A. Kraus and W. W. Lucasse, *J. Am. Chem. Soc.*, **43**, 2529 (1921).
(30) G. Lepoutre and J. P. Lelieur, ref 2, p 369.
(31) G. Lepoutre, ref 3, p 193.
(32) D. S. Kyser and J. C. Thompson, *J. Chem. Phys.*, **42**, 3910 (1965).
(33) R. D. Nasby and J. C. Thompson, *J. Chem. Phys.*, **53**, 109 (1970).
(34) J. A. Vanderhoff and J. C. Thompson, *J. Chem. Phys.*, **55**, 105 (1971).
(35) R. D. Nasby and J. C. Thompson, *J. Chem. Phys.*, **49**, 969 (1968).
(36) J. A. Morgan, J. A. Schroeder, and J. C. Thompson, *J. Chem. Phys.*, **43**, 4494 (1965).
(37) R. L. Schroeder, J. C. Thompson, and P. L. Oertel, *Phys. Rev.*, **178**, 298 (1969).
(38) J. Castel, J. P. Lelieur, and G. Lepoutre, *J. Phys. (Paris)*, **32**, 211 (1971).
(39) J. P. Lelieur, Ph.D. Thesis, Lille, 1972.
(40) J. P. Lelieur, ref 2b, p 305.
(41) J. P. Lelieur and P. Rigny, *J. Chem. Phys.*, **59**, 1142 (1974).
(42) J. P. Lelieur, *J. Chem. Phys.*, **59**, 1148 (1974).
(43) P. G. Varlashkin and J. C. Thompson, *J. Chem. Phys.*, **38**, 1904 (1963).
(44) J. F. Dewald and G. Lepoutre, *J. Am. Chem. Soc.*, **76**, 3369 (1954); **78**, 2956 (1956).
(45) J. P. Lelieur, P. Damey, and G. Lepoutre, ref 47, p 203.
(46) T. A. Beckman and K. S. Pitzer, *J. Phys. Chem.*, **65**, 1527 (1961).
(47) W. T. Cromenweth and J. C. Thompson, *Adv. Phys.*, **16**, 439 (1967).
(48) R. B. Samoans and J. C. Thompson, *Phys. Rev. A*, **1**, 376 (1970).
(49) N. F. Mott, *Proc. Phys. Soc., Ser. A*, **62**, 416 (1949).
(50) N. F. Mott, *Adv. Phys.*, **16**, 49 (1967).
(51) N. F. Mott, *Phil. Mag.*, **17**, 1259 (1966).
(52) N. F. Mott, *Phil. Mag.*, **17**, 1015 (1972).
(53) N. F. Mott, *Phil. Mag.*, **24**, 1 (1971).
(54) N. F. Mott, *Phil. Mag.*, **19**, 835 (1969).
(55) N. F. Mott, *Phil. Mag.*, **29**, 613 (1974).
(56) N. F. Mott, *Phil. Mag.*, **31**, 217 (1975).
(57) N. F. Mott, *Phys. Rev. Lett.*, **31**, 466 (1973).
(58) M. H. Cohen and J. Jortner, *Phys. Rev. Lett.*, **30**, 699 (1973).
(59) M. H. Cohen and J. Jortner, *Phys. Rev. A*, **10**, 978 (1974).
(60) J. Jortner and M. H. Cohen, *J. Chem. Phys.*, **58**, 5170 (1973); and submitted for publication.
(61) M. H. Cohen and J. Jortner, "Proceedings of the Fifth International Conference on Amorphous and Liquid Semiconductors", Taylor and Francis, London, 1974, p 167.
(62) M. H. Cohen and J. Jortner, *J. Phys. (Paris)*, **35**, C4-345 (1974).
(63) I. Webman, M. H. Cohen, and J. Jortner, submitted to *Phys. Rev.*
(64) (a) J. M. Ziman, *Phil. Mag.*, **6**, 1013 (1961); (b) *Adv. Phys.*, **16**, 578 (1967).
(65) T. E. Faber, *Adv. Phys.*, **15**, 547 (1966).
(66) H. Fukuyama, H. Ebisawa, and J. Wada, *Prof. Theor. Phys.*, **42**, 497 (1968).
(67) L. Ballentine, to be submitted for publication.
(68) A. F. Ioffe and A. R. Regel, *Profiles Semiconductors*, **4**, 237 (1960).
(69) M. H. Cohen, *J. Non-Cryst. Solids*, **4**, 391 (1970).
(70) L. Friedman, *J. Non-Cryst. Solids*, **6**, 329 (1971).
(71) U. Even and J. Jortner, *Phys. Rev. B*, **8**, 2536 (1973).

(72) C. Varea de Alvarez and J. Keller, to be submitted for publication.
(73) M. H. Cohen, H. Fritzsche, and S. R. Ovshinsky, *Phys. Rev. Lett.*, **22**, 1065 (1969).
(74) M. Cutler and N. F. Mott, *Phys. Rev.*, **181**, 1330 (1969).
(75) V. Ambegaokar, B. I. Halpern, and J. S. Langer, *Phys. Rev. B*, **4**, 2612 (1971).
(76) W. Brenig, "Proceedings of the Fifth International Conference on Amorphous and Liquid Semiconductors", Taylor and Francis, London, 1974, p 31.
(77) V. El-Hamany and W. W. Warren, *Phys. Rev. Lett.*, **34**, 1276 (1975).
(78) (a) G. Lepoutre and J. P. Lelieur, ref 2b p 369; (b) G. Lepoutre, ref 3, p 193.
(79) J. C. Thompson, ref 2a, p 307.
(80) N. W. Ashcroft and G. Russakoff, *Phys. Rev. A*, **1**, 39 (1970).
(81) R. L. Schraeder and J. C. Thompson, *Phys. Rev.*, **179**, 124 (1971).
(82) D. A. Copeland, N. R. Kestner, and J. Jortner, *J. Chem. Phys.*, **53**, 1189 (1970).
(83) J. C. Thompson and K. Ichikawa, *J. Chem. Phys.*, **59**, 1680 (1973).
(84) J. P. Lelieur and P. Rigny, *J. Chem. Phys.*, **59**, 1142 (1973).
(85) J. C. Thompson and J. P. Lelieur, *J. Phys. (Paris)*, **35**, C4-371 (1974).
(86) R. Turner, *J. Phys. F*, **3**, L57 (1973).
(87) P. W. Schmidt, *J. Chem. Phys.*, **27**, 23 (1957).
(88) P. Chieux, *Phys. Lett. A*, in press.
(89) (a) D. E. Bowen, *Phys. Lett.*, in press; (b) P. J. Sams, J. E. Rassing, and E. Wyn-Jones, *Adv. Mol. Relaxation Processes*, **6**, 255 (1975).
(90) H. Weyl, *Math. Ann.*, **71**, 441 (1912).
(91) M. H. Cohen and J. Sak, *J. Non-Cryst. Solids*, **8–10**, 696 (1972).
(92) D. A. G. Bruggeman, *Ann. Phys. (Leipzig)*, **24**, 636 (1935).
(93) V. I. Odelevskii, *J. Tech. Phys. (USSR)*, **21**, 678 (1951).
(94) R. Landauer, *J. Appl. Phys.*, **23**, 779 (1952).
(95) H. J. Juretschki, R. Landauer, and J. A. Swanson, *J. Appl. Phys.*, **27**, 838 (1956).
(96) T. P. Eggarter, *Phys. Rev. A*, **5**, 2496 (1972).
(97) M. H. Cohen and J. Jortner, *Phys. Rev. Lett.*, **30**, 696 (1973).
(98) M. H. Cohen and J. Jortner, to be submitted for publication.
(99) M. H. Cohen, I. Webman, and J. Jortner, to be submitted for publication.
(100) M. H. Cohen and J. Jortner, to be submitted for publication.
(101) D. E. Bowen, ref 2b, p 355.
(102) D. E. Bowen, private communication.
(103) D. W. Mehaffy and D. A. Jerde, *Rev. Mod. Phys.*, **40**, 710 (1968).

Discussion

G. LEPOUTRE. What would be the crucial experiment which would discriminate between the bimodal and unimodal models?

J. JORTNER. Structural data such as those of Chieux, but at smaller angles.

S. O. NIELSEN. Could you elaborate on the tunneling correction to your model and its dependence on b?

J. JORTNER. The validity of our physical picture of a continuous metal–nonmetal transition via the inhomogeneous transport regime was challenged by Mott, who argued that tunneling effects will erode local electronic structure and local transport properties. Indeed, if tunneling effects across nonmetallic regions were important, the local nonmetallic conductivity would be shortened by tunneling and the quantitative details in our theory would be wrong. We have advanced two complementary treatments of the tunneling problem. First, we have demonstrated that for a disordered model system characterized either by large potential fluctuation or by a large correlation length b, tunneling effects are negligible. In this context we have treated an electron in the field of a Gaussian distribution of local potentials [M. H. Cohen and J. Jortner, *J. Phys.*, **35**, C4-345 (1974)]. Tunneling corrections are negligible provided that

$$(b/\text{Å})(\zeta/\text{eV})^2 > 4 \qquad (1)$$

where ζ^2 is the rms of the potential fluctuations. Thus for $\zeta = 0.1$ eV tunneling effects can be disregarded provided that $b > 6$ Å, while for larger potential fluctuations the correlation length which satisfies eq 1 is even smaller. Second, we have explicitly considered tunneling corrections for the specific systems treated by us in detail. In that process we have utilized the values of b extracted from the analysis of the transport data and found that tunneling effects are indeed negligible. We assert that Mott's objection to our approach can be refuted.

The Metal–Insulator Transition in Metal–Ammonia Solutions

N. F. Mott

Cavendish Laboratory, University of Cambridge, Cambridge, England

Publication costs assisted by Cavendish Laboratory

An outline of our present knowledge of the behavior of the electrical properties of noncrystalline systems is given, and an attempt is made to apply it to metal–ammonia solutions. The solubility gap in metal–ammonia is, we believe, a direct and necessary consequence of any metal–insulator transition of band-crossing or Mott type; but above the consolute temperature the transition becomes of the Anderson type. In the range of concentration where d log σ/dT is large, an extra electron is thought to jump from one diamagnetic pair to another. A model is proposed in which the activation energy is partly of polaron type.

Metal-insulator transitions have now been studied in many noncrystalline systems, and it seems to the present author that, in spite of some unsolved problems relating for instance to the Hall effect, enough theoretical and experimental information is available to give us a fair idea of how such systems behave. Among these noncrystalline systems metal–ammonia solutions are perhaps the most complicated. The available experimental information is exceptionally extensive, but to interpret it the theory of electrons moving in a rigid noncrystalline medium may be insufficient, because the electrons themselves create their own environment. It was first shown by Jortner[1] that, for low concentrations of metal, each electron is trapped in a cavity of its own creation, the surrounding ammonia being polarized. For the interpretation of the metal-insulator transition, it may be necessary to assume that moving electrons carry

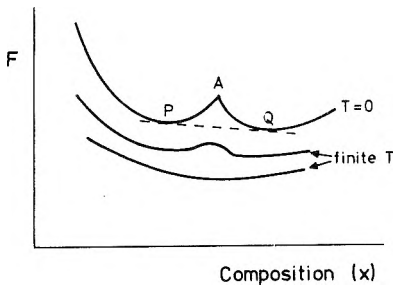

Figure 1. Free energy F of an alloy system plotted against composition x in the neighborhood of a metal-insulator transition (schematic). The discontinuity in n occurs at A.

some sort of polaron with them. A full description of the phenomenon must also include Anderson's[2] ideas on localization, those of Mott,[3] Hubbard,[4] and of Brinkman and Rice[5,6] on the effect of interaction between electrons, and some adaptation of the concept of the polaron to electrons in fluids. My aim in this paper will be to give an outline of what has been deduced about these matters from the study of simpler systems, and to show how this information can be used to give a qualitative description of the transition in metal–ammonia. This differs from that[3] put forward by the author earlier, mainly through the introduction of the polaron concept for moving electrons. It is not my aim to try to produce detailed agreement with experiment, and indeed we think this would be a very difficult computational task; my aim is rather to compare metal–ammonia with other systems and to see where they are similar and where they differ.

Inevitably this paper must be controversial; Cohen and coworkers have put forward a number of papers, some applied specifically to metal–ammonia (Cohen and Thompson,[7] Jortner and Cohen,[8] Webman, Jortner, and Cohen[9]) and others applied to noncrystalline systems in general, in which it is claimed that under certain conditions, and specifically for metal–ammonia, a treatment of conductivity by classical percolation theory is possible. I believe that for metal–ammonia this is unlikely to be so, and that their error lies in a failure to take account of the nature of tunnelling near an "Anderson transition";[3] indeed their latest paper makes no reference to the many papers[43] where this is considered.[10-13] I shall come back to their work later.

I shall first discuss metal-insulator transitions in crystalline systems. These are of two kinds, which I designate as "band-crossing" and "Mott–Hubbard". If a transition occurs as the volume changes or in an alloy system as a function of composition, the transition is believed to be first order. Though I[14] proposed this as long ago as 1949, the full understanding comes from a paper by Brinkman and Rice,[6] which considers electron-hole droplets in crystalline germanium. Taking the case of band-crossing transitions, these authors imagine a situation where the band-gap ΔE is varied, for instance, due to a change of composition. As soon as ΔE becomes comparable with the energy needed to form an exciton (constant$\cdot me^4/2\hbar^2\kappa^2$, κ = dielectric constant), some sort of excitonic phase will form, and this is usually a condensed gas of electrons and holes, the number n of each per unit volume being given by the equation

$$n^{1/3}a_H \simeq \text{constant}$$

where $a_H = \kappa\hbar^2/me^2$ and the constant depends on the form of the energy surfaces in k-space and is of order 0.2. Exactly the same is true for one-electron centers, where the

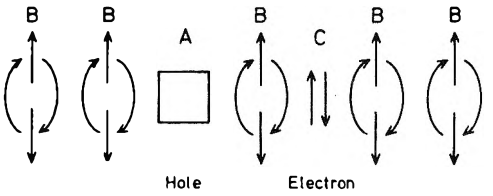

Figure 2. Showing Brinkman–Rice model of highly correlated electron gas; the arrows represent spin directions. A is a "hole"; B's are resonating spins; C is an electron.

"bands" are Hubbard bands. The transition can be from an antiferromagnetic metal (NiS_2, Gautier et al.[15]) or from a metal without magnetic order (V_2O_3, McWhan and Rice[16]).

An example of a discontinuous transition with change of composition from nonmetallic to metallic behavior is provided by the work of Endo et al.[17] on evaporated amorphous films of Cu–Ar. This system is noncrystalline. In some other noncrystalline systems (Si:P) there is no discontinuity, for a reason which is not entirely clear, though it seems that if the disorder is great enough the discontinuity disappears. When there is a discontinuity, the free energy–volume curve must *necessarily* show a kink as in Figure 1. Thus in an alloy system there *must* be a two-phase region (between P and Q in Figure 1), and the discontinuous change in n as a function of x can only be observed in the unstable region. We have little doubt that the solubility gap in metal–ammonia solutions must be due in principle to this cause. Unfortunately, no quantitative estimate exists of the form or magnitude of the solubility gap expected, except that if T_c is the temperature of the consolute point, kT_c should be of the order of the degeneracy temperature of the electron gas. Since, if m^* is the effective mass, this is

$$\frac{3}{5}\frac{\hbar^2 n^{2/3}}{m^*} \sim \frac{3\hbar^2}{5m^*}(0.2/a_H)^2 \sim 0.05m^*e^4/2\hbar^2\kappa^2$$

The experimental value (0.02 eV) would imply $\kappa \sim 5.5\ (m^*/m)^{1/2}$. Here κ should be some mean of the high frequency and static dielectric constant.

In materials containing centers each with a single localized electron, the tendency to form pairs is very marked. In Ti_4O_7, where there is an equal number of Ti^{3+} and Ti^{4+}, a range of temperature exists where mobile diamagnetic pairs carry a current (Schlenker et al.[18]). In VO_2 the interpretation of the metal-insulator transition given by Zylberzstejn and Mott[19] is that the band gap is determined by the Hubbard[44] U, and in some alloys of type $(V_{1-x}Cr_x)O_2$ a "Mott transition" occurs, but that normally an "antiferromagnetic insulator" is not observed because the V^{4+} ions form pairs. In metal–ammonia the drop in the ESR signal and in the magnetic susceptibility with increasing concentration is well known, and it is widely recognized that electrons in cavities form diamagnetic pairs.

Another important contribution to the theory also due to Brinkman and Rice[5] is that of the "highly correlated metal". According to them, an array of one-electron atoms, as it approaches the concentration for the (Mott) metal-insulator transition, has the configuration shown in Figure 2. Only a few of the sites carry two (or no) electrons and most contain only one, of which the spin resonates between its two positions. Such an electron gas has a highly enhanced paramagnetism; one way of understanding this is to say that each of the "carriers" forms a spin polaron of moment μ/x, where x is the proportion of doubly occupied

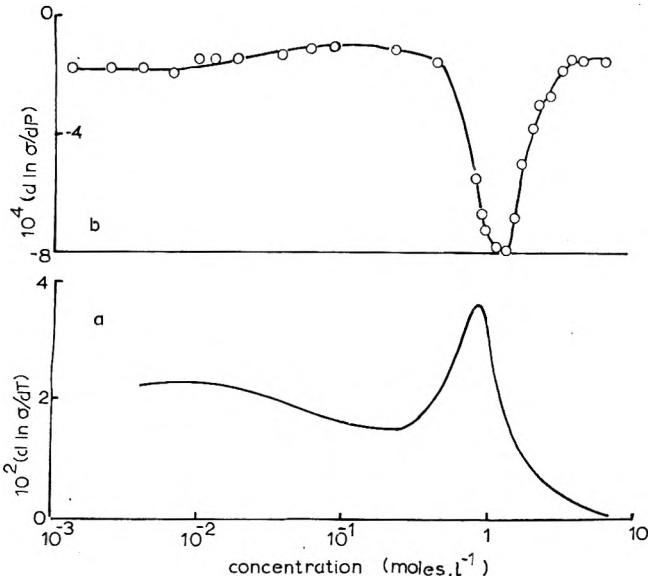

Figure 3. Pressure and temperature variation of the conductivity of $NaNH_3$. (Top) in $atm^{-1} \times 10^4$; (bottom) in $deg^{-1} \times 10^2$. Reproduced from ref 3.

sites, and the Pauli susceptibility is $Nx(\mu/x)^2/E_F$, which increases for small x. This enhancement of the magnetism is observed for Si:P near the transition and explained in this way by Chao and Berggren.[20] But the susceptibility of $Na-NH_3$ in the metallic region *decreases* as we approach the transition, as shown by direct measurements and by the Knight shift. This can only mean that, as soon as the electron gas becomes highly correlated, diamagnetic pairs begin to form. In fact, we must probably think of the metallic electron gas as consisting of an assembly of diamagnetic paired cavities, some of which contain an extra electron which can move from one to another and provide the metallic carriers. So the transition will have the electrical and magnetic characteristics rather of a band-crossing transition than a Mott transition, though a Hubbard U (as in VO_2) plays a major role in determining the gap, and is responsible for the two-phase region.

We are chiefly interested in this paper in the characteristics of the metal-insulator transition at temperatures above T_c and in particular the dependence of conductivity and thermopower[21] on concentration shown in Figure 3. To understand this we must examine the effects of disorder on a band-crossing transition. Disorder allows the occurrence of a kind of transition known as the "Anderson transition". According to Mott,[22] Cohen, Fritzsche, and Ovshinsky,[23] and quantitative calculations by Abou-Chacra and Thouless,[24] any form of disorder introduces into an energy band a range of *localized* states in the Anderson sense, which are separated from nonlocalized states by a "mobility edge" E_c (Figure 4). An Anderson transition occurs if the band is filled up to a limiting (Fermi) energy E_F, which can be varied so that $E_F - E_c$ changes sign. This can be done in the impurity band of doped and compensated germanium or silicon by varying the compensation, or at the Si/SiO_2 interface in a MOSFET device by varying the gate voltage.[25,26] The behavior of the resistivity is then as in Figure 5. If $E_F < E_c$, conductivity is of the form, at high temperatures,

$$\sigma_0 \exp(-\epsilon/\kappa T) \qquad \epsilon = E_c - E_F \tag{1}$$

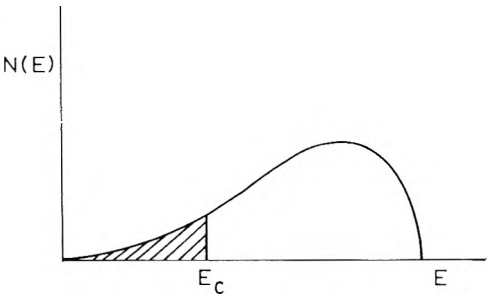

Figure 4. Conduction band, with mobility edge E_c and localized states shaded.

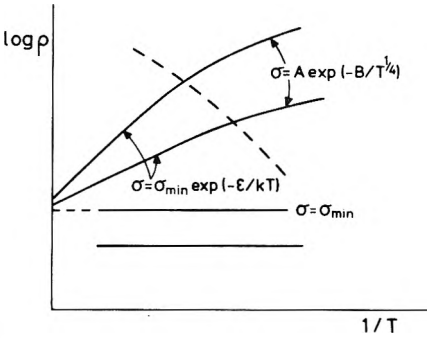

Figure 5. Typical behavior of resistivity ρ at an Anderson transition. The dotted line shows the transition between transport by carriers at mobility edge [$\rho = C \exp(+\epsilon/kT)$] and variable-range hopping [$\rho = C \exp(+\lambda/T^{1/4})$].

and at low temperatures

$$\sigma_1 \exp(-\lambda/T^{1/4}) \qquad \sigma_0 = \sigma_{min} \tag{2}$$

(in two dimensions $T^{1/4}$ becomes $T^{1/3}$). If $E_c > E_F$, conduction is metallic. A "minimum metallic conductivity"[3,27] appears, given by

$$\sigma_{min} \simeq \text{constant} \times e^2/\hbar a \tag{3}$$

with the constant in the range 0.026–0.1, or $0.1e^2/\hbar$ in two dimensions.[25] Essentially this is obtained from the idea that the mean free path L cannot be less than the distance between atoms, so that the conductivity ne^2L/mv becomes proportional to $e^2/\hbar a$, when n is taken proportional to k_F^3, mv to $\hbar k_F$, and k_F to $1/a$; k_F is the Fermi wavenumber; the numerical factor in (3) depends on the Anderson localization criterion and other considerations, but is probably a universal constant in two dimensions.

The existence of a "minimum metallic conductivity", of order 1000 Ω^{-1} cm^{-1} if $a \simeq 4$ Å, seems to be confirmed by a great many measurements as the lowest nonzero value of the conductivity as $T \to 0$. Its existence is queried by Cohen and coworkers on the following grounds. They suppose that statistical fluctuations must, near the Anderson transition, produce opaque regions through which there is no tunnelling, so that classical percolation theory can be applied. The limiting value of the conductivity as $T \to 0$ will thus drop continuously to zero as $E_F - E_c \to 0$, instead of discontinuously as in Figure 5. In making this prediction, they appear not to accept theoretical results[8,10–13] on the behavior of the *localized* wave functions when $E_c - E_F$ is small. We write one of these functions

$$\Psi = e^{-\alpha r} \Sigma a_n \phi_n \tag{4}$$

where in a tight-binding approximation ϕ_n are atomic wave functions and the a_n have random phases. Mott and

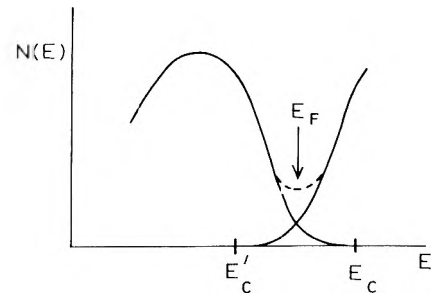

Figure 6. Density of states for noncrystalline semimetal with overlapping bands.

Davis[28] first suggested that α must tend to zero as $\epsilon \rightarrow 0$, and the investigations quoted show that

$$\alpha/\alpha_0 \simeq \{(E_c - E_F)/E_c\}^{0.6} \quad (5)$$

(the index is 0.7 in two dimensions[13]); α_0 is here the value for an isolated center, for the small fluctuations of the concentration likely between one *large* volume and another will be very small, and it is easy to show[27] that $\alpha R \ll 1$ for all but improbable fluctuations. In metal–ammonia, Jortner and Cohen make use of experimental data for the extent and magnitude of the fluctuations, and suppose that the nonmetallic regions have values of α equal effectively to α_0. Since the fluctuations are of order 5%, we think that α should be *at most*

$$\alpha \sim (0.05)^{0.6}\alpha_0$$

$$\sim 0.2\alpha_0$$

which means, contrary to what they say, that tunnelling through the "nonmetallic" fluctuations would be quite easy.

Of course, for *large* fluctuations, the theory must go over continuously to a situation when classical percolation does apply; how this will occur I have discussed elsewhere,[3,29] but it seems to me that Jortner and Cohen have left out of account an important property of the wave functions near a mobility edge, and the excellent agreement with some of the experimental evidence that they obtain I personally would regard as fortuitous.

We now go on to examine the effect of disorder on a band-crossing transition. The two bands will have localized tails, as in Figure 4, giving a pseudogap (shown in Figure 6). The conductivity is expected to behave as in Figure 5. The present author has defined the quantity

$$g = N(E_F)/N(E_F)_{free} \quad (6)$$

as giving the depth of the pseudogap. If states at the Fermi energy are not localized, but the mean free path has its minimum value a, the conductivity is given by

$$\sigma = S_F e^2 a g^2/12\pi^3\hbar = e^2 g^2/3\hbar a$$

One can estimate the value of g at which localization sets in by equating this to σ_{min}, which one can write in the form

$$\sigma_{min} = 0.1(e^2/\hbar a)(B/V)_{crit}^2 \quad (7)$$

where $(B/V)_{crit}$ is the ratio of the bandwidth to the disorder parameter in the Anderson localization criterion. Thus

$$g = (B/V)_{crit} \times 3^{1/2}$$

The "best" value of $(B/V)_{crit}$ is $\frac{1}{2}$, so for localization[45] $g \simeq \frac{1}{3}$.

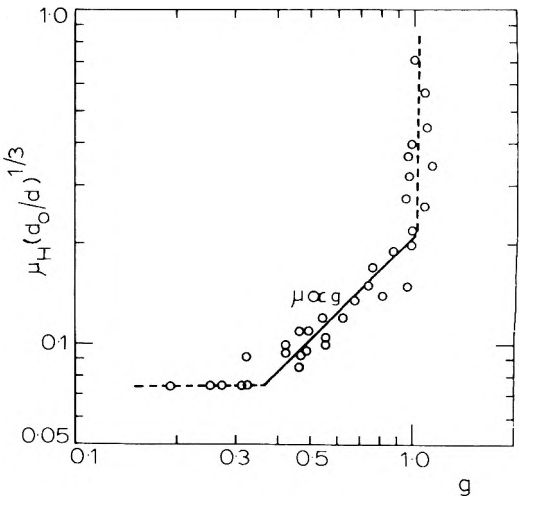

Figure 7. Hall mobility of expanded fluid mercury (Even and Jortner[33]).

Friedman[31] has discussed the Hall effect under these conditions and finds: (1) if conduction is metallic

$$R_H = 0.7/necg \quad (8)$$

(2) if conduction is due to electrons excited to the mobility edge, the Hall mobility is

$$\mu_H = 0.1ea^2/\hbar \quad (9)$$

A system in which these predictions are in quite surprising agreement with experiment is expanded fluid mercury, which has been investigated at high temperatures by Hensel and coworkers[32] and by Even and Jortner.[33] For an interpretation, see Mott.[34] As the specific volume increases, a pseudogap forms and there is a "metallic" range where $\sigma \propto g^2$, $\mu_H \propto g$. There is a sudden change in the behavior of μ_H when g (as deduced from the observed conductivity) becomes equal to $\frac{1}{3}$; this is shown in Figure 7. This we interpret as the Anderson transition, occurring when states first become localized at E_F, and the constant Hall mobility as given by (9), the variation of a being small in this range.

We turn now to the metal-insulator transition in $NaNH_3$. Figure 4 shows the well-known results of Schindewolf et al.[21] on the pressure and temperature dependence of the conductivity. We think that we have here a straightforward Anderson transition; at 2–3 mol $l.^{-1}$, d log σ/dT begins to rise, and we could interpret this as the opening up of a gap, $\epsilon = E_c - E_F$ becoming positive. Since d ln σ/d ln T is in the range 5 to 10, ϵ must be about 5–10 kT, or $\frac{1}{6}$ to $\frac{1}{3}$ eV. This interpretation is confirmed by the change of sign[35] of dS/dT, where S is the thermopower, shown in Figure 8. For S in the semiconducting region we expect

$$S = (k/e)\{\epsilon/kT + A\} \quad (10)$$

where $A = 1$ for electrons at a mobility edge.[28] Figure 8 suggests that ϵ is only of order kT, much smaller than for the conductivity.

A discrepancy between the thermopower activation energy and that deduced from the conductivity in semiconductors often occurs in the literature (e.g., for MnO),[36] and is usually ascribed to the formation of polarons, so that the activation energy for conduction includes the polaron hopping energy W_H, while that for the thermopower does not. If this is the correct description for $NaNH_3$, we could propose the following model in the region of the maximum of d

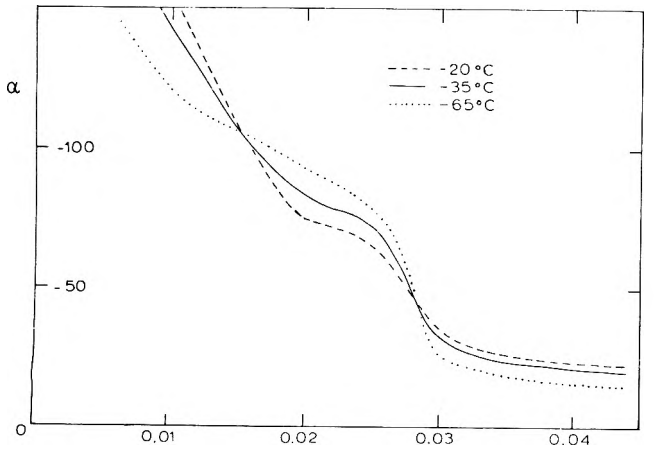

Figure 8. Thermopower of $NaNH_3$. Reproduced from ref 3.

log σ/dT. The ground state of the system consists of paired cavities. A small activation energy (that for the thermopower) is needed to form a pair carrying an extra electron. This electron is free to jump from one pair to another; but since it distorts the pair, by expanding the cavity, a polaron-type energy W_H is needed for the jump. The pressure-dependence (Figure 4) will arise because the extra electron will expand the two cavities, and therefore under pressure a greater energy is required to put the electron there. For a hopping process of this kind, probably $A \simeq 0$ in eq 10.

If this is a correct model, then for concentrations above that for the Anderson transition, the proportionality between R_H and g proposed by Acrivos and Mott[37] can still be maintained. But as soon as an excitation energy occurs in σ, conduction is by polaron hopping, and we can *not* expect the range of constant μ_H observed in mercury; it is not observed, μ_H continuing to drop, as pointed out by Jortner and Cohen[8] (but it is doubtful whether measurements at low enough concentrations have been made). The theory of the Hall effect in the case of polaron hopping has been investigated by Friedman and Holstein,[38] and they predict that μ_H should contain the term $\exp(\frac{1}{3} W_H/kT)$, a formula tested by experiment, as far as we know, in only two cases ($LiNbO_3$[39] and cerium sulfide[26,40,41]). A drop in μ_H with decreasing concentration might be due to this term.

In the low concentration region when d log σ/dT drops again, we suppose that conduction is by the drift of cavities and cavity pairs.

As I stated at the beginning, this treatment is far from giving any quantitative account of the phenomenon, such as is given so elegantly by the model of Jortner and Cohen. My aim has been to apply what one can learn from a wide study of other noncrystalline systems; I believe that, while too many effects have a role for a quantitative theory to be possible, it is possible to make some predictions that could be tested.

References and Notes

(1) J. Jortner, *J. Chem. Phys.*, **30**, 839 (1959).
(2) P. W. Anderson, *Phys. Rev.*, **109**, 1492 (1958).
(3) N. F. Mott, "Metal-Insulator Transitions", Taylor & Francis, London, 1974.
(4) J. Hubbard, *Proc. R. Soc. London, Ser. A*, **281**, 401 (1964).
(5) W. F. Brinkman and T. M. Rice, *Phys. Rev.*, **2**, 9302 (1970).
(6) W. F. Brinkman and T. M. Rice, *Phys. Rev.*, **7**, 1508 (1973).
(7) M. H. Cohen and J. C. Thompson, *Adv. Phys.*, **17**, 857 (1968).
(8) J. Jortner and M. H. Cohen, to be submitted for publication.
(9) I. Webman, J. Jortner, and M. H. Cohen, *Phys. Rev. B*, **11**, 2885 (1975).
(10) P. W. Anderson, *Proc. Nat. Acad. Sci.* U.S.A. **69**, 1097 (1972).
(11) R. A. Abram and S. F. Edwards, *J. Phys. C.*, **5**, 1183 (1972).
(12) T. Lukes, *J. Non-Cryst. Solids*, **8–10**, 470 (1972).
(13) R. A. Abram, *J. Phys. C.*, **6**, L379 (1973).
(14) N. F. Mott, *Proc. Phys. Soc., London, Sect. A*, **62**, 416 (1949).
(15) F. Gautier, G. Krill, M. F. Lapierre, P. Panissoll, C. Robert, G. Czjzek, J. Fink, and H. Schmidt, *Phys. Lett. A*, **53**, 31 (1975).
(16) D. B. McWhan and T. M. Rice, *Phys. Rev. Lett.*, **22**, 887 (1969).
(17) H. Endo, A. I. Eatah, J. G. Wright, and N. Cusack, *J. Phys. Soc. Jpn.* **34**, 666 (1973).
(18) C. Schlenker, S. Lakkis, J. M. D. Coey, and M. Marezio, *Phys. Rev. Lett.*, **32**, 1318 (1974).
(19) Z. Zylberzstejn and N. F. Mott, *Phys. Rev. B*, **11**, 4383 (1975).
(20) K. A. Chao and K. F. Berggren, to be submitted for publication.
(21) U. Schindewolf, K. W. Boddeker, and R. Vögelgesang, *Ber. Bunsenges. Phys. Chem.*, **70**, 1161 (1966).
(22) N. F. Mott, *Philos. Mag.*, **13**, 689 (1966).
(23) M. H. Cohen, H. Fritzsche, and S. R. Ovshinsky, *Phys. Rev. Lett.*, **22**, 1065 (1969).
(24) R. Abou-Chacra and D. J. Thouless, *J. Phys. C.*, **7**, 65 (1974).
(25) M. Pepper, S. Pollitt, C. J. Adkins, and R. E. Oakley, *Phys. Lett. A* **47**, 71 (1974); M. Pepper, S. Pollitt, and C. J. Adkins, *Phys. Lett. A*, **48**, 113 (1974); *J. Phys. C.*, **7**, L273 (1974).
(26) N. F. Mott, M. Pepper, S. Pollitt, R. H. Wallis, and C. J. Adkins, *Proc. R. Soc. London, Ser. A*, **345**, 169 (1975).
(27) N. F. Mott, *Philos. Mag.*, **26**, 1015 (1972).
(28) N. F. Mott and E. A. Davis, "Electronic Processes in Non-Crystalline Materials", Oxford University Press, London, 1971.
(29) N. F. Mott, *Philos. Mag.*, **3**, 613 (1974).
(30) M. H. Cohen in "Electrons in Fluids" (Colloque Weyl IV), N. R. Kestner and J. Jortner, Ed., Springer-Verlag, Berlin, 1974.
(31) L. Friedman, *J. Non-Cryst. Solids*, **6**, 329 (1971).
(32) F. Hensel and E. U. Franck, *Rev. Mod. Phys.*, **40**, 697 (1968); R. W. Schmutzler and F. Hensel, *J. Non-Cryst. Solids*, **8–10**, 531 (1972).
(33) J. Even and J. Jortner, *Philos. Mag.*, **28**, 715 (1972); *Phys. Rev. B*, **8**, 2536 (1973).
(34) N. F. Mott, *Philos. Mag.*, **31**, 217 (1975).
(35) P. Damay, Thesis (Lille), 1973.
(36) C. Crevecoeur and H. J. de Wit, *Solid State Commun.*, **6**, 2965 (1968).
(37) J. Acrivos and N. F. Mott, *Philos. Mag.*, **24**, 19 (1973).
(38) L. Friedman and T. Holstein, *Ann. Phys.*, **21**, 494 (1963).
(39) P. Nagels, R. Callaerts, and M. Denayer, to be submitted for publication.
(40) M. Cutler and J. F. Leavy, *Phys. Rev. A*, **133**, 1153 (1964).
(41) M. Cutler and N. F. Mott, *Phys. Rev.*, **181**, 1336 (1969).
(42) R. W. Schmutzler and F. Hensel, *J. Non-Cryst. Solids*, **8–10**, 718 (1972).
(43) These papers evaluate the rate of decay of a wave function as a disordered material, namely the quantity α in $\exp(-\alpha r)$. The same quantity should determine the tunnelling. Its behavior is as in eq 5 of this paper.
(44) This is defined as the average of the electrostatic repulsion between two electrons on the same site.
(45) Cohen[30] has described this numerical value as a conjecture, but given the concepts of Anderson localization and of a minimum metallic conductivity this is not so.

Microwave Electronic Properties of Metal–Ammonia Solutions

K. G. Breitschwerdt* and H. Radscheit

Institute für Angewandte Physik, Universität Heidelberg, Heidelberg, Germany *(Received June 20, 1975)*

The complex ac conductivity of a 0.1 MPM lithium–ammonia solution has been measured in the frequency range 1.2–70 GHz at temperatures between 198 and 293 K. Two theories for the ac conductivity, random range hopping and random barrier hopping in disordered systems, are used to analyze the experimental data. It is found that random barrier hopping with a distribution of electron relaxation times peaked around 10^{-10} sec gives good agreement between experimental and theoretical results.

I. Introduction

High-frequency conductivity measurements are an important means for obtaining information about the nature of the charge transport in metal–ammonia solutions at concentrations near the metal–nonmetal transition.[1] For the analysis of the experimental data, the theories of electron hopping between localized states,[2,3] which have been developed for the charge transport in amorphous materials, may be applied. In the present work, resonator perturbation measurements of the ac conductivity of a 0.1 MPM (mol percent metal) lithium–ammonia solution in the frequency range 1.2–70 GHz at temperatures between 198 and 293 K are reported.

Since the measured losses in the metal–ammonia solution consist of a number of contributions, corrections have to be made to obtain the electronic ac conductivity. The main contribution comes from the dc conductivity due to the electrons and ions in the solution. The dc conductivity of pure ammonia is comparatively small and may be neglected. The orientational polarization of the ammonia molecules causes a strong increase of the losses at frequencies near 10^{11} Hz. Experimentally only the sum of these losses can be measured, and the nonelectronic and dc contributions must be determined separately and subtracted from the total loss. Therefore the dc conductivity of the solutions had to be measured as well. The high-frequency losses of pure ammonia have been reported previously.[4]

II. Theory

Electron hopping between localized states in disordered systems may generally be described by a Debye model with a distribution of relaxation times.[2,5,6] In the following, it is assumed that no multiple hopping occurs, i.e., that all the hopping which contributes to the ac conductivity is contained within pairs of localized states. If r is the distance between two localized states, ΔE the potential difference, and W the potential barrier between them, the contribution of the electron hopping process to the complex conductivity is

$$\sigma(\omega) = [-i\omega/(1 - i\omega\tau)]D\Delta f \cos\theta \tag{1}$$

where τ is the relaxation time, $D = \frac{1}{2}er$ (the dipole moment), θ the angle between the direction of the dipole and the electric field, and Δf the change in the occupation probability of either state caused by a unit field strength. For the case $\Delta E \ll kT$, the difference Δf may be written as follows

$$\Delta f = \frac{1}{1 + \exp(\Delta E/kT)} \frac{D \cos\theta}{kT} \tag{2}$$

Averaging over the directions of n such independent pairs of possible electron sites per unit volume with a distribution of τ, ΔE, and D yields the following expression for the complex conductivity

$$\sigma(\omega) = -i \int \frac{\omega}{1 - i\omega\tau} \frac{nD^2}{3kT} \times \frac{1}{1 + \exp(\Delta E/kT)} p(\tau,\Delta E,D)\, d\tau\, d\Delta E\, dD \tag{3}$$

For small values of ΔE, the relaxation time τ does not depend on ΔE, so that integration over ΔE will only influence the temperature dependence of the conductivity but not the frequency dependence. Therefore, eq 3 can be written as follows:

$$\sigma(\omega) = -iC(T) \int \frac{\omega}{1 - i\omega\tau} D^2 p(\tau,D)\, d\tau\, dD \tag{4}$$

Two cases may be considered for the charge transport due to localized electrons: random range hopping and random barrier hopping.[7] In the case of random range hopping, the electron tunnels from one localized state to another. The tunneling probability is mainly determined by the overlap integral of the two localized wave functions. For an exponential decay of the wave functions with a decay constant α, the tunneling probability is proportional to $\exp(-2\alpha r)$, and the corresponding relaxation time is $\tau = \tau_0 \exp(2\alpha r)$. The probability of finding another localized state at a distance r is proportional to r^2 for a random distribution of localized states in three dimensions. Considering further that D^2 is also proportional to r^2, the real part of eq 4 is

$$\mathrm{Re}\ \sigma(\omega) = C'(T) \int \frac{\omega^2\tau}{1 + \omega^2\tau^2} r^4\, dr \tag{5}$$

Evaluation of the integrals yields the following results: for low frequencies, $\omega\tau_0 < 10^{-5}$, the conductivity is $\mathrm{Re}\ \sigma \propto \omega^s$, with $s \approx 0.8$. Such a power law has been found for a number of disordered systems.[8,9] At higher frequencies, $\omega\tau_0 > 10^{-2}$, the real part of conductivity is independent of frequency; i.e., a saturation of $\mathrm{Re}\ \sigma(\omega)$ occurs.

In the case of random barrier hopping, the hopping probability is proportional to $\exp(-W/kT)$, where W is the barrier height, and the corresponding relaxation time is $\tau = \tau_0 \exp(W/kT)$. For a uniform distribution of barrier heights, the analysis of eq 4 yields for lower frequencies, $\omega\tau_0 < 10^{-1}$,

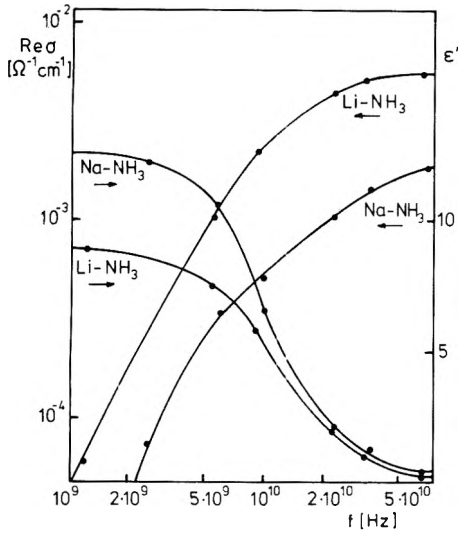

Figure 1. Conductivity Re $\sigma(\omega)$ and dielectric function $\epsilon'(\omega)$ vs. frequency for a 0.1 MPM $Li-NH_3$ and a 0.7 MPM $Na-NH_3$ solution at 238 K.

TABLE I: Conductivity Re $\sigma(\omega)$ and Dielectric Function $\epsilon'(\omega)$ for a 0.1 MPM $Li-NH_3$ Solution

	f, GHz					
	1.2	5.4	9.2	23.0	33.4	69.4
T, °K	Re $\sigma \times 10^4$ (Ω^{-1} cm^{-1})					
198	10.5	165	307	499	597	612
208	9.62	155	305	508	571	630
218	6.08	140	275	512	563	576
238	5.88	104	224	453	516	556
253	4.94	98.3	217	475	546	595
273	4.94	84.8	191	448	515	560
293	4.41	75.4	185	462	541	634
	ϵ'					
198	11.8	8.5	5.5	1.4	0.7	0.2
208	11.8	9.0	6.1	1.7	0.9	0.2
218	10.9	8.5	5.9	1.7	1.0	0.2
238	8.9	7.5	5.8	2.0	1.0	0.3
253	8.9	7.5	5.7	2.0	1.1	0.3
273	7.9	6.9	5.4	2.0	1.1	0.3
293	7.9	7.0	5.7	2.3	1.2	0.3

a power law similar to that found for random range hopping; the exponent is $s = 1$, however. The transition to saturation occurs at higher frequencies, $\omega\tau_0 \approx 10$, and in a narrower frequency range than in the case of random range hopping. For a peaked distribution of barrier heights, saturation begins at about $\omega\tau_m = 10$, where τ_m is the main relaxation time, and at lower frequencies the exponent is $s > 1$. In the extreme case of a δ-function distribution, the exponent is $s = 2$.

III. Results and Discussion

Real and imaginary parts of the electronic ac conductivity for a sodium–ammonia solution[10,11] and a lithium–ammonia solution are plotted vs. frequency in Figure 1. The imaginary part of $\sigma(\omega)$ is shown in the form of the dielectric function $\epsilon' = \text{Im } \sigma(\omega)/\omega\epsilon_0$. The complete results for the lithium–ammonia solutions are presented in Table I.

For both sodium–ammonia and lithium–ammonia solutions, the gradient of the conductivity curve is greater than 1, and at the highest frequencies, saturation occurs. The dielectric function $\epsilon'(\omega)$ is constant at lower frequencies and decreases in the frequency range where saturation begins. A Kramers–Kronig analysis shows that these frequency dependences of the real and imaginary part of conductivity are consistent with one another.

According to the theory presented in section II, both random range hopping and random barrier hopping lead to a saturation of the real part of conductivity. A gradient of the conductivity curve greater than 1 before saturation is only possible in the case of random barrier hopping, with a nonuniform distribution of barrier heights. A quantitative analysis indicates that there is a maximum in the distribution of barrier heights, so that relaxation times in the order of 10^{-10} sec are favored. From the temperature dependence of the conductivity, the dominant barrier height W is found to be approximately 0.03 eV. The frequency dependence of the conductivity at lower frequencies is required in order to determine the distribution of longer relaxation times, or larger barrier heights. The dielectric function $\epsilon'(\omega)$ is also in better agreement with random barrier hopping than with random range hopping. The latter model predicts a decrease of $\epsilon'(\omega)$ at lower frequencies than observed experimentally.

Acknowledgment. This work was supported in part by the Deutsche Forschungsgemeinschaft.

References and Notes

(1) J. Jortner and N. R. Kestner, Ed., "Electrons in Fluids", Springer-Verlag, Berlin, 1973.
(2) M. Pollak and T. H. Geballe, *Phys. Rev.*, **122**, 1742 (1961).
(3) N. F. Mott, *Philos. Mag.*, **19**, 835 (1969).
(4) K. G. Breitschwerdt and W. Schmidt, *Z. Naturforsch., Teil A*, **25**, 1467 (1970).
(5) N. F. Mott and E. A. Davis, "Electronic Processes in Non-Crystalline Materials", Clarendon Press, Oxford, 1971.
6. G. E. Pike, *Phys. Rev. B*, **6**, 1572 (1973).
(7) P. N. Butcher and P. L. Morys in "Amorphous and Liquid Semiconductors", J. Stuke and W. Brenig, Ed., Taylor and Francis, London, 1974, p 153.
(8) M. Pollak, *Philos. Mag.*, **23**, 519 (1971).
(9) H. Fritzsche in "Amorphous and Liquid Semiconductors", J. Tauc, Ed., Plenum Press, London, 1974, p 221.
(10) K. G. Breitschwerdt and H. Radscheit in ref 1, p 315.
(11) K. G. Breitschwerdt and H. Radscheit, *Ber. Bunsenges. Phys. Chem.*, **75**, 644 (1971).

Temperature and Pressure Dependence of the Nonmetal–Metal Transition in Sodium–Ammonia Solutions (Electrical Conductivity and Pressure–Volume–Temperature Data up to 150°C and 1000 Bars)

S. Hahne and U. Schindewolf*

Institut für Physikalische Chemie und Elektrochemie, Universität Karlsruhe, Karlsruhe, Germany *(Received July 23, 1975)*

Experimental details of the technique for collecting conductivity and PVT data of sodium–ammonia solutions up to 150°C and 1000 bars are given. The results can be summarized as follows: the specific conductivity σ of the solutions passes with increasing temperature through a maximum; the temperature of maximum conductivity is higher, the lower the concentration of the solution (120°C for 0.45 mol % metal (MPM), 0°C for 16.9 MPM). Below 30°C the density ρ of the solution decreases; above 60°C it increases with metal concentration. From the combination of σ and ρ data follows the molar conductivity Λ ($\sim\sigma/c$, c = molar concentration). The steep increase of the Λ/c curve, which is an indication of the nonmetal–metal transition (NMT), is shifted with increasing temperature to lower concentration (around 1.5 mol/l. at −30°C to around 0.3 mol/l. at 150°C); i.e., increasing temperature favors the NMT. Compression on the other hand, shifts the transition to higher concentrations; i.e., pressure disfavors the NMT. The temperature coefficient of Λ (d ln Λ/dT) as a function of concentration passes through a maximum at that concentration, where also the steepest slope of the Λ/c curve is found. In the concentration range of the NMT under normal conditions (0.2 to 3 MPM), the plots of ln σ vs. thermopower S and of d ln σ/dT vs. dS/dT (data taken from literature) have the slope of around e/k (e = electronic charge, k = Boltzmann constant) as to be expected for activated conduction. The reported conductivity data, especially at temperatures up to 200°C above the consulate point, do not support the percolation model but rather the qualitative theory of Mott for the interpretation of the NMT of the metal–ammonia solutions.

Considerable interest has arisen during the last years about the nature of the nonmetal–metal transition[1] (NMT) in semiconducting material, in fluid metals, and in metal–ammonia solutions (MAS), in which the electrical conductivity and other electrical transport properties can be varied in a wide range by change in composition or in volume. In MAS equivalent conductivity, Λ [($\sim\sigma/c$; σ = specific conductivity, c = molar concentration)], shows an increase by several powers of ten;[2] at low concentrations ($c < 0.1$ m or < 0.2 mol % metal (MPM)) these solutions exhibit the characteristics of an electrolyte with more or less constant equivalent conductivity (500–1000 Ω^{-1} cm^2 equiv^{-1}) as caused by the independent moving metal cations and solvated electrons, whereas at high concentrations (>5 m, >10 MPM) a metal-like behavior is found with high equivalent conductivity ($\approx 10^5$–10^6 Ω^{-1} cm^2 equiv^{-1}). The NMT is in the intermediate concentration range in which the equivalent conductivity increases strongly with concentration; it is accompanied, e.g., by abnormal, strong temperature and pressure dependencies of the conductivity, by a change of the thermoelectrical power, of the Hall coefficient, of heat conductivity, of light reflectivity, of magnetic susceptibility, etc. (see ref 3–6).

Several hypotheses and theories have been advanced to understand the NMT in MAS although a quantitative description explaining all experimental features is still missing. The most recent attempts are based on the concept of percolation theory[7] and on the theory of Mott on the Anderson transition,[1,8] respectively, both contrasting each other.

In the present investigation we have studied by conductivity measurements the temperature and pressure dependence of NMT in NaAS in the range up to 150°C and 1000 bars, hoping that the results might help to distinguish between the two opposing theories. The conductivity data were supplemented by PVT data.

The original goal was to go to supercritical conditions under which not only the metal but also the ammonia could be varied in a wide concentration range, thus learning about the influence of the dielectric ammonia on the NMT. This goal, however, had to be given up because the critical temperature of the binary system is so high that decomposition of the solutions cannot be controlled anymore.

Because of the decomposition catalyzed by metal surfaces for measurements at 150°C, a special technique had to be developed to avoid direct contact of the hot solutions with the cooled electrodes of the conductivity cell. The high-frequency method without metal electrodes was not successful, because at higher temperatures we could not get unambiguous results, as also observed by Naiditch.[9]

Experimental Procedures

(*a*) *Conductivity Measurements* (*Figure 1*). In principle, a high alternating current was passed through the solution contained in capillary a by which it could be heated up from −50 to +150°C within a few minutes. The capillary was surrounded by a thermal insulator b. The resistance of the solution followed from the current and from the voltage drop along the capillary (10 cm long, 6 mm i.d.). Attached to each end of the capillary were two wider glass compartments (20 mm i.d.) with gold electrodes c connected to a low-voltage (20 V), high-current (up to 100 A) transformer d. To obtain the voltage drop along capillary a, two platinum point electrodes e were sealed in just outside the capillary. Highly concentric in the inner portion of capillary a another capillary f (4 mm o.d.) was adjusted and attached

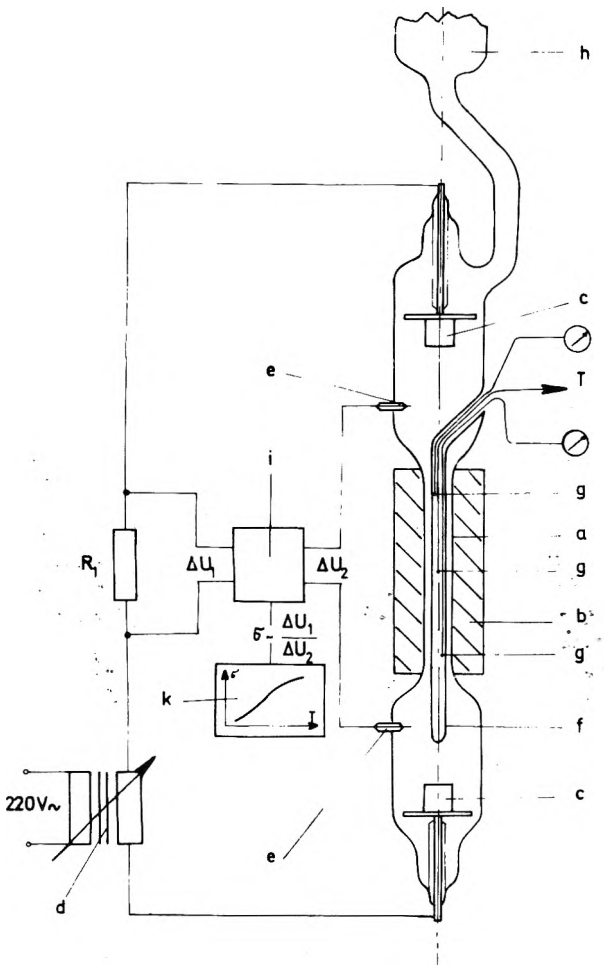

Figure 1. Conductivity cell (explanation in text).

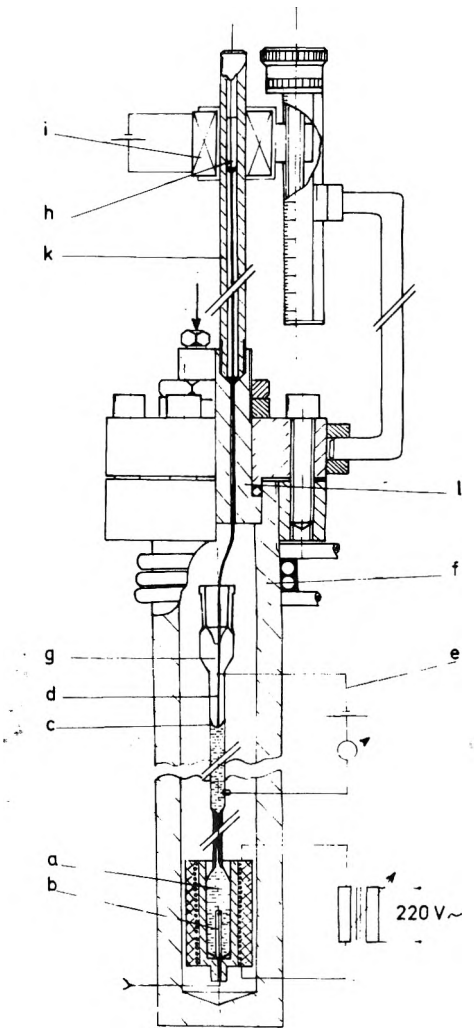

Figure 2. Cell for *PVT* data with upper section of the high-pressure autoclave (explanation in text).

to the upper electrode compartment. It could house three thermocouples g for temperature determination of the solution.

The cell was filled via h under vacuum with NaAS, prepared in a separate small glass container by multiple distillation of ammonia and sodium, and then was transferred to a cooled autoclave which with purified gas could be pressed up to 1500 bars. The electrodes and thermocouples were connected to insulated leads in the autoclave lit. Voltage drop and current signal were mixed in a divisor circuit i, the signal of which was recorded vs. the voltage of the thermocouple with an x–y recorder k, which so gave direct conductivity–temperature diagrams (error of resistivity readings 1%). The cell constant as measured with 0.1 *m* KCl and with mercury was 69.0 cm^{-1}.

Since the cross section of the electrode compartments was large relative to that of the capillary, the dissipated energy and therefore heating in the compartments was small. Because of the large cross section also, the potential drop between the platinum electrodes and capillary was small enough (less than 1% of that of the capillary) to be neglected.

The reproducibility of the curves obtained with one solution in several succeeding heating and cooling periods proves that decomposition of the solution or thermal demixing is negligible. Nevertheless, some error of the σ/T data must be assumed because the temperature reading of the two thermocouples close to the ends of the capillary was up to 5° lower than that in the middle of the capillary. Also a radial temperature gradient should influence the data. In view of the relatively large temperature range covered, we think the uncertainty of the temperature readings is not serious. Concentrations of the solutions were determined by conventional analysis and controlled by conductivity measurements under normal conditions[2] (experimental error 1%).

(*b*) *PVT Data* (*Figure* 2). The solution was filled into a 4-ml glass vessel electrically heatable from the outside. Temperature was read with a thermocouple b sealed in. The upper end of the vessel was over a capillary attached to an open glass tube c (5 mm i.d.), which was cooled and into which the solution could expand upon heating. The shift of the meniscus in this tube, which is a measure of the expansion of the solution in the vessel, was probed with a platinum wire d closing an electrical circuit e when contacting the solution. The system was housed in the same autoclave f in which the conductivity data were taken. The platinum wire was welded to a thin steel rod g, which at the upper end was attached to a ferrimagnet h. It could be moved without friction by an outside magnet i in the vertical stainless steel capillary k which was screwed in the autoclave lit (l), the upper end of which was closed. The position of the platinum wire or the height of the meniscus could be read from the position of the magnet to a preci-

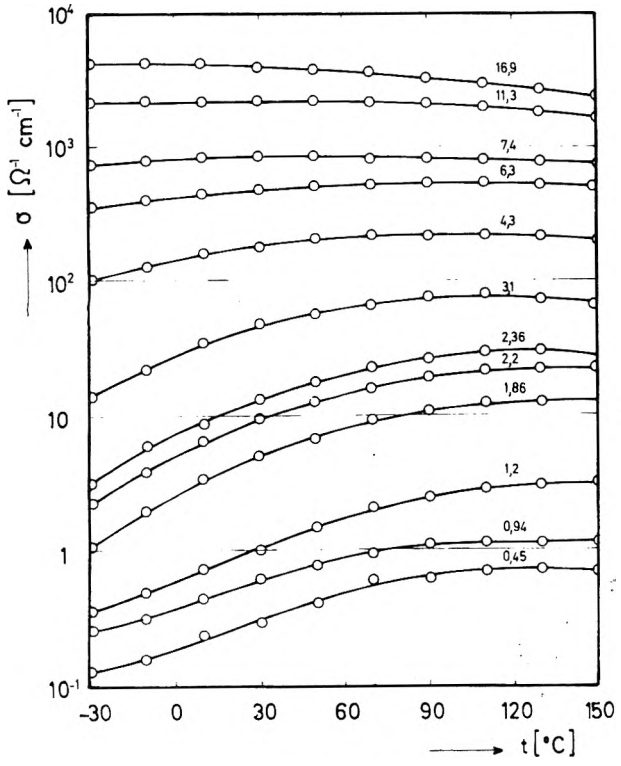

Figure 3. Specific conductivity of NaAS vs. temperature (200 bars); parameter is the Na concentration in MPM.

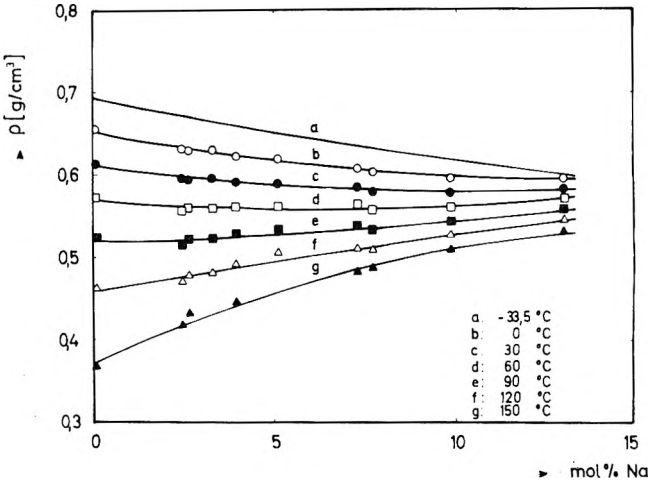

Figure 4. Density of NaAS vs. concentration (200 bars); parameter is the temperature.

sion of 0.1 mm. When thermal volume expansion was calculated by following the shift of the meniscus, the fact that the hot solution expanding into the cold glass tube contracts again was taken into consideration.

Conductivity data and *PVT* data were combined to give the equivalent conductance Λ of the solutions in the temperature and pressure ranges between −30 and 150°C and 200 to 1000 bars, respectively. The lower pressure limit is given by the vapor pressure of the ammonia at higher temperatures, which had to be compensated to avoid formation of vapor bubbles in the capillary. (Because the electrical current through the capillary is interrupted at the moment when the vapor pressure of the ammonia exceeds the outside pressure, the described cell also could be used for the determination of the vapor pressure curves of the metal–ammonia solutions at higher temperatures.) The error of the Λ data, e.g., in Figure 6, follows from the errors of σ and ρ; it is in all cases below 30%. The high error must be seen relative to changes of Λ which in the temperature range from −30 to 150°C varies by a factor of up to 100! It therefore does not invalidate any of the conclusions drawn from the experimental results.

Experimental Results

(*a*) *Specific Conductivity.* Figure 3 displays the temperature dependence of the specific conductivity σ of 0.45 to 16.9 MPM sodium–ammonia solutions under a pressure of 200 bars. At low concentrations, i.e., in nonmetallic solutions, the conductivity rises by a factor of around 10, reaching a maximum at the highest temperatures. For comparison, solutions of normal electrolytes, like potassium nitrate, under identical conditions gave only a 60% rise in conductivity, followed by a slight decrease. Here obviously the increase of the mobility of the ions due to decreased viscosity of the solvent is compensated by the decrease in volume concentration due to thermal expansion of the solutions. Since in the NaAS also the volume concentrations of the dissolved metal decreases with temperature, the observed conductivity increase is caused by a strong increase of the mobility of the electrons, indicating an activated conduction mechanism of the electrons. In concentrated solutions, the specific conductivity passes through a slight maximum at low temperatures; i.e., a change from a positive to a negative temperature coefficient of the conductivity is observed. Thus, the concentrated solutions display, at least at higher temperatures, the typical characteristics of a metal.

Our data taken at constant pressure are up to 70°C in fair agreement with the data of Naiditch[9] taken under the vapor pressure of the solutions. Deviations at higher temperatures are due to concentration changes of the solutions in Naiditch's experiments because of evaporation of ammonia.

Experimental data taken at 600 and 1000 bars are similar to those displayed in Figure 3 for 200 bars. However, in accordance with earlier experiments[10] at lower temperatures, pressure decreases the conductivity, the maximum negative pressure coefficient of the conductivity lying in the same concentration range as the maximum positive temperature coefficient. At higher temperatures, at which the thermally expanded solutions have a higher compressibility, a slight increase of conductivity is observed with pressure.

(*b*) *PVT Data.* The density–concentration relationship of the NaAS depends strongly on the temperature as follows from Figure 4, taken at 200 bars. Up to 30°C in accordance with older data,[11] density decreases with increasing concentration. This behavior which is in contrast to that of normal electrolytes is explained by the formation of cavities (radius $\simeq$ 3 to 3.5 Å) in which the electrons are caught.

At higher temperatures and relatively low pressures, the solvent already is so far expanded that the formation of cavities does not give rise to further volume expansion; the electrons can be housed in the structure holes of the solvent. Then the normal electrostriction effect of charged particles is effective; the solution density increases with concentration.

Under higher pressures, the density–concentration curves have the same tendency; they are, of course, shifted to higher densities and are lying closer together because pressure counteracts the structure-loosening effect of elec-

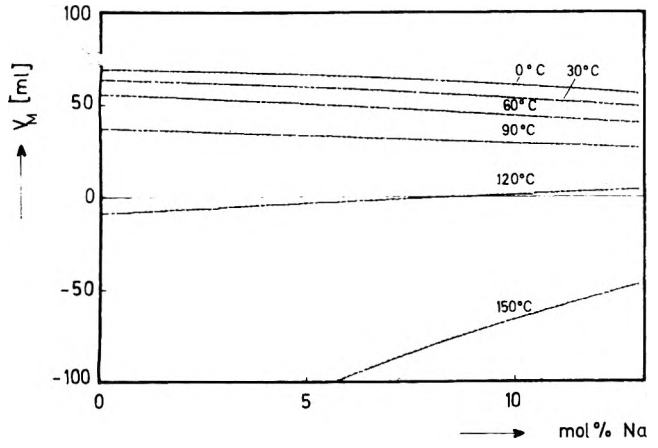

Figure 5. Apparent molar volume of sodium in NaAS vs. concentration (200 bars); parameter is the temperature.

tron cavity formation (compression of cavities) and of thermal expansion.

The apparent molar volume of the dissolved metal V_M ($V_M = (V_S - n_A, V_A)/n_M$; V_S = volume of the solution made up from n_A and n_M moles of ammonia and metal, V_A = molar volume of ammonia) in Figure 5 illustrates the counteraction of the main effects. At low temperatures it has the well-known value of ca. 65 cm^3/mol, due to cavity formation of electrons in the dense structure of ammonia. With temperature increase, i.e., expansion of the ammonia, it becomes smaller,[12] and finally negative, when the solvent structure is so loose that the electron gives no further expansion upon cavity formation, in contrast with electrostriction becoming predominant, as with normal electrolytes.

(c) *Equivalent Conductance.* The specific conductivity is proportional to the volume concentration and the mobility of the charged particles, both of which change with variation of outer conditions. To correct for the concentration changes, the specific conductivity is divided by the concentration to obtain the equivalent conductance Λ ($=1000\sigma/c$) which divided by the Faraday number (96500 A sec) gives the sum of the mobilities ($cm^2\ V^{-1}\ sec^{-1}$) of the charged particles (electrons and sodium cations, provided, of course, the dissolved metal is completely dissociated). For 200 bars the equivalent conductivity is plotted in Figure 6 vs. concentration (as calculated from density) with the temperature as parameter. All curves show the steep increase in conductivity in a narrow concentration range, as first observed by Kraus.[2] The concentration of this increase is lower the higher the temperature (≈1.5 mol/l. at −30°C, 0.3 mol/l. at 150°C). It follows that the NMT is shifted with temperature to smaller concentration, or that it sets in at larger particle distances.

Figure 7 finally gives the temperature coefficient of the equivalent conductance in dependence of the concentration, with the temperature as parameter. For all temperatures it passes through a maximum, which with higher temperature decreases and moves to lower concentrations. The concentration of the maximum coincides with that of the steepest increase of the equivalent conductivity in Figure 6. The temperature coefficient becomes negative at higher concentrations and higher temperatures.

Pressure has an adverse effect on the equivalent conductivity. For all temperatures the Λ/c curves are shifted to higher concentrations; i.e., the pressure coefficient of the equivalent conductivity is negative. Its negative value passes through a maximum in that concentration range in which the steepest conductivity increase or the maximum temperature coefficient is found as reported previously[10] for low temperatures.

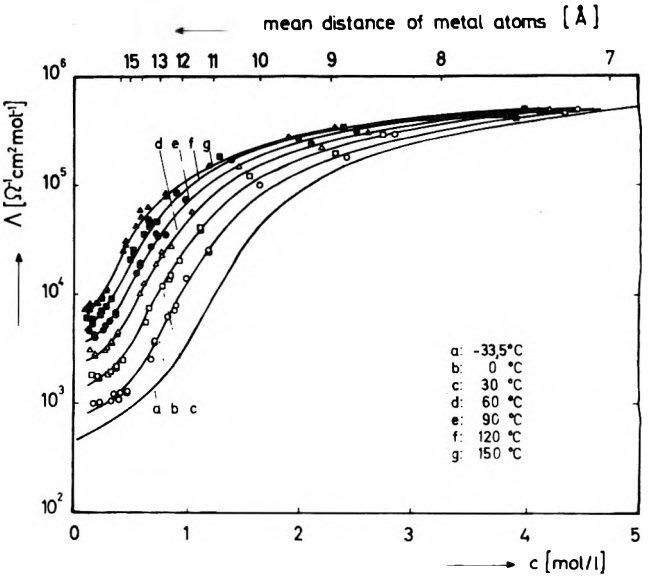

Figure 6. Equivalent conductance of NaAS vs. metal concentration in moles per liter (200 bars); parameter is the temperature. The scale on top gives the mean distance of the metal atoms.

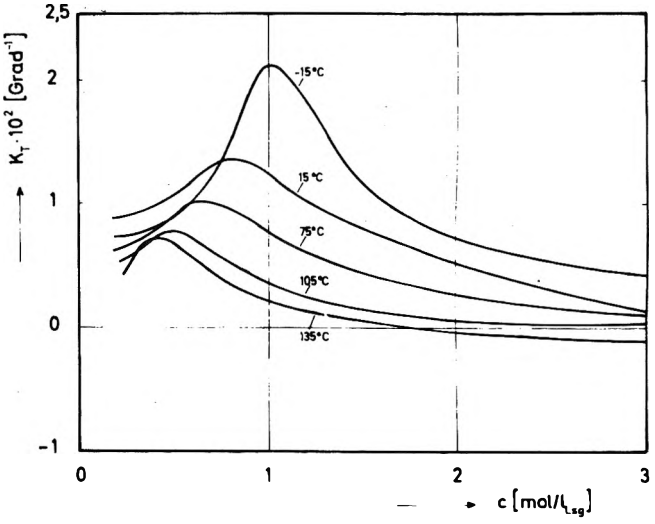

Figure 7. Temperature coefficient of the equivalent conductance of NaAS vs. molar concentration of sodium (200 bars); parameter is the temperature.

Discussion

Our discussion will be limited to a qualitative level only along the lines of the percolation theory and Mott treatment of the Anderson transition. From our data it follows that the NMT in NaAS is shifted to lower concentrations by increasing temperature and adversely to higher concentrations with increasing pressure. This statement follows only from the effect of temperature and pressure on the electrical conductivity. It does not imply any definition of the NMT, which can be given only if its mechanism is known. Different theories might locate it to different metal concentrations.

The plot of the logarithm of the specific conductivity σ vs. thermal power S of NaAS (data from Kraus[2] and Lep-

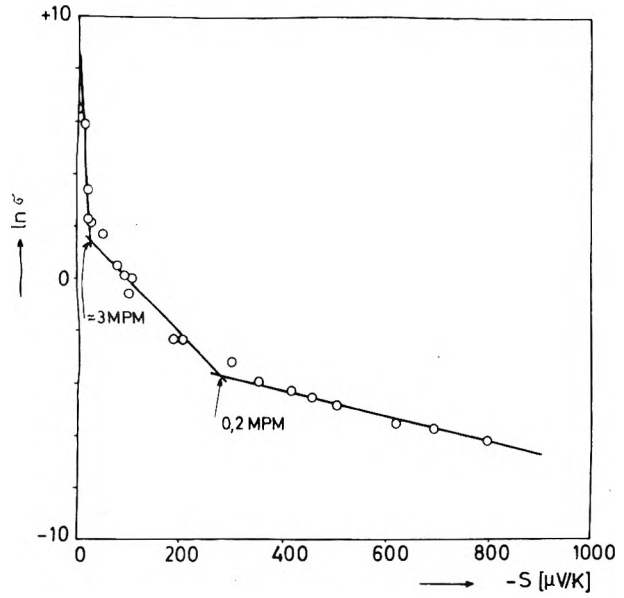

Figure 8. Logarithm of the specific conductivity vs. thermopower of NaAS (−35°C, 1 bar); data taken from literature.[2,13]

outre[13]; −35°C, 1 bar) in Figure 8 might help to distinguish the transition range from the electrolytic range and from the metallic range, i.e., to locate the NMT. In this graph three sections with linear relationship can be distinguished: (1) below 0.2 MPM with low σ and high S (this section covers the electrolytic range with concentration-independent equivalent conductance); (2) between 0.2 and 3 MPM with intermediate σ and S (here the steep increase of the equivalent conductance, the large positive temperature coefficient, and the large negative pressure coefficient were observed); (3) above 3 MPM with the strong increase of σ and the small decrease of S, both to metallic values. According to Thompson,[14] the third range can be subdivided into two or three sections with different slopes. Thus the NMT might be located in the second or the beginning of the third range.

The application of the percolation theory[7] to explain the NMT in Na- and LiAS is based on the idea that the macroscopic homogeneous solutions of intermediate concentrations are separated microscopically into two phases: one of low concentration (≈2 MPM) being nonmetallic, the other one of high concentration (≈9 MPM) being metallic. The relative volume fraction of the metallic phase, varying linearly with macroscopic concentration of the solution, determines the transport properties of the solutions. Above a critical volume fraction (0.15 to 0.3; percolation limit) of the concentrated clusters, transport originates from continuous extended metallic paths. Below the limit extended states do not exist; the solution contains isolated finite metallic clusters.

Justification for the assumption of microscopic inhomogeneity can, besides other experimental evidence, be derived from the miscibility gap of Li–, Na–, and KAS, the consulate concentration of which is around 4 MPM for all three with the consulate or critical temperature between −41 and −70°C (see ref 3–6).

With the percolation theory the electrical transport properties of Li– and NaAS close to the consulate temperature could be described on a quantitative basis. According to this theory, the NMT would set in at the percolation limit, i.e., at 3 to 4 MPM and ranging up to 9 MPM, i.e., being located in the left section of Figure 8.

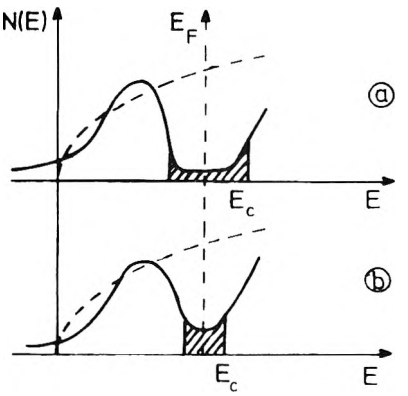

Figure 9. Schematic plot of density of states vs. electron energy (E_F = Fermi energy). (a) Overlap of the bands by density fluctuations. In the pseudogap (shaded) electrons are localized; E_C = mobility edge. (b) Increased density fluctuations or concentration increase diminishes the pseudogap.

At higher temperature, i.e, far away from the miscibility gap, formation of clusters by density fluctuation hardly can be imagined. Therefore application of the percolation theory to our data, taken at temperatures up to almost 200°C above the miscibility gap, does not seem appropriate. Here another mechanism of the NMT must be effective. However, since at all temperatures covered in this study the Λ/c curves (Figure 6) are similar in shape, only shifted to smaller concentrations with increasing temperature, we cannot think of two different mechanisms of the NMT, one being effective at low and the other at high temperatures. Therefore, we tend to exclude the percolation model also for low temperatures. We rather try to interpret our data according to the theory of Mott[1,2] for the NMT in disordered systems.

Since the solvated electrons of the MAS above 0.1 MPM are in the state of spin-compensated, diamagnetic electron pairs (see ref 3–6), we may formulate the MAS NMT as was done for divalent metals, like mercury.[15] When the electrons are approached from large distances, valency and conduction bands are formed, which in an ordered system start overlapping at a critical minimum distance. In a disordered fluid system with density fluctuations in which the bands are diffuse, the overlap may set in earlier (Figure 9a). The density of states in the overlap however is small. Therefore the states are localized in the Anderson sense, separated from the nonlocalized states by a mobility edge[1] (formation of a pseudogap). Localization of the states is expected when the density of states at the Fermi energy is below one-third that of free electrons (Mott's g factor[1] $N(E_F)/N(E_F)_{free}$). The Anderson transition occurs if the band is filled up to the limiting Fermi energy which can be varied relative to the energy of the mobility edge, so that $\epsilon = E_C - E_F$ changes sign, e.g., by varying concentration. For $\epsilon > 0$, conduction is possible by thermal activation of electrons over the mobility edge; conductivity is an activated process:

$$\sigma \sim \exp(-\epsilon/kT) \qquad (1)$$

Increasing concentration or increasing density fluctuations by temperature increase lead to a stronger band overlap with rising density of states in the pseudogap and therefore decreasing E_C (Figure 9b); i.e., the activation energy of the conductivity goes down. This can be taken from Figure 7,

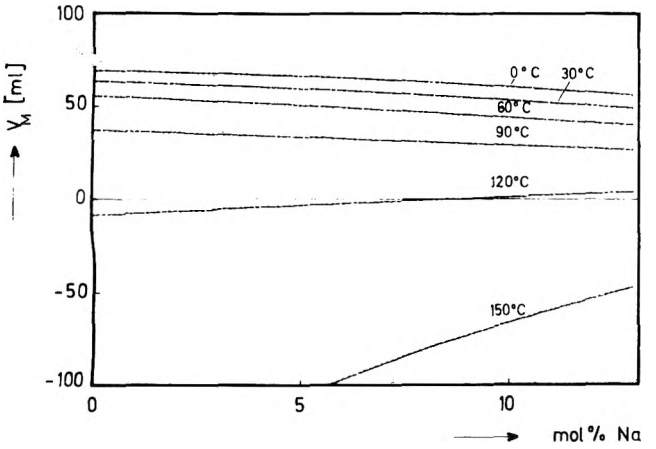

Figure 5. Apparent molar volume of sodium in NaAS vs. concentration (200 bars); parameter is the temperature.

tron cavity formation (compression of cavities) and of thermal expansion.

The apparent molar volume of the dissolved metal V_M ($V_M = (V_S - n_A, V_A)/n_M$; V_S = volume of the solution made up from n_A and n_M moles of ammonia and metal, V_A = molar volume of ammonia) in Figure 5 illustrates the counteraction of the main effects. At low temperatures it has the well-known value of ca. 65 cm^3/mol, due to cavity formation of electrons in the dense structure of ammonia. With temperature increase, i.e., expansion of the ammonia, it becomes smaller,[12] and finally negative, when the solvent structure is so loose that the electron gives no further expansion upon cavity formation, in contrast with electrostriction becoming predominant, as with normal electrolytes.

(c) *Equivalent Conductance.* The specific conductivity is proportional to the volume concentration and the mobility of the charged particles, both of which change with variation of outer conditions. To correct for the concentration changes, the specific conductivity is divided by the concentration to obtain the equivalent conductance Λ ($=1000\sigma/c$) which divided by the Faraday number (96500 A sec) gives the sum of the mobilities ($cm^2\ V^{-1}\ sec^{-1}$) of the charged particles (electrons and sodium cations, provided, of course, the dissolved metal is completely dissociated). For 200 bars the equivalent conductivity is plotted in Figure 6 vs. concentration (as calculated from density) with the temperature as parameter. All curves show the steep increase in conductivity in a narrow concentration range, as first observed by Kraus.[2] The concentration of this increase is lower the higher the temperature (≈1.5 mol/l. at −30°C, 0.3 mol/l. at 150°C). It follows that the NMT is shifted with temperature to smaller concentration, or that it sets in at larger particle distances.

Figure 7 finally gives the temperature coefficient of the equivalent conductance in dependence of the concentration, with the temperature as parameter. For all temperatures it passes through a maximum, which with higher temperature decreases and moves to lower concentrations. The concentration of the maximum coincides with that of the steepest increase of the equivalent conductivity in Figure 6. The temperature coefficient becomes negative at higher concentrations and higher temperatures.

Pressure has an adverse effect on the equivalent conductivity. For all temperatures the Λ/c curves are shifted to higher concentrations; i.e., the pressure coefficient of the equivalent conductivity is negative. Its negative value passes through a maximum in that concentration range in which the steepest conductivity increase or the maximum temperature coefficient is found as reported previously[10] for low temperatures.

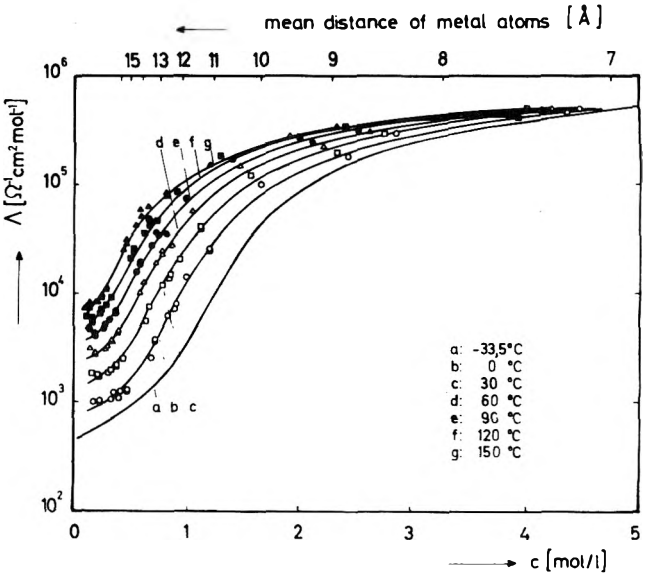

Figure 6. Equivalent conductance of NaAS vs. metal concentration in moles per liter (200 bars); parameter is the temperature. The scale on top gives the mean distance of the metal atoms.

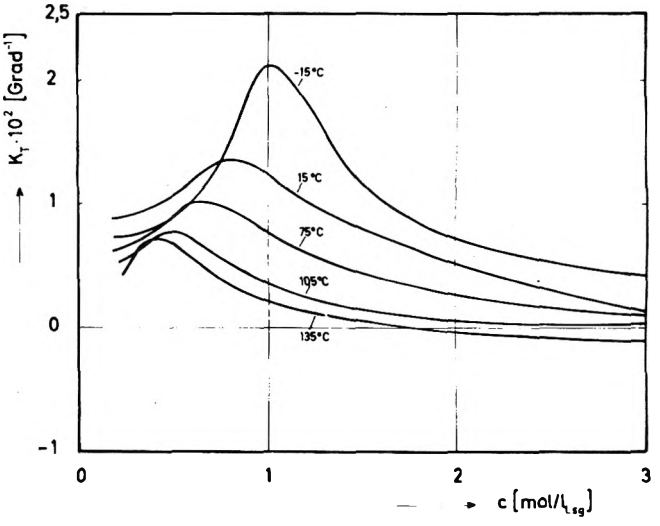

Figure 7. Temperature coefficient of the equivalent conductance of NaAS vs. molar concentration of sodium (200 bars); parameter is the temperature.

Discussion

Our discussion will be limited to a qualitative level only along the lines of the percolation theory and Mott treatment of the Anderson transition. From our data it follows that the NMT in NaAS is shifted to lower concentrations by increasing temperature and adversely to higher concentrations with increasing pressure. This statement follows only from the effect of temperature and pressure on the electrical conductivity. It does not imply any definition of the NMT, which can be given only if its mechanism is known. Different theories might locate it to different metal concentrations.

The plot of the logarithm of the specific conductivity σ vs. thermal power S of NaAS (data from Kraus[2] and Lep-

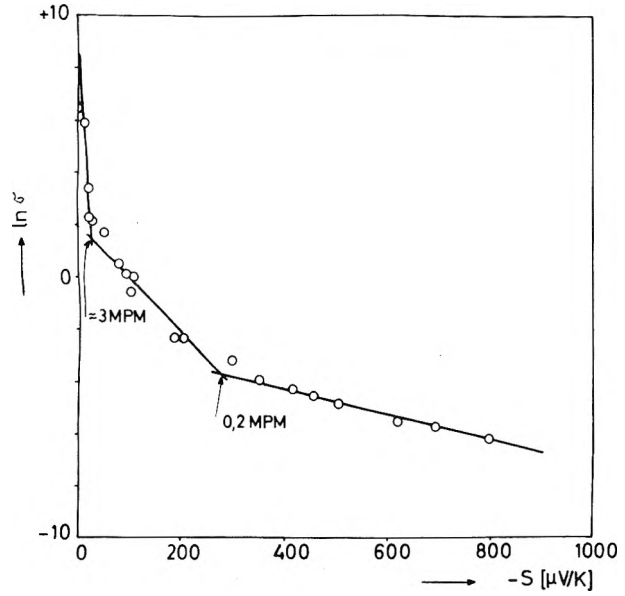

Figure 8. Logarithm of the specific conductivity vs. thermopower of NaAS (−35°C, 1 bar); data taken from literature.[2,13]

outre[13]; −35°C, 1 bar) in Figure 8 might help to distinguish the transition range from the electrolytic range and from the metallic range, i.e., to locate the NMT. In this graph three sections with linear relationship can be distinguished: (1) below 0.2 MPM with low σ and high S (this section covers the electrolytic range with concentration-independent equivalent conductance); (2) between 0.2 and 3 MPM with intermediate σ and S (here the steep increase of the equivalent conductance, the large positive temperature coefficient, and the large negative pressure coefficient were observed); (3) above 3 MPM with the strong increase of σ and the small decrease of S, both to metallic values. According to Thompson,[14] the third range can be subdivided into two or three sections with different slopes. Thus the NMT might be located in the second or the beginning of the third range.

The application of the percolation theory[7] to explain the NMT in Na- and LiAS is based on the idea that the macroscopic homogeneous solutions of intermediate concentrations are separated microscopically into two phases: one of low concentration (≈2 MPM) being nonmetallic, the other one of high concentration (≈9 MPM) being metallic. The relative volume fraction of the metallic phase, varying linearly with macroscopic concentration of the solution, determines the transport properties of the solutions. Above a critical volume fraction (0.15 to 0.3; percolation limit) of the concentrated clusters, transport originates from continuous extended metallic paths. Below the limit extended states do not exist; the solution contains isolated finite metallic clusters.

Justification for the assumption of microscopic inhomogeneity can, besides other experimental evidence, be derived from the miscibility gap of Li–, Na–, and KAS, the consulate concentration of which is around 4 MPM for all three with the consulate or critical temperature between −41 and −70°C (see ref 3–6).

With the percolation theory the electrical transport properties of Li– and NaAS close to the consulate temperature could be described on a quantitative basis. According to this theory, the NMT would set in at the percolation limit, i.e., at 3 to 4 MPM and ranging up to 9 MPM, i.e., being located in the left section of Figure 8.

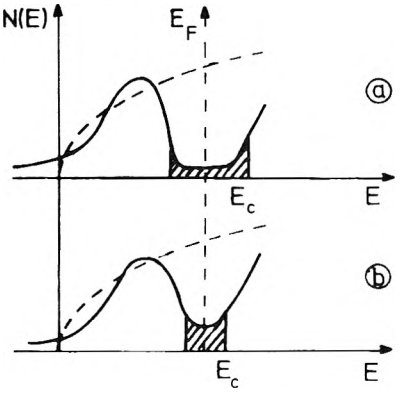

Figure 9. Schematic plot of density of states vs. electron energy (E_F = Fermi energy). (a) Overlap of the bands by density fluctuations. In the pseudogap (shaded) electrons are localized; E_C = mobility edge. (b) Increased density fluctuations or concentration increase diminishes the pseudogap.

At higher temperature, i.e, far away from the miscibility gap, formation of clusters by density fluctuation hardly can be imagined. Therefore application of the percolation theory to our data, taken at temperatures up to almost 200°C above the miscibility gap, does not seem appropriate. Here another mechanism of the NMT must be effective. However, since at all temperatures covered in this study the Λ/c curves (Figure 6) are similar in shape, only shifted to smaller concentrations with increasing temperature, we cannot think of two different mechanisms of the NMT, one being effective at low and the other at high temperatures. Therefore, we tend to exclude the percolation model also for low temperatures. We rather try to interpret our data according to the theory of Mott[1,2] for the NMT in disordered systems.

Since the solvated electrons of the MAS above 0.1 MPM are in the state of spin-compensated, diamagnetic electron pairs (see ref 3–6), we may formulate the MAS NMT as was done for divalent metals, like mercury.[15] When the electrons are approached from large distances, valency and conduction bands are formed, which in an ordered system start overlapping at a critical minimum distance. In a disordered fluid system with density fluctuations in which the bands are diffuse, the overlap may set in earlier (Figure 9a). The density of states in the overlap however is small. Therefore the states are localized in the Anderson sense, separated from the nonlocalized states by a mobility edge[1] (formation of a pseudogap). Localization of the states is expected when the density of states at the Fermi energy is below one-third that of free electrons (Mott's g factor[1] $N(E_F)/N(E_F)_{free}$). The Anderson transition occurs if the band is filled up to the limiting Fermi energy which can be varied relative to the energy of the mobility edge, so that $\epsilon = E_C - E_F$ changes sign, e.g., by varying concentration. For $\epsilon > 0$, conduction is possible by thermal activation of electrons over the mobility edge; conductivity is an activated process:

$$\sigma \sim \exp(-\epsilon/kT) \qquad (1)$$

Increasing concentration or increasing density fluctuations by temperature increase lead to a stronger band overlap with rising density of states in the pseudogap and therefore decreasing E_C (Figure 9b); i.e., the activation energy of the conductivity goes down. This can be taken from Figure 7,

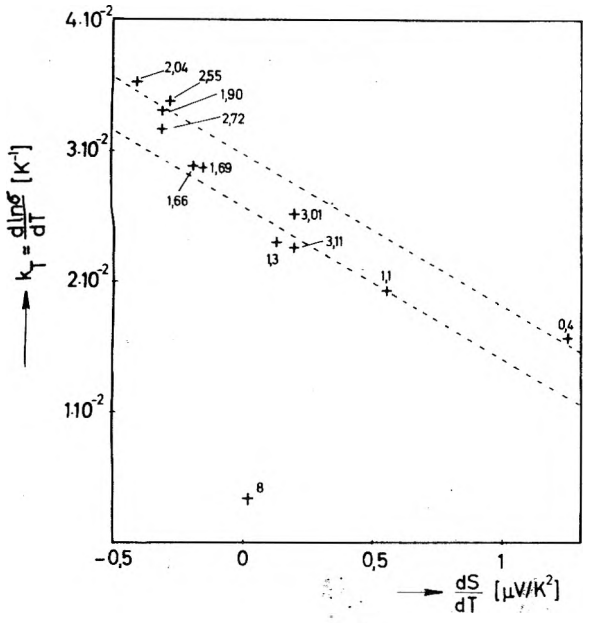

Figure 10. Temperature coefficient of the specific conductivity vs. temperature dependence of thermopower of MAS (−35°C; 1 bar); data taken from literature.[16,13] The numbers give the metal concentration in MPM.

showing the steady decrease of the T coefficient of Λ with temperature (at constant volume concentration, e.g., 1 m) or with concentration (at constant temperature). The maximum T coefficients of Figure 7, moving to lower concentrations with temperature, corresponds to about 0.1 eV.

When by further temperature or concentration increase, and therefore better band overlap, Mott's g factor rises above $\frac{1}{3}$, ϵ becomes zero or negative, the pseudogap disappears, and the conductivity shows the normal metallic behavior, rising with g^2. At room temperature g is larger than $\frac{1}{3}$ above ca. 3 MPM, as deduced by Mott and Acrivos from a wealth of experimental data.[1]

According to this simplified outline, the left range of Figure 8 (above 3 MPM) would be the range of metallic conduction ($g \gtrsim \frac{1}{3}$), the intermediate range (0.2 to 3 MPM) that of activated conduction (localized electrons, $g < \frac{1}{3}$). With increasing temperatures both ranges are shifted to smaller concentrations. Pressure diminishes density fluctuations and therefore has an effect opposing temperature.

Some proof for the assumption that the middle range of Figure 8 corresponds to activated transport follows from the following argument. For activated transport the thermopower is given by

$$S = \frac{k}{e}\left|\frac{\epsilon}{kT} + A\right| \qquad (2)$$

where $\epsilon = E_F - E_C$, k Boltzmann constant, e electron charge, and A a constant. Elimination of ϵ in the last two equations leads to

$$\ln \sigma = -(e/k)S + \text{constant} \qquad (3)$$

with $e/k = 1.16 \times 10^4$ deg K/V. The slope of the middle range of Figure 8 comes closest to this value. Furthermore, also the plot of d ln σ/dT vs. dS/dT gives for solutions in the concentration range from 0.2 to 3 MPM a slope approximately $-e/k$, although data show a larger scatter (Figure 10). The 8-MPM point, however, belonging to the metallic region is far outside.

Activated transport, however, does not necessarily mean excitation of the localized electrons to the mobility edge; it also could include transport by hopping. Mott[8] has given some arguments for this, also explaining the negative pressure coefficient of conductivity by expected volume effects associated with hopping of an electron between electron pairs. In any case it seems to us that the NMT is clearly in the range of 0.2 to 3 MPM with the large observed anomalies of the temperature and pressure coefficient of conductivity and of thermopower.

Acknowledgment. We are grateful to Professors Jortner and Mott for helpful discussions. Financial support of this work by the Deutsche Forschungsgemeinschaft is gratefully acknowledged.

References and Notes

(1) N. F. Mott, "Metal-Insulator Transitions," Taylor and Francis, London, 1974.
(2) C. A. Kraus, *J. Am. Chem. Soc.*, **43**, 749 (1921); C. A. Kraus and W. W. Lucasse, *ibid.*, **43**, 2529 (1921).
(3) G. Lepoutre and M. J. Sienko, Ed., "Solutions Metal-Ammoniac," W. A. Benjamin, New York, N.Y., 1964.
(4) J. J. Lagowsky and M. J. Sienko, Ed., "Metal-Ammonia-Solutions," Butterworths, London, 1970.
(5) *Ber. Bunsenges. Phys. Chem.*, **75**, No. 7 (1971).
(6) J. Jortner and N. R. Kestner, Ed., "Electrons in Fluids," Springer-Verlag, Berlin-Heidelberg-New York, 1973.
(7) J. Jortner and M. H. Cohen, *J. Phys. Chem.*, this issue.
(8) N. F. Mott, *J. Phys. Chem.*, this issue.
(9) S. Naiditch, ref 3, p 113.
(10) U. Schindewolf, K. W. Boddeker, and R. Vogelsgesang, *Ber. Bunsenges. Phys. Chem.*, **70**, 1164 (1966); U. Schindewolf, ref. 4, p 199.
(11) E. Huster, *Ann. Phys.* **33**, 492 (1938); C. A. Kraus, E. S. Carney, and W. C. Johnson, *J. Am. Chem. Soc.*, **49**, 2206 (1927).
(12) S. Naiditch, O. A. Paez, and J. C. Thompson, *J. Chem. Eng. Data*, **12** (2), 164 (1967).
(13) P. Damay, M. Depoorter, P. Chieux, and G. Lepoutre, ref 4, p 233; ref 5, p 642.
(14) J. C. Thompson, ref 3, p 307.
(15) F. Hensel, *Angew. Chem.*, **86**, 466 (1974).
(16) C. A. Kraus and W. W. Lucasse, *J. Am. Chem. Soc.*, **44**, 1946 (1922).

Discussion

G. R. FREEMAN. The maximum in mobility temperature coefficient as a function of metal concentration is a general phenomenon when a transport mechanism transition occurs. If one plots the mobilities of electrons for a series of alkanes and ethers at a given temperature against the corresponding temperature coefficients, one obtains a maximum in temperature coefficient similar to that shown in your work. The transport transition that occurs in ethers and alkanes (discussed in our paper) is not a metal–nonmetal transition. I simply wish to point out the maximum in activation energy as a function of mobility is a general phenomenon that is not dependent upon the specific mechanisms involved.

J. V. ACRIVOS: In the debate of how the metal–insulator transition is characterized in M–NH_3 solutions, Mott proposes that the latter is characterized by the ratio g of the density of states at the Fermi energy relative to that of a free electron gas, whereas Cohen and Jortner propose the transition is continuous over an interval and that it is characterized by the composition at the extremes of the interval and by the volume fraction of the metallic extreme. They can explain the electromagnetic properties on the basis of a microscopic inhomogeneous distribution of the two extreme compositions. There are several questions which need an answer before the controversy is resolved.

One, are the necessary and sufficient conditions for reversibility in the presence of an electromagnetic field satisfied?[1]

Two, in the trivariant system investigated by Hahne and Schindewolf is the transition characterized by the ratio g? If this is true and r is an average interatom separation then the change in enthalpy for the localization of metallic states by the formation of excitons which bind n solvent molecules is

$$\Delta H_e \simeq RT^2\{[k_T + (\partial \ln r/\partial T)_{P,g}]/k_{\mathfrak{R}} + \alpha(n-1)\} < 0$$

where k_T and $k_{\mathfrak{R}}$ are the temperature and mole ratio coefficients for the variations of conductivity (independent variables = T, P, $\mathfrak{R}$), and α is the coefficient of thermal expansivity.

Three, What are the equilibrium relations for a microscopic inhomogeneous system? Is the surface tension between the two liquid phases in contact known? The Einstein probability for fluctuations in a binary alloy have amplitudes: $\approx 4 \times 10^{-2}$ (for $Na-NH_3$) and 2×10^{-4} (for $K-NH_3$) near the boiling point of ammonia (assuming the cluster size is similar to that measured near the consolute point[2] which suggests $Na-NH_3$ is different from $K-NH_3$ at $-33°C$. However, the uncertainty principle imposes some demands on the lifetime of the fluctuations which determine the conductivity, i.e., $\tau \geq h/2E_F \sim 10^{-13}$ sec for E_F near the critical composition.[3] Unfortunately the lifetime of the solvated electron species is also being debated. Belloni, Saito, and Clerc (this issue) report the lifetimes are less than 10^{-13} sec whereas Rentzepis and Huppert report the lifetimes are greater than 10^{-13} sec. This question should be resolved and the implications of the uncertainty principle should be considered.

Reference and Notes

(1) F. O. Koenig, *J. Phys. Chem.*, **41**, 597 (1937).
(2) M. J. Sienko and P. Chieux, "Metal Ammonia Solutions", J. J. Lagowski and M. Sienko, Ed., Butterworths, London, 1969, p 339.
(3) J. C. Thompson, "Solutions Metal Ammoniac", G. Lepoutre and M. Sienko, Ed., Benjamin, New York, N.Y., 1964, p 307.

Phase Diagram for Liquid–Liquid Coexistence in the Li–ND_3 System

Masayuki Katsumoto and Pierre Damay*

Laboratoire de Chimie Physique, ERA 126 du CNRS, 13, rue de Toul, 59000 Lille, France *(Received July 23, 1975)*

A phase diagram is presented for the liquid–liquid phase separation of lithium in liquid deuterioammonia. Phase separations occur at temperatures below $-51.4°C$ for $Li-ND_3$, compared to $-63.5°C$ for $Li-NH_3$. The replacement of NH_3 by ND_3 is not accompanied by a significant change of the critical concentration. No change in natural isotopic distribution was observed between the two liquid phases of Li–ammonia solutions.

Introduction

Phase diagrams for liquid–liquid coexistence in metal–ammonia solutions have been extensively studied by many authors,[1] but in metal–deuterioammonia solutions, no phase diagram for liquid–liquid coexistence has been reported. U. Shindewolf pointed out at the Colloque Weyl II[2] that he found a large shift of the critical temperature, T_c, caused by deuteration, not accompanied by a change in the critical concentration. Up to now, no explanation has been given of this phenomenom.

The present work attempts to determine the phase diagram for liquid–liquid coexistence in $Li-ND_3$ solutions and to obtain some information on the nature of the interaction between the components from the isotopic distribution in the two liquid phases of Li–ammonia solutions.

Experimental Section

Phase Diagram. A phase separation was detected by the conventional conductance method. Two types of cells were used. In the first type, the two electrodes were at the bottom of the cell. In the second type, the two electrodes were in the vicinity of the surface of the solution.

The electrodes were made as follows. Tungsten wires (0, 5 mm, 99.9%) were sealed to Pyrex glass and totally covered by the glass. Then the glass was ground until the top of the tungsten wire was bare. The surface of the electrode was then plated with gold.

All glassware was cleaned by soaking in concentrated HNO_3, rinsing with water, soaking in 30% $HF-NH_4F$ solution, rinsing with water, drying in an oven, soaking in 1 N HNO_3 solution, rinsing, and drying in an oven.

The cell was degassed for 36–48 hr and submitted, from time to time, to a high frequency field.

99.8% deuterioammonia, provided by the French Atomic Energy Commission, was used. It was distilled onto a sodium mirror, measured quantitatively, and condensed onto a potassium mirror before being transferred to the degassed cell. After each run ND_3 was recovered.

The lithium metal was cut from a Koch-Light 99.98% ingot, weighed on a microbalance (Sartorius 4102), and transferred in a tube containing a glass covered magnet with a break seal. The tube was then pumped out then sealed off. All these operations were performed in an atmosphere of evaporating liquid nitrogen. The tube was attached to the cell. The breakseal was broken in vacuo, and the lithium was transferred in the cell by dissolving and rinsing with ND_3. Then this tube was sealed off.

The thermocontrolled bath was stable to $0.005°C$.[3a] The temperature was measured by a platinum resistance thermometer and bridge. The conductance was measured by a Wayne-Keer autobalance universal bridge B641.

Isotopic Distribution

Matheson NH_3 99.99% was used. The two phases obtained from a 4 MPM solution were analyzed for deuterium. The deuterium concentration was also measured in pure ammonia, and in ammonia gas evaporated from 18.7

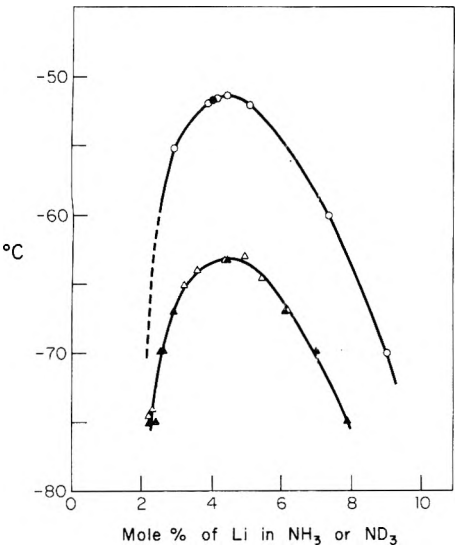

Figure 1. Phase diagram for liquid–liquid coexistence in Li–ND_3 and Li–NH_3. Li–NH_3: (Δ) Loeffler;[1a] (▲) Schettler et al.[1b] Li–ND_3: (●) Debaecker;[5] (O) this work.

to 19.7 MPM Li solution, and in various saturated Li solutions. These measurements were performed by the Centre d'Etudes Nucléaires de Saclay, France.

Results

Figure 1 shows the coexistence curve for lithium–deuterioammonia as determined in this investigation. The coexistence curve for lithium–ammonia determined by Loeffler, Schettler, et al. is also shown for comparison. The T_c for Li–ND_3 is −51.4°C compared to −63.5°C for Li–NH_3. The consolute concentrations of the two systems are not significantly different. The temperature shift is quite similar to those for Na–NH_3 and Na–ND_3 systems.

Mass spectroscopic analysis shows that in all phases the concentration of deuterium is the same as in pure NH_3.

Discussion

The shift of T_c may be discussed on the basis of a two-components model where the solute is a solvated metal, $M(NH_3)_n$, while the solvent is pure NH_3. One of the authors[3] has shown that with such a model the thermodynamic properties in the transition range can be represented by an analytical function.

The critical temperature is expressed as

$$T_c = A_{12}\, f(n, V_{NH_3 \text{ or } ND_3}, V_{Li}, x_c) \qquad (1)$$

where A_{12} is an interaction coefficient between the components of the solution, f is a function given in ref 3, n is the solvation number, V are the apparent molar volumes of ammonia and lithium in the solutions, and x_c is the analytical mole fraction at the critical point.

The analytical mole fraction at the critical point x_c is not modified when NH_3 is replaced by ND_3. The apparent molar volumes of the solvent V_{NH_3} and V_{ND_3} are also practically the same.[4] If the number n of ammonia molecules in the solvated solute was modified when NH_3 is replaced by ND_3 the critical concentration x_c would also be modified;[3] this is not the case. It is then clear that only V_{Li} and A_{12} can produce significant changes in T_c.

The apparent molar volumes V_{Li} are not known in Li–ND_3 systems. In the case of potassium the ratio V_K in $[ND_3]/V_K$ in NH_3 increases with increasing concentration and attains 1.08_5 at 2.3 MPM at −33.7°C. A similar change of 10% in V_{Li} would cause an increase of 5°C on T_c when NH_3 is replaced by ND_3. This may be a partial interpretation of the T_c shift.

The interaction coefficient A_{12} depends on the binary interactions between solvent–solvent, solute–solute, and solvent–solute. The lack of changes in the isotopic distributions when ammonia is extracted from concentrated or saturated solutions, and when it is distributed in two liquid phases, suggests that the solvent–solute interactions are not modified. However, solvent–solvent interactions are clearly modified. For instance the heat of vaporization for ND_3 is 4% higher than that for NH_3. Similarly an increase of 5% in A_{12} would yield an increase of 10°C.

Acknowledgments. The authors wish to express their thanks to Mme L. Merlivat of the Centre d'Etudes Nucleaires de Saclay, France, for her help in carrying out the mass spectroscopic analysis. Special thanks go to Mr G. Billaud for his help in preparing the Li–ND_3 solutions. M.K. is currently on a scholarship granted by the French government.

References and Notes

(1) (a) M. J. Sienko in "Metal-Ammonia Solutions", Colloque Weyl I, G. Lepoutre and M. J. Sienko, Ed., W. A. Benjamin, New York, N.Y., 1964, p 23; (b) P. D. Schettler, Jr., and A. Patterson, Jr., *J. Phys. Chem.*, **68**, 2865 (1964); (c) P. Chieux and M. J. Sienko, *J. Chem. Phys.*, **53** 566 (1970); (d) J. C. Thompson, H. Teoh, and P. R. Antoniewicz, *J. Phys. Chem.*, **75**, 399 (1971); (e) A. C. Sharp, R. L. Davis, J. A. Vanderhoff, E. W. Le Master, and J. C. Thompson, *Phys. Rev. A*, **5**, 414 (1971).
(2) U. Schindewolf in "Metal-Ammonia Solutions", Colloque Weyl II, J. J. Lagowski and M. J. Sienko, Ed., Butterworths, London, 1970, p 351.
(3) (a) P. Damay, Thesis, Paris, 1972; (b) P. Damay in "Electrons in Fluids", Colloque Weyl III, J. J. Jortner and N. R. Kestner, Ed., Springer-Verlag, Berlin, 1973, p 195.
(4) C. A. Hutchison and D. E. O'Reilly, *J. Chem. Phys.*, **34**, 163 (1961).
(5) F. Debaecker, private communication.

Discussion

J. JORTNER. Your observation of the increase of T_c from Li–NH_3 to Li–ND_3 is explained by you in terms of a large isotope effect on the molar volume of the metal. As I remember the molar volumes of ordinary ions in H_2O and D_2O are practically identical. Do you assign this volume change to different molar volumes of the electron cavity in ND_3 relative to NH_3?

P. DAMAY. Solvated electrons are not supposed to exist at these concentrations. The first question to answer would be to determine why there is a large excess volume in the whole range of concentrations in metal–ammonia systems.

J. L. DYE. Phase separation in Rb–NH_3 solutions does occur. When the EPR spectra of Rb–NH_3 solutions in this concentration region are obtained as a function of temperature, two signals occur as the tube is moved, one a narrow line from the dilute phase (more dense), the other a broad, asymmetric line from the concentrated phase. (K. D. Vos, Ph.D. Thesis, Michigan State University, 1962).

J. V. ACRIVOS. Are there any conductivity data for M–ND_3?

J. L. DYE. (Response) Yes, there are unpublished data of G. Smith (Ph.D. Thesis, Michigan State University, 1963). The results can be summarized as follows. The conductance of Na in NH_3 is higher than in ND_3 as expected from the viscosity ratio. However, as the concentration is increased the ratio $(\Lambda_{Na})_{NH_3}/(\Lambda_{Na})_{ND_3}$ increases while the inverse viscosity ratio decreases slightly. The conductivity ratio follows the expression

$$\text{ratio} = 1.22 + 0.7\sqrt{C}$$

up to $C = 0.6$ M. The intercept at zero concentration is equal to η_{ND_3}/η_{NH_3}.

U. SCHINDEWOLF. What about T_c for Li in NH_3–ND_3 mixtures? T_c for Na increases linearly with the D/H ratio.

M. KATSUMOTO. We have not investigated the phase diagrams for solutions of Li in NH_3–ND_3 mixtures.

Fluctuations in Metal–Ammonia Solutions

Pierre Damay and Paul Schettler, Jr.*

13 rue de Toul, 59000 Lille, France, and Department of Chemistry, Juniata College, Huntingdon, Pa. 16652 *(Received July 23, 1975)*

Large fluctuations of concentration occur in the vicinity of the critical point in metal–ammonia solutions. Their existence is indicated by a plateau in the activity–concentration curve. If there is no pressure work associated with fluctuations, the probability of finding a concentration x_2 different from the average concentration $\bar{x}_2$ is given by $P(x_2) = P_0 \exp\{-(n/kT)[x_1(\mu_1 - \bar{\mu}_1) + x_2(\mu_2 - \bar{\mu}_2)]\}$ where μ_1, μ_2, $\bar{\mu}_1$, $\bar{\mu}_2$ are the chemical potentials at concentrations x_2 and $\bar{x}_2$, respectively. The number n is the total number of molecules inside a characteristic volume which is related to the Ornstein, Zernike, Debye coherence length. At each average concentration $\bar{x}_2$, a distribution curve can be computed. Static and transport properties of the solutions can be interpreted by use of the distributions of concentration.

Introduction

For a long time inhomogeneities or fluctuations have been supposed to exist in the intermediate range of concentration of metal–ammonia solutions (MAS).

Thompson[1] and Cohen and Thompson[2] proposed a qualitative model of inhomogeneities based on the existence of large metallic clusters for x_2 between 10^{-3} and 0.03 (x_2 or x being the mole fraction for the metal and x_1 for the solvent). At Colloque Weyl II, Sienko and Chieux,[3] Damay, Depoorter, Chieux, and Lepoutre,[4] and Lepoutre and Lelieur[5] suggested the existence of metallic clusters in the intermediate range of concentration ($0.01 < x < 0.05$).

Since Colloque Weyl II, many authors supposed the existence of inhomogeneities to explain different properties in the same range of concentration. It is interesting to note that most of the authors used only qualitative arguments. General terms like aggregates, clusters, inhomogeneities, and density fluctuations were used. These authors were not so much interested in drawing a physical microscopic picture of the structure of the solution as in using the consequences of microscopic inhomogeneities to interpret some general properties.

More recently, Jortner and Cohen[6] used the same kind of ideas to explain the metal–nonmetal transition, but the refinement needed by their theory brought them to propose a physical picture for the inhomogeneities. They suggested that only clusters of dilute ($x_2 = 0.023$) and concentrated solutions ($x = 0.09$) of about 30 Å in size coexist in the intermediate range.

In the present paper we do not intend to discuss in detail all that has been published about inhomogeneities in MAS. Here we wish only to clarify the structure of microscopic fluctuations in the critical region from a thermodynamic and structural point of view.

It is possible to locate the fluctuations by observing the variation of chemical potential with concentration. Neutron scattering experiments conducted by Chieux[7] have brought to light the structural features of these local inhomogeneities. The thermodynamic quantities obtained from vapor pressure measurements provide another way to determine the extent of fluctuations. A characteristic length or a volume scale for correlated fluctuations can be obtained from neutron scattering data.

* Address correspondence to this author at the Department of Chemistry, Juniata College, Huntingdon, Pa. 16652.

After making a short survey of the different ways of considering fluctuations, we shall proceed to derive a general relation which would enable us to calculate the distribution of concentration around the average concentration $\bar{x}$.

Two quantities are needed to compute the distribution function, first the chemical potential of the two species as a function of concentration and a length scale which can be deduced from neutron scattering experiments.

Knowing the distribution of concentration it is possible to interpret some of the physical properties of MAS.

Concentration Fluctuation in a Two-Component Mixture

There are large fluctuations in the density of a fluid in the vicinity of its critical point. For a two-component system there are both density and concentration fluctuations near the liquid–liquid phase separation.

The density fluctuations are generally negligible compared to the concentration fluctuations. The two phases in equilibrium below the critical point are both liquid, and the change of density at the transition point is much less pronounced than in the case of the one-component critical transition. For a two-component system, concentration plays exactly the same role as density in the case of a single-component system.

In metal–ammonia solutions, the activity–concentration curve for NH_3 would clearly reveal the existence of fluctuations. In the critical region at −35°C, i.e., about 6°C above the critical temperature T_c, the curve is almost flat for the sodium–ammonia system. By using the Gibbs–Duhem equation, it can be seen that the activity of the solute also remains nearly constant in the same region.

Thus, only a small amount of energy is required to separate a volume V of concentration $\bar{x}$ into two volumes $V/2$ with two compositions $\bar{x} + \Delta x$ and $\bar{x} - \Delta x$. The energy needed to create fluctuations is provided by the temperature.

An alternative but hardly different way of looking at the fluctuations is to consider the structure factor at infinite wavelength as $q \to 0$ defined by Bhatia and Thornton.[8] The partial structure factor relative to the concentration fluctuations is

$$S_{cc}(0) = N\langle(\Delta x)^2\rangle \qquad (1)$$

where N is the total number of molecules inside the volume

V and $\langle(\Delta x)^2\rangle$ is the mean square fluctuation of concentration. But at very large wavelength, as $q \to 0$, $S_{cc}(0)$ is also a thermodynamic quantity:

$$S_{cc}(0) = Nk_bT \Big/ \left(\frac{\partial^2 G}{\partial x^2}\right)_{T,P} \tag{2}$$

where $(\partial^2 G/\partial x^2)_{T,P}$ is the second derivative of the free energy with respect to concentration.

Furthermore

$$\left(\frac{\partial^2 G}{\partial x^2}\right)_{T,P} = \frac{1}{1-x}\left(\frac{\partial \mu_2}{\partial x}\right)_{T,P} \tag{3}$$

Hence a plateau in the activity–concentration plot would correspond to a peak for $S_{cc}(0)$, and these would be strong indications for the presence of fluctuations.

Unfortunately, it is about the only thing which can be said from the $S_{cc}(0)$ in a critical region. Indeed, the thermodynamic character of $S_{cc}(0)$ can be derived from the statistical thermodynamics of fluctuations. According to the treatment of Hill,[9] if N_i and N_j are the number of molecules of the two species in a microscopic volume and ΔN_i and ΔN_j the instantaneous deviations from the mean, the probability for such deviations is given by

$$p(x) = p_0 \exp\left\{-\sum_{i,j} F_{ij}\frac{\Delta N_i \Delta N_j}{2k_bT}\right\} \tag{4}$$

where

$$F_{ij} = [\partial^2 F/\partial N_i \partial N_j]_{T,P}$$

The term within brackets can be evaluated by expanding the Helmholtz free energy in series and keeping only the first nonvanishing term which happens to be the second derivative.

If, for the sake of simplicity, it is supposed that the volume of the two components is the same and the compressibility term negligible, relation 4 becomes

$$p(x) = p_0 \exp\left\{-\frac{N}{2k_bT}\left(\frac{\partial^2 G}{\partial x^2}\right)_{T,P}(\Delta x)^2\right\} \tag{5}$$

This relation gives a pure Gaussian distribution which can also be written as

$$p(x) = p_0 \exp\left\{-\frac{N}{2}\frac{(\Delta x)^2}{\langle(\Delta x)^2\rangle}\right\} \tag{6}$$

where $\langle(\Delta x)^2\rangle = k_bT/(\partial^2 G/\partial x^2)_{P,T}$ is the mean square deviation.

Thus, this treatment keeps only the first term in the expansion, and it can be regarded as correct as long as the fluctuations are small and N is large. The higher terms in the expansion must be negligible.

It is obvious that the third derivative vanishes when $\partial S_{cc}(0)/\partial x = 0$; the expansion treatment is exact, e.g., for an ideal solution with $x = 1 - x = 0.5$. The more $S_{cc}(0)$ varies with concentration, the more the approximate treatment becomes susceptible to error, and it becomes essentially incorrect when large fluctuations occur as, for instance, in a critical region and more generally when there is a peak in $S_{cc}(0)$.

In a region where large fluctuations occur, the problem has to be solved in a more exact way. The exact form for writing the probability $p(x)$ is (Hill[9])

$$p(x) = p_0 \exp\left\{\frac{n_1\bar{\mu}_1 + n_2\bar{\mu}_2 - F}{kT}\right\} \tag{7}$$

where $\bar{\mu}_1$ and $\bar{\mu}_2$ are the chemical potentials of the species at the average concentration $\bar{x}_1$, $\bar{x}_2$. F is the Helmholtz free energy of a system of n_1, n_2 molecules at the concentration x_1, x_2.

But the Helmholtz free energy is related to the Gibbs free energy by

$$G = n_1\mu_1 + n_2\mu_2 = F + PV \tag{8}$$

If the volume is held constant, the probability $p(x)$ thus becomes:

$$p(x) = p_0 \exp\left\{-\frac{n_1(\mu_1 - \bar{\mu}_1) + n_2(\mu_2 - \bar{\mu}_2) + V\Delta p}{kT}\right\} \tag{9}$$

The main problem now is to evaluate $V\Delta p$. Two cases ought to be considered. First, if there is an excess volume of mixing at constant pressure, a given amount of solution will have a different volume when there are fluctuations and when the mixture has the average concentration $\bar{x}$. In this case, the pressure necessary to hold the volume constant can be very large and the term $V\Delta p$ in the exponential can be very important; there is thus a pressure work associated with the existence of fluctuations. On the other hand, if there is no excess volume of mixing, the same amount of mixture occupies the same volume with or without fluctuations. There is no pressure work associated with the existence of fluctuations, and the term $V\Delta p$ is therefore negligible.

In a volume V, there are n_1 and n_2 molecules. The total number n is equal to $n_1 + n_2$ with $n_1 = x_1 n$ and $n_2 = x_2 n$. Relation 9 can be slightly modified

$$p(x) = p_0 \exp\left\{-\frac{n}{kT}[x_1(\mu_1 - \bar{\mu}_1) + x_2(\mu_2 - \bar{\mu}_2) + V\Delta p]\right\} \tag{10}$$

The number n is closely related to the volume V in which fluctuations occur. If $V_m(x)$ is the volume occupied by one mole of mixture, n is simply

$$n = NV/V_m(x) \tag{11}$$

where N is the Avogadro number. The volume of 1 mol of mixture is

$$V_m(x) = x_1V_1 + x_2V_2 + \Delta V(x) \tag{11'}$$

where V_1 and V_2 are the volumes of 1 mol of the pure components and $\Delta V(x)$ is the excess volume. All the chemical potentials can be evaluated by vapor pressure measurements.

Now only the choice of the total number of molecules n or the volume V remains to be determined. If the total volume of the solution is considered, n is of the order of Avogadro's number and $p(x)$ is essentially equal to zero when x is different from $\bar{x}$. The distribution curve is a δ function. So, at the scale of the cell, i.e., for a thermodynamic measurement, no fluctuations appear. Indeed, all fluctuations which occur at a scale of a few angstroms are completely incoherent and cancel each other when the overall solution is considered. The volume V cannot be chosen as the total volume of the solution.

However, at the scale of a few tenths of an angstrom, fluctuations are actually correlated. A small local perturbation, e.g., in concentration occurring at a given place inside the solution, perturbs the neighboring system to some extent. The perturbation is propagated from the source to a given distance. A local perturbation in free energy is transmitted to the neighborhood in the same way. The decrease in the perturbation with distance must be exponential in

some way. It is thus possible to define a characteristic correlation length L.

This correlation length has been introduced by Debye[10] to explain the angular dissymmetry of the critical opalescence in liquid mixtures. At distances shorter than the length L, all fluctuations are correlated; at distances larger than L, all fluctuations are incoherent.

The solution can be conceptually split into small volume elements $V = L^3$. Inside a given volume, fluctuations are correlated or "in phase", but for molecules present in the characteristic volume, the remaining solution is subject to incoherent fluctuations which cancel out and have no effect on this volume. The solution is composed of an assembly of similar characteristic subvolumes fluctuating independently. It must be emphasized that characteristic volumes are not localized in space, but each subvolume can be generated around any point in the solution. Of course, such a splitting of the solution is a thought experiment but it reflects well what actually happens at a submacroscopic level.

The subvolume $V = L^3$ is a characteristic of the solution and, at a given temperature, it cannot be chosen arbitrarily.

Another way to define this volume is to say that it represents the smallest volume which possesses all the intensive properties of the solution. The average temperature, density, concentration, and free energy density of such a volume are just the same as for the overall solution. A smaller volume would not have this property since some correlated fluctuations would have been left out.

The correlation length gives information about the structure of the solution at a microscopic level. It is not a thermodynamic quantity. It can be determined from experiments like light scattering or neutron scattering.

Debye introduced the correlation length in the following way. Suppose that the potential energy between two molecules is only a function of their distance r. Let this energy be $-\epsilon(r)$. The range of molecular interaction between a molecule and the system is given by

$$l^2 = \int r^2\epsilon(r)\,d\tau / \int \epsilon(r)\,d\tau \qquad (12)$$

where $d\tau$ is the volume element. The integration for r must be carried out from contact to infinity. It is shown that the coherence length L at a given temperature near the critical temperature T_c is related to the range of molecular interaction l by

$$L(T) = l\epsilon^{-1/2} \qquad (13)$$

with $\epsilon = (T - T_c)/T_c$.

A similar relation has been used by Ornstein and Zernike.[11] They assumed that the net pair correlation $G(r) = g(r) - 1$ takes the form

$$G(r) = A(e^{-\varkappa r}/r) \qquad (14)$$

where $g(r)$ is the radial distribution function and $\varkappa$ the inverse of a correlation length ξ.

The variation of ξ with temperature is

$$\xi(T) = \xi_0\epsilon^{-1/2} \qquad (15)$$

Except for a numerical constant equal to $\sqrt{6}$, a dimensional factor, $\xi(T)$ can be assimilated to $L(T)$ and ξ_0 to 1. The constant $\sqrt{6}$ comes out naturally from the theory; nevertheless, this value raises some questions. Thus

$$L(T) = \sqrt{6}\,\xi(T) \text{ and } l = \sqrt{6}\,\xi_0 \qquad (16)$$

Application to Metal–Ammonia Solutions (MAS)

Two parameters are needed to compute the distribution of concentrations from relation 10, the function $\mu = f(x)$ and the total number of molecules inside the characteristic volume V.

The volume V is supposed to be independent of concentration and change with temperature according to relation 13. Debye introduces the length l by taking into account only the pair interactions between the components. He ends up with a length l independent of concentration.

Neutron scattering experiments have been recently performed on the Li–ND_3 system near the critical temperature.[7] The variation of the Ornstein–Zernike correlation length $\xi(T)$ with temperature has been determined and ξ_0 is found to be equal to 4.7 Å. This makes it possible to calculate n at any temperature and concentration using eq 16 and 11.

The value of ξ_0 is supposed to be the same for Li–ND_3 and Na–NH_3 systems. The two systems are sufficiently alike with regard to their critical phenomena so that the difference can be assumed to be negligible.

We are going to study the sodium–ammonia system at −35°C.

The variation of free energy with concentration can be determined from vapor pressure data.[11] One of us showed[12] that the vapor pressure–concentration plot can be fitted by assuming that the solution is composed of free ammonia and solvated cations. The solvation number is close to 6 or 7. The excess free energy can be written as

$$\Delta G^{ex} = A_{12}V_m\varphi_1\varphi_2 \qquad (17)$$

where $\varphi_{1,2}$ is the volume fraction, $\varphi_1 = x_1V_1/(x_1V_1 + x_2V_2)$, V_1 and V_2 are the volumes of free ammonia on one side and the other of the solvated cation $Na(NH_3)_n$, A_{12} is the coefficient of binary interaction, and V_m is the volume of 1 mol of mixture.

One analytical function for the activity vs. concentration is thus obtained. Relation 17 can be taken as a model for MAS or more simply as a semiempirical relation which enables us to fit vapor pressure data. Further, it also permits us to calculate the critical temperature and concentration. The first derivative of relation 17 with respect to concentration gives the chemical potentials of components 1 and 2:

$$(\partial G/\partial x)_{T,p} = A_{12}V_2\varphi_1^2 + RT \ln x_2 = \mu_2 \qquad (18)$$

The second derivative gives the critical temperature

$$T_c = \frac{2}{R}\left[\frac{\varphi_{1c}\varphi_{2c}V_1V_2A_{12}}{x_1V_1 + x_2V_2}\right] \qquad (19)$$

where φ_{1c}, φ_{2c} are the volume fraction at the critical point. The third derivative gives the critical concentration:

$$x_c = \frac{(V_1^2 + V_2^2 - V_1V_2)^{1/2} - V_1}{V_2 - V_1} \qquad (20)$$

There is a difference of less than 0.5% between the experimental and calculated value of the critical temperature and concentration.

Relation 17 is therefore a good analytical function for free energy in MAS in the intermediate range. The three derivatives of free energy needed to study the critical phenomena are thus in agreement with the three different experiments: vapor pressure, critical temperature, and critical concentration.

Furthermore, the excess volume of mixing between pure ammonia and the solvated cation $Na(NH_3)_n$ is negligibly small. The excess volume ΔV_m is calculated from

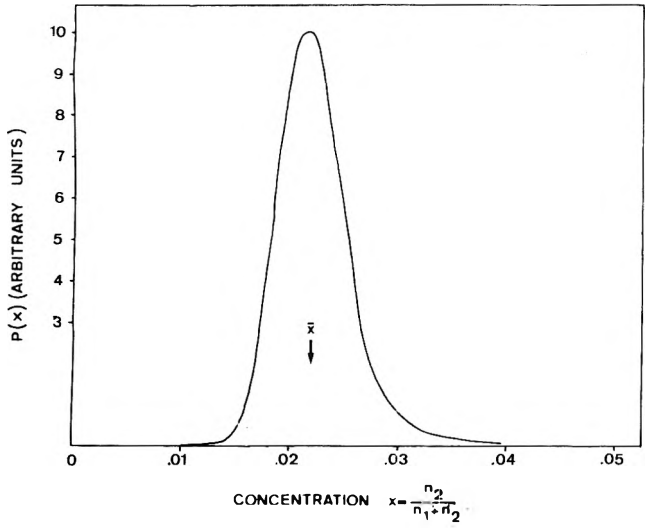

Figure 1. Concentration distribution around the mean concentration $x_2 = 0.022$ for a sodium–ammonia system at −35°C.

$$V_m = x_1V_1 + x_2V_2 + \Delta V_m = x_1\bar{V}_1 + x_2\bar{V}_2 \qquad (21)$$

$\bar{V}_1$, $\bar{V}_2$ being the partial molar volumes and V_1, V_2 the volumes of pure components.

In MAS the ratio

$$\frac{\Delta V_m}{V_m} = \frac{x_1(\bar{V}_1 - V_1) + x_2(\bar{V}_2 - V_2)}{x_1\bar{V}_1 + x_2\bar{V}_2}$$

is always smaller than 2×10^{-3}. The pressure work in relation 9 and excess volume in relation 11′ can be neglected.

Distribution of Concentrations. From relation 10 it is now possible to compute $p(x)$ for each average concentration. The curves are skewed Gaussian, and the most probable concentration may differ slightly from the average concentration $\bar{x}$. Some distribution functions are given in Figures 1–3.

It is interesting to note that the distribution curve calculated at the critical concentration $\bar{x}_c$ is broader than any other one. It corresponds to the minimum slope of the activity–concentration plot. Distribution curves are skewed on the right for concentration lower than critical concentration, and they are skewed on the left for concentrations larger than $\bar{x}_c$.

Temperature Effect. We are more interested in evaluating the temperature effect in terms of a power law in T or $T - T_c$ rather than studying the exact variation of the distributions with temperature. Considering the less precise relation 5, the square of the standard deviation (or the square of the half width of the distribution curve) is given by

$$\sigma^2 = \left[\frac{n}{kT}\left(\frac{\partial^2 G}{\partial x^2}\right)_{T,p}\right]^{-1} \qquad (22)$$

The temperature effect on the standard deviation will give the variation of the width of the distribution curve with temperature.

The characteristic length $L(T)$ is a function of $\epsilon^{-1/2}$; n is thus a function of $\epsilon^{-3/2}$. Derivation of relation 18 gives

$$\left(\frac{\partial^2 G}{\partial x^2}\right)_{T,p} = \frac{RT}{x^2} - \frac{2A_{12}V_1^2V_2^2x_1}{(x_1V_1 + x_2V_2)^3} = \frac{R}{x_2}(T - T_c) \qquad (23)$$

because

$$T_c = \frac{2}{R}\frac{\varphi_{1c}\varphi_{2c}V_1V_2A_{12}}{x_{1c}V_1 + x_{2c}V_2}$$

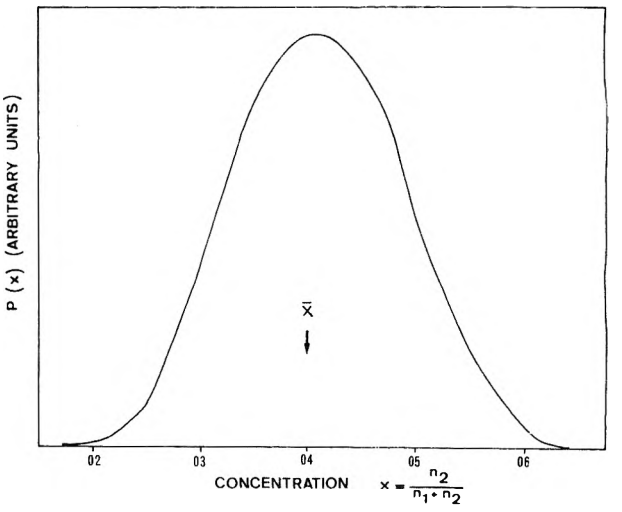

Figure 2. The same as Figure 1, but $x_2 = 0.0405$.

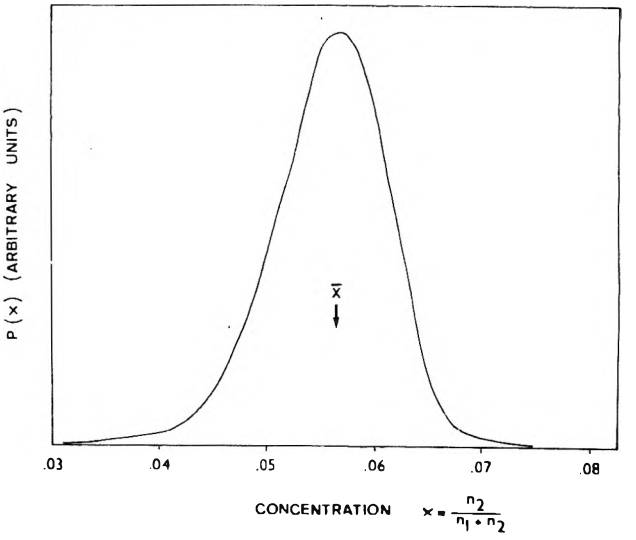

Figure 3. The same as Figure 1, but $x_2 = 0.0575$.

Application to (22) gives

$$\sigma^2 = f(T - T_c) = k(T - T_c)^{1/2}T \qquad (24)$$

and the standard deviation varies as $(T - T_c)^{1/4}T^{1/2}$.

There are two different scales of temperature, T and $T - T_c$. Close to T_c, T can be considered as a constant, and the width of the distribution curve varies slowly with temperature according to the ¼ power of $T - T_c$. Far from T_c, the $T^{1/2}$ contribution becomes larger than the $(T - T_c)^{1/4}$ contribution, and normal thermal fluctuations become more important than critical fluctuations.

Above, $T = \frac{4}{3}T_c$, the term $T - T_c$ does not play a large role any more. At this temperature the derivative of the variance $\partial(\sigma^2)/\partial T$ will show a minimum.

Discussion

Local concentration fluctuations in MAS can be studied from two experimental quantities, one purely thermodynamic, the other structural. Free energy as a function of concentration is determined from vapor pressure data, and the correlation length is obtained from neutron scattering.

The distribution curves are skewed Gaussian. The moment of skewness arises from the asymmetry of the activ-

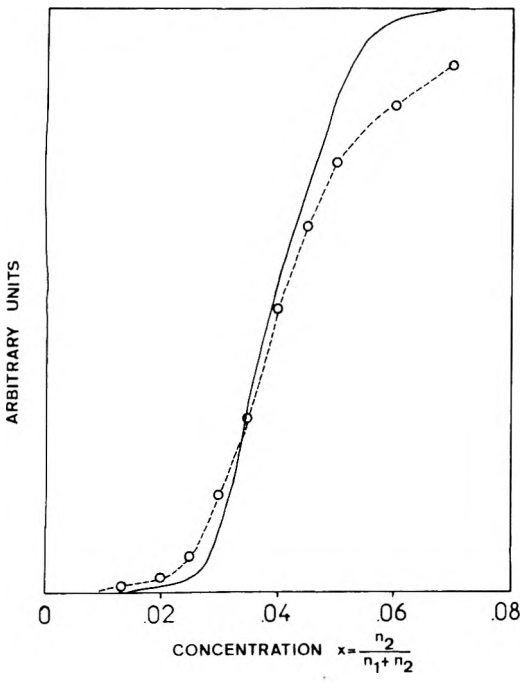

Figure 4. The calculated ESR line width of sodium–ammonia solutions at −35°C are compared with experimental data.[14]

ity–concentration function. In a critical region, concentration fluctuations are very important, and it is no more sufficient to use the second moment of free energy.

The knowledge of the distribution curves can help to interpret different properties of MAS in the intermediate range, if these properties depend on the local order.

Static or mechanical properties seem to lend themselves to easier interpretation. Let us suppose that a theoretical function f(x) can be derived for a physical property of a hypothetical MAS free from critical fluctuations. In the real fluctuating system, this property is changed into F(x) which can be derived from the relation

$$F(x) = \frac{\int_0^1 p(x)f(x)\,dx}{\int_0^1 p(x)\,dx} \tag{25}$$

The function f(x) can present any kind of particularity. In many cases it is supposed to have a sharp transition at a given concentration x_c. In the simplest case f(x) will be a step function centered on x_c with $f_1 = f(x)$ for $x < x_c$ and $f_2 = f(x)$ for $x < x_c$. Relation 25 can be simplified as

$$F(x) = \frac{f_1 \int_0^{x_c} p(x)\,dx + f_2 \int_{x_c}^1 p(x)\,dx}{\int_0^1 p(x)\,dx} \tag{26}$$

or as

$$F(x) = f_1 + (A_2/A)(f_2 - f_1) \tag{27}$$

where A_2 is the area under the distribution curve for $x_c < x < 1$, and A is the total area under the curve.

The ESR line width seems to be one of the properties which are more likely to have a step function behavior in a system free of fluctuations. Indeed, it is a constant in dilute solutions, and it varies slowly in concentrated solutions. It can be seen from Figure 4 that the experimental and calculated values are in good agreement. However, in the region above $x = 0.05$, the agreement is not so good, and this can be explained from the fact that a constant value has been chosen for concentrated solutions. Nevertheless, the two slopes are slightly different even in more dilute solutions. The two curves are found to fit perfectly on decreasing the correlation length by 10 to 15%. Other properties, like the paramagnetic susceptibility, can be interpreted in the same way.

It is less easy to use the results for interpreting transport properties. Landauer[13] showed that neither the conductivity nor the resistivity can be added up in a microscopically nonhomogeneous medium. He developed the effective medium theory (EMT) which gives good results for some alloys.

In the simplest model, two conducting states are supposed to exist in MAS, one for dilute solutions and the other for concentrated solutions. At a critical concentration, the nonmetal–metal transition occurs. EMT can be applied instead of relation 26. The results are not very different from those obtained by Jortner and Cohen[6] with their model. It comes from the fact that the ratio A_2/A gives a concentration scale not very different from that employed by Jortner and Cohen. Yet it remains that the two models imply very different physical pictures.

However, it does not seem right to suppose that the value of conductivity remains constant in the dilute as well as in the concentrated solutions of a system free from fluctuations. Indeed, at temperatures and concentrations far removed from the critical point, the conductivity varies very rapidly at all concentrations. Hence the above application of EMT appears to be an oversimplification difficult to justify.

Nevertheless, it is possible to use EMT generalized to n conducting states. The distributions curves can be split into a large number of intervals Δx. The area under the curve for one interval Δx would be

$$A(\Delta x) = \int_{x-(\Delta x/2)}^{x+(\Delta x/2)} p(x)\,dx \tag{28}$$

and

$$y_i = \frac{A_i(\Delta x)}{A} = \frac{\int_{x_i}^{x_i+\Delta x} p(x)\,dx}{\int_0^1 p(x)\,dx} \tag{29}$$

where y_i is the fraction of the solution at concentration $x_i \pm \Delta x/2$ or simply x_i if Δx is small. A conductivity can be attributed to each concentration x_i.

For two states of conductivity σ_1, σ_2, the conductivity of the solution must follow the relation

$$y_1 \frac{\sigma_1 - \bar{\sigma}}{\sigma_1 + 2\bar{\sigma}} + y_2 \frac{\sigma_2 - \bar{\sigma}}{\sigma_2 + 2\bar{\sigma}} = 0 \tag{30}$$

The extension to n states is quite direct

$$\sum_{i=1}^{n} \frac{y_i(\sigma_i - \bar{\sigma})}{\sigma_i + 2\bar{\sigma}} = 0 \tag{31}$$

Only one $\bar{\sigma}$ will satisfy (31).

In conclusion we may say that if a good theory can be derived for transport properties in MAS free from fluctuations, our treatment for fluctuations would permit one to interpret data in the intermediate range of concentration.

We want to emphasize the difference existing between the treatment of fluctuations itself, which is very close to experiment, and the application of this treatment to interpret physical properties, which requires a model for each property in an hypothetical MAS free from fluctuations.

References and Notes

(1) J. C. Thompson, *Rev. Mod. Phys.*, **40**, 704 (1968).
(2) M. H. Cohen and J. C. Thompson, *Adv. Phys.*, **17**, 857 (1968).
(3) M. J. Sienko and P. Chieux, "Proceedings Colloque Weyl II," J. J. Lagowski and M. J. Sienko, Ed., Butterworths, London, 1970.
(4) P. Damay, M. Depoorter, P. Chieux, and G. Lepoutre, "Proceedings Colloque Weyl II", see ref 3.
(5) G. Lepoutre and J. P. Lelieur, "Proceedings Colloque Weyl II", *see ref* 3.
(6) J. Jortner and M. H. Cohen, submitted for publication.
(7) P. Chieux, *Phys. Lett. A*, **48**, 493 (1974).
(8) A. B. Bhatia and D. E. Thornton, *Phys. Rev. B*, **2**, 304 (1970).
(9) T. L. Hill, "Statistical Mechanics", McGraw-Hill, New York, N.Y., 1956, Chapter 4.
(10) P. Debye, *J. Chem. Phys.*, **31**, 680 (1959).
(11) L. S. Ornstein and F. Zernike, *Proc. Acad. Sci. Amsterdam*, **17**, 793 (1914).
(12) P. Damay and G. Lepoutre, *J. Chim. Phys.*, 1276 (1972).
(13) R. Landauer, *J. Appl. Phys.*, **23**, 779 (1952).
(14) J. P. Lelieur, Thesis, Orsay, 1972.

Photoionization Spectra of Solutions as Obtained by Photoelectron Spectroscopy

Ladislav Nemec, Lucille Chia, and Paul Delahay*

Department of Chemistry, New York University, New York, New York 10003 (Received July 23, 1975)

Publication cost assisted by the Office of Naval Research and National Science Foundation

Photoelectron spectroscopic methods with variable photon energy (≈5.2 to 10 eV), which were developed in this laboratory, are applied to solutions of various photoionizable substances. A recently developed photoelectron spectrometer with continuous renewal of solution is briefly described. Experimental data include the quantum yield (per incident photon) for photoelectron emission as a function of photon energy and energy distribution curves (EDC) of emitted electrons at given photon energies over the full photon energy range. Photoionization cross sections are obtained by the method of EDC superposition as a function of photon energy. The photoionization spectra thus obtained are discussed, and mechanisms of photoionization are established: direct bound-continuum transitions and autoionization of bound excited states. The following systems are examined: lithium ferrocyanide in glycol, lithium iodide in tetraglyme, ferrocene in tetraglyme. The transfer of kinetic energy from quasi-free electrons (generated by optical excitation in the liquid phase) to the liquid medium is briefly treated. It is shown that the average loss of kinetic energy per scattering event in the liquid is constant and independent of kinetic energy. The present approach to the determination of photoionization spectra of solutions (and also pure liquids) is, to the writers' knowledge, the only one of general scope that is available at the present.

Introduction

It was shown in recent work from this laboratory[1-5] that the photoionization (PI) spectra[6] of pure liquids and solutions can be determined by photoelectron spectroscopy with variable photon energy. Basic experimental data thus obtained consist of (i) the photoelectron emission (PEE) quantum yield (per incident photon) as a function of photon energy; (ii) the derivative of the photocurrent (at a given photon energy), with respect to the retarding potential, as a function of retarding potential. The energy distribution curves (EDC), obtained under (ii), display the distribution of electrons emitted into vacuum as a function of their kinetic energy. PI spectra, that is, plots of PI cross section (in arbitrary units) against photon energy, are obtained by the method of EDC superposition.[1] A fairly detailed review of principles, methodology, and applications will be available soon.[5]

Initial applications, reviewed in ref 5, were made in the visible and ultraviolet ranges (anthracene monovalent anion radical,[1] solvated electrons,[3] sodium anion[3]). The feasibility of extension to the vacuum ultraviolet range was recently demonstrated with relatively simple equipment.[4] Methodology and instrumentation in this range have now been developed to a high degree,[7] and the number of potential applications is much greater than in the visible and ultraviolet ranges. Applications to three systems are presented here for photon energies up to 10 eV. Preliminary results on energy transfer between quasi-free electrons and the liquid medium are also given and discussed.

Experimental Section

Experimental requirements for the determination of PEE quantum yields and EDC's with a liquid emitting surface are analyzed in detail in ref 1 and 5. The new photoelectron spectrometer, used in this work, will be described and discussed elsewhere.[7] Only a few essential points will be mentioned here.

The most significant novel feature of the instrument is a *rotating disk target* (diameter, 9 cm; thickness, 0.4 cm) whose axis of rotation (72 rpm.) is horizontal. The lower

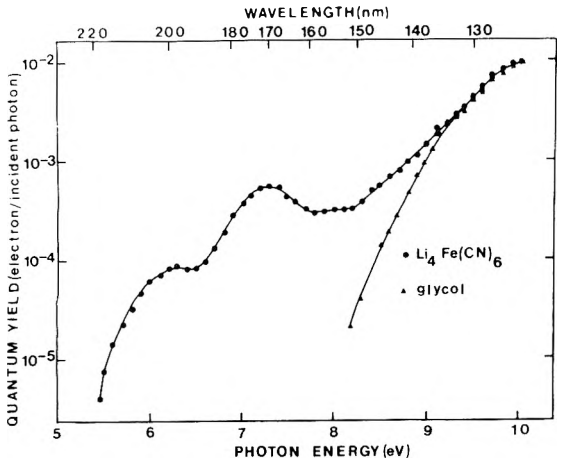

Figure 1. Quantum yield (expressed per *incident* photon) against photon energy for glycol and 0.2 *M* lithium ferrocyanide in glycol at −6°C (vapor pressure, 4 μ).

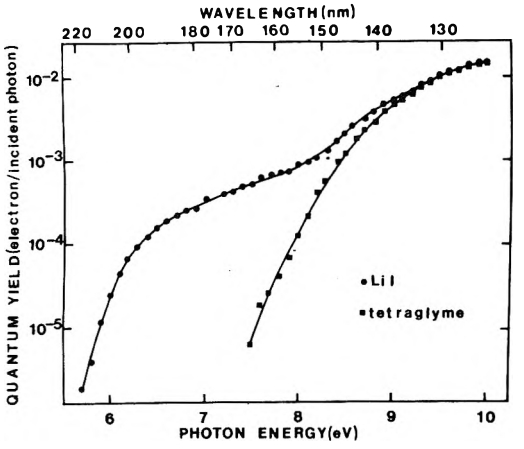

Figure 2. Quantum yield against photon energy for tetraglyme and 0.4 *M* lithium iodide in tetraglyme at 6.5°C (vapor pressure, 0.3 μ).

edge of the disk is immersed to a depth of ≈0.8 cm in the liquid or solution being studied. The latter is contained in a glass trough jacketed for a circulating coolant (to lower the vapor pressure). The liquid film on the upper edge of the disk is irradiated, and emitted electrons are collected on a cylindrical electrode made of metallic screen. The adjustable retarding potential is applied between the liquid or solution and the collector electrode. Provisions are made (slits, etc.) to minimize the evaporation of the liquid. The vacuum-tight assembly is bolted to the base plate of a 30-in. high bell jar which is evacuated continuously. Moreover, the collector electrode is surmounted by a copper plate (diameter, 36 cm) with circulating liquid nitrogen to increase, by very efficient cryogenic pumping, the pumping speed above the upper edge of the rotating disk. Cryogenic pumping is essential as it results in the establishment of a very steep gradient of pressure in the gas phase near the surface of the emitting liquid surface. In this way, the distortion of EDC's resulting from inelastic electron–gas molecule collisions is rendered negligible under correct experimental conditions.[1]

The rotating disk provides continuous renewal of the liquid emitting surface. This renewal is essential for the following reasons: (i) to minimize the enrichment in solute and the possible formation of a solid crust as a result of intense solvent evaporation (in the study of solutions); (ii) to

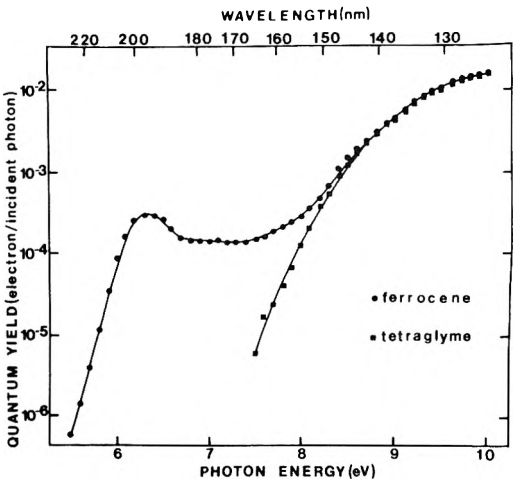

Figure 3. Quantum yield against photon energy for tetraglyme and 0.2 *M* ferrocene in tetraglyme at 6.5°C (vapor pressure, 0.3 μ).

prevent freezing of the liquid because of evaporation; (iii) to prevent accumulation of the products of possible photochemical reactions. The rotating disk is much more convenient to use and more suited to experiments in the vacuum ultraviolet range than the overflow system utilized in previous work.[1,3,8]

The light source in this work was a McPherson monochromator, Model 218, equipped either with a filament-type Hinteregger hydrogen lamp or a 250-W mercury lamp. Special attention was paid to the problems posed by stray light and calibration of the photon flux. Details on the performance of the instrument are given in ref 7. Suffice it to say that measurements can now be performed quite routinely and reliably up to 9 to 10 eV.

Solvents were purified by vacuum distillation. A small amount ($\approx 10^{-4}$ *M*) of lithium chloride was added in all cases, except for ferrocyanide and iodide, to achieve electrical conductivity of the liquid phase. Contribution to PEE by chloride was negligible under the prevailing experimental conditions.

Absorption spectra were obtained with a Cary 15 spectrometer (flushed with nitrogen) with 0.01- or 0.001-cm Suprasil cells.

Quantum Yield and Energy Distribution Curves

Quantum Yields. Quantum yields, expressed as the number of emitted electrons per *incident* photon, are plotted on a logarithmic scale against photon energy in Figures 1–3 for the solutes and solvents studied here. These curves will be discussed below in conjunction with the corresponding PI spectra, and only the following points are noted now.

(i) Quantum yields extend over a wide range, i.e., more than 3 to 4 decades.

(ii) Quantum yields for the solute are low ($\lesssim 10^{-3}$ electron emitted per incident photon). This is to be expected for PEE by solutions for the following reasons. Electrons that are emitted originate from a layer of solution adjacent to the liquid–vacuum interface.[5] The thickness of this emission layer is, on the average, of the order of magnitude of the range of quasi-free electrons at the photon energy being used. The incident photon flux is hardly attenuated over the depth of solution corresponding to the range of quasi-free electrons, and consequently the quantum yield per incident photon is very low for the solute. Most quasi-free electrons generated by optical excitation of the solute

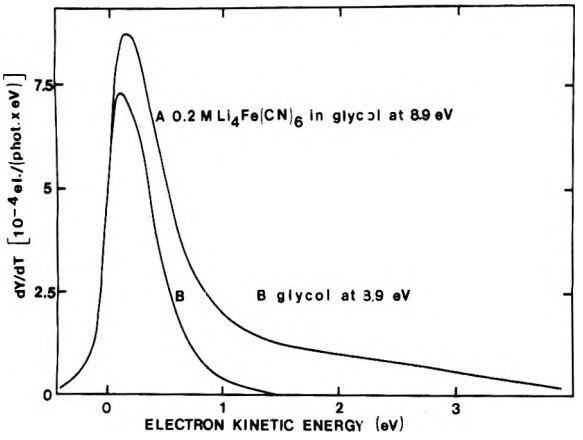

Figure 4. Energy distribution curves at photon energy of 8.9 eV for 0.2 *M* lithium ferrocyanide in glycol (curve A) and glycol (curve B) at −6°C (vapor pressure, 4 μ). *Y*, quantum yield; *T*, kinetic energy of electrons emitted into vacuum.

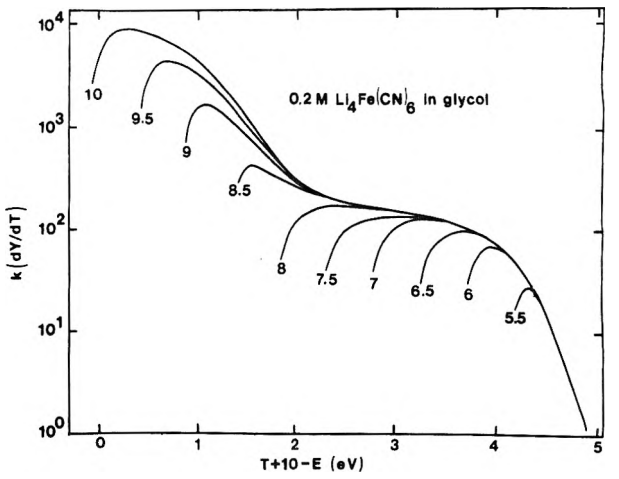

Figure 5. Superimposed EDC's for 0.2 *M* lithium ferrocyanide in glycol at −6°C, plotted with a logarithmic scale of ordinates. Photon energy marked in electron volts on each curve. EDC's were normalized to EDC at 10 eV. *Y* and *T* defined in caption to Figure 4; *E*, photon energy; *k*, proportionality factor in normalization. The zero of the abscissa was set arbitrarily at the tip of the EDC obtained at 10 eV. The logarithmic scale of ordinates is within an arbitrary constant.

are not emitted into vacuum but are solvated and ultimately lost in the liquid by scavenging or geminate recombination. At sufficiently high photon energies, the quantum yield for the solvent is higher than for the solute by a factor corresponding very roughly to the mole fractions of solvent and solute. This rule of thumb is very crude because the PI cross sections for the solvent and solute are not the same and, in fact, can be quite different.

(iii) The contribution of the solvent to PEE is quite negligible over a range of 1–2 eV. Actually, we shall see in the next section that discrimination between PEE by the solvent and the solute extends further toward higher photon energies than one would surmise from the quantum yield curves of Figures 1–3.

Energy Distribution Curves. EDC's plotted in Figure 4 have the usual expected shape for PEE by a liquid or solution.[1,2,5] The zero of kinetic energy of the electrons emitted into vacuum was set in Figure 4, by convention, at the inflection point of the ascending segment of the EDC's.[1,5] This assignment of zero kinetic energy is somewhat arbitrary, but it does not affect the interpretation whatsoever. The EDC of the solution is much richer in emitted electrons of high kinetic energy than the EDC of the pure solvent. This is the case because PI by the solvent requires higher photon energies than PI by the solution (quantum yield curves in Figure 1). Since PI spectra are obtained from the high-energy tail of EDC's, as shown below, PI cross sections of the solute can be determined even when PEE by the solvent makes a major contribution to the total PEE, as in the case in Figure 4 (see quantum yield at 8.9 eV in Figure 1). This circumstance is most fortunate in extending the range of photon energies that can be covered for given solvent and solute. Reading of EDC's is rendered easier by the use of a logarithmic amplifier in the recording of the ordinates of EDC's.

Method of EDC Superposition. PI spectra are obtained by the method of EDC superposition, the theory of which is fully developed in ref 1. The principle of the method is as follows.

Consider two EDC's for a given system measured at two different photon energies and plotted with logarithmic scale of ordinates. The EDC measured at the lower photon energy is shifted toward higher kinetic energies along the abscissa axis by an increment equal, in absolute value, to the difference in the photon energies at which the two EDC's were obtained. The shifted EDC is moved vertically until its high-energy region overlaps to the greatest feasible extent with the high-energy region of the unshifted EDC. At any given kinetic energy in the superposition range, the ratio of the ordinates of the two EDC's is independent of kinetic energy. This ratio, after normalization for the photon fluxes, is equal to the ratio of the PI cross sections at the two photon energies. The analysis is repeated for a series of EDC's at different photon energies, and the corresponding PI cross sections are obtained (in arbitrary units) as a function of photon energy.

This method of analysis was applied to all systems studied in this paper, and an example is given in Figure 5 for lithium ferrocyanide. The superposition in Figure 5 is quite remarkable and extends over a range of kinetic energies of more than 2 eV at the high photon energies. The standard deviation for superposition was typically ≈8%. The stepwise appearance of the EDC's of Figure 5 (plotted with logarithmic scale of ordinates) is due to PEE by two substances, namely lithium ferrocyanide and glycol. The EDC for the pure solvent does not exhibit any step (see section on Energy Transfer below).

The method of EDC superposition rests only on very general arguments[1] and does not presuppose any detailed model for the PEE process. Its validity was verified in ref 1 by comparison of the PI spectrum, obtained by this method, with the PI spectrum surmised from totally independent evidence. This comparison was made for anthracene monovalent anion radical. Further evidence of the validity of the method is given below (in particular for ferrocene).

Photoionization Spectra

The PI spectra presented and discussed below pertain to PI in the *liquid*, that is, the process(es) involving the production of quasi-free electrons in the liquid phase upon irradiation. Thus, PEE into vacuum is measured in this approach, but the method of EDC superposition yields the spectrum for PI in the liquid phase. This point is discussed in detail in ref 1.

Mechanisms of PI will be suggested in this section, but the spectroscopy of each substance will not be examined in

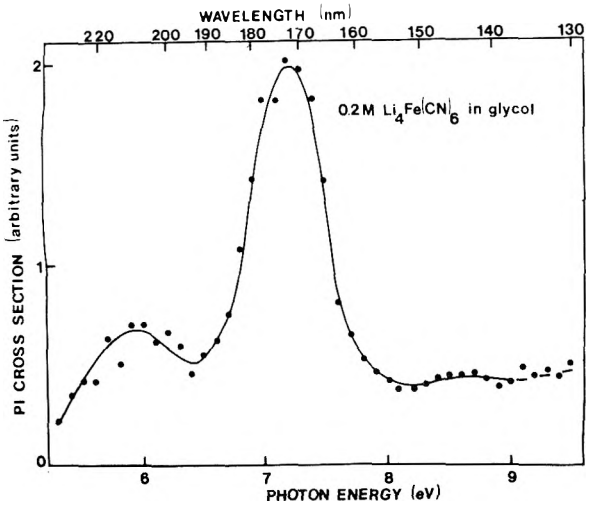

Figure 6. Photoionization cross section against photon energy for lithium ferrocyanide for the conditions of Figure 1.

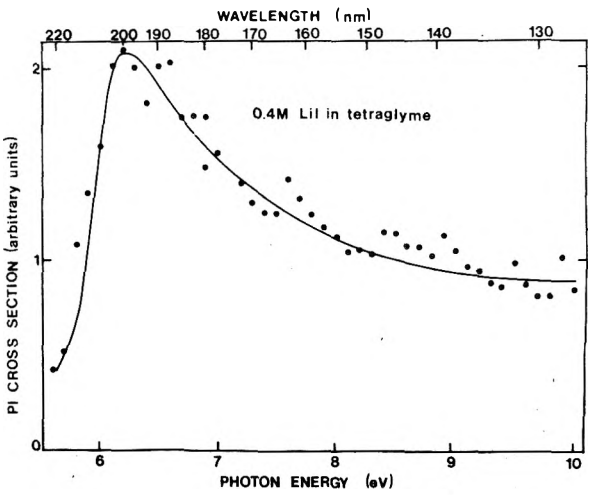

Figure 7. Same curve as Figure 6 for lithium iodide for the conditions of Figure 2.

detail. The present results are intended to show what information can be obtained rather than to constitute a fairly complete study. More complete treatment of data for these and other systems is reserved for future work now being planned.

Lithium Ferrocyanide. The PI spectrum of lithium ferrocyanide in glycol (Figure 6) exhibits two bands with maxima at ≈5.8 and 7.2 eV, respectively. Scattering of data for the band at ≈5.8 eV is pronounced because of the low intensity of the light source in this spectral range and the low quantum yields. Experimental conditions were more favorable, from this point of view, for the band at 7.2 eV. There is some indication of a third weak band at ≈8.6 eV, but this conclusion is very tentative. Cross sections above 8.8 eV are definitely uncertain because of the unfavorable spectral characteristic of the hydrogen lamp.

The PI spectrum of Figure 6 differs markedly from the quantum yield spectral response of Figure 1 for the following reasons. The quantum yield is determined to a first approximation by the product of the PI cross section and the range of quasi-free electrons generated in the liquid by optical excitation.[5] Matters are further complicated in the threshold region by the solution–vacuum interfacial barrier, but this complication need not be introduced here. The range of quasi-free electrons produced by a given PI process increases with photon energy because of the concomitant increase in kinetic energy available for transfer to the solvent. Consequently, the effect of the decrease in PI cross section on the quantum yield beyond each maximum in Figure 6 (toward higher photon energies) is minimized or eliminated in Figure 1 as a result of the increase in the range of quasi-free electrons. Further details on this matter are given in ref 5 and previous papers listed in ref 1.

The PI spectrum of Figure 6 has the appearance of the absorption spectrum of a solution. Thus, the two bands appear quite symmetrical, and their width at half-intensity is of the order of 0.6 eV. In fact, the 5.8 eV PI band matches fairly well a corresponding band in the absorption spectrum of lithium ferrocyanide in glycol. This observation was already noted in a preliminary study of ferrocyanide in glycerol with less elaborate equipment.[4] Superposition of PI and absorption bands strongly suggests[1,9] a mechanism of PI via autoionization of an excited bound state. In addition, there is a low background due to PI by direct transition into the continuum. Autoionization can also be invoked for the 7.2 eV PI band. The symmetric shape of this band rules out significant PI for this band by direct bound-continuum transitions. A markedly asymmetric band with drawn-out tail would be expected[5,10] for this type of transition (see lithium iodide below).

Direct observation of the 7.2-eV absorption band by absorption or reflectance spectroscopy would be difficult because of strong absorption by the solvent. This difficulty is avoided in PEE spectroscopy because the emission layer in the liquid (see section on Quantum Yields) is much thinner than the layer corresponding to major attenuation of the incident photon flux, even in the case of strong solvent absorption. Thus, the present approach may prove useful in determining absorption bands in the vacuum ultraviolet range when more conventional methods fail or are very difficult to apply. This method for obtaining absorption bands is valid, of course, only when PI occurs almost solely via autoionization of excited bound states. In other words, the cross section for direct bound-continuum transition, at a given photon energy, must be quite negligible in comparison with the cross section for autoionization. If this condition is not met, the band shape may be too distorted to allow reasonable identification of the PI spectrum with the absorption spectrum. Finally, it is noted that the resolution in PEE spectroscopy is somewhat lower than in absorption spectroscopy. This is the case primarily because much higher photon fluxes are needed in the present method than in absorption or reflectance spectroscopy.

Lithium Iodide. The PI spectrum of lithium iodide in tetraglyme (Figure 7) has a maximum at ≈6.2 eV and a highly asymmetric tail. The curve of Figure 7 is quite different from the quantum yield curve of Figure 2, which rises gradually even when the contribution to PEE by the solvent is quite negligible. This difference between Figures 2 and 7 arises from the increase in the range of quasi-free electrons with increasing photon energy, as was explained for lithium ferrocyanide. The shape of the PI band in Figure 7 is quite similar to that for PI of solvated electrons[3] and suggests PI via bound-continuum transitions.

The uv absorption spectrum of LiI in tetraglyme exhibits the usual doublet at 5.37 and 6.35 eV. Our results, however, indicate that the process leading to photoelectron emission into vacuum should be identified with the higher energy absorption band only. This band, after subtraction of the

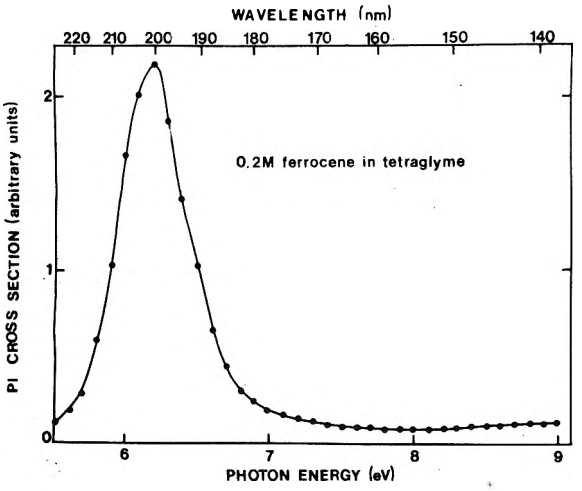

Figure 8. Same curve as Figure 6 for ferrocene for the conditions of Figure 3.

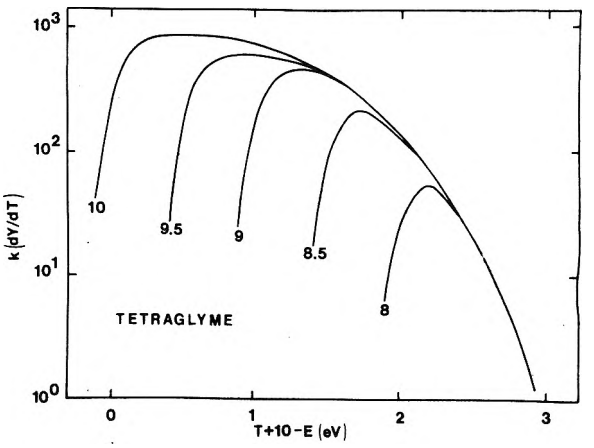

Figure 9. Superimposed EDC's for tetragiyme at 6.5°C (vapor pressure, 0.3 μ), plotted with a logarithmic scale of ordinates. Same notations as in Figure 5.

contribution of the first band (assumed symmetrical), matches quite well the corresponding part of the PI cross section of Figure 7. Similar results were reported in a work on the photoproduction of solvated electrons by I_{aq}^-.[11] According to the authors of ref 11, the energy required for escape of an electron from the solvent cavity can be more easily supplied by optical excitation within the higher photon energy band. Moreover, the absence of any steps on the experimental EDC's of LiI in tetraglyme indicates that only one process results in emission into vacuum.

In contrast, the photoelectron spectra of iodides in the gas phase exhibit two bands separated by ca. 1 eV,[12] corresponding to the spin–orbit splitting.

Ferrocene. This substance yielded a PI band (Figure 8) which is quite symmetric and has the shape of an absorption band. The corresponding absorption band of ferrocene in tetraglyme (measured up to ≈6.5 eV) indeed matches the PI band very well, and this matching very strongly suggests PI via autoionization of excited bound states. The low background above 7 eV in Figure 8 probably corresponds to a small contribution to PI by direct bound-continuum transitions. This substance and others of the same type appear to be excellent candidates for further systematic study of their PI spectroscopy.

The excellent agreement between the PI band of Figure 8 and the absorption band, as far as the latter could be measured (≲6.5 eV), confirms our previous observations that the present method indeed yields correct PI spectral response curves.

Energy Transfer between Quasi-Free Electrons and the Liquid Medium

Superposition of EDC's requires, according to the analysis of ref 1, that the average loss of kinetic energy by quasi-free electrons for any given net displacement in the liquid be independent of kinetic energy. This conclusion is based on the very general arguments of ref 1 and does not imply any detailed model for PEE by pure liquids or solutions. The foregoing implication can be stated in greater detail by application of the random walk theory of EDC's in ref 2. EDC superposition then implies that the average loss of kinetic energy by quasi-free electrons per scattering event is constant and independent of kinetic energy. This conclusion is at variance with the classical result, according to which the rate of loss of energy per unit of length along the tortuous path of the random walk is inversely proportional to the square of the kinetic energy of quasi-free electrons.

The EDC's of Figure 9 are in agreement, in their range of superposition, with the EDC's calculated from the theory of ref 2. This analysis involves two assumptions: the relationship for energy transfer, mentioned above, and a Gaussian distribution of quasi-free electrons according to their kinetic energy upon generation.

EDC superposition is an experimental fact which is observed over a wide range of kinetic energy (≈2 eV in Figure 9). EDC's are superposable only within experimental errors, but except for this obvious limitation, EDC superposition seems quite general. It was observed for all the liquids studied here and in previous work (hexamethylphosphoric triamide, glycerol, glycol, and tetraglyme). The present result is only preliminary, but it suggests some interesting possibilities: comparison of liquids with markedly different vibrational spectra, for instance. The range of energy losses could be extended to 10–13 eV by using rare-gas lamps (without monochromator and mirrors!) and a few fixed wavelengths. Indeed, the adjustment of photon energy by narrow increments, which is essential in obtaining reliable PI spectra, is not needed in energy transfer studies.

Potentialities and Limitations

Results reported here demonstrate the feasibility of obtaining the PI spectra of a wide variety of substances, either as pure liquids or in solutions in appropriate solvents. The PI spectroscopy of liquids and solutions seems ripe for systematic development. This was not the case up to now because PI spectra could be obtained by other methods (photoconductivity, electron spin resonance, production of solvated electrons, etc.) only under special favorable circumstances. The approach followed here is much more general and is applicable even when there is strong optical absorption or even PEE by the solvent (in the study of solutions). Moreover, the rotating disk target developed for this work[7] should prove useful in photoelectron spectroscopy at fixed photon energy (e.g., He-I, ESCA).

Further work on the PI spectroscopy of liquids and solutions should prove of interest for a variety of reasons: energy levels in liquids, ionization potentials, correlation with PI spectra for gases and solids, solvent effects, PI mechanisms, photochemistry at high photon energies, theoretical calculations of PI cross sections, etc.

One limitation inherent to the method must be mentioned. The vapor pressure of the liquid or the solution should not exceed the upper limit beyond which EDC's are markedly distorted by inelastic collisions between electron and molecules of the liquid in the gas phase. Methods for increasing this limit by efficient pumping are discussed in ref 1, and the maximum allowable pressure was estimated in that paper. The matter should be settled experimentally with the equipment being used because estimates are based on simplified models. We set this limit at 0.1 Torr for the equilibrium vapor pressure of the liquid with present equipment, but this value is tentative. Solvents used in this work had much lower vapor pressures (≤ 4 μ) than this upper limit. Cooling of the liquid near its freezing point should help, of course, but some pure liquids undoubtedly will have to be excluded.

There is a second possible limitation which, however, has not been encountered thus far. It arises from the sign and value V_0 of the ground-state energy of quasi-free electrons in the liquid. V_0 is expressed with reference to the vacuum level of electrons taken as zero. A negative value of V_0 indicates a positive affinity of the liquid for quasi-free electrons and vice versa. Values of V_0, or even its sign, are not known for liquids except for liquid rare gases. If V_0 is positive, it does not introduce any limitation on the determination of PI spectra by the present method. However, if V_0 is negative and quite large in absolute value (>1 eV), the PI spectrum may be truncated at the lower photon energies. Thus, PI may indeed occur in the liquid, but most quasi-free electrons generated by optical excitation do not have sufficient kinetic energy to overcome the barrier corresponding to V_0. This difficulty would be enhanced by a strong adverse surface potential arising from a layer of oriented dipoles at the liquid–vacuum interface. Significant PEE would then be observed only at sufficiently high photon energies, e.g., in the tail of the PI band.

Acknowledgment. This work was supported by the National Science Foundation and the Office of Naval Research.

References and Notes

(1) H. Aulich, P. Delahay, and L. Nemec, *J. Chem. Phys.*, **59**, 2354 (1973).
(2) L. Nemec, *J. Chem. Phys.*, **59**, 6092 (1973).
(3) H. Aulich, L. Nemec, and P. Delahay, *J. Chem. Phys.*, **61**, 4235 (1974).
(4) L. Chia, L. Nemec, and P. Delahay, *Chem. Phys. Lett.*, **32**, 90 (1975).
(5) P. Delahay in "Electron–Solvent and Anion–Solvent Interactions", L. Kevan and B. Webster, Ed., Elsevier, Amsterdam, in press.
(6) We use the expression "photoionization spectrum" both for electrically neutral and ionic species. More correctly, one should restrict this expression to electrically neutral species, and use "photodetachment spectrum" for anions. Likewise, we use autoionization in general and do not single out autodetachment for anions.
(7) H. Aulich, L. Nemec, L. Chia, and P. Delahay, *J. Electron Spectrosc. Relat. Phenom.*, in press.
(8) Hitherto unpublished details of this overflow system are given in ref 5.
(9) H. Aulich, B. Baron, and P. Delahay, *J. Chem. Phys.*, **58**, 603 (1973).
(10) Such a PI band with drawn-out tail is indeed observed for solvated electrons.[3]
(11) J. Jortner, M. Ottolenghi, and G. Stein, *J. Phys. Chem.*, **68**, 247 (1964).
(12) T. D. Goodman, J. D. Allen, Jr., L. C. Cusachs, and G. K. Schweitzer, *J Electron Spectrosc. Relat. Phenom.*, **3**, 289 (1974).

Discussion

J. JORTNER. In the spectral region where the solvent absorbs directly, electronic energy transfer from the solvent to the solute can take place resulting in photoionization of the solute. This effect will distort the solute photoionization line shapes at high energies. As solvent–solute energy transfer can occur on a fast 10^{-12}–10^{-13} sec time scale (at appropriate solute concentrations), it can compete with intramolecular indirect decay processes of the solvent molecules, such as predissociation or internal conversion. A detailed study of these effects will lead to valuable information concerning intramolecular dynamics.

P. DELAHAY. This indeed would be interesting, but it remains to be seen whether we can study the effect by our approach. The problem is as follows.

In the EDC superposition method we select the region of high kinetic energy where the contribution by the solute is overwhelmingly predominant in comparison with that of the solute. Now, energy transfer from an excited state of the solvent to an excited state of the solute would have to occur with small energy losses (by relaxation of the excited state of the solvent) to cause photoionization of the solute with production of quasi-free electrons with sufficient kinetic energy to be "picked up" in EDC superposition. If this is not the case, the effect of this type of energy transfer would not be seen to any significant extent in our photoionization spectra. So far, our spectra for photoionization via autoionization do not show any significant distortion. This problem is certainly interesting, and we are well aware of it.

R. CATTERALL. There is a supposed similarity of the ground state of e_{solv}^- and the first excited state of I_{solv}^-. The analogy seems to be supported by the form of the photoionization peak?

P. DELAHAY. Both photoionization spectra for solvated electrons in hexamethylphosphoric triamide (HMPA) and iodide in tetraglyme indicate that a particle in a box gives a fairly good but *crude* model. That is, the coulombic tail seems rather minor. The range of photon energies, however, are very different. In fact, Symons proposed a square well model for iodide ca. 1960.

M. SILVER. Can photoemission give V_0 if it is negative?

P. DELAHAY. The method of EDC superposition gives the photoionization spectrum for the internal photoelectric effect, that is, for emission of quasi-free electrons *into the liquid*. Thus, we eliminate the problem of V_0 and cannot determine V_0 by this approach. The fact that V_0 is eliminated is clearly demonstrated by the identity (position and width of bands) of the absorption band with the band for photoionization via autoionization. There is, however, a way of determining V_0 by comparing the quantum yield spectral response curve for photoconductivity (of a neutral species!) with the quantum yield spectral response curve for photoelectron emission into vacuum. Such a comparison, however, should be done very carefully because the quantum yield for the external photoeffect is complicated by the range problem. Moreover, the result for V_0 should be corrected for the surface potential which is generally unknown. Thus, only large negative V_0's (say >0.5 V in absolute value) seem accessible from such a comparison. This would already be interesting! The question of V_0 is further discussed in our paper published with the records of this conference.

Continuous Registration of Optical Absorption Spectra of Periodically Produced Solvated Electrons

P. Krebs

Institut für Physikalische Chemie und Elektrochemie, Universität Karlsruhe, Karlsruhe, Germany *(Received August 1, 1975)*

Absorption spectra of unstable intermediates, such as solvated electrons, were usually taken point by point, recording the time-dependent light absorption after their production by a flash.

The experimental arrangement for continuous recording of the spectra consists of a conventional one beam spectral photometer with a stabilized white light source, a monochromator, and a light detector. The sample is located in the light beam of the photometer, the wavelength of which can be varied continuously. The dc signal of the light detector after amplification is fed into a servo mechanism adjusting the spectrometer slit to constant light detector output, thus compensating for the wavelength dependence of the light intensity, of the transmission of the monochromator and the sample, and of the sensitivity of the detector.

By periodic production of light absorbing intermediates such as solvated electrons, e.g., by ac uv light, a small ac signal is modulated on the light detector output which after amplification can be continuously recorded as a function of wavelength. Sensitivity of the arrangement can be improved by further amplification with a lock-in amplifier, which is locked to the frequency of the ac light source. Especially this method allows the detection of absorption spectra when disturbances from the outside provide a signal-to-noise ratio smaller than 1. In this way the spectra of concentrations as low as 10^{-11} M solvated electrons (lifetime $\approx$ 1 msec) in water–ammonia mixtures can be obtained, using a 200-W high-pressure mercury lamp chopped with a frequency of 10–1600 Hz.

The technique also can be applied in combination with other methods of periodic production of solvated electrons, such as flash photolysis, pulse radiolysis, ac electrolysis, etc.

Absorption Spectra of Excess Electrons in Alkali Halide Salt Melts

W. Schmitt and U. Schindewolf*

Institut für Physikalische Chemie und Elektrochemie, Universität Karlsruhe, Karlsruhe, Germany *(Received September 8, 1975)*

The absorption spectra of excess electrons in melts of alkali halide salts have been determined by a technique described in principal by Krebs. Instead of periodic uv-induced photoionization the electrons were produced periodically by ac electrolysis on the surface of a platinum electrode. The wavelength λ_{max} of maximum absorption of different salts and salt mixtures taken in the temperature intervall between 600 and 900°C is in the range between 700 and 1150 nm. The relative half-width of the spectra (half-width/peak position) is almost 1.

For excess electrons in solid salts (F-centers) a quadratic relation between λ_{max} and the lattice parameter d ($\lambda_{max} \sim d^2$; as for an electron in a box) was given by Mollwo; d calculated from molecular weight and the density of the solids is a measure of the radius of the anion vacancy (cavity) occupied by the electrons. In the salt melts also the quadratic relationship is obtained, however, with a wider spread of data and with a steeper slope than for solids. To squeeze data for solids and melts on a single curve, it has to be assumed that the cavity radius of the electrons in melts is about 15–18% larger than deduced from its "lattice parameter". This is conceivable because in the melted state with its mobile particles the electron could expand the cavity (just as in ammonia) which is impossible in the rigid structure of the solid crystal. The large relative half-width of the spectra in the melts ($\approx$1 as compared to $\approx$0.2 in the solids) hints of a wider distribution of cavity radius than in the solids.

Discussion

A. K. PIKAEV. I would mention that we have measured the optical absorption spectra of e_s^- in molten alkaline halide compounds by the pulse radiolysis method and have obtained the same results on these spectra. Our data were published in *Radiat. Eff.*, **22**, 71 (1974).

G. R. FREEMAN. If you use the random-close-packed formula to estimate the volume of the molecule, the estimated radius of the cavity will increase.

J. JORTNER. Your correction for the Ivey law for molten alkali halides is sensible. The relation $d = (M/\rho N_c)^{1/3}$ has to be modified to account for the packing in the molten salt which will result in an increase of d.

U. SCHINDEWOLF. Yes; but of course it needs more corrections because, e.g., the effect of temperature is much larger than the thermal expansion would indicate. Our CNOE corrections are only the zeroth order approximation.

J. BELLONI. How were the solvated electrons formed?

P. KREBS. The solvated electrons were formed by uv photolysis of added methyl alcohol and potassium hydroxide which also act as scavengers for unwanted reactive photolysis products. So we actually made use of the efficient technique introduced by Mme. Belloni some years ago.

M. J. SIENKO. It would be interesting to look at +2 salts and find structure in the liquid.

U. SCHINDEWOLF. So far we studied only alkali metal halides. Nitrites, nitrates, sulfates, and others are being reduced at the cathode, so no electrons are injected. Studies with alkali earth salts will be taken up.

Discussion on paper by J. B. Weinstein and R. F. Firestone, *J. Phys. Chem.*, **79**, 1322 (1975).

M. SILVER. Your conclusion regarding the effect of preexisting sites and the correlation is not surprising. When one considers so simple a system as helium fluid, near where the localized electronic state as a function of density is becoming stable, the mobility of the electron is completely determined by preexisting density fluctuations. In this critical region, the mobility due to these preexisting "traps" can drop to 1/10 to 1/100 with only a small change in density. Above the critical density, after trapping in the preexisting traps, one does get a distortion which further lowers the energy.

R. HOLROYD. Your suggestion of reaction of the electron with preexisting aggregate rather than by reaction with an alcohol monomer, followed by aggregation (Mozumder model), is in agreement with our electron rate constant study in alkanes since we find that the rate of reaction of the electron with the methanol monomer is slow ($k \leq 10^8\ M^{-1}\ \text{sec}^{-1}$).

G. R. FREEMAN. Your work is a further indication that very long range polarization interactions are relatively unimportant in determining the observed properties of electrons in these liquids. Furthermore, you would not expect to observe spectral changes in the room temperature 50:50 mixed solvents after a microsecond. Molecular species diffuse hundreds of ångströms in that time.

J. C. THOMPSON. Do concentration variations of ΔE match those of ΔG?

R. FIRESTONE. There is no systematic relationship between the variation of ΔG vs. composition and that of ΔH or of ΔS except within a single class of solutions over limited concentration ranges; e.g., alcohols in alkanes. ΔE values are not presently available. It seems *unlikely* that a single *form* for ΔG vs. c or ΔE vs. c exists, except perhaps within single classes of solutions in limited c ranges.

No systematic dependence exists, incidentally, between $\Delta E^{E}_{\lambda max,c}$ and either ΔH or ΔS^{E} nor among ΔG^{c}, ΔH, and ΔS^{E} at constant c.

Laser-Raman Investigation of Dilute Metal–Ammonia Solutions

T. R. White and W. S. Glaunsinger*

Department of Chemistry, Arizona State University, Tempe, Arizona 85281 *(Received July 18, 1975)*

The temperature dependence of the Raman spectra of ammonia and 6×10^{-4} M lithium– and 3×10^{-4} M calcium–ammonia solutions has been studied between 195 and 300 K. A careful study has been made of the low-frequency region, using an iodine filter below 50 cm^{-1}, but no solvated-electron band was observed. Band positions, widths, and depolarization ratios have also been measured in the N–H stretching region (3100–3500 cm^{-1}). All band maxima increase linearly with temperature, and the solution bands occur at lower frequencies than those of ammonia. Uncoupled line widths have been determined using the coupled-damped-oscillator model. The uncoupled line widths decrease linearly with temperature, and the line width in the solutions is less than that in ammonia. The band shift and line width data are interpreted in terms of hydrogen bonding and nonreorientational relaxation processes, respectively.

Introduction

The nature of the solvated electron in dilute metal–ammonia solutions has been the subject of several experimental and theoretical investigations.[1-3] In very dilute solutions the solvated cations and electrons are unassociated, so that they may be treated independently. Copeland et al.[4] have proposed a configuration-coordinate model for the solvated electron, in which the electron is situated in a cavity surrounded by preferentially oriented ammonia molecules. They predict a totally symmetric, Raman-active vibration in the range 25–60 cm^{-1}. Applying the treatment of Klick and Schulman[5] to metal–ammonia solutions, Rusch[6] has suggested that the symmetric vibration may be in the 400–700-cm^{-1} region. However, Raman studies of dilute sodium–[3,6] and potassium–ammonia[7] solutions have failed to detect the predicted solvated-electron band. Possible reasons for the failure to observe the predicted band could be (1) inapplicability of present theoretical models,[4,6] (2) large band width, (3) insufficient concentration of solvated electrons, and (4) interference from intense Rayleigh scattering below 50 cm^{-1}.

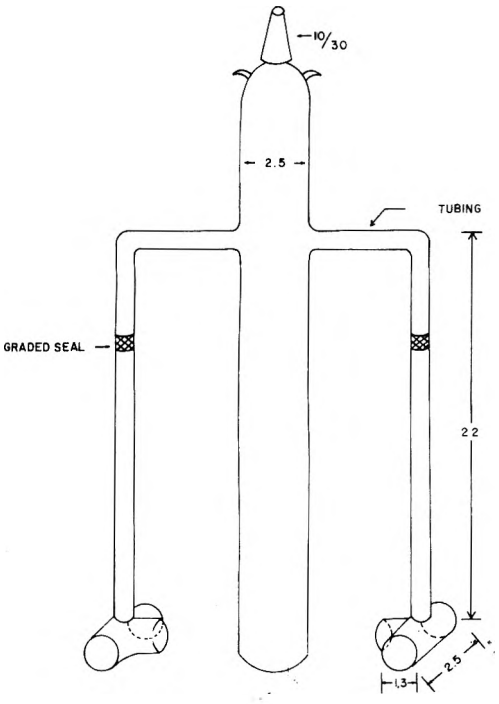

Figure 1. Sample-preparation assembly. Dimensions are in cm.

In the present study, an iodine filter has been employed to attenuate the Rayleigh-scattered light.[8,9] In order to check the possibility that the concentration of solvated electrons may be too low, dilute lithium– and calcium–ammonia solutions were employed, and a careful search conducted for symmetric metal–nitrogen stretching bands near 250 cm^{-1}.[10] If the solvated-cation bands can be detected, then there would be reason to believe that the Raman spectrometer has sufficient sensitivity to detect a solvated-electron band, if it exists and is not too broad, at the concentration used.

In addition, a careful study has been made of the band positions, widths, and depolarization ratios in the N–H stretching region in ammonia and dilute lithium– and calcium–ammonia solutions. An infrared study of lithium– and potassium–ammonia solutions indicates that the band positions shift to lower frequency with increasing concentration,[11] whereas Raman spectra of sodium–[3,6] and potassium–ammonia[7] solutions, which are of higher resolution than the infrared spectra, fail to show a shift in band positions. However, the Raman spectra of lithium– and calcium–ammonia solutions may exhibit measurable shifts due to the greater cationic influence on the solvent.

Experimental Section

Sample Preparation. 6×10^{-4} *M* lithium– and 3×10^{-4} *M* calcium–ammonia solutions were prepared by distilling a measured quantity of dry ammonia (Matheson, anhydrous, 99.99%) from a sodium–ammonia solution into the central tube of a special sample-preparation assembly, shown in Figure 1, containing the metal, which had been previously cut and weighed in an argon-filled glovebox, in amount sufficient to obtain the desired concentration. The entire assembly was then immersed in a dry ice–ethanol slush and the metal–ammonia solution poured into a specially cleaned[12] quartz sample cell, which consists of three quartz optical flats (0.5 in. dia × 1/16 in. thick) sealed at 90° to one another, and subsequently sealed. The accuracy of the sample concentration is about 10%. The cell design allows quantitative polarization measurements and spectrophotometric determination of concentration.

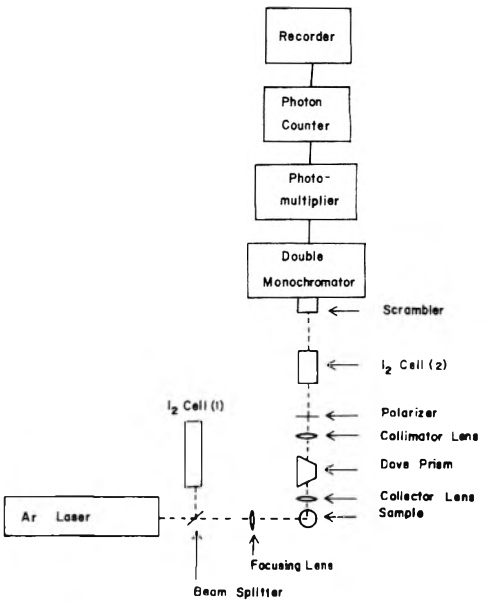

Figure 2. Schematic diagram of the Raman spectrometer.

Apparatus and Measurement Procedure. A schematic diagram of the Raman spectrometer, which uses the conventional 90° geometry, is shown in Figure 2. A Spectra Physics Model 165 argon ion laser operating at 5145 Å was the source of the incident light. The scattered light was analyzed by a Spex 1402 double monochromator followed by an SSRI photon-counting detection system. The photomultiplier tube had a dark count of 20 cps at room temperature. Prior to entering the monochromator, the scattered light was passed through a Dove prism to rotate the image 90°, which makes the image compatible with the vertical entrance slit of the monochromator, and a scrambler to remove the polarization dependence of the monochromator. In general, powers of about 100 mW were focused into the sample cell. Unpolarized, polarized, and depolarized spectra were recorded with a constant slit width (usually 200 μ) and scanned typically at 5 cm^{-1}/min. The scanning drive of the spectrometer was calibrated using indene and the resolution checked with carbon tetrachloride. All frequencies are reported accurate to ± 2 cm^{-1}. The 225-, 312-, and 459-cm^{-1} bands of carbon tetrachloride were used to determine the accuracy of the polarization measurements reported in this work. Depolarization ratios for these bands were in excellent agreement with predicted and previous experimental values.[13–15]

In order to attenuate the Rayleigh-scattered light, the laser was single moded by incorporation of an intra-cavity air-spaced etalon and an iodine filter installed before the monochromator (see Figure 2). The laser can be tuned to the iodine rotational line lying under the gain curve of the 5145-Å line of the argon-ion laser by the following procedure: (1) adjust the etalon for maximum power output causing the iodine cell to fluoresce; (2) tilt the etalon slightly, which causes the power to drop slowly and the fluorescence to disappear; and (3) continue tilting the etalon until the fluorescence reappears and the power drops suddenly. The laser is now tuned to the iodine rotational line and maximum absorption of the Rayleigh-scattered light will occur. As shown in Figure 2, two iodine cells were employed in our setup. The first cell was 50 cm long, 2.3 cm i.d., and

TABLE I: Observed Band Maxima (cm^{-1}) and Depolarization Ratios in Liquid Ammonia at 298 K

ν_2	ν_4	ν_1	$2\nu_4$	ν_3	Ref
		3215 (0.08)	3301 (0.08)	3384 (0.4)	18
1061	1645	3218	3303	3386	19
1060 (0.15)	1634 (0.5)	3215 (≈0.01)	3301 (≈0.01)	3380 (0.5)	6
1045 (0.5)	1639 (0.2)	3215 (0.04)	3298 (0.03)	3386 (1.0)	This work

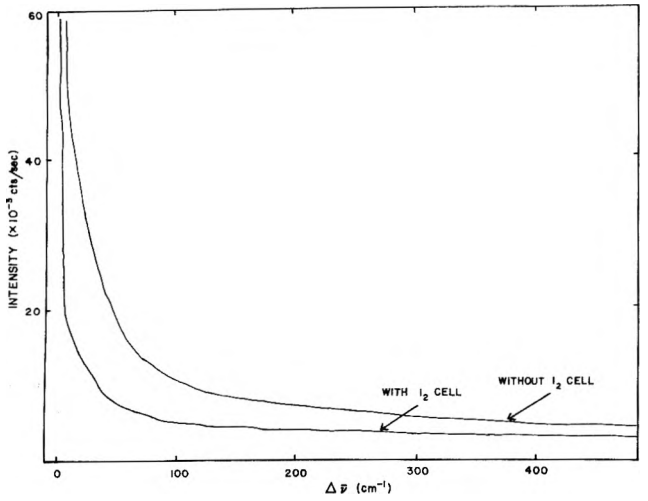

Figure 3. Typical Raman spectrum in the low-frequency region recorded with and without the iodine filter.

had a mirror attached at the far end. This cell was maintained at room temperature and used to indicate precise tuning of the laser to the iodine rotational line. The second cell was 5 cm long and 2.8 cm i.d. It was heated to 350 K and used to absorb the Rayleigh-scattered light. The iodine cell was most effective in attenuating the Rayleigh-scattered light in the range 5–50 cm^{-1}.

Temperatures between 195 and 300 K were obtained by flowing chilled nitrogen gas over the sample. Temperatures were measured with a copper–constantan thermocouple attached to the outside of the cell. The temperature gradient across the sample dimension with the laser off was about 1 K. The spectral position and widths were independent of laser power up to 100 mW, which indicates that the samples were not being heated appreciably by the laser at the powers employed in these experiments. The temperature was stabilized to within 0.5 K during the measurements.

Results and Discussion

This section is divided into two subdivisions: the first is concerned with a careful search for the solvated-electron band in dilute metal–ammonia solutions, and the second with the temperature-dependent Raman behavior in the N–H stretching region in ammonia and dilute lithium– and calcium–ammonia solutions.

Solvated-Electron Band. A careful search was conducted for the solvated-electron band in the range 5–700 cm^{-1} in the lithium– and calcium–ammonia solutions using the iodine filter in the low-frequency region to attenuate the Rayleigh-scattered light. A typical Raman spectrum in the low-frequency region is shown in Figure 3. The attenuation of the Rayleigh-scattered light is particularly evident in the range 5–50 cm^{-1}. We were unable to detect a solvated-electron band between 195 and 300 K in any of our studies. In addition, the solvated-cation bands detected in salt solutions at about 240 cm^{-1} (width about 35 cm^{-1}) for lithium salts and about 265 cm^{-1} (width about 70 cm^{-1}) for calcium salts[11] were not observed. Hence the solvated-electron band would have to be very narrow to be detected. Our failure to detect solvated-cation and electron bands indicates that the concentration of scatterers is too low to be observed by conventional laser-Raman techniques. Due to absorption problems, increasing the metallic concentration is not expected to result in a significant increase in the intensity of the Raman-scattered light.[6]

N–H Stretching Region. Five bands are observed in the Raman spectrum of liquid ammonia. At 298 K, the band maxima occur near 1045, 1640, 3215, 3300, and 3385 cm^{-1} and are assigned to the symmetric bending mode (ν_2), asymmetric bend (ν_4), symmetric stretch (ν_1), first overtone of the asymmetric bend ($2\nu_4$), and asymmetric stretch (ν_3), respectively.[10,16] The assignment of the 3215- and 3300-cm^{-1} bands to ν_1 and $2\nu_4$, respectively, is based on a recent Raman study[16] of liquid ammonia using the coupled-damped-oscillator model to analyze quantitatively the Fermi resonance between ν_1 and $2\nu_4$. If Fermi resonance is neglected, then it is possible to resolve the Raman spectrum in the N–H stretching region into four bands.[10] In addition to the ν_1, $2\nu_4$, and ν_3 bands already mentioned, a very broad fourth band centered at 3270 cm^{-1} is found and assigned to the symmetric stretch of an ammonia molecule associated through one of its hydrogens. However, neglecting the Fermi-resonance interaction in resolving the Raman spectrum into four bands in the N–H stretching region is clearly not justified. Unfortunately, after correcting a sign error in the original coupled-damped-oscillator calculation,[16] we find that both the coupled-damped-oscillator and four-band approaches provide excellent fits to the Raman spectrum of ammonia in the N–H stretching region. Hence it appears that nothing will be gained by introducing a fourth band into the coupled-damped-oscillator model. Although isotope studies provide convincing evidence for the existence of a fourth band,[17] inclusion of the Fermi-resonance interaction between ν_1 and $2\nu_4$ into the resolution calculation will lead to a significant reduction in its intensity. Hereafter, we adopt the coupled-damped-oscillator model and neglect the presence of the weak fourth band.

The observed band maxima and depolarization ratios in liquid ammonia at 298 K are summarized in Table I. The Dove prism was removed and the cell rotated 90° for the depolarization measurements. For comparison, data from recent Raman studies of liquid ammonia are also shown in Table I. The band maxima are in fair agreement with previous reports, but the depolarization ratios differ markedly from those reported previously. Due to the cell design, we believe that our depolarization measurements are the most accurate to date. The small depolarization ratios for the ν_1 and $2\nu_4$ bands means that only isotropic nonreorientational processes, such as vibrational and rotational mechanisms, contribute to the line width. In addition, the total depolarization of the ν_3 band and nonnegligible depolarization of the ν_2 and ν_4 bands indicate that both reorientational and nonreorientational processes contribute to the line width.

Now we concentrate on comparing the Raman behavior of liquid ammonia to that of the 6×10^{-4} *M* lithium– and 3

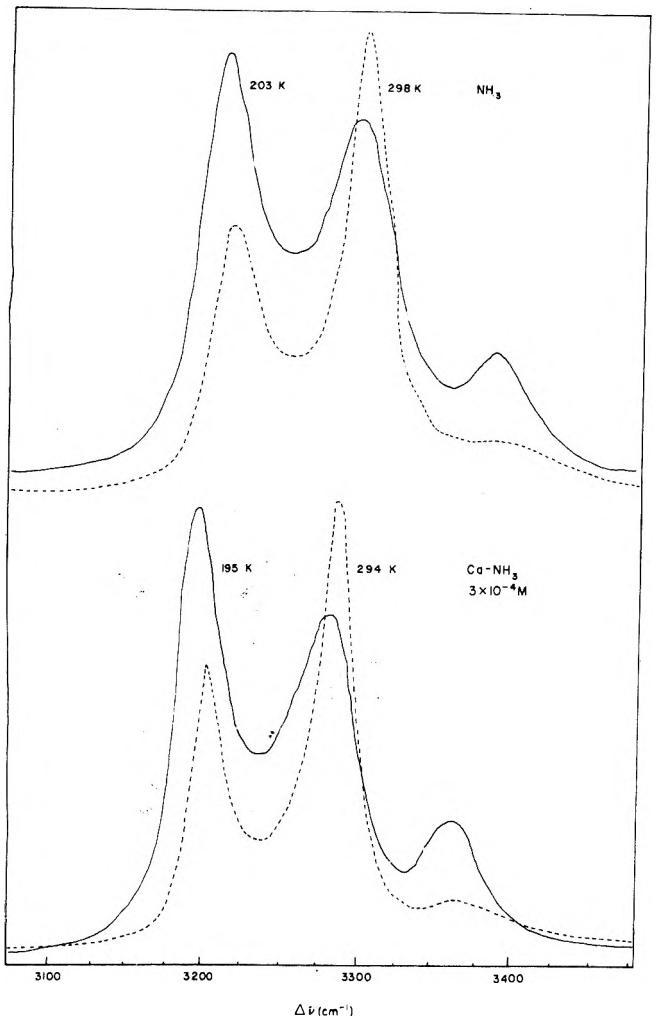

Figure 4. Raman spectra recorded at two widely separated temperatures in ammonia and 3×10^{-4} *M* calcium–ammonia solution. The low-frequency band is ν_1, the intermediate-frequency band $2\nu_4$, and the high-frequency band ν_3.

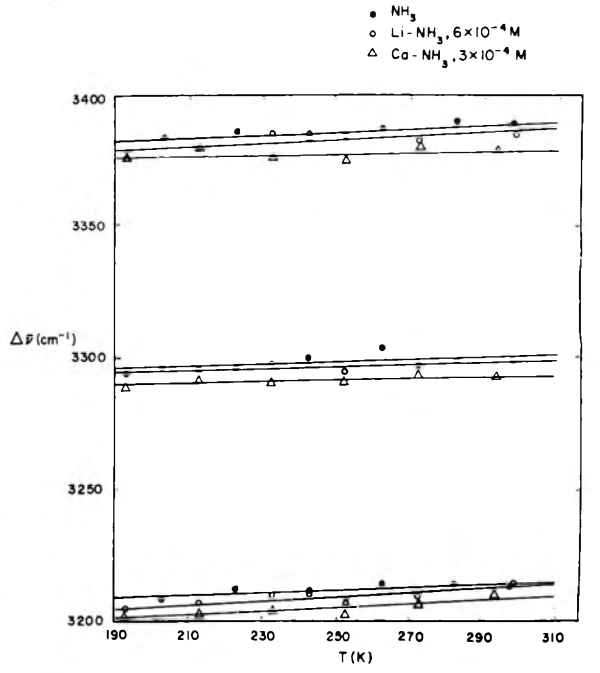

Figure 5. Band maxima $\Delta\bar{\nu}$ vs. temperature for the ν_1 (bottom), $2\nu_4$ (middle), and ν_3 (top) bands in ammonia (●), 6×10^{-4} *M* lithium–ammonia (O), and 3×10^{-4} *M* calcium–ammonia (△) solutions. The frequencies are accurate to ± 2 cm^{-1}. The lines represent least-squares fits to the data.

TABLE II: Slopes of the Band Maxima vs. Temperature Lines in Figure 5

Solution	$d\nu_1/dT$, cm^{-1}/100 K	$d(2\nu_4)/dT$, cm^{-1}/100 K	$d\nu_3/dT$, cm^{-1}/100 K
NH_3	6 ± 2	4 ± 2	6 ± 2
6×10^{-4} *M* Li–NH_3	10 ± 2	3 ± 2	8 ± 2
3×10^{-4} *M* Ca–NH_3	7 ± 2	3 ± 2	1 ± 2

$\times 10^{-4}$ *M* calcium–ammonia solutions in the N–H stretching region (3100–3500 cm^{-1}). The metallic concentrations chosen were low enough to avoid appreciable absorption at 5145 Å[6] and, since the solvated-electron concentration is the same in both solutions, permit the influence of the lithium and calcium cations on the stretching bands of ammonia to be investigated.

Raman spectra recorded at two widely separated temperatures in ammonia and the calcium–ammonia solution are shown in Figure 4. It is evident that the addition of calcium results in a narrowing of the ν_1 and $2\nu_4$ bands and a shift of all band maxima to lower frequencies. Similar, although less pronounced, behavior is observed in the lithium–ammonia solution. The observation of significant differences between the Raman spectra of ammonia and these dilute solutions is in sharp contrast to the behavior found in previous Raman studies of dilute sodium–[6] and potassium–ammonia[7] solutions. Our results indicate that Li^+, and to a larger extent Ca^{2+}, have a greater effect on ammonia than Na^+ and K^+. The larger interaction of Li^+ and Ca^{2+} with ammonia is reasonable in view of their higher charge densities.

The temperature dependence of the band maxima in ammonia and the solutions is shown in Figure 5. The important features of Figure 5 can be summarized as follows: (1) all bands shift to higher frequencies linearly with increasing temperature, (2) the solution bands occur at lower frequencies than those of ammonia at all temperatures, and (3) the calcium–ammonia bands occur at lower frequencies than those of the lithium–ammonia solution at all temperatures. The slopes of the band maxima vs. temperature lines in Figure 5 are summarized in Table II.

Since there is less thermal energy available to break hydrogen bonds at lower temperatures, it is reasonable to expect the extent of hydrogen bonding in these systems to decrease with an increase in temperature. In general, in hydrogen-bonded systems one finds that the frequency of stretching vibrations increases as the amount of hydrogen bonding decreases, whereas opposite, although less pronounced, behavior is observed for bending vibrations.[20] Similar behavior is found for overtones. Using these general rules, the increase in the frequencies of the ν_1 (symmetric stretch) and ν_3 (asymmetric stretch) bands with temperature is expected, but the similar behavior observed for the $2\nu_4$ (asymmetric bend) band is perhaps unexpected. However, the increase in frequency of the $2\nu_4$ band with temperature is smaller than the increase for the ν_1 and ν_3 bands (see Table II). In addition, the fact that ν_1 and $2\nu_4$ are in Fermi resonance means that the ν_1 and $2\nu_4$ modes are mixed, so that the $2\nu_4$ mode acquires some symmetric-stretching character. In view of the Fermi resonance be-

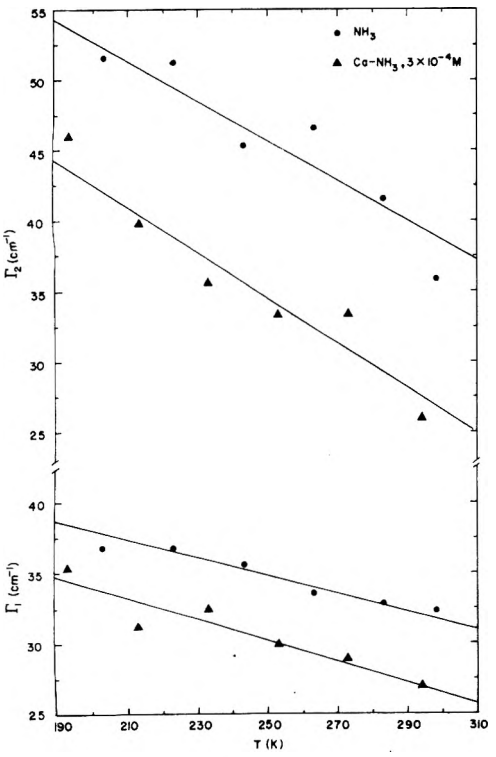

Figure 6. Uncoupled line widths Γ_1 and Γ_2 vs. temperature for the ν_1 (lower) and $2\nu_4$ (upper) bands in ammonia (●) and 3×10^{-4} *M* calcium–ammonia solution (▲). The line widths are accurate to ±2 cm^{-1}. The lines represent least-squares fits to the data.

tween ν_1 and $2\nu_4$, it is not surprising that the temperature dependence of the frequency of the $2\nu_4$ band does not exhibit the characteristic behavior observed for some bending vibrations. In fact, if the Fermi resonance between ν_1 and $2\nu_4$ is analyzed on the basis of the coupled-damped-oscillator model,[16] then it is found that the uncoupled band maxima $(\nu_1)_u$ and $(2\nu_4)_u$ do indeed show the expected behavior, with $(\nu_1)_u$ increasing with temperature more rapidly than $(2\nu_4)_u$ decreases with temperature. The results are in good agreement with a previous report,[16] which should be consulted for further details.

The fact that the lithium- and calcium–ammonia bands occur at lower frequencies than those of ammonia indicates that the N–H bond is weaker in the solutions. The weaker N–H bond arises from the coordination of the lone electron pair of an ammonia molecule to a cation. Furthermore, the weakening of the N–H bond makes the proton more available for hydrogen bonding, which in turn should result in stronger, and probably additional, hydrogen bonds in the solutions. As discussed previously, increased hydrogen bonding also causes the band maxima to shift to lower frequencies.

The occurrence of the calcium–ammonia bands at lower frequencies than those of the lithium–ammonia solution simply reflects the greater ability of Ca^{2+} to attract the lone electron pair of an ammonia molecule due to its higher charge density.

It is interesting to compare our results with those of a recent infrared study[11] of dilute lithium–ammonia solutions at 203 K. Estimating the infrared shifts in a 6×10^{-4} *M* lithium–ammonia solution by interpolation, we find about 0, −5, and −10 cm^{-1} for the shifts of the ν_1, $2\nu_4$, and ν_3 bands relative to those in ammonia, which should be compared to the Raman shifts of about −4, −2, and −4 cm^{-1}. We believe that the Raman shifts are more reliable due to the much higher resolution attained in the Raman spectra.

Uncoupled line widths of the ν_1 and $2\nu_4$ bands, which we denote by Γ_1 and Γ_2, respectively, have been obtained from the experimental Raman spectra using the coupled-damped-oscillator model.[16] The temperature dependence of Γ_1 and Γ_2 in ammonia and the calcium–ammonia solution is shown in Figure 6. The important features of Figure 6 can be summarized as follows: (1) both Γ_1 and Γ_2 decrease linearly with temperature in ammonia and in the calcium–ammonia solution, (2) the rate of decrease of the line width with temperature is the same in ammonia and in the calcium–ammonia solution, and (3) the line width in the calcium–ammonia solution is less than that in ammonia. Γ_1 and Γ_2 in the lithium–ammonia solution were between the ammonia and calcium–ammonia data and exhibited a similar temperature dependence, but for clarity the lithium–ammonia data have been omitted from Figure 6. In ammonia, the Γ_2 data are in quantitative agreement and the Γ_1 data are in qualitative agreement with a previous report.[16]

Before proceeding, it should be remembered that only nonreorientational processes contribute to Γ_1 and Γ_2. The nonreorientational processes considered to be the most important are vibrational relaxation, translational diffusion, collisional line broadening, inhomogeneous polymerization, and relaxation via low-frequency hydrogen-bond vibrations and solvent deformations; hereafter referred to as mechanisms 1–5, respectively.[16]

Mechanisms 1–3 result in an increase in line width with temperature, which is opposite to the observed behavior. In contrast, mechanisms 4 and 5 predict that the line width should decrease with temperature, as observed. Hence the decrease in the Γ's with temperature in ammonia and the solutions is attributed to mechanisms 4 and 5; however, the dominant mechanism cannot be identified solely from the temperature dependence of the line width.

The similar temperature dependence of Γ_1 and Γ_2 in ammonia and in the solutions suggests that the same line-broadening mechanism is operative in both systems. In order to estimate the activation energy E_a for the process or processes causing the observed decrease in line width with temperature, the temperature dependence of Γ_1 and Γ_2 have been fit to the Arrhenius equation

$$\Gamma = \Gamma_0 e^{E_a/RT} \tag{1}$$

Within experimental error, $E_a \approx 0.2$ kcal/mol for both Γ_1 and Γ_2. It is significant that the experimental activation energy is much less than that for the hydrogen-bond-breaking process (5–10 kcal/mol). If one mechanism makes the dominant contribution to the line width, then this result suggests that the mechanism causing Γ_1 and Γ_2 to decrease with temperature does not involve hydrogen-bond breaking, but rather perhaps a subtle structural change. However, several competing mechanisms may contribute to the line width, in which case the activation energy would have little quantitative significance.

The line narrowing observed when lithium or calcium is added to ammonia suggests that several competing mechanisms contribute to the line width. Dissolution of a metal in ammonia results in weaker N–H bonds, increased hydrogen bonding, less anharmonicity (causes vibrational relaxation), slower translational diffusion, and less-frequent collisions. Mechanisms 1, 4, and 5 predict, incorrectly, that the line should broaden upon the addition of metal. Further-

more, mechanisms 2 and 3 broaden the bands as the temperature is increased, but these mechanisms are consistent with the observed decrease in line width in the solutions. Hence it appears that (at least) mechanisms 2–5 are important in these systems.

It is now possible to understand the small activation energy found above. Mechanisms 4 and 5 cause the bands to narrow as the temperature is increased, whereas mechanisms 2 and 3 cause the opposite behavior. The net result is a line width that decreases weakly temperature, indicating that mechanisms 4 and 5 are slightly more important, and a small activation energy.

Finally, we comment upon the observation of significant differences between the Raman spectra of ammonia and the solutions, when, on the basis of concentration, one might expect the differences to be too small to be observable. We offer two possible reasons for the large cation effects observed in the Raman spectra of the solutions. First, the cation can influence a great number of ammonia molecules because the solvent is extensively polymerized,[17] and second, the cation increases the polarizability of an ammonia molecule parallel to its principle axis $\alpha_{\parallel}$ and hence increases the intensity of the Raman-scattered light, which is proportional to $\alpha_{\parallel}^2$.

Acknowledgment. We wish to thank Dr. C. T. Walker for making the light-scattering facilities in his laboratory available to us for this study, Mr. M. Anderson and Drs. W. Love and J. Potts for helpful conversations, and Ms. Lorna Glaunsinger for her drafting expertise. We gratefully acknowledge support of this research by Arizona State University and the Research Corporation.

References and Notes

(1) "Metal-Ammonia Solutions", Proceedings of Colloque Weyl I, G. Lepoutre and M. J. Sienko, Ed., W. A. Benjamin, New York, N.Y., 1964.
(2) "Metal-Ammonia Solutions", Proceedings of Colloque Weyl II, J. J. Lagowski and M. J. Sienko, Ed., Butterworths, London, 1970.
(3) "Electrons in Fluids", Proceedings of Colloque Weyl III, J. Jortner and N. R. Kestner, Ed., Springer-Verlag, New York, N.Y., 1973.
(4) D. A. Copeland, N. R. Kestner, and J. Jortner, *J. Chem. Phys.*, **53**, 1189 (1970).
(5) C. C. Klick and J. H. Schulman, *Solid State Phys.*, **5**, 97 (1957).
(6) B. I. Smith and W. H. Koehler, *J. Phys. Chem.*, **77**, 1753 (1973).
(7) Reference 3, pp 161–166.
(8) G. Hibler, J. Lippert, and W. L. Peticolas, *Spex Speaker*, **16**, 10 (1971).
(9) G. E. Devlin, J. L. Davis, L. Chase, and S. Gschwind, *Appl. Phys. Lett.*, **19**, 138 (1971).
(10) K. R. Plowman and J. J. Lagowski, *J. Phys. Chem.*, **78**, 143 (1974).
(11) P. F. Rusch and J. J. Lagowski, *J. Phys. Chem.*, **77**, 210 (1973).
(12) S. Naiditch and J. E. Werde, *J. Vacuum Sci. Technol.*, **5**, 54 (1968).
(13) A. E. Douglas and D. H. Hank, *J. Opt. Soc. Am.*, **38**, 281 (1948).
(14) A. F. Slombs, C. D. Hinman, and E. H. Siegler, Proceedings of the Conference on Analytical Chemistry and Applied Spectroscopy, 1965.
(15) W. F. Murphy, M. V. Evans, and P. Bender, *J. Chem. Phys.*, **47**, 1836 (1967).
(16) M. Schwartz and C. H. Wang, *J. Chem. Phys.*, **59**, 5258 (1973).
(17) A. T. Lemley, J. H. Roberts, K. R. Plowman, and J. J. Lagowski, *J. Phys. Chem.*, **18**, 2185 (1973).
(18) G. Seiller, M. Ceccaldi, and J. P. Leicknam, *Method. Phys. Anal.*, **4**, 388 (1968).
(19) B. Bettignies and F. Wallart, *C. R. Acad. Sci.*, **271**, 640 (1970).
(20) G. Pimentel and A. McClellan, "The Hydrogen Bond", W. H. Freeman, San Francisco, Calif., 1960.

Discussion

K. PLOWMAN. Over the concentration range at which the spectra were taken no cation-solvation mode is expected to be observed. The minimum concentration at which we were able to observe the band was 0.2 *M*.

In addition we saw no metal-solvation effect to concentration two orders of magnitude greater than that of your experiments. The calcium work is interesting but perhaps it should be repeated for confirmation.

T. WHITE. We were aware of the concentration problem in detecting these bands. However, when operating at the 5145-Å exciting line, where one can utilize the iodine filter, the method requires such concentrations to avoid absorption problems.

We too were surprised to see these effects from such a small amount of metal. We chose these metals for their small size and high charge density. We felt that if there was an effect on the spectra of the solvent, it would be greatest with these metals. I agree that the study should be repeated for confirmation, but I must add that frequency shifts reported are about the same as those we estimated from previous infrared data [P. F. Rusch and J. J. Lagowski, *J. Phys. Chem.*, **77**, 210 (1973)]. Also note that (1) the ammonia data were reproducible and agree well with previous studies ["Electrons in Fluids, The Nature of Metal-Ammonia Solutions", Colloque Weyl III, W. A. Benjamin, New York, N.Y., 1973, p 145; G. Sellier, M. Ceccaldi, and J. P. Leicknam, *Method Phys. Anal.*, **4**, 388 (1968); M. Schwartz and C. H. Wang, *J. Chem. Phys.*, **59**, 5258 (1973)], and (2) although the lithium data are close to those for ammonia, the calcium data are well outside experimental error.

Brillouin Scattering in Dilute Metal–Ammonia Solutions

W. F. Love, C. T. Walker,

Department of Physics, Arizona State University, Tempe, Arizona 85281

and W. S. Glaunsinger*

Department of Chemistry, Arizona State University, Tempe, Arizona 85281 *(Received July 30, 1975)*

Publication costs assisted by the National Science Foundation

Brillouin scattering measurements have been made on liquid ammonia and several dilute metal–ammonia solutions in the temperature range 195–300 K. Within experimental uncertainties, there are no differences in the results for pure ammonia and the dilute solutions. The hypersonic (near 6 GHz) velocities were computed from the measured Brillouin shifts and can be fitted by the relation $v = v_0 - v_1 T$, where $v_0 = 3166$ msec^{-1} and $v_1 = 5.98$ msec^{-1} K^{-1}. The temperature dependence of the adiabatic compressibility was deduced from the hypersonic velocities. The results agree with those obtained at 1 and 10 MHz using ultrasonic techniques. Intensities of the Brillouin peaks were observed to increase more rapidly with temperature than predicted by the theory outlined by Cummins and Gammon. The integrated intensities of the Rayleigh and Brillouin peaks were combined at 300 K to give a Landau–Placzek ratio ($I_R/2I_B$) of 0.83 ± 0.06, in contrast to the value of 0.71 expected when the ratio is evaluated using static values of the relevant thermodynamic parameters.

Introduction

Brillouin spectroscopy offers an interesting new light-scattering approach to the study of the properties of fluids.[1] In general, the light scattering spectrum of a liquid at small energy transfer consists of three main components, which can be identified by their frequency shift relative to the incident light. First is an unshifted component, called the Rayleigh component, which is due to scattering from nonpropagating concentration and isobaric entropy fluctuations. Second are two shifted components symmetrically placed about the Rayleigh component, called the Brillouin doublet, which arise from isentropic pressure fluctuations, i.e., sound waves.[2] The low- and high-frequency components of the doublet are termed the Stokes and anti-Stokes components, respectively. Normally all three components are relatively sharp and have widths significantly greater than the incident light, with the width of the Brillouin components being greater than the Rayleigh component. In addition, there can be another less-important contribution to the spectrum. This, typically weak fourth component, called the thermal-relaxation component, originates from the frequency dependence of the specific heats.[3,4] Usually this contribution is small enough to be neglected in analyzing the Rayleigh and Brillouin components.

A great deal of information can be extracted from the Brillouin spectrum of a liquid. The hypersonic velocity and adiabatic compressibility can be determined by accurately measuring the frequency shift of the Brillouin components from the Rayleigh component.[5] The absorption of hypersound can be studied by determining the excess width of the Brillouin components relative to the Rayleigh component.[6] Dispersion in the thermodynamic properties of a liquid can be investigated by evaluating the ratio of intensity of the Rayleigh component I_R to that of the Brillouin doublet $2I_B$,[5] which is referred to as the Landau–Placzek (LP) ratio. In addition, recently it has been shown that nonideality of solutions can be studied by measuring the LP ratio.[7]

Liquid ammonia is of interest because it is an important solvent which exhibits strong hydrogen bonding. To our knowledge there have been no reports in the literature of Brillouin scattering in liquid ammonia nor ammoniacal solutions. We have become interested in Brillouin scattering in ammoniacal systems and have examined in detail in this study the hypersonic sound velocity and adiabatic compressibility of liquid ammonia and several dilute metal–ammonia solutions. We also report measurements of the LP ratio and Brillouin intensity with the purpose of comparing theory and experiment for these systems.

Experimental Section

Sample Preparation. Metal–ammonia samples were prepared by distilling a measured quantity of dry ammonia (Matheson, anhydrous, 99.9%) from a sodium–ammonia solution into the central tube of a special sample-preparation assembly, depicted in Figure 1, containing the metal, which had been previously cut and weighted in an argon-filled glovebox, in an amount sufficient to obtain the desired concentration. The entire assembly was then immersed in a dry ice–ethanol slush and the solution poured into a specially cleaned[8] quartz cell, which consisted of three quartz optical windows (0.5 in. diameter × 1/16 in. thick) sealed at 90° to one another, and subsequently sealed. Lithium–ammonia solutions of concentration 2×10^{-4}, 4×10^{-4}, and 6×10^{-4} M, calcium–ammonia solutions of concentration 1.5×10^{-4} and 3×10^{-4} M, and a 2×10^{-4} M sodium–ammonia solution were prepared in this manner. The accuracy of the sample concentration is about 10%.

Liquid ammonia samples were prepared by distilling ammonia from a sodium–ammonia solution directly into a specially cleaned quartz cell described above. Near the completion of this study we discovered that rinsing the cell 10–15 times with absolute methanol prior to distillation reduces significantly the Tyndall scattering from particulates in the liquid. In an attempt to reduce Tyndall scattering, a nearly particulate-free sample was prepared by rinsing the cell with absolute methanol followed by double distillation of ammonia.

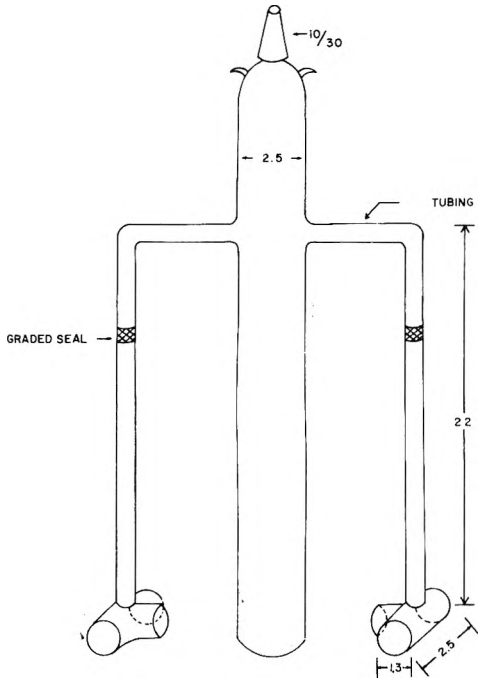

Figure 1. Sample preparation assembly. Dimensions are in centimeters.

Apparatus and Measurement Procedure. A schematic diagram of the Brillouin-scattering equipment is shown in Figure 2. A Spectra Physics Model 165 argon ion laser operating at 4880 Å and in a single longitudinal mode was used as the light source for the measurements. Approximately 15 mW of light, polarized perpendicular to the scattering plane, was focused into the sample cell. Earlier experiments with a laser intensity of 100 mW resulted in significant local heating of the solutions as observed by the Brillouin shifts. Scattered light was collected at 90° to the incident beam and passed through a piezoelectrically scanned Tropel Fabry-Perot interferometer. The interferometer plates were set for a free spectral range (FSR) of 10 GHz which ensured resolution of the Stokes and anti-Stokes Brillouin components in all samples between the freezing point of ammonia and room temperature and resulted in overlap of adjacent orders in all Brillouin spectra. A working finesse of 25 to 35 was typical, but for some spectra a finesse of 50 to 60 was attained. Light from the central spot of the fringe system was then focused onto a pinhole and detected by a Channeltron photomultiplier. The photomultiplier pulses were processed with PAR photon-counting electronics and the resulting spectrum stored in a Nicolet 1070 signal averager. Typically 512 scans of 500-msec duration were stored in the averager before final display of the spectrum on an X–Y recorder.

In the present study, the uncertainty in the scattering angle was ±0.5° at most, which gave rise to a maximum error in the hypersonic velocity of ±0.5% at our scattering angle of ≈90°.

In general, relative intensities were determined by assuming that the integrated intensity is proportional to the product of the amplitude of a component and its width. When accurate relative intensities were required, such as in the determination of the LP ratio, the area under a component was measured by numerical integration.

Temperatures between the freezing point of ammonia and room temperature were obtained by flowing chilled nitrogen gas over the sample. Temperatures were measured with a copper–constantan thermocouple attached to the outside of the cell. The temperature gradient across the sample dimension was about 1 K, which resulted in a maximum error of 0.4% in the hypersonic velocity.

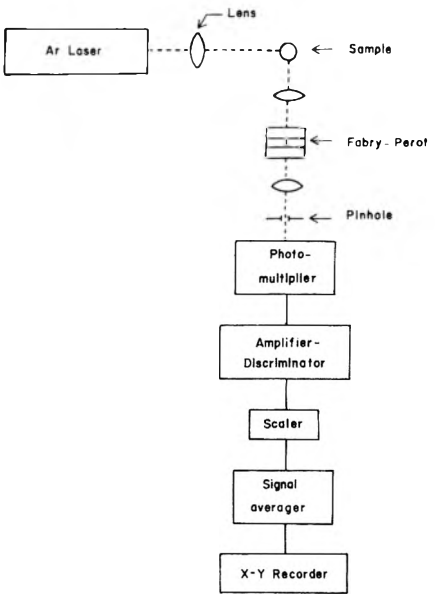

Figure 2. Schematic diagram of the Brillouin-scattering apparatus.

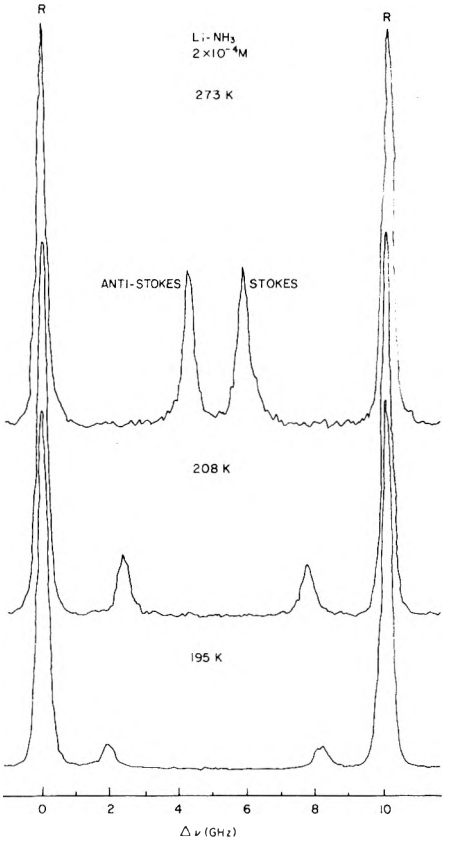

Figure 3. Brillouin spectra in a 2 × 10^{-4} *M* lithium–ammonia solution at 273, 208, and 195 K. The finesse is 30.

Results and Discussion

This section is divided into five subsections: Brillouin spectra, hypersonic velocity, adiabatic compressibility, Landau-Placzek ratio, and Brillouin intensity.

Brillouin Spectra. Figure 3 illustrates the temperature

TABLE I: Brillouin Shifts and Hypersonic Velocities in Liquid Ammonia (θ = 94.8°)

T, K	$\Delta\nu$, GHz	v_{hs}, m sec^{-1}
195.0	8.45	2007
198.0	8.33	1981
202.0	8.23	1961
207.5	8.07	1929
216.5	7.80	1874
226.0	7.41	1789
237.5	7.29	1770
246.0	6.95	1695
256.5	6.66	1634
267.5	6.36	1570
273.0	6.18	1530
278.0	6.03	1497
300.0	5.43	1365

dependence of the Brillouin spectra. Each spectrum is overlapped, i.e., the Brillouin components associated with the Rayleigh line are separated from that line by the Brillouin component of the adjacent order. It is evident that the Brillouin shift increases with decreasing temperature, which implies a corresponding increase in hypersonic velocity with decreasing temperature. The Rayleigh component is considerably more intense than the Brillouin components, indicating that the intensity of the Rayleigh component is dominated by Tyndall scattering. The origin of the particulates is either dust or insoluble metallic oxides or nitrides resulting from the degradation of the surface of the metal prior to preparation of the solution. The latter source of particulates is particularly evident is calcium–ammonia solutions due to the difficulties involved in cleaning the surface of the metal. However, the intensity of the Brillouin components is not affected by Tyndall scattering, so that the apparent increase in Brillouin intensity with temperature is an intrinsic property of the liquid. Although the Brillouin components appear to be broader than the Rayleigh components, the finesse is too low to determine the excess width of the Brillouin components reliably.

Since the thermodynamic properties of the dilute metal–ammonia solutions used in our experiments should be indistinguishable from those of ammonia, the information derived from the Brillouin spectra of these solutions should be the same as that obtained from pure ammonia. Within experimental uncertainty this was observed and hence the remainder of the discussion will be concerned only with liquid ammonia.

Hypersonic Velocity. The hypersonic velocity is given by[9]

$$v_{hs} = \pm \frac{\lambda_0 \Delta\nu}{2n \sin(\theta/2)} \quad (1)$$

where λ_0 is the vacuum wavelength of the incident light, $\pm\Delta\nu$ is the frequency shift of the Brillouin components from the central Rayleigh component, n is the refractive index of the scattering liquid, and θ is the scattering angle. In order to compute v_{hs} from the Brillouin spectrum, n must be known. Refractive-index data at 5780 Å for liquid ammonia are given in ref 10 and 11, and can be fitted by a straight line in the temperature range 196–300 K. The result is

$$n = n_0 - n_1 T \quad (2)$$

where n_0 = 1.539, $n_1 = 7.32 \times 10^{-4}$ K^{-1}, and T is the temperature in Kelvin. Using eq 2 and neglecting dispersion in the refractive index,[12] we calculate v_{hs}. The results are listed in Table I along with the measured Brillouin shifts for pure ammonia. The magnitude and temperature dependence of the hypersonic velocity is compared with ultrasound measurements conducted at 10^{13} and 10^{14} MHz in Figure 4. In the temperature range 196–300 K the hypersonic velocity decreases linearly with temperature and can be fitted by a straight line of the form

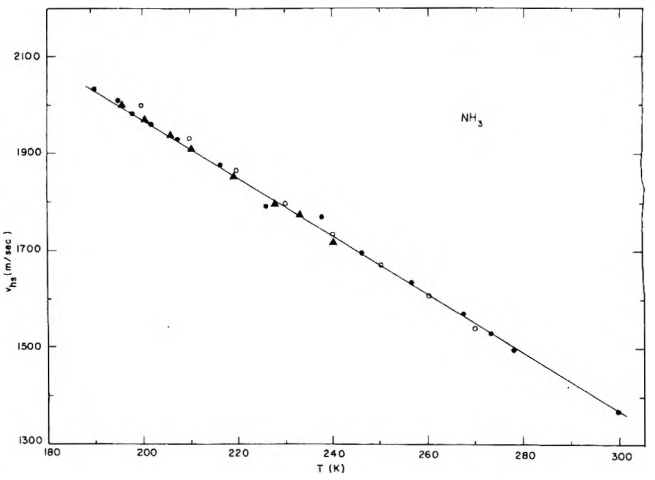

Figure 4. Hypersonic velocity vs. temperature in ammonia. The closed circles are our hypersound data, and the open circles and triangles are ultrasound data at 1 and 10 MHz from ref 13 and 14, respectively. The line represents a least-squares fit to the hypersound data.

$$v_{hs} = v_0 - v_1 T \quad (3)$$

where v_0 = 3166 m sec^{-1} and v_1 = 5.98 m sec^{-1} K^{-1}. The close agreement between the hypersonic and ultrasonic velocities indicate a lack of dispersion in the sound velocity, within experimental error (≈1%), over nearly four orders of magnitude in frequency.

The lack of dispersion in the hypersonic velocity is consistent with small absorption, as observed by the absence of appreciable broadening of the Brillouin components over the instrumentally broadened Rayleigh line. From our data we estimate that the intrinsic Brillouin width (fwhh) is less than 185 MHz at 287 K. Extrapolation of the ultrasonic attenuation[15] for ammonia at 50 MHz and 213 K, assuming a quadratic frequency dependence, gives a width equal to 60 MHz.

Adiabatic Compressibility. The adiabatic compressibility, defined by[16]

$$\beta_S = -\frac{1}{V}\left(\frac{\partial V}{\partial P}\right)_S \quad (4)$$

where V is the volume and P the pressure, was computed for liquid ammonia by using our measured hypersonic velocity, published values of the density,[17,18] and the relation[19]

$$\beta_S = 1/\rho V_{hs}^2 \quad (5)$$

The density data for ammonia between 203 and 278 K are described by the equation

$$\rho = \rho_0 - \rho_1 T - \rho_2 T^2 \quad (6)$$

where ρ_0 = 0.8899 g cm^{-3}, $\rho_1 = 4.745 \times 10^{-4}$ g cm^{-3} K^{-1}, and $\rho_2 = 1.63 \times 10^{-6}$ g cm^{-3} K^{-2}.

The temperature dependence of the adiabatic compressibility between 195 and 300 K is shown in Figure 5. The compressibility is in good agreement with that determined

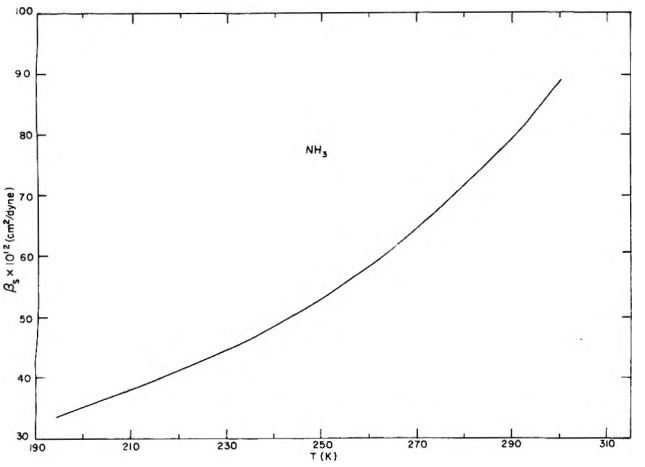

Figure 5. Adiabatic compressibility vs. temperature in ammonia.

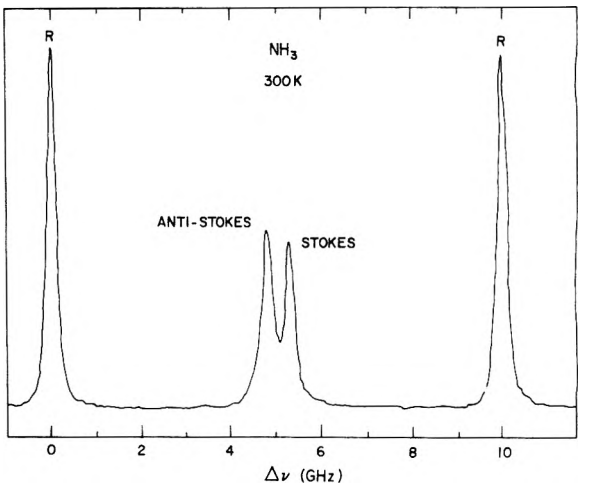

Figure 6. Brillouin spectrum of a nearly particulate-free sample of ammonia at 300 K. The finesse is 38.

from ultrasound measurements[14] in the temperature range 195–240 K. By combining eq 3, 5, and 6 the following analytical expression for the adiabatic compressibility between 195 and 300 K is obtained:

$$\beta_S = (A_0 + A_1T + A_2T^2 + A_3T^3 + A_4T^4)^{-1} \quad (7)$$

where $A_0 = \rho_0 v_0^2 = 8.92 \times 10^{10}$ dyn cm^{-2}, $A_1 = -(2\rho_0 v_0 v_1 + \rho_1 v_0^2) = -3.84 \times 10^8$ dyn cm^{-2} K^{-1}, $A_2 = \rho_0 v_1^2 + 2\rho_1 v_0 v_1 - \rho_2 v_0^2 = 3.34 \times 10^5$ dyn cm^{-2} K^{-2}, $A_3 = 2\rho_2 v_0 v_1 - \rho_1 v_1^2 = 4.48 \times 10^2$ dyn cm^{-2} K^{-3}, and $A_4 = -\rho_2 v_1^2 = -0.583$ dyn cm^{-2} K^{-4}.

From eq 5, it follows that the decrease in hypersonic velocity with temperature results because β_S increases more rapidly than ρ decreases with temperature. It is interesting to note that at room temperature the adiabatic compressibility of ammonia is about twice that of water (45.7×10^{-12} cm^2 dyn^{-1}), which reflects the more dense molecular packing in water.

Landau–Placzek Ratio. Neglecting the effects of dispersion and the intrinsic temperature dependence of the dielectric constant, viz., $(\partial\epsilon/\partial T)_\rho = 0$, the LP ratio is given by[2]

$$I_R/2I_B = \gamma - 1 \quad (8)$$

where γ is the specific heat ratio C_p/C_V. Since $\gamma = 1.71 \pm 0.10$ for liquid ammonia,[20] in this model the LP ratio is predicted to be 0.71 ± 0.10. To compare this with experiment a nearly particulate-free sample of ammonia was prepared by careful cleaning of the sample cell prior to distillation. The Brillouin spectrum for this sample at 300 K is shown in Figure 6 and the reduction in the Rayleigh intensity relative to the Brillouin components is evident. The small difference in the (peak) intensities of the Brillouin components is due to an instrumental scanning effect. The LP ratio $I_R/2I_B$ is determined from the integrated intensities and found to be 0.83 ± 0.06. The agreement between experiment and the classical theory is fairly close and within the experimental uncertainties given. There may however be some (small) contribution due to particulate scattering which would decrease our value. Alternatively, hypersonic dispersion correction of the classical LP ratio generally leads to larger values than $\gamma - 1$.[5] Since the hypersonic and ultrasonic velocities are found to be the same, the correction depends on a difference of the temperature dependence of the static and microwave (6 GHz) dielectric constants. An estimate shows that the correction is small; however, owing to inaccuracies in existing dielectric constant data a meaningful calculation is not yet possible.

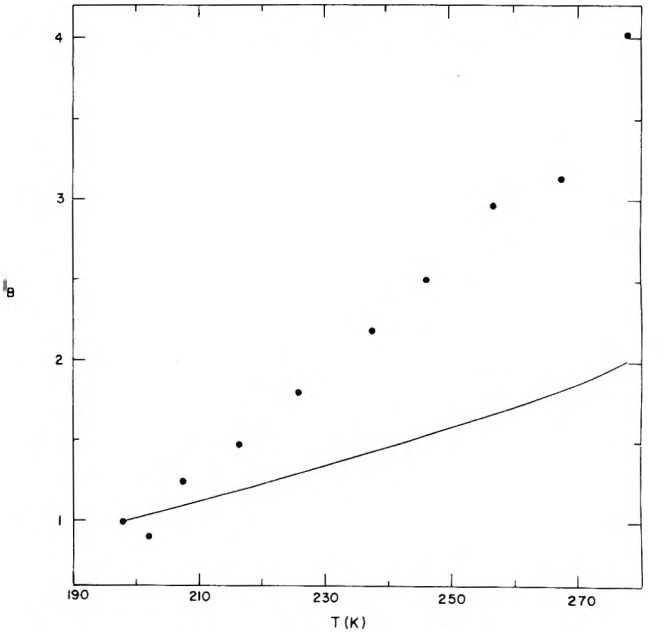

Figure 7. Relative integrated Brillouin intensity vs. temperature in ammonia. The Brillouin intensity is normalized to unity at 195 K. The closed circles are experimental intensities, and the smooth curve represents intensities calculated from eq 10.

Brillouin Intensity. Although the intensity of the Rayleigh component was normally dominated by Tyndall scattering, it was possible to determine the intensity of the Brillouin components because their intensities are not affected by Tyndall scattering.[5] The temperature dependence of the relative integrated Brillouin intensity in liquid ammonia is shown in Figure 7. The Brillouin intensity increases nonlinearly with temperature.

The intensity of the Brillouin component is given by[5]

$$I_B = A(\rho\partial\epsilon/\partial\rho)_S^2 T\beta_S \quad (9)$$

where A is a temperature-independent proportionality constant. Approximating $(\rho\partial\epsilon/\partial\rho)_S$ by $(\rho\partial\epsilon/\partial\rho)_T$, taking $(\rho\partial\epsilon/\partial\rho)_T = \epsilon - 1$, and using the classical relationship between the dielectric constant and the optical index of refraction, $\epsilon = n^2$, eq 9 becomes

$$I_B = A(n^2 - 1)^2 T\beta_S \quad (10)$$

Using eq 2 and 7, relative Brillouin intensities have been computed from eq 10. The resulting theoretical intensities in liquid ammonia appear as the smooth curve in Figure 7. The experimental Brillouin intensities increase more rapidly with temperature than the theoretical ones. Whether the origin for the discrepancy is real or simply due to the approximations used in deriving eq 10 from eq 9 is unclear at present. A determination of the temperature dependence of $(\rho\partial\epsilon/\partial\rho)_S$ in the hypersonic range would be required to resolve this question.

Acknowledgments. We wish to thank Mr. T. R. White for assistance in sample preparation and data collection, Mr. D. Kelley for expediting our mechanical work, and Ms. Lorna Glaunsinger for her drafting expertise. We gratefully acknowledge support of this research by the Research Corporation and the National Science Foundation under Grant No. GH-34248.

References and Notes

(1) For an excellent review of Brillouin scattering, see R. S. Krishnan in "The Raman Effect", Vol. I, A. Anderson, Ed., Marcel Dekker, New York, N.Y., 1971, p 343.
(2) L. Landau and G. Placzek, *Z. Phys. Sowjetunion*, **5**, 172 (1934).
(3) R. D. Mountain, *Rev. Mod. Phys.*, **38**, 205 (1966); *J. Natl. Bur. Stand., Sect. A*, **70**, 207 (1966); *J. Chem. Phys.*, **44**, 832 (1966).
(4) Reference 1, p 376.
(5) H. Z. Cummins and E. W. Gammon, *J. Chem. Phys.*, **44**, 2785 (1966).
(6) A. R. Maret and E. Yeager, *J. Acoust. Soc., Am.*, **54**, 668 (1973).
(7) G. A. Miller and C. S. Lee, *J. Phys. Chem.*, **72**, 4644 (1968).
(8) S. Naiditch and J. E. Wreede, *J. Vac. Sci. Technol.*, **5**, 54 (1968).
(9) L. Brillouin, *Ann. Phys.*, **17**, 88 (1922).
(10) R. de Mallemann, F. Suhner, and A. Malevergue, *C. R. Acad. Sci.*, **234**, 1929 (1952).
(11) "International Critical Tables", Vol. 1, McGraw-Hill, New York, N.Y., 1930, p 165.
(12) Making the same approximation in the case of water gives an error of 0.3%.
(13) Y. P. Blagoi, A. E. Butko, S. A. Mikhailenko, and V. V. Yakuba, *Russ. J. Phys. Chem.*, **42**, 564 (1968).
(14) D. E. Bowen and J. C. Thompson, *J. Chem. Eng. Data*, **13**, 206 (1968).
(15) D. E. Bowen, "Electrons in Fluids", Proceedings of Colloque Weyl III, J. Jortner and N. R. Kestner, Ed., Springer-Verlag, New York, N.Y., 1973, p 247.
(16) H. B. Callen, "Thermodynamics", Wiley, New York, N.Y., 1960.
(17) J. Timmermans, *Bull. Soc. Chim. Belg.*, **32**, 299 (1923).
(18) R. E. Lo, *Z. Anorg. Allg. Chem.*, **344**, 230 (1966).
(19) W. P. Mason, "Physical Acoustics and the Properties of Solids", Van Nostrand, Princeton, N.J., 1958.
(20) Linear extrapolation of the data for $\gamma = \beta_T/\beta_S$ to 300 K from ref 13 gives a value $\gamma = 1.71 \pm 0.10$. In the region where they overlap, near 230 K, values of γ from ref 13 and 14 are in good agreement.

Metal–Ammonia Solutions. IX. Matrix Rank Analysis as an Indicator of the Number of Species Present[1]

William Peer and J. J. Lagowski*

The Robert A. Welch Laboratories, The University of Texas at Austin, Austin, Texas 78712 *(Received July 23, 1975)*

Publication costs assisted by the Robert A. Welch Foundation

Matrix rank analysis was applied to the broad 1500-nm band of sodium–ammonia solutions and sodium in sodium iodide–ammonia solution. The data used are those of Rubinstein at temperatures of −55, −65, and −75°C in the concentration ranges of 10^{-5} to 10^{-3} *M* Na and 10^{-5} to 5×10^{-4} *M* Na in 0.08 *M* NaI. Two linearly independent absorbing species were found in each type of solution at each temperature. The salt and nonsalt solutions analyzed together at each temperature yielded a matrix rank of 3; three possible interpretations are discussed.

Introduction

Presently, models which describe the behavior of dilute metal–ammonia solutions include a specification of the number and the nature of two or more species related through equilibrium processes.[2,3] For the most part, these models attempt to correlate experimental results obtained from several types of experiments. This, of course, should be the goal of any acceptable general theory of metal–ammonia solutions. In the development of such theories, there may be confusion between questions concerning the number of species and those addressing the nature of the species. Indeed, in attempting to devise a general theory encompassing the results of several types of experiments, it is often difficult to separate these questions and to consider them independently of each other. In our attempt to separate these questions, it appeared logical to consider methods which would lead to a statement of the number of species present in metal–ammonia solutions first, and then to identify them, either by experimental or theoretical arguments. Accordingly, we address the problem here of determining the number of optically important species in metal–ammonia solutions.

The 1500-nm band observed for sodium–ammonia solutions and for sodium solutions containing NaI has been resolved assuming a two species model.[3] We are interested here in establishing the number of absorbing species present in such solutions directly from experimental evidence without recourse to a model. Consequently, we have applied the method of matrix rank analysis[4,5] to the 1500-nm band exhibited by these solutions. The method, which has been well demonstrated to give the number of optically

absorbing species in other chemical systems,[6,7] depends only upon the linear independence of the concentrations of species in a series of metal–ammonia solutions at different concentrations (or, for the case of pulse radiolysis experiments, in the absorption spectra recorded as a function of time).

Outline of Method

The only assumption required for the matrix rank method is that Beer's law obtains at all wavelengths (eq 1). In eq 1, $D_{\lambda i}$ is the absorbance per unit cell length at the λth wavelength in the ith solution, $\epsilon_{\lambda k}$ is the extinction coefficient of the kth species at the λth wavelength, c_{ki} is the concentration of the kth species in the ith solution, and n_c is the total number of species that contribute to the absorption of light at any wavelength studied. The term "species" is taken to mean "that entity which produces an absorption which obeys Beer's Law", which implies that band shapes attributed to individual species cannot change as a function of total metal concentration; no assumption concerning line shapes needs to be made.

$$D_{\lambda i} = \sum_{k}^{n_c} \epsilon_{\lambda k} c_{ki} \tag{1}$$

In matrix form, Beer's law is given by eq 2:

$$D = EC \tag{2}$$

For

$$M = D\bar{D} \tag{3}$$

where $\bar{D}$ is the transpose of D, the number of nonzero eigenvalues of M is the rank of M and of D. The rank of D is always less than or equal to the rank of C if the number of solutions (n_s) and number of wavelengths (n_w) are both greater than the number of species (n_c). The rank of C is normally n_c unless the concentration of one species is linearly dependent upon the concentrations of the other species. In metal–ammonia solutions such a situation may occur as in reactions 4 and 6; the corresponding equilibrium constants are given by eq 5 and 7. Even if the two differently solvated electrons had two distinct absorption bands, only one of the two species would contribute to the rank of C (and therefore of M) since the ratio of their concentrations would always be a constant (eq 5). Similarly, if the concentration of metal ion is essentially constant for all solutions studied, then reaction 6 would contribute only one species to the rank even if the monomer (or ion pair) and the electron both have separate absorption peaks. This situation could occur, for example, in concentrated salt–ammonia solutions containing a relatively small amount of metal.

$$e^-(NH_3)_x + (y - x)NH_3 \rightarrow e^-(NH_3)_y \tag{4}$$

$$K[NH_3]^{y-x} = [e^-(NH_3)_y]/[e^-(NH_3)_x] \tag{5}$$

$$M^0 \rightarrow M^+ + e^- \tag{6}$$

$$K/[M^+] = [e^-]/[M^0] \tag{7}$$

If no error in the absorbance measurements occurred, an orthogonal transformation of M would yield the number of linearly independent absorbing species contributing to the 1500-nm band. However, because of experimental error, the number of eigenvalues will equal the order of matrix M. So statistical criteria must be developed to determine whether or not a given eigenvalue is zero. We have adapted a program by Hugus and El-Awady to analyze the available data for metal–ammonia solutions. These investigators have developed three criteria for deciding whether an eigenvalue is zero within experimental error.[5]

The first criterion Hugus and El-Awady developed is eq 8, to determine the variance of the lth eigenvalue:

$$\sigma_{v_{ll}}^2 = \sum_{j,k}^{n_w} S_{jl}^2 S_{kl}^2 \sigma_{M_{jk}}^2 \tag{8}$$

S_{jl} and S_{kl} are the jth and kth components of the lth eigenvector of M and

$$\sigma_{M_{jk}}^2 = \sum_{i}^{n_s} [D_{ki}^2 \sigma_{D_{ji}}^2 + D_{ji}^2 \sigma_{D_{ki}}^2] \qquad j \neq k \tag{9}$$

$$\sigma_{M_{jk}}^2 = \sum_{i}^{n_s} 4 D_{ji}^2 \sigma_{D_{ji}}^2 \qquad j = k \tag{10}$$

where $\sigma_{D_{ji}}$ is the standard deviation of the jth point in the ith solution. Thus, by comparing an eigenvalue to the square root of its variance, we have a statistical criterion for determining if an eigenvalue is zero within experimental error. However, in deriving this equation, the correlation coefficients were set equal to zero, except for the case of self-correlation. Two additional criteria were therefore developed to test for the number of nonzero eigenvalues.

Since M is symmetric and real it can be expressed in terms of its eigenvalues and eigenvectors. If the rank of matrix M is m then only m eigenvalues should be necessary to satisfactorily regenerate the absorbance data. Specifically, if the eigenvalues are arranged in order of decreasing value, Hugus and El-Awady showed that the approximation $B_{il}^{(m)}$ to the measured absorbance at the lth wavelength in the ith solution, $\bar{D}_{il}$, using the first m eigenvalues is given by eq 11 where T_{ij} is defined by eq 12:

$$B_{il}^{(m)} = \sum_{j}^{m} T_{ij} \bar{S}_{jl} \tag{11}$$

$$T_{ij} = \sum_{k}^{n_w} \bar{D}_{ik} S_{kj} \tag{12}$$

In eq 11 and 12 the quantities S_{kj} and $\bar{S}_{jl}$ are the jth components of the kth and lth eigenvectors, respectively. Then, for each absorbance point one can compute the normalized residual d_{il}:

$$d_{il} = |B_{il} - \bar{D}_{il}|/\sigma_{D_{il}} \tag{13}$$

As a whole the residuals should follow the normal probability density function if the errors, $\sigma_{D_{il}}$, are really the standard deviations for the absorbances. The distribution of residuals within various ranges can be compared to that expected from the normal probability density function; the minimum number of eigenvalues required to achieve a satisfactory distribution would then be the rank of the matrix. Finally, an estimate of χ^2 using the first m eigenvalues to regenerate the data is given by eq 14. This value can be compared to the expectation value of χ^2, which, when the rank is m, is given by eq 15. $\langle \chi_m^2 \rangle$ should be near χ_m^2 when m is the rank of matrix M.

$$\chi_m^2 = \sum_{i,l} [(B_{il}^{(m)} - \bar{D}_{il})^2/\sigma_{D_{il}}^2] \tag{14}$$

$$\langle \chi_m^2 \rangle = (n_w - m)(n_s - m) \tag{15}$$

Results

Optical data for metal–ammonia solutions abound in the

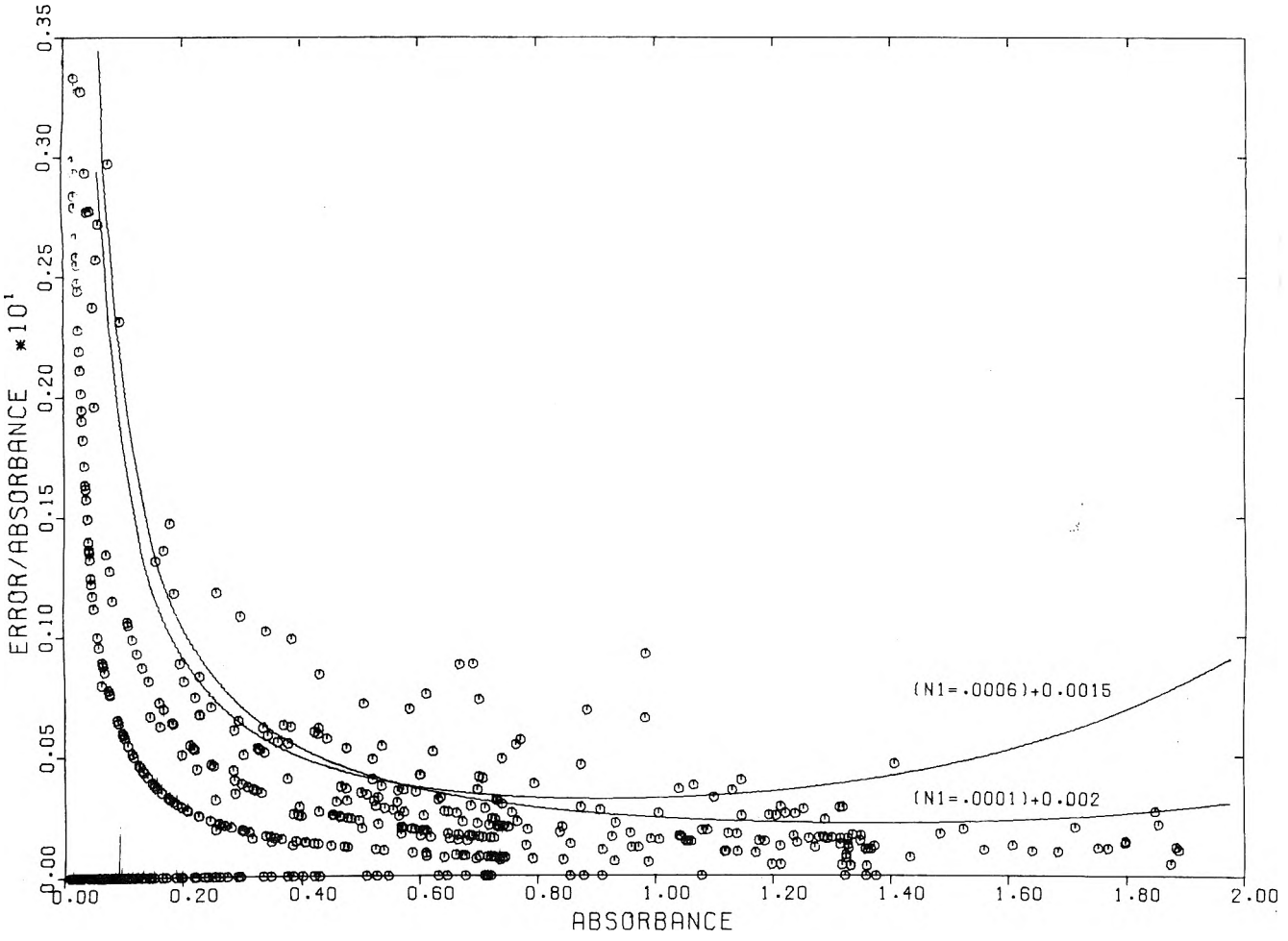

Figure 1. The estimation of the photometric and chart reading errors: points are relative errors in nondecomposing solutions; lines are the error functions used in this analysis.

literature but we required data from only one experimenter as it has been shown that only well-calibrated spectrophotometers will give the proper results when the data from two or more spectrophotometers are combined.[7] Rubinstein's data[8] which we employed in this analysis are the most extensive, consistent, and precise available. The Na–NH_3 solutions encompass a concentration range of about 10^{-5} to 10^{-3} M at three temperatures, −55, −65, and −75°C. Rubinstein also recorded the spectra of sodium in 0.08 M NaI–NH_3 solutions. The concentration of sodium was about 10^{-5} to 5×10^{-4} M, again at the three temperatures. In most cases multiple scans were made so that the amount of decomposition during a run could be determined.

We used 51 wavelengths from 450 to 1825 nm; those points at the highest energy recorded by Rubinstein were not used because some negative absorbances existed. There were seven, and in one instance six, solutions available for analysis in the concentration ranges at each temperature. Thus, six separate sets of data are available to test for the number of species. The data were normalized since multiplying a row by a factor does not change the rank of the matrix. This process eliminates errors due to path length measurements and makes all the solutions of approximately equal weight.

Since many different results can be obtained depending upon the error assumed, it is very important to properly calculate the errors. Three types of errors exist: the thermal noise from the lead sulfide detector, chart reading error, and decomposition of the solutions.

The proper error for thermal noise for the Cary Model 14 is given by eq 16:

$$\Delta D = -0.434 \times \mathrm{N1} \times [1 + (1/T^2)]^{1/2} \qquad (16)$$

where N1 is the root mean square noise at 100% T, in units of transmittance.[9] For our own Cary Model 14, we calculate a value of 0.0006 for N1 with a reading error of ±0.0015. However, this may not be the error for Rubinstein's instrument but it does provide a reasonable basis for comparison. Fortunately, among the 41 solutions reported by Rubinstein, 9 did not appear to decompose during the three or four runs made on each solution. Thus, by averaging the runs and calculating a standard deviation based on the three or four points at each wavelength, a plot of relative error vs. absorbance was made. This plot is given in Figure 1 and shows that, except at high absorbances, the error we found appears to be a good estimate for Rubinstein's data. However, matrix rank analysis is not a least-squares procedure, and the high absorbances contribute more to the eigenvalues and therefore to the standard errors than the lower absorbances. Thus, the correct error function at high absorbances is crucial. We chose to use a reading error of ±0.002 and an N1 of 0.0001.

We must also deal with solution decomposition because

the concentrations of the species changed as the spectrum of the solution was recorded. This phenomenon would affect the rank of the absorption matrix unless this error is accounted for. So a linearly graduated error, based on the estimated percent decomposition per spectrum, was added to each succeeding absorbance point recorded. However, this decomposition error is systematic, rather than random. Thus, the total calculated errors will not follow a χ^2 distribution so standard statistical tests cannot properly be made.

TABLE I: Distribution of Normalized Residuals for $Na–NH_3$ Solutions at −65°C

No. of eigenvectors	No. of normalized residuals in the given ranges							
	0–1	1–2	2–3	3–4	4–5	5–6	6–7	7+
1	161	60	26	14	26	16	14	40
2	294	53	8	1	1	0	0	0
3	305	46	6	0	0	0	0	0
Expected distribution	244	97	15	1	0	0	0	0

Table I shows a typical result of our analysis of Rubinstein's data. The seven $Na–NH_3$ solutions at −65°C have a distribution of residuals using only one eigenvalue and eigenvector which is obviously insufficient. However, the use of two eigenvalues gives a distribution close to that expected. So the residual distribution shows a rank of 2 for the M matrix.

Tables II and III show that χ_2^2 at each temperature is the closest to its expectation value. In fact, all the other χ_m^2 are far from their expectation values. Also, the first two eigenvalues are much greater than their errors, whereas the third and succeeding eigenvalues are much smaller than their errors and so are certainly zero within experimental error. Thus, for each set of data, all three error criteria show that two linearly independent bands are necessary and sufficient to regenerate the data. Furthermore, we have applied this analysis to the less extensive data of Gold and Jolly[10] for $Na–NH_3$ solutions at −65°C. Again, two species were found within the rather large experimental error.

If Na^+ is involved in an equilibrium with one of the absorbing species in $Na–NH_3$ solutions, then the addition of

TABLE II: Results of the Matrix Rank Analysis for $Na–NH_3$ Solutions

	Eigenvalue	Standard error	No. of residuals $>3\sigma_{est}$	Expected no. $>3\sigma_{est}$	χ_m^2	$\langle\chi_m^2\rangle$
−55°C	107.0	0.0129	65	1	3884	300
(357 pts.)	0.03920	0.0097	0	1	169	245
	0.00054	0.0080	0	1	121	192
−65°C	104.7	0.0115	110	1	13224	300
(357 pts.)	0.10780	0.0082	2	1	237	245
	0.00062	0.0078	0	1	173	192
−75°C	102.3	0.0155	137	1	29157	300
(357 pts.)	0.23786	0.0094	2	1	230	245
	0.00071	0.0080	1	1	159	192

TABLE III: Results of the Matrix Rank Analysis for $NaI/Na–NH_3$ Solutions

	Eigenvalue	Standard error	No. of residuals $>3\sigma_{est}$	Expected no. $>3\sigma_{est}$	χ_m^2	$\langle\chi_m^2\rangle$
−55°C	91.9	0.0297	70	1	6215	250
(306 pts.)	0.08083	0.0210	1	1	236	196
	0.00193	0.0060	0	1	42	144
−65°C	104.4	0.0422	86	1	10098	300
(357 pts.)	0.19523	0.0274	0	1	110	245
	0.00098	0.0123	0	1	24	192
−75°C	100.7	0.0194	169	1	46746	300
(357 pts.)	0.31058	0.0125	0	1	192	245
	0.00068	0.0128	0	1	134	192

TABLE IV: Results of the Matrix Rank Analysis for $NaI/Na–NH_3$ with $Na–NH_3$ Solutions

	Eigenvalue	Standard error	No. of residuals $>3\sigma_{est}$	Expected no. $>3\sigma_{est}$	χ_m^2	$\langle\chi_m^2\rangle$
−55°C	198.9	0.0324	165	2	11887	600
(663 pts.)	0.12393	0.0225	57	2	1841	539
	0.00862	0.0093	1	2	355	480
	0.00136	0.0242	0	2	229	423
−65°C	209.1	0.0437	241	2	25402	650
(714 pts.)	0.30387	0.0277	46	2	1927	588
	0.00851	0.0142	7	2	578	528
	0.00277	0.0313	0	2	275	470
−75°C	203.1	0.0249	325	2	77470	650
(714 pts.)	0.54413	0.0155	63	2	2913	588
	0.01133	0.0136	7	2	685	528
	0.00304	0.0146	0	2	337	470

sodium salts to these solutions might change the relative concentrations of species sufficiently so that one species would appear to predominate, or, if a third, very minor species existed in the relatively dilute $Na–NH_3$ solutions studied by Rubinstein, which might be a major constituent of the more concentrated solutions of Gold and Jolly, the addition of sodium salts to the $Na–NH_3$ solutions would also change the rank of the M matrix. Yet, analysis of the $NaI/Na–NH_3$ solution yields only two species. Therefore, an analysis of the $NaI/Na–NH_3$ and $Na–NH_3$ solutions at the same temperature was made. The results given in Table IV show the matrix M no longer has a rank of 2, but rather it has a rank of 3. The third eigenvalues are slightly less than their errors but neglecting the correlation error in deriving the formula for the standard error could account for the differences. The other two criteria discussed previously indicate two species to be insufficient, but three species will account for the spectrum.

There are three ways to interpret our results. First, it is possible that the band shapes and positions of the two species in ammonia are changed by the addition of salt, a suggestion originally made by Rubinstein;[8] such behavior corresponds to a noncompliance of the system to Beer's law and for small deviations could lead to a rank of 3. An alternate explanation is that one of the two species found in the $Na–NH_3$ solutions is not the same as either of the two species found in the salt solutions. Finally, the salt solutions may contain three species but one of them is equivalent to M^0 because a rank of two would be expected for the solutions containing only salt. However, upon adding solutions from the $Na–NH_3$ set, the monomer would become linearly independent of all other species because the metal ion concentration is variable for the added $Na–NH_3$ solutions.

Our analysis of the $Na–NH_3$ and $NaI/Na–NH_3$ solutions together was an attempt to elucidate the nature of the species present. Unfortunately, a firm conclusion cannot be reached. Of course, with a sufficient number of solutions, it should be possible to find the band shapes and equilibrium constants by a least-squares procedure. However, Rubinstein's data do not contain enough solutions because there are only about 2.5 degrees of freedom available per required variable. In addition, the total metal concentrations are not known with sufficient accuracy to obtain good equilibrium constants. We hope to remedy this situation by obtaining more spectral data, over a wider concentration range, than are currently available.

Although we are presently unable to identify the species present in $Na–NH_3$ and $NaI/Na–NH_3$ solutions without resorting to other data, we have shown *conclusively that* two linearly independent absorbing species (possibly three species in the salt solutions) are necessary and sufficient to regenerate the data for $Na–NH_3$ solutions in the concentration range of 10^{-5} to 10^{-3} M and for 0.08 M NaI solutions with Na concentrations of about 10^{-5} to 5×10^{-4} M. This conclusion is independent of the band shape function.

Acknowledgment. We gratefully acknowledge the generous financial assistance of the National Science Foundation and the Robert A. Welch Foundation. Dr. A. A. El-Awady provided us with a copy of the matrix rank analysis program which saved a considerable amount of time.

References and Notes

(1) Presented at Colloque Weyl IV under the title "The Number of Absorbing Species in the 1.5 μ Band as Determined by Matrix Rank Analysis".
(2) E. Becker, R. H. Lindquist, and B. J. Alder, *J. Chem. Phys.*, **25**, 971 (1956); M. Gold, W. L. Jolly, and K. S. Pitzer, *J. Am. Chem. Soc.*, **84**, 2264 (1962); E. Arnold and A. Patterson, Jr., *J. Chem. Phys.*, **41**, 3089 (1964); S. Golden, C. Guttman, and T. R. Tuttle, Jr., *ibid.*, **44**, 3791 (1966); A. Demortier and G. Lepoutre, *C. R. Hebd. Seances Acad. Sci., Ser. C*, **268**, 453 (1969).
(3) G. Rubinstein, T. R. Tuttle, Jr., and S. Golden, *J. Phys. Chem.*, **77**, 2872 (1973).
(4) R. M. Wallace, *J. Phys. Chem.*, **64**, 899 (1960); S. Ainsworth, *ibid.*, **65**, 1968 (1961); J. L. Simonds, *J. Opt. Soc. Am.*, **53**, 968 (1963); R. M. Wallace and S. M. Katz, *J. Phys. Chem.*, **68**, 3890 (1964); D. Katakis, *Anal. Chem.*, **37**, 876 (1965); J. S. Coleman, L. P. Varga, and S. H. Mastin, *Inorg. Chem.*, **9**, 1015 (1970); J. J. Kankare, *Anal. Chem.*, **42**, 1322 (1970).
(5) Z. Z. Hugus and A. A. El-Awady, *J. Phys. Chem.*, **75**, 2954 (1971).
(6) L. P. Varga and F. C. Veatch, *Anal. Chem.*, **39**, 1101 (1967); W. D. Wakley and L. P. Varga, *ibid.*, **44**, 169 (1972); P. H. Rieger, *Aust. J. Chem.*, **26**, 1173 (1973); J. T. Bulmer and H. F. Shurvell, *J. Phys. Chem.*, **77**, 256 (1973).
(7) G. Wernimont, *Anal. Chem.*, **39**, 554 (1967).
(8) G. Rubinstein, Ph.D. Dissertation, Brandeis University, 1973; University Microfilms No. 73-15458.
(9) Cary Instruments, Application Report AR 14-2, Sept, 1964.
(10) M. Gold and W. L. Jolly, *Inorg. Chem.*, **1**, 818 (1962).

Liquid Ammonia. A Comparative Study of Models via Raman Spectroscopy

James W. Lundeen and William H. Koehler*

Department of Chemistry, Texas Christian University, Fort Worth, Texas 76129 *(Received July 23, 1975)*

Publication costs assisted by the Robert A. Welch Foundation

High-density digital Raman spectra of pure ammonia in the 3000–3500-cm^{-1} region have been collected as a function of temperature. The data were used to critically evaluate two previously suggested models. One model interprets the spectrum in terms of associated and unassociated species. Resolution of the N–H region into four bands, three attributed to the unassociated (C_{3v}) species and one attributed to the associated (C_s) species, forms the basis for interpretation of the Raman spectrum of pure ammonia and ammonia solutions. This interpretation raises questions concerning line shapes due to the C_s species, variation of line shapes with temperature, relative intensities of ν_1 and ν_1', and coincidences necessary to explain the absence of other C_s bands. The second model, the damped, coupled oscillator model, attempts to interpret the spectrum in terms of coupling of vibrational states. Correction of a sign error in the original formulation and the use of only the isotropic Raman scattering resulted in a satisfactory explanation of the changes observed in the spectrum as temperature is varied. The band at ca. 3290 cm^{-1} (at high temperatures) is assigned to ν_1, the totally symmetric N–H stretching mode, and the same band is assigned to $2\nu_4$ at low temperatures (below 240 K). The change in assignments is due to a lowering in frequency of the nonresonating symmetric stretch with increased hydrogen bonding. Fermi resonance between ν_1 and $2\nu_4$ gives rise to an observed spectrum in which observed peak positions do not change appreciably.

Introduction

The Raman spectrum of liquid ammonia is characterized by weak scattering around 1060 and 1640 cm^{-1} and strong scattering around 3300 cm^{-1}. The 1060- and 1640-cm^{-1} bands have been unambiguously assigned as ν_2, symmetric bending mode, and ν_4, asymmetric bending mode, respectively. The 3300-cm^{-1} region is characterized by an envelope which appears to be three overlapping bands. Little doubt exists concerning the assignment of the highest energy band (ca. 3380 cm^{-1}) to ν_3, asymmetric stretching mode; however, controversy exists concerning the assignment of the two lower energy bands. It is not the purpose of this paper to review comprehensively all band assignments. Suffice it to say that various investigators[1,2] have assigned the bands at ca. 3220 and 3305 cm^{-1} to $2\nu_4$ and ν_1, symmetric stretching mode, respectively, whereas other investigators[3] have reversed these assignments. The problem of band assignments is complicated by the existence of Fermi resonance[4] between $2\nu_4$ and ν_1, and the intensity reversals which occur with increasing (decreasing) temperature.[5] The importance of the correct interpretation of the N–H stretching region cannot be minimized if meaningful conclusions concerning solute–solute and solute–solvent interactions in liquid ammonia solutions are to be forthcoming.

Recently, two models have been proposed to explain the spectral features observed in the 3300-cm^{-1} region. One model, henceforth referred to as the four-band model, suggests that there are two types of ammonia molecules present in liquid ammonia.[6,7] One type of ammonia molecule is unassociated and has C_{3v} symmetry, whereas the second type is associated with another ammonia molecule via hydrogen bonding and has C_s symmetry. Resolution of the 3300-cm^{-1} envelope into three, four, and five bands revealed that a four-band fit was statistically more meaningful than either a three- or five-band fit.[8] The fourth band at ca. 3265 cm^{-1} is polarized and has been assigned as ν_1', the totally symmetric stretching mode of the C_s species. This band is reported to increase in intensity as the temperature is decreased, and such an intensity change accounts for the observed intensity reversals with temperature. The four-band model has been used to explain the bands observed in the N–H stretching region in salt solutions,[6–8] in ND_2H,[7] and most recently in solutions of ammonia in deuteriobenzene.[9]

Inspection of the results presented by the aforementioned investigators[8] raises certain questions. Although complete band parameter data are not given, the shape of the band assigned to ν_1' appears significantly different than the shape of the band assigned to ν_1. If these are both due to totally symmetric vibrations, their band shapes might be expected to be more similar. The fact that the C_s species could have six Raman active modes yet only one is observed necessitates fortuitous coincidences. Finally, the intensity of ν_1' is always less than that of ν_1. One of two conclusions must be drawn: either the vibration giving rise to ν_1' is not as efficient a scattering center as the vibration giving rise to ν_1, and/or the concentration of associated molecules is less than that of the unassociated molecules.

An alternative model based on coupling of vibrational modes has been proposed.[10] This model is an extension of the model used to explain the low-frequency photon coupling in solids.[11] While a complete derivation will not be given here, the basic equations are presented for reference purposes:

$$I_{zz}(\omega) = \frac{1}{2\pi}(\eta(\omega)+1)\left(C_1^2\frac{(\Omega_2^2-\omega^2)B-\omega\Gamma_2 A}{A^2+B^2} + 2C_1C_2\frac{bB}{A^2+B^2} + C_2^2\frac{(\Omega_1^2-\omega^2)B-\omega\Gamma_1 A}{A^2+B^2}\right) \quad (1)$$

where

$$A = \Omega_1^2\Omega_2^2 - \omega(\Omega_1^2+\Omega_2^2) + \omega^4 - \omega^2\Gamma_1\Gamma_2 - b^2 \quad (2)$$

and

$$B = \omega(\Omega_2^2\Gamma_1 + \Omega_1^2\Gamma_2) - \omega^3(\Gamma_1+\Gamma_2) \quad (3)$$

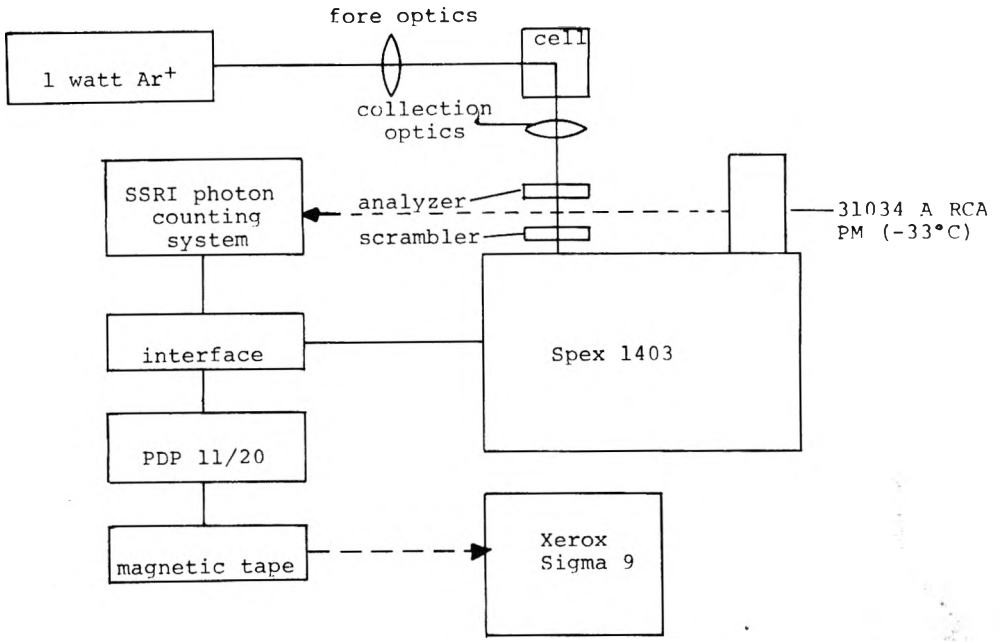

Figure 1. Laser Raman spectrometer.

In the above formulation $I_{zz}(\omega)$ is the isotropic Raman intensity. $\eta(\omega)$ is the Bose–Einstein population factor, b is the interaction energy or coupling parameter, C_1 and C_2 are the relative scattering strengths of the uncoupled oscillators, Γ_1 and Γ_2 are the damping constants and are equivalent to the line widths normally observed for vibrations which are not in Fermi resonance, ω_1 and ω_2 are the observed frequencies, and Ω_1 and Ω_2 are the frequencies of the uncoupled vibrations. Ω_1 and Ω_2 are calculated as follows:

$$\Omega_1^2 = \tfrac{1}{2}(\omega_1^2 + \omega_2^2) + \tfrac{1}{2}[(\omega_1^2 - \omega_2^2)^2 - 4b^2]^{1/2} \quad (4)$$

and

$$\Omega_2^2 = \tfrac{1}{2}(\omega_1^2 + \omega_2^2) - \tfrac{1}{2}[(\omega_1^2 - \omega_2^2)^2 - 4b^2]^{1/2} \quad (5)$$

where ω_1 and ω_2 are the observed peak frequencies.

Although the results of this model appear promising, it too raises questions. Some of the data are reported[10] at 182 K but ammonia solidifies at 193 K. In the original publication, the sign preceding the term $2C_1C_2[bB/(A^2 + B^2)]$ in eq 1 was reported as negative; however, an analysis of the deviation yields a positive sign.[12] Close examination of the curve fitting reveals a deficiency in intensity in the valley between the peaks. This is the same region where the four-band model suggests ν_1' should be. Regardless of band assignments $C_2/C_1 = 0.3$ appears too large; such a ratio suggests that either the intrinsic scattering of $2\nu_4$ is greater than that of ν_1 or that it is 30% of ν_1. Certainly the intensity of the overtone would not be greater than the fundamental, and it is doubtful that it would be as large as 30%. Finally, the anisotropic scattering, although small, should be removed from the isotropic scattering since the model is applicable only to isotropic scattering.

The four-band model results in assignment of the bands in the 3300-cm^{-1} region as 3214 ($2\nu_4$), 3271 (ν_1'), 3300 (ν_1), and 3385 cm^{-1} (ν_3) at 25°C. The assignments based on the coupled oscillator model are 3220 (ν_1), 3305 ($2\nu_4$), and 3388 cm^{-1} (ν_3) at 25°C. Unfortunately the assignment dilemma remains unresolved. Because of the questions which have been raised, a review of both models seemed in order. High-density Raman scattering data obtained under carefully controlled experimental conditions are necessary to critically evaluate the proposed models. Only when the two models are subjected to analyses using the same data can meaningful conclusions be drawn. The acquisition of Raman scattering data, treatment of the data using the four-band model and a corrected version of the coupled oscillator model, and assignment of the bands in the Raman spectrum of liquid ammonia form the subject of this work.

Experimental Section

A laser Raman spectrometer was constructed using five primary components: (1) control Laser-Orlando 1-W Ar^+ ion laser fitted with an optical feedback loop for power stabilization; (2) Spex 1403 double monochromator; (3) SSRI photon counting detection system with buffered binary scaler; (4) RCA 31034A photomultiplier tube housed in a Products for Research thermoelectric cooler (dark count ~50 Hz at −30°C); and (5) PDP-11/20 minicomputer with magnetic tape drive. The instrument geometry is shown schematically in Figure 1. The laser beam (4880 Å, maximum power 400 mW) was focused on the sample after deflection into a vertical plane parallel to the monochromator entrance slit. The scattered light was focused on the entrance slit by a 75 mm $f/1.0$ lens. Prior to reaching the slit, the light passed through an analyzer followed by a calcite wedge scrambler. The analyzer permitted accurate depolarization measurements. Measured depolarization values for carbon tetrachloride were 0.0092, 0.740, and 0.752 for the 459-, 314-, and 218-cm^{-1} bands, respectively, using the same slit width as for the ammonia spectra (10.7-cm^{-1} band-pass). Comparison to literature values[13] of 0.0039, 0.751, and 0.758, which were obtained using narrower slits, demonstrated that the analyzer was satisfactory.

The monochromator drive motor was controlled by the minicomputer with spectral data accumulated only when the drive was stationary. Since the scaler input did not involve an RC time constant the effective time constant was zero, and there was no time constant distortion of the band contours. The Raman spectral data were written on magnetic tape by the PDP-11 minicomputer for off-line pro-

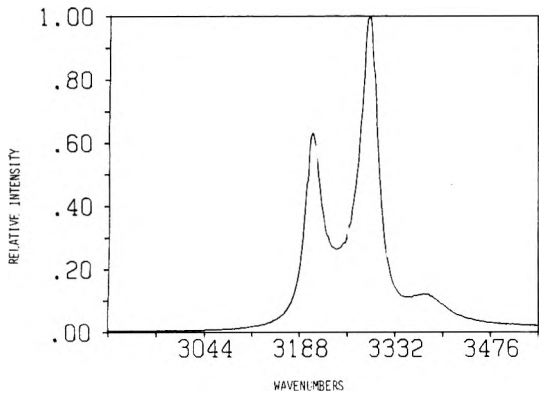

Figure 2. N–H stretching region (polarized) (22°C).

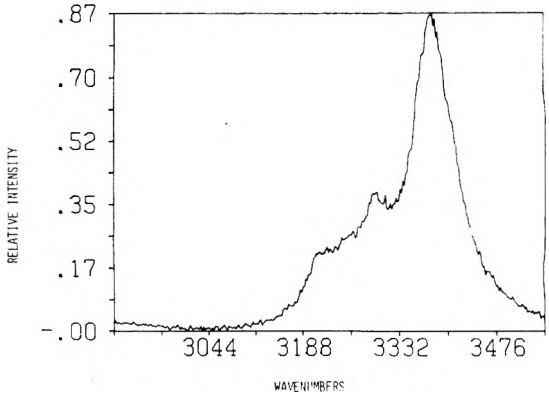

Figure 3. N–H stretching region (depolarized) (22°C).

cessing on a Xerox Sigma 9 computer.

Samples were prepared by condensing ammonia (Matheson, 99.99%), which had been distilled twice from sodium metal, into glass Raman sample tubes on a vacuum line. The samples were frozen in liquid nitrogen and sealed off under vacuum. The samples were held in a vertical orientation in a metal block which was cooled by recirculating cold methanol. A plexiglass cube filled with dry nitrogen surrounded the sample block preventing condensation on the sample. Temperatures were monitored with a thermistor and are accurate to ±3°C.

Data Treatment

Any slit distortion was removed by deconvoluting[14-16] using an observed slit function for this instrument. This function was derived from a mercury emission line contour measured as a function of slit width. The Raman scattering polarized in the z direction is given[17,18] by

$$I_z = k(45(\bar{\alpha}')^2 + 4(\gamma')^2)E_y^2 \quad (6)$$

which corresponds to the matrix equation

$$\alpha_{zz} = (1/3)(\mathrm{Tr}(\alpha)) + (1/3)(3\alpha_{zz} - \mathrm{Tr}(\alpha)) \quad (7)$$

of Schwartz and Wang.[10] Since these authors formulated a model in which only scattering due to the first term is considered, it was necessary to isolate the Raman scattering due to the $\bar{\alpha}'$ term in eq 6. This was accomplished by utilizing the scattering polarized in the y direction[17,18] given by:

$$I_y = k(3\gamma')^2E_y^2 \quad (8)$$

and applying the relation shown by eq 9 at each frequency.

$$\bar{\alpha}' = k(I_z - (4/3)I_y) \quad (9)$$

The resulting isotropic spectrum was resolved by a nonlinear damped least-squares program[19] into symmetrical bands described as a sum of a Gaussian and a Lorentzian having the same band centers and half-widths. The function used is given by eq 10, where ω_0 is the band center, h is the band half-width, and G and L are the Gaussian and Lorentzian intensities, respectively. This analysis was done using the same computer program used in references 8 and 9.

$$I(\omega) = Ge^{-4\ln 2((\omega-\omega_0)/h)^2} + L/(1 + 4[(\omega - \omega_0)/h]^2) \quad (10)$$

The coupled oscillator model was programmed so that all seven parameters (b, Γ_1, Γ_2, C_1, C_2/C_1, ω_1, and ω_2) could be refined simultaneously. Due to the complexity of the model, the partial derivatives of intensity with respect to each parameter were approximated by relations of the type shown in eq 11, where $\Delta = 0.005(\Gamma_1)$.

$$\partial f(\Gamma_1)/\partial\Gamma_1 = [f(\Gamma_1 + \Delta) - f(\Gamma_1 - \Delta)]/2\Delta \quad (11)$$

The computer used, a Xerox Sigma 9, was capable of only six significant figures in floating point notation, and therefore all computations were performed in double precision mode since significant figures were lost in the subtraction step as well as during the solution of the matrix equation in the least-squares iteration. It was found that the best results were obtained by constraining the observed peak maxima (which were found quite accurately using program RESOL[19]) and allowing only five parameters to be adjusted. If all seven parameters were varied, oscillation around the final solution occurred. A "manual regression" was performed on the observed peak maxima by making small adjustments in these parameters. The values which gave the smallest weighted sum of squares of residuals were accepted as the final solution in all cases. The weighting scheme w = (number of counts)$^{-1}$, which is appropriate for counting experiments, was applied during all computations.

Results and Discussion

Raman scattering data in liquid ammonia as a function of temperature were collected. Polarized and depolarized spectra in the 3300-cm^{-1} region are shown in Figures 2 and 3. Prior to any analysis, the data were deconvoluted with a slit function. The data in the 3300-cm^{-1} region were subjected to a curve fitting procedure using program RESOL.[19] Using Hamilton's R factors[30] as a criteria of "goodness" of fit, these analyses confirmed[7] that a four-band fit was statistically better than either a three- or five-band fit. Results of the curve fitting for both the polarized and depolarized spectra are presented in Tables I and II, and representative plots of the data are shown in Figures 4 and 5. The error curve shown at the bottom is on the same scale as the ordinate.

Inspection of Table I reveals several interesting and unexpected results. The bands at ca. 3205 and 3290 cm^{-1}, assigned[8] as $2\nu_4$ and ν_1, respectively, exhibit a high percentage of Lorentzian character. This is not unexpected because a Lorentzian or Voigt function is generally regarded as a satisfactory description of most Raman bands.[20-22] The lower percentage of Lorentzian character observed in the 3380-cm^{-1} band, assigned to ν_3, seems reasonable, since studies[23-25] have shown that line widths corresponding to non-totally symmetric vibrations are considerably greater than those corresponding to totally symmetric vibrations.

TABLE I: Four-Band Model Parameters (Polarized)

Temp, K	ν, cm^{-1}	Intensity, Hz		Half-width, cm^{-1}	Area, Hz × cm^{-1} × 10^5	% Lorentzian
		Gaussian	Lorentzian			
295	3209	2650	12720	28	6.4	83
	3258	3950	0	67	2.8	0
	3294	2680	22150	29	10.9	89
	3383	1350	790	66	1.8	37
258	3207	3370	15290	35	8.5	82
	3256	5820	0	77	4.7	0
	3293	3850	15490	35	9.9	80
	3376	1240	1720	57	2.2	58
243	3204	4370	13050	32	8.1	75
	3249	6150	0	92	6.0	0
	3291	3250	11590	41	8.9	78
	3374	1700	3080	51	3.4	64
228	3203	180	1190	32	0.7	87
	3252	400	0	80	0.3	0
	3291	40	1080	42	0.7	96
	3375	0	350	19	0.3	100

Table II: Four Band Model Parameters (Depolarized)

Temp, K	ν, cm^{-1}	Intensity, Hz		Half-width, cm^{-1}	Area, Hz × cm^{-1} × 10^5	% Lorentzian
		Gaussian	Lorentzian			
295	3213	170	140	50	2.0	44
	3254	10	260	43	1.8	97
	3294	10	470	44	3.3	98
	3381	0	1920	77	23	100
258	3207	100	470	42	3.5	82
	3254	380	170	65	4.3	31
	3296	210	390	42	3.5	65
	3377	0	3220	59	30	100
243	3208	380	500	46	5.5	57
	3246	340	0	31	1.2	0
	3287	720	160	63	6.4	18
	3375	690	3090	52	29	82
228	3207	40	40	43	0.04	49
	3256	30	1	45	0.01	4
	3292	40	40	44	0.04	46
	3374	60	110	49	0.11	64

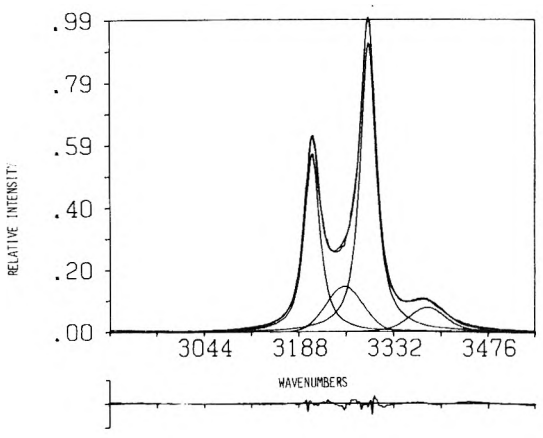

Figure 4. Resolution of polarized N–H stretching region into four bands (22°C).

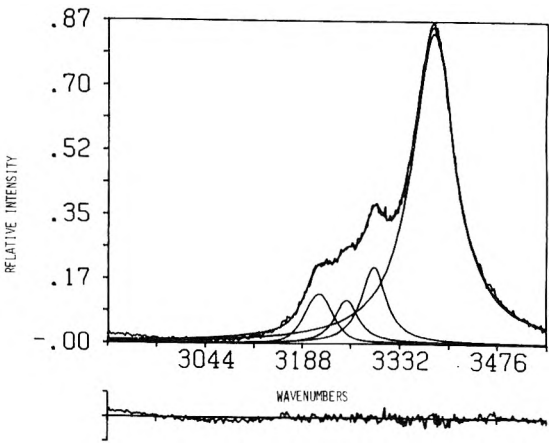

Figure 5. Resolution of depolarized N–H stretching region into four bands (22°C).

The unexpected result is the total Gaussian character of the band at 3255 cm^{-1}. This band is assigned as ν_1', the totally symmetric stretching mode of the associated species. That the band parameters describing this totally symmetric vibration should differ so markedly from the parameters describing the totally symmetric vibration of the unassociated species is difficult to rationalize.

Although the parameters (Table I) describing the bands at 3205, 3290, and 3380 cm^{-1} vary with temperature in a not unreasonable manner, the band parameters set forth in Table II seem to vary in a nonsystematic way with temperature. This variation may be due to the greater uncertainty caused by the lower intensities.

Examination of the spectra at various temperatures did

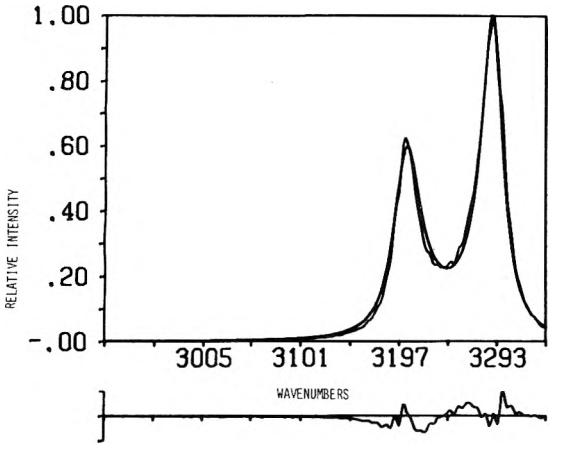

Figure 6. Isotropic component of N–H stretching region fit with coupled oscillator model (22°C).

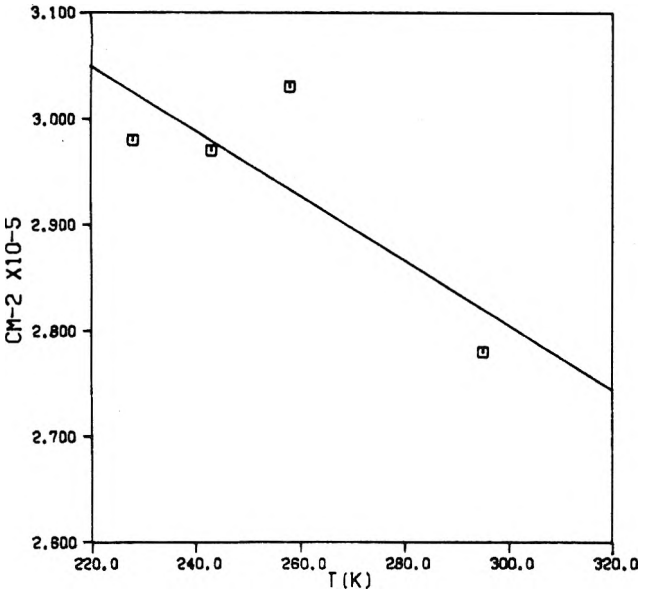

Figure 7. Coupling constant, b, as a function of temperature.

not reveal any new bands; changes in spectral features were limited to a sharpening of the band at 3380 cm^{-1} with decreasing temperature and an intensity reversal involving the bands at 3205 and 3290 cm^{-1}. These results are perplexing if the four-band model is used to interpret the spectrum, since the associated species has C_s symmetry and could have six Raman active fundamental modes. Furthermore, the symmetry of the modes is such that Fermi resonance is allowed between any overtone and any A' fundamental. In light of the fact that at −30°C the band (ν_1') attributed to the associated species accounts for ~23% of the area under the computed envelope, the absence of other bands attributable to the C_s species seems somewhat astonishing. To explain the apparent absence of these bands a great many fortuitous coincidences must be invoked. The possibility of such coincidences raises questions involving the quality of the band parameters ascribed to the ν_1, $2\nu_4$, and ν_3 of the unassociated species.

The coupled oscillator model[10] was investigated using the same Raman scattering data as was used to evaluate the four-band model. Prior to fitting the data, a sign error in the second term of eq 11 in the original publication[10] was

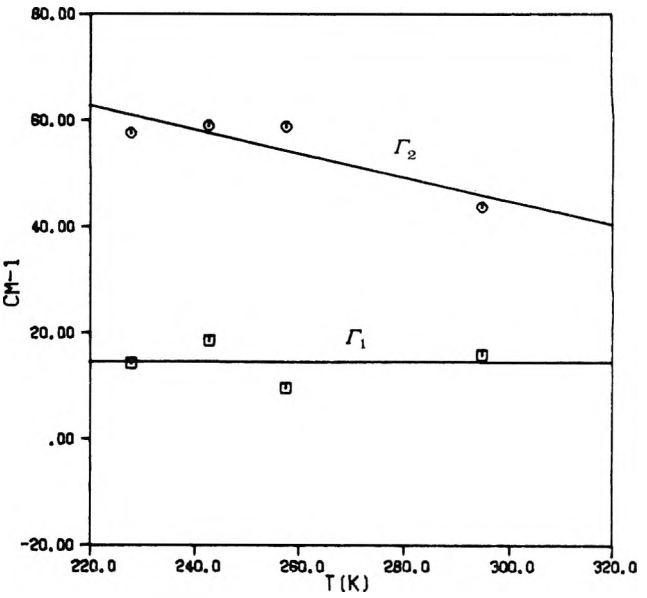

Figure 8. Damping factors, Γ_1 and Γ_2, as a function of temperature.

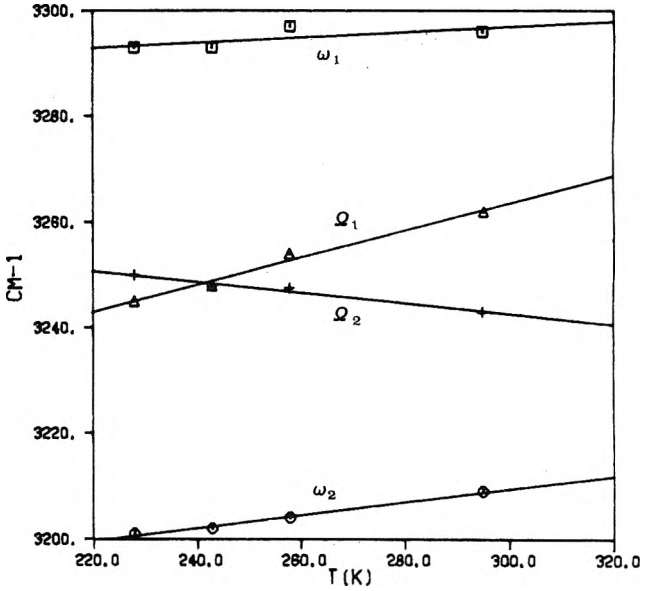

Figure 9. Observed frequencies, ω_1 and ω_2, and uncoupled frequencies, Ω_1 and Ω_2, as a function of temperature.

changed.[12] The data were deconvoluted with a slit function, and the anisotropic contribution to the spectrum was removed (vide supra). Although Schwartz and Wang held the ratio C_2/C_1 constant after establishing a "best" value of 0.3 via a manual regression technique, C_2/C_1 and C_1 were treated as adjustable parameters during the present study. As a consequence five parameters were refined simultaneously.

A representative result of the curve fitting procedure is shown in Figure 6. Variation of the parameters b, Γ_1 and Γ_2, and ω_1, ω_2, Ω_1, and Ω_2 with temperature is shown in Figures 7, 8, and 9. In these figures, the line(s) shown are the result of a linear least-squares analysis. The data are presented in tabular form in Table III. Comparison of these results with those presented by Schwartz and Wang reveals certain similarities and some distinct differences. In general, the computed curve in this study fits the experimental data better in the region between the peaks than does the

TABLE III: Coupled Oscillator Model Parameters

	Temp, K			
	295	258	243	228
Γ_1, cm^{-1}	15.8	9.6	18.5	14.3
Γ_2, cm^{-1}	43.7	58.8	59.0	57.6
b, cm^{-2}	2.78×10^5	3.03×10^5	2.97×10^5	2.98×10^5
C_2/C_1	7×10^{-3}	4×10^{-3}	1×10^{-2}	7×10^{-3}
ω_1, cm^{-1}	3296	3297	3293	3293
ω_2, cm^{-1}	3208	3204	3202	3201
Ω_1, cm^{-1}	3262	3254	3248	3245
Ω_2, cm^{-1}	3243	3247	3248	3250

curve reported in the original publication;[10] however, there is still some problem with the fit at the top of the peaks and on the wings. The values of b reported in this study are of similar magnitude to those previously reported, but b increases rather than decreases with decreasing temperature. Values of Γ_1 and Γ_2 agree quite well with those reported. The variation of Ω_1 and Ω_2 with temperature is very significant in that they cross around 240 K. Ω_1 decreases with decreasing temperature whereas Ω_2 appears to increase. Whether a variation of 5 cm^{-1} in the value of Ω_2 over 50°C can be considered a significant change is dubious. The variation of Ω_2 with temperature is very similar to the variation of the corresponding fundamental ν_4 with temperature (Figure 10). An unexpected but satisfying result concerns the ratio C_2/C_1 (Table III). Although treated as an adjustable parameter, C_2/C_1 always converged to a value of ~0.01. This value lends support to the conclusions which follow.

The results of this study indicate that the Raman spectrum of liquid ammonia can be interpreted as follows. There is little question that the bands at ca. 1060, 1640, and 3380 cm^{-1} can be assigned to ν_2, ν_4, and ν_3, respectively. The controversy has centered around the bands at 3205 and 3290 cm^{-1}. The two modes are coupled via Fermi resonance as indicated by a nonzero value of b, and as a result of this resonance, both bands are combinations of ν_1 and $2\nu_4$. At high temperatures (300 K) the band at 3290 cm^{-1} has more ν_1 character than $2\nu_4$ character and likewise the 3205-cm^{-1} band has more $2\nu_4$ character than ν_1 character. As the temperature is decreased the ammonia molecules are subjected to environmental changes, probably through increased hydrogen bonding, which perturb the molecules and shift Ω_1, the frequency of the uncoupled oscillator, to lower frequency with decreasing temperature. Such frequency shifts are expected as a result of increased hydrogen bonding. The coupling between the two energy levels increases because they are now closer together. As a result of increased coupling the observed frequencies (ω_1 and ω_2) appear relatively constant. The fact that Ω_1 decreases and Ω_2 remains constant or increases supports the supposition that at 300 K the band at 3290 cm^{-1} is primarily of ν_1 character and the band at 3205 cm^{-1} is primarily of $2\nu_4$ character because a symmetric stretching mode should be more affected by hydrogen bonding than a bending mode. As coupling increases, the 3290-cm^{-1} band increases in $2\nu_4$ character and the 3205-cm^{-1} band increases in ν_1 character. As a consequence of the increasing $2\nu_4$ character of the 3290-cm^{-1} band, the intensity decreases, whereas the intensity of the 3205-cm^{-1} band increases because of increasing ν_1 character. Around 240 K, Ω_1 has shifted such that it is equal to Ω_2 and, therefore, each band is of equal ν_1 and

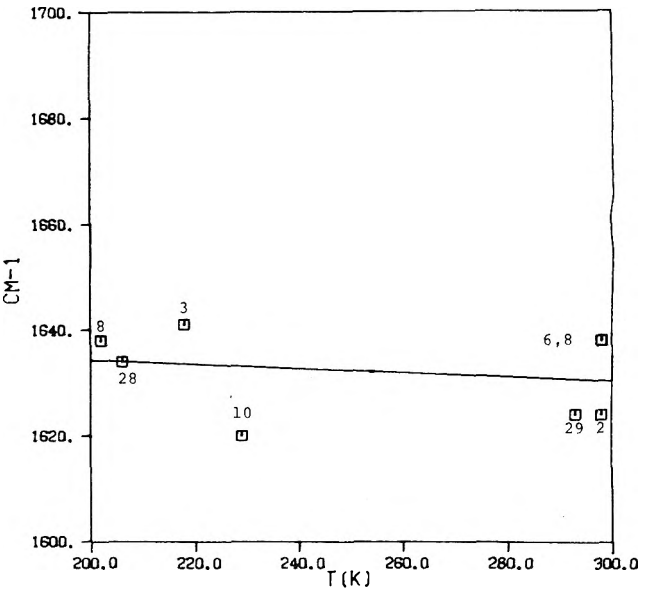

Figure 10. Position of ν_4 as a function of temperature.

$2\nu_4$ character. This result confirms those previously reported.[5] Below 240 K, the band at 3290 cm^{-1} has more $2\nu_4$ character, whereas the 3205-cm^{-1} band has more ν_1 character. In other words, if definite labels must be placed on these bands, above 240 K, the higher energy band is ν_1 and the lower energy band is $2\nu_4$; below 240 K the higher energy band is $2\nu_4$ and the lower energy band is ν_1. Such labels should be summarily rejected because the resonance phenomenon requires that both bands be combinations of states (modes) and only the degree of mixing holds any significance. The value of C_2/C_1 = 0.01 lends support to the aforementioned assignments. Intuitively an overtone is expected to scatter much less than a fundamental, and a ratio of 0.01, $C_{2\nu_4}/C_{\nu_1}$, is more plausible than the reported ratio of 0.30.

In summary, the results of this study suggest that until questions involving band shapes and frequency coincidences are resolved, interpreting the N–H stretching region in terms of two species of ammonia should be viewed with a great deal of skepticism. In addition to these questions, the four-band model requires 12 adjustable parameters (for the isotropic spectrum) whereas the coupled oscillator model requires only 7. Application of the coupled oscillator model permits a reasonable interpretation of the observed spectrum. This model also fits the spectrum of ammonia in carbon tetrachloride, benzene, and pentane[26] as well as the spectrum of alkali halide–liquid ammonia solutions.[27] Further refinement of the model is possible but in the present form it seems to offer a satisfying solution to the controversy involving band assignments in the N–H stretching region.

Acknowledgments. We wish to thank the Robert A. Welch Foundation and the Research Corporation for their financial support.

References and Notes

(1) C. A. Plint, R. M. B. Small, and H. L. Welsh, *Can. J. Phys.*, **32**, 653 (1954).
(2) S. Kinumaki and K. Aida, *Sci. Rep. Res. Inst. Tohoku Univ., Ser. A*, **6**, 186 (1954).
(3) T. Birchall and I. Drummond, *J. Chem. Soc. A*, 1859 (1970).
(4) G. Herzberg, "Infrared and Raman Spectra", D. Van Nostrand Co., Princeton, N.J., 1966.

(5) B. De Bettignies and F. Wallert, *C. R. Hebd. Seances Acad. Sci., Ser. B*, 640 (1970).
(6) D. J. Gardiner, R. E. Hester, and W. E. L. Grossman, *J. Chem. Phys.*, **59**, 175 (1973).
(7) J. H. Roberts, A. T. Lemley, and J. J. Lagowski, *Spectrosc. Lett.*, **5**, 271 (1972).
(8) A. T. Lemley, J. H. Roberts, K. R. Plowman, and J. J. Lagowski, *J. Phys. Chem.*, **77**, 2185 (1973).
(9) J. H. Roberts and B. De Bettignies, *J. Phys. Chem.*, **78**, 2106 (1974).
(10) M. Schwartz and C. H. Wang, *J. Chem. Phys.*, **59**, 5258 (1973).
(11) J. F. Scott, "Light Scattering in Solids", M. Balkanski, Ed., Flammarion, Paris, 1972.
(12) M. Schwartz, North Texas State University, Denton, Tex., private communication.
(13) W. F. Murphy, M. E. Evans, and P. Bender, *J. Chem Phys.*, **47**, 1836 (1967).
(14) K. S. Seshadri and R. N. Jones, *Spectrochim. Acta*, **19**, 1013 (1963).
(15) R. N. Jones, R. Venkataraghavan, and J. W. Hopkins, *Spectrochim. Acta, Part A*, **23**, 925 (1967).
(16) R. N. Jones, T. E. Bach, H. Fuhrer, V. B. Kartha, J. Pitha, K. S. Seshadri, R. Venkataraghavan, and R. P. Young, *NRC Bull.*, **No. 11** (1968).
(17) T. C. Damen, S. P. S. Porto, and B. Tell, *Phys. Rev. (Ser. 2)*, **142**, 570 (1966).
(18) T. R. Gilson and P. J. Hendra, "Laser Raman Spectroscopy", Wiley-Interscience, New York, N.Y., 1970.
(19) P. F. Rusch, Ph.D. Dissertation, University of Texas, Austin, Tex., 1971.
(20) H. S. Goldberg and P. S. Pershan, *J. Chem. Phys.*, **58**, 3816 (1973).
(21) M. McClintock, D. A. Jennings, and M. Mizushima, *Phys. Rev. Lett.*, **21**, 276 (1968).
(22) W. L. Greer, S. A. Rice, and G. Morris, *J. Chem. Phys.*, **52**, 5622 (1970).
(23) W. R. L. Clements and B. P. Stoicheff, *Appl. Phys. Lett.*, **12**, 246 (1968).
(24) J. D. Masso, Y. D. Harker, and D. F. Edwards, *J. Chem. Phys.*, **50**, 5420 (1969).
(25) M. Scotto, *J. Chem. Phys.*, **49**, 5362 (1968).
(26) J. W. Lundeen and W. H. Koehler, to be submitted for publication.
(27) J. W. Lundeen and W. H. Koehler, to be submitted for publication.
(28) B. L. Smith, Masters Thesis, Texas Christian University, Fort Worth, Tex., 1973.
(29) Present work.
(30) W. C. Hamilton, *Acta Crystallogr.*, **18**, 502 (1965).

Correlation of Optical and Magnetic Data for Sodium–Ammonia Solutions

Gabriel Rubinstein

School of Theoretical and Applied Science, Ramapo College, Mahwah, New Jersey 07430 *(Received July 25, 1975)*

The resolution of the optical spectra of Na–NH_3 solutions into two bands,[1-3] one of which may be associated with a species incorporating two electrons, permits the correlation of the optical data with the magnetic data of Huster[4] and of Freed and Sugarman[5], without reference to any particular model for the solutions. With the aid of the redox model,[6] the optical data are shown also to correlate with the spin susceptibility data of Hutchinson and Pastor.[7] The latter correlation requires identification of the diamagnetic species as one of stoichiometry M^-.

The resolution of the broad infrared spectra of dilute (10^{-5}–10^{-3} M) solutions of Na–NH_3 at −75, −65, and −55°C reveals the presence of two distinct, yet similar bands separated by about 600 cm^{-1}. At −65°C their maxima occur at 7067 and 6494 cm^{-1}, respectively. The shape function $f_1(\nu)$ for the band occurring at the higher frequencies was obtained by extrapolation to infinite dilution and was assigned to a species composed of two electrons in some form.

Since the optical analysis revealed the presence of two bands and that $f_2(\nu)$ is due to a species containing two electrons, it is natural to suppose that this species is diamagnetic. Figure 1 compares Huster's[4] static susceptibility data for Na–NH_3 solutions with optical data at −75°C. As can be seen, a good correlation is obtained at the overlapping metal concentrations (about 10^{-3}), and the trend established at low sodium concentrations (optical data) is carried over to the more concentrated metal solutions (magnetic data).

The fraction of unpaired spins, Y, derived from the magnetic data is obtained from the ratio of the measured, net molar static susceptibility (χ_m) to the theoretical magnetic susceptibility of a mole of free electrons ($\chi_T = N^0\beta/kT$). The reported χ_m values have been corrected for the solvent's diamagnetism, while the relative diamagnetic–paramagnetic contributions from the other species is expected to be small for the more dilute solutions. Since χ_m for 0.105 and 7.63×10^{-3} M solutions were -19.0×10^{-6} and 202×10^{-6} erg/(mol G^2), the diamagnetic contributions are expected to be less than 10% for the solutions more dilute than the latter concentration. It is assumed that the minimum negative Y values were characteristic of essentially 100% diamagnetic solutions and that the molar diamagnetic susceptibility decreases with decreasing metal concentrations.

Since the sodium metal concentrations were not experimentally determined, the Y values obtained from the optical data were calculated from

$$Y = C_1/[\mathrm{Na}]$$

where

$$[\mathrm{Na}] = A_{1m}/\epsilon_{1m}L + A_{2m}/\epsilon_{2m}L$$

A_{1m} and A_{2m} are the absorbances at the maximum for each band determined in this work, while the extinction coefficients at the maxima are those calculated by other investigators[8,9] ($\epsilon_{1m} = 5.0 \times 10^4$ and $\epsilon_{2m} = 4.5 \times 10^4$ M^{-1} cm^{-1}) and were both based on total metal concentrations. It is reasonable to assume that both ϵ_{1m} and ϵ_{2m} were determined for solutions characterized mainly by either species 1 or species 2, respectively. C_1 represents the concentration of all paramagnetic species and is equal to $A_{1m}/\epsilon_{1m}L$, where L is the path length (cm).

Figure 2 correlates Freed and Sugarman's[5] static suscep-

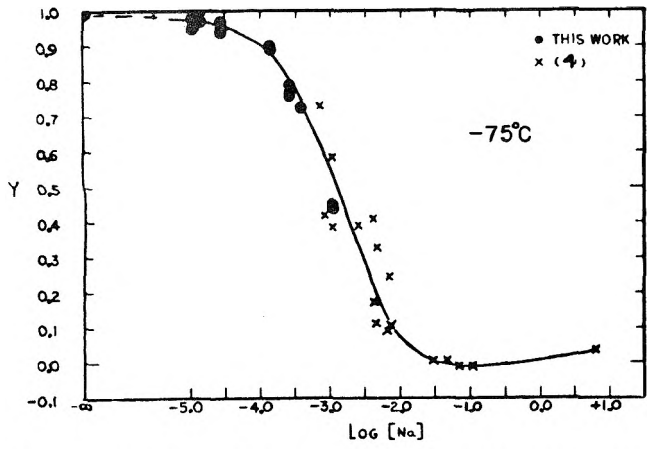

Figure 1. Comparison of the fraction of paramagnetic species derived from optical and static susceptibility data at −75°C.

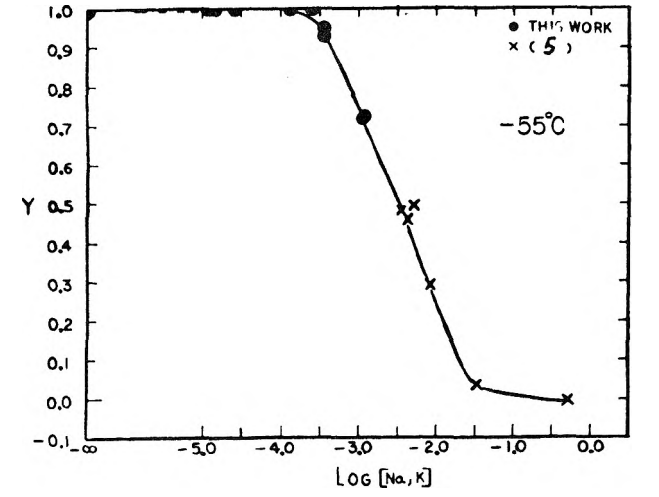

Figure 2. Comparison of the fraction of paramagnetic species derived from optical and static susceptibility data at −55°C.

tibility data for K–NH_3 solutions at −53 ± 1°C with Y values derived from the optical data for Na–NH_3 solutions investigated at −55 ± 0.1°C. It is quite reasonable to compare these to metals (in ammonia), since other investigations have shown that their optical[9,10] and magnetic[7,11] characteristics differ very little.

In order to obtain the spin-pairing equilibrium constant, the following equilibria were assumed:

$$Na^+ + S^- \rightleftharpoons Na^+ \cdot S^- \quad (1)$$

$$Na^+ + 2S^- \rightleftharpoons Na^- + 2S \quad (2)$$

$$Na^+ + Na^- \rightleftharpoons Na^+ \cdot Na^- \quad (3)$$

S^- and $Na^+ \cdot S^-$ (ion pair) are the paramagnetic species while the Na^- and $Na^+ \cdot Na^-$ (ion pair) entities are diamagnetic.

By assuming that the ion-pairing dissociation constants for equilibria 1 and 3 have the same value,[6] and that the respective anions and their ion pairs with Na^+ absorb light identically, the following expression can be derived:[3]

$$A_{1T}(\nu)^2(1 - \alpha) = (f_1(\nu)\epsilon_{1m}L)^2 A_{2T}/(f_2(\nu)\epsilon_{2m}L)KK_{sp}$$

where $A_{1T}(\nu), A_{2T}(\nu)$ = total absorbance of each anion and their respective ion pairs at frequency ν; $f_1(\nu), f_2(\nu)$ = normalized shape function for the paramagnetic and diamagnetic species, respectively; α, K = degree of ion pair dissociation and dissociation constants; K_{sp} = spin-pairing constant for equilibrium 2; $\epsilon_{1m} = 5.0 \times 10^4\ M^{-1}\ cm^{-1}$. Extinction coefficient for dilute solutions;[8] $\epsilon_{2m} = 9.0 \times 10^4\ M^{-1}\ cm^{-1} = 2 \times 4.5 \times 10^4$, where 4.5×10^4 was obtained[9] for solutions characterized by diamagnetic species and was based on total metal concentration.

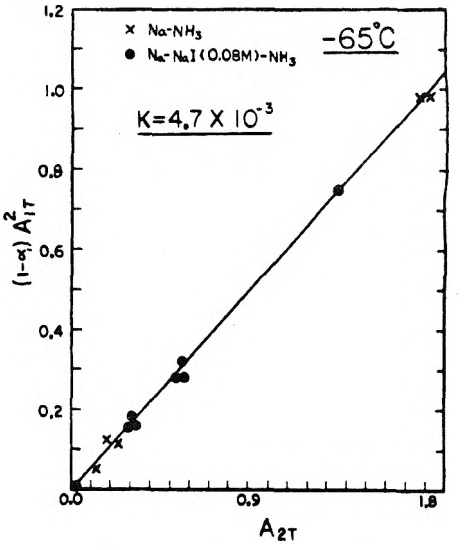

Figure 3. Test for Na^- (stoichiometry) equilibria at −65°C.

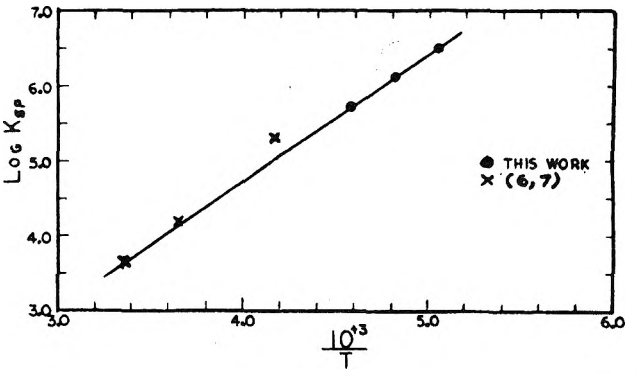

Figure 4. Van't Hoff plot for the spin-pairing reaction $2e^- + Na^+ \rightleftharpoons Na^-$.

TABLE I: Calculated Ion-pairing Dissociation (K) and Spin-Pairing Constants (K_{sp}) Obtained from Optical Data

T, °C	K	K_{sp}
−75	9.0×10^{-3}	3.0×10^6
−65	4.7×10^{-3}	1.3×10^6
−55	7.5×10^{-3}	4.8×10^5

By choosing the proper values of K (and thus α), linear plots of $A_{1T}(\nu)^2(1 - \alpha)$ vs. $A_{2T}(\nu)$ were obtained for Na–NH_3 and Na–NH_3–NaI (0.08 M) solutions at each temperature investigated (Figure 3). K_{sp} was then calculated from the slopes of the lines. The values for K and K_{sp} obtained are summarized in Table I.

The values of K thus obtained are typical of ion-pairing dissociation constants for $Na^+ \cdot S^-$ in liquid ammonia as calculated from conductance data.[12]

The van't Hoff plot in Figure 4 compares the optically derived K_{sp} with those calculated by Golden, Guttman, and Tuttle[6] based on spin paramagnetic susceptibility data of Hutchinson and Pastor[7] (−33, +1, and +25°C). A linear

correlation is obtained yielding the expected negative spin-pairing enthalpy change (−7.55 kcal/mol).

These observations substantiate the assignment of the two optical bands found in Na–NH_3 solutions, $f_1(\nu)$ and $f_2(\nu)$, to paramagnetic and diamagnetic species, respectively.

References and Notes

(1) T. R. Tuttle, G. Rubinstein, and S. Golden, *J. Phys. Chem.*, **75**, 3635 (1971).
(2) G. Rubinstein, T. R. Tuttle, Jr., and S. Golden, *J. Phys. Chem.*, **77**, 2872 (1973).
(3) G. Rubinstein, Ph.D. Thesis, Brandeis University, 1973.
(4) E. Huster, *Ann. Phys.*, **33**, 477 (1938).
(5) S. Freed and N. Sugarman, *J. Chem. Phys.*, **11**, 354 (1943).
(6) S. Golden, C. Guttman, and T. R. Tuttle Jr., *J. Chem. Phys.*, **44**, 3791 (1966).
(7) C. A. Hutchinson, Jr., and R. C. Pastor, *Rev. Mod. Phys.*, **25**, 285 (1953).
(8) R. K. Quinn and J. J. Lagowsky, *J. Phys. Chem.*, **73**, 2326 (1969).
(9) M. Gold and W. L. Jolly, *Inorg. Chem.*, **1**, 818 (1962).
(10) R. C. Douthit and J. L. Dye, *J. Am. Chem. Soc.*, **82**, 4472 (1960).
(11) A. Demortier and G. Lepoutre, *C. R. Acad. Sci., Ser. C*, **268**, 453 (1969).
(12) R. R. Dewald and J. H. Roberts, *J. Phys. Chem.*, **72**, 4224 (1968).

Discussion

R. CATERALL (to Rubinstein). In your plot of log K_2 against $1000/T$ you seem to have used the Hutchinson and Pastor magnetic data for Na or potassium. The Na and K data differ at higher temperatures. A. Demortier measured some spin-pairing fraction in our laboratory for Na–NH_3 found close agreement for Na and K.

(To Peer). The possibility of a third species in the Na–NaI–NH_3 solutions is interesting. At Colloque Weyl I, I reported a strong interaction between the unpaired electron spin and solvated iodide ions, this showing up as a strong g shift and increase in line width. At Colloque Weyl II, I reported some measurements of I Knight shifts in these systems (confirmed by O'Reilly). Both these factors confirm a tendency for e^-–I^- interactions, and we have attributed the species responsible to the triple ion $I^-Na^+e_{sol}^-$.

Martyn Symons (1959) reported a band at 12500 cm^{-1} in Na–NaI–NH_3 which has been the subject of considerable controversy.

J. L. DYE (to Rubinstein). In response to the comment of R. Caterall on the magnetic susceptibility data of Demortier et al., let me note that our ESR studies (Abstracts, Dallas ACS meeting 1964) from −60 to −5°C for solutions of Na, K, Rb, and Cs in NH_3 show that there is no apparent effect of the cation on the temperature dependence of the spin susceptibility.

W. A. SEDDON (to Rubinstein). Using pulse radiolysis we have detected two absorption bands in basic solutions of liquid ND_3. Immediately after the pulse, the spectrum corresponds to that reported at infinite dilution by Hurley *et al.* at Colloque Weyl II. On a longer time scale, the band maximum is shifted to the infrared by about 140 nm. This I believe corresponds to the difference calculated by Rubinstein et al.

G. RUBINSTEIN. The difference in ν_{max} of the two bands of Na–NH_3 solutions at −65°C is 573 cm^{-1} (7067 and 6494 cm^{-1}) or 125 nm.

S. GOLDEN (to Peer and Lagowski). The matrix rank analysis serves to provide an elegant way of establishing the number of distinct and independent line shapes needed to account for the spectral data, two in the present case of added salt or no added salt. If the effect of adding salt is to produce only a shift in the two line shapes that obtain in the absence of salt, and the shift in both cases is the same, it seems to me that the combined data of both salt-containing and salt-absent metal–ammonia solutions will require only three independent line shapes but four distinct ones. I wonder if the result that three independent line shapes are needed for the combined data is not, in fact, in accord with the foregoing possibility. This is what the experimental results of Rubinstein did turn out to be.

T. TUTTLE. Rubinstein's data are consistent with the idea that the spectra are the superposition of two components each of which is shifted slightly by a salt effect. The spectra have been interpreted successfully, quantitatively on this basis (see G. Rubinstein, T. R. Tuttle, Jr., and S. Golden, *J. Phys. Chem.*, **77**, 2872 (1973)). These salt shifts are directly obtained from Rubinstein's data. Such salt shifts are well known for charge-transfer-to-solvent transitions and on this account may be anticipated for these absorptions in Na–NH_3 solutions containing NaI. Consequently, it would not appear necessary to introduce a third independent species in order to analyze the spectra.

W. PEER. Without data from more measurements, we cannot decide what the result of a rank of 3 for the Na plus NaI/Na solutions means. However, it seems to us that if there are the same two species in both types of solutions but that the band shapes shift for NaI/Na solutions, then either a rank of 2 or a rank of 4 for M should be expected. We are only presenting some possibilities other than band shifts to explain the rank of 3 which was found. You may be right, but a decision is impossible now.

B. DEBETTIGNIES. Your calculation and assignment are a nice confirmation of the assignment we have suggested from spectra obtained under the same conditions (*C. R. Acad. Sci., Ser. B*, **271**, 640 (1970)).

KEITH PLOWMAN. Our resolution statistics are only supportive of a fourth band in the N–H stretching region. The primary species arguments are the spectra of ND_2H and NH_2D where a second band is definitely observed. If species arguments are valid, a Fermi resonance study is not a reasonable method if only a diad is considered. I think the isotopic data must be explained before the Fermi resonance arguments can be accepted to explain the temperature dependence.

Trapped Electrons in Organic Glasses[1]

John E. Willard

Department of Chemistry, University of Wisconsin, Madison, Wisconsin 53706 *(Received July 23, 1975)*

Publication costs assisted by the U.S. Energy Research and Development Administration

The experimental observations dealing with trapped electrons in organic glasses which are most revealing as to the nature of the trapping process are discussed, and a model of trapping which they suggest is outlined. Data from optical and ESR spectrometry, differential thermal analysis, bleaching, decay, and scavenger studies are cited. It appears that after mobile electrons produced by γ irradiation or photoionization of solutes are thermalized they first become stabilized in weak traps through polarization and dipole interactions and then deepen these traps by molecular orientation at rates dependent on the polarity of the matrix molecules and the temperature. The data suggest that the stabilized condition at any temperature involves a continuum of trap depths in which the electrons give optical spectra of different λ_{max} which add up to give the broad observed spectrum. The energy of a photon absorbed by an electron in excess of the detrapping threshold for that electron determines whether the electron can migrate far enough to encounter a capturing entity. If the energy is too low the electron is retrapped rather than being bleached. Evidence for capture of epithermal subexcitation electrons by some scavengers and on the heats of solvation of electrons and cations in organic glasses is also noted.

Introduction

Starting in 1962 it was demonstrated[2] that electrons liberated by ionizing radiation in several glassy matrices at cryogenic temperatures can be stabilized in chemically uncombined states observable by optical and ESR spectra. Such trapping has now been observed in such widely different glasses as alkaline ices (e.g., 10 *M* NaOH), aqueous sugar solutions, alcohols, ethers, amines, alkenes, and alkanes. By contrast, significant yields of trapped electrons have not been found in similar crystalline systems.[3]

This paper evaluates the current understanding of the electron trapping process in glasses, as deduced from experiments in many laboratories, including the author's. Illustrations will be taken largely from pure hydrocarbon and methyltetrahydrofuran matrices.

Electron spin resonance and optical absorption spectrometry are the most direct methods of detecting trapped electrons (e_t^-) in glasses and give some of the most revealing evidence as to the nature of the interaction of electrons with the matrix molecules. Significant corollary evidence has been obtained from luminescence, electrical conductivity, and differential thermal analysis studies; from investigations of photobleaching and thermal decay; and from comparative studies with different matrices and different electron scavengers. Endeavors to provide a theoretical understanding of the observed phenomena are in progress in several groups.[4]

Among the questions raised by the trapping of electrons in the glasses are the following. Does the stabilization occur at preexisting sites or are the traps formed by electronic polarization and bond dipole interaction with the coulomb field of the electron (i.e., does the electron "dig its own hole")? Are all electrons in a given matrix trapped with the same energy? What accounts for the broad optical spectra of the trapped electrons? What are the distances between cations and electrons? Does photoexcitation promote to a bound state of the trap or to the conduction band? How far do mobilized electrons travel? Do they inevitably combine with the geminate cation? Can trapped electrons tunnel to deeper traps, cations, and scavengers? What are the heats of solvation of trapped ion pairs? Some of these questions are now answered and others are under continuing investigation. The step-by-step evolution of understanding of the phenomena may be traced in review articles dealing with irradiated glassy solids.[5]

Physical Properties of Organic Glasses

In general glasses used in the study of trapped electrons are formed by immersing a tube of the liquid at room temperature in liquid nitrogen. Typically this results in a density increase of ~30%.[6] As the viscosity increases on cooling, the glass transition temperature (T_g) is reached (typically at 10^{12} to 10^{13} P), below which the rate of molecular relaxation becomes too slow for the enthalpy and free volume to keep up with the rate of cooling in maintaining their equilibrium value (Figure 1). Glasses formed by rapid cooling to below T_g anneal toward the equilibrium state with time. This is evidenced by an increase in the endothermic differential thermal analysis (DTA) peak which appears on warming the sample[8] and by a decrease in the decay rate of trapped electrons.[9] Annealing is much slower at temperatures considerably below T_g than near T_g.[8]

Partial orientation of the molecules of 3-methylpentane (3MP), methylcyclohexane (MCHx), and 2-methyltetrahydrofuran (MTHF) glasses in electric fields as low as 10^4 V cm^{-1} has been demonstrated[10] at temperatures near T_g, suggesting that the much more intense field in the vicinity of a trapped electron may aid it in producing molecular orientations which result in trapping. The orientation is much greater in MTHF, which has a molecular dipole, than in the hydrocarbons where interaction with bond dipoles must predominate.

The glasses are transparent to visible light. If cooled much below the glass transition temperature, they often crack. Some (e.g., MCHx and ethyl alcohol) crystallize on warming while others (e.g., 3MP and MTHF) do not.

Production of Electrons in Glassy Solids

Free electrons may be produced in glassy solids by exposure to high energy electrons from accelerators or the high energy electrons ejected by γ rays or x rays. These electrons (e.g., >0.1 MeV) eject secondary electrons every 1000 Å or so along their tracks and each secondary electron ejects some two to four electrons which are trapped within "spurs" of some 150 Å or less radius in the glasses.

Electrons may also be formed in glasses by photoionization of solutes (e.g., *N,N,N′,N′*-tetramethyl-*p*-phenylenediamine (TMPD)[5g] or sodium metal[11]). In contrast to γ irradiation, this method gives random distribution, the nature of the cation is definitively known, and if monochromatic light is used the energy given to the electron is known. Also, if the ionization potential of the solute is less than that of the solvent, it may be assumed that the positive charge does not migrate.

A chemical method has proved effective for generating electrons in water and alcohols deposited from the vapor phase on a rotating metal drum in vacuo. When sodium or potassium vapor is allowed to condense on such a deposit at 77 K, trapped electrons are produced.[12]

Trapped Electron Yields as a Function of Matrix and Dose

Hydrocarbon glasses typically give G values for trapped electrons (number of electrons trapped per 100 eV of ionizing radiation absorbed) of <0.8 at 77 and 4 K, whereas the values for more polar molecules are commonly >2.[13] These values are lower than the values of 3 to 4[14] for the yield of primary ionization events determined by charge collection in the gas phase, but higher than the G(free electrons) detectable by charge collection in the liquid phase (e.g., $G(e_t^-)$ in glassy 3MP at 77 K is 0.65 while G(free electron) in the liquid at 300 K is 0.15[15]). In the gas, the long mean free path of the electron precludes geminate recombination with the parent cation following thermalization; in the much more dense liquid, thermalization occurs within a relatively short distance and geminate recombination is probable. In glasses the densities, and hence the thermalization distances, are similar to the liquid case (unless the probability of energy loss per collision is less in the glass because of fewer vibrational and rotational degrees of freedom), but return of the electron to the cation is often prevented by trapping. Similar traps in the liquid are mobile, allowing rapid neutralization, and are also less stable to thermal destruction.

Although the yields of trapped electrons are uniformly higher in polar compounds than hydrocarbons, molecular structure plays a role independent of polarity. For example, the $G(e_t^-)$ values in 3-methylheptane (3MHp), 3-methylhexane (3MHx), and 3MP glasses are about 0.5, 0.7, and 0.7, whereas in 2,4-dimethylpentane (2,4-DMP) and 2,4-dimethylhexane (2,4-DMHx) they are 0.09 and 0.17, and in polycrystalline hydrocarbons negligible trapping of e^- occurs.

In hydrocarbon glasses some of the electrons produced by ionizing radiation are chemically trapped by radicals, forming carbanions.[16] Since no method has yet been developed for determining the yields of either the carbanions or cations, it is possible that G(total charged pairs) is similar for all hydrocarbon matrices. In this case the differences in $G(e_t^-)$ between different hydrocarbons would be accounted for by the effect of differences in the pathlength for thermalization of the electrons on the competition between physical trapping and carbanion formation. Large differences in thermalization distances are suggested by the observation that electron mobilities in liquids of spherical molecular structure (e.g., CH_4 and neopentane) are as much as 10^3 greater than for molecules of linear structure (e.g., *n*-pentane).[17]

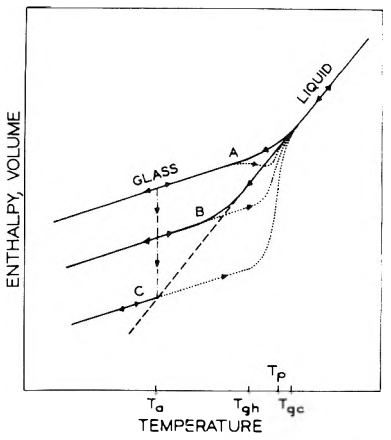

Figure 1. Schematic diagram of enthalpy and volume changes during cooling, heating, and annealing of glasses near the glass transition temperature: (curve A) rapid cooling; (curve B) slower cooling; (line C) equilibrium enthalpy and volume achieved after prolonged annealing from A or B; (– · – · –) direction of change on annealing; (· · · · ·) changes on warming after different extents of annealing; (- - - - -) extrapolated behavior of liquid.

In principle an attractive method for determining the relative electron trapping efficiency of different matrices without interference from electron capture by radicals would be to determine the quantum yields for production of e_t^- in glasses by photoionization of solutes. However, factors such as bleaching of the e_t^- by the photoionizing light, absorption of activating light by the cation product and radical formation by photosensitized mechanisms complicate the interpretation of such studies.

With increasing γ dose to organic glasses at 77 K, the concentration of e_t^- passes through a maximum (at about 10^{20} eV g^{-1} for hydrocarbons and higher for polar glasses) and then decreases.[16a,18] This must result from increasing probability of electron reaction with cations and radicals as the concentration increases to a value where the spurs overlap. Thus studies of the mechanisms of trap formation can best be made at lower doses.

Characteristics of the Trapping Process Deduced from Optical Spectra

Electrons trapped in organic and alkaline ice glasses all give broad (>3 eV) absorption spectra in the visible or near infrared.[19] These spectra have bandwidths at half-height ranging from ~0.5 eV for hydrocarbons to >1 eV for some alcohols, long tails on the high energy side of λ_{max} and shorter tails on the low energy side, and extinction coefficients at λ_{max} of 10^3 to 10^4. They have been the single most fruitful source of evidence on the properties of the traps and the dynamics of trapping.

Effects of Polarity and Phase. A plot of the photon energy at λ_{max} at 77 K vs. the static dielectric constant (D_s) of the matrix compound for D_s values for 12 compounds, from 2 for the hydrocarbons to 42 for glycerol, gives a smooth curve.[20] This suggests that trap depths increase with increasing polarity of the matrix molecules, as do similar data on blue shifts with increasing polarity in a series of glassy alcohols,[21] in liquid alcohols,[22] and in liquid ethers as com-

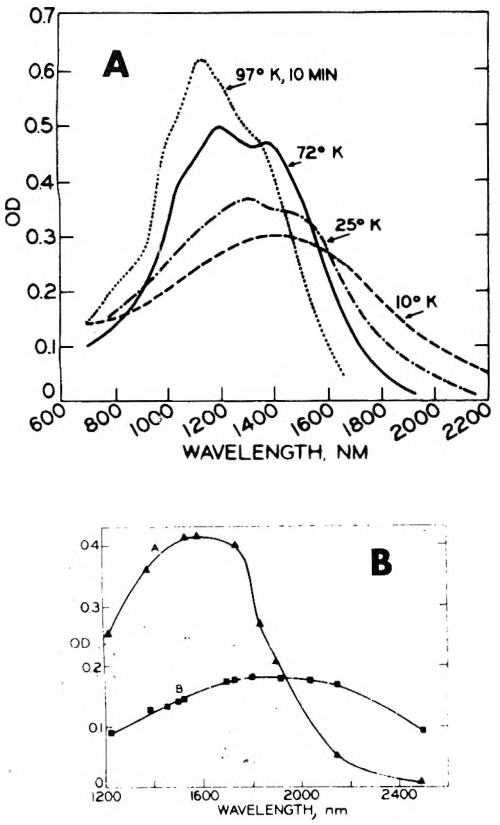

Figure 2. (A) Spectra of e_t^- produced in MTHF glass by photoionization of TMPD at different temperatures. At 97 K, the 3-min photoionization was followed by 10 min in the dark prior to cooling to 50 K for measurement. The other spectra, produced by 3-min illuminations, were measured at the temperature of production after 10-min stabilization. (B) Spectra of trapped electrons in 3MP-d_{14} at 23 K: (A) electrons produced by photoionization of TMPD at 72 K and cooled to 23 K; (B) after partial photobleaching of A at 23 K with 700–1000-nm light.

pared to alcohols.[23] The spectra of e_t^- in glassy alcohols are similar to those in liquid alcohols but are blue shifted and narrowed[20] in a manner suggesting that the trapping configuration in the glass at 77 K is of the same type responsible for solvation in the liquid but is contracted and stabilized. The optical spectra of electrons in liquid hydrocarbons,[24] measured on the nanosecond time scale, appear to be shifted relative to the e_t^- spectra in glasses in a manner similar to the shifts in liquid alcohols relative to the glasses.

While recognizing the correlations of λ_{max} with polarity, it is important to note that molecular structure may play an equally important role in determining the solvation energies and spectra of electrons. This is indicated by data on longer chain and branched chain liquid alcohols,[23b] and is also illustrated by noting that λ_{max} for the absorption by solvated electrons in liquid dimethyl sulfoxide (D_s = 48) is >1500 nm[25] which is more similar to λ_{max} values observed in hydrocarbons ($D_s \simeq 2$) than in the more polar compounds such as glycerol (D_s = 42) for which λ_{max} of e_{solv}^- is ~510 nm at 300 K.

When electrons are produced in glasses made from mixtures of similar types of molecules such as isopropyl alcohol and ethylene glycol, there is a single absorption peak and λ_{max} shifts from its value in the less polar compound toward that in the more polar as the concentration of the latter is increased,[20,26] suggesting that each e_t^- is interacting with the two types of molecules to an extent dependent on their concentration. By contrast, when a glassy matrix is prepared from such dissimilar molecules as 3MP and n-C_3H_7OH,[20,26] two well-separated e_t^- absorption peaks characteristic of the two components are found, indicating aggregation of each type of molecule with others of the same kind. The fraction of the trapped electrons which are in the alcohol is greater than the alcohol mole fraction, and the e_t^- concentration in the alcohol increases as thermal decay of the e_t^- in the 3MP occurs, indicating that the e^- born in the 3MP can move to the alcohol regions. Preferential solvation by the alcohol environment has also been observed in methanol and ethanol solutions in several *liquid* hydrocarbons.[27]

Evidence for Self-Induced Traps with a Continuum of Trapping Energies. Three types of evidence, (1) the time dependence of spectral shapes, (2) the temperature dependence of spectral shapes, and (3) preferential bleaching of narrow regions of the spectra by monochromatic light, indicate that electrons which become trapped in organic glasses are first localized in weak traps and then deepen their traps by orientation of molecules through polarization forces and interaction with bond or molecular dipoles.[28] The same evidence indicates that the observed broad spectra are envelopes of the spectra of electrons in a continuum of trap depths. Some examples will be cited.

The spectra of e_t^- produced in alcohols at 77 K by a <40 nsec pulse of 13-MeV electrons[31] are not stable but undergo continual blue shifting during the interval from 10^{-7} to 2 sec after production. The rate of shifting (i.e., of molecular orientation at 77 K) is ~10^5 faster in CH_3OH than C_2H_5OH and C_3H_7OH.[31] Similar observations on alcohol glasses have been made in several laboratories[29,32,33] and analogous changes have also been found in liquid 1-propanol at 152 K on the time scale of 5 nsec to 1 μsec.[34] As with alcohols, the initial spectra of electrons produced in the glassy hydrocarbons 3MP and 3MHx at 76 K by short electron pulses undergo major blue shifts, but on a slower time scale.[30] Change continues for as much as 380 sec.[30] Electrons trapped in 3MP at 72 K long enough to achieve their "stable" spectra and then detrapped by exposure to 700–1000-nm light are retrapped in weaker traps as indicated by an increase in OD of the spectrum at wavelengths >1900 nm and a decrease at lower wavelengths.[35] When the light is turned off, the OD at <1900 nm grows back over a period of several minutes as the traps deepen.

If the blue shifting of the spectra of e_t^- in organic glasses at ~77 K with increasing time after e^- formation is the result of molecular orientation by the Coulombic field of the electrons, it should be possible to more nearly capture the "original" spectra by producing the electrons at lower temperatures where the ease of molecular orientation is reduced and subsequent warming should allow trap deepening to occur with an accompanying blue shift in the spectrum. Such effects are illustrated in Figure 2 for MTHF and MCHx.[36] They have also been observed in C_2H_5OH[37] and C_2H_5OD.

The shifts in the spectra of e_t^- with time and temperature strongly suggest that each spectrum represents a continuum of trap depths rather than electrons all trapped with the same energy. Even more convincing is the reversible partial photobleaching of the blue side of spectra accompanied by enhancement of the red side.[35] The most conclusive evidence is the selective reduction of the OD of spectra at wavelengths in the region of monochromatic

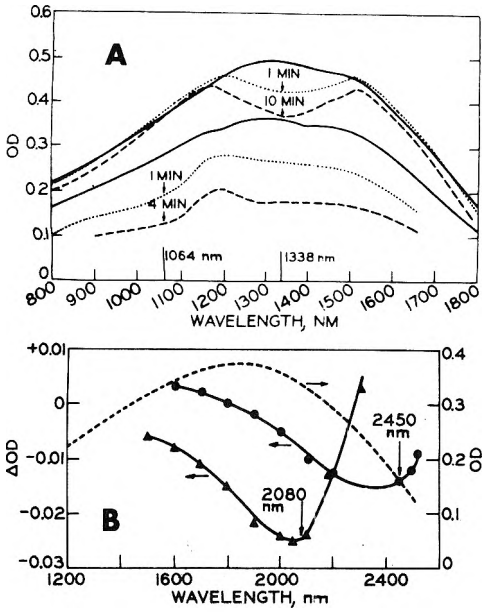

Figure 3. (A) Effect of bleaching with 1338- and 1064-nm light on the spectrum of e_t^- in MTHF: (solid lines) before bleaching; (upper three lines) 1338-nm experiment, e_t^- produced and bleached at 20 K; (lower three lines) 1064-nm experiment, 25 K. Intensities ~30 mW cm^{-2}. (B) Effect of bleaching with 2450- and 2080-nm light on the spectrum of e_t^- produced and bleached in 3MP-d_{14} at 25 K. Dashed line shows unbleached spectrum (scale at right); solid lines show the ΔOD caused by 2-min bleaching at ~0.3 mW cm^{-2} at the indicated wavelengths (scale at left).

bleaching light in MTHF, 3MP (Fig. 3),[36] and C_2H_5OH,[37c] and selective bleaching of the red end of the e_t^- spectrum in C_2H_5OH at 4 K.[19,37] Selective wavelength bleaching of a more complex type has been observed in MTHF glass at 77 K on fast time scales using pulsed laser light.[38]

Thresholds, Quantum Yields, and Light Intensity Dependence for Photodetrapping. Electrons trapped in hydrocarbon glasses can be detrapped by a monophotonic process[39] at all wavelengths of their absorption spectra from far on the low energy side[36] (~2500 nm, 0.5 eV) to far on the high energy side (<400 nm)[40] as indicated by photobleaching[36] and photoconductivity.[40] This implies that the absorbed photon raises the electron to the conduction band of the matrix. However, not all electrons so activated move far enough to react with a cation or radical (and so be "bleached") or contribute significantly to conductivity before being retrapped, since the quantum yields for photobleaching at wavelengths on the red tail are low.[41] These yields increase with increasing photon energy.[41] In the slightly more polar matrix MTHF, for which λ_{max} at 77 K is at 1200 nm, monophotonic photobleaching[36] and photoconductivity[40] occur up to ~1200 nm but not at longer wavelengths. This implies that the amount of energy given to the electrons by the longer wavelengths in excess of that necessary to reach the conduction band is insufficient to prevent prompt return to the oriented coulomb well of the parent trap, or formation of a new trap without appreciable migration. The relatively high probability of prompt trapping in MTHF as compared to hydrocarbons is reflected in its $G(e_t^-)$ value of 2.6 as compared to that of 0.65 for 3MP glass.

Spectra of Individual e_t^-. If, as indicated above, the observed spectra of trapped electron populations are envelopes of the spectra of individual electrons with a continuum of trapping energies, it is important to deduce, if possible, the shape of the individual spectra. The experimental data available allow only a speculative hypothesis, illustrated formalistically in Figure 4. The hypothesis is capable of rationalizing the four main relevant observations. (1) The initial rate of hole burning in the spectrum of MTHF at 1338 nm at 20 K (Figure 3A) decreases rapidly as the hole deepens. (2) The same MTHF spectrum bleaches nearly uniformly when 1064-nm rather than 1338-nm light is used. (3) The quantum yield at 1064 nm for bleaching of electrons produced in MTHF at 25 K (Figure 2A) and bleached at 25 K is several fold greater than for electrons produced at 67 K and bleached at 67 or 25 K.[36] (4) The quantum yields of photobleaching of e_t^- in 3MP[42] and MTHF[43] with broad band light decrease rapidly with fraction bleached (reversible spectral shifting[35] may also contribute to this effect).

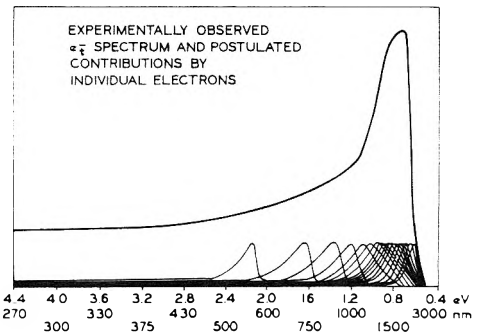

Figure 4. Schematic representation of hypothetical spectra of individual electrons in different trap depths (lower lines), the summation of which gives the envelope (upper line) typical of the observed absorption by e_t^- in alkanes at 77 K.

It is assumed that the red end of the spectrum of each e_t^- is the photoionization threshold for the trap but that a photon of energy on the blue side of the maximum is required to give the electron enough energy to move far enough to "encounter" a cation or radical with which it can react rather than being retrapped. To account for the uniform bleaching of the spectrum of Figure 3A at 1064 nm, all of the spectra of individual electrons must extend at least that far on the short wavelength side of the observed spectral maximum. The selective bleaching at 1338 nm, which decreases in rate with fraction bleached, indicates that (1) a portion of the 1338-nm optical density is due to electrons which have a significant quantum yield for bleaching at this wavelength; (2) another portion is due to e_t^- for which 1338 nm is too far on the red side of their spectra to give a significant quantum yield of bleaching; (3) trapped electrons which have their λ_{max} substantially to the longer wavelength side of 1338 nm make only minor contributions to the optical density at 1338 nm relative to the contributions of the other populations. Similar considerations may account for observation (4) above. The failure of e_t^- produced at 67 K to bleach as readily with 1064-nm photons as those produced at 23 K is ascribed to the production of deeper traps on the average at 67 K than 23 K, with a more homogeneous and blue-shifted continuum of spectra, such that 1064-nm photons have insufficient energy relative to most of the trapping energies to remove the electrons far enough from their traps to be captured by electrons or radicals.

Characteristics of Traps Deduced from ESR Techniques

Proximity and Configuration of Trap Walls. Consistent

with the trapping model suggested by the evidence from optical spectra discussed above, the line widths of the ESR singlet of the trapped electron in glasses at 77 K in general increase with increasing polarity of the matrix molecules,[20] indicating increasing hyperfine interaction with atoms in the walls as the traps become deeper.

More specific information on the orientation of molecules around trapped electrons in alcohol glasses comes from the observation that the width of the ESR singlet in C_2H_5OD is smaller than that in C_2H_5OH by a factor approximating the ratio predicted if hyperfine interaction with deuterons replaces that with protons, indicating that the alcohol molecules in the walls of the traps are aligned with the hydroxyl groups toward the electrons.[2i,45]

A quantitative model of the organization of molecules around trapped electrons in MTHF glass at 77 K, based on electron spin echo studies, indicates that three or four MTHF molecules are oriented around each electron with the plane of each molecule facing the electron at a distance of ~3.7 Å and the CH_3 group on the side away from the electron.[46] The shortest electron to proton distance is ~3.1 Å. If this model is correct, the randomly oriented MTHF molecules in glassy MTHF at 77 K can be readily converted to the suggested configuration by the field of an electron and the electron becomes centered in a hole of ~6 Å diameter, the walls of which have large gaps. The model does not assist in explaining the three peaks in the optical spectrum of e_t^- in MTHF at 77 K (Figure 2A) which have been ascribed[26,36] to different discrete preferred orientations of MTHF molecules giving different trap depths. Similar spin echo results on electrons trapped in MTHF at 4 K where the optical spectra indicate that the traps are much weaker and more homogeneous would be valuable.

Spatial Distribution of e_t^- and Cations. Concentrations of trapped electrons $>10^{17}$ g^{-1} ($>10^{-5}$ mole fraction) in MCHx[47] and 3MP[16a] and $>10^{19}$ g^{-1} ($>10^{-3}$ mole fraction) in ethanol[18b] can be produced by γ irradiation of the glasses at 77 K. If cations were evenly spaced in the glass and the e_t^- randomly distributed, the nearest neighbor cation–cation distance for 3MP sould be ~200 Å and the average electron–cation distance ~60 Å. The corresponding distances for C_2H_5OH would be ~40 and 12 Å. For isolated ion pairs with these intrapair separations (i.e., with no influence from the other charges present), and assuming dielectric constants of 2 and 25, respectively, the Coulombic energy of separation between the e_t^- and cation would be 0.12 and 0.05 eV. In actual γ-irradiated organic glasses the upper limit of e_t^- concentration achievable is determined as much or more by the growth in concentration of radicals,[16] with which the electrons can react to form carbanions, as by the cations.

The above considerations of charge separation were related to glasses which have received sufficiently high radiation doses so that the spurs in which the radiation energy is deposited overlap. Studies of the spin–spin relaxation times (T_2) of e_t^- and trapped radicals as a function of dose give indication of the minimum doses at which spur overlap is significant and allow estimates of the spur sizes. The upper limits of the "spur radii" for e_t^- in MTHF, triethylamine, and 3MP so obtained are 60, 100, and 130 Å, respectively.[18a,48] Earlier ESR saturation studies in MTHF give ~45 Å. The intraspur separations of the radicals are less,[49] consistent with the expectation that the latter are trapped at the site of formation whereas the electrons migrate while being thermalized before trapping.

Electron Decay Processes

Spontaneous removal of e_t^- by combination with cations, radicals, or additives in γ-irradiated organic glasses and alkaline ice occurs with half-lives of the order of tens of minutes near the glass transition temperature. The rates increase rapidly with increase in temperature and decrease rapidly with decrease in temperature. Possible mechanisms of the electron migration include: (1) thermal detrapping and movement to a reaction partner by a hopping mechanism (This appears improbable since the photodetrapping thresholds are ~0.5 eV in hydrocarbons and much higher in more polar matrices, while kT at 77 K is 0.006 eV); (2) diffusion of the e_t^- coupled with its "solvation shell" of surrounding molecules; (3) diffusion of e_t^- without molecular movement, the polarization passing to new molecules as the e_t^- moves; (4) quantum mechanical tunneling to a cation, a radical, or added scavenger of greater electron affinity than the trap.

Electron Tunneling. Present evidence[50] suggests that diffusion is the rate-controlling step in e_t^- decay observed on the time scale of tens of minutes in 3MP near the glass transition temperature but that tunneling predominates as the mode of removal of e^- which are trapped relatively close to a cation, radical, or scavenger molecule and disappear on the time scale of 10^{-9} to 10^2 sec, and also of electrons trapped at greater distances at temperatures far below T_g.

Convincing evidence for tunneling includes (1) temperature independent decay over wide temperature ranges from 4 K up; (2) transfer of e_t^- to scavengers at rates which decrease linearly with increase in the log of the time over many decades in the range of 10^{-9} to 1 sec; (3) enhancement of the yield of the anion of a strong scavenger by the added presence of a weaker scavenger; (4) linear dependence of the log of trapped electron yields on the concentration of scavengers as contrasted to the linear dependence of the reciprocal yields on the scavenger concentration expected for competitive diffusive encounters. The results seem to indicate that scavenging in glasses occurs to a great extent by tunneling after trapping rather than by competition between traps and scavengers for mobile electrons.

Electron Decay in 3MP and MTHF at 77 K at Longer Times. Electron decay in pure 3MP and MTHF at 77 K observed on the time scale of minutes and longer appears to involve diffusion and the kinetics are revealing as to the distribution of the e_t^- relative to cations and radicals.

Several types of evidence[5b,c] indicate that a substantial fraction (perhaps 50%) of the e_t^- present after γ irradiation of organic glasses combine with a positive ion or radical within the parent spur when they are detrapped by absorption of light or diffuse. Likewise, there is evidence that many e_t^- produced by photoionization of TMPD in 3MP combine with the geminate $TMPD^+$ cation.[5g] The evidence includes the following. (1) The fractional rates of electron decay after short irradiations are independent of the radiation dose, and hence of the concentration of electrons, cations, and radicals.[5c,48] (2) The decrease in the quantum yields for photobleaching of e_t^- with increasing fraction bleached is independent of the initial electron (and hence cation and radical) concentration.[42,43] (3) When e_t^- produced in 3MP glass by photoionization of TMPD by vertically polarized light are photobleached in the presence of a large population of cations produced by horizontally polar-

ized light, the fluorescence is predominately vertically polarized.[5g,51] (4) Application of an electric field to a photoionized sample of TMPD in 3MP causes a burst of luminescence, which is repeated with a second application of the field with reversed polarity,[5g,52] indicating that some or all the electrons are trapped within the coulomb field of the geminate cation and overcome the potential barrier for recombination with the aid of the external field.

Despite the pattern of predestined combination indicated by the above evidence, all of the electrons that can be physically trapped in the pure matrices are captured to form biphenylide ion when as little as 10^{-3} mole fraction of biphenyl solute is present.[5c,53] Furthermore, many of the e_t^- in pure matrices can be detrapped by photon absorption and retrapped many times without capture by a cation or radical.[16b,35] From the combined data it may be concluded that about 50% of the e_t^- react within the parent spur, the fractional rate of thermal decay decreasing as the spur population is depleted, and that the remaining e_t^- escape intraspur combination. If the molecules of the 10^{-3} mole fraction biphenyl which remove all trapped electrons were uniformly distributed, they would be ~10 molecular diameters apart, the maximum distance of a trapped electron from a scavenger molecule would be ~7 molecular diameters and the average distance ~3 molecular diameters (~15 Å). These are distances over which tunneling may be expected to occur[50] before observations of γ-irradiated samples are started.

In both 3MP[53] and MTHF[48] at 77 K, the fractional decay rates of e_t^- produced by γ irradiation show composite first-order kinetics, i.e., they decrease as the fraction decayed increases, but are independent of γ dose (i.e., of initial concentration). After 40–50% decay the rates are discontinuously slower than for the earlier decay. This pattern is similar to that of the decay of 3-methylpentyl radicals[54] in 3MP at 77 K, for which intraspur radical–radical reaction accounts for the composite first-order fast portion of the decay (57%) and random radical–radical reaction after diffusion accounts for a second-order slow portion. The second-order rate constant for the slow portion is independent of dose. The electron decay kinetics differ from the radical decay kinetics in that the rate of the slow portion is not proportional to the square of the dose.[55] Several factors may cause the slow electron decay kinetics to be different than those for radicals: (1) coulomb interactions may result in a larger fraction decaying by intraspur reaction; (2) electrons may decay by reaction with radicals to form carbanions as well as by reaction with cations, so the concentration of potential reaction partners is much greater than the concentration of e_t^-, leading, in the limiting case, to pseudo-first-order kinetics; (3) tunneling may contribute to the decay.

Since the decreases in quantum yields of photobleaching of e_t^- in 3MP[42] and MTHF[43] with fraction bleached are independent of dose, they indicate that the initial bleaching involves intraspur reactions of the e^- with cations and radicals rather than reactions dependent on the average acceptor concentration in the matrix.

Presumably geminate recombination with the sibling cation occurs for some e_t^- produced by γ irradiation as it appears to for some formed by photoionization of TMPD.[51,52] One feature of γ-irradiated hydrocarbons which reduces the probability of the geminate process is the ability of positive charge to migrate,[5c] whereas this cannot occur when the charge is initially on TMPD, which has a lower ionization potential than the hydrocarbon. The migration of positive charge to a localizing center is indicated by increases in $G(e_t^-)$ and by slow decay rates of e_t^- when positive charge scavengers such as alkenes, ethers, or alcohols are present as solutes in the hydrocarbon.[2e]

Trapped electrons produced by photoionization of TMPD in 3MP at 77 K have characteristics strikingly similar to e_t^- formed by γ irradiation[53,56] (infrared absorption, decay rates, saturation of their ESR signal, and photobleaching). However, prolonged illumination of TMPD produces a relatively randomized steady state population,[5g,56] with a lower fraction of geminate pairs and slower decay rate.[57]

The characteristics of the ESR singlet and decay of e_t^- formed by photoionization of Na in 3MP are similar to those of e_t^- produced by γ irradiation,[11] again indicating that the nature of the cation is not a dominant factor in determining the properties of the traps.

Effect of Annealing on Decay Rates. Differential thermal analysis measurements on 3MP glass held at 77 K (i.e., near the glass transition temperature) for different lengths of time following quenching of the liquid to 77 K show that free volume and enthalpy are progressively lost over a period of several hours.[8] Parallel experiments on the rate of decay of e_t^- produced in such glass following different times of annealing show initial half-lives ranging from 6 min for minimal annealing of 3MP to a limit of 60 min for completely relaxed samples, but no change in $G(e_t^-)$ or the shape of the optical spectrum of the e_t^-.[9] This implies that in 3MP at 77 K annealing does not change the probability of trapping or the characteristics of the traps formed but decreases the rate of diffusion of the e_t^- (and perhaps also of positive holes).

Preirradiation annealing has also been found to cause a decrease in luminescence intensity[58] and in radical decay rates[54] in 3MP, a lengthening of the phosphorescence lifetime of deuteriobenzene solute,[59] and spectral shifts in luminescence photoexcitation spectra.[60] Preirradiation annealing of the polar glass C_2H_5OH at 77 K for 500 hr causes decrease in $G(e_t^-)$, a red shift in the e_t^- spectrum, and an increase in the decay rate,[18b] in contrast to the effects in 3MP.

Epithermal Electron Capture

Enhanced yields of C_6H_{13} radicals during γ irradiation of 3MP glass containing HCl, HI, CH_3Cl, CH_3Br, or CH_3I as compared to the yields in pure 3MP imply that electrons are captured by the solutes before complete thermalization. The increase in radical production is presumed to occur by dissociative electron capture by the additive, followed by abstraction of H from 3MP by a hot H or CH_3. Both the thermochemistry of the reactions and the similarities of electron capture cross sections for different additives in the glass as compared to the gas can be rationalized if electrons in the epithermal subexcitation energy range of the matrix are captured. Little is known about the migration distance of such electrons but it may be presumed to be considerable. The first singlet excitation level of 3MP is at 7–8 eV; triplet levels at 6 eV and possibly 3 eV have been indicated by thin film studies.[61]

Heats of Reaction of e_t^- and Solvation Energies

The heat released when e_t^- produced in 3MP by γ irradiation at 77 K are photobleached is ~150 kcal mol^{-1} when extrapolated to zero dose.[8] This sets an upper limit of −80

kcal mol^{-1} on the heat of solvation of the cation plus any solvation of the mobilized electron. The heat of bleaching decreases with increasing dose, as the probability that the e_t^- can react with radicals rather than cations increases. This decrease, which implies increasing spur overlap, occurs in a dose range ($>1 \times 10^{19}$ eV g^{-1}) where the ESR data on spin–spin relaxation times[18a] also indicate increasing overlap.

DTA measurements on γ-irradiated MTHF glass suggest that on warm-up e_t^- react predominately with radicals to form carbanions which then react with cations and indicate that the total heat of the e_t^- + radical + cation reaction → products is ~80 kcal mol^{-1}. From this it may be estimated that the sum of the heats of solvation of the e_t^- and cation is −120 to −150 kcal mol^{-1}.[8] (The products and heat of neutralization of e_t^- via the carbanion may be different than via the direct e_t^- + cation → products reaction, but this cannot affect the estimated heat of solvation significantly.)

The energy released on bringing two charges together from infinity to a distance d in a medium of dielectric constant ϵ is $-e^2/\epsilon d$. At distances $\lesssim$10 Å the effective dielectric constant changes due to dielectric saturation effects. It is also dependent on the extent to which dipoles can be saturated during the ion neutralization process. Assuming the heat of neutralization of $MTHF^+$ in the gas phase is 220 kcal/mol and that d, the charge separation after neutralization, is the same in the gas and solid phases and taking ϵ_0 as the permittivity of free space, ϵ_{eff} for the neutralization in MTHF glass may be estimated from the relation $\epsilon_{eff} = (e^2/\epsilon_0 d)/(e^2/d) = 220/80 = 2.8$. This value is slightly greater than the optical dielectric constant (~2.4) of MTHF, but 60% less than the static dielectric constant (4.6). These estimates neglect the possibility that the electron is trapped within the field of a positive ion. However, for the energy of combination to be reduced to 80 kcal mol^{-1} the charged partners would have to be trapped within ~1 Å of each other assuming a dielectric constant of only 2. For a trapping distance of 25 Å, the reduction in energy of combination from that at infinite separation would be only 8 kcal mol^{-1} for $\epsilon = 2$.

References and Notes

(1) This work has been supported in part by the U.S. Atomic Energy Commission under Contract No. AT(11-1)-1715 and by the W. F. Vilas Trust of the University of Wisconsin.

(2) For examples and references see: (a) D. Schulte-Frohlinde and K. Eiben, *Z. Naturforsch. A*, **17**, 445 (1962); (b) P. S. Rao, J. R. Nash, J. P. Guarino, M. R. Ronayne, and W. H. Hamill, *J. Am. Chem. Soc.*, **84**, 500 (1962); (c) M. R. Ronayne, J. P. Guarino, and W. H. Hamill, *ibid.*, **84**, 4230 (1962); (d) C. Chachaty and E. Hayon, *J. Chim. Phys.*, **61**, 1115 (1964); (e) J. P. Guarino and W. H. Hamill, *J. Am. Chem. Soc.*, **86**, 777 (1964); (f) J. B. Gallivan and W. H. Hamill, *Trans. Faraday Soc.*, **61**, 1960 (1965); (g) D. R. Smith and J. Pieroni, *J. Phys. Chem.*, **70**, 2379 (1966); (h) K. Tsuji and F. Williams, *J. Am. Chem. Soc.*, **89**, 1526 (1967); (i) D. R. Smith and J. J. Pieroni, *Can. J. Chem.*, **45**, 2723 (1967); (j) F. S. Dainton, G. A. Salmon, P. Wardman, and U. Zucker, *Proc. Second Tihany Symp. Radiat. Chem.*, 247 (1967).

(3) (a) H. Barzynski and D. Schulte-Frohlinde, *Z. Naturforsch. A*, **22**, 2131 (1967) (methanol); (b) H. Fenrick and J. E. Willard, unpublished (*n*-hexane); (c) T. Ichikawa and H. Yoshida, private communication (*n*-hexane to *n*-hexadecane).

(4) For examples and references see: (a) S. A. Rice, *Acc. Chem. Res.*, **1**, 81 (1968); (b) D. A. Copeland, N. R. Kestner, and J. Jortner, *J. Chem. Phys.*, **53**, 1189 (1970); (c) J. Jortner, *Actions Chim. Biol. Radiat.*, **14**, 7 (1970); (d) K. Funabashi and Y. Maruyama, *J. Chem. Phys.*, **55**, 4494 (1971); (e) G. W. Robinson in "Computational Methods on Large Molecules and Localized States in Solids", F. Herman, A. D. McLean, and R. K. Nesbet, Ed., Plenum Press, New York, N.Y., 1973, p 29; (f) L. Kevan, *Int. J. Radiat. Phys. Chem.*, **6**, 297 (1974). (g) A review of the problems and methods involved in developing a theory of trapping is given by L. Kevan, "Advances in Radiation Chemistry", M. Burton and J. L. Magee, Ed., Wiley-Interscience, New York, N.Y., 1974, pp 275–298.

(5) For examples and references see: (a) V. A. Rojinskii and B. B. Kotov, *High Energy Chem.*, **1**, 254 (1967); (b) J. E. Willard, "Radiation Chemistry of Organic Solids", in "Fundamentals of Radiation Chemistry", P. Ausloos, Ed., Wiley, New York, N.Y., 1968, p 599; (c) W. H. Hamill, "Ionic Processes in γ-Irradiated Organic Solids at −196°C", in "Radical Ions", E. T. Kaiser and L. Kevan, Ed., Wiley, New York, N.Y., 1968, p 321; (d) L. Kevan, *Actions Chim. Biol. Radiat., Ser. 13e*, 57–117 (1969); (e) A. Ekstrom, *Radiat. Res. Rev.*, **2**, 381 (1970); (f) F. Kieffer and M. Magat, *Actions Chim. Biol. Radiat., Ser. 14e*, 135 (1970); (g) A. C. Albrecht, *Acc. Chem. Res.*, **3**, 238 (1970); (h) L. Kevan, *ibid., 81–143* (1971); (i) J. E. Willard, *Science*, **180**, 553 (1973); (j) L. Kevan in "Advances in Radiation Chemistry", Vol. 4, M. Burton and J. L. Magee, Ed., Interscience, New York, N.Y., 1974, pp 181–298; (k) *Int. J. Radiat. Phys. Chem.*, **6**, 281–515 (1974), is devoted to autoreviews of work on trapped charged species in glasses by investigators from 12 laboratories.

(6) For example, the densities of 3-methylpentane (3MP)[7] at 298 and 77 K are 0.676 and 0.866 g cm^{-3}, respectively. The densities of 3MP-d_{14} are 0.766 and 0.944 g cm^{-3} at 298 and 77 K, respectively, the number of molecules per (centimeter)^3 being the same in the two systems at the same temperature.

(7) B. Dietrich, Ph.D. thesis, University of Wisconsin—Madison, 1971.

(8) S. L. Hager and J. E. Willard, *J. Chem. Phys.*, **63**, 942 (1975).

(9) D. Shooter and J. E. Willard, *J. Phys. Chem.*, **76**, 3167 (1972).

(10) A. C. Ling and J. E. Willard, *J. Phys. Chem.*, **73**, 2408 (1969).

(11) S. C. Srinivasan and J. E. Willard, *J. Phys. Chem.*, **77**, 2171 (1973).

(12) J. Bennett, B. Mile, D. Thomas, and B. Ward, *Adv. Phys. Org. Chem.*, **8**, 1 (1970).

(13) See yield summaries of M. A. Bonin, J. Lin, K. Tsuji, and F. Williams, *Adv. Chem. Ser.*, No. **81**, 269 (1968), and in ref 5j.

(14) Summarized by J. T. Myers in "Radiation Dosimetry", Vol. I., 2nd ed, F. H. Attix and W. C. Roesch, Ed., Academic Press, New York, N.Y., 1968, p 317.

(15) (a) P. H. Tewari and G. R. Freemen, *J. Chem. Phys.*, **49**, 4394 (1968); (b) W. F. Schmidt and A. O. Allen, *ibid.*, **52**, 2345 (1970).

(16) (a) A. Ekstrom, R. Suenram, and J. E. Willard, *J. Phys. Chem.*, **74**, 1888 (1970); (b) D. P. Lin and J. E. Willard, *ibid.*, **78**, 1135 (1974).

(17) For examples and references see A. O. Allen and R. A. Holroyd, *J. Phys. Chem.*, 78, 796 (1974).

(18) (a) D. P. Lin and L. Kevan, *J. Chem. Phys.*, **55**, 2629 (1971); (b) S. Fujii and J. E. Willard, *J. Phys. Chem.*, **74**, 4313 (1970).

(19) For many examples of spectra of e_t^- in alkanes, alcohols, ethers, amines, and alkaline ice, see T. Shida, S. Iwata, and T. Watanabe, *J. Phys. Chem.*, **76**, 3683 (1972).

(20) A. Ekstrom and J. E. Willard, *J. Phys. Chem.*, **72**, 4599 (1968).

(21) B. G. Ershov, J. E. Makarov, and A. K. Pikaev, *High Energy Chem.*, **1**, 414 (1967).

(22) (a) M. C. Sauer, S. Arai, and L. M. Dorfman, *J. Chem. Phys.*, **42**, 708 (1965); (b) S. Arai and M. C. Sauer, *ibid.*, **44**, 2297 (1966).

(23) (a) L. M. Dorfman and F. Y. Jou, a chapter in "Electrons in Fluids", J. Jortner and N. R. Kestner, Ed., Springer-Verlag, New York, N.Y., 1973; (b) R. H. Hentz and G. Kenney-Wallace, *J. Phys. Chem.*, **78**, 2931 (1972).

(24) (a) H. A. Gillis, N. V. Klassen, G. G. Teather, and K. H. Lokan, *Chem. Phys. Lett.*, **10**, 481 (1971); (b) L. B. Magnussen, J. T. Richards, and J. K. Thomas, *Int. J. Radiat. Phys. Chem.*, **3**, 295 (1971); (c) J. H. Baxendale, C. Bell, and P. Wardman, *Chem. Phys. Lett.*, **12**, 347 (1971).

(25) D. C. Walker, N. V. Klassen, and H. A. Gilles, *Chem. Phys. Lett.*, **10**, 636 (1971).

(26) T. Sawai and W. H. Hamill, *J. Phys. Chem.*, **74**, 3452 (1969).

(27) (a) J. R. Brandon and R. F. Firestone, *J. Phys. Chem.*, **78**, 792 (1974); (b) B. J. Brown, N. T. Barker, and D. F. Sangster, *ibid.*, **75**, 3639 (1971); *Aust. J. Chem.*, **26**, 2089 (1973); **27**, 2529 (1974); (c) F. Smith and I. Brown, *ibid.*, **26**, 691, 705 (1973).

(28) The alternative hypothesis that weakly trapped electrons migrate to deeper preformed traps by thermally activated hopping seems to be ruled out[29,30] by the observations that (1) the rate of the spectral shifts increases with polarity of the matrix, and (2) the spectral shifts are not altered by the presence of electron scavengers.

(29) L. Kevan, *J. Chem. Phys.*, **56**, 838 (1972).

(30) N. V. Klassen, H. A. Gillis, and G. G. Teather, *J. Phys. Chem.*, **76**, 3847 (1972).

(31) J. R. Miller, B. E. Clift, J. J. Hines, R. F. Runowski, and K. W. Johnson, *J. Phys. Chem.*, submitted for publication.

(32) N. V. Klassen, H. A. Gillis, G. G. Teather, and L. Kevan, *J. Chem. Phys.*, **62**, 2474 (1975).

(33) J. T. Richards and J. K. Thomas, *J. Chem. Phys.*, **53**, 218 (1970).

(34) J. H. Baxendale and P. Wardman, *Nature (London)*, **230**, 449 (1971).

(35) S. L. Hager and J. E. Willard, *Chem. Phys. Lett.*, **24**, 102 (1974).

(36) S. L. Hager and J. E. Willard, *J. Chem. Phys.*, **61**, 3244 (1974).

(37) (a) H. Hase, M. Noda, and T. Higashimura, *J. Chem. Phys.*, **54**, 2975 (1971); (b) L. M. Perkey, Farhataziz, and R. R. Hentz, *ibid.*, **61**, 2979 (1974); (c) A. Namiki, M. Noda, and T. Higashimura, *Chem. Phys. Lett.*, **23**, 402 (1973).

(38) D. C. Walker and R. May, *Int. J. Radiat. Phys. Chem.*, **6**, 345 (1974).

(39) G. C. Dismukes, S. L. Hager, G. H. Morine, and J. E. Willard, *J. Chem. Phys.*, **61**, 426 (1974).

(40) G. C. Dismukes, Ph.D. Thesis, University of Wisconsin—Madison, 1975.

(41) J. R. Miller and J. E. Willard, *J. Phys. Chem.*, **76**, 2341 (1972).

(42) D. W. Skelly and W. H. Hamill, *J. Chem. Phys.*, **44**, 2892 (1966).

(43) P. J. Dyne and O. A. Miller, *Can. J. Chem.*, **43**, 2696 (1965).

(44) H. Yoshida and T. Higashimura, *Can. J. Chem.*, **48**, 504 (1970).
(45) M. J. Blandemer, L. Shields, and M. C. R. Symons, *J. Chem. Soc.*, 1127 (1965).
(46) L. Kevan, M. K. Bowman, P. A. Narayana, R. K. Boeckman, V. F. Yudanov, and Y. D. Tsvetkov, *J. Chem. Phys.*, **63**, 409 (1975).
(47) M. Shirom and J. E. Willard, *J. Am. Chem. Soc.*, **90**, 2184 (1968).
(48) D. R. Smith and J. J. Pieroni, *Can. J. Chem.*, **43**, 876 (1965).
(49) (a) D. P. Lin, P. Hamlet, and L. Kevan, *J. Phys. Chem.*, **76**, 1226 (1972); (b) D. P. Lin and J. E. Willard, *ibid.*, **78**, 2233 (1974).
(50) For examples and references see (a) J. R. Miller, *J. Phys. Chem.*, **79**, 1070 (1975); (b) *J. Chem. Phys.*, **56**, 5173 (1972).
(51) W. M. McClain and A. C. Albrecht, *J. Chem. Phys.*, **43**, 465 (1965).
(52) J. Bullot and A. C. Albrecht, *J. Chem. Phys.*, **51**, 2220 (1969).
(53) J. B. Gallivan and W. H. Hamill, *J. Chem. Phys.*, **44**, 1279 (1966).
(54) M. A. Neiss and J. E. Willard, *J. Phys. Chem.*, **79**, 783 (1975).
(55) Although the authors[48,53] have spoken of the decays as "second order", their data show that the processes are more nearly first order than second order in dose.
(56) K. Tsuji and F. Williams, *J. Chem. Phys.*, **46**, 1986 (1967).
(57) S. Hager, Ph.D. Thesis, University of Wisconsin—Madison, 1974.
(58) K. Funabashi, P. F. Herley, and M. Burton, *J. Chem. Phys.*, **43**, 3939 (1965).
(59) T. E. Martin and A. H. Kalantar, *J. Phys. Chem.*, **72**, 2265 (1968).
(60) T. B. Truong and A. Bernas, *J. Phys. Chem.*, 76, 3894 (1972).
(61) K. Hiraoka and W. H. Hamill, *J. Chem. Phys.*, **59**, 5749 (1973).

Discussion

G. R. FREEMAN. Do you know whether the Kirkwood g factor of 1-butanol is larger than that of 1-propanol or ethanol? If so, that might help to rationalize the slightly high absorption energy of electrons in 1-butanol.

J. E. WILLARD. No. It is of interest to note that the results of Hentz and Kenney-Wallace on $E_{\lambda_{max}}$ vs. D_s for liquid alcohols show "high" $E_{\lambda_{max}}$ values for all straight chain alcohols with more C atoms than propanol and that the values for the branched alcohols are lower than the straight chain alcohols, emphasizing the importance of structural as well as polarity effects.

G. R. FREEMAN. Your bleaching experiments at different wavelengths indicate that the experiments of Rentzepis and Struve (this conference), in which they bleached electrons in ammonia (λ_{max} 1.4 μ) with 1.06 μ-photons, referred in fact to homogeneous bleaching rather than to homogeneous broadening. The distinction is worth emphasizing.

J. E. WILLARD. It is a possibility that they might have observed hole burning with light on the long wavelength side of λ_{max} but it is also quite possible that the energy distribution of the traps is much narrower (more homogeneous) in liquid ammonia than in our work in the glassy state at below 25 K.

J. JORTNER. There is a close analogy between your interesting experimental results on the inhomogeneous broadening of the absorption bands of trapped electrons in solid matrices and recent optical studies of organic molecules trapped in solid hydrocarbons. In the latter case irradiation by a laser source into a very broad, structureless, absorption band results in very sharp emission spectrum, indicating that only a single trapping site of the guest molecule was optically selected.

I would like to inquire whether you have studied preparation conditions of the solid samples (annealing, etc.). In spectroscopic absorption studies appropriate hydrocarbon samples prepared by slow cooling resulted in exceedingly narrow line widths in absorption. Thus inhomogeneous broadening effects can be eliminated to a large extent.

J. E. WILLARD. When unannealed samples of 3MP and samples annealed for several days at 77 K, which is near the glass transition temperature, are γ irradiated at 77 K the spectra of the e_t^- produced are similar. It would be interesting to see whether the same is true for irradiation at 4 K where molecular relaxation induced by the field of the electron is very slow so that the chance that the spectrum will indicate distribution of the virgin trapping sites is greater.

L. KEVAN. Does the amount of hole burning in the trapped electron spectrum in MTHF depend on the temperature at which the electrons are produced or, in other words, on the degree of relaxation of the molecules around the electron? The lack of hole burning found for the electron in liquid ammonia reported by Struve and Rentzepis presumably refers to an equilibrium configuration around the electron.

J. E. WILLARD. The hole burning experiments reported from our work on MTHF and 3MP and Higashimura's work with ethanol were all done at 25 K or below. It is to be presumed that the bleaching characteristics at any wavelength *will be* different at higher temperatures where the average trap depths are greater because of the greater ease of molecular relaxation. We have observed that electrons produced and trapped in MTHF at 23 K, and exposed to 1064-nm light, bleach readily throughout the spectrum, whereas electrons trapped at 67 K are not readily bleached by 1064-nm light either at 67 K or when the same sample is lowered to 23 K.

R. CATTERALL. When you burn a hole in the optical absorption band you are presumably exciting an electron out of its trap into the continuum from where it finds a new home. You cannot rearrange solvent molecules by photolysis (Franck–Condon). If the spectrum than relaxes slowly back (the hole fills in), this has to correspond to a motion of molecular reorientation energy through the lattice. The recovery process should lead to information about the distribution of electron traps and to the transfer of energy—you are changing from a favorable distribution of trapping sites to an unfavorable one by photolysis, followed by a relaxation back to the favorable distribution. It is the distribution function of trapping sites which is changed by photolysis, not the structure around a specific trap. In order to get any recovery back to the original distribution function the system must respond cooperatively.

J. E. WILLARD. No detailed studies have yet been made of spectral changes in the dark following hole burning. All of the hole burning experiments have been done at 25 K or lower where removal of the bleaching effect is very slow. In experiments at 67 K the increase in absorption on the long wavelength side of the spectrum caused by bleaching on the short wavelength side partially reverses within a few minutes in the dark. This is presumed to be because some of the e^- which are detrapped are retrapped at random in weak traps which deepen with time. The old trap is no longer involved in the spectrum. Its configuration relaxes on the time scale of thermal motions of the molecules in the matrix.

Trapped Electrons Studied through Stimulated Neutralization Luminescence

A. Bernas,* D. Grand, and T. B. Truong

Laboratoire Chimie Physique, 91405 Orsay, France *(Received July 23, 1975)*

Publication costs assisted by CNRS

The optically induced or "stimulated" neutralization luminescence (SL) following γ irradiation of rigid matrices can provide two types of information: (1) the emission spectrum characterizes the neutralization process, i.e., the neutralized cation or one of its dissociation fragments; (2) the excitation spectrum gives information on the nature and depths of the electron traps and occasionally on the trapped electrons e_t^- spatial distribution.

Examples of type 2 experiments performed at 77 K on crystalline or glassy polar matrices will be presented and discussed.

(2a) The photodetrapping threshold values are found at 2.3 eV for ethanol glasses (λ_{an} 345 nm) at 1.9 eV for crystalline H_2O or D_2O ices (λ_{an} 380 nm). No detrapping threshold appears in the SL spectra recorded from γ-irradiated alkaline ices. These SL results confirm previously reported data obtained by photoconductivity and optical absorption or ESR spectroscopy.

(2b) In some particular cases, as alkaline ices for example, SL spectra may further lead to specific results. A comparison of SL excitation spectrum with photoconductivity measurements indicates that only part of the detrapped electrons give rise to a luminescent cation neutralization. Additional photoionization experiments in presence or absence of an electron scavenger substantiate the view that the red side of the e_t^- absorption band corresponds to e_t^- which are close to their parent cations and give rise to geminate recombination whereas e_t^- corresponding to the blue component of the absorption band disappear by reacting with O^-.

Discussion

N. KLASSEN. I should like to suggest that the reaction of bleached electrons with H_3O^+ occurs from a retrapped state rather than from a mobile state. H_3O^+ is found to be a poor scavenger of "dry" electrons in aqueous solutions and we believe it is also a very poor scavenger of mobile electrons in LiCl and $MgCl_2$ glasses at 77 K.

A. BERNAS. From our luminescence measurements, it is not possible to determine whether charge neutralization occurs from a mobile state or from a retrapped state after successive hoppings of the electron toward the cation and, in the latter case, whether tunnelling is operative or not—what I essentially meant to show was that an optical excitation of e_s^-, and hence an initial detrapping and "mobilization", was necessary for neutralization luminescence and that H_3O^+ was the most probable neutralized cation in pure ice as well as in alkaline aqueous glasses.

S. A. RICE. Essentially electrons do not react with electron scavengers in glasses until the electron has been trapped. Thereafter the electron tunnels to the scavenger. See F. S. Dainton, M. J. Pilling, and S. A. Rice, *J. Chem. Soc. Faraday Trans. 2*, **71**, 1311 (1975).

A. BERNAS. From the experimental results I have just presented, one cannot conclude whether charge neutralization occurs through tunnelling or not.

However, in the tryptophan photoionization in alkaline glasses, we have observed that the two e_{solv}^- stimulated luminescence bands are affected differently upon N_2O addition. This seems to imply that at least part of the N_2O scavenging action occurs after the electron trapping and detrapping process.

R. HOLROYD. To what do you attribute the 380-nm emission in pure ice?

A. BERNAS. (1) From arguments developed previously and based on the low kinetic energy of the detrapped electrons ($\simeq$1 eV) we can be certain that the latter are unable to electronically excite stabilized radiolysis products, e.g., OH, HO_2, OH^- .... (2) Luminescent neutralization of alkali cation impurities seems also impossible on energetic grounds: in ice at 77 K alkali metal $\rightarrow M^+ + e_{sol}^-$ hence the inverse reaction neutralization would be endothermic. Besides, we find that adding NaCl or KCl does not enhance but quenches the stimulated luminescence of γ-irradiated ice. (3) From the value reported in the literature for the ionization potential of H_3O (~4.0–4.2 eV for the isolated radical), a value which is expected to be lowered by almost 2 eV in ice, we think that we can also disregard H_3O as the possible emitting species.

The most plausible species responsible for the emission remains a low-lying triplet state of water with unknown configuration since theoretical calculations predict that no vertical transition exists below about 6.7 eV.

(These remarks and conclusions have been published recently (A. Bernas and T. B. Truong, *Chem. Phys. Lett.*, **29**, 585 (1974)).

Capture of the Trapped Electron in Alcohol Glasses

A. Namiki, M. Noda, and T. Higashimura*

Research Reactor Institute, Kyoto University, Kyoto, Japan *(Received July 23, 1975)*

Publication costs assisted by the Research Reactor Institute

This is a paper on the scavenging of the presolvated electron. In many matrices, the secondary electron is stabilized in shallow traps at first, and then it becomes solvated to deepen the potential well. Because the tunneling rate depends strongly on the height of the potential, scavenging by tunneling from the presolvated state possibly overcomes the tunneling from the solvated state even if the lifetime of the presolvated state is very short.

Scavengers (benzene, fluorobenzene, chlorobenzene, bromobenzene, iodobenzene, *o*-chlorotoluene, *o*-bromotoluene, and *o*-dichlorobenzene) were added to alcohols (methanol, ethanol, 1-propanol, and 2-propanol) and were cooled rapidly to make clear glasses. These glasses were irradiated by γ rays at 77 K with the dose of about 0.2 Mrad. The yield of the solvated electron was estimated from the optical density of the wavelength of the peak of the absorption spectrum.

The scavenging efficiency is defined as $1/[S]^{1/2}$ where $[S]^{1/2}$ is the concentration at which the yield of the solvated electron becomes half of that in pure matrices.

When the scavenging efficiency is plotted against the adiabatic electron affinity of the scavenger molecule (see Table I), we obtain the linear relationships for every matrice. For every scavenger, the efficiencies in the 1-propanol glasses are larger than those in the ethanol glass. This suggests that the electron tunneling does not occur from the solvated state but from the unsolvated state, because the absorption spectra of the solvated electrons in both matrices are very similar to each other. The solvation time of the trapped electron in 1-propanol is larger than that in ethanol. Therefore, the former electron has larger chance of tunneling than that of the latter electron. If we assume the same depths of the trapped electron levels in both solvents, the difference between the tunneling distances in both matrices is expressed as

$$\frac{1}{\sqrt{\text{V-E}}} \ln \frac{\tau(\text{1-PrOH})}{\tau(\text{EtOH})}$$

where V-E is the energy level of the trapped electron and τ's are the solvation times. From the experimental values of the scavenging efficiencies, one obtains τ(1-PrOH) = 175 μsec. Similar calculation gives 10 nsec for the solvation time of methanol.

In order to explain the dependence on the electron affinity, one must introduce a factor F (inefficiency factor called by J. Miller) into a usual equation for the tunneling rate. F is expressed as $F = \theta p(E_v)\Delta E_v$, where θ is the fractional solid angle within which the trapped electron sees the scavenger molecule, and ΔE_v is the width of the resonant vibrational level of the scavenger. $p(E_v)$ is the probability density of the nuclear configuration of the scavenger molecule at which the difference of the energy between potential curves of the neutral molecule and that of the anion is equal to E_v. E_v is the energy which is given to the electron upon tunneling and is expressed as $E_v = V_0 - (\text{V-E}) - p_-$, where V_0 is the energy of the quasi-free electron in the matrix and p_- is the polarization energy of the matrix. Taking $E_v = 0.5$ eV, $\theta = 10^{-2}$, and $\Delta E_v = 10^{-2}$ eV and using the Morse function for the molecular potential (following Steelhammer and Wentworth), one can obtain the tunneling radius numerically. Calculated values are shown in Table I.

TABLE I: Data for $1/[S]_{1/2}$ (M^{-1}), Experimental Tunneling Radius, a, and Calculated One, a' (in Å)

Solvent	MeOH			EtOH			1-PrOH		
τ	10 nsec			2.5 μsec			14 μsec		
	$1/[S]_{1/2}$	a	a'	$1/[S]_{1/2}$	a	a'	$1/[S]_{1/2}$	a	a'
o-$PhCH_3Cl$	9.0	12.1	6.4	16.4	16.6	10.2	34.9	23.3	12.7
PhCl	9.3	12.2	12.4	21.7	18.2	20.3	41.1	24.6	22.7
o-$PhCH_3Br$	11.1	12.9	10.7	23.0	18.5	28.5	39.7	24.3	21.0
PhBr	11.7	13.2	13.1	25.0	19.1	21.0	46.0	25.5	23.4
o-$PhCl_2$	12.4	13.4	15.5	31.9	20.7	23.4	52.3	26.6	25.9

Discussion

S. RICE. That semilogarithmic electron yields vs. scavenger concentration give straight-line plots merely reflects the fact that the electron reaction is pseudo first order.

G. R. FREEMAN. The semilogarithmic relationship between solvated electron concentration and scavenger concentration could be obtained by several mechanisms. One is the tunneling process that you mentioned. Another is the stochastic model of nonhomogeneous kinetics that is often used for charge scavenging in irradiated systems. What you have called tunneling distances might actually be related to the migration distances of the electrons before becoming localized in deep traps. However, this would not affect the other conclusions in your interesting paper.

T. HIGASHIMURA. The semilogarithmic relationship can be obtained in the case of capture of the epithermal electron, as you say. What I wanted to emphasize in my talk is the strong correlation between the scavenging efficiency and the solvation time.

N. KLASSEN. Your estimate of 10 nsec for the solvation time in MeOH at 77 K agrees with our pulse radiolysis experiments in which we see very little ir absorption component to the absorption band at a time of ~20 nsec in a pure MeOH glass. Our pulse radiolysis results with ethanol glasses at 77 K show that the stable spectrum of e_t^- is largely reached only after milliseconds which is much slower than the 2.4 μsec reported by Richards and Thomas.

A. K. PIKAEV. (1) Have you measured the scavenging effects at different temperatures? (2) Did you make any attempts to observe the spontaneous decay of e_{tr}^- after γ-irradiation in your systems?

T. HIGASHIMURA. (1) No, we have not obtained scavenging efficiencies at different temperatures. In cases of solutions different from those which I mentioned, we obtained larger scavenging efficiencies at 4.2 K than at 77 K. This phenomenon supports the tunneling mechanism. [*J. Phys. Chem.* **76**, 3744 (1972) and *Int. J. Radiat. Phys. Chem.*, **6**, 393 (1974)]. (2) No, all data are at 5 min after radiolysis.

L. KEVAN. Would you predict the same $S_{1/2}$ values for a solute in EtOH and in 1-PrOH at 4 K where the trapped electron is unsolvated in both matrices? At 4 K the relaxation times in both matrices are so long that they should not enter in.

T. HIGASHIMURA. Yes. The tunneling distance at 4 K, a_4', and that at 77 K, a_{77}', satisfy the equation $a_4' - a_{77}' = (1/\sqrt{V-E}) \ln (\tau_4/\tau_{77})$ for each solvent. Here, τ_4 must be taken as the time interval between irradiation and measurement. Taking 5 min for τ_4 and values in the table for τ_{77}, a_4' becomes 26.3 Å larger than a_{77}' in ethanol and 23.9 Å larger than a_{77}' in 1-PrOH. In this simplification, the scavenging efficiency becomes dependent only on the depth of the trapped state, V-E, for the 4 K experiment. If we take the same depth in both EtOH and 1-PrOH, the scavenging efficiency at 4 K becomes the same in both matrices.

Proton Magnetic Resonance Study of Metal–Ammonia Compounds

R. F. Marzke

Department of Physics, Arizona State University, Tempe, Arizona 85281

W. S. Glaunsinger*

Department of Chemistry, Arizona State University, Tempe, Arizona 85281 *(Received August 4, 1975)*

The proton magnetic resonance (^{1}H NMR) spectra of $Ca(NH_3)_6$, $Ba(NH_3)_6$, and $Li(NH_3)_4$ have been recorded in the temperature range 20–150 K using a broad-line, symmetrical-bridge spectrometer. In the hexaammines very narrow first-derivative line widths are observed (<2.5 G in the range 20–150 K). Significant changes occur in the ^{1}H NMR spectra of $Ca(NH_3)_6$ in the ranges 20–50, 60–80, and 100–130 K, whereas in $Ba(NH_3)_6$ changes occur between 70 and 100 K and above 140 K. The line width and its temperature dependence are interpreted in terms of structure, phase transitions, and molecular motion. In the high-temperature region very large, temperature-independent, high-field shifts of about 0.3 G (160 ppm) have been measured in both $Ca(NH_3)_6$ and $Ba(NH_3)_6$. The shifts are tentatively interpreted in terms of indirect coupling of the type found in aromatic radicals.

Introduction

When Li, Ca, Sr, Ba, Eu, or Yb is dissolved in liquid ammonia and the resulting solution frozen, metallic compounds having the compositions $Li(NH_3)_4$ and $M(NH_3)_6$, where M is Ca, Sr, Ba, Eu, or Yb, are formed. The metallic nature of these compounds arises from the loss of one, in the case of $Li(NH_3)_4$, and two, in the case of $M(NH_3)_6$, electrons from the molecular complex to a conduction band. Preliminary x-ray studies[1-4] indicate that the molecular ions thus formed are arranged in the solid state in either a cubic or hexagonal array. The large ionic radius of the molecular ions, as well as Brillouin-zone-contact effects, lead to the classification of these materials as low-electron-density metals, and as such are of great theoretical interest. Electrical transport,[5,6] magnetic susceptibility,[7,8] and electron spin resonance[9] studies suggest that metal–ammonia compounds should also be experimentally suitable model systems for investigating the electronic behavior of metals in the low-electron-density regime.

Previously, it was believed that in these compounds ammonia molecules were tetrahedrally arranged around Li and octahedrally disposed around Ca, Sr, Ba, Eu, and Yb in a regular fashion. However, a recent neutron diffraction study of $Ca(ND_3)_6$[10] has disclosed that, although the calcium atoms occupy body-centered-cubic positions, they are surrounded by a distorted octahedron of highly distorted ammonia molecules having C_s symmetry. Similar structural complexities are anticipated in other metal–ammonia compounds.

Recent research has suggested that molecular motion could play an important role in determining the properties of metal–ammonia compounds. Abrupt changes in electrical resistivity[6,11] and Mössbauer resonant absorption[12] near 69 K in $Li(NH_3)_4$ and $Eu(NH_3)_6$, respectively, may be due to a rotational transition. Since rotational lockup occurs near 65 K in pure ammonia,[13] the observed transitions near 69 K in $Li(NH_3)_4$ and $Eu(NH_3)_6$ may be due to the onset of thermally activated rotation of the ammonia molecules in a molecular ion about their principal axes. If the transitions near 69 K in $Li(NH_3)_4$ and $Eu(NH_3)_6$ are indeed due to ammonia rotational lockup, then the other metal–ammonia compounds should exhibit similar rotational transitions.

One of the most direct ways to study molecular motion is proton magnetic resonance (^{1}H NMR). Here we report the

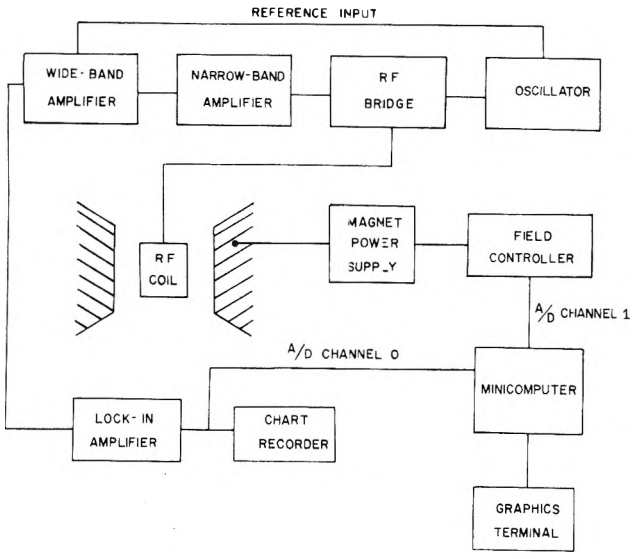

Figure 1. Block diagram of the NMR spectrometer.

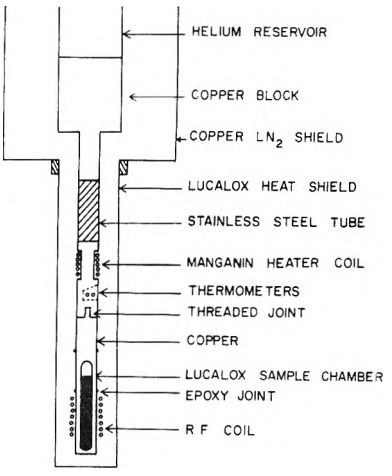

Figure 2. Cross-sectional view of the cryostat tail assembly.

first observation of ^1H NMR in metal–ammonia compounds. $Ca(NH_3)_6$ and $Ba(NH_3)_6$ have been studied in detail, and $Li(NH_3)_4$ has been studied over a narrow temperature range. The results are interpreted in terms of structure, phase transitions, and molecular motion.

Experimental Section

Sample Preparation. Samples were prepared by distilling a measured quantity of dry ammonia (Matheson, anhydrous, 99.99%) from a sodium–ammonia solution into a specially cleaned[14] 2 × 3 mm Pyrex tube containing the elemental metal, which had been previously cut and weighed in an argon-filled glovebox, in amount sufficient to give a slight excess of the elemental metal. Metal-rich samples were used to eliminate the possibility of observing ^1H NMR from pure ammonia. The tube was sealed and allowed to warm to room temperature to ensure complete reaction. The accuracy of the sample composition is about 4%. Some of the samples studied showed visible signs of decomposition near the top of the tube, but this caused no difficulty because the rf coil surrounded only the lower portion of the tube.

Apparatus and Measurement Procedure. First-derivative ^1H NMR spectra were obtained using field modulation and a symmetrical-bridge spectrometer. The spectrometer was interfaced to a PDP-11 minicomputer with graphics terminal to facilitate data analysis and processing. A block diagram of the spectrometer is shown in Figure 1. The rf bridge operates close to 8 MHz and is driven by a stable, crystal-controlled oscillator. An rf amplitude of 0.13 G was usually employed, but fields as high as 2 G could be used without degrading the signal-to-noise ratio. The field modulation amplitude and frequency were about 0.10 G and 460 Hz, respectively. Although some modulation broadening is expected for the narrowest lines observed (0.4 G), the broadening is within the experimental error in measuring the line width, so that the line-width data have not been corrected for it. The magnetic field sweep was calibrated before each run using a separate ^1H NMR spectrometer of the marginal oscillator type, with a room-temperature water sample located in the magnet gap. Most spectra were recorded using a 45-min field sweep and 30-sec lock-in amplifier time constant.

A cross-sectional view of the cryostat tail assembly is shown in Figure 2. The rf coil was wound around the Lucalox sample chamber to maximize the filling factor. The epoxy used to seal the rf coil to the sample chamber produced a broad, temperature-independent ^1H NMR line (about 14 G wide), which appears as background superimposed on the sharp spectra of the metal–ammonia compounds. Good thermal contact was established between the sample tube and Lucalox chamber via a thin layer of Apiezon N grease, which gave no ^1H NMR signal above background in the range 20–150 K. Temperatures were measured with a calibrated gallium arsenide thermometer mounted directly above the sample. Calibration of the thermometer was checked by using the large change in bridge balance that accompanied the melting of $Li(NH_3)_4$ at 88.8 K and was found to be accurate to better than 0.5 K. Liquid nitrogen was placed in the central chamber of the cryostat for temperatures between 80 and 150 K, and liquid helium was used for the range 20–80 K. To avoid possible hysteresis, spectra were recorded as the sample was warmed from 20 to 150 K.

Results

Calcium Hexaammine. Significant changes in the ^1H NMR spectra of $Ca(NH_3)_6$ occur in the ranges 20–50, 60–80, and 100–130 K. Typical spectra for these ranges are given in Figures 3–5. All spectra exhibit the asymmetry expected for metallic samples having dimensions much larger than the skin depth. The apparent baseline drift is due to the proton background mentioned earlier. Between 20 and 50 K, the line broadens with increasing temperature, and below 30 K the line shape and asymmetry parameter become temperature-dependent. In the ranges 60–80 and 100–130 K, the line narrows with increasing temperature. Above 30 K, the spectra can be fitted to a Gaussian lineshape function, which is characterized by an asymmetry parameter of 1.82.[15]

The temperature dependence of the first-derivative peak-to-peak line width ΔH_{p-p} is shown in Figure 6. The line broadening in the range 20–50 K and line narrowing in the ranges 60–70 and 100–130 K are evident. Unfortunately, the diffuse wings of the signals in these metals prevented the determination of reliable second moments.

The temperature dependence of the proton shift k_H is shown in Figure 7. Proton shifts were determined using the relation[15]

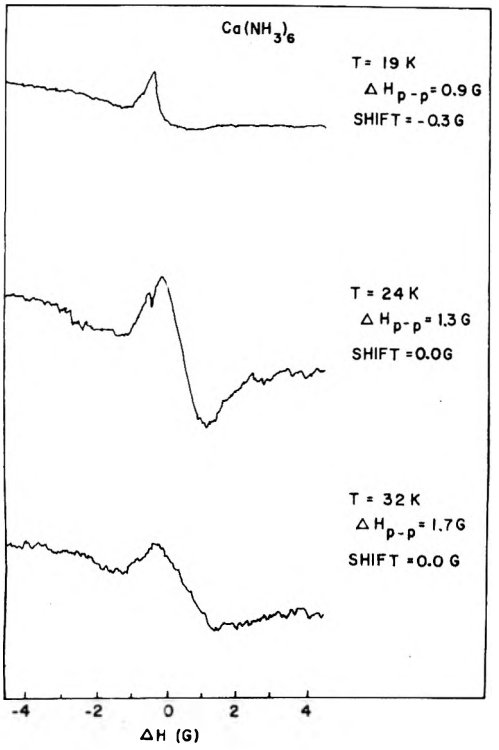

Figure 3. Low-temperature ^{1}H NMR spectra of $Ca(NH_3)_6$.

$$k_H = H_{max} + 0.2\Delta H_{p-p} \quad (1)$$

where H_{max} is the field at the highest amplitude lobe of a first-derivative spectrum. Within our experimental error, eq 1 is valid for both Lorentzian and Gaussian metallic line shapes. We have assumed that eq 1 can be used below 30 K, where the line shape is not Gaussian. This is not unreasonable in view of the apparent insensitivity of the metallic shift to the details of the line shape. Since the resonant field is 1.88 kG, the shifts can be converted from G to ppm by multiplying by 532, i.e., k_H (ppm) = $532k_H$ (G). The shift is zero at lower temperatures within experimental error, but at higher temperatures where the accuracy is much greater, a very large shift to high fields of about 0.3G (160 ppm) has been measured.

Barium Hexaammine. Significant changes occur in the ^{1}H NMR spectra of $Ba(NH_3)_6$ between 70 and 100 K and above 140 K. Typical spectra above 70 K are illustrated in Figure 8. The line narrows between 70 and 100 K as the temperature is increased, and above 140 K it is evident that the spectrum is composed of at least three closely spaced lines.

Above 100 K the spectra exhibited saturation at an rf amplitude of 0.13 G, as shown in the trace at 99 K in Figure 8, so that lower rf amplitudes were required. At very large rf levels (1 G), it was possible to saturate the absorption component of the signal completely, so that a pure dispersion signal was observed with the spectrometer adjusted for normal absorption. The line-shape asymmetry parameter was nearly Gaussian (i.e., approximately 1.8) for spectra consisting of a single line (below 140 K).

The temperature dependence of ΔH_{p-p} is shown in Figure 9. The line narrowing between 70 and 100 K is apparent, as well as a slight narrowing between 40 and 50 K. In contrast to $Ca(NH_3)_6$, the line width is independent of temperature between 20 and 40 K. Above 40 K, the line

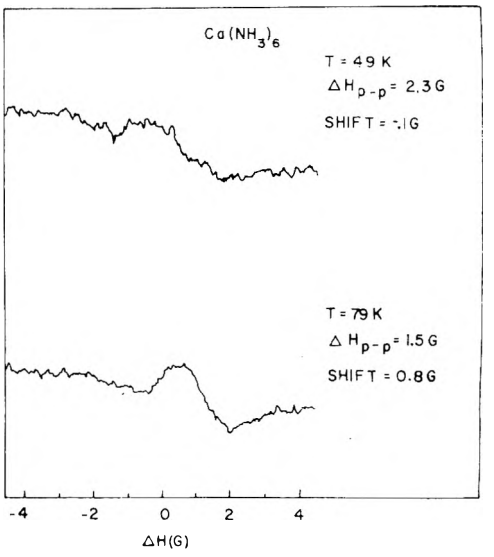

Figure 4. Low-temperature line-narrowing transition in $Ca(NH_3)_6$.

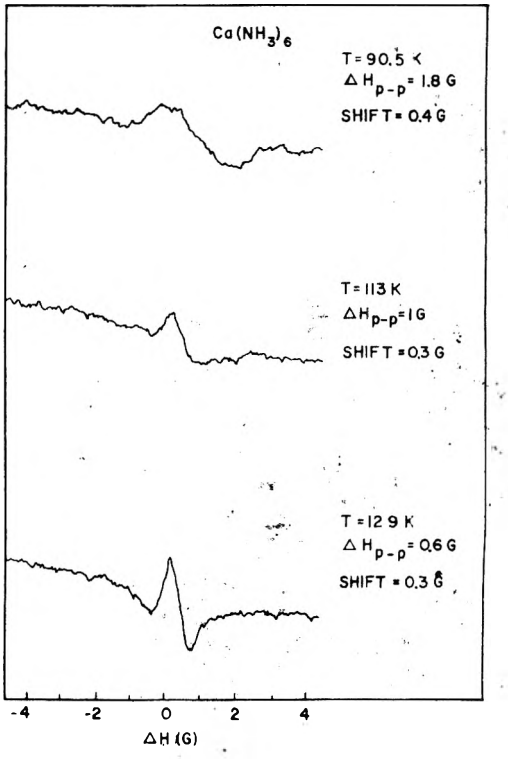

Figure 5. High-temperature line-narrowing transition in $Ca(NH_3)_6$.

widths in $Ba(NH_3)_6$ are even smaller than those in $Ca(NH_3)_6$.

The temperature dependence of k_H is shown in Figure 10. In analogy to $Ca(NH_3)_6$, the shift is zero at lower temperatures within experimental error, but at higher temperatures the shift is about 0.3 G (160 ppm).

Lithium Tetraammine. Spectra could be observed only in the cubic phase of $Li(NH_3)_4$, i.e., between 82 and 88 K. The ^{1}H NMR line was too broad to be detected above background in the low-temperature hexagonal phase. Considering the spectrometer sensitivity and difference in skin depth between the two phases, we estimate that the line width must exceed 4 G in the hexagonal phase.

A typical spectrum in the cubic phase is shown in Figure

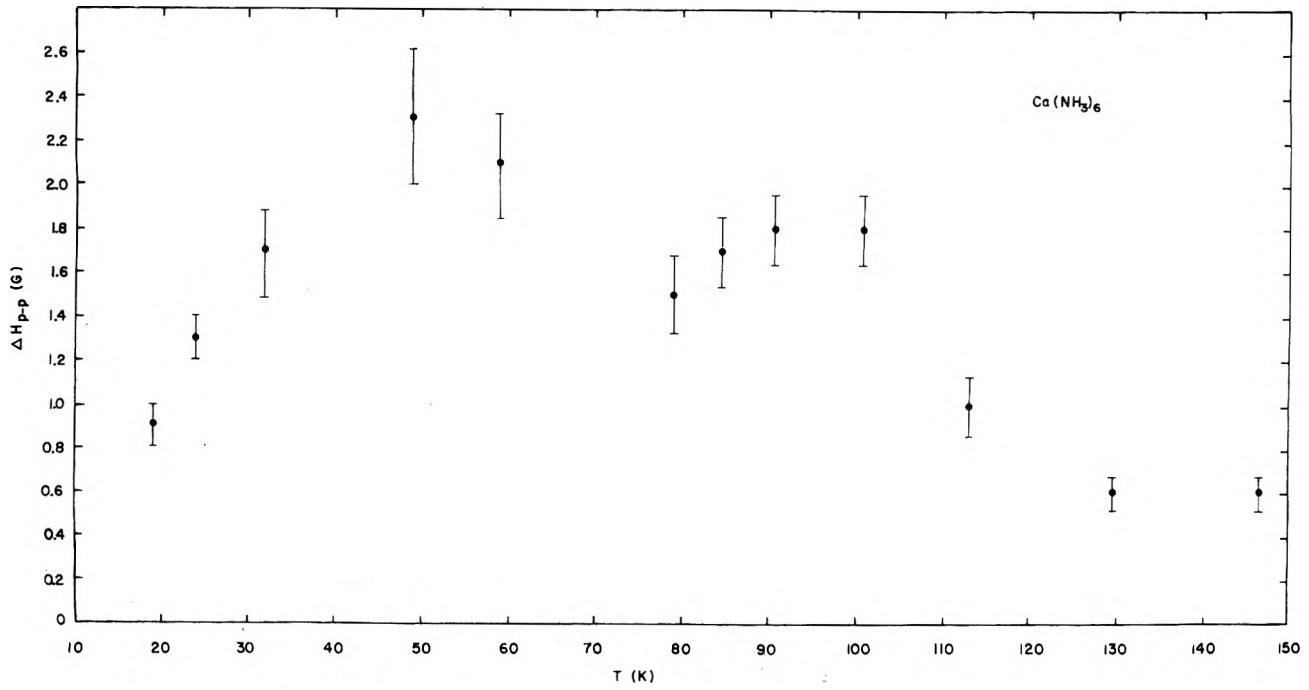

Figure 6. Temperature dependence of the first-derivative peak-to-peak line width in $Ca(NH_3)_6$.

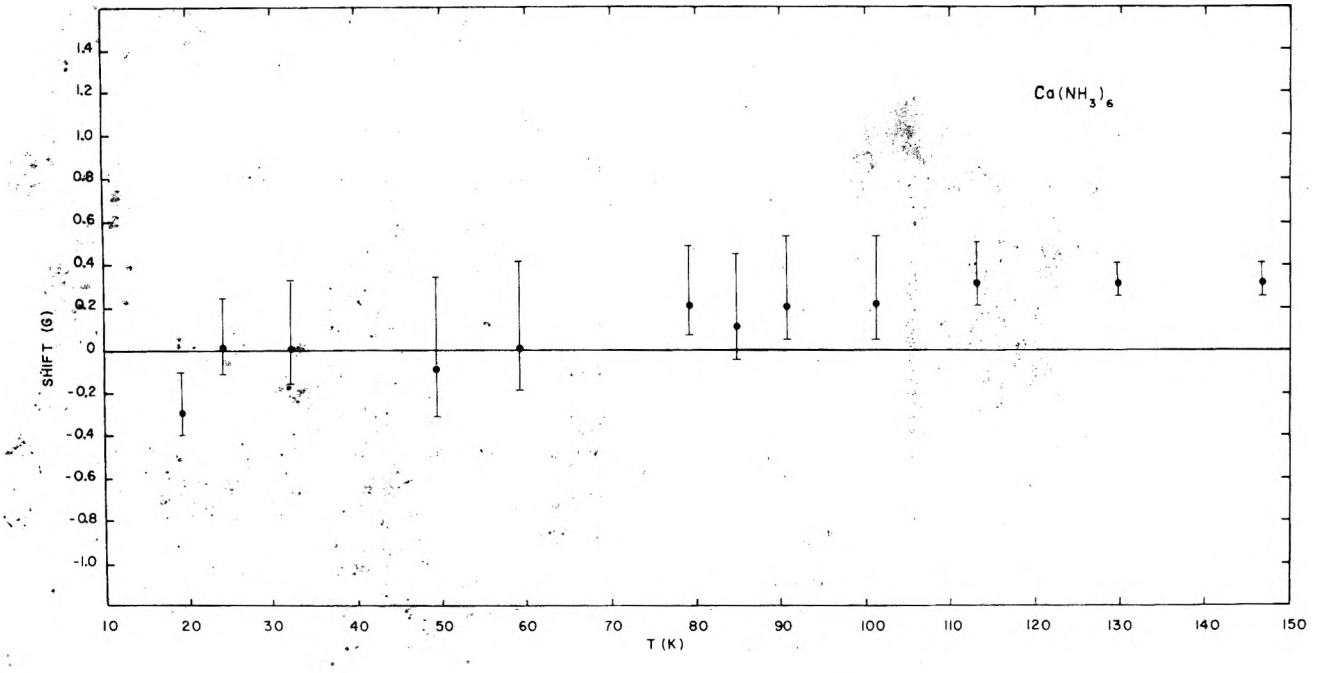

Figure 7. Temperature dependence of the proton shift in $Ca(NH_3)_6$.

11. The line shape is Gaussian, the width is temperature independent and equal to 1.3 ± 0.2 G, and the shift is zero within experimental error.

Discussion

It is useful to review the results of a recent NMR study of solid ammonia[13] before discussing the results of this study. In solid ammonia, ΔH_{p-p} is about 10 G between 20 and 60 K and shows a slight increase below 20 K. As the temperature is increased from 60 to 80 K, the line narrows from 10 to 7.5 G, and the line width remains about 7.5 G up to 160 K. Quantum-mechanical tunneling of the ammonia molecule about its principal axis was required to explain the small line width observed below 60 K, and it was concluded that the line-width transition between 60 and 80 K reflected a transition from quantum-mechanical tunneling to thermally activated rotation of an ammonia molecule.

Calcium Hexaammine. An important feature of the ^1H NMR spectra in $Ca(NH_3)_6$ is that they are very narrow (<2.5 G) compared to those in solid ammonia. The observed Gaussian line shape above 30 K indicates that dipolar interactions determine the line width. For a Gaussian line shape, the theoretical rigid-lattice first-derivative peak-to-peak line width can be obtained from the relation

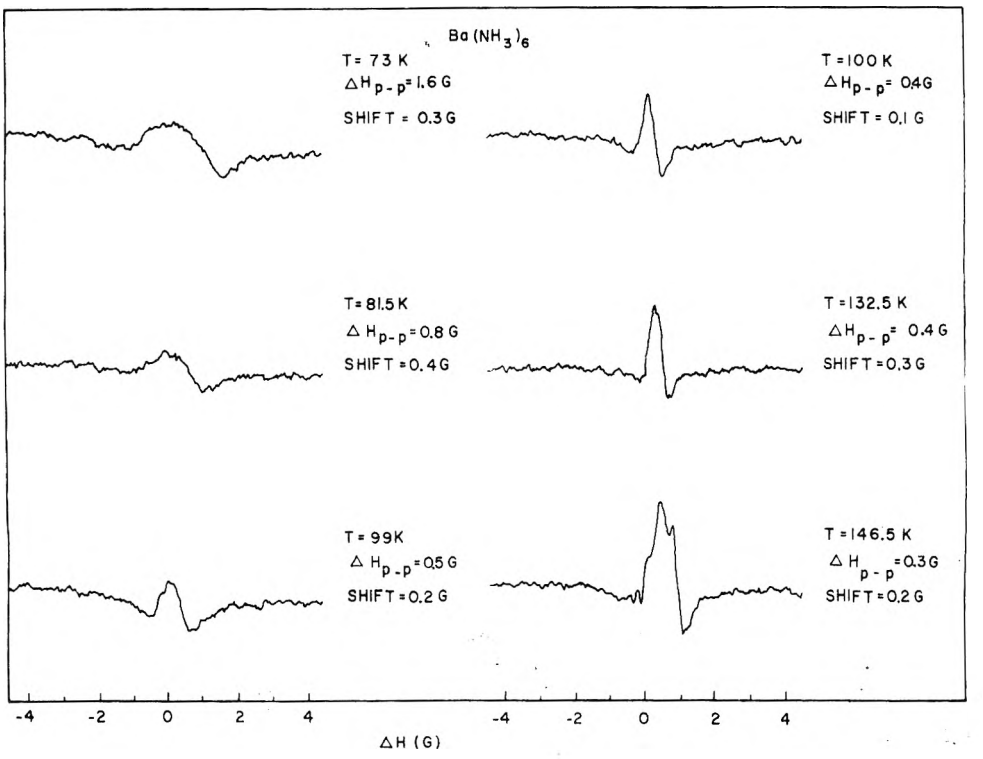

Figure 8. ^{1}H NMR spectra in $Ba(NH_3)_6$.

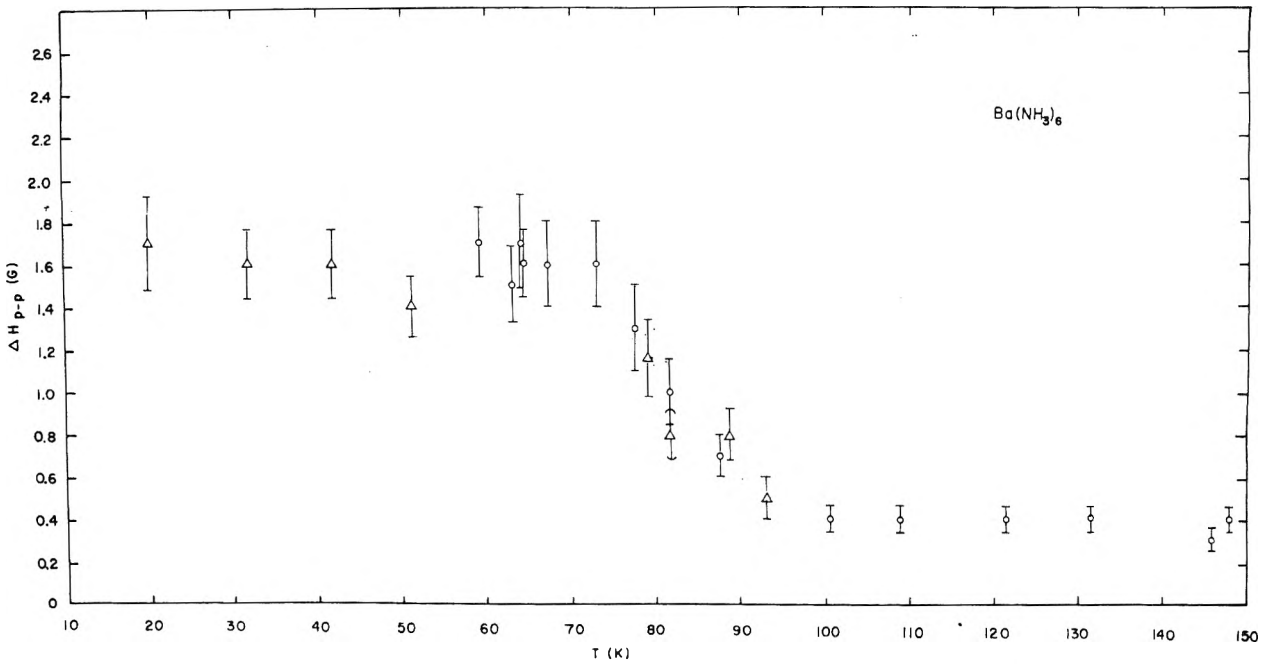

Figure 9. Temperature dependence of the first-derivative peak-to-peak line width in $Ba(NH_3)_6$. Open circles and triangles represent data from two independent experiments.

$$\Delta H_{p-p}{}^{R} = 2\sqrt{M_2{}^{R}} \quad (2)$$

where $M_2{}^{R}$ is the rigid-lattice proton second moment. $M_2{}^{R}$ is given by[16]

$$M_2{}^{R} = (3/5)g_H{}^2\beta^2 I_H(I_H + 1)\frac{1}{n_H}\sum_{jk} r_{jk}{}^{-6} + (4/15)g_X{}^2\beta^2 I_X(I_X + 1)\frac{1}{n_H}\sum_{jk'} r_{jk'}{}^{-6} \quad (3)$$

where n_H is the number of protons per unit cell, r_{jk} is the internuclear distance between nuclei j and k, and β, g, and I are the nuclear magneton, g-factor, and spin, respectively. In eq 3, the first term gives the contribution due to the proton–proton interactions, while the second term gives the contribution of proton–nitrogen interactions. The second term is very small for metal–ammonia compounds and has been neglected.

A complete calculation of the rigid lattice $M_2{}^{R}$ cannot be made without full knowledge of the crystal structure. A re-

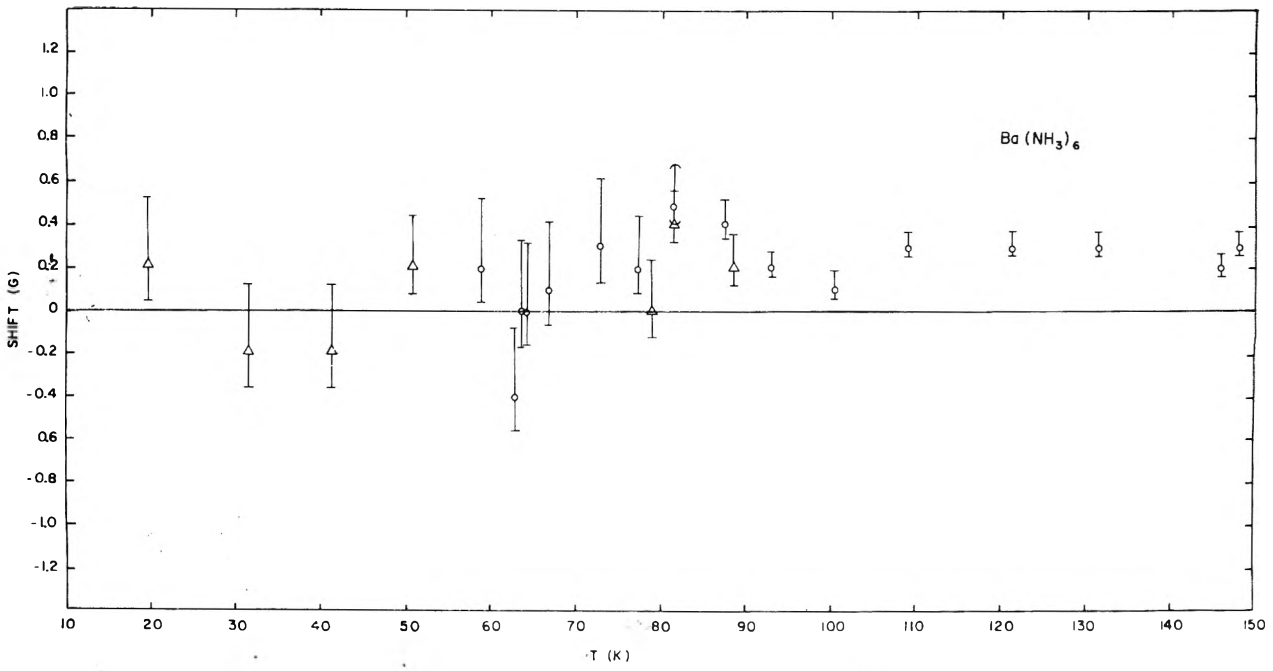

Figure 10. Temperature dependence of the proton shift in $Ba(NH_3)_6$. Open circles and triangles represent data from two independent experiments.

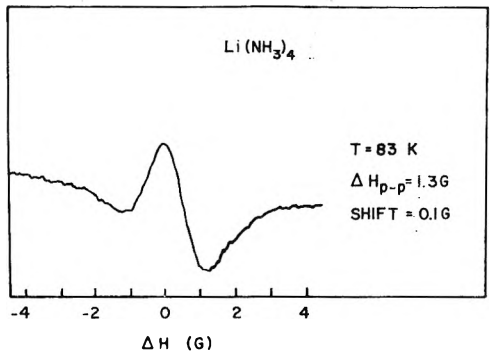

Figure 11. ^1H NMR spectrum in the cubic phase of $Li(NH_3)_4$.

cent neutron diffraction study of $Ca(ND_3)_6$[10] at 75 K leaves undetermined the relative orientation of neighboring NH_3 molecules, and thus allows only estimates of the longer range proton–proton interactions. This does not affect the contribution to M_2^R from the nearest-neighbor protons in the ammonia molecule itself, i.e., the "intra-ammonia" protons. Their contribution, which will be seen to be dominant, is readily obtained from the neutron-diffraction proton–proton distance. The other "intraionic" protons, contained within the near octahedron of NH_3 molecules surrounding each calcium, contribute to M_2^R according to the relative NH_3 orientations, which are about 4^6 in number, since each NH_3 can have four orientations. A simple statistical estimate shows that the intraionic proton contribution is between 30 and 50% of that of the intra-ammonia protons. More distant protons should make a very much smaller contribution to M_2^R, as found in solid ammonia[13] and tetramethylammonium compounds,[17,18] so that their contribution will be neglected.

Using the proton–proton distances 2.05 and 2.35 Å from the neutron diffraction study,[10] we get a contribution to M_2^R of 6.05 G^2 from the intraammonia protons. Taking the second moment of the intraionic protons to be 30% of that of the intra-ammonia protons, the intraionic-proton contribution to M_2^R is then about 1.81 G^2. Using eq 2, the rigid-lattice line width is estimated to be 5.61 G. This value is in poor agreement with the maximum low-temperature line width of 2.3 ± 0.3 G at about 50 K. Below about 60 K, thermally activated reorientation of ammonia molecules is slow on the NMR time scale, so that a line-narrowing process other than thermally activated reorientation must be present below 60 K. If the ammonia molecules tunnel about their principle axes through a potential barrier of less than 3 kcal/mol at low temperatures, then the intra-ammonia proton contribution to the second moment will be reduced by a factor of $\frac{1}{4}$,[19] and the intraionic-proton contribution will be reduced by a smaller factor. Assuming that the latter contribution is reduced by a factor of $\frac{1}{2}$, as found for the intermolecular contribution in solid ammonia,[13] the calculated line width is 3.11 G, which is slightly larger than the experimental value. If the intraionic proton contribution is neglected, then the predicted line width is 2.46 G, which is in excellent agreement with experiment. On this basis, we tentatively conclude that the ammonia molecules in $Ca(NH_3)_6$ quantum mechanically tunnel below 60 K.

We emphasize that the line-width results support the structure of $Ca(ND_3)_6$ determined by neutron diffraction.[10] In particular, if the structural parameters for an ammonia molecule in solid ammonia were used, i.e., r(N–H) = 1.005 Å and angle H–N–H = 110.4°,[20] then the calculated low-temperature line width in $Ca(NH_3)_6$ is about 8 G, which is over a factor of 3 larger than the experimental value.

The increase in line width with temperature between 20 and 50 K is unexpected. On the basis of dipolar interactions, the low-temperature line width should be independent of temperature. Since the expected behavior is found in solid ammonia[13] and $Ba(NH_3)_6$, the situation in $Ca(NH_3)_6$ becomes even more puzzling. Magnetic susceptibility studies[8] have indicated significant changes in electronic behavior below 30 K, which coincides with the temperature below which the unusual changes in line width

and line shape occur. This suggests that electron–nuclear interactions may play an important role in determining the ^1H NMR behavior at low temperatures. Data below 20 K would be very helpful in elucidating the interesting low-temperature behavior in $Ca(NH_3)_6$, and to this end a ^1H NMR study below 20 K is being undertaken.

We know of no way to calculate the line narrowing expected when the ammonia molecules go from the quantum-mechanical tunneling to the thermally activated reorientation regime. However, in analogy to solid ammonia, where a similar transition has been observed,[13] it is reasonable to attribute the line-narrowing transition between 60 and 80 K to a transition from quantum-mechanical to classical behavior. The changes in electrical resistivity[6,11] and Mössbauer resonant absorption[12] near 69 K in $Li(NH_3)_4$ and $Eu(NH_3)_6$, respectively, which have been attributed to the onset of thermally activated rotation of the ammonia molecules about their principal axes, further substantiates the interpretation of the line-narrowing transition given above.

The dramatic line narrowing between 100 and 130 K must be associated with a more general motion than ammonia-molecule rotation. The most likely possibilities are isotropic reorientation and perhaps diffusion of molecular ions. Isotropic reorientation averages the intraionic contribution to the second moment to zero, so that the second moment is entirely interionic in nature. The calculation of the interionic contribution is facilitated by noting that the effect of isotropic reorientation is to concentrate the 18 protons of $Ca(NH_3)_6^{2+}$ at the calcium site.[21,22] For a body-centered-cubic array of molecular ions having $a_0 = 9.01$ Å,[10] we find a second moment of 0.34 G^2 and line width of 1.17 G by summing over the four nearest shells of molecular ions and then integrating to estimate the remaining contribution. About 70% of this value arises from the eight nearest neighbors at $\sqrt{3}a_0/2$. Since the observed line width above 130 K is a factor of 2 less than that calculated on the basis of isotropic reorientation of molecular ions, we conclude that diffusion of molecular ions probably occurs above 130 K. The occurrence of diffusion at this relatively low temperature is not unreasonable in view of the large deviation from stoichiometry in the alkaline earth hexaammines,[3] which should lower considerably the activation energy for the diffusion process.

The motional activation energies can be estimated from the equation[23]

$$E_a \approx 37T_c \tag{4}$$

where E_a is the activation energy in cal/mol and T_c is the temperature where the NMR begins to narrow in K. Since line narrowing begins near 60 and 100 K for ammonia-molecule and molecular-ion rotations, respectively, the resulting activation energies are 2.2 and 3.7 kcal/mol. Since the activation energy for ammonia-molecule rotation is less than 3 kcal/mol, quantum-mechanical tunneling of ammonia molecules about their principal axes is expected to occur below 60 K, as assumed in computing the low-temperature line width.

The direction of the proton shift at higher temperatures is characteristic of a chemical shift, but it is about an order of magnitude larger than typical proton chemical shifts. Although a similar shift is observed in dilute metal–ammonia solutions, its magnitude is very small (7 ppm).[24] The direction and magnitude of the shift can perhaps be accounted for by assuming, in analogy to indirect coupling through a C–H bond in aromatic radicals, appreciable π-electron spin density at nitrogen and indirect coupling to the proton via the N–H bond. The π-electron spin density at nitrogen could arise from the conduction electrons since a recent conduction electron spin resonance study has shown that the conduction–electron wave function contains appreciable ammonia character.[9] In such a case, the spin density at the proton would be negative, which results in a high-field shift, and the resulting proton shift could be rather large. If this suggestion is valid, then the nitrogen nucleus should exhibit a rather large low-field shift. We are currently attempting to measure the nitrogen shift to test this hypothesis.

Barium Hexaammine. An abrupt transition in the temperature dependence of the magnetic susceptibility of $Ba(NH_3)_6$ at 76 K may be associated with a crystallographic transition,[8] so that below 76 K the structure may not be body-centered cubic. If the structural parameters of $Ba(NH_3)_6^{2+}$ are the same as those of $Ca(NH_3)_6^{2+}$, then the low-temperature line-width estimate of 5.61 G in $Ca(NH_3)_6$ should apply to $Ba(NH_3)_6$. The considerably narrower low-temperature line width in $Ba(NH_3)_6$ suggests that at least some of the intraionic proton–proton distances in $Ba(NH_3)_6$ are greater than those in $Ca(NH_3)_6$. In analogy to $Ca(NH_3)_6$, the narrow low-temperature line width probably results from quantum-mechanical tunneling of the ammonia molecules about their principal axes, which requires an activation energy for rotation of less than 3 kcal/mol.[19] A significant difference between $Ca(NH_3)_6$ and $Ba(NH_3)_6$ is that the low-temperature line width in $Ba(NH_3)_6$ is independent of temperature within experimental error, as expected for a line width determined by dipolar interactions.

In analogy to $Ca(NH_3)_6$, decrease in line width between 40 and 50 K probably reflects a transition from quantum-mechanical tunneling to classical rotation of ammonia molecules.

The large decrease in line width between 70 and 100 K is most likely mainly due to isotropic reorientation and diffusion of molecular ions, since the line narrowing associated with the possible solid–solid transition at 76 K is only about 0.3 G. Using the same computational procedure as in $Ca(NH_3)_6$ and assuming a body-centered-cubic array of molecular ions having $a_0 = 9.77$ Å,[3] we predict a second moment and line width of 0.21 G^2 and 0.92 G, respectively, if the molecular ions undergo isotropic reorientation. Since the observed line width above 100 K is over a factor of 2 less than the value predicted on the basis of isotropic orientation, we conclude that diffusion of molecular ions probably occurs above 100 K.

Using eq 4, the activation energies for ammonia-molecule and molecular-ion rotations are estimated to be 1.5 and 2.8 kcal/mol, respectively. Again the activation energy for ammonia-molecule rotation is less than 3 kcal/mol, as required for quantum-mechanical tunneling of ammonia molecules at low temperatures. These activation energies are both lower than those in $Ca(NH_3)_6$, indicating that the ammonia molecules and molecular ions in $Ba(NH_3)_6$ have greater rotational freedom than in $Ca(NH_3)_6$. Greater rotational freedom implies larger interionic proton–proton distances, which is consistent with the smaller line widths found in $Ba(NH_3)_6$. The lower molecular-ion rotational activation energy is probably a consequence of the lower packing density of molecular ions in $Ba(NH_3)_6$, as indicated by its 25% larger cell volume.

The origin of the three closely spaced lines observed in $Ba(NH_3)_6$ above 140 K is unclear. The splitting could be a

result of anisotropy, or possibly the existance of three phases differing slightly in lattice parameter. A structural study above 140 K is required to elucidate this behavior.

The proton shifts in $Ba(NH_3)_6$ and $Ca(NH_3)_6$ are the same within experimental error. The discussion of the $Ca(NH_3)_6$ data should be consulted for a discussion of the proton shift.

Lithium Tetraammine. In analogy to the behavior of $Ca(NH_3)_6$ and $Ba(NH_3)_6$ at higher temperatures, it is likely that the molecular ions in the cubic phase of $Li(NH_3)_4$ undergo isotropic reorientation and possibly diffusion. Using the same computational procedure as in $Ca(NH_3)_6$ and assuming a face-centered-cubic array of molecular ions having $a_0 = 9.55$ Å,[1] for isotropic reorientation, a second moment and line width of 0.68 G[2] and 1.65 G, respectively, are predicted. This value is close enough to the experimental one that it cannot be unequivocally established whether diffusion occurs or not.

In $Ca(NH_3)_6$ and $Ba(NH_3)_6$, the cessation of isotropic reorientation resulted in about a threefold increase in line width. If isotropic reorientation ceases upon transforming to the hexagonal phase at 82 K and a similar increase in line width occurs, then the line width in the hexagonal phase would be about 4 G, which is too broad to be detected with the present spectrometer.

Acknowledgments. The authors wish to thank Mr. T. White for assistance in sample preparation, Dr. D. Irwin and Ms. F. Robb for help in recording spectra and data analysis, and Ms. Lorna Glaunsinger for her drafting expertise. We gratefully acknowledge support of this research by the Research Corporation and Arizona State University.

References and Notes

(1) N. Mammano and M. J. Sienko, *J. Am. Chem. Soc.*, **90**, 6322 (1968).
(2) H. Oesterreicher, N. Mammano, and M. J. Sienko, *J. Solid State Chem.*, **1**, 10 (1969).
(3) N. Mammano and M. J. Sienko, *J. Solid State Chem.*, **1**, 534 (1970).
(4) L. Kleinman, S. B. Hyde, C. M. Thompson, and J. C. Thompson, "Metal–Ammonia Solutions", Proceedings of Colloque Weyl II, J. J. Lagowski and M. J. Sienko, Ed., Butterworths, London, 1970, p 229.
(5) E. W. LeMaster and J. C. Thompson, *J. Solid State Chem.*, **4**, 163 (1972).
(6) M. D. Rosenthal and B. W. Maxfield, *J. Solid State Chem.*, **7**, 109 (1973).
(7) W. S. Glaunsinger, S. Zolotov, and M. J. Sienko, *J. Chem. Phys.*, **56**, 4756 (1972).
(8) T. David, W. S. Glaunsinger, S. Zolotov, and M. J. Sienko, "Electrons in Fluids", Proceedings of Colloque Weyl III, J. Jortner and N. R. Kestner, Ed., Springer-Verlag, New York, N.Y., 1973, p 323.
(9) W. S. Glaunsinger and M. J. Sienko, *J. Chem. Phys.*, **62**, 1873 (1975).
(10) R. B. Von Dreele and W. S. Glaunsinger, *J. Phys. Chem.*, in this issue.
(11) J. A. Morgan, R. L. Schroeder, and J. C. Thompson, *J. Chem. Phys.*, **43**, 4494 (1965).
(12) F. T. Parker and M. Kaplan, *Chem. Phys. Lett.*, **24**, 280 (1974).
(13) J. L. Carolan and T. A. Scott, *J. Magn. Reson.*, **2**, 243 (1970).
(14) S. Naiditch and J. E. Wreede, *J. Vac. Sci. Technol.*, **5**, 54 (1968).
(15) A. C. Chapman, P. Rhodes, and E. F. W. Seymour, *Proc. Phys. Soc., London*, **70**, 345 (1957).
(16) J. H. Van Vleck, *Phys. Rev.*, **74**, 1168 (1948).
(17) E. R. Andrew and P. C. Canepa, *J. Magn. Reson.*, **7**, 429 (1972).
(18) M. Mahajan and B. D. Nageswara Rao, *J. Phys. C*, **7**, 995 (1974).
(19) P. S. Allen, *J. Chem. Phys.*, **48**, 3031 (1968).
(20) J. W. Reed and P. M. Harris, *J. Chem. Phys.*, **35**, 1730 (1961).
(21) E. R. Andrew and R. G. Eades, *Proc. Roy. Soc., Ser. A*, **216**, 398 (1953).
(22) D. J. Kroon, *Philips Res. Rep.*, 15, 501 (1960).
(23) J. S. Waugh and E. I. Fedin, *Sov. Phys. - Solid State (Engl. Transl.)*, **4**, 1633 (1963).
(24) T. R. Hughes, Jr., *J. Chem. Phys.*, **38**, 202 (1968).

Discussion

M. H. COHEN. There can be a conduction–electron intermediated interaction between the hydrogen nuclei, which can be quite long ranged—the so-called RKKY interaction. This could act so as to give an exchange narrowing, but there is no reason to expect the Ca^{2+} and Ba^{2+} compounds to differ significantly in this regard. An anomaly in the electron paramagnetic susceptibility, however, can in some circumstances show up in the RKKY interaction. Also temperature effects can enter through the mean free path, which limits the range of the interaction when it becomes as small as a few interatomic separations.

J. V. ACRIVOS. The negative ^1H Knight shifts observed in $Ca(NH_3)_6$ and $Ba(NH_3)_6$ are greater than those reported by Hughes in $Na–NH_3$ at Colloque Weyl I. This was assumed to be due to the fact that hydrogen bonds are broken in the solvation process. Therefore, since the ammonia molecules were found to be much farther apart in the above compounds (Von Dreele, this meeting) than in pure ammonia, the effect may be of the same nature.

Optical Properties of Concentrated Li–NH_3 Solutions and Solid $Li(NH_3)_4$

W. H. McKnight and J. C. Thompson*

The University of Texas at Austin, Austin, Texas *(Received June 12, 1975)*

Publication costs assisted by the National Science Foundation

The reflectivity has been measured at 0 and 45° angles of incidence on 10, 12, and 20 mol % metal Li–NH_3 solutions and on $Li(NH_3)_4$ at 77 and 87 K. The photon energies cover 0.25–5 eV. The results are compared with free-electron models.

I. Introduction

Previous reports on the optical properties[1-5] of concentrated metal–ammonia solutions have left out the spectral regions well outside the visible or have failed to provide a proper reference.[6] In an attempt to rectify that situation, we have investigated the normal and 45° reflectance of several concentrated Li–NH_3 solutions and of solid $Li(NH_3)_4$ over the spectral range 0.25–5.0 eV.

The apparatus used was that developed by Mueller[7] and briefly described at Colloque Weyl II.[3] The incident light is reflected (twice) at incident angles of either 0 or 45°, then analyzed, and the intensity compared with a signal derived from light totally internally reflected at a sapphire–air interface. The resultant, raw data is R_0^2 and R_{45}^2 as a function of photon energy.

The frequency-dependent dielectric constant $\epsilon(\omega) = \epsilon_1(\omega) + i\epsilon_2(\omega)$ may then be computed using the Fresnel equations.[8] Unfortunately, the equations used to derive ϵ_1 and ϵ_2 from R_0^2 and R_{45}^2 contain terms where the two reflectivities are subtracted. Since the original data are accurate to no more than two significant figures, the values of ϵ_1 and ϵ_2 obtained when R_0 is near R_{45} are meaningless. Furthermore, in a free electron metal wherein ϵ_1 and ϵ_2 may be obtained from the Drude equations,[1] R_0 and R_{45} become very close, indeed, at low energies. These problems in analysis for certain values of R_0 and R_{45} have obliged us to simply report R_0 and R_{45} (in some cases) rather than analyzing the data to give the more useful dielectric constant. Other experimental details are treated more thoroughly in the dissertation of one of us.[9]

II. Liquid Results

Data were obtained at 10, 12, and 20 mol % metal (MPM) at 195 K in Li–NH_3 solutions. The liquid reflectances (with respect to sapphire) at 45° and at 0° are shown in Figures 1 and 2, respectively, together with computations based on Drude parameters derived from dc values of conductivities and Hall coefficients.[10] Though the observed reflectivities at 45° are somewhat lower than those calculated, the trend in the 45° reflectance data with respect to photon energy is in reasonable agreement with the free electron curves. The dip near 4.2 eV is, in our opinion, an artifact resulting from a contaminated sapphire prism.[9] The normal reflectivities are again somewhat lower than those calculated, and perhaps the agreement with the free electron trends is not so good as in the case of the 45° reflectance. The reflectance of a 20 MPM Li–NH_3 solution exceeds considerably that of liquid Hg.[11]

The plasma frequency, identified by the sharp drop in R_0^2 in Figure 2, is in substantial agreement with dc determinations of carrier densities. The value of the relaxation

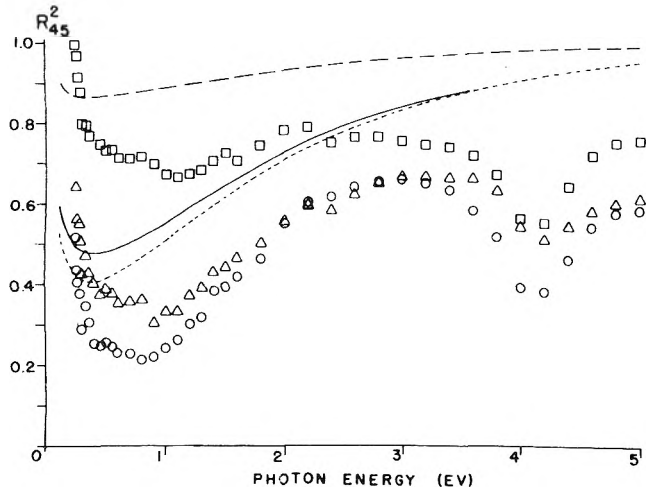

Figure 1. Reflectance data (45°) for 10, 12, and 20 MPM Li–NH_3 solutions at 195 K: (O) 10%, (- - - -) free electron calculation; (△) 12%, (——) free electron calculation; (□) 20%, (— —) free electron calculation.

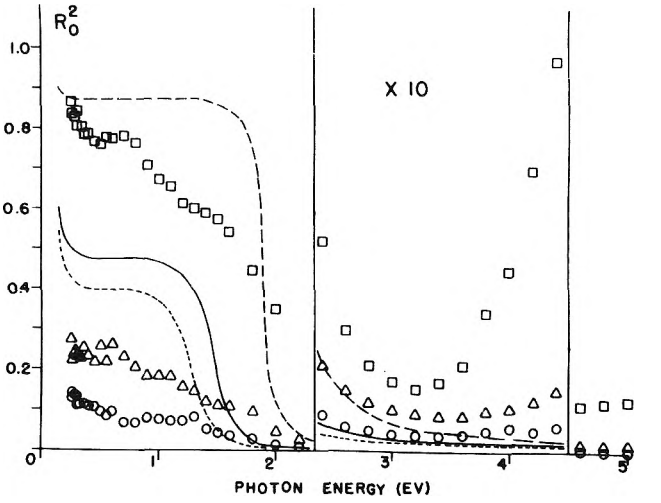

Figure 2. R_0^2 measurements (with respect to sapphire) at 195 K: (O) 10 MPM Li–NH_3, (- - - -) free electron calculation; (△) 12 MPM Li–NH_3, (——) free electron calculation; (□) 20 MPM Li–NH_3 (— — —) free electron calculation.

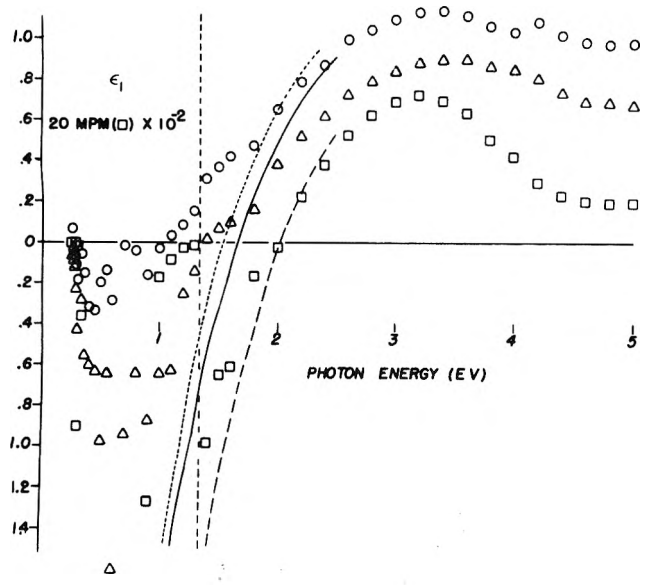

Figure 3. ϵ_1 vs. photon energy for 10, 12, and 20 MPM Li-NH_3 solutions at 195 K: (□) 20%, (- - -) 20% Li-NH_3 at 213 K (ref 1); (△) 12%, (——) 12% Li-NH_3 at 213 K (ref 1); (○) 10%, (- - - -) 20% Li-NH_3 at 213 K (ref 2).

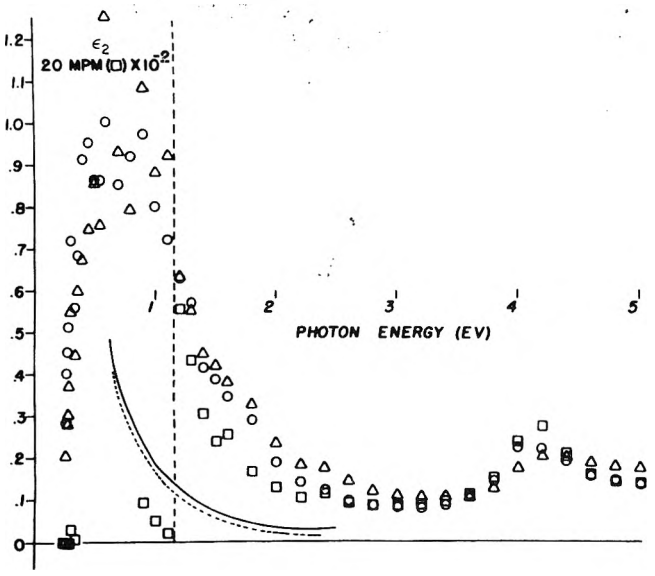

Figure 4. ϵ_2 vs. photon energy for 10, 12, and 20 MPM Li-NH_3 solutions at 195 K: (□) 20%; (△) 12%, (——) 12% Li-NH_3 at 213 K (ref 1); (○) 10%, (- - - -) 10% Na-NH_3 at 213 K (ref 2).

time at optical frequencies must be significantly lower than at dc to account for the smearing of the plasma edge. In addition, there is some evidence of an extra loss at the lowest frequencies since the observed values of R_{45}^2 exceed the Drude values there.

For that frequency range over which R_0 and R_{45} are not close to equality, ϵ_1 and ϵ_2 may be computed. These results are shown in Figures 3 and 4, together with results previously obtained by ellipsometric techniques.[1,2] As there is a long literature displaying[12] differences between ellipsometric and reflectance results, the differences shown in Figure 3 and 4 are not to be regarded as significant. Reflectance results are generally regarded as less susceptible to surface effects.[12] Errors resulting from the near-equality of R_0 and R_{45} are the source of the scatter near 1 eV in the 10- and 12-MPM curves, while nothing could be computed from the 20-MPM data in this region.

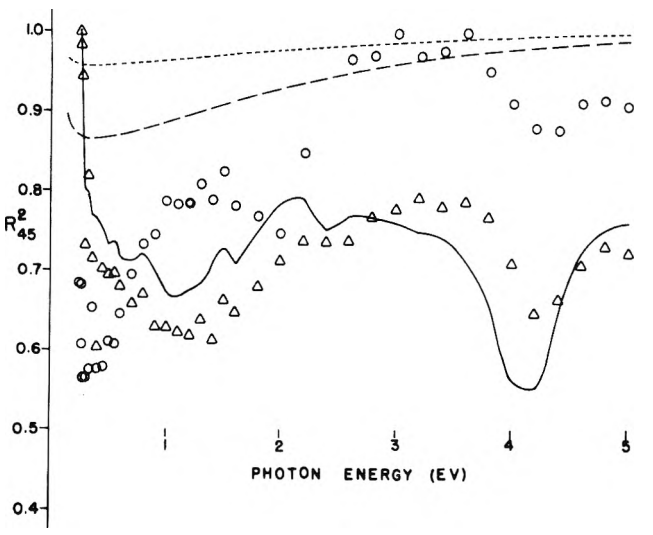

Figure 5. Raw 45° reflectance (R_{45}^2) data vs. photon energy: (○) hexagonal phase of Li(NH_3)$_4$ at 77 K; (△) cubic phase of Li(NH_3)$_4$ at 87 K; (——) 20 MPM Li-NH_3 solution (liquid) at 195 K; (- - - -) Drude calculation for cubic phase; (— —) Drude calculation for hexagonal phase.

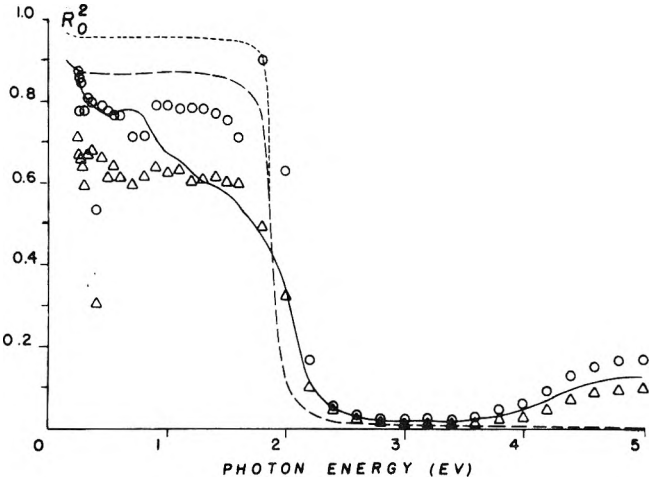

Figure 6. Raw normal reflectance (R_0^2) data vs. photon energy: (○) hexagonal phase of Li(NH_3)$_4$ at 77 K; (△) cubic phase of Li(NH_3)$_4$ at 87 K; (——) 20 MPM Li-NH_3 solution (liquid) at 195 K; (- - - -) Drude calculation for cubic phase; (— —) Drude calculation for hexagonal phase.

The qualitative trend of Drude behavior is maintained in these results, except at the lowest frequencies and where the prism contamination intervenes, as would be expected from Figures 1 and 2.

III. Solid Results

Data were taken on solid Li(NH_3)$_4$ in the cubic phase[14] at 87 K and in the hexagonal phase at 77 K. Figure 5 shows the raw 45° reflectance data for both the cubic and hexagonal phases and for a 20-MPM Li-NH_3 solution at 195 K. The dashed curve represents a free electron calculation for the cubic phase, with the usual corrections for the fact that the sample is in contact with sapphire.[9] Figure 6 shows similar data for normal reflectances. Clearly the hexagonal phase is not describable by a free-electron model. The cubic phase is similar in behavior to the 20-MPM liquid, when the higher conductivity is taken into account.

IV. Discussion

The present results tend to confirm those obtained previously on M–NH_3 solutions in the visible part of the spectrum. Free electron parameters do, however, show somewhat lower values of the relaxation times. Whether this is a consequence of the change from ellipsometric to reflectance techniques, or some other effect, cannot be determined from these data.

All the results show an extra loss at low energies (<0.8 eV) which is most likely due to some level in the NH_3 molecule. The solvated electron does not appear, at least not in the form familiar from dilute solutions.

The cubic solid is also describable by the conventional free-electron models, but the hexagonal phase shows the effects of interband transition and deserves the kind of analysis described by Ashcroft and Sturm.[15]

Acknowledgment. This work was supported in part by R. A. Welch Foundation of Texas and the National Science Foundation.

References and Notes

(1) J. C. Thompson and W. T. Cronenwett, *Adv. Phys.*, **16**, 439 (1967).
(2) R. B. Somoano and J. C. Thompson, *Phys. Rev. A*, **1**, 376 (1970).
(3) W. E. Mueller and J. C. Thompson, Colloque Weyl II: "Metal-Ammonia Solutions", J. J. Lagowski and M. J. Sienko, Ed., Butterworths, London, 1970, p 293.
(4) J. A. Vanderhoff, E. W. LeMaster, W. H. McKnight, J. C. Thompson, and P. R. Antoniewicz, *Phys. Rev. A*, **4**, 427 (1971).
(5) H. Aullch, B. Baron, P. Delahay, and R. Lugo, *J. Chem. Phys.*, **58**, 4439 (1973).
(6) T. A. Beckman and K. S. Pitzer, *J. Phys. Chem.*, **65**, 1527 (1961).
(7) W. E. Mueller, *Appl. Opt.*, **8**, 2083 (1969).
(8) K. Kudo, *Sci. Light (Tokyo)*, **13**, 11 (1964).
(9) W. H. McKnight, Ph.D. Dissertation, The University of Texas at Austin, 1975.
(10) R. D. Nasby and J. C. Thompson, *J. Chem. Phys.*, **53**, 109 (1970).
(11) W. E. Mueller, *J. Opt. Soc. Am.*, **59**, 1246 (1969).
(12) F. Abeles, Ed., "Optical Properties of Solids", North-Holland Publishing Co., Amsterdam, 1972.
(13) A. N. Bloch and S. A. Rice, *Phys. Rev.*, **185**, 933 (1969).
(14) N. Mammano, in ref 3, p 367.
(15) N. W. Ashcroft and K. Sturm, *Phys. Rev. B*, **3**, 1898 (1971).

Electronic Band Structure in Solid Hexaamminecalcium(0)[1]

Thérèse David Pfeuty and M. J. Sienko*

Baker Laboratory of Chemistry, Cornell University, Ithaca, New York 14853 *(Received July 23, 1975)*

Publication costs assisted by the National Science Foundation

In order to account for highly unusual magnetic and magnetic resonance properties observed in hexaamminecalcium(0), band calculations have been carried out to order $l = 2$ by the KKR method. Due to the very unusual form of the $Ca(NH_3)_6$ potential it appears that convergence of the KKR method requires expansion of the trial wave function up to $l = 4$. By extension of the calculations to $l_{max} = 4$ at points Γ, H, N, and P in the bccub zone scheme a preliminary band scheme has been constructed for $Ca(NH_3)_6$ solid. Behavior is different along the Σ direction compared to that along Δ and Λ. The lowest band, which lies entirely below the Fermi energy, is a very flat Σ_4 band that joins the Γ_1 state to the p-like state N_1'. A Λ_1 band connecting Γ_1 to P_1 and a Δ_1 band connecting Γ_1 to H_{12} intersect the Fermi level. Thus, the Fermi surface may deviate sensibly from a sphere. An upper band Σ_1 which comes down to point N_1 may also intersect the Fermi level, in which case electron pockets would be generated around the point N. Extended Hückel molecular orbital calculations are developed for the molecule $Ca(NH_3)_6$; the muffin-tin potential calculation for $Ca(NH_3)_6$ solid is described.

The metal–ammonia compounds[2] $Li(NH_3)_4$ and $Ca(NH_3)_6$ are of considerable interest as possible prototypes for expanded-metal systems on the verge of a metal–nonmetal transition. Recent studies of the magnetic susceptibility and conduction electron spin resonance[3-5] have indeed confirmed that the thermal behavior of these compounds is quite unusual. In order to understand the origin of the thermal behavior, the present calculation of band structure was undertaken. The compound $Ca(NH_3)_6$ was chosen since its structural relations are relatively simple. In the hexagonal phase, $Li(NH_3)_4$ has a twofold screw axis that would considerably complicate a band-structure calculation.

The crystal structure of $Ca(NH_3)_6$, as deduced from x-ray investigations of Cagle and Holland,[6] consists of octahedral $Ca(NH_3)_6$ molecules located at the body-centered cubic positions of a unit cell having edge length equal to 0.91 nm. In this research molecular orbitals were calculated for an isolated $Ca(NH_3)_6$ molecule, the potential function sphericalized, and the molecules brought together in a muffin-tin potential. In the muffin-tin approximation, the potential is assumed to be spherically symmetric within a sphere of radius R (equal to or less than half the nearest-neighbor distance) and very nearly equal to the electrostatic potential produced by all the nuclei and electrons of the neutral $Ca(NH_3)_6$ molecule. Outside the spheres, the potential is assumed to be constant; it is adjusted to zero for convenience.

Two models were selected for calculation of the muffin-tin potential. In one, the electrostatic potential was derived

from the whole neutral molecular unit $Ca(NH_3)_6$. In the other, separate consideration was given to the electrostatic potential created by the twice ionized entity $Ca(NH_3)_6^{2+}$ and the screening potential due to the conduction electrons, i.e., two electrons per molecule were assumed to have been set free through the molecular potential overlap. Clearly, the first model does not account for the observed metallic appearance of the material, since the valence electrons contribute to the potential as if they were localized. The second potential model was considered more appropriate for the band structure calculations.

EHMO Calculation and Results

The distribution of the electron cloud in the $Ca(NH_3)_6^{2+}$ ion was calculated by the extended Hückel molecular orbital (EHMO) approximation. Wave functions of the molecular orbitals are expressed as linear combinations of atomic orbitals

$$\psi_i = N_i \sum_j a_{ij} \varphi_j$$

where ψ_i is a molecular orbital wave function and the φ_j's are atomic wave functions. N_i is a normalizing factor such that

$$|\psi_i|^2 = 1 = \frac{1}{N_i^2} \int_\tau \left(\sum_j a_{ij} \varphi_j \right)^2 \delta\tau$$

The Hückel molecular orbital approximation assumes each atomic orbital φ_j is normalized and its overlap with neighboring φ_j's is negligible. This restriction that interaction is significant only between electrons on adjacent atoms is relaxed in the EHMO theory as developed by Hoffman.[7] All interactions are now considered and the full eigenvalue problem is solved. The input data fed into the EHMO program, which was kindly made available to us by Professor Hoffmann, were bond lengths and bond angles as follows: d(Ca–N), the Ca to N separation = 0.282 nm (from x-ray data); d(N–H), the N to H distance = 0.101 nm (as for NH_3); θ (Ca–N–H), the angle between the Ca–N bond and the N–H bond = 111° (chosen to be consistent with an angle of 107° between the N–H bonds in NH_3). The 48 valence electrons of the $Ca(NH_3)_6^{2+}$ ion [18 from the 18 1s orbitals of the 18 hydrogen atoms and 30 from the six 2s and 18 2p orbitals of the six nitrogen atoms] were to be distributed in the 51 atomic orbitals considered in the expansion. In addition to the 42 atomic orbitals indicated above, one 4s, three 4p, and five 3d orbitals of the calcium were included in the expansion. The atomic orbitals were Slater-type functions

$$\psi_{AO}(r, \theta, \varphi) = R_n(r) Y_{l,m}(\theta, \varphi)$$

where $R_n(r)$, the radial part of the atomic wave function, has the form

$$R_n(r) = \frac{2\zeta^{n+1/2}}{(2n!)^{1/2}} r^{n-1} e^{-\zeta r}$$

and $Y_{l,m}(\theta, \varphi)$ are the usual spherical harmonics. For the atomic screening constants ζ and orbital energy levels E, the following parameters were used: hydrogen 1s, ζ = 1.3 and E = −13.6 eV; nitrogen 2s, ζ = 1.95 and E = −26 eV; nitrogen 2p, ζ = 1.95 and E = −13.4 eV; calcium 4s, ζ = 1.05 and E = −7.5 eV; calcium 4p, ζ = 0.95 and E = −4 eV; calcium 3d, ζ = 1.05 and E = −3.2 eV.

The results of the computation are represented schematically in Figure 1. The diagram has been simplified in showing only the interactions between the highest energy levels: the six sp^3-hybridized lone pairs of the ammonia molecules and the 4s, 4p, and 3d orbitals of the calcium. The character of the molecular orbitals is not so well defined as the picture indicates since the presence of the C_3 symmetry axis in the NH_3 molecule destroys the perfect octahedral symmetry of the $Ca(NH_3)_6^{2+}$ ion, lifting all the remaining degeneracies. This fact, however, does not appear to be a real problem as the molecular orbitals and energies proved relatively insensitive to change in the orientation of the hydrogen atoms in one ammonia relative to the orientation in another.

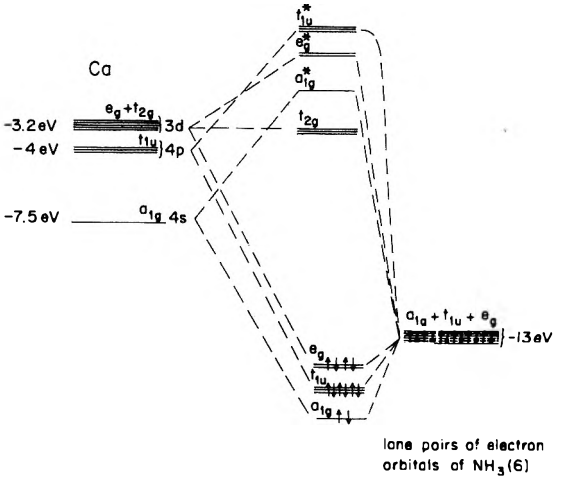

Figure 1. Schematic representation of the molecular orbital energy levels in $Ca(NH_3)_6^{2+}$.

Electronic Charge Density Distribution

Twenty-four occupied molecular orbitals were obtained from the above calculation. To obtain the full electronic charge density, the 15 core orbitals of the calcium, left behind as unperturbed atomic orbitals in the EHMO approximation, had to be added. The electronic charge density may be expressed as

$$\rho(r) = \sum_{i(\text{occupied levels})} |\psi_i|^2$$

where ψ_i are atomic or molecular wave functions. To spherically the charge distribution, a surface $S(r)$ was drawn at a given distance r from the center of the muffin-tin sphere, 1/48 of it (because of the cubic symmetry) cut into a thousand elementary solid angles, and the amplitude of the wave functions evaluated at each elementary surface $dS(r)$. Finally, the sum of the properly weighted elementary contributions was obtained and the average electronic charge density at the position r determined. Figure 2 shows a plot of the resulting electronic charge density distribution.

Electronic Potential

Starting from the electronic charge density, the electronic potential $V_e(r)$ can be calculated from Poisson's equation

$$\nabla^2 V_e(r) = -4\pi e^2 \rho(r)$$

using a program from Loucks[8] as extended to include exchange contribution. The exchange contribution $V_{ex}(r)$ was treated in the Slater approximation[9]

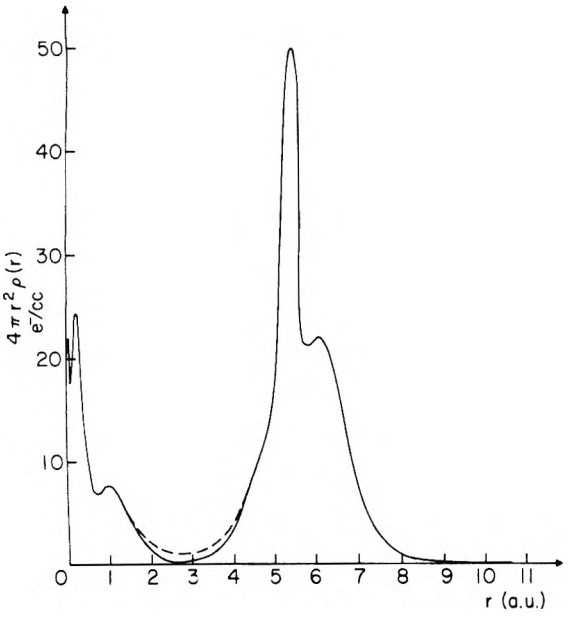

Figure 2. Radial electron density distribution in $Ca(NH_3)_6^{2+}$ (shown by solid curve) and in $Ca(NH_3)_6^{0}$ (shown by dashed curve).

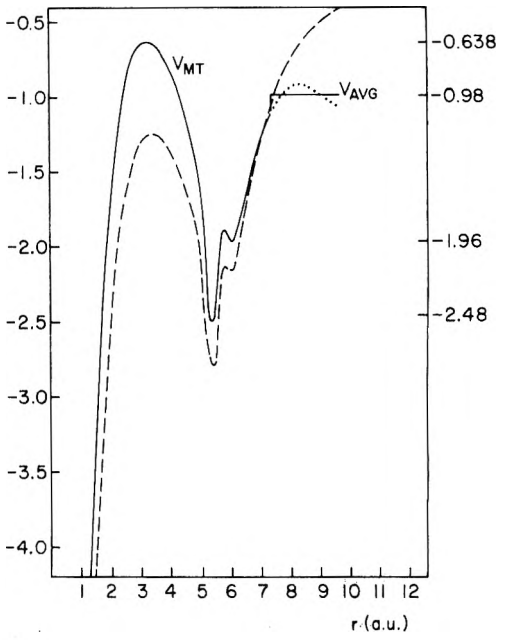

Figure 3. Potential curve for $Ca(NH_3)_6^{2+}$ ion (shown by dashed curve) and muffin-tin potential in bcc solid $Ca(NH_3)_6$ (shown by solid curve).

$$V_{ex}(r) = -6\left[\frac{3}{8\pi}\rho'(r)\right]^{1/3}$$

where $\rho'(r)$ is the crystal electronic density and differs from the atomic electronic density wherever the density from neighboring ions encroaches upon the particular muffin-tin sphere considered. The nuclear potential has the simple form

$$V_N(r) = -e^2\sum_i \frac{z_i}{r}$$

where z_i, the nuclear charge, is 20, 7, and 1 for Ca, N, and H, respectively. The nuclear potential was evaluated relative to the center of the muffin-tin sphere, then spherically averaged as for the electronic density.

The total potential for the $Ca(NH_3)_6^{2+}$ ion, obtained by summarizing $V_e(r)$, $V_{ex}(r)$, and $V_N(r)$, is shown (by the dashed curve) in Figure 3. Also shown in Figure 3 (full curve is the final form of the muffin-tin potential for solid $Ca(NH_3)_6$. Including a contribution for screening by conduction electrons and a correction for neighboring potential overlap, it can be written

$$V_{MT}(r) = V'(r) + \Delta V' - E_{ee} + \Sigma V'(a_i/r)$$

$V'(r)$ is the screened potential and can be derived from the unscreened potential, following Harrison,[10] as follows. If $W^0(r)$ is the sum of the potentials due to the positive ions $W^0(r) = \Sigma_j V(r - r_j)$ and $W^1(r)$ is the unknown potential due to the conduction electrons, then the total potential seen by the electrons is $W(r) = W^0(r) + W^1(r)$. Assuming the wave functions of the conduction electrons to be represented by plane waves, one may calculate the electronic density distribution by summing over all the occupied electron states. For a particular Fourier component, the electron density n_q can be expressed in terms of the total potential

$$n_q = -mk_F\frac{\langle \mathbf{k}+\mathbf{q}|W|\mathbf{k}\rangle}{2\pi^2\hbar^2}\left[\frac{1-\eta^2}{2\eta}\ln\left|\frac{1+\eta}{1-\eta}\right| + 1\right]$$

where $\eta = q/2k_F$, k_F is the Fermi wave number, and $\mathbf{k}$ and $\mathbf{q}$ are conduction electron wave vectors. Once we have the electron density in terms of the total potential, we may compute through Poisson's equation the screening potential in terms of the electron density

$$W_q^1 = \frac{4\pi e^2}{q^2}n_q$$

Elimination of n_q leads to

$$\langle \mathbf{k}+\mathbf{q}|W|\mathbf{k}\rangle = \langle \mathbf{k}+\mathbf{q}|W^0|\mathbf{k}\rangle/\epsilon(\mathbf{q})$$

with

$$\epsilon(\mathbf{q}) = 1 + \frac{me^2}{2\pi k_F\hbar^2\eta^2}\left[\frac{1-\eta^2}{2\eta}\ln\left|\frac{1+\eta}{1-\eta}\right| + 1\right]$$

where it may be noted that the screened potential may be derived from the unscreened potential by dividing with a simple function of wave number. The function $\epsilon(\mathbf{q})$, the static Hartree dielectric function for free electrons, goes to infinity as $\mathbf{q}$ becomes infinite, corresponding, respectively, to strong screening of long-wavelength and weak screening of short-wavelength components of the potential. In the final calculation, $\epsilon(\mathbf{q})$ is replaced by $\epsilon^*(\mathbf{q})$, where $\epsilon^*(\mathbf{q})$ is the Hartree dielectric function corrected for exchange and correlation between the conduction electrons. The latter correction can be made by adding to the screening potential a term X_q which, according to the treatment of Heine and Abarenkov,[11] has the form

$$X_q = \frac{-2\pi e^2}{q^2 + k_F^2 + k_S^2}$$

where k_S^{-2} equals half the square of the Thomas–Fermi screening length $k_{TF} = (6\pi n_0 e^2/\epsilon_F)^{-1/2}$. The final screened potential as a function of r has the form

$$V'(r) = \frac{\Omega}{2\pi^2}\int_0^\infty \frac{\langle \mathbf{k}+\mathbf{q}|V|\mathbf{k}\rangle}{\epsilon^*(\mathbf{q})}\frac{\sin \mathbf{qr}}{\mathbf{qr}}q^2\,dq$$

To compute it, we need to know, aside from $V(r)$, the value of k_F. For a bccub lattice, the volume of the first Brillouin zone is given by $V_{BZ} = (8\pi^3/\Omega_0) = 16\pi^3/a^3$ where Ω_0 is the

volume of the direct lattice primitive cell. Since for $Ca(NH_3)_6$ there are two electrons per primitive cell, and since each state can accommodate two electrons, the volume of the Fermi sphere will be given by

$$\frac{4\pi}{3}k_F^3 = \frac{16\pi^3}{a^3}$$

which leads to $k_F = 1.56(\pi/a)$, or 0.2855 au (atomic units). From k_F, we can determine $\epsilon^*(\mathbf{q})$ as a function of $\mathbf{q}$.

The correction term $\Delta V'$ represents the average potential due to the ions of valence z and the uniform background of conduction electrons. This average may be approximated[12] by the value computed for a uniform sphere of the molecular volume with z electronic charges, viz. $(-9/5)(ze^2/r_0)$, where r_0 is the radius of the molecular sphere. With $r_0 = (3\Omega_0/4\pi)^{1/3} = 8.45$ au and $\Omega_0 = 2544$ au^3, $\Delta V' = -0.8502$ Ry.

The correction term E_{ee} is needed because, by adding the electron-electron interaction and the Coulomb potential of the ions, we have computed the energy of each electron in the potential field of the ions and in the field of every other electron but, in so doing, we have counted the Coulomb interaction between any pair of electrons twice. The right measure may be reestablished by subtraction of an electron–electron interaction energy as given by

$$E_{ee} = \frac{\Omega_0}{8\pi e^2}\Sigma_q W_q^{1*} W_q^1 \cdot q^2$$

This extra term was evaluated to be +0.55 Ry.

The final correction term, that due to neighboring potential overlap, was obtained in a way described by Loucks[8] by expanding the neighboring potentials in spherical harmonics about the origin of the muffin-tin sphere. Since we had to retain only the spherically symmetric contributions, the expansion resulted in very simple form:

$$V'(a/r_2) = \frac{1}{2ar_2}\int_{|a-r_2|}^{a+r_2} r_1 V'(r_1)\, dr_1$$

which gives the contribution at distance r_2, measured from origin 2, due to the potential $V'(r_1)$ centered at origin 1, the two origins being separated by the distance a.

The required constancy of the muffin-tin potential between the muffin-tin spheres was determined by averaging the potential over the region between the muffin-tin sphere radius R and the Wigner–Seitz sphere radius R_{WS}.

$$V_{av} = 3\int_R^{R_{WS}} \frac{V_{MT}(r) r^2\, dr}{(R_{WS}^3 - R^3)}$$

With $R_{WS} = 8.45$ a and $R = 7.27$ au, V_{av} comes out to be -0.983 Ry. For convenience in the band structure calculation $V_{MT}(r)$ was set equal to zero at distances greater than the muffin-tin radius. Hence, in the discussion that follows, the potential was as follows:

$$U_{MT}(r) = V_{MT}(r) + 0.983 \qquad r < R$$
$$= 0 \qquad r > R$$

Band Structure Calculation

The calculation method was the Green function or KKR method. The two names derive from the Green function formalism and from Korringa,[13] Kohn, and Rostoker,[14] who first worked out the application. The procedure actually used, details of which are given elsewhere,[15] is essentially that of Segall and Ham.[16] Within the muffin-tin sphere, the assumption of spherical symmetry dictates a trial function of the form

$$\psi(r) = \sum_{l=0}^{l_{max}} \sum_j i^l C_{lj} R_l(r) Y_{lj}(r)$$

where $Y_{lj}(r)$ are linear combinations of spherical harmonics of angular momentum l, chosen so as to transform under the irreducible representations of the symmetry group of the wave vector $\mathbf{k}$ and, in addition, be normalized, real, and mutually orthogonal. The $R_l(r)$ are radial functions for the same energy E utilized in the construction of the Green function $G(\mathbf{r}, \mathbf{r}')$. The Green function has the form

$$G(\mathbf{r}, \mathbf{r}') = -\frac{1}{\tau'}\sum_n \frac{\exp[i(\mathbf{K}_n + \mathbf{k})\cdot(\mathbf{r} - \mathbf{r}')]}{(\mathbf{K}_n + \mathbf{k})^2 - E}$$

where τ' is the volume of the unit cell, $\mathbf{K}_n$ is a reciprocal lattice vector, and E is the energy eigenvalue for the Bloch function solution of the integral equation

$$\psi(\mathbf{r}) = \int_{\tau'} G(\mathbf{r}, \mathbf{r}') V(\mathbf{r}') \psi(\mathbf{r}')\, \delta\tau'$$

This integral equation is equivalent to the variational principle $\delta\Lambda = 0$ with

$$\Lambda = \int_\tau \psi^*(\mathbf{r}) V(\mathbf{r}) \psi(\mathbf{r})\, \delta\tau - \int_\tau \int_{\tau'} \psi^*(\mathbf{r}) V(\mathbf{r}) G(\mathbf{r}, \mathbf{r}') V(\mathbf{r}') \psi(\mathbf{r}')\, \delta\tau\, \delta\tau'$$

The conditions $\delta\Lambda/\delta dC_{lj} = 0$ lead to a set of linear equations which give a nontrivial solution if the determinant $\Lambda_{lj,l'j'}$ is zero. The secular equation has a very simple form if expressed in terms of the scattering phase shifts η_l of the muffin-tin potential.

$$\det\{B_{lj,l'j'} \tan \eta_{l'} + K\delta_{ll'}\delta_{jj'}\} = 0$$

Roots of this determinant, where $K = E^{1/2}$ for $E > 0$ and $i(-E)^{1/2}$ for $E < 0$, approach quite closely to the eigenvalues $E(\mathbf{k})$ of the Bloch-function Schrödinger equation, provided the expansion of the trial function is carried to sufficiently large values of l_{max}. According to Segall and Ham, convergence is extremely good and $l_{max} = 2$ is sufficient, at least for crystals built up from elements belonging to the top half of the periodic table. For the heavier elements, in order to account for states generating from or hybridizing with f levels, they recommend extending the expansion up to $l_{max} = 3$. As noted below, in the case of $Ca(NH_3)_6$, convergence of the KKR method requires expansion up to $l_{max} = 4$ at least.

The parameter $B_{lj,l'j'}$ is a function of structure constants which are evaluated by use of an Ewald procedure that includes summations in both coordinate and reciprocal space. A structure constant program written for an fccub lattice by Dr. Edwin Pollock was adapted to a bccub lattice in this work and extended at the Γ point (center of the Brillouin zone), at the point H[$\mathbf{k} = (1, 0, 0)$], at the point N[$\mathbf{k} = (1, 1, 0)$], and at the point P[$\mathbf{k} = (1, 1, 1)$], to include structure constants up to $L = 8$. Details of the program as well as of that utilized to calculate the phase shift tangents are given elsewhere.[15] Figure 4, which shows the variation of phase shift tangent with energy, indicates that the convergence appears to be less rapid than usual. Since $\tan \eta_l$ determines how far the eigenvalues deviate from their free-electron analog, there may be a problem arising from premature truncation of the wave function expansion.

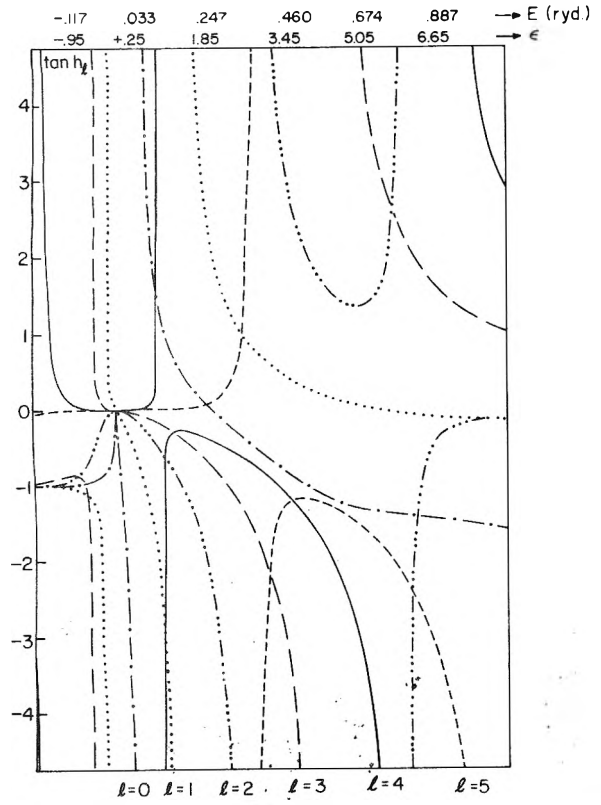

Figure 4. Tangents of the phase shifts vs. energy for $l = 0$ (–·–·), $l = 1$ (···), $l = 2$ (–···), $l = 3$ (– – –), $l = 4$ (——), and $l = 5$ (- - -).

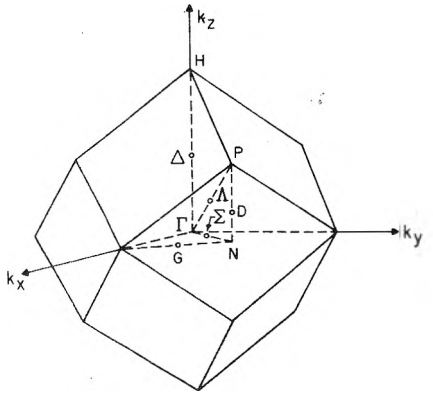

Figure 5. First Brillouin zone of the bccub lattice with symmetry points and axes as shown.

The first Brillouin zone of the bccub lattice, together with the designations of the symmetry points and the symmetry directions, is as shown in Figure 5. In the direction Δ([100]axis), the distance ΓH is $2\pi/a$; along Λ([111] axis), ΓP is $1.732\pi/a$; along Σ([110] axis), ΓN is $1.414\pi/a$. As noted above, the Fermi wave number $\mathbf{k}_F$ is $1.56\pi/a$, so on a free-electron basis one might expect some spill-over of the Fermi sphere into the second Brillouin zone and possibly formation of hole pockets around the point H.

In the free-electron limit (i.e., when the periodic potential of the lattice structure is made arbitrarily weak while the symmetry properties of the wave functions are preserved) the energy bands of the bccub structure are as shown in Figure 6. These have been calculated following the procedure of Callaway.[17] The energy roots at the symmetry points have been labeled according to the symmetry

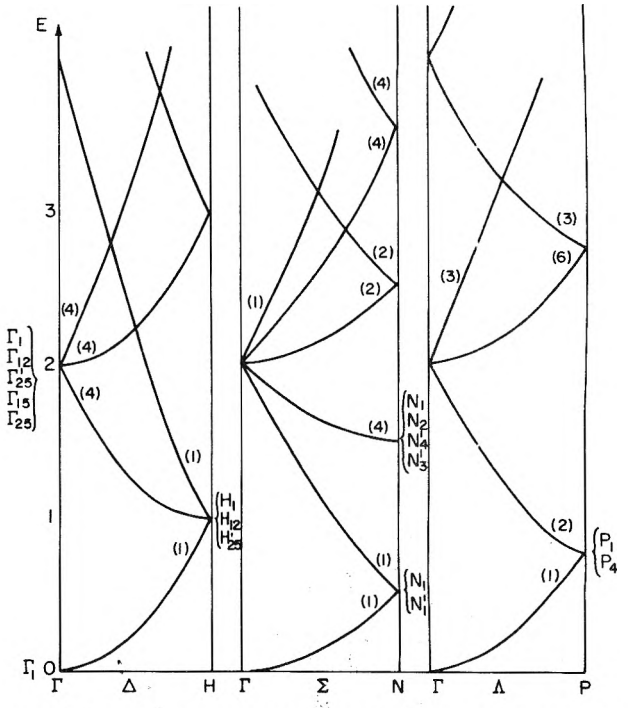

Figure 6. Free electron bands in the bccub lattice. Energy scale is in units of $4\pi^2/a^2$, which for $Ca(NH_3)_6$ is 0.133 Ry.

of the wave function at these points.[18] The parenthetical numbers on the curves are the degeneracies. Introduction of the $Ca(NH_3)_6$ periodic potential lifts some of the degeneracy and changes the band structure. Successive calculations were performed first up to $l_{max} = 2$ for values of $\mathbf{k}$ along Δ, Σ, Λ and at the symmetry points Γ, H, N, and P and then for $l_{max} = 3$, $l_{max} = 4$ at the symmetry points Γ, H, N, and P. As shown in Figure 7, calculations carried out to $l_{max} = 2$ along Δ, Σ, Λ and at Γ, H, N, P gave rise to fictitious bands corresponding to $l = 3$, generated from mixing terms of order $l = 2$ and $l = 1$ or corresponding to $l = 2$, generated from mixing terms of order $l = 0$ and $l = 2$. Table I gives the results for points Γ, H, N, and P up to $l_{max} = 2$, $l_{max} = 3$, and $l_{max} = 4$, respectively. For Γ, H, and N, extension to $l_{max} = 3$ readjusted the roots corresponding to $l = 1$ (Γ_{15}, H_{15}, H_2', N_3'), whereas extension to $l_{max} = 4$ corrected the roots corresponding to $l = 0$ (Γ_1, H_1, N_1) and $l = 2$ (Γ_{12}, Γ_{25}', H_{12}, H_{25}', N_2) and generated the pure $l = 3$ state (Γ_{25}). At point P, where $l = 1$, $l = 2$, $l = 3$, and $l = 4$ states are admixed together, both P_1 and P_4 were perturbed by extension to $l_{max} = 3$ and $l_{max} = 4$. Inasmuch as the domain of importance for tan η_l shifts toward higher energies as l increases (see Figure 4), components in $l > 4$ are not expected to come into play, at least for the lowest bands.

From the results of the above calculations, the first band in $Ca(NH_3)_6$ solid is expected to have roughly the features shown in Figure 8.

Discussion

According to the calculations carried out to $l_{max} = 4$, the first band along the Δ axis (Δ_1 in Figure 8) should connect Γ_1 to H_{12}. Furthermore, if there is not much distortion from the free-electron band (Figure 6), we would expect along Δ a band width of 0.108 Ry. The next band, a Δ_2 band, would join H_{12} or H_{15} to Γ_{25}; to be specific, one would need more points along that direction. In any case, if a

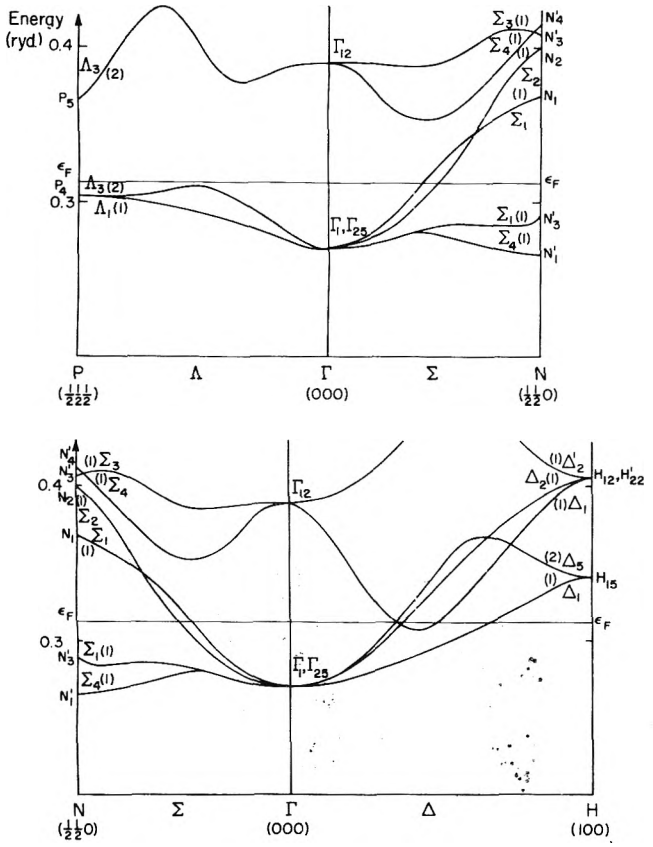

Figure 7. Electronic bands in $Ca(NH_3)_6$ solid as calculated by expansion up to $l_{max} = 2$.

TABLE I: Energy Eigenvalues (in Rydbergs) at the Points Γ, H, N, and P for $Ca(NH_3)_6$ Solid up to Order $l = 2$, $l = 3$, $l = 4$

	$l_{max} = 2$	$l_{max} = 3$	$l_{max} = 4$
Γ_1	0.269	0.269	0.302
	0.571	0.571	
Γ_{15}	0.522	0.674	0.674
Γ_{12}	0.39	0.39	0.720
	0.746	0.746	
Γ_{25}'	0.648	0.648	0.682
Γ_{25}			0.579
H_1	0.437	0.437	
H_{15}	0.342	0.452	0.452
	0.660	0.660	0.660
H_{12}	0.406	0.406	0.410
H_{25}'	0.570	0.570	
N_1'	0.266	0.300	0.300
	0.458	0.447	0.447
N_3'	0.290	0.352	0.352
	0.408		
N_1	0.367	0.367	0.346
			0.391
N_2	0.397	0.397	0.369
			0.454
N_4'	0.409	0.409	0.386
	0.436	0.436	
P_4	0.304	0.392	0.468
P_1	0.420	0.330	0.378

Fermi energy of 0.044 Ry (0.61 eV), as derived from magnetic susceptibility measurements,[4] is not unreasonable, then we should not expect a second band close to the Fermi level in the Δ direction. Along the Λ direction, a free-electron-like band connecting Γ_1 to P_1 would give a width of

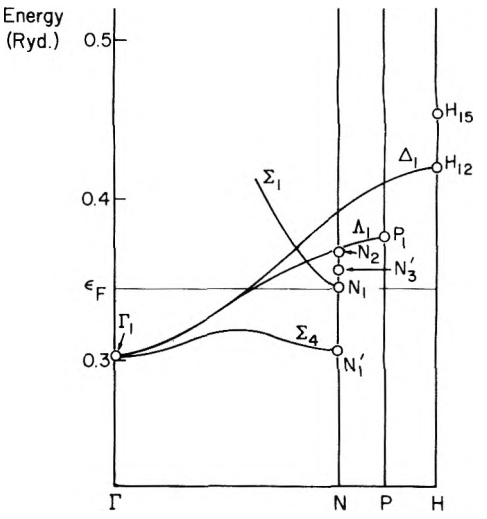

Figure 8. Electronic band structure in $Ca(NH_3)_6$ solid as deduced from calculations up to order $l = 4$ at the symmetry points Γ, H, N, and P.

0.076 Ry, and a very large bandgap should exist between the first band and the next one starting at the point P_4 situated 0.09 Ry above P_1. We note that the features of the first band around the Fermi energy level appear very similar in the directions Δ and Λ. In order to be more explicit, one would need to calculate the electronic energies between the symmetry points N, P, and H. However, consideration of only the symmetry points makes us anticipate a behavior of the solid drastically different along the Σ direction compared to the Δ and Λ directions. Indeed we find below the Fermi level a very flat band Σ_4 joining the Γ_1 state to the p-like state N_1' and a second band Σ_1 starting at the point N_1 situated at an energy about equal to the Fermi level. The Fermi surface must then deviate sensibly from a sphere. If the Fermi energy level intersects the Σ_1 band, electron pockets should be generated around the point N. Confirmation of our results could be afforded by measurements (conductivity, Hall effect, magnetic susceptibility) on monocrystals of $Ca(NH_3)_6$ solid. In order to interpret the anomalous thermal behavior of the magnetic susceptibility and conduction electron spin resonance observed on polycrystalline $Ca(NH_3)_6$ solid, one should extend the present calculation to include all the **k** vectors and derive the density of states.

In conclusion, a comparison might be noted between our M–NH_3 system and the elements Ca, Sr, and Ba. The electronic band structure of these elements has been calculated[19] for the fccub phase as a function of atomic volume up to 60% compression. The band structure, which appears nearly free-electron-like, is dominated near the Fermi level by admixture of d components, the effect increasing with pressure and from Ca to Ba. Figure 8 suggests that an analogous effect has occurred on introduction of the ammonias into the Ca lattice, since H_{12}, a d-like state, has descended below H_{15} and H_1 and the p-like state N_1' has been shifted down. Such an effect could be rationalized by considering that the ammonia lone-pair electrons, by donation to the empty 3d, 4s, and 4p states of the Ca, cause these states to depress so that the 4s and 4p states, which are partially filled, descend below the Fermi level and the partially filled d states merge at the Fermi level.

NOTE ADDED IN PROOF. Data presented elsewhere in this symposium suggest that $Ca(NH_3)_6$ has bond distances

different from those used above. However, changes in H positions do not affect the major conclusion that expansion needs to be carried out to higher order than in normal metals. The new neutron data are difficult to accept on a simple chemical basis and raise a question as to the chemical identity of the sample investigated.

Acknowledgment. We wish to thank the National Science Foundation, the Air Force Office of Scientific Research, and the Materials Science Center of Cornell University for their support of this research. We are grateful to Professor Roald Hoffmann and his research group for use of their EHMO programs, to Doctor Edwin Pollock for use of his structure constant program, and to Professor Neil Ashcroft and Doctor Pierre Pfeuty for their encouragement and advice in carrying out this work. We also wish to thank Professor Hans Nowotny of the Institut für Physikalische Chemie, Universität Wien, for his kind hospitality to one of us (M.J.S.) during the time this report was prepared.

References and Notes

(1) This research was sponsored by the National Science Foundation under Grant No. GP-17706 and was supported in part by the Air Force Office of Scientific Research and the Materials Science Center at Cornell University.
(2) A review of metal–ammonia compounds has been given by N. Mammano in "Metal-Ammonia Solutions", Colloque Weyl II, J. J. Lagowski and M. J. Sienko, Ed., Butterworths, London, 1970, pp 367–393.
(3) W. S. Glaunsinger, S. Zolotov, and M. J. Sienko, *J. Chem. Phys.*, **56**, 4756 (1972).
(4) T. David, P. Damay, and M. J. Sienko, *J. Chem. Phys.* **62**, 1526 (1975).
(5) W. Glaunsinger and M. J. Sienko, *J. Chem. Phys.*, **62**, 1873, 1883 (1975).
(6) F. W. Cagle and H. J. Holland, presented at the 145th National Meeting of the American Chemical Society, New York, Sept 1963.
(7) R. Hoffman, *J. Chem. Phys.*, **39**, 1397 (1963).
(8) T. L. Loucks, "Augmented Plane Wave Method", W. A. Benjamin, Reading, Mass., 1966.
(9) J. C. Slater, *Phys. Rev.*, **81**, 385 (1951).
(10) W. A. Harrison, "Pseudopotentials in the Theory of Metals", W. A. Benjamin, Reading, Mass., 1966, p 46.
(11) V. Heine and I. Abarenkov, *Phil. Mag.*, **9**, 451 (1964).
(12) Reference 10, p 275.
(13) J. Korringa, *Physica*, **13**, 392 (1947).
(14) W. Kohn and N. Rostoker, *Phys. Rev.*, **94**, 111 (1954).
(15) Thérèse David, Ph.D. Thesis, Cornell University, 1974.
(16) B. Segall and F. S. Ham, *Methods Comput. Phys.*, **8**, 251 (1968).
(17) J. Callaway, "Energy Band Theory", Academic Press, New York, N.Y., 1964, p 9.
(18) H. Jones, "The Theory of Brillouin Zones and Electronic States in Crystals", North-Holland Publishing Co., Amsterdam, 1960, p 116.
(19) B. Vasvari, A. O. E. Animalu, and V. Heine, *Phys. Rev.*, **154**, 535 (1967).

Discussion

J. THOMPSON. What do you believe would be the effect on the electrical resistivity of sphericalizing the potential of $Ca(NH_3)_6$?

M. J. SIENKO. I do not know. Sphericalizing was the only way we could handle the computation problem. We did find that trying various positions of the hydrogen atoms did not seem to make much difference in the energy band eigenvalues. However, changing the Ca–N distance did.

A Neutron Diffraction Study of Hexaammine-d_3-calcium(0) at 75 K[1]

R. B. Von Dreele,* W. S. Glaunsinger

Department of Chemistry, Arizona State University, Tempe, Arizona, 85281

A. L. Bowman, and J. L. Yarnell

Los Alamos Scientific Laboratory, Los Alamos, New Mexico, 87544 *(Received July 28, 1975)*

The structure of $Ca(ND_3)_6$ was determined by powder neutron diffraction at 75 K. The atomic parameters were refined by least-squares fitting of the diffraction profile. $Ca(ND_3)_6$ crystallizes in the space group $Im3m$ with $a = 9.0137(4)$ Å and $Z = 2$. The standard profile residual was 0.109 for eight parameters and a profile range $10° \leq 2\theta \leq 50°$ for $\lambda = 1.27963$ Å. $Ca(ND_3)_6$ has highly distorted ND_3 molecules arranged in an exact octahedron around the Ca atoms with fourfold rotational disorder for each ND_3. The Ca–N distance is 2.69 Å. One N–D bond is normal, 0.94 Å, while the other two are extremely long, 1.39 Å. There is no hydrogen bonding in the structure and virtually all nonbonded contacts are greater than van der Waals distances.

Introduction

Previous investigations of the alkaline earth and lanthanide metal–liquid ammonia systems showed that a hexammine metal [$M(NH_3)_6$, M = Ca, Sr, Ba, Eu, and Yb] compound was formed and that it had unusual metallic properties similar to those of $Li(NH_3)_4$.[2-5] X ray powder diffraction studies[6,7] of these compounds indicated that they have a body-centered cubic structure which is maintained down to at least 77 K. However, because of the high scattering power of the metal atoms, these studies could not establish in detail the structural arrangement of the ammonia molecules. It is clear that this detailed structural information for these compounds is required before their properties can be understood, therefore we have performed a neutron powder diffraction analysis of one of the hexam-

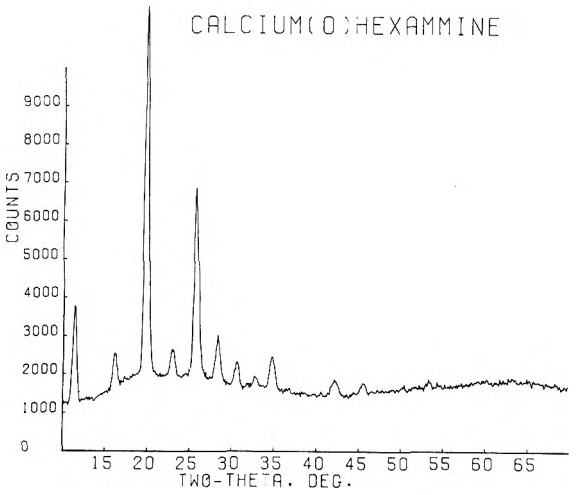

Figure 1. Neutron powder diffraction pattern for $Ca(ND_3)_6$ taken at 75 K.

mines, $Ca(ND_3)_6$, to establish the structure and thermal motion of the ammonia molecules at 75 K.

Experimental Section

Sample Preparation. Deuterated ammonia was prepared by allowing sodium cyanide to react with deuterated water at 140°C for 1 hr in a 75-ml stainless steel bomb capable of withstanding 300 atm.[8] The ND_3 thus prepared was dried and purified by repeated distillation onto sodium metal. A $Ca(ND_3)_6$ sample for neutron diffraction was prepared by distilling a stoichiometric quantity of ND_3 onto freshly cut calcium metal placed in a specially cleaned[9] 2 × 4 cm cylindrical quartz ampule. The ampule was sealed off and allowed to warm to room temperature to ensure complete reaction. This sample showed no visible signs of decomposition during the preparation and subsequent neutron data collection.

Neutron Data Collection. Neutron powder diffraction data (Figure 1) were collected at 75 K on a modified triple-axis diffractometer at the Omega West Reactor, Los Alamos Scientific Laboratory. A mean neutron wavelength of 1.27963(8) Å was obtained by reflection from the (220) planes of a Cu monochromator at a $2\theta_m$ of 60°. The flux at the sample was $\sim 10^5$ n cm^{-2} sec^{-1}. The wavelength was calculated from the diffraction pattern of a NbO standard; these diffraction peaks were accurately Gaussian in shape. The sample was cooled by conduction in the tail of a liquid nitrogen Dewar. (Liquid nitrogen boils at 75 K under ambient pressure at Los Alamos, New Mexico.) The data were collected over the range $10.0 \leq 2\theta \leq 70.0°$ in steps of $0.10°2\theta$.

The counting time at each step was determined by the time required for an incident beam monitor count of 100K obtained with a fission counter. Absorption and extinction effects proved to be negligible and no corrections were necessary. Since the peaks were completely resolved, background corrections were made at points bracketing each peak with a linear interpolation across the base of each peak. The observed background can be entirely ascribed to scatter from the quartz sample tube.

Structure Analysis and Refinement. Since both the observed neutron diffraction pattern (Figure 1) and the x-ray results indicate a body centered structure with two $Ca(ND_3)_6$ molecules per cell,[6] only the space groups $Im3$, $Im3m$, $I23$, and $I43m$ are compatible with this result. The

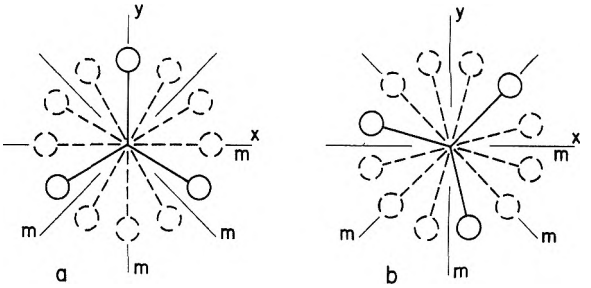

Figure 2. View down the Ca–N bond (z axis) showing the disposition of the disordered ND_3 molecules for model a and model b. The lines marked m denote the positions of the mirror planes for the space group $Im3m$.

two noncentrosymmetric space groups $I23$ and $I43m$ were rejected because they required a disorder of the ammonia molecules which leads to a set of positions very nearly the same as those for the centrosymmetric space groups $Im3$ and $Im3m$, respectively, and hence would be indistinguishable from them. A plausable model in the space group $Im3$ was subsequently shown to give a poorer refinement than the same model in $Im3m$ and that space group was also rejected.

Two models (Figure 2) for the orientation of a disordered ammonia molecule in the space group $Im3m$ were developed and refined. In both models the Ca atoms are in fixed positions at the origin and body center of the cell surrounded by an exact octahedron of nitrogen atoms. The nitrogen atoms are in the 12 e special positions $(0, 0, Z)$ with one variable coordinate. One deuterium atom occupies for 25% of the time the special position 48j $(0, Y, Z)$ for the first model (Figure 2a) and 48k (X, X, Z) for the second model (Figure 2b). In both models the two other deuteriums are accommodated in a general position with 50% occupancy placed such that the threefold symmetry of the ammonia molecule is maintained. Thus both models have a fourfold rotational disorder of the ammonia molecules with the ND_3 in the second model rotated 45° from the first.

These models were refined by a least-squares fitting of the diffraction profile, the details of which are described elsewhere.[10,11] The computer program used in this analysis enabled the use of some simple constraints which allowed the testing of models of varying complexity. (A modified version of a Fortran program written by H. M. Rietveld was used in this analysis.) Since the diffraction pattern shows no identifiable peaks above $2\theta = 50°$ only the data in the range $10° \leq 2\theta \leq 50°$ was used in the analysis.

Initially the position of the idealized ND_3 molecule was refined for the two models (three parameters). The ND_3 molecule was oriented with its threefold axis coincident with the Ca–N bond. Both models gave identical results with a diffraction profile residual[11] Rp = 0.248, a weighted profile residual[11] Rpw = 0.272, and a Ca–N distance of 2.45 Å for the first model and Rp = 0.249, Rpw = 0.272, and a Ca–N distance of 2.46 Å for the second model. The two models had virtually identical overall temperature factors at 7.5 and 7.3 $Å^2$, respectively. A much better refinement for both models resulted when two additional parameters, which in effect describe the N–D bond distance and the Ca–N–D bond angle, were allowed to vary; the threefold symmetry of the ND_3 molecules was still maintained. For the first model an N–D distance of 1.18 Å, a Ca–N distance of 2.78 Å, and a Ca–N–D angle of 83.8° was obtained with Rp = 0.155 and Rpw = 0.147. The second model gave ex-

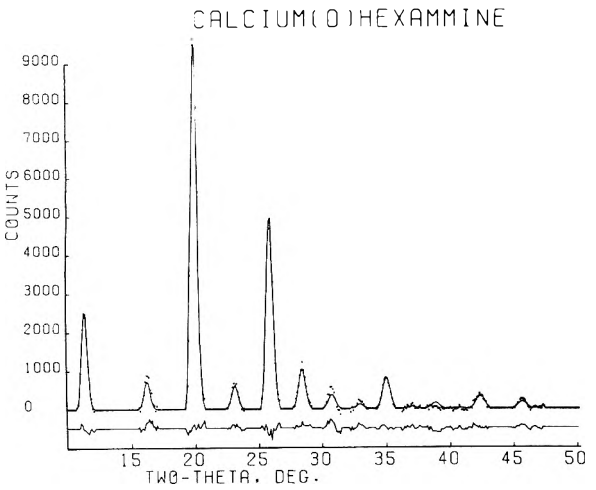

Figure 3. Observed and calculated neutron powder diffraction profile from least-squares refinement of $Ca(ND_3)_6$. The points are the observed intensities corrected for background and the solid line is the calculated diffraction profile. A difference curve is also shown.

TABLE I: Atomic Positions for Hexaammine-d_3-calcium(0)[a]

Atom	x	y	z
Ca	0	0	0
N	0	0	0.298 (2)
D1	0	0.100 (4)	0.328 (6)
D2	0.130 (2)	−0.082 (2)	0.286 (2)

[a] Value in parentheses is the estimated standard deviation in the last significant figure.

actly the same results with a N–D bond length of 1.16 Å, a Ca–N bond of 2.77 Å, and a Ca–N–D angle of 84.1° for the residuals Rp = 0.159 and Rpw = 0.147. The temperature factors remained unchanged for this refinement and was 7.4 Å^2 for both models. A further significant improvement was obtained for the first model when the positions of each deuterium atom were allowed to refine independently (eight parameters) to give the residuals Rp = 0.109 and Rpw = 0.098. This breaks the threefold symmetry of the ND_3 molecules. The attempt to refine the second model in the same way failed because the two deuterium atoms in the general position moved toward the special position 48j occupied in the first model whereupon the least-squares diverged. Because of this result, it seems clear that the first model more properly represents the distribution of deutrium atoms in the structure and it will be discussed below.

Three other structural models were also refined. A model based on the first positional model with individual temperature factors for the atoms showed no change in the residuals despite large changes in the temperature factors from the average value. Clearly, there is not enough diffraction data to be able to refine individual temperature factors. Another model which was a composite of both positional models was also refined. In this model the angular relationship of the deuterium atoms to each other was fixed while effectively allowing the N–D distance and the Ca–N–D angle for each to vary. This refinement did not significantly reduce the residuals from those obtained from the best refinement of the first positional model. This result suggests that the first positional model better represents the true structure rather than a completely disordered model or one in which there is unhindered free rotation of the ammonia molecules about the Ca–N bond. A third model in which half of the possible positions in the first positional model

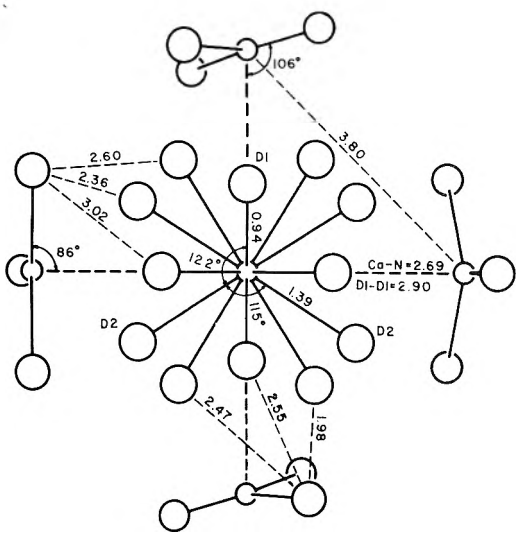

Figure 4. A perspective representation of the structure of $Ca(ND_3)_6$. One disordered ND_3 molecule is shown with four adjacent ND_3 molecules each in one of their possible orientations. A number of interatomic distances and angles are also shown.

was occupied according to the space group $Im3$ was refined and gave higher residuals than the best refinement in $Im3m$. Because of the restrictions imposed by the space group $Im3$, it requires a high correlation of possible disorder positions for neighboring ammonia molecules. There are no restrictions for the space group $Im3m$; this result is consistent with the fact that nearly all the nearest neighbor contacts between ammonia molecules are greater than the van der Waals distance regardless of their orientation.

Results and Discussion

The observed and calculated neutron powder diffraction profile intensities from the best refinement of the first positional model for $Ca(ND_3)_6$ are shown in Figure 3. A difference curve is also shown. The atomic coordinates obtained in this refinement are given in Table I along with the estimated standard deviations given by the least-squares analysis. Drawings showing the relative positions of the ammonia molecules about the calcium atom are shown in Figure 4. Pertinant bond lengths and angles are shown on this drawing. The lattice parameter obtained in this analysis is a_0 = 9.0137(4) Å at 75 K.

The most striking feature of the structure of $Ca(ND_3)_6$ is the considerable distortion of the ammonia molecule. The principal distortion is an elongation of two of the N–D bonds to 1.39 Å; the third N–D bond, 0.94 Å, is essentially normal as compared to N–D bonds of 1.00 Å found[12] in solid ND_3. In addition, these ammonia molecules are much flatter with D–N–D angles of 122 and 115° as compared to solid ND_3 where the D–N–D angles are 110°. This makes the D–D distances in each molecule much longer, 2.05 and 2.35 Å, than in normal ND_3, 1.65 Å. These results are entirely consistent with the very narrow proton NMR linewidths observed[13] for $Ca(NH_3)_6$ and $Ba(NH_3)_6$. The reduction in dipolar coupling by the long N–D bonds and long D–D distances along with the indicated thermal motion provides a complete explanation of the line widths. These effects will be discussed in more detail in the accompanying paper.[13]

Although the ammonia molecules are coordinated to the calcium via the nitrogen, the pseudotrigonal axis of each ammonia is not coincident with the Ca–N bond but makes

an angle of 13° with it. As a result the Ca–N–D bond angles are quite different. The angle for the normal N–D bond is 106° which is close to the ideal tetrahedral angle of 109.5° but the two long N–D bonds are very nearly at right angles, 86°, to the Ca–N bond. The Ca–N distance is 2.69 Å which is greater than the sum of the Ca metallic radius[14] of 1.736 Å and the N tetrahedral covalent radius[15] of 0.70 Å. It is also longer than the Ca–NH_2R coordinate bonds, 2.59 Å, found[16] in the eight-coordinate compound, $Ca(NH_2NHCOO)_2 \cdot H_2O$. The high degree of thermal motion, $B_{ov} = 7.7(6)$ Å^2, as is evident in the rapid fall-off of intensity in the neutron diffraction pattern is consistent with the disorder required by the space group $Im3m$. A consideration of the possible intermolecular D–D contacts show that a pair of adjacent ND_3 molecules are in contact, 1.98 Å, for only one of the positions allowed for each as compared to the van der Waals contact distance. This one restriction in the relative positions of the ND_3 molecules would prevent completely free rotation about the Ca–N bond hence the deuterium atoms are found in fixed but disordered positions. However, it does appear from the narrow proton NMR line observed at this temperature[13] that the ammonia molecules are undergoing hindered rotation or tunneling which is also consistent with these results. The intramolecular contacts between $Ca(ND_3)_6$ groups are all much greater than the van der Waals distances regardless of the orientation of any of the ND_3 molecules. There appears to be no hydrogen bonding in this structure, the closest nonbonded N- - -D distance is 3.08 Å.

References and Notes

(1) Work supported in part by the United States Energy Research and Development Administration (ERDA).
(2) (a) E. W. Lemaster and J. C. Thompson, *J. Solid State Chem.*, **4**, 163 (1972); (b) M. D. Rosenthal and B. W. Maxfield, *ibid.*, **7**, 109 (1973).
(3) W. S. Glaunsinger, S. Zolotov, and M. J. Sienko, *J. Chem. Phys.*, **56**, 4756 (1972).
(4) T. David, W. S. Glaunsinger, S. Zolotov, and M. J. Sienko, "Electrons in Fluids", Colloque Weyl III, J. Jortner and N. R. Kestner, Ed., Springer-Verlag, New York, N.Y., 1973, pp 323–339.
(5) W. S. Glaunsinger and M. J. Sienko, *J. Chem. Phys.*, **62**, 1873 (1975).
(6) N. Mammano and M. J. Sienko, *J. Solid State Chem.*, **1**, 534 (1970).
(7) F. W. Cagle and H. J. Holland, presented at the 145th National Meeting of the American Chemical Society, New York, N.Y., Sept 1963.
(8) U. Schindewolf, "Metal-Ammonia Solutions", Colloque Weyl II, J. J. Lagowski and M. J. Sienko, Ed., Butterworths, London, 1970, pp 495–496.
(9) S. Naiditch and J. E. Wreede, *J. Vac. Sci. Technol.*, **5**, 54 (1968).
(10) H. M. Rietveld, *Acta Crystallogr.*, **22**, 151 (1967).
(11) H. M. Rietveld, *J. Appl. Cryst.*, **2**, 65 (1969).
(12) J. W. Reed and P. M. Harris, *J. Chem. Phys.*, **35**, 1730 (1961).
(13) R. F. Marzke and W. S. Glaunsinger, *J. Phys. Chem.*, this issue.
(14) L. Pauling, "The Nature of the Chemical Bond", Cornell University Press, Ithaca, N.Y., 1960, p 403.
(15) L. Pauling, ref 14, Chapter 7.
(16) A. Bralbanti, A. M. M. Lanfredi, M. A. Pellinghelli, and A. Tiripicchio, *Acta Crystallogr., Sect. B*, **27**, 2261 (1971).

Discussion

M. J. SIENKO. What would be the effect on the neutron diffraction results of a rotation or an oscillation of the ammonia group about an axis that is not the Ca–N axis? Could that account for the apparent two N–D bond lengths?

R. VON DREELE. Any oscillation or rotation of a normal ammonia molecule about an axis that passes through or near the nitrogen, i.e., near the center of mass, will not result in longer apparent N–D distances. If anything the N–D distances in this situation would appear to be shorter than they actually are. In any case, for the degree of thermal motion indicated in this structure such corrections would be of the order of 0.01 Å or less.

W. GLAUNSINGER. Experimental evidence in favor of the structure of the ammonia molecule in $Ca(NH_3)_6$ derived from our neutron diffraction study is provided by the observed low-temperature proton NMR line width in $Ca(NH_3)_6$. Making the reasonable assumption that the intramolecular contribution to the proton line width is dominant and that the hydrogen atoms in an ammonia molecule tunnel rapidly at low temperatures, for the observed Gaussian line shapes the calculated line width is about 6 G for the conventional NH_3 molecule and about 2 G for the NH_3 geometry found by neutron diffraction. The experimental line width of about 2 G at 50 K in $Ca(NH_3)_6$ is in very good agreement with our proposed neutron-diffraction structure.

I would like to point out that further evidence for the unusual ammonia-molecule geometry found in our neutron diffraction study could be obtained by investigating the N–H stretching region for the ammonia molecules in $Ca(NH_3)_6$.

A Neutron Diffraction Study and Phase Diagram Investigation of the Solid Lithium–Ammonia Compound

P. Chieux,

Institut Laue Langevin, Grenoble, France

M. J. Sienko,*

Cornell Universtly, Ithaca, New York 14853

and F. DeBaecker

Laboratoire de Chimie Physique, Lille, France *(Received July 30, 1975)*

Publication costs assisted by the National Science Foundation

Low-temperature neutron-diffraction experiments have been carried out on the lithium-deuterated ammonia system in the vicinity of $Li(ND_3)_4$. In all the samples, there was observed a strong background scattering similar to that displayed by the liquid, suggesting either highly strained regions or coexistence of an amorphous phase with the solid compound. The structure of the compound at 3 K was indexed as bccub with $a_0 = 14.80 \pm 0.01$ Å; at 85 K, $a_0 = 15.03$ Å. No phase change was observed in the interval 60–85 K. Partial results are also presented for the $Li–NH_3$ compound, where significant changes were observed in the neutron diffraction patterns between 60 and 85 K. Low temperature DTA on a 20 mol % $Li–ND_3$ sample showed a thermal effect at 27 ± 5 K, which may be related to appearance of a few additional neutron diffraction lines in all the $Li–ND_3$ samples below 30 K.

Ammonia forms compounds with the alkali element lithium, the alkaline earth elements Ca, Sr, Ba, and the rare earth elements Eu and Yb.[1] The compounds are of special interest because they are metallic, are apparently composed of only ammoniated cations at the lattice points, and are relatively low in electron density compared to normal metals. The last point may be especially important as these materials may be on the verge of the metal–nonmetal transition.

The lithium compound, $Li(NH_3)_4$, has been the one most extensively studied. From x-ray powder studies at 77 K, Mammano and Sienko[2] suggested that the solid compound exists in two phases: a cubic form with $a_0 = 9.55$ Å, stable between 82.2 and 88.8 K, and a hexagonal form having $a = 7.0$ Å and $c = 11.1$ Å, stable below 82.2 K. Kleinman et al.[3] also performed x-ray measurements at 77 K and found $a = 7.12$ Å and $c = 11.29$ Å. Both sets of investigators found the same c/a ratio (1.585) for the hexagonal phase.

The magnetic susceptibility of $Li(NH_3)_4$ shows typical Pauli–Peierls metallic behavior in the cubic phase between 82 and 89 K but a surprisingly strong temperature dependence below 82 K and a flattening out below 10 K.[4] The apparent appearance of localized moments below 82 K, and their possible antiferromagnetic coupling below 10 K, was the driving motive behind this investigation. It was believed that neutron diffraction study might disclose the ordering of magnetic moments. However, because of the large incoherent scattering by protium atoms, it was not possible to examine $Li(NH_3)_4$. Therefore, $Li(ND_3)_4$ was investigated instead.

I. The Experimental Setup

(*a*) *The Spectrometer.* The experiments were performed on the D1B Spectrometer of the Institut Laue Langevin (Grenoble). The spectrometer is installed on a thermal neutron guide-tube (see Figure 1). A pyrolytic graphite monochromator gives a wavelength λ of 2.398 Å. A graphite filter prevents higher order contamination. The detection is assured by a BF_3 Multidetector. Two different multidetectors were employed for our work, covering respectively 60 or 80 angular degrees (i.e., 300 or 400 cells of 0.2° steps). The detection efficiency is about 60% at λ 2.4 Å. The resolution accessible $\Delta d/d$ is at best 0.8%. Two detector positions were generally used in order to cover 100° (or 120°) of scattering angle. The relative efficiency of each cell was always calibrated from a vanadium run and stayed constant to 3% over several days. A typical run took from 1 to 6 hr.

(*b*) *The Cryostat.* A variable-temperature liquid helium cryostat was employed for all the experiments. Cold helium gas was continuously pumped from the liquid helium reservoir into the cryostat tail through a sintered metal disk. The helium gas temperature was monitored and stabilized to better than 0.1°C. The quartz sample container was inserted in a 0.04-mm-thick vanadium sample holder. The temperature of the sample holder was recorded independently. The 20-mm diameter cryostat tail was also made out of a vanadium foil (0.2-mm thick). Since vanadium is essentially an incoherent scatterer, perturbing Bragg peaks are absent. The aluminum external wall of the cryostat as well as an aluminum thermal screen kept at liquid nitrogen temperature were both of large diameter (about 500 mm). Here again several cadmium masks could suppress all the aluminum Bragg peaks except for one around 70° (2θ) when the detector was at high θ position.

II. Sample Preparation

The ammonia was either 99.99% pure Matheson or deuterated (99.8% isotopic purity) ammonia from Saclay. Since ^6Li has a very strong neutron absorption cross section, we used ^7Li isotope from Oak Ridge (sample no. 4726330). The solutions were prepared directly in the quartz sample cells. The cells were about 10 cm long and made mostly out of $^8/_{10}$

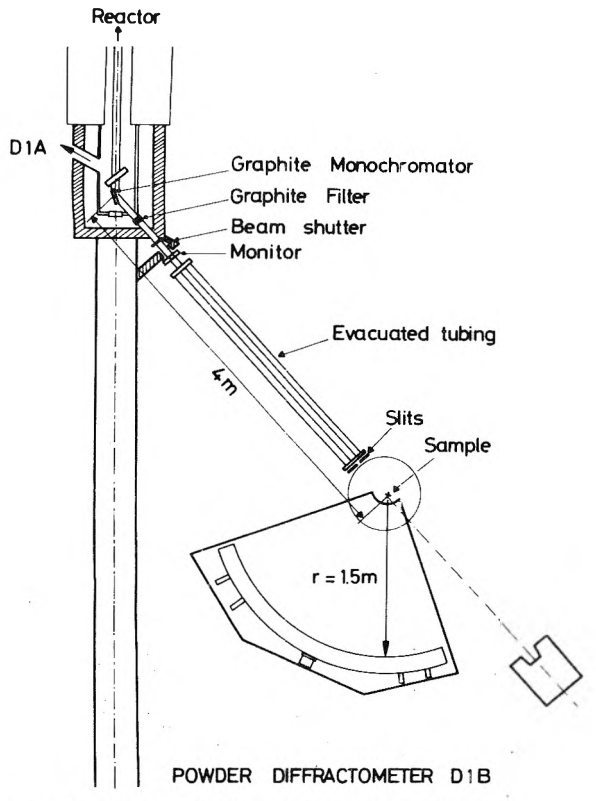

Figure 1. The D1B powder diffractometer. General view.

mm quartz tubing. The ¼ and ⅜ size were also occasionally prepared. The lithium was cut, weighed, and introduced bright in the sample cells mounted on the vacuum line, all operations being done under inert atmosphere. Its weight was measured with a Sartorius microbalance to 0.1% precision. The ammonia was dried by the usual procedure (over alkali metal) and distilled on the lithium. Gas volumetric measurements allowed us to condense known quantities of solvent and thus prepare a priori calculated concentrations. The glassware was cleaned with great care (ammonium fluoride treatment) and degassed. The vacuum could be as good as 10^{-7} Torr. Some samples kept at liquid nitrogen temperature and handled several times under various experimental conditions, including periods at room temperature, did not show any sign of decomposition or change in scattering pattern.

Problems Related to a Powder Sample Preparation. "Prepare a good powder sample" was considered as being the major difficulty encountered in these experiments. The standard technique of cooling the liquid sample in the cryostat with various cooling speeds (we tried speeds as fast as 5 min from room temperature to liquid helium, and as slow as 3 hr to go from 90 to 80 K) gives very poor results. The powder always contained very large single crystals, and the problems of preferential orientation were overwhelming.

We therefore decided to rotate the sample in situ. The whole sample holder was rotated in the cryostat at turning speeds of 12 to 25 rpm, which is quite sufficient for the multidetector assembly. A double "O ring" ensured the tightness of the low-pressure helium atmosphere of the cryostat tail. Rotating contacts allowed for a continuous recording of the sample holder temperature. It was thus possible to achieve a 30% reproducibility on the peak intensities of a given sample. No improvement could be made by

TABLE I: Sample Compositions

	No.	Formula	MPM[a]
Li–ND_3	1	$Li(ND_3)_{4.5}$	18.1
	2	$Li(ND_3)_{4.2}$	19.2
	3	$Li(ND_3)_{3.0}$	25.2
	5	$Li(ND_3)_{5.5}$	15.3
	6	$Li(ND_3)_{4.0}$	20.0
	7	$Li(ND_3)_{4.0}$	19.9
Li–NH_3	G	$Li(NH_3)_{3.1}$	24.5
	H	$Li(NH_3)_{4.1}$	19.7

[a] MPM values accurate to at least 1%.

varying the size of the cells from 8 to 4 mm internal diameter. For the tests, as well as for all the subsequent experiments, the cooling rate was chosen as fast as possible. The tail of the cryostat was filled with liquid helium and the sample and sample holder were immersed directly in it.

Sample Concentrations. Considering the complexity of the phase diagram, it was decided to prepare, as described above, a series of samples of different concentrations as listed in Table I. It must be emphasized that these are the concentrations of the ingredients, not necessarily of the liquid phase where we are limited by the saturation line at room temperature. (We always kept the solution for a while at room temperature with vigorous shaking to ensure complete dissolution of the metal.) On the other hand, it must also be noted that the solidification occurs always as the eutectic concentration.

III. Existence of an Amorphous Phase Coexisting with the Compound

We have already indicated that the knowledge of the ratio of metal and ammonia or of the liquid concentration was of little use for fixing the compound composition. Moreover, for all samples investigated we noticed in the background and extending over many Bragg peaks a quite strong scattering pattern similar to that displayed by these systems in the liquid state. (The strong incoherent scattering of hydrogen atoms prevented a study of the hydrogenated samples.) The pattern was corrected for the cryostat, sample holder, and quartz container[5] as is usually done in liquid investigations.

The results are presented in Figure 2. The (a) line represents the background (corrected for the cryostat and quartz container) for a pure ND_3 sample at 80 K. Within the experimental errors it is flat. The same background is obtained at 3 K when a Li–ND_3 sample is cooled for the first time (the samples stored permanently in liquid nitrogen were defrosted at room temperature for 10–15 min before being introduced in the cryostat). There is little change of signal on warming from 3 to 20 K. At 30 K we get the (b) line, then (c) at 60 K, and (d) at 85 K. The central part of the signal between 1.9 and 2.2 $Å^{-1}$ is subject to a larger error because of the presence of several closely spaced Bragg peaks in that region. The overall reproducibility of the curves is, however, quite good and evaluated to 15% in area and 0.05 $Å^{-1}$ in peak position. Within that accuracy, no significant difference could be observed between the samples 3, 5, 6, and 7. Samples 3 and 7 were studied in greater detail for temperature cycling effects. When after a first run the samples were defrosted again at room temperature and rerun at 3 K, we never came back to the (a) curve but to at least the (b) curve level. Subsequent temperature cycling did not change that result. The cycling, however,

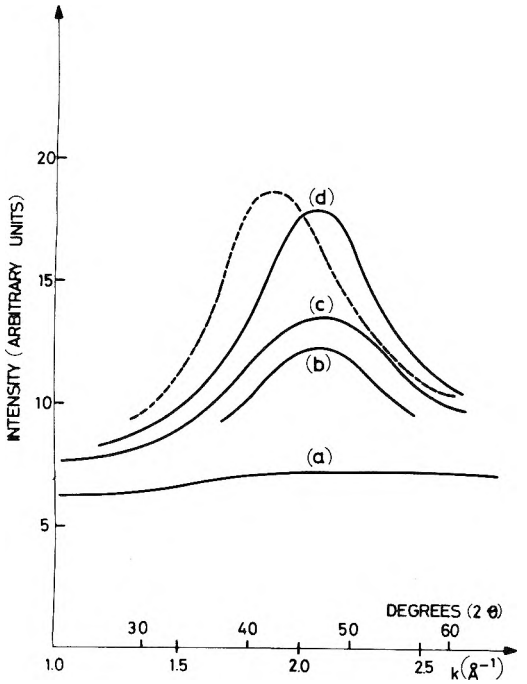

Figure 2. Scattering signal observed in the background: (a) Pure ND_3 at 80 K or Li–ND_3 sample cooled for the first time at 3 K, (b) Li–ND_3 samples at 30 K or Li–ND_3 samples at 3 K after temperature cycling, (c) Li–ND_3 samples at 60 K, (d) Li–ND_3 samples at 85 K. Dashed line: scattering pattern (intensity X0.25) of a 20 MPM Li–ND_3 solution at 95 K.

had much less effect on the 60 and 80 K lines. These observations give a structural support to the necessity noticed by several authors of cycling the sample in order to get reproducible low-temperature measurements.

We have also drawn on Figure 2 a dashed line representing the signal produced by $Li(ND_3)_{4.0}$ (sample 6 or 7) at 95 K in the liquid state. The height of that signal was actually reduced to one-quarter of its size and the (a) line taken as the origin for the drawing. We notice the similarity. A pure ND_3 signal would have exactly the same shape but centered at 2.11 $Å^{-1}$. A 12.5 MPM solution ($Li(ND_3)_{7.0}$) would give a signal centered at 2.00 ± 0.03 $Å^{-1}$.

We therefore must have here either an amorphous phase coexisting with the solid compound or highly strained regions in the compound. Since the lithium atoms contribute very little to the neutron scattering (about 1% at 20 MPM), we conclude that an amorphous phase would take up to about one-fourth of the ammonia molecules of the eutectic concentration. The reproducibility of the signal independent of the starting concentrations is understandable since we always reach the eutectic concentration while cooling along the liquidus lines after precipitation of excess ND_3 or Li. It is not clear whether an amorphous phase would consist of pure ND_3 or of a dilute solid solution of metal. We do not know either if we have concomitant precipitation of excess lithium. Furthermore, the cycling effects observed at very low temperatures are quite unique.

IV. Structure of the Solid Compound

Many runs were made on the solid compound as a function of temperature (3 to 85 K), initial composition, and cooling techniques. As stated above, the rotation of the sample was necessary but could not, however, give a better reproducibility than about 30% on peak intensities for a given initial composition. A typical diagram is shown on Figure 3. A list of peak positions and intensities is given in Table II. The structure was indexed as bccub with parameter a_0 = 14.80 ± 0.01 Å at 3 K.

The concentration effect on the solid lithium compound was very small. No variation in the lattice parameter could be detected. A few peaks had, however, an apparent concentration dependency of their intensities, sometimes twice as large as the recorded reproducibility. As expected, the dilute samples, but also to a lesser extent samples 6 and 7, presented small ND_3 Bragg peaks. These peaks were not detectable in sample 3. Their identification was easily made since they almost did not shift with temperature. They corresponded to the known[6] cubic ND_3 structure with a parameter a_0 = 5.06 Å at 3°K and 5.07 Å at 60°K.

TABLE II: Comparison of Neutron Diffraction Spectra of $Li(ND_3)_4$ and $Li(NH_3)_4$

	Li–ND_3		Li–NH_3[a]			
No.	3 K		60 K		85 K	
2	13.12	vw				
6	22.85	m	22.8	vw	22.2	s
8	26.44	vw			26.0	vw
10	29.65	w				
14	35.23	ms	35.4	vw		
16	37.75	vw				
20	42.42	m	42.0	vw		
22	44.60	s	44.4	vw	44.0	w
24	46.72	ms				
26	48.70	vs	48.6	s		
30	52.62	w	52.3	w	52.0	s
32	54.47	w	54.2	w		
34					55.8	s
36					57.4	vw
38	59.87	w	59.6	s	60.5	ms
40	61.50	vvw				
42	63.20	m	62.8	m		
44					64.1	s
46	66.50	vw	66.2	m		
48			67.8	m	66.0	vw
52	71.20	vvw	70.8	vw	70.2	vw
54	73.00	w	72.4	ms	72.2	vw
56	74.50	vw	73.8	vw		
58	76.00	w				
62	79.20	w				
66	82.20	w	81.8	ms		
68						
72	86.70	w				
74	88.20	w	87.6	s		
82			93.6	vw		
84	95.80	vvw				
86	97.20	w	96.6	w		
88	98.80	vw				
90	100.3	w				
94	103.4	w	102.8	w		
96	105.0	vvw				
98	106.6	vvw	105.6	w		
102	109.6	vw				
104	111.5	vw				
106	113.4	vvw				
110	116.2	w				

[a] Data of poor quality. Values listed are 2θ values.

TABLE III: Unit Cell Parameters of $Li(ND_3)_4$

Temp, K	a_0, Å	Temp, K	a_0, Å
3	14.80	30	14.83
10	14.80	60	14.93
20	14.80	85	15.03

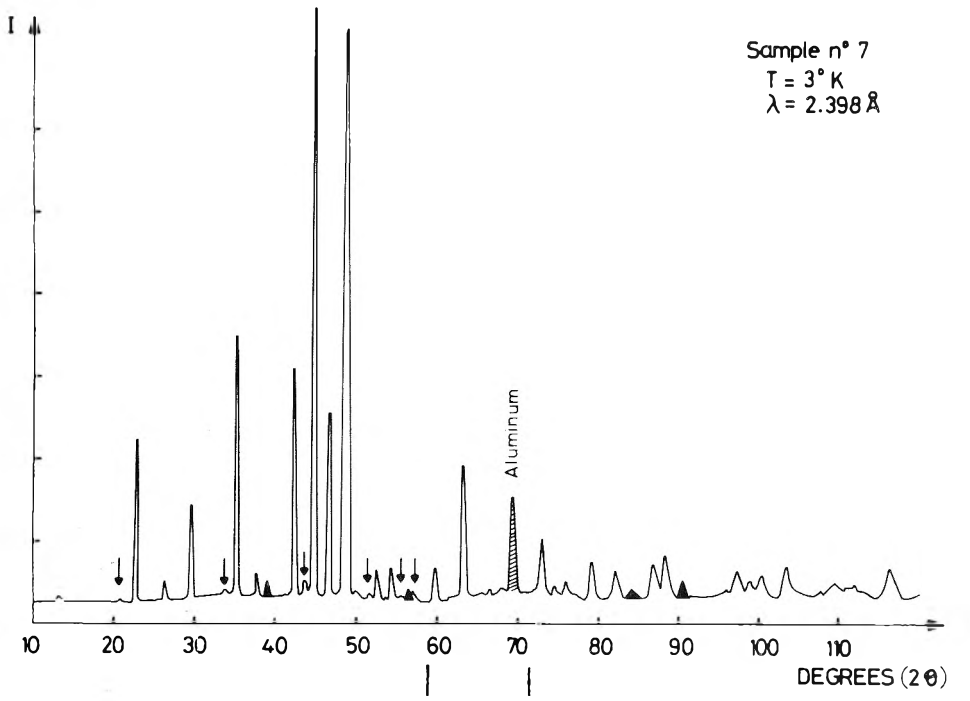

Figure 3. A typical diagram: sample 7 at 3 K; raw data. The black peaks are ND_3 peaks. The arrows show peaks disappearing at high temperature ($T > 30$ K).

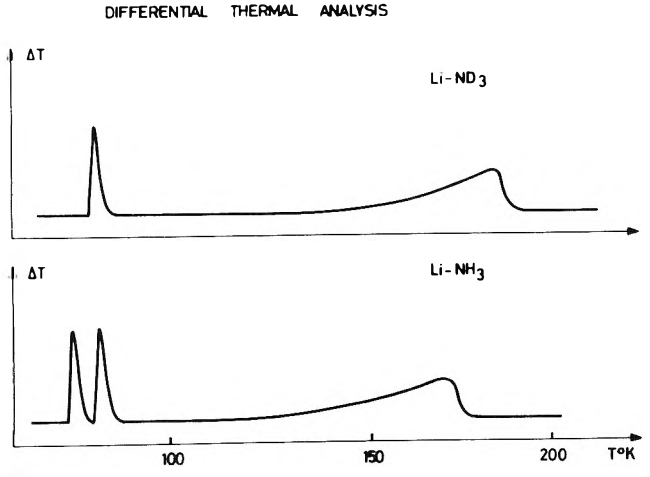

Figure 4. A differential thermal analysis of two typical samples.

The bccub solid lithium peaks[7] could never be detected, which was expected considering their small scattering power.

On the other hand, the lithium compound has a noticeable temperature dependency of its a_0 parameter as listed in Table III. It is interesting to note that below about 30 K the parameter is temperature independent.

V. Structure of the Hydrogenated Compound

The uniqueness of the structure found for the deuterated compound raises some questions about the hydrogenated one which was reported differently.[2,3] It was possible to analyze the neutron diffraction pattern of some Li–NH_3 samples. The background is, however, extremely high in that case, and only the strongest lines could be significantly detected. The results are presented in Table II. Samples H and G were investigated at 60 K and gave the same peak positions as for Li–ND_3. The variations of line intensities were expected since H and D have different scattering lengths. The a_0 parameter determined is $a_0 = 14.90$ Å at 60 K.

Sample G was also studied at 85 K. The pattern observed showed significant changes from the 60 K one (see Table II). The transition reported at 82 K for the Li–NH_3 compound is thus confirmed, but the structure at 85 K needs further investigation.

As we have said, no phase change on going from 60 to 85°K was observed on the deuterated system. This is confirmed by a differential thermal analysis of a series of 22 deuterated and 6 hydrogenated lithium–ammonia samples of concentrations varying from 10 to 22.4 MPM over a temperature scale from 77.4 K to room temperature. That investigation[8] was made in order to get a better knowledge of the liquidus shape. A typical run is presented on Figure 4. The single peak obtained on the warming curves of Li–ND_3 is at 82.4 ± 0.3 K. However, for the concentrations around the eutectic composition, a metastable peak could also be obtained, but on cooling curves only, at 85.6 K.[8]

VI. Existence of a Low-Temperature Phase

Several peaks were detected at 3 K on the Li–ND_3 samples, especially at 2θ = 20.80, 33.80, 43.50, 51.20, 55.40, and 57.20° (see Figure 3). These peaks disappear at temperatures higher than 30 K. They indicate the existence of a new low-temperature phase.

A low-temperature differential thermal analysis made on a 20 MPM sample confirmed the existence of a thermal effect at 27 ± 5 K, detected both on cooling and warming curves.

Considering the difficulty of sample preparation and the complexity of the phase diagram, it is clear that these findings need further investigation. A polarized neutron experiment would be of real interest to check the possibility of magnetic ordering. In any event, it is clear that $Li(ND_3)_4$ is a different material from $Li(NH_3)_4$, with different structure and different transitions, perhaps because of subtle

differences in hydrogen bonding or small effects on rotational motions.

References and Notes

(1) See the review article by N. Mammano in "Metal-Ammonia Solutions: Colloque Weyl II", J. J. Lagowski and M. J. Sienko, Ed., Butterworths, London, 1970, pp 367–393.
(2) N. Mammano and M. J. Sienko, *J. Am. Chem. Soc.*, **90**, 6322 (1968).
(3) L. Kleinman, S. B. Hyde, C. M. Thompson, and J. C. Thompson in ref 1, p 229.
(4) W. S. Glaunsinger, S. Zolotov, and M. J. Sienko, *J. Chem. Phys.*, **56**, 4756 (1972).
(5) H. H. Paalman and C. J. Pings, *J. Appl. Phys.*, **33**, 2635 (1962).
(6) J. W. Reed and P. M. Harris, *J. Chem. Phys.*, **35**, 1730 (1961).
(7) J. Donohue in "The Structure of the Elements", Wiley, New York, N.Y., 1974, p 29.
(8) F. DeBaecker, Diplôme d'Etudes Approfondies—Uiversité Paris-Sud, Faculté des Sciences d'Orsay, 1973.

Discussion

C. S. JAIN. Some years ago Kleinman and others (Colloque Weyl II, 1969) reported an fccub structure of $Li(NH_3)_4$ compound above 82 K (say between 82 and 89 K), with a transition to the hexagonal phase at 82 K. The same was also established by Mammano and Sienko (*J. Am. Chem. Soc.*, **90**, 6322 (1968)), although the space groups suggested in these two works were different. Results of your studies presented in this conference indicate a CsCl (bccub) structure for this compound around 85 K. However, if the bccub structure is correct, how would you fit NH_3 molecules in this structure since there is a fourfold coordination of NH_3 molecules around the Li^+ ion? Existence of a fourfold coordination of NH_3 around Li^+ is fairly well established from our experience with the Li–NH_3 system. However, if you do not consider this to be the correct coordination, what coordination do you think exists, and how would you explain the persistence of a bccub structure with this coordination?

M. SIENKO. Von Dreele indicated there are sites in bccub that have tetrahedral symmetry.

P. CHIEUX. First of all I want to emphasize that the neutron diffraction study of the hydrogenated samples is of poor quality and that new x-ray work should really be made on that system. Moreover, we must be careful when we speak of tetrahedral environment, since nobody has ever determined experimentally the composition of the compound.

L. V. COULTER. In an attempt to remove some of the ambiguity of the nature of the transition of the ~88.8 K transition in the solid Li–NH_3 system, we (Susan Lee and L. Coulter) have reexamined the thermal behavior of a 55 MPM (Li) system. Warming curves, into and out of the transition, at the rate of about 6×10^{-3} deg min^{-1} from about 86 to 90 K confirm the previously observed (by N. Mammano and L. Coulter, *J. Chem. Phys.*, **50**, 393 (1969)) existence of only a single sharp isothermal transition in this range. It is also relevant to note that the heat capacity of a 22.5 MPM system above the 88° transition rises smoothly up to 225 K with no indication of additional transitions.

Conduction Electron Spin Resonance of Lithium Tetraammine, $Li(NH_3)_4$

P. Damay

Laboratoire de Chimie Physique, CNRS, E.R.A. 126, 59046 Lille, France

and M. J. Sienko*

Cornell University, Ithaca, New York 14853

(Received July 23, 1975)

Publication costs assisted by the National Science Foundation

New results of electron spin resonance have been obtained for the hexagonal phase of solid $Li(NH_3)_4$; they are compared with previous data. Existence of stresses prevented obtainment of a narrow signal. The line is about 1 G wide, and the width decreases with temperature as expected for a metal. The spin–lattice relaxation time is calculated as a function of temperature.

Introduction

Conduction electron spin resonance (CESR) of lithium–ammonia solutions and of solid compound $Li(NH_3)_4$ has been reported first by Levy.[1] The lithium–ammonia phase diagram was not established at this time, and Levy attributed the narrowing of the ESR line at 80 K to a transition in metallic lithium. More complete results have been published recently by Glaunsinger and Sienko.[2]

The Li–NH_3 phase diagram is not yet completely understood. There exists a liquid–solid transition at 88 K and a solid–solid transition at 82 K. X-ray experiments[3] indicated that a hexagonal solid compound existed below 82 K. It was assumed that the solid is cubic between 82 and 88 K although no x-ray experiments have been performed in this temperature range. From the liquid, the transition seems to be a simple eutectic, but the solid is actually a well-defined compound.

The recent results obtained by Glaunsinger and Sienko[2] indicate some interesting and puzzling effects. If the generally accepted phase diagram is correct, the same resonance line should be observed when a Li–NH_3 solution of any composition is frozen below 88 and 82 K.

The same signal was indeed observed for the so-called "cubic compound" $Li(NH_3)_4$ for any composition between 82 and 88 K. Below 82 K, however, Glaunsinger and Sienko observed a symmetric narrow line for frozen dilute solutions but a broader and not well-defined signal for frozen concentrated solutions. The authors attributed the first signal to persistence of the cubic phase below 82 K, assum-

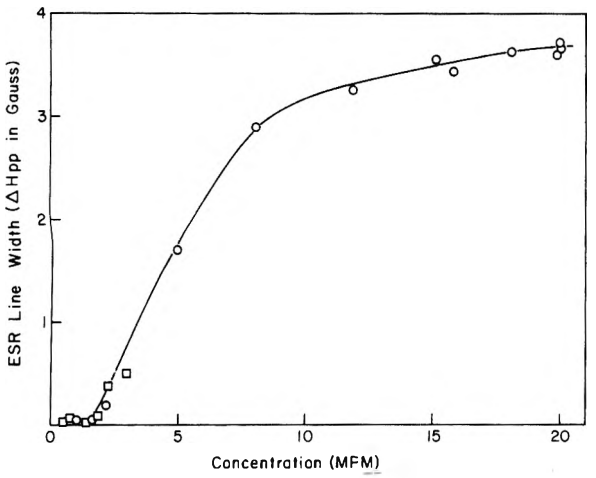

Figure 1. CESR line width of Li–NH_3 solutions at −35°C: (□) previous data reported by O'Reilly;[5] (○) this work. The line width is the peak-to-peak width ΔH_{pp} of the second-derivative signal.

ing that solid ammonia stabilized the cubic phase below 82 K. As a possible mechanism, epitaxial growth of the compound at the surface of crystals of cubic ammonia at the freezing point was proposed.

In order to clarify this problem, a systematic investigation of resonance experiments was carried out for a large number of mixtures with composition between 1 and 99 MPM (Li) (MPM is 100 times the mole fraction). The concentration range below 20 MPM was investigated more carefully.

Results for the "cubic phase", as well as for the liquid, were similar to those reported previously; nevertheless, somewhat narrower lines were systematically observed.

Two main differences from the previous work appeared for the hexagonal phase between 1 and 20 MPM. First, a single line was always observed for all concentrations in contrast to the mixture of two lines previously reported. Second, at the exact composition $Li(NH_3)_4$, depending on the sample and on the rate of cooling, either a very broad (15 G) asymmetric line or sometimes no line at all was observed. It was assumed that the line was broadened owing to stresses that occurred in the sample at the solid–solid transition, persisting to lower temperatures in the hexagonal phase. This supposition was confirmed by the observation that a narrow line (~1 G) was obtained when the 20 MPM solution was finely dispersed in paraffin oil so as to remove stresses in the crystals. The line observed was the same as that for the dilute mixtures.

Experimental Section

CESR measurements were performed at X-band frequency. First and second derivatives of absorption could be detected. Temperatures from 4 K to room temperature were attained using a cryogenic flow system based on liquid nitrogen or liquid helium.

The ammonia used was Matheson 99.99%; the lithium, which was obtained from Lithium Corporation of America, was 99.99%. Preparation of the samples, as well as detailed experimental techniques, have been reported elsewhere.[4]

Results and Data Analysis

Four different regions corresponding to different properties must be considered: the liquid phase, the cubic phase between 82 and 88 K, the hexagonal phase below 82 K, and the very concentrated range above 99% lithium.

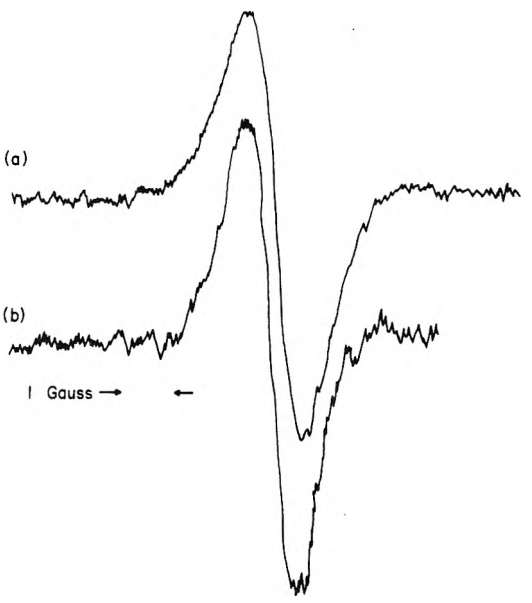

Figure 2. (a) Second-derivative ESR spectrum of 6.2 MPM lithium–ammonia at 60 K; (b) second-derivative ESR spectrum of 20 MPM lithium–ammonia dispersed in paraffin oil at 43 K.

(a) *The Liquid Phase.* Our results, compared with previous data reported by O'Reilly[5] at 7 MHz, are given in Figure 1. The variation of line width with concentration shows the same trend as for the sodium–NH_3 system.[6] The width is almost constant in the dilute range as well as in the concentrated range. In the intermediate range, the variation of the signal can be accounted for by assuming that the line is actually formed of two signals in rapid exchange, one line representing the dilute solutions and the other the metallic range. Damay and Schettler[7] have recently studied concentration fluctuations in this region. They showed that the local concentration may be far from equal to the average concentration and calculated concentration distribution curves at each average composition. Assuming that the ESR line width is a step function in an hypothetical solution free of fluctuations, the width being constant on each side of a critical concentration x_c, the ESR line width can be calculated in the real fluctuating system using the concentrations distribution. Calculated and experimental results are in good agreement.

(b) *Cubic Phase.* Our results are very similar to those previously reported by Glaunsinger and Sienko for all concentrations, although the line widths are systematically about 15% narrower. The signal is asymmetric in accord with Dyson's theory for samples thicker than the skin depth.[8]

(c) *Hexagonal Phase.* All samples between 1 and 20 MPM presented a single ESR line below 82 K. The signal was easy to obtain for frozen solutions between 1 and 12 MPM. The line shape is typically dysonian; the signal for a 6.2 MPM frozen solution at 60 K is given in Figure 2. Line width decreases linearly with temperature. The signal was more difficult to observe for solutions just above 12 MPM; it was somewhat less intense and broader, probably because amplitude modulation had to be increased.

A 15-G-wide line was observed for 16, 17, and 20 MPM mixtures. The width increased with decreasing temperature, and the signal disappeared completely around 50 K. This effect was very reproducible though signal intensity could depend upon the cooling rate. For one 20 MPM sample, no signal at all was detected below 82 K. This behavior

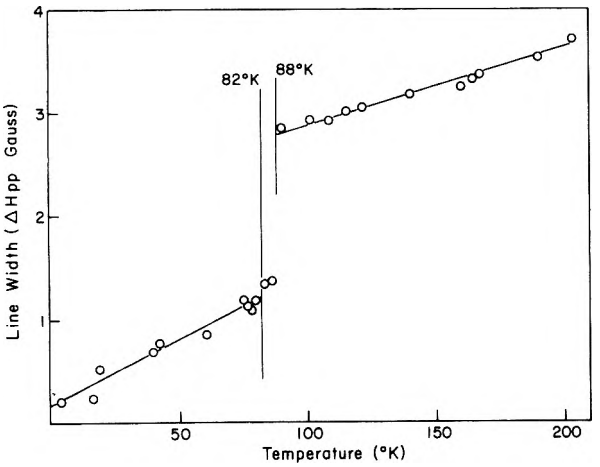

Figure 3. Peak-to-peak line width ΔH_{pp} of $Li(NH_3)_4$ as a function of temperature. Below 82 K, the data come from the compound dispersed in paraffin oil.

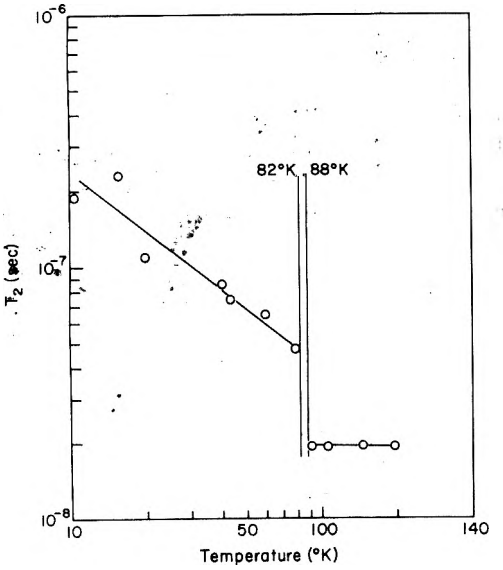

Figure 4. Relaxation time T_2 for the compound $Li(NH_3)_4$ as a function of temperature.

seems to indicate that some inhomogeneous broadening occurs at the solid–solid transition. Such broadening could very well come from stresses that occur in the polycrystal at the transition. Stresses are known to broaden resonance lines in crystals, and it is likely that they could exist in the hexagonal phase. There is indeed a change of density at the transition, and several physical properties such as the electrical conductivity and the Hall effect show important hysteresis effects that do not disappear completely on annealing.

A dispersion of $Li(NH_3)_4$ in paraffin oil was prepared in order to get rid of the stresses. The emulsion was made in an ultrasonic bath at −30°C. Small droplets of bronze solutions of size less than a tenth of a millimeter were formed. The signals of the liquid and the cubic phases remained unchanged, but a narrow (~1 G) asymmetric line appeared below 82 K. The ESR spectrum at 43 K is given in Figure 2b. Resemblance with Figure 2a is striking; hence, there is little doubt that stresses are the broadening factor in the pure hexagonal compound. The effect of stresses does not occur in more dilute mixtures because the compound there is actually dispersed in excess ammonia.

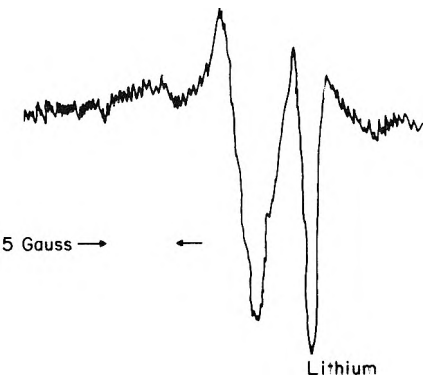

Figure 5. Second-derivative ESR signal for a 99% solution of lithium in ammonia. The second line is due to excess metallic lithium.

Our conclusion, then, is that only the hexagonal phase compound, $Li(NH_3)_4$, exists in the frozen solutions between 1 and 20 MPM below 82 K. As expected for metals, the line width of the hexagonal phase decreases with temperature. The line width for a 20 MPM [i.e., exact $Li(NH_3)_4$] sample as a function of temperature is given in Figure 3, and the relaxation time T_2, in Figure 4.

(d) *Very Concentrated Range.* Between 20 and 90 MPM, the CESR signal was the same as that for a saturated solution or the cubic phase below 88 K, as expected from the phase diagram. For concentration around 99 MPM, the line of excess metallic lithium appeared, and at the same time the liquid or solid signal was replaced by a much narrower line. The line width was 220 mG at 184 K. The g shift was -2.30×10^{-4} compared with -8×10^{-4} as observed for the compound $Li(NH_3)_4$. The sample signal was obtained at all temperatures investigated from 200 to 50 K. Too large amplitude modulation prevented reliable determination of the temperature effect on the line width. The new line is reported in Figure 5.

The observed effect could be accounted for by formation of a compound for concentrations larger than 90 MPM. The exact composition of the compound could not be determined because there was a large amount of excess metallic lithium in the three samples that presented the effect (97, 99, and 99.5 MPM). Only a few drops of bronze solution were visible on the metallic lithium when the new line was observed. Other mechanisms could also be involved, such as slow exchange of electrons between $Li(NH_3)_4$ compound and metallic lithium.

Discussion

It has been shown that for concentrations between 1 and 20 MPM, only a single line was observed below 82 K. Furthermore, the intrinsic line of the hexagonal phase could be obtained by dispersing the compound in paraffin oil. Its line width decreased linearly with temperature as expected for a metal.

According to Dyson,[8] if the asymmetry parameter of the line is constant with temperature, the relaxation time should vary with temperature as the square of the electrical conductivity σ^2. The temperature dependence of the electrical conductivity of $Li(NH_3)_4$ presents some anomalies between 60 and 80 K.[9] These anomalies are not observed for the relaxation time T_2, which decreases linearly over the whole temperature range. The anomalies in the conductivity could be explained by the fact that the experiments were performed on polycrystals produced from freezing of a

concentrated solution and not on single crystals. This disadvantage does not affect ESR measurements.

Glaunsinger and Sienko attributed the line observed in the very dilute range (0.05 and 0.001 MPM) to stabilization of a cubic phase at low temperature by an epitaxial mechanism. In the light of the present results, this interpretation seems doubtful. There is not much difference between the cubic signal above 82 K and the hexagonal phase signal just below the transition. Both line widths are similar, and only the asymmetry parameter permits one to differentiate the two signals easily. In the very dilute range, however, the signal is symmetric because the particles are smaller than the skin depth. It would be very difficult to differentiate signals in such a case. Furthermore, the relaxation times observed for the hexagonal phase are very comparable to those reported in the more dilute range. Thus, it seems probable that the signal observed below 82 K by Glaunsinger and Sienko was indeed the line of hexagonal phase $Li(NH_3)_4$ dispersed in excess ammonia.

Acknowledgment. This research was sponsored by the National Science Foundation under Grant No. GP-17706. It was supported in part by AFOSR, the Materials Science Center at Cornell University, and CNRS.

References and Notes

(1) R. A. Levy, *Phys. Rev.*, **102**, 31 (1956).
(2) W. S. Glaunsinger and M. J. Sienko, *J. Chem. Phys.*, **62**, 1873, 1883 (1975).
(3) N. Mammano and M. J. Sienko, *J. Am. Chem. Soc.*, **90**, 6322 (1968).
(4) T. David, P. Damay, and M. J. Sienko, *J. Chem. Phys.*, **62**, 1526 (1975).
(5) D. E. O'Reilly, *J. Chem. Phys.*, **50**, 4743 (1969).
(6) J. P. Lelieur, Thesis, Orsay, 1972.
(7) P. Damay and P. Schettler, to be submitted for publication.
(8) F. J. Dyson, *Phys. Rev.*, **98**, 349 (1955).
(9) M. D. Rosenthal and B. W. Maxfield, *J. Solid State Chem.*, **7**, 109 (1973).

Discussion

J. V. ACRIVOS. The additional ESR signal observed when excess Li is present is very similar to the signals observed when Pb is added to $Na-NH_3$. (J. Azebu and J. V. Acrivos, unpublished results and Colloque Weyl II).

Insertion of NH_3 and N_2H_4 into Layer Disulfides

J. V. Acrivos,*[1] C. Delios, N. Y. Topsøe, and J. R. Salem

San José State University, San José, California 95192 *(Received June 18, 1975)*

The stoichiometry and mechanism for insertion of gases into a layer disulfide, $2H-TaS_2 + I(g) = 2H_I-TaS_2 \cdot I_n$ (1), where I = NH_3 and N_2H_4, have been investigated by gravimetry and by Cu $K\alpha$ x-ray diffraction measurements. The results are *one*, the equilibrium weight gain is constant for I = N_2H_4 ($n = 0.66 \pm 0.03$) but depends on temperature and pressure when I = NH_3; *two*, the integrated intensities of the x-ray diffraction spectra lines of powdered samples interacting with both NH_3 and N_2H_4 indicate the initial rate of disappearance of the reactant is at least one order of magnitude greater than the rate of appearance of the ordered first-stage intercalated product; and *three*, the rate of weight gain is first order in the number of sites remaining unoccupied by I = NH_3 and N_2H_4 to within 10% accuracy. A rate mechanism consistent with the data is used to discuss the results.

I. Introduction

The changes produced in the optical absorbancy of layer disulfides by the insertion of atoms and molecules suggest the formation of a molecular complex.[2,3] The structural changes are summarized in Figure 1.[4-6]

At Colloque Weyl III a hypothesis was advanced to explain the stability of intercalated compounds using the Mulliken concept of electron donor–acceptor (EDA) complexes[7] since then the shifts produced on the optical absorbancy of $2H-TaS_2$ by intercalating pyridine, *N*-methylformamide, cyclohexylamine, and hydrazine suggest that the former is the acceptor in the EDA complex.[2b,3] The changes produced by intercalation on the heat capacity and transport properties of TaS_2 and $NbSe_2$ polytypes[6c] also support the semiempirical model. However, the reaction is complex and the effects of structure, dipole moment, and ionization potential of the gas I on the process may give further information on the nature of the product.

The purpose of this work is to investigate the mechanism and stoichiometry of

$$2H-TaS_2 + I(g) = 2H_I-TaS_2 \cdot I_n \quad (1)$$

This may be accomplished under conditions where (1) is the only process present as follows.

II. Experimental Section

A. *Measurements.* A McBain–Bakr[8a,b] type balance was constructed for quantitative measurements as a function of time (t), temperature, and pressure (T = 250 to 300 K and $P_I = 10^{-3}$ Torr to 5 atm). The balance, enclosed in LabCrest pipe (Fisher and Porter 0.5 in. i.d.), consists of a Worden Quartz Products Spring No. 4501-E (with extensions of 1 mg/mm). The increase in weight is reported as the ratio x^0 of moles of I to the moles of $TX_2(TaS_2)$:

$$x^0 = [MW(TX_2)/MW(I)][(l_3 - l_2)/(l_2 - l_1)] \quad (2)$$

where MW is the molecular weight and the l_i are spring extensions (i = 1 for the empty sample boat, i = 2 for the boat loaded with TX_2 after being pumped to 10^{-5} Torr for 24 hr, and i = 3 during the intercalation reaction) x_∞^0 is

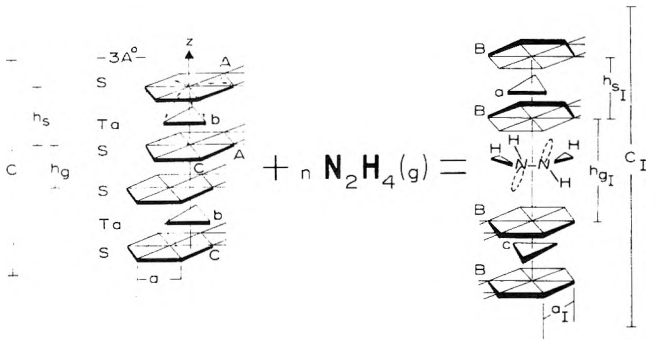

Figure 1. Effects produced by the insertion reaction. The parameters h_s and a do not change appreciably but h_g increases to accommodate the I molecules and produce a stacking rearrangement. The x-ray diffraction data given in ref 6b–d indicate the unit cell changes from |AbA|CbC| to ||BcB||BaB|| (capital and lower case letters identify the hexagonal close-packed sites occupied by the sulfur and Ta atoms along the 110 axis, respectively, and the sites occupied by I are not known).

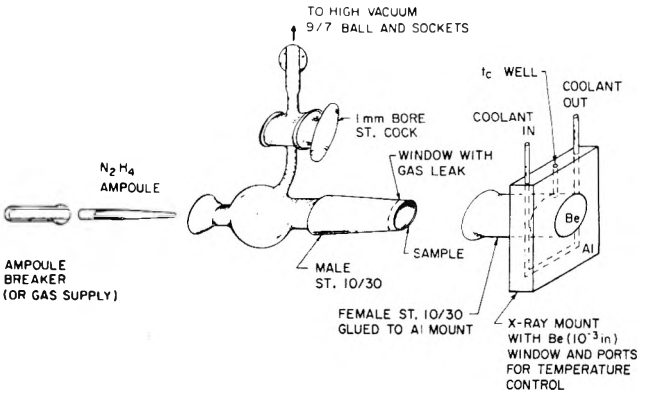

Figure 2. Reaction cell used with Picker and GE x-ray diffractometers.

the extrapolated value as $t \rightarrow \infty$. The uncertainty Δx^0 was determined by the reproducibility of l_i, i.e.[8b]

$$\Delta x^0 = 2[\mathrm{MW}(TX_2)/\mathrm{MW}(I) + x^0]\Delta l/(l_2 - l_1) \qquad (3)$$

where $\Delta l/(l_2 - l_1) < 10^{-3}$ was estimated by measuring each extension three times with a Cenco (Model 72730) universal type cathetometer. A calibration curve verified the linearity of the spring extension vs. weight. This was obtained using weights made of clean nichrome wire (calibrated on a Cahn electrobalance to within 0.01 mg). The effect of buoyancy was determined by calibrating in air and in vacuo and the deviation was found to be 0.05 mm in the total extension of 3×10^2 mm at 1 atm of air relative to vacuum.

The fraction of a phase present in a powdered mixture may be determined from the integrated intensity of the corresponding x-ray diffraction lines.[8c,d] For powders with $\mu d \ll 1$ ($\mu \simeq 10^3$ cm^{-1} is the linear absorption coefficient and d is the normal dimension) the rate of change of the latter is then a measure of the rate of change of the corresponding phase. The reaction cell shown in Figure 2 was constructed for use with a GE XRD-6 x-ray diffractometer. The sequence of measurements involved (a) measurement of the x-ray spectrum of a blank cell (using a CA-8-S/Cu tube with a 0.4° slit and a Ni filter) from $2\theta = 3$ to 80° at the highest spectrometer sensitivity, (b) loading and pumping of cell to 10^{-5} Torr overnight, (c) measurement of reactant spectrum in same range as in (a), (d) starting the reaction by letting gas flow into the cell from an ampule or from a gas reservoir and measuring the time intervals with the synchronous motor of the recorder, and (e) scanning from $2\theta = 15$ to 8° and back at the rate of 2°/min after earlier runs showed there were no base line changes from 3 to 9° for both gases investigated within the first 3 min of the reaction. The Be line at $2\theta = 50.98°$ was used as a reference for intensity as well as alignment.

B. *Chemicals.* The 2H–TaS_2 powder samples were prepared by heating reagent grade elements (Merck S and ESPI Ta) in quartz evacuated tubes below 800°C for several weeks and annealing at 400°C; the phase present was determined by x-ray diffraction.[6a–c] Single crystals grown by vapor transport were kindly given to us by Dr. S. F. Meyer. The powders were used as grown (or ground in vacuo) and then separated according to size using U.S.A. Standard Testing Sieves (ASTME-11) and stored in vacuo. The average particle size is $d_a^2\bar{d}_c$, where d_a is the basal dimension (in the plane of the crystalline a-axis shown in Figure 1) selected by the sieve and $\bar{d}_c$ is the mean of the dimension parallel to the c axis. Observation under the microscope shows that $\bar{d}_c \ll d_a$.

The ammonia was purified by vacuum line procedures described elsewhere.[9] The pressure was measured at the beginning and at the end of a reaction to within ±1 Torr with a Hg manometer (which was isolated from the system by a gold dust trap) and/or a Wallace Tiernan gauge (0 to 760 Torr). This remained constant during the reaction within the uncertainty limits because the manifold had a buffer volume $v = 2 \times 10^3$ ml.

The 97% anhydrous hydrazine (reagent grade Matheson Coleman and Bell) was distilled in vacuo at room temperature and stored in ampules at 0°C. These were later broken inside the reaction vessel (previously evacuated to 10^{-5} Torr). The magnitude of the vapor pressure P_I was determined by calibration curves of P_I vs. the liquid temperature T_I where the latter was controlled to 0.1°C. The values reported in Table I are equal to those evaluated from the literature interpolation curves[10] within the experimental uncertainty. Below 50°C the sample temperature (T) was controlled by a 2095 Forma Scientific bath. A heated oil bath was used above 50°C.

C. *Analyses.* The intercalated gas removed from samples was analyzed in order to determine the stability of the complexes. After a sample was intercalated to equilibrium at (0°C, $P_{NH_3} = 1$ atm), the ammonia pressure was reduced to 10^{-5} Torr without appreciable change in the composition of the intercalated compound. However, when the temperature was raised at 10^{-5} Torr, the ammonia content decreased to $x^0 = 0.34 \pm 0.02$ at room temperature. The gaseous mixtures removed at several temperature intervals were collected for mass spectrometer analysis. It was found that the samples were stable to at least room temperature, because only peaks due to fragments of NH_3 and no trace of sulfur were observed in the mass spectra. However, when samples were heated to $T \geq 66$°C, the gas fraction revealed traces of sulfur. The same analyses carried out for the N_2H_4 complexes also revealed the presence of sulfur traces at $T > 30$°C. Therefore reaction 1 is assumed to be the only one present at or below these temperatures.

A BET surface area measurement was carried out on a constant volume apparatus in the laboratory of Professor M. Boudart of Stanford University. The maximum surface area measured for 2H–TaS_2 ($d_a < 75$ μm) of 0.278 m^2/g is (within the accuracy of the measurement) equal to the basal area of the powder, i.e., nitrogen gas was not interca-

TABLE I: Parameters for the Rate of Insertion of Gases into 2H–TaS_2[a-c]

Run no.	d_a, 10^{-4} cm (powders)	T_I,[a] °C (±0.5 max)	T, °C (±0.1 max)	τ,[a] min	$100\Delta\tau/\tau$[a]	$t_{1/2}$, min (±0.1 max)	t_0/τ[b] (±0.1 max)	P_I,[a] Torr	$(10^6 d_a/\nu_T P_I)$,[c] $Torr^{-1}$	$(d_a^2/\tau D_\parallel)$[d]
I = NH_3										
T-1	<38		24	0.84×10^3	1		−0.2	308	0.03	8×10^{-6}
T-2	<38		24	4.3×10^3	6		−0.2	98		
I = N_2H_4										
DP-11	38–53	5.6	17.2	1.56	6	1.3	0.1	4.2 (3.4)		
DP-13	38–53	5.6	24.3	1.58	5	1.3	0.1	4.2 (3.4)		
DP-14	38–53	5.6	52.7	1.4	5	0.9	−0.4	4.2 (3.4)		
DP-15	38–53	5.6	73.3	2.8	5	1.5	−0.2	4.2 (3.4)		
DP-16	38–53	5.6	33.6	1.3	6	1.0	0.2	4.2 (3.4)		
DP-17	38–53	5.6	42.3	1.3	5	1.0	0.1	4.2 (3.4)		
DP-18	38–53	5.6	50.1	1.4	4	1.0	0	4.2 (3.4)		
D-21	38–53	0	14.7	39.1	15	9.2	−0.4	2.9 (2.7)		
D-22	38–53	0	21.5	15.6	2	7.2	−0.1	2.9 (2.7)	20	2×10^{-3}
D-23	38–53	0	33.67	2.5	2	2.0	0.1	2.9 (2.7)		
D-25	38–53	0	54.7	28.0	4	8.8	0.5	2.9 (2.7)		
D-26	38–53	0	91.1	31.3	7	10.6	0.3	2.9 (2.7)		
D-27	38–53	0	71.7	27.0		8.6	0.3	2.9 (2.7)		
D-31	38–53	0	34.8	6.37	3	3.2	−0.2	2.9 (2.7)		
D-32	38–53	0	33.9	5.13	3	2.5	−0.2	2.9 (2.7)		
D-33	38–53	0	29.1	7.8	3	3.6	−0.2	2.9 (2.7)		
D-34	38–53	0	30.5	4.1	2	2.3	−0.2	2.9 (2.7)		
D-35	38–53	0	38.6	11.5	4	5.3	−0.2	2.9 (2.7)		
DP-1	38–53	−9.3	29.9	39.2	2	19.5	−0.2	1.4 (1.2)		
DP-2	38–53	−9.6	24.6	64.0	3	46.2	−0.1	1.4 (1.2)		
DP-3	38–53	−9.4	25.9	18.9	8	3.0	−0.5	1.4 (1.2)		
DP-4	38–53	−9.0	27.3	4.48	8	1.4	−0.4	1.4 (1.2)		
DP-5	38–53	−9.4	30.5	37.3	5	17.5	−0.2	1.4 (1.2)		
DP-6	38–53	−9.0	17.10	53.2	3	27	−0.2	1.4 (1.2)		
DP-7	38–53	−9.5	54.8	50	10	19.2	−0.2	1.4 (1.2)		
Single crystals[e]	$(d_a^2)^{1/2}$, cm									
DX-6	0.45	24	24	4.3×10^3	10		0.0	12		
DX-7	0.30	24	24	1.8×10^3	1		−0.4	12	28	
DX-9	0.60	24	24	2.0×10^3	7		−0.2	12	±12	10^{-1}

[a] τ was determined using a weighted least-squares computer program of ref 16 to fit the data in Figures 5–9 to eq 8′ when the uncertainty is $\Delta(\ln (x_\infty/(x_\infty - x^0)) = 3\Delta x^0/(2 - 3x^0)$, $x_\infty = 2/3$ and Δx^0 is given in eq 3. $100\Delta\tau/\tau$ is the percent uncertainty. The values reported for P_I were obtained from calibration curves of P_I vs. T_I using N_2H_4 purified as described in the Experimental Section. The values in parentheses were obtained from the interpolation curves in the literature 10. [b] The lack of correlation between t_0/τ and the experimentally controlled parameters suggests the intercept arises from crystal imperfections. [c] ν is the kinematic viscosity of the liquid ($\nu = 4 \times 10^{-3}$ and 10^{-2} St for NH_3 and N_2H_4). [d] Assuming $D_\parallel = 10^{-5}$ cm^2 sec^{-1} for both NH_3 and N_2H_4 during the insertion reaction. [e] The single crystals remained intact after intercalation. In ref 3 and 21 electron micrographs indicate intercalation has created ridges on the surface and on cleaved lamellae from within the body of the crystal of dimensions 10^{-6} m.

lated. However, the intercalation of NH_3 could not be carried out on the sample after the BET measurement. The reaction when I = N_2H_4 under the same conditions of sample D-22 in Table I was slowed down by a factor greater than 10 after N_2 at 760 Torr was adsorbed to TaS_2 at 77 K and the sample subsequently pumped at 10^{-5} Torr for 24 hr.

D. *Results.* Typical x-ray spectra are shown in Figures 3 and 4. The weight increase vs. time is shown in Figures 5–9 and the NH_3 isotherms and isosteres in Figures 10 and 11.

For powder TaS_2 ($d_a < 38$ μm and $d_c \ll d_a$) the rate of change of the phases present was estimated by measuring the relative areas under the 00*l* x-ray diffraction lines vs. time. The spectra of the product phases recorded within 30 min after the start of reaction (P_I = 12 and 256 Torr for N_2H_4 and NH_3, respectively, at room temperature) are similar to those obtained after the end of reaction and exposure to air of 2H–$TaS_2(NH_3)_n$, n = 1, 0.34, 0.36, and 0.13[6c,11] except for the following reproducible observations: *one*, the rate of disappearance of the reactant phase in Figure 3 is one order of magnitude greater than the rate of appearance of the product phase but changes in the base line of the x-ray diffraction spectra as shown in Figures 3 and 4 suggest the presence of an intermediate disordered phase; *two*, the magnitude of the *c* axis of the product does not remain constant during the reaction. $c_I/2$ changes from 9.3 Å (30 min after the start of reaction for both bases) to 9.03 and 9.04 ± 0.01 Å when I = N_2H_4 and NH_3, respectively, whereas a_I remains at 3.32 Å under the experimental conditions described above; and *three*, although when the sample is pumped to $P_I < 10^{-5}$ Torr the c_I axis remains the same, when the sample is exposed to air after pumping at the end of reaction $c_I/2$ changes to 9.10 Å as reported in earlier cases.[6c,11] This is unlike the effects of moisture[6f] because our earlier work excluded moisture but the N_2 atmosphere[6c] was not purified of O_2. The effects of both N_2 and O_2 are being investigated in our laboratory.

The value of x^0 vs. time at room temperature but different P_I(I = NH_3) and sample size are shown in Figure 5. The rate of weight gain is: *one*, first order in the number of unreacted sites ($1 - x^0/x_\infty^0$) to within 6% accuracy (as shown in Table I) and *two*, linear in P_I. For I = N_2H_4 all

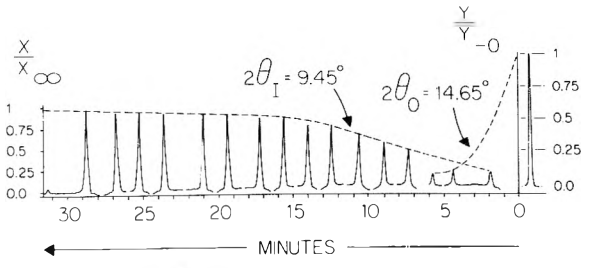

Figure 3. Typical variation of the integrated intensity of the 002 diffraction lines at $2\theta_0 = 14.65°$ for the original phase and $2\theta_I = 9.4°$ for the product phase vs. t (I = N_2H_4). The ordinate was normalized using the intensity of the original phase before the reaction Y_{-0} and that of the product as $t \rightarrow \infty$, X_∞.

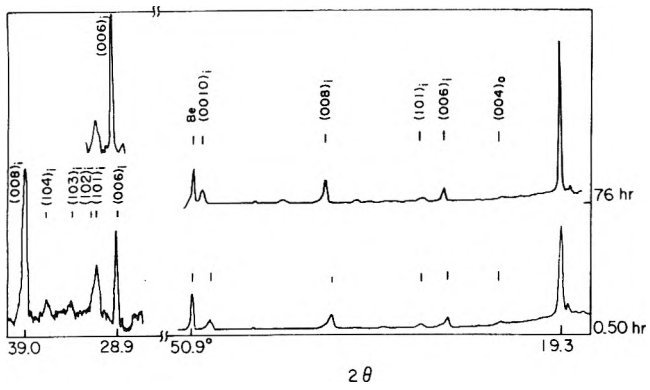

Figure 4. Sections of x-ray diffraction spectra at $t = 0.5$ and 76 hr after I = N_2H_4 was allowed into the evacuated vessel at room temperature and $P_I = 12$ Torr show only two phases are present. The 0010 x-ray diffraction is compared with the Be reference (in an experiment where the cell remained in the diffractometer) to indicate the appreciable change in c_I after the reaction is completed.

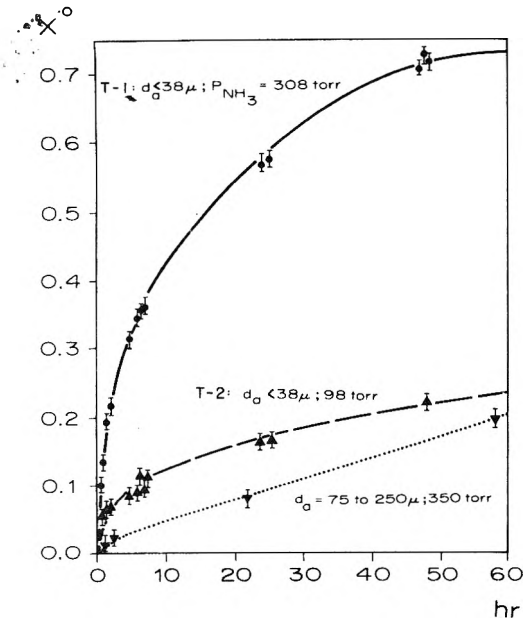

Figure 5. Weight increase vs. time for I = NH_3 with the experimental conditions described in Table I. The ordinate was normalized to $t_{1/2}$ in order to include all the experimental points in the least number of plots.

the data points may be included in Figures 6–8 by plotting $\ln (1 - x^0/x_\infty{}^0)$ vs. $t/t_{1/2}$ where $x^0/x_\infty{}^0 = 1/2$ at $t_{1/2}$. The rates of weight gain were found to be linear in P_I only for $T > 50°C$ at the two lowest pressures as reported in Table I.

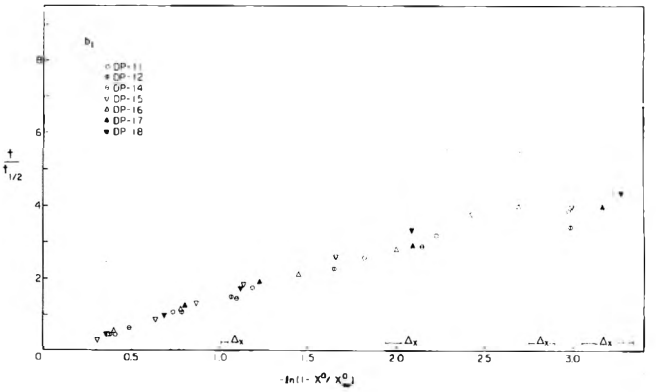

Figure 6. Weight increase vs. time for I = N_2H_4. See caption to Figure 5.

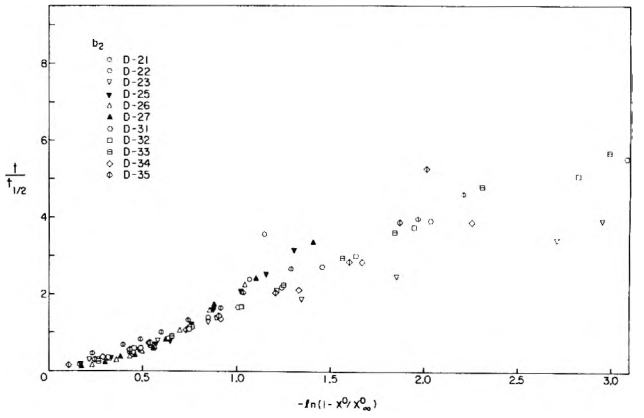

Figure 7. Weight increase vs. time for I = N_2H_4. See caption to Figure 5.

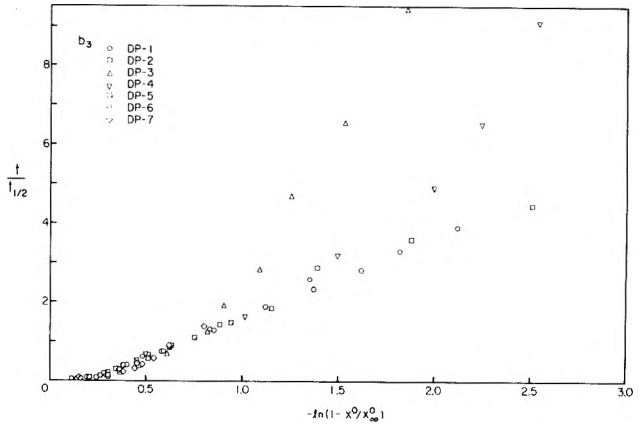

Figure 8. Weight increase vs. time for I = N_2H_4. See caption to Figure 5.

Although N_2 does not intercalate 2H–TaS_2, the adsorption of a monolayer at 77 K slows the intercalation of other gases (beyond measurement when I = NH_3 and by a factor of 10 when I = N_2H_4). The surface of a lamellar crystal is given by the basal planes and a monolayer of N_2 is expected to affect the latter to the greatest extent. However, in order to answer the questions of how the lameallae (which are a distance from the basal plane) start to react the following experiment was carried out. In powders (2H–TaS_2, $d_c \ll d_a < 38$ μm) the rate of disappearance of the integrated intensity of the 100 x-ray reflection (y_{hkl}) is nearly equal to that for the 004 reflection of the reactant phase.

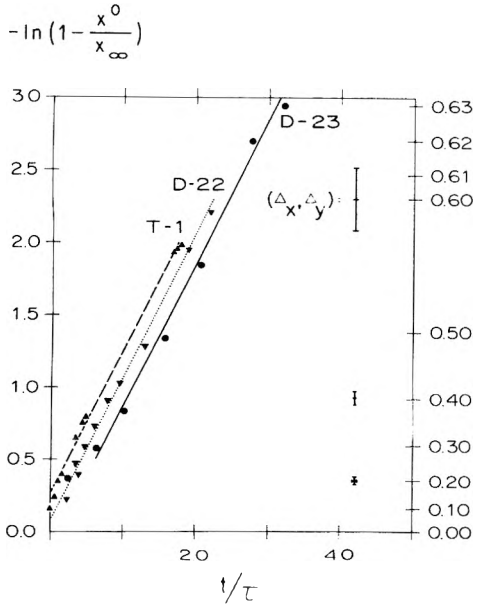

Figure 9. Comparison of first-order rate law behavior of I = NH_3 and N_2H_4 with the experimental conditions described in Table I.

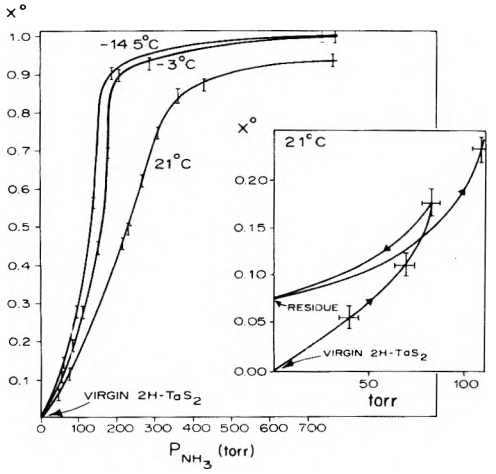

Figure 10. Equilibrium data (isotherms) for $2H_I$-TaS_2-$(NH_3)_n$ complexes. The presence of hysteresis is indicated in the insert.

Two single crystals (2H-TaS_2) of approximately equal weight (19 mg) and $d_a^2 \sim 0.2$–0.1 cm^2 were allowed to react in separate cells as shown in Figure 2 with N_2H_4 (P_I = 5 Torr at room temperature). One crystal was aligned with the c axis normal to the Be window, the other with the a axis normal to the window. For the former only the 00l lines can be measured and the initial rate of disappearance of the integrated intensity for the 002 line is $-(1/y_{002})(dy_{002}/dt = 0.02\ min^{-1}$. For the latter only the h00 lines could be measured. The 100 and 200 lines had sufficient intensity but the 100 line was selected. The spectrometer was adjusted for 2θ (maximum intensity of 100) = 31.14° and the reaction was carried out as described above except that 2θ was left constant. The rate of disappearance of the maximum in the integrated intensity was recorded continuously over a 24-hr period. The rate of disappearance

$$\frac{1}{y_{100}}\frac{dy_{100}}{dt} \leq 2 \times 10^{-3}\ min^{-1}$$

is nearly an order of magnitude slower than that observed

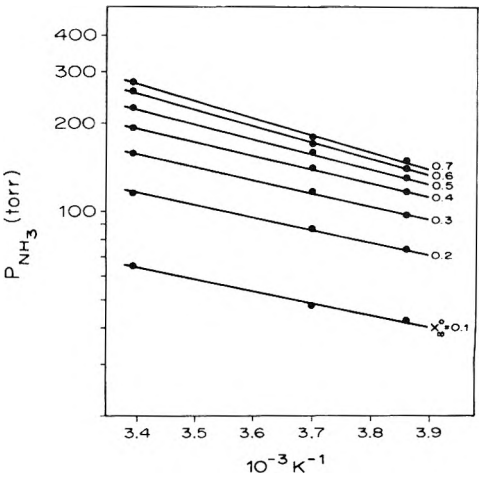

Figure 11. Equilibrium data (isosteres) for $2H_I$-TaS_2-$(NH_3)_n$ complexes. The isosteric heats were evaluated as follows: 7.49, 8.36, 8.61, 9.16, 9.71, 10.29, and 10.83 kJ-mol^{-1} for x_∞^0 = 0.1–0.7, respectively, and the total increase (25%) is greater than the propagated uncertainty ($\Delta q_{st}/q_{st} = 2[\Delta P/P|\ln(P/760)| + \Delta T/(T\delta T)] < 0.02$ in the temperature interval δT = 40°C).

for the 00l lines. After 24 hr the integrated intensity for both the 100 and 200 reflections was reduced by more than 80%. For single crystals with a dimension parallel to c axis $d_c > 10^2$ μm gives $\mu d_c \gg 1$. Therefore the 00l x-ray diffractions sample only the top layers of the crystal. When a crystal is oriented with the a^* axis normal to the Be window the x-ray diffractions do not sample the entire sample either but they do sample the edges of all the lamellae constituting the crystal. Thus the slower rate of disappearance of the h00 lines relative to the 00l lines in single crystals is additional evidence in support that all the lamellae do not start to react simultaneously and that the reaction starts at the basal planes.

The observed first-order rate laws are similar to those measured under very different conditions for the intercalation of TaS_2 by alkaline hydroxides from aqueous solutions.[12] These results may be discussed using the available rate theory for solid–gas reactions as follows.

III. Discussion of Results

The true mechanism of reaction 1 must be consistent with the above experimental observations. Thus using the concepts of absolute reaction rate theory[8e] the first step in the insertion reaction is assumed to be the formation of an activated complex and a mobile species on the top TaS_2 lamella of the reactant phase ϕ_1, i.e.

$$TaS_2(\phi_1) + I(g) \underset{b_-}{\overset{b_+}{\rightleftarrows}} (I \cdot TaS_2)_0^{\ddagger} \underset{k_-}{\overset{k}{\rightleftarrows}} (I_x^0 \cdot TaS_2)_0 \quad (4a)$$

At the lowest pressures measured, the deviations from first-order rate laws in Figure 8 suggest the evaporation of I as well as I^0 is competing with the insertion of I^0 between the TaS_2 lamellae. Thus if the subindex i labels the TaS_2 lamellae starting at the basal planes, the intercalation must proceed in at least two steps: the separation of the TaS_2 lamellae to allow the diffusion of I^0 and the formation of the ordered product phase ϕ_2, i.e.

$$(I_x^0 \cdot TaS_2)_0 \xrightarrow[\text{diffusion of } I^0]{\text{convective}} \sum_i (I_x^0 \cdot TaS_2)_i \xrightarrow[\text{reaction}]{\text{cooperative}} TaS_2 \cdot I_n(\phi_2) \quad (4b)$$

$$b_-^0 \searrow \quad I(g)$$

The rate constants are identified in eq 4 and $b = b_+/b_-$ is the Langmuir adsorption coefficient.[8f] The general mass conservation relations[13] must be satisfied by the fractions of basal surface covered by the activated complex and I^0, θ_s, and θ_0, respectively, i.e.

$$d\theta_s/dt = b_+P_I(1 - \theta_0 - \theta_s) - b_-\theta_s - k\theta_s + k_-\theta_0 = 0 \quad (5)$$

and

$$d\theta_0/dt = k\theta_s + \text{div } \mathbf{D} \cdot [\text{grad } \theta_0 + K \text{ grad } T] - \text{div } \theta_0\mathbf{u} - b_-{}^0\theta_0 - k_-\theta_0 \quad (5')$$

D is the diffusion tensor, K is the coefficient for thermal diffusion, and u is the speed of convection created by the potential gradient under which I^0 penetrates between the $i - 1$ and ith lamellae.

The diffusion time in the direction parallel to the plane of the lamellae (measured by Carr–Purcell–Meiboom–Gill proton NMR echoes) is $\tau_\parallel = 2.3 \times 10^{-10}$ sec for $2H_I$–TaS_2·NH_3.[14] Here, the component of **D** parallel to the layers is of the same order of magnitude as that measured by the same technique for motion of liquids within a mica stack[15] (e.g., $D_\parallel$(water) $= 2.2 \times 10^{-5}$ cm^2 sec^{-1}). However when (4b) is assumed to be the rate-determining step, the data for I = NH_3 in Figure 5 give $D \sim 10^{-12}$ cm^2 sec^{-1} [11] which is inconsistent with the NMR data and the fact that the NH_3 content of the complex is easily decreased by reducing P_I to 10^{-5} Torr at room temperature. Thus, in a first-order approximation eq 4a will be assumed to be the rate-determining step. In this case θ_0 also achieves a steady state value which is equal to the bulk distribution (i.e., $\theta_0 = x^0/x_\infty{}^0$). From eq 5 it then follows that

$$\theta_s = [1 + bP_I + k/b_-]^{-1}[(1 - \theta_0)bP_I + \theta_0 k_-/b_-] \quad (6)$$

and the excess I^0 produced in (4a) reaches the edge of the basal plane at the rate

$$(d[I^0]/dt)_0 = (k\theta_s - k_-\theta_0 - b_-{}^0\theta_0)N_0 \quad (7)$$

where N_0 is the total number of sites available for reaction on the top lamella. Intercalation between the lamellae within the body of the crystal occurs when a positive flux is created (by the concentration gradient and the attractive potential due to the affinity of I^0 for the TaS_2 lamellae) at the edge of the basal plane in the direction of the c axis.

The rate of weight gain is equal to the rate of excess I^0 produced on the basal surface per site available for intercalation in the entire crystalline particle. Thus for crystalline particles made-up by $2d_c/c$ lamellae of equal dimensions $\sim d_a{}^2$ (where c is the magnitude of the c axis in the reactant phase), the initial rate of weight gain is given by

$$dx^0/dt = (d[I^0]/dt)_0[N_0(dc/c)]^{-1} = k\theta_s(d_c/c)^{-1} \quad (8)$$

and from eq 6–8 an initial rate of reaction which is first order in the number of unreacted sites in the bulk is obtained, i.e.

$$d\{\ln (1 - x^0/x_\infty{}^0)\} \simeq -\tau^{-1}d(t - t_0) \quad (8')$$

where

$$\tau = \left[\frac{b_-}{kb_+P_I} + \frac{1}{k} + \frac{1}{b_+P_I}\right] d_c/c$$

subject to the condition that the particle basal dimension is $d_a \ll 4(\tau D_\parallel)^{1/2}$ because in step 4b the time of diffusion to the center between two lamellae of area $d_a{}^2$, $d_a{}^2/16D_\parallel$, must be shorter than τ. Thus $d_a{}^2/16\tau D_\parallel \ll 1$ is satisfied in Table I. Here τ was obtained by fitting the data in Figures 5–9 using a weighted least-squares analysis,[16] and $D_\parallel$ was estimated from the NMR data.[14,15] The finite intercept indicates the integrating constant t_0/τ is small but nonzero. However, the physical significance of t_0 is hard to ascertain because crystalline imperfections on the surface can introduce a delay time for the start of reaction and induce evaporation of I^0. A delay time for the start of diffusion between the lameallae in the order of their distance from the basal plane has already been suggested as a possibility.[11,17] The experimental observation may be discussed using eq 4 as follows:

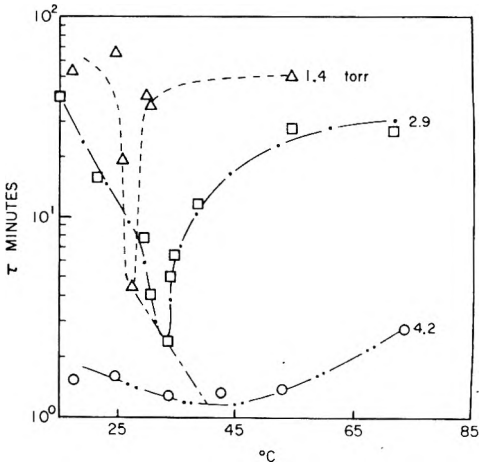

Figure 12. τ vs. T for I = N_2H_4 at different pressures for the data reported in Table I: (△) P_i = 1.4 Torr; (□) 2.9 Torr; (○) 4.2 Torr.

One, a correlation of τ with the linear dimension of the reactant is consistent with (8′). Also the fact that straight lines are observed in Figure 9 for $t/\tau > 1$ suggests $b_-{}^0$, $k_- \ll k$ in step (4a) for both I = NH_3 and N_2H_4.

Two, the difference in the affinity of NH_3 and N_2H_4 for TaS_2 is indicated by the pressures at which measurable rates are observed. However at sufficiently high temperatures the rates are linear in P_I within the uncertainties reported in Table I suggesting that under these conditions b_+P_I is the rate-determining step.

Three, the hysteresis effects observed in the isotherms shown in Figure 10 should be related to the variation in the magnitude of the c axis of the product during the reaction. No attempt will be made to interpret these results until extensive rate of c_I change vs. T,P is realized except to note that (4b) must involve at least two steps.

Four, careful rate studies reported in Figures 6–8 were used to test the mechanism postulated in eq 4a as follows. In Figure 12, τ vs. T at constant P_I goes through a minimum value (τ^0). This follows from eq 4a assuming typical activation energies for b_+ and k, $-E_+$ and $E_a(E_+, E_a > 0)$, and zero for b_-.[8f] A minimum is reached when $E_+(1 + k/b_-) = E_a(1 + bP_I)$ because in (8′)

$$(\partial \ln \tau/\partial\beta)_{P_I} = E_a - E_+ + [E_+bP_I - E_ak/b_-][1 + bP_I + k/b_-]^{-1}$$

and

$$(\partial^2 \ln \tau/\partial\beta^2)_{P_I} = [(E_+ + E_a)^2kbP_I/b_- + E_+{}^2bP_I + E_a{}^2k/b_-] \times [1 + bP_I + k/b_-]^{-2} > 0 \quad (9)$$

where

$$(\tau k)_{\beta=\beta^0} = (d_c/c)[1 + (E_a/E_+)(1 + 1/bP_I)]_{\beta=\beta^0}$$

and $\beta = 1/RT$. The shift in the temperature $T^0 = 1/R\beta^0$ at which the minima are observed vs. P_I is consistent with the relation

$$d\beta^0/dP_I = -bE_+^{-1}(k/b_- + bP_I)^{-1} < 0 \quad (10)$$

and

$$d \ln \tau^0 = \left(\frac{\partial \ln \tau^0}{\partial \beta}\right) d\beta + \left(\frac{\partial \ln \tau^0}{\partial P_I}\right) dP_I \quad (11)$$

gives a pseudo-activation energy

$$E^0 = d \ln \tau^0/d\beta^0 = E_a[1 + (d_c/c)(\tau^0 b_- b^2 P_I^2)^{-1}]_{\beta^0} \quad (12)$$

which is estimated from the data in Figure 12 to be $E^0(N_2H_4) \sim 70$ kJ mol^{-1}. A lower limit for $(E_aE_+)^{1/2}$ of 7×10^2 kJ mol^{-1} was estimated as follows. A Taylor series expansion about the minimum τ^0 leads to

$$(\tau - \tau^0)/\tau^0 = \frac{1}{2}(\beta - \beta^0)^2(\partial^2 \ln \tau/\partial\beta^2)_{\beta^0} + \ldots \quad (13)$$

where

$$(\partial^2 \ln \tau/\partial\beta^2)_{\beta^0} = E_+E_a[(k/b_- + bP_I)/(1 + bP_I + k/b_-)]_{\beta^0}$$

and if $\tau(\beta_2) = 2\tau^0$

$$\Delta\beta = |\beta^0 - \beta_2| = (2/E_aE_+)^{1/2}[(1 + bP_I + k/b_-)/(k/b_- + bP_I)]_{\beta^0}^{1/2} \quad (14)$$

defines a breadth which increases with P_I as indicated by the data in Figure 12. Also from (14) $(E_aE_+)^{1/2} > 2^{1/2}/\Delta\beta \approx 7 \times 10^2$ kJ mol^{-1} and in (9) $(\tau k)_{\beta^0} \approx d_c/c$ or $E_a \approx E^0$.

Five, the isotherms measured for I = NH_3 in Figure 10 led to the determination of the isosteres shown in Figure 11. Langmuir adsorption isotherms[8f] cannot explain the data because the isosteric heats reported in Figure 11

$$q_{st} = -(\partial \ln P_I/\partial\beta)_{x_\infty{}^0} \quad (15)$$

do not remain constant with $x_\infty{}^0$. These increase with $x_\infty{}^0$. This change is in the opposite direction predicted by the Temkin and Freundlich isotherms. However simple arguments based on Henry's law for solid solutions can be used to discuss the data. Here the fugacity of the solute is

$$f_I = \gamma_I P_I = \mathcal{K}_I x_\infty{}^0/(1 + x_\infty{}^0) \quad (16)$$

where $\gamma_I \sim \exp[-\beta P_I(V_{ideal} - V_{real})] \sim \exp\beta P_I(b - a\beta)$ when I behaves to first order as a van der Waals or Dieterici gas with constants a and b and $\mathcal{K}_I$ is the Henry law constant. Then

$$-q_{st} = [(\partial \ln \mathcal{K}_I/\partial\beta)_{x_\infty{}^0} - 2a\beta P_I]/[1 + \beta P_I(b - a\beta)] \quad (17)$$

Langmuir adsorption cannot explain the data because the correction terms for a nonideal gas in (17) are of the order of $2\beta a P_{NH_3} \sim 10$ J mol^{-1} [10] which is two orders of magnitude smaller than the changes in q_{st} reported in Figure 11. Therefore, since the measurements on the superconducting transition temperature T_c indicate the presence of more than one well-defined complex (where T_c increases with the NH_3 content[7]), the data suggest q_{st} increases with $x_\infty{}^0$ because the change in enthalpy for (1) is negative and decreases as n increases and that $\bar{\mathcal{K}}_I$ is an average of several chemical equilibrium constants.

IV. Conclusions

The experimental observations lead to the following conclusions and/or conjectures:

One, the self-consistency of eq 4 with all the phenomena observed suggest that the ratio greater than two orders of magnitude for the measured τ when I = NH_3 relative to I = N_2H_4 arises in step 4a.

Two, N_2H_4 is more tightly bound than NH_3 in the TaS_2 complexes as shown by the fact that the NH_3 content can be decreased by reducing P_I to 10^{-5} Torr at room temperature whereas $n = 2/3$ remains constant with N_2H_4 under similar conditions. This supports the concept that EDA complexes are formed since the interaction with the latter is expected to be stronger than with the former because the respective dipole moments and ionization potentials are 0.58 and 1.75 D and 10.2 and 8.7 eV for NH_3 and N_2H_4. The 2% contraction in the c axis of the product phase at the end of reaction may also be the result of stabilization of the EDA complex. Thus, the magnitude of the interactions in the EDA complex[18] determine whether the charge density waves found for the 1T, 2H, and 4Hb polytypes of TaS_2[19] are suppressed by intercalation and how the latter affect the physical properties.

Three, finally in the spirit of the Colloque Weyl it is important to note that the interaction of gases with metals such as 2H–TaS_2 lead to the formation of new types of compounds where even M–NH_3 can be intercalated up to the limiting solubility of M in NH_3.[20]

Acknowledgments. This work was supported by San José State University President Fellows Program, the Research Corporation, and NSF grants in aid GP 21293 and DMR 74-11752. J.V.A. is grateful for released time as a San José State President Fellow during 1974–1975. We are grateful to Dr. H. Topsøe for enlightened discussion and to Dr. S.F. Meyer for some of the TaS_2 samples.

References and Notes

(1) San José State University Fellow.
(2) (a) J. V. Acrivos, W. Y. Liang, J. A. Wilson, and A. Yoffe, *J. Phys. C.*, **4**, L18 (1971); (b) A. R. Beal and W. Y. Liang, *Phil. Mag.*, **27**, 1397 (1973); *J. Phys. C.*, **6**, L482 (1973).
(3) J. V. Acrivos and J. R. Salem, *Phil. Mag.*, **30**, 603 (1974).
(4) W. Rudorff, *Chimia*, **19**, 489 (1965).
(5) A. Weiss and R. Ruthardt, *Z. Naturforsch. B*, **24**, 356 (1969); **28**, 249 (1973).
(6) (a) F. R. Gamble, J. H. Osiecke, M. Cais, R. Pisharody, F. J. DiSalvo, and T. H. Geballe, *Science*, **174**, 493 (1971); (b) J. F. Revelli, Ph.D. Thesis, Stanford, University, 1972; (c) S. F. Meyer, R. Howard, G. Stewart, J. V. Acrivos, and T. H. Geballe, *J. Chem. Phys.*, **62**, 4411 (1975); (d) G. S. Parry, C. B. Scruby, and P. M. Williams, *Phil. Mag.*, **29**, 601 (1974); (e) P. W. Williams and B. A. Robinson, *Nature (London)*, **245**, 79 (1973); (f) M. S. Wittingham, *Mater. Res. Bull.*, **9**, 1681 (1974).
(7) J. V. Acrivos, S. F. Meyer, and T. H. Geballe, "Proceedings of Colloque Weyl III", 1972, "Electron in Fluids", J. Jortner and N. Kestner, Ed., Springer Verlag, West Berlin, 1973, p 341.
(8) (a) J. W. McBain and A. M. Bakr, *J. Am. Chem. Soc.*, **48**, 690 (1926); (b) D. P. Shoemaker, C. W. Garland, and J. I. Steinfeld, "Experiments in Physical Chemistry", 3rd ed, McGraw-Hill, New York, N.Y., 1974; (c) H. P. Klug and L. E. Alexander, "X-Ray Diffraction Procedures", Wiley, New York, N.Y., 1954; (d) W. H. Zachariasen, "Theory of X-Ray Diffraction in Crystals", Wiley, New York, N.Y., 1946; (e) S. Glasstone, K. J. Laidler, and H. Eyring, "The Theory of Rate Processes", McGraw-Hill, New York, N.Y., 1942; (f) T. L. Hill, "An Introduction to Statistical Thermodynamics", Addison-Wesley, Reading, Mass., 1960, Chapter 7.
(9) J. V. Acrivos and J. Azebu, *J. Magn. Reson.*, **4**, 1 (1971).
(10) (a) "CRC Handbook of Physics and Chemistry", 49th ed, R. C. Weast, Ed., The Chemical Rubber Co., Cleveland, Ohio, 1969; (b) L. F. Audrieth and B. Ackerson Ogg, "The Chemistry of Hydrazine", Wiley, New York, N.Y., 1951; (c) "Handbook of Chemistry", 10th ed, E. Lange, Ed., McGraw-Hill, New York, N.Y., 1967.
(11) N. Y. Topsøe, M.S. Thesis, San José State Unitversity, San José, Calif., 1974.
(12) G. B. Subba Rao and M. W. Shafer, *J. Phys. Chem.*, **79**, 557 (1975).
(13) (a) V. G. Levich, "Physicochemical Hydrodynamics", translated by

Scripta Technica, Inc., Prentice Hall, New York, N.Y., 1962; (b) V. V. Rachinskii, "General Theory of Surface Dynamics and Chromatography", translated from Russian by Consultants Bureau, New York, N.Y., 1965.
(14) B. Silbernagel and F. J. Gamble, Phys. Rev. Lett., **37**, (1974).
(15) (a) E. O. Stejskal, *J. Chem. Phys.*, **43**, 3597 (1965); (b) J. E. Tanner and E. O. Stejskal, *ibid.*, **49**, 1768 (1968).
(16) F. Daniels, J. W. Williams, P. Bender, R. A. Alberty, C. D. Cornwell, and J. F. Harriman, "Experimental Physical Chemistry", 7th ed, McGraw-Hill, New York, N.Y., 1970, p 451.
(17) G. Hooley, *Can. J. Chem.*, **35**, 374 (1957); *Carbon*, **2**, 131 (1964).
(18) J. V. Acrivos, *J. Phys. Chem.*, **78**, 2399 (1974).
(19) (a) J. A. Wilson, F. J. DiSalvo, and S. Mahajan, *Bull. Am. Phys. Soc.*, **18**, 386 (1973); *Phys. Rev. Lett.*, **32**, 16, 882 (1974); (b) C. B. Scruby, P. M. Williams, and G. S. Parry, *Phil. Mag.*, **31**, 255 (1975).
(20) S. F. Meyer, J. V. Acrivos, and T. H. Geballe, *Proc. Natl. Acad. Sci. U.S.*, **72**, 464 (1975).

Discussion

M. J. SIENKO. (a) Where does the N_2H_4 go? Does it go between each pair of layers or leave some unchanged? (b) Does TaS_2 stay in 2H polytype? (c) NH_3 on side in TaS_2. Similar for N_2H_4. Lone pair avoids layer.

J. V. ACRIVOS. The complete x-ray diffraction spectra taken 0.50 and 76 hr after the start of reaction were analyzed by a weighted least-squares program [S. F. Meyer, R. E. Howard, G. R. Stewart, J. V. Acrivos, and T. H. Geballe, *J. Chem. Phys.*, **62**, 4411 (1975)]. These show that there is only one ordered phase present at all times and that the sequence of the Ta and S layers is as indicated in the figure shown. We have not determined the structure of the hydrazine layer. However the most important observation is that although the magnitude of the a axis in the hcp 2H phase does not change appreciably, the magnitude of the c axis changes from 18.5 Å at 0.5 hr after the start of reaction to 18.0 Å 76 hr after the start of reaction. This is dramatically shown by comparing the 0010 reflection with the Be reference given by the window of the cell in Figure 3. The changes in base line suggest also the presence of other disordered phases.

(c) We cannot answer the last question without doing a neutron diffraction study of N_2D_4 intercalated compounds. Please give reference of NH_3 intercalated compound. Our work with NH_3 + TaS_2 indicates that the final product depends strongly on the pressure of the gas during the reaction.

Electron Spin Resonance Studies of Localized Excess Electron States in Frozen Solutions of Alkali Metals in Hexamethylphosphoramide

Ron Catterall* and Peter P. Edwards

Department of Chemistry and Applied Chemistry, University of Salford, Salford M5 4WT, England *(Received July 25, 1975)*

Electron spin resonance spectra of frozen solutions of sodium, potassium, rubidium, and cesium metals in HMPA are reported. Spectra at low microwave power levels ($\lesssim$1 mW) showed the existence of several, discrete, localized excess electron states with unpaired electron spin density lying between ~36 and ~80% of the free atom value. In potassium, rubidium, and cesium solutions, a localized state with spin density $\lesssim$1% of the free atom value was also identified. Magnetic parameters (hyperfine coupling constant, electronic g factor) for both the high and low atomic character states in frozen metal–HMPA solutions showed similarities with results for fluid metal–amine solutions. The relevance of our observations to current models for metal–amine solutions is discussed. The experimental distribution function for localized excess electron states provides strong support for a multistate model for fluid metal–amine solutions. The high atomic character states are described in terms of intermediate impurity states in the host (HMPA) matrix, while the low atomic character state approximates closely to a true Wannier–Mott impurity ground state.

Introduction

Fluid solutions of alkali metals in ammonia,[1,2] HMPA,[3] amines,[4-8] and ethers[9,10] have electron spin resonance (ESR) spectra which can be classified into two groups: those for which only a single, time-averaged signal is observed, and those for which two signals are observed, a hyperfine multiplet from electron–cation aggregates, and a central singlet from isolated solvated electrons. A quantitative explanation for these differences in spectra is possible[11] in terms of simple ion-pairing theory

$$M_{solv}^{+} + e_{solv}^{-} \rightleftharpoons M_{solv} \qquad (1)$$

In solvents of high dielectric constant (ammonia, HMPA) the rate constants for (1) are such that the average lifetime, $\langle\tau_M\rangle$, of M_{solv} is short compared to the inverse of the metal hyperfine coupling constant (A_{iso}^{-1}), and $\langle\tau_M\rangle A_{iso} \ll 1$. A time averaging of signals from e_{solv}^{-} and M_{solv} occurs and only a single absorption line is observed.

In solvents of low dielectric constant (amines, ethers) $\langle\tau_M\rangle A_{iso} \gg 1$ and signals from both paramagnetic centers are observed. Calculated values[11] of $\langle\tau_M\rangle A_{iso}$ for a wide range of metal–solvent systems are illustrated in Figure 1.

Perhaps the most intriguing aspect of fluid amine and ether solutions lying above the critical region, $\langle\tau_M\rangle A_{iso} \sim 1$, is the marked temperature dependence of the metal hyperfine coupling constants.[4-10] In some cases A_{iso} varies by almost two orders of magnitude over a relatively small temperature interval, and two conceptually different models have been proposed to explain this behavior.

In a "continuum" model, a single species is proposed whose structure is markedly temperature dependent,[4,12] while a "multistate" model pictures a dynamic and temperature-dependent equilibrium between two (or more) species of the same stoichiometry whose structures are relatively insensitive to temperature.[6a,8b] Both models are equally capable of explaining both the temperature dependence of A_{iso} and the strong dependence of line widths upon nuclear spin configuration. Again both models contain too many parameters for adequate testing to be carried out.

An unambiguous distinction between the models should be possible by examination of ESR spectra of frozen solutions,[13] but unfortunately several factors have contributed to an almost complete failure to obtain frozen metal solutions which preserve the structure of the liquid state: (i) solutions in more polar solvents show a strong tendency to separate out on freezing into crystalline phases of pure metal and pure solvent;[14–16] (ii) although crystallization is more readily avoided in the less polar amines and ethers, solubilities are much lower;[10] (iii) the spin-pairing equilibrium in less polar solvents is generally shifted strongly away from states involving unpaired electron spin.[9b] This problem is further enhanced at lower temperatures.[4a,8a]

Although the high static dielectric constant[18] of fluid HMPA (Figure 1) ensures that only a single, time-averaged ESR absorption is found a room temperature,[3] the presence of metal-dependent bands in the visible region[3,19] establishes a strong link with amine and ether solutions. In addition, the high solubilities[3] of alkali metals in HMPA, the high fraction of unpaired electron spins (~10%),[3,9b] and the high freezing point (~7°C) and viscosity[20] of HMPA all suggest strongly that homogeneous frozen solutions might be obtained with sufficient concentrations of unpaired electron spins for practical study. In accord with these suggestions we have found that rapid freezing of solutions of alkali metals in HMPA does give rise to homogeneous blue glasses, and in this paper we report some preliminary results of ESR investigations of frozen solutions of sodium, potassium, rubidium, and cesium metals in HMPA.

Experimental Section

Samples were prepared using conventional high vacuum techniques modified for use with a high boiling solvent. Spectra were recorded on a Varian V4502 spectrometer using standard accessories and operating at ~9.1 GHz. Microwave power levels incident upon the cavity were ~1.0 mW.

Results

Spectra (77 K) of frozen solutions of sodium, potassium, rubidium, and cesium are shown in Figure 2. The main characteristics of the spectra are summarized as follows. (i) Strong central singlets had line widths and g factors which varied from one metal to another. (ii) Isotropic multiplet signals consisted of $2I + 1$ lines, where I is the nuclear spin of the alkali metal. (iii) Line width of multiplet spectra were dependent upon the nuclear magnetic quantum number, m_I, of the alkali metal. Line width variations were particularly marked for rubidium and cesium solutions. (iv) Spectra at high machine amplification revealed a multitude of weaker signals (Figures 3, 6, and 7). (v) Both singlet and multiplet resonances had line shapes approximating closely to Gaussian. (vi) Microwave power saturation behavior of both singlet and multiplet resonances was characteristic of

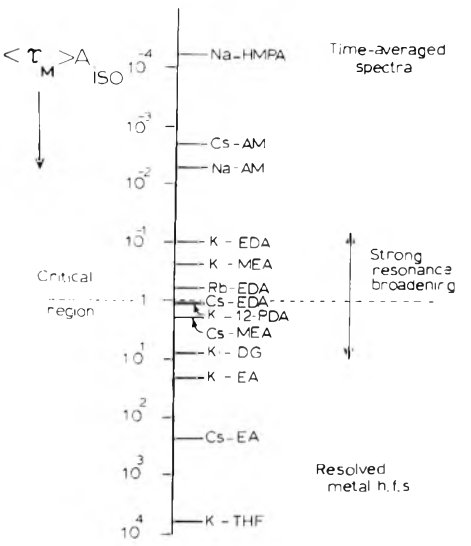

Figure 1. Classification of ESR spectra (~296 K) of fluid metal solutions on the basis of the product $\langle \tau_m \rangle A_{iso}$: THF = tetrahydrofuran, EA = ethylamine, DG = diglyme, MEA = methylamine (~220 K), 1,2PDA = 1,2-propanediamine, EDA = ethylenediamine, AM = ammonia (~240 K).

inhomogeneously broadened lines.[21] Saturation curves for the narrowest hyperfine components ($\Delta H_{ms} \sim 4.4$ G) of potassium, rubidium, and cesium spectra are compared in Figure 4. For potassium through cesium, the onset of saturation moves to higher microwave power in accord with enhanced spin–orbit coupling for the heavier atoms. (vii) All line positions, widths and shapes, and all relative and absolute intensities were independent of temperature over the accessible range (77–180 K).

Analysis of Spectra. Singlet Resonances. Line widths showed a marked dependence upon the nature of the metal in solution (Table I) and spectra were simulated to first order to obtain metal hyperfine coupling constants. Assuming coupling to a single metal nucleus and an intrinsic width of 4.3 G, comparable to the narrowest of the hyperfine components of multiplet spectra, the hyperfine coupling constant was adjusted to fit the observed line shapes. Results are given in Table I.

Multiplet Resonances. Experimental line positions for the dominant multiplets were fitted to the Breit–Rabi equation[22]

$$W_{(F,m_F)} = \frac{-\Delta W}{2(2I+1)} - \frac{\mu_I H_0 m_F}{I} \pm \frac{\Delta W}{2} Q \qquad (2)$$

where $W_{(F,m_F)}$ is the energy of a state with magnetic quantum numbers F and m_F, and

$$Q = \left\{1 + \left(\frac{4m_F x}{2I+1}\right) + x^2\right\}^{1/2} \qquad (3)$$

The zero field splitting, ΔW, is given by

$$\Delta W = \frac{hA_{iso}}{2}(2I+1) \qquad (4)$$

and

$$x = (g_e - g_I)\mu_B H_0/\Delta W \qquad (5)$$

where g_I is the nuclear g factor and μ_B the Bohr magneton.

A comparison of observed and calculated line positions, together with the derived magnetic parameters (g_e and A_{iso}), is given in Table II.

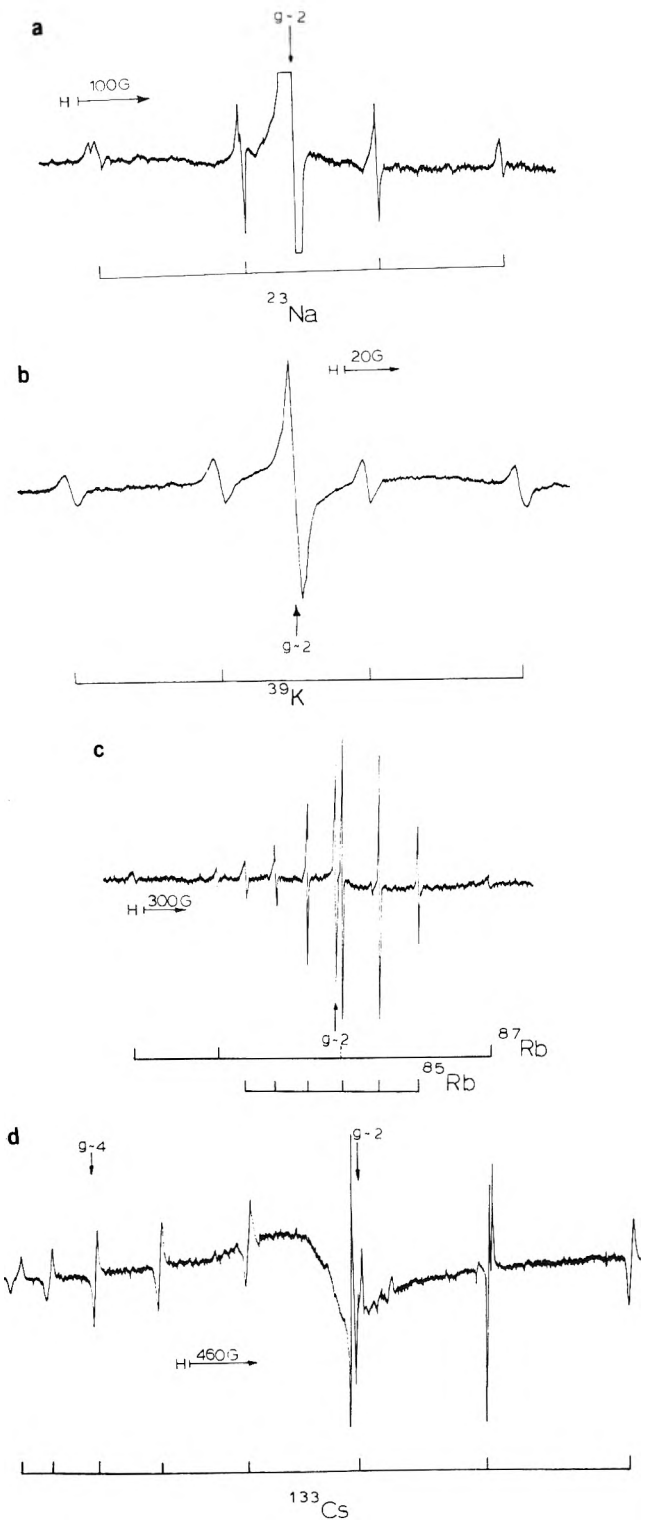

Figure 2. Electron spin resonance spectra (77 K) of frozen solutions of (a) sodium, (b) potassium, (c) rubidium, and (d) cesium in HMPA.

Analysis of spectra obtained at high machine amplification was more complicated; spectra of rubidium and cesium solutions in particular gave resonance patterns which at first sight appeared unrelated. In these cases, analysis in the first instance relied heavily upon calculated plots such as that given in Figure 5 which show the variation of resonant field position of a given line as a function of the metal hyperfine coupling constant. Our identification of lines in rubidium and cesium spectra are given in Figures 6 and 7. Lines correlated in this manner were then subjected to a full least-squares analysis to yield final values of A_{iso} and g_e.

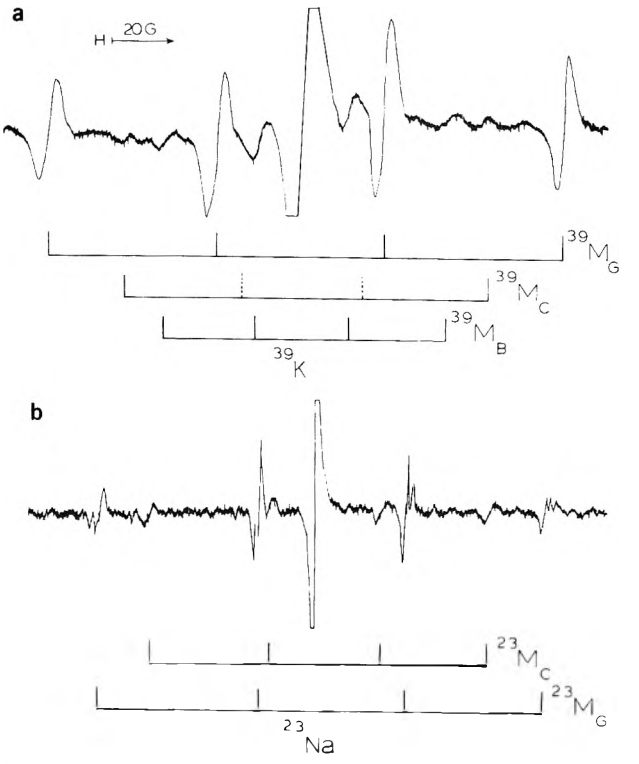

Figure 3. Electron spin resonance spectra at higher amplification of frozen solutions of (a) potassium and (b) sodium in HMPA.

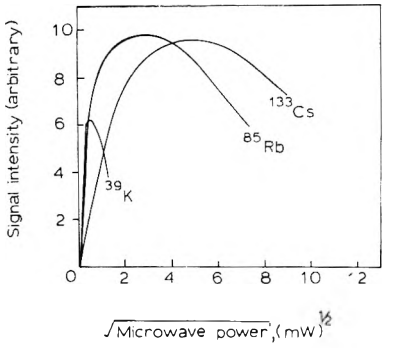

Figure 4. Microwave power saturation of the narrowest hyperfine components ($\Delta H_{ms} \sim 4.4$ G) of the species M_G in potassium, rubidium, and cesium solutions in HMPA (77 K).

TABLE I: Magnetic Parameters for the Central Singlet Resonance in Frozen Solutions of Potassium, Rubidium, and Cesium Metals in HMPA[a]

Isotope	ΔH_{ms}, G	g_e (±0.0004)	A_{iso}, G	% atomic character
^{39}K	4.9 ± 0.3[b]	2.0018	0.80 ± 0.1	0.97 ± 0.10
^{85}Rb	9.4 ± 0.5[c]	2.0009	1.48 ± 0.1	0.41 ± 0.03
^{133}Cs	14.9 ± 0.8[d]	1.9994	1.85 ± 0.1	0.23 ± 0.02

[a] The intense colloidal metal resonance from sodium solutions (Figure 1a) effectively obscures all other resonances in the $g_e \sim 2$ region (*ca.* 3200 G). [b] Average of five samples examined. [c] Average of two samples examined. [d] Average of four samples examined.

TABLE II: Magnetic Parameters Derived from the Dominant Multiplet Resonance in the ESR Spectra (77 K) of Frozen M–HMPA Solutions[a]

Line positions	+7/2	+5/2	+3/2	+1/2	−1/2	−3/2	−5/2	−7/2	Isotope, sample	Magnetic parameters[b] (frequency), GHz
Obsd[c]			2946.2	3132.3	3329.3	3543.1			^{23}Na	198.36
			(2.0)	(1.0)	(1.0)	(2.0)				2.00135
Calcd			2945.6	3131.9	3330.4	3541.0			Na-3	(9.1138)
Obsd			3184.3	3238.3	3292.8	3348.7			^{39}K	54.75
			(0.3)	(0.3)	(0.3)	(0.3)				2.00090
Calcd			3184.4	3238.2	3238.2	3348.6			K-5	(9.1504)
Obsd		2626.8	2838.6	3072.2	3322.8	3594.0	3885.9		^{85}Rb	251.34
		(2.0)	(0.5)	(1.0)	(0.1)	(0.2)	(1.0)			1.99806
Calcd		2626.6	2839.1	3071.1	3322.7	3594.2	3885.0		Rb-1	(9.1735)
Obsd			1815.8	2430	*d*	4406			^{87}Rb	849.0
			(1.0)	(1.5)		(1.5)				1.99802
Calcd			1816.7	2430.4	3293.4	4405.9			Rb-1	(9.1735)
Obsd	924.6	1153.8	1473.3	1936	2534	*d*	4200.5	5198.5	^{133}Cs	604.0
	(5.0)	(3.0)	(3.0)	(10)	(3.0)		(1.0)	(1.5)		1.99213
Calcd	934.6	1156.2	1472.3	1920.5	2529.6	3299.8	4201.9	5198.5	Cs-3	(9.1019)

[a] Calculated line positions are given by the Breit–Rabi equation (eq 2). [b] To conserve space we have adopted the following convention for tabulating parameters: e.g., 198.4, value of A_{iso}(G); 2.0014, g_e derived from Breit Rabi analysis; (9.1134), experimental frequency, GHz. [c] Values in parentheses denote estimated error (G) in line positions. [d] Line obscured by strong central singlet.

TABLE III: Magnetic Parameters[a] for the Localized States (M_B–M_H) in Frozen Solutions of the Alkali Metals in HMPA (77 K)

Isotope	A_{iso}, G	$\|\psi(0)\|_M^2 \times 10^{-24}$	% atomic[b] character	g_e	$\Delta g_e \times 10^4$ [c]	Designation
^{23}Na	198.36	3.173	62.75	2.00135	9.6	$^{23}M_G$[d]
	150.95	2.415	47.75	2.00119	11.0	$^{23}M_C$
^{39}K	54.75	4.964	66.45	2.00090	15.1	$^{39}M_G$[d]
	~38	~3.51	~47	2.0009	15	$^{39}M_C$
	30.16	2.734	36.60	2.00082	14.9	$^{39}M_B$
^{85}Rb	277.3	12.153	76.8	1.99824	41.7	$^{85}M_I$
	268	11.74	74.2	1.9982	42	$^{85}M_H$
	251.34	11.015	69.61	1.99806	43.5	$^{85}M_G$[d]
	233.2	10.223	64.6	1.9992	32	$^{85}M_E$
	210	9.210	58.2	1.9985	39	$^{85}M_D$
	179.1	7.851	49.6	1.9988	36.1	$^{85}M_C$
^{87}Rb	849.0	10.978	69.63	1.99802	43.9	$^{87}M_G$[d]
	706.3	9.134	57.93	1.9986	38	$^{87}M_D$
^{133}Cs	655	21.16	80	~1.992		$^{133}M_H$
	604.0	19.440	73.5	1.99213	104.5	$^{133}M_G$[d]
	595	19.18	72.5	~1.992		$^{133}M_F$
	555	17.91	67.7	~1.992		$^{133}M_E$
	493	15.92	60.2	~1.992		$^{133}M_D$

[a] Taken from experimental data at 77 K which gave the smallest rms deviation in the Breit–Rabi analysis. [b] Calculated from free atom hyperfine coupling constants (A), given in P. Kusch and V. W. Hughes, "Handbuch der Physik", Vol. XXXVII/1, Springer-Verlag, Berlin, 1959, pp 100 and 117. [c] $\Delta g_e = (g_e(\text{free atom}) - g_e)$. Free atom values:

	^{23}Na	^{39}K	^{85}Rb	^{87}Rb	^{133}Cs
A, G	316.109	82.38	361.07	1219.25	819.84
g_e	2.00231	2.00231	2.00241	2.00241	2.00258

[d] Dominant states.

A full listing of magnetic parameters for states identified so far is given in Table III where we have provisionally classified states on the basis of their percentage occupation of the outer metal *n*s orbital. We use a system[24] which labels, for example, the lowest atomic character state (^xM_A), where x denotes the mass number of the particular isotope. We stress that there are still some unidentified lines in the spectra; more complete analysis will be attempted elsewhere on the basis of further experimental studies.

Line Width Variations. The m_I dependence of line widths in the solid state spectra (Figure 2) was superficially similar to that observed for fluid solutions of alkali metals in amines.[4-6] However, we stress that the interpretation of this behavior for fluid solutions (i.e., rapidly fluctuating structural changes) *cannot* be applied to our spectra obtained from rigid solutions. Likewise, the explanation we propose below cannot be applied to fluid solutions.

We first express the observed line width as sums of m_I-dependent (ΔH_{m_I}) and m_I-independent (ΔH_{res}) contributions

$$\Delta H_{obsd}^2 = \Delta H_{m_I}^2 + \Delta H_{res}^2 \quad (6)$$

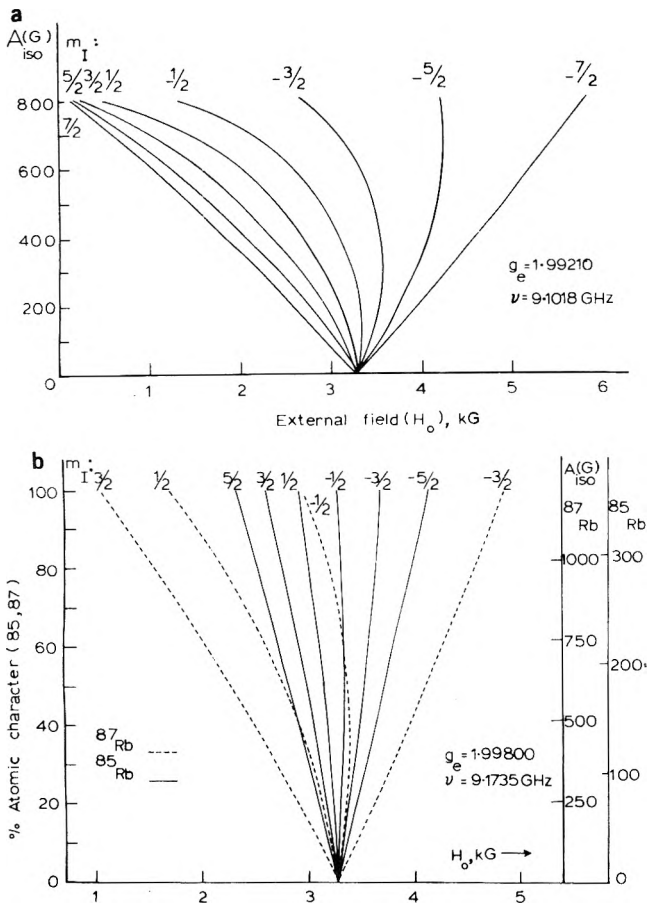

Figure 5. Variation in the resonant field positions with metal hyperfine coupling constant for (a) ^{133}Cs (I = 7/2) and (b) ^{85}Rb (I = 5/2) and ^{87}Rb (I = 3/2). Calculated using eq 2.

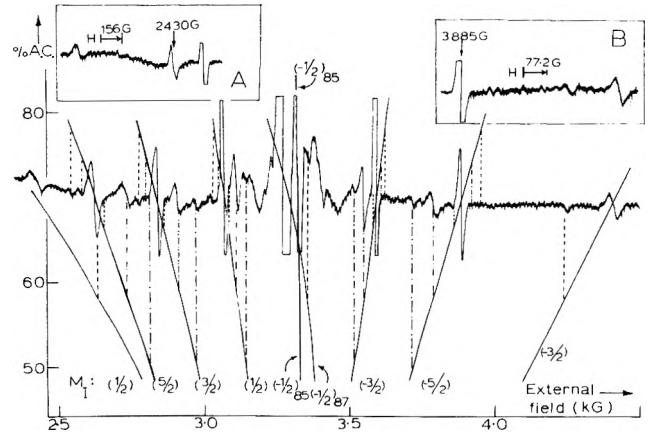

Figure 6. Analysis of the ESR spectrum of a solution of rubidium in HMPA (77 K). Full lines show the variation of resonant field position with A_{iso} (eq 2) for g_e = 1.99800 and a microwave frequency of 9.1735 GHz. The lines are anchored at the crossovers of the M_G species (A_{iso} = 251.3 G). Insert A shows the low-field (m_I = +3/2) ^{87}Rb line; insert B gives a rerun of the high-field section.

and postulate the existence of normal (Gaussian) distributions of hyperfine coupling constants to metal nuclei centered on each of the derived A_{iso} values. The width of the distributions must be small to account for the narrow line widths and could, for example, arise from centers differing slightly in the orientation and density of HMPA molecules

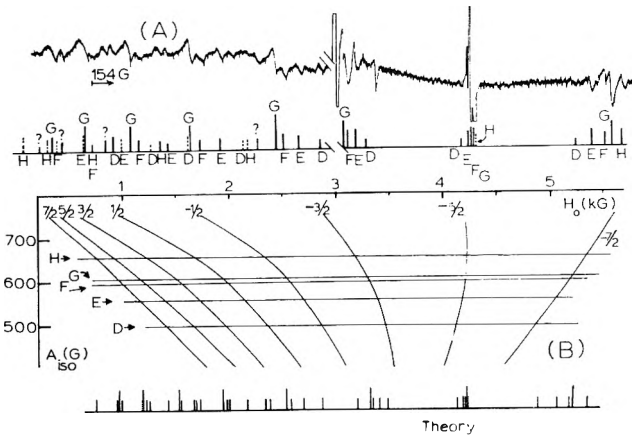

Figure 7. Analysis of the ESR spectrum of a solution of cesium in HMPA (77 K). (A) is the observed spectrum and (B) the calculated stick spectrum for the five Cs states with A_{iso} values given in Table III. Resonant field positions as functions of A_{iso} were obtained from eq 2 with g_e = 1.9921 at a microwave frequency of 0.1018 GHz.

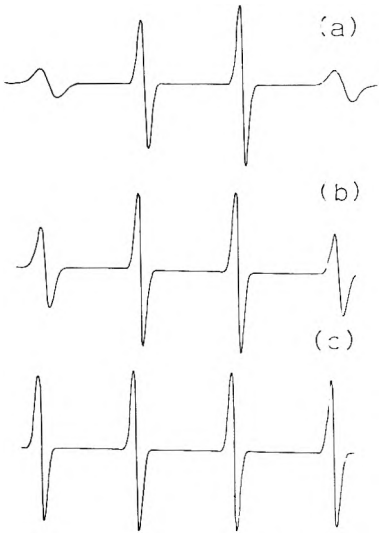

Figure 8. Computer simulation of the ESR spectra of the $^{39}M_G$ state (potassium) for residual line widths (ΔH_{res}) (a) 3.18, (b) 4.00, and (c) 4.18 G.

about the metal atom. To first order, the m_I-dependent contribution is given by

$$\Delta H_{m_I} = 2\delta A(\partial H/\partial A_{iso})_{m_I} \quad (7)$$

where δA is the half-width at half-height of the Gaussian distribution.

Numerical convolution of the distribution function with a Gaussian line shape using gradients ($\partial H/\partial A_{iso}$) obtained from the Breit–Rabi equation, yielded a two-parameter model (δA and ΔH_{res}) capable of a precise simulation of ESR spectra. To illustrate the process, potassium spectra simulated for various values of ΔH_{res} are given in Figure 8. A least-squares fit yielded optimum values of ΔH_{res} and δA, and experimental and simulated spectra for potassium and rubidium solutions are compared in Figure 9. It should be stressed that the equations defining the fit are particularly well defined, and the minimum in the least-squares surface is both sharp and deep permitting considerable confidence to be placed on the derived parameters given in Table IV.

Variations in g_e factors, while undoubtedly present, cannot account for the m_I-dependence in the line widths since

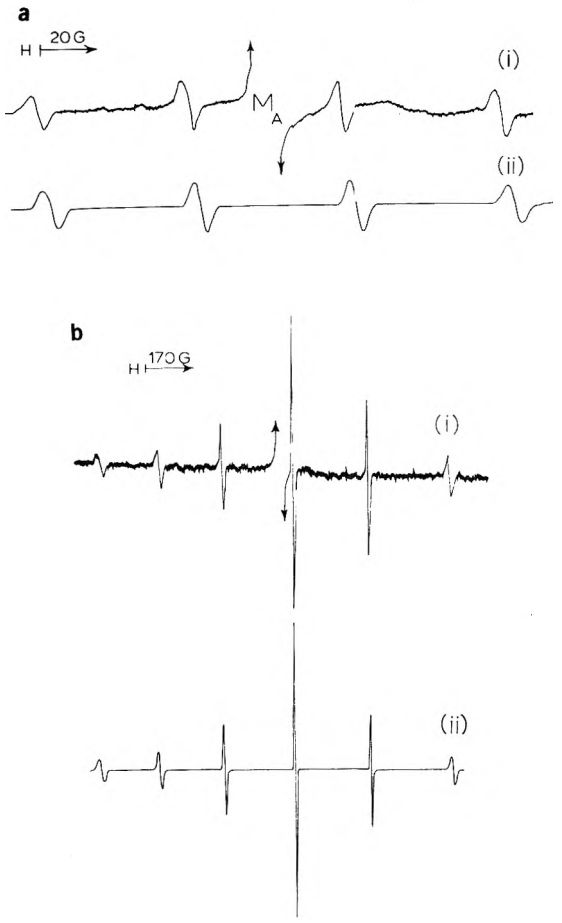

Figure 9. Comparison of observed (i) and simulated (ii) ESR spectra of (a) the $^{39}M_G$ quartet in potassium solutions and (b) the $^{85}M_G$ sextet in rubidium solutions in HMPA.

TABLE IV: Analysis of Multiplet Line Widths in the ESR Spectra of Frozen M–HMPA Solutions[a]

Isotope	Species	ΔH_{res}, G	Std dev, δA, G	δA^b (% atomic character)
^{23}Na	$^{23}M_G$	4.2	2.1	0.7
^{39}K	$^{39}M_G$	4.12	0.92	1.1
^{85}Rb	$^{85}M_G$	4.320 (+½)	2.34	0.648
		4.285 (−½)	2.66	0.737
^{85}Rb	$^{85}M_D$	4.3	≲5	≲1.5
^{133}Cs	$^{133}M_E$	4.3	4.1	0.5

[a] Final estimates of the residual widths (ΔH_{res}) and the standard deviations (δA) for the species $^{X}M_{G,D,E}$. [b] δA = (δA(G)/A(free atom)) × 100%.

gradients $\partial H/\partial g_e$ are approximately independent of m_I. Any line width contributions from g_e factor variations appear in ΔH_{res}.

Discussion

The significance of our solid state results lies first in their relevance to current models for solutions of alkali metals in amines, and secondly in the nature of the wide variety of solvated atoms detected.

Magnetic Parameters from Solid and Liquid Phase Spectra. In Figure 10 we compare available metal hyperfine coupling constants, expressed in terms of percent atomic character, for fluid solutions of potassium and cesium in various amines and ethers together with our results

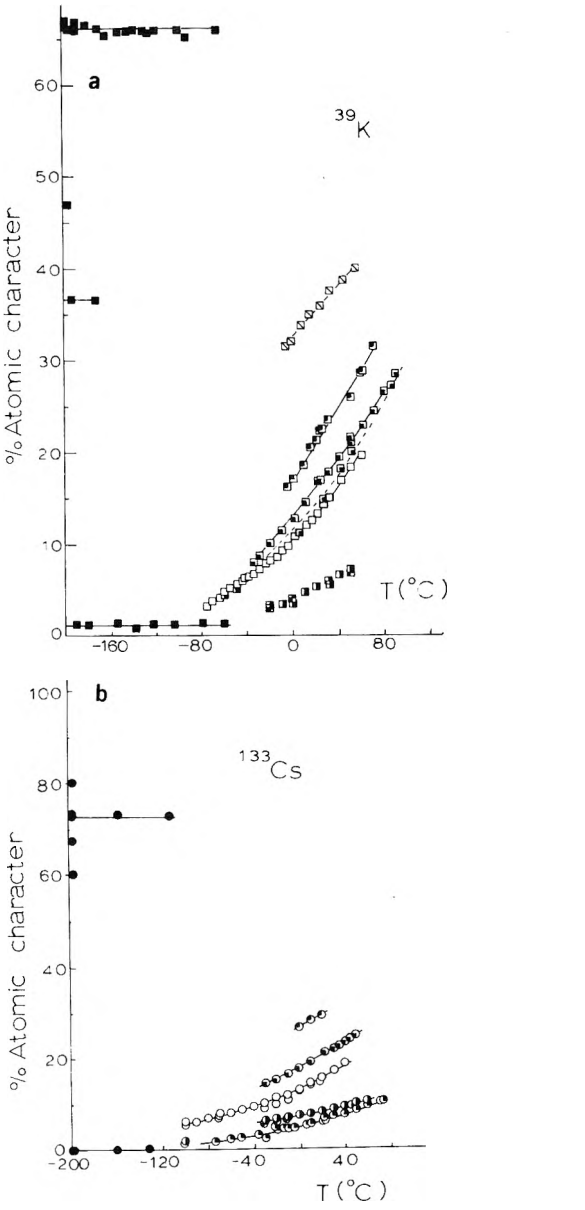

Figure 10. Temperature dependence of the metal hyperfine coupling constant in (a) fluid solutions of potassium in amines and ethers, and frozen potassium solutions in HMPA, and (b) solutions of cesium in amines (fluid) and HMPA (solid): (□) ethylamine (EA), ref 8d; (◔) methylamine (MEA); (◪) butylamine (BUA), ref 8a; (◫) *n*-propylamine (nPA) ref 6b and 8a; (◩) isopropylamine (iPA) ref 6b and 8a; (◧◨) 1,2- and 1,3-propylenediamine (1,2- and 1,3-PDA), ref 6b; (□) tetrahydrofuran (THF), ref 9 and 10; (■) HMPA, this work. Cesium solutions: MEA, ref 5b and 6b; EA, ref 4b and 6b; nPA, iPA, and 1,2- and 1,3-PDA, ref 6b.

for frozen solutions of these metals in HMPA. Coupling constants in the fluid amine and ether solutions always lie intermediate between the values for the two dominant states in HMPA (M_A and M_G), but tend toward these values at low and high temperature, respectively.

In Figure 11 we show $\Delta g_e = g_e$(free atom) $- g_e$ as a function of percent atomic character for the species M_A to M_H together with values for fluid solutions. For all systems a common trend emerges; as the A_{iso} factor moves toward the free atom value, so the g_e factor moves away from the corresponding atomic g_e factor. This substantiates earlier predictions[8b,c] that the limiting high atomic character state in fluid solutions is *not* the free alkali atom. However, for

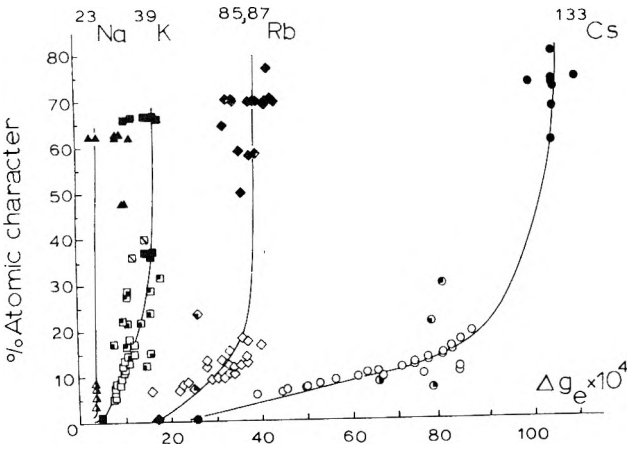

Figure 11. Correlation of percentage atomic character with Δg_e for frozen solutions of sodium, potassium, rubidium, and cesium in HMPA and for fluid solutions in amines and ethers. Solvent identification as in Figure 10: (▲) ammonia–ethylamine mixtures (*ca.* 40 mol % ammonia, ref 8b). Metal identification; (▲) Na; (■) K; (♦) ^{85}Rb; (♦) ^{87}Rb; (●) Cs.

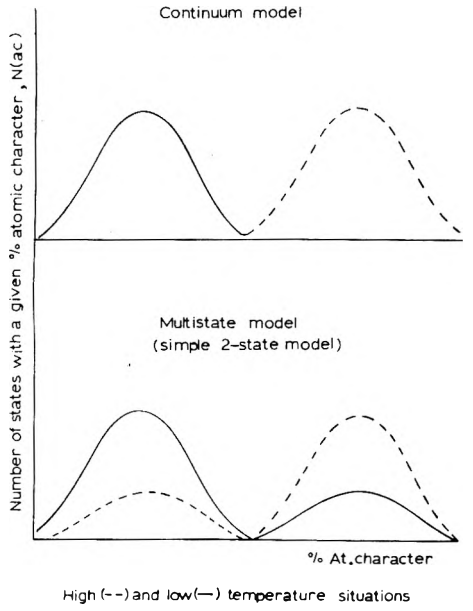

Figure 12. Schematic representation of multistate and continuum models.

each metal there is a maximum Δg_e which increases from sodium through cesium, in line with greater spin–orbit coupling in the higher alkali atoms (Table III).

The points made in Figures 10 and 11 are adequate confirmation of the underlying similarity between fluid amine solutions and our frozen HMPA solutions and justify our use of results from rigid solutions to distinguish models for fluid solutions.

Relevance to Current Models for Fluid Amine Solutions. The two conceptually different models currently in vogue to explain the temperature dependence of A_{iso} and the m_I dependence of ΔH_{ms} for fluid solutions have been outlined in the Introduction. A schematic representation of the fundamental difference between the two models is given in Figure 12 where the distribution functions for the A_{iso} factor are shown at different temperatures. In Figure 13 we present a typical distribution function obtained from a frozen rubidium–HMPA solution, independent of temperature 77–180 K. The latter clearly provides strong support for the multistate model[6a,8b] and is at variance with the postulates of the continuum model.[4,12] We conclude that the spectra of fluid metal–amine and ether solutions arise from a dynamic equilibrium between several (three or more are required[10,23]) species whose structures are approximately independent of temperature.

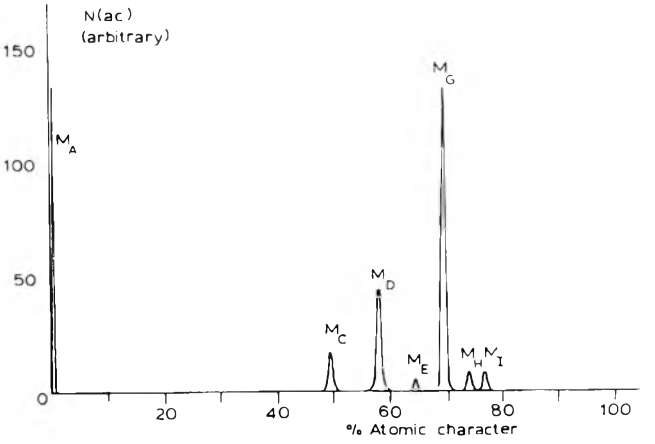

Figure 13. Observed density of states for solutions of rubidium in HMPA.

The High Percent Atomic Character States, M_B–M_H. Strong matrix perturbations on gas-phase alkali atom eigenstates bring about large deviations in both A_{iso} and g_e factors from their free atom values (Table III). The parameter ΔA defined by

$$\Delta A = 100(A_{iso} - A(\text{free atom}))/A(\text{free atom}) \quad (8)$$

represents a quantitative measure of the perturbation of the alkali atom gas phase *n*s wave function by the surrounding matrix. Alkali atoms trapped in rare gas matrices have been reported,[26] but in general deviations from free atom coupling constants are small $|\Delta A| < 10\%$, and negative, i.e., $A_{iso} < A$(free atom), and arise from second-order dispersion-type interactions between the trapped alkali atom and the surrounding matrix. In marked contrast, our values of ΔA range from ~30 to ~99%. A description[26a] in terms of an atomic interaction potential between the trapped atom and a rare gas atom accounts semiquantitatively[27] for the observed shifts (ΔA), while similar calculations[24] for the interaction between an alkali atom and an HMPA "atom" predict maximum shifts of ~3%

	^{23}Na	^{39}K	^{85}Rb	^{133}Cs
$-\Delta A_{calcd}$, %	2.35	2.70	2.50	2.60

We may therefore rule out this mechanism for species M_B–M_H and conclude that our species cannot be described as trapped atoms, but must involve more specific bonding interactions with the solvent. A general molecular orbital scheme, originally proposed[28] to explain results for trapped silver atoms,[29,30] gives a qualitative picture of the observed deviations in both A_{iso} and g_e from free atom values.[23]

Alternatively we might describe the centers M_B–M_H as "intermediate impurity states" in the host (HMPA) matrix, that is, as states which retain a unique parentage in the states of the gas-phase alkali atoms, but are subject to large perturbations from the host. A theoretical description[31] of such states must be either in terms of a strongly perturbed Heitler–London scheme, or by a modified Wan-

TABLE V: Unpaired Electron Spin Densities, $|\psi_{(0)}|_D^2$, at the Donor Nucleus in Shallow Impurity States

Donor	Host	$\|\psi_{(0)}\|_D^2 \times 10^{-24}$, cm^{-3}
P	Si[a]	0.43
As		1.73
Sb		1.18
P	Ge[b]	0.17
As		0.69
K	HMPA[c]	0.073 ± 0.007
Rb		0.065 ± 0.005
Cs		0.060 ± 0.006

[a] See ref 32. [b] See ref 34. [c] This work.

nier–Mott formalism (see below). In any description of intermediate impurity states dielectric screening reduces the electron–parent ion (M^+) coulomb interaction and the unpaired donor electron moves in an expanded centrosymmetric Bohr orbit about the parent ion.

The Low Atomic Character State, M_A. The extremely low unpaired electron spin density on the metal nucleus in this state (Table V) suggests considerable dielectric screening and a correspondingly large Bohr radius. However, the Gaussian line shape requires that the unpaired electron remain associated with a particular metal nucleus for $\gtrsim 10^{-6}$ sec. The effective mass formalism for Wannier–Mott impurity states gives the ground state wave function for the donor electron[33]

$$\psi_D(r) = \sum_{j=1}^{N} \alpha_j F_j(r) \phi_j(r) \qquad (9)$$

where $F_j(r)$ is the hydrogenic envelope function at the jth conduction band minimum, of which there are N. $\phi_j(r)$ is the Bloch function at the same minimum and α_j the relative contribution from the jth valley. A wave function of the form (9) requires that $|\psi(0)|_D^2$, the unpaired electron spin density at the donor nucleus, be independent of the nature of the donor atom. Our observed values for the states labeled M_A are consistent with this (Table V).

To a first approximation, shallow impurity states in group 4 semiconductors are also described by (9), but in these systems $|\psi(0)|_D^2$ is dependent upon the donor atom,[32,34] and the effective mass formalism obviously breaks down as $r \rightarrow 0$ and requires a significant admixture of donor atom wave functions in the ground state. So far as we know, therefore, the states M_A characterized in this investigation represent the closest approximation to true Wannier–Mott impurity ground states. Wannier–Mott excited states (excitons) have been characterized in doped liquid and solid rare gases.[31b,c]

Acknowledgments. We thank the Science Research Council for financial assistance.

References and Notes

(1) C. A. Hutchison, Jr., and R. C. Pastor, *J. Chem. Phys.*, **21**, 1959 (1953).
(2) R. Catterall and M. C. R. Symons, *J. Chem. Soc.*, 4342 (1964).
(3) (a) R. Catterall, L. P. Stodulski, and M. C. R. Symons, *J. Chem. Soc. A*, 437 (1968); (b) *Pure Appl. Chem.* (Metal Ammonia Solutions Suppl.), 151 (1970); (c) L. P. Stodulski, Ph.D. Thesis, Leicester University, 1969.
(4) (a) K. Bar-Eli and T. R. Tuttle, Jr., *J. Chem. Phys.*, **40**, 2508 (1964); (b) *ibid.*, **44**, 114 (1966).
(5) (a) K. D. Vos and J. L. Dye, *J. Chem. Phys.*, **38**, 2033 (1963); (b) K. D. Vos, Ph.D. Thesis, Michigan State University, 1962.
(6) (a) J. L. Dye and L. R. Dalton, *J. Phys. Chem.*, this issue; (b) L. R. Dalton, M.Sc. Thesis, Michigan State University, 1966.
(7) R. Catterall and M. C. R. Symons, *J. Chem. Soc.*, 6656 (1965).
(8) (a) R. Catterall, M. C. R. Symons, and J. W. Tipping, *J. Chem. Soc.*, 1529 (1966); (b) *ibid.*, 1234 (1967); (c) J. L. Dye and L. R. Dalton, *J. Phys. Chem.*, **71**, 184 (1967), see Discussion on p 190; (d) R. Catterall, unpublished results.
(9) (a) R. Catterall, J. Slater, and M. C. R. Symons, *J. Chem. Phys.*, **52**, 1003 (1970); (b) *Pure Appl. Chem.* (Metal Ammonia Solutions Suppl.), 329 (1970).
(10) J. Slater, Ph.D. Thesis, Leicester University, 1970.
(11) R. Catterall, P. P. Edwards, M. C. R. Symons, and J. Slater, *Chem. Phys. Lett.*, submitted for publication.
(12) D. E. O'Reilly and T. Tsang, *J. Chem. Phys.*, **42**, 3333 (1965).
(13) R. Catterall and P. P. Edwards, *J. Chem. Soc., Chem. Commun.*, 96 (1975).
(14) R. A. Levy, *Phys. Rev.*, **102**, 31 (1956).
(15) R. Catterall, W. T. Cronenwett, R. J. Egland, and M. C. R. Symons, *J. Chem. Soc. A*, 2396 (1971).
(16) R. Catterall and P. P. Edwards, *Adv. Mol. Relaxation Processes*, submitted for publication.
(17) R. Catterall, I. Hurley, and M. C. R. Symons, *J. Chem. Soc., Dalton Trans.*, 139 (1972).
(18) J. E. Dubois and H. Viellard, *J. Chim. Phys.*, **62**, 699 (1965).
(19) J. M. Brooks and R. Dewald, *J. Phys. Chem.*, **72**, 2655 (1968).
(20) H. Normant, *Angew. Chem., Int. Edit. Engl.*, **6**, 1046 (1967).
(21) T. G. Castner, *Phys. Rev.*, **115**, 1506 (1959).
(22) G. Breit and I. I. Rabi, *Phys. Rev.*, **38**, 2082 (1931).
(23) R. Catterall and P. P. Edwards, *J. Chem. Soc.*, submitted for publication.
(24) R. Catterall and P. P. Edwards, *Chem. Phys. Lett.*, submitted for publication.
(25) (a) V. A. Nicely and J. L. Dye, *J. Chem. Phys.*, **52**, 119 (1970); (b) V. A. Nicely, Ph.D. Thesis, Michigan State University, 1969.
(26) (a) C. K. Jen, V. A. Bowers, E. L. Cochran, and S. N. Foner, *Phys. Rev.*, **126**, 1749 (1962); (b) S. L. Kupferman and F. M. Pipkin, *ibid.*, **166**, 207 (1968).
(27) P. P. Edwards, Ph.D. Thesis, Salford University, 1974.
(28) M. C. R. Symons, *J. Chem. Soc.*, 1482 (1964).
(29) C. J. Delbecq, W. Hayes, M. C. M. O'Brien, and P. H. Yuster, *Proc. R. Soc. (London)*, **271**, 243 (1963).
(30) (a) R. A. Zhitnikov, N. V. Kolesnikov, and V. I. Kosyakov, *Soviet Phys. JETP (Engl. Transl.)*, **17**, 815 (1963); (b) A. Zhitnikov and A. L. Orbeli, *Soviet Phys. Solid State (Engl. Transl.)*, **7**, 1559 (1966).
(31) (a) S. Webber, S. A. Rice, and J. Jortner, *J. Chem. Phys.*, **42**, 1907 (1965); (b) B. Raz and J. Jortner, *Chem. Phys. Lett.*, **4**, 511 (1970); (c) B. Raz and J. Jortner, *Proc. R. Soc. (London), Ser. A*, **317**, 113 (1970).
(32) G. Feher, *Phys. Rev.*, **114**, 1219 (1959).
(33) W. Kohn in "Solid State Physics", Vol. 5, F. Seitz and D. Turnbull, Ed., Academic Press, New York, N.Y., 1957.
(34) D. K. Wilson, *Phys. Rev.*, **134**, A265 (1964).

Discussion

W. GLAUNSINGER. Your ESR analysis is very impressive, but is it not possible that these frozen solutions may contain a greater number of distinct localized centers than the solutions? In other words, do you believe that the spectra of quick-frozen solids really represent the state of affairs in the liquid state?

R. CATTERALL. First our spectra are reproducible from one preparation to another which argues against any accidental changes on freezing. Secondly a rough spin count from the area under the ESR lines shows, by comparison with the static susceptibility measurements on fluid solutions (reported at Colloque Weyl II), that there is no great change in the concentration of unpaired spins on freezing. We believe that these two points, coupled with the observation of very precise states in the frozen solutions, provide very strong evidence for the trapping out of fluid solution structure.

Electron Spin Resonance Studies of Extended Excess Electron States in Frozen Solutions of Alkali Metals in Hexamethylphosphoramide

Ron Catterall* and Peter P. Edwards

Department of Chemistry and Applied Chemistry, University of Salford, Salford M5 4WT, England *(Received September 2, 1975)*

In this paper we report the observation of delocalized excess electron states in frozen solutions of lithium, potassium, rubidium, and cesium in HMPA. The delocalized states are identified as mobile electrons residing in a metallic impurity band within the host (HMPA) bandgap. In potassium, rubidium, and cesium solutions both delocalized (metallic) and localized (insulating) states coexist within the same sample. It is proposed that spin exchange between localized and delocalized electrons in these amorphous materials is very inefficient. The implications of these observations to an inhomogeneous model for metal solutions are discussed. A transition from delocalized to localized states was monitored in frozen lithium–HMPA solutions at metal concentrations of the order of 5×10^{-3} M. A simple criterion is proposed which relates the observed magnetic properties of localized Wannier-type impurity states to the critical density (n_c) of free carriers at the metal–insulator (M–I) transition. Critical densities obtained from this relation are in good agreement with both experimental values and theoretical estimates (Hubbard model) for n_c in doped group 4 semiconductors and in frozen lithium–HMPA solutions. It is proposed that the M–I transition in a *homogeneous* fluid metal–HMPA solution would proceed via a Mott transition, although the presence of microscopic inhomogeneities in the solution will almost certainly preclude its direct experimental verification at the predicted metal concentration.

Introduction

The presence of a metal–insulator (M–I) transition in fluid metal–ammonia solutions appears to have gained universal acceptance,[2-4] although considerable controversy[5] still surrounds the exact nature and critical concentration of the transition. Experimentally, both magnetic resonance and transport properties suggest[4] delocalization of the electronic wave function at high concentration although the critical metal concentration obtained from magnetic resonance studies[6,7] (and in particular electron spin resonance,[6] ESR) is considerably lower than that determined from transport properties.[3b-7] In this connection Silsbee[8] has emphasized the high intrinsic sensitivity of the ESR technique when monitoring the onset of delocalization.

A simple model of a metal solution in which the excess electron centers are randomly (and hence uniformly) distributed is almost certainly complicated by the presence of microscopic inhomogeneities which give rise to the coexistence of insulating (localized) and metallic (delocalized) regions within the sample. In fluid solutions electrons in both localized and delocalized states contribute to the observed ESR signal and only a time-averaged signal is recorded experimentally.

A magnetic resonance study of frozen metal solutions is therefore attractive for the following reasons. (i) Any metallic and insulating regions which are present in the fluid metal–solution at temperatures just above the freezing point should be sufficiently isolated in the rigid solution to give rise to separate ESR spectra. (ii) If the concentration of metal is reduced sufficiently, a transition from delocalized to localized states should be amenable to experimental observation by ESR.

Electron spin resonance studies of frozen metal–solutions have been reported by several authors,[10-14] but spectra are generally characteristic of colloidal metal. In general the presence of deep eutectic points in the phase diagrams of lithium–, sodium–, and potassium–ammonia solutions[15] ensure that frozen solutions below the eutectic temperature (Li, 88 K; Na, 163 K; K, 116 K) consist predominantly of crystalline ammonia and either pure metal[15] (in the case of sodium and potassium solutions) or the metallic compounds[16] $M(NH_3)_x$ (M = Li, x = 4; M = Ca, Sr, Ba, Eu, or Yb, x = 6).

Catterall[17] has obtained homogeneous blue solid solutions by rapid freezing of solutions (ca. 0.1–0.4 M) of sodium and potassium in ammonia in the presence of high concentrations (ca. 1 M) of structure-breaking salts. In these vitreous samples, solvent and metal crystallization were reduced considerably and the presence of a sharp, motionally narrowed singlet in the ESR spectra clearly demonstrated high intrinsic mobility in the solid state. Unfortunately, attempts[17] to glassify more dilute solutions were unsuccessful and no transition to the localized state was observed.

Thus so far ESR studies of frozen metal solutions have been confined to systems which are trully metallic in nature, and only a very limited amount of information has been obtained[13,17] about the M–I transition.

In this paper we report the observation of delocalized excess electron states in frozen solutions of lithium, potassium, rubidium, and cesium in HMPA (often coexisting with spectra attributed to localized states) and demonstrate the existence of a concentration-dependent metal–insulator transition in lithium solutions.

Results

Electron Spin Resonance Spectra of Delocalized Electrons in Frozen Metal–HMPA Solutions. Concentrated Solutions. (i) *Lithium Solutions.* A typical ESR spectra of a frozen solution of lithium (^{7}Li isotope) in HMPA (ca. 0.1 M) is shown in Figure 1a and consisted of a single narrow

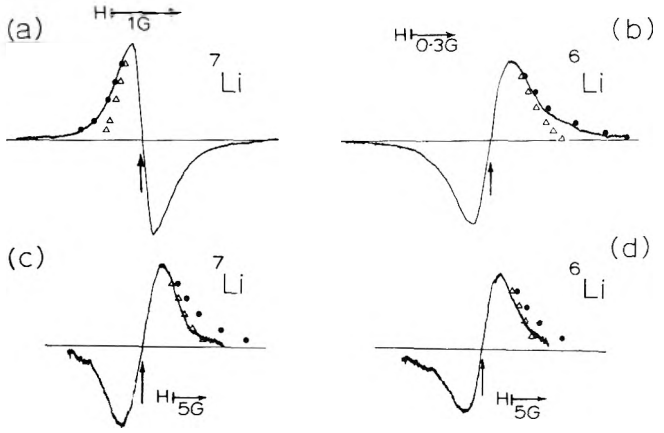

Figure 1. Electron spin resonance spectra of frozen lithium–HMPA solutions (ca 77 K): (a) ca. 0.1 *M* ^{7}Li solution; (b) ca. 0.1 *M* ^{6}Li solution; (c) ca. 5×10^{-3} *M* ^{7}Li solution; (d) ca. 5×10^{-3} *M* ^{6}Li solution. In all spectra the vertical arrow corresponds to $g_e = 2.0018$. Shaded circles and open triangles represent respectively the theoretical Lorentzian and Gaussian line shapes for a resonance of this width.

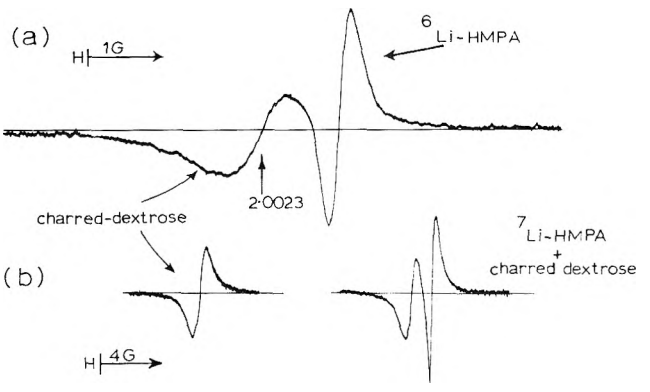

Figure 2. Electron spin resonance spectra (90 K) of frozen lithium–HMPA solutions (ca. 0.1 *M*) with an evacuated charred dextrose standard: (a) ^{6}Li solution; (b) ^{7}Li solution.

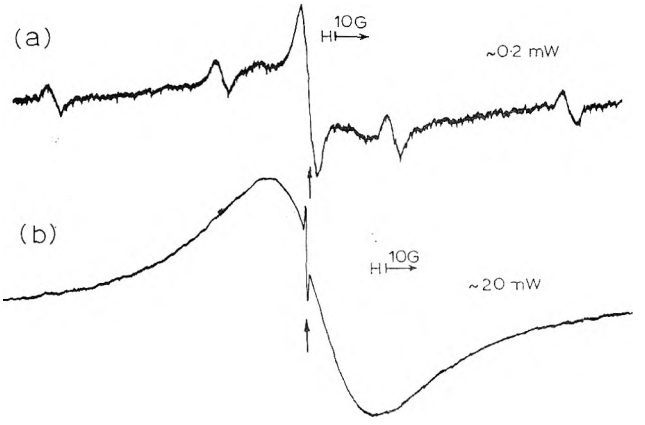

Figure 3. Electron spin resonance spectra (77 K) of a frozen potassium–HMPA solution (ca. 0.1 *M*) recorded at (a) low microwave power (ca. 0.2 mW), (b) high microwave power (ca. 20 mW). The vertical arrows correspond to $g_e = 2.0018$.

Lorentzian line ($\Delta H_{ms} = 0.32 \pm 0.05$ G, $g = 2.0019 \pm 0.0004$) which had saturation behavior characteristic of a homogeneously broadened line, both properties reminiscent of a delocalized electron state.

Frozen solutions (ca. 0.1 *M*) of lithium-6 (^{6}Li) in HMPA gave a very similar Lorentzian absorption (Figure 1b) with $\Delta H_{ms} = 0.32 \pm 0.05$ G, $g_e = 2.0017 \pm 0.0004$), and within experimental accuracy line widths and g_e factors of the *delocalized* center are independent of magnetic moment although $g_N(^7\text{Li})/g_N(^6\text{Li}) = 2.65$.

Conduction electron spin resonance (CESR) in metallic lithium has been observed in frozen lithium–ammonia solutions[10,13,14,18] and in various other systems.[19-22] Line widths vary considerably and depend strongly upon particle size,[18] purity of sample,[18,19] etc., but one universal feature of CESR in metallic lithium in all samples is the very small g_e factor shift,[21] $\Delta g_e (= 2.00231 - g_e) \simeq -0.6 \times 10^{-4}$. Accurate g_e shifts for the resonance in frozen lithium–HMPA solutions were determined by comparison with a charred dextrose standard[23] ($g_e = 2.0023 \pm 0.0002$) closely adjacent to the sample in the microwave cavity. Figure 2a shows a typical spectrum of the superimposed signals for a ca. 0.1 *M* lithium (^{6}Li)–HMPA solution and the charred dextrose standard both at 90 K, while Figure 2b shows the corresponding ^{7}Li spectra. The average g_e shift for both isotopes was

$$\Delta g_e(^6\text{Li}) = +6.0 \pm 1.0 \times 10^{-4} (g_e = 2.00171 \pm 0.0001)$$

$$\Delta g_e(^7\text{Li}) = +5.1 \pm 2.0 \times 10^{-4} (g_e = 2.00180 \pm 0.0002)$$

In contrast the g_e shift in metallic lithium,[21] $(-0.61 \pm 0.02) \times 10^{-4}$, is an order of magnitude smaller and of opposite sign.

We therefore conclude that the signal does not arise from particles of metallic lithium. We presume that the very high solvating power of Li^+ prevents any precipitation of lithium metal.

(ii) *Sodium Solutions.* Samples at 77 K gave ESR spectra of localized excess electron centers and a strong Lorentzian absorption ($\Delta H_{ms} = 2.5$ G, $g_e = 2.0013 \pm 0.0004$) close to the free-spin position. The latter resonance has been identified as originating from colloidal sodium metal.[12] This signal was generally very strong and sufficient to obscure any other resonances in the central region.

(iii) *Potassium Solutions.* The ESR spectrum (77 K), recorded at low microwave power (~0.2 mW), of a frozen potassium–HMPA solution (ca. 0.1 *M*) is shown in Figure 3a. The corresponding spectrum obtained from the same sample at higher power (~20 mW) is shown in Figure 3b. The isotropic quartet and narrow Gaussian absorption (Figure 3a) originate from localized excess electron centers and are discussed in our previous paper.[24] At high microwave power (Figure 3b), two new absorptions were recorded, both having line shapes approximating closely to Lorentzian but differing markedly in their line widths ($\Delta H_{ms} =$ 0.5 and 35 G) and to a lesser extent in their g_e factors ($g_e =$ 2.0014 ± 0.0004 and 1.9984 ± 0.0004, respectively). The line width and g_e factor of the narrow line were independent of both temperature (77–133 K) and (over a very limited range) metal concentration.

In contrast, the width of the broad Lorentzian line was markedly temperature dependent and we have identified[12] this signal as arising from CESR in colloidal potassium metal particles small compared to the microwave skin depth.

(iv) *Rubidium and Cesium Solutions (ca. 0.1 M).* At high microwave power (~6 mW (Rb), ~10 mW (Cs)), narrow Lorentzian signals ($\Delta H_{ms}(^{85}\text{Rb}) = 0.8 \pm 0.2$ G; $\Delta H_{ms}(^{133}\text{Cs}) = 1.0 \pm 0.2$ G; $g_e(^{85}\text{Rb}) = 2.00073 \pm 0.0002$;

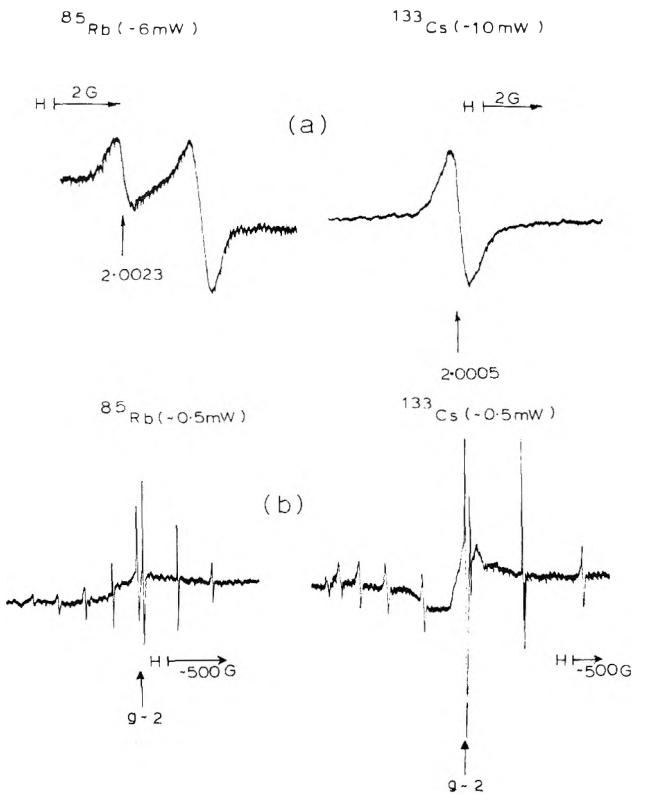

Figure 4. Electron spin resonance spectra (77 K) of frozen rubidium– and cesium–HMPA solutions (ca. 0.1 *M*) recorded at (a) high microwave power, (b) low microwave power (specific values shown in the figure). In rubidium–HMPA spectra at high power (a) the resonance at $g = 2.0023$ arises from a signal in the Dewar.

$g_e(^{133}Cs) = 2.0005 \pm 0.0004$, Figure 4a) were observed from samples prepared in both Pyrex and quartz vessels. ESR spectra of the same samples at low microwave power (Figure 4b) (~0.5 mW) gave signals attributed to the localized centers M_A–M_H.[24] The observation of CESR in colloidal rubidium and cesium particles at 77 K is precluded by the large spin–orbit coupling in these metals. On the basis of a Block–Grüneisen relation for T_1^{-1} in metallic particles,[12] we estimate (very approximateley) $\Delta H_{ms}(^{85}Rb) \sim 300$ G and $\Delta H_{ms}(^{133}Cs) \sim 2000$ G at 77 K, from experimental data[25] for these metals at 1.3 K.

Microwave Power Saturation. In Figure 5 we compare the power saturation behavior of the narrow ($\Delta H_{ms} = 0.5$ G) Lorentzian resonance in frozen potassium–HMPA solutions (77 K) with that of the inhomogeneously broadened lines from the M_G localized centers[24] in frozen potassium ($\Delta H_{ms} = 4.4$ G), rubidium (4.4 G), and cesium (10.8 G) solutions (77 K). The narrow line starts to saturate at microwave powers in order of magnitude greater than for the broader resonances associated with the localized centers. The figure emphasizes the intrinsic differences between spin relaxation in the two species.

Concentration Dependence. Experimental difficulties have been encountered[17] in freezing dilute metal–ammonia solutions and we have found similar problems in freezing dilute solutions of sodium, potassium, rubidium, and cesium in HMPA. However, dilute solutions of lithium in HMPA were found to glassify readily and samples with metal concentrations $< 5 \times 10^{-3}$ *M* had ESR spectra comprising a Gaussian singlet for both ^7Li and ^6Li solutions (Figure 1c,d). Line widths were *dependent* on the isotope

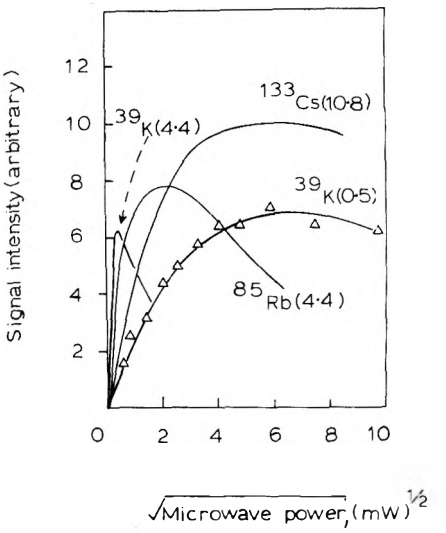

Figure 5. Comparison of the saturation behavior (open triangles) of the 0.5-G resonance from a frozen potassium–HMPA solution (sample K-5) with several *inhomogeneously* broadened resonances from potassium–, rubidium–, and cesium–HMPA spectra Values of ΔH_{ms} are given in brackets.

TABLE I: ESR Parameters from Spectra of Frozen Solutions of the Alkali Metals in HMPA[a]

Isotope	*T*, K	ΔH_{ms}, G	g_e
^6Li	(i) 77	4.3 ± 0.3	2.0019 ± 0.0004
^6Li	(ii) 77	0.32 ± 0.05	2.00171 ± 0.0001
^7Li	(i) 77	6.4 ± 0.3	2.0020 ± 0.0004
^7Li	(ii) 77	0.32 ± 0.05	2.0018 ± 0.0002
Na–K (alloy)	77	0.3 ± 0.1	2.0013 ± 0.0004
^{39}K	77	0.5 ± 0.1	2.0015 ± 0.0004
	133	0.5 ± 0.1	2.0014 ± 0.0004
^{85}Rb	77	0.8 ± 0.2	2.00073 ± 0.0002
	118	1.2 ± 0.2	2.0010 ± 0.0004
^{133}Cs	77	0.8 ± 0.2	2.0005 ± 0.0004
	93	1.1 ± 0.2	2.0009 ± 0.0004

[a] Parameters only for spectra showing no resolved hyperfine coupling to metal. All parameters shown are for concentrated (ca. 0.1–0.2 *M*) solutions with Lorentzian ESR absorptions, except for lithium solutions where (i) denotes metal concentration $\lesssim 5 \times 10^{-3}$ *M* (Gaussian absorption) and (ii) denotes metal concentration $\gtrsim 5 \times 10^{-3}$ *M* (Lorentzian absorption).

with $\Delta H_{ms}(^6Li) = 4.3 \pm 0.3$ G, $\Delta H_{ms}(^7Li) = 6.4 \pm 0.3$, while g_e factors were isotope independent within experimental uncertainty (±0.0004) with $g_e(^6Li) = 2.0019$, $g_e(^7Li) = 2.0020$.

The microwave power saturation characteristics of these signals from dilute solutions were markedly different from these of the narrow lines obtained from the more concentrated solutions, and showed close affinities with the saturation properties observed for localized states.[24]

Results for all systems examined are collected in Table I.

Discussion

Delocalized Excess Electron States in Frozen Lithium–, Potassium–, Rubidium–, and Cesium–HMPA Solutions. We identify the narrow Lorentzian signal (Table I) as arising from spin transitions of delocalized electron states in a narrow metallic-like impurity band within the host (HMPA) bandgap. Our assignment is based on the following considerations.

(*i*) *Line Shape.* The Lorentzian line shape (Figure 1) is characteristic of rapidly fluctuating electron–lattice interactions occurring on a time scale short compared to the electron spin relaxation time. This sets an upper limit to the electron–nuclear correlation time, τ, as

$$\tau \ll 10^{-6} \text{ sec.}$$

(*ii*) *Power Saturation Behavior.* In Figure 6 we compare the saturation behavior of the 0.5-G line from *frozen* potassium–HMPA solutions (77 K) with corresponding curves for the motionally narrowed solvated electron resonance in *fluid* (296 K) potassium–tetrahydrofuran solutions.[26] Our solid-state results clearly show very close similarities with the fluid state studies, with the onset of saturation moving steadily to higher microwave power levels for the broader lines.

(iii) In contrast to spectra of localized states reported earlier,[24] the present spectra show only a very minor dependence upon the nature of the cation.

Electron Relaxation Mechanism. Lattice–phonon modulation of the electron spin–orbit coupling is the dominant relaxation mechanism in the localized centers in frozen potassium–, rubidium–, and cesium–HMPA solutions,[24,37] but this mechanism clearly cannot be responsible for the much faster electron relaxation observed in these studies (Figure 5). We propose that the dominant spin relaxation mechanism in this instance is via modulation either of the exchange coupling between electrons in the impurity band states,[27] or (more likely) of the electron–metal nuclear hyperfine interactions.

Alexander and Holcomb[9] have pointed out that the nature of the impurity band in doped group 4 semiconductors is poorly understood. As a first approximation[9,29] the impurity band is expected to possess the characteristics of the host material; this appears a reasonable hypothesis if the band is constructed by overlap of Wannier–Mott type localized states (which are in fact composed predominantly of Bloch waves from the bottom of the host conduction band).[24,28] Martino et al.[29] have suggested that this simple viewpoint must only be taken as a first approximation. Our results (Table I) for the impurity band in the M–HMPA system require that in any realistic description of the band, contributions from both *n*s (ground state) and *n*p (excited state) wave functions of the donor (alkali) atom must also be taken into consideration. Nevertheless, the relatively small cation dependence of the time-averaged signals suggests strongly that metal contributions to the band are only of minor importance.

Implications for an Imhomogeneous Model of Metal–Ammonia Solutions. An inhomogeneous model proposes the simultaneous existence, within a disordered system, of both metallic and nonmetallic regions. The specific form of the model was developed by Cohen and Jortner[30] while Lelieur and Thompson[31] have applied the model to an analysis of transport properties in moderately concentrated metal–ammonia solutions. They[31] suggest that in this concentration region (1–9 MPM), the solution may be considered as 1 MPM (ca. 0.3 *M*) dilute clusters embedded in a 9 MPM (ca. 3 *M*) metallic matrix.

Our observations (Figures 3 and 4) of electron spin resonance signals from both metallic (delocalized) and insulating (localized) states *within the same sample* are then consistent with an inhomogeneous model. The intrinsic differences in electron spin-relaxation behavior for localized and delocalized states are responsible for their simultaneous

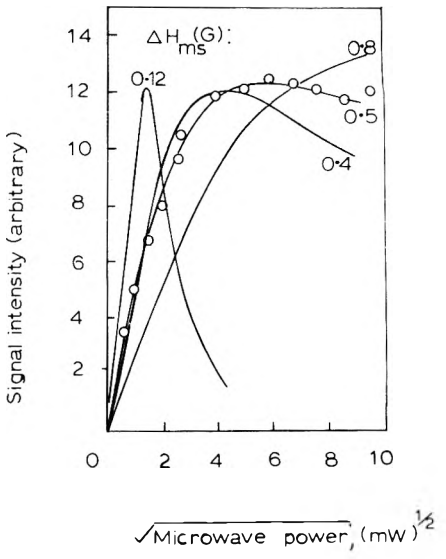

Figure 6. Comparison of the saturation behavior (77 K) of the 0.5-G motionally narrowed resonance from a frozen potassium–HMPA solution (sample K-3, open circles) with several fluid-state (296 K) homogeneously broadened resonances from fluid potassium–tetrahydrofuran solutions.[26]

observation and highlight the possible future use of the ESR technique in this respect. The experimental distinction between both types of relaxation behavior requires that spin exchange[27] between localized and delocalized electrons in amorphous materials is very slow.

Although at first sight our results appear to provide strong support for an inhomogeneous model, a cautionary point must be noted. If the "metallic" regions are the result of local fluctuations in the density of excess electron states, then one must consider that *all* the localized states observed in the "insulator" regions are also present in the "metallic" clusters, and that the ESR signal from these metallic regions is a weighted time average over all states. Without doubt the most prominent features in the spectra of the localized states[24] are those originating from species with approximately 1 ($^{x}M_A$) and 70% ($^{x}M_G$) outer metal *n*s character (see Figure 12b of ref 24), so that electron-relaxation proceeding via rapid modulation of the electron–metal nuclear hyperfine coupling is given approximately[32] by

$$\Delta H_{ms} \simeq g_e g_M^2 I_M(I_M + 1)|\psi(0)|_{M_G}^4 \tau_M$$

and $\tau_K/\tau_{Cs} \simeq 280$. Such a disparity between correlation times for electron motion in potassium and cesium clusters appears most unlikely, and we must conclude that the high percent atomic character states are not involved in the metal–insulator transition. If this is the case, then the observation of the two types of signals cannot be used to support the existence of microscopic inhomogeneities. It appears that only states of low atomic character are capable of contributing to impurity band formation *in the concentration range we have studied.* Alternatively, electron relaxation may be dominated by some mechanism other than the modulation of the hyperfine interactions, but we feel this is unlikely.

The Nature of the Localized State in Frozen Lithium Solutions. In contrast to results for concentrated ($\gtrsim 5 \times 10^{-3}$ *M*) lithium solutions, the isotope dependence of the observed line width in dilute solutions ($\lesssim 5 \times 10^{-3}$ *M*, Table I) suggests a hyperfine interaction with lithium nuclei, while the Gaussian lineshapes (Figure 1c,d) require

that the interaction between unpaired electrons and lithium nuclei is long lived. Assuming a pairwise interaction, computer simulation of spectra yielded a best fit for a residual width[24] (ΔH_{res}) of ca. 4.3 G and a hyperfine coupling to ^{7}Li of 1.45 G, giving $|\psi(0)|_{Li}^2 \simeq 0.016\ (\pm 0.006) \times 10^{24}$ cm^{-3}.

Although the value of $|\psi(0)|_{Li}^2$ is approximately four times smaller than corresponding values for the M_A localized states identified in frozen potassium–, rubidium–, and cesium–HMPA solutions,[24] and although we might attribute this difference to the solvating power of lithium cations, we do not feel the difference is too significant. The localized excess electron states are best described as Wannier–Mott impurity states,[33] very similar to the M_A states defined in the previous paper.[24]

The Transition Region. We have monitored a transition from delocalized to localized states in frozen lithium solutions at metal concentrations of the order of ca. 5×10^{-3} *M*. The experimental results are summarized below.

(i) For metal concentrations down to ca. 5×10^{-3} *M* the sharp ESR signal attributed to mobile electrons in a metallic impurity band was observed in all lithium (both ^{6}Li and ^{7}Li) samples examined.

(ii) For metal concentrations below ca. 5×10^{-3} *M*, an ESR absorption was observed in both ^{6}Li and ^{7}Li solutions which has been identified as a Wannier–Mott type localized impurity state.

This experimental data provides direct evidence for a M–I transition in these systems, the localized Wannier-type states being the source of electrons in the delocalized impurity band. In the following section we calculate critical donor concentrations assuming that frozen solutions of lithium in HMPA approximate closely to a homogeneous system.

Thomas-Fermi (T–F) Screening of Wannier–Mott Impurity States. Localized States. In Wannier–Mott type impurity states,[24,33] the electron–parent core Coulomb attraction is dielectrically screened. From simple effective mass theory[28,34] (SEMT) the ground state wave function, ψ_j, satisfies the Schrödinger equation.

$$\left\{-\left(\frac{\hbar^2}{2m^*}\right)\nabla^2 + V(r) - E_{\text{eff mass}}\right\}\psi_j(r) = 0 \qquad (1)$$

where $V(r)$, the long-range electron–hole potential, is given by

$$V(r) = -e^2/\gamma t \qquad (2)$$

and γ is the static dielectric constant of the host lattice. The lowest eigenvalue of (1) is then[28,34]

$$E_{\text{eff mass}} = -m^*e^4/2\hbar^2 \qquad (3)$$

and the corresponding eigenfunction[28,34]

$$\psi_j(r) = \sum_{j=1}^{N} \alpha_j F_j(r)\phi_j(r) \qquad (4)$$

where $\phi_j(r)$ is the Bloch function at the jth conduction band minimum (of which there are N), α_j describes the relative contribution from the jth valley, and $F_j(r)$ is the hydrogenic envelope function.

For an anisotropic conduction band, the function $F_j(r)$ should be written[28,34] as

$$F_j(x, y, z) = (\pi a^2 b)^{-1/2} \exp\{-[(x^2 + y^2)/a^2 + z^2/b^2]^{1/2}\} \qquad (5)$$

The z axis is defined parallel to the axis containing the jth minimum and a and b are the effective transverse and longitudinal Bohr radii, respectively.

However, if we are interested purely in the unpaired electron spin density at the donor nucleus, $|\psi(0)|^2$, then a simpler version of (5) is given by the isotropic envelope function

$$F_j(r) = \{1/(\pi a^{*3})^{1/2}\} \exp(-r/a^*) \qquad (6)$$

where a^* is a mean Bohr radius of the order of

$$a^* \simeq \hbar^2\gamma/m^*e^2 \qquad (7)$$

and m^* is an appropriate average between the transverse and longitudinal effective masses. Hence

$$|\psi(0)|^2_{\text{eff mass}} = N|\phi_j(0)|^2|F_j(0)|^2 \qquad (8)$$

For group 5 shallow donor states in silicon and germanium, the SEMT approach (eq 8) predicts[28,34] unpaired electron spin densities at the donor nuclei roughly an order-of-magnitude smaller than those observed experimentally. The discrepancy is attributed[28,34] to the breakdown of the Coulomb potential (2) in the vicinity of the donor impurity. Kohn and Luttinger[28] proposed a corrected effected mass formalism (CEMF) in which the corrected envelope function, $F_{corr}(r)$, was obtained using the observed ionization potential E_{obsd}. For distances greater than a critical value (r_{WS}, the Wigner–Seitz radius enclosing an impurity atom) the envelope function is given[28] by

$$F_{corr}(r) = A\{(n/2r)W_{n,1/2}(2r/n)\} \qquad (9)$$

where A is a normalization constant, $W_{n,1/2}(2r/n)$ is the Whittaker function, and

$$n = \{E_{obsd}/E_{\text{eff mass}}\}^{1/2} \qquad (10)$$

One disadvantage of this approximate solution is that $F_{corr}(r \to 0) \to \infty$ and a direct evaluation of $|F_{corr}(0)|^2$ is thereby ruled out.[34] However Kohn and Luttinger[28] set $|F_{corr}(0)|^2 \simeq |F_{corr}(r_{WS})|^2$ and the calculated value of $|\psi(0)|^2$ for phosphorus doped silicon is in good agreement with experimental values.[28,34] Therefore, on the CEMF, the corrected value of the unpaired electron spin density is given[34] by

$$|\psi(0)|^2_{corr} = N|\phi_j(0)|^2|F_{corr}(r_{WS})|^2 \qquad (11)$$

In order to retain the physically attractive concept of an isotropic Bohr radius we rewrite (11) as

$$|\psi(0)|^2_{corr} = \mathcal{K}|\psi(0)|^2_{\text{eff mass}} \qquad (12)$$

where the Kohn enhancement factor, $\mathcal{K}$, is given by[34]

$$\mathcal{K} = \frac{|F_{corr}(r_{WS})|^2}{|F_j(0)|^2} \qquad (13)$$

Equation 12 then predicts values of $|\psi(0)|^2$ which are in reasonable agreement with experimental values.[28,34,37]

Delocalized States. As the concentration of donors is increased, donor wave functions begin to overlap until at a critical concentration, n_c, the long-range Coulomb potential (2) is replaced by a short-range potential. In the Thomas–Fermi approximation this is given by

$$V(r) \simeq (-e^2/\gamma r)\exp(-qr) \qquad (14)$$

where the screening length, q, is given by

$$q^2 = 4m^*e^2(3n/\pi)^{1/3}/\hbar\gamma \qquad (15)$$

and n corresponds to the free electron density. The ground state eigenfunctions are now described in terms of extend-

TABLE II: Thomas–Fermi Screening of Wannier–Mott Impurity Ground States

Host	Donor	N	$\lvert\psi(0)\rvert^2_{obsd} \times 10^{-24}$	$\lvert\phi_j(0)\rvert^2$	$\mathcal{K}$	Mott constant,[d] C	n_c(calcd)[e] (ESR)	n_c(obsd)[f] (empirical)	n_c(calcd)[g] (Hubbard)
Si	^{31}P	6	0.43[a]	178[b]	9.8[c,h]	0.23	1.6×10^{18}		
						0.25	2.0×10^{18}	3×10^{18}	3.9×10^{18}
						0.295	3.3×10^{18}		
Si	^{75}As	6	1.73[a]	178	12.3[h]	0.23	5.0×10^{18}		
						0.25	6.5×10^{18}	5×10^{18}	4.6×10^{18}
						0.295	1.1×10^{19}		
Si	^{121}Sb	6	1.18[a]	178	7.1[h]	0.23	6×10^{18}		
						0.25	7.7×10^{18}		3.2×10^{18}
						0.295	1.3×10^{19}		
Ge	^{31}P	4	0.17[b]	1700[b]	27.1[h]	0.23	3.5×10^{16}		
						0.25	4.6×10^{16}	2.5×10^{17}	1.3×10^{17}
						0.305	8.2×10^{16}		
Ge	^{75}As	4	0.69[b]	1700	40.8[h]	0.23	9.5×10^{16}		
						0.25	1.2×10^{17}	3.5×10^{17}	1.4×10^{17}
						0.305	2.2×10^{17}		
HMPA	^{7}Li	4	0.016[j]	~100[j]	~1.4[h,i]	0.23	1.2×10^{18}		
						0.25	1.5×10^{18}	~3×10^{18}[j]	1.7×10^{18}[j]
						0.305	2.7×10^{18}		
HMPA	^{7}Li	6	0.016	~100	~1.4[h,i]	0.23	7.7×10^{17}		
						0.25	1.0×10^{18}	~3×10^{18}	2.0×10^{18}
						0.295	1.6×10^{18}		

[a] Reference 35. [b] Reference 36. [c] Reference 34. [d] Values taken from ref 29. [e] Equation 19. [f] For donors in Si and Ge, taken from ref 9. [g] Reference 40. [h] Values of the Kohn enhancement factor, $\mathcal{K}$, calculated from eq 5.11 of W. Kohn and J. M. Luttinger, *Phys. Rev.*, 97, 1721 (1955). [i] An estimate for $n \to 1$, eq 10. [j] This work.

ed Bloch functions and unpaired electrons propagate freely through the system. Approached from the metallic side, the transition from delocalized to localized states occurs[38,39] when

$$qa^* \simeq 1 \tag{16}$$

In its more familiar form, the Mott criterion[38,39] (17) relates the critical number of free carriers, n_c, at the M–I transition to the isotropic Bohr radius

$$n_c^{1/3}a^* \simeq C \tag{17}$$

where C represents a constant, originally taken[38] as 0.25. However, recent calculations[29] have shown that C is particularly sensitive to the number (N) of conduction band minima; ranging from 0.295 for $N = 6$ to 0.435 for $N = 1$.

It is interesting to the relate the Mott criterion (17) to the basic observation of an ESR experiment on localized donor stakes, namely $\lvert\psi(0)\rvert^2_{obsd}$. To a reasonable approximation[37] $\lvert\psi(0)\rvert^2_{obsd} \simeq \lvert\psi(0)\rvert^2_{corr}$ (eq 11) and from eq 6, 8, and 12 the isotropic Bohr radius is given by

$$a^* = \left|\frac{N\mathcal{K}\lvert\phi_r(0)\rvert^2}{\pi\lvert\psi(0)\rvert^2_{obsd}}\right|^{1/3} \tag{18}$$

Substituting for a^* in (17) leads to an expression which relates the observed magnetic properties of the localized centers to the critical density at which short-range Thomas–Fermi screening overcomes the long-range Coulcomb potential between the localized electron–parent hole, viz.

$$n_C = \left|\frac{C^3\pi\lvert\psi(0)\rvert^2_{obsd}}{N\mathcal{K}\lvert\phi_j(0)\rvert^2}\right| \tag{19}$$

Before applying this relation to our system, we first test it on the well-documented properties of Wannier-type impurity states in silicon and germanium. From experimental values[28,34-36] of $\lvert\psi(0)\rvert^2_{obsd}\mathcal{K}$ and $\lvert\phi_j(0)\rvert^2$ in these systems we use (19) to calculate the critical density at which T–F screening of shallow impurity states occurs. The results are given in Table II, together with available experimental values[9] of n_c. The calculations were performed for three values of C, namely, 0.23, 0.25, and 0.305 in germanium and 0.23, 0.25, and 0.295 in silicon. Between the lowest and highest values of C, computed critical densities changed by a factor of ca. 2. In Table II we also give critical densities from calculations[40] based on Hubbards model for the M–I transition.

The results obtained from eq 19 are in good agreement with both the experimental data[9] and the values calculated[40] from Hubbards model, especially when one considers the order-of-magnitude difference in the function $\lvert\phi_j(0)\rvert^2$ in silicon and germanium[35,36] (178 and 1700, respectively).

Similar calculations (eq 19) for Wannier–Mott impurity states in HMPA are difficult in that the nature of the conduction band wave function is at present unknown. An order-of-magnitude estimate of $\lvert\phi_j(0)\rvert^2$ can be obtained from the tight-binding approximation[28] as applied to the conduction band wave function in HMPA. In this approach we approximate the conduction band wave function by unoccupied atomic s functions from each of the atoms of the HMPA molecule, thus

$$\phi_j(r) = \left(\frac{\Omega}{2}\right)^{1/2}\{\alpha\psi_{4s(P)} + \beta\psi_{3s(N)} + \gamma\psi_{3s(O)}\} \tag{20}$$

(as a first approximation we neglect contributions from the C (2s) and H (1s) functions) where $\Omega/2$ is the volume per atom and e.g., $\psi_{4s(P)}$ is the 4s orbital on phosphorus. In addition

$$\alpha^2 + \beta^2 + \gamma^2 = 1 \tag{21}$$

and we set

$$\lvert\alpha\rvert^2 = \lvert\beta\rvert^2 = \lvert\gamma\rvert^2 = \tfrac{1}{3} \tag{22}$$

giving finally

$$\lvert\phi_j(0)\rvert^2 \simeq 100 \tag{23}$$

Results of calculations for the HMPA system are given in Table II.

As before the agreement between calculated (eq 19) and experimental critical densities is good, in view of the approximations introduced, although this might be fortuitous. However, as in the silicon and germanium calculations we note that the value of n_c calculated from the Hubbard model compares well with both the experimental value and with our criterion (19) for T–F screening of Wannier-type impurity states, and we must conclude that eq 19 represents a useful empirical correlation between an observed quantity and n_c.

The details of the Hubbard calculations are somewhat cumbersome and will be discussed elsewhere,[41] but briefly a transition from delocalized to localized states occurs when the unperturbed band width (Δ) of a *crystalline* array of isolated donors falls below the value of the repulsion integral ($\cup$) associated with electron correlation. Berggren[40] has shown that because of the common factor ($e^2/\gamma a^*$) occurring in expressions for both Δ and $\cup$, the critical density is determined solely by the dimensionless parameter $1/n^{1/3}a^*$, as in the Mott criterion (eq 17).

This correspondance with Motts criterion therefore establishes a direct link between the Hubbard calculations and our interpretation of eq 17 in terms of the magnetic properties of isolated donor states.

On the basis of the good agreement between the experimental and calculated critical values we conclude that the M–I transition in a *homogeneous* fluid metal–HMPA solution would proceed via a Mott transition although the presence of microscopic inhomogeneities might preclude its direct experimental verification. Nevertheless, the model outlined is quite capable of accommodating the results of the present investigation, and the empirical relation (19) should find application elsewhere.

Acknowledgment. We thank the S.R.C. for financial support.

References and Notes

(1) British Fulbright Scholar, 1975–1976.
(2) (a) "Solutions Métal-Ammoniac" (Propriétés Physico-Chimiques), G. Lepoutre and M. J. Sienko, Benjamin, New York, N.Y., 1964; (b) "Metal Ammonia Solutions", J. J. Lugowski and M. J. Sienko, Ed., Butterworths, London, 1970; (c) "Electrons in Fluids" (The Nature of Metal Ammonia Solutions), J. Jortner and N. R. Kestner, Ed., Springer-Verlag, Berlin, 1973.
(3) (a) R. Catterall and N. F. Mott, *Adv. Phys.*, **18**, 665 (1969); (b) M. H. Cohen and J. C. Thompson, *ibid.*, **17**, 857 (1968).
(4) J. C. Thompson, *Rev. Mod. Phys.*, **40**, 704 (1968).
(5) (a) J. C. Thompson and J. Jortner comments in ref 2b, p 315; (b) N. F. Mott, this conference.
(6) R. Catterall, *J. Chem. Phys.*, **43**, 2262 (1965).
(7) R. A. Newmark, J. C. Stephenson, and J. S. Waugh, *J. Chem. Phys.*, **46**, 3514 (1967).
(8) R. H. Silsbee, private communication to M. N. Alexander and D. F. Holcomb (cited in ref 9, p 828).
(9) M. N. Alexander and D. F. Holcomb, *Rev. Mod. Phys.*, **40**, 815 (1968).
(10) R. A. Levy, *Phys. Rev.*, **102**, 31 (1956).
(11) R. Catterall, W. T. Cronenwett, R. J. Egland, and M. C. R. Symons, *J. Chem. Soc. A*, 2396 (1971).
(12) R. Catterall and P. P. Edwards, *Adv. Mol. Relaxation Processes*, in press.
(13) W. Glausinger and M. J. Sienko, *J. Chem. Phys.*, **62**, 1873 (1975).
(14) W. Glausinger and M. J. Sienko, *J. Chem. Phys.*, **62**, 1883 (1975).
(15) M. J. Sienko, in ref 2a, p 23.
(16) N. Mammano in ref 2b, p 376.
(17) R. Catterall, *Phil. Mag.*, **22**, 779 (1970).
(18) P. Damay and M. J. Sienko, *J. Chem. Phys.*, in press.
(19) G. Feher and A. F. Kip, *Phys. Rev.*, **98**, 337 (1955).
(20) A. J. Watts and J. E. Cousins, *Phys. Status Solidi*, **30**, 105 (1968).
(21) N. S. VanderVen, *Phys. Rev.*, **168**, 787 (1968).
(22) R. J. Pressley and H. L. Berk, *Phys. Rev. A*, **140**, 1207 (1965).
(23) R. H. Hoskins and R. C. Pastor, *J. Appl. Phys.*, **31**, 1506 (1960).
(24) R. Catterall and P. P. Edwards, preceding paper in this issue.
(25) W. M. Walsh, Jr., L. W. Rupp, Jr., and P. H. Schmidt, *Phys. Rev. Lett.*, **16**, 181 (1966).
(26) J. Slater, Ph.D. Thesis, Leicester University, 1970.
(27) D. Pines, J. Bardeen, and C. P. Slichter, *Phys. Rev.*, **106**, 489 (1957).
(28) W. Kohn and J. M. Luttinger, *Phys. Rev.*, **97**, 883 (1955).
(29) F. Martino, G. Lindell, and K. F. Berggren, *Phys. Rev.*, **8**, 6030 (1973).
(30) M. H. Cohen and J. Jortner, *Phys. Rev. Lett.*, **30**, 699 (1973).
(31) J. P. Lelieur and J. C. Thompson, *J. Phys. (Paris)*, C4-371 (1974).
(32) R. Catterall in ref 2b, p 105.
(33) (a) B. Raz and J. Jortner, *Chem. Phys. Lett.*, **4**, 511 (1970); (b) B. Raz and J. Jortner, *Proc. R. Soc. (London)*, **317**, 113 (1970).
(34) W. Kohn in "Solid State Physics", Vol. 5, F. Seitz and D. Turnbull, Ed., Academic Press, New York, N.Y., 1957.
(35) G. Feher, *Phys. Rev.*, **114**, 1219 (1959).
(36) D. K. Wilson, *Phys. Rev.*, **134**, A265 (1964).
(37) R. Catterall and P. P. Edwards, unpublished work.
(38) N. F. Mott, *Proc. Phys. Soc.*, **62**, 416 (1949).
(39) N. F. Mott and E. A. Davis, "Electronic Processes in Non-Crystalline Materials", Clarendon, Oxford, England, 1971.
(40) K. F. Berggren, *Phil. Mag.*, **27**, 1027 (1973).
(41) R. Catterall and P. P. Edwards, *Phil. Mag.*, submitted for publication.

Discussion

J. JORTNER. I am worried about the analogy between your HMPA solid solutions and doped Si and Ge, as the dielectric constant in the former case is lower by one order of magnitude. Thus metallic screening effects in the homogeneous low dielectric constant HMPA–metal solid solution will set in at much higher donor concentration than in the case of Si or Ge. On the experimental side I would like to ask whether you have measured the electrical conductivity of your solids above 5×10^{-3} M and whether is there any indication for metallic behavior?

R. CATTERALL. We can only get an insulator–metal transition if we assume all the valence electrons of the alkali metals are equally effective in the formation of the impurity band. Nevertheless, we only see about 1% of these electrons as area under the electron resonance signal. The point is well made and the problem remains.

We have not yet measured any of the properties of these solids.

J. V. ACRIVOS. The lower than free electron value observed for the g factor of the ESR absorption of extended states suggests a spin–orbit coupling interaction which may allow its identification.

R. CATTERALL. The g shifts observed correlate quantitatively with the spin–orbit coupling constants for the free alkali atoms in the case of the spectra of the M_G species and are qualitatively in accord with the observed shifts for the species of lower atomic character. Spin relaxation studies (not reported in the paper) show T_1 for K_G, Rb_G, and Cs_G are also quantitatively correlated with spin–orbit coupling.

T. TUTTLE. (1) Could spin exchange be responsible for the narrowness of the single line resonance?

(2) Does the breadth of the single line resonance depend on metal concentration?

R. CATTERALL. (1) The concentration of unpaired spins is too low for significant spin exchange between the sites of the solids.

(2) Not significantly, but if the mobility were increasing further it would not have much effect on the line width since we are already very close to the exchange narrowed limit.

M. H. COHEN. The possibility of a transition from localized states to more extended states at such low concentration remains even though the idea of a Mott transition in a uniform system is out if some clustering occurs during quenching. The transition could then take place within a locally dense region and would contribute a local conductivity. Such could be detected by microwave dielectric constant and microwave conductivity measurements, which cannot fail to be interesting in any event.

R. CATTERALL. We hope to make further measurements and thank you for your suggestions.

Influence of the Nature of a Matrix on the Reactivity of Electrons in Irradiated Systems

A. K. Pikaev,* B. G. Ershov, and I. E. Makarov

Institute of Physical Chemistry of the Academy of Sciences of the USSR, Moscow, USSR *(Received July 23, 1975)*

In this paper experimental data on the reactivity of solvated and mobile electrons in different irradiated systems are considered and generalized. Special attention is paid to the reactivity of solvated electrons toward ions of transuranium elements in dilute and concentrated alkali and carbonate aqueous solutions, toward some compounds in alcohols and melted alkali halide salts, and to the reactivity of mobile electrons in some glassy systems. Also the results of a study of decay kinetics of F centers in alkali halide crystals at different temperatures by pulse radiolysis method are described. These data are discussed from the point of view of the influence of dielectric constant, viscosity of the medium, and other parameters on the reaction rate of solvated electrons. The problem of a tunnel mechanism of electron reactions in irradiated systems is also considered.

1. Introduction

Immediately after the detection of hydrated electrons (e_{aq}^-) in irradiated liquid water a great number of works on the reactivity of this particle were performed. Reviews of these works are available, for example, in book form.[1,2] At that time the reactivity of solvated electrons (e_s^-) in other liquids was studied occasionally. That was a reason why in radiation chemistry the idea of similar reactivity of e_s^-, in particular, in water and simple alcohols, was widespread. However, in a 1971 paper[3] it was shown that the rate constants for the reactions between e_s^- and anions in methyl alcohol are considerably lower than the rate constants of the reactions of e_{aq}^- with the same anions in water. The rate constants of the reactions of e_s^- with electroneutral molecules, as was measured in cited work, are approximately the same in water and methyl alcohol. A decrease of the rate constant of the reaction of e_s^- with the NO_3^- ion during the transition from water to methyl alcohol was also observed.[4] Later a similar phenomenon was observed for ethyl alcohol.[5] Due to lower dielectric constants, rate constants for the reactions of e_s^- with cations in simple alcohols may be larger than in water; for example, it is true for $k(e_s^- + Zn^{2+})$ in water–ethanol mixtures[5] and for $k(e_s^- + ROH_2^+)$ in methanol[6,7] and ethanol.[6] According to work[8] in glycerine rate constants for all the studied e_s^- reactions are much lower than the rate constants of the same reactions of e_{aq}^-. This effect was explained by the high viscosity of glycerine.

The above-mentioned variation of e_s^- reactivity during the transition from water to alcohols is illustrated in Table I. In this table literature data on absolute rate constants of e_s^- reactions in these liquids which were measured by pulse radiolysis method are listed.

In addition to the reactivity of e_s^- in water and alcohols in the literature there are values of the rate constants of some reactions of e_s^- in other irradiated liquids: ammonia,[13,14] amines,[15,16] hexamethylphosphoric triamide,[17,18] tetrahydrofuran[19-22] and other ethers,[19,23] water–ethanol,[5] water–dioxane,[5] and water–dimethyl sulfoxide[24] mixtures, etc. These data also testify to the influence of the matrix nature on e_s^- reactivity.

At sufficiently low temperatures the mobile solvated electron is stabilized; this is the trapped electron (e_{tr}^-). In the case of e_{tr}^- the question about far electron transfer by a tunnel mechanism is widely discussed in the literature (see, for example, ref 25–29). The tunnel mechanism is also postulated by some authors[2,28,30] for the reactions of e_{aq}^- in liquid water.

In the present work data on the reactivity of e_s^- toward ions of transuranium elements in dilute and concentrated alkali and carbonate aqueous solutions and toward some compounds in alcohols are presented and discussed. The choice of ions of transuranium elements is due to the variety of forms of their existence and, as a consequence, to the possibility of the investigation of the e_{aq}^- reactivity toward ions of these elements in different valence states.

Experiments with alcohols were undertaken for two reasons. First there is the contradiction in literature data on the reactivity of e_s^- toward the NO_3^- ion (see Table I). Second, recent new information on the properties of e_s^- in alcohols has been published (for example, on the mobility of these species[31,32]). This makes possible more definite conclusions about the influence of solvent nature on e_s^- reactivity.

Also in this work the results of the investigation of electron reactivity toward some acceptors during γ radiolysis of glassy alcohols and water–alcohol mixtures at 77 K are described. The purposes of this investigation are the comparison of the reactivity of electrons toward the same solutes in liquid and solid phases and the elucidation of the influence of electron trap depth on the probability of a tunnel transfer of an electron to the acceptor molecule.

Another type of electron center is the F center. It is an electron localized in an anion vacancy. F centers are formed, for example, during the irradiation of alkali halide crystals. Many years ago the important role of tunnel processes in the behavior of F-centers was noted.[33] It is interesting to obtain experimental evidence for electron tunneling in these systems. Alkali halide crystals are solids and for these systems the diffusion processes, under ordinary conditions, are slightly characteristic in the comparison with liquids. This circumstance favors the search of such evidence. To obtain this evidence the kinetics of F-center decay at different temperatures has been studied by the pulse radiolysis method.

Melts of alkali halide compounds were also an object of the investigation in the present work. It has been shown[34,35] that irradiation of these systems results in the formation of short-lived solvated electrons. In this case the study of e_s^- reactivity was stimulated by specific peculiari-

TABLE I: Comparison of Reactivity of Solvated Electrons in Water and Alcohols at Room Temperature

Scavenger	k, M^{-1} sec^{-1}			
	Water	Methanol	Ethanol	Glycerine
Hydrogen ion	2.2×10^{10} [b]	3.9×10^{10};[d] 6.8×10^{10};[e] 5.2×10^{10} [f]	2.0×10^{10};[d] 2.8×10^{10};[e] 4.5×10^{10} [f]	2×10^{9} [l]
Cd^{2+}	5.2×10^{10} [b]			5.6×10^{8} [l]
O_2	2×10^{10} [b]	1.9×10^{10} [d]	1.9×10^{10} [d]	
Acetone	$(5.6–6.5) \times 10^{9}$ [b,c]	$(2–3) \times 10^{9}$ [g]	6×10^{9} [c]	1.3×10^{8} [l]
Nitrobenzene	4.2×10^{10} [c]		1.5×10^{10} [c]	
Naphthalene	5.4×10^{9} [b]	2.7×10^{9};[g] $\sim 2 \times 10^{9}$ [h]	4.3×10^{9} [k]	
Benzyl alcohol	1.3×10^{8} [b]			5.5×10^{7} [l]
Benzyl chloride	5.5×10^{9} [b]	5.0×10^{9} [d]	5.1×10^{9} [d]	
Chloroacetate ion	1.2×10^{9} [b]	1.7×10^{8} [a,i]		1.9×10^{8} [l]
NO_3^-	8.5×10^{9} [b]	4×10^{7} [a,i] 2.1×10^{8} [a,i]	3×10^{7} [c]	
NO_2^-	3.7×10^{9} [b]	9.1×10^{7} [a,i]		

[a] The correction caused by kinetic salt effect is introduced into the values of the rate constants shown in ref 3. [b] Reference 2. [c] Reference 5. [d] References 9 and 10. [e] Reference 6. [f] Reference 7. [g] Reference 3. [h] Reference 12. [i] Reference, 3. [j] Reference 4. [k] Reference 11. [l] Reference 8.

ties of these liquids (by their ionic character, high temperature, etc.).

The results discussed in this work were partially published previously.[36-40]

2. Experimental Section

The pulse radiolysis method with optical registration of short-lived species was used for the measurement of rate constants of the e_s^- reactions in liquids and the kinetics of F-center decay in alkali halide crystals. The radiation source was a linear electron accelerator U-12 (the pulse duration is 2.3 μsec; the energy of electrons is ca. 5 MeV; the current in the pulse is 0.2 A). The transient optical absorption was recorded with a fast spectrophotometric apparatus, which has been mainly described earlier.[41,42] The small modification was that the signal from the exit of the photomultiplier passed to the operational amplifier and then to the oscilloscope with a frequency range of 0–100 MHz. This equipment allowed one to record optical absorption signals from 10^{-6} to 10^{-2} sec duration.

For low-temperature radiolysis of glassy systems ^{60}Co γ radiation was used. The dose rate was 5.5×10^{16} eV g^{-1} sec^{-1}. The concentration of e_{tr}^- formed was measured by an optical method using SF-4A and Specord uv-vis spectrophotometers which had special set for measurements at 77 K.

Aqueous solutions have been prepared using triply distilled water. Alcohols have been purified by continuous refluxing with 2,4-dinitrophenylhydrazine and then by double distillation under reduced pressure in an atmosphere of nitrogen or argon. Sodium hydroxide (CP grade), which was used for the preparation of concentrated alkali solutions, was recrystallized from doubly distilled water. All salts used have been recrystallized also from doubly distilled water. The kinetics of F-center decay in alkali halide compounds was measured using single crystals in which the impurity content had been determined earlier.[42]

In pulse radiolysis experiments, aqueous or alcoholic solutions were introduced for irradiation into the quartz cells with plane-parallel windows. The removal of the air from the solutions in the cases when it was necessary was accomplished by continuous bubbling with purified argon. Solutions in the melts of alkaline halide crystals were prepared by the introduction of a known amount of aqueous solution of the compound under investigation into the cell and then by the evaporation of water and the addition of alkali halide compound. After these operations the mixture obtained was kept under vacuum for 2–3 days (for the removal of oxygen and moisture), and then the cell was sealed.

Irradiation of alkali halide single crystals at high temperatures and of their melts has been performed in a special electric heater. Its construction has been described earlier.[35] The temperature was maintained within ±5°C (for single crystals) and ±2°C (for melts).

3. Results and Discussion

Reactivity of e_{aq}^- toward Ions of Neptunium and Plutonium. The measurement of rate constants of the reactions between e_{aq}^- and these ions was performed in alkali and carbonate media. This choice results from the stability of different valence states of these ions in these media. Rate constants were determined from optical density decay curves at wavelengths which correspond to the optical absorption band of e_{aq}^-, in the absence and in the presence of neptunium or plutonium ions. In alkaline solutions at OH^- concentrations more and less than 7.5 M, measurements were carried out respectively at 650 and 700 nm. In carbonate solutions the absorption of e_{aq}^- was registered at 800 nm because CO_3^- radical ions do not absorb light at this wavelength. Methanol (5×10^{-3} M) was added to ≤ 5 M solutions to increase the e_{aq}^- lifetime.

Usually the e_{aq}^- lifetime was decreased several fold as a result of the addition of transuranium element ions, and the e_{aq}^- decay was followed in accordance with the pseudo-first-order kinetic equation. The correction because of e_{aq}^- decay in the absence of transuranium element ions was introduced into the calculations of rate constants. In Tables II and III are shown the rate constants of the reactions between e_{aq}^- and ions of neptunium and plutonium determined in such a way. From the values obtained it is possible to make the following general conclusions.

In alkaline solutions Np(VI), Pu(VI), and especially Np(VII) and Pu(VII) are characterized by the high reactivity toward e_{aq}^-, the rate constants for Pu(VII) being higher than for Np(VII). Rate constants for Np(V) are less by a factor of 2–4 than for Np(VI) and Np(VII).

The reaction rate for all ions investigated is appreciably decreased at $[OH^-] \geq 7.5$ M. Note that the decrease of the rate constants of the e_{aq}^- reactions toward some compounds (NO_3^-, N_2O, etc.) in very concentrated solutions of

TABLE II: Rate Constants k of Reactions between e_{aq}^- and Ions of Neptunium and Plutonium in Alkali Aqueous Solutions at Room Temperature[a,b]

Ion	Concn, M	$[OH^-]$, M	k, M^{-1} sec^{-1}
Np(VII)	2×10^{-5}	0.1	2.9×10^{10}
Np(VII)	2×10^{-5}	0.5	3.2×10^{10}
Np(VII)	4×10^{-5}	1.0	2.0×10^{10}
Np(VII)	3×10^{-5}	2.0	2.1×10^{10}
Np(VII)	4×10^{-5}	5.0	1.7×10^{10}
Np(VII)	4×10^{-5}	7.5	1.3×10^{10}
Np(VII)	4×10^{-5}	10.0	8.8×10^{9}
Np(VII)	4×10^{-5}	12.5	6.0×10^{9}
Np(VII)	8×10^{-5}	12.5	8.0×10^{9}
Np(VI)	1.5×10^{-5}	0.5	2.3×10^{10}
Np(VI)	5.3×10^{-5}	1.0	1.3×10^{10}
Np(VI)	2×10^{-5}	2.0	1.3×10^{10}
Np(VI)	5.3×10^{-5}	2.0	1.1×10^{10}
Np(VI)	5.3×10^{-5}	5.0	2.0×10^{10}
Np(VI)	5.3×10^{-5}	7.5	1.1×10^{10}
Np(VI)	5.3×10^{-5}	10.0	8.3×10^{9}
Np(VI)	5.3×10^{-5}	12.5	6.8×10^{9}
Np(V)	4.4×10^{-5}	1.0	5.0×10^{9}
Np(V)	4.4×10^{-5}	2.0	6.1×10^{9}
Np(V)	4.4×10^{-5}	5.0	6.6×10^{9}
Np(V)	5.3×10^{-5}	5.0	5.2×10^{9}
Np(V)	4.4×10^{-5}	7.5	3.2×10^{9}
Np(V)	7.5×10^{-5}	7.5	3.0×10^{9}
Pu(VII)	2×10^{-5}	1.0	3.5×10^{10}
Pu(VII)	2×10^{-5}	2.0	4.2×10^{10}
Pu(VII)	2.7×10^{-5}	5.0	2.3×10^{10}
Pu(VII)	4×10^{-5}	7.5	2.0×10^{10}
Pu(VI)	2.6×10^{-5}	2.0	1.9×10^{10}
Pu(VI)	5.2×10^{-5}	5.0	2.0×10^{10}
Pu(VI)	5.2×10^{-5}	7.5	6.6×10^{9}

[a] Here and further (in the cases without special remarks) the errors in the rate constant measurements are ±10–12%. [b] Reference 36.

electrolyte (12.4 M solution of KF was used) was observed earlier.[43] A similar effect was described[44] for rate constants of the reactions $e_{aq}^- + e_{aq}^-$ and $e_{aq}^- + O^-$. It is possible to propose several explanations for such a decrease of the rate constants. Principally, they are the increase of the viscosity of the solutions and the capture of electrons in deeper traps.

It seems most probable[45] that in alkaline solutions heptavalent neptunium and plutonium exist as the ions $MeO_4(OH)_2^{3-}$ (Me is Np or Pu). On this basis it is possible by means of the well-known equation

$$\log \frac{k}{k_0} = 1.02 Z_X \frac{\mu^{1/2}}{1 + a\mu^{1/2}} \quad (1)$$

where k is the rate constant at ionic strength μ, k_0 is the same at $\mu = 0$; Z_X is the charge of the ion X reacting with e_{aq}^-, $a = r/3$ (r is the sum of the radii of e_{aq}^- and the ion, in Å), to introduce the kinetic salt effect correction in the rate constant of the reaction between e_{aq}^- and Np(VII) in 0.1 M solution of KOH (at higher alkali concentrations eq 1 obviously is not valid). If we take $a = 1.8$ Å (see below), then $k_0 = 7.2 \times 10^9\ M^{-1}$ sec^{-1} ($Z_X = -3$) or $1.1 \times 10^{10}\ M^{-1}$ sec^{-1} ($Z_X = -2$ if in 0.1 M solution of KOH there is ion-pair formation with K^+).

Let us evaluate $k[e_{aq}^- + Np(VII)]$, if we propose that the rate of this reaction is limited by diffusion. The rate constants k_{dif} of such reactions in the case of ions are expressed by Debye equation:

$$k_{dif} = \frac{4\pi N(r_{e^-} + r_X)(D_{e^-} + D_X)Q}{1000(e^Q - 1)} \quad (2)$$

TABLE III: Rate Constants k of Reactions between e_{aq}^- and Ions of Neptunium and Plutonium in Carbonate Aqueous Solutions at Room Temperature[a]

Ion	Concn, M	Carbonate concn, M	k, M^{-1} sec^{-1}
Np(VI)	2.7×10^{-5}	0.05 M Na_2CO_3 + 0.05 M $NaHCO_3$	1.9×10^{10}
Np(VI)	5.4×10^{-5}	The same	1.7×10^{10}
Np(VI)	5.4×10^{-5}	0.1	1.9×10^{10}
Np(VI)	2.7×10^{-5}	1.0	1.3×10^{10}
Np(VI)	5.4×10^{-5}	1.0	1.1×10^{10}
Np(VI)	5.4×10^{-5}	5.0	6.2×10^{9}
Np(V)	2.0×10^{-4}	0.1	2.5×10^{9}
Np(V)	2.0×10^{-4}	1.0	2.0×10^{9}
Np(V)	2.0×10^{-4}	5.0	2.0×10^{9}
Np(IV)	5.0×10^{-5}	0.1	5.0×10^{9}
Np(IV)	5.0×10^{-5}	1.0	4.0×10^{9}
Np(IV)	6.7×10^{-5}	1.0	4.0×10^{9}
Np(IV)	6.7×10^{-5}	4.3	4.0×10^{9}
Np(IV)	5.0×10^{-5}	4.5	3.7×10^{9}
Pu(VI)	3.85×10^{-5}	0.1	2.3×10^{10}
Pu(VI)	4.85×10^{-5}	0.1	2.2×10^{10}
Pu(VI)	3.85×10^{-5}	1.0	1.4×10^{10}
Pu(VI)	3.85×10^{-5}	5.0	6.3×10^{9}
Pu(VI)	4.85×10^{-5}	5.0	7.2×10^{9}

[a] Reference 38.

where N is Avogadro's number, r_{e^-} and r_X are the radii of e_s^- and X, D_{e^-} and D_X are the diffusion coefficients of e_s^- and X, $Q = -Z_X e^2/\epsilon kT(r_{e^-} + r_X)$ (Z_X is the charge of X, e is the electron charge, ϵ is dielectric constant of the medium, k is Boltzmann's constant, and T is the temperature, K), and k_{dif} is given in M^{-1} sec^{-1}. For water $D_{e^-} = 4.9 \times 10^{-5}$ cm^2 sec^{-1}.[46] Usually it is accepted[47] that the radius of e_{aq}^- is equal to 2.5 Å. The values of r_X and D_X for $NpO_4(OH)_2^{3-}$ are unknown. However, in analogy with other ions of similar structure it is possible to assume that in this case $2.5 \leq r_X \leq 3.5$ Å and $D_X \sim 10^{-5}$ cm^2 sec^{-1}. Then for Np(VII) $1.4 \times 10^9 \leq k_{dif} \leq 2.4 \times 10^9\ M^{-1}$ sec^{-1} ($Z_X = -3$) or $3.8 \times 10^9 \leq k_{dif} \leq 6.5 \times 10^9\ M^{-1}$ sec^{-1} ($Z_X = -2$). As is seen, k_{dif} is considerably less than k_0. From this it may be supposed that in the reactions of e_{aq}^- with Np(VII) and, obviously with Pu(VII), as in the case of other effective oxidants, tunnel transfer of electrons plays an important role. It is interesting to note that $k[e_{aq}^- + Pu(VII)] > k[e_{aq}^- + Np(VII)]$. This is apparently because Pu(VII) is a stronger oxidant than Np(VII); the difference in redox potentials (1 M OH^-) is 0.27 V.[48]

Information on the structure of Np(VI), Pu(VI), and Np(V) ions in alkaline aqueous solutions is absent. Therefore it is impossible to make definite conclusions on the reasons for the different reactivity of these ions toward e_{aq}^-. It is possible only to suggest that the lower rate constants of Np(V) ions in comparison with the rate constants of Np(VI) and Np(VII) are caused by the necessity of the reconstruction of Np(V) anion into Np(IV) cation as a result of e_{aq}^- reaction.

The forms of neptunium and plutonium ions in carbonate aqueous solutions are known. Np(VI) and Pu(VI) exist as $MeO_2(CO_3)_3^{4-}$ ions.[49,50] Np(V) and Np(IV) exist as the ions $NpO_2(CO_3)_2^{3-}$ and $Np(CO_3)_5^{6-}$,[49,50] respectively. To a certain extent this information favors the interpretation of the reactivity of Np(IV), Np(V), Np(VI), and Pu(VI) carbonate complexes toward e_{aq}^-.

The r_X values for the carbonate complexes under consideration are unknown. They have been calculated from the radii[51] of Np^{4+}, Np^{5+}, Np^{6+}, and Pu^{6+} and the bond

TABLE IV: Evaluation of k_0 and k_{dif} for Reactions of Carbonate Complex Ions of Neptunium and Plutonium with Hydrated Electrons

Ion	k_0, M^{-1} sec^{-1}	r_X, Å	D_X, cm^2 sec^{-1}	k_{dif}, M^{-1} sec^{-1}
$NpO_2(CO_3)_3^{4-}$	2.1×10^9	3.5	0.8×10^{-5}	1.1×10^9
$PuO_2(CO_3)_3^{4-}$	2.2×10^9	3.5	0.8×10^{-5}	1.1×10^9
$NpO_2(CO_3)_2^{3-}$	4.5×10^8	3.5	0.9×10^{-5}	2.7×10^9
$Np(CO_3)_5^{6-}$	1.3×10^8	3.0	0.9×10^{-5}	8.3×10^7

lengths in similar complexes of uranium[52] (it has been assumed that for neptunium and plutonium complexes the bond lengths are the same). The r_X values obtained in such a way are given in Table IV. On the basis of these r_X values the coefficients a for calculations of k_0 using eq 1 have been taken as 2 (for $MeO_2(CO_3)_3^{4-}$ and $NpO_2(CO_3)_2^{3-}$) and 1.8 (for $Np(CO_3)_5^{6-}$). In these calculations rate constants for 0.1 M solutions of K_2CO_3 and solution of the composition 0.05 M Na_2CO_3 + 0.05 M $NaHCO_3$ were used. To calculate k_{dif} by means of eq 2 it is necessary to know D_X. Information on D_X values for the complex ions under consideration is absent. In the calculations of k_{dif} the diffusion coefficients shown in Table IV have been used, chosen by analogy with similar complex ions.

From the data of Table IV it is possible to conclude that the reaction rate of e_{aq}^- with $MeO_2(CO_3)_3^{4-}$ seems to be limited by diffusion. For $NpO_2(CO_3)_2^{3-}$ k_0 is less than k_{dif}. Obviously it is caused by the necessity of considerable reconstruction of ions during the transition from Np(V) to Np(IV). For the reaction between e_{aq}^- and $Np(CO_3)_5^{6-}$ the values of k_0 and k_{dif} are close to each other. The redox potential of the Np(IV)–Np(III) pair in carbonate solutions is considerably higher than that of the Np(VI)–Np(V) pair. However, the transition of Np(IV) into Np(III) occurs without a change in the ion structure.

It is necessary to stress that the ions under consideration can form the ion pairs with gegenions. Because of this effect the charge of these ions may be more positive than is indicated in Table IV. However, this effect has no influence on the above-mentioned conclusions. For example, if the charge of Pu(VI) ion is −3 or −2 then k_0 and k_{dif} are equal to 3.6×10^9 or 6.6×10^9 M^{-1} sec^{-1} and 2.6×10^9 or 6.2×10^9 M^{-1} sec^{-1}, respectively. In the case of Np(V) ion k_0 is 7.3×10^8 (for $Z_X = -2$) or 1.4×10^9 M^{-1} sec^{-1} (for $Z_X = -1$) and k_{dif} is 6.3×10^9 (for $Z_X = -2$) or 1.4×10^{10} M^{-1} sec^{-1} (for $Z_X = -1$). If the charge of Np(IV) ions is −5 or −4 then k_0 is 2.1×10^8 or 4×10^8 M^{-1} sec^{-1} and k_{dif} is 2.3×10^8 and 6.8×10^8 M^{-1} sec^{-1}, 2.0 are respectively.

Apparently the decreases of the rate constants of the e_{aq}^- reactions with carbonate complex ions of neptunium and plutonium in concentrated solutions of K_2CO_3 are due to the same reasons as in the case of alkaline solutions.

Reactivity of e_s^- in Alcohols. Almost all published values of absolute rate constants of e_s^- reactions in alcohols are shown in Table I. Because of contradictory data on the value of $k(e_s^- + NO_3^-)$ we have performed a redetermination of this rate constant. Also this constant has been measured for ethylene glycol.

The rate constants were determined using alcohols containing 5×10^{-2} M KOH or NaOH. The addition of alkali increased the lifetime of e_s^- in alcohol and as a consequence favored the measurement of the rate constant. It was found that the rate constants of the reaction between e_{aq}^- and NO_3^- in methanol and ethylene glycol in the presence of 5×10^{-2} M KOH (the content of water in alcohols was ca. 1%) are the same and are 8×10^8 M^{-1} sec^{-1}. The kinetic salt effect correction was made by means of eq 1. The coefficient a in this equation is equal to $0.51r$ and $0.47r$ respectively for methanol and ethylene glycol; the coefficient preceding Z_X is equal to 3.84 and 2.98, respectively. As in the case with water[47] it has been taken that r = 4 Å. Then the k_0 values are 2.0×10^8 and 2.7×10^8 M^{-1} sec^{-1} respectively for methanol and ethylene glycol. The k_0 value coincides with the value measured in an earlier work.[3]

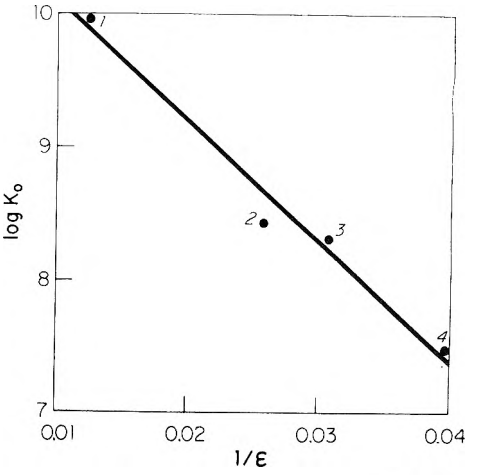

Figure 1. Dependence of log k_0 for the reaction of e_s^- with NO_3^- on $1/\epsilon$: (1) water; (2) ethylene glycol; (3) methanol; (4) ethanol.

The dependence of log k_0 on $1/\epsilon$ is shown in Figure 1 for the reaction of e_s^- with NO_3^- in water and alcohols. The k_0 values for water and ethanol were taken from ref 2 and 5. It is seen that log k_0 is almost linearly decreased with an increase of $1/\epsilon$. The same dependence of log k_0 on $1/\epsilon$ has been found earlier in work[5] for this reaction in water, water–ethanol, and water–dioxane mixtures. As it follows from the theory of chemical kinetics (see, for example, ref 53), such a dependence takes place for comparatively slow reactions.

The reaction rate of e_s^- with NO_3^- is not limited by diffusion. It follows from the calculations using eq 2. It was supposed that the radius of e_s^- is the same in water, methanol, ethanol, and ethylene glycol and equal to ~2.5 Å. Such a supposition is confirmed by the almost linear dependence of log k_0 on $1/\epsilon$. Also, the proximity of the r_{e^-} values in water and methanol were noted as well in an earlier work.[54] According to recent data,[31,32] for methanol and ethylene glycol D_{e^-} is equal to 7×10^{-5} and 7×10^{-6} cm^2 sec^{-1}, respectively. In accordance with previous conclusions[23] for ethanol D_{e^-} has been taken as 3.75×10^{-5} cm^2 sec^{-1}. The choice of D_X values for methanol and r_X values was based on a previous work.[3] The $D_{NO_3^-}$ values for ethanol and ethylene glycol were taken respectively as 6.9×10^{-6}[5] and 1.5×10^{-6} cm^2 sec^{-1}. In the case of ethylene glycol it was assumed that $D_{NO_3^-}$, like D_{e^-}, is a factor of 10 less than that in methanol. Results of the calculations are shown in Table V. In this table results of k_{dif} calculations for some other solutes in methanol, chloroacetate ion in water, and for a comparison literature data[47,55] on k_{dif} values for some solutes in water are also included. In the case of oxygen the k_{dif} value was determined by means of

TABLE V: Values of k_{dif} for e_s^- Reactions in Water and Alcohols[a]

Solvent	Scavenger	r_X, Å	D_X, cm² sec⁻¹	k_0, M^{-1} sec⁻¹	k_{dif}, M^{-1} sec⁻¹
Water	O_2 [b]	1.6	2.4×10^{-5}	2.0×10^{10}	2.3×10^{10}
	H^+ [b]	2.5	9.3×10^{-5}	2.2×10^{10}	1.03×10^{11}
	NO_3^- [c]	1.4	1.8×10^{-5}	8.5×10^{9}	6.7×10^{9}
	NO_2^- [c]	1.1	1.4×10^{-5}	4.6×10^{9}	5.2×10^{9}
	$ClCH_2COO^-$	2.65	1.1×10^{-5}	1.2×10^{9}	7.8×10^{9}
Methanol	O_2	1.6	4.3×10^{-5}	1.9×10^{10}	3.5×10^{10}
	H^+	1.35	3.8×10^{-5}	5.2×10^{10}	1.4×10^{11}
	NO_3^- [c]	1.4	1.5×10^{-5}	2.2×10^{8}	1.3×10^{9}
	NO_2^- [c]	1.1	1.35×10^{-5}	9.1×10^{7}	9×10^{8}
	$ClCH_2COO^-$	2.65	8×10^{-6}	1.7×10^{8}	3.6×10^{9}
Ethanol	NO_3^-	1.4	6.9×10^{-6}	3×10^{7}	2.5×10^{8}
Ethylene glycol	NO_3^-	1.4	1.5×10^{-6}	2.7×10^{8}	2.3×10^{8}

[a] The references to the papers from which the values of k_0 have been taken for the reactions in water, methanol, and ethanol are presented in Table I. [b] From ref 55. [c] From ref 47.

Smoluchovsky equation: $k_{dif} = 4\pi N(r_{e^-} + r_X)(D_{e^-} + D_X)/1000$.

As it is seen from Table V, the reaction rate of e_s^- with O_2 is limited by diffusion both in water and methanol. For the reactions of e_s^- with H^+ and $ClCH_2COO^-$ the k_0 values are less than the k_{dif} values for both solvents. However $k_0 < k_{dif}$ for the reactions of e_s^- with NO_3^- and NO_2^- in methanol and with NO_3^- in ethanol, while in water the rate of these reactions is diffusion controlled. For the reaction of e_s^- with NO_3^- in ethylene glycol $k_0 \sim k_{dif}$.

The sufficiently lower values of k_0 in comparison with k_{dif} for the reactions of e_s^- with NO_3^- in methanol and ethanol seem to result from the fact that the radical ion NO_3^{2-} has less solvation energy in alcohols.

Obviously a very similar phenomenon takes place in ethylene glycol. However, in ethylene glycol because of its high viscosity the reacting species (NO_3^- and e_s^-) can be in a "solvent cage" for a comparatively long time, and they can suffer several encounters before diffusing away. Apparently this can draw together the values of k_0 and k_{dif}. The important role of this effect has been noted earlier in work[8] for the reactions of e_s^- in glycerine.

Reactivity of Electrons in Glassy Alcohols and Water–Alcohol Mixtures at 77 K. In glassy systems the electron is stabilized under definite conditions. If in the system the electron acceptor is present, the following competition processes take place (T is trap, A is acceptor):

$$e^- + T \rightarrow e_{tr}^- \quad (3)$$

$$e^- + A \rightarrow A^- \quad (4)$$

Then

$$\frac{G_0}{G} = 1 + \frac{k_4[A]}{k_3[T]} \quad (5)$$

where G_0 and G are the yields of e_{tr}^- in the absence and in the presence of an acceptor and k_3 and k_4 are the rate constants of reactions 3 and 4.

From eq 5 it follows that the ratio of G_0/G should depend linearly on [A]. However in many works (see, for example, ref 26 and 56–60) it has been shown that the deviation of this dependence from linearity is observed in aqueous "glasses" at sufficiently high concentrations of acceptors. According to some authors[56,58,59] this deviation is due to the decrese of electron trap concentration. In the opinion of other authors[26,28,29,60] it is caused by tunneling of the electrons. In ref 37 the study of this effect has been extended to glassy alcohols and water–alcohol mixtures.

It has been found that the linear dependence of the ratio D_0/D (D_0 and D are the optical densities of the irradiated system in the maximum of the e_{tr}^- band in the absence and in the presence of A), which is proportional to G_0/G, on [A] up to 0.2 M occurs in the γ radiolysis of methanol for all acceptors investigated (acetone, $HClO_4$, H_2O_2, biphenyl, and $LiNO_3$). D_0 and D have been measured for 40 min after the irradiation. Such a dependence has also been observed in the above-mentioned range of concentrations for some other systems: H_2O_2, $ClCH_2COO^-$ and FCH_2COO^- in water–methanol mixture (1:1), $ClCH_2COO^-$ and FCH_2COO^- in water–methanol mixture (2:1), and FCH_2COO^- in 2-propanol (from here on the composition of mixtures is given in mole percent). At the same time the deviation of the dependence under consideration from linearity has been found for some systems: H_2O_2 in water–methanol mixture (2:1), NO_3^- in water–methanol mixture (1:1 and 2:1), 2-propanol, and 2-methyl-2-propanol, $ClCH_2COO^-$ and H_2O_2 in 2-propanol.

During the interpretation of the deviation under discussion it was suggested that the trapped electrons, which are inside the reaction volumes V_{eff} of the acceptor molecules, decay via the reaction:

$$e_{tr}^- + A \rightarrow A^- \quad (6)$$

Then it is easy to obtain that

$$\frac{G_0}{G} = \left(1 + \frac{k_4[A]}{k_3[T]}\right) e^{V_{eff}[A]} \quad (7)$$

It is possible to simplify eq 7 by the decomposition of its exponential term in a series. During this operation for small values of [A] it is possible to be limited by the first items of the series. As a result we have

$$\left(\frac{G_0}{G} - 1\right)\frac{1}{[A]} = \frac{k_4}{k_3[T]} + V_{eff} + \frac{k_4[A]}{k_3[T]} V_{eff} \quad (8)$$

We note that eq 7 is general. It takes into account the competition of reactions 3 and 4 and also the spontaneous decay of e_{tr}^- (reaction 6). At V_{eff} [A] $\rightarrow$ 0 eq 7 is transformed into eq 5. Experimentally we observe such linear dependence at V_{eff} [A] $\approx$ 0.05. Therefore the linear dependence of D_0/D on [A] at comparatively small values of D_0/D (for example in the case of methanol) indicates only that here the spontaneous decay of e_{tr}^- after irradiation can be neglected.

Using eq 8 at small [A] the values of V_{eff} and k_4/k_3[T] were found for systems in which the deviation of the dependence of D_0/D on [A] from linearity takes place. For the

TABLE VI: Values of $k_4/k_3[T]$ in Different Glassy Systems at 77 K

Matrix	$k_4/k_3[T]$, M^{-1}							
	NO_3^-	NO_2^-	H_2O_2	$ClCH_2COO^-$	Acetone	Biphenyl	$HClO_4$	FCH_2COO^-
Methanol	10	6	7	4	5	9	6	
Methanol–water (1:1)	20		10					
Methanol–water (1:2)	170	80	45	15			20	
Ethanol	20							
2-Propanol	180		105	30				14
2-Methyl-2-propanol	220							
6 *M* NaOH	60	40						

TABLE VII: Values of V_{eff} and R for Different Acceptors and Matrices

Matrix	Acceptor	$E_{\lambda_{max}}$, eV	V_{eff}, Å^3	R, Å
Methanol–water (1:1)	NO_3^-	2.3	7.7×10^3	12
Ethanol	NO_3^-	2.4	6.7×10^3	12
2-Propanol	NO_3^-	2.0	7.5×10^4	26
2-Propanol	H_2O_2	2.0	3.3×10^4	19
2-Propanol	$ClCH_2COO^-$	2.0	1.4×10^4	15
2-Methyl-2-propanol	NO_3^-	1.7	1.3×10^5	31
6 *M* NaOH	$Fe(CN)_6^{3-}$	2.2	1.1×10^5	29
6 *M* NaOH	NO_3^-	2.2	5.0×10^4	23
6 *M* NaOH	NO_2^-	2.2	4.6×10^4	22

systems for which this deviation is not observed, the values of $k_4/k_3[T]$ were determined via eq 5. The results obtained are shown in Tables VI and VII. From the values of V_{eff} the radii R of the effective reaction volumes were calculated (see Table VII). In these tables for the purpose of comparison the values of $k_4/k_3[T]$, V_{eff}, and R are listed for acceptors in alkaline "glass", which have been calculated on the basis of the results of previous work.[26]

The radius R determines the distance of electron transfer to a molecule of the acceptor. These large distance values (several tens of angstroms) testify to tunneling by the electron. This conclusion is confirmed by the fact that for the same acceptor the larger V_{eff} and R the smaller the energy of optical transfer ($E_{\lambda_{max}}$) in the maximum of the e_{tr}^- band in the matrix. Since for solvated and trapped electrons the larger $E_{\lambda_{max}}$ the deeper the electron trap, the dependence obtained may be connected with the energy of the ground state of the electron. Obviously the deeper the electron trap the smaller the values of V_{eff} and R.

There are other evidences of tunneling by the electron in irradiated glassy systems at low temperatures. Let us consider the evidence which has been obtained recently at our laboratory by the pulse radiolysis method. This investigation will be described in detail in a separate paper.[61]

Obviously, the probability of tunneling is increased with the increase of [A] and the time of the contact of the reacting species. Therefore eq 5 characterizes the initial yields of e_{tr}^-. Speaking in other words, in the general case, it is valid for times during which the reaction of e_{tr}^- with an acceptor does not occur at all. Apparently this time is smaller the larger the probability of tunneling by the electron from the trap to the acceptor molecule.

It was found by the pulse radiolysis method[61] (glassy 10 *M* aqueous solution of NaOH in the presence of different acceptors at 77 K) that eq 5 is valid for NO_2^- and NO_3^- for short times after pulse. As an example the dependence of

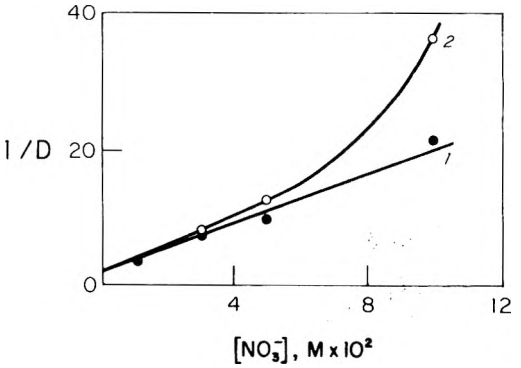

Figure 2. Dependence of $1/D$ (D is the optical density in the maximum of the e_{tr}^- band) on NO_3^- concentration in glassy 10 *M* aqueous solution of NaOH irradiated by an electron pulse of duration 2.3 μsec at 77 K: (1) immediately after the pulse; (2) for 400 μsec after the pulse.

$1/D$ (D is the optical density in the maximum of the e_{tr}^- band at a given concentration of A and at a given time after the pulse) on $[NO_3^-]$ is shown in Figure 2. In the cases of $Fe(CN)_6^{3-}$ and CrO_4^{2-} there was the same deviation from linearity if the yield of e_{tr}^- was measured immediately after the pulse. It is caused by the fact that these ions are more effective electron acceptors than NO_2^- and NO_3^-. However, if we take into consideration the data in ref 62 then for a time of 10^{-7} sec after the pulse the dependence for CrO_4^{2-} is also close to linearity. Equation 5 does not take into account the decay of e_{tr}^- after the pulse. Because of it the longer the period of time from the end of the pulse to the measurement the larger the deviation of above-mentioned dependence from linearity. The fraction of e_{tr}^- at a given time t is determined by the probability that a molecule of the acceptor is absent in the reaction volume V_{eff}:

$$G_t = G_0 e^{-V_{eff}[A]} \quad (9)$$

where G_0 and G_t are the yields of e_{tr}^- at the initial and measured moments of time.

It has been obtained that for all four acceptors studied eq 9 is sufficiently valid. On the basis of this equation the distances of tunneling by the electrons were calculated, for example, for the time of 400 μsec after the pulse. They are equal to 9.5, 10.5, 14.4, and 17.3 Å respectively for NO_2^-, NO_3^-, $Fe(CN)_6^{3-}$, and CrO_4^{2-}.

Note that the rate of e_{tr}^- decay after the pulse in glassy 10 *M* aqueous solution of NaOH in the presence of acceptors does not depend on temperature from 77 to 150 K. This fact testifies to the resonance tunnel mechanism of e_{tr}^- decay.

Other evidence of tunneling of electrons in irradiated glassy systems are presented in reviews[28,29] and papers,[25-27,60,62-67] including works[25,26,66,67] which were car-

TABLE VIII: Values of E, T_{lim}, and k_{lim} for Single Crystals of Alkaline Halide Compounds

Compound	E, kcal/mol	T_{lim}, °C	k_{lim}, sec^{-1}
NaCl	20.9	350	1.1×10^2
KCl	15.9	250	1.2×10^2
KBr	19.2	200	0.6×10^3
CsI	25.6	170	0.6×10^2

ried out with the participation of the authors of the present paper.

Kinetics of Decay of F Centers in Alkali Halide Crystals at High Temperatures. According to the calculations described in a previous paper,[33] in alkali halide crystals tunneling of the electrons of F centers and the primary hole centers is possible up to distances of 30–40 Å. We consider the results of work[40] which can serve as evidence of F-center decay in alkali halide crystals under definite conditions via the tunnel mechanism.

It was found in a previous work[42] that at room temperature not all the F centers, which were formed in a single crystal of alkali halide compound as a result of the action of the electron pulse, are stable. There was a partial decay during the times which were on the order of milliseconds. As was obtained later[40] practically all the F centers decay at high temperatures. The decay kinetics obey a complex law. Therefore it is necessary to mention the following main peculiarities of this process. First, the kinetic curve has at least two pronounced parts: fast decay ($\tau_{1/2}$ is ca. 3–6 μsec, its time depends on temperature slightly) and slower decay (its rate constant is determined by temperature). Second, the concentration contribution of the first part depends considerably on temperature and dose per pulse. This contribution is changed from 0 to 50%. Here the decay of the main fraction of F centers is considered which corresponds to the second kinetic part.

In Figure 3 the time dependences of the normalized optical density of a KCl single crystal are shown in the maximum F-center optical absorption band at 500, 550, and 600°C. The linear dependence of log (D/D_0) on time t testifies to the occurrence of the process via the first-order law: $[F] = [F]_0 e^{-kt}$. The dependences of k values on temperature (plots of log k vs. $1/T$) for single crystals of different alkali halide compounds are shown in Figure 4. As is seen in the case of each single crystal the rate of the F-center decay is constant when the temperature is lower than a certain limit value (its designation is T_{lim}). In Table VIII values of activation energies E, T_{lim}, and rate constants k_{lim} not depending on the temperature are listed.

To determine whether the registering light influences the process under consideration or not, the action of light of different intensity on the decay kinetics was studied. Verification was made in the case of KBr single crystals at 100, 150, and 200°C. It was found that the kinetic curves measured at full light intensity and light intensities reduced by a factor of 10 are the same.

Hence the spontaneous decay of F centers with a rate which did not depend on temperature has been observed. It is possible to assume that this process is due to tunneling by the F-center electrons. It is necessary to note that the primary hole centers at room and higher temperatures are mobile. Their decay is a fast process; there is no connection of this decay with the decay of F-centers. It is possible to suggest that during this fast process the hole centers are

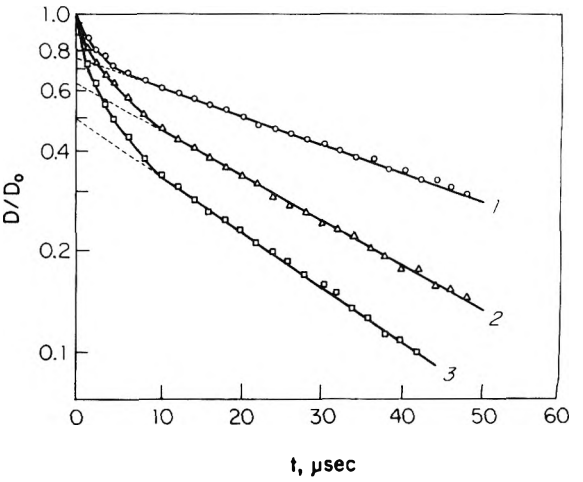

Figure 3. Dependence of normalized optical density of a KCl single crystal in the maximum of the F-center optical absorption band on time t after the electron pulse at 500 (1), 550 (2), and 600°C (3).

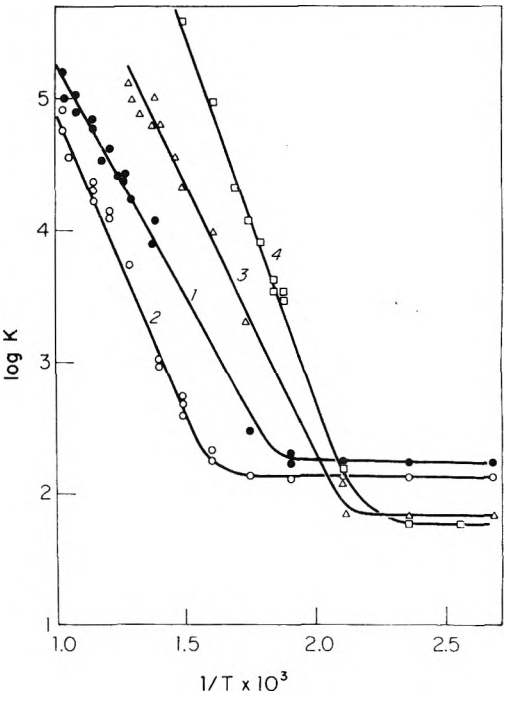

Figure 4. Dependence of the rate constants of the F-center decay in single crystals of alkali halide compounds on temperature (Arrhenius plot): (1) KCl; (2) NaCl; (3) KBr; (4) CsI.

transformed into more stable centers (perhaps into aggregated centers) localized on dislocations of the crystal lattice. Obviously at $T \leq T_{lim}$ the mobility of F centers is negligible and the rate of their decay is determined by tunneling of the electrons of F centers to the dislocations. According to the conclusions of previous work[33] the k_{lim} value of $\sim 10^2$ sec^{-1} corresponds to the mean distance of tunneling which is equal to approximately 20–25 Å (from unexcited state). Apparently the number of F centers decaying via this mechanism depends on the concentration and mobility of the dislocations in the sample at a given temperature.

Consequently in the case of single crystals of alkali halide compounds, which are comparatively "rigid" systems, tunneling of the electrons can take place even at comparatively high temperatures. However, it is necessary to stress that k_{lim} does not describe the entire process because it has

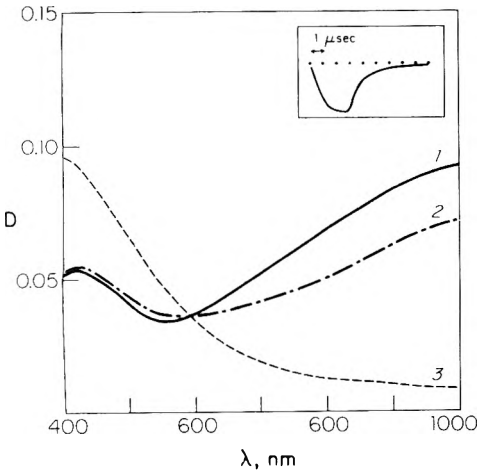

Figure 5. Optical absorption spectra of a pure melt of KBr (1) and melts of KBr, containing 10^{-2} *M* Ca^{2+} (2) or Cd^{2+} (3) measured immediately after the electron pulse. The insert shows the optical absorption of a pure melt of KBr during the electron pulse (duration 2.3 μsec), monitored at 900 nm.

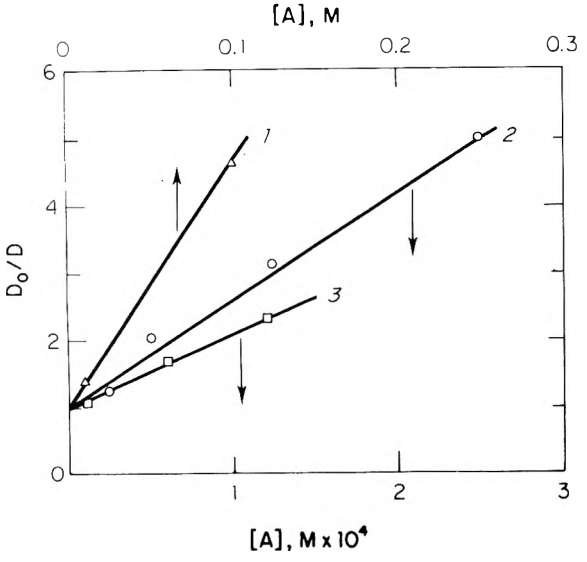

Figure 6. Dependence of D_0/D for KBr melt on the acceptor concentration: (1) Ca^{2+}; (2) Cd^{2+}; (3) Zn^{2+}.

been determined from a small part of a plot of ln [F] vs. time.

Reactivity of Solvated Electrons in Melted Alkali Halide Compounds. As it follows from previous works[34,35] short-lived solvated electrons are formed in melted alkali halide compounds as a result of irradiation. According to previous work[35] e_s^- in melted alkali halide compounds is an electron which is localized in a potential well formed by a displacement of positive charges of alkali metal cations. Apparently e_s^- is an electron surrounded by alkali metal cations and it can be considered as a peculiar F center of near order.

The reactivity of e_s^- was studied in the case of the melts of KBr (temperature 800°C) and NaCl (temperature 850°C). In these systems the decay of e_s^- even in the absence of an acceptor occurs very fast (during 1–2 μsec). Therefore it is impossible to study directly the influence of the acceptor concentration on the kinetics of the e_s^- decay by means of the apparatus used. The evaluation of the e_s^- reactivity was performed on the basis of the dependence of

TABLE IX: Values of Relative Rate Constants k_A/k for Melted Alkali Halide Compounds

	k_A/k, M^{-1}					
Melt	Ba^{2+}	Sr^{2+}	Ca^{2+}	Cd^{2+}	Zn^{2+}	Ag^+
KBr (800° C)	7	16	37	2.2×10^4	1.1×10^4	1.4×10^3
NaCl (850° C)			7.6	5.2×10^3	1.3×10^3	5.4×10^2

the limiting concentration of the solvated electron during the pulse time on acceptor concentration. An example of the optical absorption spectra of the pure melt of KBr and the melt of KBr with addition of Cd^{2+} or Ca^{2+} recorded at the end of the pulse is shown in Figure 5. It is seen that at the concentration of Cd^{2+} which is equal to 10^{-2} *M* the formation of e_s^- is practically completely suppressed; however, at the same concentration of Ca^{2+} there is only a 50% suppression. Quantitatively, although approximately, the reactivity of e_s^- was evaluated on the basis of the following considerations. The concentration of e_s^- at the end of the pulse is close to the steady-state concentration even in the absence of the acceptor (see an insert in Figure 5). Then

$$d[e_s^-]/dt = GI - V([e_s^-]) - k_A[e_s^-][A] = 0 \quad (10)$$

where G is the yield of e_s^-, I is the dose rate, $V([e_s^-])$ is the rate of reaction between e_s^- and the matrix, k_A is the rate constant of the reaction between e_s^- and the acceptor, and $[e_s^-]$ and [A] are the concentrations of e_s^- and the acceptor.

If we take

$$V([e_s^-]) = k[e_s^-] \quad (11)$$

where k is the rate constant of the pseudomonomolecular reaction of e_s^- decay, then

$$\frac{[e_s^-]_s^0}{[e_s^-]_s} = 1 + \frac{k_A[A]}{k} \quad (12)$$

In eq 12 $[e_s^-]_s^0$ is the concentration of e_s^- in the absence of acceptor at the end of the pulse, $[e_s^-]_s$ is the same at a given concentration of acceptor. After the transition to optical densities in the absence of acceptor (D_0) and in the presence of acceptor (D) we have

$$\frac{D_0}{D} = 1 + \frac{k_A[A]}{k} \quad (13)$$

The decay of e_s^- in the pure matrix via the pseudomonomolecular process (eq 11) may be explained by the occurrence of the reaction (Me^+ is the cation of the alkaline metal):

$$e_s^- + Me^+ \rightarrow Me \quad (14)$$

or by transition into unbounded state, i.e., by transition into the conductivity zone.

Some of the observed dependences of D_0/D on [A] are shown in Figure 6. These dependences are linear within sufficient accuracy. This confirms the foregoing consideration. The k_A/k values obtained are listed in Table IX.

The data obtained indicate that there are the following peculiarities of the e_s^- reactivity in melts of alkali halide compounds. First there is a satisfactory correlation between the electron affinity U of the cation and the rate constant of its reaction with e_s^- (see Figure 7). The values corresponding to the ionization potentials of Na and K and to the second ionization potentials of Ba, Sr, Ca, Cd, and Zn[68] have been taken as the U values. The rate constant k'

TABLE X: Rate Constants of Reactions of e_s^- with Cations in Melted Alkaline Halide Compounds

	k, M^{-1} sec^{-1}							
Melt	Na^+	K^+	Ba^{2+}	Sr^{2+}	Ca^{2+}	Cd^{2+}	Zn^{2+}	Ag^+
KBr (800°C)		$\sim 8 \times 10^4$	1×10^7	2.2×10^7	5.2×10^7	3×10^{10}	1.5×10^{10}	2.1×10^9
NaCl (850°C)	$\sim 5 \times 10^4$				1×10^7	7×10^9	1.7×10^9	7×10^8

of the second-order reaction of e_s^- with the matrix (i.e., the ratio of $k/[K^+]$ for KBr and $k/[Na^+]$ for NaCl) has been taken as unity. As is seen the points for K^+ and Na^+ are not deviated from these dependences. This confirms the above-mentioned assumption about the decay of e_s^- in a pure matrix via reaction 14. The values of k for melts of KBr and NaCl are equal respectively to $\sim 1.4 \times 10^6$ and $\sim 1.3 \times 10^6$ sec^{-1}. Then $k(e_s^- + K^+) \approx 8 \times 10^4$ and $k(e_s^- + Na^+) \approx 5 \times 10^4$ M^{-1} sec^{-1}. The absolute values of k_A (see Table X) were determined on the basis of these considerations and from the experimental values of k_A/k. The rate constants of the e_s^- reaction with Ag^+ in both melts deviated from the dependences shown in Figure 7. Apparently it is due to the peculiarities of the mechanism of this reaction.

Second the rate of the e_s^- reaction depends on the nature of the matrix. In a melt of KBr the solvated electron reacts faster than in a melt of NaCl. It is interesting to note that in the second melt the electron is localized in a deeper trap ($E_{\lambda_{max}}$ for e_s^- in a melt of NaCl is larger than for e_s^- in a melt of KBr[35]). It is not excluded that the dependence under discussion is caused by a tunnel mechanism of the reactions of e_s^-.

Third in melts of alkali halide compounds the solvated electrons are characterized by the comparatively high reactivity toward the cations of alkaline earth elements. The ratio of the rate constants of the reactions of e_s^- with Cd^{2+} and Ca^{2+} is equal to ~ 600 for a KBr melt and ~ 700 for a NaCl melt. In water these constants are greater by more than 5 orders of the magnitude.[2] The higher reactivity of e_s^- in the melts investigated toward the cations under consideration is connected with the considerably smaller "solvation" of the cations in comparison with aqueous solutions.

One of the peculiarities of the melts is that they are at very high temperatures. However, rate constants for the reactions of e_s^- with such an effective acceptor as the Cd^{2+} ion in both melts are slightly less than the rate constant of this reaction in water at room temperature. This effect may be explained by two reasons. First the lower reactivity of e_s^- toward acceptor cations in the melt may be caused by the screening of the electron by the ions of alkali metal. Second it is possible to suggest that at such high temperatures reactions of e_s^- are reversible. In this case the deviation of $k(e_s^- + Ag^+)$ from the foregoing correlation between the rate constants and the electron affinity of the acceptor molecule may be due to the considerable higher stability of the Ag atom in comparison with the products of other reactions investigated.

4. Conclusion

From the considered experimental data on the reactivity of the electrons in different irradiated systems it is possible to make the following general conclusions. First many peculiarities of the behavior of trapped electrons in glassy systems are satisfactorily explained by electron transfer via the tunnel mechanism. Apparently this mechanism plays also an important role in the process of F-center decay in alkali halide crystals. Second data obtained do not contradict the hypothesis of the tunnel mechanism of the reactions of solvated electrons in liquids including such specific ionic liquids as the melts of alkali halide compounds. This mechanism explains the exceeding of the cross section of the reactions of e_{aq}^- with the ions of Np(VII) and Pu(VII), which are strong oxidants, over the sum of the radii of reacting species, the decrease of the rate in the case of the reaction with Np(V) ion in which the ion with the different structure in comparison with the initial ion is formed, the dependence of the reaction rate on the nature of alkali halide compound in the case of the melts, etc. Third in some cases (for example in the case of reaction between e_s^- and NO_3^-) considerable variation of the reaction rate takes place during the transition from one liquid to another. It may be due to the different solvation energy of the reaction product.

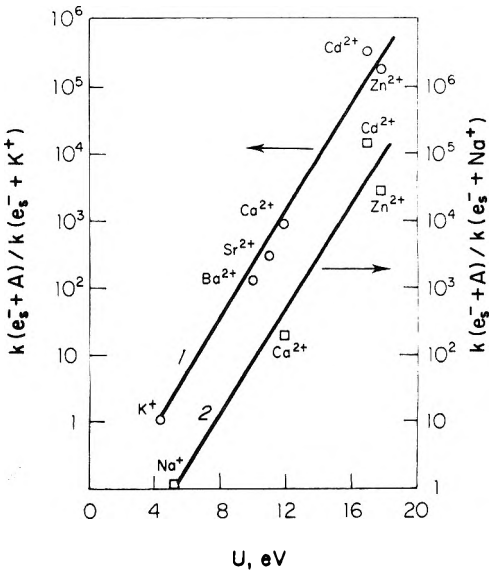

Figure 7. Dependence of $k(e_s^- + A)/k(e_s^- + Me^+)$ (Me^+ is Na^+ in NaCl melt and K^+ in KBr melt) on the electron affinity U of the acceptor A: (1) KBr melt (800°C); (2) NaCl melt (850°C). The constant $k(e_s^- + Me^+)$ has been taken as unity.

References and Notes

(1) A. K. Pikaev, "Sol'vatirovannyi electron v radiatsionnoi khimii", Izd-vo Nauka, Moscow, 1969.
(2) E. J. Hart and M. Anbar, "The Hydrated Electron", Wiley-Interscience, New York, N.Y., 1970.
(3) A. K. Pikaev, G. K. Sibirskaya, and S. A. Kabakchi, *Dokl. Akad. Nauk SSSR*, **198**, 1374 (1971).
(4) I. Janovsky, *Proc. Tihany Symp. Radiat. Chem., 3rd*, 1119 (1973).
(5) F. Barat, L. Gilles, B. Hickel, and B. Lesigne, *J. Phys. Chem.*, **77**, 1711 (1973).
(6) P. Fowles, *Trans. Faraday Soc.*, **67**, 428 (1971).
(7) J. H. Baxendale, *Int. J. Radiat. Phys. Chem.*, **4**, 113 (1972).
(8) T. Kajiwara and J. K. Thomas, *J. Phys. Chem.*, **76**, 1700 (1972).
(9) I. A. Taub, M. C. Sauer, and L. M. Dorfman, *Discuss. Faraday Soc.*, **36**, 206 (1963).
(10) I. A. Taub, D. A. Harter, M. C. Sauer, and L. M. Dorfman, *J. Chem. Phys.*, **41**, 979 (1964).
(11) S. Aral and L. M. Dorfman, *J. Chem. Phys.*, **41**, 2190 (1964).

(12) F. S. Dainton, J. P. Keene, T. J. Kemp, G. A. Salmon, and J. Teply, *Proc. Chem. Soc.*, 265 (1964).
(13) G. I. Khaikin, V. A. Zhigunov, and P. I. Dolin, *Khim. Vys. Energ.*, **5**, 54 (1971).
(14) G. I. Khaikin, V. A. Zhigunov, and P. I. Dolin, *Khim. Vys. Energ.*, **5**, 84 (1971).
(15) J. W. Fletcher, W. A. Seddon, J. Jevcak, and F. C. Sopchyshyn, *Chem. Phys. Lett.*, **18**, 592 (1973).
(16) J. W. Fletcher, W. A. Seddon, and F. C. Sopchyshyn, *Can. J. Chem.*, **51**, 2975 (1973).
(17) E. I. Mal'tsev and A. V. Vannikov, *Radiat. Effects*, **20**, 137 (1973).
(18) E. I. Mal'tsev and A. V. Vannikov, *Khim. Vys. Energ.*, **8**, 328 (1974).
(19) F. Y. You and L. M. Dorfman, *J. Chem. Phys.*, **58**, 4715 (1973).
(20) B. Bockrath and L. M. Dorfman, *J. Phys. Chem.*, **77**, 1002 (1973).
(21) B. Bockrath and L. M. Dorfman, *J. Am. Chem. Soc.*, **96**, 5708 (1974).
(22) G. A. Salmon, W. A. Seddon, and J. W. Fletcher, *Can. J. Chem.*, **52**, 3259 (1974).
(23) R. A. Vermeer and G. R. Freeman, *Can. J. Chem.*, **52**, 1181 (1974).
(24) A. M. Koulkes-Pujo, L. Gilles, and J. Sutton, *J. Chem. Soc., Chem. Commun.*, 912 (1974).
(25) B. G. Ershov and E. L. Tseitlin, *Khim. Vys. Energ.*, **4**, 186 (1970).
(26) B. G. Ershov and E. L. Girina, *Izv. Akad. Nauk. SSSR, Ser. Khim.*, 278 (1972).
(27) J. R. Miller, *J. Chem. Phys.*, **56**, 5173 (1972).
(28) K. I. Zamaraev and R. F. Khairutdinov, *Chem. Phys.*, **4**, 181 (1974).
(29) J. Kroh and C. Stradowski, *Int. J. Radiat. Phys. Chem.*, **7**, 23 (1975).
(30) A. Henglein, *Ber. Bunsenges. Phys. Chem.*, **78**, 1078 (1974).
(31) A. V. Rudnev, A. V. Vannikov, and N. A. Bach, *Khim. Vys. Energ.*, **6**, 473 (1972).
(32) A. V. Vannikov, *Usp. Khim.* **44**, 1931 (1975).
(33) D. L. Dexter, *Phys. Rev.*, **93**, 985 (1954).
(34) S. J. Black and D. M. J. Compton, *J. Phys. Chem.*, **69**, 4421 (1965).
(35) I. E. Makarov, T. N. Zhukova, and A. K. Pikaev, *Radiat. Effects*, **22**, 71 (1974).
(36) A. K. Pikaev, M. P. Mefod'eva, N. N. Krot, and V. I. Spitsyn, *Khim. Vys. Energ.*, **7**, 505 (1973).
(37) E. L. Girina, B. G. Ershov, and A. K. Pikaev, *Khim. Vys. Energ.*, **8**, 334 (1974).
(38) A. K. Pikaev, M. P. Mefod'eva, N. N. Krot, and V. I. Spitsyn, *Izv. Akad. Nauk SSSR, Ser. Khim.*, 2847 (1974).
(39) I. E. Makarov, T. N. Zhukova, and A. K. Pikaev, *Dolk. Akad. Nauk SSSR*, in press.
(40) I. E. Makarov, T. N. Zhukova, and A. K. Pikaev, *Izv. Akad. Nauk SSSR, Ser. Khim.*, in press.
(41) A. K. Pikaev, G. K. Sibirskaya, E. M. Shirshov, P. Ya. Glazunov, and V. I. Spitsyn, *Dokl. Akad. Nauk SSSR*, **200**, 383 (1971).
(42) I. E. Makarov, T. N. Zhukova, and A. K. Pikaev, *Khim. Vys. Energ.*, **8**, 74 (1974).
(43) M. Anbar and E. J. Hart, *J. Phys. Chem.*, **69**, 1244 (1965).
(44) A. K. Pikaev, T. P. Zhestkova, and G. K. Sibirskaya, *J. Phys. Chem.*, **76**, 3765 (1972).
(45) J. H. Burns, W. H. Baldwin, and J. R. Stokely, *Inorg. Chem.*, **12**, 466 (1973).
(46) K. H. Schmidt and S. M. Ander, *J. Phys. Chem.*, **73**, 2846 (1969).
(47) M. Anbar and E. J. Hart, *Adv. Chem. Ser.*, **No. 81**, 79 (1969).
(48) V. F. Peretrukhin, N. N. Krot, and A. D. Gel'man, *Radiokhimiya*, **14**, 72 (1972).
(49) G. T. Seaborg and J. J. Katz, "The Chemistry of the Actinide Elements", Wiley, New York N.Y., 1957.
(50) A. D. Gel'man, M. P. Mefod'eva, A. I. Moskvin, and L. M. Zaitsev, "Kompleksnye soedineniya transuranovykh elementov", Izd-vo Akademic Nauk SSSR, Moscow, 1961.
(51) G. T. Seaborg and J. J. Katz, Ed., "The Actinide Elements", New York, N.Y., 1954.
(52) "Kompleksnye soedineniya urana", pod red. I. I. Chernyaeva, Izd-vo Nauka, Moscow, 1964.
(53) G. Scatchard, *Chem. Rev.*, **10**, 229 (1932).
(54) G. V. Buxton, F. S. Dainton, and A. Hammerli, *Trans. Faraday Soc.*, **63**, 1191 (1967).
(55) M. S. Mahteson and L. M. Dorfman, "Pulse Radiolysis", The M.I.T. Press, Cambridge, Mass., 1969, p 107.
(56) L. T. Bugaenko and O. S. Povolotskaya, *Dokl. Akad. Nauk SSSR*, **174**, 378 (1967).
(57) I. A. Batyuk, E. N. Borisova, L. T. Bugaenko, and V. M. Byakov, *Khim. Vys. Energ.*, **4**, 143 (1970).
(58) H. Hase and L. Kevan, *J. Phys. Chem.*, **74**, 3358 (1970).
(59) H. B. Steen, O. Kaalhus, and H. Kongshaug, *J. Phys. Chem.*, **75**, 1941 (1971).
(60) R. F. Khairutdinov, A. I. Mikhailov, and K. I. Zamaraev, *Dokl. Akad. Nauk SSSR*, **200**, 905 (1971).
(61) B. G. Ershov, E. L. Girina, and A. K. Pikaev, *Khim. Vys. Energ.*, in press.
(62) J. R. Miller, *Chem. Phys. Lett.*, **22**, 180 (1973).
(63) K. I. Zamaraev, R. F. Khairutdinov, A. I. Mikhailov, and V. I. Gol'dansky, *Dokl. Akad. Nauk SSSR*, **199**, 640 (1971).
(64) J. Kroh and C. Stradowski, *Radiochem. Radioanal. Lett.*, **9**, 169 (1972).
(65) J. Kroh and C. Stradowski, *Int. J. Radiat. Phys. Chem.*, **5**, 1239 (1973).
(66) E. L. Girina, B. G. Ershov, and A. K. Pikaev, *Khim. Vys. Energ.*, **8**, 470 (1974).
(67) B. G. Ershov and F. Kiffer, *Nature (London)*, **252**, 118 (1974).
(68) "Energii razryva khimicheskikh svyazei. Potentsialy ionizatsii i srodstvo k electronu", Izd-vo Nauka, Moscow, 1974.

Discussion

A. M. KOULKES-PUJO. Is the reaction of NO_3^- with solvated electrons in ethylene glycol related only to viscosity? In the case of H_2O–DMSO mixtures, it seems that this parameter is not the only one to be taken into account even if the effect of dielectric constant is added to it.

A. K. PIKAEV. Rate constants of diffusion-limited reactions of e_s^- in some solvents are approximately proportional to $\eta^{-1/2}$ where η is viscosity (see T. Kajiwara and J. K. Thomas, *J. Phys. Chem.*, **76**, 1200 (1972), and B. Cercek, *Int. J. Radiat. Phys. Chem.*, issue dedicated to R. L. Platzman). In alcohols $k(e_s^- + NO_3^-)$'s are less than k_{diff}. I explained this phenomenon by peculiarities of the reaction itself.

U. SCHINDEWOLF. What are the products of the reaction of e^- with cations like K^+, Na^+, in salt melts? Are neutral melt atoms formed? With this respect I would like to mention: in our experiments of injection of electrons by electrolysis into salt melts we observed slight changes of the absorption spectra with time, indicating that some other light absorbing species are formed from electrons + cations in a consecutive reaction, e.g., neutral atoms as you also might have.

A. K. PIKAEV. We propose that they are metal atoms K, Na, etc. However, we do not have yet any direct evidences for this proposition. This is open for further investigation.

J. JORTNER. You have stated that some rate constants of the solvated electron are slower than those expected on the basis of a diffusion-controlled reaction and interpreted this result in terms of configurational changes in the ion. Most of the rate constants are, however, close to the diffusion-limited rates. Large configurational changes occur as the solvated electron reacts and the solvent structure around it is drastically modified. I must admit that it is very surprising that these electron transfer rates are so fast. This can originate from the following possible factors: (1) large free energy changes in the process; (2) vibrational excitation; (3) electron transfer to electronically excited states. The conventional theory of electron transfer processes in solutions is inadequate to describe the reactivity of the solvated electron.

A. K. PIKAEV. I talked about large *structural* changes in reactions which have comparatively low rate constants. For example, $k[e_{aq}^- + Np(V)] < k[e_{aq}^- + Np(VI)]$. In the reaction $e_{aq}^- + Np(V)$ the transition from NpO_2^+ to Np^{4+} occurs. However, in the reaction $e_{aq}^- + Np(VI)$ the ion NpO_2^{2+} is transformed into NpO_2^+. From such general considerations it is obvious that $k[e_{aq}^- + Np(VI)]$ must be higher than $k[e_{aq}^- + Np(V)]$.

Effect of the Charge of an Electron Scavenger on the Rate of Electron Tunneling in Glasses and Liquids

M. J. Pilling* and Stephen A. Rice

Physical Chemistry Laboratory, South Parks Road, Oxford, OX1 3QZ, England *(Received July 23, 1975)*

A theoretical model for electron reactions with ions and molecules (scavengers) in liquids and glasses has been developed. To represent quantum mechanical tunneling an exponential sink term was added to Fick's second law. The reaction path was analyzed in terms of encounter pair formation and direct electron tunneling to the scavenger. Analytic expressions for the rate of these processes were obtained by using Gauss's theorem. Electron reactions in glasses are not at steady state and are strongly influenced by the electron trap depth. In liquids, electron reactions rapidly reach the steady state and the rate of reaction is enhanced compared to the predictions of the Smoluchowski theory. The effect of scavenger's charge on the rate of reaction in glasses was considered. As the dominant reaction path between electrons and scavengers is tunneling even in mobile liquids, the Debye correction to the Smoluchowski theory is too large.

Introduction

Recently there has been considerable experimental evidence supporting the concept of electron tunneling to a scavenger molecule in both liquids and glasses.[1-11] Time-resolved electron decays,[1-5] isothermal luminescence decays,[6-9] and electron yields in γ irradiated[10,11] aqueous and organic glasses support the exponential dependence on distance of the electron transfer probability through a potential barrier.

The Gamow equation[12-14] and Fermi's golden rule[15] predict that the rate of electron tunneling through a potential barrier is of the form

$$l_s(r) = \alpha\chi(r) \exp(-\beta(r - R)) \tag{1}$$

where α is a frequency factor $\sim 10^{14}$ sec^{-1}, $\chi(r)$ is a polynomial in the distance of separation between the electron and the scavenger r, R is the crystallographic encounter distance and

$$\beta \simeq \frac{2}{\hbar}(2m^*(\langle V_0\rangle - E))^{1/2} \tag{2}$$

Here m^* is the electron's effective mass and $\langle V_0\rangle - E$ is the appropriately averaged barrier height, which is approximately equal to the electron trap depth.[14]

In liquids, direct tunneling to a scavenger provides an alternative reaction path to the diffusive formation of encounter pairs and their subsequent reaction. This situation can be described by adding a first-order sink term to Fick's second law of diffusion[16]

$$\frac{\partial S}{\partial t} = \frac{D}{r}\frac{\partial^2 Sr}{\partial r^2} - l_s(r)S(r, t) \tag{3}$$

where D is the coefficient of relative diffusion, and $S(r, t)$ is the ensemble averaged concentration of scavenger molecules around electrons. Gauss's theorem equates the volume integral of the divergence of the flux per unit area to the flux leaving that volume. Now the volume integral of the sink term in eq 3 is the total tunneling flux. The rate of reaction is the sum of the rate of formation of encounter pairs and the total tunneling flux.[16] Following Smoluckowski,[17] the rate constant for the diffusive formation of encounter pairs is

$$k_D(t) = \frac{4\pi R^2 D}{S_0}\frac{\partial S}{\partial r}\bigg|_R \tag{4}$$

and the total tunneling rate constant is[16]

$$k_T(t) = \int_R^\infty \frac{4\pi r^2 l_s(r)S(r, t)}{S_0}\,dr \tag{5}$$

where S_0 is the bulk scavenger concentration. In the steady state, the total rate constant is the sum of the infinite time limit of eq 4 and 5[16]

$$k(\infty) = \lim_{t\to\infty}\left(\lim_{r\to\infty}\frac{4\pi r^2 D}{S_0}\frac{\partial S(r, t)}{\partial r}\right) \tag{6}$$

It is the purpose of this paper to consider how the charge of a scavenger modifies the rate of reaction with electrons in liquids and glasses. Both the rate of diffusion and tunneling are altered, but to different degrees. The density of states and the symmetry of the acceptor orbital of the scavenger (orbital overlap) also affect the rate of tunneling and the effect of these is briefly considered.

Direct Electron Tunneling in Glasses

A. Uncharged Scavengers. The diffusion coefficient of glasses is so small that cooperative diffusion of reactants cannot be an important reaction path. Hence electrons may be expected to react only by tunneling.[14] Thus, the solution of eq (3) is

$$S(r, t) = S(r, 0) \exp(-l_s(r)t) \tag{7}$$

where $S(r, 0)$ is the initial ensemble averaged scavenger concentration around electrons.

Dainton et al.[14] equated $\chi(r)$ to $\sigma^2/4r^2$; that is, the solid angle subtended by a scavenger of electron capture cross sectional area $\pi\sigma^2$ at an electron distant r from the scavenger. Equation 7 was substituted into eq 5 and the integral evaluated numerically. Figure 1 shows the time dependence of the rate constant for $\alpha = 10^{15}$ sec^{-1}, $\sigma = 0.5$ nm, $R = 0.6$ nm, with $\beta = 7.0$, 9.9, and 14.0 nm^{-1}. For times greater than $t_1 = 4r_c^2 \ln 2/\alpha\sigma^2 \exp(\beta R)$, where r_c is an unspecified length $\sim R$, the total tunneling rate constant (5) is approximately

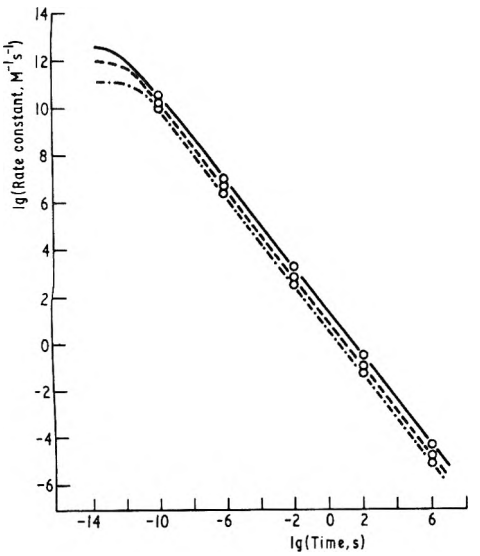

Figure 1. The numerically evaluated rate constant, $k_T(t)$, for $R = 0.6$ nm, $\sigma = 0.5$ nm, $\alpha = 10^{15}$ sec^{-1}, and $\beta = 7.0$ nm^{-1}, trap depth 0.5 eV (——); 9.9 nm^{-1}, 1.0 eV (- - - -); and 14.0 nm^{-1}, 2.0 eV (- · - · - · - · -). The analytic expression (eq 8) is also shown using the same parameters as above (O).

$$k_T(t) = \frac{4\pi}{\beta^3 t}\left(\ln\frac{t}{t_1}\right)^2 \tag{8}$$

This is the rate constant for the psuedo-first-order reaction between scavengers and electrons, of bulk concentration $C(t)$. If the electron concentration is C_0 at a time t_0, which is greater than t_1, then[14]

$$\ln\frac{C(t)}{C_0} = -\frac{4\pi S_0}{3\beta^3}\left[\left(\ln\frac{t}{t_1}\right)^3 - \left(\ln\frac{t_0}{t_1}\right)^3\right] \tag{9}$$

A similar expression has been derived by Miller[10] and by Tachiya and Mozumder.[18]

B. Charged Scavengers. The Coulombic field of the scavenger of charge Ze, where e is the electronic charge, alters the potential barrier shape and height through which the electron tunnels. The relative permittivity of the glass is ϵ_s which is approximately n^2, with n the refractive index (as molecular orientations are frozen-in). If the electron and scavenger have square well potentials out to distances equal to their respective radii, r_e and r_s, then the potential which the electron experiences is shown in Figure 2. For simplicity the long-range polarization field and the effect of molecular reorientation around the scavenger have been ignored. A distance y from the scavenger the potential is

$$V(y) = V_0 - E - \frac{Ze^2}{4\pi\epsilon_0\epsilon_s}\left(\frac{1}{r - r_e} - \frac{1}{y}\right)$$

where ϵ_0 is the permittivity of free space. From the Gamow equation the electron tunneling rate constant is

$$l_s(r) = \frac{\alpha\sigma^2}{4r^2}\exp\left\{-\beta\int_{y_1}^{r-r_e}\left(1 - \frac{b}{r - r_e} + \frac{b}{y}\right)^{1/2} dy\right\} \tag{10}$$

where $b = Ze^2/4\pi\epsilon_0\epsilon_s(V_0 - E)$. y_1 is the barrier limit nearer to the scavenger, being r_s for negative and neutral scavengers, but may be greater than r_s for positive scavengers (as shown in Figure 2) from the inequality

$$1 - \frac{b}{r - r_e} + \frac{b}{y} \geq 0$$

From eq 10 the total tunneling rate constant of eq 5 was

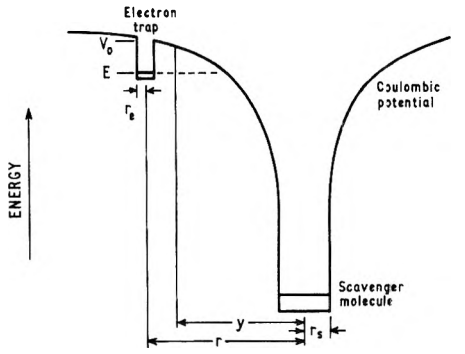

Figure 2. The potential energy diagram for an electron in the presence of a positively charged scavenger.

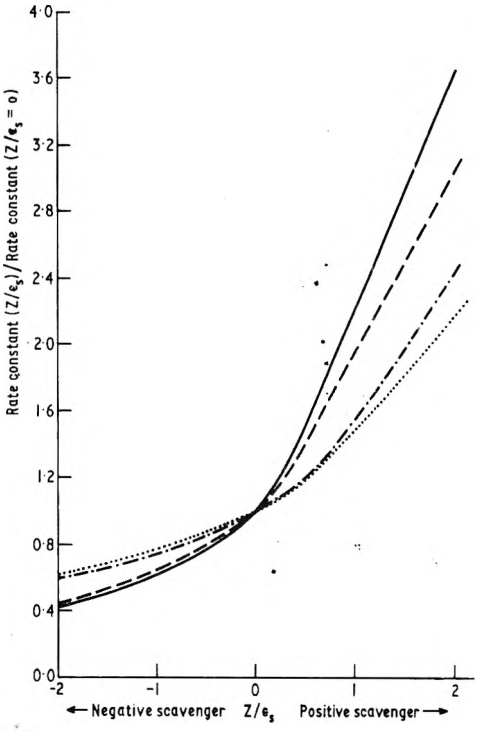

Figure 3. Relative effect of (scavenger charge/relative permittivity) on the rate constant for electron tunneling in glasses with traps of depth 1 eV, $\beta = 9.9$ nm^{-1}: (——) 10^{-3} sec, (- - - -) 10^3 sec; and 2 eV, $\beta = 14.0$ nm^{-1}: (- · - · - · -) 10^{-3} sec, (· · · · ·) 10^3 sec.

computed. With the same parameters as used for Figure 1 the ratio of the total tunneling rate constant for a charged vs. uncharged scavenger was found as a function of Z/ϵ_s, and is shown in Figure 3. The rate constant is enhanced by positive scavengers but reduced by negative scavengers. As expected the effect of charge is also more noticeable with less deeply trapped electrons. Figure 3 compares the rate constant for electron tunneling from traps of depth 1 and 2 eV. Except at times less than 1 μsec the ratio of the rate constant for charged vs. uncharged scavengers is essentially independent of time. Thus the same theory of tunneling may be used for uncharged and for charged scavengers but with the value of β replaced by an effective value.

The ratio $|Z/\epsilon_s|$ is unlikely to be greater than unity, and may be significantly less than this because of the omission of the polarization potential and the effect of solvent reorientation around the scavenger. Even for a trap depth of 1 eV, the effect of charge is small; decreasing the rate constant by 50% for negative scavengers and increasing it by 100% for positive scavengers. It should be emphasized that

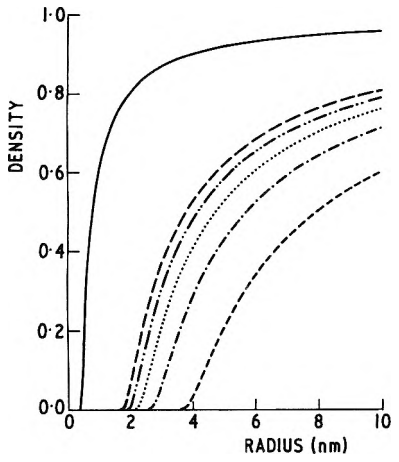

Figure 4. Steady-state density profile for electron tunneling and diffusion, with $\alpha = 10^{14}$ sec^{-1}, $D = 10^{-16}$ m^2 sec^{-1}, and $\beta = 7.0$ nm^{-1}, trap depth 0.5 eV (- - - -); 9.9 nm^{-1}, 1.0 eV (- · · · · · · · · -); 12.1 nm^{-1}, 1.5 eV (· · · · ·); 14.0 nm^{-1}, 2.0 eV (– · · – · · –); and 15.7 nm^{-1}, 2.5 eV (– –). The Smoluchowski limit ($1 - R/r$) is also included (——).

the observed rate of electron tunneling is proportional to the ensemble averaged rate constant (5) and not to the rate constant (1). The ensemble averaged rate constant depends on β^{-3} whereas the barrier permeability depends on an exponential of β. Thus the observed rate of tunneling is very much less affected by scavenger change than is the barrier permeability.

Keiffer et al.[19] chose a similar model for electrons tunneling toward scavengers but only evaluated the rate constant $l_s(r)$.

Miller[2] and Marshall et al.[11] have found that the efficiency of the electron scavengers CrO_4^{2-}, NO_3^-, acrylamide, and Tl^+ in aqueous hydroxide glasses at 77 K decreases from chromate to thallous. This trend is more pronounced and in the opposite sense to that predicted by the above model for charged scavengers. The charge of the scavenger is not the most important factor controlling the rate of electron tunneling to different scavengers.

C. The Density of States and Acceptor Orbital Symmetry. From eq 9, the rate of electron decay is strongly dependent on β and thus on the electron trap depth. However, the term t_1 affects the electron decay rate very much less strongly than β. If the density of states of scavengers are different, the frequency factor will depend on the nature of the electron trap and the scavenger molecule.[15] This in turn will make t_1 dependent on the scavenger used. Equation 9 indicates that a variation of t_1 will only alter the relative time scales of the scavenging process when different scavengers are used, as Miller noted.[2] On accepting an electron the molecular geometry of the scavenger may change, so that the Franck–Condon factor[15] should also be considered; it will be different for each scavenger and will depend on the nature of the glass. Like the density of states, this only modifies t_1, and so does not explain the observed differences in scavenger efficiency.

Marshall et al.[11] suggested that the decrease in scavenging efficiency of CrO_4^{2-} through NO_3^- to acrylamide (β respectively 10, 16, and 19 nm^{-1}) approximately correlates with the symmetry or "freedom of access to" the acceptor orbital of the scavenger molecule. The nitrate ion is planar and has a partial positive charge on the nitrogen.[20] Presumably the electron will enter the 2p like orbital centered on the nitrogen. This orbital overlap factor affects α and hence t_1, but not β. However, if the acceptor orbital of the scavenger is discontinuous, with the orbital overlap factor zero outside a cone of semiangle θ_0, the rate constant of eq 8 must be multiplied by $2\theta_0/\pi$.[21] This effectively increases the value of β and would account for the different efficiencies of the electron scavengers CrO_4^{2-}, NO_3^-, and acrylamide.

Electron Reactions in Liquids

Equation 3 can be solved in the steady state if the polynomial $\chi(r)$ is equated to unity.[16] With $\alpha = 10^{14}$ sec^{-1}, $D = 10^{-16}$ m^2 sec^{-1}, and an encounter distance of 0.4 nm, the steady-state density profile is as shown in Figure 4.[16] The electron trap depths are 0.5, 1.0, 1.5, 2.0, and 2.5 eV ($\beta \simeq$ 7.0, 9.9, 12.1, 14.0, and 15.7 nm^{-1}). The Smoluchowski limit is also shown and arises as $\beta \to \infty$. Both the steady-state diffusive and total rate constants can be evaluated[16] from the eq 4 and 6

$$k_D(\infty) = 4\pi RD/I_0(w_0) \tag{11}$$

$$k(\infty) = 4\pi RD\left[1 + \frac{1}{\beta R}\left(2\gamma + \ln\frac{w_0^2}{4} + \frac{2K_0(w_0)}{I_0(w_0)}\right)\right] = 4\pi R_{\text{eff}}D \tag{12}$$

where $w_0^2 = 4\alpha/\beta^2 D$, γ is Euler's constant (0.57721 . . .) and $I_0(w_0)$ and $K_0(w_0)$ are the modified first and second kind Bessel's functions of zero order. The dimensionless parameter w_0 compares the rate of tunneling to the rate of diffusion.

Buxton et al.[4] found that the encounter distance in 10 M aqueous hydroxide in the region 190–260 K was 2.01 ± 0.54 nm for CrO_4^{2-} and 1.05 ± 0.37 nm for NO_3^-. They suggested that in these concentrated ionic solutions ionic association occurs to such an extent that the Debye[21] correction to the Smoluchowski theory is unnecessary. However, in aqueous hydroxide glasses at 77 K, the values of α and β are $\sim 10^{13}$ sec^{-1} and 10 nm^{-1} for CrO_4^{2-} and 16 nm^{-1} for NO_3^-.[10,11,14] The diffusion coefficient of 10 M aqueous hydroxide[4] at 215 K is $\sim 10^{-12}$ m^2 sec^{-1}. From eq 12 the effective encounter distance is ~2 nm for CrO_4^{2-} and ~1 nm for NO_3^-.

To apply the Debye correction[22] to eq 3 the Coulombic potential $U(r)$ should be incorporated

$$\frac{\partial S}{\partial t} = \frac{D}{r^2}\frac{\partial}{\partial r}r^2\left[\frac{\partial S}{\partial r} + \frac{S}{kT}\frac{\partial U(r)}{\partial r}\right] - l_s(r)S(r,t)$$

where k is Boltzmann's constant and T is the absolute temperature. Since this equation cannot be solved except by numerical techniques, the importance of scavenger charge will only be assessed qualitatively. As the electron and scavenger diffuse nearer to each other, the probability of electron tunneling increases. This depletes the scavenger concentration, particularly at short distances (Figure 4) where the Coulombic interaction is strongest. When tunneling is significant ($w_0 > 3$) the diffusive formation of encounter pairs (eq 11) is a very much less important reaction path than the tunneling process (eq 12). In liquids $|Z/\epsilon_s| < 0.1$, so that for an electron trap depth of 1 eV the tunneling rate constant is altered by no more than 10%. However, the Debye–Smoluchowski theory predicts that with an encounter distance of 0.4 nm the rate constant is altered by more than an order of magnitude. Thus the effect of the scavenger's charge is less than that predicted by the Debye–Smoluchowski theory.

Acknowledgment. One of us (S.A.R.) thanks the Salters' Company for a Scholarship.

References and Notes

(1) J. R. Miller and J. E. Willard, *J. Phys. Chem.*, **76**, 2641 (1972).
(2) J. R. Miller, *Chem. Phys. Lett.*, **22**, 180 (1973).
(3) J. Kroh and C. Stradowski, *Int. J. Radiat. Phys. Chem.*, **5**, 243 (1973).
(4) G. V. Buxton, F. C. R. Cattell, and F. S. Dainton, *J. Chem. Soc., Faraday Trans. 1*, **71**, 115 (1975).
(5) G. V. Buxton and K. G. Kemsley, *J. Chem. Soc., Faraday Trans. 1*, **71**, 568 (1975).
(6) F. Keiffer, C. Meyer, and J. Regnault, *Chem. Phys. Lett.*, **11**, 359 (1971).
(7) J. Moan, *Ber. Bunsenges. Phys. Chem.*, **75**, 668 (1971).
(8) B. G. Ershov and F. Keiffer, *Chem. Phys. Lett.*, **25**, 576 (1974).
(9) M. Aubailly, M. Bazin, and R. Santus, *Chem. Phys. Lett.*, **31**, 340 (1975).
(10) J. R. Miller, *J. Chem. Phys.*, **56**, 5173 (1972).
(11) E. J. Marshall, M. J. Pilling, and S. A. Rice, *J. Chem. Soc., Faraday Trans. 2*, **71**, 1555 (1975).
(12) G. Gamow, *Z. Phys.*, **51**, 204 (1928).
(13) D. I. Blokhintsev, "Quantum Mechanics", D. Reidel Publishing Co., Dordrecht, Holland, 1964, p 337.
(14) F. S. Dainton, M. J. Pilling, and S. A. Rice, *J. Chem. Soc. Faraday Trans. 2*, **71**, 1311 (1975).
(15) B. Brocklehurst, *Chem. Phys.*, **2**, 6 (1972).
(16) M. J. Pilling and S. A. Rice, *J. Chem. Soc., Faraday Trans. 2*, **71**, 1563 (1975).
(17) M. van Smoluchowski, *Z. Phys. Chem.*, **92**, 129 (1917).
(18) M. Tachiya and A. Mozumder, *Chem. Phys. Lett.*, **28**, 87 (1974).
(19) F. Keiffer, C. Lapersonne-Meyer, and J. Regnault, *Int. J. Radiat. Phys. Chem.*, **6**, 79 (1974).
(20) J. F. Wyatt, I. H. Hillier, V. R. Saunders, J. A. Connor, and M. Barber, *J. Chem. Phys.*, **54**, 5311 (1971).
(21) S. A. Rice, D.Phil. Thesis, Oxford University, 1975.

Discussion

J. JORTNER. During an American Chemical Society meeting at San Francisco in 1949 physical chemists were trying to understand thermal electron transfer (ET) processes between simple ions in solutions. J. Franck, quoting Libby, pointed out that electron tunneling at fixed nuclear configuration cannot be implied in this context. Such an approach violates the Franck–Condon principle and implies, in fact, that the nuclei follow the motion of the electron. The Franck–Condon principle has to be applied to ET processes as well as to optical excitation processes. Indeed, thermal ET can be considered as an optical process in the limit of zero photon energy. The electron tunneling concept was recently revived by biochemists in an attempt to rationalize ET in biological systems. I believe that this approach is wrong, violating the Franck–Condon principle. The reactivity of the solvated electron as well as the quasifree electron in solutions and glasses has to be accounted for in terms of a theory which incorporates explicitly nuclear configurational changes.

J. W. HUNT. In your tunneling model, I am interested in the history of the electron yields, and how your analysis of J. R. Miller's data is extrapolated back to ~100 psec. I believe that certain scavengers reduce the yield of electrons at this time. This could be explained by formation of the encounter pair as suggested by Czapski, or a fast initial rate of e^- decay. I wonder if you can discuss your present thoughts on this process.

S. A. RICE. If the electron can be trapped about an encounter radius away from the scavenger molecule then Czapski and Peled's treatment is relevant and a further reduction in the electron yield occurs over the reduction due to dry electron scavenging, since such reactive pairs would react rapidly. Electrons trapped further away from scavengers would decay by electron tunneling. If the electron enters an unrelaxed trap the rate of tunneling from this will be faster than from the extrapolated long time decay. To assess what fraction of electrons decay by "dry" electron and encounter pair formation it is necessary to determine whether or not the electron trap relaxes and over what time scale.

Kinetics Study of Selective Solvation of Electrons in Water–Dimethyl Sulfoxide Mixtures

A. M. Koulkes-Pujo,

C.N.R.S., 91190 Gif Sur Yvette, France

L. Gilles, and J. Sutton

Cen-Saclay, 91190 Gif Sur Yvette, France *(Received September 10, 1975)*

Publication costs assisted by Cen-Saclay

Dimethyl sulfoxide (DMSO) is known to solvate with difficulty anions including the electron and hence the addition of DMSO to a medium increases the anionic reaction rates. We attempted to study this effect in mixtures of H_2O–DMSO for specific reactions of the solvated electron using the pulse radiolysis technique. To begin with we chose different solutes among those known as good scavengers of electrons, neutral ones, N_2O, and positive and negative ionic ones (NO_3^- and H^+). The experiments were carried out with a Febetron delivering 10-nsec pulses of 1.8-MeV electrons. The rate of disappearance of the solvated electron formed by the pulse was measured by direct observation of the decay absorption at 870 or 600 nm. The ultrapure products were used as supplied except for DMSO which was distilled before use.

We first of all determined the value of the rate constant $k_{e_{aq}^- + \text{DMSO}}$ as a function of the DMSO concentration. The reaction is pseudo-first order and the results obtained were in good agreement with those of Cooper, Walker, Gillis and Klassen.[1] The mixture H_2O–DMSO has a viscosity and a density greater than water. The viscosity is maximum for a concentration of 0.3 mole fraction.[2] It is known that for diffusion rate-controlled reactions, the diffusion coefficient is related to the reciprocal of the viscosity of the medium, by the Stokes–Einstein law ($D = kT/6\pi\eta r$). So the rate constant of the solvated electron with a solute must vary as $1/\eta$ on addition of DMSO, if this parameter alone is taken into account.

With all the solutes investigated, the disappearance of

the electron remained pseudo-first order, so the rate constant was calculated by subtracting from the total rate of disappearance the rate of disappearance of the electron with DMSO, then dividing by the concentration of the solute. The results are the following.

(1) *N_2O.* The rate constant is not always varying with the concentration of DMSO in the mixture, as the reciprocal of the viscosity of the medium (theoretical curve).[3] Three zones may be distinguished.

Up to 50% volume of DMSO (0.21 mole fraction) the experimental and the theoretical curves are identical, suggesting that the electron is solvated only by water. Above 90% of DMSO (0.68 mole fraction), the experimental rate constant increases too rapidly to be measured. The effect of viscosity cannot only be taken into account and we suggest that the electron formed under these conditions is extremely reactive and is different from the hydrated electron, this conclusion being borne out by the displacement of the absorption spectrum maximum from 720 to above 1500 nm. Between 66 and 90% DMSO, the measured rate constant seems to be lower than that indicated by the theoretical curve. Around 66% DMSO, the solution is known to be especially strongly structured by hydrogen bonding and under these conditions, one may expect that the electron is "heavier" and is thus less mobile and also less reactive than the hydrated electron.

The existence of three zones as a function of the concentration of DMSO has already been seen particularly by Morel[4] who studied the ionic conductivity of Cl^- in such media.

(2) *$NaNO_3$.* This case is completely different from the previous one. The experimental curve is always below the theoretical one, contrary to what happens in the case of N_2O. For low concentrations of DMSO, the rate constant of $e_{aq}^- + N_2O$ was correctly correlated to the viscosity of the medium. In the case of the reaction of two anions, a second phenomena seems to be superimposed on the effect of viscosity.

For concentrations of DMSO equal to or greater than 0.33 mole fraction, the rate of disappearance of the solvated electron is the same as in absence of NO_3^-. We relate this effect to the desolvation of both the anions and to the increased repulsive coulombic interaction between NO_3^- and the electron. If this hypothesis is confirmed, this may have implications in the radioprotective properties of DMSO.

(3) *$HClO_4$.* In general, cations are more solvated in DMSO than in water. The case of the proton in $HClO_4$ seemed interesting to investigate because $HClO_4$ is completely dissociated in these mixtures.[5] Moreover, this case seems simple because we can avoid complex formation with different cations in DMSO and which could have been used as good electron scavengers. Although this work is still in progress, we find that, for small concentrations of DMSO ($\leq$0.1 mole fraction) and $HClO_4$ 10^{-3} M, the rate constant $k_{e_s^- + H^+}$ is increased from 1.9×10^{10} to 2.2×10^{10} M^{-1} sec^{-1}. The difference is not very large but it is significant if we take into account the effect of viscosity. We have very recently obtained results from a greater concentration of $HClO_4$ (5.6×10^{-3} M). They confirm the shape of the curve but there is a shift of the maximum to 0.1 mole fraction DMSO and the rate becomes equal to 2.4×10^{10} M^{-1} sec^{-1}. As the curve passes through a maximum at low concentrations of DMSO, it seems difficult to correlate the increase in rate constant with an increase in the solvation of the proton by DMSO. We suggest that an effect of structure breaking of water either by DMSO or ClO_4^- may be involved. This property was already suggested by MacDonald et al.[6] who studied the influence of DMSO on the temperature of maximum density of water. They concluded that this compound destabilizes the structure of water over the entire concentration range studied ($0.1–3 \times 10^{-2}$ mole fraction). However, Le Narvor et al.[7] arrived at an opposite conclusion in their work on the ir spectrum of water containing low concentrations of DMSO, where they found no change in comparison with pure water. Our own results seem to support the conclusion of MacDonald et al. but we also suspect the effect of ClO_4^- ions which are known as effective structure breakers. It would be interesting to look at the ir spectrum of water–DMSO mixtures in presence of ClO_4^-.

In conclusion, these previous results show that the rate constant of a scavenger with solvated electrons is markedly affected by the presence of DMSO. In spite of the complexity of these solvent mixtures, it seems possible to obtain from them more informations than from the constituents taken separately. Particularly the effect of strength of hydrogen bonding on the energy degradation of a slow electron seems interesting to follow up.

References and Notes

(1) T. K. Cooper, D. C. Walker, H. A. Gillis, and N. V. Klassen, *Can. J. Chem.*, **51**, 2195 (1973).
(2) J. M. G. Cowie, and P. M. Toporowski, *Can. J. Chem.*, **39**, 2241 (1961).
(3) A. M. Koulkes-Pujo, L. Gilles, and J. Sutton, *J. Chem. Soc., Chem. Commun.*, 912 (1974).
(4) J. P. Morel, *Bull. Soc. Chim. Fr.*, 1408 (1967).
(5) J. Courtot-Coupez, and M. Le Demezet, *Bull. Soc. Chim. Fr.*, 1033 (1969).
(6) D. D. MacDonald, M. D. Smith, and J. B. Hyne, *Can. J. Chem.*, **49**, 2817 (1971).
(7) A. Le Narvor, E. Gentric, and P. Saumagne, *Can. J. Chem.*, **49**, 1933 (1971).

Discussion

L. M. DORFMAN. Two brief questions with regard to the rate constant. (1) Is the heat of mixing known for the system and do values correlate with your "structure-breaking" proposal? (2) Does the value of the rate constant come back down to lower values at 0.9 or 0.95 mole fraction of DMSO, or in pure DMSO?

A. M. KOULKES-PUJO. (1) Yes, they are known; after discussion with Dr. Firestone, he will look at this point to see if his correlations may be applied to this case. (2) No, in pure DMSO and around 0.9 mole fraction, N_2O reacts too rapidly with electrons and the rate constant could not be measured.

G. R. FREEMAN. You mentioned that the rapid increase in rate constant for reaction between electrons and N_2O at mole fractions greater than 0.5 of DMSO might be due to dry electrons. In hydrocarbons the rate constant of reaction of quasi-free electrons with nitrous oxide is smaller than that of solvated electrons. The increased rate constant might be attributable to an increasing electron mobility without involving reaction from the quasi-free state.

Your value of the rate constant for reaction of electrons with acid in water, 1.9×10^{10} M^{-1} sec^{-1}, is lower than literature values, $\sim 2.2 \times 10^{10}$ M^{-1} sec^{-1}. Your curve would extrapolate to near the latter value. Is the maximum real?

A. M. KOULKES-PUJO. Yes, we think that the difference is significant; moreover, the viscosity effect is taken into account.

N. KESTNER. How does the optical spectrum of DMSO–H_2O mixtures change as a function of DMSO concentration? Does that spectrum indicate the same strong preference of the electron for coordination by water in accord with your kinetic data?

N. KLASSEN. The λ_{max} of the e_s^- in H_2O–DMSO solutions changes smoothly between λ_{max} in pure H_2O to λ_{max} in pure DMSO. This smooth change occurs at low DMSO concentrations.

J. BELLONI. I would note an important point: in polar media where we have difficulty getting experimental values of the mobilities of e_{solv}^-, the rate constant values of e^- reactions give an indication of the mobility. In your case, if I remember, the maximum of e_{solv}^- spectrum is far away in the ir, despite the high static dielectric rate constants you observe for the decay in pure DMSO.

A. M. KOULKES-PUJO. We correlated the high rate constant we observed to the solvation (or nonsolvation) of the electrons; an electron which absorbs in the ir, as you say, is less solvated so more reactive, so I agree with you. But I do not agree completely to a correlation of any anomaly between high dielectric constant and maximum absorptions of the solvated electrons. Other parameters have to be taken into account.

The Solvated Electron as Reducing Species in the Submicrosecond Formation of Reactive Transients. Carbanions in Solution

Leon M. Dorfman* and Bradley Bockrath

Department of Chemistry, The Ohio State University, Columbus, Ohio 43210 *(Received July 23, 1975)*

Publication costs assisted by the U.S. Energy Research and Development Administration

The solvated electron, generated by pulse radiolysis, has proved to be extremely useful in fast reaction studies as the primary reducing species which forms organic intermediates of interest in other areas of chemistry. Organic free radicals[1] have been generated by dissociative attachment to appropriate solutes in a variety of solvents.

$$e_s^- + RCl \rightarrow R\cdot + Cl^- \quad (1)$$

Aromatic radical anions[2] have been formed by nondissociative attachment to aromatic compounds.

$$e_s^- + A \rightarrow A\cdot^- \quad (2)$$

In the work we report here, carbanions have been generated[3] by dissociative attachment to organomercury compounds in tetrahydrofuran.

$$e_s^- + R_2Hg \rightarrow R^- + RHg\cdot \quad (3)$$

In this way, the benzyl carbanion, $PhCH_2^-$, has been formed and studied. It exhibits a uv absorption band with maximum at 362 nm. Absolute rate constants[3,4] for its formation, as well as for the formation of $(PhCH_2^-,Na^+)$, in the following reactions, have been determined.

$$e_s^- + (PhCH_2)_2Hg \rightarrow PhCH_2^- + PhCH_2Hg\cdot \quad (4)$$

$$k_4 = 2.7 \times 10^{10}\ M^{-1}\ sec^{-1}$$

$$PhCH_2^- + Na^+ \rightarrow PhCH_2^-,Na^+ \quad (5)$$

$$k_5 = 1.5 \times 10^{11}\ M^{-1}\ sec^{-1}$$

$$e_s^- + Na^+ \rightarrow (Na^+,e_s^-) \quad (6)$$

$$k_6 = 7.9 \times 10^{11}\ M^{-1}\ sec^{-1}$$

$$(Na^+,e_s^-) + (PhCH_2)_2Hg \rightarrow PhCH_2^-,Na^+ + PhCH_2Hg\cdot$$

$$k_7 = 7.9 \times 10^{9}\ M^{-1}\ sec^{-1} \quad (7)$$

This is a convenient way of generating benzyl carbanion for fast reaction studies, and much information about its absolute reactivity has been obtained. The method may be extended to other carbanions[5] and other solvents.

Acknowledgment. This work was supported by the United States Energy Research and Development Administration.

References and Notes

(1) M. S. Matheson and L. M. Dorfman, *J. Chem. Phys.*, **32**, 1870 (1960).
(2) L. M. Dorfman, *Acc. Chem. Res.*, **3**, 224 (1970).
(3) B. Bockrath and L. M. Dorfman, *J. Am. Chem. Soc.*, **96**, 5708 (1974).
(4) B. Bockrath and L. M. Dorfman, *J. Phys. Chem.*, **77**, 1002 (1973).
(5) B. Bockrath and L. M. Dorfman, *J. Am. Chem. Soc.*, **97**, 3307 (1975).

Discussion

T. TUTTLE. While the stoichiometry of the species you identify as Na^+,e_s^- is undoubtedly correct, in view of the very large shift in the optical spectrum attributed to the association, I wonder whether some more substantial interaction between the electron and Na^+ is involved as for example in the solvated monomer.

B. BOCKRATH. It would seem that the question of the structure of the 890-nm band cannot be answered solely upon the basis of the magnitude of the shift of the absorption maximum observed upon association.

L. M. DORFMAN. The question to which you are drawing attention, the structure of the ion pair, involves the degree of interposition of solvent, i.e., to what extent is it a solvent-separated ion pair? J. W. Fletcher's paper will likely deal with this, as will the comparison I shall make with other alkali metals, notably lithium. In our kinetic studies we refer only to the stoichiometry.

J. W. FLETCHER. We have attempted to correlate the position of the absorption of Na^+,e_s^- in THF and other solvents with percent atomic character of the monomer as determined by ESR. This is considered in our paper.

Electron Attachment to Sulfur Hexafluoride in Nonpolar Liquids

George Bakale,*

Department of Radiology, Case Western Reserve University, Cleveland, Ohio 44106

U. Sowada, and W. F. Schmidt

Hahn-Meitner-Institut für Kernforschung Berlin GmbH, Bereich Strahlenchemie, 1 Berlin 39, Germany *(Received July 23, 1975)*

Publication costs assisted by the U.S. Energy Research and Development Administration and Case Western Reserve University

The rates of electron attachment to SF_6 were measured in liquid methane, ethane, and propane as a function of the temperature. The data are discussed with relation to the models proposed for the electron motion in these liquids.

Introduction

Excess electron transport in nonpolar liquids for many years was an area of interest primarily restricted to studies of condensed rare gases.[1] With the development of improved purification techniques and faster electronic recording devices, the observation of excess electrons was extended to liquid hydrocarbons[2-4] which resulted in an intense study of these species by radiation chemists. Using the techniques of pulse radiolysis[5-11] and laser flash photolysis,[12,13] measurements of electron reaction rate constants for a large number of solute–solvent systems were carried out within the last few years. The rate constants obtained for good electron scavengers (e.g., SF_6, N_2O, biphenyl, etc.) depend strongly on the molecular structure of the solvent as does the electron mobility.[4,10]

Several models have been proposed for the explanation of the variation of the reaction rates in various liquids;[10-14] whereas Allen et al.[10] assumed that reaction takes place when the electron is in the quasi-free state, Yakovlev et al.[11] derived a model in which the reaction is thought to occur while the electron is in the trapped state.

From our investigations of the electron transport in liquid hydrocarbons, we conclude that at least two different cases should be distinguished: (a) liquids in which the electron is strongly localized (e.g., ethane, propane, *n*-hexane) and (b) liquids in which the electron spends a larger fraction of its lifetime in the extended state. In addition, one must distinguish between purely diffusion-controlled reactions and reactions which require an activation energy.

Sulfur hexafluoride is one of the most efficient electron scavengers in gases and liquids, and in the gas phase the attachment cross section approaches the theoretical limit.[15] The attachment cross section for the reaction

$$e^- + SF_6 \rightarrow SF_6^- \qquad (I)$$

shows a maximum at low electron energies and decreases rapidly with increasing electron energy.[16,17]

Here we report results on the scavenging of excess electrons in liquid ethane, propane, and methane by SF_6.

2. Experimental Section

The measurements were carried out with conductivity cells and electronic circuits described earlier in detail.[18] A short burst of Bremsstrahlung (10 nsec) generated by 15-MeV electrons from a linear accelerator was used to ionize the liquid and to generate an initial concentration of excess electrons of $\sim 10^8$ cm^{-3}. With $[SF_6] > 10^{12}$ cm^{-3}, the decay of the electron current due to the transformation of highly mobile electrons into slow anions is pseudo first order and is given by

$$i(t) = i_0 e^{-k_{ap}t} \qquad (1)$$

By varying the SF_6 concentration, the dependence of the apparent rate constant on the solute concentration was obtained, and from

$$k_{ap} = k_s[S] \qquad (2)$$

the bimolecular rate constant k_s was derived.

Liquid samples were prepared from Phillips Petroleum Co. research grade hydrocarbons. Gaseous ethane and propane were passed through activated columns of charcoal, silica gel, and molecular sieve, and then condensed into an evacuated bottle containing activated silica gel. Cells were evacuated to pressures of $<10^{-5}$ Torr and filled by vacuum condensation. Defined concentrations of SF_6 were prepared by filling a cell having a calibrated volume with SF_6 to a specified pressure and then cooling the cell with liquid air and filling it with methane, ethane, or propane. The dead space above the liquid level was less than 20% of the total cell volume, and the quantity of solute in the gas phase was regarded as negligible. The cell was maintained at a defined temperature by storing it in a cooling bath during the measurement of k_{ap}.

The decay of the electron current was measured with external fields sufficiently low so that the condition

$$k_{ap}^{-1} \ll t_d \qquad (3)$$

was fulfilled (t_d, electron drift time to the electrode).

3. Results

The decay of the electron current was recorded with an oscilloscope; Figure 1a shows a typical oscillograph. In Figure 1b this decay is shown in a semilogarithmic plot, and the straight line indicates that the decrease in electron concentration was mainly due to attachment and not due to neutralization at the electrodes. The bimolecular rate constant was obtained from the dependence of the apparent rate constant on the scavenger concentration. Measurements were made as a function of the temperature, and in Figure 2 the data are presented in an Arrhenius plot. In liquid ethane and propane, activation energies, E_a, of 0.12 and 0.14 eV, respectively, were obtained. The data for a mix-

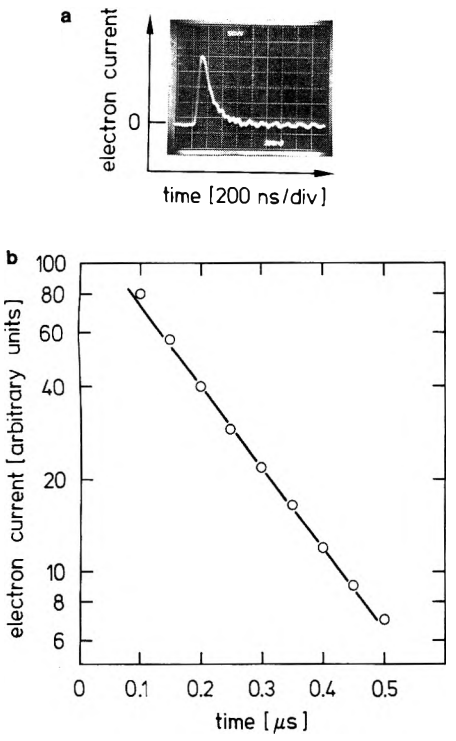

Figure 1. (a) Oscilloscopic trace of the electron current in liquid ethane at 174 K with 0.72 μmol/l. of SF_6 following a 20-nsec pulse of x rays. (b) First-order plot of data of Figure 1a.

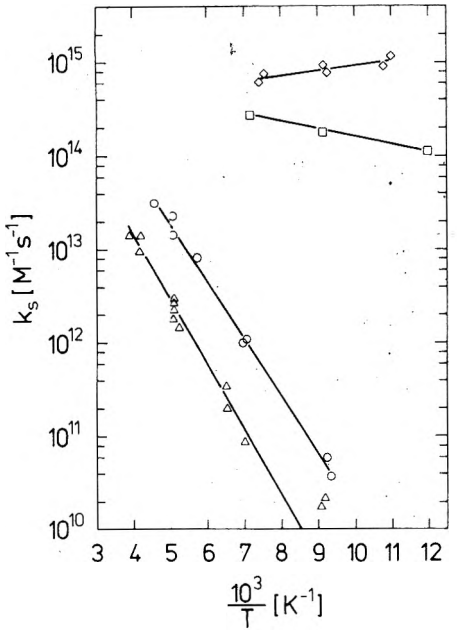

Figure 2. Arrhenius plot of the rate constants for electron scavenging by SF_6 in propane (△), ethane (○), methane (◇), and an equimolar mixture of methane and ethane (□).

ture of 50 mol % ethane and methane showed a small temperature dependence with an activation energy of 0.017 eV. In liquid methane the temperature coefficient of the reaction was negative.

4. Discussion

Liquid ethane and propane exhibit electron mobilities <1 cm^2 V^{-1} sec^{-1} in the temperature range where the rate

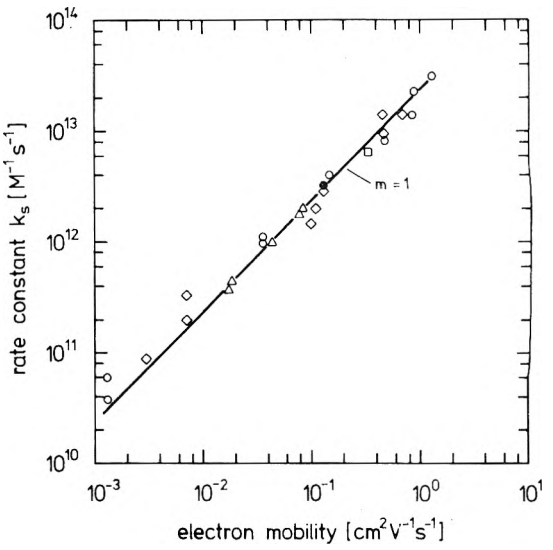

Figure 3. Electron scavenging rate constant as a function of electron mobility: ethane (○), propane (◇), *n*-pentane (●), *n*-butane (□), and, from ref 10, *n*-hexane (△).

constants for reaction with SF_6 were measured.[19,20] The electron transport in low-mobility liquids is discussed either on the basis of an equilibrium model[19-21] or a hopping model.

In the hopping model it is assumed that the electron transport occurs by jumps of the electron between localized states which are separated by barriers of average height E_a. In the equilibrium model the electrons are thought to exist in two states, a trapped state and an extended state, with the population of the two states governed by the temperature. In the extended state the electrons exhibit a mobility μ_0 which also may depend on the temperature

The electron may in principle react with SF_6 in both states. Reactions in the extended state have been reported for liquid argon and xenon where the electrons are quasi-free.[22] For this case, the rate constant is limited by the de Broglie wavelength.

The reaction rate of electrons in liquid methane shows a temperature dependence similar to the mobility, and the reaction is thought to occur in the quasi-free state. In liquid propane and ethane the reaction rate depends strongly upon temperature with an activation energy comparable to that of the electron mobility. Therefore, a close correlation between rate constant and mobility should exist and, in fact, plotting log k_s vs. log μ yields a straight line with a slope of 1 over more than three orders of magnitude (Figure 3). A similar dependence of k_s on μ in various liquids was also observed by Allen et al.;[10] however, their rate constants for the high mobility liquids (isooctane, neopentane, and tetramethylsilane) and our methane k_s values fall below an extension of the line in Figure 3 to higher mobilities.

The proportionality of k_s to the electron mobility can be rationalized with the Smoluchowski equation[23]

$$k_s = 4\pi(D_{el} + D_s)\beta N \times 10^{-3}\ (M^{-1}\ \mathrm{sec}^{-1}) \qquad (4)$$

where D_{el} and D_s are the diffusion coefficients of the electron and solute, respectively, N is Avogadro's number, and β is an effective reaction distance, which for electron attachment to a nonpolar molecule may be expressed by

$$\beta^{-1} = \int_{\rho}^{\infty} r^{-2} \exp[V(r)/kT]\, dr \qquad (5)$$

In eq 5, $V(r)$ is the interaction potential between e^- and S, and ρ is the effective encounter radius of e^- and S, or R_{el} and R_s, respectively. With these assumptions, integration of eq 5 yields

$$\beta \simeq (R_{el} + R_s) \tag{6}$$

Assuming $D_{el} \gg D_s$ and substitution of eq 6 into eq 4 results in

$$k_s \simeq 4\pi D_{el}(R_{el} + R_s)10^{-3}N \tag{7}$$

If we now assume that the Nernst–Einstein equation

$$D = \mu kT/e \tag{8}$$

is applicable to electrons in liquids, then

$$k_s \propto \mu_{el}(kT/e)(R_{el} + R_s) \tag{9}$$

If R_{el} decreases with increasing temperature as T^{-n} and $0.5 < n < 1$,

$$k_s \propto \mu_{el} \tag{10}$$

approximately follows. For instance $R \propto T^{-0.5}$ follows if $R \propto \lambda$, the de Broglie wavelength.

Proportionality between k_s and μ_{el} has been proposed for acceptor–solvent systems where the overlap of corresponding electrons redox levels is sufficient.[14] This condition is fulfilled in the case of SF_6–low mobility hydrocarbons where the encounter time is sufficiently long to assure reaction with each encounter.

A more detailed treatment of the reaction requires a more detailed knowledge of the energy levels of the electron and the SF_6 molecule. The relative energy of the conducting state with respect to the vacuum level is given by V_0, which can be measured by a technique based on the photoelectric effect.[24] In Figure 4 we plotted the dependence of k_s on V_0 for liquid ethane, where V_0 as a function of temperature was determined by Tauchert.[25] The data of Allen et al.[10] obtained in various liquids follow this dependence, while our data for liquid methane deviate considerably. The points for liquid argon and xenon follow the ethane data.

The meaning of this apparent correlation between k_s and V_0 is still unclear as it is for the relation between V_0 and the electron mobility. The attachment of electrons to SF_6 in the gas phase proceeds via two channels

$$e^- + SF_6 \rightarrow SF_6^- \tag{I}$$

and

$$e^- + SF_6 \rightarrow SF_5^- + F \tag{II}$$

where reaction I has its maximum cross section at 0.02 eV while reaction II exhibits a maximum at 0.37 eV. The absolute values of the two cross sections depend on the temperature. Allen et al.[10] interpret Figure 4 by identifying V_0 with the mean electron energy and assume that the maximum rate occurs if the energy of the electron matches a certain energy level of the anion. A maximum rate occurs at $V_0(\max)$, where

$$V_0(\max) = E_{\max} - P^-$$

with $E_{\max}$ the energy of the electrons necessary to obtain the maximum rate in the gas phase and P^- is the polarization energy of the product ion.

For the attachment of electrons to SF_6 in the gas phase $E_{\max} \approx 0$ has been found.[16,17] The highest rate constant in the liquid was determined in liquid xenon. With V_0 increasing in the other liquids $|V_0(\max) - V_0|$ increases and the rate constant decreases.

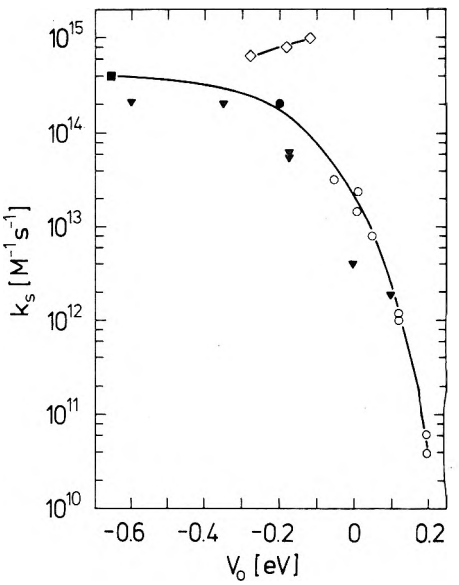

Figure 4. Electron scavenging rate constant as a function of V_0, the energy of the conduction state: ethane (O), data in various liquids from ref 10 (▼), methane (◊), argon (●), xenon (■).

Clearly more experiments, especially the influence of high electric fields, are necessary in order to get a more complete picture of the dynamics of electron attachment to SF_6 in dielectric liquids.

Acknowledgment. We thank Professor K. Yoshino for stimulating discussions and are grateful to Deutsche Forschungsgemeinschaft and U.S. ERDA for support of this work.

References and Notes

(1) S. A. Rice, *Acc. Chem. Res.*, **1**, 81 (1968).
(2) P. H. Tewari and G. R. Freeman, *J. Chem. Phys.*, **49**, 4394 (1968).
(3) R. M. Minday, L. D. Schmidt, and H. T. Davis, *J. Chem. Phys.*, **50**, 1473 (1969).
(4) W. F. Schmidt and A. O. Allen, *J. Chem. Phys.*, **52**, 4788 (1970).
(5) G. Bakale, E. C. Gregg, and R. D. McCreary, *J. Chem. Phys.*, **57**, 4246 (1972).
(6) J. H. Baxendale, C. Bell, and P. Wardman, *J. Chem. Soc., Faraday Trans. 1*, **69**, 776 (1973).
(7) J. H. Baxendale and E. J. Rasburn, *J. Chem. Soc., Faraday Trans. 1*, **70**, 705 (1974).
(8) J. H. Baxendale, J. P. Keene, and E. J. Rasburn, *J. Chem. Soc., Faraday Trans. 1*, 718 (1974).
(9) A. O. Allen and R. A. Holroyd, *J. Phys. Chem.*, **78**, 796 (1974).
(10) A. O. Allen, T. E. Gangwer, and R. A. Holroyd, *J. Phys. Chem.*, **79**, 25 (1975).
(11) B. S. Yakovlev, I. A. Boriev, and A. A. Balakin, *Int. J. Radiat. Phys. Chem.*, **6**, 23 (1974).
(12) G. Beck and J. K. Thomas, *J. Chem. Phys.*, **57**, 3659 (1972).
(13) G. Beck and J. K. Thomas, *J. Chem. Phys.*, **60**, 1705 (1974).
(14) A. Henglein, *Ber. Bunsenges. Phys. Chem.*, **79**, 129 (1975).
(15) A. Herzenberg, Abstracts of the VIIth International Conference on the Physics of Electronic and Atomic Collisions, Amsterdam, The Netherlands, 1971, North Holland Publishing Co., Amsterdam, 1971, pp 1161–63.
(16) R. K. Asundi and J. D. Craggs, *Proc. Phys. Soc., London*, **83**, 611 (1964).
(17) L. G. Christophorou, D. L. McCorkle, and J. G. Carter, *J. Chem. Phys.*, **54**, 253 (1971).
(18) G. Bakale and W. F. Schmidt, *Z. Naturforsch., Teil A*, **28**, 511 (1973).
(19) W. F. Schmidt, G. Bakale, and U. Sowada, *J. Chem. Phys.*, **61**, 5275 (1974).
(20) G. Bakale, U. Sowada, and W. F. Schmidt, presented at the 1974 Conference Electrical Insulation and Dielectric Phenomena, Downingtown, Pa., and to be published in the 1974 Annual Report, National Academy of Sciences, Washington, D.C., 1975.
(21) R. M. Minday, L. D. Schmidt, and H. T. Davis, *J. Phys. Chem.*, **76**, 442 (1972).

(22) U. Sowada, G. Bakale, K. Yoshino, and W. F. Schmidt, *Chem. Phys. Lett.*, **34**, 466 (1975).
(23) E.g., R. E. Weston and H. A. Schwarz, "Chemical Kinetics", Prentice-Hall, Englewood Cliffs, N.J., 1972.
(24) R. A. Holroyd and M. Allen, *J. Chem. Phys.*, **54**, 5014 (1971).
(25) W. Tauchert and W. F. Schmidt, Proceedings of the 5th International Conference on Conduction and Breakdown in Dielectric Liquids, Noordwijkerhout, The Netherlands, July 1975.

Discussion

D. A. ARMSTRONG. Would you say whether the rate constants that you plotted against V_0 were zero-field-strength rate constants; also tell us which liquids they were for?

G. BAKALE. The rate constants in the k vs. V_0 plot were all low-field results where v_d is proportional to E, the electric field. (The symbols are explained in Figure legend.)

L. KEVAN. (1) It is interesting in your electron mobility data vs. temperature in ethane that you find a break near 180 K (see ref 19 and 20). This is about where the simple electron localization criterion Fueki and I developed (paper in this issue) changes sign. In liquid propane, your data vs. temperature do not show a break and the electron localization criterion does not change sign.

G. BAKALE. We agree that this temperature region should be studied further since it may provide information on electron localization; however, we could not do these experiments in our glass cells.

L. KEVAN. (2) In alkaline ice glass (10 m NaOH–H_2O) hot electrons may also be produced at moderate electric fields. (T. Huang, I. Eisele, and L. Kevan, *J. Chem. Phys.*, 1973). Thus it appears that scavenger rate constant effects on field-dependent mobilities of hot electrons could be studied to compare with your results in liquids.

G. BAKALE. We would like to see such studies done since we believe such studies would provide information on the electronic states in both liquids and glasses.

M. SILVER. One must be very careful when applying the Bagley "sink" formula for the field emptying out of traps (see ref 19 and 20). This comes from a one-dimensional analysis. One should use the Onsgaer three-dimensional field-dependent escape probability from a localized center. The two approaches agree at very high fields but disagree at moderate to low fields.

G. BAKALE. We recognize that the Bagley model may be an oversimplification but consider it adequate as a first-order approximation to explain the apparent increase in the electron mobilities at high (~100 kV/cm) fields which we observed.

R. A. HOLROYD. What is the temperature dependence of the rate constant in xenon?

G. BAKALE. We saw a slight negative temperature dependence of $k(e^- + SF_6)$ in liquid xenon, but the narrow liquidus range of xenon over which we could make measurements prevented our accurately determining this dependence.

M. SILVER. The result that the rate constant in high mobility systems decreases with electric field is very interesting. From the standpoint of bias random walk [D. Haarer and H. Mohwald, *Phys. Rev. Lett.*, **34**, 1447 (1975)], in the hot electron regime, the distribution of velocities is distorted in the field direction and the number of new sites encountered per unit time is increased and therefore the rate constant for attachment should go up. It would be very important to compare these field effects (for high mobility electrons) at many temperatures and for different scavengers. Your results might be in conformity with the random walk ideas if the cross-section for attachment was decreasing with increasing electron energy faster than the encounter rate with new sites was increasing.

Mechanistic Studies of Metal–Ammonia Reductions

Robert R. Dewald

Department of Chemistry, Tufts University, Medford, Massachusetts 02155 *(Received July 23, 1975)*

Mechanisms are discussed for the reactions of the ammoniated electron with alkyl sulfides, alkyl sulfones, acetone, bromate ion, ammonium nitrate, nitrous oxide, and benzylaniline. Mechanisms for the reactions of protonic acids with metal–ammonia solutions are also discussed. The ionization constant for ethanol in liquid ammonia at −45° has been estimated from conductivity studies. Kinetic data are presented for the reaction of ethanol with sodium in liquid ammonia at −45°. Mechanisms are suggested for the reduction of benzene by the alcohol–metal–ammonia system.

The unique properties of metal–ammonia solutions present unusual opportunities for the study of reduction reactions. A large variety of organic and inorganic molecules are reduced by reaction with the metals, either in the presence or absence of a proton donor. Encyclopedic summaries[1–8] of the chemistry of metal–ammonia solutions indicate the magnitude of scientific expenditure in this area. In view of the synthetic utility of metal–ammonia solutions, it is surprising to still find a paucity of available kinetic data necessary in formulating mechanisms.

The objective of this paper is to review some recent studies of the reactions of metal–ammonia solutions and to suggest mechanisms for a number of other metal–ammonia reactions. Because of the abundance of synthetic data, it has been necessary to be selective, and the choice of the systems discussed does not in any way reflect upon the merit of other work.

Bond Cleavage Reactions. Several overall general mechanisms have been suggested previously to characterize bond cleavage reactions.[9,10] In Figure 1, a general scheme is presented in this paper where A and B can represent either individual atoms or radical groups. Note that the different possible net reactions and corresponding sets of products are indicated by Roman numerals. A more general scheme is obtained when the scheme given in Figure 1 is coupled with the one presented by Jolly.[9]

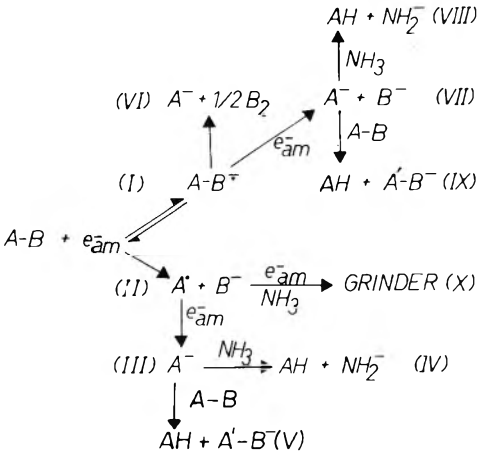

Figure 1. A proposed general mechanism to explain bond cleavage reactions.

Net reaction I corresponds to radical anion formation. There exists an almost complete lack of rate data reported for reactions of this type. The rate constant for the reaction of the ammoniated electron with pyridine[11] has been reported to be $4 \times 10^4\ M^{-1}\ \text{sec}^{-1}$ at −34°. In this case, the pyridine radical anion dimerizes and hence does not lead to bond cleavage.[1]

Examples corresponding to net reaction VI are found in the reactions of propionamide, hydroquinone, and phenol with the ammoniated electron.[12] These compounds[2] react as weak acids with the ammoniated electron according to the following general scheme:

$$HA + e_{am}^- \rightarrow A^- + \tfrac{1}{2}H_2 \quad (1)$$

Moreover, these weak acids are capable of forming radical anions prior to bond cleavage. Radical anions of monobenzenoid substances[1,13,14] have been reported in a number of solvent systems, and, in the case of propionamide, the carbonyl group can facilitate electron attachment as previously suggested for acetamide.[15] For these reactions, the following scheme has been suggested[12] to account for the observed second-order rate expression:

$$e_{am}^- + HA \rightleftharpoons HA\cdot^- \quad (2)$$

$$HA\cdot^- \rightarrow A^- + \tfrac{1}{2}H_2 \quad (3)$$

If reaction 3 is the slow step, then the rate expression becomes

$$-d(e_{am}^-)/dt = k_3K_2(e_{am}^-)(HA) \quad (4)$$

where $K_2 = (HA\cdot^-)/(e_{am}^-)(HA)$ and the observed second-order rate constant is k_3K_2.

The reactions of sodium with simple alkyl sulfides in liquid ammonia are in accord with net reaction IV. The following scheme has been suggested[16] for these reactions:

$$e_{am}^- + R\text{–}S\text{–}R \rightarrow R\text{–}S^- + R\cdot \text{ (slow)} \quad (5)$$

$$R\cdot + e_{am}^- \rightarrow R^- \quad (6)$$

$$R^- + NH_3 \rightarrow RH + NH_2^- \quad (7)$$

where R denotes an alkyl group. Figure 2, obtained from the results reported by Jones and Dewald,[16] gives a plot of $\Delta H^\ddagger$ vs. $\Delta S^\ddagger$ for these reactions. The linearity of the plot supports their suggestion of a common rate-determining step for the reactions in this series. The isokinetic temperature (348° in Figure 2) indicates that the reaction rates are

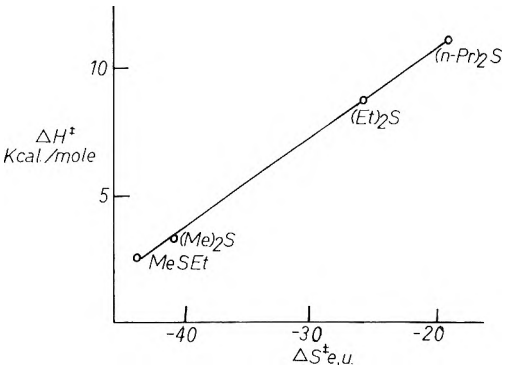

Figure 2. Isokinetic plot for the reaction of sodium with simple alkyl sulfides in ammonia.[16]

controlled by $\Delta H^\ddagger$ values, consistent with the electronic effects being paramount.[17] Moreover, the inductive effects of the alkyl groups were found to strongly influence the rates of cleavage. The cleavage of diphenyl sulfide also has been reported to proceed via the phenyl radical.[18] This was shown by using the acetone enolate ion to trap phenyl radicals.

The cleavage of alkyl sulfones by the ammoniated electron[19] conforms to net reaction V. Using dimethyl sulfone as an example, the following mechanism[19] has been suggested:

$$CH_3SO_2CH_3 + e_{am}^- \rightarrow CH_3SO_2^- + CH_3\cdot \text{ (slow)} \quad (8)$$

$$CH_3\cdot + e_{am}^- \rightarrow CH_3^- \quad (9)$$

$$CH_3^- + CH_3SO_2CH_3 \rightarrow CH_3SO_2CH_2^- + CH_4 \quad (10)$$

For these reactions, the rate expression was found to be second-order, first-order with respect to both the alkyl sulfone and the ammoniated electron.[19] One would predict that the oxygens on the sulfone group should dominate the electronic effects governing the cleavage process. Hence, one would expect that the activation energies of a series of simple alkyl sulfones should be essentially invariant. This was found to be the case.[19] The reaction of diphenyl sulfone was found to be too rapid to permit rate studies by conventional methods. However, unlike the simple alkyl sulfones, the phenyl group can readily accept an electron forming a radical anion, and the following scheme presents a possible mechanism for the overall reaction (net reaction VIII):

$$C_6H_5SO_2C_6H_5 + e_{am}^- \rightleftharpoons C_6H_5SO_2C_6H_5\cdot^- \quad (11)$$

$$C_6H_5SO_2C_6H_5\cdot^- + e_{am}^- \rightarrow C_6H_5SO_2^- + C_6H_5^- \quad (12)$$

$$C_6H_5^- + NH_3 \rightarrow C_6H_6 + NH_2^- \quad (13)$$

The above mechanism is consistent with a third-order rate expression, that is, second-order with respect to the ammoniated electron and first-order with respect to diphenyl sulfone. Moreover, the above scheme is in agreement with the observations of Rossi and Bunnett.[18]

Benzylaniline is reduced by metal–ammonia solutions according to the overall reaction[2]

$$2C_6H_5CH_2NHC_6H_5 + 2e_{am}^- \rightarrow C_6H_5NH^- + C_6H_5CH_3 + C_6H_5CH_2NC_6H_5^- \quad (14)$$

In this reaction, one can speculate that the substrate is initially cleaved to anilide and benzyl anions with the carbanion being protonated by the substrate giving toluene and the diphenylamide ion as shown by the following sequence:

$$C_6H_5CH_2NHC_6H_5 + e_{am}^- \rightleftharpoons C_6H_5CH_2NHC_6H_5^{\cdot -} \quad (15)$$

$$C_6H_5CH_2NHC_6H_5^{\cdot -} + e_{am}^- \rightarrow C_6H_5CH_2^- + C_6H_5NH^- \quad (16)$$

$$C_6H_5CH_2^- + C_6H_5CH_2NHC_6H_5 \rightarrow C_6H_5CH_3 + C_6H_5CH_2NC_6H_5^- \quad (17)$$

The above mechanism is representative of net reaction IX.

Kraus and White[21] reported that acetone reacts with sodium in a 1:1 mole ratio without the evolution of hydrogen. On the other hand, Birch[22] reported that acetone is recovered largely unchanged on treatment with sodium in liquid ammonia, and suggested that the lack of reduction resulted because of the enolate salt formation. Recently, Rossi and Bunnett[18] reported that the reaction of acetone with potassium metal in ammonia yields the acetone enolate ion and produces approximately 40% isopropoxide ion as a by-product. We suggest the following scheme for the reaction of acetone with the ammoniated electron:

$$CH_3{-}\overset{\overset{O}{\|}}{C}{-}CH_3 \leftrightarrow CH_3{-}\overset{\overset{O^-}{|}}{C^+}{-}CH_3 + e_{am}^- \rightarrow CH_3{-}\overset{\overset{O^-}{|}}{C}{-}CH_3 \quad (18)$$

$$CH_3{-}\overset{\overset{O}{|}}{C}{-}CH_3 + CH_3{-}\overset{\overset{O}{\|}}{C}{-}CH_3 \rightarrow CH_3{-}\overset{\overset{O^-}{|}}{C}{-}CH_2^+ + CH_3{-}\overset{\overset{O^-}{|}}{CH}{-}CH_3 \quad (19)$$

$$CH_3{-}\overset{\overset{O^-}{|}}{C}{-}CH_2^+ + e_{am}^- \rightarrow CH_3{-}\overset{\overset{O^-}{|}}{C}{=}CH_2 \quad (20)$$

The mechanism is consistent with the following stoichiometric reaction:

$$2CH_3COCH_3 + 2e_{am}^- \rightarrow CH_3{-}\overset{\overset{O^-}{|}}{C}{=}CH_2 + CH_3{-}\overset{\overset{O^-}{|}}{CH}{-}CH_3 \quad (21)$$

Note the 1:1 mole ratio which was recently confirmed by Jones and Dewald.[23] Moreover, the acetone enolate ion can readily be prepared by the reaction of acetone with the amide ion.[18] Evidence for the radical formed by reaction 18 has been demonstrated by pulse radiolysis and by ESR for a number of carbonyl compounds.[24]

The reaction of ammonium nitrate with metal–ammonia solutions is an interesting system in that virtually no hydrogen is evolved.[2] Burgess and Holden reported that ammonium nitrate and potassium react in a 1:3.1 ratio.[25] The following overall reaction has been proposed[2,26]

$$2NH_4NO_3 + 6K \rightarrow 2NH_3 + K_4N_2O_4 + 2KOH \quad (22)$$

The following scheme can account for the products of the above reaction:

$$NO_3^- + e_{am}^- \rightarrow NO_3^{\cdot 2-} \quad (23)$$

$$NO_3^{\cdot 2-} + NH_4^+ \rightarrow NO_2 + NH_3 + OH^- \quad (24)$$

$$NO_2 + e_{am}^- \rightarrow NO_2^- \quad (25)$$

$$NO_2^- + e_{am}^- \rightarrow NO_2^{\cdot 2-} \quad (26)$$

$$2NO_2^{\cdot 2-} \rightarrow N_2O_4^{4-} \quad (27)$$

We have found that some hydrogen is indeed evolved in this reaction. In a typical experiment in which 6.72×10^{-4} mol of NH_4NO_3 was allowed to react with 3.10×10^{-4} mol of Na, 6.58×10^{-6} mol of hydrogen was recovered. This would indicate that the rate constants for reactions 23 and 24 are much larger than $k(NH_4^+ + e_{am}^-)$.

Nitrous oxide reacts with metal–ammonia solutions according to the following:[9]

$$N_2O + 2e_{am}^- + NH_3 \rightarrow N_2 + OH^- + NH_2^- \quad (28)$$

Since nitrous oxide is capable of readily accepting an electron, a possible pathway for the reaction is as follows:

$$N_2O + e_{am}^- \rightarrow N_2O^{\cdot -} \quad (29)$$

$$N_2O^{\cdot -} + NH_3 \rightarrow N_2 + OH^- + NH_2^{\cdot} \quad (30)$$

$$NH_2^{\cdot} + e_{am}^- \rightarrow NH_2^- \quad (31)$$

In addition, the following side reaction occurs:[9]

$$N_2O + 2NH_2^- \rightarrow N_3^- + OH^- + NH_3 \quad (32)$$

We have found that sodium bromate reacts upon mixing with sodium–ammonia solutions at −65°. The following stoichiometric reaction has been reported:[2]

$$NaBrO_3 + 6Na + 3NH_2 \rightarrow NaBR + 3NaOH + 3NaNH_2 \quad (33)$$

We suggest the following mechanism in order to account for the reaction products:

$$BrO_3^- + e_{am}^- \xrightarrow{NH_3} BrO_2^- + OH^- + NH_2^{\cdot} \quad (34)$$

$$BrO_2^- + e_{am}^- \xrightarrow{NH_3} BrO^- + OH^- + NH_2^{\cdot} \quad (35)$$

$$BrO^- + e_{am}^- \xrightarrow{NH_3} Br^- + OH^- + NH_2^{\cdot} \quad (36)$$

where the amide ion is formed by the reaction of $NH_2^{\cdot}$ with e_{am}^-. The above mechanism is an example of the scheme which we termed "grinder" in Figure 1.

The reaction of hexamethylphosphoramide (HMPA) with alkali metals has been reported to yield two anions,[27] the dimethylamine anion and the diamidophosphite anion. Therefore, the following scheme appears to be operative:

$$[(CH_3)_2N]_3P{=}O + e_{sol}^- \rightarrow [(CH_3)_2N]_3PO^{\cdot -} \quad (37)$$

$$[(CH_3)_2N]_3PO^{\cdot -} + e_{sol}^- \rightarrow [(CH_3)_2N]_2PO^- + (CH_3)_2N^- \quad (38)$$

Here the nature of the decomposition products is now governed by the reactions of the dimethylamine anion. Analysis of the decomposition products showed the presence of dimethylamine, and lesser amounts of trimethylamine and methane.[28] Also, it is interesting to note that the stability of metal–HMPA solutions increases by a factor of 3 to 4 when the temperature is lowered from 25 to 10°.[28] This variation in stability with temperature would correspond to an activation energy of approximately 11 to 15 kcal/mol. At −45°, we have found that HMPA is not readily cleaved by sodium–ammonia solutions. The slowness of this reaction would correspond to a second-order rate constant of less than $10^{-6}\ M^{-1}\ sec^{-1}$.

Reactions of Weak Acids. One of the most important class of reactions that metal–ammonia solutions undergo is the reaction with a protonic acid to give hydrogen and the corresponding salt of the acid.[9] Weak acids, especially ethanol, are frequently used as the proton source in the reduc-

TABLE I: Summary of Rate Constants for the Reaction of Ethanol with Sodium in Liquid Ammonia at −45°

Run no.	$(e_{am}^-)_i$ 10^3 M	$(EtOH)_i$ 10^2 M	$10^5 k_{obsd}$, sec^{-1}	$10^6 k'$, M sec^{-1}
R41R	1.26	1.13	7.0 ± 1.0[a]	1.1 ± 0.3[a]
R42R	1.44	2.30	9.0 ± 0.5	2.4 ± 0.2
R37R	1.34	3.79	8.2 ± 0.2	5.5 ± 0.4
R36R	6.90	1.10	8.6 ± 0.8	1.0 ± 0.1
R35R	1.67	1.14	8.1 ± 0.5	0.40 ± 0.04
R39R	0.809	1.30	7.4 ± 0.3	0.66 ± 0.03
		Av	8.0 ± 0.7	

[a] Standard deviation.

TABLE II: Summary for the Conductance Data for the Determination of the Ionization Constant for Ethanol in Liquid Ammonia at −45°

EtOH 10^3 M	Λ	$\alpha = \Lambda/\Lambda_0$	K_{eq}, M
2.39	0.0620	2.34×10^{-4}	1.5×10^{-10}
8.56	0.0294	1.11×10^{-4}	1.2×10^{-10}
15.8	0.0232	8.75×10^{-5}	1.4×10^{-10}
28.6	0.0152	5.77×10^{-5}	1.1×10^{-10}
42.7	0.0129	4.87×10^{-5}	1.2×10^{-10}
		Av	1.3×10^{-10}

tion of aromatic compounds by metal–ammonia solutions.[5,8] A mechanism in which the weak acid can readily form a radical anion has been discussed above. For the case wherein a weak acid cannot initially form a radical anion, Jolly[9,29] has suggested the following mechanism:

$$HA \rightleftharpoons NH_4^+ + A^- \quad (39)$$

$$NH_4^+ + e_{am}^- \rightarrow NH_3 + \tfrac{1}{2}H_2 \quad (40)$$

The kinetics of the reactions of sodium with water,[30] alcohols,[30-32] and urea[33] have been studied. The results of these studies appear to substantiate Jolly's mechanism. Krapcho and Bothner-By[34] reported findings that provide strong evidence that the reverse step of reaction 39 is much faster than reaction 40. Brooks and Dewald,[35] using the stopped-flow technique, reported that $k_{40} = (1.2 \pm 0.2) \times 10^6$ M^{-1} sec^{-1} at −34°. There is agreement that k_{-39} is expected to have a magnitude characteristic of a diffusion-controlled reaction.[9] Therefore, assuming equilibrium conditions exist in reaction 39, the rate expression for ethanol becomes

$$-d(e_{am}^-)/dt = k_{40}K_{39}[(e_{am}^-)(EtOH)/(EtO^-)] \quad (41)$$

where $K_{39} = (NH_4^+)(EtO^-)/(EtOH)$. Furthermore, the following side reactions should be considered:

$$NH_3 + e_{am}^- \rightarrow NH_2^- + \tfrac{1}{2}H_2 \quad (42)$$

$$NH_2^- + EtOH \rightarrow NH_3 + EtO^- \quad (43)$$

Kinetic studies have shown that the platinum-catalyzed decomposition reaction 42 is zero order in dissolved alkali metal.[36] We also have investigated the decomposition reaction in our glass system containing bright platinum electrodes and found that the reaction is consistent with zero-order kinetics. Therefore, the rate expression becomes

$$-d(e_{am}^-)/dt = k_{40}K_{39}[(e_{am}^-)(EtOH)/(EtO^-)] + k' \quad (44)$$

where k' corresponds to the zero-order decomposition reaction. The general curve fitting program developed by Dye and Nicely[37] was used to evaluate the kinetic data for the reaction of sodium with ethyl alcohol. The results of the study are summarized in Table I. Note the constancy of the observed rate constants ($k_{obsd} = k_{40}K_{39}$). Moreover, the zero-order decomposition constant, k', is small and varies by approximately an order of magnitude depending on the experiment. An example of the fit of the data to the rate expression (eq 44) is shown in Figure 3. Electrical conductivity experiments were performed in order to determine the ionization constant for ethyl alcohol in liquid ammonia according to eq 39 at −45°. The results of this study are given in Table II. The ionization constant was calculated by using the simple Ostwald dilution equation[38] assuming unit activity coefficients. The value of the equivalent conductance of ammonium ethoxide at infinite dilution has not been reported. A value of 265 (Kohlrausch units) for ammonium ethoxide was used in the calculations. This value was obtained by assuming that NH_4EtO and NH_4BrO_3 should have similar equivalent conductivities, and hence the reported value for NH_4BrO_3[39] was corrected for viscosity to yield 265. Note the constancy of the ionization constants given in Table II. Assuming an activation energy of 5.0 kcal/mol for reaction 40,[11] k_{40} is estimated to be 7.2×10^5 M^{-1} sec^{-1} at −45°. Therefore, we calculate a value of 9.4×10^{-5} for $k_{40}K_{39}$, which is in good agreement with the observed rate constant.

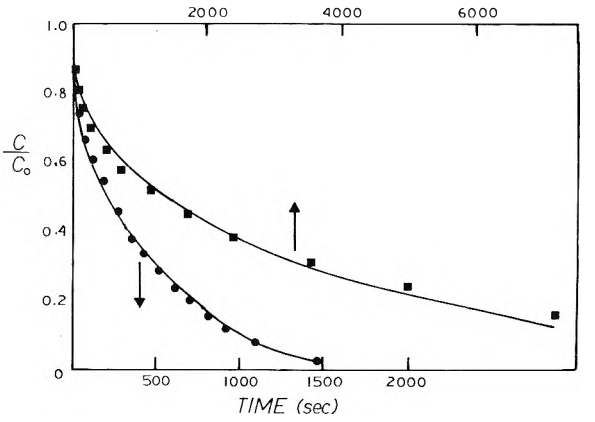

Figure 3. Typical C/C_0 vs. time plots for the reaction of sodium with ethanol in liquid ammonia. The circles are run no. R39R, and the squares are data reported by Kelly, et al.[31] The solid lines represent calculated curves.

Figure 3 also shows the fit of the data reported by Kelly *et al.*[31] to eq 44. Taking their data and estimating the initial ethoxide ion concentration by using the ionization constant for ethanol at −45°, k_{obsd} was calculated to be 4.3×10^{-5}. This value is about a factor of 4 smaller than one would expect based on our results. However, the magnitude of the calculated rate constant is highly sensitive to the initial ethoxide concentration which may account for the above disparity.

Hydrogenation of Unsaturated Compounds. The only reported kinetic studies of the hydrogenation reactions (Birch reductions) have been for the reduction of benzene to 1,4-cyclohexadiene by alkali metals and alcohols in liquid ammonia. The overall reaction is

$$C_6H_6 + 2e_{am}^- + 2ROH \rightarrow C_6H_8 + 2RO^- \quad (45)$$

The mechanism originally suggested by Birch[5] appeared to be in agreement with kinetic data reported by Krapcho and Bothner-By.[34] These investigators reported that the reduction of benzene proceeds by the third-order rate law

$$-d(C_6H_6)/dt = k_{46}(C_6H_6)(ROH)(Li) \quad (46)$$

However, Jacobus and Eastham[40] later questioned the va-

lidity of the above rate expression and observed that the reaction rate in the presence of an initially saturated solution of ethoxide ions is

$$-d(C_6H_6)/dt = k_{47}(C_6H_6)(EtOH)(Li)^2 \quad (47)$$

Jolly[29] suggested a mechanism in which protonation proceeds via the ammonium ion. Protonation of sodium naphthalide[41] by ethanol in liquid ammonia also was found to proceed via the ammonium ion. It is of interest to consider a modification of the mechanism for the reduction of benzene as suggested previously by Jolly.[29] In this scheme we again assume protonation via the ammonium ion as follows:

$$EtOH \rightleftharpoons NH_4^+ + EtO^- \quad (48)$$

$$e_{am}^- + C_6H_6 \rightleftharpoons C_6H_6\cdot^- \quad (49)$$

$$C_6H_6\cdot^- + NH_4^+ \rightarrow C_6H_7\cdot + NH_3 \quad (50)$$

$$C_6H_7\cdot + e_{am}^- \rightarrow C_6H_7^- \quad (51)$$

$$C_6H_7^- + EtOH \rightarrow C_6H_8 + EtO^- \quad (52)$$

Applying steady-state treatment to $C_6H_7\cdot$ and $C_6H_7^-$, one obtains

$$\frac{d(C_6H_8)}{dt} = k_{50}K_{48}K_{49}\frac{(EtOH)(C_6H_6)(e_{am}^-)}{(EtO^-)} \quad (53)$$

where $K_{48} = (NH_4^+)(EtO^-)/(EtOH)$ and $K_{49} = (C_6H_6\cdot^-)/(e_{am}^-)(C_6H_6)$.

The above rate expression can be shown to be equivalent to the fourth-order rate law reported by Jacobus and Eastham[40] if one considers the limited solubility product constant for lithium ethoxide is about 10^{-7}. In addition, charge balance requires that

$$(Li^+) = (e_{am}^-) + (C_6H_6\cdot^-) + (C_6H_7^-) + (EtO^-) \quad (54)$$

and at high-metal concentrations eq 54 reduces to

$$(Li^+) \approx (e_{am}^-) \quad (55)$$

Hence, the rate expression becomes:

$$\frac{d(C_6H_8)}{dt} = \frac{k_{50}K_{48}K_{49}}{K_{sp}}(EtOH)(C_6H_6)(e_{am}^-)^2 \quad (56)$$

where $K_{sp} = (Li^+)(EtO^-)$. Note that the above expression is in agreement with that found by Jacobus and Eastham.[40] Unfortunately, not all of the constants in eq 56 are known. In order to have 95% reduction,[34] k_{50} should be about two orders of magnitude greater than $k(e_{am}^- + NH_4^+)$. Hence, if $k_{50} \approx 10^8\ M^{-1}\ sec^{-1}$ and $K_{49} \approx 10^{-4}\ M^{-1}$ (estimated from the lack of an observed ESR signal for the $C_6H_6\cdot^-$ species when pure ammonia is the solvent), one calculates $k_{obsd} = 13$ which is in good agreement with the values reported by Jacobus and Eastham.[40] Furthermore, as pointed out by Jolly,[29] the observation[34] that the reduction rates with lithium, sodium, and potassium decreases in that order is predictable from the increase expected in the solubility of the alkoxides. The major defects of the above mechanism are the inability to explain low product yields when low concentrations of metal [(Na) < $10^{-2}\ M$] are used, and the role of a cosolvent which is frequently added.[5] In this connection, from the studies reported on the protonation of aromatic radical anions in solvent systems of lower dielectric constant than liquid ammonia, it has been shown that the state of ion pairing plays a major role in determining the reaction mechanism.[42-44] Therefore, we propose the following alternative mechanism involving ion pairing:

$$e_{am}^- + C_6H_6 \rightleftharpoons C_6H_6\cdot^- \quad (49)$$

$$C_6H_6\cdot^- + M^+ \rightleftharpoons (C_6H_6\cdot^- - M^+)\ \text{ion pair} \quad (57)$$

$$(C_6H_6\cdot^- - M^+) + EtOH \rightarrow C_6H_7\cdot + EtO^- \quad (58)$$

$$C_6H_7\cdot + e_{am}^- \rightarrow C_6H_7^- \quad (51)$$

$$C_6H_7^- + EtOH \rightarrow C_6H_8 + EtO^- \quad (52)$$

Applying steady-state treatment to the intermediates $C_6H_7\cdot$ and $C_6H_7^-$, and letting $(e_{am}^-) \approx (M^+)$, the following rate expression is obtained:

$$d(C_6H_8)/dt = k_{58}K_{57}K_{49}(e_{am}^-)^2(C_6H_6)(EtOH) \quad (59)$$

where K_{57} is the ion-pairing constant. Note that eq 59 is again consistent with the observations of Jacobus and Eastham.[40] If one assumes that $K_{49} \approx 10^{-4}$ as before, K_{57} to be in the neighborhood of 10^3 for ion pairing,[45] and using the fourth-order rate constants reported by Jacobus and Eastham,[40] one calculates $k_{58} \approx 10^2$ to 10^3. This range of values is comparable to the rate constants reported for the protonation of various radical anions in other solvents.[42,43] Moreover, the influence of the ethoxide ion on the rate constant[40] can be explained by its formation of complex ions with ethanol.[9,31] We are presently undertaking a systematic study of the yield obtained for the reduction of benzene as a function of ionic strength and dielectric constant in the hope of obtaining experimental results that would enable us to distinguish between the above suggested mechanisms.

Acknowledgment. This work was supported in part by the National Science Foundation. I especially acknowledge the efforts of M. A. Latina, D. E. Gannon, S. I. Bearman, and E. Petrillo, and the many helpful discussions regarding this subject with Professor T. R. Tuttle, Jr.

References and Notes

(1) H. O. House, "Modern Synthetic Reactions", 2nd ed, W. A. Benjamin, Menlo Park, Calif., 1972, Chapter 3.
(2) G. W. Watt, *Chem. Rev.*, **46**, 289, 317 (1950).
(3) G. Jander, "Chemistry in Nonaqueous Ionizing Solvents", Vol. I, Part 1, Interscience Publishers, New York, N.Y., 1966.
(4) H. Smith, "Chemistry of Nonaqueous Ionizing Solvents", Vol. I, Part 2, Interscience Publishers, New York, N.Y., 1963.
(5) A. J. Birch, *Q. Rev., Chem. Soc.*, 69, (1950); 12, 17 (1958).
(6) W. L. Jolly, *Prog. Inorg. Chem.*, **1**, 235 (1956).
(7) R. G. Harvey, *Synthesis*, 161 (1970).
(8) A. J. Birch and G. Subba Rao, *Adv. Org. Chem.*, **8**, 1 (1972).
(9) W. L. Jolly, "Metal-Ammonia Solutions", J. J. Lagowski and M. J. Sienko, Ed., Butterworths, London, 1970, p 167.
(10) Reference 4, p 153.
(11) R. R. Dewald, R. L. Jones, and H. Boll, "Electrons in Fluids", J. Jortner and N. R. Kestner, Ed., Springer-Verlag, Heidelberg, 1973, p 473.
(12) H. Boll, P. S. Childs, R. R. Dewald, and R. L. Jones, *J. Chem. Phys.*, in press.
(13) U. Schindewolf, R. Vogelsgesang, and K. W. Boeddeker, *Angew. Chem., Int. Ed., Engl.* **6**, 1076 (1967).
(14) T. R. Tuttle, Jr., and S. I. Weissman, *J. Am. Chem. Soc.*, **80**, 5342 (1958).
(15) M. Simic and E. Hayon, *J. Phys. Chem.*, **77**, 996 (1973).
(16) R. L. Jones and R. R. Dewald, *J. Am. Chem. Soc.*, **96**, 2315 (1974).
(17) R. G. Wilkins, "The Study of Kinetics and Mechanism of Reactions of Transition Metal Complexes", Allyn and Bacon, Boston, Mass., 1974, p 101.
(18) R. A. Rossi and J. F. Bunnett, *J. Am. Chem. Soc.*, **96**, 112 (1974).
(19) R. R. Dewald, D. Gannon, S. Bearman, and E. Petrillo, to be submitted for publication.
(20) Reference 4, p 185.
(21) C. A. Kraus and G. F. White, *J. Am. Chem. Soc.*, **45**, 768 (1923).
(22) A. J. Birch, *J. Proc. R. Soc. N.S.W.*, **83**, 245 (1950).
(23) R. L. Jones and R. R. Dewald, *Anal. Chem.*, **45**, 1753 (1973).
(24) E. J. Hart and M. Anbar, "The Hydrated Electron", Wiley, New York, N.Y., 1970, p 136.
(25) W. M. Burgess and F. R. Holden, *J. Am. Chem. Soc.*, **59**, 459 (1937).
(26) Reference 3, p 443.
(27) H. Normat, *Angew. Chem. Int. Ed. Engl.*, **6**, 1046 (1967).
(28) J. M. Brooks, M.S. Thesis, Tufts University, 1968.

(29) W. L. Jolly, *Adv. Chem. Ser.*, **No. 50**, 27 (1965).
(30) R. R. Dewald and R. V. Tsina, *J. Phys. Chem.*, **72**, 4520 (1968).
(31) E. J. Kelly, H. V. Secor, C. W. Keenan, and J. F. Eastham, *J. Am. Chem. Soc.*, **84**, 3611 (1962).
(32) R. R. Dewald, "Metal–Ammonia Solutions", J. J. Lagowski and M. J. Sienko, Ed., Butterworths, London, 1970, p 193.
(33) W. L. Jolly and L. Prizant, *Chem. Commun.*, 1345 (1968).
(34) A. P. Krapcho and A. A. Bothner-By, *J. Am. Chem. Soc.*, **81**, 3658 (1959).
(35) J. M. Brooks and R. R. Dewald, *J. Phys. Chem.*, **75**, 968 (1971).
(36) I. Warshawsky, *J. Catal.*, **3**, 291 (1964).
(37) J. L. Dye and V. A. Nicely, *J. Chem. Educ.*, **48**, 443 (1971).
(38) G. W. Castellan, "Physical Chemistry", 2nd ed, Addison-Wesley, Reading, Mass., 1971, p 715.
(39) Reference 3, p 169.
(40) O. J. Jacobus and J. F. Eastham, *J. Am. Chem. Soc.*, **87**, 5799 (1965).
(41) H. Boll and R. R. Dewald, data to be submitted for publication.
(42) G. Levin, C. Sutphen, and M. Szwarc, *J. Am. Chem. Soc.*, **94**, 2652 (1972).
(43) S. Bank and B. Bockrath, *J. Am. Chem. Soc.*, **94**, 6076 (1972).
(44) E. R. Minnich, L. D. Long, J. M. Ceraso, and J. L. Dye, *J. Am. Chem. Soc.*, **95**, 1061 (1973).
(45) R. M. Fuoss, *J. Am. Chem. Soc.*, **80**, 5059 (1958).

Discussion

J. BELLONI. How do you explain the differences between the kinetics and hence mechanisms of e_{am}^-–hydrazine and e_{am}^--substituted hydrazine reactions? Why can you definitely rule out a mechanism for phenylhydrazine beginning by ionization of the molecule as we showed for N_2H_4 similar to the ethanol mechanism?

R. R. DEWALD. Hydrazine does not react with the ammoniated electron. However, substituted hydrazines, especially those having electron-withdrawing groups, are acidic in ammonia and hence react with the ammoniated electron. In other cases, resonance effects can facilitate electron attachment which leads to bond cleavage. In the phenylhydrazine case, a mechanism similar to the alcohol reaction would not account for the products of the reaction. I would like to point out, however, that the mechanism we presented is formulated to account for the reaction products and we have no kinetic data to support the mechanism.

U. SCHINDEWOLF. The equilibrium for the reaction

$$e^- + C_6H_6 \rightleftarrows C_6H_6{\cdot}^-$$

in mixtures of methylamine and liquid ammonia is shifted to left with increasing temperature. This indicates that ΔH is negative and also that $\Delta S > 0$.

J. L. DYE. The temperature dependence of the equilibrium constant for the formation of benzenide radical anion in tetrahydrofuran also shows a decreasing equilibrium constant with increasing temperature. By ESR techniques the benzenide signal disappears as the temperature is raised above about −50°C, similar to the results of Tuttle and Weissman.

U. SCHINDEWOLF. What is the catalyzed zero-order reaction that you were referring to

R. R. DEWALD. I was referring to the following reaction

$$e_{am}^- + NH_3 \rightleftarrows NH_2^- + \tfrac{1}{2}H_2$$

which is platinum catalyzed.[9]

U. SCHINDEWOLF. Why do you assume that ion pairing, $C_6H_6{\cdot}^- + M^+ \rightleftarrows C_6H_6{\cdot}^-,M^+$, is important in the reduction of benzene? What is the evidence?

R. R. DEWALD. It is well established[42-44] that ion pairing plays an important role in the protonation of a number of aromatic radical anions in solvent systems of lower dielectric constants than liquid ammonia. Moreover, Krapcho and Bothner-By[34] reported that the addition of salts, particularly LiBr, resulted in a marked increase in the reduction rate.

A. M. KOULKES-PUJO. In the case of HMPA, were you referring to the reaction of e_{am}^- with HMPA? The reaction of e_{HMPA}^- + HMPA is very slow, if there is a reaction occurring at all.

R. R. DEWALD. Yes, I was referring to e_{am}^-. I agree that the reaction of e_{HMPA}^- + HMPA is very slow corresponding to second-order rate constant of less than $10^{-2}\ M^{-1}\ sec^{-1}$ at room temperature.

A. M. KOULKES-PUJO. For reaction of DMSO with e_{am}^-, you suggested an intermediate step involving the formation of $DMSO{\cdot}^-$. Is there any evidence for a $DMSO{\cdot}^-$ species?

R. R. DEWALD. Chung et al. (*J. Phys. Chem.*, **78**, 1882 (1974)) reported the formation of methyl-radical–methanesulfenate anion pairs by dissociative electron capture in γ-irradiated crystalline dimethyl-d_6 sulfoxide at 77 K. These authors also regarded $Me_2SO{\cdot}^-$ as an unstable product of electron capture whose structure naturally lends itself to a facile dissociation process.

Surface Tension of Metal–Ammonia Solutions

Pierre Damay

Laboratoire de Chimie Physique, CNRS, E.R.A. 126, 59000 Lille, France *(Received July 23, 1975)*

A phenomenological study of surface tension at −35 and −40°C from the Gibbs equation indicates that the minimum thickness of the interphase is very large just above the critical point (160 Å at −35°C and 360 Å at −40°C). In the interphase, the solution is much more dilute than in the bulk. These effects can be explained by the proximity of the critical point and by the large difference of surface tension between pure ammonia and concentrated solutions. Our results could help to interpret reflection spectroscopy data reported by Burrow and Lagowski.

Introduction

Surface tension of sodium–ammonia solutions at −35°C is largely influenced by the proximity of the critical point (−41°C). A method is described which allows the thickness of the surface phase where gradients occur to be evaluated. It appears that the minimum thickness of the surface phase is 160 Å at −35°C and 360 Å at −40°C at the critical concentration. The structure of the surface can be proposed as follows: there exists a sharp density gradient at the surface corresponding to the liquid–vapor equilibrium. Inside the liquid, close to the surface, the concentration varies over a large distance. The surface phase becomes thicker as the critical point is approached.

Generalities

Thermodynamics permits energy balance of macroscopic systems to be studied. The simplest way to apply thermodynamic formalism to surface properties is, as did van der Waals or Guggenheim, to consider the surface of a liquid in equilibrium with its vapor as a third phase of a given thickness τ. All gradients between the vapor and liquid phases take place in the surface phase. It is supposed that average thermodynamic quantities, pressure, temperature, density, and free energy can be defined in this phase.

The surface phase is not isotropic and therefore pressure is a tensor. The pressure on a plane parallel to the surface is assumed to be the same as the pressure inside the vessel, but the pressure perpendicular to the surface is

$$p - \gamma/\tau \tag{1}$$

This expression can be used as a definition for surface tension γ.

From there the Gibbs equation can be derived quite simply for a two-component mixture as

$$\frac{\partial\gamma}{\partial x_2} = -\frac{RT}{x_1}\left[\Gamma_2 x_1 - \Gamma_1 x_2\right]\frac{\partial \ln a_2}{\partial x_2} \tag{2}$$

at constant pressure and temperature. $\Gamma_{1,2}$ is the number of molecules of components 1,2 in the surface phase per unit surface; a_2 is the activity of component 2, and $x_{1,2}$ are the mole fraction of components 1,2.

We are going to focus all our attention on the term $u = \Gamma_2 x_1 - \Gamma_1 x_2$. It appears that this quantity can be easily determined if both the surface tension and the chemical potentials of the solution as a function of concentration are known.

It must be pointed out that $\Gamma_{1,2}$ is closely related to the mole fraction x_1', x_2' in the surface phase; if k is a factor taking care of the dimensionality, it is found that

$$u = \Gamma_2 x_1 - \Gamma_1 x_2 = k(x_2' x_1 - x_2 x_1') \tag{3}$$

Hence, if the average concentration of the solute in the surface phase is the same as in the bulk of the solution, u vanishes, and it is shown from eq 2 that the surface tension should not vary with concentration. Conversely, any change of surface tension with concentration indicates that the concentration in the surface phase is different from that in the bulk.

In all of the textbooks except Guggenheim's,[1] the concentration of the solvent is supposed to be the same in the surface phase and in the bulk, and thus u/x_1 in eq 2 becomes simply $k(x_2' - x_2)$, which indicates the excess solute in the surface phase.

Some very interesting points coming from a more complete analysis of u are missed by this simplification, which is just one of the many ways to locate the surface plane. As is shown from Figure 1, this procedure consists of choosing B as the surface plane. This figure gives the number of species 1,2 per unit surface as a function of distance. The number of molecules contained between planes A and B represents the excess concentrations in the surface phase.

Actually there is no need to choose a surface plane at this point, and Guggenheim[1] showed that u does not depend on this choice.

It is seen from Figure 1 that the distance through which gradients occur must be related in some way tc the value of τ. The interface thickness cannot be chosen as τ since the concentration gradients are not sharp but display smooth profiles. It will be shown that τ is the minimum thickness of the surface phase, and that the actual thickness can be well approximated by 2τ.

By some rearrangements, it can be seen that τ is a linear function of u

$$\tau = -uV_m/x_1x_2 \tag{4}$$

V_m being the volume of 1 mol of mixture. Using eq 2 and 4, τ can be determined directly from surface tension and activity data by

$$\tau = \frac{V_m}{x_2 RT}\frac{\partial\gamma/\partial x_2}{\partial \ln a_2/\partial x_2} \tag{5}$$

For example for an ideal solution

$$\partial \ln a_2/\partial x_2 = 1/x_2$$

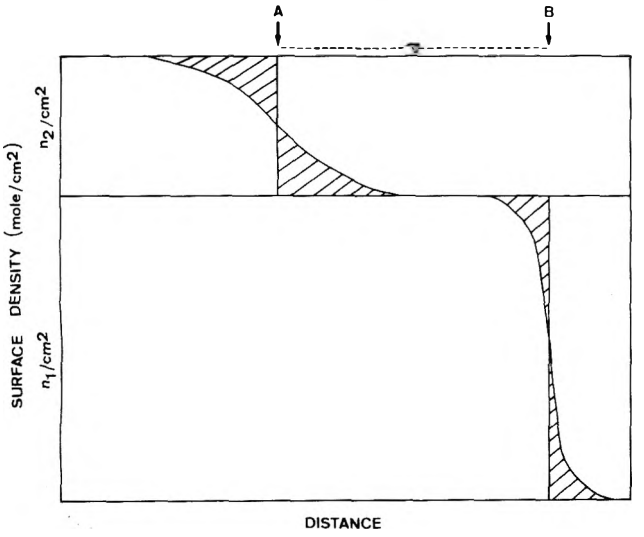

Figure 1. Surface density for a two-component mixture. A and B represent the planes where the excess concentration of the solute and the solvent, respectively, is zero. The smooth curves are the actual density profiles. Dashed areas on the left and on the right of each plane are equal.

and

$$\tau = \frac{V_m}{RT}\frac{\partial\gamma}{\partial x_2} \tag{6}$$

For a perfect ideal mixture of two liquids for which the surface tension varies linearly with concentration between γ_1 and γ_2, the values of the pure components, $\partial\gamma/\partial x_2$ and therefore τ are constants. The surface thickness depends mainly on the difference $\gamma_2 - \gamma_1$. The absolute value of $\gamma_2 - \gamma_1$ must be chosen because negative values of τ would be meaningless.

It seems very important to determine τ before making any model for the structure of the surface of a two-component mixture. Most models assume that gradients occur only in a monolayer. Very often there is no quantitative basis to make this assumption. The determination of τ could test the applicability of such models. If τ is of the order of a few angstroms, a monolayer surface is probable; but if it happens to be of the order of a few tens of angstroms, such models must be dicarded.

Application to Metal–Ammonia Solutions

The Sodium–Ammonia System at −35 and −40°C. Surface tension measurements on sodium–ammonia solutions have been performed by Holly,[2] and the results have been reviewed by Sienko at Colloque Weyl I.[3] It is seen from eq 2 that $\partial\gamma/\partial x_2$ must be compared to $\partial \ln a_2/\partial x_2$ in order to determine u. The surface tension and the activity of the solute at −35°C are given on the same plot in Figure 2 as functions of the concentration. It is seen that both curves show a plateau and a point of inflection, but it is interesting to note that the minimum slope does not occur at the same concentration for the two properties. Values of τ have been calculated from eq 5 and are shown in Figure 3. The minimum surface thickness τ shows a maximum at the critical concentration, i.e., at the minimum slope of the activity–concentration plot. At this concentration, $\partial\gamma/\partial x_2$ is already quite large as can be seen from Figure 2. At its maximum value, τ reaches 160 Å −35°C and 360 Å at −40°C.

The surface plane can now be chosen close to plane B since it is near this plane that a large density gradient occurs. It has been said that concentration profiles were not taken into account when calculating τ. The minimum requirement for concentration profiles is that x_2 must not vanish between planes B and A. Thus in Figure 1 the solute profile must be extended from A to B. Assuming symmetry on both sides of plane A, it can be concluded that a value of 2τ is a good approximation for the thickness of the interface. For metal–ammonia solutions, the surface phase is furthermore much more dilute than the bulk phase.

The thickness of the surface phase increases as the critical point is approached. It probably diverges near the criti-

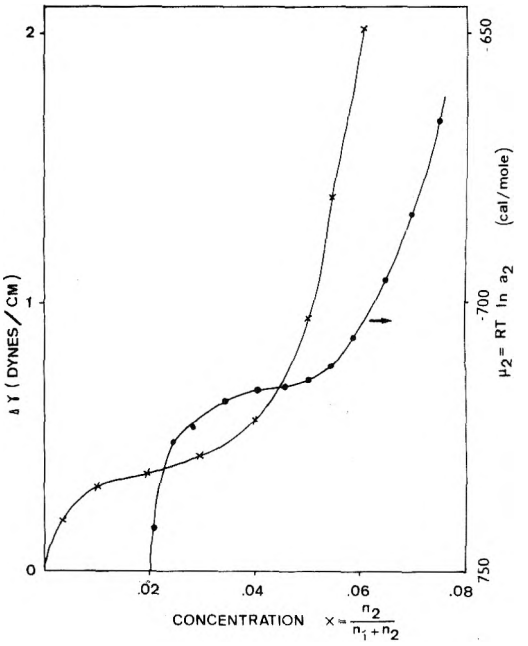

Figure 2. Surface tension and chemical potential of a sodium–ammonia system at −35°C as functions of concentration. $\Delta\gamma$ is the difference between the surface tension of the solution and that of the pure solvent.

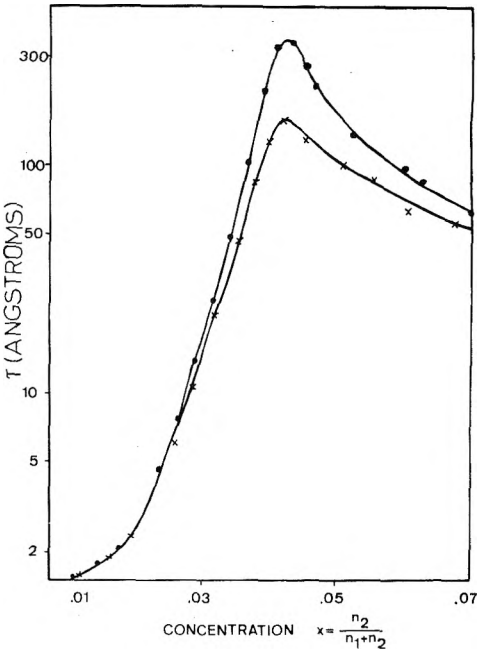

Figure 3. The minimum surface thickness τ as a function of concentration at −35°C (×) and −40°C (●).

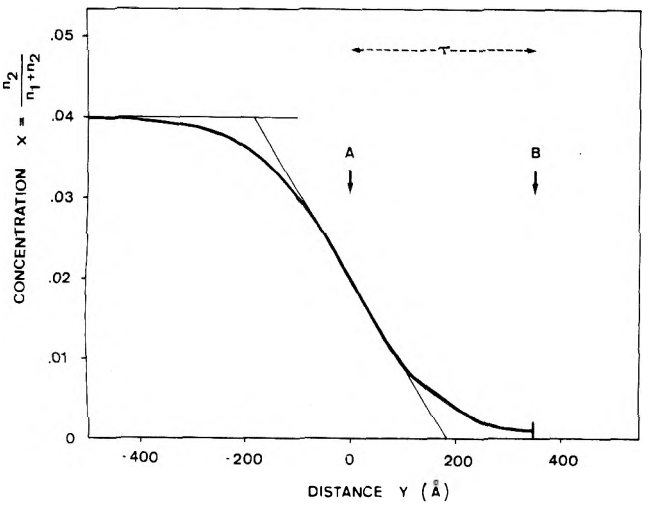

Figure 4. A tentative concentration profile for a sodium–ammonia solution at −40°C at the critical concentration. Positions of planes A and B in Figure 1 are indicated by the arrows.

cal temperature. At the critical point itself, both $\partial\tau/\partial x_2$ and $\partial \ln a_2/\partial x_2$ vanish and τ is not defined.

Discussion

If we assume that sodium–ammonia solutions consist of a mixture of free ammonia and solvated sodium, $Na(NH_3)_n$, it is evident from Figure 2 that the surface tension of the solvated metal is much larger than that of pure ammonia; it is probably of the order of 100 or 200 dyn/cm as for most liquid metals. In order to minimize the surface energy, ammonia tends to replace the solute at surface sites, but energy is required to make the solution more dilute. This energy can be calculated from the difference in free energy coming from different concentrations in the surface phase and in the bulk. Damay and Schettler[4] showed that the energy required to make large concentration fluctuations in the intermediate range is small because of the proximity of the critical point. A minimization is operated between these two opposite energies.

Very often profiles are represented by hyperbolic tangents in order to take into account the exponential gradient of concentration which occurs on both sides of the midpoint (Figure 1). Figure 4 represents a tentative concentration profile for a sodium–ammonia system at −35°C at the critical concentration. The concentration gradient at plane A is taken as x_2/τ. The surface plane is chosen very close to B because it is at this plane that a large density gradient occurs. This density gradient is very sharp due to the fact that the critical temperature of pure ammonia is far from −35°C.

Hence the surface structure in the intermediate range of concentration can be summarized as follows: a concentration gradient exists through several hundred angstroms, the surface itself presents a sharp density gradient. The concentration at the surface is much more dilute than in the bulk. Semiquantative arguments (hyperbolic tangent profile and $\partial x_2/\partial z = x_2/\tau$ at plane A) allows the concentration to be calculated in the few angstroms close to the surface. It appears that the molar fraction of the solute at the surface is of the order of 10^{-3} and is surprisingly quite independent of concentration.

Those results could help to interpret reflection spectroscopy data obtained by Burrow and Lagowski.[5] Their results show that the vibrational spectra of ammonia for all concentrations is the same as for the pure solvent. These spectra could very well be attributed to the surface phase which is always much more dilute than the bulk. The same argument could be applied to the data of Beckman and Pitzer[6] who found the reflection spectrum of solvated electrons in the intermediate range.

It can also be suggested that the work function of electrons should be strongly affected by these surface effects.

Conclusion

The surface tension of metal–ammonia solutions has been studied from a thermodynamic point of view. It has been shown that concentration gradients occur through large distances in the intermediate range of concentration. A semiquantitative concentration profile has been suggested. It indicates that the concentration in the few angstroms close to the surface remains nearly constant and is more dilute than in the bulk.

More work has to be done in order to define a more probable structure of the interface. Widom[7] showed that the surface and interfacial tension could be interpreted in terms of concentration and density fluctuations. In the light of recent results obtained by Chieux[8] on neutron diffraction near the critical point and by Damay and Schettler[4] on the microscopic structure of these solutions in the intermediate range, it should be possible to make a more quantitative model for both surface and interface structure (the interface separating the two liquid phases below the critical point).

Acknowledgments. The author is grateful to Professeur M. J. Sienko for having extended to him the hospitality of the Chemistry Department of Cornell University, where this work was completed, and to the National Science Foundation for the award of a fellowship which made possible his stay at Cornell.

References and Notes

(1) E. A. Guggenheim, "Thermodynamique", Dunod, Paris, 1965.
(2) F. Holly, Ph.D. Dissertation, Cornell University, 1962.
(3) M. J. Sienko in "Metal–Ammonia Solutions", G. Lepoutre and M. J. Sienko, Ed., W. A. Benjamin, New York, N.Y., 1964.
(4) P. Damay and P. Schettler, *J. Phys. Chem.*, this issue.
(5) D. F. Burrow and J. J. Lagowski, *J. Phys. Chem.*, **72**, 163 (1968).
(6) T. A. Beckman and K. S. Pitzer, *J. Phys. Chem.*, **65**, 1527 (1961).
(7) B. Widom, *J. Chem. Phys.*, **43**, 3892 (1965).
(8) P. Chieux, *Phys. Lett A*, **48**, 493 (1974).

Dielectric Constant of Liquid Ammonia from −35 to +50°C and Its Influence on the Association between Solvated Electrons and Cation

Gérard Billaud and Antoine Demortier*

13, rue de Toul, 59000 Lille, France *(Received July 23, 1975)*

The dielectric constant of pure liquid ammonia has been measured from −35 to +50°C. In addition previous works have been reviewed so as to allow the estimation of a "best" value for the dielectric constant anywhere between −75 and +50°C. Anomalies had been reported in the temperature coefficient of the association between solvated electrons and cations. They are explained in the light of these new measurements.

Many measurements of the dielectric constant of liquid ammonia have been made at different temperatures and the resulting values are scattered in the literature.[1-13] Most of these measurements have been made as a subsidiary part of some other experimental program and as a result there are few values at high temperatures, few series of measurements as a function of temperature, and, in addition, intercomparison of the results from different authors leads to considerable uncertainty.[14,15]

We have measured the dielectric constants from −35 to +50°C. In addition we have briefly reviewed other works so as to allow the estimation of a "best" value of the dielectric constant anywhere within the extended range from −75 to +50°C.[16]

Experimental Section

Our dielectric constant measurements were made by the capacity method. Following the method of Baldwin and Gill[3] we have measured the capacity of a condenser with an impedance bridge. This choice was conditioned by the characteristics of the high-pressure bomb at our disposition. In order to avoid loss of precision special care was taken with regard to two experimental points. First, parasitic parallel capacitance can be a serious cause of error; our cell design eliminated problems from this quarter. Second, because the impedance is a function both of capacitance (c) and conductance (G), high precision capacitance measurements are not possible if the ammonia has even trace amounts of ionic (or ionizable) impurities. Thus particular care was taken in purifying the ammonia.

The cell consisted of two concentric cylinders constructed of stainless steel with the following dimensions: outer cylinder exterior diameter 59.8 mm, interior diameter 51.2 mm, height 50.0 mm; inner cylinder exterior diameter 56.0 mm, interior diameter 53.4 mm, height 30.0 mm. Thus the space between the two plates was 6 mm.

Gaps smaller than this risk serious difficulties arising from capillary effects and trapped bubbles. The outer cylinder was longer than the inner cylinder by 10 mm at each end in order to minimize edge effects. The cylinders were placed in a cylindrical cell of Teflon which served to fix the cylinders in relationships to one another. Appropriate channels were constructed in the Teflon to allow for circulation of the ammonia, escape of bubbles between the inox plates, and connection of insulated wires to the plates.

This assembly was then placed in a grounded stainless steel bomb. Appropriate provisions were made for magnetic stirring. It was found that this form of agitation could be augmented by the pumping of ammonia.

Measurements of capacitance and conductance were made simultaneously, utilizing a Wayne Kerr B 641 impedance bridge (frequency 1522 Hz, resolution 0.01% of full scale).

Because of the temperature range considered the vessel containing the cell as described was a high-pressure reactor which was made of stainless steel along with its accessories which include apparatus for control of liquid level and pressure values for filling and emptying, etc.

Temperature was controlled to ±0.02°C with a proportional regulator and a resistance heater located on the inside of the reactor. For temperatures lower than ambient, the outside of the reactor was cooled by circulation of cold alcohol.

Ammonia is a difficult substance to maintain at high purity levels. Our ammonia was purified by distilling over sodium to obtain maximum dehydration. It was then distilled into a storage cylinder containing sodium amide. This method has been used by Kraus to maintain the ammonia in a perfectly anhydrous state, in addition the use of this slightly soluble salt restricted contamination of the distillate by the dehydrating agent to negligible levels. After each series of measurements four to five successive distillations were necessary in order to obtain a conductivity less than 5×10^{-7} ohm^{-1} cm^{-1} at 20°C.

For calibration we first tried to measure the capacitance of the cell under vacuum and with 1 atm of helium as a function of temperature utilizing the method of Baldwin and Gill. However, these results were not of sufficient accuracy. Therefore we utilized n-hexane and chlorobenzene (Carlo Erba pure reagents kept under molecular sieve). The dielectric constant of both of these substances has been measured by Smyth and Morgan[17] in the range of temperatures of interest. This calibration also permitted verifying that the cell did not have measurable parasitic capacitance.

Results

The values of dielectric constant which we obtained are shown in Table I. Measurements were made in four series. Each series contains a succession of points taken as a function of both increasing and decreasing temperature. The ammonia was siphoned out and redistilled between each series ensuring that the conductivity remained approximately 2.5×10^{-7} at −30°C, 5×10^{-7} at +20°C, and 1×10^{-6} ohm^{-1} cm^{-1} at +50°C. In the table column 1 shows the series number, column 2 the temperature, and column 3, the average value of the cell capacitance under vacuum as deduced from calibration with hexane and chlorobenzene. Column 4 is the apparent capacitance under vacuum

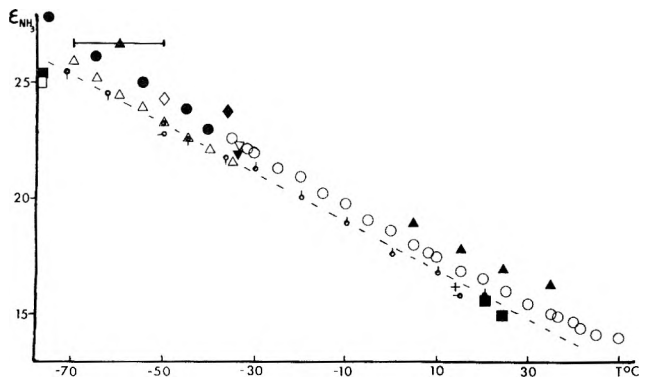

Figure 1. Dielectric constant of liquid ammonia: (●) ref 1; (▲) ref 2; (△) ref 3; (■) ref 4; (+) ref 5; (▽) ref 6; (◇) ref 7; (▼) ref 8; (◆) ref 9; (□) ref 10; (-○-) ref 11; (♀) ref 12; (◇) ref 13; (- - -) "best values" of ref 14 and 15; (○) our values.

as measured by n-hexane minus the apparent capacitance under vacuum as measured by chlorobenzene. Because these differences are very slight and the signs are not constant we concluded that parasitic capacitance is negligible. Columns 5 and 6 are the measured capacitance and dielectric constant of ammonia.

Discussion

The new results are compared in Figure 1 with those already existing. A thorough discussion of these data has been made by Cronenwett.[14,15] Data obtained by various authors above 3000 MHz have not been included because the measurement techniques are questionable at these frequencies.[14] The new results fit very well with those of Breitschwerdt, Zintl, and Hooper. Grubb's data are isolated at higher values. The values obtained by Burow, Baldwin, Hasted, Palmer, and Schlundt are lower by 4–8%.

Such deviations can be accounted for by edge effects, parallel capacitance, and by calibration procedures. In the beginning of this work, when edge effects and parallel capacitance through the Teflon holders were not minimized, a calibration of the cell with benzene always resulted in a lower value for the dielectric constant of other liquids (for example, nitromethane). In order to avoid this difficulty the cell was designed as described above and two liquids of different dielectric constants were used for a double calibration. In this case it has been possible to prove that these effects had become negligible.[16] Moreover calibration of the cell has been made at each experimental temperature (Table I). The same care was not taken by Burow, Baldwin, Hasted, Palmer, and Schlundt. The work of Baldwin is also questionable for the purity of ammonia.

The accuracy of our data gives significance to the slight curvature of the dielectric constant vs. temperature curve. Cronenwett[14,15] had made a best provisional estimate by drawing a straight line through the results of Burow and Hasted. Our results can be summarized by the following parabolic equation where t is the temperature in degrees centigrade

$$\epsilon = 16.024 - 9.483 \times 10^{-2}(t - 25) + 2.6 \times 10^{-4}(t - 25)^2$$

with this equation the standard deviation is 0.08. The results also fit the exponential equation

$$\epsilon = 4.515 \exp(-T/171.2)$$

where T is the absolute temperature. However the standard deviation, 0.10, is slightly greater than with the parabolic equation.

TABLE I

Series no.	T, °C	C_0, pF	ΔC_0, pF	C_{NH_3}, pF	ϵ_{NH_3}
1	50.0	78.39	0.61	1098	14.01
2	45.0	78.26	0.45	1109	14.17
3	41.5	78.18	0.40	1125	14.39
1	40.0	78.18	0.22	1155	14.77
3	36.5	78.35	0.17	1168	14.91
2	35.0	78.15	0.34	1176	15.05
1	30.0	78.34	0.19	1215	15.51
2	25.0	78.63	−0.10	1260	16.03
1–2	20.0	79.00	−0.09	1312	16.61
3	15.0	80.46	−0.06	1356	16.85
1	10.0	81.07	0.02	1420	17.52
3	8.0	81.29	−0.05	1435	17.65
2	5.0	81.61	−0.01	1468	17.99
1	0.0	82.03	−0.20	1529	18.64
2	−5.0	82.47	−0.41	1577	19.12
1–4	−10.0	82.84	−0.52	1643	19.83
2	−15.0	83.55	−0.54	1691	20.24
1	−20.0	84.09	−0.35	1762	20.95
2	−25.0	84.73	−0.66	1815	21.42
3	−30.0	85.36	−0.22	1880	22.01
1	−31.7	85.74	−0.12	1907	22.24
1	−35.0	86.16	0.18	1950	22.63

Application to Metal–Ammonia Solution

In a previous paper[18] a peculiar behavior had been found for the association of alkali cations and solvated electrons into ion pairs. The association decreases with the increasing temperature from −65 to −35°C. The association increases with increasing temperature from 0 to 25°C.

Along the terms of Bjerrum's theory the association increases when the Bjerrum distance (or $(\epsilon T)^{-1}$) increases and when the distance a (of "closest approach") decreases. With the present values of ϵ, the variations in the product ϵT are negligible from −65 to −35°C ($\epsilon T = 5.4 \times 10^3$). The Bjerrum distance remains therefore almost constant. In this range, the distance a increases sharply with increasing temperature.[18] The later increase is sufficient to account for the decrease of the association with increasing temperature.

The product ϵT decreases from −35 to +25°C (where $\epsilon T = 4.6 \times 10^3$). The Bjerrum distance increases and is responsible for increasing association. However its variation is not sufficient to account for the magnitude of the effect. A simultaneous decrease of a would be necessary. No data are available on a at these temperatures, but a decreasing solvation with increasing temperature is reasonable.

As a conclusion the temperature dependence of the dielectric constant is partly but only partly responsible for the behavior of the association. A larger role has to be played by the distance parameter a, which is related to the solvation of cation and electron.

Acknowledgments. The authors are grateful to W. T. Cronenwett who has made his discussion of previous data[15] available at Colloque Weyl IV and to G. Lepoutre who has revised and rewritten the Discussion of the present paper. They also thank the referee who suggested a fit of the results to an exponential expression.

References and Notes

(1) K. G. Breitschwerdt and W. Schmidt, *Z. Naturforsh A*, **25**, 1467 (1970).

(2) H. M. Grubb, J. F. Chittum, and H. Hunt, *J. Am. Chem. Soc.*, **58**, 776 (1936).
(3) J. Baldwin and J. B. Gill, *Phys. Chem. Liquids*, **2**, 25 (1970).
(4) R. C. Palmer and H. Schlundt, *J. Phys. Chem.*, **15**, 381 (1911).
(5) W. D. Coolidge, *Ann. Phys.*, **305**, 125 (1899).
(6) G. S. Hooper, and C. A. Kraus, *J. Am. Chem. Soc.*, **56**, 2265 (1934).
(7) E. Zintl and S. Neumayr, *Ber. Dtsch, Chem. Ges.*, **63**, 237 (1930).
(8) H. M. Goodwin and M. Thompson, *Phys. Rev.*, **8**, 38 (1899).
(9) J. Sedlet and T. De Vries, *J. Am. Chem. Soc.*, **73**, 5808 (1951).
(10) C. P. Smyth and C. S. Hitchcock, *J. Am. Chem. Soc.*, **56**, 1804 (1934).
(11) H. Schlundt and O. C. Schaefer, *J. Phys. Chem.*, **16**, 253 (1912).
(12) D. F. Burow, Ph.D. Dissertation, University of Texas, 1966.
(13) J. B. Hasted and S. H. Tirmazi, *J. Chem. Phys.*, **50**, 4116 (1969).
(14) W. T. Cronenwett, School of Electrical Engineering Report No. OUEE-WTC-1973-01, College of Engineering, University of Oklahoma, Norman, Okla., 1973.
(15) W. T. Cronenwett, "Measurements of the Low Frequency Dielectric Constant of Liquid Ammonia", submitted to Colloque Weyl IV, Michigan State University, July 1975.
(16) For more details see G. Billaud, "Constantes diélectriques de l'ammoniac liquide", D.E.A. Universite de Lille-I, France, Oct 1974.
(17) C. P. Smyth and S. O. Morgan, *J. Am. Chem. Soc.*, **50**, 1547 (1928).
(18) A. Demortier, M. De Backer, and G. Lepoutre, *J. Chim. Phys.*, **69**, 380 (1972).

Alkali Metal Species in Liquid Amines, Ammonia, and Ethers. Formation by Pulse Radiolysis†

J. W. Fletcher* and W. A. Seddon

Physical Chemistry Branch, Atomic Energy of Canada Limited, Chalk River Nuclear Laboratories, Chalk River, Ontario K0J 1J0 *(Received July 23, 1975)*

Publication costs assisted by Atomic Energy of Canada Limited

Pulse radiolysis of solutions of alkali metal cations in methylamine, ethylamine, liquid ammonia, tetrahydrofuran, and diethyl ether demonstrates the formation of solvated electrons, e_s^-, ion pairs (M^+, e_s^-), and alkali metal anions M^-. This paper correlates previous work and presents kinetic evidence for the formation of a triple ion intermediate (Na_2^{2+}, e_s^-) in the formation of Na^- in methylamine. Studies on the formation of Na^- in metal–ethylamine or –methylamine solutions containing trace amounts of Na^+ show a marked difference in the rate depending on the metal in excess. Evidence is presented which suggests the formation of a complex with sodium in Li, Mg, or Ca solutions, whereas in K, Cs, or Rb solutions, the reaction proceeds via the corresponding K^-, Cs^-, or Rb^- species. The spectrum of (Na^+, e_s^-) has been investigated in binary mixtures of THF–ethylamine and ethylamine–ammonia. In each case, a single absorption is observed, which shows a shift in the band maximum to a wavelength intermediate to that obtained in pure solvents. The effects of ammonia on the formation of, and equilibrium between, (M^-, e_s^-) and M^- in ethylamine are also discussed.

Introduction

A comprehensive introduction to the subject of alkali metal solutions in liquid ammonia, amines, and ethers is contained in the proceedings of Colloque Weyl I, II, and III.[1-3] Numerous investigations have demonstrated that in general at least three species, the solvated electron e_s^-, ion pairs (M^+, e_s^-), or M and alkali metal anions M^- coexist in equilibrium.

$$e_s^- + M^+ \rightleftharpoons (M^+, e_s^-) \text{ or } M \quad (1)$$

$$(M^+, e_s^-) + e_s^- \rightleftharpoons M^- \quad (2)$$

Absorption spectra characteristic of e_s^- [4-8] and M^- [7-11] are well established, but it is only recently that flash photolysis[11-15] and pulse radiolysis[16-20] studies have demonstrated the existence of transient absorption bands attributed to (M^+, e_s^-). However, very little is known about the corresponding rate or equilibrium constants associated with reactions such as (1) and (2) since the alkali metal systems are normally observed at equilibrium. Using pulse radiolysis in conjunction with fast infrared detectors,[21-23] it is now possible to obtain this type of information by first producing e_s^- and then observing the subsequent formation of metal dependent species.

This paper describes work on the effect of solvent, alkali metal, crown ether (dicyclohexyl-18-crown-6), mixed solvent, and mixed metals on the overall equilibria and absorption spectra of e_s^-, (M^+, e_s^-), and M^- in methylamine, ethylamine, liquid ammonia, tetrahydrofuran (THF), and diethyl ether (DEE).

Experimental Section

Detailed accounts of the pulse radiolysis techniques and solvent preparations have been described elsewhere.[17,20,24,25] Briefly, solutions were irradiated in either Pyrex or quartz flow systems with 0.3- to 1-μsec pulses of electrons from a 2.5-MeV Van de Graaff accelerator. Optical absorptions were monitored in rectangular quartz cells with an optical path length of 0.5–2.0 cm.

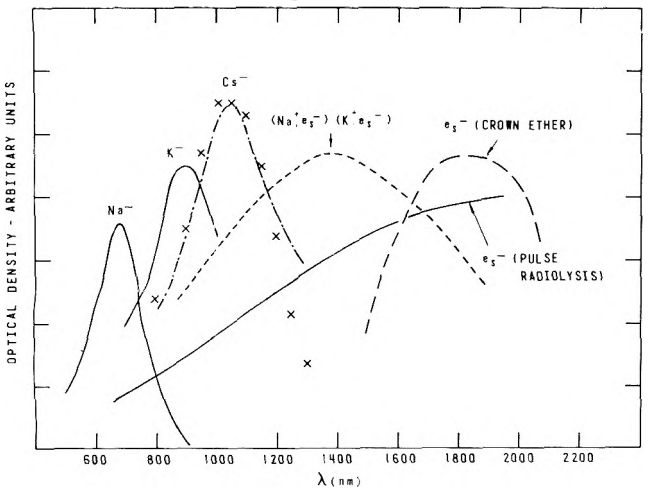

Figure 1. Optical absorption spectra observed in ethylamine. Pulse radiolysis; Na^-, K^-, and Cs^- (crosses, difference spectrum from Figure 2) observed in solutions containing sodium, potassium, or cesium ethylamide. Solid e_s^- line obtained in pure or basic solutions in the absence or presence of crown ether; - - - - represents the spectrum observed in sodium or potassium ethylamide, $NaBPh_4$, $NaAlH_4$, or $KBPh_4$ solutions. Experimental points are omitted because of close overlap. Alkali metal solutions at equilibrium: — —, Na or K solutions plus crown ether: – • – • – • –, Cs solutions (ref 27). The e_s^- spectra are normalized relative to each other at 1600 nm, while the remainder are arbitrarily enhanced to different peak heights for clarity in presentation. See text and ref 17 for further details.

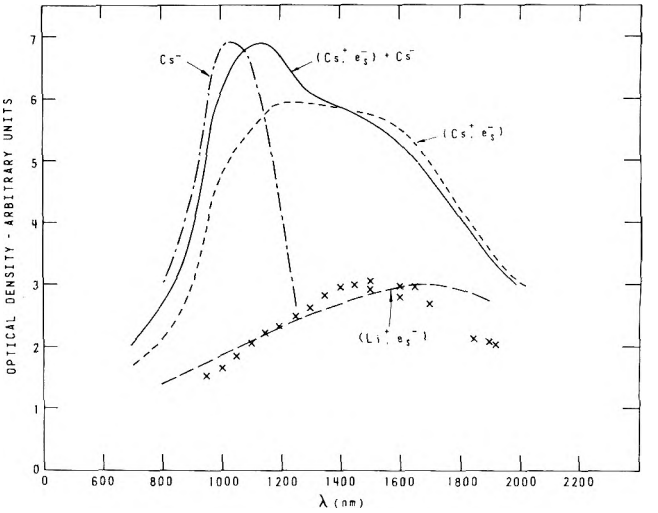

Figure 2. Optical absorption spectra observed by pulse radiolysis in lithium and cesium solutions in ethylamine, $\sim 6 \times 10^{-5}$ *M* cesium ethylamide; solid (≥ 7 μsec) and - - - - - (2.5 μsec) lines are normalized relative to each other at 1400 nm. The difference spectrum due to Cs^- (– • – • –) is arbitrarily normalized to a peak height of 6.9 units for clarity: dashed line, $\sim 10^{-3}$ *M* lithium ethylamide solutions; ×, ~ 0.1 *M* $LiAlH_4$. See text and ref 17 for further details.

Results and Discussion

Spectra. General Review. Optical spectra of alkali metal solutions in amines and ethers at equilibrium are in general composed of two absorption bands ascribed to metal-dependent and metal-independent species.[7-9] The former or "visible" band maximum occurs at relatively short wavelengths, ≤ 1100 nm, and is assigned to the species of stoichiometry M^-.[7-10] The latter band is often much broader and extends further into the infrared with a pronounced solvent dependence of both the maximum and band shape.[8]

Until recently it has been common to assign this infrared component to the solvated electron.[26-28] This is supported by comparisons of the spectra of metal solutions with those obtained by pulse radiolysis and flash photolysis.[7,8,14,21] However, the agreement is not exact, and it has been noted[7,8] that the metal solution bands are in general broader and at slightly higher energies than those found by pulse radiolysis. Furthermore, the pulse radiolysis solutions were not always completely free of alkali cations since it was necessary to add base ($\sim 10^{-4}$ *M*) to prevent rapid reaction of e_s^- with oxidizing species produced by the pulse.[7]

It has been emphasized, therefore, that the shape and band width of the infrared absorption may also be concentration dependent, because of either the formation of spin-paired species or of ion-paired species.[7-9] Consequently, correlations between pulse radiolysis of solutions of alkali metals and alkali metal solutions at equilibrium are more difficult to interpret unambiguously than was originally supposed.

With the possible exception of solutions containing crown ether or cryptate,[7,8] which can shift the equilibria in favor of e_s^-, the infrared absorption band is, in our view, more likely a composite spectrum with the proportions of e_s^-, (M^+, e_s^-), or M^- being dependent on the solvent and alkali metal. Comparisons relating to e_s^- spectra would be most reliable at infinite dilution, a region effectively covered by pulse radiolysis, but difficult to achieve with alkali metal systems.

In our pulse radiolysis experiments we have, therefore, investigated the spectra as a function of time both in the pure solvent and in the presence of alkali metal salts. Details of specific systems are discussed below.

Ethylamine. Figures 1 and 2 show the absorption spectra obtained at room temperature by pulse radiolysis in pure, slightly basic ($\geq 10^{-4}$ *M* CH_3CH_2NHM, where M = Li, Na, K, or Cs) and solutions containing $\geq 10^{-4}$ *M* $NaAlH_4$, $LiAlH_4$, salts of tetraphenylboron ($NaBPh_4$, $KBPh_4$), or crown ether in ethylamine.

In pure or basic solutions, a broad infrared absorption due to e_s^- is observed immediately after the pulse.[17] The "maximum" occurs at ≥ 1800 nm, but cannot be clearly resolved owing to the large solvent absorption at longer wavelengths. This "peak" is, however, consistent with that attributed to e_s^- in alkali metal ethylamine solutions containing crown ether[8] (dashed line in Figure 1). However, in the latter case the overall envelope has a different shape, indicating that crown ether may also modify the initial e_s^- spectrum. This phenomenon is also observed in THF and DEE (see below).

In basic solutions the initial e_s^- absorbance is followed by a further substantial growth in absorption which shows a slight, but distinct shift in the maximum toward the blue. This growth is first order with the rate dependent on the nature of the alkali metal ethylamide. The absorption then subsequently decays (except for Li) with the concomitant second-order formation of the corresponding long-lived M^- species.[17] Both the growth and decay are eliminated in the presence of an excess of crown ether, and only the broad initial spectrum due to e_s^- is observed (Figure 1).

We conclude therefore that this transient, blue-shifted, infrared band corresponds to the formation of an ion-pair intermediate (M^+, e_s^-). For sodium and potassium solutions this species has a maximum at 1400 nm.

This assignment is supported in that identical spectra are observed immediately after the pulse in ethylamine solutions containing $\geq 10^{-4}$ *M* $NaBPh_4$ or $KBPh_4$ or 10^{-2} *M*

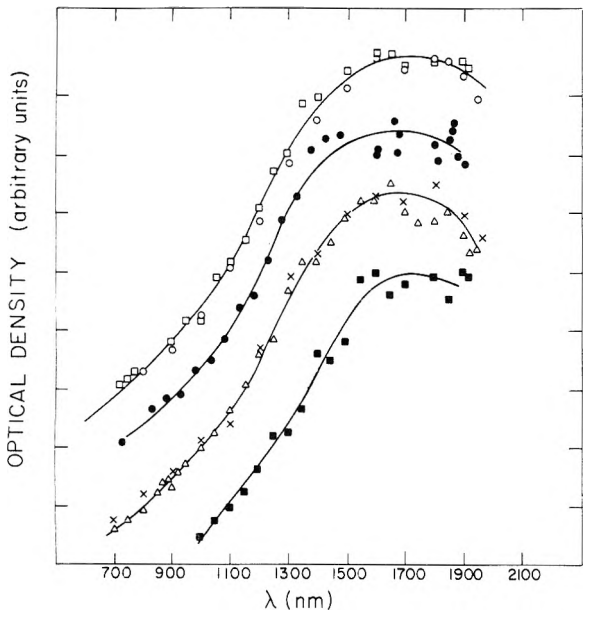

Figure 3. Optical absorption spectra observed immediately after the pulse in pure methylamine, $\leq 10^{-5}$ *M* alkali metal methylamide solutions and solutions containing $\sim 10^{-3}$ *M* CH_3NHK and $\sim 10^{-3}$ *M* crown ether: (●) pure CH_3NH_2, (■) K with crown ether, (O) Li, (□) Na, (△) K, (×) Cs. The curves are normalized to a common peak height but arbitrarily displaced for clarity.

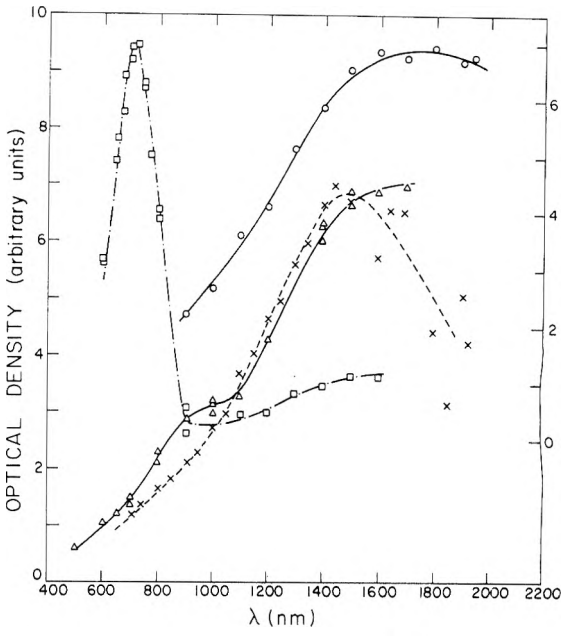

Figure 4. Optical absorption spectra observed 400 μsec after the pulse in $\geq 10^{-3}$ *M* alkali metal methylamide solutions in methylamine: (O) Li, (□) Na, (△) K, (×) Cs. The curves are normalized to a peak height of 6.9 units but with O and □ displaced 2.5 units for clarity (right-hand scale).

$NaAlH_4$. In these systems the initial ion-pair absorption decays completely on a microsecond time scale with only a small amount of Na^- being detected in $NaAlH_4$ or $NaBPh_4$ solutions. In this respect the results are similar to those observed in THF[20] where, in the absence of base, the ion pairs disappear by reaction with radiolytically produced radicals.

In lithium ethylamide solutions the corresponding ion-pair maximum is shifted toward 1600–1700 nm (Figure 2). As indicated by ESR,[9,29] it is likely that this latter absorption contains an equilibrium contribution from e_s^- which may mask the true peak due to (Li^+, e_s^-). The 1600–1700-nm peak position correlates well with the band maximum of 1400 nm reported for lithium solutions at −17°C and the temperature coefficient of ~6 nm/deg.[9] In $LiAlH_4$ solutions the spectrum observed immediately after the pulse shows a gradual shift toward the blue with the maximum changing from ~1800 to 1500 nm with increasing concentration from 10^{-4} to 10^{-1} *M*. This again is consistent with the formation of (Li^+, e_s^-), the spectrum of which is very similar to that of (Na^+, e_s^-) and (K^+, e_s^-). Unlike $NaAlH_4$ solutions, no evidence is observed for the formation of a long-lived species analogous to Na^-.

For $\sim 6 \times 10^{-5}$ *M* cesium ethylamide solutions (Figure 2), the long time scale (≥ 7 μsec) spectrum very closely resembles the steady-state spectrum observed in cesium–ethylamine solutions.[9] In this case we believe the maximum at 1100 nm is due to a contribution from Cs^-, while the broad long-wavelength shoulder, which is more predominant at shorter time scales (2.5 μsec), is largely due to an equilibrium mixture of (Cs^+, e_s^-) and Cs^-. The difference between the short and long time scale spectra does, in fact, correspond to that expected for Cs^-.[8]

In summary, our results suggest that in ethylamine[17] the true e_s^- absorption has a maximum at ≥1800 nm, while the infrared bands at 1400–1600 nm, formerly assigned to e_s^-,[26-28] are, in fact, predominantly due to ion-pair formation. The visible bands attributed to M^- are consistent with those observed in alkali metal solutions.

Methylamine. The spectra observed in methylamine–methylamide solutions are, in some respects, significantly different from those obtained in ethylamine. Figure 3 shows the e_s^- spectrum obtained immediately after the pulse in pure methylamine, dilute solutions ($\leq 10^{-5}$ *M*) of lithium, sodium, potassium, or cesium methylamide, and 10^{-3} *M* potassium methylamide solutions containing excess crown ether. In each case the maximum is difficult to resolve because of solvent absorption. However, the "peak" appears to be somewhat better defined than in ethylamine with a slight blue shift toward ~1700 nm. It is significant that the intensity represented by $G_{e_s^-}\epsilon_{1700} \sim 8 \times 10^4$ is about four times greater than the corresponding value obtained in ethylamine.[17] ($G_{e_s^-}\epsilon_{1700}$ is the product of *G*, the radiation chemical yield in units of molecules per 100 eV, and ϵ_{1700} the molar decadic extinction coefficient at 1700 nm.) Taking $G_{e_s^-} \sim 2$[30] and assuming the same general spectral shape as found for e_s^- in ND_3,[25] we estimate an oscillator strength for e_s^- in methylamine of ~1.

A similar oscillator strength would be expected for e_s^- in ethylamine. However, since $G_{e_s^-}$ is also ~2,[30] this implies that the absorption maximum must be further into the infrared than is the case for methylamine. The absence, in pulse radiolysis, of a clearly resolved e_s^- peak in ethylamine is consistent with this view and draws further attention to the modifying effect, in alkali metal solutions, of crown ether on the overall band shape.

Following the pulse, the infrared absorption again continues to increase in intensity and, with the exception of sodium methylamide solutions, shows no decay over a period of ≤1 msec. Figure 4 shows the spectra observed 400 μsec after the pulse for $\geq 10^{-3}$ *M* solutions of lithium, sodium, potassium, and cesium methylamide. The infrared "peak" at ~1700 nm remains independent of the alkali metal for Li, Na, and K and shows no distinct shift from that due to e_s^-. A blue shift to 1500 nm is observed with Cs, and in K

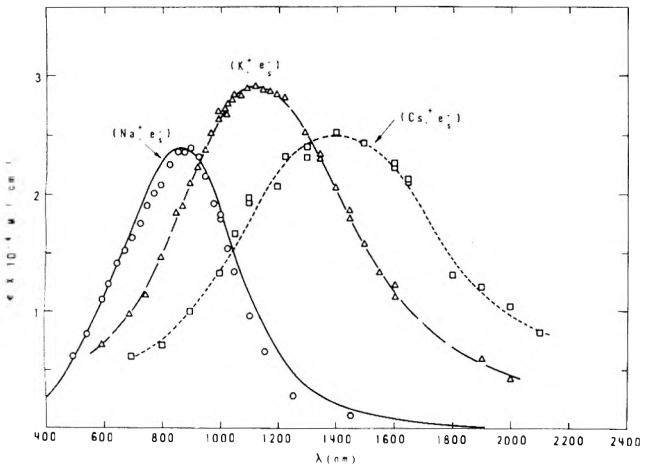

Figure 5. Ion-pair absorption spectra observed immediately after the pulse in solutions containing $NaBPh_4$, $KBPh_4$ or $CsBPh_4$: O, (Na^+, e_s^-); △, (K^+, e_s^-); □, (Cs^+, e_s^-). The solid line represents the spectrum of (Na^+, e_s^-) observed by Bockrath and Dorfman.[18]

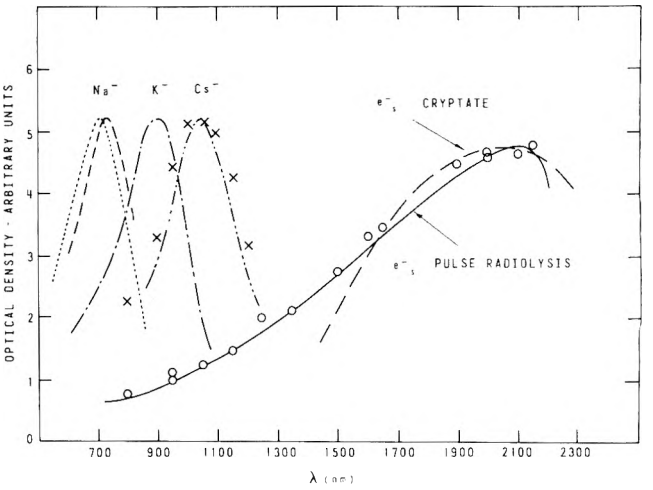

Figure 6. Optical absorption spectra observed in THF. Alkali metal solutions at equilibrium in the presence of crown ether or cryptate (ref 8): — —, e_s^- and Na^-; - • - • -, K^- (identical spectrum observed in pure K solutions, ref 20); - •• - •• -, Cs^-. Pulse radiolysis: O, pure THF; - - - -, $NaAlH_4$ solutions; ×, in ethylamine for comparison. The solid line represents the spectrum from ref 21 normalized to open circles at 2100 nm. The e_s^- cryptate spectrum is normalized to the same e_s^- peak height.

solutions a shoulder, due to K^-, is evident at 900 nm.

The relative predominance and stability of the potassium infrared bands are consistent with absorption spectra observed by others in potassium–methylamine solutions[31] and contrast sharply with the behavior in ethylamine solutions described in the previous section and in ref 17 and 31.

For Cs solutions the shift to ~1500 nm may be due to the presence of some unresolved Cs^-.

In Na solutions the infrared band decays completely to form Na^-.

We conclude again that the enhanced infrared absorption is due to the formation of the corresponding ion pairs (M^+, e_s^-). Furthermore, the equilibria in methylamine (except for Na) are predominantly in favor of (M^+, e_s^-). The lack of a significant change in the spectral shape with ion-pair formation is comparable to the situation observed in ethylenediamine[21,32-34] and liquid ammonia[7,25,35] (see below).

Ammonia. The results obtained by pulse radiolysis in pure and basic ammonia solutions are quite different from those observed in amines. Using potassium or sodium amide solutions in ND_3, the absorption consists of an initial transient followed by a rapid decay to a long-lived component.[25]

At −15°C the initial absorption has a maximum at 1500 nm, while the spectrum of the long-lived absorption, observed after 150 μsec, has a maximum shifted slightly to 1640 nm. We concluded that the initial absorption was equivalent to that of e_s^- at infinite dilution,[36] whereas the residual absorption represented a composite of two or more, overlapping bands corresponding to e_s^- and a metal–electron species.[25]

The latter suggestion is consistent with the conclusion deduced in Na–NH_3 solutions that the infrared absorption band, previously attributed to e_s^-, can be resolved into two components.[37,38] In this case the species absorbing at the longer wavelengths is considered to contain two solvated electrons.[38]

In progressing from ammonia to methylamine to ethylamine, the general trend in the e_s^- absorption maximum at room temperature is toward the red, whereas the maximum arising from electron association with alkali metal cations appears to be more toward the blue.

Tetrahydrofuran. Since the solubility of alkali metals is low (~2×10^{-6}) in THF, solutions of alkali metal ions were prepared from the more soluble tetraphenylboron salts (Na, K, Cs) or the aluminum hydride salts (Li, Na). Studies of such solutions provide the clearest optical evidence for the formation and conversion of e_s^- to (M^+, e_s^-) and ultimately M^-.[18-20] Figures 5 and 6 show the spectra of e_s^-, (Na^+, e_s^-), (K^+, e_s^-), (Cs^+, e_s^-), and Na^- as observed by pulse radiolysis.[4,18-21] Superimposed in Figure 6 is the spectrum of e_s^- as obtained in the presence of cryptate along with the spectra of Na^-, K^-, and Cs^- in the presence of crown ether or cryptate.[8] While peaking at about the same wavelength, the e_s^- cryptate spectrum is again (compare ethylamine) a different shape from that observed by pulse radiolysis.

Spectra indistinguishable from that of e_s^- in pure THF were obtained in the presence of $LiAlH_4$ or LiCl, although $G\epsilon$ at 2000 nm increases with solute concentration.[20] It was suggested that this represented the formation of (Li^+, e_s^-), but recent experiments[39] indicate this species has a maximum at 1180 nm.

Diethyl Ether. The optical spectrum of e_s^- observed by pulse radiolysis in DEE[4,5,21] is similar to that in THF and again slightly different from that observed in the presence of cryptate.[7,8,40] However, (as shown in Figure 7) the addition of $NaBPh_4$ (~10^{-4} *M*) or a saturated mixture of $NaAlH_4$–$LiAlH_4$, shifts the absorption maximum to ~700 nm, corresponding to that expected for Na^-. Unlike THF, no evidence was obtained for (Na^+, e_s^-), unless coincidentally, both species were to absorb at the same wavelength in DEE. Extinction coefficients for each species in the different solvents are summarized in Table I.

Mixed Solvents. In view of the considerable wavelength difference in the band maximum of (Na^+, e_s^-) from THF to ethylamine to ammonia, it was of interest to examine this shift as a function of solvent composition. Figure 8 shows the spectral shift for THF–ethylamine mixtures containing ~10^{-4} *M* $NaBPh_4$. Similar behavior was noted for ethylamine–ammonia mixtures containing ~10^{-3} *M* sodium or potassium amides. In each case only a single band is observed, the maximum of which is at a wavelength inter-

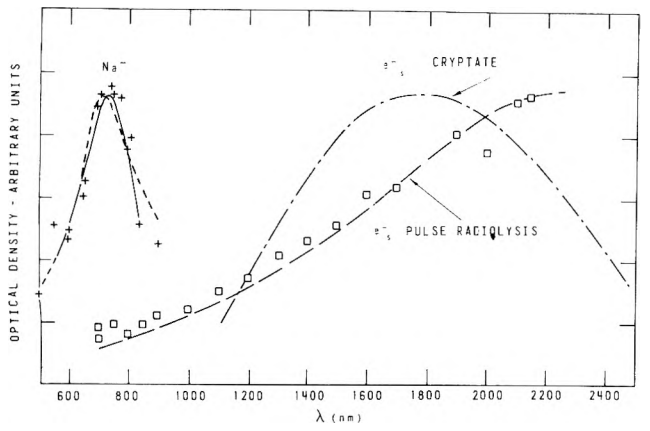

Figure 7. Optical absorption spectra observed in DEE. Alkali metal solutions at equilibrium in the presence of crown ether or cryptate (ref 8, 40): – • – • –, e_s^-; - - - -, Na^-; solid line, in THF for comparison. Pulse radiolysis: □, pure DEE; +, solutions containing ~10^{-4} *M* $NaBPh_4$ or saturated with $NaAlH_4$ and $LiAlH_4$; – – – –, spectrum from ref 4 and 5 normalized to open squares at 2100 nm. The e_s^- cryptate spectrum is normalized to the same e_s^- peak height.

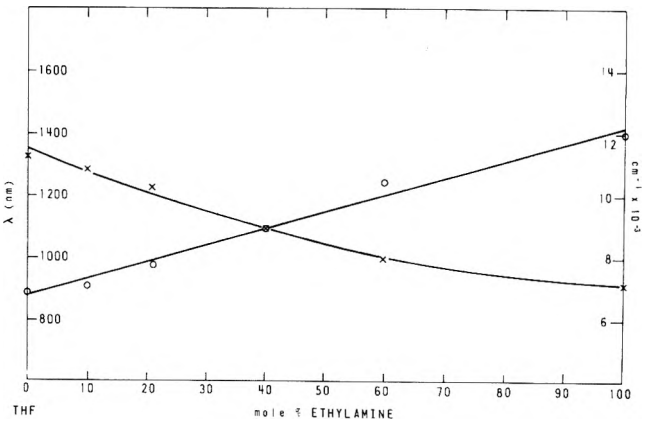

Figure 8. Optical absorption maximum in terms of wavelength or wavenumber for (Na^+, e_s^-) obtained immediately after the pulse in THF–ethylamine mixtures containing 10^{-4} *M* $NaBPh_4$: O, nm, X, cm^{-1}.

mediate to that observed in the pure components. This change with composition is similar to the situation observed for the optical absorption spectrum of e_s^- in similar binary solutions[4,5] and indicates that the ion-pair spectrum is largely dependent upon the aggregate properties of the mixture and not a selective solvation process. A correlation can also be made between the shift in band maximum for the ion pair and the observed hyperfine splitting constant in THF–ethylamine mixtures.[41] In such solutions the percent atomic character decreases from THF to ethylamine and parallels the shift in frequency. This trend can be extended to other solvents. For example, in ammonia the ion-pair optical spectrum is very similar to that of e_s^-, and likewise its percent atomic character is very small. In general (for the solvents used in our work), as the blue shift associated with ion-pair formation increases from that of the parent e_s^-, so does the hyperfine constant.[7,42,43] As noted above, (Na^+, e_s^-) in DEE may absorb at the same wavelength as Na^-. This would require an even greater blue shift than observed in THF, which would be consistent with ESR data from dioxane–ethylamine mixtures which show the largest percent atomic character.[41]

Within experimental error the bandwidth for THF–ethylamine mixtures remains constant at 7000 cm^{-1} throughout the entire composition range. For ethylamine–ammonia mixtures the bandwidth gradually decreases to ~3500 cm^{-1} in pure ammonia.

In the amine–ammonia system the ion-pair spectra appear to be virtually independent of the cation, whereas in THF a significant dependence on cation is observed.[18,20,39]

It is interesting to note that, unlike e_s^- and (M^+, e_s^-), the M^- spectra observed in our work show no large solvent dependence. However, a dependence on solvent composition has recently been observed for alkali metal solutions in mixtures of ethylenediamine and hexamethylphosphoric acid.[44]

Reaction Kinetics. Formation of (M^+, e_s^-). In the kinetic analysis of these systems, two important features should be recognized. First, the radiolytic experiments are complicated by the existence of competing radical or solvent positive ion processes,[20] and, second, very little information exists concerning the dissociation constants (K_d) of the dissolved salts and hence the effective concentration of M^+ in solution.

TABLE I: Molar Extinction Coefficient at the Band Maximum (× 10^{-4} M^{-1} cm^{-1})

Solvent	e_s^-	(M^+, e_s^-)	M^-	Ref
Ethylamine	~1.0[a]	1.9–3.5[b]	7.5–9.6[b]	17
		2.4[a]		This work with $NaBPh_4$
Methylamine	~4.0[a]	2.5–3.8[b]	9.2–10.0[b]	This work, 56
Ammonia	4.9			68
THF	4–5	2.4–2.9		4, 18, 20
DEE	3.5			4

[a] Assumes $G_{e_s^-} \sim 2$. [b] $-G_{(M^+,e_s^-)} = 4.8$ (ref 30).

TABLE II: Rate Constants for the Formation of (M^+, e_s^-) in Different Solvents

Alkali metal	Rate constant, k_1, M^{-1} sec^{-1}		
	Methylamine[a]	Ethylamine[a]	THF[d]
Li	5 × 10^6	4 × 10^6	
Na	2 × 10^8	1.2 × 10^9 [b]	7.8 × 10^{11}
K	1.2 × 10^7	1.6 × 10^8 [c]	4.6 × 10^{11}
Cs	1 × 10^9	2 × 10^{10}	~5 × 10^{11}

[a] Based on total concentration of RNHM. [b] Estimated $\geq 10^{10}$ M^{-1} sec^{-1} in $NaBPh_4$ solutions (see text). [c] Estimated $\geq 10^9$ M^{-1} sec^{-1} in $KBPh_4$ solutions (see text). [d] References 18–20.

Studies of dilute solutions of lithium, sodium, potassium, and cesium alkylamides in methylamine and ethylamine[17] show that the rate of formation of (M^+, e_s^-) is first order and consistent with reaction 1.

$$e_s^- + M^+ \rightarrow (M^+, e_s^-) \quad (1)$$

However, $K_d = 4 \times 10^{-7}$ *M* for CH_3NHK in methylamine at −62.2°C,[45] and therefore it is likely that the methyl- and ethylamides are predominantly associated at room temperature. Consequently, we make no attempt to distinguish between reaction 1 and 3.

$$e_s^- + RNHM \rightarrow RNH^- + (M^+, e_s^-) \quad (3)$$

For comparative purposes, values for the rate constant k_1 (Table II) are based on the total concentration of alkylamide in solution.

In general, such rate constants increase significantly in the series lithium–cesium and are an order of magnitude less in methylamine than the corresponding values in ethylamine. We believe that such differences are, in part, due

to differing degrees of dissociation for the appropriate alkylamides.

Support for this latter contention is indicated by the appearance of the (Na^+, e_s^-) and (K^+, e_s^-) spectrum at the end of the pulse in ethylamine solutions containing $\sim 10^{-4}$ M $NaBPh_4$ or $\sim 10^{-3}$ M $KBPh_4$. This implies that k_1 for Na^+ in ethylamine should be $\geq 10^{10}$ M^{-1} sec^{-1}, and hence K_d for $NaBPh_4 \geq 10^{-5}$ $M > K_d$ for CH_3NHNa. Similarly k_1 for K^+ is on this basis probably $>10^9$ M^{-1} sec^{-1}. The entries in Table II show these estimates.

In THF, assuming the dissociation constants of 8.22×10^{-5}, 3.22×10^{-5} and 1.87×10^{-6} M for $NaBPh_4$, $KBPh_4$ and $CsBPh_4$, respectively,[18,20] the pseudo-first-order rate constant k_1 is proportional to the concentration of free M^+ and not to the concentration of salt. In this case k_3 appears to be much slower than k_1.

The significant differences in k_1 between THF and the amines again suggest that the latter values are, in effect, lower limits which are subject to revision when the appropriate K_d values are established. Overall it is difficult to rationalize these apparent trends because of the complexities of ion and ion-pair solvation processes[46,47] and triple ion and aggregate formation.[48-51] In liquid ammonia, for example, K_d for the amide salts at −33.5°C increases from Na to K and/or Cs,[52] whereas for the corresponding nitrate salts the reverse is true.[53,54]

Formation of M^-. The kinetics of formation of M^- have been investigated recently by pulse radiolysis in ethylenediamine,[33] ethylamine,[17] and THF,[20] and earlier by flash photolysis in dimethoxyethane,[11,55] THF,[55] and ethylamine.[27] However, earlier investigations[27,55] need reinterpretation in view of the complication arising from incorrect spectral assignments which did not recognize the presence of Na^-.

It is important to note that the nature of the added salt has a significant role in the overall radiolytic processes leading to the formation of M^-. In THF appreciable concentrations of M^+ can only be added in the form of soluble salts such as $NaBPh_4$ or $NaAlH_4$. In $NaBPh_4$ solutions, (Na^+, e_s^-) disappears almost entirely by reaction with radiolytically produced radicals, whereas in ~ 1 M $NaAlH_4$ solutions, about 25% of the (Na^+, e_s^-) decays to produce Na^-.[19,20]

Qualitatively similar observations are obtained in DEE and in $\sim 10^{-2}$ M $NaAlH_4$ solutions in ethylamine, whereas, in ethylamide solutions[17] and methylamide solutions, the conversion from (Na^+, e_s^-) to Na^- appears to be quantitative.

In basic solutions of ethylenediamine,[33] ethylamine,[17] and methylamine, the formation of Na^- is second order and consistent with an overall pseudo-second-order reaction

$$e_s^- + e_s^- \overset{Na^+}{\rightleftharpoons} Na^- \qquad (4)$$

Significant differences in rate are observed in the three solvents with k_4 in $\sim 10^{-4}$ M alkylamide solutions varying respectively from 1×10^8 to 1.6×10^9 and 1×10^{10} M^{-1} sec^{-1} in ethylenediamine, methylamine, and ethylamine. (The value of 2.4×10^{10} quoted in ref 17 assumed $G_{e_s^-} = 2.0$, whereas later experiments give $G_{e_s^-} = 4.8$.[30])

For potassium solutions, the corresponding value in ethylamine is 6.2×10^9 M^{-1} sec^{-1}, and that in methylamine is too slow, $\leq 10^4$ M^{-1} sec^{-1}, to be measured by our technique.

In potassium solutions in THF[20] and DEE[11] the formation of K^- is consistent with the reactions

$$e_s^- + K^+ \rightleftharpoons (K^+, e_s^-) \qquad (5)$$

$$(K^+, e_s^-) + e_s^- \rightleftharpoons K^- \qquad (6)$$

whereas in solutions containing Na^+ [20] it is necessary to invoke reaction 8 in addition to the analogous reactions 7 and 9.

$$e_s^- + Na^+ \rightleftharpoons (Na^+, e_s^-) \qquad (7)$$

$$(Na^+, e_s^-) + (Na^+ + e_s^-) \rightarrow Na^+ + Na^- \qquad (8)$$

$$(Na^+, e_s^-) + e_s^- \rightarrow Na^- \qquad (9)$$

A similar sequence was considered in ethylenediamine but subsequently rejected, since k_4 was observed to be independent of other cations, in favor of the reactions

$$e_s^- + e_s^- \rightleftharpoons e_2^{2-} \qquad (10)$$

$$e_2^{2-} + Na^+ \rightarrow Na^- \qquad (11)$$

However, studies on mixed metal solutions in ethylamine (see below) demonstrate that the formation of Na^- can occur via the formation of M^- and subsequent electron transfer processes to Na^+.

More detail will be presented elsewhere,[56] but Figure 9 shows a comparison of k_4 as observed in methylamine and ethylenediamine.[33] In the case of ethylenediamine, the Na^+ concentration refers to the total concentration of added sodium (metal plus salt). In methylamine we have assumed that added NaI is fully dissociated since the halide salts are, in liquid ammonia, two to three orders of magnitude more dissociated than the corresponding amides.[53] We have taken K_d for $CH_3NHNa = 2 \times 10^{-5}$ M since this gave the best fit judged by the slope at the lowest Na^+ concentrations in Figure 9-1. The solid curves in Figure 9 represent the calculated best fit to the data based on reactions 7 to 9 and the rate constants summarized in Table III. It can be seen that this mechanism fits the ethylenediamine results equally as well as the one composed of reactions 10 and 11 (dotted line, Figure 9-2).[33]

These calculations imply that K_7^{-1} for reaction in methylamine is about two orders of magnitude less than that in ethylenediamine. Values for K_1^{-1} have been determined by conductance measurements for Li, K, Cs, and Rb in ethylenediamine[32] and Cs in methylamine[57] and are typically about 1×10^{-4} M. The conductance behavior of Na solutions differs markedly from that of solutions of the other alkali metals, and therefore conductance data cannot be used to deduce an equilibrium constant for sodium for comparison with our pulse radiolysis estimates.

In THF the corresponding ion pairs are much less dissociated with estimates for K_1^{-1} in the range 3×10^{-8} to 3×10^{-7} M for both (Na^+, e_s^-) and (K^+, e_s^-).[12,18,20]

Using the computer program WR20,[58] we therefore sought to check the validity of the reaction sequence 7 to 9 in methylamine by comparing the calculated formation and decay of (Na^+, e_s^-) and Na^- with experiment. It was shown, however, that no one set of rate constants would predict the observed effects of increasing Na^- on the build-up and decay of (Na^+, e_s^-) or the concomitant formation of Na^-.[56]

To resolve this difficulty we are forced to invoke the formation of a triple ion,[48-50] such as (Na_2^{2+}, e_s^-), which can perhaps be regarded as analogous to the triple ions suggested in polymerization processes.[59,60]

TABLE III: Reactions and Rate Constants Used to Calculate the Best Fit to the Data Points Shown in Figures 9-1 and 9-2

Reaction	Rate constant: Methylamine	Rate constant: Ethylenediamine
(7) $e_s^- + Na^+ \rightarrow (Na^+, e_s^-)$	$1.0 \times 10^8\ M^{-1}\ sec^{-1}$	$3.3 \times 10^7\ M^{-1}\ sec^{-1}$
(−7) $(Na^+, e_s^-) \rightarrow e_s^- + Na^+$	$1.2 \times 10^4\ sec^{-1}$	$5.0 \times 10^5\ sec^{-1}$
(8) $(Na^+, e_s^-) + (Na^+, e_s^-) \rightarrow Na^- + Na^+$	$2.0 \times 10^9\ M^{-1}\ sec^{-1}$	$1.5 \times 10^9\ M^{-1}\ sec^{-1}$
(9) $(Na^+, e_s^-) + e_s^- \rightarrow Na^-$	$6.7 \times 10^9\ M^{-1}\ sec^{-1}$	$5.0 \times 10^9\ M^{-1}\ sec^{-1}$

$$(Na^+, e_s^-) + Na^+ \rightleftharpoons (Na_2^{2+}, e_s^-) \quad (12)$$

This additional species must also absorb in the infrared but have a lower extinction coefficient than (Na^+, e_s^-) at 1400 nm. Likewise it must also react in a manner analogous to (Na^+, e_s^-) to produce Na^-.

$$(Na_2^{2+}, e_s^-) + e_s^- \rightarrow Na^- + Na^+ \quad (13)$$

$$(Na_2^{2+}, e_s^-) + (Na^+, e_s^-) \rightarrow Na^- + 2Na^+ \quad (14)$$

$$(Na_2^{2+}, e_s^-) + (Na_2^{2+}, e_s^-) \rightarrow Na^- + 3Na^+ \quad (15)$$

At low methylamide concentrations and/or high doses per pulse, additional refinements are necessary to account for the reaction of e_s^- and metal–electron species with radiolytically produced radicals. For example

$$e_s^- + R \rightarrow \text{product} \quad (16)$$

$$(Na^+, e_s^-) \text{ or } (Na_2^{2+}, e_s^-) \text{ or } Na^- + R \rightarrow \text{product} \quad (17)$$

For a given dose per pulse this effect decreases with increasing concentrations of methylamide, suggesting that the solvent base differs from other solute anions in that the radicals (or geminate and parent positive ions) are converted into a less reactive basic form. For example

$$CH_2NH_2 + CH_3NH^- \rightarrow CH_2{=}NH^- + CH_3NH_2 \quad (18)$$

$$CH_3NH_2^+ + CH_3NH^- \rightarrow \dot{C}H_2{-}NH_2 + CH_3NH_2 \quad (19)$$

$$CH_3NH_3^+ + CH_3NH^- \rightarrow 2CH_3NH_2 \quad (20)$$

In summary, Table IV lists the various reactions, rate constants, and extinction coefficients we have found necessary to obtain satisfactory agreement with experiment as a function of dose per pulse and Na^+ concentration. However, we do not imply that the reactions and rate constants proposed here represent a unique solution since more information is obviously needed on solute and ion-pair dissociation constants, or aggregates, before further detail is justified.

Formation of Na^- in Solutions Containing Other Alkali Metals. Regardless of the metal used in the preparation, it is now well established that in alkali metal solutions the presence of trace amounts of Na^+ results in the formation of Na^-.[9,61,62] In an effort to resolve the main features of this process, we have monitored the formation of Na^- in methylamine and ethylamine in solutions containing varying amounts of Na^+ and an excess of lithium, potassium, cesium, rubidium, magnesium, or calcium methyl- or ethylamides.

The results can be separated into two categories, those involving K, Cs, and Rb, and those involving Li, Mg, and Ca. In the former category, there is clear evidence for the initial formation of the corresponding M^- species of the metal in excess. This, in turn, decays with the concomitant formation of Na^- by an overall second-order process.

$$M^- \xrightarrow{Na^+} Na^- + M^+ \quad (21)$$

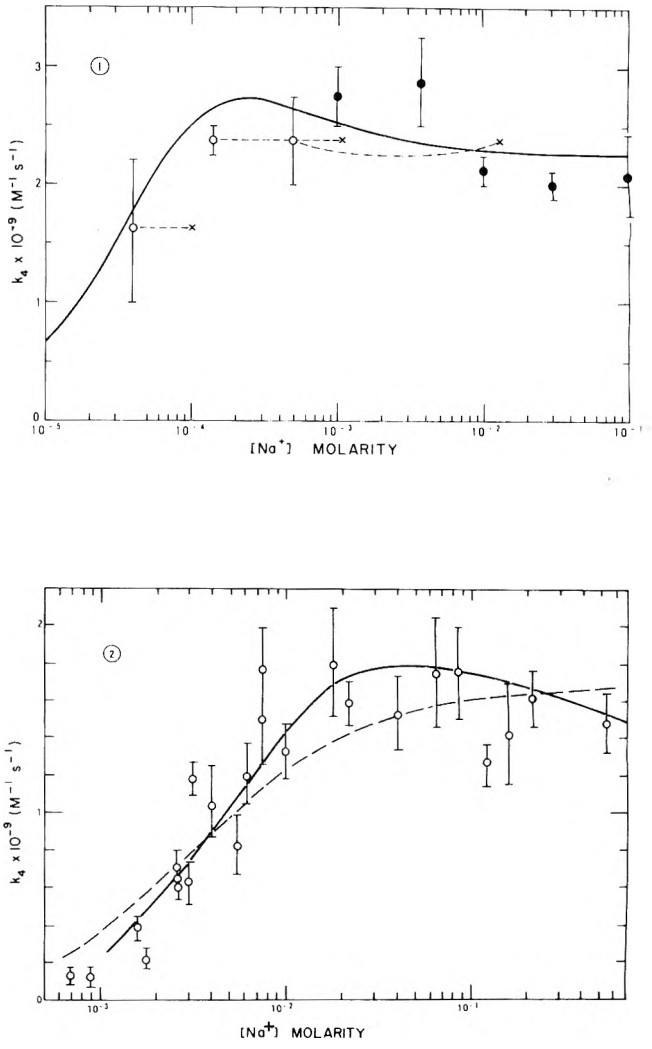

Figure 9. Pseudo-second-order rate constants for the formation of Na^- by reaction 4 in methylamine and ethylenediamine. (1) Methylamine: O, Na^+ added as CH_3NHNa taking $K_d = 2 \times 10^{-5}$ *M*; ×, total CH_3NHNa concentration (dotted lines show relative displacement); ●, Na^+ added as $\sim 5 \times 10^{-4}$ *M* CH_3NHNa + NaI and assumes fully dissociated NaI. The solid line represents the calculated best fit using the rate constants in Table III and K_d (CH_3NH_2Na) = 2×10^{-5} *M*. (2) Ethylenediamine: Na^+ added as NaBr plus sodium, potassium, or cesium ethylenediamide; see ref 33 for details. The dotted line was calculated[33] on the basis of reactions 10 and 11 and the solid line according to reactions 7 to 9 (see text).

The kinetics are obviously complex but probably proceed via the intermediate formation of (Na^+, e_s^-) and (M^+, e_s^-)

$$M^- + Na^+ \rightleftharpoons (Na^+, e_s^-) + (M^+, e_s^-) \quad (22)$$

For potassium–sodium solutions this would be consistent with both ESR[9,42,63,64] and optical spectra[9,62] provided that the subsequent reactions of (Na^+, e_s^-) with itself or e_s^- are significantly faster than the corresponding (K^+, e_s^-) reactions. Evidence for this behavior has been noted in

TABLE IV: Reactions, Rate Constants, and Extinction Coefficients Used in the Computer Simulation of the Pulse Radiolysis of CH_3NHNa in CH_3NH_2

	Reaction	Rate constant
(7)	$e_s^- + Na^+ \rightarrow (Na^+, e_s^-)$	$2.0 \times 10^8\ M^{-1}\ sec^{-1}$
(−7)	$(Na^+, e_s^-) \rightarrow e_s^- + Na^+$	$3.0 \times 10^3\ sec^{-1}$
(9)	$(Na^+, e_s^-) + e_s^- \rightarrow Na^-$	$2.0 \times 10^9\ M^{-1}\ sec^{-1}$
(−9)	$Na^- \rightarrow (Na^+, e_s^-) + e_s^-$	$8.0 \times 10^2\ sec^{-1}$
(8)	$(Na^+, e_s^-) + (Na^+, e_s^-) \rightarrow Na^- + Na^+$	$2.0 \times 10^9\ M^{-1}\ sec^{-1}$
(12)	$(Na^+, e_s^-) + Na^+ \rightarrow (Na_2^{2+}, e_s^-)$	$5.0 \times 10^7\ M^{-1}\ sec^{-1}$
(−12)	$(Na_2^{2+}, e_s^-) \rightarrow (Na^+, e_s^-) + Na^+$	$1.2 \times 10^5\ sec^{-1}$
(13)	$(Na_2^{2+}, e_s^-) + e_s^- \rightarrow Na^- + Na^+$	$6.7 \times 10^9\ M^{-1}\ sec^{-1}$
(14)	$(Na_2^{2+}, e_s^-) + (Na^+, e_s^-) \rightarrow Na^- + 2Na^+$	$6.7 \times 10^9\ M^{-1}\ sec^{-1}$
(15)	$(Na_2^{2+}, e_s^-) + (Na_2^{2+}, e_s^-) \rightarrow Na^- + 3Na^+$	$2.0 \times 10^9\ M^{-1}\ sec^{-1}$
(16)	$e_s^- + R \rightarrow$ product	$6.6 \times 10^{10}\ M^{-1}\ sec^{-1}$
(17)	$(Na^+, e_s^-) + R \rightarrow$ product	$6.6 \times 10^{10}\ M^{-1}\ sec^{-1}$
	$(Na_2^{2+}, e_s^-) + R \rightarrow$ product	$1.0 \times 10^{10}\ M^{-1}\ sec^{-1}$
	$Na^- + R \rightarrow$ product	$1.0 \times 10^{10}\ M^{-1}\ sec^{-1}$
(18)	$R + CH_3NH^- \rightarrow CH_2{=}NH^- + CH_3NH_2$	$3.3 \times 10^9\ M^{-1}\ sec^{-1}$
	$R + R \rightarrow$ product	$6.6 \times 10^{10}\ M^{-1}\ sec^{-1}$

Species	$G\epsilon$[a] 680 nm	1485 nm
e_s^-	1.0×10^4	8.0×10^4
(Na^+, e_s^-)	1.0×10^4	2.0×10^5
(Na^{2+}, e_s^-)	1.0×10^4	8.0×10^4
Na^-	2.4×10^5	

[a] $G(e_s^-) = 4.8$; $G(R) = 5.4$.

THF.[11,20] In general the overall rate of formation of Na^- is not significantly different from that expected in solutions containing just Na^+.

In the second, or "alkaline earth" category, the situation is much different. Here the metals Li, Mg, or Ca considerably decrease the rate of Na^- formation from that observed in pure Na^+ solutions of the same concentration. In these solutions, the Na^+ appears to be associated with the excess metal such that the unassociated Na^+ in solution is drastically reduced. We are forced to speculate that some complex or triple amide ion aggregates[48-50] are formed in these solutions. The Na^- is then formed at a rate dependent on the e_s^-–(M^+, e_s^-) equilibrium characteristics of the "alkaline earth" system and the dissociation constant of the complex.

For example, in lithium solutions the equilibrium mixture contains predominantly (Li^+, e_s^-). However, in the presence of Na^+ ions the rate of formation of the infrared absorption is greater than in pure lithium solutions, but much less than in pure sodium solutions.[17] This suggests the formation of (Na^+, e_s^-) from the equilibrium mixture via reaction 7, rather than via the reaction

$$(Li^+, e_s^-) + Na^+ \rightarrow (Na^+, e_s^-) + Li^+ \qquad (23)$$

Subsequent Na^- formation presumably can occur via a sequence of reactions such as indicated in Table IV.

Further studies on these systems are continuing, but the present results certainly indicate their complexity and that normal competition kinetics based on initial concentrations simply do not apply.

Formation of (M^+, e_s^-) and M^- in Mixed Ethylamine–Ammonia Solutions. From the results so far, it is clear that both solvent and cation have a significant effect on the rate of formation of (M^+, e_s^-) and M^- and their respective equilibrium concentrations. Strongly solvating media such as ammonia shift the equilibria toward e_s^-, whereas in THF and, to a progressively lesser extent, from ethylamine to methylamine, the equilibrium is displaced in favor of M^-. Solutions containing Na^+ (except NH_3) give entirely Na^-, whereas K^+ and Cs^+ solutions give mixtures of M^- and (M^+, e_s^-), the proportion of M^- decreasing from ethylamine to methylamine.

It was of interest, therefore, to see to what extent the trend toward ammonia-like properties from ethylamine to methylamine could be observed in mixtures of ethylamine and ammonia. In such mixtures containing either sodium or potassium amides, we find that the initial $G\epsilon_{1450}$ and the rate of buildup of (M^+, e_s^-) both increase with ammonia concentration. In Na solutions both the yield and rate of formation of Na^- decrease with increasing concentrations ($\leq$20 mol %) of ammonia, whereas in K solutions, K^- is not observed at concentrations $\geq$10 mol % NH_3.

These observations are consistent with a shift of the overall equilibrium toward e_s^- and (M^-, e_s^-), with the effect more pronounced in K solutions as might be expected from previous ESR[42,63-67] studies and our pulse radiolysis data. Work is continuing on the more detailed kinetics in such mixtures.

Summary

Pulse radiolysis of solutions of alkali metal cations demonstrates the formation of transient infrared absorption bands attributed to the ion pairs (M^+, e_s^-). The THF, the band maxima are metal dependent and widely separated from that of e_s^-, whereas in amines and ammonia the converse is true. In mixed solvent systems, the ion-pair spectra lie at wavelengths intermediate to those observed in the pure components.

With the exception of lithium solutions, the ion pairs subsequently decay with the concomitant formation of M^-, the final equilibrium being both solvent and cation dependent. The overall kinetics are complex, but in methylamine the evidence suggests a triple ion (Na_2^{2+}, e_s^-) is an intermediate in the formation of Na^-. In solutions of Na^+ and Li^+, Mg^+ or Ca^+, a complex with Na^+ limits the rate of formation of Na^-, whereas in K^+, Cs^+, or Rb^+–Na^+ mixtures

the reaction proceeds via the corresponding K^-, Cs^-, or Rb^- species.

Acknowledgments. The authors are indebted to Messrs. E. B. Selkirk, F. C. Sopchyshyn, and J. J. Jevcak for their technical assistance throughout this work.

References and Notes

†AECL No. 5277.
(1) G. Lepoutre and M. J. Sienko, Ed., "Metal-Ammonia Solutions", Colloque Weyl I, W. A. Benjamin, New York, N.Y., 1964.
(2) J. J. Lagowski and M. J. Sienko, Ed., "Metal-Ammonia Solutions". Colloque Weyl II (IUPAC), Butterworths, London, 1970.
(3) J. Jortner and N. R. Kestner, Ed., "Electrons in Fluids", Colloque Weyl III, Springer-Verlag, Berlin, 1973.
(4) F. Y. Jou and L. M. Dorfman, *J. Chem. Phys.*, **58**, 4715 (1973).
(5) L. M. Dorfman and F. Y. Jou in ref 3, p 447.
(6) J. F. Gavlas, F. Y. Jou, and L. M. Dorfman, *J. Phys. Chem.*, **78**, 2361 (1974).
(7) J. L. Dye in ref 3, p 77.
(8) M. T. Lok, F. J. Tehan, and J. L. Dye, *J. Phys. Chem.*, **76**, 2975 (1972).
(9) I. Hurley, T. R. Tuttle, Jr., and S. Golden in ref 2, p 449.
(10) S. Matalon, S. Golden, and M. Ottolenghi, *J. Phys. Chem.*, **73**, 3098 (1969).
(11) S. H. Glarum and J. H. Marshall, *J. Chem. Phys.*, **52**, 5555 (1970).
(12) M. Fisher, G. Ramme, S. Claesson, and M. Szwarc, *Chem. Phys. Lett.*, **9**, 309 (1971).
(13) M. Fisher, G. Ramme, S. Claesson, and M. Szwarc, *Proc. R. Soc. London, Ser. A*, **327**, 481 (1972).
(14) L. J. Giling, J. G. Kloosterboer, R. P. H. Rettschnick, and J. D. W. van Voorst, *Chem. Phys. Lett.*, **8**, 457 (1971).
(15) J. G. Kloosterboer, L. J. Giling, R. P. H. Rettschnick, and J. D. W. van Voorst, *Chem. Phys. Lett.*, **8**, 462 (1971).
(16) J. W. Fletcher, W. A. Seddon, and F. C. Sopchyshyn, *Chem. Phys. Lett.*, **18**, 592 (1973).
(17) J. W. Fletcher, W. A. Seddon, and F. C. Sopchyshyn, *Can. J. Chem.*, **51**, 2975 (1973).
(18) B. Bockrath and L. M. Dorfman, *J. Phys. Chem.*, **77**, 1002 (1973).
(19) G. A. Salmon and W. A. Seddon, *Chem. Phys. Lett.*, **24**, 366 (1974).
(20) G. A. Salmon, W. A. Seddon, and J. W. Fletcher, *Can. J. Chem.*, **52**, 3259 (1974).
(21) L. M. Dorfman, F. Y. Jou, and R. Wageman, *Ber. Bunsenges. Phys. Chem.*, **75**, 681 (1971).
(22) W. A. Seddon, E. B. Selkirk, and J. W. Fletcher, *Int. J. Radiat. Phys. Chem.*, **5**, 323 (1973).
(23) J. H. Baxendale, C. Bell, and J. Mayer *Int. J. Radiat. Phys. Chem.*, **6**, 117 (1974).
(24) W. A. Seddon, C. Willis, M. J. Young, and E. B. Selkirk, Atomic Energy of Canada Limited Report AECL-3853.
(25) W. A. Seddon, J. W. Fletcher, J. Jevcak, and F. C. Sopchyshyn, *Can. J. Chem.*, **51**, 3653 (1973).
(26) H. Blades and J. W. Hodgins, *Can. J. Chem.*, **33**, 411 (1955).
(27) M. Ottolenghi, K. Bar-Eli, and H. Linschitz, *J. Chem. Phys.*, **43**, 206 (1965).
(28) J. L. Dye and R. R. Dewald, *J. Phys. Chem.*, **68**, 135 (1964).
(29) K. Bar-Eli and T. R. Tuttle, Jr., *J. Chem. Phys.*, **40**, 2508 (1964).
(30) W. A. Seddon, J. W. Fletcher, F. C. Sopchyshyn, and J. J. Jevcak, *Can. J. Chem.*, **52**, 3269 (1974).
(31) K. Bar-Eli and G. Gabor, *J. Phys. Chem.*, **77**, 323 (1973).
(32) R. R. Dewald and J. L. Dye, *J. Phys. Chem.*, **68**, 128 (1964).
(33) J. L. Dye, M. G. DeBacker, J. A. Eyre, and L. M. Dorfman, *J. Phys. Chem.*, **76**, 839 (1972).
(34) J. L. Dye, M. G. DeBacker, and L. M. Dorfman, *J. Chem. Phys.*, **52**, 6251 (1970).
(35) J. L. Dye in ref 2, p 1.
(36) I. Hurley, T. R. Tuttle, Jr., and S. Golden in ref 2, p 503.
(37) T. R. Tuttle, Jr., G. Rubinstein, and S. Golden, *J. Phys. Chem.*, **75**, 3635 (1971).
(38) G. Rubinstein, T. R. Tuttle, Jr., and S. Golden, *J. Phys. Chem.*, **77**, 2872 (1973).
(39) B. Bockrath and L. M. Dorfman, *J. Phys. Chem.*, **79**, 1509 (1975).
(40) J. L. Dye, M. T. Lok, F. J. Tehan, R. B. Coolen, N. Papadakis, J. M. Ceraso, and M. G. DeBacker, *Ber. Bunsenges. Phys. Chem.*, **75**, 659 (1971).
(41) R. Catterall, personal communication.
(42) R. Catterall, J. Slater, and M. C. R. Symons in ref 2, p 329.
(43) R. Catterall, M. C. R. Symons, and J. W. Tipping in ref 2, p 317.
(44) P. S. Childs and R. R. Dewald, *J. Phys. Chem.*, **79**, 58 (1975).
(45) E. Rochard and J. Raviore, *J. Chim. Phys.*, **68**, 1183 (1971).
(46) M. Szwarc, *Prog. Phys. Org. Chem.*, **6**, 323 (1968).
(47) M. Szwarc, *Acc. Chem. Res.*, **2**, 87 (1969).
(48) R. M. Fuoss and C. A. Kraus, *J. Am. Chem. Soc.*, **55**, 21, 476, 1019, 2387 (1933).
(49) N. L. Cox, C. A. Kraus, and R. M. Fuoss, *Trans. Faraday Soc.*, **31**, 749 (1935).
(50) C. A. Kraus, *J. Phys. Chem.*, **58**, 673 (1954).
(51) H. S. Harned and B. B. Owen, "The Physical Chemistry of Electrolytic Solutions", Reinhold, New York, N.Y., 1958, p 297.
(52) R. Delmas, P. Courvoisier, and J. Ravoire, *Adv. Chem. Ser.*, **No. 89**, 25 (1969); R. Delmas, Report CEA-R-3377, CEN, Saclay.
(53) A. M. Monoszon and V. A. Pleskov, *Z. Phys. Chem., Abt. A*, **156**, 176 (1931).
(54) A. M. Monoszon and V. A. Pleskov, *Zh. Fiz. Khim.*, **3**, 221 (1932).
(55) J. Eloranta and H. Linschitz, *J. Chem. Phys.*, **38**, 2214 (1953).
(56) J. W. Fletcher, W. A. Seddon, J. J. Jevcak, and F. C. Sopchyshyn, *Can. J. Chem.*, in press.
(57) R. R. Dewald and K. W. Browall, *J. Phys. Chem.*, **74**, 129 (1970).
(58) K. H. Schmidt, Argonne National Laboratory Report ANL-7693.
(59) D. N. Bhattacharyya, J. Smid, and M. Szwarc, *J. Am. Chem. Soc.*, **86**, 5024 (1964).
(60) D. N. Bhattacharyya, C. L. Lee, J. Smid, and M. Szwarc, *J. Phys. Chem.*, **69**, 612 (1965).
(61) I. Hurley, T. R. Tuttle, Jr., and S. Golden, *J. Chem. Phys.*, **48**, 2818 (1968).
(62) M. G. DeBacker and J. L. Dye, *J. Phys. Chem.*, **75**, 3092 (1971).
(63) R. Catterall, J. Slater, and M. C. R. Symons, *J. Chem. Phys.*, **52**, 1003, (1970).
(64) R. Catterall in ref 2, p 479.
(65) L. R. Dalton, J. D. Rynbrandt, E. M. Hansen, and J. L. Dye, *J. Chem. Phys.*, **44**, 3969 (1966).
(66) R. Catterall, M. C. R. Symons, and J. W. Tipping, *J. Chem. Soc. A*, 1529 (1966).
(67) R. Catterall, M. C. R. Symons, and J. W. Tipping, *J. Chem. Soc. A*, 1234 (1967).
(68) D. F. Burow and J. J. Lagowski, *Adv. Chem. Ser.*, **No. 50**, 125 (1965).

Discussion

R. CATTERALL. In the comparison made between the shift in the optical band of M^+e^- in pulsed $EtNH_2$–THF mixtures with the corresponding change in the A_{iso} value for the metal solutions in the same mixtures, the agreement is quite temperature dependent. In Figure 1D we have the variation of A_{iso} with temperature for these solvent mixtures. The data used by Dr. Fletcher were at 20°C. If we used data at a somewhat higher temperature, the deviation from linearity in the A_{iso} composition plot would be less and the agreement better. What temperature were your optical measurements made?

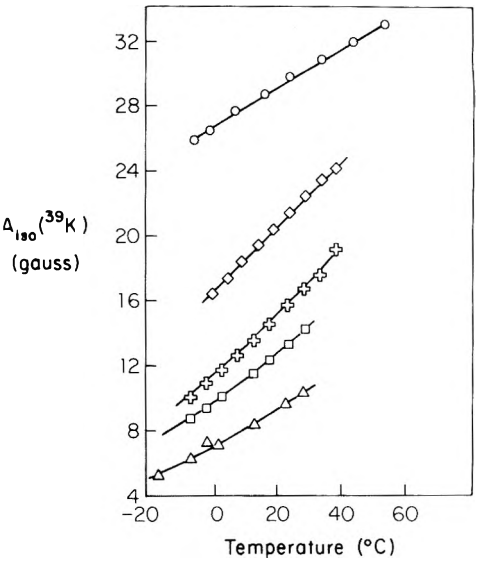

Figure 1D. Temperature dependence of the ^{39}K hyperfine splitting constant for solutions of potassium in ethylamine–tetrahydrofuran (THF) mixed solvents containing 1.0 (○), 0.8 (◇), 0.56 (+), 0.31 (□), and 0.0 (△) mole fraction of THF.

J. W. FLETCHER. Our results were at ≃25°C.

J. V. ACRIVOS. Evidence for the existence of a triple ion $Na^+ \cdot S^- \cdot Na^+$ has been observed (J. V. Acrivos, *J. Chem. Phys.*, **47**, 5389 (1967)) by ESR. In alcohol solutions for S^- ≡ *p*-benzosemiquinone the species is stable at t = 15°C and the hyperfine structure at low magnetic fields suggest a D_{2h} point symmetry for the complex.

J. W. FLETCHER. Can you also relate this to the triple ions $[M^+(base^-)M^+]$ referred to by Fuoss?

J. V. ACRIVOS. Yes.

U. SCHINDEWOLF. The evidence of M^- cannot be doubted any more under certain experimental conditions so I raise the question about H^-; is it stable in the solutions and does it absorb light as Na^-, K^-, etc., do? During electrolysis in, e.g., ether between two sodium electrodes, will sodium dissolve at the cathode forming anions or at the anode forming cations or on both sides?

Comment: Pulse radiolysis should be done in connection with polarography to get other than optical evidence for M^- formation; it also would yield redox potentials.

J. W. FLETCHER. H^- is not stable in these solutions.

J. L. DYE. The major remaining difference between the results of pulse radiolysis and of metal solution studies is the difference in the ir band of e_s^- and of metal solutions with crown or cryptand present. This may tell us something about the nature of the species in the latter case. We must remember that the metal solutions are several orders of magnitude more concentrated in the reducing species (10^{-4} to 10^{-3} M) than in pulse radiolysis so we may have e_2^{2-} or $e^-{\cdot}M{\cdot}e^-$ or other spin-paired species.

Spectra of the Solvated Electron Coupled with Metal Cations. Lithium in Tetrahydrofuran

Bradley Bockrath, James F. Gavlas, and Leon M. Dorfman*

Department of Chemistry, The Ohio State University, Columbus, Ohio 43210 *(Received July 23, 1975)*

Publication costs assisted by the U.S. Energy Research and Development Administration

Our purpose in this paper is to present some recent data on the aggregation of the solvated electron with alkali metal cation for one specific system, namely lithium in tetrahydrofuran. We had reported earlier[1] the results of pulse radiolysis investigations of the nature of the aggregation of e_{sol}^- with sodium in ethylenediamine. More recently, the solvated electron in tetrahydrofuran[2] and its ion pair with sodium[3] were reported from our laboratory. Coupling of e_{sol}^- with K^+ and with Cs^+ has been reported by Salmon et al.[4] In their work[4] it was concluded that, although the ion pair (Li^+,e_{sol}^-) might be formed, its spectrum in tetrahydrofuran was indistinguishable from that of e_{sol}^-.

We find,[5] to the contrary, that the ion pair (Li^+,e_{sol}^-) formed in tetrahydrofuran exhibits an absorption band with maximum at 1180 nm. The molar extinction coefficient at the maximum is 2.3×10^4 M^{-1} cm^{-1}, which gives an oscillator strength of 0.9 for the band. This absorption band is shown in Figure 1, in which data for three lithium salts, $LiClO_4$, LiBr, and LiCl, obtained by two investigators, are seen to clearly define the band. Evidence for the identity of this band has been presented.[5] Because of the similarity of this band to that of (K^+,e_{sol}^-),[4] we have taken the trouble to show, by atomic absorption analyses, that the potassium content of the solutions was below 0.04 ppm and could not possibly have entered into observable reaction on the time scale of our experiments.

The absorption maximum of 1180 nm for (Li^+,e_{sol}^-) may be compared with 890 nm for sodium,[3] 1125 nm for potassium,[4] 1400 nm for cesium,[4] and 2120 nm for the solvated electron[2] itself in THF. The smaller shift, from e_{sol}^-, for Li^+ than for Na^+ may be the result of a greater degree of solvation of the former cation in THF than of the latter.

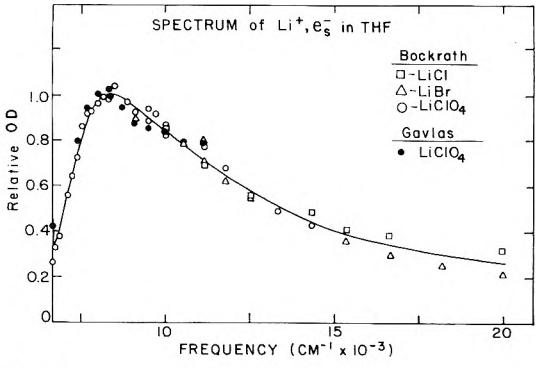

Figure 1.

Absolute rate constants for the reaction of (Li^+,e_{sol}^-) with anthracene, biphenyl, and dibenzylmercury in THF, at 25°C, were found to be 2.65×10^{10}, 1.00×10^{10}, and 1.8×10^{10} M^{-1} sec^{-1}, respectively. The latter two values are twofold higher than the corresponding rate constants for (Na^+,e_{sol}^-)[3,6] and an order of magnitude lower than the corresponding rate constants[3,6] for e_{sol}^-.

Acknowledgment. This work was supported by the United States Energy Research and Development Administration.

References and Notes

(1) J. L. Dye, M. G. DeBacker, J. A. Eyre, and L. M. Dorfman, *J. Phys. Chem.*, **76**, 839 (1972).
(2) L. M. Dorfman, F. Y. Jou, and R. Wageman, *Ber. Bunsenges. Phys. Chem.*, **75**, 681 (1971).
(3) B. Bockrath and L. M. Dorfman, *J. Phys. Chem.*, **77**, 1002 (1973).
(4) G. A. Salmon, W. A. Seddon, and J. W. Fletcher, *Can. J. Chem.*, **52**, 3259 (1974).
(5) B. Bockrath and L. M. Dorfman, *J. Phys. Chem.*, **79**, 1509 (1975).
(6) B. Bockrath and L. M. Dorfman, *J. Am. Chem. Soc.*, **96**, 5708 (1974).

Discussion

J. W. FREEMAN. The mobility of electrons in the cyclic polyether *p*-dioxane is lower than that in *n*-alkyl ethers. This seemed surprising in view of the relatively low dielectric constant of *p*-dioxane. The low mobility indicated that the optical absorption spectrum in the latter should lie at a higher energy than those in *n*-alkyl ethers. F.-Y. Jou recently measured the spectra and verified the prediction. This indicates that there is an unusual interaction between electrons and cyclic polyethers. It might not be necessary to postulate $(e^-)_{2,sol}$ to explain the spectrum shift in the presence of crown ethers.

A. M. KOULKES-PUJO. Have you tried the pulse radiolysis in presence of a crown compound and is there any shift of the position of λ_{max} of e_s^-?

L. M. DORFMAN. Yes, no shift.

Comment by A. M. K-PUJO. We obtained a similar result for pulse radiolysis of aqueous solutions in the presence of 2,2,2 cryptand. We added it to try to scavenge either H_2O^+ or H_3O^+ formed by ionization process. There is no shift in the position of the maximum of e_{aq}^-, but the G value seems to be markedly increased. This work is in progress.

Strategies for the Preparation of Compounds of Alkali Metal Anions

J. L. Dye,* C. W. Andrews, and S. E. Mathews

Department of Chemistry, Michigan State University, East Lansing, Michigan 48824 *(Received July 28, 1975)*

Publication costs assisted by the U.S. Energy Research and Development Administration

By using alkali cation complexing agents of the crown and cryptand classes (C) and appropriate solvents, solutions can be prepared which contain essentially only M^+C and M^- in equal concentrations. From estimates of the metal solubility in the absence of the complexing agent and of the cation complexation constant, the solubility in the presence of the complexing agent can be predicted. If, in the metal solution with C absent, the e_{solv}^-/M^- ratio is appreciable, then when C is used and the solution is allowed to contact excess metal, this ratio will remain nearly the same. Therefore, in addition to MC^+ and M^-, the solution may contain relatively high concentrations of e_{solv}^-. Examples of the application of these equilibrium considerations to various metal–solvent combinations are described. Only $Na^+C{\cdot}Na^-$, in which C is 2,2,2 cryptand has been prepared as a crystalline solid. Gold-colored solid films have been obtained by rapid evaporation of solutions of Na, K, Rb, and Cs in one or more of the solvents methylamine (MA), ethylamine (EA), and tetrahydrofuran (THF) when the complexing agent 2,2,2 cryptand is present. In addition, gold-colored films are obtained with Na and K when 18-crown-6 is used. The former metal gives the film when MA is the solvent while the latter gives it with THF. In these cases, the gold film apparently yields the metal plus 18-crown-6 when the solvent vapors are removed. The criteria for thermodynamic vs. kinetic stability of salts of M^- are considered.

Introduction

Part of the fascination of metal–ammonia solutions stems from their complexity. We are accustomed to describing them as solutions which contain metal cations and solvated electrons. However, it has been evident since the days of Kraus[1] that these solutions are more complex. In particular, electron spin-pairing occurs as the concentration increases. For example, at −33°C only about 30% of the electron spins are unpaired at 0.02 *M*.[2] A large number of models have been proposed[3] for this spin-pairing phenomenon. Species of stoichiometry M^- were proposed by Bingel[4] as early as 1953. Arnold and Patterson[5] used electrochemical and magnetic data to argue that species of stoichiometry M^- were to be preferred over those of stoichiometry M_2. However, Golden, Guttman, and Tuttle[6,7] first suggested the presence of "genuine" spherically symmetric alkali metal anions in metal–ammonia solutions. Their arguments were based largely on the stability of M^- in the gas phase, which made its existence in solutions plausible. However, even today there is no *specific* evidence for alkali anions in metal–ammonia solutions although species of *stoichiometry* M^- probably are present.

The situation is very different in metal–amine and metal–ether solutions. In these solvents, metal-dependent optical absorption bands exist,[8,9] which demand that the alkali metal play more than a mere "bystander" role. The variation of the optical spectrum with metal, solvent, and temperature prompted Matalon, Golden, and Ottolenghi[10] to suggest that this species in metal–amine and metal–ether solutions is a centrosymmetric anion of large radius. This assumption is reasonable and has been confirmed by alkali metal NMR studies[11,12] and by the isolation of a solvent-free solid salt of Na^-.[13,14] The evidence for *stoichiometry* M^- is overwhelming. It includes the diamagnetic nature of the species,[15,16] its conductivity,[17,18] the Faraday effect,[19] oscillator strength,[20] behavior upon photolysis,[21–24] and the rate of its formation from M^+ and e_{solv}^-.[25–27] We can safely conclude that, at least in amines and ethers, the formation of alkali metal anions for all members of the family except lithium is a common occurrence. Diamagnetic species of stoichiometry M^- undoubtedly also exist in metal–ammonia solutions, but the present evidence indicates that they are probably best described as ion clusters or pairs with two solvated electrons or with the dielectron, e_2^{2-}. Since infrared bands attributable to "the solvated electron" also exist in metal–amine and metal–ether solutions, it is likely that ion clusters of stoichiometry M^- as well as ion pairs of stoichiometry M are also present whenever the solvated electron concentration becomes appreciable. Such ion clusters, which in metal–amine solutions absorb in the infrared region, should not be confused with the alkali metal anions, M^-. The latter species, which absorb at shorter wavelengths, are the subject of this paper.

Equilibria Involving M^- in Solution

The species which can exist in metal solutions may be described by the following equilibria[28,29] in which C represents a cation-complexing agent of either the crown[30] or cryptand[31,32,33] class:

$$M(s) \rightleftarrows M^+ + e_{solv}^- \quad (1)$$

$$M^+ + e_{solv}^- \rightleftarrows M \quad (2)$$

$$M^+ + 2e_{solv}^- \rightleftarrows M^- \quad (3)$$

$$M^+ + C \rightleftarrows M^+C \quad (4)$$

It is convenient for some cases to combine equilibria 1 and 3 to give

$$2M(s) \rightleftarrows M^+ + M^- \quad (5)$$

with $K_5 = K_1^2 K_3$.

Very little quantitative information is available for these reactions. However, by considering solubilities, conductances, and optical spectra, some qualitative trends can be es-

TABLE I: Qualitative Trends in Metal Solution Equilibria

Reaction	Effect of solvent[a] on equilibrium constant	Order of decreasing equilibrium constant
(1) $M(s) \overset{K_1}{\rightleftharpoons} M^+ + e^-$	Decrease	Li, Cs, Rb, K, Na
(2) $M^+ + e^- \overset{K_2}{\rightleftharpoons} M^b$	Increase	Cs, Rb, K, Na (Li)[c]
(3) $M^+ + 2e^- \overset{K_3}{\rightleftharpoons} M^-$	Increase	Na, K, Rb, Cs, (Li)[d]
(4) $M^+ + C \overset{K_4}{\rightleftharpoons} M^+C$	Unknown but expected to increase	Depends upon nature of C

[a] Solvent order: NH_3, HMPA, MA ~ EDA, EA, THF, DEE. [b] M refers to the monomer species which gives hyperfine splitting in the ESR spectrum. [c] No Li hyperfine splitting has been observed. [d] Li^- has not been observed.

TABLE II: Estimated Concentrations of Various Species in Equilibrium with Pure Sodium Metal in Two Solvents

Solvent	Complexing agent (0.1 M)	Value[a] used for K_3	K_4	K_5	Computed concentrations M^-	e^-	M^+	M^+C	C
MA	None	10^{11}		10^{-8}	10^{-4}	3×10^{-6}	10^{-4}		
MA	C_{222}	10^{11}	10^{10}	10^{-8}	0.097	3.1×10^{-3}	10^{-7}	0.10	10^{-4}
MA	18-C-6	10^{11}	10^{8}	10^{-8}	0.089	2.8×10^{-3}	1.1×10^{-7}	0.092	8.2×10^{-3}
THF	C_{222}	10^{13}	10^{11}	10^{-12}	0.050	0.016	2×10^{-11}	0.066	0.34
THF	18-C-6	10^{13}	10^{9}	10^{-12}	0.008	0.003	1×10^{-10}	0.01	0.09

[a] As discussed in the text, these constants have not been measured but are estimated from solubilities, optical spectra, and conductivities where these data are available.

tablished. The various equilibria are dependent upon the metal, solvent, and (for reaction 4) the complexing agent which is used. The general trends are summarized in Table I. Solvents which are referred to are ammonia, hexamethylphosphoric triamide (HMPA), methylamine (MA), ethylenediamine (EDA), ethylamine (EA), tetrahydrofuran (THF), and diethyl ether (DEE). Other solvents such as the longer chain primary amines and diamines, dimethoxyethane, and other linear polyethers could be added to the list. The value of K_4 will generally be larger when the appropriate cryptand is used rather than a crown ether. Since equilibria 1–3 will still be applicable even when the complexing agent is present, the relative values of K_1, K_2, and K_3 will determine the $(e^-)/(M^-)$ ratio even when C is added to enhance the solubility, provided equilibrium with the metal is retained.

Estimates of the solubility in the absence of C and of the complexation constant, K_4, permit one to predict whether the metal solubility will be large or small when C is used. In the examples considered in this paper, a liberal amount of guesswork has been used to arrive at equilibrium constants. These examples should be considered illustrative only since they are not based upon firmly established data. Furthermore, such data are not easily obtained. Solubilities in the absence of C are very low, the saturated solutions are only slowly formed, and decomposition problems are severe. The values of K_4 are so large in these nonaqueous solvents that they cannot be readily measured. To determine K_3 would require quantitative measurements of absorption spectra or conductances, or combined ESR and optical spectra. Finally, the determination of the extent of reaction 2 to form the monomer species which shows hyperfine splitting by the metal nucleus in the ESR spectra would require quantitative ESR and optical spectra. We do not include the formation of loose ion pairs, $M^+ \cdot e^-$, in considering reaction 2. In the present treatment the formation of monomers is considered negligible.

In spite of these difficulties, we have found estimates of the type illustrated here to be useful in predicting which metal–solvent–complexing agent combinations can be expected to yield relatively high concentrations of M^-. In all cases, activity coefficient effects are neglected.

The first illustrative example is sodium in methylamine at temperatures of −30 to −80°C. The solubility of sodium in this solvent is at least 1.2×10^{-4} M based upon the conductance data of Dewald and Browall.[34] Their conductance data also indicate that the ratio $(e^-)/(Na^-)$ is probably less than 0.04. These data yield $K_5 \geq 10^{-8}$ and $K_3 \geq 10^{11}$. By examining the variation of K_4 from one solvent to another,[35] we estimate $K_4 \geq 10^{10}$ for 2,2,2 cryptand (C_{222}) and $K_4 \geq 10^8$ for 18-crown-6 (18-C-6). (See the companion paper[12] for the structures of these complexing agents.) Suppose we prepare solutions of Na in MA by three methods: (1) a saturated solution of Na in MA; (2) a saturated solution of Na in MA which contains 0.1 M total C_{222} concentration; (3) same as (2) but with 18-C-6.

By using the *limits* given above for K_3, K_4, and K_5, we obtain the results shown in Table II. Note the prediction that both 18-C-6 and C_{222} yield high concentrations of M^-, nearly equal to the concentration of added C and that the concentration of e_{solv}^- remains relatively low. Both of these predictions have been shown to be correct in this case. The solubility of sodium in MA in the presence of either complexing agent is at least 0.1 M and the integrated intensities of the ^{23}Na NMR absorptions of Na^+C_{222} and Na^- are equal within experimental error,[11,12] showing that the relative concentration of e_{solv}^- is low.

The relative concentration of e_{solv}^- can be increased by increasing the concentration of C in a solution which does not contact the metal. For the constants given in Table II for Na in MA with C_{222} as the complexing agent, removal of the solution from the metal and the addition of enough C_{222} to make its total concentration 0.2 M would yield $(M^-) = 0.068$ M, $(e_{solv}^-) = 0.061$ M, $(M^+C) = 0.13$ M, and $(C) = 0.071$ M. Even in this favorable solvent, the addition of excess cryptand away from the metal does not complete-

TABLE III: Solvent and Complexing Agent Combinations Which Have Been Used to Enhance Metal Solubility

Solvent	Complexing agents	Metal
MA	DCH 18-C-6,[a] 18-C-6, C_{222}	Na, K, Rb, Cs
EA	DCH 18-C-6, 18-C-6, C_{222}	Na, K, Rb, Cs
Diglyme	DCH 18-C-6	K
THF	18-C-6	Na, K
THF	C_{222}	Na, K, Rb, Cs
THF	DCH 18-C-6	K, Cs
DEE	18-C-6	K
DEE	C_{222}	Na,[b] K
DEE	DCH 18-C-6	K, Cs
Dimethyloxyethane	C_{222}	K
1,2-Propanediamine	DCH 18-C-6	K
Diethylamine	C_{222}	K
Diisopropyl ether	C_{222}	K
Di-*n*-propylamine	C_{222}	K
Di-*n*-propyl ether	C_{222}	K

[a] Dicyclohexyl-18-crown-6. [b] Light blue solution indicates low solubility.

ly dissociate M^-.

The second example shows the effect of solvent on the solubility equilibria. Consider a saturated solution of Na in THF in the presence of 0.1 *M* total C_{222} or 18-C-6. Sodium does not dissolve in THF, but potassium does, to an extent of about 10^{-5} *M*.[36-38] Let us assume that Na in the saturated solution has a concentration which is less than 10^{-6} *M*. Otherwise a blue color would be easily discernible. Since the solvation of cations by THF is not as favored as their solvation by MA, we assume that the complexation constants, K_4, for both C_{222} and 18-C-6 are an order of magnitude greater in THF than in MA. Also in accord with the qualitative trends shown in Table I, K_3 is assumed to be two orders of magnitude greater in THF than in MA. As shown in Table II, these assumptions predict a total sodium solubility of about 0.2 *M* with 0.1 *M* C_{222} and about 0.02 *M* with 18-C-6. We find that C_{222} actually gives high concentrations of sodium in THF (C > 0.1 *M*) while 18-C-6 produces a dark blue solution which is, however, easily transparent in thin cells and has an estimated concentration of 10^{-3} to 10^{-4} *M*. On the other hand, potassium dissolves readily to high concentrations in THF when either complexing agent is used. The narrow NMR line of Na^- in THF and the equal integrated intensities for the Na^+C_{222} and the Na^- NMR absorptions[11,12] indicate that K_3 is probably much larger than that used to prepare Table II.

Preparation of Solutions

The combinations of metal, complexing agent, and solvent which have been used to obtain metal solutions are summarized in Table III. These results show that the solubilization of metals by C_{222} and by crown ethers is very general. It may be of particular interest to chemists who are engaged in synthesis, that concentrations of sodium as high as 0.4 *M* can be obtained in methylamine by using the relatively inexpensive complexing agent 18-crown-6. If a solvent such as THF is to be used instead with this complexing agent, then a switch to potassium still permits the production of high concentrations of M^-. The metals will even dissolve in benzene and toluene[39,40] with the aid of complexing agents of this type, although in these cases the aromatic radical anion is formed rather than M^-.

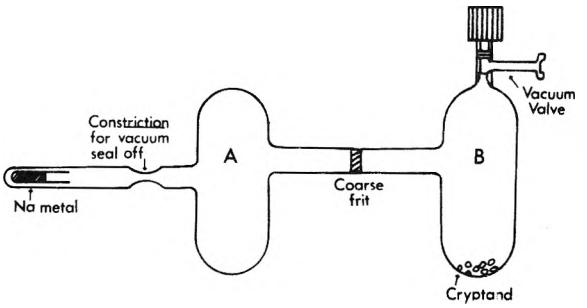

Figure 1. Apparatus for the preparation of solutions of M^+C,M^-

Solutions with the maximum $(M^-)/(e^-)$ ratio are easily prepared in an apparatus such as that shown in Figure 1. Provision is made for the separate addition of metal and complexing agent. Following evacuation, the metal is distilled from the side arm to form a mirror on the walls of vessel A. Then the solvent is distilled under vacuum into B. When the complexing agent has been dissolved, the solution is poured through the coarse frit onto the metal. Agitation at about 0°C produces a saturated solution which can then be poured back through the frit to remove it from the metal. Solutions of sodium in MA, EA, and THF in the presence of C_{222} prepared in this way were studied by ^{23}Na NMR,[12] and in each case the area under the Na^+C peak was equal to the area under the Na^- peak within a few percent. This shows that the stoichiometry of the dissolved metal was essentially Na^+C,Na^-.

Solids Which Contain M^-

When a ~0.2 *M* solution of sodium in EA with C_{222} is cooled from about +10 to −20°C, shiny gold-colored hexagonal crystals form spontaneously.[13,14] Their analysis and crystal structure show that the solid has the composition $Na^+C{\cdot}Na^-$. The Na^+C moiety has virtually the same structure as it does in salts such as $Na^+C{\cdot}I^-$. Since the $Na^+C{\cdot}Na^-$ salt forms spontaneously and reversibly in the solution even in the presence of pure solid sodium, it appears that this compound is thermodynamically stable with respect to Na(s) and C(soln). When the solid is rapidly heated in a sealed tube, it melts at 83°C (compared with 68°C for the pure cryptand) to yield C_{222} and free sodium.[14] It is also possible, however, that other decomposition products form.

The existence of salts which contain alkali metal anions is not altogether unexpected. Because of the relatively low lattice energies and ionization potentials of the alkali metals, and particularly because of the positive electron affinities of the gaseous alkali atoms,[6,7,41,42] the energy required to convert the metallic solid into a *hypothetical* ionic solid according to

$$2M(s) \rightarrow M^+{\cdot}M^-(s)$$

is less than about 15 kcal mol^{-1}. The calculation of the enthalpy of this reaction is made by means of a Born–Haber cycle of the type shown in Figure 2 for sodium. Known thermodynamic quantities are used throughout except for the lattice energy of the hypothetical salt. This was estimated by assuming that the structure would be the same as that of sodium iodide but with a different interionic distance. The M^+M^- distance in the hypothetical salt was set equal to the interatomic distance in the corresponding metal. This implies a decrease in density because of the change in crystal structure from body-centered cubic

TABLE IV: Estimated Enthalpy Changes for Various Reaction Steps

Metal	M–M distance in metal, Å	Enthalpy change, kcal mol^{-1} (see Figure 2) ΔH_{vap}	ΔH_{ip}	ΔH_{ea}	ΔH_{le}	ΔH_F	Radius of cryptated cation, Å	ΔH°_{10}, kcal mol^{-1}	$(\Delta H^\circ_9 - \Delta H^\circ_{9'})_{max}$, kcal mol^{-1}	$(\Delta H^\circ_9 - \Delta H^\circ_{9'})_{est}$, kcal mol^{-1}
Li	3.03	33.17	124.3	−14.3	−175.0	0.4	5.06	−73.1	−12.4	−22.3
Na	3.72	24.03	118.5	−12.5	−142.7	10.2	5.50	−66.6		
K	4.5	19.35	100.1	−11.8	−117.9	7.9	5.52	−65.2	24.0	14.8
Rb	4.87	18.64	96.3	−11.1	−109.4	11.9	5.53	−62.2	24.7	21.4
Cs	5.42	16.82	89.7	−10.8	−97.9	13.5	5.56	−61.3	31.8	38.1

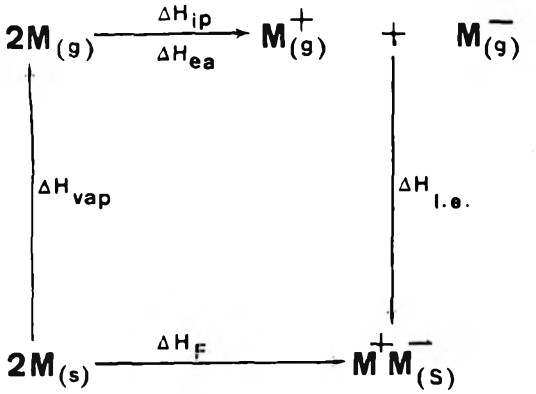

Figure 2. Born–Haber cycle for the formation of the hypothetical ionic solid, $M^+ \cdot M^-$(s).

(bccub) in the metal to interpenetrating face-centered cubic (fccub) in the ionic solid. Alternative choices, such as retention of the bccub structure or keeping the density constant, lead to even larger lattice energies than the original choice. The lattice energy of $M^+ \cdot M^-$(s) is computed by scaling that of Na^+I^- by the ratio of the interionic distances since the lattice energy varies nearly as $1/r$. The computed results for all of the alkali metals are given in Table IV.

Two conclusions may be drawn from these estimated enthalpies of formation of $M^+ \cdot M^-$(s). First, the values are only slightly endothermic. This indicates that it would not require much stabilization of M^+ to create an ionic solid. Second, all of the alkali metals yield similar results so that one might expect to be able to produce negative alkali metal anions for all members of the family under suitable circumstances.

Stabilization of the cation by complexation with crown or cryptand leads to an increase in size which decreases the ionic lattice energy. Since the size of M^+C is comparable to that of M^-, the crystal structure can be expected to approximate the closest packing of the ions. Indeed, the $Na^+C \cdot Na^-$ crystal structure shows hexagonal closest packing of the sodium species.[14] By estimating the effective size of M^+C[32] and using the Kapustinskii equation,[43] the lattice energy can be computed.

Unfortunately, neither the enthalpy of sublimation of the cryptands nor the enthalpy of complexation of the gaseous cations is known. If they were known, then by a simple cycle we could compute ΔH for the process

$$2M(s) + C(s) \rightarrow M^+C \cdot M^-(s) \qquad (6)$$

Rather than attempt calculation of the absolute values of ΔH°_6 and ΔS°_6, we choose to use the fact that one member of this class of compounds, $Na^+C_{222} \cdot Na^-$(s), is thermodynamically stable to estimate whether the other alkali metals should form similar compounds. Because of the thermodynamic stability of the sodium compound, we know that for the process

$$2Na(s) + C_{222}(s) \rightarrow Na^+C_{222} \cdot Na^-(s) \qquad (6')$$

$$\Delta G^\circ_{6'} = \Delta H^\circ_{6'} - T\Delta S^\circ_{6'} \leq 0$$

(Throughout the balance of this section, the primed values will refer to the sodium case and C_{222} will be represented by C.)

In order for the other alkali metals to form thermodynamically stable salts of the same type, we must have

$$\Delta G^\circ_6 = \Delta H^\circ_6 - T\Delta S^\circ_6 \leq 0$$

This will necessarily be the case if

$$\Delta G^\circ_6 - \Delta G^\circ_{6'} = (\Delta H^\circ_6 - \Delta H^\circ_{6'}) - T(\Delta S^\circ_6 - \Delta S^\circ_{6'}) \leq 0$$

Note that ΔG°_6 may be negative even if $\Delta G^\circ_6 - \Delta G^\circ_{6'}$ is not, but we will refer to the more stringent condition as the "stability criterion" for the salt $M^+C \cdot M^-$(s). We will first develop this stability criterion for all of the alkali metals, and then we will proceed to estimate the values of $\Delta G^\circ_6 - \Delta G^\circ_{6'}$. If the estimates are more negative than that given by the stability criterion, the existence of stable solid salts is indicated. Because lithium forms only very weak complexes with the cryptand C_{222},[44] we substitute C_{211} for this case. Such a substitution makes the calculation in the lithium case less valid because terms which cancel when the same complexing agent is used will not cancel in this case. Nevertheless, to obtain an estimate of the stability of $Li^+C_{211} \cdot Li^-$(s), we assume these differences to be small.

Consider the series of reaction steps

$$2M(s) \rightarrow M^+(g) + M^-(g) \qquad (7)$$

$$C(s) \rightarrow C(g) \qquad (8)$$

$$M^+(g) + C(g) \rightarrow M^+C(g) \qquad (9)$$

$$M^+C(g) + M^-(g) \rightarrow M^+C \cdot M^-(s) \qquad (10)$$

We note that ΔH°_7 is known for all of the metals, ΔH°_{10} can be calculated by using the Kapustinskii equation, and ΔH°_8 will cancel out when the *difference* between M and Na is computed. Therefore in the expression

$$(\Delta H^\circ_6 - \Delta H^\circ_{6'}) = (\Delta H^\circ_7 - \Delta H^\circ_{7'}) + (\Delta H^\circ_9 - \Delta H^\circ_{9'}) + (\Delta H^\circ_{10} - \Delta H^\circ_{10'})$$

only $(\Delta H^\circ_9 - \Delta H^\circ_{9'})$ is unknown.

The stability criterion can then be replaced by

$$(\Delta H^\circ_9 - \Delta H^\circ_{9'}) \leq (\Delta H^\circ_9 - \Delta H^\circ_{9'})_{max} = -(\Delta H^\circ_7 - \Delta H^\circ_{7'}) - (\Delta H^\circ_{10} - \Delta H^\circ_{10'}) + T[\bar{S}^\circ_{M^+C \cdot M^-(s)} - \bar{S}^\circ_{Na^+C \cdot Na^-(s)}] - 2T[\bar{S}^\circ_{M(s)} - \bar{S}^\circ_{Na(s)}]$$

Everything on the right-hand side of this equation is known or calculable except the molar entropy difference between the salt and the corresponding sodium salt. In order to proceed, we assume that this difference is small. When this is done, the value of $(\Delta H^\circ_9 - \Delta H^\circ_{9'})_{max}$ can be

TABLE V: Conditions Which Have Yielded Gold-Colored Films upon Solvent Evaporation

Metal	Complexing agent	Solvent	Remarks
Na	C_{222}	THF	
Na	C_{222}	EA	Crystal growth also occurs
Na	C_{222}	MA	
Na	18-C-6	MA	MA vapor required
K	18-C-6	THF	Dark bronze color, THF vapor required
K	C_{222}	THF	Dark bronze color
Na–K	C_{222}	EA	Film has a greenish-gold color
Rb	C_{222}	THF	
Rb	C_{222}	EA	
Cs	C_{222}	THF	Dark bronze color

numerically evaluated. The results, together with the calculated values of $\Delta H°_{10}$, are given in Table IV.

Having made an estimate of the maximum value of $\Delta H°_9 - \Delta H°_{9'}$, we next proceed to use another cycle to estimate the actual value of $\Delta H°_9 - \Delta H°_{9'}$. Consider the series of reaction steps

$$M^+(g) + C(g) \rightarrow M^-C(g) \quad (9)$$

$$M^+C(g) \rightarrow M^+C(aq) \quad (11)$$

$$M^+(g) \rightarrow M^+(aq) \quad (12)$$

$$C(g) \rightarrow C(aq) \quad (13)$$

$$M^+(aq) + C(aq) \rightarrow M^+C(aq) \quad (14)$$

From this sequence of steps, we see that

$$\Delta H°_9 = -\Delta H°_{11} + \Delta H°_{12} + \Delta H°_{13} + \Delta H°_{14} \quad (15)$$

Again we will compute only differences in ΔH rather than absolute values. The Born equation[45] may be used, together with the radii of the cryptated cations, to calculate $\Delta H°_{11} - \Delta H°_{11'}$. While absolute values of hydration enthalpies may be seriously in error when the Born equation is used, the calculation of the difference should be reliable for such large ions. The value of $\Delta H°_{12}$ is reasonably well known[46] for all of the alkali cations (again differences are more reliable than absolute values), and $\Delta H°_{13}$ will cancel out of the difference calculations. Measured values of $\Delta H°_{14}$ are available[34] for all of the alkali metal cations except Cs^+. For the case of cesium we assume, on the basis of the magnitude of the complexation constants, that $\Delta H°_{14} - \Delta H°_{14'} = 3.8$ kcal mol^{-1}. As indicated previously the values for the 2,1,1 cryptand are used for lithium. The estimates of $\Delta H°_9 - \Delta H°_{9'}$ made in this way are given in Table IV.

The results shown in Table IV indicate that, with the exception of $Cs^+C_{222}{\cdot}Cs^-(s)$, all of the alkali metals can probably form salts of the type $M^+C{\cdot}M^-(s)$ which are thermodynamically stable with respect to the dissociation reaction

$$M^+C{\cdot}M^-(s) \rightarrow 2M(s) + C(s) \quad (16)$$

Even in the case of cesium, the use of 3,2,2 cryptand might provide a stable salt.

Of course, these calculations do not preclude the decomposition of the salt into other reaction products. For example, the reaction

$$M^+C{\cdot}M^-(s) \rightarrow M^+C{\cdot}e^-(s) + M(s) \quad (17)$$

might occur. In addition, decomposition of the cryptand could limit the stability.

In spite of the relative ease with which crystals of $Na^+C_{222}{\cdot}Na^-$ can be obtained and the favorable calculations described above, we have not yet been able to grow crystals with any other combination of metal and complexing agent. Gold-colored solid films are, however, readily obtained by rapid evaporation of the solvent from a concentrated solution in many cases. Table V gives the metal–solvent combinations which have so far yielded such films with either 18-C-6 or C_{222}. Other complexing agents of the cryptand class have not been used. Neither dibenzo-18-crown-6 nor dicyclohexyl-18-crown-6 have yielded gold-colored films although dark blue solids which show strong ESR signals have been obtained[14] in these cases and in many cases when cryptands are used.

TABLE VI: Effect of Temperature and Methylamine Vapor Pressure on the Stability of a Sodium–18-C-6–Methylamine Gold-Colored Film

Temp of film, °C	Approx methylamine pressure, Torr	Effect on gold-colored film
24	10–250	Turns gray-purple rapidly
0	1140	Forms blue solution rapidly
0	260	Forms blue solution in ~3 min
0	100–400	Stable for at least 12 min
0	1–10	Turns gray-purple in 6–8 min
−11	100–250	Stable for at least 10 min
−11	10	Turns purple in ~6 min
−32	1–10	Stable for at least 10 min
−32	<1	Turns purple in ~10 min
−77	10	Forms blue solution rapidly
−77	~1	Stable for at least 10 min
−77	≪1	Turns purple in <10 min

The failure to obtain crystals by precipitation from appropriate solvents or solvent mixtures might mean simply that the proper solvent has not yet been used. However, it could also signify thermodynamic instability of the solid salt, $M^+C{\cdot}M^-(s)$. If the gold-colored solid films obtained by rapid evaporation of solvent are similar to $Na^+C_{222}{\cdot}Na^-$, then the formation of these films might represent kinetic rather than thermodynamic stability. This is possible because the rate of release of M^+ from M^+C is very slow at low temperatures.[14]

The gold-colored films which are formed by evaporating methylamine from solutions of Na^+C,Na^- when 18-C-6 is used are interesting since they require the presence of solvent in order to exist. Stability of such films for many minutes can be obtained provided the methylamine vapor pressure is maintained between certain upper and lower limits which depend upon the temperature of the film. If the vapor pressure is too low or if the system is evacuated, the gold-colored film turns to a dull gray-purple to purple color. This process cannot be reversed by increasing the methylamine vapor pressure. The gray-purple deposit can be dissolved in methylamine to yield a dark blue solution from which gold-colored films can again be produced. Therefore, removal of solvent from the original film probably yields metal, and 18-C-6 and this process is not reversible on the time scale used. On the other hand, when the methylamine vapor pressure is sufficiently high, the gold-colored film dissolves to form a dark blue solution. All of these phenomena are sensitive to the temperature of the film. Some typical results are given in Table VI.

We conclude that the formation of solid salts of the alkali anions, while thermodynamically favored in at least one case, is very dependent upon the metal, complexing agent, and solvent used. In some cases, the salt may be thermodynamically unstable with respect to the free metal and the

complexing agent. Even in such cases, however, the major species *in solution* can be M^+C and M^-.

Acknowledgments. We are grateful to J. Ceraso, M. DaGue, M. Lok, E. Mei, F. Tehan, J. Tracy, J. Whitman, and M. Yemen for making some of the observations described in this paper. This research was supported by the U.S. Energy Research and Development Administration under Contract No. E(11-1)-958.

References and Notes

(1) C. A. Kraus, *J. Am. Chem. Soc.*, **36**, 864 (1914).
(2) C. A. Hutchison and R. C. Pastor, *Rev. Mod. Phys.*, **25**, 285 (1963); *J. Chem. Phys.*, **21**, 7959 (1953).
(3) J. L. Dye, *Pure Appl. Chem.*, 1 (1970).
(4) W. Bingel, *Ann. Phys.* (Leipzig), **12**, 57 (1953).
(5) E. Arnold and A. Patterson, Jr., *J. Chem. Phys.*, **41**, 3089, 3098 (1964).
(6) S. Golden, C. Guttman, and T. R. Tuttle, Jr., *J. Am. Chem. Soc.*, **87**, 135 (1965).
(7) S. Golden, C. Guttman, and T. R. Tuttle, Jr., *J. Chem. Phys.*, **44**, 3791 (1966).
(8) M. T. Lok, F. J. Tehan, and J. L. Dye, *J. Phys. Chem.*, **76**, 2975 (1972).
(9) For earlier reference to optical properties of metal amine solutions, see T. R. Tuttle, Jr., and S. Golden, *Pure Appl. Chem.*, 449 (1970).
(10) S. Matalon, S. Golden, and M. Ottolenghi, *J. Phys. Chem.*, **73**, 3098 (1969).
(11) J. M. Ceraso and J. L. Dye, *J. Chem. Phys.*, **61**, 1587 (1974).
(12) J. L. Dye, C. W. Andrews, and J. M. Ceraso, *J. Phys. Chem.*, paper in this issue.
(13) J. L. Dye, J. M. Ceraso, M. T. Lok, B. L. Barnett, and F. J. Tehan, *J. Am. Chem. Soc.*, **96**, 608 (1974).
(14) F. J. Tehan, B. L. Barnett, and J. L. Dye, *J. Am. Chem. Soc.*, **96**, 7203 (1974).
(15) L. R. Dalton, J. D. Rynbrandt, E. M. Hansen, and J. L. Dye, *J. Chem. Phys.*, **44**, 3969 (1966).
(16) S. H. Glarum and J. H. Marshall, *J. Chem. Phys.*, **52**, 5555 (1970).
(17) R. R. Dewald and J. L. Dye, *J. Phys. Chem.*, **68**, 128 (1964).
(18) R. R. Dewald and K. W. Browall, *J. Phys. Chem.*, **74**, 129 (1970).
(19) T. R. Tuttle, Jr., *Chem. Phys. Lett.*, **20**, 371, (1973).
(20) M. G. DeBacker and J. L. Dye, *J. Phys. Chem.*, **75**, 3092 (1971).
(21) S. H. Glarum and J. H. Marshall, *J. Chem. Phys.*, **52**, 5555 (1970).
(22) L. J. Gilling, J. G. Kloosterboer, R. P. H. Rettschnick, and J. D. W. Van Voorst, *Chem. Phys. Lett.*, **8**, 457, 462 (1971).
(23) A. Gaathon and M. Ottolenghi, *Isr. J. Chem.*, **8**, 165 (1970).
(24) D. Huppert and K. H. Bar-Eli, *J. Phys. Chem.*, **74**, 3285 (1970).
(25) J. L. Dye, M. G. DeBacker, J. A. Eyre, and L. M. Dorfman, *J. Phys. Chem.*, 76, 839 (1972).
(26) J. W. Fletcher, W. A. Seddon, and F. C. Sopchyshyn, *Chem. Phys. Lett.*, **18**, 592 (1973).
(27) G. A. Salmon, W. A. Seddon, and J. W. Fletcher, *Can. J. Chem.*, **52**, 3259 (1974).
(28) J. L. Dye, M. T. Lok, F. J. Tehan, R. B. Coolen, N. Papadakis, J. M. Ceraso, and M. G. DeBacker, *Ber. Bunsenges. Phys. Chem.*, **75**, 659 (1971).
(29) J. L. Dye in "Electrons in Fluids", J. Jortner and L. R. Kestner, Ed., Springer-Verlag, West Berlin, 1973, p 77.
(30) C. J. Pedersen, *J. Am. Chem. Soc.*, **89**, 7017 (1967); **92**, 386 (1970).
(31) B. Dietrich, J. M. Lehn, and J. P. Sauvage, *Tetrahedron Lett.*, 2885, 2889 (1969).
(32) J. M. Lehn, *Struct. Bonding (Berlin)*, **16**, 1 (1973).
(33) J. M. Lehn and J. P. Sauvage, *Chem. Commun.*, 440 (1971).
(34) R. R. Dewald and K. W. Browall, *J. Phys. Chem.*, **74**, 129 (1970).
(35) J. J. Christensen, D. J. Eatough, and B. M. Izatt, *Chem. Rev.*, **74**, 351 (1974).
(36) I. Hurley, T. R. Tuttle, Jr., and S. Golden, *Pure Appl. Chem.*, 449 (1970).
(37) Comment of R. Catterall in general discussion: I. Hurley, T. R. Tuttle, Jr., and S. Golden, *Pure Appl. Chem.*, 449 (1975).
(38) R. Catterall, J. Slater, and M. C. R. Symons, *Pure Appl. Chem.*, 329 (1970).
(39) B. Kaempf, S. Raynal, A. Collet, F. Schué, S. Boileau, and J. M. Lehn, *Angew. Chem.*, **86**, 670 (1974).
(40) M. A. Komarynsky and S. I. Weissman, *J. Am. Chem. Soc.*, **97**, 1589 (1975).
(41) E. C. M. Chen and W. E. Wentworth, *J. Chem. Educ.*, **52**, 486 (1975).
(42) W. H. E. Schwarz, *Chem. Phys. Lett.*, **10**, 478 (1971). See this paper for earlier references to experimental and theoretical electron affinities of the alkali atoms.
(43) A. F. Kapustinskii, *Q. Rev., Chem. Soc.*, **10**, 283 (1956).
(44) Y. M. Cahen, J. L. Dye, and A. I. Popov, *J. Phys. Chem.*, **79**, 1289 (1975).
(45) G. N. Lewis, M. Randall, K. S. Pitzer, and L. Brewer, "Thermodynamics," McGraw-Hill, New York, N.Y., 1961, pp 503, 523.
(46) S. Goldman and R. G. Bates, *J. Am. Chem. Soc.*, **94**, 1476 (1972).

Discussion

J. W. FLETCHER. Have you estimated the solubility product for Na^+ and Na^- in the presence of complexing agent?

J. L. DYE. Yes. Based upon the maximum concentrations used in the measurements of conductivity by Dewald and coworkers in methylamine we estimate $K \approx 10^{-8}$ for the solubility equilibrium in the absence of C. Over excess metal with C present it should be the same.

R. CATTERALL. The band shape of M^- anions is very similar to that of e_{solv}^- in its asymmetric high energy tail and different from the I^- bands (CTTS) which (after resolution) are very symmetrical. Would you or any theoretician care to comment?

J. L. DYE. I would have to defer to theoreticians for an answer to this question. We do know that excitation in the optical absorption band leads to dissociation according to the work of Glarum and Marshall.

The Monomer and Its Paramagnetic Companion in Some Potassium Solutions in Alkylated Amines

T. R. Tuttle, Jr.

Department of Chemistry, Brandeis University, Waltham, Massachusetts 02154 *(Received July 23, 1975)*

Evidence is obtained from ESR spectra of potassium metal solutions in ethylamine and in a mixed ethylamine–methylamine solvent to show that the central component in these spectra may be attributed to the solvated electron in very dilute solutions, but that in more concentrated metal solutions this single line resonance must be assigned to an ion pair of the solvated electron with K^+. As a consequence of this assignment, the temperature dependence of the metal nuclear hyperfine coupling constant, a_M, cannot arise on account of a rapid equilibrium between the ion pair and isomeric species of metal with fixed values of the hyperfine coupling constant. In addition, the shape of the hyperfine lines for pure ethylamine solutions is found to deviate appreciably from the Lorentzian shape expected if such a rapid equilibrium would be operative. However, the facts available are consistent with the idea that the temperature dependence of a_M arises on account of the presence of thermally accessible vibrational states with a distribution of values of a_M.

The electron spin resonance spectra of solutions of alkali metals in amines and other solvents often show the presence of at least two distinct species.[1-12] One of these displays a particularly simple spectrum consisting of a single line which is often, but not always, quite narrow. This single line spectrum has usually been attributed to the solvated electron. However, in one investigation,[5] the rather erratic behavior of this line, with respect to its presence or appearance in spectra of potassium, rubidium, and cesium solutions in various alkylamines, caused the authors to attribute it to an impurity. In another investigation,[11] the single line component in the spectra of potassium and rubidium solutions in glassy hexamethylphophoramide has been attributed to a form of monomeric metal. Whether the single line absorption observed in the ESR spectra of alkali metals is sometimes, always, or never due to an impurity appears to be still an unsettled question.

The second of the species displays a spectrum composed of many hyperfine components. In the cases for which the hyperfine structure may be attributed to the interaction of the unpaired electron with an alkali metal nuclear spin, the responsible species has been identified as a monomeric, electrically neutral species of metal. One interpretation of the temperature dependence of the metal hyperfine coupling involves rapid equilibria between two or more monomeric species.[6,9] A second interpretation attributes this temperature dependence to the presence of thermally accessible vibrational states,[2] which are associated with different values of the hyperfine coupling constant.[13] Accordingly, the structure of the monomer and the relationship between its structure and its ESR spectra are still a matter for speculation and a source of controversy.

In this paper we present data on solutions of potassium in pure ethylamine and an ethylamine–methylamine mixture. These data indicate that the single line component in the ESR spectra may be attributed to the solvated electron or its ion pair with potassium ion and that on this account the ^{39}K hyperfine spectrum cannot be described as an average between the $K^+ \cdot e^-$ ion pair and a monomeric species with hyperfine splitting near that of the free atom.

Experimental Procedures

The experimental procedures used have been described in detail elsewhere.[14] In the present case, the glassware used in fabricating apparatuses was rinsed several times with absolute methanol and subsequently with distilled water prior to fabrication.

Electron spin resonance spectra of potassium in pure ethylamine and potassium in ethylamine containing approximately 15% by volume of methylamine were obtained with the aid of our Strand Labs 602BX spectrometer[2,4] operating at 20-kc/sec modulation frequency. The apparatuses housing the sample solutions were of designs previously described.[14] The apparatuses were of Pyrex glass except for the quartz optical cell on the apparatus containing pure ethylamine. Each of the apparatuses had a trap in which decomposition products could be deposited. The apparatus containing pure ethylamine also incorporated a calibrated tube which permitted dilutions by known volumes to be made.

Field sweeps were calibrated using a sample of potassium naphthalenide dissolved in 1,2-dimethoxyethane assuming a separation between the two outermost lines on the high-field side of the spectrum of 1.86 G.[15]

Solutions of potassium naphthalenide in DME were also used as standards in estimating spin concentrations. Concentrations of naphthalenide were determined by measuring the optical density of solutions at 8000 Å and using the measured value of the extinction coefficient.[16] Since the Q of the loaded cavity was essentially the same for standard solutions and samples, relative spin concentrations were determined by measuring the true peak-to-peak breadth δH_p and the maximum amplitude of the derivative curve a_{1pm}, and using the relationship[17]

$$a_{1pm}\delta H_p^2 = k[\text{spins}] \quad (1)$$

where k is a constant evaluated by using the standard. The line which occurs at highest field in the naphthalenide spectrum was used for this purpose. Application of this procedure, for example, led to a monomer concentration of

Figure 1. (a) ESR spectrum of a solution of K dissolved in ethylamine containing approximately 15% by volume methylamine. The concentration of monomer is 1.4×10^{-6} *M*. The central component due to the solvated electron, as well as weak lines due to ^{41}K monomers, is clearly in evidence here. (b) Same at somewhat lower concentration. At this lower concentration, the central component due to the solvated electron is essentially equal in amplitude to the monomer lines.

Figure 2. ESR spectra of a solution of K dissolved in pure ethylamine. Upper spectrum was taken with peak-to-peak modulation amplitude, $2h_m = 0.8$ G, while for the lower spectrum $2h_m = 0.2$ G. In the upper spectrum, a weak central line due to the solvated electron is barely perceptible, while in the lower spectrum no central component can be detected. The upper spectrum also shows some weak lines due to the ^{41}K (~7% natural abundance) monomer.

1.4×10^{-6} *M* for the solution of K in ethylamine–methylamine which gave the spectrum shown in Figure 1a.

Experimental Results

The spectra shown in Figure 2 are typical of those obtained for potassium solutions in pure ethylamine. These tracings are successive spectra of the same solution, differing otherwise only in the modulation amplitude employed (0.8 G peak to peak for the upper spectrum and 0.2 G for the lower one). This comparison illustrates one of the aspects of apparent nonreproducibility in the spectra of such solutions. Although both spectra display the four-line ^{39}K hyperfine pattern, the spectrum taken at higher modulation displays additional features including the appearance of a weak central component. The central component often behaves in an extraordinary manner. Over an appreciable concentration range, the amplitude of this central component *increases* absolutely with increasing dilution, as well as with respect to the amplitude of the hyperfine spectrum. This behavior is exemplified by the data plotted in Figure 3. A decrease in the breadth of the central line accompanies the increasing amplitude of the derivative curve. This peculiar behavior, which also occurs while the solution decomposes, has led one set of investigators to attribute this central component to an impurity.[6]

Addition of methylamine to a solution of K in ethylamine had two principal effects. The ^{39}K hyperfine coupling constant decreased, and the relative amount of the central component increased. Empirically, this behavior is

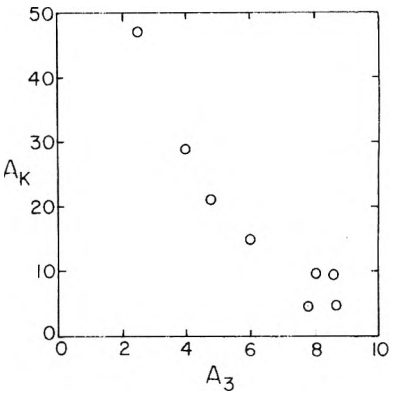

Figure 3. The amplitude of the central component, A_3, in spectra of solutions of K in ethylamine plotted vs. the amplitude by a hyperfine line. Concentration changes were effected by successive dilutions. The solution of lowest concentration is about 30-fold more dilute than the highest concentration solution. A_K decreases monotonically with increasing dilution.

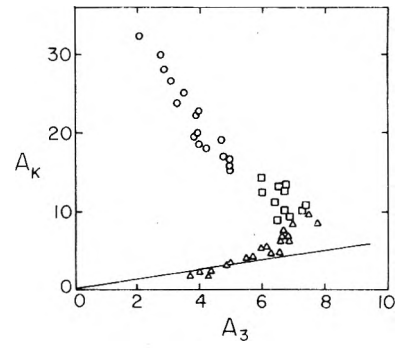

Figure 4. The amplitude of the central component, A_3, in spectra of solutions of K in ethylamine–methylamine plotted vs. the amplitude of a hyperfine line. All the points refer to a single solution which decomposed over a period of several hours. The solid line emanating from the origin gives a visual indication that A_K and A_3 do not vary in direct proportion to one another. The three different symbols used, O, □, and Δ, simply denote different gain settings on the spectrometer. Thes symbols are also used to represent the same data in the plots of Figures 7 and 8.

to be expected because the central component is characteristically relatively more important and the hyperfine coupling constant smaller for pure methylamine solutions.[1,2,4] Typical spectra of K in ethylamine, plus about 15% by volume methylamine, are shown in Figure 1. The larger amplitude of the central component makes its study easier so that most of our experiments were carried out on solutions in this mixed solvent. The behavior of the central component in the mixed solvent was qualitatively similar to that observed in pure ethylamine. For example, compare Figure 4 with Figure 3. An advantage of the mixed solvent is that amplitude changes may be easily followed to sufficiently low concentrations so that the amplitude of both the single line and the hyperfine components decrease together, as is shown in Figure 4. As was the case in the pure ethylamine solutions, the breadth of the central component increased rapidly with increasing metal concentration, as is shown by the plot in Figure 5.

In the absence of excessive amounts of decomposition products, the line shapes for the hyperfine components in pure ethylamine were nearer Gaussian than Lorentzian. A comparison between one of the hyperfine lines for K in pure ethylamine and Gaussian and Lorentzian shapes is given in Figure 6. Clearly the observed line shape is far from being Lorentzian.

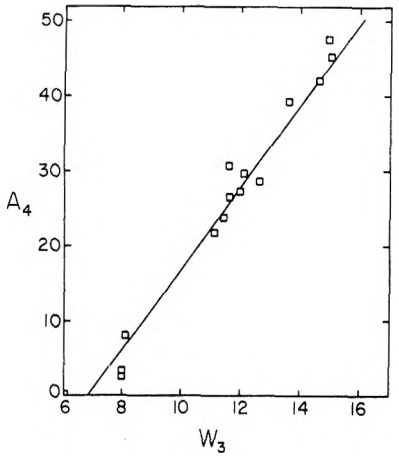

Figure 5. Width of the central line, W_3, vs. amplitude of the hyperfine spectrum for mixed solvent. Line widths are not corrected for the effect of modulation.

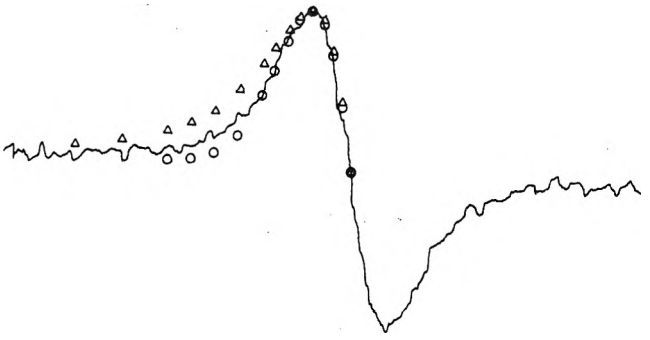

Figure 6. The shape of hyperfine lines for K dissolved in pure ethylamine: Δ, Lorentzian line shape; O, Gaussian line shape.

The hyperfine coupling constant for K in ethylamine was 9.6 G and that for K in the mixed solvent, 7.8 G.

Analysis of Data

Catterall and Symons[3] have invoked an ion-pair-type equilibrium

$$K \rightleftarrows K^+ + e^- \qquad (2)$$

to account for the changes[12] they observed in ESR spectra of potassium solutions in ethylamine on changing metal concentration. We find that our data on K solutions in the mixed solvent are also in accord with such an equilibrium in very dilute solutions, as is shown in Figure 7 in which the square root of the amplitude of one of the hyperfine components, $A_K^{1/2}$, is plotted vs. the amplitude of the central component, A_3. The points in the dilute range follow a straight line which extrapolates to the origin. In these dilute solutions, the breadth of the central line remains essentially constant at a value less than 0.1 G. The breadth of the hyperfine components remains constant over the entire concentration range investigated. Since the modulation amplitude remained fixed, the amplitudes of the derivative curves are proportional to concentrations when the line breadths do not change. In the more concentrated solutions, the points deviate violently from this straight line, as is to be expected on account of the rapidly changing breadth of the central component. In this range of concentrations a different correlation between the amplitude of the central line and that of the hyperfine component appears as is shown in Figure 8. Remarkably, the two amplitudes are inversely proportional to one another. Because we are overmodulating (modulation amplitude = 0.8 G peak to peak) during this set of experiments, we expect the proportionality

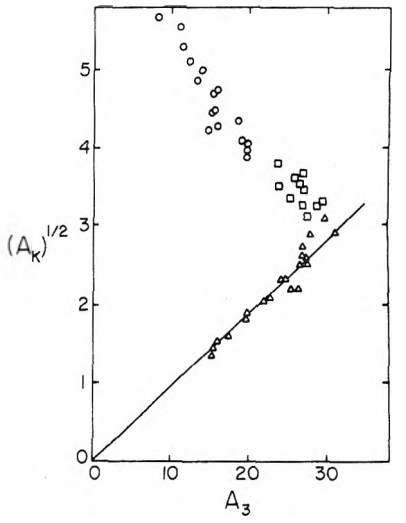

Figure 7. The amplitude of the central component A_3 vs. the square root of the amplitude of the hyperfine lines.

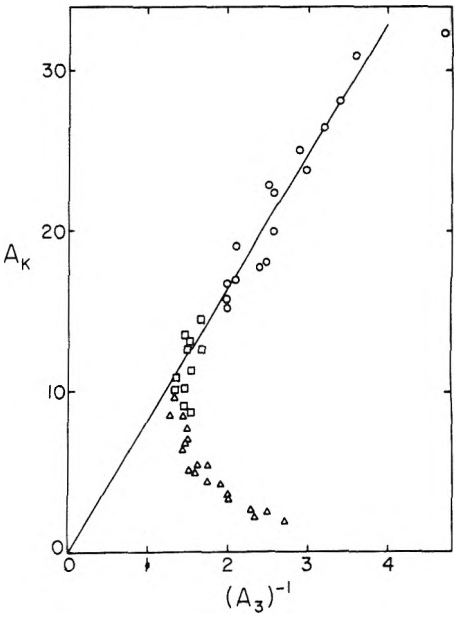

Figure 8. The reciprocal of the amplitude of the central component, A_3, vs. the amplitude of the hyperfine lines.

$$A_3 W_3^2 \propto [S^-] \qquad (3)$$

to hold approximately in which S^- denotes the species responsible for the single line resonance. Empirically, $A_3 \propto (A_K)^{-1}$ (see Figure 8) and $W_3 \propto (A_K)$ (see Figure 5). Combining these proportionalties with eq 3 and $A_K \propto [K]$ gives

$$[S^-] \propto [K] \qquad (4)$$

Thus we are led to the conclusion that in the higher concentration range the species responsible for the single line resonance is no longer related to the monomer through an equilibrium of the type given in eq 2. Rather, the two species must be isomeric. This situation can be accounted for by introducing a new species, the ion pair of the solvated electron with K^+, so that

$$K \rightleftarrows K^+ \cdot e^- \quad (5)$$

is the important equilibrium in the higher concentration range. However, the rates of the processes by which the central line becomes broadened depend linearly on [K]. Spin exchange between monomer and the solvated electron according to

$$K(\uparrow) + e^-(\downarrow) \rightleftarrows K(\downarrow) + e^-(\uparrow)$$
$$K(\uparrow) + K^+ \cdot e^-(\downarrow) \rightleftarrows K(\downarrow) + K^+ \cdot e^-(\uparrow) \quad (6)$$

satisfy this criterion. The broadening produced in a solution in which [K] $\approx 2 \times 10^{-6}$ M is about 0.3 G. Consequently, the lifetime of the solvated electron spin is

$$\tau = \frac{1}{\gamma_e \Delta H} \approx \frac{1}{5 \times 10^6} = 2 \times 10^{-7} \text{ sec} \quad (7)$$

and the rate constant for spin exchange is

$$k = 1/\tau[K] \approx 3 \times 10^{12} \text{ l./(mol sec)} \quad (8)$$

The magnitude of this rate constant appears to be well above the diffusion-controlled limit. This exceptionally large value may perhaps be attributed to a high cross section for spin exchange due in part to the large sizes of solvated electron and monomer.

One consequence of the above analysis is that it is inconsistent with the explanation of the temperature dependence of the hyperfine coupling constant through a rapid interconversion of K and $K^+ \cdot e^-$ because $K^+ \cdot e^-$ contributes to the single line resonance. In addition, it has been previously reported[6] and we also find (see Figure 6) that the shapes of the lines of the hyperfine patterns are often more nearly Gaussian than Lorentzian. Since the explanation based on rapid interconversion requires that the lines be Lorentzian, it is difficult to see how this explanation can be entirely correct. On the other hand, the model in which the temperature dependence of a_K is attributed to thermally accessible vibrationally excited states does not require the lines to be Lorentzian. The observed line shape merely reflects the distribution in the values of a_K over the vibrational states. In this model the lines of the hyperfine pattern are expected to increase in breadth at greater values of m_I as is actually observed. Actually the distribution in a_K must be related to the temperature dependence of the average coupling constant $\bar{a}_K$ through

$$\frac{d\bar{a}_K}{dT} = \frac{1}{kT^2}(\overline{a_K \epsilon} - \bar{a}_K \bar{\epsilon}) \quad (9)$$

in which ϵ is the energy of the state with coupling constant a_K. Consequently, observation of a temperature dependence implies a distribution and vice versa.

Recently Catterall and Edwards[11] have reported observation of two metal-dependent species in ESR spectra of alkali metals in a hexamethylphosphoramide glass at low temperatures. These authors claim that these species are the ones which are interconverting rapidly in solution to give a temperature-dependent hyperfine coupling. An alternative interpretation of their data is that the two species which they observe are the monomer and the ion pair of the solvated electron with the metal cation, the same species which are observed in liquid solutions. The lack of temperature dependence of the metal hyperfine coupling constants in their glasses is puzzling. If the states with different values of a_M are all degenerate, then $d\bar{a}_M/dT = 0$. Otherwise, the dependence of a_M on ϵ may be such that over a limited temperature range the variation in $\bar{a}_M$ is negligibly small.

References and Notes

(1) K. D. Vos and J. L. Dye, *J. Chem. Phys.*, **38**, 2033 (1963).
(2) K. Bar-Eli and T. R. Tuttle, Jr., *J. Chem. Phys.*, **40**, 2508 (1964).
(3) R. Catterall and M. C. R. Symons, *J. Chem. Soc.*, 6656 (1965).
(4) K. Bar-Eli and T. R. Tuttle, Jr., *J. Chem. Phys.*, **44**, 114 (1966).
(5) L. R. Dalton, J. D. Rynbrandt, E. M. Hansen, and J. L. Dye, *J. Chem. Phys.*, **44**, 3969 (1966).
(6) J. L. Dye and L. R. Dalton, *J. Phys. Chem.*, **71**, 184 (1967).
(7) R. Catterall, M. C. R. Symons, and J. W. Tipping, *J. Chem. Soc. A*, 1529 (1966).
(8) R. Catterall, J. Slater, and M. C. R. Symons, *J. Chem. Phys.*, **52**, 1003 (1970).
(9) V. A. Nicely and J. L. Dye, *J. Chem. Phys.*, **53**, 119 (1970).
(10) R. Catterall, I. Hurley, and M. C. R. Symons, *J. Chem. Soc. A*, 139 (1972).
(11) R. Catterall and P. P. Edwards, *J. Chem. Soc., Chem. Commun.*, 96 (1975).
(12) R. Catterall, M. C. R. Symons, and J. W. Tipping, *J. Chem. Soc. A*, 1234 (1967).
(13) D. E. O'Reilly and T. Tsang, *J. Chem. Phys.*, **42**, 3333 (1965).
(14) I. Hurley, T. R. Tuttle, Jr., and S. Golden, "Metal Ammonia Solutions", Butterworths, London, 1970.
(15) N. M. Atherton and S. I. Weissman, *J. Am. Chem. Soc.*, **83**, 1330 (1961).
(16) J. Danner, Thesis, Brandeis University, 1966.
(17) H. Wahlquist, *J. Chem. Phys.*, **35**, 1708 (1961); G. W. Smith, *J. Appl. Phys.*, **35**, 1217 (1964).

Discussion

R. CATTERALL. (1) Modulation amplitude is not the critical factor in observing the central singlet; we observe it easily at much lower modulation amplitude. It is simply a problem of machine sensitivity.

(2) To carry out the correlations of amplitude of ESR lines from multiplet and singlet spectra, it is essential to correct for microwave power saturation. We have carried out an analysis of spectra corrected in this way together with optical spectra. We cannot fit the observed data with either a one-equilibrium model,

$$M^+ + e^- \rightleftarrows M$$

or with a two-equilibrium model including

$$M + M \rightleftarrows M_2$$

but we can get a good fit if we use a three-equilibrium scheme

$$M^+ + e^- \overset{K_1}{\rightleftarrows} M$$
$$M + e^- \overset{K_2}{\rightleftarrows} M^-$$
$$M^+ + M^- \overset{K_3}{\rightleftarrows} M^+M^-$$

and find $K_1 = (10 \pm 0.4) \times 10^6$, $K_2 = (3.2 \pm 0.04) \times 10^8$, $K_3 = (2.3 \pm 1.0) \times 10^4$ for a concentration range 5×10^{-5} down to 10^{-7} M. Over a limited concentration region, the correlation of $(A_K)^{1/2}$ vs. A_3 and A_K vs. $(A_3)^{-1}$ does indeed hold as shown by Tuttle, the singlet being due to a mixture of e_{sol}^- and its ion pair $M^+e_{sol}^-$.

(3) The point about the temperature dependence of the A_{iso} value in our HMPA work I do not really understand. We have completely separate distribution functions for each of our "solvated atom species", and while your analysis certainly applies *within* a single peak in the distribution function, it should not affect the A values very much. It should, I agree, affect the m_I dependence, but this we do not observe. Since the peaks in the distribution function are very sharp (e.g., standard deviation ~2 G in Cs atoms with an A value of 600 G), the temperature dependence of the A value may simply be within our experimental error.

T. R. TUTTLE. (1) Modulation amplitude often is an important factor in determining what is observed in a spectrum containing lines of different widths. Apart from any question of spectrometer sensitivity, Figure 1 in our paper shows how the central component may be missed entirely, even though it is present, by employing too low a modulation amplitude. We too find that the central component may be observed at lower modulation amplitudes in solutions of lower metal concentrations. This is part of the curious behavior of the central component to which we draw attention.

(2) During our experiments, the spectrometer was operated at a power of less than 1 mW incident on the cavity.

(3) The spectra for glassy solutions (see the paper by R. Catterall and P. P. Edwards, *J. Phys. Chem.*, this issue) which Catterall presents are not qualitatively different from those which are observed in liquid solutions. For example, the spectra in glassy HMPA show a similar variation in line breadth with changing m_I as is observed generally for spectra of the monomer in liquid solutions. This variable line breadth has been accounted for by the two or multistate model of the monomer through rapid exchange between the states in liquid solutions. In the glassy HMPA solutions, on the other hand, Catterall claims to have trapped the two or more species which undergo rapid exchange in liquid solution. Yet, the variation of line breadth with changing m_I persists even though the process which is supposed to give rise to this phenomenon in liquid solutions is supposedly quenched in the glasses. Consequently, a different mechanism for line broadening in the glasses is postulated by Catterall, namely that the breadths are due to a distribution of values for the metal hyperfine coupling constant. This is essentially the model originally proposed by Bar-Eli and myself for liquid solutions. This model apparently applies equally well for liquid and glassy solutions. Catterall presents no evidence to suggest otherwise. However, apart from any particular model, the observation of a distribution of values for the metal hyperfine coupling constant a_M implies a temperature dependence in the average value, $\bar{a}_M$, according to general statistical considerations (see eq D1). Only under special circumstances will the temperature coefficient vanish. One such circumstance would be if the states with different values of a_M all have the same energy. The point is that the lack of temperature dependence of $\bar{a}_M$ observed by Catterall must be considered "accidental" in view of the observed distribution in a_M.

In recent experiments we have found that for potassium solutions in a mixed methylamine–ethylamine solvent the hyperfine lines are Lorentzian in contrast to the situation in pure ethylamine where the lines were found to deviate substantially from the Lorentzian shape. Nicely and Dye[9] have also reported Lorentzian lines in a mixed ethylamine–ammonia solvent for cesium solutions while Dye and Dalton[6] have reported near-Gaussian lines for metal solutions in pure ethylamine. This difference in line shape between pure and mixed solvents is naturally accounted for within the context of the model in which the temperature dependence of $\bar{a}_M$ is attributed to a distribution over thermally accessible excited states. In the pure solvent, the exchange of solvent between bulk solvent and the solvation sphere of the monomer does not change $\bar{a}_M$ appreciably, while in the mixed solvent, exchange of one kind of solvent molecule for another in the solvation sphere modulates $\bar{a}_M$. If the exchange is rapid compared to the corresponding difference in hyperfine frequencies, the result will be an exchange-narrowed Lorentzian line, as is observed.

In addition, the enhanced temperature coefficient which Catterall observes for metal hyperfine coupling constants in mixed solvents (see Figure D1 in comments of R. Catterall on the paper by Fletcher and Seddon) may be accounted for in the following way. Whatever structural features are responsible for the spread of coupling constants in the pure solvent, the addition of a second solvent will almost inevitably increase the spread, because to all the structural possibilities involving just one solvent must be added those involving mixed solvent. Of course the change in the temperature coefficient will depend on how the a_M of the various structures correlate with their energies. Since better solvating solvents always seem to lower $\bar{a}_M$, there appears to be a direct relationship between a_M and the corresponding energy. For simplicity let us assume a direct proportionality, i.e., $a_M = \beta\epsilon_M$ in which β is the proportionality constant. Inserting this proportionality into eq 9 of the paper leads to

$$\frac{d\bar{a}_M}{dT} = \frac{\beta}{kT^2}(\overline{\epsilon_M^2} - \bar{\epsilon}_M^2) = \frac{1}{\beta kT^2}(\overline{a_M^2} - \bar{a}_M^2) \qquad \text{(D1)}$$

i.e., the temperature coefficient of $\bar{a}_M$ is proportional to the dispersion in energy, or the dispersion in coupling constant. Thus, if the spread in coupling constant, which is measured by its dispersion, is increased on addition of a second solvent, we may expect an enhanced temperature coefficient. In contrast, the multistate model does not appear to offer any ready explanation of the observed enhanced temperature coefficients in mixed solvents.

Nuclear Magnetic Resonance Studies of Alkali Metal Anions

James L. Dye,* Charles W. Andrews, and Joseph M. Ceraso

Department of Chemistry, Michigan State University, East Lansing, Michigan 48824 *(Received July 28, 1975)*

Publication costs assisted by the U.S. Energy Research and Development Administration

The NMR chemical shift and line width has been measured for $^{23}Na^-$ in tetrahydrofuran (THF), ethylamine (EA), and methylamine (MA), for $^{87}Rb^-$ in THF and EA, and for $^{133}Cs^-$ in THF. In all cases, the counterion was the 2,2,2 cryptate complex of the corresponding cation. The chemical shift of Na^- is, within experimental error, the same as that calculated for the gaseous anion (based upon the measured value for the gaseous atom) and is independent of solvent. Comparison with the solvent-dependent chemical shift of Na^+ provides conclusive evidence that Na^- is a "genuine" anion with two electrons in a 3s orbital which shield the 2p electrons from the influence of the solvent. The line width increases from THF to EA to MA, suggesting either an increasing exchange rate with the cryptated cation or, more probably, the influence of an increasing concentration of solvated electrons. In the case of sodium solutions in all solvents, both Na^+C and Na^- are detected by their NMR peaks. However, probably because of extreme line broadening, Rb^+C and Cs^+C are not observed, but only the relatively narrow line of the corresponding anion. The chemical shifts (diamagnetic shift in ppm from the infinitely dilute aqueous ion) are 185 and 197 for Rb^- in EA and THF, respectively, and 292 for Cs^- in THF, compared with 212 and 344, respectively, for the gaseous Rb and Cs atoms. When 18-crown-6 is used instead of the 2,2,2 cryptand complex, it is still possible to obtain solutions which are about 0.4 *M* in total metal when methylamine is used as the solvent. However, in this case, both the Na^- and the Na^+C NMR peaks are exchange broadened, even at −50°C, and coalesce as the temperature is raised to about −15 to 0°C, depending upon the concentrations. The variation of the rate of exchange of the sodium nucleus between Na^+C and Na^- with concentration should permit determination of the exchange mechanism. Possible exchange mechanisms and the information obtainable from them are discussed.

Introduction

The evidence for the existence of species of stoichiometry M^- in metal–amine and metal–ether solutions is very convincing.[1] The shift of the optical absorption band with metal, solvent, and temperature[2,3] suggests strongly that the species is a centrosymmetric anion. However, other models cannot be ruled out on the basis of optical evidence alone. Figure 1 shows three other contenders for the M^- structure. Indeed, one or more of such structures might be responsible for the diamagnetic species in metal–*ammonia* solutions which, to date, show no *specific* evidence for the existence of centrosymmetric anions. We believe that the $^{23}Na^-$ NMR spectra in ethylamine (EA) and tetrahydrofuran (THF),[4] and the data described in this paper, provide the best evidence so far available that the anion in these solvents is centrosymmetric with two electrons in the outer s orbital.

Optical pumping,[5,6] atomic beam,[7] and NMR[8-11] techniques have established the shielding constants of the aqueous cations $^{23}Na^+$, $^{87}Rb^+$, and $^{133}Cs^+$ relative to the gaseous atoms with an accuracy of at least 2%. It is possible to make reliable calculations[12] of the shielding constants of $Na^+(g)$ and $Na^-(g)$ relative to the free atom by using Lamb's complete expression for atomic diamagnetic shielding[13] and analytic Hartree–Fock wave functions.[14] The changes in shielding constants are relatively small, amounting to only 7.7 ppm (diamagnetic) for the addition of two 3s electrons to gaseous Na^+ to form $Na^-(g)$. Corresponding shifts for $Rb^-(g)$ and $Cs^-(g)$ are also expected to be small. Diamagnetic contributions from solvation are generally only a few parts per million,[15-17] and the major effect of the solvent, both from theoretical expectations and experimental results,[18] is a substantial paramagnetic shift (45 to 75 ppm) upon solvation. The magnitude of this shift correlates very well with the donicity of the solvent,[19-23] that is, the ability of the solvent to donate electron density to the cation. It is via the interaction of this solvent electron density with the outer p orbitals of the alkali metal cation which gives the observed paramagnetic shifts.

Experimental Section

Solvents and metals were purified as previously described.[3] The 2,2,2 cryptand, **1** (C_{222}), was synthesized by a modification[24] of the method of Dietrich, Lehn, and Sauvage.[25] The second complexing agent, 18-crown-6, **2** (18-C-6), from PCR Inc., Gainesville, Fla., was recrystallized twice from acetonitrile and vacuum dried. The NMR system has been previously described[4] except that multinuclear capabilities[26] have been added.

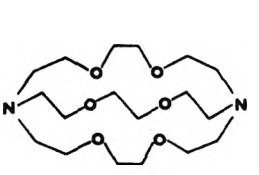

1
2,2,2 Cryptand
(C_{222})

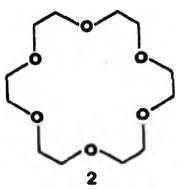

2
18-Crown-6
(18-C-6)

Chemical Shifts and Line Widths

The key factor which permits us to study the NMR spectra of alkali metal anions is the complexation of the *cation*

TABLE I: Selected List of Shielding Constants and Line Widths

Ion	Concn, M	Temp, °C	Solvent	$\sigma(M_{solv}$ vs. $M_g)$,[a] ppm	$\Delta\nu_{1/2}$,[b] Hz	Ref[c] σ	Ref[c] $\Delta\nu_{1/2}$
Na^+	∞ dil	25	H_2O	−60.5 ± 1	5.16	7	43
Rb^+	∞ dil	25	H_2O	−211.6 ± 1.2		7	
Cs^+	∞ dil	25	H_2O	−344.3 ± 5.8	0.02	7	43
F^-	∞ dil	25	H_2O	−168 ± 2[d]		16,44	
Br^-	∞ dil	25	H_2O	−194 (calcd)[d]		17	
Na^+	Sat NaCl	25	H_2O	−61.2	8.0	11	
Na^+	0.3 NaI	−15	MA	−72.2	9.0		
Na^+	0.25 NaI	25	EA	−74.4	17.9		
Na^+	0.2 $NaPh_4B$	25	THF	−52.9	23.0		
Na^+C	0.15 Na^+C,Na^-	−15	MA	−49.8	30.8		
Na^+C	0.15 Na^+C,Na^-	−17 to +1	EA	−50.8	120–170		
Na^+C	0.15 Na^+C,Na^-	−4	THF	−50.4	51		
Na^-	Gas			+2.6 (calcd)		12	
Na^-	0.15 Na^+C,Na^-	−15	MA	+1.4	11		
Na^-	0.15 Na^+C,Na^-	−17 to +1	EA	+1.6	6–9		
Na^-	0.15 Na^+C,Na^-	−4	THF	+2.3	<3		
Rb^+	0.1 RbI	25	H_2O	−212.7	158	11	
Rb^+	0.4 RbI	25	CH_3OH	−199.6	300		
Rb^+C	0.4 Rb^+C,I^-	25	H_2O	−262	1300		
Rb^+C	0.4 Rb^+C,I^-	25	CH_3OH	~−300	4000		
Rb^-	0.1 Rb^+C,Rb^-	−40	EA	−26.2	220		
Rb^-	0.1 Rb^+C,Rb^-	−46	THF	−14.4	15		
Cs^+	0.1 CsI	25	H_2O	−348.4	<3	45	
Cs^+	0.08 CsI	25	CH_3OH	−315.3	<3		
Cs^+C	0.08 Cs^+C,I^-	25	CH_3OH	−476.7	30		
Cs^-	0.1 Cs^+C,Cs^-	−71	THF	−52.3	10		

[a] Shielding constant, σ, defined by $\omega = \gamma(1 - \sigma)H_0$, where H_0 is the static magnetic field and γ is the gyromagnetic ratio for the neutral gaseous atom. [b] $\Delta\nu_{1/2}$ = full width at half-height. [c] Where no reference is cited, data refer to the present work. [d] Reference state is the gaseous anion.

by macrocyclic polyethers of the crown[27] and cryptand[25,28] classes. There are two reasons for the importance of this complexation. First, the pronounced enhancement of metal solubility[3,29-33] permits the use of metal concentrations which are high enough to study by alkali metal NMR techniques. Second, the complexed cation is released slowly enough by the complexing agent so that, at low enough temperatures, the exchange of M^+C with solvated cations is slow on the NMR time scale.[34-42] This makes it possible to observe separate resonances for M^+C and M^-.

The ^{23}Na NMR spectrum of Na^+C_{222}, Na^- has been studied as a function of temperature in three solvents: THF, EA, and methylamine (MA). The results are summarized in Table I. Typical spectra are displayed in Figure 2. The most striking features are the virtual absence of a solvent-induced paramagnetic shift for Na^- and the narrowness of this line. The complexed cation, Na^+C_{222}, has a chemical shift which is also nearly independent of the solvent and is at the same position as for ordinary salts of Na^+C_{222} in these solvents. By contrast, the chemical shift of the solvated cation, Na^+, is strongly solvent dependent. The values of the various shielding constants relative to the free gaseous atom are given in Table I. Since the cryptated cation is enclosed within the same "crypt" in all three solvents and is therefore separated from the solvent, it is not surprising that its chemical shift is nearly solvent independent.

The chemical shift of Na^- is not only independent of solvent, but is also nearly the same as that of Na^- in the gas phase. This behavior is completely different from that of any ion with filled outer p orbitals as indicated in Table I. Marked paramagnetic shifts are caused by the orbital angular momentum introduced by interaction of solvent electron density with the filled outer p orbital. In the case of

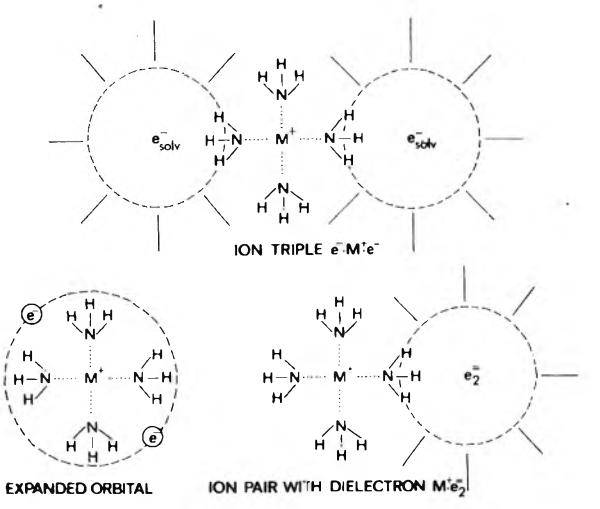

Figure 1. Three possible models for a species of stoichiometry M^-. All of these models permit solvent interaction with the outer p electrons of the cation. Ammonia is used to represent any amine or ether solvent.

halide anions, the paramagnetic shift probably results from donation of electron density from the filled outer p orbitals to the solvent. The absence of a chemical shift for Na^- shows that the 2p orbitals are well shielded from the solvent by the presence of the filled 3s orbital. This would not be the case for any of the models shown in Figure 1. We conclude, therefore, that the most reasonable model for Na^- is that of a centrosymmetric anion with two electrons in the outer s orbital. It is not obvious why the shift is as small as it is, since electron donation to or from the solvent and the mixing of s and p character could yield a paramagnetic shift. Perhaps the large size of the anion causes the chemical shift to be small.

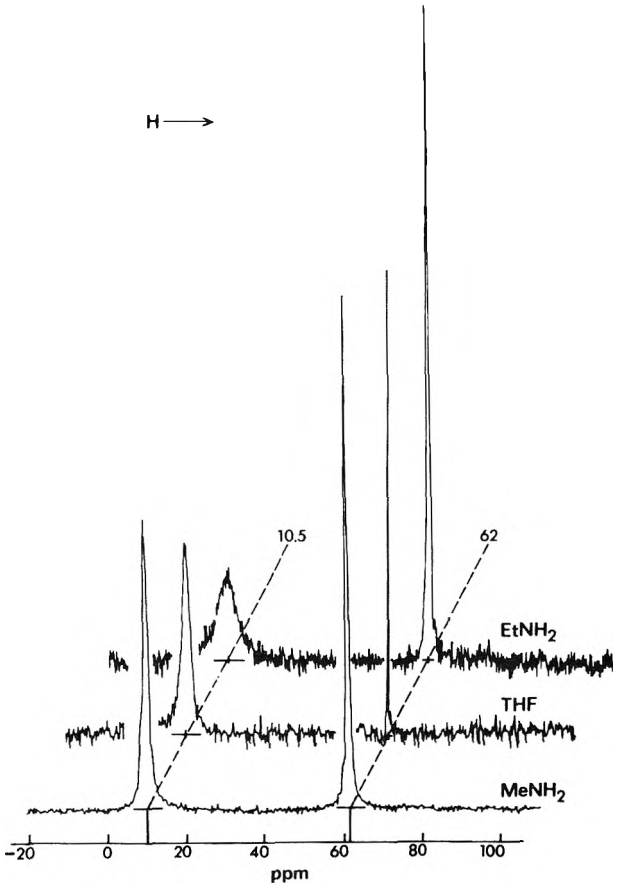

Figure 2. ^{23}Na NMR spectra of Na^+C_{222},Na^- solutions (~0.1 *M*) in three solvents. All chemical shifts are referenced to aqueous Na^+ at infinite dilution.

The extreme narrowness of the line for Na^- also attests to the high spherical symmetry of this species. Quadrupolar broadening of ^{23}Na NMR lines is common (see Table I) and results from an electric field gradient at the nucleus. Even such presumably symmetric cations as $Na^+(aq)$ are quadrupole broadened to 5 Hz (full width at half-height). By contrast, the true line width of Na^- in THF is less than 3 Hz compared with 23 Hz for Na^+ in THF. Since the lines may also be broadened by the presence of e_{solv}^- via a paramagnetic interaction, it is difficult to obtain the true quadrupole-broadened line width. The relative concentration of e_{solv}^- tends to vary from one sample to another, depending upon the solvent used and the method of preparation.[1] Therefore, we find that the line widths are not completely reproducible. Since exchange of sodium between Na^- and either Na^+C or Na^+ would also broaden the line (see below), we cannot completely rule this out. However, it seems unlikely since the line width of Na^- does not decrease markedly as the temperature is lowered. Within experimental error, the area under the Na^+C peak is equal to that under the Na^- peak, in agreement with the proposed stoichiometry.

NMR Spectra of Rb^- and Cs^-

Preliminary NMR studies of $^{87}Rb^-$ in EA and THF and of $^{133}Cs^-$ in THF have been made. The results are given in Table I. Just as for Na^-, these anions give narrow lines which are diamagnetically shifted from the corresponding cations by a large amount. The NMR absorptions of Rb^+C and Cs^+C were not observed in the M^+C,M^- samples,

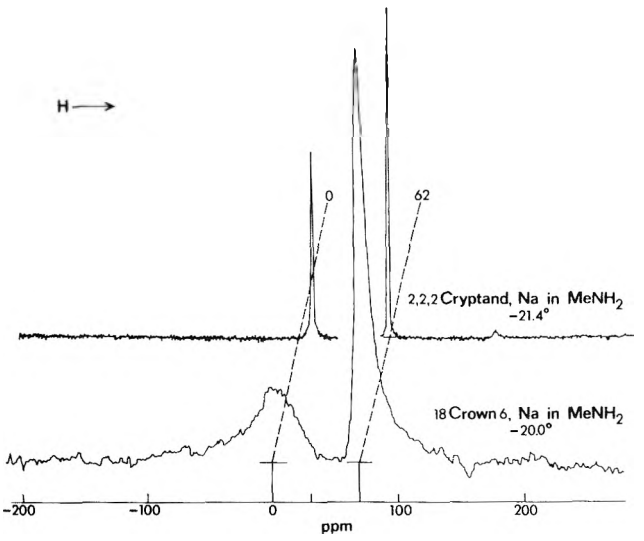

Figure 3. ^{23}Na NMR spectra of Na^+C_{222},Na^- and Na^+(18-C-6), Na^- (~0.1 *M*) in methylamine.

probably because of line broadening. The signal-to-noise ratio was satisfactory for observation of the narrow Rb^- and Cs^- lines but not for the broad lines expected for Rb^+C and Cs^+C. Studies with salts indicate that the line width of Rb^+C is far too broad to have been observed in the metal solution case. The situation for the case of Cs^+C is not as clear. If the line width were in excess of 200 Hz, the signal would have been lost in the noise. In methanol at 25°C the line width of Cs^+C (iodide salt) is 30 Hz. It might be expected to be much broader in THF at −71°C. The aqueous Rb^+ and Cs^+ ions are paramagnetically shifted 212 and 344 ppm from the respective gaseous atoms. Values for the gaseous anions are not known but are presumably shifted diamagnetically a few parts per million from the atoms. The resonance positions of Rb^- in EA and THF are shifted 26 and 14 ppm paramagnetically from the atom, and Cs^- in THF is shifted 52 ppm. Although the shielding constants are not as close to the gaseous anions as for the case of sodium, they are very close compared with the range of chemical shifts for the corresponding solvated cations.[45,46] The line width of Rb^- in THF, 15 Hz, is much narrower than that of the Rb^+ ion in any solvent. However, this is not the case for Rb^- in EA or Cs^- in THF which have line widths comparable to those of the solvated cations. It is likely that the lines of Rb^- and Cs^- are either paramagnetically broadened by e_{solv}^- or are broadened by exchange.

NMR Spectrum of Na^+(18-C-6),Na^-

Although the exchange rate of Na^+C_{222} with Na^+ is relatively slow in these solvents, the exchange between the crown complexes and the solvated ion is fast.[35,38] However, the complexation constant is large enough to permit formation of sodium solutions in MA as concentrated as 0.4 *M* in total sodium. Preliminary NMR studies show that in this case sodium exchanges at a measurable rate between Na^+C and Na^-. As shown in Figure 3, the chemical shift of Na^- is the same as that obtained by using C_{222} as the complexing agent. However, the NMR lines of both Na^+(18-C-6) and Na^- are very much broader than the corresponding lines obtained with the 2,2,2 cryptand complexing agent. As the temperature is raised, a classical line-collapse pattern is observed as shown in Figure 4. Note the extreme width of the

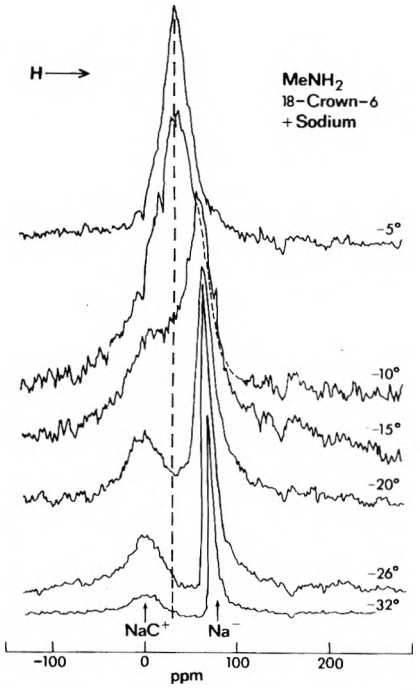

Figure 4. ^{23}Na NMR spectra of Na^+(18-C-6),Na^- (~0.1 *M*) in methylamine at various temperatures.

line near coalescence (≈700 Hz) which tends to degrade the signal-to-noise ratio.

The exchange could occur directly via the process

$$Na^- + Na^+C \rightleftarrows Na^+C + Na^- \quad (1)$$

or indirectly through Na^+ via such processes as

$$Na^+C \rightleftarrows Na^+ + C \quad (2)$$

$$Na^+ + Na^- \rightleftarrows Na^- + Na^+ \quad (3)$$

$$Na^- + C \rightleftarrows Na^+C + 2e_{solv}^- \quad (4)$$

$$Na^- \rightleftarrows Na^+ + 2e_{solv}^- \quad (5)$$

From the changes in the lifetimes τ_{Na^-} and τ_{Na^+C} with concentration of the various species present, it should be possible to determine the exchange mechanism which is operative. For equimolar concentrations of Na^+C and Na^- of ~0.15 *M*, the mean lifetime, τ, varies from ~7 msec at −33°C to ~0.2 msec at the coalescence temperature of −5°C to ~0.05 msec at +6°C. Additional studies are needed to obtain the mechanism and the rate constants.

Acknowledgment. This research was supported by the U.S. Energy Research and Development Administration under Contract No. E(11-1)-958.

References and Notes

(1) See J. L. Dye, C. W. Andrews, and S. E. Mathews, *J. Phys. Chem.*, paper in this issue, for appropriate references.
(2) S. Matalon, S. Golden, and M. Ottolenghi, *J. Phys. Chem.*, **73**, 3098 (1969).
(3) M. T. Lok, F. J. Tehan, and J. L. Dye, *J. Phys. Chem.*, **76**, 2975 (1972).
(4) J. M. Ceraso and J. L. Dye, *J. Chem. Phys.*, **61**, 1585 (1974).
(5) C. W. White, W. M. Hughes, G. S. Hayne, and H. G. Robinson, *Phys. Rev.*, **174**, 23 (1968).
(6) G. S. Hayne, C. W. White, W. M. Hughes, and H. G. Robinson, *Bull. Am. Phys. Soc.*, **13**, 20 (1968).
(7) A. Beckmann, K. D. Böklen, and D. Elke, *Z. Phys.*, **270**, 173 (1974).
(8) O. Lutz, *Phys. Lett. A*, **25**, 440 (1967).
(9) O. Lutz, *Z. Naturforsch., Teil A*, **23**, 1202 (1968).
(10) O. Lutz and A. Schwenk, *Phys. Lett. A*, **24**, 122 (1967).
(11) C. Deverell and R. E. Richards, *Mol. Phys.*, **10**, 551 (1966).
(12) G. Malli and S. Fraga, *Theor. Chim. Acta*, **5**, 275 (1966).
(13) W. Lamb, *Phys. Rev.*, **60**, 817 (1941).
(14) E. Clementi, "Tables of Atomic Wave Functions", IBM Corp., San Jose, Calif., 1965.
(15) A. Saika and C. P. Slichter, *J. Chem. Phys.*, **22**, 26 (1954).
(16) C. Deverell, *Mol. Phys.*, **16**, 491 (1969).
(17) D. Ikenberry and T. P. Das, *Phys. Rev.*, **138**, A822 (1965).
(18) C. Deverell, *Progr. Nucl. Magn. Reson. Spectrosc.*, **4**, 278 (1969).
(19) E. G. Bloor and R. G. Kidd, *Can. J. Chem.*, **46**, 3425 (1968).
(20) R. H. Erlich, E. Roach, and A. I. Popov, *J. Am. Chem. Soc.*, **92**, 4989 (1970).
(21) R. H. Erlich and A. I. Popov, *J. Am. Chem. Soc.*, **93**, 5620 (1971).
(22) M. Herlem and A. I. Popov, *J. Am. Chem. Soc.*, **94**, 1431 (1972).
(23) M. S. Greenberg, R. L. Bodner, and A. I. Popov, *J. Phys. Chem.*, **77**, 2449 (1973).
(24) J. L. Dye, M. T. Lok, F. J. Tehan, J. M. Ceraso, and K. J. Voorhees, *J. Org. Chem.*, **38**, 1773 (1973).
(25) B. Dietrich, J. M. Lehn, and J. P. Sauvage, *Tetrahedron Lett.*, 2885, 2889 (1969).
(26) D. D. Traficante and J. A. Simms, *J. Magn. Reson.*, **15**, 484 (1974).
(27) C. J. Pederson, *J. Am. Chem. Soc.*, **89**, 7017 (1967).
(28) J. M. Lehn, *Struct. Bonding (Berlin)*, **16**, 1 (1973).
(29) J. L. Dye, M. G. DeBacker, and V. A. Nicely, *J. Am. Chem. Soc.*, **92**, 5226 (1970).
(30) J. L. Dye, M. T. Lok, F. J. Tehan, R. B. Coolen, N. Papadakis, J. M. Ceraso, and M. G. DeBacker, *Ber. Bunsenges. Phys. Chem.*, **75**, 659 (1971).
(31) J. L. Dye in "Electrons in Fluids", J. Jortner and N. R. Kestner, Ed., Springer-Verlag, West Berlin, 1973, p 77.
(32) J. L. Dye, J. M. Ceraso, M. T. Lok, B. L. Barnett, and F. J. Tehan, *J. Am. Chem. Soc.*, **96**, 608 (1974).
(33) F. J. Tehan, B. L. Barnett, and J. L. Dye, *J. Am. Chem. Soc.*, **96**, 7203 (1974).
(34) J. M. Lehn, J. P. Sauvage, and B. Dietrich, *J. Am. Chem. Soc.*, **92**, 2916 (1970).
(35) E. Shchori, J. Jagur-Grodzinski, Z. Luz, and M. Shporer, *J. Am. Chem. Soc.*, **93**, 7133 (1971).
(36) J. M. Ceraso and J. L. Dye, *J. Am. Chem. Soc.*, **95**, 4432 (1973).
(37) J. P. Kintzinger and J. M. Lehn, *J. Am. Chem. Soc.*, **96**, 3313 (1974).
(38) E. Shchori, J. Jagur-Grodzinski, and M. Shporer, *J. Am. Chem. Soc.*, **95**, 3842 (1973).
(39) Y. M. Cahen, J. L. Dye, and A. I. Popov, *Inorg. Nucl. Chem. Lett.*, **10**, 899 (1974).
(40) Y. M. Cahen, J. L. Dye, and A. I. Popov, *J. Phys. Chem.*, **79**, 1289 (1975).
(41) Y. M. Cahen, J. L. Dye, and A. I. Popov, *J. Phys. Chem.*, **79**, 1292 (1975).
(42) J. M. Ceraso, P. B. Smith, S. Landers, and J. L. Dye, to be published.
(43) H. G. Hertz, *Ber. Bunsenges. Phys. Chem.*, **77**, 531 (1973).
(44) M. R. Baker, C. H. Anderson, and N. F. Ramsey, *Phys. Rev. A*, **133**, 1533 (1964).
(45) J. D. Halliday, R. E. Richards, and R. R. Sharp, *Proc. R. Soc. Lond., Ser. A*, **313**, 45 (1969).
(46) Unpublished work, this laboratory.

Discussion

J. V. ACRIVOS. The optical work suggests that the presence of the crown compound influences the absorption spectrum of e^-, and the large diamagnetic shift you observe for Na^- suggests a large orbital contribution; i.e., the electrons may be delocalized in the crown compound. Have you measured the proton NMR absorption of the latter in your system?

J. L. DYE. Pulse radiolysis studies show that the e^- spectrum is *not* affected by the addition of the complexing agent. At the much higher concentrations used in metal solution studies, it is likely that species such as e_2^{2-} or ion clusters form and alter the spectrum. The NMR spectrum does not show a diamagnetic shift of Na^- but rather the absence of the usual paramagnetic shift of Na^+. The complexing agent is all used to complex Na^+ as indicated by the usual chemical shift and line width of Na^+C and the fact that only half as much C as total sodium is present. Therefore, Na^- is not associated with the complexing agent, at least not as intimately as is Na^+.

ADDITIONS AND CORRECTIONS

1958, Volume 62

John B. Greenshields and Frederick D. Rossini: Molecular Structure and Properties of Hydrocarbons and Related Compounds.

Page 273. In eq 6 the negative sign of the first term on the right has been omitted, so that the correct form of eq 6 is

$$\Delta Hv^0(\text{isomer}) - \Delta Hv^0(\text{normal}) = -0.118C_3 - 0.307C_4 + 0.164\Delta P_3 + 3.081\Delta W/(n^2 - n) \text{ kcal mol}^{-1}$$

Further, when this eq 6 is combined with eq 5, one obtains the correct equation for the difference between the standard enthalpy of formation of a given isomer and the corresponding normal paraffin hydrocarbon, at 25°C, for the gaseous state, as follows:

$$\Delta Hf^0(\text{isomer}) - \Delta Hf^0(\text{normal}) = -0.469C_3 - 1.364C_4 + 1.139\Delta P_3 + 12.508\Delta W/(n^2 - n) + 1.978P''_4 + 5.19P'_4 \text{ kcal mol}^{-1}$$

We thank Martin B. Smith for calling our attention to this typographical error in eq 6, which is given correctly in the doctoral thesis (J.B.G.) from which the paper was prepared.—Frederick D. Rossini

1971, Volume 75

Sheffield Gordon, W. Mulac, and P. Nangia: Pulse Radiolysis of Ammonia Gas. II. Rate of Disappearance of the $NH_2(X^2B_1)$ Radical.

Page 2093. In eq 19 and Figure 14, the value reported for $k_{NH_2+NO} = 1.6 \times 10^{10}\ M^{-1}\ \text{sec}^{-1}$ was incorrectly stated. The value for this rate constant at a total pressure of the system (NH_3 + NO) of 300 Torr and a temperature of 300 K as calculated from this slope should be $1.2 \times 10^{10}\ M^{-1}\ \text{sec}^{-1}$. This agrees within 5% of the value obtained by G. Hancock, W. Langi, M. Lenzi, and K. H. Welge obtained by laser fluorescence of NH_2 (private communication).—Sheffield Gordon

1973, Volume 77

F. Barat, L. Gilles, B. Hickel, and B. Lesigne: Effect of the Dielectric Constant on the Reactivity of the Solvated Electron.

Page 1713. Equation III should read

$$k_{\text{diff}} = \frac{4\pi N(r_A + r_B)(D_A + D_B)}{1000} \times \frac{Q}{(\exp Q) - 1} \quad \text{(III)}$$

Equation III′ should read

$$\log k_{\text{diff}} = \log \frac{4\pi N(r_A + r_B)(D_A + D_B)}{1000} - \frac{Q}{2.3} + \log Q \quad \text{(III′)}$$

Equation III″ should read

$$\log k_{\text{diff}} = \frac{\log 4\pi N(r_A/r_B)(D_A + D_B)}{1000} + \log(-Q) \quad \text{(III″)}$$

B. Hickel

1974, Volume 78

C. C. Chou and William L. Hase: Rice–Ramsperger–Kassel–Marcus Theory Applied to Decomposition of Hot Atom Substitution Products. c-C_4H_7T and c-C_4D_7T.

Page 2310. The second line of eq 1 should be changed to read

$$E_{ri} = L_i^2/2I_i \qquad i = x, y, \text{ or } z$$

Page 2313. The abscissa of Figures 3 and 4 should be changed to $1/P(\times 10^{-3}\ \text{Torr}^{-1})$.—William L. Hase

1975, Volume 79

Robert B. Hermann: Theory of Hydrophobic Bonding. III. A Method for the Calculation of the Hydrophobic Interaction Based on Liquid State Perturbation Theory and a Simple Liquid Model.

Page 164. The left-hand side of eq 3 should read d_{ii}. Omit the factor kT from both the second and third terms on the right-hand side of eq 8. The left-hand side of eq 12 should read $u_{11}(r)$. Column 2, line 23 should read "The quantity ρ_1 was . . ." instead of "The quantity σ_1 was . . .".

Page 165. Omit the factor kT from the right-hand side of eq 14, 15, and 18. In column 2, line 10, delete the symbols $S_A =$.

Page 166. In the caption under Figure 2, line 4 "μ_{in}" should read "$-\mu_{in}$".

The correct formulas were used in the calculations.—Robert B. Hermann

Raymond M. Fuoss: Conductance–Concentration Function for Associated Symmetrical Electrolytes.

Page 525. Corrections to this article have been published (*J. Phys. Chem.*, **79**, 1983 (1975)).—R. M. Fuoss

M. K. Chantooni, Jr., and I. M. Kolthoff: Acid–Base Equilibria in Methanol, Acetonitrile, and Dimethyl Sulfoxide in Acids and Salts of Oxalic Acid and Homologs, Fumaric and o-Phthalic Acids. Transfer Activity Coefficients of Acids and Ions.

Page 1176. In the third line of the Abstract delete the bar over HA^- in denominator, i.e., ... values of $K' = [\overline{HA}^-]/[HA^-]$, ...; in the tenth line delete the bar over second HA^-, i.e., ... in contrast to that in HA^-.

Page 1180. In the third line from bottom and bottom line of the right-hand column a bar should be placed over HA^-.

Page 1181. In the third line of the left-hand column, replace the word latter with former.

Page 1182. In the eighth line of the left-hand column, delete sentence: For fumaric acid, whose monoanion is intramolecularly hydrogen bonded in any of the solvents used, ${}^{AN}\Delta^{DMSO}pK(HE) = {}^{AN}\Delta^{DMSO}pK(HA) = 9.7 \pm 0.1_5$.—I. M. Kolthoff

Vaclav Zabransky and Robert W. Carr, Jr.: Photodissociation of Ketene at 313 nm.

Page 1618. The last paragraph in the Introduction should read as follows.

Since the pressure dependence of singlet and triplet products is diagnostic of whether or not $CH_2(^1A_1)$ and $CH_2(^3B_1)$ are formed by competing first-order and second-order processes, and hence to the details of excited state behavior, we have reinvestigated this aspect of ketene photolysis at 313 nm. In all of the above mentioned work, the yields of singlet and triplet products were obtained from relative product yields. Since many of the reactions and products of $CH_2(^1A_1)$ and $CH_2(^3B_1)$ with hydrocarbons are identical the relative contributions of singlet and triplet products may be difficult to determine. In this work we have used a pairwise photolysis technique which we have previously demonstrated to be reliable, to obtain relative *total* singlet and triplet product yields without having to separate individual products into their singlet and triplet components.[6]—Robert W. Carr, Jr.

John C. Owicki, Lester L. Shipman, and Harold A. Scheraga: Structure, Energetics, and Dynamics of Small Water Clusters.

Page 1795. In the right-hand column, lines 15 and 16, we neglected to note that, for clusters larger than the dimer, our definition of the hydrogen-bond nonlinearity (δ) was the deviation from linearity of the O–H···O angle rather than the H–O···O angle as in Figure 2. Deviations calculated with the latter definition are roughly 70% of those based on the O–H···O angle, for the geometries encountered in this study.

Page 1803. In the right-hand column, line 23, substitute "a free-energy" for "an enthalpic".—H. A. Scheraga

Frederick R. Duke and Vernon C. Bulgrin: Copper Catalysis in the Hexacyanoferrate(III) Oxidation of Mercaptoacetate.

Page 2323. The correct Table I for this article appears on page 2326.

George C. Levy, Tadeusz Holak, and Alois Steigel: Intra- and Intermolecular Hydrogen Bonding in Chlorinated Phenols and Related Compounds.

Page 2326. The correct Table I for this article appears on page 2323.

AUTHOR INDEX to Volume 79, 1975

Note: In this Author Index, titles of papers are listed after the name of each author of the paper. Multiple authorship is not indicated. Complete authorship may be ascertained by consulting the original paper.

KEYWORD INDEX to Volume 79, 1975

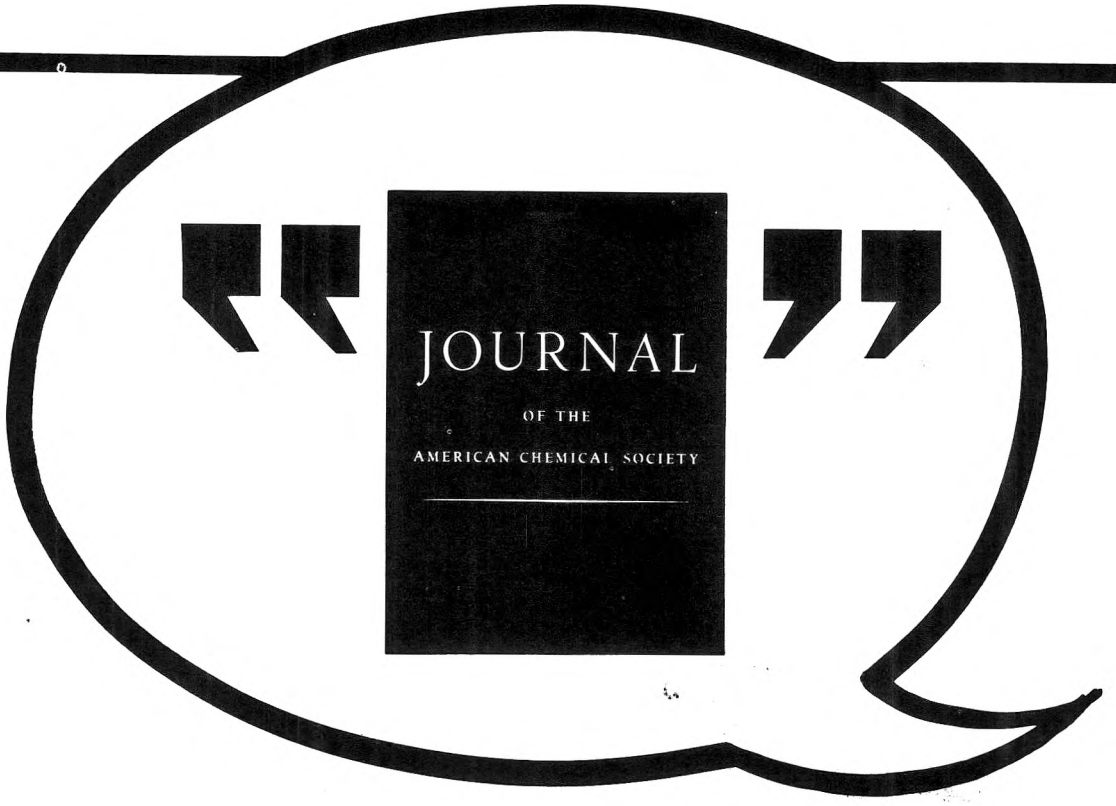

More chemists quote the Journal of The American Chemical Society than any other journal in the world BECAUSE ...

Each year the JOURNAL OF THE AMERICAN CHEMICAL SOCIETY publishes nearly 9,000 pages of new chemistry—original research of the widest possible interest in all fields of chemistry.

Each biweekly issue includes up to 50 definitive articles, and about the same number of concise, up-to-the-minute communications by the world's leading chemists.

No wonder the JOURNAL OF THE AMERICAN CHEMICAL SOCIETY is one of chemistry's great subscription values . . . no wonder it is read, studied and quoted by more working chemists than any other publication.

Take advantage of this extraordinary value now . . . complete and send in the coupon today.

Journal of the American Chemical Society
American Chemical Society **1976**
1155 Sixteenth Street, N.W.
Washington, D.C. 20036

Yes, I would like to receive the JOURNAL OF THE AMERICAN CHEMICAL SOCIETY at the one-year rate checked below:

	U.S.	*Canada***	*Latin America***	*Other Nations***
ACS Member One-Year Rate*	☐ $28.00	☐ $40.75	☐ $38.75	☐ $40.75
Nonmember	☐ $112.00	☐ $124.75	☐ $122.75	☐ $124.75

Bill me ☐ Bill company ☐ Payment enclosed ☐

Air freight rates available on request.

Name _____

Street _____ Home ☐ Business ☐

City _____ State _____ Zip _____

Journal subscriptions start January '76

*NOTE: Subscriptions at ACS member rates are for personal use only. **Payment must be made in U.S. currency, by international money order, UNESCO coupons, U.S. bank draft, or order through your book dealer.